THE JOURNAL OF

PHYSICAL CHEMISTRY

Volume 73, Number 4 April 1969

Thermodynamics of Iodine Trichloride. Entropy and Heat Capacity from 15 to 325°K. Composition of the Equilibrium ICl and Cl_2 Gas Phase . . . . . **R. H. Lamoreaux and W. F. Giauque** 755

A Thermodynamic Study of the Urania–Uranium System . . . **R. J. Ackermann, E. G. Rauh, and M. S. Chandrasekharaiah** 762

The Vapor Pressure of Liquid Uranium; Effects of Dissolved Tantalum, Phosphorus, Sulfur, Carbon, and Oxygen . . . **R. J. Ackermann and E. G. Rauh** 769

Electron Spin Resonance Studies of Hyperconjugation in 2,3-, 2,6-, and 2,7-Dimethylanthracene Cation and Anion Radicals . . . . . **Jorge A. Valenzuela and Allen J. Bard** 779

High-Temperature Vacuum Ultraviolet Photolysis of *n*-Butane . . **James R. McNesby and Rudolph V. Kelley** 789

The Mercury $6(^3P_1)$ Photosensitized Decomposition of Methyl Ethyl Ether. . . . . **S. V. Filseth** 793

The Diffusion of Polyelectrolyte in the Presence of Added Salt . . . **Yasuko Suzuki, Ichiro Noda, and Mitsuru Nagasawa** 797

The Electron Spin Resonance of Low-Spin Isocyanide Complexes of Cobalt(II). I. Halides . . . **Nobuko Kataoka and Hideo Kon** 803

Photolysis of Perfluorocyclobutane . . . . . **John E. Davenport and Glenn H. Miller** 809

Localized Adsorption on Graphite and Absolute Surface Areas . . . . . **Conway Pierce** 813

An Electron Spin Resonance Study of Radiation-Induced Centers of Chemical Activity in a Silica–Alumina Gel . . . **Robert R. Hentz and Dennis K. Wickenden** 817

Vacuum-Ultraviolet Photolysis of Polydimethylsiloxane. Gas Yields and Energy Transfer . . . **Seymour Siegel and Thomas Stewart** 823

Ionic Reactions in Unsaturated Compounds. IV. Vinyl Chloride . . . **B. Mason Hughes, Thomas O. Tiernan, and Jean H. Futrell** 829

Chemical Effects of Charge-Transfer Absorption. I. The Photoinduced Chain Reaction between Thallium(I) and Thallium(III) . . . . . **D. R. Stranks and J. K. Yandell** 840

The Use of Tritiated H_2S as a Radical Scavenger in the γ Radiolysis of Organic Liquids . . . **William A. Pryor and Umberto Tonellato** 850

A Molecular Orbital Description of TcH_9^{2-}. . . . . **Harold Basch and A. P. Ginsberg** 854

Proton Magnetic Resonance Study of Water–Ammonia Proton Exchange in Water–Ammonia Solutions Containing Added Potassium Hydroxide . . . . . **Mohammed Alei, Jr., and Alan E. Florin** 857

The Nature of Water Species in Water–Ammonia Solutions as Inferred from Proton and Oxygen-17 Nuclear Magnetic Resonance Observations . . . . . **Mohammed Alei, Jr., and Alan E. Florin** 863

Aqueous Chemistry of Inorganic Free Radicals. VI. The Effect of Oxygen on the Rate of Photolysis of Hydrogen Peroxide in Aqueous Solutions Containing Carbon Monoxide . . . **F. P. Laming, George Buxton, and W. K. Wilmarth** 867

A Mass Spectrometric Investigation of the Low-Pressure Pyrolysis of Borane Carbonyl. The Bond Dissociation Energy of Diborane . . . . . **T. P. Fehlner and G. W. Mappes** 873

Positronium Interactions in Aqueous Oxyacids and Hydrogen Compounds . . . . . **S. J. Tao and J. H. Greene** 882

Absolute Intensity of Thin-Film $C_6H_6(s)$ from Reflectance and Transmittance near 680 Cm^{-1} . . . **Donald E. Glover and J. Leland Hollenberg** 889

The Orthohydrogen–Parahydrogen Conversion and Hydrogen–Deuterium Equilibration on Sodium Tungsten Bronzes . . . . . **F. T. Jones and E. M. Loebl** 894

Relation between Local Structure and Thermodynamic Properties in Aqueous Fluids . . . **Frank H. Stillinger, Jr., and Arieh Ben-Naim** 900

Infrared Spectra of the Surface Species Produced by Reactions of Ammonia with Germania Gel . . . **M. J. D. Low and Kun-ichi Matsushita** 908

Infrared Studies of the Reactions between Silica and Trimethylaluminum . . . **D. J. C. Yates, G. W. Dembinski, W. R. Kroll, and J. J. Elliott** 911

Ultrasonic Absorption in Hydrated Melts. I. Systems of $Ca(NO_3)_2 \cdot 4H_2O$ and Its Mixtures with Water . . . **G. S. Darbari and S. Petrucci** 921

Thermodynamics of Aqueous Mixtures of Electrolytes and Nonelectrolytes. VII. Enthalpies of Transfer of Perchloric and Hydrochloric Acids from Pure Water to Aqueous Ethylene Glycol and Aqueous Acetic Acid at 25° . . . . . **J. H. Stern and J. M. Nobilione** 928

Electron Scavenging in the Radiolysis of Cyclohexane Solutions of Alkyl Halides . . . **John M. Warman, K.-D. Asmus, and Robert H. Schuler** 931

The Behavior of Entropy at Low Temperatures . . . . . **Alan J. Brainard** 940

A Parametric Study of Bimolecular Exchange Reactions . . . . . **Don L. Bunker and Tiang-Shing Chang** 943

Bonding in C_1 and C_2 Fluorides . . . . . **Thomas C. Ehlert** 949

Catalytic Polarographic Current of a Metal Complex. VI. Correlation of the Nickel(II)–*o*-Phenylenediamine Prewave Height with the Surface Concentration of the Ligand . . . **Lowell R. McCoy and Harry B. Mark, Jr.** 953

Photolysis of Ketene. Mechanism of Hydrogen Production and the Reaction of Methylene with Methane . . . **A. H. Laufer** 959

A Theoretical Study of Alkane Positive Ions in γ-Irradiated Organic Solids . . . . **K. Narita and K. Funabashi** 964

Argon–Ethylene Layer Formation on Graphitized Carbon Black . . . **Carl F. Prenzlow, H. Richard Beard, and Robert S. Brundage** 969

The Electrical Conductances of Some Alkali Metal Halides in Aqueous Solutions from 0 to 800° and at Pressures to 4000 Bars . . . . . **Arvin S. Quist and William L. Marshall** 978

Apparent Molal Heat Capacities of Aqueous Solutions of Alkali Halides and Alkylammonium Salts . . . **H. Rüterjans, F. Schreiner, U. Sage, and Th. Ackermann** 986

Spectrofluorometric Studies. IV. Some New Aspects of the Photochemistry of Monofluorobenzene . . . **M. E. MacBeath, G. P. Semeluk, and I. Unger** 995

Mass Spectrometric Investigation of the High-Temperature Reaction of Hydrogen with Boron Carbide . . . **Sara J. Steck, George A. Pressley, Jr., and Fred E. Stafford** 1000

The Electronic Density Distributions in Carbon Monoxide, Carbonyl Sulfide, and Carbon Dioxide . . . **Mark J. Hazelrigg, Jr., and Peter Politzer** 1008

Primary Processes in the Acetone Photochemical System . . . . . **H. Edward O'Neal and Carl W. Larson** 1011

The Effect of Normal Aliphatic Alcohols on Electrode Kinetics . . . **Katsumi Kanzaki Niki and Norman Hackerman** 1023

Far-Ultraviolet Spectra of Hydrogen and Hydroxyl Radicals from Pulse Radiolysis of Aqueous Solutions. Direct Measurement of the Rate of H + H . . . **P. Pagsberg, H. Christensen, J. Rabani, G. Nilsson, J. Fenger, and S. O. Nielsen** 1029

Enthalpy of Hydrolysis of Rhenium Trichloride. Enthalpy and Free Energy of Formation of Rhenium Sesquioxide . . . . . **R. H. Busey, E. D. Sprague, and R. B. Bevan, Jr.** 1039

The Proton Magnetic Resonance Spectra of Five *ortho*-Substituted Phenols . . . **James L. Roark and William B. Smith** 1043

The Nuclear Magnetic Resonance Spectra of Six *ortho*-Substituted Fluorobenzenes . . . **James L. Roark and William B. Smith** 1046

The Proton Magnetic Resonance Spectra of Several 2-Substituted Pyridines . . . **William B. Smith and James L. Roark** 1049

A Contribution to the Theory of Dielectric Dispersion of Colloidal Particles . . . . . **Robert S. Alwitt** 1052

The Dielectric Dispersion of Paper Impregnated with a Glycol Electrolyte . . . . . **Robert S. Alwitt** 1056

The Secondary Electroviscous Effect. Paths of Approach of Two Charged Spheres in a Viscous Medium . . . **J. Blachford, F. S. Chan, and D. A. I. Goring** 1062

Interpretation of Chlorophyll Electron Spin Resonance Spectra . . . **M. Garcia-Morin, R. A. Uphaus, J. R. Norris, and J. J. Katz** 1066

Foreign Gas Quenching of Sulfur Dioxide Vapor Emission . . . . . **H. D. Mettee** 1071

Aspects of the Pulse Radiolysis and γ Radiolysis of Alkyl Iodides and Their Mixtures . . . **C. Capellos and A. J. Swallow** 1077

Solubilities of Ammonia in Alkali Nitrate and Perchlorate Melts . . . . . **S. Allulli** 1084

The Distribution of Hydrogen Isotopes between $H_2PO_4^-$ and Water in Partially Deuterated Solutions . . . **Maurice M. Kreevoy, Richard A. Landholm, and Robert Eliason** 1088

Reduction of Cobalt(III) Complexes by Monovalent Zinc, Cadmium, and Nickel Ions in Aqueous Solutions . . . **D. Meyerstein and W. A. Mulac** 1091

Transport in Concentrated Solutions of 1:1 Electrolytes . . . . . **P. C. Carman** 1095

Ionization Potentials, Electronic and Molecular Structures of Metal Halides from Extended Hückel Theory . . . **J. W. Hastie and J. L. Margrave** 1105

The Role of Polar Factors in Collision Complex Models for the Solvent and Concentration Dependence of Nuclear Magnetic Resonance Parameters . . . . **Raymond L. Schmidt, Robert S. Butler, and J. H. Goldstein** 1117

Analysis of the Proton Nuclear Magnetic Resonance Spectrum of Trimethylene Selenide . . . **William B. Moniz** 1124

Thermodynamics of Solutions with Liquid Crystal Solvents. II. Surface Effects with Nematogenic Compounds . . . **Laurence C. Chow and Daniel E. Martire** 1127

Physical Properties and Chemical Reactivity of Alternant Hydrocarbons and Related Compounds. XVI. Electronic Absorption and Phosphorescence Spectra of Aryl Phenyl Ketones . . . **C. Párkányi, E. J. Baum, J. Wyatt, and J. N. Pitts, Jr.** 1132

Aromatic Hydroxylation Catalyzed by Fenton's Reagent. An Electron Paramagnetic Resonance Study. I. Furans. . . . . **Takeshi Shiga and Akio Isomoto** 1139

NOTES

Effect of Density and Electron Scavengers in Nitrous Oxide Radiolysis . . . . . **John T. Sears** 1143

The Dielectric Relaxation of Binary Liquid Mixtures . . . . . **K. Baba, T. Fujimura, and K. Kamiyoshi** 1146

Hyperfine and *g*-Tensor Anisotropy of the Tropenyl Radical . . . . . **Walter V. Volland and Gershon Vincow** 1147

Fluorescent Yields of 1,2,3,4-Tetrahydronaphthalene Excited in the 2850–3100-Å Region . . . **M. Grossman, G. P. Semeluk, and I. Unger** 1149

Direct Observation of Intrinsic Diastereotopic Magnetic Nonequivalence . . . . . **G. Redl and G. J. D. Peddle** 1150

Ion–Solvent Interactions. Relation to Solvent Dielectric Constant . . . . . **C. N. Hammonds and M. C. Day** 1151

Nuclear Magnetic Resonance Study of Concentrated Lithium Chloride Solutions. . . . . **Robert G. Bryant** 1153

Diffusion of Alcohols and Amides in Water from 4 to 37° . . . . . **C. M. Gary-Bobo and Heather W. Weber** 1155

Adhesive Forces in Mixed Films of Cholesterol and Octadecyl Sulfate as Detected by Desorption . . . **M. Muramatsu and N. L. Gershfeld** 1157

Kinetics of Hot Hydrogen Atoms from H_2S Photodissociation at 1850 Å . . . **L. E. Compton, J. L. Gole, and R. M. Martin** 1158

Activity Coefficients for Ionic Melts . . . . . **R. Haase** 1160

Determination of Water Activities of Dilute Electrolyte Solutions . . . . . **S. Amdur** 1163

Negative Partial Molal Volumes in the Critical Region. Mixtures of Ethylene and Vinyl Chloride . . . **Paul Ehrlich and Robert H. Fariss** 1164

Fluorescence of 2-Pentanone . . . . . **F. Sheldon Wettack** 1167

The *cis–trans* Effect in the H-Atom Addition to Olefins . . . **Richard D. Kelley, Ralph Klein, and Milton D. Scheer** 1169

The Apparent Molecular Area of Adsorbed Carbon Tetrachloride . . . . . **W. D. Machin** 1170

Photolysis of 1,5-Cyclooctadiene Vapor. Molecular Elimination of Ethylene from 1,5-Dienes . . . **Setsuo Takamuku and Hiroshi Sakurai** 1171

COMMUNICATIONS TO THE EDITOR

Catalytic Synthesis of Ammonia over the Electron Donor–Acceptor Complexes of Alkali Metals with Graphite or Phthalocyanines . . . **Mizuo Sudo, Masaru Ichikawa, Mitsuyuki Soma, Takaharu Onishi, and Kenzi Tamaru** 1174

Subnanosecond Observations of the Solvated Electron . . . . . **M. J. Bronskill, R. K. Wolff, and J. W. Hunt** 1175

Electron-Transfer Spectra and the II–III Oxidation Potentials of Some Lanthanide and Actinide Halides in Solution . . . **L. J. Nugent, R. D. Baybarz, and J. L. Burnett** 1177

Langmuir–Hinshelwood Mechanism as Revealed by Thermal Desorption Study. The Catalytic Decomposition of Methyl Formate on Copper Surface . . . . . **Naohiro Momma and Iwao Yasumori** 1179

AUTHOR INDEX

Ackermann, R. J., 762, 769
Ackermann, Th., 986
Alei, M., Jr., 857, 863
Allulli, S., 1084
Alwitt, R. S., 1052, 1056
Amdur, S., 1163
Asmus, K.-D., 931

Baba, K., 1146
Bard, A. J., 779
Basch, H., 854
Baum, E. J., 1132
Baybarz, R. D., 1177
Beard, H. R., 969
Ben-Naim, A., 900
Bevan, R. B., Jr., 1039
Blachford, J., 1062
Brainard, A. J., 940
Bronskill, M. J., 1175
Brundage, R. S., 969
Bryant, R. G., 1153
Bunker, D. L., 943
Burnett, J. L., 1177
Busey, R. H., 1039
Butler, R. S., 1117
Buxton, G., 867

Capellos, C., 1077
Carman, P. C., 1095
Chan, F. S., 1062
Chandrasekharaiah, M. S., 762
Chang, T.-S., 943
Chow, L. C., 1127
Christensen, H., 1029
Compton, L. E., 1158

Darbari, G. S., 921
Davenport, J. E., 809
Day, M. C., 1151
Dembinski, G. W., 911

Ehlert, T. C., 949
Ehrlich, P., 1164
Eliason, R., 1088
Elliott, J. J., 911

Fariss, R. H., 1164
Fehlner, T. P., 873
Fenger, J., 1029
Filseth, S. V., 793
Florin, A. E., 857, 863
Fujimura, T., 1146
Funabashi, K., 964
Futrell, J. H., 829

Garcia-Morin, M., 1066
Gary-Bobo, C. M., 1155
Gershfeld, N. L., 1157
Giauque, W. F., 755
Ginsberg, A. P., 854
Glover, D. E., 889
Goldstein, J. H., 1117
Gole, J. L., 1158
Goring, D. A. I., 1062
Greene, J. H., 882
Grossman, M., 1149

Haase, R., 1160
Hackerman, N., 1023
Hammonds, C. N., 1151
Hastie, J. W., 1105
Hazelrigg, M. J., Jr., 1008
Hentz, R. R., 817
Hollenberg, J. L., 889
Hughes, B. M., 829
Hunt, J. W., 1175

Ichikawa, M., 1174
Isomoto, A., 1139

Jones, F. T., 894

Kamiyoshi, K., 1146
Kataoka, N., 803
Katz, J. J., 1066
Kelley, R. D., 1169
Kelley, R. V., 789
Klein, R., 1169
Kon, H., 803
Kreevoy, M. M., 1088
Kroll, W. R., 911

Laming, F. P., 867
Lamoreaux, R. H., 755
Landholm, R. A., 1088
Larson, C. W., 1011
Laufer, A. H., 959
Loebl, E. M., 894
Low, M. J. D., 908

MacBeath, M. E., 995
Machin, W. D., 1170
Mappes, G. W., 873
Margrave, J. L., 1105
Mark, H. B., Jr., 953
Marshall, W. L., 978
Martin, R. M., 1158
Martire, D. E., 1127
Matsushita, K., 908
McCoy, L. R., 953
McNesby, J. R., 789
Mettee, H. D., 1071
Meyerstein, D., 1091
Miller, G. H., 809
Momma, N., 1179
Moniz, W. B., 1124
Mulac, W. A., 1091
Muramatsu, M., 1157

Nagasawa, M., 797
Narita, K., 964
Nielsen, S. O., 1029
Niki, K. K., 1023
Nilsson, G., 1029
Nobilione, J. M., 928
Noda, I., 797
Norris, J. R., 1066
Nugent, L. J., 1177

O'Neal, H. E., 1011
Onishi, T., 1174

Pagsberg, P., 1029
Párkányi, C., 1132
Peddle, G. J. D., 1150
Petrucci, S., 921
Pierce, C., 813
Pitts, J. N., Jr., 1132
Politzer, P., 1008
Prenzlow, C. F., 969
Pressley, G. A., Jr., 1000
Pryor, W. A., 850

Quist, A. S., 978

Rabani, J., 1029
Rauh, E. G., 762, 769
Redl, G., 1150
Roark, J. L., 1043, 1046, 1049
Rüterjans, H., 986

Sage, U., 986
Sakurai, H., 1171
Scheer, M. D., 1169
Schmidt, R. L., 1117
Schreiner, F., 986
Schuler, R. H., 931
Sears, J. T., 1143
Semeluk, G. P., 995, 1149
Shiga, T., 1139
Siegel, S., 823
Smith, W. B., 1043, 1046, 1049
Soma, M., 1174
Sprague, E. D., 1039
Stafford, F. E., 1000
Steck, S. J., 1000
Stern, J. H., 928
Stewart, T., 823
Stillinger, F. H., Jr., 900
Stranks, D. R., 840
Sudo, M., 1174
Suzuki, Y., 797
Swallow, A. J., 1077

Takamuku, S., 1171
Tamaru, K., 1174
Tao, S. J., 882
Tiernan, T. O., 829
Tonellato, U., 850

Unger, I., 995, 1149
Uphaus, R. A., 1066

Valenzuela, J. A., 779
Vincon, G., 1147
Volland, W. V., 1147

Warman, J. M., 931
Weber, H. W., 1155
Wettack, F. S., 1167
Wickenden, D. K., 817
Wilmarth, W. K., 867
Wolff, R. K., 1175
Wyatt, J., 1132

Yandell, J. K., 840
Yasumori, I., 1179
Yates, D. J. C., 911

THE JOURNAL OF
PHYSICAL CHEMISTRY

Registered in U. S. Patent Office © Copyright, 1969, by the American Chemical Society

VOLUME 73, NUMBER 4 APRIL 1969

Thermodynamics of Iodine Trichloride. Entropy and Heat Capacity from 15 to 325°K. Composition of the Equilibrium ICl and Cl_2 Gas Phase[1]

by R. H. Lamoreaux and W. F. Giauque

Low Temperature Laboratory, Departments of Chemistry and Chemical Engineering, University of California, Berkeley, California 94720 *(Received October 14, 1968)*

The heat capacity of ICl_3 has been measured from 13 to 325°K. Its entropy was found to be 40.40 gibbs/mol and its free energy and heat of formation from the elements, $\Delta F^\circ = -5413$ cal/mol, $\Delta H^\circ = -21{,}340$ cal/mol, each at 298.15°K. $\Delta H^\circ_0 = -21{,}723$ cal/mol. Values of C_p°, S°, $(F^\circ - H^\circ_0)/T$, and $(H^\circ - H^\circ_0)/T$ have been tabulated. The temperature of the ICl_3–ICl eutectic has been found to be 296.21°K and the partial pressures over the eutectic are $P(ICl) = 23.9$ Torr and $P(Cl_2) = 19.7$ Torr. For the reaction $ICl_3(s) = ICl(g) + Cl_2(g)$, $\Delta H^\circ_0 = 26{,}297$ cal/mol. The vapor over $ICl_3(s)$ and the equilibrium liquid on the ICl side is known to consist of ICl and Cl_2. Their partial pressures have been evaluated over the range 296.56–312.78°K. Below 301.5°K, ICl predominates in the vapor and above this temperature an excess of Cl_2 increases rapidly. An error in the calculations of Calder and Giauque, *J. Phys. Chem.*, **69**, 2443 (1965), has been noted for the reaction $ICl(s)(l) = ICl(g)$. ΔH°_0 should have been 13,245 cal/mol instead of 13,273 cal/mol used in their calculations. Revised values of the vapor pressure of ICl and data relating to ΔF and ΔH for several reactions are given in an addendum to the present paper.

This paper reports a continuation of the work in this laboratory on the thermodynamics of the iodine–chlorine system. A previous paper[2] has reported heat capacity data to low temperatures on iodine monochloride together with measurements of the composition and pressure of the equilibrium vapor over the liquid. The present paper reports heat capacity data on ICl_3 over the range 15–320°K and measurements of the Cl/I atomic composition ratio in the gas over solid ICl_3 and the liquid which is in equilibrium with it on the ICl side of its melting curve. The above ratio at the ICl_3:ICl eutectic temperature, which was evaluated from the measurements, enabled the calculation of the partial pressures of ICl and Cl_2 gases over this solid–liquid equilibrium system. These data, combined with the previous work on ICl,[2] determine the free energy of formation of ICl_3, which, with the entropy values based on the third law of thermodynamics, enables evaluation of its heat of formation from ICl and Cl_2 or from $\frac{1}{2}I_2$ and $\frac{3}{2}Cl_2$.

Previous measurements on this system, including the above Cl/I composition ratio in the gas, have been made by Stortenbeker[3,4] and by Nies and Yost.[5]

The present measurements of the Cl/I composition ratio should be considerably more accurate due to the use of constant stirring in the thermostated solid–liquid system, and the taking of large samples for analysis through a fine capillary over a very long time period, so as not to disturb the equilibrium.

Experimental Section

Calorimetric Apparatus. The calorimetric apparatus of Giauque and Egan[6] was used except that a Hastelloy Type C alloy[7] calorimeter was substituted for the

(1) This work was supported in part by National Science Foundation Grant GP-8137.

(2) G. V. Calder and W. F. Giauque, *J. Phys. Chem.*, **69**, 2443 (1965).

(3) W. Stortenbeker, *Rec. Trav. Chim.*, **7**, 152 (1888).

(4) W. Stortenbeker, *Z. Physik. Chem.*, **3**, 11 (1889); **10**, 183 (1893).

(5) N. P. Nies and D. M. Yost, *J. Amer. Chem. Soc.*, **57**, 306 (1935).

(6) W. F. Giauque and C. J. Egan, *J. Chem. Phys.*, **5**, 45 (1937).

(7) Union Carbide Co., Kokomo, Ind.

original gold calorimeter to avoid corrosion. The ability of Hastelloy to successfully resist corrosion in this interhalogen system had been investigated in connection with the work on ICl.[2] A sample of ICl_3 was kept in the Hastelloy shell of the final calorimeter for 20 days and then removed. The vessel was rinsed with aqueous KI, then with distilled water, and baked at 110° while being flushed with dry N_2 gas.

The thermal conductivity of Hastelloy is so low that it is far from an ideal material to assist the attainment of equilibrium in a calorimeter. In an attempt to improve this situation, we tried the suggestion of Calder and Giauque,[2] who suggested the addition of a copper layer made from a tube soldered to the exterior of the Hastelloy. The idea might have succeeded if the copper had been welded to the Hastelloy; however, the solder could not resist the differential contraction on cooling, leading to breakage of the gold thermometer–heater wound on the exterior of the calorimeter, which was discarded. To avoid this difficulty, a second Hastelloy calorimeter was enclosed in a slightly loose copper jacket, onto which the gold thermometer–heater was wound. The space between the Hastelloy and copper was filled with helium gas. The arrangement was a substantial improvement over the original Hastelloy calorimeter. The completed calorimeter is shown in Figure 1. Hastelloy C tubes, 0.254 cm o.d.

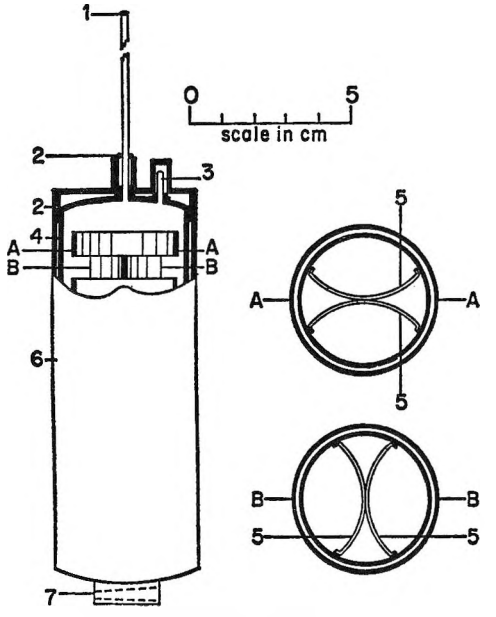


Figure 1. Hastelloy calorimeter, with internal Hastelloy jacketed copper heat conductors and external copper jacket, for use with halogens.

and 0.17 cm i.d., are shown as 1 and 3. They were used in the procedure for filling the calorimeter with ICl_3, as described later. The Hastelloy C calorimeter is indicated by 4. The dimensions of the Hastelloy shell were identical with those given by Calder and Giauque.[2] In addition, sections A–A and B–B show flattened Hastelloy tubes, 5, which were welded into the cylindrical calorimeter as indicated. These 0.475-cm diameter tube sections were 6.5 cm long with a 0.013-cm wall. They were rolled nearly flat so that copper strips 5.5 cm long and 0.013 cm thick could be inserted before the final rolling. The Hastelloy ends were sealed with an atomic hydrogen torch before they were formed into semicircles and electrically spot-welded in place. Thirteen pairs of vanes, arranged in a staggered configuration, were placed in the calorimeter to improve lateral thermal conductivity. The volume of the calorimeter was 144 cm^3. It seems probable that a very small amount of hydrogen gas was enclosed in these tubes during the welding operation. This would assist heat transfer between the copper strips and their enclosing Hastelloy jackets. The outer cylindrical copper jacket, 6, was added to provide longitudinal thermal conductivity, after the calorimeter had been filled with ICl_3. It was desirable not to have longitudinal conductivity during the filling operation to be described later. Epoxy joints, 2,2, were used for the final closure of the copper jacket to avoid the heat required for soldered joints. A detachable thermocouple well is shown at 7. This device has been described by Busey and Giauque.[8]

A gold thermometer–heater constructed as described by Murch and Giauque[9] was wound on the exterior of the copper jacket. Standard copper–constantan thermocouple No. W-23 was used as a temperature reference. It was compared with normal hydrogen triple point, 13.95°K, and boiling point, 20.37°K; and nitrogen triple point, 63.15°K, and boiling point, 77.33°K. Appropriate corrections were made for the small change since the original calibration in 1933. 0°C was taken as 273.15°K. One defined calorie was taken as 4.18400 absolute joules.

Preparation of ICl_3. The general procedure was similar to that described by Calder and Giauque[2] for the preparation of ICl. The chlorine was purified in a low-temperature vacuum-jacketed silvered fractionation column as described previously.[2]

The Mallinckrodt iodine used was stated to contain only 0.005% Cl + Br and 0.01% of nonvolatile material.

All analyses were made by weighing the combined halogens followed by conversion to I_3^- ion with aqueous KI solution and weight titration with aqueous $Na_2S_2O_3$.

Filling the Calorimeter. According to Stortenbeker,[3] ICl_3 "melts" only at some temperature near 101°, and at a pressure of some 16 atm.[3] The problem of introducing such a material to a calorimeter is somewhat complex. An attempt was made with the first calorimeter by

(8) R. H. Busey and W. F. Giauque, *J. Amer. Chem. Soc.*, **74**, 4443 (1952).

(9) L. E. Murch and W. F. Giauque, *J. Phys. Chem.*, **66**, 2052 (1962).

adding a known amount of the I_2–ICl eutectic as liquid, because of its low vapor pressure. This was followed by the condensation of an amount of liquid chlorine which was slightly less than the amount required to form stoichiometric ICl_3. After sufficient cooling and the addition of some helium for thermal conduction, the filling tube of the Hastelloy calorimeter was closed by pinching it, followed by heliarc welding. The calorimeter was then heated to 110° to facilitate reaction. Some preliminary heat capacity measurements showed heat effects near the melting point of chlorine and were taken as a definite indication that equilibrium combination had not occurred. It is probable that the helium interferred with the reaction since the necessary diffusion would be slow. Also, since the substance is considerably decomposed into Cl_2 and ICl gases near 100°, with a substantial excess of Cl_2, stoichiometric recombination with the resultant ICl rich liquid may have been difficult in the range below 100°. We visualize an ICl-rich liquid at the bottom, the ICl_3 solid intermediate, with the Cl_2 rich gas above. Although the calorimeter was repeatedly turned end over end during the cooling, complete recombination was not attained. An alternate procedure was then substituted.

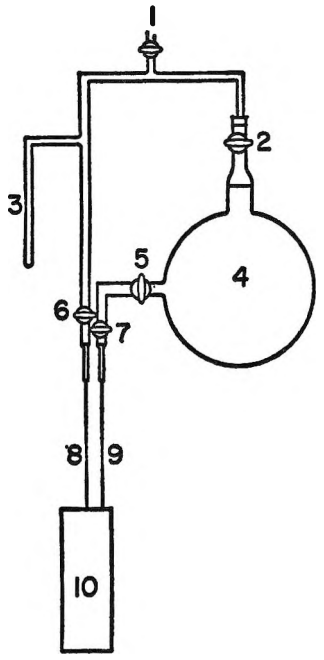


Figure 2. Schematic diagram of apparatus used for filling calorimeter with solid iodine trichloride by using chlorine as a carrier gas.

Figure 2 is a schematic drawing of the arrangement used for condensing the solid ICl_3 within the second Hastelloy calorimeter, 10, of Figure 2. The Hastelloy tubes, 8 and 9 of Figure 2, were sealed to common glass which was attached to the Pyrex apparatus by means of graded seals. A 1:3 mixture of Kel-F200 wax with Kel-F210 grease[10] was used[2] to lubricate stopcocks. The method of transfer recognizes the fact that solid ICl_3 decomposes to give only ICl and Cl_2 in the vapor. This was shown by the early but accurate gas density experiment of Melikoff.[11]

The present experiments show that above 301.5°K the vapor contains a Cl_2/ICl molecular ratio in excess of unity. At first it was thought that a simple circulating system, with the lower part of the calorimeter cooled to the ice point and the ICl_3 supply flask, 4 of Figure 2, and other upper portions of the system heated to about 333°K would transport the material to the calorimeter by simple convection, using the Cl_2 as a temporary carrier gas. The Hastelloy inlet and outlet tubes of the calorimeter, 8 and 9 in Figure 2, were heated electrically. This method was undoubtedly correct in principle but too slow.

The method was then modified with the assistance of stopcocks 2, 5, 6, and 7 and a side tube, 3, which could be cooled to 196°K, the temperature of solid CO_2. At the ice point the vapor pressure over ICl_3 is quite low and the partial pressure of ICl exceeds that of Cl_2 unless Cl_2 is present in excess. The vapor pressure of liquid chlorine at 196°K is too high to remove chlorine from ICl_3 at 273°K by decomposition. At 333°K the vapor pressure is of the order of 1 atm and the Cl_2 partial pressure is greatly in excess of the ICl pressure. The Hastelloy calorimeter was filled before the copper jacket was added; thus it had quite poor longitudinal conductivity and the lower portions could easily be maintained near the ice point while the top and tubes 8 and 9 remained warm. The sequence of the filling operation was as follows.

(A) Stopcocks 5, 6, and 7 were open and stopcock 2 was closed. The side tube, 3, was at 196°K, the supply bulb, 4, was at 333°K, and the bottom of the calorimeter, 10, was at 273°K. The condensation of liquid Cl_2 in the side tube greatly accelerated the transfer. However, the removal of Cl_2 eventually depleted the chlorine fraction of the original ICl_3 in supply bulb 4 and the process slowed.

(B) Stopcocks 5 and 6 were closed and 2 was opened. Side tube 3 was warmed and supply bulb 4 cooled somewhat until the chlorine was transferred to it. Sequence A was then repeated.

After three cycles, the ICl_3 was nearly all condensed in the calorimeter as a solid. Stopcocks 6 and 7 were then closed and 2 was opened so that all residual amounts of halogen in side tube 3 and supply bulb 4 could be removed through stopcock 1 for analysis. The final result showed a small deficiency of chlorine, which was considered preferable to an excess, since data were available[2] to correct the heat capacity for a small amount of solid ICl obtained as eutectic mixture in the cooled sample. The calorimeter contained 0.99922 mol

(10) Minnesota Mining and Manufacturing Co., St. Paul, Minn.
(11) P. Melikoff, *Ber. Deut. Chem. Ges.* (Berlin), 8, 490 (1875).

of ICl_3 and the chlorine deficiency produced 0.00584 mol of ICl in the solid sample investigated.

The calorimeter was then cooled in ice and an atmosphere of helium was added. Tubes 1 and 3 of Figure 1 were then pinched off and sealed by heliarc welding. The copper jacket, 6, of Figure 1, was then added.

The Eutectic Temperature of Iodine Monochloride and Iodine Trichloride. Since the eutectic equilibrium gives an important relation between the ICl and ICl_3 systems, its temperature was determined in separate experiments.

ICl_3 (0.65 mol) and ICl (1.60 mol) were added to a closed Pyrex glass bulb with a well for a copper–constantan thermocouple. Thermal contact between the well and thermocouple junction was obtained by means of kerosene.

After cooling the assembly to about 0°, it was allowed to warm slowly and the temperature stayed constant for a long period (days) at 23.06° = 296.21 ± 0.01°K. The experiment was repeated with an identical result.

Heat Capacity Observations. The heat capacity data are recorded in Table I. As mentioned above, the sample was slightly deficient with respect to chlorine and was shown by analysis to consist of 0.99922 mol of ICl_3 and 0.00584 mol of ICl.

All of the runs above the eutectic temperature, 296.21°K, show the effect of some ICl_3 melting into the equilibrium liquid phase due to the very small excess of ICl. The principal heat of eutectic melting is included in the run at T_{av} = 293.87°K. However, there were other minor disturbances which extended for some 25° below the eutectic temperature. These are typical of eutectic behavior when one of the phases is present in such small proportion that much of the minor phase cannot form macroscopic crystals. As is well known, microscopic crystals melt at various temperatures below the melting point of the macroscopic phase. The two runs at 272.17 and 280.00°K, which were obviously low and high, respectively, were examined with considerable care. These heat capacities were confirmed by the use of the thermocouple data in addition to the more precise resistance thermometer observations. A plausible explanation can be found in the assumption that some of the microscopic regions of ICl were so small that crystallization did not occur during the slow but relatively rapid initial cooling. Additional crystallization could have occurred during the heat capacity measurement at 272.17°K, which would appear low due to the uncounted heat evolution. Similarly, the high run following, at 280.00°K, can be explained by the melting of most of the newly formed microscopic crystals. While the effect is noticeable on the heat capacity measurements, the effect on the data as a whole is trivial. The temperature rise for each run is given so that the total energy input is a matter of record. In extrapolating the heat capacity data through the above region practically all of the observations have been assumed to be somewhat high for the above reasons.

Table I: Heat Capacity of Iodine Trichloride Sample[a,b,c]

T_{av}, °K	ΔT, °K	C_{measd}	T_{av}, °K	ΔT, °K	C_{measd}
13.83	1.859	1.61	159.55	7.874	20.81
15.85	2.021	2.12	167.59	7.954	21.13
18.27	2.110	2.72	173.55	7.616	21.37
20.90	2.677	3.55	181.17	7.231	21.46
24.70	4.606	4.64	188.39	7.295	21.55
29.92	4.089	6.20	196.54	7.960	21.80
34.12	3.818	7.17	204.81	7.279	22.13
37.95	3.630	8.05	206.66	8.416	22.26
41.32	3.000	8.89	215.38	7.992	22.47
45.15	4.563	9.73	223.75	7.638	22.61
49.83	4.766	10.69	232.11	7.889	22.92
54.84	5.327	11.71	240.33	7.549	22.97
60.63	6.258	12.70	248.49	7.107	23.38
64.85	7.151	13.35	256.15	6.933	23.42
71.89	6.942	14.33	263.76	7.220	23.41
78.78	6.776	15.04	272.17	7.032	23.20[d]
85.91	7.304	15.81	280.00	6.573	24.13[d]
93.10	6.934	16.48	283.13	7.364	23.71
100.46	7.663	17.14	286.74	6.418	23.93
107.91	7.514	17.77	290.33	7.110	25.92[d]
115.49	7.593	18.31	293.87	5.807	30.11[d]
122.93	7.398	18.88	298.21	7.488	28.84[d]
130.55	7.795	19.39	303.89	7.673	24.92[d]
138.08	7.205	19.80	312.77	7.171	25.72[d]
144.86	6.696	20.16	321.14	6.929	26.71[d]
151.90	7.149	20.46			

[a] 0°C = 273.15°K; mol wt: ICl_3 = 233.2634, ICl = 162.3574. [b] *C* in gibbs/mol, 1 gibbs = 1 defined cal/defined deg. [c] 234.0285 g (*in vacuo*) = 0.99922 mol of ICl_3 + 0.00584 mol of ICl in calorimeter. [d] These points were given no weight when the smooth curve was drawn.

Thermodynamic Properties of Iodine Trichloride. The molal heat capacity of pure ICl_3 was calculated from the observations in Table I by correcting the heat capacity of the sample for the small fraction of ICl, using the data of Calder and Giauque.[2] The resulting thermodynamic properties are given in Table II.

As previously noted,[2] the crystal structure of α-ICl[12] is an ordered chain that should have no residual entropy. Similarly, the structure of ICl_3[13] is ordered into symmetrical I_2Cl_6 units of such a nature that no third-law discrepancy should occur. Thus each of these systems has been assumed to approach zero entropy at 0°K. The extrapolation to 0°K was made on a C_p/T *vs.* T^2 plot.

Composition of the Vapor in Equilibrium with ICl_3 and Liquid. The pressure and composition of the vapor over solid ICl_3 and the equilibrium liquid on the ICl side of the pure trichloride have fixed values for each

(12) K. H. Boswijk, J. van der Heide, A. Vos, and E. H. Wiebenga, *Acta Cryst.*, 9, 274 (1956).

(13) K. H. Boswijk and E. H. Wiebenga, *ibid.*, 7, 417 (1954).

Table II: Thermodynamic Properties of Iodine Trichloride[a]

T, °K	$C_p°$	$S°$	$-F° - H°_0/T$	$H° - H°_0/T$
15	1.90	0.764	0.208	0.557
20	3.28	1.497	0.435	1.062
25	4.74	2.384	0.734	1.651
30	6.23	3.382	1.091	2.291
35	7.39	4.428	1.493	2.936
40	8.57	5.492	1.926	3.567
45	9.71	6.568	2.382	4.187
50	10.76	7.646	2.854	4.792
55	11.75	8.725	3.339	5.386
60	12.62	9.785	3.832	5.953
65	13.39	10.826	4.330	6.496
70	14.09	11.844	4.831	7.014
75	14.70	12.838	5.332	7.507
80	15.23	13.804	5.831	7.973
85	15.64	14.742	6.328	8.414
90	16.21	15.654	6.821	8.833
95	16.67	16.543	7.309	9.234
100	17.11	17.410	7.793	9.617
110	17.95	19.080	8.743	10.337
120	18.68	20.673	9.672	11.002
130	19.39	22.198	10.577	11.621
140	19.93	23.655	11.460	12.196
150	20.40	25.047	12.319	12.728
160	20.84	26.377	13.157	13.221
170	21.23	27.653	13.972	13.681
180	21.52	28.875	14.766	14.109
190	21.78	30.045	15.540	14.505
200	22.03	31.169	16.294	14.875
210	22.29	32.248	17.028	15.220
220	22.56	33.291	17.743	15.548
230	22.81	34.299	18.441	15.858
240	23.07	35.276	19.123	16.153
250	23.29	36.222	19.788	16.434
260	23.48	37.139	20.438	16.702
270	23.65	38.029	21.073	16.956
273.15	23.69	38.303	21.270	17.033
280	23.80	38.891	21.694	17.198
290	23.96	39.730	22.301	17.428
298.15	24.08	40.395	22.787	17.609
300	24.11	40.544	22.896	17.649
310	24.25	41.337	23.478	17.859
320	24.38	42.109	24.048	18.061
330	24.50	42.861	24.607	18.254

[a] Units are gibbs/mol (1 gibbs ≡ 1 defined cal/defined deg).

temperature. The present work has included a determination of the vapor composition over the range 296.56–312.78°K.

The principal sources of error in such a determination are related to the difficulty in obtaining large enough representative samples of the gas to give high analytical accuracy without disturbing the solid–liquid–gas equilibrium. Even if an equilibrium sample of the vapor could be enclosed in a thermostated bulb of practicable size, adsorption effects could interfere.

To avoid the above difficulties and obtain increased accuracy over previous work, we used essentially the same procedure as that of Calder and Giauque;[2] namely, the samples were withdrawn through a fine electrically heated capillary over a very long period, with complete condensation at liquid nitrogen temperature. The heated capillary is essential since otherwise the expansion and cooling of the ICl gas within the capillary would cause error through loss of deposited solid and possible blockage of the tube. However, the magnetic stirrer used in the earlier experiments with ICl[2] was unsuitable for the present solid–liquid mixture. As a substitute, the sample was contained in a disk-shaped Pyrex flask 22 cm in diameter with a volume of 1520 cm³. The flask, which was completely immersed in a thermostat, controlled to 0.01°, was connected to a 140-cm length of 0.4-mm i.d. capillary, which was in turn connected to a sample take-off manifold. The whole assembly was mounted horizontally on a rocker within the thermostat so that the liquid–solid mixture flowed gently from side to side with a period of 4.6 sec to ensure equilibrium.

The first sample, initally composed of 3.885 g-atoms of I_2 and 6.442 g-atoms of Cl_2 was used for measurements at temperatures below and including 28.48°. Depletion of this sample made a second amount composed of 5.007 g-atoms of I_2 and 10.92 g-atoms of Cl_2 necessary. At higher temperatures the results were somewhat erratic and it became obvious that the increasing vapor pressure was causing the removal of material too fast to maintain equilibrium between the three phases within the sample chamber. When the 0.4-mm i.d. capillary length was increased to 371 cm to reduce flow rate, the results were still somewhat erratic. It was then realized that the diffusion rate at the higher temperatures was causing a disproportionate loss of Cl_2 back into the sample chamber. A train of two 1.0-cm long capillaries, 0.1 mm i.d., separated by a 1-cm³ bulb was added below the water level of the thermostat in the manner used by Calder and Giauque.[2] This eliminated the difficulty. The last point recorded at 28.38° in Table III was a repeated observation, made as a check that error had not occurred before it became apparent with the initial take-off arrangement. The chlorine:iodine ratio in the gas was determined from the weight of each sample, followed by its complete conversion to I_3^-, by means of aqueous KI, and weight titration with aqueous $Na_2S_2O_3$. In order to avoid excess pressure during the weighing of the warmed condensation bulbs when chlorine was in considerable excess, either some solid KI, or usually KI with a little water, was added to the bulbs before taking the sample. The data are given in Table III.

By extrapolation over the 0.35° interval below the measurement at 296.56°K to the eutectic temperature, 296.21°K, the value of $r_{eut} = (n_{Cl}/n_I)_{eut} = 2.6520$, where the n's refer to the number of g-atoms. Since the vapor consists only of ICl and Cl_2,[11] the atomic ratio r_{eut} evaluates the molecular ratio at the eutectic as $(Cl_2/ICl)_{eut} = 0.8260$.

Table III: Composition of the Vapor over Solid ICl_3 and the Equilibrium Liquid on the ICl Side of Its Melting Curve (Experimental)

T, °K	n, g-atoms in sample	Time, hr	Atomic ratio = r	Molec. ratio P_{Cl_2}/P_{ICl}
296.56	0.07738	24.0	2.670	0.8350
296.56	0.07612	23.8	2.669	0.8345
296.56	0.07800	24.2	2.670	0.8350
298.97	0.09376	20.9	2.821	0.9105
298.95	0.10776	24.0	2.822	0.9110
298.95	0.10147	22.8	2.823	0.9115
301.48	0.13433	21.0	2.994	0.9970
301.50	0.15233	23.7	2.995	0.9975
301.58	0.15243	23.0	3.002	1.0010
301.63	0.16083	24.2	3.004	1.0020
301.59	0.15544	23.5	3.001	1.0005
303.11	0.11299	26.0	3.123	1.0615
303.11	0.10879	25.0	3.128	1.0640
303.11	0.10349	23.7	3.122	1.0610
303.11	0.09019	23.8	3.128	1.0640
303.11	0.10510	24.0	3.123	1.0615
307.35	0.15963	20.1	3 476	1.2380
307.35	0.13742	17.3	3.474	1.2370
312.78	0.13582	8.1	4.017	1.5085
312.78	0.11582	6.9	4.023	1.5115
301.53	0.08410	24.4	2.995	0.9975

The work of Calder and Giauque[2] produced data for the indirect evaluation of the partial pressures of ICl and Cl_2 over liquid and solid ICl. Since the crystal structures of ICl and ICl_3 are so different,[12,13] it is considered improbable that the ICl_3–ICl eutectic involves solid solutions. Thus the partial pressure of ICl over this eutectic should be the same as that for pure ICl. Also, since the molecular Cl_2/ICl composition ratio is known

$$P_{Cl_2} = (Cl_2/ICl)P_{ICl} \quad (1)$$

and

$$P_{total} = P_{ICl}(1 + Cl_2/ICl) \quad (2)$$

Nies and Yost[5] made two determinations of the vapor pressure over solid ICl_3 and its equilibrium liquid at 24.8 and 34.8°, respectively, by means of a "click" gauge. When these values were plotted as log P *vs.* $1/T$ and extrapolated over the short interval to the eutectic temperature, the result was 1.9 Torr higher than the result obtained from eq 2. While a "click" gauge is a little less accurate than the presssure balance against a buffered column of mercury, as used by Calder and Giauque, the difference was more than we had expected because of the close connection with the direct ICl vapor pressure measurement. Calder and Giauque[2] had used third-law data for calculating the vapor pressure of the solid from the actual observations on the liquid.

$$ICl(s)(l) = ICl(g) \quad (3)$$

$$\Delta F^\circ/T = R \ln (760/P) = \Delta(F^\circ - H^\circ_0)/T + \Delta H^\circ_0/T \quad (4)$$

where P is the partial pressure of ICl expressed in Torr. A check of their calculation showed that the ΔH°_0 evaluated from their data should have been 13,245 cal/mol instead of the incorrect value 13,273 cal/mol given in their paper.[2] We shall add corrections of Calder and Giauque's equations 11, 12, 13, 20, 22, and 23, and their Tables VII and IX (vapor pressures) as an Addendum to the present paper.

When the above correction is made, $P_{ICl} = 23.9$ Torr at the ICl_3–ICl eutectic, 296.21°K, and the use of this value in our eq 2 gives $P_{Cl_2} = 19.7$ Torr and a total pressure of 43.6 Torr. This is in agreement with the 43.3 Torr value obtained by an assumed linear extrapolation of the two vapor pressure values of Nies and Yost[5] to the eutectic temperature, and differs within the limits of their 0.1° measurements.

The Free Energy of Formation of ICl_3. The vapor pressure equilibrium over the ICl_3–ICl eutectic determines the free energy of formation of $ICl_3(s)$ from ICl(s) and $Cl_2(g)$ at the eutectic temperature

$$ICl(s) + Cl_2(g) = ICl_3(s) \quad (5)$$

$$(\Delta F^\circ/296.21) = -R \ln (760/P_{Cl_2}) = -7.259 \text{ gibbs/mol} = \Delta(F^\circ - H^\circ_0)/T + \Delta H^\circ_0/T$$

From the table of thermodynamic properties for $Cl_2(g)$ given by Evans, Munson, and Wagman,[14] the similar table for ICl(s)(l)[2] and Table II for $ICl_3(s)$, ΔH°_0 is found to be −13,052 cal/mol, $\Delta H^\circ_{298.15°K} =$ 12,902 cal/mol, and $\Delta F^\circ_{298.15°K} = -2079$ cal/mol for reaction 5. Subtracting eq 3 from eq 5, and using the corrected values of Calder and Giauque as given in the Addendum below, one obtains

$$ICl(g) + Cl_2(g) = ICl_3(s) \quad (6)$$

for which $\Delta H^\circ_0 = -26{,}297$ cal/mol, $\Delta H^\circ_{298.15°K} =$ −25,524 cal/mol, and $\Delta F^\circ_{298.15°K} = -4045$ cal/mol.

From Calder and Giauque,[2] we obtain

$$\tfrac{1}{2}Cl_2 + \tfrac{1}{2}I_2(g) = ICl(g) \quad (7)$$

$$\Delta H^\circ_0 = -3255 \pm 25 \text{ cal/mol}$$

$$\Delta H^\circ_{299.15°K} = -3277 \pm 25 \text{ cal/mol}$$

$$\Delta F^\circ_{298.15°K} = -3682 \pm 25 \text{ cal/mol}$$

and for

$$\tfrac{1}{2}I_2(s) = \tfrac{1}{2}I_2(g) \quad (8)$$

we obtain from Shirley and Giauque[15]

$$\Delta H^\circ_0 = 7829 \text{ cal/mol}$$

$$\Delta H^\circ_{298.15°K} = 7461 \text{ cal/mol}$$

$$\Delta F^\circ_{298.15°K} = 2314 \text{ cal/mol}$$

(14) W. H. Evans, T. R. Munson, and D. D. Wagman, *J. Res. Natl. Bur. Std.*, **55**, 147 (1955).

(15) D. A. Shirley and W. F. Giauque, *J. Amer. Chem. Soc.*, **81**, 4778 (1959).

Table IV: Total Pressure and Composition of the Vapor over Solid ICl_3 and the Equilibrium Liquid on the ICl Side of Its Melting Curve

T, °K	Atomic ratio Cl/I	Molec. ratio P_{Cl_2}/P_{ICl}	$K^a = P_{Cl_2}P_{ICl}$, Torr²	P_{Cl_2}, Torr	P_{ICl}, Torr	P_{total}, Torr
296.21[b]	2.652	0.8260	471	19.7	23.9[c]	43.6
298.15	2.770	0.8850	624	23.5	26.6	50.1
300	2.890	0.9450	813	27.7	29.3	56.9
305	3.273	1.1365	1640	43.2	38.0	81.2
310	3.733	1.3665	3240	66.5	48.7	115
315	4.254	1.627	6230	101	61.9	163

[a] Equilibrium constants, expressed in Torr², are calculated from $\Delta H°_0$ = 26,297 cal/mol for vaporization. [b] ICl_3–ICl eutectic. [c] P_{ICl} from corrected data of Calder and Giauque (see Addendum) to set equilibrium values at the eutectic.

Adding reactions 6, 7, and 8

$$\tfrac{1}{2}I_2(s) + \tfrac{3}{2}Cl_2(g) = ICl_3(s) \qquad (9)$$

$$\Delta H°_0 = -21{,}723 \pm 25 \text{ cal/mol}$$

$$\Delta H°_{298.15°K} = -21{,}340 \pm 25 \text{ cal/mol}$$

$$\Delta F°_{298.15°K} = -5413 \pm 25 \text{ cal/mol}$$

Returning to reaction 6, we may use the free-energy data and $\Delta H°_0$ for this reaction, in combination with the vapor composition data in Table III to calculate the total and partial pressures in the vapor over $ICl_3(s)$ and the liquid which is in equilibrium with it on the ICl side of its melting curve.

$$\Delta F°/T = \Delta(F° - H°_0)/T + \Delta H°_0/T = R \ln P_{Cl_2}P_{ICl} \qquad (10)$$

From Table III we find by interpolation P_{Cl_2}/P_{ICl} at each of the several temperatures. Combining the product and quotient

$$P_{Cl_2} = [(P_{Cl_2}P_{ICl})(P_{Cl_2}/P_{ICl})]^{1/2} \qquad (11)$$

$$P_{ICl} = P_{Cl_2}(P_{ICl}/P_{Cl_2}) \qquad (12)$$

$$P_{total} = P_{Cl_2} + P_{ICl} \qquad (13)$$

The results of the calculation are collected in Table IV. Although eq 10–13 require the use of fugacities rather than pressures, the difference should be less than 0.1% over the range of pressures in Table IV.

Acknowledgment. We thank P. R. Siemens for assistance with the heat capacity measurements.

Addendum

Corrections to the ICl Data of G. V. Calder and W. F. Giauque, Ref 2. $\Delta H°_0$ for the reaction ICl(s) (l) = ICl(g) was given as 13,273 cal/mol instead of the correct value 13,245 cal/mol. This affects the calculated values of vapor pressure of ICl and the ΔF and ΔH values for several reactions.

$$ICl(s)\,(l) = ICl(g) \qquad \text{(C \& G-10)}$$

$$4.5758 \log (760/38.52) = -37.701 + \Delta H°_0/303.60 \qquad \text{(C \& G-11)}$$

from which $\Delta H°_0$ = 13,245 cal/mol and $\Delta F_{298.15°K}$ = 1966 cal/mol. Also

$$\Delta H°_{298.15} = 298.15[\Delta(H° - H°_0)/298.15] + 13{,}245 \text{ cal/mol}$$
$$= 298.15[-2.090] + 13{,}245$$
$$= 12{,}622 \text{ cal/mol} \qquad \text{(C \& G-12)}$$

for the solid.

C. and G. Table VII: Vapor Pressure of Solid Iodine Monochloride

T, °C	Total P, mm (Cornog and Bauer)	Partial P, ICl (this research)	P, I_2(s)	P, ICl + I_2(s) (this research)
−15	1.2	1.027	0.006	1.033
−10	2.0	1.647	0.011	1.658
−5	3.1	2.599	0.018	2.617
0	4.6	3.883	0.031	3.914
5	6.8	6.129	0.050	6.179

C. and G. Table IX: The Partial Pressure of ICl over Stoichiometric ICl

T, °K	P, Torr	T, °K	P, Torr
250	0.44	300	31.40
260	1.18	300.53[a]	32.62
270	2.96	Liquid	Liquid
273.15	3.88	303.60	38.52
280	6.89	310	53.71
290	15.29	320	87.40
298.15	27.55	330	135.5

[a] Melting point.

ห้องสมุด กรมวิทยาศาสตร์

For the heat of vaporization of the liquid which can easily be supercooled to 298.15°K

$$\Delta H^\circ_{298.15^\circ K} = \Delta H_{sub,298.15^\circ K} - \Delta H_{m,300.53^\circ K} + (300.53 - 298.15^\circ K)\Delta C_{p,m}$$
$$= 12{,}622 - 2773 + 11{,}360 \times 2.38$$
$$= 9876 \text{ cal/mol} \quad \text{(C \& G-13)}$$
$$\Delta F^\circ_{298.15^\circ K} = 1946 \text{ cal/mol}$$
$$ICl(s) = (\tfrac{1}{2})Cl_2 + (\tfrac{1}{2})I_2(g) \quad \text{(C \& G-20)}$$
$$\Delta H^\circ_0 = 16{,}500 \pm 25 \text{ cal/mol}$$
$$\Delta F^\circ_{298.15^\circ K} = 5648 \pm 25 \text{ cal/mol}$$
$$ICl(s) = (\tfrac{1}{2})Cl_2 + (\tfrac{1}{2})I_2(s) \quad \text{(C \& G-22)}$$
$$\Delta H^\circ_0 = 8671 \pm 25 \text{ cal/mol}$$
$$\Delta F^\circ_{298.15^\circ K} = 3334 \pm 25 \text{ cal/mol}$$

and finally

$$ICl(l) = (\tfrac{1}{2})Cl_2 + (\tfrac{1}{2})I_2(s) \quad \text{(C \& G-23)}$$
$$\Delta F^\circ_{298.15^\circ K} = 3314 \pm 25 \text{ cal/mol}$$

A Thermodynamic Study of the Urania-Uranium System[1]

by R. J. Ackermann, E. G. Rauh,

Chemistry Division, Argonne National Laboratory, Argonne, Illinois 60439

and M. S. Chandrasekharaiah[2]

Chemical Engineering Division, Argonne National Laboratory, Argonne, Illinois 60439 *(Received May 9, 1968)*

The phase diagram (temperature–pressure–composition) for the uranium–oxygen system from 1600 to 2500°K in the composition range of the unvariant system $UO_2(s) + U(l)$ was investigated in three steps. The composition of the urania phase in equilibrium with liquid uranium from 1900 to 2500°K was determined by an isopiestic method. The mole fraction of uranium dissolved in the UO_2 phase is given by $\log N_U = (1.63 \pm 0.11) - (6270 \pm 240)/T$. The total effusion rates were measured by means of the effusion method from 1580 to 2400°K. An "effective" vapor pressure p_e was calculated from the measured effusion rates, assuming the vapor to be UO(g). The least-squares treatment of the data resulted in the expression, $\log p_e(\text{atm}) = (7.25 \pm 0.15) - (27{,}020 \pm 250)/T$. The mass spectrometric investigation of the same system has shown the vapor to be predominantly UO(g) with smaller amounts of U(g) and $UO_2(g)$. The temperature dependence and relative intensities of the species were measured mass spectrometrically and combined with the total effusion rates to yield the partial pressures for each species: $\log p_U(\text{atm}) = (5.21 \pm 0.14) - (25{,}640 \pm 300)/T$; $\log p_{UO}(\text{atm}) = (7.11 \pm 0.14) - (26{,}880 \pm 300)/T$; $\log p_{UO_2}(\text{atm}) = (7.74 \pm 0.14) - (30{,}180 \pm 300)/T$. The standard free energy of formation of UO(g) is given by the equation $\Delta G_f^\circ(UO) = -7800 - 13.8T$ (kcal/mol).

I. Introduction

It is now generally recognized that many so-called chemical compounds can exist as phases of variable composition.[3] Uranium dioxide (urania) is certainly no exception and, in fact, experimental evidence suggests that its composition can vary continuously within wide limits. The crystallographic and thermodynamic properties of the superstoichiometric phase which extends up to a composition given approximately by the oxygen-to-uranium ratio, $O/U \cong 2.2$, have been most extensively investigated in recent years.[4] Early evidence which suggests the existence of a substoichiometric urania phase which may extend down to $O/U = 1.75$ was compiled by Brewer,[5] but more recently others including Anderson, Sawyer, Worner, Willis, and Bannister,[6] Rothwell,[7] Aitken, Brassfield, and Fryxell,[8] Martin and Edwards,[9] and Ackermann, Rauh, and Chandrasekharaiah[10] have demonstrated the stability of substoichiometric compositions at high

(1) Based on work performed under the auspices of the U. S. Atomic Energy Commission.

(2) Chemistry Division, Bhabha Atomic Research Centre, Trombay, Bombay 74, India.

(3) R. F. Gould, Ed., "Non-stoichiometric Compounds," Advances in Chemistry Series, American Chemical Society, Washington, D. C., 1963.

(4) Report of the Panel on "Thermodynamic and Transport Properties of Uranium Dioxide and Related Phases," Technical Reports Series No. 39, International Atomic Energy Agency, Vienna, 1965.

(5) L. Brewer, *Chem. Rev.*, 52, 1 (1953).

(6) J. S. Anderson, J. O. Sawyer, H. W. Worner, G. M. Willis, and M. J. Bannister, *Nature*, 185, 915 (1960).

(7) E. Rothwell, *J. Nucl. Mat.*, 6, 229 (1962).

(8) E. A. Aitken, H. C. Brassfield, and R. E. Fryxell, "Thermodynamics," Vol. II, International Atomic Energy Agency, Vienna, 1965, p 435.

(9) A. E. Martin and R. K. Edwards, *J. Phys. Chem.*, 69, 1788 (1965).

(10) R. J. Ackermann, E. G. Rauh, and M. S. Chandrasekharaiah, Argonne National Laboratory Report, ANL-7048, July 1965.

temperatures. The mass spectrometric observations of DeMaria, Burns, Drowart, and Inghram,[11] Pattoret, Drowart, and Smoes,[12] and Ackermann, *et al.*,[10] indicate that the total vapor pressure (predominantly UO) of the urania phase saturated with liquid uranium is greater by a factor of approximately 10 at 2000°K than that (predominantly UO_2) measured by Ackermann, *et al.*,[10] and Ackermann, Gilles, and Thorn[13] for nearly stoichiometric urania. In view of these observations a comprehensive investigation of the evaporation behavior of the urania phase especially near its lower phase boundary was initiated. The present investigation includes the following: (1) the measurement of the total effusion rate of various mixtures of urania–liquid uranium at randomly chosen temperatures from 1540 to 2315°K; (2) the mass spectrometric determination of the vapor species in equilibrium with urania–liquid uranium mixtures and the temperature dependence of their partial pressures in the range 1820–2330°K; (3) the determination of the lower boundary of the urania phase from 1860 to 2525°K by an isopiestic method; (4) a demonstrated consistency of the total effusion data with the mass spectrometric data to yield partial pressures of U, UO, and UO_2 for these mixtures; and (5) the reevaluation of the standard free energy of UO(g) based on these findings and more recent measurements of the vapor pressure of liquid uranium.

II. Experimental Methods and Results

A. Measurement of the Total Effusion Rate. The effusion rates of the vapors in equilibrium with the mutually saturated urania–liquid uranium phases were measured by the condensation on platinum targets of a known fraction of the effusate from an effusion cell and the analysis of the target deposit for uranium content by α or fission counting. The experimental details, apparatus, preparation of targets, and temperature measurements of this method have been described elsewhere.[13]

Before measurements could be made, it was necessary to find a suitable container for liquid uranium, particularly at the higher temperatures. Tungsten and molybdenum were found generally to be unsatisfactory above 1600°, tantalum above 1750°; penetration of the liquid uranium along the grain boundaries ultimately resulted in the virtual loss of sample. After some experimentation urania cups were found to be satisfactory containers at temperatures as high as 2300°.

The effusion measurements were carried out over the temperature range 1540–2315°K. For measurements at the higher temperatures, 1825–2315°K, the samples used consisted of normal uranium in a normal urania cup located inside either a tungsten or tantalum effusion cell. At the lower temperatures, 1540–2030°K, the sample consisted of enriched (in ^{234}U and ^{235}U) uranium metal and urania prepared from the same metal contained in a tantalum cup.

The uranium content of the targets was determined by radiochemical methods, α counting of the natural uranium sublimates, and both α and fission counting of the enriched sublimates. For the latter case suitable targets previously analyzed by α counting were used as standards. The condensation efficiency of the targets was checked as before[13,14] and found to be greater than 99.5%.

When a fraction of the effusate is collected on a circular target of area much larger than that of the orifice and parallel to the plane of the orifice, the rate of collection is related to the pressure of the vapors inside the cell by means of the equation

$$p_i = \frac{w_i}{at}\sqrt{\frac{2\pi RT}{M_i}}\left(\frac{d^2 + r^2}{r^2}\right) \quad (1)$$

where p_i is the partial pressure of species i, w_i and M_i are the mass and molecular weight, respectively, of species i collected on the target in time t, a is the area of the orifice, d is the orifice-to-collimator distance, r is the radius of the collimator, and R and T are the gas constant and temperature, respectively. The composition of the vapor was shown mass spectrometrically to be predominantly UO and is described later. Hence, an apparent or "effective" vapor pressure, p_e, for the system was calculated from the measured effusion rates by assuming UO to be the only molecular species in the vapor. The results are shown on the log p_e *vs.* $1/T$ plot of Figure 1. The open circles are the data obtained from a sample of natural uranium in a natural UO_2 cup in a tantalum cell over the temperature range 1825–2320°K; the remaining points are the results of four series of measurements on enriched U and UO_2 in a tantalum cup in tantalum or tungsten cells with orifice areas varying by a factor of about 30, over the temperature range 1470–2200°K. The detailed information on the conditions of the measurements and the variety of samples and effusion cells is given in ref 10.

The combined data of the five series are expressible by the least-squares equation

$$\log p_e = (7.25 \pm 0.15) - (27{,}020 \pm 250)/T \quad (2)$$

The errors quoted here and elsewhere are standard deviations. The agreement between the results from samples of natural isotopic content and those with enriched uranium and between α and fission counting is

(11) G. DeMaria, R. P. Burns, J. Drowart, and M. G. Inghram, *J. Chem. Phys.*, 32, 1373 (1960).

(12) A. Pattoret, J. Drowart and S. Smoes, Paper Sm.98/49 published in the Proceedings of the Symposium on Thermodynamics of Nuclear Materials, with Emphasis on Solution Systems, International Atomic Energy Agency, Vienna, Sept 4–8, 1967.

(13) R. J. Ackermann, P. W. Gilles, and R. J. Thorn, *J. Chem. Phys.*, 25, 1089 (1956).

(14) E. G. Rauh and R. J. Thorn, *ibid.*, 22, 1414 (1954).

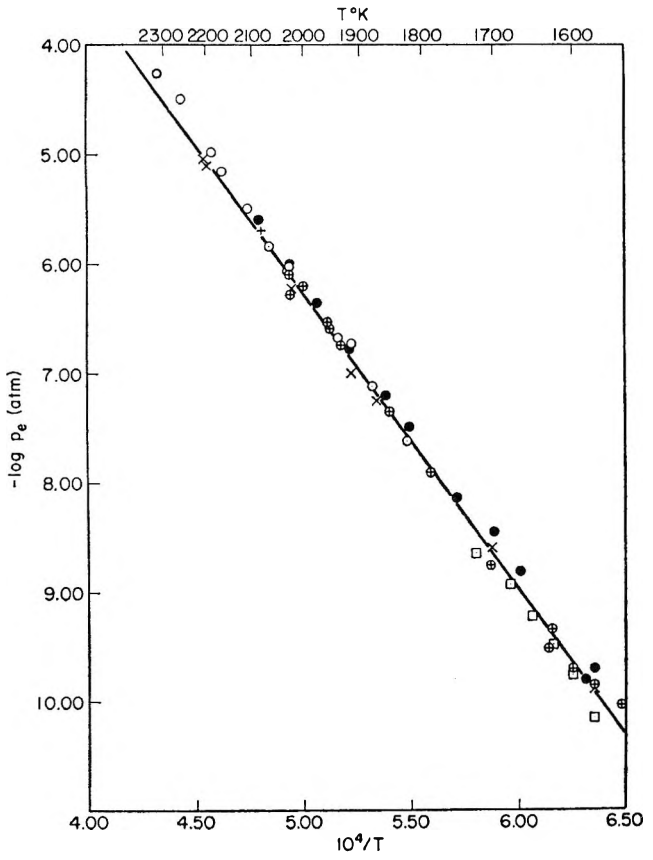


Figure 1. Plot of log p_e(atm) *vs.* $10^4/T$ for mixtures of urania–liquid uranium. Five series of measurements are shown, differing only in the orifice area, the isotopic content of the sample, and the method of target assay.

good. Also, the variation of the orifice area from 7.7×10^{-4} to 2.5×10^{-2} cm^2 produced no apparent effect on the observed rates of effusion. Furthermore, the results of the present investigation and those of Ackermann, Gilles, and Thorn[13] for the system U(l) + UO_2(s) are in close agreement; the data of these investigators corrected to the molecular weight of UO yield a pressure of 1.45×10^{-6} atm at 2077°K which is to be compared with 1.59×10^{-6} atm evaluated from eq 2.

B. Mass Spectrometric Measurements. Several mass spectrometric measurements with a Bendix time-of-flight spectrometer were made on the U–UO_2 system. The instrumentation, methods, and techniques used have been reported previously.[15]

To eliminate the difficulties arising from the creep of liquid uranium and the dissolution of tantalum in liquid uranium, a sample consisting of an 80-mg pellet of uranium metal placed in a shallow cavity in a 200-mg disk of sintered UO_2 was used; the relatively small sample was used to minimize the time required to reach equilibrium.

Since the appearance potentials of U^+, UO^+, and UO_2^+ lie between 5 and 6 eV,[12] and since the dissociation energy of the U–O bond is of the order of 8 eV,[11] U^+ and UO^+ ions from fragmentation of UO and UO_2, respectively, may be expected above 13 or 14 eV. Appearance potential measurements did indeed demonstrate this behavior which has also been demonstrated in the fragmentation of YO to Y^+ [16] and NpO_2 to NpO^+.[17] Hence, in all the following observations an ionizing electron energy of 10 eV was used.

The ions observed at 1800°K were UO^+, UO_2^+, and U^+ in the approximate ratios 10:1:1 in general agreement with the observations of DeMaria, *et al.*[11] Three series of measurements of the temperature dependences of the ion currents over the temperature range 1800–2200°K were made after various lengths of time at temperature. The data of Series 1 were taken after 20 min at 2150°K, those of series 2 after an additional 200 min at 2150°K, and those of series 3 after an additional 150 min at 2200°K. The least-squares equations of the data and the measured heats of evaporation are given in Table I.

Table I: Summary of Mass Spectrometric Results: Log $I^+T = A + B/T$

Species	A	$-B$	ΔH, kcal/mol
	Series 1. 10 Experimental Points, Temperature Range 1870–2150°K		
U^+	14.950 ± 0.259	24,390 ± 530	111.6 ± 2.4
UO^+	17.079 ± 0.220	26,080 ± 450	119.3 ± 2.1
UO_2^+	17.994 ± 0.122	29,920 ± 250	136.9 ± 1.1
	Series 2. 11 Experimental Points, Temperature Range 1830–2170°K		
U^+	15.647 ± 0.054	25,540 ± 110	116.9 ± 0.5
UO^+	17.566 ± 0.072	26,810 ± 150	122.7 ± 0.7
UO_2^+	18.185 ± 0.078	30,100 ± 160	137.7 ± 0.7
	Series 3. 7 Experimental Points, Temperature Range 1820–2190°K		
U^+	15.621 ± 0.123	25,360 ± 250	116.0 ± 1.1
UO^+	17.593 ± 0.102	26,730 ± 200	122.3 ± 0.9
UO_2^+	18.314 ± 0.153	30,240 ± 310	138.4 ± 1.4

The measured heats of evaporation of UO_2 agree in all three series within the standard deviations. However, ΔH(U) and ΔH(UO) for Series 1 are low and do not agree within the standard deviations with the corresponding heats in Series 2 and 3. This suggests that even with a relatively small sample an appreciable time at temperature is required to bring both phases into equilibrium. Since the results of Series 2 and 3

(15) R. J. Ackermann and E. G. Rauh, *J. Chem. Phys.*, 36, 448 (1962).

(16) R. J. Ackermann, E. G. Rauh, and R. J. Thorn, *ibid.*, 40, 883 (1964).

(17) R. J. Ackermann, R. L. Faircloth, E. G. Rauh, and R. J. Thorn, *J. Inorg. Nucl. Chem.*, 28, 111 (1966).

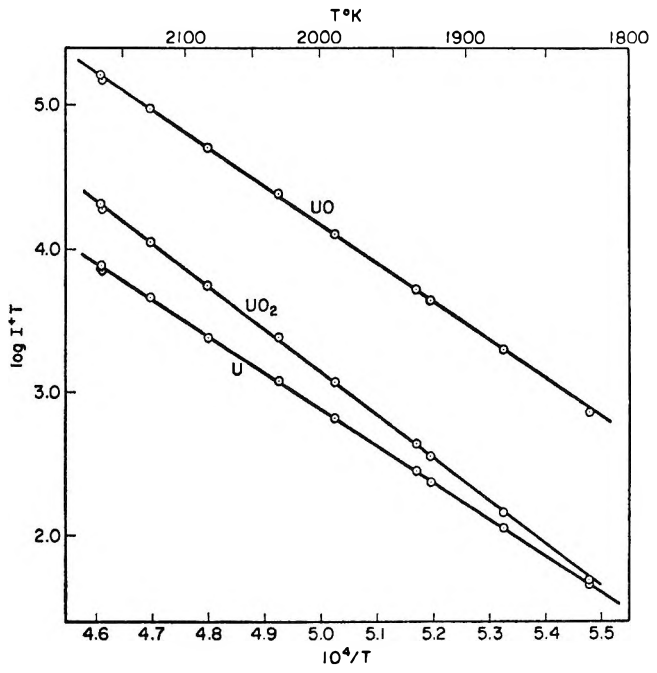


Figure 2. Plot of log I^+T *vs.* $10^4/T$ for mass spectrometric measurements of U, UO, and UO_2 in equilibrium with urania–liquid uranium, Series 2.

are in agreement within the standard deviations, only the data of Series 2 are shown in Figure 2.

C. Measurement of the Composition of the Urania Phase in Equilibrium with Liquid Uranium. The temperature *vs.* composition phase diagram of the uranium–oxygen system between the metal and dioxide is generally characterized by the absence of a stable monoxide or suboxides and hence there exists a rather extensive miscibility gap between the metal and dioxide phases. Thompson, Cleaves, Cron, and Sterling[18] reported a small solubility of urania in liquid uranium up to 2000° at which temperature the atom ratio O/U is approximately equal to 0.05 for the liquid metal. Martin and Edwards[9] have amplified these measurements and have essentially confirmed the results of Thompson, *et al.*,[18] but Guinet, Vaugoyeau, and Blum[19] report a substantially greater solubility which at 2000° is equal to an atom ratio O/U = 0.3.

Martin and Edwards,[9] Bates,[20] and Guinet, *et al.*,[19] have reported measurements of the lower phase boundary of the dioxide phase and the results generally agree although the compositions reported by Bates are somewhat more substoichiometric. In all cases the dioxide phase was equilibrated with liquid metal and the intergrowth layer of oxide subsequently analyzed. These investigations indicate that the dioxide phase can become as substoichiometric as O/U = 1.6 at the monotectic temperature, 2470°. Perhaps some doubt remains concerning the extent of phase separation in the UO_{2-x} intergrowth upon cooling and the subsequent gain or loss of uranium from the analyzed sample that had been in direct contact with the liquid metal. To circumvent this difficulty in the present investigation, the composition was determined by an isopiestic method which consisted of equilibrating a sample of urania with the vapor arising from a saturated mixture of urania–liquid uranium inside a closed container.

The assembly used in these determinations is shown in Figure 3. A small pre-outgassed disk (~1 g) of

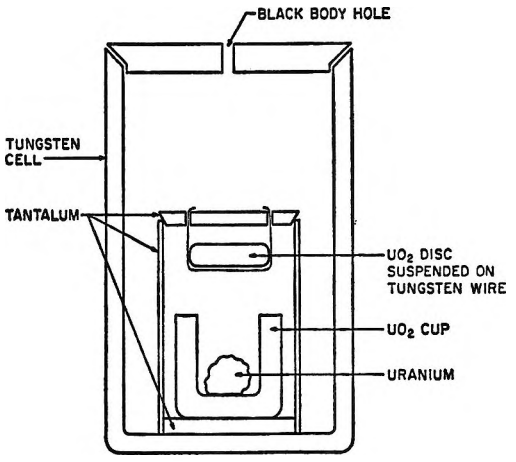


Figure 3. Experimental assembly for determination of the lower phase boundary of urania.

pure UO_2 was suspended on fine tungsten wires inside a closed tantalum cylinder, also pre-outgassed, containing a slipcast cup of UO_2 (3–4 g) within which a 1–2-g sample of uranium metal had been placed. This capsule was then placed inside a larger tungsten cell and the complete assembly heated *in vacuo* to the desired temperature for sufficient time to achieve equilibrium throughout. The times allowed were greater by factors of 2–20 than the minimum time calculated from the measured vapor pressure of the urania–liquid uranium mixture and the quantities of UO required to reduce the UO_2 in the disk to compositions near those observed in previous studies.[9] After equilibration the composition of the UO_2 phase was determined by oxidation of the urania disk to U_3O_8 by heating in air to 850°. The results, shown in Figure 4, are in agreement within the respective experimental errors with those of Martin and Edwards.[9] The solid curve is the best fit of the data obtained from a nonlinear least-squares treatment of T°C *vs.* O/U.

If the solubility data are fitted to a linear equation of the form $\log N_u = A + B/T$, in which N_u is the mole fraction of uranium dissolved in the urania phase, the equation shown in Figure 4 results. The reconstruction of the curve of T°C *vs.* O/U from the least-squares

(18) J. G. Thompson, H. E. Cleaves, M. M. Cron, and J. T. Sterling, Report CT-2618, 1945.

(19) P. Guinet, H. Vaugoyeau, and P. L. Blum, Commissariat a L'Energie Atomic Report CEA-R-3060, Nov 1966.

(20) J. L. Bates, "Thermodynamics," Vol. II, International Atomic Energy Agency, Vienna, 1965, p 73.

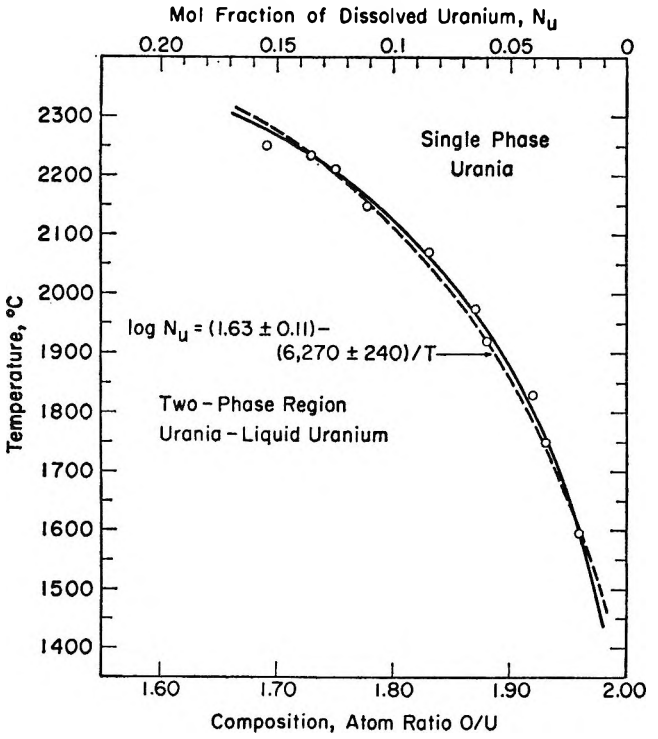


Figure 4. Composition of urania saturated with uranium as a function of temperature. The dashed line is calculated from the expression for log N_U, the solid line from a nonlinear least-squares treatment of T *vs.* O/U.

values of N_u yields the dashed curve in Figure 4. This treatment indicates that the proposed linear equation does not appear to best fit the experimental data but is essentially adequate within the experimental scatter. The constant B multiplied by $2.303R$ in the equation yields the average value for the heat of solution of the solute uranium, 28.7 ± 1.1 kcal/mol. In the case of an ideal solution, this quantity should be the heat of fusion of the solute. However, the heat of fusion of uranium is estimated to be 3.1 kcal/mol,[21] and consequently the solid solution that results from the dissolution of uranium in uranium dioxide must be, in fact, quite nonideal. The deviation from ideality will be discussed further in the following section.

III. Thermodynamic Analysis and Discussion

A. Calculations of the Partial Pressures in Equilibrium with Urania–Liquid Uranium. It can be shown by means of eq 1 that the "effective" pressure of the uranium-bearing species given by eq 2 is related to the individual partial pressures of species observed mass spectrometrically *via* the equation

$$p_e = P_{UO} + \left(\frac{M_{UO}}{M_{UO_2}}\right)^{1/2} p_{UO_2} + \left(\frac{M_{UO}}{M_U}\right)^{1/2} p_U \quad (3)$$

The individual partial pressures can be evaluated from the effective pressure and the ion currents, I^+, by means of eq 3 and the relationship

$$I_i^+ T = \sigma_i \epsilon_i p_i G \quad (4)$$

where σ_i and ϵ_i are the relative ionization cross sections and multiplier efficiencies, respectively, and G is a geometry factor.

The appearance potentials of U^+ and US^+ are nearly equal (6.0 and 6.3 eV, respectively) and Cater, Rauh, and Thorn[22] have calculated equal instrumental sensitivities ($\sigma \cdot \epsilon$) at 11 eV from the mass effusion and mass spectrometric measurements of US(s). Ackermann and Rauh[23] were able to fit an exact functional form to the curve of log p_e *vs.* $1/T$ involving these two vapor species arising from US(s) + U(l) mixtures. The relative instrumental sensitivities were shown to lie within the limits $\frac{1}{2}$ to 2. Further, the appearance potentials of Y^+ and YO^+ are nearly equal (6.0 and 5.5 eV, respectively)[16] and the assumption of equal instrumental sensitivities at 10 eV is consistent with the thermodynamic data. Since the appearance potentials of U^+, UO^+, and UO_2^+ are nearly equal (6.1, 5.7, and 5.5 eV, respectively),[12] equal relative instrumental sensitivities have been assumed.[24] In principle, this reasoning seems more compelling, particularly at low energies, than the estimations of the cross sections from Otvos and Stevenson[25] and the multiplier efficiencies of Plock and Walcher[26] even though in the present case the same conclusions would have been reached.

Equation 3 can be rewritten to yield the partial pressure of UO(g), *viz.*

$$p_{UO} = p_e/[1 + (0.970)(p_{UO_2}/p_{UO}) + (1.033)(p_U/p_{UO})] \quad (5)$$

and the assumption of equal relative instrumental sensitivities permits the direct substitution of ratios of ion intensities from the appropriate equations in Table I, Series 2, for the respective ratios of pressures in eq 5. Similarly, eq 3 can be rewritten to yield the pressures of U(g) and UO_2(g). Equations for the partial pressures of the vapor species are given in the form log $p_i = A_i + B_i/T$, in Table II.

The agreement between the values of the coefficients of reciprocal temperature, B_i, with those given in Table I, Series 2 and Series 3, is quite good and emphasizes,

(21) R. Hultgren, R. L. Orr, P. D. Anderson, and K. K. Kelley, "Selected Values of Thermodynamic Properties of Metals and Alloys," John Wiley and Sons, Inc., New York, N. Y., 1963.

(22) E. D. Cater, E. G. Rauh, and R. J. Thorn, *J. Chem. Phys.*, **44**, 3106 (1966); Erratum, *ibid.*, **48**, 538 (1968).

(23) R. J. Ackermann and E. G. Rauh, *J. Phys. Chem.*, **73**, 769 (1969).

(24) Furthermore, the approximate equality of the appearance potentials of U^+, UO^+, and UO_2^+ compared with the much larger value for UO_2^+ (~11 eV)[12] suggests that the ionization process of each of the first three species involves the loss of an antibonding electron.

(25) J. W. Otvos and D. P. Stevenson, *J. Amer. Chem. Soc.*, **78**, 545 (1956).

(26) W. Plock and W. Walcher, *Rev. Sci. Instr.*, **22**, 1028 (1951).

Table II: The Partial Pressures of U, UO, UO_2, and O in Equilibrium with Mutually Saturated Urania–Liquid Uranium: Log $p_i = A + B/T$

Vapor species	A_i	$-B_i$
U	5.21 ± 0.14	25,640 ± 300
UO	7.11 ± 0.14	26,880 ± 300
UO_2	7.74 ± 0.14	30,180 ± 300
O[a]	8.10	41,500

[a] Calculated from the equation $UO_2(g) = UO(g) + O(g)$.

in particular, the accord between the temperature dependence of the quantity log I_iT and that of log p_e given by eq 2. It should be noted that in addition to the dependence of pressure on the temperature, these measurements reflect substantial changes in composition as a function of temperature within each of the two condensed phases. The lack of large random errors and, in particular, hysteresis effects with increasing or decreasing temperature suggests that the equilibrium state was indeed observed.

The overall precision of the mass spectrometric data can be viewed *via* the study of the equilibrium

$$U(g) + UO_2(g) = 2UO(g) \qquad (6)$$

If the respective measured ion intensities[10] are used to calculate individual values of the equilibrium constant, $K = p_{UO}^2/p_U p_{UO_2}$, at each measured temperature, the plot of log K *vs.* reciprocal temperature shown in Figure 5 results. The combined data are seen to possess good precision with the exception of a few points, two of which correspond to the initial observations in Series 1 in which case the equilibration of the system was very likely not complete. These points were discarded in the calculation of the solid line drawn through the points in Figure 5 by the least-squares method. The resultant equation is

$$\log K_6 = (1.268 \pm 0.058) + (2091 \pm 117)/T \qquad (7)$$

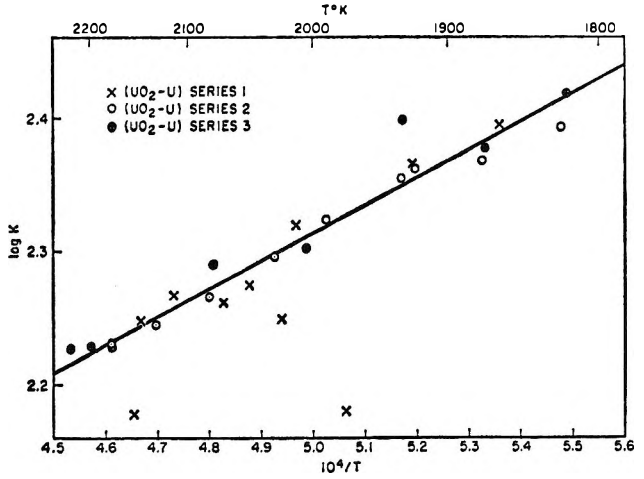


Figure 5. Plot of log K *vs.* $10^4/T$ for the equilibrium $UO_2(g) + U(g) = 2UO(g)$.

B. The Standard Free Energy of Formation of UO(g). The equilibrium represented by eq 6 can be utilized to derive an expression for the standard free energy of formation of UO(g)

$$\Delta G_f^\circ(UO, g) = \tfrac{1}{2}\Delta G_f^\circ(UO_2, g) + \tfrac{1}{2}\Delta G_f^\circ(U, g) + \tfrac{1}{2}R'T \log K_6 \qquad (8)$$

The standard free energy of formation of $UO_2(g)$, $\Delta G_f^\circ(UO_2, g) = -121{,}500 + 4.24T$, can be evaluated from the known free energy of formation[27] and vapor pressure of $UO_2(s)$.[13] The standard free energy of formation of U(g), $\Delta G_f^\circ(U, g) = 115{,}430 - 26.12T$ ($\Delta H^\circ_{298} = 126.3 \pm 1.0$), has been recently determined by Ackermann and Rauh.[23] The substitution of these expressions along with eq 7 yields the resulting equation

$$\Delta G_f^\circ(UO, g) = -7{,}800 - 13.84T \qquad (9)$$

The temperature coefficient in eq 9 is the average value, in the temperature range of this study, of the standard entropy of formation of UO(g), namely, $\Delta S_f^\circ(UO, g) = 13.8$ eu. This value, when compared with the values for ThO(g)[28] and PuO(g),[29] 14.4 and 12.1 eu, respectively, indicates that the entropy change associated with essentially isostructural processes involving only the change in the metal atom is relatively constant as might be expected. The apparent trend with atomic number of the metal in the values of $\Delta S_f^\circ(MO, g)$ for the three monoxides in question may not be real when one considers that an uncertainty of ±1 eu is likely in each case.

The absolute entropy of UO(g) exclusive of the electronic contribution can be estimated with some reliability from available molecular parameters which can be used to approximate those of UO(g). The molecular parameters used in the calculation of the entropy are 1.75 Å for the interatomic distance[30] and 860 cm^{-1} for the vibrational constant[31] which is the symmetrical stretching constant for the uranyl ion. This latter estimate may be quite reliable since a value of 877–881 cm^{-1} has been recently measured for ThO(g) by means of the matrix isolation technique.[32] The employment of these parameters in the proper statistical mechanical relationships yields a value of the absolute entropy of UO(g) at 2000°K which is 73.3 eu mol^{-1}. The combination of this value with those of liquid

(27) J. P. Coughlin, U. S. Bureau of Mines Bulletin 542, U. S. Government Printing Office, Washington, D. C., 1954. See also M. H. Rand and O. Kubaschewski, "The Thermochemical Properties of Uranium Compounds," Oliver and Boyd, London, 1963.

(28) R. J. Ackermann, E. G. Rauh, R. J. Thorn, and M. C. Cannon, *J. Phys. Chem.*, **67**, 762 (1963).

(29) R. J. Ackermann, R. L. Faircloth, and M. H. Rand, *ibid.*, **70**, 3698 (1966).

(30) H. R. Hoekstra, *Inorg. Chem.*, **2**, 492 (1963).

(31) E. Rabinowitch, ANL-5122 (1953).

(32) M. J. Linevsky, Air Force Materials Laboratory, Wright-Patterson Air Force Base Technical Report AFML-TR-64-420 (Feb 1965).

uranium[21] and molecular oxygen[33] permits the calculation of the entropy of formation of UO(g), 8.7 eu mol^{-1}. The discrepancy between this value and the measured value from eq 9 suggests that the electronic contribution to the absolute entropy of UO(g) may be approximately 5 eu mol^{-1}. A similar magnitude has been suggested previously for ThO(g).[28]

C. The Partial Pressure of Oxygen in Equilibrium with Urania–Liquid Uranium. The calculation of the partial pressure of oxygen in equilibrium with the lower phase boundary of the urania (see Figure 4) can be accomplished by consideration of the equilibrium

$$UO_2(g) = UO(g) + O(g) \qquad (10)$$

For this equilibrium one writes

$$\Delta\bar{G}_O = R'T \log p_O = -R'T \log (p_{UO}/p_{UO_2}) - \Delta\bar{G}_f^\circ(UO) - \Delta G_f^\circ(O) + \Delta G_f^\circ(UO_2) \qquad (11)$$

Substitution into eq 11 of the appropriate equations for log p_{UO} and log p_{UO_2} from Table II, eq 9, the equation, $\Delta G_f^\circ(O) = 61{,}245 - 16.07T$,[33] and the equation for $\Delta G_f^\circ(UO, g)$ given earlier leads to the equation for atomic oxygen given in Table II. The partial pressures of O, U, UO, and UO_2 are plotted in Figure 6, together with the "effective" pressure given by eq 2.

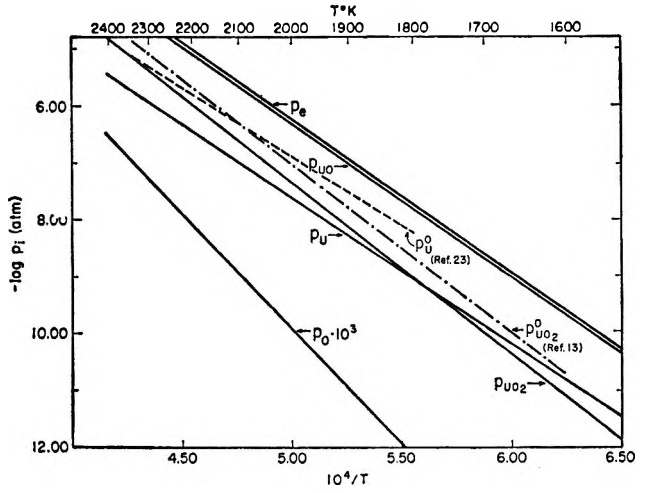


Figure 6. Partial pressures of U, UO, UO_2, and O in equilibrium with urania–liquid uranium and the "effective" pressure from Figure 1.

D. General Discussion. A comparison of these partial pressures with the most recent values reported by Pattoret, *et al.*,[12] obtained from mass spectrometric observations indicates a general agreement within a factor of 3, which magnitude of discrepancy is often considered unavoidable in high-temperature studies. It is noteworthy to point out that such errors are seldom random in nature but rather are frequently systematic; *i.e.*, the discrepancy between two sets of measurements exceeds the scatter within each. In the present comparison the discrepancies are indeed systematic in that the pressures of U, UO, and UO_2 reported by Pattoret, *et al.*, are all very nearly a factor of 3 larger than those evaluated in the present study. The partial pressure of $UO_2(g)$ in equilibrium with the lower phase boundary of the urania phase obtained in the present study is ostensibly a factor of one-half the measured vapor pressure of stoichiometric urania. The vapor pressure of nearly stoichiometric urania has been established by the effusion method (collection type) over a relatively wide range of temperature by Ackermann, *et al.*,[13] confirmed over a portion of the range by Ohse,[34] and by the transpiration method by Alexander, Ogden, and Cunningham[35] and by Tetenbaum.[36] The magnitude of discrepancy expressed as a standard deviation among these investigations in the range 1600–2200°K is of the order of ±20% in the pressure of $UO_2(g)$ which is known to be the grossly predominant vapor species.[10,12] Hence, one is inclined to accept the reliability of the absolute measurements of the vapor pressure of $UO_2(s)$. It can be proved that the pressure of $UO_2(g)$ is a maximum for the stoichiometric composition of the solid phase[37] and, consequently, must decrease as the composition of the solid phase becomes substoichiometric. Since the partial pressure of $UO_2(g)$ in equilibrium with urania–liquid uranium reported by Pattoret, *et al.*,[12] is approximately 60% greater at ~2000°K than the vapor pressure of stoichiometric urania, the result (eq 3, Table II) of the present study appears to be the more realistic one. The thermodynamic description of the vaporization behavior of the substoichiometric plutonium dioxide phase supports the present conclusion in that the partial pressure of $PuO_2(g)$ decreases gradually as the composition of the condensed phase becomes progressively more substoichiometric.[29]

Another systematic difference occurs with the heat of vaporization of UO(g) from the urania–liquid uranium system. In the temperature range 1700–2100°K the data of Pattoret, *et al.*,[12] yield a value of 129.4 kcal/mol compared with the value of 123.0 ± 1.4 kcal/mol obtained from eq 2 in Table II. The latter (smaller) value has been shown to be consistent with the mass effusion data of the present investigation obtained over the temperature range 1500–2300°K and which correspond primarily to the effusion rate of UO(g) as seen in Figure 6.

The nonideality of the urania solid solution with respect to the solute uranium is further manifested by

(33) D. R. Stull and G. C. Sinke, "Thermodynamic Properties of the Elements," American Chemical Society, Washington, D. C., 1956.

(34) R. W. Ohse, *J. Chem. Phys.*, 44, 1375 (1966).

(35) C. A. Alexander, J. S. Ogden, and G. W. Cunningham, Battelle Memorial Institute Report, BMI-1789, Jan 1967.

(36) M. Tetenbaum, Chemical Engineering Division, Argonne National Laboratory, private communication.

(37) R. K. Edwards, Argonne National Laboratory Report, ANL-7020, May 1964–Apr 1965, p 155.

the variation of the partial pressure of uranium over its range of composition. From the equilibrium reaction, eq 6, it is possible to calculate the partial pressure of U(g) in equilibrium with the stoichiometric solid and to compare it with the value measured at the lower phase boundary. By means of eq 7 and 9, the equations for $\Delta G_f^\circ(U, g)$ and $\Delta G_f^\circ(UO_2, g)$ given in the text, and the observation of Ackermann, *et al.*,[10] that at 2000°K $p_{UO} \simeq 0.03 p_{UO}$ for nearly stoichiometric dioxide, $UO_{1.994}(s)$, one calculates that at this temperature the partial pressure of uranium is 3.8×10^{-13} atm, which is to be compared with the value at the lower phase boundary, 2.5×10^{-8} atm, obtained from the equation in Table II. Hence, this rather large change in the partial pressure relative to the vapor pressure of uranium over a relatively small change of composition indicates a positive deviation from Raoult's law.

Acknowledgments. The authors are grateful to Dr. Russell K. Edwards of the Chemical Engineering Division and to Dr. R. J. Thorn of the Chemistry Division for pertinent discussion throughout the course of the investigation, to Dr. Allan E. Martin of the Chemical Engineering Division for discussions dealing with liquid–solid phase equilibria, to John J. Hines and Michael A. Essling of the Chemistry Division for their assistance with the fission counting, and to Reactor Operations for the use of the Juggernaut reactor facilities.

The Vapor Pressure of Liquid Uranium; Effects of Dissolved Tantalum, Phosphorus, Sulfur, Carbon, and Oxygen[1]

by R. J. Ackermann and E. G. Rauh

Chemistry Division, Argonne National Laboratory, Argonne, Illinois 60439 *(Received May 9, 1968)*

The vaporization behavior of liquid uranium saturated with tantalum, phosphorus, sulfur, and carbon has been studied by mass effusion and mass spectrometric techniques in the temperature range 1800–2400°K. The results, combined with those previously reported for uranium saturated with oxygen, show that the activity coefficient of uranium decreases with increasing electronegativity of the dissolved component, varying from nearly unity in the case of tantalum and phosphorus to approximately 0.2 for oxygen. The vapor pressure of liquid uranium is given by the equation $\log p(\text{atm}) = (5.71 \pm 0.17) - (25{,}230 \pm 370)/T$, and the heat of sublimation, ΔH°_{298}, is 126.3 ± 1.0 kcal/mol. At high temperatures uranium monophosphide and uranium monosulfide are converted to the two-phase systems UP(s) + U(l) and US(s) + U(l).

Introduction

The vapor pressure and heat of sublimation of uranium appear thus far to have escaped experimental verification by two or more laboratories. Several studies have yielded values of the heat of sublimation, ΔH°_{298}, that lie within the range 117–129 kcal/mol and pressures that differ by an order of magnitude. More recently, the high limit of the heat of sublimation has been favored but values derived from experimental measurements and thermochemical cycles show systematic differences that lie outside the agreement that hopefully could be expected in high-temperature systems. Rauh and Thorn,[2] using the effusion method and radiochemical analysis for uranium, measured the vapor pressure in the temperature range 1630–1970°K and derived a value of 116.6 kcal/mol for the heat of sublimation at 0°K. The effusion measurements of Alcock and Grieveson[3] also support this value of the heat of sublimation. DeMaria, Burns, Drowart, and Inghram,[4] using mass spectrometric analysis of the vapor effusing from an initially constituted system of uranium metal and aluminum oxide, measured partial pressures of uranium that were approximately 0.1 those of Rauh and Thorn and reported a heat of sublimation, $\Delta H^\circ_{298} = 126 \pm 5$ kcal/mol. (The change of reference temperature from 0 to 298°K is numerically unimpor-

(1) Based on work performed under the auspices of the U. S. Atomic Energy Commission.

(2) E. G. Rauh and R. J. Thorn, *J. Chem. Phys.*, 22, 1414 (1954).

(3) C. B. Alcock and P. Grieveson, *J. Inst. Metals*, 90, 304 (1962).

(4) G. DeMaria, R. P. Burns, J. Drowart, and M. G. Inghram, *J. Chem. Phys.*, 32, 1373 (1960).

tant.) Ackermann, Rauh, and Thorn[5] concluded that these two investigations need not be inconsistent if the activity of uranium is reduced to approximately 0.05 by the presence of dissolved oxygen. Drowart, Pattoret, and Smoes[6] have reported mass spectrometric studies of $UO_2(s) + U(l)$ mixtures and pure liquid uranium which yield an average value of the heat of sublimation at 298°K of 125.5 ± 2.5 kcal/mol. That study indicated that the pressures measured by Rauh and Thorn[2] and Alcock and Grieveson[3] were too high as a result of oxygen contamination which vaporizes as UO(g). Furthermore, the reduction of the vapor pressure of pure liquid uranium by dissolved oxygen was indicated to be less than a factor of 1.6. These authors[7] also reviewed the thermochemical data for the vaporization of uranium oxides and carbides and concluded that the use of the thermochemical data in the thermodynamic cycles was reasonably consistent with the latter value. Leitnaker and Godfrey[8] recently analyzed the thermochemical data for the uranium–carbon system and calculated $\Delta H°_{298} = 123.7 \pm 1.3$ kcal/mol. Pattoret, Drowart, and Smoes[9] have recently reported new mass spectrometric data that yield an even higher value of the heat of sublimation, $\Delta H°_{298} = 128.5 \pm 2.0$ kcal/mol.

The general intent of the present investigation is to directly measure by mass spectrometric and absolute effusion techniques the partial pressures of U(g) in equilibrium with liquid uranium saturated with tantalum, UP, US, and UC, to include those of $UO_2(s) + U(l)$ previously reported,[10] and to demonstrate the significance of any observed trend of nonideality of the liquid solutions from the chemical and thermodynamic properties of the dissolved components.

Experimental Methods and Results

A. Mass Spectrometric Observations and Measurements. Mass spectrometric observations were made on the initially constituted systems UP(s), $UP(s) + U(l)$, US(s), $US(s) + U(l)$, UC(s), and $UC(s) + U(l)$. The instrument used was a Bendix Model 12–101 time-of-flight mass spectrometer equipped with an electron-bombarded effusion cell. Details of the cell assembly,[11] the power regulator,[12] and the methods, techniques, and measurement of temperature have been described elsewhere.[13] The observations included identification of species, behavior of impurities (principally oxygen bearing species from oxide contamination of the starting materials), indications of changes in composition by a time dependence of the ion currents, and measurement of the temperature dependences of the ion currents. A typical behavior of the ion currents accompanying a change of composition has been demonstrated in the thorium–oxygen system.[14] As the composition adjusts to the equilibrium value, the ion currents increase or decrease at varying rates and the rate of adjustment may become quite slow at the lower temperatures, for large temperature changes, and when the temperature has been decreased. In order to ensure steady-state conditions within reasonable times, large temperature changes were avoided and the ion currents were recorded at temperatures sequentially decreased, then increased. The data for each series of measurements of the equilibrium ion currents as a function of temperature will be given by the least-squares equations of $\log I_i T$ *vs.* $1/T$ with the standard deviations. As shown previously,[14] the data can reflect changes in partial pressures with both temperature and composition if the composition variable is important.

An ionizing electron energy of 10 eV was used when there existed the possibility of U^+ ions being formed from fragmentation of higher molecular weight species;[10] when fragmentation was not possible 20 eV was used. Tungsten effusion cells were used throughout.

The samples in all cases were in the form of dense cups of the monophosphide, sulfide, or carbide weighing about 1 g to which 50–200 mg of uranium metal was added after impurities had been removed by vaporization.

1. The Systems UP(s) and UP(s) + U(l). Before the addition of uranium, oxide contamination in the UP was removed by vaporization as UO gas. At 2350°K the ions observed (20 eV) were U^+, UO^+, P^+, and a trace of P_2^+. No UP^+ or UO_2^+ ions were observed. Initially the U^+ and UO^+ were of equal intensity but during a 7-hr period at 2350°K, the U^+ increased by about a factor of 2 and the UO^+ and P^+ decreased by factors of about 200 and 2, respectively, and thereafter both the U^+ and P^+ remained constant. The temperature dependences of the partial pressures of U(g) and P(g) were then determined at 20 eV over the temperature range 1890–2350°K. The least-squares representation of the data and the measured heats of vaporization are given in Table I under Series UP-1. The errors quoted here and in the remainder of the paper are standard deviations. After an additional 4 hr at 2350°K the temperature dependences were remeasured; the least-squares representation of these data is given in Table I under Series UP-2. Since the heats of the two series agree within the standard devia-

(5) R. J. Ackermann, E. G. Rauh, and R. J. Thorn, *J. Chem. Phys.*, **37**, 2993 (1962).

(6) J. Drowart, A. Pattoret, and S. Smoes, *ibid.*, **42**, 2629 (1965).

(7) J. Drowart, A. Pattoret, and S. Smoes, *J. Nuclear Mat.*, **12**, 319 (1964).

(8) J. M. Leitnaker and T. G. Godfrey, *ibid.*, **21**, 175 (1967).

(9) A. Pattoret, J. Drowart, and S. Smoes, Paper Sm.98/49, published in the Proceedings of the Symposium on Thermodynamics of Nuclear Materials with Emphasis on Solution Systems, International Atomic Energy Agency, Vienna, Sept 4–8, 1967.

(10) R. J. Ackermann, E. G. Rauh, and M. S. Chandrasekharaiah, *J. Phys. Chem.*, **73**, 762 (1969).

(11) E. G. Rauh, R. C. Sadler, and R. J. Thorn, Argonne National Laboratory Report, ANL-6536, April 1962.

(12) H. H. Cremer, *Z. Instr.*, **72**, 209 (1964).

(13) R. J. Ackermann and E. G. Rauh, *J. Chem. Phys.*, **36**, 448 (1962).

(14) R. J. Ackermann, E. G. Rauh, R. J. Thorn, and M. C. Cannon, *J. Phys. Chem.* **67**, 762 (1963).

Table I: Mass Spectrometric Determinations of Temperature Dependence of Partial Pressures of U and P in Equilibrium with the System UP(s) + U(l): Linear Least-Squares Representation, Log $I_iT = A_i + B_i/T$. Measured Heats of Vaporization of U(g) and P(g)

Series[a]	Species	A	$-B$	ΔH_v, kcal/mol
UP-1	U	15.391 ± 0.086	25,030 ± 180	114.5 ± 0.8
	P	17.447 ± 0.164	31,990 ± 360	146.4 ± 1.6
UP-2	U	15.628 ± 0.125	25,330 ± 260	115.9 ± 1.2
	P	17.896 ± 0.255	32,720 ± 560	149.7 ± 2.6
UP-U-1	U	15.315 ± 0.086	25,170 ± 180	115.2 ± 0.8
	P	17.706 ± 0.246	33,050 ± 530	151.2 ± 2.4

[a]UP-1: eight experimental points, temperature range 1890–2340°K. UP-2: ten experimental points, temperature range 1890–2400°K. UP-U-1: seven experimental points, temperature range 1885–2310°K.

tions, it was apparent that equilibrium had been established and a 50-mg sample of anodically cleaned uranium was added. Again, at 2350°K, approximately equal intensities of U^+ and UO^+ were observed initially but after 3 hr the UO^+ had decreased by a factor of about 250 and the U^+ and P^+ remained constant within a few per cent. A third measurement of the temperature dependences of the partial pressures of U(g) and P(g) resulted in the data given in Table I under Series UP-U-1 and shown in Figure 1.

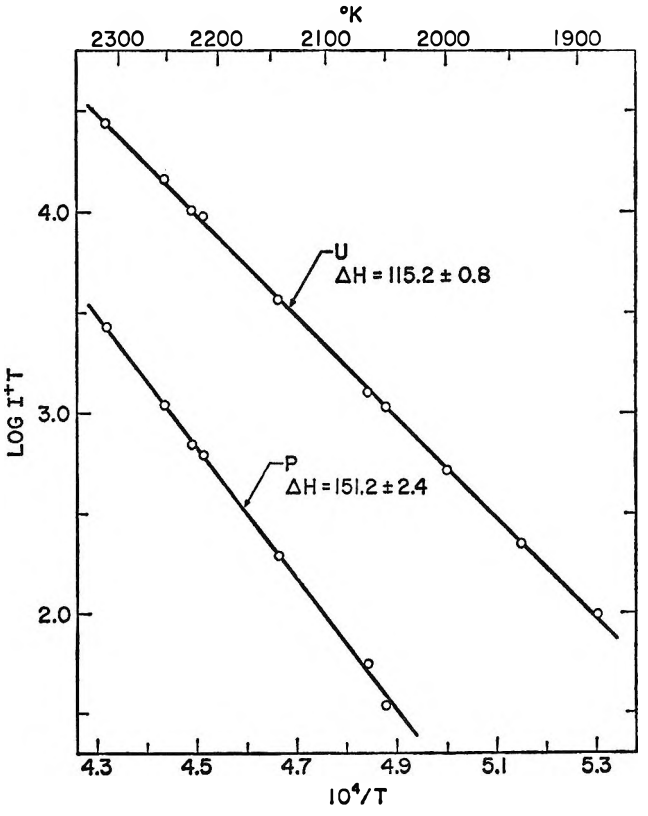


Figure 1. Mass spectrometric measurements of the temperature dependence of U(g) and P(g) in equilibrium with UP(s) + U(l), Series UP-U-1, Table I; log $I_iT = A_i + B_i/T$.

The measured heats of evaporation of U agree within the standard deviations in all three series and there is agreement between the measured values of ΔH(P) of Series UP-2 and UP-U-1 although that of Series UP-1 is slightly low.

The mass spectrometric evidence given here indicates that oxide contamination in UP(s) and UP(s) + U(l) can be reduced to trace amounts by vaporization as UO but that during the time required, in this case 7 hr at 2350°K, phosphorus is lost preferentially and the composition shifts into the two-phase region, UP(s) + U(l). The observations are in agreement with those of Reishus, Gunderson, and Edwards.[15]

2. The Systems US(s) and US(s) + U(l). During the high-temperature purification of the US the general vaporization behavior observed was essentially that described earlier.[16] Initially at 2110°K the ions observed were U^+, UO^+, US^+, and $UO_2^+ + US^+$ (mass 270), and UOS^+ (not UO_3 because of reducing conditions) in the approximate ratios 1:45:15:1. During a period of 15 hr at 2110°K, the U^+ increased by a factor of 5 and the UO^+, $US^+ + UO_2^+$, and UOS^+ decreased by factors of 2, 3, and 8, respectively. During an additional 10-hr period at 2270°K, the U^+ increased slightly, the US^+ remained constant, the UO^+ decreased by a factor of 10^3, and the UOS^+ decreased beyond the limit of detection. The temperature dependences of the ion currents U^+ and US^+ were then determined over the temperature range 1920–2270°K. In this range the ion currents showed no increase or decrease with time at each temperature indicating that the composition of the solid, stoichiometric or otherwise, did not change appreciably. However, when the temperature was raised to 2320°K, the U^+ showed a small but steady increase while the US^+ remained constant. After 1 hr at 2320°K, the temperature dependences of U^+ and US^+ were remeasured over the temperature range 1920–2320°K. Again there appeared to be no change in composition at temperatures below 2320°K. The temperature was then raised to 2400°K for 1 hr during which time the U^+ increased slightly, then became constant while the US^+ remained unchanged. A third series of measurements of the temperature dependences was made in the range 1920–2320°K. The data for the three series of measurements are given in Table II under Series US-1, US-2, and US-3.

An 85-mg sample of uranium metal was added to the US cup and the temperature raised to 2270°K for 5 hr during which time the U^+ and US^+ were essentially constant and a small ion current of UO^+, initially about 3% of the total, decreased by a factor of 20. Three series of measurements of the temperature dependences

(15) J. W. Reishus, G. E. Gunderson, P. M. Danielson, and R. K. Edwards, Argonne National Laboratory Report, ANL-7514, Nov 1968.

(16) E. D. Cater, E. G. Rauh, and R. J. Thorn, *J. Chem. Phys.*, 44, 3106 (1966); Erratum, *ibid.*, 48, 538 (1968).

Table II: Mass Spectrometric Determinations of Temperature Dependence of Partial Pressures of U and US in Equilibrium with US(s) and US(s) + U(l): Linear Least-Squares Representation, Log $I_iT = A_i + B_i/T$. Measured Heats of Vaporization of U(g) and US(g)

Series[a]	Species	A	$-B$	ΔH_v, kcal/mol
US-1	U	17.268 ± 0.085	28,750 ± 180	131.6 ± 0.8
	US	18.720 ± 0.129	31,550 ± 270	144.4 ± 1.2
US-2	U	16.463 ± 0.077	26,850 ± 160	122.9 ± 0.7
	US	18.172 ± 0.180	31,270 ± 380	143.1 ± 1.7
US-3	U	16.221 ± 0.076	26,210 ± 160	119.9 ± 0.7
	US	18.221 ± 0.129	31,310 ± 270	143.3 ± 1.2
US-U-1	U	16.201 ± 0.063	26,240 ± 130	120.1 ± 0.6
	US	18.104 ± 0.088	31,170 ± 180	142.6 ± 0.8
US-U-2	U	16.209 ± 0.030	26,340 ± 60	120.5 ± 0.3
	US	18.065 ± 0.110	31,170 ± 240	142.0 ± 1.1
US-U-3	U	16.207 ± 0.032	26,280 ± 70	120.2 ± 0.3
	US	18.124 ± 0.090	31,240 ± 190	143.0 ± 0.9

[a] US-1: ten experimental points, temperature range 1910–2310°K. US-2: seven experimental points, temperature range 1930–2320°K. US-3: seven experimental points, temperature range 1930–2240°K. US-U-1: ten experimental points, temperature range 1930–2300°K. US-U-2: eight experimental points, temperature range 1945–2345°K. US-U-3: nine experimental points, temperature range 1925–2390°K.

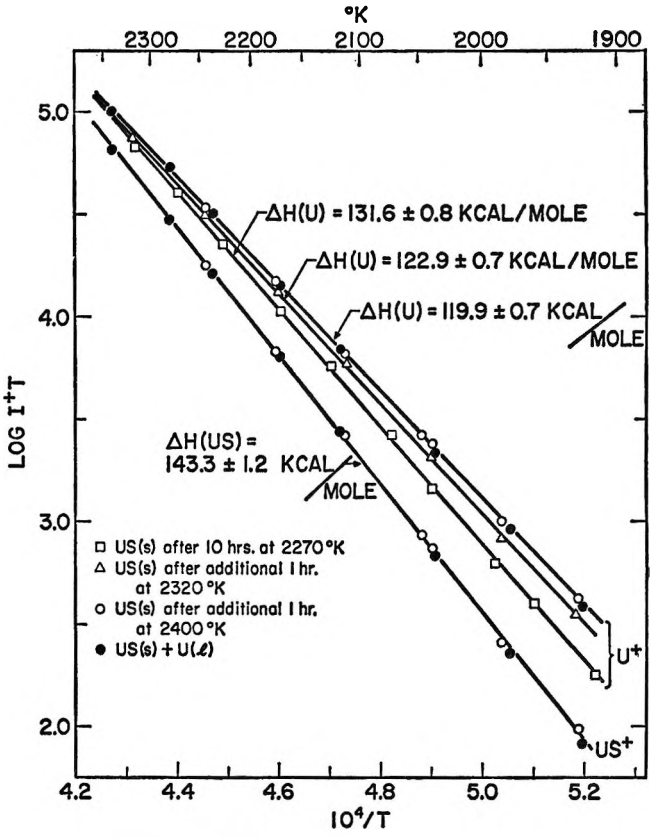


Figure 2. Mass spectrometric measurements of the temperature dependence of U(g) and US(g) in equilibrium with systems in various stages of decomposition of US(s) to US(s) + U(l); log $I_iT = A_i + B_i/T$ for Series US-1, 2, 3 and US-U-3, Table II.

of U^+ and US^+ from the system US(s) + U(l) were carried out over the temperature range 1920–2320°K: US-U-1 after the original 5 hr at 2270°K, US-U-2 after an additional 5 hr at 2350°K, and US-U-3 after an additional 1 hr at 2400°K. The data are given in Table II.

Plotted in Figure 2 are the data for U^+ from Series US-1, US-2, US-3, and US-U-3 and the data for US^+ from Series US-3 and US-U-3. The data for U^+ from Series US-U-1 and US-U-2 reproduce those of US-3 and US-U-3 and all six sets of data for US^+ agree within the standard deviations.

These mass spectrometric observations show that oxygen contamination in these condensed phases can be reduced to trace amounts by the evaporation of a small fraction of the total sample at 2270°K. The decrease in the measured heats of evaporation of U over US (US-1, US-2, US-3) as the sample was heated at progressively higher temperatures suggests that the composition was becoming more substoichiometric. The agreement between the measured heats of Series US-3 and US-U-1, US-U-2, and US-U-3 indicates that in Series US-3 the composition had already been driven into the two-phase region, US(s) + U(l), *via* the preferential vaporization of sulfur. The insensitivity of the measured heats of evaporation of US to changes in composition suggests that the solubility of U in US is small and that the activity of the US remains near unity.

3. The Systems UC(s) and UC(s) + U(l). The UC cup was heated for a total of 30 hr at 2475°K during which time only the ions U^+ and CO^+ were observed, initially in the ratio 1:1 (at 20 eV) and finally at about 20:1. The ion intensity U^+ did not change appreciably. The temperature dependence of U^+ over the range 1960–2475°K was measured at the end of the 4th, 9th, 14th, 20th, and 30th hours. The measured heats of evaporation, each with a standard deviation of ±1 kcal/mol, were successively, 141, 131, 126, 124, and 122 kcal/mol, while the partial pressure of uranium at 2000°K increased by a factor of 2.5. This behavior indicates a progressive increase in the activity of uranium in the solid phase as the partial pressure of CO(g) decreases and possibly can be associated with the diminishing effect of stabilization of the carbide by oxygen and/or the preferential loss of carbon *via* CO(g) although this would require a ratio of partial pressure of U/CO less than the observed ratio of the ion currents.

A sample of 175 mg of uranium metal was added to the UC and the temperature raised to 2385°K. Only U^+ and CO^+ were observed, in the ratio 1:3 initially and 3:1 after 1.5 hr. A measurement of the temperature dependence of U^+ over the range 1940–2385°K was made after 7 hr at 2385°K. An average slope of 116 ± 1.6 kcal/mol was measured but an examination of the residuals in the data indicated a departure from a linear relationship of log U^+T *vs.* $1/T$. After 27 hr at 2385°K the temperature dependence data shown in Figure 3

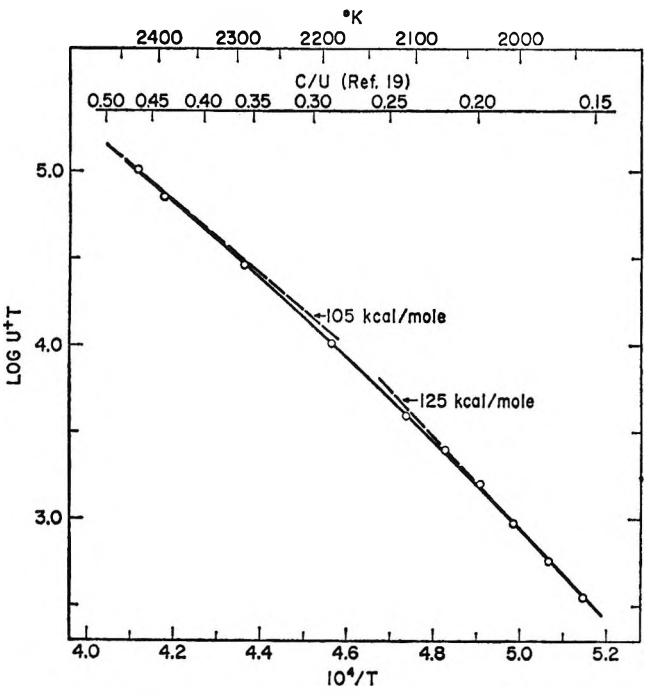


Figure 3. Mass spectrometric measurements of the temperature dependence of U(g) in equilibrium with UC(s) + U(l). The limiting slopes have been included to show the departure from linearity.

indicated a definite curvature with a limiting slope of approximately 125 kcal/mol at 2000°K and 105 kcal/mol at 2400°K and could well reflect the effect of the increasing solubility of carbon in liquid uranium with temperature.

B. Measurements of the Total Effusion Rate of Uranium. The effusion rates of the vapor species containing uranium in equilibrium with the heterogeneous systems cited in the preceding section were measured by the collection of known fractions of the effusate on platinum targets and the subsequent radiochemical analysis for uranium. Both tantalum and tungsten effusion cells of the same design were used interchangeably. The rate of collection is related to the vapor pressure inside the effusion cell by the equation

$$p_i = \frac{n_i}{at}\sqrt{2\pi M_i RT}\left(\frac{d^2 + r^2}{r^2}\right) \qquad (1)$$

in which p_i is the pressure of species i, n_i and M_i are the number of moles and atomic or molecular weight, respectively, of the uranium species collected on the target in time t, a is the area of the orifice, d is the orifice-to-collimator distance, r is the radius of the collimator, and R and T are the gas constant and temperature, respectively.

The choice of the collection technique in which a relatively small fraction of the total effusate is collected in the forward direction, *i.e.*, normal to the plane of the orifice, was made for several reasons. Such a technique closely parallels the geometrical arrangement used in the mass spectrometer and possesses the advantage of sensing only the vapor flux emitted directly from the evaporating surface of the sample. The utility of this method with sensitive radiochemical analysis is well established.[2] More importantly, the spatial distribution of the vapor for a small solid angle located in the forward direction approaches closely the theoretical value for a cosine or random distribution whereas at solid angles away from the normal the intensity may be markedly less than the theoretical values. Ward, Mulford, and Kahn[17] have shown very striking departures from a cosine distribution for a variety of systems, samples, and cell geometries. In view of these findings an experiment was performed in which a direct comparison was made between the weight of uranium collected on platinum targets which intercepted a known solid angle, $r^2/(r^2 + d^2) = 0.011$ in eq 1, and the total weight lost from a tantalum effusion cell containing liquid uranium located in the bottom of a single crystal tantalum cup. At 2320°K this experimental arrangement yielded a ratio of the measured weight loss to that expected for a cosine distribution equal to 0.60. This value less than unity indicates a significant loss of particle intensity at larger angles from the normal, as do Ward's results, and demonstrates the unreliability of total weight loss measurements for these systems.

In all cases except one, either the predominant or only vapor species was shown mass spectrometrically to be atomic uranium, and consequently, an apparent or "effective" vapor pressure of a particular system, p_e, was calculated by assuming uranium to be the only uranium-containing species present in the vapor. Correction of this assumption will be effected when necessary in the subsequent thermodynamic analysis. The results are given in Table III and in Figure 4 and are compared with those of pertinent previous studies.

Curve 1 represents the vapor pressure of liquid uranium reported by Rauh and Thorn[2] and curve 2 represents the effective pressure which is predominantly that of UO(g) in equilibrium with mutually saturated UO_2(s) + U(l).[10]

Curve 3 corresponds to the system US(s) + U(l) and an additional phase which was detected in the residue by metallographic sectioning of the sample. This additional phase was probably UO_2 since the X-ray diffraction pattern did not show the lines of a third phase such as UOS; the diffraction lines of UO_2 and US are virtually coincident. Mass spectrometric observations of the vapor arising from US contaminated with oxide indicated that UO(g) is the major component. At the present time, however, this system has not been quantitatively characterized and it is possible that the additional phase (if other than UO_2) may have escaped detection in the X-ray pattern as a result of inadequate sampling. It is important, however, to retain the

(17) J. W. Ward, R. N. R. Mulford, and M. Kahn, *J. Chem. Phys.*, 47, 1710 (1967); see also J. W. Ward, *ibid.*, 47, 4030 (1967), and J. W. Ward, Los Alamos Scientific Report LA-3509, Jan 1966.

Table III: Experimental Results of the Effusion Measurements

Curve and designation		System	Remarks	Least-squares equation	Temp range, °K
1		U(l) + (oxide)	Ref 2	$\log p_e(\text{atm}) = (5.702 \pm 0.011) - (23{,}330 \pm 21)/T$	1630–1970
2		U(l) + UO_2(s)	Ref 10	$\log p_e(\text{atm}) = (7.250 \pm 0.146) - (27{,}020 \pm 250)/T$	1580–2400
3	○	U(l) + US(s) + (UO_2)	Normal uranium	$\log p_e(\text{atm}) = (7.450 \pm 0.200) - (28{,}050 \pm 420)/T$	1984–2330
	⊙	U(l) + UP(s)	Normal uranium		
4	×	U(l) + Ta(s)	Normal uranium	$\log p_U(\text{atm}) = (5.493 \pm 0.170) - (24{,}910 \pm 370)/T$	1980–2416
	+	U(l) + Ta(s)	^{235}U enriched		
5	▲	U(l) + US(s)	Normal uranium	$\log p_e(\text{atm}) = (10.340 \pm 1.783) - (4.388 \pm 0.751)10^4/T + (0.1787 \pm 0.0787)10^8/T^2$	1874–2383
	●	U(l) + US(s) + Ta(s)	^{235}U enriched		
6	○	U(l) + UC(s)	^{235}U enriched	$\log p_U(\text{atm}) = (4.880 \pm 0.230) - (24{,}400 \pm 450)/T$	1792–2138

effusion data at least for the purpose of qualitative comparison.

Curve 4 represents several sets of data which are statistically indistinguishable. The circle points correspond to the partial pressure of U(g) in equilibrium with liquid uranium contained in a UP cup. The × points and + points correspond to normal and ^{235}U-enriched uranium contained in a cup made from single crystal tantalum. It is noteworthy to point out that single crystal tantalum as well as tungsten appear to be excellent container materials for liquid uranium at temperatures up to at least 2400°K as the liquid metal

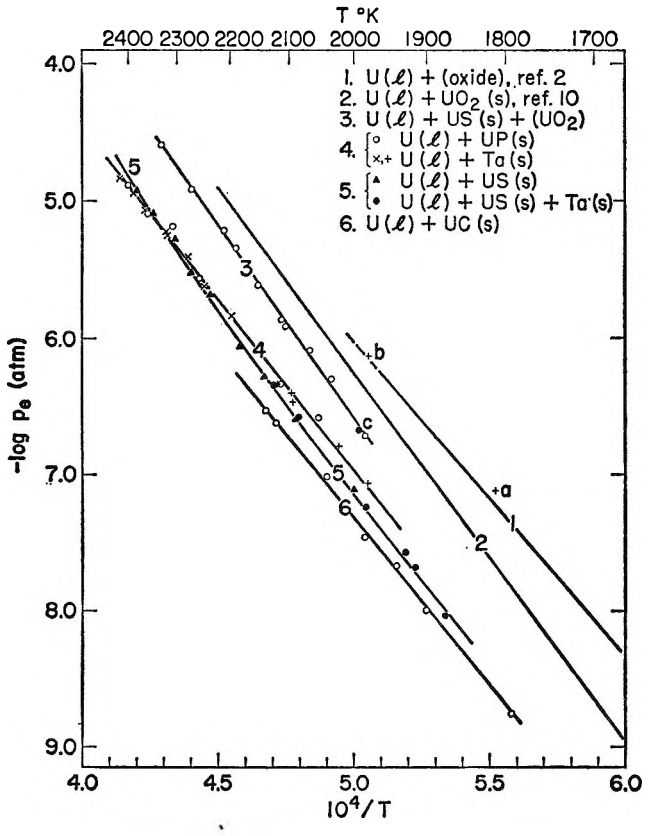


Figure 4. Log p_e *vs.* $10^4/T$ for various multiphase systems containing liquid uranium. The "effective pressure," p_e, is the total pressure of uranium-bearing species as calculated from eq 1. The significance of points a, b, and c is given in the text.

was confined entirely within the cup. Containers fabricated from polycrystalline tantalum and tungsten are useful only up to approximately 2050 and 1900°K, respectively, above which the liquid metal rapidly disappears *via* creep into the grain-boundary network. The capability of heating liquid uranium to temperatures at which the vapor pressure is relatively large ensures the complete loss of oxide contamination which vaporizes as UO(g). It is interesting to note that the initially measured volatility of liquid uranium containing a surface film of oxide shown by points a and b in Figure 4 appears to be significantly higher than that corresponding to the system UO_2(s) + U(l) given by curve 2. In fact, the two points agree more closely with the pressures measured by Rauh and Thorn.[2] However, after 5 hr of heating at approximately 1980°K, the pressure had decreased to the value shown on curve 4. Mass spectrometric observations of the vapor at this temperature resulting from metal possessing a surface layer of oxide showed amounts of UO(g) that were substantially larger than U(g) but which decreased steadily with time. Consequently, it doubtful whether these initial observations could have corresponded to the equilibrium state of the univariant system UO_2(s) + U(l).

A comparison of the results of the system UP(s) + U(l) with those recently reported by Reishus, *et al.*,[15] shows that the present values of the partial pressure of uranium are approximately a factor of 2 larger and the apparent heat of vaporization of uranium from the system is 115.5 ± 1.7 kcal/mol compared with 118.5 ± 0.9 kcal/mol for the latter. The factor of 2 discrepancy in the pressures is perhaps explainable in terms of the difference between the total weight loss and that calculated from the collection of effusate in the forward direction; Reishus, *et al.*,[15] calibrated their mass spectrometric observations by the total weight loss method, and hence their pressures are possibly too small by approximately a factor of 2. The partial pressures of uranium reported by Gingerich and Lee[18] are approximately a factor of 5 larger than the present results and

(18) K. A. Gingerich and P. K. Lee, *J. Chem. Phys.*, **40**, 3520 (1964).

their validity very likely should be discounted because the partial pressure of uranium above one of its compounds cannot be larger than the vapor pressure of the pure metal; in the present study, as seen in Figure 4, the system UP(s) + U(l) essentially yields the vapor pressure of uranium. Pattoret, *et al.*,[9] report a value of the heat of sublimation $\Delta H°_0(U) = 128.5$ kcal/g-atom which corresponds to vapor pressures that are approximately one-half of those obtained in the present study.

Curve 5 represents the data obtained from a tungsten cell for the univariant system, US(s) + U(l) + vapor. The measurements designated by solid triangles were carried out with normal uranium contained within a normal US cup. The measurements designated by solid circles were obtained from a mixture of liquid uranium and US(s), both enriched in ^{235}U, contained in a tantalum cup. The pressure calculated from this first collection of effusate in this case, shown by point c on curve 3, Figure 4, is seen to be markedly greater than the remaining points on curve 5, which behavior indicates that the system was initially contaminated with oxygen which vaporized as UO(g). Similarly, the first two collections obtained near 2300°K from samples containing normal uranium were approximately 25% higher than subsequent ones, and consequently these points were also not included in the analysis of the data. In order to prove that the vapor phase was relatively free of oxygen contamination during the remainder of the collections, a sample of the US cup was removed from the effusion cell at the termination of the measurements and transferred to the mass spectrometer. Only a few per cent of UO^+ relative to U^+ was observed initially and it decreased rapidly with time, probably indicating that a small but insignificant oxide contamination resulted from the brief exposure to air which occurred in the transfer operation.

It is obvious from Figure 4 that curve 5 is not a simple linear plot as typified by all the other curves. The mass spectrometric observations indicate that both U(g) and US(g) are present in the vapor phase, the latter becoming more important at higher temperatures. Hence, the composite curve appears to possess a positive curvature with increasing temperature. The empirical least-squares equation together with the standard deviations in the coefficients given in Table III demonstrates this curvature. A comparison of the results of the US(s) + U(l) system with the previous studies by Cater, Rauh, and Thorn[16] for US(s) is discussed in the next section.

Curve 6 represents the data obtained for the system UC(s) + U(l). The mixture was prepared *in situ* by the reaction of uranium metal and graphite which had been outgassed previously at 2200°. The desired proportion of the two condensed phases was estimated to be nearly equal from the phase diagram given by Storms.[19] The measured partial pressures of U(g), the only significant species observed mass spectrometrically, agree well with those reported by Storms, the latter being approximately 30% lower. The average heat of vaporization of uranium, 111.7 ± 2.1 kcal/mol, virtually agrees with the value 114.4 ± 0.5 kcal/mol given by Storms. Both values are consistent with the range of values resulting from the curvature of log U^+T *vs.* $1/T$ (see Figure 3) observed mass spectrometrically. Some caution must be exercised in this case, as well as in the previously described systems, in the interpretation of the temperature dependence of the partial pressure. This dependence can be interpreted as the partial molar enthalpy *only* if the change in temperature produces no change of composition within each of the condensed phases. Such an idealized behavior was certainly not obtained throughout most of the upper portions of the temperature ranges of these heterogeneous systems, in particular the U(l) + UC(s) system as shown in Figure 3.

Thermodynamic Analysis and Discussion

The data shown in curve 4, Figure 1, *i.e.*, the partial pressure of U(g) in equilibrium with liquid uranium saturated with phosphorus or tantalum, must represent the lower limit of the vapor pressure of liquid uranium. The calculation of the heat of sublimation, $\Delta H°_{298}(U)$, at each experimental temperature *via* the measured pressures and the free energy functions for liquid and gaseous uranium yields values that display a small but significant increase (~0.5 kcal) with increasing temperature. This trend suggests that the observed pressure is systematically lowered by the presence of a dissolved component. The solubility of tantalum in liquid uranium has been measured by Schramm, Gordon, and Kaufman.[20] The correction of the partial pressure of uranium (equation for curve 4, Table IV) for dissolved tantalum according to Raoult's law yields values of $\Delta H°_{298}(U)$ which show no trend with temperature. These results are given in Table IV. The data for the system UP(s) + U(l) are statistically indistinguishable from those obtained with liquid uranium contained in tantalum and have been given the numerical corrections for dissolved tantalum since the effects of dissolved phosphorus and tantalum on the measured partial pressure of U(g) are nearly equal. The demonstrated constancy of the values of the heat of sublimation indicates the concordance of the present data with the thermodynamic data for liquid and gaseous uranium and the virtual ideality of the liquid solutions containing tantalum or phosphorus. The derived vapor pressure of pure liquid uranium in the temperature range 1980 to 2420°K is given by the

(19) E. Storms, "Thermodynamics," Vol. I, International Atomic Energy Agency, Vienna, 1966, p 318.

(20) C. H. Schramm, P. Gordon, and A. R. Kaufmann, *J. Metals*, 188, 195 (1950).

Table IV: Thermodynamic Analysis of the Vaporization of Liquid Uranium

T, °K	$-R'T \log p_U$,[a] kcal/mol	$-\Delta(G°_T - H°_{298})$,[b] kcal/mol	$\Delta H°_{298}$(U), kcal/mol
1980	63.43	62.45	125.8_8
2023	62.35	63.60	125.9_5
2053	61.21[c]	64.40	125.6_1
2095	61.33	65.51	126.8_4
2097	60.79	65.57	126.3_6
2114	60.62[c]	66.02	126.6_4
2120	60.78	66.19	126.9_7
2198	58.00	68.25	126.2_5
2248	57.01	69.58	126.5_9
2256	56.64[c]	69.80	126.4_4
2278	55.49	70.37	125.8_6
2309	53.89[c]	71.19	125.0_8
2319	54.81	71.45	126.2_6
2322	54.84	71.54	126.3_8
2358	54.04[c]	72.48	126.5_2
2363	53.94	72.61	126.5_5
2387	53.12	73.28	126.4_5
2399	52.64[c]	73.59	126.2_3
2416	52.56	74.05	126.6_1
		Av =	126.3 ± 0.1[d]

[a] Values corrected for the solubility of tantalum by means of Raoult's law. [b] Values obtained from a smoothed curve of the points taken from the compilation of Hultgren, *et al.*[21] [c] Measurement of the system U(l) + UP(s). All other points correspond to the system U(l) + Ta(s). [d] The error quoted is the standard deviation in the average; the total uncertainty is estimated to be $< \pm 1.0$ kcal.

equation

$$\log p°_U(\text{atm}) = (5.71 \pm 0.17) - (25{,}230 \pm 370)/T \quad (2)$$

The heat of vaporization at the average temperature of the experimental range, $\Delta H°_{2200}(U)$, is 115.5 ± 1.7 kcal/mol which is in agreement with the average value at 298°K from Table IV corrected to 2200°K by means of the heat content functions,[21] *i.e.*, 116.5 ± 1.0 kcal/mol.

Since the mass spectrometric data show that the vaporization of US(s) + U(l) mixtures occurs *via* two modes of vaporization involving U(g) and US(g), it can be easily shown by means of eq 1 that the "effective" pressure of uranium-bearing species p_e in curve 4, Figure 4, is related to the individual partial pressures of U(g) and US(g) *via* the equation

$$p_e = p_U + (M_U/M_{US})^{1/2} p_{US} \quad (3)$$

From Table II it is seen that the quantities $\log I_i T$ are linear with reciprocal temperature and since the ion current I_i of a given species is related to its partial pressure p_i *via* the instrumental sensitivity K_i according to the equation

$$I_i T = K_i p_i \quad (4)$$

the partial pressures of U(g) and US(g) can be functionally expressed by the equations

$$p_U = \exp(\Delta S_U/R) \exp(-\Delta H_U/RT) \quad (5)$$

and

$$p_{US} = \exp(\Delta S_{US}/R) \exp(-\Delta H_{US}/RT) \quad (6)$$

Since both eq 5 and 6 reduce to the form $p_i = C_i \exp(B_i/T)$, eq 3 can be rewritten as

$$p_e = C_U \exp(B_U/T) + (0.939) C_{US} \exp(B_{US}/T) \quad (7)$$

The application of the method of least squares to obtain values of the parameters C_U and C_{US} using the individual measured values of p_e(atm) and T and the values of B_U and B_{US} multiplied by 2.303 from Series US-U-1 in Table II leads to the numerical results shown in Table V. The effect of variation of the constants

Table V: Calculated Instrumental Sensitivities for U(g) and US(g)

B_U	B_{US}	C_U ($\times 10^{-5}$)	$(0.939)C_{US}$ ($\times 10^{-7}$)	K_U/K_{US}[a]
−26,240	−31,170	7.390	5.859	1.06
$B_U + 130$	$B_{US} + 180$	8.824	6.429	0.97
$B_U + 130$	$B_{US} - 180$	8.466	4.849	0.76
$B_U - 130$	$B_{US} + 180$	6.456	7.070	1.46
$B_U - 130$	$B_{US} - 180$	6.170	5.130	1.15

[a] Considering the errors in both A_i and B_i, Table II, the error in K_U/K_{US} as given by $\log K_U/K_{US} = 0 \pm 0.3$. The range of K_U/K_{US} is thus $\frac{1}{2}$ to 2.

B_i by the upper and lower limits of their respective standard deviations is shown to produce significant variations in the least-squares values of C_U and C_{US}. The instrumental sensitivity K_i is the product of the ionization cross section and the detection efficiency of a given species and the relative values for U(g) and US(g) are shown in the last column of Table V; an average value near unity is obtained.

The least-squares analysis of curve 5, Figure 4, just described yields the partial pressures of U(g) and US(g) in the temperature range 1900–2400°K expressed in logarithmic form

$$\log p_U(\text{atm}) = (5.87 \pm 0.15) - (26{,}240 \pm 130)/T \quad (8)$$

and

$$\log p_{US}(\text{atm}) = (7.80 \pm 0.15) - (31{,}170 \pm 180)/T \quad (9)$$

The accuracy of this method of analysis of this system, or other systems involving two or more vapor

(21) R. Hultgren, R. L. Orr, P. D. Anderson, and K. K. Kelley, "Selected Values of Thermodynamic Properties of Metals and Alloys," John Wiley and Sons, Inc., New York, N. Y., 1963.

Table VI: Derived Results of the Activity of Uranium Saturated with Various Components

System	$\log a_U = A_U + B_U/T$ A_U	B_U	a_U (2000°K)[a]	$\log N_i = A_i + B_i/T$[b] A_i	B_i	γ_U (2000°K)
U(pure)	...	...	1	...	...	1
U(Ta)	−0.22	330	0.9	~0	1800[19]	1
U(P)	...	...	~0.9	...	...	~1
U(S)	0.16	−1010	0.45	(1.70)[23]	(5540)[23]	0.5
U(C)	−0.83	830	0.4	1.56	4590	0.5
U(O)[10]	−0.50	−410	0.2[c]	1.18[24]	4400[24]	0.2_2

[a] ±10% estimated from average of residuals in log p_e, Table III. [b] Dissolved components are Ta, US, UC, and UO_2. [c] Value involves estimated relative cross section of U:UO:UO_2 = 1:1:1.[10]

species, is subject to three limiting criteria: (1) the partial pressures of the vapor species must be comparable; (2) their slopes or temperature dependencies must differ significantly; and (3) the values of log p_e must be sufficiently precise to display a curvature with reciprocal temperature or an average slope between those of the two species. In the present case the resolution of the data into the partial pressures of U(g) and US(g) is somewhat marginal with respect to the relatively small curvature seen in curve 4 of Figure 4. For example, the inclusion of two initial measurements of p_e near 2300°K that were too high by approximately 25% due to suspected oxide contamination produced a ratio of K_U/K_{US} near 12 rather than unity. Such a result appears to be quite unreasonable in view of what is presently known or believed about relative cross sections. The work of Otvos and Stevenson[22] and the nearly equal appearance potentials of US^+ and U^+ [10,16] indicate a value near unity. Nevertheless, the illustration serves well to caution the investigator of the problems inherent in the three criteria previously cited. The apparently good agreement of the present values of the ratio with the average value 0.86 reported by Cater, *et al.*,[16] in the study of the vaporization behavior of nearly stoichiometric US(s) may be somewhat fortuitous because both are subject to the same criticism. Furthermore, the lack of observed curvature in log p_e *vs.* $1/T$ and the less pronounced difference in the slopes of U(g) and US(g) in the latter case would in general be expected to result in a less definitive ratio.

It is noteworthy to point out the close correspondence between the results of this study with those of Cater, *et al.*[16] The mass spectrometric data shown in Figure 2 demonstrate the ultimate conversion of the US(s) phase to the univariant system US(s) + U(l) above approximately 2300°K. It was observed that the partial pressure of U(g) substantially increased, for example, by a factor of 2 at $10^4/T = 5.2$. The present measurement of p_e at the same value of reciprocal temperature is a factor of 2 larger than the value obtained by Cater, *et al.* Since the partial pressure of US(g) is relatively small at this temperature, the increase in p_e is essentially that of U(*g*) and the consistency between the effusion and mass spectrometric measurements is adequately demonstrated. Furthermore, the derived pressures of U(g) and US(g), which are based on instrumental sensitivities near unity in both studies, are also consistent with the measured increases in p_e and the ion currents of U^+ and the relative constancy of US^+ for both systems.

The results and conclusions of the present study are summarized in Table VI. Expressions for log a_U ($a_U = p_U/p°_U$) are given for various systems of liquid uranium saturated with tantalum, phosphorus, sulfur, carbon, and oxygen; specific values of a_U at 2000°K are given in the fourth column. Approximate linear expressions for the measured solubilities in terms of mole fractions are given for tantalum,[20] sulfur,[23] carbon,[19] and oxygen.[24] Calculated values of the activity coefficients for uranium, $\gamma_U = a_U/N_U$, are shown in the last column. The solubility of tantalum (and probably phosphorus) in liquid uranium appears to produce virtually ideal solutions since the correction of dissolved tantalum *via* Raoult's law yields constant values of $\Delta H°_{298}$ given in Table IV. However, sulfur, carbon, and oxygen cause increasingly negative deviations from ideality and, in fact, the activity of uranium in these various systems appears to follow the trend predicted by the scale of electronegativities.[25] Hence, these results indicate that it is not always possible to measure directly the vapor pressure of a pure metal when the liquid is in equilibrium and saturated with one of its compounds. In a previous study, Drowart, *et al.*,[6] and most recently Pattoret, Drowart and Smoes[26] report that the effect of dissolved oxygen in liquid uranium reduces the activity of uranium by no more than a factor of approximately 2 as compared to a factor of 5 shown in Table

(22) J. W. Otvos and D. P. Stevenson, *J. Amer. Chem. Soc.*, **78**, 546 (1956).

(23) L. N. Yannopoulos and R. K. Edwards, Argonne National Laboratory Report, ANL-7020 May 1964–April 1965.

(24) P. Guinet, H. Vaugoyeau, and P. Blum, Commissariat a L'Energie Atomique Report, CEA-R 3060, Nov 1966.

(25) E. J. Little, Jr., and M. M. Jones, *J. Chem. Educ.*, **37**, 231 (1960).

(26) A. Pattoret, J. Drowart, and S. Smoes, *Trans. Faraday Soc.*, **65**, 98 (1969).

VI. This disagreement is disturbing but the explanation is not obvious at the present time.

The apparently substantial reductions of the activity of metals by saturated amounts of electronegative components is supported by data available for the Ti(O) and Zr(O) systems. Komarek and Silver[27] measured the partial pressure of oxygen as a function of the atom fraction of oxygen in solid solution from 1000 to 1300°K. The activity of the metal components, titanium and zirconium, can be obtained from the measured activity of oxygen by integration of the Gibbs–Duhem equation. Such calculations demonstrate the nonideality of these solutions and yield values at 1300°K of the activities of titanium and zirconium at the saturation limit (~30 at. % oxygen) which are 0.35 and 0.25, respectively.

It is possible to offer an additional explanation, albeit speculative, of the high vapor pressures observed by Rauh and Thorn.[2] Drowart, *et al.*,[6] have attributed these measurements to the system $UO_2(s) + U(l)$. Since the pressures of Rauh and Thorn were somewhat greater[28] than those reported by Ackermann, *et al.*,[10] for $UO_2(s) + U(l)$ mixtures, and since points a and b of Figure 1 obtained in the present study lie close to Rauh and Thorn's results, neither appears to correspond to equilibrium mixtures of $UO_2(s) + U(l)$ as given by curve 2, Figure 4. The explanation of this difference rests in the assumption that, at the relatively low temperatures employed, the rate of solution of the oxide contamination on the surface of the metal was relatively slow and therefore the vaporization reaction that occurred involved liquid uranium near unit activity with a surface coating of oxide (probably UO_2). Hence, a process of the type, $U(l, a \simeq 1) + UO_2(\text{surface}) \rightarrow 2UO(g)$, could produce a total pressure of uranium-bearing species higher than that of the fully equilibrated system.

As previously indicated by DeMaria, *et al.*,[4] and by Drowart, *et al.*,[6] the heat of sublimation, $\Delta H°_0 = 116.6$ kcal/mol derived by Rauh and Thorn[2] is incorrect due to the vaporization of significant amounts of UO(g). Because of the relatively low temperatures of their measurements, it was apparently not possible to remove the initial oxide contamination. The heat of sublimation, $\Delta H°_{298}$, derived from the results of the present study, 126.3 ± 1.0 kcal/mol, is to be compared with the value of 129.0 ± 2.0 kcal/mol most recently reported by Pattoret, *et al.*,[26] the value of 123.7 ± 1.3 kcal/mol reported by Leitnaker and Godfrey[8] based on thermochemical cycles involving UC(s) and $UC_2(s)$, and the value of 126.5 ± 0.5 kcal/mol recommended by Storms[29] in a recent appraisal of the same thermochemical cycles.

(27) K. L. Komarek and M. Silver, "Thermodynamics of Nuclear Materials," International Atomic Energy Agency, Vienna, 1962, p 749.

(28) The actual collector plates of Series 3 were reassayed for uranium by fission counting with new standards; the results agreed within 5% of those originally reported by Rauh and Thorn.[2]

(29) E. K. Storms, "The Refractory Carbides," Academic Press, New York, N. Y., 1967.

Electron Spin Resonance Studies of Hyperconjugation in 2,3-, 2,6-, and 2,7-Dimethylanthracene Cation and Anion Radicals

by Jorge A. Valenzuela and Allen J. Bard[1]

Department of Chemistry, The University of Texas at Austin, Austin, Texas, 78712 *(Received May 15, 1968)*

The electron spin resonance (esr) spectra of the 2,3-, 2,6-, and 2,7-dimethylanthracene cation and anion radicals, prepared by oxidation with sulfuric acid and by reduction with either potassium metal in dimethoxyethane or electrochemically in dimethylformamide, are given. The experimental coupling constants arising from the interaction of the unpaired electron with the ring protons were found to be in good agreement with those calculated using simple Hückel molecular orbital theory. The experimental coupling constants arising from the interaction of the unpaired electron with the methyl protons were found to be in good agreement with those calculated using simple Hückel molecular orbital theory considering a hyperconjugative model and Levy's formula. Polarographic reduction half-wave potentials of 30 methyl-substituted anthracenes and naphthalenes were correlated with the energies of the lowest vacant π-molecular orbital. Molecular orbital calculations using different models (inductive, heteroatom, hyperconjugation) showed that the best results were obtained with the hyperconjugation model with a small inductive effect; this model also yielded spin densities which were in good agreement with the electron spin resonance results.

The effects that are produced by the substitution of a methyl group for a hydrogen into an aromatic hydrocarbon have been discussed in terms of inductive and hyperconjugative models. The inductive effect of a methyl group upon an aromatic hydrocarbon is considered as a direct electrostatic effect modifying the electric potential in the aromatic ring, with the carbon of the aromatic ring adjacent to the methyl group made more electropositive. The latter effect causes a charge redistribution around this ring carbon, but no transference of actual charge is allowed between the aromatic ring and the methyl group.[2] On the other hand, the hyperconjugative effect has been defined in the most general sense as the conjugation of alkyl groups with a multiple bond.[3,4] Among the alkyl groups, the methyl group, due to its higher symmetry, can conjugate more effectively with multiple bonds than other alkyl groups. For example, the hyperconjugative effect for a methyl group and an aromatic hydrocarbon can be explained theoretically, on the basis of molecular orbital theory, in the following way. It is possible to construct, by a proper combination, orbitals for a methyl group which possess π symmetry and can combine with the π orbitals of the aromatic ring. This combination allows a flow of electrons between the methyl group and the aromatic ring, producing a redistribution of electrons in the aromatic ring.

The assessment of the alkyl substitution effects in terms of an inductive or a hyperconjugative model has been discussed extensively.[5] Among the experimental techniques used to study this problem, electron spin resonance (esr) seems to be one of the best for ion and neutral radicals which involve alkyl substitution effects.[2b,6,7] The main value of esr in these studies is based on the fact that hyperfine splitting from methyl protons will be observed only if the unpaired spin density penetrates in some way into the methyl group and interacts with the protons of this group. Experimentally this effect has been observed several times, for example in 9-methyl- and 9,10-dimethylanthracene cation and anion radicals,[2b,8] and in several dimethylnaphthalene anion radicals.[9]

The observation of hyperfine splittings arising from methyl protons can be explained by a hyperconjugative mechanism, since the combination of the methyl group π-electron orbitals (pseudo π orbitals)[7] with the π orbitals of the aromatic rings allows the delocalization of the unpaired electron (unpaired spin density) onto the methyl groups. This leads directly to hyperfine splittings from the interactions of this unpaired spin density with the methyl protons.

The experimental observation of hyperfine splittings from methyl protons apparently rules out the impor-

(1) To whom all correspondence and requests for reprints should be directed.

(2) (a) G. W. Wheland and L. Pauling, *J. Amer. Chem. Soc.*, **57**, 2086 (1935); (b) J. R. Bolton, A. Carrington, and A. D. McLachlan, *Mol. Phys.*, **5**, 31 (1962).

(3) (a) R. S. Mulliken, *J. Chem. Phys.*, **7**, 339 (1939); (b) R. S. Mulliken, C. A. Rieke, and W. G. Brown, *J. Amer. Chem. Soc.*, **63**, 41 (1941).

(4) C. A. Coulson and V. A. Crawford, *J. Chem. Soc.*, 2052 (1953).

(5) (a) "Conference on Hyperconjugation," Indiana University, June, 1958, in *Tetrahedron*, **5**, 105 (1959); (b) R. S. Mulliken, *ibid.*, **6**, 68 (1959); (c) M. J. S. Dewar, "Hyperconjugation," The Ronald Press Company, New York, N. Y., 1962.

(6) M. C. R. Symons, *Tetrahedron*, **18**, 333 (1962).

(7) J. P. Colpa and E. de Boer, *Mol. Phys.*, **7**, 333 (1964).

(8) J. A. Brivati, R. Hulme, and M. C. R. Symons, *Proc. Chem. Soc.*, 384 (1961).

(9) F. Gerson, B. Weidmann, and E. Heilbronner, *Helv. Chim. Acta*, **47**, 1951 (1964).

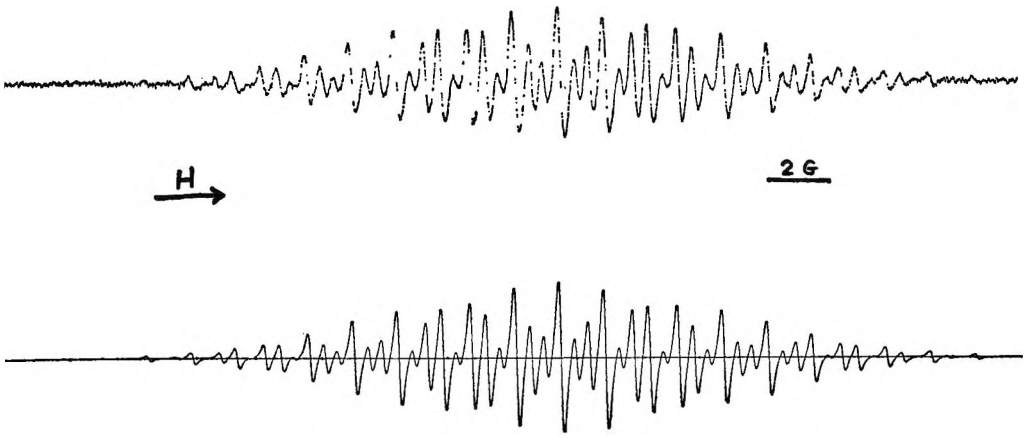


Figure 1. Top: esr spectrum of 2,3-dimethylanthracene anion radical prepared by potassium metal reduction in DME and examined at −80°. Bottom: theoretical simulated esr spectrum using the coupling constants listed in Table I and a line width of 0.160 G.

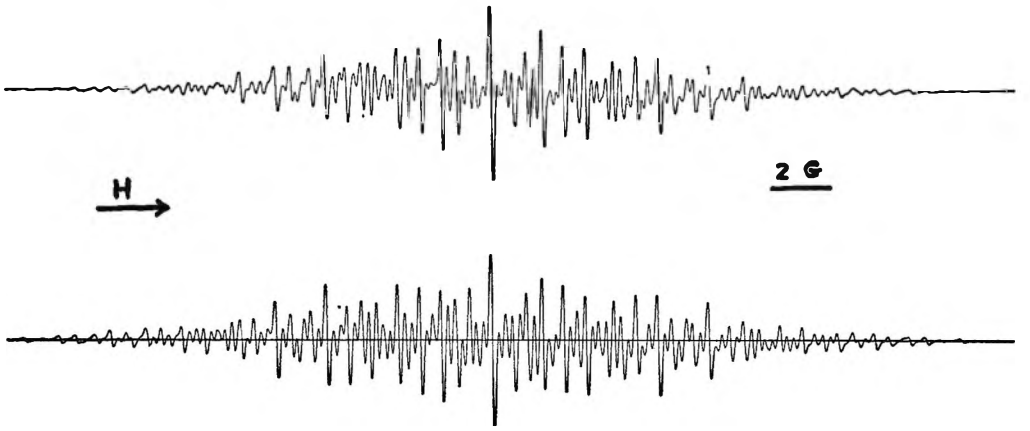


Figure 2. Top: esr spectrum of 2,3-dimethylanthracene cation radical prepared by sulfuric acid oxidation. Bottom: theoretical simulated esr spectrum using the coupling constants given in the Table I and a line width of 0.160 G.

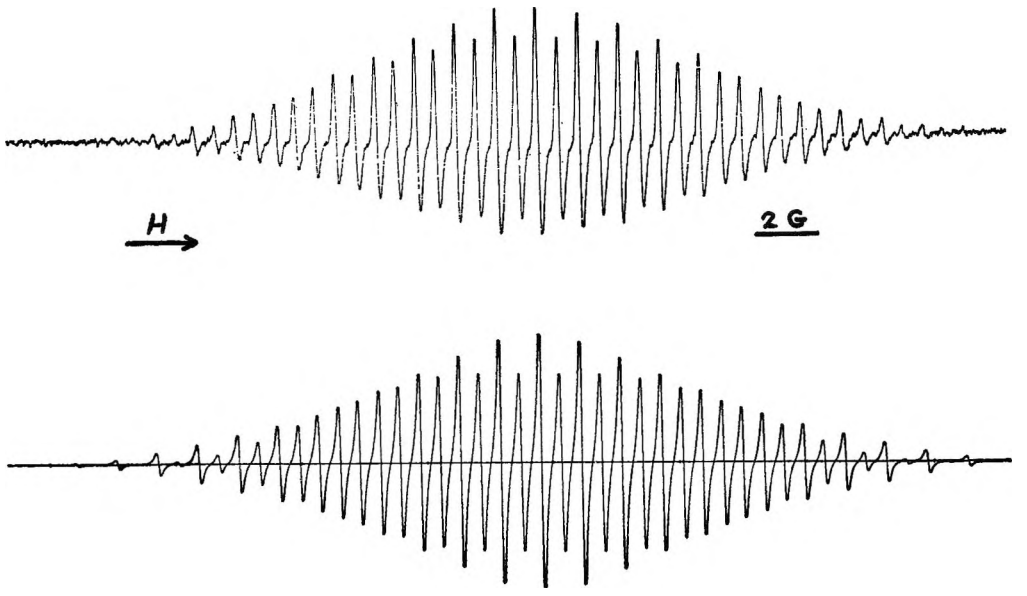


Figure 3. Top: esr spectrum of 2,6-dimethylanthracene anion radical prepared by electrochemical reduction in DMF and examined at −50°. Bottom: theoretical simulated esr spectrum using the coupling constants listed in Table I and a line width of 0.130 G.

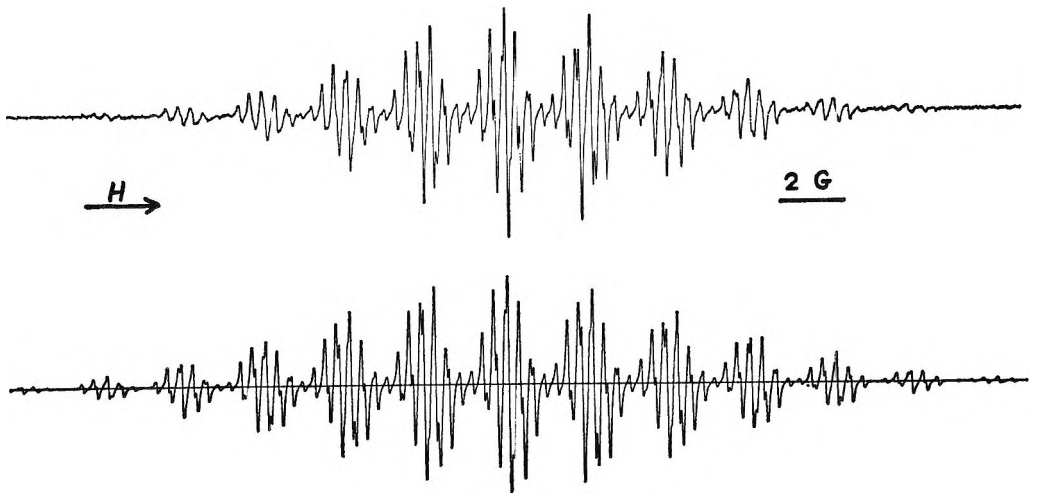
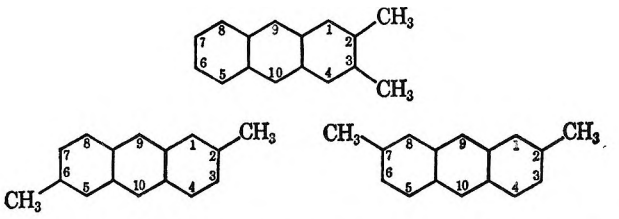


Figure 4: Top: esr spectrum of 2,6-dimethylanthracene cation radical prepared by sulfuric acid oxidation. Bottom: theoretical simulated esr spectrum using the coupling constants given in Table I and a line width of 0.090 G.

tance of an inductive model to explain the methyl substitution effects, since there is no provision in this model for a charge transference between the aromatic ring and the methyl group. However, those hyperfine splittings from the methyl protons could also arise through a spin-exchange polarization mechanism similar to that which produces proton hyperfine splittings in aromatic ion radicals, which arise by spin-exchange polarization between the unpaired π electron and the σ electrons in the C–H bond.[10,11] In the case of methyl proton hyperfine splittings Colpa and de Boer[7] suggested that "spin polarization merely rearranges the spins in the σ orbitals of the aliphatic C–C and C–H bonds, without a net transfer of spin into these orbitals, spin density now arises through correlation effects between the unpaired electron and the paired electron in the σ bonds." However, if the methyl proton coupling constants arise only from a spin-exchange polarization mechanism, one would expect these coupling constants to be very similar in the cation and anion radicals of a given alternant hydrocarbon. This is because, in the case of a spin polarization mechanism, the hyperfine splittings arising from the methyl protons should be proportional to the unpaired spin density in the substituted ring carbon. Molecular orbital calculations show that the spin densities in the substituted ring carbons in cations and anions are very similar. Experimentally, Bolton, *et al.*,[2b] and Colpa and de Boer[7] have shown that the methyl (and also methylene) proton coupling constants are nearly twice as large for the cation radicals as the corresponding constants for the anion radicals (for example, 8.00 and 3.88 G in 9,10-dimethylanthracene, 7.79 and 4.27 G in 9-methylanthracene, and 12.80 and 6.58 G in pyracene cation and anion radicals, respectively). Hence the experimental facts cannot be explained exclusively by spin-exchange polarization, and it is also necessary to consider an alternate mechanism, *e.g.*, hyperconjugation, to account for them. Indeed, the hyperconjugative model can predict correctly that the methyl (or methylene) proton coupling constants in the cation radical will be nearly twice as large as in the anion radicals of these aromatic hydrocarbons, and the contribution of spin polarization to the methyl or methylene splitting is very small, probably no more than a few per cent of the total observed hyperfine splittings.[7,12]

The objectives of the present work were: (1) to examine the esr spectra of the 2,3, 2,6-, and 2,7-dimethylanthracene (DMA) cation and anion radicals



(2) to discuss the different models used in the molecular orbital calculations of methyl-sbustituted aromatic hydrocarbons and to correlate the experimental coupling constants arising from the interaction of the unpaired electron with both the ring protons and the methyl protons; (3) to correlate polarographic reduction half-wave potentials of methyl-substituted anthracenes and naphthalenes with molecular orbital theory to test the different models considered in these calculations.

Results

Preparation of Radicals. Anion radicals were prepared either by exhaustive controlled-potential electrolysis in an external cell at a mercury pool electrode

(10) (a) H. M. McConnell, *J. Chem. Phys.*, **24**, 632, 764 (1956); (b) H. M. McConnell and H. H. Dearman, *ibid.*, **28**, 51 (1958); (c) H. M. McConnell and D. B. Chesnut, *ibid.*, **28**, 107 (1958).

(11) (a) S. I. Weissman, *ibid.*, **25**, 890 (1956); (b) H. S. Jarret, *ibid.*, **25**, 1289 (1956).

(12) D. H. Levy, *Mol. Phys.*, **10**, 233 (1966).

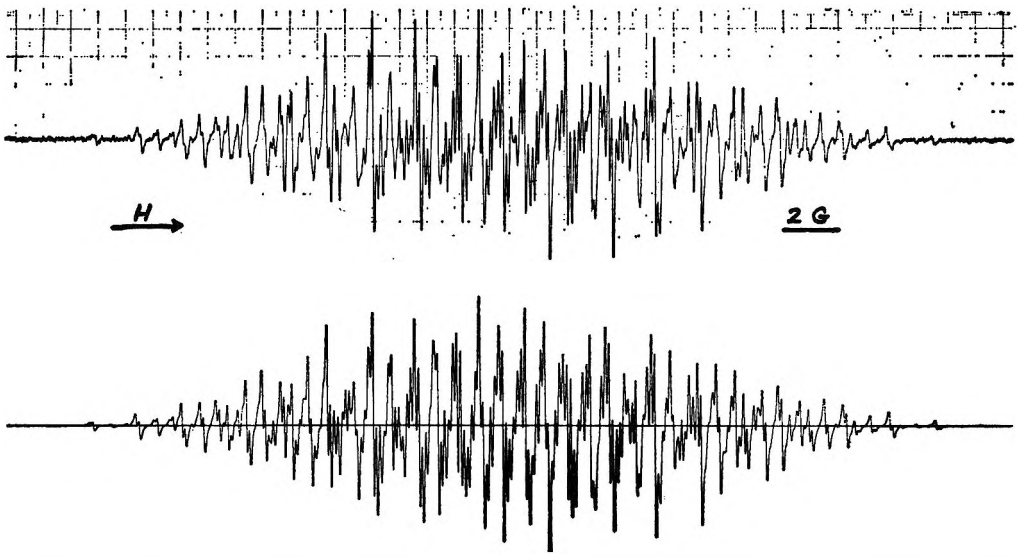


Figure 5. Top: esr spectrum of 2,7-dimethylanthracene anion radical prepared by potassium metal reduction in DME and examined at −80°. Bottom: theoretical simulated esr spectrum using the coupling constants listed in Table I and a line width of 0.096 G.

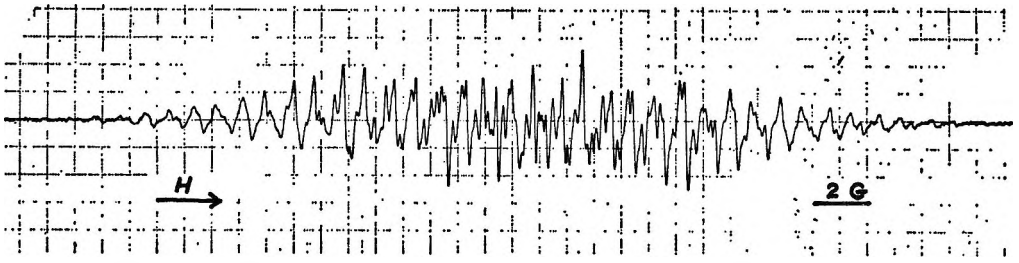


Figure 6. Esr spectrum of 2,7-dimethylanthracene cation radical prepared by sulfuric acid oxidation.

in dimethylformamide (DMF) solutions containing 0.1 *M* tetra-*n*-butylammonium iodide (TBAI) as supporting electrolyte and concentrations of the hydrocarbons of 2 to 6 × 10^{-4} *M* or by potassium metal reduction in dimethoxyethane (DME). Cation radicals were obtained by dissolving a few milligrams of the hydrocarbon in concentrated sulfuric acid at room temperature. Hydrocarbon concentrations of 0.001 to 0.02 *M* were employed. Details are given in the Experimental Section.

The spectra of the anion radicals prepared by electrolytic reduction in DMF and potassium metal reduction in DME were vitually identical. Typical spectra for 2,3-DMA, 2,6-DMA, and 2,7-DMA anion and cation radicals are shown in Figures 1 through 6.

Assignment of the Esr Spectra. The coupling constants for the radicals were assigned by comparing the experimental spectra with those simulated by a computer. The values of the assigned coupling constants are given in Table I. The computer-simulated spectra based on the coupling constants, assuming a Lorentzian line shape, are shown in Figures 1 through 5. Linewidth variations and lack of good resolution in the experimental spectrum of 2,7-DMA cation radical prevented a complete assignment of coupling constants. The approximate values given in Table I were obtained by inspection of an esr spectrum produced by overmodulation.

Discussion

Molecular Orbital Treatment of Methyl-Substituted Aromatic Hydrocarbons. To account for the effects produced by a methyl group substitution in an aromatic hydrocarbon, three models are commonly used in molecular orbital theory: (1) the inductive model,[1] (2) the heteroatom model,[13] and (3) the hyperconjugation model.[3]

Inductive Model. The substitution of a methyl group for a hydrogen atom in an aromatic hydrocarbon produces a change in the magnitude of the coulomb integral of the substituted aromatic carbon due to the electron-donating inductive effect of the methyl group. This inductive effect is treated in Hückel molecular orbital (HMO) theory[14] by assigning a small negative value to the coulomb parameter h_r for the carbon atom r of the π system to which the methyl group has been attached. It has been found that suitable values for

(13) F. A. Matsen, *J. Amer. Chem. Soc.*, 72, 5243 (1950).
(14) E. Hückel, *Z. Physik*, 70, 204 (1931).

Table I: Experimental Coupling Constants of Esr Spectra of 2,3-, 2,6-, and 3,7-Dimethylanthracene Cation and Anion Radicals

	Ring position									
	1	2	3	4	5	6	7	8	9	10
2,3-DMA$^+$	3.60	1.95[a]	1.95[a]	3.60	2.76	1.35	1.35	2.76	6.38	6.38
2,3-DMA$^-$	2.37	1.46[a]	1.46[a]	2.37	2.87	1.46	1.46	2.87	5.30	5.30
2,6-DMA$^+$	3.18	2.76[a]	0.56	3.18	3.18	2.76[a]	0.56	3.18	6.33	6.33
2,6-DMA$^-$	2.67	1.33[a]	1.33	3.32	2.67	1.33[a]	1.33	3.32	5.25	5.25
2,7-DMA$^+$	2.7	2.7[a]	0.9	2.7	2.7	0.9	2.7[a]	2.7	6.3	5.5
2,7-DMA$^-$	2.40	1.72[a]	1.60	3.00	3.00	1.60	1.72[a]	2.40	4.83	5.66

[a] Denotes a methyl proton hyperfine splitting.

h_r range from -0.3 to -0.5.[15] In this work the coulomb integral parameter, h_r, was given a value of -0.3.[2b]

Heteroatom Model. In this model, the methyl group is regarded as a pseudo-heteroatom, m, which contributes a pair of electrons to the π system. Therefore, two parameters have to be considered: (1) a resonance integral parameter, k_{rm}, for the evaluation of the resonance integral, β_{rm}, corresponding to the bond between the carbon of the pseudo-heteroatom (methyl group), m, and the substituted carbon atom of the π system, r, and (2) a coulomb integral parameter, h_m, to calculate the coulomb integral, α_m, of the pseudo-heteroatom, m. Parameter values covering the ranges 1.4–3.3 and 0.5–0.8 have been used for h_m and k_{rm}, respectively. In this work, the resonance integral parameter, k_{rm}, was given a value of 0.5, and the coulomb integral parameter, h_m, was given a value of 1.5.[2b]

Hyperconjugation Model. In this model, the methyl group is treated as a modified vinyl group, C′–C–H_3, where C′ is the substituted carbon atom belonging to the original π system, C corresponds to the carbon atom of the methyl group, and H_3 is the pseudo-atom corresponding to a group of three hydrogens. In this model, there are several parameters to consider: the coulomb integral parameters, $h_{C'}$, h_C, and h_{H_3}, and the resonance integral parameters, $k_{C'C}$ and k_{CH_3}. Mulliken, *et al.*,[3] in their original calculations using this model, assumed $h_{C'}$, h_C, and h_{H_3} were zero, and $k_{C'C} = 0.8$ and $k_{CH_3} = 5$. Coulson and Crawford[4] modified these original parameters based on the following arguments. (1) The *ortho–para* directing property of the methyl substituent in electrophilic reactions implies that a π-electron migration from the methyl group into the aromatic hydrocarbon must be involved. To account for this effect, the coulomb integral parameter for the pseudo-atom, h_{H_3}, was given a value of -0.5, making it more electropositive than the ring carbon atom, C′. The electropositive nature of H_3 was also assumed to be shared with the adjacent carbon atom, C, whose coulomb integral parameter was then given a value of -0.1. (2) The resonance integrals were assumed to vary with distance and be proportional to the overlap integrals; $k_{C'C} = 0.7$ and $k_{CH_3} = 2.5$ were used. Coulson and Crawford's parameters were chosen in order to reproduce the dipole moment of toluene. This set of parameters with small variations has been employed by the majority of researchers in this field. In this work Levy's values of the coulombs integral parameters, $h_{C'} = 0$, $h_C = -0.1$, and $h_{H_3} = -0.5$, and the resonance integral parameters, $k_{C'C} = 0.76$ and $k_{CH3} = 2.00$, were employed.

It has been suggested from electronic spectra studies[16] and from the interpretation of esr spectra of toluene and other anions[17] that it is necessary to introduce a small inductive effect together with hyperconjugation. In this work, we have also considered this possibility by giving to the coulomb integral parameter, $h_{C'}$, a value of -0.1.

Calculated Coupling Constants. Ring Protons. Values of the spin densities (ρ) were calculated using the different models; the results are listed in Table II. The calculated ρ values were compared with those derived from the experimental coupling constants (a_H) using the following relations: (1) the McConnell relation:[10] $a_H = Q\rho$, with $Q = 32$ for cations, and $Q = 28$ for anions; (2) the Colpa–Bolton relation:[18] $a_H = (Q\rho \pm K\rho^2)$, where $Q = 27$ and $K = 12$; (3) the Giacometti–Nordio–Pavan relation:[19] $a_H = Q_1\rho \pm Q_2 \mid \Sigma_j c_r c_j \mid$, where $Q_1 = 31.5$ and $Q_2 = 7.0$. Values of the ring coupling constants for the different models and the above relations are given in Tables III to V. Since there are no major differences among the magnitudes of the spin densities of a specific ring position calculated using the different models (Table II), when the same relation (*e.g.* McConnell) is used for the calculation of the theoretical coupling constants of a specific ring position, no major differences are found

(15) A. Streitweiser, Jr., "Molecular Orbital Theory for Organic Chemists," John Wiley and Sons, Inc., New York, N. Y., 1961.

(16) A. Denis and A Pullman, *Theoret. Chim. Acta*, 7, 110 (1967).

(17) (a) J. P. Malrieu, A. Pullman, and M. Rossi, *ibid.*, 3, 261 (1965); (b) D. Lazdins and M. Karplus, *J. Amer. Chem. Soc.*, 87, 920 (1965); (c) E. de Boer and J. P. Colpa, *J. Phys. Chem.*, 71, 21 (1967).

(18) (a) J. P. Colpa and J. R. Bolton, *Mol. Phys.*, 6, 273 (1963); (b) J. R. Bolton, *J. Chem. Phys.*, 43, 309 (1965).

(19) G. Giacometti, P. L. Nordio, and M. V. Pavan, *Theoret. Chim. Acta*, 1, 404 (1963).

Table II: Hückel Spin Densities of the Ring Carbon Atoms of Dimethylanthracene Cation and Anion Radicals Calculated Using Several Models

Carbon atom	Model: Inductive	Hetero-atom	Hyperconjugation: With inductive effect	Hyperconjugation: Without inductive effect
	2,3-Dimethylanthracene			
	Cation radical			
1	0.1162	0.1098	0.1108	0.1046
5	0.0897	0.0897	0.0892	0.0913
6	0.0466	0.0462	0.0460	0.0465
9	0.1918	0.1890	0.1887	01.890
	Anion radical			
1	0.0741	0.0866	0.0874	0.0945
5	0.1054	0.0995	0.0982	0.0957
6	0.0504	0.0489	0.0484	0.0478
9	0.1938	0.1924	0.1909	0.1908
	2,6-Dimethylanthracene			
	Cation radical			
1	0.1137	0.1069	0.1077	0.1023
3	0.0304	0.0339	0.0328	0.0385
4	0.0931	0.0922	0.0917	0.0931
9	0.1907	0.1875	0.1869	0.1881
	Anion radical			
1	0.0822	0.0895	0.0899	0.0947
3	0.0669	0.0561	0.0545	0.0484
4	0.0982	0.0970	0.0962	0.0955
9	0.1931	0.1924	0.1911	0.1908
	2,7-Dimethylanthracene			
	Cation radical			
1	0.1195	0.1115	0.1127	0.1053
3	0.0376	0.0394	0.0387	0.0420
4	0.0877	0.0883	0.0876	0.0905
9	0.2113	0.2028	0.2036	0.1979
10	0.1726	0.1743	0.1728	0.1794
	Anion radical			
1	0.0761	0.0869	0.0876	0.0945
3	0.0641	0.0530	0.0519	0.0481
4	0.1045	0.0996	0.0984	0.0957
9	0.1755	0.1844	0.1842	0.1900
10	0.2127	0.2007	0.1980	0.1915

from one model to another. Hence a study of only the ring proton coupling constants is not useful for deciding the magnitude of hyperconjugation or inductive effects in these dimethylanthracenes. This argument can be extended to other methyl-substituted anthracenes using perturbation theory.[2]

Calculated Coupling Constants. Methyl Protons. The experimental methyl proton coupling constants are listed in Table VI. The methyl proton coupling constants of 9-methyl- and 9,10-dimethylanthracenes are also listed in Table VI. Note that the methyl proton coupling constants for the cation radicals are larger than the corresponding anion radicals, and the ratio of cation to anion coupling constants is, in most cases, close to a factor of 2. The experimental findings suggest that the large differences in the cation and anion coupling constants are due to a predominantly hyperconjugative mechanism. Therefore, since an inductive model in which the methyl proton hyperfine splittings arise exclusively through a spin-exchange polarization mechanism could not account for these differences in methyl proton coupling constants, the hyperconjugation models were tested. Bolton, *et al.*,[2] observed that the

Table III: Experimental and Theoretical Ring Proton Coupling Constants in 2,3-Dimethylanthracene Cation and Anion Radicals Assuming Different Models and Relations

Carbon atom	$\lvert a_H \rvert$, G: Inductive	Hetero-atom	Hyperconjugation: With inductive effect	Hyperconjugation: Without inductive effect	Exptl
	McConnell Relation				
	Cation radical				
1	3.72	3.51	3.55	3.35	3.60[a]
5	2.87	2.87	2.85	2.92	2.76[a]
6	1.49	1.48	1.47	1.49	1.35
9	6.14	6.05	6.04	6.05	6.38
	Anion radical				
1	2.07	2.43	2.45	2.65	2.37[a]
5	2.95	2.78	2.75	2.73	2.87[a]
6	1.41	1.37	1.35	1.40	1.46
9	5.43	5.39	5.35	5.67	5.30
	Giacometti–Nordio–Pavan Relation				
	Cation radical				
1	3.98	3.76	3.80	3.59	3.60[a]
5	3.07	3.07	3.06	3.13	2.76
6	1.59	1.58	1.58	1.60	1.35
9	6.56	6.47	6.46	6.48	6.38
	Anion radical				
1	2.10	2.47	2.49	2.70	2.37[a]
5	3.32	2.84	2.80	2.74	2.87[a]
6	1.43	1.39	1.38	1.37	1.46
9	5.50	5.49	5.46	5.45	5.30
	Colpa–Bolton Relation				
	Cation radical				
1	3.30	3.11	3.14	2.96	3.60[a]
5	2.52	2.52	2.51	2.56	2.76[a]
6	1.28	1.27	1.30	1.28	1.35
9	5.62	5.53	5.52	5.53	6.38
	Anion radical				
1	1.93	2.25	2.27	2.45	2.37[a]
5	2.71	2.57	2.54	2.47	2.87[a]
6	1.33	1.29	1.28	1.26	1.46
9	4.78	4.75	4.72	4.71	5.30

[a] Assigned to this position on the basis of MO theory.

heteroatom model could predict fairly well the ratios of the methyl proton coupling constants of the cation and anion radicals of 9-methyl- and 9,10-dimethylanthracenes. The following theoretical and experimental ratios, respectively, were obtained:[2] *9-methylanthracene*, 3.638 and 1.82, and *9,10-dimethylanthracene*, 3.095 and 2.06. In the present work the following theoretical and experimental ratios were found: *2,3-dimethylanthracene*, 2.471 and 1.34; *2,6-dimethylanthracene*, 3.657 and 2.08; and *2,7-dimethylanthracene*, 3.078 and 1.57. Note that the experimental ratio for 2,3-dimethylanthracene is lower than for the other members of the group, probably because the steric interaction between the methyl groups in positions 2 and 3 reduces to some extent the conjugation between the methyl groups and the aromatic ring. However, although this model predicts the methyl proton coupling constant ratios in the right direction, there is a serious discrepancy between the observed and predicted split-

Table IV: Experimental and Theoretical Ring Proton Coupling Constants in 2,6-Dimethylanthracene Cation and Anion Radicals Assuming Different Models and Relations

	$\lvert a_H \rvert$, G				
			Hyperconjugation		
Carbon atom	Inductive	Heteroatom	With inductive effect	Without inductive effect	Expt[a]
	McConnell Relation				
	Cation radical				
1	3.64	3.42	3.45	3.27	3.18
3	0.97	1.08	1.05	1.23	0.54
4	2.98	2.95	2.93	2.98	3.18
9	6.10	6.00	5.98	6.02	6.33
	Anion radical				
1	2.30	2.51	2.52	2.65	2.67[a]
3	1.87	1.57	1.53	1.39	1.33
4	2.75	2.72	2.69	2.73	3.32[a]
9	5.41	5.39	5.35	5.46	5.25
	Giacometti–Nordio–Pavan Relation				
	Cation radical				
1	3.89	3.66	3.69	3.51	3.18
3	1.04	1.16	1.12	1.32	0.54
4	3.18	3.16	3.14	3.19	3.18
9	6.52	6.42	6.40	6.45	6.33
	Anion radical				
1	2.34	2.55	2.56	2.71	2.67[a]
3	1.90	1.60	1.57	1.39	1.33
4	2.79	2.77	2.75	2.73	3.32[a]
9	5.49	5.49	5.45	5.46	5.25
	Colpa–Bolton Relation				
	Cation radical				
1	3.22	3.02	3.05	2.89	3.18
3	0.83	0.93	0.90	1.05	0.54
4	2.62	2.59	2.58	2.62	3.18
9	5.58	5.48	5.47	5.50	6.33
	Anion radical				
1	2.14	2.32	2.33	2.45	2.67[a]
3	1.75	1.48	1.44	1.28	1.33
4	2.54	2.51	2.49	2.47	3.32[a]
9	5.49	4.75	4.72	4.72	5.25

[a] Assigned to this position on the basis of MO theory.

Table V: Experimental and Theoretical Ring Proton Coupling Constants in 2,7-Dimethylanthracene Cation and Anion Radicals Assuming Different Models and Relations

	$\lvert a_H \rvert$, G				
			Hyperconjugation		
Carbon atom	Inductive	Heteroatom	With inductive effect	Without inductive effect	Expt[a]
	McConnell Relation				
	Cation radical				
1	3.82	3.57	3.61	3.37	2.7
3	1.20	1.26	1.24	1.34	0.9
4	2.81	2.83	2.80	2.90	2.7
9	6.76	6.49	6.52	6.33	6.3[a]
10	5.52	5.58	5.53	5.74	5.5[a]
	Anion radical				
1	2.13	2.43	2.45	2.65	2.40[a]
3	1.68	1.48	1.45	1.35	1.60
4	2.93	2.79	2.76	2.68	3.00[a]
9	4.91	5.16	5.16	5.32	4.83[a]
10	5.96	5.62	5.55	5.36	5.66[a]
	Giavometti–Nordio–Pavan Relation				
	Cation radical				
1	4.09	3.82	3.86	3.61	2.7
3	1.29	1.35	1.32	1.44	0.9
4	3.00	3.02	3.00	3.10	2.7
9	7.23	6.95	6.97	6.79	6.3
10	5.90	5.97	5.92	6.16	5.5
	Anion radical				
1	2.16	2.48	2.45	2.70	2.40[a]
3	1.71	1.51	1.48	1.38	1.60
4	2.97	2.84	2.81	2.74	3.00[a]
9	4.99	5.26	5.26	5.43	4.83[a]
10	6.04	5.72	5.65	5.48	5.66[a]
	Colpa–Bolton Relation				
	Cation radical				
1	3.40	3.16	3.20	2.98	2.7
3	1.03	1.08	1.05	1.16	0.9
4	2.46	2.48	2.46	2.54	2.7
9	6.24	5.97	6.00	5.81	6.3[a]
10	5.02	5.07	5.02	5.23	5.5[a]
	Anion radical				
1	1.99	2.26	2.27	2.44	2.40[a]
3	1.58	1.40	1.37	1.27	1.60
4	2.69	2.57	2.54	2.47	3.00[a]
9	4.37	4.57	4.57	4.70	4.83[a]
10	5.20	4.94	4.88	4.73	5.66[a]

[a] Assigned to this position on the basis of MO theory.

tings themselves, as noted by Colpa and de Boer[7]. They found, for example, that the heteroatom model for the ions of 9,10-DMA gave values for the methyl coupling constants that were roughly too low by a factor of 4. This same disparity was found for the DMA ion radicals in this study.

Levy[12] derived the following general formula for the calculation of methyl proton hyperfine splittings to be used with Mulliken's hyperconjugation model[3] with or without overlap

$$a_{\text{methyl}} = 219.8c_H^2 + 13.17c_C^2 + 107.0c_Hc_C + 3.997c_Hc_{C'} + 0.973c_{CC'} - 3.09c_{C'}^2$$

where c_H is the coefficient of the pseudo orbital (H_3), c_C is the coefficient of the methyl carbon (C) in the modified vinyl group, and $c_{C'}$ is the coefficient of the carbon atom (C′) of the original π system to which the methyl group is attached. In addition to the hyperconjugation contribution, a small spin polarization contribution is considered in this formula, given by a term $3.09c_{C'}^2$. Levy used this formula only for anion radicals, but we have extended it to cation radicals with good success; the results are listed in Table VI. Coefficients were calculated by the HMO method without overlap using Mulliken's hyperconjugation model with and without a small inductive effect and the parameters listed previously. We have also carried out calculations of methyl proton coupling constants of several dimethylnaphthalene (DMN) anion radicals using Levy's formula. These results are listed in Table VII. The agreement found between the experimental and theoretically calculated coupling constants was excellent in most of the cases.

Table VI: Experimental and Theoretical Methyl Proton Coupling Constants of Methylanthracene Cation and Anion Radicals. The Theoretical Methyl Proton Coupling Constants Have Been Calculated by Using Levy's Formula and the Hyperconjugation Model (with and without a Small Inductive Effect)

Hydrocarbon	$\lvert a_H \rvert$, G: Levy's formula without inductive effect	Levy's formula with inductive effect	Exptl
	Cation radical		
9-Methylanthracene	7.85	7.46	7.79[a]
9,10-Dimethylanthracene	7.97	7.85	8.00[a]
2,3-Dimethylanthracene	1.95	1.83	1.95
2,6-Dimethylanthracene	2.30	2.39	2.76
2,7-Dimethylanthracene	2.14	2.12	2.7
	Anion radical		
9-Methanthracene	5.16	5.25	4.27[a]
9,10-Dimethylanthracene	4.99	4.78	3.88[a]
2,3-Dimethylanthracene	1.31	1.38	1.46
2,6-Dimethylanthracene	1.30	1.22	1.33
2,7-Dimethylanthracene	1.30	1.29	1.72

[a] Taken from ref 2b.

Table VII: Experimental and Theoretical Methyl Proton Coupling Constants of Dimethylnaphthalene Anion Radicals. The Theoretical Methyl Proton Coupling Constants Have Been Calculated by Using Levy's Formula and the Hyperconjugation Model (with or without a Small Inductive Effect)

Hydrocarbon	$\lvert a_H \rvert$, G: Levy's formula without inductive effect	Levy's formula with inductive effect	Exptl[a]
1,4-Dimethylnaphthalene	4.71	4.43	3.26
1,5-Dimethylnaphthalene	4.65	4.76	4.41
1,8-Dimethylnaphthalene	4.63	4.82	4.61
2,3-Dimethylnaphthalene	1.82	1.94	1.69
2,6-Dimethylnaphthalene	1.89	1.63	1.22
2,7-Dimethylnaphthalene	1.85	1.81	2.16

[a] From ref 9.

Polarographic Correlations. Esr–HMO correlations only serve to compare the experimental coupling constants with the theoretical spin densities, *i.e.*, the square of the various elements of the eigenvector associated with the π-MO where the unpaired electron moves. It is also of interest to attempt a correlation of polarographic reduction half-wave potentials with the eigenvalue of the lowest available antibonding π-MO. In this way both the eigenvector and the eigenvalue of a model can be tested.[20]

The usual correlation equation is given by[15]

$$E_{1/2} = -bm_{m+1} + c$$

where $E_{1/2}$ is the polarographic reduction half-wave potential, m_{m+1} is the energy of the lowest vacant π-MO in units of β_{CC}, and b, the slope of the correlation line, is regarded as the effective value of β for the system under study. In the present work, $E_{1/2}$ for 12 methylanthracenes and anthracene itself and 16 methylnapthalenes and naphthalene itself, measured in 75% aqueous dioxane by Klemm, *et al.*,[21] have been correlated. The m_{m+1} energies were calculated from HMO theory using, as previously, the inductive, the heteroatom, and the hyperconjugation, with and without inductive effect, models. The $E_{1/2}$ and m_{m+1} values are listed in Table VIII. The following correlation equations were obtained: *inductive model*, $E_{1/2} = (2.085 \pm 0.125)m_{m+1} - 1.025 \pm 0.076$; *heteroatom model*, $E_{1/2} = (2.387 \pm 0.057)m_{m+1} - 0.941 \pm 0.032$; *hyperconjuga-*

(20) A. J. Bard, K. S. V. Santhanam, J. T. Maloy, J. Phelps, and L. O. Wheeler, *Discussions Faraday Soc.*, 45, 167 (1968).

(21) (a) L. H. Klemm, A. J. Kohlik, and K. B. Desai, *J. Org. Chem.*, 28, 625 (1963); (b) L. H. Klemm and A. J. Kohlik, *ibid.*, 28, 2044 (1963).

Table VIII: Polarographic Reduction Half-Wave Potentials for Methylnaphthalenes and Energies of Lowest Vacant Molecular Orbitals Calculated Using Various Models

Hydrocarbon	$-E_{1/2}$,[a] V *vs.* sce	$-m_{m+1}$ in β_{CC} units: Inductive	Heteroatom	Hyperconjugation: Without inductive effect	Hyperconjugation: With inductive effect
Anthracene	1.925	0.414	0.414	0.414	0.414
1-MA	1.937	0.442	0.427	0.415	0.428
2-MA	1.956	0.428	0.420	0.415	0.419
9-MA	1.940	0.474	0.439	0.417	0.436
2,3-DMA	1.991	0.446	0.427	0.415	0.425
2,6-DMA	1.988	0.441	0.426	0.415	0.425
2,7-DMA	1.991	0.443	0.427	0.415	0.425
9,10-DMA	1.976	0.523	0.462	0.419	0.455
2,3,9-TMA	2.007	0.505	0.452	0.418	0.446
2,6,9-TMA	2.003	0.500	0.451	0.418	0.445
2,3,6,7-TeMA	2.054	0.478	0.440	0.417	0.436
2,3,9,10-TeMA	2.044	0.554	0.475	0.420	0.465
2,3,6,7,9,10-HMA	2.109	0.589	0.487	0.421	0.474
Naphthalene	2.437	0.618	0.618	0.618	0.618
1-MN	2.458	0.671	0.639	0.615	0.633
2 MN	2.460	0.636	0.626	0.617	0.624
1,2-DMN	2.479	0.682	0.645	0.614	0.637
1,3-DMN	2.483	0.690	0.647	0.614	0.638
1,4-DMN	2.471	0.714	0.658	0.612	0.646
1,5-DMN	2.475	0.730	0.660	0.612	0.647
1,6-DMN	2.476	0.692	0.647	0.614	0.638
1,7-DMN	2.469	0.688	0.646	0.614	0.638
1,8-DMN	2.521	0.732	0.661	0.612	0.647
2,3-DMN	2.501	0.664	0.635	0.616	0.530
2,6-DMN	2.476	0.651	0.633	0.616	0.629
2,7-DMN	2.485	0.658	0.634	0.616	0.629
1,3,7-TMN	2.496	0.703	0.654	0.613	0.643
1,4,5-TMN	2.529	0.783	0.681	0.609	0.660
2,3,5-TMN	2.515	0.720	0.656	0.613	0.644
2,3,6-TMN	2.523	0.682	0.642	0.615	0.635

[a] From ref 21.

tion model (without a small inductive effect), $E_{1/2} = (2.494 \pm 0.072)m_{m+1} - 0.055 \pm 0.037$; *hyperconjugation model* (with a small inductive effect, $E_{1/2} = (2.456 \pm 0.051)m_{m+1} - 0.920 \pm 0.028$.

The best least-squares fit (*i.e.*, the smallest standard deviation in the coefficient of m_{m+1}) was obtained with the hyperconjugation model employing a small inductive effect. Note that the hyperconjugation model without a small inductive effect predicts nearly the same energy eigenvalue for each type of molecule considered, even though this model gives a fairly good overall least-squares correlation. These results support the suggestion based on studies of electronic spectra and esr spectra of toluene and other anions, that is the introduction of a small inductive effect together with hyperconjugation produces more satisfactory results.

Conclusions

(1) The methyl proton hyperfine splittings arise in these dimethylanthracenes predominantly from a hyperconjugative mechanism rather than from a spin-exchange polarization mechanism. This effect is more pronounced in cation radicals than in anion radicals.

(2) A hyperconjugation model (with or without a small inductive effect) where the methyl group is treated as a modified vinyl group and using slightly modified Coulson and Crawford parameters and Levy's formula is very satisfactory in accounting for methyl proton hyperfine splittings.

(3) A study of the correlations between the polarographic reduction half-wave potentials of methyl substituted anthracenes and naphthalenes *vs.* the energies of the lowest vacant π-MO's showed that a hyperconjugation model with a small inductive effect correlated very well.

Experimental Section

Electrochemical Experiments. The electrochemical cell and the vacuum line used were essentially the same as reported by Santhanam and Bard.[22] The electro-

(22) K. S. V. Santhanam and A. J. Bard, *J. Amer. Chem. Soc.*, **88**, 2669 (1966).

chemical reduction was carried out in the following way. Mercury, TBAI (0.1 *M*), and stirring bar were introduced into the electrochemical cell. The auxiliary compartment was introduced, and the cell was connected to the vacuum line by means of O-ring ball joint. The cell was evacuated overnight to remove traces of air and water. Evacuation to about 10^{-5} mm was considered satisfactory for performing the electrochemical experiment and the esr examinations. After the evacuation process the stopcocks which connect the main body of the cell with the side arms (3-mm Pyrex tubing) were closed. Then the cell was cooled down at liquid nitrogen temperature and the solvent (DMF) was distilled into it from a storage flask. After the distillation had been completed, the cell was warmed to room temperature without ceasing continuous evacuation. As soon as the room temperature had been reached, the cell was brought to the atmospheric pressure by introducing helium through the vacuum line. A helium blanket was kept over the cell during the entire experiment to prevent air from coming into contact with the solution. The cell prepared in this way was ready for electrochemical measurements. The reference electrode (sce) and the working electrode (hanging mercury drop electrode) were introduced at this moment. A cyclic voltammogram of the background was recorded to check the purity of the solution. Then, the hanging mercury drop electrode was removed and the mercury pool was connected to serve as a working electrode. As soon as this step had been completed a weighed sample was introduced into the cell by means of a small glass tube. When the sample had dissolved in the DMF, new cyclic voltammetric measurements were carried out, and finally controlled potential coulometry was performed. When the coulometry had been completed, the evacuated bulb of one of the stopcocks which was connected with the esr tube was opened to the cell. A few milliliters was pulled into this bulb to be subsequently discarded. This was carried out to get a homogeneous solution between the cell and the stopcock. The 3-mm evacuated side arm was cooled down and the stopcock was opened for a brief time to this tube. After this the 3-mm Pyrex tubing was sealed and cut with a torch. A second sample was usually taken at a different stage of the reduction in order to study the changes in the esr spectra.

Tetra-*n*-butylammonium iodide (TBAI) was obtained from Southwestern Analytical Chemicals (Austin, Texas) and was used without further purification. N,N-Dimethylformamide (DMF) was obtained from Eastman Organic Chemicals. It was purified by storing overnight over anhydrous copper sulfate and then was distilled under vacuum.[22] Helium of 99.995% purity was obtained from the Matheson Co. (La Porte, Texas). It was passed successively through anhydrous magnesium perchlorate, copper turnings heated to 350°, activated charcoal at liquid nitrogen temperature, and finally to the vacuum line. The reference electrode employed was an aqueous saturated calomel electrode (sce) with a fresh 3% agar–1 *M* potassium nitrate salt bridge. The end of the sce which was immersed in the electrolytic solution was closed by a medium porosity sintered glass disk. The auxiliary electrode was a silver wire.

Alkali Metal Reductions. Alkali metal reductions were carried out in an apparatus described by Wheeler, *et al.*;[23] details of the technique have been described.[24] Dimethoxyethane (DME) was obtained from the Ansul Co. It was stored over calcium hydride for 12 hr with continuous stirring and was then refluxed over lithium aluminum hydride for 16 hr. Then it was distilled under nitrogen and stored in the vacuum line.[25]

Potassium metal was obtained from Matheson Coleman and Bell. It was stored under mineral oil and was carefully washed with purified solvent at the time of the experiment.

Compounds. 2,3-, 2,6-, and 2,7-dimethylanthracenes (*ca.* 0.050 g of each one) were donated by Dr. L. H. Klemm (The University of Oregon) and were used as received.

Electron Spin Resonance Spectrometer. A Varian Associates V-4502 spectrometer employing 100 kcps field modulation and a Varian V-153C Klystron (output 300 mW) were used. The field sweep was calibrated by using Fremy salt in one side of a V-4532 dual sample cavity. The high- and low-field coupling constants for the Fremy salt were taken as 13.160 ± 0.008 and 13.101 ± 0.004 G.[26] A Moseley 7100 dual channel recorder was used to record the spectra. A Varian V-4540 variable temperature unit was used for low-temperature studies.

Computer Calculations. The molecular orbital calculations were done on a Control Data Corporation (CDC) 6600 Computer. The theoretical simulated spectra were calculated on the CDC 6600 Computer and plotted on the CDC 160 plotter.

Acknowledgments. The support of this research by the Robert A. Welch Foundation and the National Science Foundation (GP-6688X) is gratefully acknowledged. The esr instrument was purchased with funds provided by the National Science Foundation (Grant No. GP-2090). We extend these acknowledgements to Mr. T. V. Atkinson for helpful discussions and Dr. L. H. Klemm (The University of Oregon) for the samples of 2,3-, 2,6-, and 2,7-dimethylanthracene.

(23) L. O. Wheeler, K. S. V. Santhanam, and A. J. Bard, *J. Phys. Chem.*, 71, 2223 (1967).

(24) (a) D. E. Paul, D. Lipkin, and S. I. Weissman, *J. Amer. Chem. Soc.*, 78, 116 (1956); (b) P. Balk, G. J. Hoijtink, and J. W. H. Schreurs, *Rec. Trav. Chim.*, 76, 813 (1957).

(25) D. F. Scriver, D. E. Smith, and P. Smith, *J. Amer. Chem. Soc.*, 86, 5153 (1964).

(26) J. A. Valenzuela and A. J. Bard, *J. Phys. Chem.*, 72, 286 (1968).

High-Temperature Vacuum Ultraviolet Photolysis of *n*-Butane

by James R. McNesby and Rudolph V. Kelley

Institute for Materials Research, National Bureau of Standards, Washington, D. C. 20234 *(Received May 22, 1968)*

Mixtures of *n*-butane and *n*-butane-d_{10} have been photolyzed at 1470 Å over the temperature range 308–671°K. The mechanism of methane formation is shown to be largely intramolecular at 308°K and becomes increasingly dominated by a chain reaction carried by methyl radicals as the temperature is raised. At 671°K, the mechanism of methane formation is almost entirely a free-radical process. Estimates have been made of average chain lengths as a function of temperature and from this, the chain length in the pyrolysis of *n*-butane is calculated to be about 2000. It is suggested that none of the methods of detecting molecular elimination of methane in the pyrolysis of butane has been sufficiently sensitive. Molecular elimination of methane in pyrolysis may be at least as important as methyl radical formation and still escape detection.

Among the products of the photolysis of mixtures of *n*-butane and *n*-butane-d_{10} in the presence of NO at 1470 A is methane of which more than 80% is $CH_4 + CD_4$. Nevertheless, appreciable amounts of CH_3D and CD_3H are present. Their presence is even more apparent in the absence of NO.[1] These results suggest that methane is formed in two ways, molecular elimination and abstraction of hydrogen by methyl radicals. Moreover, in the presence of NO where the molecular elimination of methane is dominant,[2] photolysis of $CH_3CD_2CD_2CH_3$ gives primarily CH_4 and CH_3D. The photolysis of $CD_3CD_2CH_2CH_3$ at 1236 Å gives mainly CH_4 and CD_4.[2] The dominant mechanism for molecular elimination of methane is, therefore

$$CH_3CH_2CH_2CH_3 \longrightarrow CH_4 + CHCH_2CH_3^* \quad (1)$$

The excited propylidene rearranges rapidly to excited propylene which may be stabilized by collision or decompose further as

$$CHCH_2CH_3^* \longrightarrow CH_2{=}CHCH_3^* \quad (2)$$

Similarly, *n*-butane-d_{10} photolysis produces CD_4 as in

$$CD_3CD_2CD_2CD_3 \longrightarrow CD_4 + CDCD_2CD_3^* \quad (3)$$

Methyl radicals are also formed in the primary process

$$n\text{-}C_4H_{10} \longrightarrow CH_3 + n\text{-}C_3H_7 \quad (4)$$

$$n\text{-}C_4D_{10} \longrightarrow CD_3 + n\text{-}C_3D_7 \quad (5)$$

The methyl radicals may be expected to abstract hydrogen from the parent increasingly as the temperature rises as shown by

$$CH_3 + n\text{-}C_4H_{10} \longrightarrow CH_4 + C_4H_9 \quad (6)$$

$$CH_3 + n\text{-}C_4D_{10} \longrightarrow CH_3D + C_4D_9 \quad (7)$$

$$CD_3 + n\text{-}C_4H_{10} \longrightarrow CD_3H + C_4H_9 \quad (8)$$

$$CD_3 + n\text{-}C_4D_{10} \longrightarrow CD_4 + C_4D_9 \quad (9)$$

At low temperatures most methyl radicals disappear by association, *e.g.*

$$2CH_3 + M \longrightarrow C_2H_6 + M \quad (10)$$

and the methanes are dominated by molecular elimination reactions 1 and 3. As the temperature is raised and abstraction reactions 6–9 assume greater importance, additional methyls are formed by decomposition of the *s*-butyl radical which is formed preferentially over the *n*-butyl radicals.[3] Thus, all of the elements of a chain reaction are present. This presentation is considerably oversimplified because (a) propyl radicals formed in the primary process decompose to give methyl radicals, (b) H atoms and ethyl radicals formed in primary photochemical processes abstract hydrogen to produce *s*-butyl radicals, and (c) those abstractions which occur at the primary CH or CD bonds produce *n*-butyl radicals which decompose thermally to give ethyl radicals which in turn can carry a chain.

In spite of all of these complexities it is of interest to understand the nature of the competition between the modes of methane formation, molecular and free radical, and to obtain an estimate of the length of the chains in the photolysis of *n*-butane as a function of temperature.

Two studies of chain reactions in hydrocarbon photolysis have already been reported for ethane and propane.[4,5] The propagation of the chain reactions in these cases involved the necessity of abstracting the primary hydrogen atom. It was felt that the chains might be propagated at a somewhat lower temperature in the *n*-butane photolysis (or be longer at the same temperature) since the propagation step involves the abstraction of the more labile secondary hydrogen atom.

(1) H. Okabe and D. A. Becker, *J. Chem. Phys.*, **39**, 2549 (1963).
(2) R. P. Borkowski and P. J. Ausloos, *ibid.*, **39**, 818 (1963).
(3) J. R. McNesby and A. S. Gordon, *J. Am. Chem. Soc.*, **78**, 3570 (1956).
(4) R. F. Hampson, Jr., and J. R. McNesby, *J. Chem. Phys.*, **42**, 2200 (1965).
(5) A. H. Laufer and J. R. McNesby, *J. Phys. Chem.*, **70**, 4094 (1966).

Table I: Relative Amounts of Products of Photolysis of Mixture of *n*-Butane and *n*-Butane-d_{10}[a]

Temp, °C	CH_4	CH_3D	CH_2D_2	CD_3H	CD_4	H_2	HD	D_2
35	100.0	3.27	0.64	11.10	5.75	1015	62.7	126.0
70	...	...	...	11.85	100.0	283	93.0	1415.0
75	100.0	3.64	0.0	11.71	3.70	573	31.3	70.5
125	100.0	4.49	0.0	13.70	3.06	340	22.7	39.6
157	100.0	4.03	0.74	14.38	3.69	421.7	27.8	42.1
189	100.0	4.25	0.0	13.22	3.72	...	...	...
206	100.0	4.32	0.32	14.56	3.35	406.6	33.8	39.3
239	100.0	4.32	0.33	14.33	3.11	365	30.9	35.0
272	100.0	5.84	0.0	15.41	3.00	182.3	27.4	27.3
314	100.0	5.25	0.0	14.68	1.87	...	...	...
349	100.0	5.85	1.08	12.66	1.40	123.8	6.3	6.1
397	100.0	8.20	0.0	10.94	1.24	48.3	4.5	3.2
398	100.0	8.30	0.0	9.83	1.18	58.1	3.5	2.5

[a] $[n\text{-}C_4H_{10}]/[n\text{-}C_4D_{10}] = 3.70$.

Experimental Method

The details of the apparatus have already been described[4,5] and involve the use of a lithium fluoride–silver chloride–silver–Pyrex graded seal to facilitate working at temperatures up to about 400°. A conventional xenon resonance lamp powered by a 2450-MHz microwave generator was used as the light source. About 2% of the intensity of the 1470-Å line appeared at 1295 Å and no other radiation absorbed by *n*-butane was present. The *n*-butane was research grade material and the isotopic purity of the *n*-C_4D_{10} is characterized by $D:(D + H) > 0.99$. The *n*-C_4D_{10} was purified by gas chromatography, dried over P_2O_5, and purged of CO_2 with Ascarite. Blank experiments showed no detectable methane prior to photolysis. After photolysis, the fraction of the reaction mixture (methane and hydrogen) volatile at 77°K was sampled and analyzed on an analytical mass spectrometer of resolution $1/4000$. Thus, H_2O^+, OH^+, and N^+ presented no problem in the methane analysis. Cracking patterns were measured on authentic isotopic methanes. Most experiments were done on a master mixture with the ratio *n*-C_4D_{10}:*n*-$C_4H_{10} = 0.27$.

Results

Table I shows the isotopic methane analyses measured in experiments done in the temperature range 308–671°K. Figure 1 shows the Arrhenius plots of the ratios $[CH_4]/[CH_3D]$ and $[CD_3H]/[CD_4]$. Two experiments not reported in the table were done with a 1:1 mixture of *n*-C_4D_{10} at the same total butane pressure as those experiments reported in Table I and at 308°K. These experiments were done to test for kinetically "hot" methyl radicals. A pressure of 66,500 N/m² (500 Torr) of helium was added prior to photolysis and pumped away after photolysis by means of a liquid hydrogen cold trap. It was found that the presence of helium had no effect on either ratio $[CH_4]/[CH_3D]$ or $[CD_3H]/[CD_4]$. All reactions were carried out to less than 1% conversion.

Discussion

The sources of methane are considered to be reactions 1, 3, 6–9. In eq I and II [BuH] and [Bu_dD] are concentrations of *n*-butane and *n*-butane-d_{10}, respectively, φ_1 and φ_3 are quantum yields of reactions 1 and 3, respectively, and I_a is the rate of light absorption. Inspection of eq I and II reveals that when the temperature is so low that reactions 6 and 7 are negligible, the ratio $[CH_4]/CH_3D]$ approaches infinity. On the other hand, at low temperature where reactions 8 and 9 are also negligible, $[CD_3H]/[CD_4]$ approaches zero. Consequently an increasing divergence in the two ratios should occur as the temperature decreases. As the temperature increases, (6) dominates (1) and (9) dominates (3) with the result that eq I and II reduce to eq III and IV.

$$[CH_4]/[CH_3D] = (\varphi_1 I_{a_1} + k_6[CH_3][BuH])/(k_7[CH_3][Bu_dD]) \quad (I)$$

$$[CD_3H]/[CD_4] = k_8[CD_3][BuH]/(k_9[CD_3][Bu_dD] + \varphi_3 I_{a_3}) \quad (II)$$

$$[CH_4]/[CH_3D] \approx k_6[BuH]/(k_7[Bu_dD]) \quad (III)$$

$$[CD_3H]/[CD_4] \approx k_8[BuH]/(k_9[Bu_dD]) \quad (IV)$$

It is well documented[6] that $k_6/k_7 = k_8/k_9$ and it follows that the ratios $[CH_3D]/[CH_4]$ and $[CD_3H]/[CD_4]$ should approach asymptotically the same Arrhenius line defined by the kinetic isotope effect measured for *n*-butane by McNesby and Gordon.[3] The data in Figure 1 show that this is the case for the highest temperatures at which experiments were possible.

(6) W. M. Jackson, J. R. McNesby, and B. deB. Darwent, *J. Chem. Phys.*, **37**, 1610 (1962).

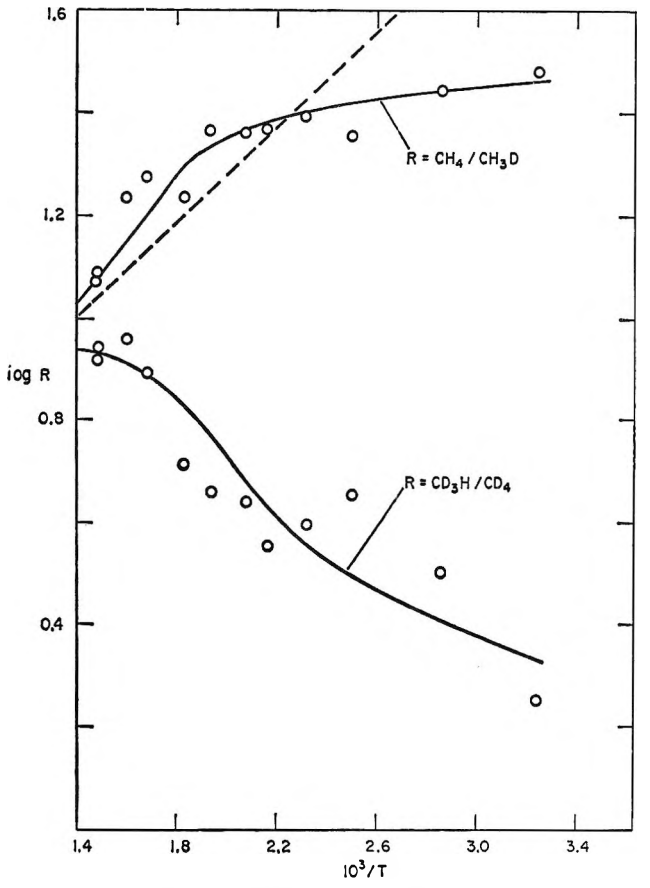


Figure 1. Effect of temperature on isotopic methanes.

A most striking feature of Figure 1 is that the divergence expected on the basis of the proposed mechanism becomes markedly less severe below about 523°K, with the ratio $[CH_4]/[CH_3D]$ actually falling to a value well below that expected from a pure free-radical abstraction mechanism. There are two explanations for this observation that may be advanced. (1) Some of the methyl radicals are "hot" and those that are should abstract hydrogen and deuterium approximately in the ratio[7] 4:1 to give $([CH_4]/[CH_3D])_{hot} = ([CD_3H]/[CD_4])_{hot} = 4$. The observed ratios log $\{[CH_4]/[CH_3D]\}$ and log $\{[CD_3H]/[CD_4]\}$ should tend toward the value log 4 = 0.60 as observed in Figure 1. The addition of inert gas in sufficient quantity to quench "hot" methyl radicals should cause a very large increase in $[CH_4]/[CH_3D]$ and a corresponding decrease in $[CD_3H]/[CD_4]$. The observation that large amounts of helium have no effect on these ratios proves the point that their depressed divergence at low temperatures cannot be due to hot radicals. An alternative explanation is (2) disproportionation of methyl with other radicals such as *n*-propyl and butyl. It is approximately true that at temperatures too low for efficient decomposition of butyl and *n*-propyl the numbers of C_xH_{2x+1} radicals are 3.7 × 1.6 or 5.9 times as abundant as C_xD_{2x+1} radicals, where the factor 1.6 is the ratio of absorption coefficients[8] of C_4H_{10} and C_4D_{10} present in the ratio 3.7:1. Since disproportionation reactions have very low activation energies, the methanes formed will be approximately in the ratio $[CH_4]/[CH_3D] = [CD_3H]/[CD_4] = 5.9$. The disproportionation hypothesis, therefore, predicts a result in the same direction as that predicted by the "hot" methyl hypothesis with the exception that no effect of inert gas is expected. Disproportionation of methyl and other free radicals as an explanation of the depressed divergence of $[CH_4]/[CH_3D]$ and $[CD_3H]/[CD_4]$ is in good agreement with all experimental observations. A further possible explanation that wall reactions are involved may be dismissed since the walls of the vessel are certainly vastly richer in H than in D. Abstraction of H from the walls could not, therefore, cause the observed drop in the $[CH_4]/[CH_3D]$ ratio.

$$CH_3 + n\text{-}C_3H_7 \longrightarrow CH_4 + C_3H_6 \qquad (11)$$

A rough estimate of the chain length may be made as follows. Assume all D_2 to be formed by molecular elimination. Okabe and Becker[1] have estimated that methyl radicals are produced at a rate 17% of that at which molecular hydrogen is formed. However 12% of the molecular hydrogen in our system is D_2. Thus, 17:12 = 1.4 is the ratio of production of methyl radicals to production of D_2. At 671°K, the ratio of [methane] (formed from methyl radical abstraction of hydrogen from *n*-butane) to $[D_2]$ is 42 ± 6. If it is assumed that the quantum yield for molecular elimination of D_2 at 671°K is the same as at room temperature, the ratio of [methane] formed to [methyl radicals] formed in the primary process, *i.e.*, the chain length, is 30 ± 4. At 622°K, a similar calculation gives a chain length of 14, and at 546°K the chain length is 3.2

These results cannot be compared with the chain lengths in propane photolysis[5] since chain length is a function of light intensity and the relative light intensities in the two studies are not known with sufficient accuracy. Nevertheless, the chain lengths are approximately correct for light intensities of about 10^{14} quanta sec^{-1} and are comparable to those measured for propane. The depression in the divergence of the $[CH_4]/[CH_3D]$ and $[CD_3H]/[CD_4]$ ratios was not apparent in the propane photolysis and this may be due to the fact that the average disproportionation:recombination ratio is higher for [methyl]/[butyl, *n*-propyl] than for [methyl]/[propyl, ethyl];[9] *i.e.*, methyl and alkyl radical collisions will produce methane by disproportionation with a higher probability in the *n*-butane system than in the propane system.

The Effect of Temperature on Chain Length. The mechanism of the chain reaction may be written in terms of the parent molecule, BuH, the methyl radical,

(7) R. D. Doepker and P. J. Ausloos, *J. Chem. Phys.*, **41**, 1865 (1964).
(8) M. C. Sauer, Jr., and L. M Dorfman, *ibid.*, **35**, 497 (1961).
(9) A. F. Trotman-Dickenson and G. S. Milne, "Tables of Biomolecular Gas Reactions," NSRDS-NBS-9, 1967, p 110.

CH_3, and the butyl radical, Bu, which gives rise to the methyl radical at temperatures where Bu does not decompose rapidly

$$BuH \longrightarrow CH_3 \quad (12)$$

$$CH_3 + BuH \longrightarrow CH_4 + Bu \quad (13)$$

$$Bu \longrightarrow CH_3 + C_3H_6 \quad (14)$$

$$CH_3 + Bu \longrightarrow CH_3Bu \quad (15)$$

The stationary-state treatment gives the relationship

$$[CH_3] = R_i/2k_{15}[Bu] \quad (V)$$

where R_i is the rate of initiation. The concentration of butyl is given by

$$Bu = (-R_i/4k_{14}) + [(R_i/4k_{14})^2 + (R_i k_{13}[BuH]/2k_{14}k_{15})]^{1/2} \quad (VI)$$

The chain length is defined by

$$CL = \frac{R_m}{R_i} = \frac{k_{13}[BuH]}{2k_{15}\left\{\frac{-R_i}{4k_{14}} + \left[\left(\frac{R_i}{4k_{14}}\right)^2 + \frac{R_i k_{13}[BuH]}{2k_{14}k_{15}}\right]^{1/2}\right\}} \quad (VII)$$

where R_m is the rate of free-radical methane formation. We assign the following values to the parameters in eq VII

$$R_i = 10^{14} \text{ molecules cm}^{-3} \text{ sec}^{-1}$$

$$k_{14} = 10^{14.35}e^{-33,000/RT} \text{ sec}^{-1}$$ [10]

$$k_{13} = 1.6 \times 10^{-12}e^{-4444/RT} \text{ molecule}^{-1} \text{ cm}^3 \text{ sec}^{-1}$$ [9]

$$k_{15} = 1.0 \times 10^{-10} \text{ molecule}^{-1} \text{ cm}^3 \text{ sec}^{-1}$$ [11]

$$[BuH] = 3 \times 10^{17} \text{ molecules cm}^{-3}$$

The temperature at which $(R_i/4k_{14})^2 = R_i k_{13}[BuH]/2k_{14}k_{15}$ is 548°K. The second term in the square root of eq VII dominates the first as the temperature rises above 548°K so that their ratio is 38 at 600°K. The physical meaning of this is that the butyl radicals are decomposing rapidly above about 548°K and the termination reaction (eq 15) is replaced by reaction 16 because of the increased relative abundance of methyl radicals. The stationary-state assumption now

$$CH_3 + CH_3 + M \longrightarrow C_2H_6 + M \quad (16)$$

leads to the value

$$[CH_3] = (R_i k_{16})^{1/2} \quad (VIII)$$

The average chain length is given by

$$CL = R_m/R_i = k_1[BuH](R_i k_{16})^{1/2}/R_i = k_{13}[BuH]/(k_{16}R_i)^{1/2} \quad (IX)$$

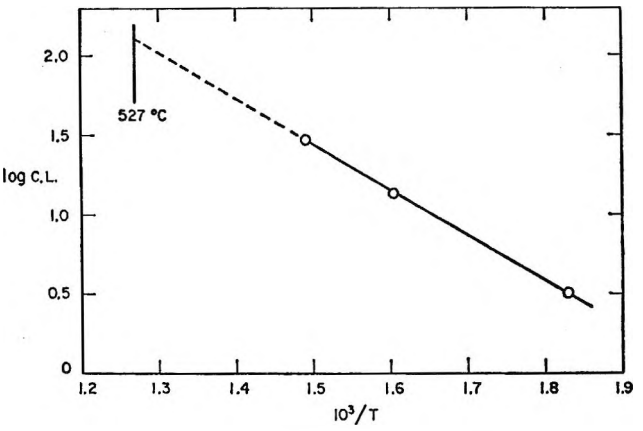


Figure 2. Chain length as function of temperature.

Thus, at temperatures (>548°K) above which the decomposition of Bu is so fast that reaction 16 dominates reaction 15 as the chain-terminating process, the temperature effect on chain length is given by

$$\ln CL = [(\ln [BuH])/R_i^{1/2}] + [(\ln k_{13})/k_{16}^{1/2}] \quad (X)$$

$$\log CL = [(\log [BuH])/R_i^{1/2}] + [(\log A_{13})/A_{16}^{1/2}] - [(E_{13} - {}^1/_2E_{16})/2.303RT] \quad (XI)$$

The plot of log CL *vs.* $1/T$ should be linear above 548°K and the slope should equal approximately the average $-(E - {}^1/_2E)/2.303R$. Figure 2 shows the plot of eq XI and the slope gives $E_{13} - {}^1/_2E_{16} = 13$ kcal. This is in reasonable agreement with the experimental average value of about 11 kcal.[3]

Pyrolysis of n-Butane. Figure 2 shows the average chain length extrapolated to a typical pyrolysis temperature of 800°K. Evidently at the rate of chain initiation used in the present work, the chain length at this temperature would be about 140. In pyrolysis, the initiation rate,[12] $R_i = k[BuH] = 5 \times 10^{11}$ molecules sec^{-1}, is a factor of about 200 lower than the photochemical initiation rate. Since the average chain length is approximately inversely proportional to the square root of the initiation rate, it is expected that at 800°K the chain length in *n*-butane pyrolysis will be approximately given by

$$CL \approx 140 \times 200^{1/2} \approx 2000$$

Now it has been shown by Kupperman and Larson[13] that, in the *n*-butane pyrolysis fully inhibited by NO, the residual reaction is completely free radical in nature and no molecular elimination is detected. It must be remembered, however, that the maximally inhibited

(10) B. S. Rabinovitch and D. W. Setser, *Advan. Photochem.*, **3**, 70 (1964).

(11) R. Gomer and G. B. Kistiakowsky, *J. Chem. Phys.*, **19**, 85 (1951).

(12) W. Tsang (unpublished results) gives $k = 10^{16.3} \exp(-81,200/RT)$.

(13) A. Kupperman and J. G. Larson, *J. Chem. Phys.*, **33**, 1264 (1960).

reaction proceeds at a rate at least 1% of that of the uninhibited reaction[14] at a pressure of 1330 N/m^2 (10 Torr). Therefore, the maximally inhibited reaction proceeds as a chain reaction of average length ~20.

It is obvious from this result that the detection of a molecular elimination

$$n\text{-}C_4H_{10} \longrightarrow CH_4 + CH_3CH{=}CH_2 \qquad (17)$$

competitive with the free-radical elimination

$$n\text{-}C_4H_{10} \longrightarrow CH_3 + C_3H_7 \qquad (18)$$

would be quite impossible even if the molecular elimination were equally as important as the free-radical elimination. Thus, we are confronted with an old fundamental problem: Why does the highly favored (energetically) intramolecular reaction not dominate the less favorable radical elimination reaction? The answer is that molecular elimination may very well dominate free-radical formation but that the chains are so long even when "fully inhibited" by NO that the free-radical reaction dominates molecular elimination reactions. Thus, the early notion of the entire residual fully inhibited reaction being intramolecular is certainly incorrect, but a small fraction of the residual reaction may be intramolecular and may have escaped detection.

Acknowledgment. The authors are indebted to Dr. Allan H. Laufer for performing some of the experiments and to Dr. Wing Tsang for making some of his results available before their publication. This work was carried out at the National Bureau of Standards under the sponsorship of the Atomic Energy Commission.

(14) E. W. R. Steacie, "Atomic and Free Radical Reactions," Reinhold Publishing Corp., New York, N. Y., 1954, p 108.

The Mercury 6($^3P_1$) Photosensitized Decomposition of Methyl Ethyl Ether

by S. V. Filseth

Department of Chemistry, Harvey Mudd College, Claremont, California 91711 *(Received May 23, 1968)*

The mercury 6($^3P_1$) photosensitized decomposition of methyl ethyl ether has been studied in the vapor phase in a static system at 55° and between 0.25 and 10.0 Torr. Gas chromatographic and mass spectroscopic analysis of the distribution of reaction products was carried out at varying times, intensities, and ether and added gas pressures. The principal products are hydrogen, 2,3-dimethoxybutane, 1-ethoxy-2-methoxypropane, and methyl vinyl ether. It is concluded that the principal primary process involves breaking of a carbon–hydrogen bond and that a competing step involving the breaking of a carbon–oxygen bond occurs with no more and probably considerably less than 3% probability.

Introduction

The mercury 6($^3P_1$) photosensitized decomposition of dimethyl ether has been the subject of several investigations.[1-5] A conclusion common to these studies is that the primary interaction results, at least in part, in the formation of the methoxymethyl radical near ambient temperatures at moderate pressures. An equally important primary process has been observed, however, in a fast flow system[2] at pressures of the order of 0.01 Torr, to produce methyl and methoxy radicals. No evidence of this latter process was observed in a recent[4] thorough investigation in the pressure range from 3 to 600 Torr. The present study was begun in an attempt to determine the importance of possible competing primary processes in methyl ethyl ether.

Experimental Section

Methyl ethyl ether was prepared in a Williamson-type synthesis from sodium ethoxide and dimethyl sulfate. After purification by trap-to-trap distillation, it was stored at −78° behind a metal valve. Gas chromatographic analysis revealed it to be 99.95% pure with dimethyl ether the only impurity.

The reaction was studied in a static system in a

(1) R. A. Marcus, B. deB. Darwent, and E. W. R. Steacie, *J. Chem. Phys.*, **16**, 987 (1948).

(2) R. F. Pottie, A. G. Harrison, and R. P. Lossing, *Can. J. Chem.*, **39**, 102 (1961).

(3) Y. Takezaki, S. Mori, and H. Kawasaki, *Bull. Chem. Soc. Jap.*, **39**, 1643 (1966).

(4) L. F. Loucks and K. J. Laidler, *Can. J. Chem.*, **45**, 2763, 2767, 2775 (1967).

(5) R. Payette, M. Bertrand, and Y. Rousseau, *ibid.*, **46**, 2693 (1968).

cylindrical quartz reaction vessel of 2-in. diameter and 10-cm light path. The vessel was contained in a tubular aluminum furnace which was heated with cartridge type heaters and controlled at 55 ± 1°. The vessel was connected by a heated side arm to a small mercury reservoir, about which thermostated water at 25.0 ± 0.05° was circulated, and by a metal valve to a conventional glass vacuum system.

The light source was a Hanovia SC 2537 low-pressure mercury discharge in the form of a flat spiral which was mounted parallel to the face of the vessel. Two different such lamps were employed during the course of this study. Preliminary experiments indicated that the output intensity of the lamps was a marked function of the envelope temperature as has been reported previously.[6] In all the work reported here, the lamp was held at constant temperature by flowing heated air through an enclosure which surrounded it. The enclosure was fitted with a Vycor quartz window which prevented the transmission of wavelengths below 2000 Å. The lamps were run continuously during the course of this study in an attempt to ensure reproducible conditions. After prolonged usage, the intensity of 2537-Å light emitted by these lamps was found to vary in a periodic manner with a frequency of about 45 sec. The amplitude of the oscillation increased with the age of the lamp, and its origin was not determined. An approximately 2% scatter exists in the data reported here as a result of this effect.

Following irradiation, the products were initially removed from the reaction vessel into two traps kept at −196°. The noncondensable fraction was found to be over 98% hydrogen by mass spectrometer analysis, and except during the volumetric analyses for hydrogen, all subsequent analyses were made by gas chromatography.

Irradiations were performed under identical conditions, and product analyses were made on three different columns. A 6-ft silica gel column operated at 50° gave good separation of the low-molecular-weight hydrocarbons. The condensable oxygenated products were determined on a tandem column: 10-ft, 20% Carbowax 20M on 100–120 acid-washed firebrick and 20-ft 15% tricresyl phosphate on 60–80 HMDS-treated Chromosorb W. Finally a 6-ft column of 30% silver nitrate and diethylene glycol on 80–100 GC-22 was employed to separate methyl vinyl ether from undecomposed substrate.

The identification of all compounds was made on the basis of chromatographic retention volumes and was confirmed by combined gas chromatography and mass spectrometry. The mass spectra of products were compared with spectra obtained from authentic samples.

To measure the efficiency of the primary processes involved, actinometry was carried out upon the low-pressure mercury lamp. Propane was used as the actinometer at pressures of the order of 150 Torr using published[7] values for the quantum yield of hydrogen formation under these conditions. This measurement necessitated the determination of the fractional transmission of 2537-Å radiation through the vessel as a function of both methyl ethyl ether and propane pressures. These measurements were made with a photomultiplier tube on light transmitted through a chemical filter containing the cyanine dye recommended by Kasha.[8] During a 2-month period of this investigation the intensity of the lamp at 2537 Å was found to diminish by about 15% with an average value of about 5×10^{14} quanta cm^{-2} sec^{-1} reaching the interior of the vessel.

Results

The sensitized decomposition of methyl ethyl ether was studied at 55° at pressures between 0.25 and 10.0 Torr. The principal products were hydrogen, 2,3-dimethoxybutane, 1-ethoxy-2-methoxypropane, and methyl vinyl ether. In addition, smaller amounts of methyl isopropyl ether, acetaldehyde, and other ethers, ketones, alcohols, and hydrocarbons were produced. Compounds positively identified but present in small quantities include 1,4-dimethoxybutane, 1,3-dimethoxybutane, 1,2-diethoxyethane, and 1,3-methoxyethoxypropane. Several compounds formed in very small amounts were tentatively identified on the basis of either chromatographic retention volumes or mass spectral fragmentation patterns alone. These compounds include diethyl ether, propylene oxide, methyl-*n*-propyl ether, 1,1-dimethoxyethane, 3-methoxy-2-butanone, and 2,3-butanedione. Formaldehyde, although definitely present, was not measured because of the lack of a quantitative and reliable method for the analysis of submicromolar amounts of this material. No trimeric products were observed as had been previously reported in a study of the dimethyl ether system.[3] The 2,3-dimethoxybutane was observed chromatographically as two well-separated peaks of approximately equal area. With identical mass spectra, these peaks are undoubtedly due to the *meso* and *dl* forms of the compound.

To determine which of the many products were the result of a primary process and which had their origin in subsequent decomposition of primary products, a study was made of product yield as a function of varying irradiation time. The results of these studies are presented in part in Table I. The shortest irradiation time corresponds to a conversion of about 0.5%. Also observed with a quantum yield of the order of 0.001 for an irradiation time of 20 sec were: propane, methanol, ethanol, acetone, 2-butanone, carbon monoxide, ethyl-*n*-propyl ether and methyl-*sec*-butyl ether.

(6) L. J. Heidt and H. B. Boyles, *J. Amer. Chem. Soc.*, **73**, 5728 (1951).
(7) S. Bywater and E. W. R. Steacie, *J. Chem. Phys.*, **19**, 319 (1951).
(8) M. Kasha, *J. Opt. Soc. Amer.*, **38**, 929 (1948).

Table I: Product Quantum Yields in the Irradiation of 2.05-Torr Methyl Ethyl Ether for Varying Periods

Product	Irradiation time, sec						
	10	20	40	65	90	120	170
Hydrogen	0.51	0.55	0.49	0.44	...	0.49	0.47
2,3-Dimethoxybutane	0.34	0.34	0.29	0.30	0.27	0.28	0.27
1-Ethoxy-2-methoxypropane	0.25	0.20	0.12	0.14	0.14	0.13	0.12
Methyl vinyl ether	0.15	0.13	0.10	0.09	0.07	0.06	0.04
Methyl isopropyl ether[a]	0.025	0.025	0.030	0.040	0.045	0.045	0.055
Acetaldehyde	...	0.020	0.015	0.025	0.030	0.035	0.040
Ethylene	0.020	0.015	0.013	0.010	0.010	0.009	0.007
Methane	...	0.003	0.004	0.005	0.005	0.006	0.007
Ethane	...	0.002	0.003	0.003	0.004	0.004	0.005

[a] Includes an estimated 25–35 mol % diethyl ether.

In contrast to the major products the formation of propane appears to occur at very small and probably zero rate initially and at increasing rate as the irradiation is prolonged. A similar behavior was observed for the yields of acetone, 2-butanone, 2,3-butanedione, and 3-methoxy-2-butanone. It is, therefore, felt that none of these compounds are primary products of the decomposition of the ether.

In other experiments designed to provide information about possible excited molecule mechanisms, the product distribution was studied at varying pressures of the ether. The results of these studies are represented in part in Figures 1 and 2.

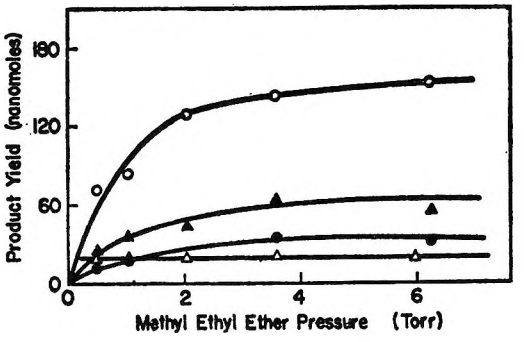


Figure 1. Product yields for 20-sec irradiation of methyl ethyl ether at varying pressures: ○, hydrogen; ▲, 2,3-dimethoxybutane; ●, 1-ethoxy-2-methoxypropane; △, methyl vinyl ether.

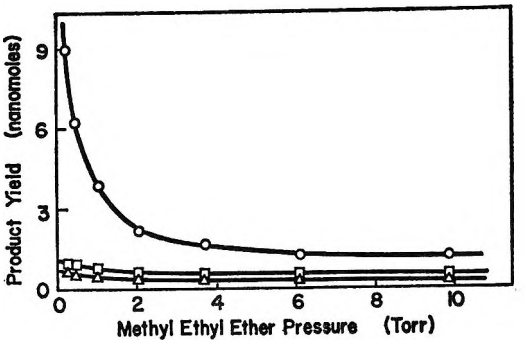


Figure 2. Product yields for 20-sec irradiation of methyl ethyl ether at varying pressures; ○, ethylene; □, methane; △, ethane.

In additional experiments, the distribution of certain products was studied as a function of incident intensity and added $(C_2H_5)_2Hg$. The results of the intensity measurements are recorded in Table II. In a hydrogen atom scavenging experiment, addition of 0.25 Torr of isobutene reduced the yield of hydrogen in the irradiation of 3.0-Torr ether for 100 sec by a factor of 5. Finally, the quenching cross section of methyl ethyl ether has been determined by the competitive N_2O technique. A value of 10.3 Å^2 was obtained which is consistent with the values of 2.8 and 15.1 Å^2 reported[9] for dimethyl and diethyl ethers, respectively.

Table II: Yields of Selected Products from the Irradiation of 1.82-Torr Methyl Ethyl Ether at Varying Intensities

Intensity	0.010	0.275	1.000
Irradiation time, sec	10,000	364	100
	Product yields, nmol		
2,3-Dimethoxybutane[a]	107.2	89.5	69.0
Methyl isopropyl ether	36.3	42.8	45.3
Methyl vinyl ether	27.0	38.0	50.9
Acetaldehyde	19.2	24.9	30.5
Methane[b]	2.9	3.9	4.5
Ethane[b]	1.5	2.8	3.5
Ethylene[b]	0.9	2.0	2.5
Acetone	2.9	2.5	2.2
Methyl-*sec*-butyl ether	1.3	1.5	1.5
2-Butanone	1.1	0.9	3.1
Ethanol	0.5	1.9	4.1

[a] Represents only one of the two peaks of approximately equal area which are due to 2,3-dimethoxybutane. [b] Pressure of methyl ether was 2.40 Torr.

Discussion

The composition and behavior of the product distribution as studied in these experiments is consistent with a primary process involving a carbon–hydrogen bond rupture as, for example

$$Hg\,6(^3P_1) + CH_3OCH_2CH_3 \rightarrow CH_3OCHCH_3 + H + Hg\,6(^1S_0) \quad (1)$$

(9) M. G. Bellas, Y. Rousseau, O. P. Strausz, and H. E. Gunning, *J. Chem. Phys.*, 41, 768 (1964).

In addition to the 1-methoxyethyl radical, two other alkoxyalkyl radicals would be produced, and in recombination, these three would form six dialkoxyalkanes. All six are observed with 2,3-dimethoxybutane in highest yield and 1,4-dimethoxy butane in lowest yield. Experiments designed to measure the primary branching ratio between the three alkoxyalkyl radicals in reaction 1 have not been quantitatively unambiguous because of incomplete analytical resolution. It can only be approximately stated that the order of decreasing yield is 1-methoxyethyl, ethoxymethyl, and 2-methoxyethyl.

In addition to combination, disproportionation of alkoxyalkyl radicals must be considered as

$$2CH_3OCHCH_3 \rightarrow CH_3OCH_2CH_3 + CH_3OCH{=}CH_2 \quad (2)$$

Methyl vinyl ether will also be formed, however, in the competing hydrogen abstraction reaction

$$H + CH_3OCHCH_3 \rightarrow CH_3OCH{=}CH_2 + H_2 \quad (3)$$

It is possible to make a qualitative comparison of reactions 2 and 3 as sources of methyl vinyl ether by noting the effect of intensity on product yields as shown in Table II. If (2) were the predominant source of methyl vinyl ether, the yield of this disproportionation product should parallel the yield of the 2,3-dimethoxybutane combination product. However, the reverse is observed. The intensity results are consistent with (3) serving as the principal source of methyl vinyl ether. At low intensities, hydrogen atoms will be relatively more likely to abstract hydrogen from the substrate which should increase the yield of the resulting radical combination product. At higher intensities, radical–radical reactions are relatively more important, and methyl vinyl ether should be produced in increasing yield at the expense of 2,3-dimethoxybutane. The ratio of methyl vinyl ether to 2,3-dimethoxybutane will, therefore, most closely approach the ratio of rate constants for disproportionation to combination for the 1-methoxyethyl radical in the limit of low intensities. This ratio is 0.12 in this system. This is consistent with an upper limit of 0.14 determined for the corresponding ratio of rate constants for the 1-ethoxyethyl radical.[10]

Alternative primary processes which may be considered include a carbon–oxygen bond breaking step observed in an earlier study of dimethyl ether.[2] Thus, in this system by analogy

$$Hg\,6(^3P_1) + CH_3OCH_2CH_3 \rightarrow CH_3 + C_2H_5O + Hg\,6(^1S_0) \quad (4)$$

$$Hg\,6(^3P_1) + CH_3OCH_2CH_3 \rightarrow CH_3O + C_2H_5 + Hg\,6(^1S_0) \quad (5)$$

An upper limit to the extent of participation of these processes may be evaluated by comparing the yields of all alkoxy radical derived products with those of all alkoxyalkyl radical derived products. This limit is approximately 3%. In fact, reaction 4 is inconsistent with the effect of intensity on the yield of ethanol as shown in Table II, and it is unlikely that (4) and (5) make any contribution as primary processes.

It has been suggested[2] that an excited molecule may be produced in the primary process and that its deactivation at higher pressures would account for the failure to observe the carbon–oxygen split in other studies of dimethyl ether. The aliphatic ethers, however, are not known to possess the low-lying triplets which would be required by conservation. There is some evidence for an excited molecule in this system in the form of the pressure dependence of the yields of methane, ethane, ethylene, and methyl vinyl ether. This excited molecule may result from an atomic cracking reaction as

$$H + CH_3OCHCH_3 \rightarrow CH_3OCH_2CH_3^* \quad (6)$$

Subsequent decomposition of the excited molecule to produce the radicals indicated in (4) and (5) is consistent with the observed effect of intensity on the ethanol yield.

The considerable excess of products containing the methyl radical over ethanol makes it clear that another source of methyl radical is important from very short irradiation times. It is suggested that this process is

$$Hg\,6(^3P_1) + CH_3OCHCH_3 \rightarrow CH_3CHO + CH_3 + Hg\,6(^1S_0) \quad (7)$$

An analogous process has been proposed[2] to account for the formation of formaldehyde at low temperatures in the dimethyl ether system. The same process, however, was not observed more recently.[5] The observation that acetaldehyde is completely eliminated by the addition of small amounts of diethyl mercury is consistent with step 7.

If the yield of methane is attributed solely to the disproportionation reaction

$$CH_3 + CH_3OCHCH_3 \rightarrow CH_4 + CH_3OCH{=}CH_2 \quad (8)$$

then an upper limit can be obtained for the ratio of rate constants for disproportionation to combination

$$CH_3 + CH_3OCHCH_3 \rightarrow CH_3OCH(CH_3)_2 \quad (9)$$

k_8/k_9 of 0.10. This value can be compared with the corresponding upper limit of 0.07 obtained[10] for the reaction of ethyl radicals with the 1-ethoxyethyl radical.

Additional primary processes which have not already been considered include

$$Hg\,6(^3P_1) + CH_3OCH_2CH_3 \rightarrow CH_3OCH_2 + CH_3 + Hg\,6(^1S_0) \quad (10)$$

$$\rightarrow CH_3OCH{=}CH_2 + H_2 + Hg\,6(^1S_0) \quad (11)$$

$$\rightarrow C_2H_4 + CH_3OH + Hg\,6(^1S_0) \quad (12)$$

(10) K. M. Bansal and G. R. Freeman, *J. Amer. Chem. Soc.*, **88**, 1639, 4326 (1966).

Step 10 can be eliminated on the basis of the failure to observe products containing the methoxymethyl radical. Intramolecular formation of hydrogen as in step 11 would be uninfluenced by the presence of an olefin. However, a plot of the quantum yield of hydrogen against the reciprocal of added isobutylene extrapolates easily to zero suggesting that step 11 is unimportant in this system. Finally, the difference qualitatively and quantitatively in the yields of ethylene and methanol rule out (12) as an important source of ethylene.

The pressure dependence of the ethylene yield appears to be a characteristic of the process in which it is formed. An alternative explanation involves a competition between stabilization and decomposition of a vibrationally excited ethyl radical formed by addition of a hydrogen atom to ethylene. However, this explanation would predict that the difference between the zero-pressure ethylene quantum yield and the one reported in Table I would appear as products containing the ethyl radical. This is not observed. The sensitized decomposition of methyl vinyl ether as

$$\mathrm{Hg}\,6(^3P_1) + CH_3OCH{=}CH_2 \rightarrow CH_3OCH{=}CH_2^* + \mathrm{Hg}\,6(^1S_0)$$

$$CH_3OCH{=}CH_2^* \rightarrow C_2H_4 + CH_2O \qquad (13)$$

may be considered as a possible source of pressure-dependent ethylene. However, preliminary work[11] indicates that this process is unimportant, and the origin of ethylene consequently remains unknown.

Acknowledgment. It is a pleasure to acknowledge the undergraduate senior research contributions of Brian W. Dorman and John Y. Morimoto to this project. In addition, the author thanks the Consolidated Electrodynamics Corporation and the Pomona College Chemistry Department for the use of their mass spectrometers. This research was supported by grants from the National Science Foundation, the Petroleum Research Fund of the American Chemical Society, and Harvey Mudd College.

(11) R. V. Morris and S. V. Filseth, to be published.

The Diffusion of Polyelectrolyte in the Presence of Added Salt

by Yasuko Suzuki,

The Textile Research Institute of the Japanese Government, Kanagawa-ku, Yokohama, Japan

Ichiro Noda, and Mitsuru Nagasawa

Department of Synthetic Chemistry, Nagoya University, Chikusa-ku, Nagoya, Japan *(Received June 13, 1968)*

The diffusion process of polyelectrolyte in the presence of added salt is analyzed based on the assumption that the Donnan equilibrium is always maintained between the sample solution and the solvent. The apparent diffusion coefficient determined by an interference optical system is given as a function of the concentrations of both polyelectrolyte and added salt. Consequently, it is shown that the polymer concentration dependence of the apparent diffusion coefficient is expressed by an equation valid for two-component systems if the polymer solution is dialyzed against the solvent. That is, the second virial coefficient of the sample solution can be expressed by the sum of the concentration dependence coefficients of both sedimentation and diffusion divided by the molecular weight. The diffusion coefficient of poly(sodium styrenesulfonate) in sodium chloride solutions is determined by a Rayleigh optical system to be compared with the theory. The second virial coefficient calculated from the concentration dependence coefficient of diffusion thus obtained and that of sedimentation reported previously is found to agree with the value determined by the light-scattering method.

Introduction

In diffusion experiments of charged macromolecules, the sample solution is, in general, dialyzed against solvent which contains a neutral salt. That is, the electrochemical potentials of simple ions as well as of water molecules, except that of the macromolecule, are equal over the whole solution before start of the diffusion process, since otherwise, the diffusion of polyion would be accelerated by osmotic flow of water from the solvent phase to the solution phase. Consequently, the concentration of the neutral salt in the solvent phase is higher than the concentration in the solution phase, and as the diffusion of a macromolecule proceeds from the solution phase to the solvent phase, the neutral salt must diffuse in the opposite direction. Therefore, if

we use an optical system making use of refractive index such as the schlieren or interference method, we observe the sum of the diffusions of both macromolecule and neutral salt. On the other hand, if such an optical system as uv absorption is employed to measure the concentration of macromolecule, the counterdiffusion of added salt is not observed. In the analysis of diffusion processes of charged macromolecule so far published,[1-6] however, it seems to us that the counterdiffusion of neutral salts has not fully been discussed.

The purpose of the present paper is to analyze the diffusion process of polyelectrolyte in a neutral salt solution and to clarify the dependence of the observed diffusion coefficient on polymer concentration at various ionic strengths, paying attention to the counterdiffusion of the neutral salt.

Dependence of the Apparent Diffusion Coefficient on Polymer and Added Salt Concentrations

Neglecting the cross terms, the flux of a charged solute k relative to the cell is given by

$$(J_k)_c = \left(-D_k^0 \frac{\partial \ln m_k}{\partial x} + l_k^0 \frac{\partial \psi}{\partial x}\right) m_k \qquad (1)$$

where D_k^0, l_k^0, and m_k are the diffusion coefficient, mobility of the solute k, and concentration (number/ml), respectively, and $\partial\psi/\partial x$ is the diffusion potential created in the cell. Here, it is assumed that the activity coefficients of all solutes are unity. The diffusion potential is calculated from the condition that no electric current should pass through the solution at the steady state. That is

$$\sum_k (Z_k e)(J_k)_c = 0 \qquad (2)$$

where Z_k is the analytical charge number of the solute k. From eq 2, we have

$$\frac{\partial \psi}{\partial x} = \frac{\sum_k (Z_k e) D_k^0 m_k (\partial \ln m_k)/\partial x}{\sum_k (Z_k e) l_k^0 m_k} \qquad (3)$$

The insertion of eq 3 into eq 1 gives

$$(J_k)_c = \frac{[-\sum_{j\neq k}(Z_j e) l_j^0 m_j] D_k^0 (\partial m_k/\partial x) + l_k^0 m_k [\sum_{j\neq k}(Z_j e) D_j^0 (\partial m_j/\partial x)]}{\sum_k (Z_k e) l_k^0 m_k} \qquad (4)$$

Here, it is assumed that the sample solution is fully dialyzed against the solvent before start of the diffusion and also that the diffusion of polyion is so slow that the chemical potentials of all simple ions and water molecules may be equal over the whole solution at any stage of the diffusion. That is, the diffusion is assumed to proceed keeping the Donnan equilibrium between the sample and the solvent phases. Then, there must always be the following relationship between the concentrations of ions, m_+, m_-, and m_p at any position in the cell.

$$(Zm_p + m_-)m_- = m_s^2$$
$$m_+ = Zm_p + m_- \qquad (5)$$

where m_s is the concentration of neutral salt in the solvent which is assumed to be of a 1:1 type for simplifying the discussion and Z is the absolute charge number of the polyion (*i.e.*, $Z_p = -Z$). From the relationship of eq 5, m_+, m_-, and their gradients can be calculated as a function of m_p and m_s as

$$m_\pm = \tfrac{1}{2}(\sqrt{Z^2 m_p^2 + 4m_s^2} \pm Zm_p) \qquad (6)$$

$$\frac{\partial m_\pm}{\partial x} = \frac{Z}{2}\left(\frac{Zm_p}{\sqrt{Z^2 m_p^2 + 4m_s^2}} \pm 1\right)\frac{\partial m_p}{\partial x} \qquad (7)$$

Here, it is to be noted that m_s is a constant but m_p is a function of x.

If we use an optical system making use of refractive index such as the Rayleigh interference method used in this work, not only the flux of polyion, $(J_p)_c$, but also fluxes of other ions, $(J_+)_c$ and $(J_-)_c$, are observed together since all ions contribute to the refractive index. If we denote the partial molar refractive index of a solute k by Δn_k, the gradient of the refractive index at a position x, $\partial n/\partial x$, is given by

$$\frac{\partial n}{\partial x} = \sum_k \Delta n_k \frac{\partial m_k}{\partial x} \qquad (8)$$

By inserting eq 7 into eq 8, it follows that

$$\frac{\partial n}{\partial x} = \Delta n_{app} \frac{\partial m_p}{\partial x} \qquad (9)$$

$$\Delta n_{app} = \left[\Delta n_p + \frac{Z}{2}(\Delta n_+ - \Delta n_-) + \frac{1}{2}\frac{Z^2 m_p}{\sqrt{Z^2 m_p^2 + 4m_s^2}}(\Delta n_+ + \Delta n_-)\right] \qquad (10)$$

The rate of change in the refractive index of solution at x, $\partial n/\partial t$, is determined by the rates of change in the amounts of all diffusing solutes at the position. That is

$$\frac{\partial n}{\partial t} = -\frac{\partial}{\partial x}[\sum_k \Delta n_k (J_k)_c] \qquad (11)$$

Inserting eq 4 into $(J_k)_c$ of eq 11 and using the relation-

(1) Z. Alexandrowicz and E. Daniel, *Biopolymers*, **1**, 447, 473 (1963).
(2) P. J. Mijnlieff, "Effect of Charges on the Sedimentation, the Diffusion and the Sedimentation Equilibrium of Colloidal Electrolytes" in "Ultracentrifugal Analysis," J. W. Williams, Ed., Academic Press, New York, N. Y., 1963.
(3) V. N. Tsvetkov, V. S. Skazka, G. V. Tarasova, V. M. Yamshchikov, and S. Ya. Lyubina, *Vysokomol. Soed.*, **10**, 74 (1968).
(4) B. R. Record and R. G. Wallis, *J. Chim. Phys.*, **55**, 110 (1958).
(5) A. Soda and I. Kagawa, *Nippon Kagaku Zasshi*, **83**, 412 (1962).
(6) K. Iso, *ibid.*, **84**, 95 (1963).

ships of eq 7 and 9, we can transform eq 11 into the form

$$\frac{\partial n}{\partial t} = \frac{\partial}{\partial x}\left[D_p \frac{\partial n}{\partial x}\right] \tag{12}$$

which we generally use to calculate the diffusion coefficient from the Rayleigh or schlieren patterns. While in two-component systems D_p in eq 12 is the same as the diffusion coefficient of solute in the present three-component system, it must have the meaning

$$D_p = -\frac{1}{\kappa \Delta n_{app}}\Big[\{(\Delta n_p + Z\Delta n_+)l_+^0 m_+ - (\Delta n_p - Z\Delta n_-)l_-^0 m_-\}D_p^0 + \{-(\Delta n_p + Z\Delta n_+)l_p^0 m_p - (\Delta n_+ + \Delta n_-)l_-^0 m_-\}D_+^0 \times \frac{Z}{2}\left(\frac{Zm_p}{\sqrt{Z^2 m_p^2 + 4m_s^2}} + 1\right) + \{-(-\Delta n_p + Z\Delta n_-)l_p^0 m_p + (\Delta n_+ + \Delta n_-)l_+^0 m_+\}D_-^0 \times \frac{Z}{2}\left(\frac{Zm_p}{\sqrt{Z^2 m_p^2 + 4m_s^2}} - 1\right)\Big] \tag{13}$$

where

$$\kappa = -Zl_p m_p + l_+ m_+ - l_- m_- \tag{14}$$

To simplify our discussion, here, it is assumed that

$$\begin{aligned} \Delta n_+ &= \Delta n_- = \Delta n_\pm \\ l_+^0 &= -l_-^0 = l_\pm^0 \\ D_+^0 &= D_-^0 = D_\pm^0 \end{aligned} \tag{15}$$

and the units of concentrations are converted from m_k (number/ml) to C_p (g/ml) for polyion and to C_s (mol/l) for added salt. Then, eq 13 can be simplified at the limit of $Zm_p/2m_s \ll 1$ as

$$D_p = D_p^0[1 + k_D C_p + \cdots] \tag{16}$$

where

$$k_D = -k_s + 2A_2^0 M \tag{17}$$

and

$$k_s = \frac{10^3}{2}\frac{l_p^0}{l_\pm^0}\frac{Z}{M}\frac{1}{C_s} \tag{18}$$

$$A_2^0 = \frac{10^3}{4}\left(\frac{l_p^0}{l_\pm^0}\frac{D_\pm^0}{D_p^0}\right)\frac{Z}{M^2}\frac{1}{C_s} \tag{19}$$

If the polyelectrolyte solution is thermodynamically and hydrodynamically ideal, *i.e.*, if there is no thermodynamic and hydrodynamic interaction between solutes and, moreover, no hydrodynamic interaction between segments, there must be the following relationship between the electric mobility and the diffusion coefficient.

$$D_i^0/kT = l_i^0/Z_i e \tag{20}$$

with which eq 19 can be recast into

$$A_2^0 = \frac{10^3}{4}\frac{Z^2}{M^2}\frac{1}{C_s} \tag{21}$$

If we compare eq 18 with eq 17 of ref 7 and eq 21 with eq 1 of ref 8, we can know that k_s is the concentration dependence coefficient of sedimentation coefficient of the same polyion in the same solvent, while A_2^0 is the second virial coefficient of the polyelectrolyte solution if the solution is ideal. Equation 17 is well known to be valid for two-component systems. Thus, it may be concluded that the diffusion of a polyelectrolyte in the presence of added salt can be interpreted as that in a two-component system if the polyelectrolyte solution is dialyzed against the solvent. This conclusion is understandable if we remember the theory of Casassa and Eisenberg[9] that the refractive index increment relative to that of a solvent as well as other thermodynamic properties of the polyelectrolyte solution can be expressed by the equations valid for two-component systems if the polyelectrolyte solution is dialyzed against the solvent.

In general, however, polyelectrolyte solutions are not ideal but extremely nonideal thermodynamically and there are hydrodynamic interactions between polymer molecules as well as between segments.[10] The method to analyze the nonideal behavior of polyelectrolyte has not yet fully been established. Moreover, eq 20 is not valid for polyion if there is hydrodynamic interaction between segments.[11] However, it is well known that the nonideal behavior of polyelectrolyte solutions can be approximately explained if we use the effective charge of polyion instead of the analytical charge.[10] Moreover, the theory of Casassa and Eisenberg is valid for nonideal solutions. Therefore, it may be assumed that eq 22 must be applicable to real polyelectrolyte solutions if we use the values of k_s and A_2 determined experimentally.

$$k_D = -k_s + 2A_2 M \tag{22}$$

Moreover, if we use such an optical system as the uv system to determine the polymer concentration directly, instead of a refractive index method, we can observe the diffusion of polymer only, so that the apparent diffusion coefficient obtained, D_p', may be defined by

$$\frac{\partial C_p}{\partial t} = \frac{\partial}{\partial x}\left[D_p' \frac{\partial C_p}{\partial x}\right] \tag{23}$$

(7) M. Nagasawa and Y. Eguchi, *J. Phys. Chem.*, **71**, 880 (1967).

(8) A. Takahashi, T. Kato, and M. Nagasawa, *ibid.*, **71**, 2001 (1967).

(9) E. F. Casassa and H. Eisenberg, *ibid.*, **65**, 427 (1961).

(10) S. A. Rice and M. Nagasawa, "Polyelectrolyte Solutions," Academic Press, New York, N. Y., 1961.

(11) M. Nagasawa, A. Soda, and I. Kagawa, *J. Polymer Sci.*, **31**, 439 (1958); I. Noda, M. Nagasawa, and M. Ōta, *J. Amer. Chem. Soc.*, **86**, 5075 (1964).

Table I: The Apparent Diffusion Coefficients of the Sample in Sodium Chloride Solutions

NaCl concn, M							
0.2	Polymer concn, g/dl	0.0688	0.1493	0.2181	0.3802		
	$D_p \times 10^7$, cm²/sec	1.92	2.01	2.10	2.52		
0.05	Polymer concn, g/dl	0.0639	0.1113	0.1399	0.2044	0.3018	
	$D_p \times 10^7$, cm²/sec	1.68	1.93	1.94	2.44	2.94	
0.02	Polymer concn, g/dl	0.0440	0.0872	0.1465	0.2140	0.3716	
	$D_p \times 10^7$, cm²/sec	1.65	2.10	2.66	3.30	5.64	
0.01	Polymer concn, g/dl	0.0326	0.0652	0.0991	0.1317	0.2063	0.2753
	$D_p \times 10^7$, cm²/sec	1.65	2.26	2.83	3.38	5.29	7.14
0.005	Polymer concn g/dl	0.0361	0.0662	0.1445	0.1807	0.2107	0.3717
	$D_p \times 10^7$, cm²/sec	1.61	3.05	6.44	8.07	9.90	19.96

Inserting eq 6 and 7 into $(J_p)_c$ of eq 4 and comparing it with eq 23, we have the same equations for D_p' as eq 16 to 19, though the higher terms with respect to C_p are different. The derivation was already reported by Alexandrowicz and Daniel.[1] Thus, it may be concluded that eq 16 and 22 are valid irrespective of the optical system used.

However, if the assumptions of eq 15 are not applicable, D_p of eq 16 and D_p' of eq 23 do not completely agree with each other. For example, the limiting value of D_p at $C_p = 0$ is given by

$$\lim_{C_p \to 0} D_p = D_p^0 \times \left[1 + \frac{(l_+ - l_-)Z(\Delta n_+ - \Delta n_-)}{2(l_+ - l_-)\Delta n_p + (l_+ + l_-)Z(\Delta n_+ + \Delta n_-)}\right] \quad (24)$$

whereas

$$\lim_{C_p \to 0} D_p' = D_p^0$$

Only if $\Delta n_+ = \Delta n_-$, we have

$$\lim_{C_p \to 0} D_p = \lim_{C_p \to 0} D_p' = D_p^0$$

An additional term must appear in k_D of eq 17, too. However, it can be shown that both additional terms in D_p^0 and k_D are of secondary importance, at least in the present experimental system.

Experimental Section

Samples. Sodium polystyrenesulfonate used is the same as used in previous work.[7,8] The crude sample was purified by precipitation from aqueous solution with isopropyl alcohol and was then fractionated. The details in the fractionation procedure were described in a previous paper.[8] Among nine fractions obtained, a fraction having a suitable molecular weight was selected. The number and weight average molecular weights of the sample were found to be 3.20×10^5 and 4.91×10^5 from osmotic pressure measurements[12] and light scattering measurements,[8] respectively. Sodium chloride was of an analytical grade and the specific conductivity of the deionized distilled water used was lower than 5×10^{-7} ohm^{-1} cm^{-1}.

The polymer sample purified was dissolved in NaCl aqueous solutions used as solvent and was fully dialyzed against the solvent at 25 ± 3°. The arrival at the equilibrium was confirmed by measuring the specific conductivity of the solvent.

Diffusion Experiments. The diffusion was observed with Rayleigh interference optics of a Beckman Spinco Model H electrophoresis and diffusion instrument. The optical alignment was examined by measuring the diffusion coefficient of NaCl in 0.05 N solution. The measured value (1.502 ± 0.001) agreed with the literature value[13] within the error of 0.3%. All measurements were carried out at 25.00 ± 0.01° in the bath of the Spinco H which was filled with 3% aqueous solution of ethylene glycol. Distances between fringes were read by a microcomparator of Shimazu Seisakusho.

The diffusion coefficient of a polyelectrolyte in the presence of added salt depends on the concentration of the polyelectrolyte so highly that the diffusion pattern is skewed. Therefore, the diffusion experiments carried out between a polymer solution and solvent is not suitable to clarify the concentration dependence of diffusion coefficient of polyelectrolyte. In this work, the diffusion was performed between two polyelectrolyte solutions whose concentrations were different by about 25 fringes in most experiments and by 10 fringes in the most dilute solution. Since the concentration difference between two solutions is so small that the diffusion coefficient may be assumed to be linear with respect to concentration in this range, the diffusion

(12) To be published.

(13) R. H. Stokes, *J. Amer. Chem. Soc.*, **72**, 2243 (1950).

coefficient at the arithmetic average concentration between two concentrations used can be calculated from Rayleigh patterns using the method of Creeth.[14] The diffusion coefficients thus determined at various concentrations were plotted against the average concentrations. The standard deviation in diffusion coefficient thus determined was about 1%.

To eliminate the initial boundary disturbance, the apparent diffusion coefficients thus calculated at different times, $D_p(C_p, t)$, are extrapolated to infinite time. The diffusion coefficient at C_p, $D_p(C_p)$, can be obtained as the intercept at $1/t = 0$, while the slope of the straight line gives the initial time correction which was about 10 min.

Results

The values of the apparent diffusion coefficient, D_p, obtained are listed in Table I as functions of concentration of both polyelectrolyte and sodium chloride. The relationship between D_p and C_p is also shown in Figure 1. The concentration dependence of the diffusion coefficient can well be approximated by straight lines at low polymer concentrations and at high ionic strengths, but deviate from the linearity at high polymer concentrations and low ionic strength. The concentration dependence of the diffusion coefficient is determined by combination of the concentration dependences of both osmotic pressure (or light-scattering data) and sedimentation coefficient.[15] The deviation of D_p from linearity observed in Figure 1 appears reasonable, if we compare the figure with the concentration dependences of the osmotic pressure[12] (or light-scattering data[8]) and the sedimentation coefficient[7] of the same sample reported previously.

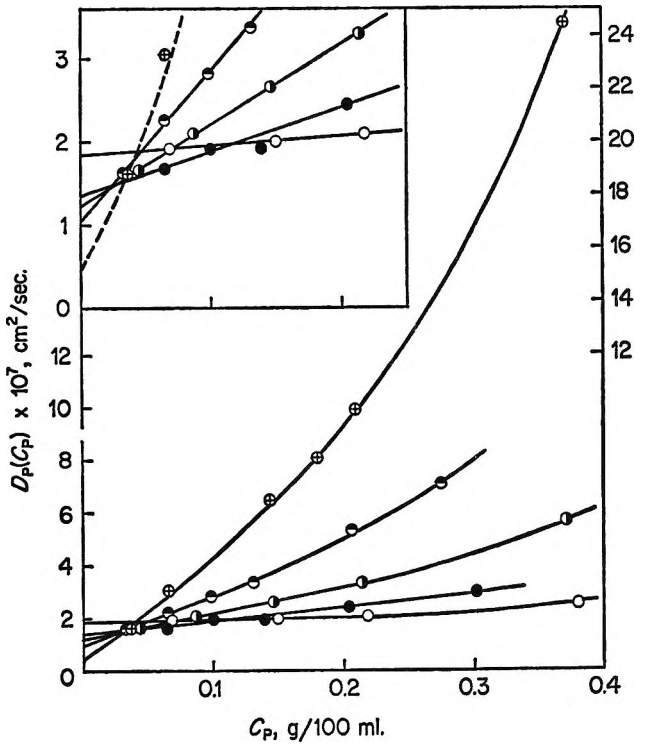


Figure 1. The concentration dependence of the apparent diffusion coefficient. NaCl concentrations: ○, 0.2 *M*; ●, 0.05 *M*; ◑, 0.02 *M*; ◒, 0.01 *M*; ⊕, 0.005 *M*.

The diffusion coefficient at zero polymer concentration, which is called the limiting diffusion coefficient in this paper, can be obtained as the intercept at $C_p = 0$ in the figure, while the concentration dependence coefficient of diffusion coefficient, k_D, can be obtained from the slope. The values of D_p^0 and k_D of the present sample at various ionic strengths are listed in Table II, in which both the concentration dependence coefficient of sedimentation coefficient, k_s,[7] and second virial coefficient, A_2,[8] are also listed. The values in parentheses are estimated by interpolation of the observed values. The concentration dependence of the diffusion coefficient of polyelectrolyte is so high that the limiting diffusion coefficient cannot be obtained so accurately as the limiting sedimentation coefficient, particularly if the molecular weight is higher than that of the present sample.

Discussion

As is well known, an average molecular weight of polymer, M_{SD}, can be calculated from the limiting sedimentation and diffusion coefficients of the polymer using the Svedberg equation[16]

$$M_{SD} = \frac{S_p^0 RT}{D_p^0(1 - \bar{v}\rho)} \tag{25}$$

where $\bar{v}$ is the partial specific volume of polymer and ρ is the density of the solvent. The value of M_{SD} calculated is also shown in Table II to be compared with M_n and M_w. The agreement is reasonable if we take into account the polydispersity of the sample[17–19] and the ambiguity in D_p^0 due to the second term in eq 24.

The limiting diffusion coefficient D_p^0 is found to differ markedly with ionic strength. The variation in D_p^0 with ionic strength is due to two factors as was discussed in a previous paper:[7] the change in the radius of gyration with ionic strength and the electrophoretic force of ionic atmosphere. However, the change in D_p^0 with expansion of polyion can be canceled by combining D_p^0 with the intrinsic viscosity $[\eta]$, so that the following Mandelkern–Flory coefficient[20–22] may be influenced

(14) J. M. Creeth, *J. Amer. Chem. Soc.*, **77**, 6428 (1955).
(15) L. Mandelkern and P. J. Flory, *J. Chem. Phys.*, **19**, 984 (1951).
(16) T. Svedberg and K. O. Pederson, "Die Ultrazentrifuge," Steinkoff, Dresden and Leipzig, 1940.
(17) S. Singer, *J. Polymer Sci.*, **1**, 445 (1946).
(18) N. Yamada and H. Matsuda, *Kobunshi Kagaku*, **18**, 110 (1961).
(19) S. Ya. Frenkel, *Vysokomol. Soed.*, **2**, 731 (1960).
(20) L. Mandelkern and P. J. Flory, *J. Chem. Phys.*, **20**, 212 (1952).
(21) L. Mandelkern, W. R. Krigbaum, H. A. Sheraga, and P. J. Flory, *ibid.*, **20**, 1392 (1952).
(22) T. G Fox, Jr., and L. Mandelkern, *ibid.*, **21**, 187 (1953).

ห้องสมุด กรมวิทยาศาสตร์

only by the effect of ionic atmosphere on the limiting diffusion coefficient.

$$\Phi_0^{1/3}P_0^{-1} = [\eta]^{1/3}M^{1/3}\eta_0 D_p^0/kT \qquad (26)$$

where all notations are the same as in the previous paper.[7]

The values of $\Phi_0^{1/3}P_0^{-1}$ obtained by inserting the experimental values of D_p^0 into eq 26 are shown in Table II. In the case of the present sample, the values of $\Phi_0^{1/3}P_0^{-1}$ are found to be independent of ionic strength and similar to the results obtained from S_p^0, except that the value of $\Phi_0^{1/3}P_0^{-1}$ extrapolated to infinite ionic strength is a little higher than the value accepted for nonionic polymers (2.5×10^6). It was reported that the value of $\Phi_0^{1/3}P_0^{-1}$ at infinite ionic strength determined by sedimentation experiments is lower than 2.5×10^6. The disagreement between the

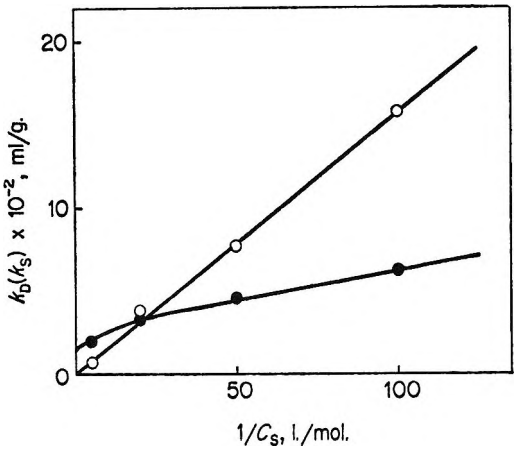


Figure 2. Relationship between the concentration dependence coefficient of diffusion coefficient, k_D, and the ionic strength (open circles). The filled circles show the concentration dependence coefficient of sedimentation coefficient, k_S, reported previously.[7]

values of $\Phi_0^{1/3}P_0^{-1}$ determined by sedimentation and diffusion and also the deviation of those values from 2.5×10^6 is eliminated if we use M_{SD} instead of M_w to calculate $\Phi_0^{1/3}P_0^{-1}$.

The second virial coefficient, A_2, is calculated from the experimental values of k_S and k_D with M_w using eq 22. The values obtained are also listed in Table II to be compared with the values determined by a light-scattering method.[8] Since the hydrodynamic interaction between expanded polyion coils was neglected in the derivation of k_S, the theoretical prediction of the linear relationship between k_S and $1/C_s$ was not accounted for by experiments.[7] However, the hydrodynamic interaction term is canceled when we add k_S and k_D and, hence, the agreement between the second virial coefficient determined from the combination of k_S and k_D and that from light-scattering measurements is satisfactory. As is seen in Figure 2, moreover, k_D is found to be linear with respect to $1/C_s$ as predicted by

Table II[a]

C_S, M	$D_p^0 \times 10^7$, cm²/sec	$S_p^0 \times 10^{13}$, sec	$M_{SD} \times 10^{-5}$, g/mol	$k_0 \times 10^{-2}$, ml/g	$k_S \times 10^{-2}$, ml/g	$(k_D + k_S)/2M_w \times 10^{-4}$, ml mol/g²	$A_2 \times 10^{-4}$, ml mol/g²	$\Phi_0^{1/3}P_0^{-1} \times 10^{-6}$ from $[\eta]$, D, M_w	$\Phi_0^{1/3}P_0^{-1} \times 10^{-6}$ from $[\eta]$, S, M_w	$\Phi_0^{1/3}P_0^{-1} \times 10^{-6}$ from $[\eta]$, D, M_{SD}	$\Phi_0^{1/3}P_0^{-1} \times 10^{-6}$ from $[\eta]$, S, M_{SD}
0.2	1.83	8.13	2.78	0.680	1.97	2.70	(4.1)	2.90	1.88	2.46	2.62
0.05	1.35	7.25	3.28	3.91	3.25	7.29	(8.6)	2.86	2.09	2.54	2.63
0.02	1.25	6.41	3.20	7.75	4.56	12.5_3	14.8	2.92	1.94	2.50	2.66
0.01	1.09	5.88	3.28	16.1_7	6.18	22.7_7	(22)	2.75	1.96	2.45	2.59
0.005	(0.6)	5.13	(4.6)	(64)	7.65	(73)	(41)				

[a] $M_n = 3.2 \times 10^6$; $M_w = 4.9 \times 10^6$.

eq 17–22, probably because the contribution of the hydrodynamic interaction to k_D is not high compared with the $2A_2M$ term. Here, however, it is to be noted that in this paper we discussed only the relationship among k_D, k_S, and A_2. The quantitative analysis of k_D as well as of k_S and A_2 in terms of the polymer characteristics and salt concentration is beyond the purpose of this paper.

Acknowledgment. Y. S. wishes to thank the Science and Technology Agency for giving her the opportunity of carrying out this work in Nagoya.

The Electron Spin Resonance of Low-Spin Isocyanide Complexes of Cobalt(II). I. Halides

by Nobuko Kataoka and Hideo Kon

Laboratory of Physical Biology, National Institute of Arthritis and Metabolic Diseases, National Institutes of Health, Bethesda, Maryland 20014 *(Received June 19, 1968)*

The electron spin resonance (esr) spectra of the low-spin Co^{II}(phenyl isocyanide)$_4X_2$, where X = Cl^-, Br^-, or I^-, show that the two halogen ions are equivalently coordinated in liquid as well as in frozen solution and the molecule shows rhombic distortion for X^- = Cl^- and Br^-. From the observed large halogen hyperfine splittings the fractional spin transfer to the halogen ion is calculated as 8.7, 15.3, and 14.3% per halogen ion, respectively, for the chloride, bromide, and iodide. The fact that the ^{59}Co hyperfine structure was resolved only in the parallel band is attributed to the positive isotropic contact term which means that the unpaired electron orbital of the complexes consists of predominant $3d_{3z^2-r^2}$ *plus* a small amount of s orbitals. The existence of an equilibrium between the para- and the diamagnetic forms was demonstrated for the bromide and iodide by esr and by visible absorption spectra.

When a transition metal ion is surrounded by ligands octahedrally, the 3d orbital levels are split into two groups: $e_g(d_{x^2-y^2}, d_{3z^2-r^2})$ orbitals with probability distributions pointing toward the ligands are higher in energy while t_{2g} (d_{xy}, d_{yz}, d_{zz}) orbitals pointing in the in-between directions have lower orbital energy. When a tetragonal distortion exists, each of the two groups is split further, and $d_{x^2-y^2}$ and $d_{3z^2-r^2}$ become separated, the latter being of lower energy in most complexes studied thus far. Cu(II) complexes which have nine electrons in the d-shell (an unpaired electron in $d_{x^2-y^2}$) are very common and have been studied extensively by esr. On the contrary, the system with one unpaired electron in $d_{3z^2-r^2}$ orbital, such as low-spin Co(II) complexes, is much less common, mainly because the complex tends to dimerize to become diamagnetic or, otherwise, the ligand field is not strong enough to bring about the low-spin state. When this state is realized, however, the magnetic properties of the system due to the unpaired electron in the out-of-plane ($d_{3z^2-r^2}$) orbital depends in a more sensitive manner upon the presence, absence, or the nature of the ligand in the axial sites than in the system with the unpaired electron in $d_{x^2-y^2}$ orbitals. One typical example may be seen in the large variations of the spin-Hamiltonian parameters observed with cobalt(II) tetraphenylporphine[1] and phthalocyanines[2,3] accompanying the change in the molecular environment.

The understanding of such phenomena in terms of the electronic structure of the metal ion is made difficult mainly because of the scarcity of esr studies on such low-spin Co(II) systems.

In this report we present the results of investigation by esr of the low-spin Co^{II}(phenyl isocyanide)$_4X_2$, where X^- = Cl^-, Br^-, or I^-. The synthesis and the magnetic susceptibility of these compounds and analogs were reported by Malatesta, *et al.*[4,5] It will be shown that the spin transfer to the axial ligand is relatively small and that the participation of a small amount of the metal s orbitals plays a significant role in the metal hyperfine (hf) interaction.

Esr spectra at room temperature of analogous complexes have been reported[6] previously, with which the

(1) J. M. Assour, *J. Chem. Phys.*, **43**, 2477 (1965).
(2) J. M. Assour and W. K. Kahn, *J. Amer. Chem. Soc.*, **87**, 207 (1965).
(3) J. M. Assour, *ibid.*, **87**, 4701 (1965).
(4) L. Malatesta and L. Giuffre, *Atti acad. nazl. Lincei, Rend. Classe sci. fis. mat. e nat.*, **11**, 206 (1951).
(5) L. Malatesta and A. Sacco, *Gazz. Chim. Ital.*, **83**, 499 (1953).
(6) J. P. Maher, *Chem. Commun.*, 632 (1967).

corresponding part of the present results is in good agreement.

Experimental Section

Preparation of tetrakis(phenyl isocyanide)cobalt(II) bromide and iodide were carried out according to the method of Malatesta and Sacco[5] from phenyl isocyanide and $CoBr_2 \cdot 6H_2O$ and $CoI_2 \cdot 6H_2O$, respectively. The chloride, which is unstable in solution at room temperature, was obtained by adding dropwise the cold EtOH (95%) solution of $CoCl_2 \cdot 6H_2O$ to EtOH (95%) solution of isocyanide in an ice bath. The pale green crystals were washed with cold EtOH and dried. The results of analysis showed good agreement with the calculated values. *Anal.* Calcd for $Co(C_7H_5N)_4Cl_2$: C, 62.01; H, 3.72; N, 10.33; Cl, 13.08; Co, 10.87. Found: C, 62.11; H, 3.77; N, 10.20; Cl, 12.86; Co, 10.60. Calcd for $Co(C_7H_5N)_4Br_2$: C, 53.27; H, 3.19; N, 8.88; Br, 25.32; Co, 9.34. Found: C, 53.49; H, 3.50; N, 8.46; Br, 25.70; Co, 9.29. Calcd for $Co(C_7H_5N)_4I_2$: C, 46.37; H, 2.78; N, 7.73; I, 35.00; Co, 8.13. Found: C, 46.26; H, 2.84; N, 7.59; I, 35.31; Co, 8.4.

The esr spectra at room temperature were taken in chloroform solution at a concentration of 5×10^{-3} *M*. The frozen spectra (77°K) were obtained in: CH_2Cl_2 *plus* $CHCl_3$ (1:1) for the bromide and chloride, and benzene *plus* toluene (1:1) for the iodide. Proper choice of mixed solvent was found critically important for good resolution of the spectra in frozen solution. The number of spins in the solution at room temperature was measured by the dual cavity method[7] by comparing the integrated intensity of absorption with that of a Cu(II) solution of known concentration.

All esr spectra were recorded as the first derivative using a Varian V-4500 spectrometer with a 6-in. magnet regulated by Fieldial.

The least-square curve fitting was carried out to obtain the esr parameters from the solution spectra: the spectral shape was computed as the superposition of appropriate number of the first derivatives of Lorentzian, each with theoretical integrated intensity. The peak-to-peak width and the interval were adjusted to reproduce the experimental spectra.

The optical spectra at and below room temperature were observed in solution with a Cary-14 spectrophotometer. A cylindrical quartz cell with a jacket was used. Low temperature was obtained by passing precooled nitrogen gas through the jacket. The solvent used was $CHCl_3$ containing 10% EtOH to prevent the formation of ice from traces of water in the solvent. Because of its instability in solution at room temperature the absorption spectrum of the chloride was not observed.

Results

Esr of Powder. Malatesta and Sacco[5] reported that both bromide and iodide exist in two different forms depending upon the condition of precipitation. The green bromide and the black iodide showed a paramagnetic susceptibility attributable to approximately one spin moment. The dark green iodide was found to be diamagnetic, and the orange form of the bromide, which rapidly changes to the green form, was assumed to be diamagnetic. The chloride, the green bromide, and the black iodide showed strong, structureless signals at 77°K at room temperature with g factors near the free-spin value 2.116 (chloride), 2.088 (bromide), and 2.058 (iodide), indicating relatively little orbital contribution to magnetic moment, whereas no signal was detected from the dark green iodide.

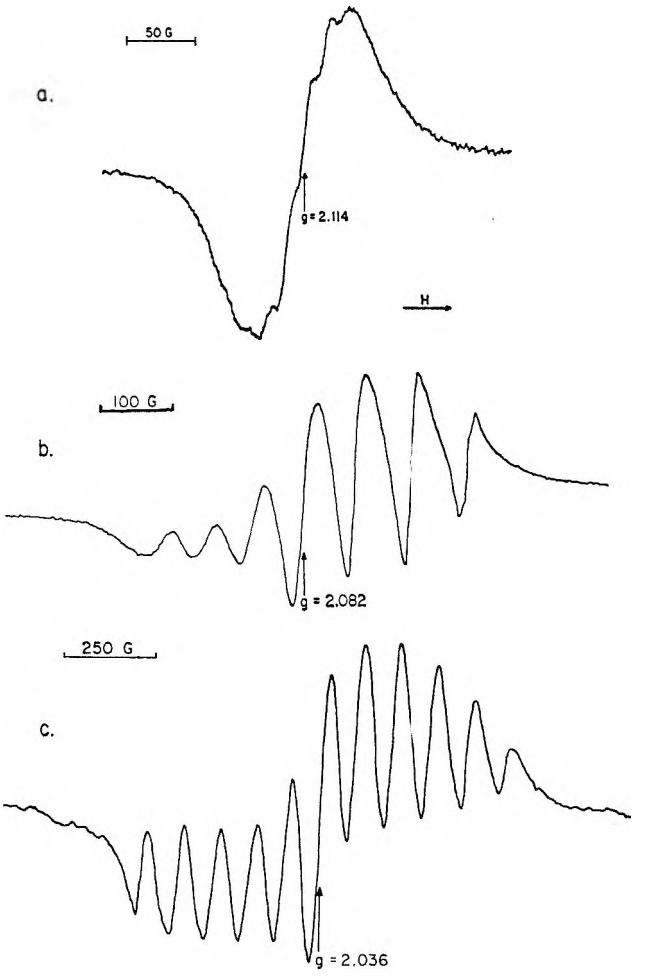


Figure 1. Esr spectra of $Co^{II}(C_7H_5N)_4X_2$ in solution at room temperature: a, chloride; b, bromide; c, iodide.

Esr of Solution. At room temperature the chloride solution in $CHCl_3$ showed a poorly resolved seven-line pattern due, probably, to the two chloride nuclei (^{35}Cl, 75.4%; ^{37}Cl, 24.6%) with $I = 3/2$ (Figure 1a). The resolution improves slightly but significantly toward higher temperature (~50°), indicating that some relatively slow averaging process is taking place. Under the

(7) W. Köhnlein and A. Müller, "Free Radicals in Biological Systems," M. S. Blois, Jr., Ed., Academic Press, New York, N. Y., 1961, p 113.

same condition the green bromide solution gave a better resolved seven-line pattern, some of the peaks showing barely discernible secondary structure (Figure 1b), while the brown iodide solution showed an eleven-line pattern with no substructure (Figure 1c). These spectra are interpreted as the hyperfine (hf) structure due to the halogen nuclei. There are two Br isotopes with almost equal nuclear magnetic moment, ^{79}Br (μ = 2.099, 50.57%) and ^{81}Br (μ = 2.2626, 49.43%), and with identical nuclear spin $I = {}^3/_2$. Thus the two equivalent Br nuclei would give a seven-line spectrum with intensity ratio of (1:2:3:4...) at low resolution. The observed secondary structure is most likely the result of superposition of three spectra corresponding to the combinations, ^{79}Br–^{79}Br, ^{79}Br–^{81}Br, and ^{81}Br–^{81}Br. The interpretation of the iodide spectrum is straightforward: the eleven lines with intensity ratio of 1:2:3:4:5:6:... are predicted from two equivalent ^{127}I with $I = {}^5/_2$, μ = 2.7937. No ^{59}Co hf structure was resolved in any of the solution spectra.

Because the iodide solutions made from either the para- or diamagnetic forms showed identical magnetic susceptibility and electric conductivity, Malatesta and Sacco[5] suggested the existence of some equilibrium between the para- and diamagnetic form in solution. Our esr spectra of $CHCl_3$ solution at 20° were found to respresent approximately 85 ± 10 and 30 ± 10% of the number of solute molecules of the bromide and the iodide complex, respectively. Furthermore, the signal intensity decreases continuously and reversibly from 55 to −46°, a fact demonstrating the equilibrium mentioned above. No attempt was made to obtain more quantitative information about the equilibrium.

Esr in Frozen Solution. On freezing at 77°K the bromide and iodide solutions changed color to brown-orange and dark violet, respectively, probably as a result of partial conversion to the diamagnetic form. No color change was observed with the chloride. All solutions showed intense resonance absorption but with no hf structure when observed in frozen single solvents such as $CHCl_3$, CH_2Cl_2, or benzene. On the other hand, very well resolved hf structures were obtained in mixed solvents, *e.g.*, $CHCl_3$ + CH_2Cl_2 (1:1).

A typical chloride spectrum is shown in Figure 2a. It shows three distinct groups of absorptions, presumably corresponding to the canonical molecular orientations, indicating that the complex has rhombic symmetry. The parallel peaks can be ascribed to the ^{59}Co (91.35 G) and the two equivalent chlorine (27.25 G) hf structures. The predicted intensity ratio is in agreement with apparent relative peak height. Also, the peaks which correspond to zero chlorine nuclear quantum number, and in which the ^{35}Cl and ^{37}Cl components should coincide, when carefully examined, show in fact narrower line widths. Each of the two perpendicular bands consists of seven peaks due to the two equivalent chlorines. There is no indication of

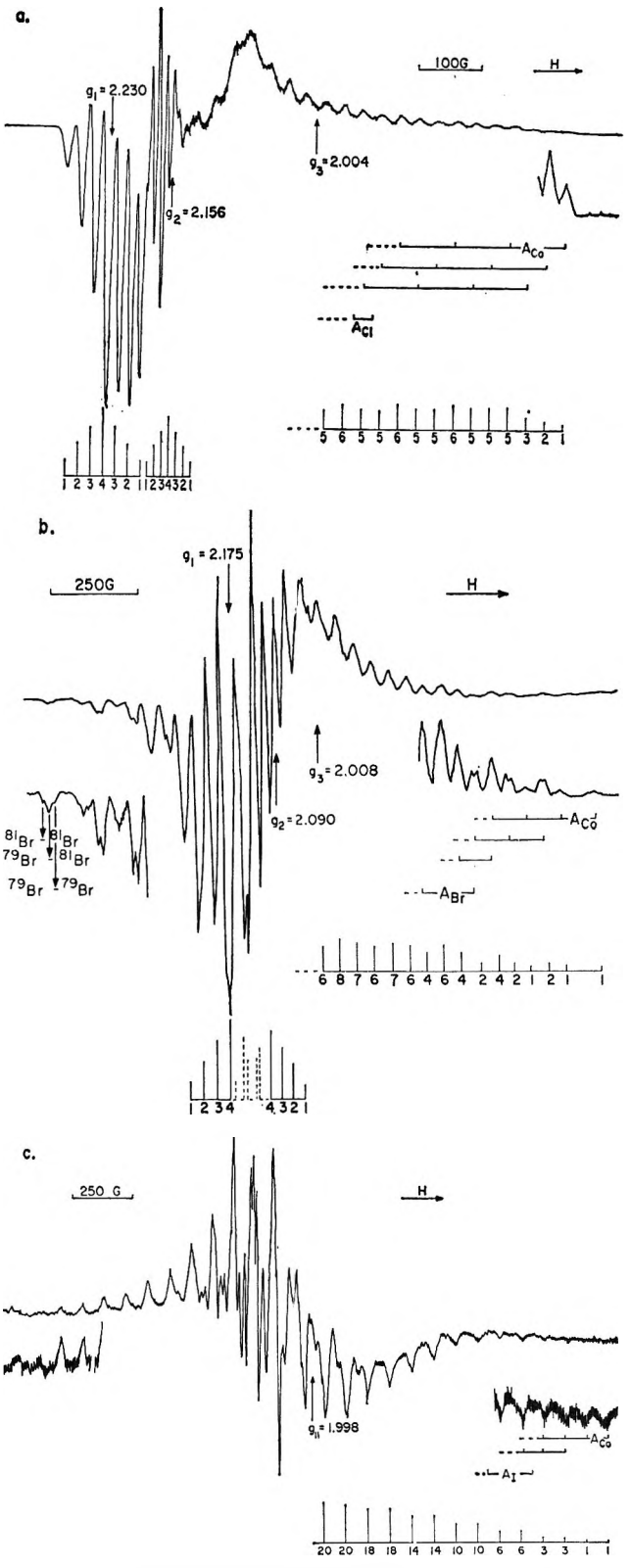


Figure 2. Esr spectra of $Co^{II}(C_7H_5N)_4X_2$ in frozen solution and the reconstructions: a, chloride; b, bromide; c, iodide.

further splitting by ^{59}Co hf interaction, the upper limit of which may, therefore, be estimated to be ~3 G.

In the frozen spectrum of the bromide solution (Figure 2b), the parallel band, which covers almost 1600 G, can be best interpreted as seven groups of hf

structure due to the two equivalent Br nuclei (I_{total} = 3), each group being further split into eight lines by a ^{59}Co ($I = {}^7/_2$) with coupling constant roughly $^2/_3$ of that of Br. Of the expected 31 lines, 25 were resolved, the rest being obscured by the overlapping perpendicular band. The ^{59}Co hf coupling constant (96.71 G) was obtained as the average of the two outermost pairs. Careful examination of the components at the higher and lower field ends of the spectrum revealed further structures which can be ascribed to the combinations, ^{79}Br–^{79}Br, ^{79}Br–^{81}Br, ^{81}Br–^{81}Br. In fact, the ratio 1.073 of the coupling constant of ^{81}Br to that of ^{79}Br obtained on this assumption agrees very well with the theoretical ratio, 1.078. The two perpendicular bands, although they partly overlap, can be analyzed analogously to the chloride spectrum: there are two superimposed seven-line patterns due to two Br nuclei and no ^{59}Co hf structures.

The frozen iodide solution in CH_3Cl + CH_2Cl_2 (1:1) gave a resolved but very weak absorption probably as the result of conversion to the diamagnetic form, whereas a much stronger signal was obtained in benzene + toluene (1:1) (Figure 2c). Evidently the higher freezing point of the latter mixture is helpful for preventing the conversion from taking place before freezing. The general aspect of the frozen pattern of iodide is similar to that of the other two, except that the perpendicular band is too complicated for analysis. The g factors and the hf coupling constants are summarized in Table I.

Optical Absorption Spectra. The temperature dependence of the visible absorption spectra in solution ($CHCl_3$ + EtOH) is shown in Figure 3. An immediately noticeable difference between the bromide and the iodide spectra is that in the iodide the absorption around 430–650 mμ, as well as the temperature dependence, is much greater than in the bromide. In the bromide spectrum the absorption at 390 and 575

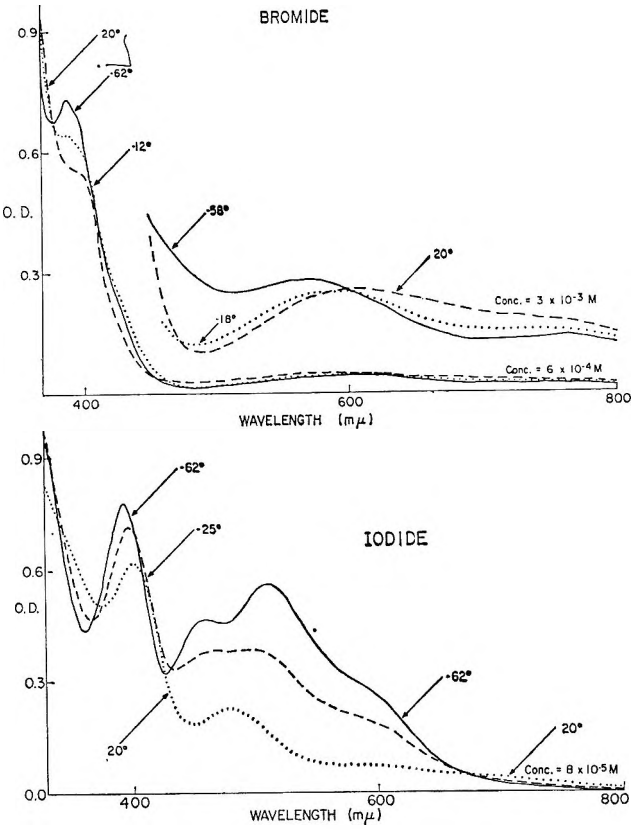


Figure 3. The temperature dependence of the visible absorption of $Co^{II}(C_7H_5N)_4X_2$ in solution; solvent, $CHCl_3$ + EtOH (5%); path length, 1 cm.

mμ increased and at around 422 mμ and in the longer wavelength region than 600 mμ the absorption decreased as the temperature was lowered, while in the iodide an increase in absorption was observed at 401- and 482-mμ bands. Below −15° the latter was split into two bands, the separation steadily becoming larger toward lower temperatures. Beyond 670 mμ the intensity also decreased in the iodide spectrum.

These reversible changes in absorption spectrum can be ascribed to the equilibrium between the para- and the diamagnetic species. The lack of exact isosbestic points, however, indicates that more than two species are involved in the equilibrium, *viz.*, the association of the paramagnetic monomer may go beyond dimerization. The observed splitting of the 480-mμ band of the iodide into 458- and 511-mμ bands, the latter becoming dominant as the temperature is lowered, could be interpreted similarly, although other possibilities are conceivable.

The weak visible absorption bands of the bromide are considered to be the d–d transitions, whereas the more intense (~30 times) bands of the iodide in the same region can be explained as charge-transfer transitions in which the filled iodide orbital and an empty d orbital may be involved. The corresponding transitions in the bromide are conceivably shifted toward shorter wavelength region because of the larger elec-

Table I: g Factors and Hyperfine Coupling Constants (in G) of $Co^{II}(C_7H_5N)_4X_2$

			Frozen state		
	g_{powder}[a]	$g_{solution}$	g_3	g_2	g_1
Chloride	2.116	2.114	2.004	2.156	2.230
Bromide	2.089	2.082	2.008	2.090	2.175
Iodide	2.058	2.036	2.005	(2.052)[b]	

			Halogen		
	$a_{solution}$	A	B_1	B_2	A_{Co}
Chloride	16	27.2	19.5	10.7	91.4
Bromide	70.0	144.6[c]	39.0	28.6	96.7
Iodide	94.5	169.0	(58.9)[d]		96.7

[a] Estimated from the crossing point of the first derivative of absorption and the base line. [b] Average of g_1 and g_2, calculated from $g_{solution}$ and g_3. [c] Average of ^{79}Br and ^{81}Br hf couplings. [d] Average of B_1 and B_2, calculated from $a_{solution}$ and A.

tronegativity of the bromine, showing only the weak d–d transitions. Since an unknown number of components are involved in the spectra, a more definite assignment is difficult.

Discussion

Unpaired Electron Orbital and Fractional Spin Transfer. Since the esr results show that the two halogen ions are coordinated equivalently and that the symmetry of the ligand field is rhombic, it would be reasonable to assume for the paramagnetic monomer a distorted octahedral structure with the isocyanides in the xy plane and the halogen ions on the z axis.

The phenyl groups of isocyanide can be either perpendicular to or coplanar with the xy plane at equilibrium positions. There are two kinds of π-molecular orbital in phenyl isocyanide, which are oriented in mutually perpendicular directions, the one (π_a) delocalized over an entire phenyl isocyanide and the other (π_b) localized on a C–N group, either of which can interact with $3d_{xy}$ or $3d_{xz}$ ($3d_{yz}$) when properly oriented. When all four phenyl groups are coplanar in the xy plane π_a orbitals would interact with $3d_{xz}$ and $3d_{yz}$ to form two out-of-plane π-molecular orbitals, and π_b and $3d_{xy}$ an in-plane π orbital. The situation will be reversed when all four phenyl groups are perpendicular to the xy plane. In any case, the molecular symmetry would be of D_{4h}. When, however, phenyl groups are alternately in and out of the xy plane, $3d_{xz}$, say, would interact with two π_a orbitals in the x direction, while $3d_{yz}$ will conjugate with π_b in the y direction; also, $3d_{xy}$ will interact with π_b and π_a, respectively, in the x and y direction. In this case the degeneracy ($3d_{xz}$, $3d_{yz}$) may be lifted and the symmetry D_{2h} would apply. The observed rhombic distortions are consistent with the last case, although other possible mechanisms (interaction with solvent) for the distortion cannot be ruled out.

The observed relation between the magnitudes of the g tensor components, *i.e.*, $g_\perp > g_{||} = 2.0023$, is in good agreement with the criterion for the unpaired electron to be in $d_{3z^2-r^2}$ orbital.[8] As will be shown, there is some spin transfer to the ligand halogen orbitals. The above criterion, which applies generally to an electron in a pure $d_{3z^2-r^2}$ orbital within the scheme of the perturbation treatment, may still be applied here, since the transfer of the unpaired electron in this case is from $d_{3z^2-r^2}$ to the halogen p_z and s orbitals, and, consequently, the matrix elements of the angular momentum operator l_z in the second-order term will vanish, making, $g_{||} = 2.0023$. The effect of the spin transfer may make some contribution to $g_\perp$, but the relation $g_\perp > 2.0023$ should be unaffected.

The molecular orbital for the unpaired electron is expressed in terms of the metal 3d and the halogen p_z and s orbitals as

$$\Psi_{3z^2-r^2} = N_\sigma\{d_{3z^2-r^2} - \alpha_\sigma(-z_1 + z_2) - \alpha_s(s_1 + s_2)\} \quad (1)$$

where the contribution from equatorial ligand σ orbitals is assumed to be negligible for the present purpose. The fractional spin transfer to the halogen p_z and s orbitals is then

$$f_\sigma = N_\sigma^2\alpha_\sigma^2; \qquad f_s = N_\sigma^2\alpha_s^2 \quad (2)$$

and

$$N_\sigma^{-2} = 1 + 2\alpha_\sigma^2 + 2\alpha_s^2 - 4\alpha_\sigma\langle 3d_{3z^2-r^2} \mid 4p_z\rangle - 4\alpha_s\langle 3d_{3z^2-r^2} \mid 4s\rangle \quad (3)$$

or

$$1 = N_\sigma^2 + 2f_\sigma + 2f_s - 4\sqrt{f_\sigma}N_\sigma\langle 3d_{3z^2-r^2} \mid 4p_z\rangle - 4\sqrt{f_s}N_\sigma\langle 3d_{3z^2-r^2} \mid 4s\rangle$$

The fractional spin transfers f_σ and f_s can be obtained from the observed halogen nuclear hyperfine components A (parallel) and B (perpendicular)

$$A = A_s + A_0 + 2A_\sigma + 2A_d$$
$$B = A_s + A_0 - A_\sigma - A_d \quad (4)$$

where A_s and A_0 are the contact terms for the valence shell and the core s orbital of halogen, respectively, A_σ is the dipolar term for the valence shell p_z electron, and A_d the direct dipole–dipole interaction between the unpaired electron in the d orbital of the metal ion and a ligand nucleus at a distance R. These are related to f_σ and f_s by

$$A_s = f_sA_s^0/2S; \qquad A_s^0 = (8\pi/3)gg_N\beta\beta_N \mid \Psi_s(0) \mid^2$$
$$A_\sigma = f_{p\sigma}A_p/2S; \qquad A_p = \tfrac{2}{5}gg_N\beta\beta_N\langle r^{-3}\rangle_p$$
$$A_0 = -f_{p\sigma}k/2S; \qquad k = gg_N\beta\beta_N\langle r^{-3}\rangle_p\kappa$$

κ is an empirical parameter called core polarization factor. The direct dipole term A_d can be approximated by the fixed dipole interaction, $A_d = gg_N\beta\beta_NR^{-3}$. Thus if the values of the relevant quantities are known, the fractional spin transfer f's can be derived from (4), and the molecular orbital determined from (2) and (3).

$|\Psi_s(0)|^2$ for chlorine and bromine was calculated by using the Roothaan–Hartree–Fock functions[9] of the appropriate orbitals for neutral atoms. The use of the neutral atomic function is based upon the more satisfactory account of the magnetic properties of octahedral complexes obtained by the covalent bonding model.[10] However, since $|\Psi_s(0)|^2$ calculated by the neutral atom functions is larger than that by the anion functions for Cl and Br by only 5.1%, the choice of the atomic functions does not cause much difference in the present case. A significant difference may result when the amount of the spin transfer is much greater. $|\Psi_s(0)|^2$ for I^- obtained[11] from the Hartree–Fock func-

(8) C. Ballhausen, "Introduction to Ligand Field Theory," McGraw-Hill Book Co., Inc., New York, N. Y., 1962, p 134.
(9) E. Clementi, *IBM J. Res. Develop.*, **9**, 2 (1965).
(10) J. Owen and J. H. M. Thornley, *Rep. Progr. Phys.*, **29**, 675 (1966).
(11) C. G. Windsor, J. H. M. Thornley, J. H. E. Griffiths, and J. Owen, *Proc. Phys. Soc.*, **80**, 803 (1962).

tion was used after the correction (5%) was made. For $\langle r^{-3} \rangle$ the values calculated by Barnes and Smith[12] were used. The core $\kappa = 0.1$ was assumed following Windsor, *et al.*[11] The overlap integrals were calculated for Cl and Br by using the minimal basis SCF atomic orbitals.[13] Similar calculation was not carried out for I because of lack of proper atomic functions. The numerical values used and the results of calculation are summarized in Table II.

Table II: The Numerical Values Used and the Results of Calculation

	Chloride	Bromide	Iodide
$\lvert\Psi_s(0)\rvert^2 \times 10^{-24}$ cm^{-3}	71.9[a]	130.8[a]	158[b]
$\langle r^{-3} \rangle_p \times 10^{-24}$ cm^{-3}	48.3[c]	91.5[c]	121.5[c]
R(Co–X), Å	2.509[d]	2.619[d]	2.827[d]
$\langle 3d_{z^2-r^2} \mid p_z \rangle$	0.095[e]	−0.0390[e]	...
$\langle 3d_{z^2-r^2} \mid s \rangle$	0.0889[e]	0.0795[e]	...
f_σ	0.075	0.135	0.130
f_s	0.012	0.018	0.013
N_σ	0.988	0.826	...
α_σ	0.276	0.444	...
α_s	0.110	0.162	...

[a] Roothaan–Hartree–Fock function, ref 9. [b] Hartree SCF function for I^- (ref 11) increased by 5%. [c] Reference 11. [d] Calculated from the crystallographic data of CoX_2 (X = Cl, Br, I). R. W. G. Wyckoff, "Crystal Structures" 2nd ed, Vol. I, Interscience Publishers, New York, N.Y., 1960. [e] Minimal basis set SCF function, ref 13.

Although the fractional spin transfer per halogen (f) is roughly twice as much here as in the high-spin CoX_6^{4-} (X = F, Cl, I) studied by Windsor, *et al.*,[11] the total transfer to the ligand is much lower in the isocyanide complexes than in CoX_6^{4-}. In fact, the spin density on Co^{2+} in the latter is 50–65% while it is more than 70% here. It must be noted that in the present treatment the effect of the ligand inner s and p orbitals is not included, the examination of the effect being outside the scope of this work. The result obtained, however, can be compared with those in other works derived by the same approximation.

^{59}Co Hyperfine Coupling. It is well known that the isotropic metal hf interaction in a transition metal complex is the result of spin imbalance (χ) in the s orbitals caused by the unpaired electron in the d shell.[14] Thus, χ normally has a negative sign and is rather insensitive to the change of electronic state of the metal ion, the actual magnitude being $2 \sim 4$ (atomic units) in many cases.[15] For Co^{2+} complexes, if we assume $\chi \simeq 3$ amu, we would expect the isotropic coupling of ~70 G, even with the reduction due to the spin transfer of 20%, whereas in none of the present complexes ^{59}Co hf structure was observed. A similar situation is found in $Co(CN)_5^{3-}$ where only a single absorption with peak-to-peak width of about 80 G was observed in liquid solution,[16,17] for which no explanation has been offered.

Characteristically in all these complexes, the perpendicular splitting, B, is much smaller than the parallel, A; in the bromide and the chloride the upper limit of the unresolved ^{59}Co perpendicular splitting is estimated from the line widths as only 5 and 3 G, respectively, while the corresponding A is 97 and 91 G. Also, $B = 28$ and $A = 87$ G in $Co(CN)_5^{3-}$.

In order to understand the reason for such small B's, the isotropic contact term ($-K$) was estimated[18] from the observed esr data by using the equations for A and B given by McGarvey.[15] In these equations the orbital contributions $L \cdot I$, which in the present cases turned out to be small, are taken into account by perturbation methods. The results (in G) are $Co(CN)_5^{3-}$, −11.6; chloride, 8.5; bromide, 17.2; iodide, 23.3, and $A > 0$, $B < 0$. The quantitative aspect of the results may not be significant. Nevertheless, it turns out that the isotropic contact term is either a very small negative value (much smaller than that expected for $\chi \simeq -3$ amu) or it can even be positive. These results clearly account for the large difference in magnitude of A and B.

The unusually small negative or the positive isotropic contact term can be best explained by direct participation of the s (mostly 4s with minor 3s and 2s contribution) orbitals. In the symmetry group assumed for the above molecules (D_{4h} or D_{2h} for the isocyanide complexes, C_{4v}[17] for $Co(CN)_5^{3-}$) the $d_{3z^2-r^2}$ and s orbitals belong to the totally symmetric representation and can mix directly in the formation of the molecular orbital. The result would be an increased positive contribution to the spin imbalance χ. Being of first order, the effect could be quite significant with a rather small fractional s character. Thus, if we ignore the 2s and 1s contribution on the ground of too low energy and if we make a reasonable assumption that the contribution of 4s and 3s would be inversely proportional to the orbital energy difference from 3d, it can be shown[19] that the inclusion of, for example, $\Psi(s) = 0.18\,\Psi_{4s} - 0.032\,\Psi_{3s}$ would be sufficient to give rise to ^{59}Co isotropic hf splitting of 100 G, which can easily override the negative spin polarization effect, −90 G

(12) R. G. Barnes and W. V. Smith, *Phys. Rev.*, **93**, 95 (1954).

(13) E. Clementi and D. L. Raimondi, *J. Chem. Phys.*, **38**, 2686 (1963).

(14) A. J. Freeman and R. E. Watson, "Magnetism," Vol. IIA, G. T. Rado and H. Suhl, Ed., Academic Press, Inc., New York, N. Y., 1965.

(15) B. R. McGarvey, *J. Phys. Chem.*, **71**, 51 (1967).

(16) J. H. Bayston, F. D. Looney, and M. E. Winfield, *Aust. J. Chem.*, **16**, 557 (1963).

(17) J. J. Alexander and H. B. Gray, *J. Amer. Chem. Soc.*, **89**, 3350 (1960).

(18) The average of the two $g_\perp$ was taken in halides. The upper limit of B estimated from the line width of the perpendicular band was used as B for the chloride and the bromide. For the iodide, in which the perpendicular band is not analyzed, B was arbitrarily assumed as 10 G. The authors are grateful to the referee for pointing out the importance of the orbital contributions in these calculations.

(19) Using the Roothaan–Hartree–Fock 3s and 4s function, and the corresponding orbital energies in $(4s)^2(3d)^6\ ^5D$ (ref 9).

(or $\chi = -3$ amu). The molecular orbital in eq 1 should then be $\Psi_{3z^2-r^2} = N_\sigma\{d_{3z^2-r^2} + 1/N_\sigma\ (0.18\ \Psi_{4s} - 0.032\ \Psi_{3s}) - \alpha_\sigma\ (-Z_1 + Z_2) - \alpha_s(s_1 + s_2)\}$. The N_σ given in Table II are not corrected for this small effect.

The participation of the metal s orbitals may be considered a general phenomenon in the complexes with $(d_{3z^2-r^2})^1$ configuration, where the fractional s character should in large part be determined by the relative heights of the s and d orbitals and, consequently, may depend on the nature of the axial ligand. The explanation may be sought along this line for the observed large variation in ^{59}Co hf parameters in Co-phthalocyanines.[1,2]

Acknowledgment. The authors are grateful to Mr. R. Shrager and Mrs. M. McNeel for the least-square curve fitting.

Photolysis of Perfluorocyclobutane

by John E. Davenport[1] and Glenn H. Miller

Department of Chemistry, University of California, Santa Barbara, California 93106 *(Received June 24, 1968)*

Perfluorocyclobutane mixed with small amounts of xenon was photolyzed using 1470-Å radiation from a xenon resonance lamp. No evidence was found for XeF_2 formation. Reaction products included CF_4, C_2F_4, C_2F_6, C_3F_6, C_3F_8, 1-C_4F_8, 2-C_4F_8, C_4F_{10}, and higher fluorocarbons to polytetrafluoroethylene. *trans*-2-C_4F_8 was the main product. A reaction mechanism is proposed to account for the experimental observations.

The 1470-Å xenon-sensitized reaction of CF_4 was studied by Dacey and Hodgins[2] in 1950. Fluorine was shown to be present in the reaction products and a quantum yield of one eliminated chain processes as possible steps leading to the assumed product polytetrafluoroethylene. The only other reported photolysis of a perfluoroalkane was the preliminary note by Miller and Dacey[3] on the photolysis of perfluorocyclobutane. This work indicated the presence of XeF_2 and a dimer as important reaction products.

The mercury-sensitized photolyses of tetrafluoroethylene,[4,5] perfluoropropene,[6] and *cis*- and *trans*-2-perfluorobutene[7] have been reported as well as the thermal decomposition of perfluorocyclobutane[8] and tetrafluoroethylene.[9,10]

The purpose of the present investigation was to confirm the presence or absence of XeF_2 as a reaction product or intermediate in the xenon-photosensitized photolysis of perfluorocyclobutane and to elucidate the reaction mechanism.

Experimental Section

Equipment. The vacuum system was of conventional design and utilized an oil diffusion pump, ionization gauge, and Teflon stopcocks with Viton O rings. Two arrangements were used for the reaction system; both, however, utilized the xenon resonance lamp and reaction chamber previously described.[11]

In the first arrangement, the reaction system consisted of a closed loop containing the reaction cell, lamp, an induction-operated circulating pump (Teflon bearings), a Wallace–Tiernan pressure gauge (Model FA-141), U-trap, and a KBr-windowed 10-cm infrared cell. The latter was positioned in the beam of a Beckman IR-10 spectrometer. Product samples were condensed and transferred for mass spectrographic analysis.

In the second arrangement, the infrared cell was replaced with a vpc sampling valve (Teflon stopcocks) by means of which a sample could be isolated and passed directly from the reaction loop into the column of the chromatography apparatus. The 90-P3 Aerograph gas chromatograph was equipped with a Sargent SR

(1) Taken in part from a dissertation presented to the Graduate Division, UCSB, in partial fulfillment of the requirement for the M.A. degree.

(2) J. R. Dacey and J. W. Hodgins, *Can. J. Res.*, **28B**, 173 (1950).
(3) G. H. Miller and J. R. Dacey, *J. Phys. Chem.*, **69**, 1434 (1965).
(4) B. Atkinson, *J. Chem. Soc.*, 2684 (1952).
(5) J. Heicklen, V. Knight, and S. A. Greene, *J. Chem. Phys.*, **42**, 221 (1965).
(6) J. Heicklen and V. Knight, *J. Phys. Chem.*, **69**, 3600 (1965).
(7) D. Saunders and J. Heicklen, *ibid.*, **69**, 3205 (1965).
(8) B. F. Gray and H. O. Pritchard, *J. Chem. Soc.*, 1002 (1956).
(9) B. Atkinson and V. A. Atkinson, *ibid.*, 2086 (1957).
(10) B. Atkinon and A. B. Trenwith, *ibid.*, 2082 (1953).
(11) G. H. Miller and J. R. Dacey, *Rev. Sci. Instrum.*, **36**, 1041 (1965).

recorder, disk integrator, and fraction collector to remove samples for mass spectrographic analysis. The total volume of the reaction loop was 285 ml.

The ambient temperature was 23°, the temperature of the reaction chamber about 150°, and the surface of the lamp was estimated to be approximately 240°; thus during the photolyses the cell had a temperature gradient from 23° on the outer wall to 240° on the lamp window.

Several chromatography columns were used; all were constructed from 1/4-in. copper tubing. Column A, 20 ft, consisted of $CH_2{=}CHCO_2CH_2(CF_2CF_2)_3H$[12] on Chromosorb W. It was prepared as previously described[13] and operated at 0°. Column B was a 1-m, 40–60 mesh silica gel column operated at 200°. Column C was a tandem arrangement consisting of column A plus a 1-m squalane on silica gel section. Helium at 60 cc/min was used as the carrier gas.

Table I: Summary of Experiments

Expt no.	Initial pressures,[a] Torr Xe	Initial pressures,[a] Torr c-C_4F_8	Reaction time, min	Final pressures,[a] Torr Xe	Final pressures,[a] Torr c-C_4F_8	Analysis
2	0.32	31.28	5600	Total 16.09		Ir
3	trace	10.51	1040	Total 9.35		Ir
4	12.42	18.78	1501	Total 24.73		Ir
5	6.90	28.61	76	Total 33.98		Vpc column A
6	15.10	11.73	20	Total 26.80		Vpc column A
7	3.56	31.32	90	Total 34.80		Vpc column A
8	0.18	35.07	97	Total 35.20		Vpc column A
11	0.22	17.62	50	Total 18.20		Vpc column A
12	0.13	25.57	1987	Total 17.25		Vpc column A
13	1.2	28.6	246	Total 27.30		Vpc column A
14	3.01	22.43	5	3.0	21	Vpc column B
15	3.03	22.61	10	3.0	20.8	Vpc column B
16	3.01	22.7	20	3.0	18.2	Vpc column B
17	3.01	22.60	33	3.1	18.9	Vpc column B
18	3.01	22.66	35	3.2	22.2	Vpc column B
19	3.29	26.72	20	3.1	25.6	Vpc column B
21	3.29	30.01	60	3.3	24.1	Vpc column B
22	3.34	22.72	32	3.3	22.6	Vpc column C
23	3.29	26.75	50	3.29	26.1	Vpc column C
24	3.29	26.70	62	3.34	26.0	Vpc column C
25	3.31	26.93	40	...	25.9	Vpc column C
26	3.31	26.99	585	3.3	17.4	Vpc column C
27	3.34	27.21	10	3.32	26.9	Vpc column C
28	3.34	27.21	20	3.34	26.0	Vpc column C
29	3.35	27.24	95	3.36	25.58	Vpc column C
30	3.34	27.24	125	3.35	25.0	Vpc column C
31	3.34	27.23	20	3.33	26.8	Vpc column C
32	3.34	27.23	303	3.35	23.2	Vpc column C
33	3.01	27.00	7194	Total 16.20		Vpc column C
34	0.78	29.26	1000	Total 21.4		Vpc column C
35	0.80	29.26	2840	...		
36	0.51	18.78	15	0.51	18.70	Vpc column C
37	0.51	18.79	31	0.51	18.74	Vpc column C
38	0.52	18.92	45	9 52	18.37	Vpc column C
39	0.51	18.79	60	0.51	18.51	Vpc column C
40	0.53	19.39	100	0.53	18.37	Vpc column C

[a] Partial pressures were determined from vpc data.

Perfluorocyclobutane from Columbia Organic Chemicals Inc. was purified by bulb-to-bulb distillation. The ms and vpc analyses showed no detectable impurities. Airco ultrapure xenon was used without further purification.

Experimental Results and Techniques

Table I contains a summary of the reported experiments. Experiments 2, 3, and 4 were made with the ir cell as part of the reaction system loop. The system was evacuated to less than 10^{-6} Torr, the gases were admitted from their storage bulbs, the lamp was turned on, and after thermal equilibrium was established the total pressure was followed as a function of time. Typical total pressure–time curves are shown in Figure 1. The

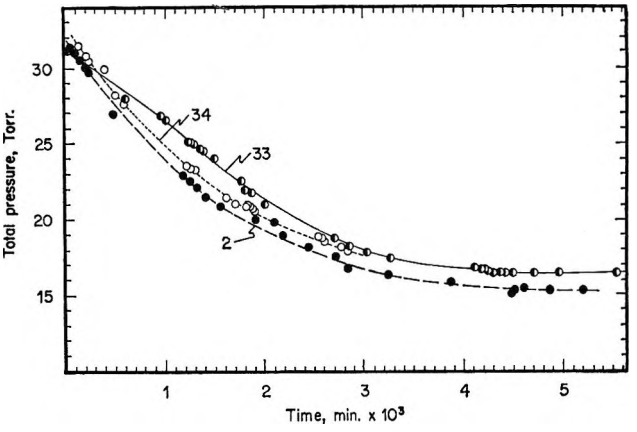


Figure 1. Total pressure of reaction system as a function of time for experiments 2, 33, and 34.

lamp had to be turned off and the reaction interrupted to obtain ir spectra; all attempts to shield the spectrograph from microwave interference were unsuccessful. No ir absorption peaks due to XeF_2 were observed. The peaks previously believed to be due to XeF_2 were shown to originate from various fluorocarbons in the reaction product mixture.

For all the remaining experiments the ir cell was replaced by the vpc sampling valve arrangement. Experiments 5–13 were made to determine the composition of the reaction product mixture. Following a run the total product was collected in the liquid nitrogen cooled trap of the valve system and after warming to room temperature it was passed directly into the vpc column. The pressure due to noncondensables never exceeded 0.5 Torr.

A total of 47 vpc peaks were observed for experiment 12 over a total elution time of 920 min. Xenon, C_2F_6, C_2F_4, C_3F_8, C_3F_6, c-C_4F_8 (8.7 min), C_4F_{10}, *trans*-2-C_4F_8 (14.8 min), and C_5F_{12}'s were identified. Additional major product peaks (relative areas greater than 6000, compared to *trans*-2-C_4F_8 at 30,800) were observed at elution times of 34.0, 35.1, 37.8, 338, and 685 min.

(12) Courtesy of the E. I. Dupont de Nemour and Co.

(13) S. A. Greene and F. M. Wachi, *Anal. Chem.*, **35**, 928 (1963).

Other product peaks with relative areas greater than 2000 were eluted after 43, 104, 115, 137, 380, 470, and 500 min.

For experiments 13–40 the Xe and c-C_4F_8 were premixed and stored in a glass storage bulb. The vpc column was calibrated with known amounts of Xe and c-C_4F_8 and the partial pressures of these gases were determined quantitatively before and after the reaction. Within experimental error no loss of xenon was observed. Photolyses were made for various lengths of time in order to obtain plots of c-C_4F_8 disappearance as a function of time; several of these are shown in Figure 2.

Attempts were made to obtain the quantum yield for c-C_4F_8 disappearance by using CO_2 actinometry. The method, however, is subject to many restrictions and the results can only be considered approximate. The values obtained varied from 0.75 to 1.5.

Exposure of c-C_4F_8 to a helium discharge in the same apparatus produced no pressure change. Thus, thermal decomposition of c-C_4F_8 did not occur on the lamp window.

Calibration of the vpc column with available fluorocarbons gave the following relative partial pressures for the listed reaction products: *trans*-2-C_4F_8 > C_2F_6 > C_3F_8 > C_4F_{10} > C_2F_4 ≃ 1-C_4F_8 ≃ C_3F_6 > individual higher molecular mass products. Some free carbon was found and polytetrafluoroethylene was identified by ir analysis.

CF_4 production was followed by observing an ir absorption peak. The concentration of CF_4 increased rapidly during a photolysis to a relatively high partial pressure and then decreased slowly. These data are shown in Figure 3.

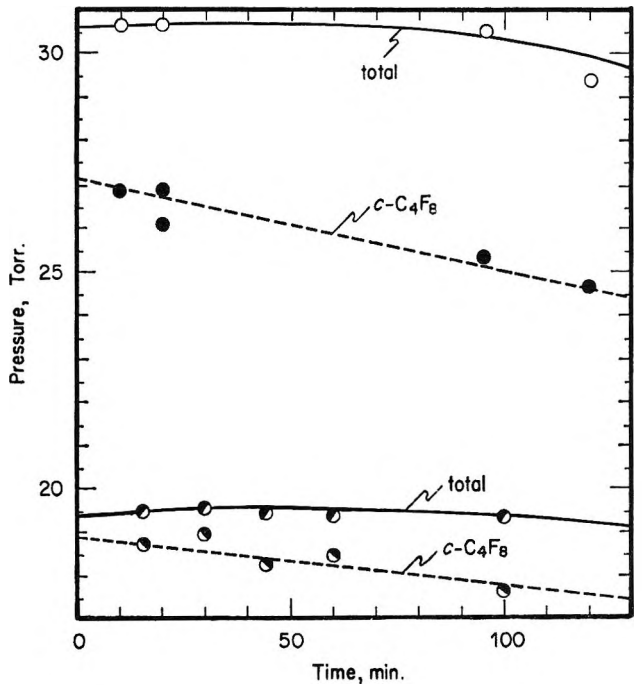


Figure 2. Total and c-C_4F_8 pressures for experiments 27–31 (top) and experiments 36–40 (bottom).

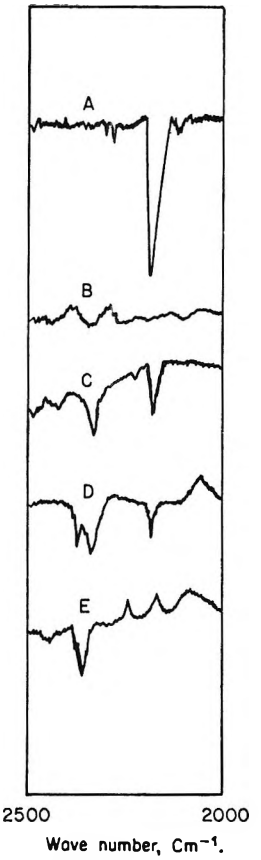


Figure 3. Infrared spectra of CF_4. A, 10.4-Torr standard CF_4 sample; B, Xe and c-C_4F_8 at start of reaction C, reaction mixture after 189 min; D, after 1202 min; E, after 1925 min.

Separate photolysis experiments showed that *trans*-2-C_4F_8 is photolyzed directly by 1470-Å radiation. These results will be presented in a separate communication.

Discussion

On the basis of the above experimental results it is possible to propose a tentative mechanism for the c-C_4F_8 photolysis. The initial step is undoubtedly

$$Xe^* + c\text{-}C_4F_8 \longrightarrow Xe + c\text{-}C_4F_8^* \qquad (1)$$

followed by

$$c\text{-}C_4F_8^* \longrightarrow (-CF_2CF_2CF_2CF_2-)^* \begin{cases} \xrightarrow{a} CF_3CF{=}CFCF_3 \\ \xrightarrow{b} CF_2 + CF_3CF{=}CF_2 \\ \xrightarrow{c} 2C_2F_4 \\ \xrightarrow{d} 4CF_2 \end{cases} \qquad (2)$$

Step a is favored. *trans*-2-C_4F_8 is the major product. Also, there is no overall pressure decrease during the initial stages of the reaction, Figure 2, but actually a slight pressure increase due to fragmentation reactions which precede polymerization. During this time,

c-C_4F_8 is being converted to 2-C_4F_8 and the overall pressure decrease occurs only when the latter is photolyzed and polymerization reactions become important.

Photolysis of the 2-C_4F_8 produces CF_3CF species

$$2\text{-}C_4F_8 \longrightarrow (2\text{-}C_4F_8)^* \longrightarrow 2CF_3CF \qquad (3)$$

These react as

$$2CF_3CF \longrightarrow C_4F_8 \qquad (4)$$

$$CF_3CF \longrightarrow C_2F_4 \qquad (5)$$

$$CF_3CF \xrightarrow{\text{wall}} CF_4 + \text{carbon} \qquad (6)$$

Dalby[14] in his study of CF_2 reactions assumed that no CF_3CF radicals rearranged to C_2F_4; however, Heicklen and Knight[6] have proposed this reaction for some energetic state of CF_3CF.

Step 6 accounts for the formation of CF_4 and free carbon. The decrease in CF_4 partial pressure during photolysis can be explained by assuming this reaction to be dependent on available wall space; large areas are available at the beginning of the reaction, but as other products are formed and adsorbed the available space decreases. CF_4 also disappears by photolysis[2]

$$CF_4 + Xe^* \longrightarrow CF_2 + F_2 + Xe \qquad (7)$$

Polymer is formed by polymerization of $C_2F_4^*$ species

$$nC_2F_4^* \longrightarrow (C_2F_4)_n \qquad (8)$$

and not by combination of CF_2 radicals since the preferred reaction is the recombination of CF_2 radicals to form C_2F_4.

The formation of the major products C_2F_6, C_3F_8, and other saturated fluorocarbons is more difficult to explain. It is doubtful if sufficient free fluorine from reaction 7 is present. A reaction analogous to the formation of CF_3 radicals from perfluoroisobutene proposed by Atkinson[9]

$$CF_3C(CF_3)=CF_2 \longrightarrow CF_3 + CF_3CF=CF$$

might occur

$$CF_3CF=CFCF_3 \longrightarrow CF_3 + CF_3CF=CF \qquad (9)$$

This would be followed by

$$2CF_3 \longrightarrow C_2F_6$$

$$CF_3 + CF_2 \longrightarrow C_2F_5$$

$$C_2F_5 + CF_3 \longrightarrow C_3F_8 \text{ etc.} \qquad (10)$$

It is necessary to assume the presence of either free fluorine, CF_3 radicals, or both to account for the products. Further speculation concerning the reaction mechanism must await additional experimental evidence.

Acknowledgment. We wish to thank the National Science Foundation (Grant GP-4346) for support of this work.

(14) F. W. Dalby, *J. Chem. Phys.*, 41, 2297 (1964).

Localized Adsorption on Graphite and Absolute Surface Areas

by Conway Pierce

Department of Chemistry, University of California, Riverside, California 92502 *(Received July 5, 1968)*

Adsorption isotherms for C_6F_6 on a graphitized carbon black appear to lend support to the hypothesis that a six-carbon aromatic ring adsorbs at localized graphite lattice positions. The C_6F_6 isotherms, like those for C_6H_6, are concave to the p axis up to completion of a localized monolayer but at this point there is an abrupt change to a convex shape and there appears to be a transition from localized to mobile adsorption up to completion of a tightly packed first layer. The cross sections computed with reference to a benzene cross section of 47.2 Å^2 are in agreement with predictions from scale models in both localized and mobile arrangements. It is shown that a benzene cross section of 47.2 Å^2 is an absolute value, based on lattice dimensions only. Using this standard it is established that (1) the accepted value of 16.2 Å^2 as the cross section for the N_2 molecule in a close-packed monolayer is correct and (2) that at the apparent monolayer point for nitrogen adsorption on graphite the effective area is 19.3 Å^2. Apparent nitrogen areas for graphites should therefore be increased by the factor 1.19.

Previously the writer noted[1] that when nitrogen is adsorbed on graphitized carbon blacks the BET or point B monolayer volume is less than the one computed by application of the universal nitrogen isotherm to adsorption in the multilayer region. This raised doubts concerning surface areas based upon the apparent nitrogen monolayer volume and the assumption that there is normal packing at V_m. Further work[2-4] indicated that at the monolayer point the N_2 molecules are apparently localized at lattice positions so that the cross section is somewhat greater than the normal value for a close-packed monolayer. When adsorption is carried past the V_m point it appears that additional molecules crowd into the first layer and there is a change from a localized to a mobile condition. This additional adsorption in the first layer leads to a step-like rise in the N_2 isotherm in the relative pressure region between 0.2 and 0.4.

Later it was observed[5,6] that the adsorption of benzene on uniform surface graphites gives isotherms with unusual properties. These are (1) the concave shape throughout the submonolayer region, (2) lack of lateral interactions between first layer molecules as the surface population increases, (3) isotherms for different temperatures (below the normal melting point) superimpose when plotted as relative pressures, and (4) the monolayer volume is independent of temperature over a wide range. To explain these unique features for benzene it was postulated that the six-carbon ring is localized at preferred lattice positions.

When the suggestion was first made that six-carbon aromatic rings are held at preferred positions on a graphite lattice, there was no precedent for assuming such an arrangement other than the fact that there are such localizations in alternate layers of graphite itself, with the unit hexagons of a given layer centered above C atoms of the next layer. Recently, however, it has been found that similar arrangements prevail in equimolar π-molecular compounds containing aromatic rings. One such, the compound of naphthalene with pyromellitic dianhydride, has been shown[7] to consist of alternate layers at a mean separation of 3.23 Å, with the aromatic rings of each layer centered opposite C atoms of the adjacent one (the graphite structure). It seems logical to assume, therefore, that a similar arrangement will prevail in an adsorbed layer of aromatic molecules on a graphite surface, since the layer separation is approximately the same as that found in the naphthalene compound.

The localization hypothesis appeared to provide self-consistent explanations for the adsorption of benzene and nitrogen by graphite but the results with these two alone are still somewhat inconclusive. Further studies have therefore been made with another aromatic compound, hexafluorobenzene, whose physical properties are very similar to those of benzene[8] but whose molecules have larger cross sections. The results of these studies provide additional evidence in support of the previous assumptions.

Experimental Section

Details of the isotherm measurements using diaphragm gauges[9] to determine pressures have been given previously.[10] The original Series 78 gauges with ranges of 3 and 30 Torr have been replaced by all-

(1) C. Pierce, *J. Phys. Chem.*, **63**, 1076 (1959).
(2) C. Pierce, *ibid.*, **64**, 1184 (1960).
(3) C. Pierce and B. Ewing, *J. Amer. Chem. Soc.*, **84**, 4070 (1962).
(4) C. Pierce and B. Ewing, *J. Phys. Chem.*, **68**, 2562 (1964).
(5) B. W. Davis and C. Pierce, *ibid.*, **70**, 1051 (1966).
(6) C. Pierce and B. Ewing, *ibid.*, **71**, 3408 (1967).
(7) J. C. A. Boeyens and F. H. Herbstein, *ibid.*, **69**, 2153, 2160 (1965).
(8) W. T. Plummer and L. A. Wall, *J. Chem. Eng. Data*, **6**, 76 (1961).
(9) MKS Instruments, Inc., Burlington, Mass.
(10) C. Pierce, *J. Phys. Chem.*, **72**, 1955 (1968).

welded Series 90 sensors (with ranges of 10 and 100 Torr, respectively) in order to permit use of organic vapors which might attack O-rings of the older model sensors and to increase the available pressure ranges of measurements.

The adsorbent, designated MTg, is the same 6.3-g sample of Sterling MT (3100°) used in previous work. The conventional nitrogen area is 7.65 m^2/g if $\sigma(N_2)$ is assumed to be 16.2 Å^2 but as previously shown,[4,6] 9.1 m^2/g is preferred.

The sample[11] of C_6F_6 used was purified in a glpc preparative column and showed no side peaks when tested by an analytical column. Isotherms were measured at two temperatures, 0 and −17.75°, both of which are below the bulk melting point. At these temperatures p_0 values for C_6F_6 are 19.6 and 4.22 Torr, respectively, and for C_6H_6 are 23.9 and 5.75 Torr. Heats of sublimation computed from these are 11.9 kcal/mol for C_6F_6 and 11.1 for C_6H_6.

Isotherms for benzene and hexafluorobenzene at 0 and −17.75° are shown in Figure 1. Also given are a few points for a C_6H_6 isotherm at 20°. These points were measured in order to permit comparison of the data with those given by Isirikyan and Kiselev[12] at this temperature, as an independent check for accuracy. In the pressure region attainable with our equipment the agreement was very close, an indication that both isotherms are accurate in the absolute amounts adsorbed. The fact that the 20° points of Figure 1 lie so close to the isotherms for much lower temperatures is surprising, especially so since the latter are below the melting point and the former above it. This behavior too is indicative of adsorption at localized sites.

Results and Discussion

Comparison of the C_6F_6 and C_6H_6 isotherms of Figure 1 shows the following similarities (1) both sets of isotherms are concave to the p axis throughout the submonolayer region, (2) isotherms at different temperature coincide up to the V_m point, which shows that heats of adsorption for first layer molecules are identical with heats of sublimation, and (3) the V_m values are independent of temperature (V_m for C_6F_6 appears to be near 22 μmol/g, the point at which isotherms for different temperatures diverge from one another). These similarities in isotherms indicate that in the first layer C_6F_6 molecules are localized at lattice positions in the same way as C_6F_6 molecules.

After completion of a localized first layer the C_6F_6 isotherm becomes entirely different from that for C_6H_6. Instead of flattening out as the C_6H_6 isotherm does, the C_6F_6 isotherm changes from a concave shape to one that is convex to the p axis and there is a sharp rise of the type associated with lateral interaction effects in mobile adsorption. The separation for isotherms at two temperatures, which occurs at this point, shows that there is now an increase in the heat of adsorption.

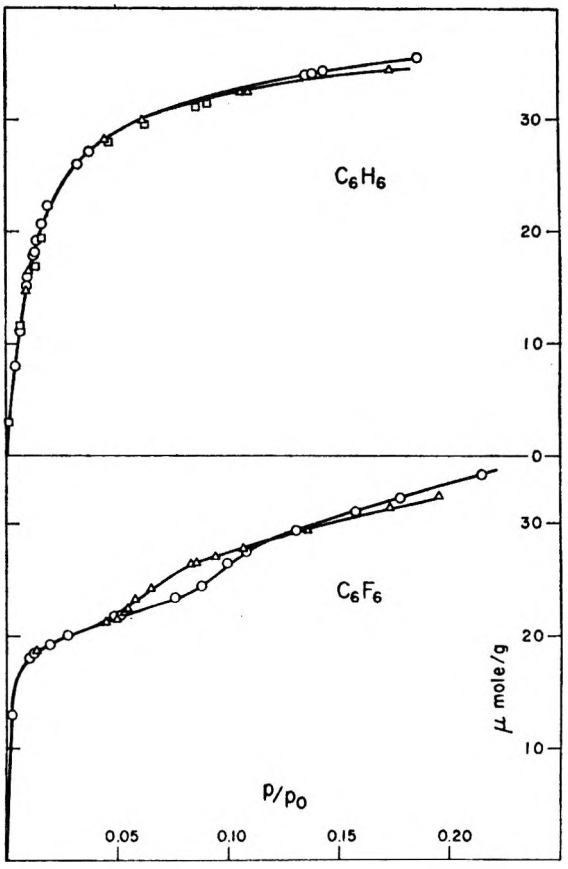


Figure 1. Isotherms for adsorption of C_6H_6 (upper) and C_6F_6 (lower) on graphitized carbon black at 0°, circles, and −17.75°, triangles. The points shown as squares for C_6H_6 are at 20°.

The convex region of the isotherm is followed by a well-defined point B that apparently marks completion of the first layer. At this point isotherms for the two temperatures cross and thereafter adsorption in the multilayer region shows the same type of temperature dependence as previously noted for benzene, with an increase in adsorption as the temperature is raised. This effect, which now appears to be quite common for multilayer adsorption at temperatures where the bulk adsorbate is a solid, is attributed to the fact that the first layer molecules on which further crystallization occurs are often not in the same orientation or spacing as the molecules in a crystal surface and consequently an increase in temperature, which increases thermal disorder, may facilitate a more ready accommodation of molecules deposited on the surface layer.

The convex portion of the isotherm suggests that the initially localized adsorption is followed by a change to mobile adsorption with lateral interactions as additional molecules crowd into the first layer. Thus there appear to be two well defined V_m points in the C_6F_6 isotherm, the first at 22 μmol/g for a localized monolayer and the second at 28 μmol/g, the

(11) We wish to thank Professor Corwin Hansch, Pomona College, Claremont, Calif., for providing the purified sample.

(12) A. A. Isirikyan and A. V. Kiselev, *J. Phys. Chem.*, 65, 601 (1961).

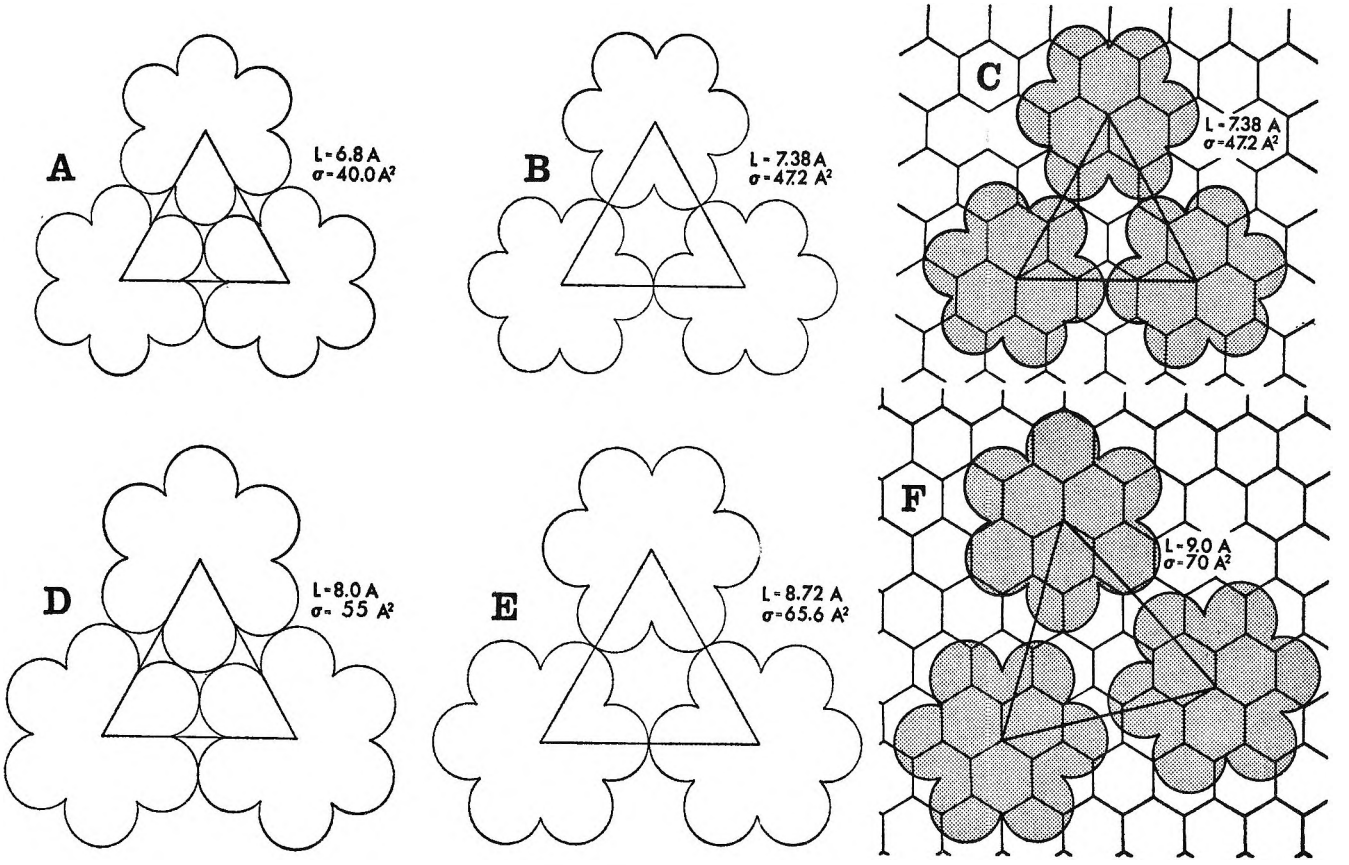


Figure 2. Packing arrangements of models. C_6H_6, close packed (A), with free rotation (B), localized on graphite (C); C_6F_6, close packed (D), with free rotation (E), and localized on graphite (F). Values of L and σ are shown for each arrangement.

point where the 0 and $-17.75°$ isotherms cross and the mobile monolayer is completed.

This isotherm is the first one we know of to demonstrate so clearly a dual adsorption in filling of the first layer. It was previously postulated[4] that there is such a change from localized to mobile first layer adsorption of nitrogen by graphite but the isotherm itself does not show the two regions as distinctly as we find for the present one. Instead it appears that in N_2 adsorption the mobile first layer is not completed until there is also a considerable amount of adsorption in the second layer, for in the V–n plot of Figure 3 the isotherm points fall below the straight line portion until the number of statistical layers is near 1.6. (The significance of this plot is discussed later.) The C_6F_6 isotherm indicates that a localized monolayer is essentially completed before there is a change to mobile adsorption and that in turn the mobile monolayer is completed before there is any significant amount of adsorption in the second layer.

With the additional evidence from the C_6F_6 data we are now in a position to examine the localization hypothesis more critically, for we have three sets of data for comparison and two separate V_m points for C_6F_6. The various V_m points are first used to compute relative cross sections on the assumptions that either (1) $\sigma(C_6H_6)$ is 47.2 Å^2 as deduced from the localization theory or (2) that $\sigma(N_2)$ is 16.2 Å^2. The relative values obtained in this way are then compared with calculations from scale models in various assumed packing arrangements. The isotherm V_m values used, each expressed as micromoles per gram of MTg, are 78 for N_2, 32 for C_6H_6, 22 for C_6F_6 when localized, and 28 when in a close-packed mobile layer.

When the standard is assumed to be 47.2 Å^2 for C_6H_6 we have

$$\sigma(N_2) \times \frac{32}{78} \times 47.2 \text{ Å}^2 = 19.3 \text{ Å}^2$$

$$\sigma(C_6F_6 \text{ localized}) = \frac{32}{22} \times 47.2 \text{ Å}^2 = 69 \text{ Å}^2$$

$$\sigma(C_6F_6 \text{ mobile}) = \frac{32}{28} \times 47.2 \text{ Å}^2 = 54 \text{ Å}^2$$

The values based on 16.2 Å^2 for N_2 are

$$\sigma(C_6H_6) = \frac{78}{32} \times 16.2 \text{ Å}^2 = 39.5 \text{ Å}^2$$

$$\sigma(C_6F_6 \text{ localized}) = \frac{78}{22} \times 16.2 \text{ Å}^2 = 58 \text{ Å}^2$$

$$\sigma(C_6F_6 \text{ mobile}) = \frac{78}{28} \times 16.2 \text{ Å}^2 = 45 \text{ Å}^2$$

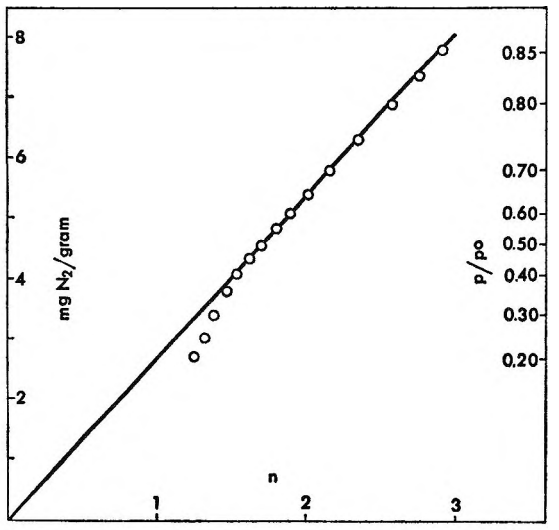


Figure 3. V–n plot for adsorption of N_2 on MTg.

Two-dimensional scale models constructed for C_6H_6 and C_6F_6 molecules using covalent radii from Pauling[13] and van der Waals radii from Bondi[14] give for r, the distance from the center of the ring to the outer edge of the H or F atom

$$r(C_6H_6) = 1.40\ \text{Å} + 0.77\ \text{Å} + 0.32\ \text{Å} + 1.20\ \text{Å} = 3.69\ \text{Å}$$

$$r(C_6F_6) = 1.40\ \text{Å} + 0.77\ \text{Å} + 0.72\ \text{Å} + 1.47\ \text{Å} = 4.36\ \text{Å}$$

Three different packing arrangements of these models, all based on a six-neighbor arrangement, are shown to scale in Figure 2. With each arrangement there are shown L, the center-to-center distance and σ, the cross section for this L value.

We see by comparing these figures from the models with the relative values given above that there is good agreement with the cross sections for C_6F_6 that are based on 47.2 Å^2 for C_6H_6. For a localized arrangement we find a cross section of 70 Å^2 *vs.* 69 Å^2 from the V_m value and for mobile we have 55 Å^2 *vs.* 54 Å^2 from the V_m value. The N_2 cross section on this basis is 19.3 Å^2. On the other hand, when $\sigma(N_2)$ is taken as 16.2 Å^2 the C_6F_6 value for the mobile monolayer is an impossibly small one of 45 Å^2. We see no way to reconcile such an area with scale models unless the molecules are tilted on the surface, an orientation that does not seem probable in view of the fact that the heat of adsorption is 11.9 kcal/mol, which is identical with the heat of sublimation. We feel therefore that the assumption of a localized model for C_6H_6 with a cross section of 47.2 Å^2 is correct and that consequently the apparent nitrogen areas of graphitized carbon blacks should be increased by the factor 19.3 Å^2/16.2 Å^2 or 1.19.

Analysis of the nitrogen isotherm for graphite by a V–n plot, as described previously,[15] leads to the same conclusion regarding the graphite area. When the volume adsorbed in plotted *vs.* n ($n = V/V_m$, or the number of statistical layers at given relative pressures) the plot normally yields a straight line which passes through the BET V_m and whose slope V/n is another measure of V_m. This line should, if correct, pass through the origin when extrapolated back to $V = 0$. A V–n plot for the nitrogen isotherm of MTg is shown in Figure 3, based upon isotherm data from four different laboratories. The points above $n = 1.6$ do fall on a linear plot which extrapolates to the origin. This fit shows that in the region where the points fit the standard n values the first layer cross section for the N_2 molecule must be the same as that on other surfaces. Below $n = 1.6$ the points fall below the straight line and at the apparent V_m point the amount adsorbed is less than predicted from the slope of the line. Taking V_m from the slope of the plot gives a value of 2.62 mg of N_2/g while the point B V_m (not shown here) is 2.19 mg of N_2/g. The ratio in the two is 1.19, the same as the figure we obtained from benzene adsorption.

The fact that 47.2 Å^2 for $\sigma(C_6H_6)$ on graphite is an absolute[16] value provides a means for testing the commonly used $\sigma(N_2)$ of 16.2 Å^2. This figure, first established by Emmett and Brunauer[17] in 1937, has become the recognized standard for area measurements, even though its validity has from time to time been questioned. As shown in the V–n plot of Figure 3, V_m for mobile adsorption of N_2 on MTg is 2.62 mg/g or 93.6 μmol/g. The value for C_6H_6 is 32 μmol/g. These give

$$\sigma(N_2) = \frac{32}{93.6} \times 47.2\ \text{Å}^2 = 16.1\ \text{Å}^2$$

which agrees within experimental error with the cross section computed from the liquid density. This value, incidentally, is also in agreement with estimates made from scale models. Using the atomic radii cited above gives

$$\text{length of } N_2 \text{ molecule} = 2 \times 0.55\ \text{Å} + 2 \times 1.60\ \text{Å} = 4.30\ \text{Å}$$

If a hexagonal packing with center-to-center distances equal to this length is assumed, the cross section is

$$\sigma(N_2) = \frac{\sqrt{3}}{2}(4.30)^2 = 16.1\ \text{Å}$$

(13) L. Pauling, "The Nature of the Chemical Bond" Cornell University Press, Ithaca, N. Y., 1960.

(14) A. Bondi, *J. Phys. Chem.*, **68**, 441 (1964).

(15) C. Pierce, *ibid.*, **72**, 3673 (1968).

(16) Because it is based on the C–C distances in the basal plane of graphite instead of the relative value compared to another molecular. See ref 6.

(17) P. H. Emmett and S. Brunauer, *J. Amer. Chem. Soc.*, **59**, 1553 (1937).

It must be concluded, therefore, that in normal surface packing each molecule is free to rotate on the surface independently of its neighbors.

Acknowledgment. This research was supported in part by grants from the Petroleum Research Fund administered by the American Chemical Society and from the Intramural Research Funds of the University of California. Grateful acknowledgment is made to the donors of both these funds.

An Electron Spin Resonance Study of Radiation-Induced Centers of Chemical Activity in a Silica–Alumina Gel

by Robert R. Hentz and Dennis K. Wickenden

Department of Chemistry and the Radiation Laboratory,[1] University of Notre Dame, Notre Dame, Indiana 46556
(Received July 10, 1968)

The esr spectrum of a γ-irradiated silica–alumina gel has a line 44.5 ± 0.5 G wide at $g = 2.0088 \pm 0.0005$ which is partially resolved into six components separated by 8.5 ± 0.2 G; superimposed on this broad line is a narrow line at $g = 2.0010 \pm 0.0005$. The broad line is identified with a positive hole trapped at an aluminum atom present substitutionally in the silica matrix. The narrow line is attributed to an electron trapped at one of several kinds of oxygen vacancies and seems to result from a reaction of H atoms. An appreciable number of electrons are trapped in such a manner as to be undetectable in the esr spectrum. At large doses, the positive-hole intensity reaches a limiting value that corresponds to 16×10^{17} spins/g; such a value is comparable with a previously determined value of 13×10^{17} centers/g as the limiting yield of radiation-induced centers of chemical activity. On exposure of irradiated solid to each of 18 reagents and on irradiation in the presence of each of 12 reagents, without exception, behavior of the visible coloration parallels that of the broad esr signal. With H_2 and H_2O as the only exceptions, a correlation exists between ionization potential of a reagent and its reactivity with the trapped positive holes; such a correlation permits an estimate of the effective electron affinity of the positive hole as lying between 9.8 and 12.1 eV. When present during irradiation, O_2, N_2O, and CO_2 act as traps for free electrons and enhance color and positive-hole signal of the solid; CO and SO_2 apparently act as traps for free positive holes (unstabilized O^-) to give CO_2^- and SO_3^-. A model is presented to describe the generality of results obtained in radiation studies with silica–alumina gel.

Introduction

Studies of the dealkylation of isopropylbenzene on γ-irradiated silica–alumina[2] and silica gels[3] have been reported in a series of papers. The results indicate that an appreciable portion of the dealkylation on a γ-irradiated silica–alumina is associated with the radiation-induced visible color centers, the visible color being bleached concomitantly with occurrence of the dealkylation reaction. The visible color of an irradiated silica–alumina or silica gel also is bleached by hydrogen,[2,4-7] ethylene,[4] ammonia,[4] and water[4] but not by oxygen.[2,4-6] In a variety of silica-base solids, radiation-induced visible color centers have been identified, by certain correlations with the esr spectrum of the irradiated solid, as positive holes trapped at aluminum atoms present substitutionally in the silica matrix.[7-10] Both the aluminum positive-hole center[7-10] and certain trapped-electron centers[7,9,11-16] have characteristic esr spectra in a silica matrix. Consequently, study of the effect on the esr spectrum of an irradiated silica–alumina gel of various gases, either present during irradiation or added subsequently, provides additional insight into the mechanism of formation and chemical reactivity of the radiation-induced visible color centers.

(1) The Radiation Laboratory of the University of Notre Dame is operated under contract with the U. S. Atomic Energy Commission. This is AEC Document No. COO-38-617.
(2) *Cf.* R. R. Hentz, L. M. Perkey, and R. H. Williams, *J. Phys. Chem.*, **70**, 731 (1966), which includes references to earlier papers in this series.
(3) E. A. Rojo and R. R. Hentz, *ibid.*, **70**, 2919 (1966).
(4) H. W. Kohn, *Nature*, **184**, 630 (1959).
(5) G. F. Shipman, *J. Phys. Chem.*, **70**, 1120 (1966).
(6) H. W. Kohn and E. H. Taylor, *Proc. Intern. Congr. Catalyse, 2e, Paris, 1960*, **2**, 1461 (1961).
(7) G. K. Boreskov, V. B. Kazanskii, Yu. A. Mishchenko, and G. B. Pariiskii, *Dokl. Akad. Nauk SSSR*, **157**, 384 (1964); G. B. Pariiskii, Yu. A. Mishchenko, and V. B. Kazanskii, *Kinetika i Kataliz*, **6**, 625 (1965).
(8) J. H. E. Griffiths, J. Owen, and I. M. Ward, Bristol Conference on Defects in Crystalline Solids, The Physical Society, London, 1955, p 81; M. C. M. O'Brien and M. H. L. Pryce, *ibid.*, p 88.
(9) S. Lee and P. J. Bray, *Phys. Chem. Glasses*, **3**, 37 (1962).
(10) J. H. Mackey, Jr., *J. Chem. Phys.*, **39**, 74 (1963); A. Halperin and J. E. Ralph, *ibid.*, **39**, 63 (1963).
(11) S. Lee and P. J. Bray, *ibid.*, **39**, 2863 (1963).
(12) G. M. Muha, *J. Phys. Chem.*, **70**, 1390 (1966).
(13) J. S. van Wieringen and A. Kats, *Philips Research Repts.*, **12**, 432 (1957).
(14) R. A. Weeks and C. M. Nelson, *J. Appl. Phys.*, **31**, 1555 (1960).
(15) R. A. Weeks and C. M. Nelson, *J. Am. Ceram. Soc.*, **43**, 399 (1960).
(16) H. W. Kohn, *J. Chem. Phys.*, **33**, 1588 (1960).

Experimental Section

Materials. The silica–alumina used in this work is a conventional catalyst (10 wt % alumina and surface area = 400 m^2/g) that has been designated as solid A in a previous publication[17] in which its properties are described. Hydrogen sulfide was obtained from Air Products and Chemicals. All other gases were obtained from Matheson Co. Gases noncondensable at 77°K were dried by passage through a silica gel column and through traps at 77°K. Condensable gases were passed through the silica gel column and were purified by trap-to-trap distillation at 77°K; the middle fraction was retained for use.

Procedures. The solid was crushed with a Diamonite mortar and pestle and passed through sieves of 20 and 40 mesh. After heating in a muffle furnace at 500° for 19 hr, the solid was stored in a desiccator over silica gel. Approximately 0.3 g of solid was placed in a 4-mm o.d. Suprasil sample tube which was equipped with a quartz-to-Pyrex graded seal and a full-length inner 12/30 standard-taper joint. The sample was degassed on a vacuum line by heating for 18–20 hr at 500° and less than 10^{-5} Torr. The sample tube then was sealed off above the standard-taper joint, and the sample was irradiated in a 4-kCi ^{60}Co source. The dose rate to a $CsNO_3$ dosimeter, based on $G(NO_2^-) = 1.65$,[18] was 1.64×10^{18} eV g^{-1} min^{-1}. Doses to silica–alumina were determined by correction for its electron density relative to that of the dosimeter and for decay of the ^{60}Co. Prior to recording of the esr spectrum, the sample was kept in one end of the tube while the Suprasil was heated with a flame to anneal paramagnetic centers produced in the Suprasil.

For study of the effect of various gases, the sample tube was attached by the standard-taper joint to an apparatus with two ~110-ml bulbs and a tip breaker (*cf.* Figure 1). After evacuation of the apparatus on a vacuum line, selected gases were admitted to the desired pressure into the storage bulbs and excess gas was removed. The apparatus then was shut off from the vacuum system and transferred to the esr spectrometer.

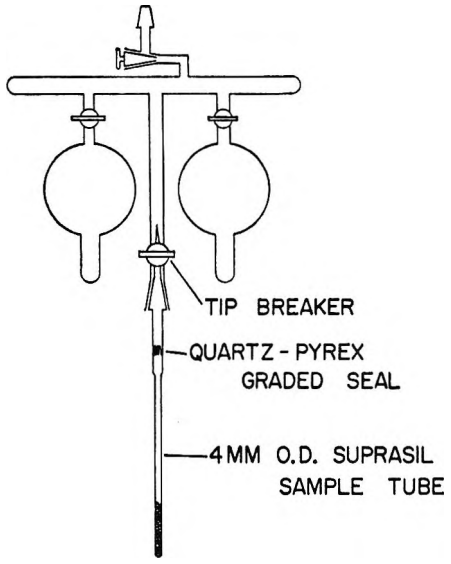


Figure 1. Apparatus for exposure of an irradiated solid to a gaseous reagent.

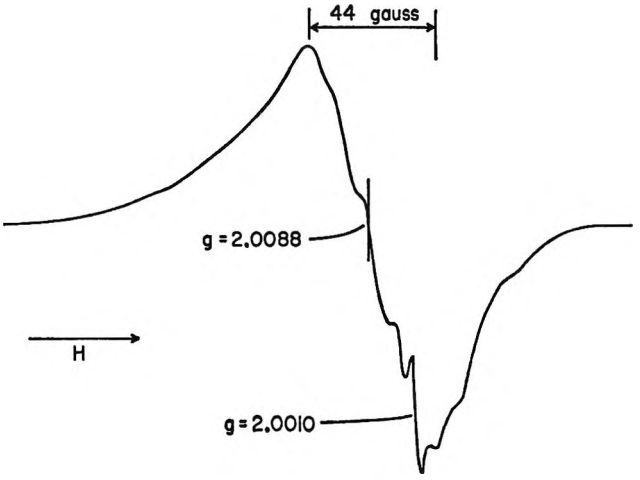


Figure 2. The esr spectrum of silica–alumina gel irradiated and observed at room temperature.

A Varian Model 4502 spectrometer, operating at 9485 Mcps and in the TE_{102} mode, was employed. The magnetic field was modulated at 100 kcps and was controlled by a Field-Dial regulator V-FR-2503. Such a system permits observation of signal height relative to the base line at a particular value of the magnetic field. Values of g were determined by comparison with samples of α,α-diphenyl-β-picrylhydrazyl (g = 2.0036), freshly recrystallized from benzene, which were taped to the outside of the sample tube. A single crystal of $CuSO_4 \cdot 5H_2O$ was used as the standard for estimation of absolute spin concentrations.

Results

The Esr Spectrum of Irradiated Silica–Alumina Gel. Prior to irradiation all samples exhibited a small esr signal at $g = 4.28$ which was unaffected by irradiation. This signal is attributed to the trace amount of Fe^{3+} impurity[19] present in the silica–alumina.[17] A typical spectrum of the γ-irradiated solid at room temperature is presented in Figure 2. The spectrum consists of two distinguishable signals. There is a broad line with a width of 44.5 ± 0.5 G and g = 2.0088 ± 0.0005 which is partially resolved into six components with a splitting of 8.5 ± 0.2 G; superimposed on the broad line is a narrow line at g = 2.0010 ± 0.0005.

The esr spectrum of irradiated silica–alumina gel (*cf.* Figure 2) is almost identical with that reported by Lee and Bray[9] for irradiated aluminosilicate glasses.

(17) R. R. Hentz, *J. Phys. Chem.*, **68**, 2889 (1964).
(18) T. H. Chen and E. R. Johnson, *ibid.*, **66**, 2249 (1962).
(19) T. Castner, Jr., G. S. Newell, W. C. Holton, and C. P. Slichter, *J. Chem. Phys.*, **32**, 668 (1960).

These authors identify the partially resolved broad line with the center observed by Griffiths, *et al.*,[8] in irradiated quartz single crystals; this center was interpreted by O'Brien and Pryce[8] as a positive hole trapped on a bridging oxygen atom that is bonded to a substitutional Al^- ion. A line similar to the narrow line at $g = 2.0010$ has been reported in a variety of irradiated silica-base solids (*e.g.*, crystalline quartz,[15] fused quartz and synthetic fused silicas,[13,14] borosilicate[11,12] and aluminosilicate[9] glasses, and silica gels[7,16]). Height[20] of the signal at $g = 2.0010$ is about fourfold larger when the Suprasil sample tube is not annealed. As noted by Muha,[12] such a line must be associated with defects in the silica matrix rather than impurities or peculiarities of a high-surface sample. Thus, the line at $g = 2.0010$ appears to derive from a center of the type described as an electron trapped at one of several kinds of oxygen vacancies in the silica matrix.[21]

Visual comparison of the broad and narrow lines in the spectrum of Figure 2 suggests that the number of electrons observed at $g = 2.0010$ represents a small fraction of the number of Al positive-hole centers; *i.e.*, an appreciable number of electrons are trapped in such a manner as to escape detection in the esr spectrum. Other observations support such a conclusion. When an irradiated sample is heated for 10 min at 250°, the color and hole signal are destroyed; however, height of the signal at $g = 2.0010$ is decreased by only 30% and is not eliminated by 20 min at ∽500°. The esr spectrum of a sample irradiated and observed at 77°K is shown in Figure 3a. Resolution of the positive-hole signal is improved; there is no evidence of the signal at $g = 2.0010$; and the characteristic H-atom signal with a splitting of ∽510 G is present. Thus, a large positive-hole signal is produced without an observable trapped-electron signal. After the sample was warmed and kept at room temperature for 2 hr, the spectrum was recorded again at 77°K with the result shown in Figure 3b. The H-atom signal is absent while the narrow line at $g = 2.0010$ is now present and height of the positive-hole signal has decreased by ∽37%. No hydrogen gas is detectable after irradiation of the silica–alumina gel.[2] Thus, formation of the trapped-electron center at $g = 2.0010$ appears to be a consequence of some reaction of the H atoms produced by irradiation or of H_2 formed from them.

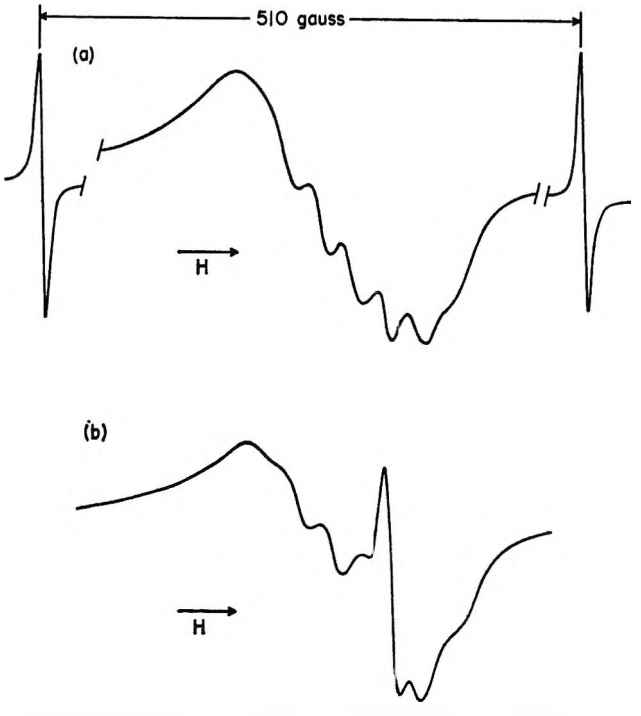


Figure 3. (a) The esr spectrum of silica–alumina gel irradiated and observed at 77°K. (b) Spectrum of the same sample observed at 77°K, with a 63/40 amplification factor relative to (a), after 2 hr at room temperature.

Height of the positive-hole signal increases and reaches a limiting value as dose to the solid is increased. A limiting yield of 16×10^{17} positive-hole centers per gram is obtained by comparison of areas under the absorption curves (obtained by integration of the first-derivative signals) of the positive-hole center and the $CuSO_4 \cdot 5H_2O$ standard.

Exposure of Irradiated Solid to Reagents. In all experiments the solid received a dose of at least 1.8×10^{21} eV g^{-1}. Such a dose exceeds that required to attain the limiting yield of positive-hole centers and of benzene produced in isopropylbenzene dealkylation (∽1×10^{21} eV g^{-1}). For study of the effect of various reagents on the hole signal, the magnetic field was set at the value corresponding to the maximum in the first-derivative spectrum of the hole signal (*cf.* Figure 2), and height relative to the base line was recorded as a function of time of exposure. Height of the trapped-electron signal (maximum-to-minimum of the narrow line at $g = 2.0010$) was determined before and after exposure to a reagent. Unless otherwise noted, gaseous reagents were used at a pressure of 150 Torr in one of the 110-ml storage bulbs which gave a pressure of ∽130 Torr over the sample (assuming no adsorption). Isopropylbenzene, benzene, and cyclohexane were adsorbed on the irradiated solid at their room-temperature vapor pressures by opening the sample tube to a bulb containing the liquid.

A 30-min exposure of irradiated solid to the gases O_2, N_2, N_2O, and CO_2 produced no effect on the visible color or the positive-hole signal. However, both the visible color and hole signal disappear completely in less than 1 min of exposure to each of the gases NH_3, H_2S, NO, NO_2, propylene, 1-butene, and 2-butene; ethylene requires 5–10 min to produce the same effect. Benzene,

(20) Except for measurements at fixed magnetic field, when height relative to the base line is measured, height is measured from maximum to minimum of the first-derivative spectrum of a signal.

(21) R. A. Weeks, *Phys. Rev.*, **130**, 570 (1963); R. A. Weeks and E. Lell, *J. Appl. Phys.*, **35**, 1932 (1964).

isopropylbenzene, and cyclohexane also rapidly remove the visible color and hole signal. Each of the foregoing reagents has little or no effect on the height of the trapped-electron signal.

The effects of H_2, CO, and SO_2 on the esr spectrum of irradiated silica–alumina gel are more complicated. On exposure of irradiated solid to H_2, the hole signal height drops essentially instantaneously to ~50% of its original value, reaches 30% in ~2 min, and thereafter decreases slowly to ~24% after 20 min. With the decrease in positive-hole signal height there is a concomitant bleaching of the visible color. The esr spectrum after a 20 min exposure to H_2 is shown in Figure 4. Height of the trapped-electron signal has

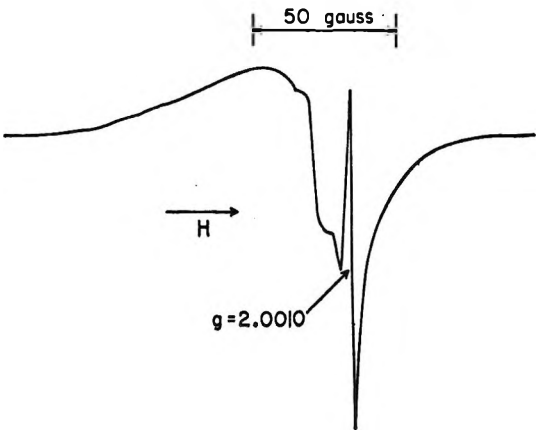


Figure 4. The esr spectrum of irradiated silica–alumina gel after a 20-min exposure to H_2.

increased by a factor of ~2. Such a result supports the conclusion (*cf.* preceding section) that formation of the center at $g = 2.0010$ is a consequence of some reaction of H or H_2. Aside from the trapped-electron signal, the residual spectrum in Figure 4 is not of the same form as the original spectrum (*cf.* Figure 2). The effect of H_2 on the esr spectrum suggests that more than one kind of center contributes to the spectrum in the region of the Al positive-hole signal[22] and that H_2 does not react with all such centers with equal facility (whereas the other effective reagents do). It is also possible, but difficult to conceive, that the reaction with H_2 yields a product which gives a signal in the region of the Al positive-hole signal.

On exposure of the irradiated solid to CO or SO_2, height (relative to the base line) of the positive-hole signal decreases to ~85% of the original value in 10 min and thereafter remains constant. There is a slight bleaching of the visible color and, as shown in Figures 5 and 6, a large new signal appears with both reagents. An expanded trace of the new signal obtained with CO is shown in Figure 5b; this signal looks very similar to that region in the spectrum of the irradiated solid in which the signal associated with a trapped electron occurs (*cf.* Figure 2). However, the

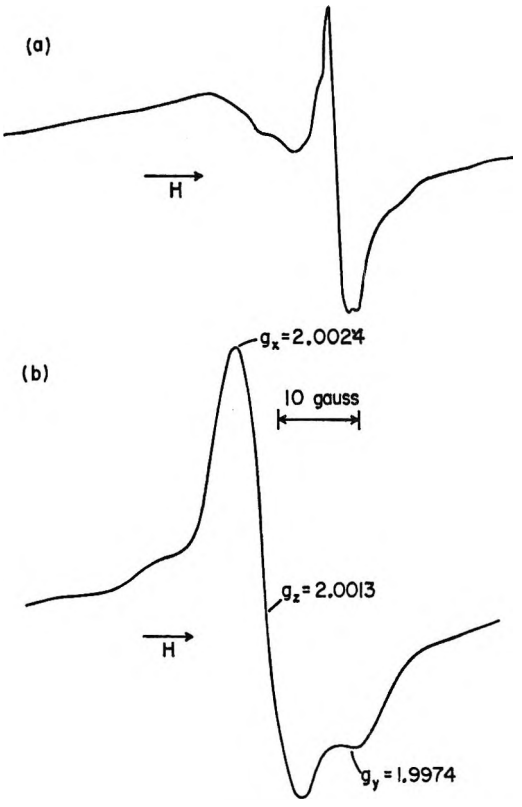


Figure 5. (a) The esr spectrum of irradiated silica–alumina gel after exposure to CO for more than 10 min. (b) An expanded trace of the large signal in (a).

behavior of what will be referred to as the CO signal is very different from that of the trapped-electron signal in several respects: (1) pumping off the added CO reduces the CO signal, but pumping has no effect on the trapped-electron signal; (2) exposure to air removes the CO signal and restores the original signal, but air has no effect on the trapped-electron signal; (3) subsequent exposure to H_2 (of irradiated solid previously exposed to CO) removes both the hole signal and the CO signal, but direct exposure of irradiated solid to H_2 removes the hole signal and approximately doubles the electron signal; (4) CO produces no change in the residual spectrum of an irradiated solid previously exposed to H_2. Because of the close resemblance of the spectrum in Figure 5b to the reported spectrum[23] of CO_2^-, the CO signal is attributed tentatively to CO_2^-. Thus, it appears that CO reacts with O^- centers on the surface of irradiated silica–alumina gel to form CO_2^- with concomitant destruction of certain of the centers

(22) Lee and Bray (ref 9) report a broad, structureless, asymmetric line of ~10-fold lower intensity than the Al positive-hole signal. This line, which appears at $g = 2.0091$ with a peak-to-peak width of 18 G, underlies the Al positive-hole signal and remains unaffected after removal of the Al center by annealing at 350°. The authors identify the signal with a positive hole trapped on nonbridging oxygen.

(23) J. H. Lunsford and J. P. Jayne, *J. Phys. Chem.*, **69**, 2182 (1965); D. W. Ovenall and D. H. Whiffen, *Mol. Phys.*, **4**, 135 (1961); S. A. Marshall, A. R. Reinberg, R. A. Serway, and J. A. Hodges, *ibid.*, **8**, 225 (1964).

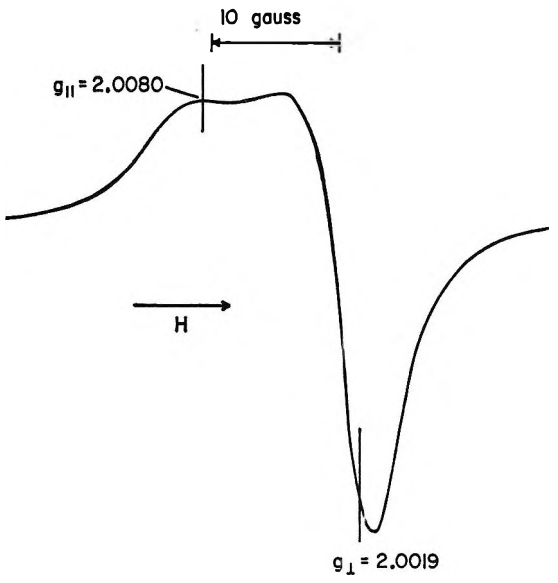


Figure 6. An expanded trace of the large new signal obtained after exposure of irradiated silica–alumina gel to SO_2 for more than 10 min.

that contribute to the spectrum in the region of the Al positive hole.

The SO_2 signal shown in Figure 6 is typical of that obtained with polycrystalline substances showing uniaxial g anisotropy. On the basis of a line-shape analysis,[24] the signal can be described as Gaussian with the values of g shown in Figure 6 and a single crystal line width of 5.8 G. Because of the absence of any similarity between the SO_2 signal and the spectrum[25] of SO_2^- and the absence of a CO_2^- signal when CO_2 is admitted to irradiated solid, assignment of the SO_2 signal to SO_2^- seems inadmissible. The similarity in effect of CO and SO_2 suggests that the SO_2 signal is attributable to SO_3^- formed in reaction of SO_2 with surface O^-. If so, anisotropy of the signal must result from some distortion of SO_3^- on the surface.[26]

Irradiation of Solid in the Presence of Reagents. Irradiation of silica–alumina gel in the presence of H_2, NH_3, H_2S, NO, or NO_2 gives no visible coloration after doses in excess of 10^{22} eV g^{-1}. The esr spectrum in each case consists of an ill-defined broad signal of very low intensity and a trapped-electron signal of about the same height as that obtained in irradiation of the solid alone. Irradiation of solid in the presence of CO or SO_2 gives very intense signals of the type attributed to CO_2^- (Figure 5b) and SO_3^- (Figure 6), respectively, but no visible coloration. When the solid is irradiated in the presence of CO_2, O_2, or N_2O (which have no effect on the hole signal or color of solid irradiated alone), the solid becomes very much darker and height of the hole signal is 2–3 times greater than that obtained in irradiation of solid alone to the same dose. Irradiation in the presence of CO_2 yields an esr spectrum like that shown in Figure 5a. Such a result suggests that CO_2 captures free electrons to give CO_2^- and provides support for identification of the CO signal (*cf.* the preceding section) with CO_2^-. Irradiation of solid in the presence of Ar or N_2 gives a visible coloration and esr spectrum identical with that obtained in irradiation of the solid alone.

Discussion

On exposure of irradiated silica–alumina gel to each of 18 reagents and on irradiation in the presence of each of 12 reagents, without exception, the behavior of visible coloration parallels that of the esr signal attributed to an Al positive-hole center. Such a correlation provides strong support for identification of the visible color centers in silica–alumina gel as Al positive-hole centers.[2] Identity of positive-hole centers and centers of chemical activity for isopropylbenzene dealkylation is indicated by comparison of the limiting yield of 16×10^{17} positive-hole centers per gram with that of $\sim 13 \times 10^{17}$ benzene molecules per gram obtained in isopropylbenzene dealkylation.[2]

A model is proposed which describes the generality of results obtained in radiation studies with silica–alumina gel. Radiation generates H atoms, free electrons, and free positive holes in the solid. The free positive hole may be thought of as an O^- ion the position of which moves through the solid by electron-transfer processes until the hole is trapped at a site of lower energy—*e.g.*, on a bridging oxygen atom bonded to a substitutional Al atom,[8,9] on a nonbridging oxygen,[9] or perhaps on some kind of O^{2-} on the solid surface. An appreciable number of electrons (perhaps equal to the number of Al positive-hole centers; *cf.* results at 77°K) are trapped in such a way as to escape detection in the esr spectrum. At room temperature, H atoms react with some kind of defect (probably in competition with neutralization of positive holes) at which ionization occurs to give the trapped-electron signal at g = 2.0010. Of particular interest in this regard is the observation of Lee and Bray[9] that their trapped-electron signal at g = 2.0012 is produced in neutron irradiation of an aluminosilicate glass but not in X irradiation; the Al positive-hole signal was of about the same intensity in both cases. Apparently, the kind of defect necessary for the detectable trapped electron is present in silica–alumina gel but must be created in the glass.

Such effective electron scavengers as O_2, N_2O, and CO_2, when present during irradiation, function as additional traps for free electrons (with CO_2 the signal attributed to CO_2^- is observed) and thereby enhance the visible color and positive-hole signal. As suggested earlier with regard to the limiting yield of benzene in

(24) J. W. Searl, R. C. Smith, and S. J. Wyard, *Proc. Phys. Soc.* (London), **78**, 1174 (1961).

(25) P. W. Atkins, A. Hirsfield, and M. C. R. Symons, *J. Chem. Soc.*, 5220 (1964).

(26) A completely symmetric signal with g = 2.004 is reported for SO_3^- by G. W. Chantry, A. Hirsfield, J. R. Morton, J. R. Rowlands, and D. H. Whiffen, *Mol. Phys.*, **5**, 233 (1962).

dealkylation of isopropylbenzene,[3] the limiting yield of positive holes appears to be determined by the availability of stable electron traps. Because of the absence of visible coloration on irradiation of silica–alumina gel in the presence of CO or SO_2 and development of the large signals attributed to CO_2^- and SO_3^-, respectively, it is suggested that these reagents are very effective traps for the free positive hole (unstabilized O^-). Reaction of CO and SO_2 with trapped positive holes may be limited (note their small effect on visible color and positive-hole signal of a previously irradiated silica–alumina gel) to O^- stabilized at certain specific sites on the solid surface.

The trapped electron with $g = 2.0010$ is not removed by the electron scavengers O_2, N_2O, and CO_2 or by any of the reactions in which various reagents remove the positive-hole signal. Those trapped electrons not detected in the esr spectrum also appear to be in relatively stable traps. For example, exposure of the irradiated solid to CO_2 does not give the signal attributed to CO_2^-, nor does O_2, N_2O, or CO_2 affect the positive-hole signal (which might be expected were, *e.g.*, CO_2^- being formed and subsequently neutralized).

Ability of a reagent to react with the positive-hole center clearly is not related to the ability to scavenge electrons. Neither is any correlation possible between reactivity and effectiveness of a reagent as a free-radical scavenger. Among the reactive reagents are effective and ineffective free-radical scavengers; oxygen, an effective free-radical scavenger, is not reactive. Also, the paramagnetic molecules NO and O_2 differ in their reactivity.

A correlation appears to exist, as might be expected for reaction with a positive hole, between reactivity and ionization potential of a reagent. The reagents, with their ionization potentials[27] in eV in parentheses, are divided into unreactive and reactive groups as follows: unreactive—N_2(15.6), CO(14.0), CO_2(13.8), N_2O(12.9), SO_2(12.3), and O_2(12.1); reactive—H_2(15.4), H_2O[28] (12.6), H_2S(10.5), C_2H_4(10.5), NH_3(10.2), *c*-C_6H_{12}(9.9), NO_2(9.8), C_3H_6(9.7), 1-C_4H_8(9.6), NO(9.2), C_6H_6(9.2), 2-C_4H_8(9.1), and $C_6H_5C_3H_7$(8.7). With H_2 and H_2O as the only exceptions, reagents with an ionization potential of at least 12.1 eV are unreactive and reagents with an ionization potential no greater than 10.5 eV are reactive. Thus, the positive hole appears to have an effective electron affinity (including changes in binding energy of reagent to the solid owing to the charged species produced) between 10.5 and 12.1 eV. However, some additional factor must be involved in the reactions with H_2 and H_2O. In these cases, it is suggested that the additional energy necessary for electron transfer to the positive hole is provided by an accompanying proton transfer to O^{2-} of the lattice. For H_2 the reaction may be written as

$$H_2 + P^+ + O^{2-} \longrightarrow H + P + H^+ \cdot O^{2-}$$

in which P^+ represents a positive hole. The H atoms formed in the case of H_2 enhance the trapped-electron signal at $g = 2.0010$ in competition with neutralization of positive holes. Because other of the reagents containing H may react *via* the mechanism suggested for H_2 and H_2O, the effective electron affinity of the positive hole is estimated more conservatively as lying between the O_2 ionization potential of 12.1 eV and the NO_2 ionization potential of 9.8 eV. The ultimate fate of radicals or radical ions formed in reactions of reagents other than H_2 with the positive holes cannot be ascertained from results of the present study.

(27) K. Watanabe, T. Nakayama, and J. Mottl, *J. Quant. Spectrosc. Radiation Transfer*, 2, 369 (1962).

(28) Though not used in the present study, water decolorizes irradiated silica–alumina gel (unpublished work; also, see ref 4).

Vacuum-Ultraviolet Photolysis of Polydimethylsiloxane. Gas Yields and Energy Transfer[1]

by Seymour Siegel and Thomas Stewart

Aerospace Corporation, El Segundo, California *(Received July 10, 1968)*

A polydimethylsiloxane polymer was irradiated with 1470- and 1236-Å radiation, and the quantum yields of the gas products were determined. Analysis of the data indicates that the breaking of the Si–CH_3 bond is the most probable reaction occurring at both wavelengths. For surface irradiations, C_2H_6, CH_4, and H_2 are primary products, while for immersion irradiations, only CH_4 and H_2 are produced. The differences in the two types of experiments are ascribed to the competition between bimolecular CH_3 combination and radical abstraction reactions; the surface irradiation favors the former mechanism. The quantum yields for 1470 Å were 0.033, 0.020, and 0 009 for C_2H_6, CH_4, and H_2, respectively, with surface irradiation. Quantum yields for the immersion irradiation were 0.087 and 0.021 for CH_4 and H_2. The precision of these numbers is ± 0.002 for all values. For 1236-Å surface irradiations, secondary photolytic reactions were complicating factors and quantum yields were not obtained. In the immersion irradiations, 1236-Å radiation gave quantum yields of 0.087 ± 0.016 and 0.049 ± 0.005 for CH_4 and H_2, respectively. A mixed methyl–phenyl polymer $[(CH_3)(Ph)_2Si\text{-}O\text{-}Si(CH_3)_2\text{-}O\text{-}Si(CH_3)(Ph)_2]$ was also irradiated at 1470 Å, and quantum yields of $1.0 \pm 0.5 \times 10^{-3}$ and $\leq 4 \times 10^{-3}$ were found for CH_4 and H_2, respectively, in both surface and immersion irradiations. No C_2H_6 was found for this polymer. Also solutions of the phenyl-containing polymer in the polydimethylsiloxane were irradiated. It was found that the gas yields were reduced by both radical addition to the phenyl groups as well as intermolecular energy transfer between the two polymers; however, there is no evidence for the presence of long-range transfer involving energy transfer along the chain. Analysis of the data indicates that the rate constant for H atom addition to a phenyl group is ~ 10 times larger than the corresponding rate constant for CH_3 radicals.

Introduction

The vacuum-ultraviolet (vuv) region of the electromagnetic spectrum is commonly considered to start at about 2000 Å (6.2 eV) and extend to shorter wavelengths where it merges with the X-ray region. Many studies have been published[2] dealing with the vuv photochemistry of low molecular weight molecules with the major emphasis on gas-phase reactions. Two of the more popular vuv photolytic wavelengths have been 1470 Å (8.4 eV) and 1236 Å (10.0 eV) because of the development of easily constructed resonance lamps. These studies have shown very interesting reactions occurring as a function of wavelength, perhaps the most striking example being the wavelength dependence of molecular hydrogen elimination mechanisms. While the early work concentrated on gas-phase reactions, the vuv photochemistry of the solid and liquid phase has been receiving more attention recently.[3–7] However, the vuv photochemistry of polymeric materials has not been examined at all.

This paper describes the results of a study which examined the evolved gas products produced by the irradiation of polydimethylsiloxane (DMS) with 1470- and 1236-Å radiation. The inter- and intramolecular effects of phenyl groups on the efficiency of production of these products were also studied. One complicating factor in this type of investigation is the very small ($\sim$500 Å) penetration depth of the radiation. This small penetration depth results in emphasizing the importance of gas-phase reactions or surface reactions. This point will be discussed in more detail later.

The high-energy ionizing radiation chemistry of DMS at room temperature has been shown to be predominantly controlled by free-radical mechanisms with ionic reactions having little, if any, contribution.[8] However, the excitation by X-rays or fast electrons is random in character with the chemistry occurring after considerable intramolecular and/or intermolecular migration of energy. With vuv radiation, the excitation is much more specific with well-characterized initial transitions occurring such as $\sigma \rightarrow \sigma^*$, $n \rightarrow \pi^*$, and $n \rightarrow \sigma^*$ transitions. Also, it has been commonly assumed that the particulate radiation chemistry occurring *via* excited electronic states involves the same electronic states excited by uv light. Therefore, it is of interest to compare the results of the two types of radiation in order to observe the effects of differences in the nature of the deposition of energy and in the excitation of the molecules present.

(1) This paper was prepared under U. S. Air Force Contract F04695-67-C-0158.

(2) J. R. McNesby and H. Okabe, "Advances in Photochemistry," Vol. II, Interscience Publishers, New York, N. Y., 1963, p 157.

(3) (a) P. Ausloos, R. E. Rebbert, and S. G. Lias, *J. Chem. Phys.*, **42**, 540 (1965); (b) W. M. Jackson, J. Faris, and N. J. Buccos, *ibid.*, **45**, 4145 (1966).

(4) R. E. Rebbert and P. Ausloos, *ibid.*, **46**, 4333 (1967).

(5) J. Y. Yang, F. M. Servedio, and R. A. Holroyd, *ibid.*, **48**, 1331 (1968).

(6) R. A. Holroyd, J. Y. Yang, and F. M. Servedio, *ibid.*, **46**, 4540 (1967).

(7) H. R. Ward and J. S. Wishnok, *J. Amer. Chem. Soc.*, **90**, 1085 (1968).

(8) A. A. Miller, *ibid.*, **82**, 3519 (1960); **83**, 31 (1961).

Experimental Section

Materials. The primary DMS used in this study was a Dow-Corning 360 dimethylsilicone medical fluid with a viscosity of 350 cP and a molecular weight of 10^4. A higher viscosity DMS fluid with a viscosity of 12,500 cP and a molecular weight of 5×10^4 was also used in several experiments. The methylphenylsiloxane used was also a Dow-Corning fluid with a molecular weight of 408. The fluids were purified by vacuum distillation; the medium-boiling fraction of the distillate was used. The gases used in making the rare gas resonance lamps were research grade xenon and krypton obtained from J. T. Baker Co.

Photolysis Apparatus. The xenon resonance lamp was constructed by attaching a piece of 12-mm glass tubing with a fritted disk to a 34/45 greaseless inner joint. A 1-in. diameter sapphire-to-Pyrex graded seal window was attached to the joint. Barium alloy getters were placed in the lamp to remove any impurities that might alter the spectral content of the lamp. After the lamp was thoroughly outgassed at 10^{-5} Torr, it was filled with 1 mm of xenon. The lamp was sealed and the getters flashed.

The krypton lamp was constructed by attaching a U-tube to a 34/45 inner joint. A magnesium fluoride window was put on the lamp with an epoxy adhesive. The lamp was filled with 0.5 mm of krypton. This gas pressure resulted in the best lamp performance. Barium getters were not used because the krypton seems to be gettered by the barium alloy; therefore, a liquid nitrogen trap was used to trap any impurities present.

The spectral purity of the lamps was examined with a McPherson (Model 218) monochromator. With the xenon lamp, only the 1470-Å resonance line in the vuv was observed. However, with the krypton lamp both the 1236- and 1165-Å lines were observed; the 1165-Å line contributed ~10 to 15% of the total output of the lamp. In this paper, the output of the krypton lamp will be considered to be all at 1236 Å; any uncertainties arising from the small amount of 1165-Å radiation present is probably less than the errors inherent in the various measurement techniques.

The cells were fabricated from the 34/45 outer O-ring seal joint. Holders were placed 1 in. above the bottom of the cells so that the calibrated screens used in the relative light intensity experiments could be fastened. The lamps mated into the cells. Power was supplied to the lamps by a Raytheon PG10 microwave power generator through an Evenson cavity.

Photolysis Procedure. For the surface mode experiments, 1 mm of silicone fluid was placed in the cell and thoroughly outgassed at 10^{-5} Torr. The irradiations at 1470 Å were usually 45 min in duration with readings of gas yields taken at 5-min intervals. The duration of 1236-Å experiments varied from 5 min for 100% lamp intensity to 12 min for 25% intensity; product readings were taken at 1-min intervals. Samples were stirred constantly during the irradiations.

Immersion mode experiments at 1470 Å were made by immersing the window of the xenon lamp 6 mm into the polymer fluid. Despite the fact that the samples were vigorously stirred, effects of bulk diffusion of the product gases were observed. When the gas evolution data were analyzed, a straight line was obtained, but the line intersected the time axis at $t > 0$. To correct for the effects of diffusion, the samples were irradiated for 10 min and the gas yield was measured. The lamp was then turned off and the sample stirred very vigorously for an additional 10 min; then a second set of gas measurements was made. The gas yields went up by a factor of 5 upon standing without irradiation. For example, the CH_4 yield went from 8 to 39 μ. The gas yields obtained from the stirring in the dark method of analysis were considered to be the more representative of the true yields and are the values given in this paper.

The immersion mode experiments with the krypton lamp were performed somewhat differently than with the xenon lamp. Because of the geometry of the krypton lamp and cell, the immersion experiments at this wavelength were made by putting a 6-mm layer of liquid on the surface of the lamp window and stirring the liquid. Under these conditions, the liquid volume was small and the product gas diffusion problem was minimized; the gas evolution curves intersected the time axis at $t = 0$, and the slopes of the lines were used to obtain gas yields.

With the immersion mode irradiations, polymer films were formed on the windows of both lamps; however, the problem was considerably more pronounced with the krypton lamp. A similar problem occurred in the surface mode irradiations using the krypton lamp, but not with the xenon lamp. The polymer film was removed by polishing the windows after each irradiation experiment.

Actinometry. The photolysis of CO_2 was used as an actinometer in calibrating the photon flux of the lamps. The quantum efficiency for production of CO from CO_2 was taken to be unity.[9,10] Seventy-six millimeters of CO_2 was placed in a cell designed for actinometry with a cold finger attached to the cell that trapped the CO_2. The cold trap was isolated from the cell by a stopcock. The lamps were started and allowed to run for 5 min, at which time CO_2 was expanded into the cell from the cold finger. The photolysis period was exactly 5 min. The photon flux at 1470 Å was $3.3 \pm 0.2 \times 10^{15}$ photons/sec, and at 1236 Å it was $3.3 \pm 0.7 \times 10^{15}$ photons/sec. At

(9) B. H. Mahan, *J. Chem. Phys.*, 33, 959 (1960). This paper gives $\Phi(CO) = 1.1 \pm 0.1$ and 1.2 ± 0.1 at 1470 and 1236 Å, respectively, where both values are upper limits.

(10) J. Y. Yang and F. M. Servedio, *Can. J. Chem.*, 46, 338 (1968).

1236 Å, a decrease in production rate of CO was observed after 10 min of exposure. A similar effect was observed by Yang and Servedio,[10] which they attributed to polymer formation on the window. The window was cleaned by operating the lamp in air for 15 min. The polymer formation was not observed with the 1470 Å lamp.

Analysis. The photolysis cells were connected directly to an Electronic Associates Series 200 residual gas analyzer (a quadrupole mass spectrometer). The gases were introduced into the mass spectrometer chamber by a manually controlled variable leak. The mass spectrometer was calibrated for determining absolute product yields. Total gas pressures were measured with a McLeod gauge. The mass spectral peak heights were read out on a dual-trace oscilloscope. Polaroid photos were taken of the peak responses on the oscilloscope, and quantitative measurements were made from them. Peak height deflection was directly proportional to the pressure of gas introduced into the mass spectrometer chamber. For the 1470-Å experiments, reproducibility errors were 10% or less, whereas with the 1236-Å experiments, errors were 25% or less. The uncertainties given in this paper are reproducibility errors.

Results

1470-Å Irradiation. When DMS was irradiated in the surface mode, the gas products consisted of H_2, CH_4, and C_2H_6. For stirred samples the yields for all three products were linear with irradiation time for a constant incident radiation intensity (I); typical gas evolution *vs.* time plots are shown in Figure 1. Within experimental error the quantum yields (Φ) are independent of I over a factor of 10 in the magnitude of I, as illustrated in Figure 2. The values of Φ are given in Table I.

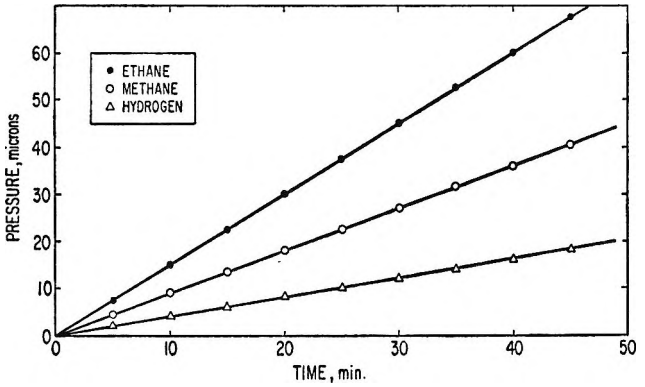


Figure 1. Gas evolution *vs.* irradiation time curves for 1470-Å irradiation.

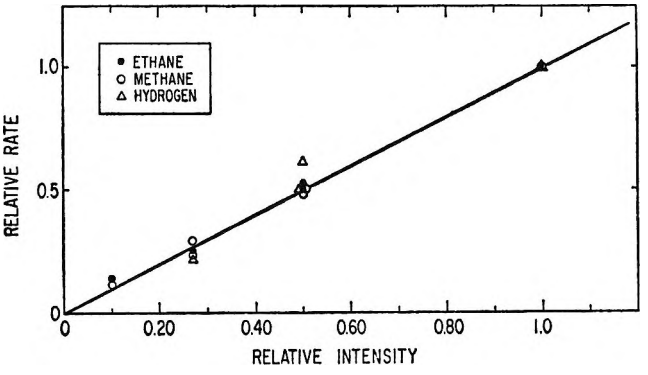


Figure 2. Relative gas yields *vs.* light intensity.

Table I: Quantum Yields (Φ) of Gas Products from 1470-Å Irradiation of DMS

Product	Φ^a (surface)	Φ^a (immersion)
C_2H_6	0.033	N.d.
CH_4	0.020	0.087
H_2	0.009	0.021
Total CH_3[b]	0.086	0.087

[a] The precision of all the quantum yields is ±0.002 with the exception of $\Phi(CH_3)$, which has an estimated precision of ±0.006. [b] The quantum yield for total CH_3 was taken to be equal to $2\Phi(C_2H_6) + \Phi(CH_4)$.

The values of Φ for the immersion mode experiments are also given in Table I. As can be seen from the values of Φ for the two irradiation modes, the relative quantum yields for CH_4 and C_2H_6 are strongly dependent upon the experimental irradiation conditions. This point is further illustrated by the data given in Table II, which lists the slopes (k) of the gas evolution curves for several experimental conditions. The important point to be noted is that while the yield of total CH_3 is constant, the fraction of CH_4 and H_2 produced increases with conditions which promote

Table II: Variation of k^a with Experimental Conditions (1470-Å Irradiation)

	Mode				
Product	Surface (stirred)	Surface[b] (not stirred)	Surface[c] (not stirred)	Surface[d] (high viscosity)	Immersion
C_2H_6	1.50	1.36	1.20	1.10	N.d.
CH_4	0.90	1.44	1.88	1.80	3.90
H_2	0.40	0.60	0.82	1.02	0.95
Total CH_3	3.90	4.10	4.20	4.00	3.90

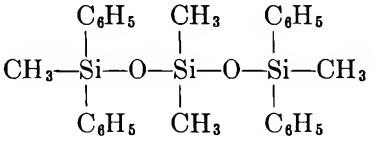
[a] k = slope of experimental gas evolution curves with units of μ/min. The values of k can be converted into quantum yields by multiplying by 0.022. The reproducibility is ±10%. [b] These values of k were obtained by taking the slopes during the first 45 min of irradiation, which was the normal irradiation time in these experiments. [c] These values of k were obtained by irradiating to 120 min and then taking the slopes of the gas evolution curves evolved during the subsequent 45 min of irradiation. [d] The high-viscosity material has a mol wt of 5×10^4 and a viscosity of 12,500 cP; the low-viscosity material used in the rest of the experiments has a mol wt of 1×10^4 and a viscosity of 350 cP. The sample was stirred but the efficiency of stirring was low because of the high viscosity of the material.

homogeneous reactions and minimize diffusion to the surface. In the extreme of the immersion irradiation mode, no C_2H_6 is formed.

1236-Å Irradiation. Analysis of the data from the 1236-Å irradiations in the surface mode was complicated by the secondary photolysis of the C_2H_6 formed. The primary products were still C_2H_6, CH_4, and H_2, but C_2H_4, C_2H_2, and H_2 were also formed as secondary products.[2,3b] The gas evolution curves were nonlinear with irradiation time, and the quantum yields were a function of incident light intensity. Formation of the polymer on the window during the irradiation which reduced the photon flux at the sample was an added complication. Because of these complications, meaningful quantum yields could not be derived from the data obtained from the surface mode irradiations.

The secondary products C_2H_2 and C_2H_4 were not observed when the 1236-Å irradiation was performed in the immersion mode. Despite the absence of secondary photolytic reactions, the immersion mode experiments still gave nonlinear gas–time evolution curves. However, in this case the nonlinearity arises only from the rapid formation of the polymer film on the lamp window. The initial slopes of the evolution curves were used to approximate the quantum yields. As in the case of the 1470-Å irradiations, no C_2H_6 is found in the immersion experiments; the only products observed were CH_4 and H_2. The quantum yields were $\Phi(CH_4) = 0.087 \pm 0.016$ and $\Phi(H_2) = 0.049 \pm 0.005$.

Energy Transfer. In order to study the protective effect of aromatic substituents on the vuv photochemistry of silicone polymers, a mixed methyl phenyl silicone (MPS) was examined. The polymer has the structure[11]



The gas yields from MPS irradiated with 1470-Å radiation were much less than those found for DMS. In the surface mode a value of $1.0 \pm 0.5 \times 10^{-3}$ was observed for $\Phi(CH_4)$. No C_2H_6 was observed, and $\Phi(H_2)$ was less than 4×10^{-3}. (The background production of H_2 was too high to obtain a more accurate value for the latter quantum yield.) In the immersion mode the corresponding yields were essentially the same, *i.e.*, $\Phi(CH_4) = 1.0 \pm 0.5 \times 10^{-3}$ and $\Phi(H_2) \leq 3 \pm 1 \times 10^{-3}$. These results demonstrate the strong protective effect produced by aromatic substituents on the vuv photochemistry of these types of polymers. However, it should be pointed out that these quantum yields are significantly higher than those found in the 2537-Å photolysis of MPS,[11] where $\Phi(H_2) = 2.6 \times 10^{-5}$ and $\Phi(CH_4) = 0.6 \times 10^{-5}$.

Solutions of MPS in DMS were also examined. These experiments were performed in the immersion mode. Concentrations of MPS ranged from 0.11 (saturated solution) to 0.01 *M*; the concentrations of phenyl groups are four times larger. The results of these experiments are given in Table III in terms of the values of *k*. Measurements of the absorption of 1470-Å radiation as a function of MPS concentration show that the radiation is being absorbed by the DMS even at the highest concentrations of MPS used.[12,13] Therefore, the variations in gas yields are not due to competition between solvent and solute for the available radiation.

Table III: Variation of k^a with MPS Concentration in Immersion Mode

[MPS], *M*	$k(CH_4)^b$	$k(H_2)^c$
0	3.9	0.95
0.01	3.7	0.80
0.025	3.6	0.51
0.05	3.2	0.30
0.08	2.3	0.20
0.11	1.8	0.20

[a] *k* is the slope of the experimental gas evolution curves with units of μ/min. The values of *k* can be converted into quantum yields by multiplying by 0.022. [b] The precision is ± 0.1 μ/min. [c] The precision is ± 0.05 μ/min.

The H_2 yield is more sensitive to the presence of MPS than is the CH_4 yield, and the effect on the H_2 yield is significant, even in the 0.01 *M* solution. This difference in sensitivity is probably due, at least in part, to the relative efficiencies of H and CH_3 additions to phenyl groups. The leveling off of the H_2 yield at high MPS concentrations is probably due to insufficient corrections for background H_2 production from the lamp walls and other sources. It should be pointed out that the value of H_2 production obtained at 0.11 *M* MPS is essentially that found for the irradiation of pure MPS. Considering the known efficiency of energy conversion in phenyl groups as well as their large radical-scavenging power, it seems likely that a significant fraction of the value of $\Phi(H_2)$ obtained for pure MPS may be due to background H_2 evolution.

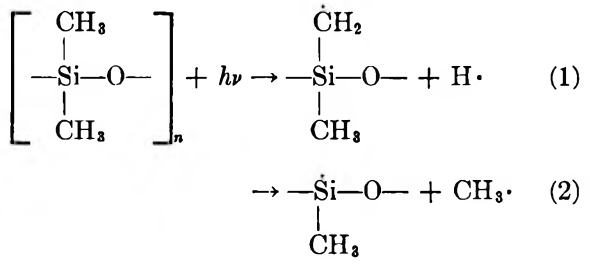
(11) S. Siegel, R. J. Champetier, and A. R. Calloway, *J. Polym. Sci., Part A*, **4**, 2107 (1966).

(12) S. Siegel and T. Stewart, Aerospace Corp., unpublished data.

(13) This conclusion is also supported by published measurements on other systems. For example, using the absorption coefficients for benzene at 1470 Å of ~5000 cm^{-1} [A. Quemarais, M. Morlais, and S. Robin, *C. R. Acad. Sci. Paris, Ser. B*, **265**, 649 (1967)], we calculate that for a 0.4 *M* solution only 10% of 1470-Å radiation would be absorbed in a path length of 5500 Å. The data on the absorption of polystyrene [R. H. Partridge, *J. Chem. Phys.*, **47**, 4223 (1967)] also indicate that the phenyl groups do not make a larger contribution to the absorption than the CH_2 backbone. The penetration depth for polyethylene [R. H. Partridge, *ibid.*, **45**, 1685 (1966)] at 1470 Å is approximately 500–1000 Å.

Discussion

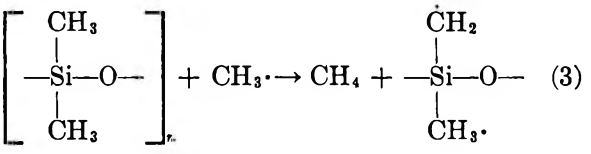
The primary reactions occurring during the 1236- and 1470-Å irradiations of DMS are



(1)

(2)

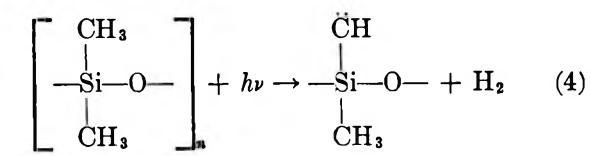
All the data obtained in this study are consistent with the postulate that C_2H_6 is produced only in the gas phase, or on the cell walls, by the combination of methyl radicals. The penetration depth of vuv radiation is very shallow; therefore, when the irradiation is performed in the surface mode, some of the CH_3 radicals can diffuse to the surface before interacting with the matrix. The rest of the CH_3 radicals produced by reaction 2 abstract a hydrogen atom from the solvent, *i.e.*



(3)

As the viscosity of the material is increased, diffusion is hindered and reaction 3 plays a more important role. Since no C_2H_6 is produced in the immersion mode irradiations, CH_3 radicals are consumed exclusively by the abstraction reactions. The quantum yield for reaction 2 is independent of the experimental conditions; only the fate of the methyl radicals is variable.

Similar considerations pertain to the fate of the H atoms formed by reaction 1. The H atoms formed in the immersion mode are most probably consumed by hydrogen abstraction to form H_2. When surface mode irradiations are considered, the observed H_2 comes almost entirely from H + H combination reactions after H atoms escape from the liquid, since $\Phi(H_2)$ drops by about a factor of 2. Also, some of the H atoms may be involved in CH_3 + H combination processes. Unfortunately, it is not possible to definitely determine from the available data what fractions of CH_4 and H_2 formed in the surface mode irradiations arise from the combination reactions. The quantitative assessment of the relative importance of molecular elimination reactions such as[14]



(4)

also can not be made. However, consideration of the large increase in $\Phi(H_2)$ in going from the surface to immersion modes would indicate that reaction 4 is not a large contributor to the observed H_2 yield. Some preliminary experiments, using NO as a radical scavenger, and the results in Table III support the latter conclusion.[15]

The results from the immersion experiments in Table I, together with the assumption that the radicals are totally consumed by abstraction reactions, indicate that for 1470 Å reaction 2 is four times more probable than reaction 1 after the absorption of a photon. When 1236-Å radiation is used, the observed quantum yields indicate that reaction 2 is only twice as probable as reaction 1. The significant increase in the probability of the H-atom elimination at shorter wavelengths may be due to the differences in the nature of the electrons being excited.[16] With 1236-Å radiation, the electrons in the C–H bonds are being excited directly, while for 1470-Å irradiations it is likely that the polymer backbone and the Si–C electrons are being primarily excited.

It is of interest to compare the results of the present study with the published results obtained from particulate ionizing radiation experiments. Gases are evolved under ionizing irradiation[17] with G values (*i.e.*, molecules produced per 100 eV of absorbed energy) as follows: $G(H_2) = 0.8$, $G(CH_4) = 1.2$, $G(C_2H_6) = 0.3$, and $G(CH_3) = 1.8$. The value of $G(H)$ can be calculated from these data only if the mechanism of H_2 and CH_4 production is assumed; the radical combination processes give $G(H) = 2.8$ and the abstraction mechanism $G(H) = 0.8$. Analysis of the vuv immersion mode irradiation results in the same units and, using the abstraction assumption, gives (a) 1470 Å: $G(CH_3) = 1.0$, $G(H) = 0.25$ and (b) 1236 Å: $G(CH_3) = 0.87$, $G(H) = 0.49$. Comparison of the relative gas yields shows that for the immersion vuv experiments no C_2H_6 was found, while approximately one-third of the total CH_3 yield appeared as C_2H_6 in the ionizing radiation studies. Part of the C_2H_6 in the latter studies may arise from spur reactions where the local concentration of CH_3 is large. However, the variations in ratios of the various products with type of radiation may also indicate that different excited

(14) O. P. Strausz, K. Obi, and W. K. Duholke, *J. Amer. Chem. Soc.*, 90, 1359 (1968).

(15) Some preliminary experiments using various pressures of NO as a radical scavenger and the surface irradiation mode were also performed. At the highest concentration of NO used (*i.e.*, 200 μ), we found that the C_2H_6 yield was decreased by a factor of 2 while the H_2 yield was reduced by 25%. The CH_4 yield was essentially unaffected by the presence of NO. These data confirm the conclusion that C_2H_6 is formed in the gas phase. They also indicate that the CH_4 from the surface mode is mainly formed in the bulk material, while an appreciable fraction of the H_2 arises from H atoms that have escaped. The result that $\Phi(H_2)$ from the immersion mode is twice the value found from the surface mode also indicates that most of the H atoms formed in the surface irradiations escape from the liquid.

(16) J. W. Raymonda and W. T. Simpson, *J. Chem. Phys.*, 47, 430 (1967).

(17) M. G. Ormerod and A. Charlesby, *Polymer*, 4, 459 (1963).

states are involved. Also, it is possible that ionic species play a more important role in the particulate radiation chemistry of DMS than has been previously thought.[18] It is interesting to note that the uv radiation is less efficient than the ionizing radiation in producing gas products.

Yang, Servedio, and Holroyd[5,6] have shown in recent papers that benzene reduces the product yields from the 1470-Å irradiation of cyclohexane by two mechanisms. One mechanism that is effective at low concentrations is the attachment of H atoms to benzene. This process is 300 times more effective than H-atom abstraction from cyclohexane. The second mechanism that predominates at high concentrations is energy transfer from excited cyclohexane to benzene. For our system (*i.e.*, MPS dissolved in DMS) these two mechanisms would yield the following expression for the MPS concentration dependence of the observed CH_4 and H_2 quantum yields in the immersion mode

$$\frac{\Phi_0}{\Phi} = \frac{P_0}{P}\left[1 + \frac{k_a[\text{MPS}]}{k_m[\text{DMS}]}\right] \qquad (5)$$

where Φ_0 is the quantum yield at [MPS] = 0, Φ is the quantum yield at [MPS] $\neq$ 0, P_0 is the radical production rate at [MPS] = 0, P is the radical production rate at [MPS] $\neq$ 0, k_a is the rate constant for radical addition to MPS, and k_m is the rate constant for radical abstraction from DMS. The value of P_0/P is a function of the probability of energy transfer.

Analysis of the data in Table III in terms of eq 5 can be performed only with some approximations. First, since the CH_4 yield decreases by only 20% at [MPS] = 0.05 M, while the H_2 yield decreases by a factor of 3, it is apparent that at low concentrations of MPS the H_2 yield is affected mainly by the radical addition reaction. Therefore, we assumed that up to 0.05 M MPS, $P_0/P = 1$. With this assumption, we find that the slope of the straight line obtained yields $k_a/k_m \approx 1100$. Considering the fact that each MPS molecule contains four phenyl groups, the latter ratio is in good agreement with the results of Yang, *et al.* Making the same assumption for CH_4 yields as for H_2 yields, at [MPS] = 0.05 M, $k_a/k_m \approx 100$. This supports the above conclusion that the phenyl groups are less efficient scavengers of CH_3 radicals than of H atoms. The latter estimate is probably too high, since energy transfer was completely ignored. However, using this value of k_a/k_m, we find that for CH_4, P_0/P at 0.11 M MPS = 1.5, whereas, if radical addition is ignored, $P_0/P = 2.2$ at the same concentration. If diffusion is neglected and an active volume concept[19] is adopted, these values for P_0/P correspond to an interaction radius for energy transfer of 11.4 to 14.0 Å. Obviously, the interaction requires very close overlap of the electron distribution of the two molecules for transfer to occur. There does not seem to be any migration of energy involved along the polymer chain. The data for H_2 at the high concentrations of MPS are too uncertain to perform a similar calculation.

(18) While it is not known with any certainty if ionization occurs in the 1236- and 1470-Å irradiation of DMS, the results of Partridge (ref 13) on polyethylene and polystyrene indicate that, at least for 1470-Å radiation, ionization is not an important process. It is most probable that the results reported here are due to primary excitation into nonionized states.

(19) S. Siegel and H. Judeikis, *J. Chem. Phys.*, **48**, 1613 (1968).

Ionic Reactions in Unsaturated Compounds. IV. Vinyl Chloride

by B. Mason Hughes,[1] Thomas O. Tiernan,[2] and Jean H. Futrell[3]

Aerospace Research Laboratories, Office of Aerospace Research, Wright-Patterson Air Force Base, Ohio 45433 *(Received July 11, 1968)*

Mass spectrometric studies of ion–molecule reactions in vinyl chloride have resulted in the identification of three ionic polymerization sequences

$$\xrightarrow{M} C_3H_4Cl^+ \xrightarrow{M} C_5H_6Cl^+$$

$$C_2H_2^+ \xrightarrow{M} C_2H_3Cl^+ \xrightarrow{M} C_4H_5Cl^+$$

$$\xrightarrow{M} C_4H_6Cl^+$$

$$C_2H_3^+ \xrightarrow{M} C_4H_5^+ \xrightarrow{M} C_6H_7^+$$

$$C_2H_3^+ \xrightarrow{M} C_2H_4Cl^+ \xrightarrow{M} C_4H_6Cl^+ \xrightarrow{M} C_6H_8Cl^+$$

In most cases the indicated condensation reactions proceed with elimination of HCl or C_2H_2. Isotopic studies show that the principal reaction of low velocity parent ions is charge transfer, the rate constant for this process being some 30 times larger than the summation of rates for other ion–molecule reactions It is further observed that vinyl chloride parent ions produced directly by electron impact react to give a distribution of condensation products which is substantially different from that which results from the reactions of parent ions formed by charge transfer. This is interpreted in terms of differences in the internal energy of the collision complexes formed by the two types of reactant ions. An examination of the dependence of the product distribution from this reaction on both internal and translational energy of the reactants shows that the former is the more important factor in this system. The results of the present investigation are compared with data on ionic processes in vinyl chloride obtained by other techniques.

Introduction

The radiolysis of vinyl chloride in the gaseous phase, using an α-particle source, was investigated some time ago by Mund and coworkers.[4–8] These studies indicated that the "ionic" yield of monomer consumption is strongly dependent upon the experimental conditions for radiolysis, but they provided little information concerning the actual nature of the ionic reactions which occur in the vinyl chloride system. It seems likely, however, that degradation products, such as hydrogen and methane, which are produced by radiolysis, may result from ionic condensation reactions.[9]

Recently, ion–molecule reactions in vinyl chloride have been examined by the use of a new technique which employs ion cyclotron resonance spectroscopy.[10] Condensation reactions were indeed observed for this compound but most of these were found to involve elimination of HCl as the neutral species. Some interesting isotope effects were also reported in this study. In view of the considerable number of uncertainties which are still associated with the use of a cyclotron resonance instrument for the investigation of ion–molecule reactions, it seemed appropriate to undertake a study of vinyl chloride using the more conventional mass spectrometric techniques which we have employed in earlier studies in this laboratory.[11–13] Because of the somewhat larger polarizability of the halocarbon and its permanent dipole moment, the reactivity of the vinyl chloride might be expected to be significantly greater than that of the simple hydrocarbons previously studied. For these several reasons the detailed mass spectrometric study of vinyl chloride described in this paper was therefore initiated.

(1) National Research Council–Office of Aerospace Research Postdoctoral Research Associate, 1967–1968.

(2) Author to whom reprint requests and correspondence should be addressed.

(3) Department of Chemistry, University of Utah, Salt Lake City, Utah 84112.

(4) W. Mund and J. A. Herman, *Bull. Acad. Roy. Belg.*, **37**, 333 (1951).

(5) W. Mund, J. A. Herman, and P. Huyskens, *ibid.*, **37**, 696 (1951).

(6) W. Mund, J. A. Herman, and G. Verfaillie, *ibid.*, **35**, 656 (1949).

(7) W. Mund, M. Van Meerssche, and J. Momigny, *Bull. Soc. Chim. Belges*, **62**, 109 (1953).

(8) W. Mund, M. Van Meerssche, and J. Momigny, *ibid.*, **62**, 645 (1953).

(9) A. Chapiro, "Radiation Chemistry of Polymeric Systems," Interscience Publishers, Inc., New York, N. Y., 1962.

(10) J. L. Beauchamp, L. R. Anders, and J. D. Baldeschwieler, *J. Amer. Chem. Soc.*, **89**, 4569 (1967).

(11) J. H. Futrell and T. O. Tiernan, *J. Phys. Chem.*, **72**, 158 (1968).

(12) T. O. Tiernan and J. H. Futrell, *ibid.*, **72**, 3080 (1968).

(13) F. P. Abramson and J. H. Futrell, *ibid*, **72**, 1994 (1968).

Experimental Section

The experimental approach applied in this study is similar to that used in the previous investigations in this series.[11-13] High-pressure single-source experiments were accomplished with a modified time-of-flight mass spectrometer, which has recently been described in some detail,[14] in order to search for sequential reaction processes and to evaluate kinetic parameters. In this instrument the ion path length from the collimated electron beam to the source exit aperture is 0.28 cm. For all the experiments reported here, the electric field strength in the source was maintained at 10.6 V/cm by applying an appropriate repeller potential to the source backing grid. The source temperature was held at 250° for all these studies and the ionizing voltage was set at 100 V. In order to minimize space charge effects, the electron current was adjusted to approximately 1×10^{-8} Å with no gas in the source prior to a particular experiment. Gas was then introduced into the ion source from a reservoir by means of a motor-driven gas leak which is controlled by a Granville-Phillips Series 213 automatic pressure controller. The input signal for the controller was an MKS Baratron Model 77H1 pressure transducer, connected by a static pressure tap directly to the ion source chamber. The latter was set to the desired ion source pressure and the pressure is held constant within about 1% of the selected value throughout an experiment. After introducing the gas and allowing a short period for stabilization of the source, the mass range of interest was scanned and recorded. Data reduction requires a correction for mass discrimination, as already described,[14] because of the technique used to achieve space-focus for time-of-flight mass analysis.

Studies of elementary ion–molecule reactions of individually selected ions were carried out using the ARL tandem mass spectrometer, which has also been described previously.[15] For the experiments reported in this paper, the kinetic energy of the mass-analyzed impacting ion beam was maintained at 0–0.4 eV except where otherwise indicated. Pulse-counting techniques were used for measuring product ion intensities.

Vinyl chloride used in these experiments was obtained from the Matheson Co. and was purified by conventional vacuum distillation. Gas chromatographic analysis indicated only trace impurities.

Results and Discussion

The low-pressure mass spectrum of vinyl chloride is comparatively simple, consisting of only four ions of appreciable intensity which have the relative abundances: $C_2H_2^+$, 32.3%; $C_2H_3^+$, 100%; $C_2H_3{}^{35}Cl^+$, 84.5%; $C_2H_3{}^{37}Cl^+$, 26.6%. Therefore, it is the ion–molecule reactions of these four principal primary ions which will be of significance for the vinyl chloride system. The reaction of each of these ions with the parent molecule was examined in the tandem mass spectrometer at a reaction chamber pressure of 5 μ. The observed ionic products and their relative intensities in each case are indicated by the series of reactions 1–3c.

	Relative intensity	
$C_2H_2^+ + C_2H_3Cl \rightarrow C_2H_3Cl^+ + C_2H_2$	1.0	(1)
$C_2H_3^+ + C_2H_3Cl \rightarrow C_4H_5^+ + HCl$	0.21	(2a)
$\rightarrow C_2H_4Cl^+ + C_2H_2$	0.79	(2b)
$C_2H_3Cl^+ + C_2H_3Cl \rightarrow C_3H_4Cl^+ + CH_2Cl$	0.80	(3a)
$\rightarrow C_4H_5Cl^+ + HCl$	0.06	(3b)
$\rightarrow C_4H_6Cl^+ + Cl$	0.14	(3c)

In order to investigate the details of reactions 1 and 2, the acetylene and vinyl ions were treated with vinyl chloride-d_3.

	Relative intensity	
$C_2H_2^+ + C_2D_3Cl \rightarrow C_2D_3Cl^+ + C_2H_2$	1.00	(4)
$C_2H_3^+ + C_2D_3Cl \rightarrow C_2D_3^+ + (C_2H_3Cl)$	0.24	(5a)
$\rightarrow C_4H_3D_2^+ + DCl$	0.09	(5b)
$\rightarrow C_4H_2D_3^+ + HCl$	0.11	(5c)
$\rightarrow C_2D_3HCl^+ + C_2H_2$	0.56	(5d)

Reaction 4 shows that the charge-transfer reaction of acetylene ion with vinyl chloride-d_3 does not involve an intimately bonded intermediate complex since no hydrogen is incorporated in the charge-transfer product. It can probably best be interpreted as an electron-transfer reaction. However, reactions 5a–5d show that in addition to the $C_4X_5^+$ product and $C_2X_4Cl^+$ products observed in reactions 2a and 2b, about 24% of the total reaction of vinyl ions yields a $C_2D_3^+$ product. The corresponding product from reaction 2 is not detected since it would be obscured by the primary signal. This reaction could proceed either by a Cl^- transfer from the vinyl chloride molecule to the vinyl ion, by proton transfer from the ion to the neutral species, followed by dissociation of the excited protonated ion to yield the products indicated, or by dissociative charge transfer. Both the latter reactions are highly endothermic for ground-state ions and tentatively may be ruled out. Reaction 5d shows that simple proton transfer is the most important reaction in which the vinyl ion participates, while reactions 5b and 5c suggest that the $C_4X_5^+$ product is formed from an intermediate complex which eliminates HCl and DCl with about equal probability. An identical distribution for the $C_4X_5^+$ products was obtained when $C_2D_3^+$ reacted with C_2H_3Cl. This suggests that the products in both of these cases result from decomposition of $(C_4D_3H_3Cl^+)^*$ complexes which are very similar in structure and internal energy, and a normal isotope effect in the decomposition of the complex is responsible for the fact that $C_4H_3D_2^+$ constitutes 44% of the total $C_4X_5^+$ product.

(14) J. H. Futrell, T. O. Tiernan, F. P. Abramson, and C. D. Miller *Rev. Sci. Instr.*, 39, 340 (1968).

(15) J. H. Futrell and C. D. Miller, *Rev. Sci. Instr.*, 37, 1521 (1966).

In addition to reactions 3a–3c of the parent vinyl chloride ion, reaction 6, the charge-transfer reaction, was also observed.

$$C_2H_3{}^{35}Cl^+ + C_2H_3{}^{37}Cl \rightarrow C_2H_3{}^{37}Cl^+ + C_2H_3{}^{35}Cl \quad (6)$$

The corresponding reaction with $C_2H_3{}^{35}Cl$ neutrals cannot be observed in the tandem spectrometer, but if it is assumed to occur with the same cross section as reaction 6, then simply on the basis of the relative abundances of the ^{35}Cl and ^{37}Cl neutrals in the vinyl chloride reactant, this reaction should be more intense by a factor of 3 than reaction 6. This would mean that the total charge-transfer reaction of $C_2H_3Cl^+$ ions with vinyl chloride has a cross section which is larger by a factor of 30 than the other ion–molecule reactions of this ion. Reactions of $C_2D_3Cl^-$ with C_2H_3Cl are reported in Table VI and will be discussed in a later section.

Further information on reactions 3a–3c can be obtained from a study of the isotopic chlorine distribution in the product ion resulting from impact of ^{35}Cl or ^{37}Cl reactant ions. Since the minor chlorine isotope is of substantial natural abundance and since the reactant ion is mass selected in the tandem instrument, it is possible to investigate the source of the chlorine atom which ultimately appears in the product ion. Three limiting cases for a given reaction may be considered. The product ions may retain the chlorine isotope of the reactant ions (case A), the chlorine isotope of the reactant neutrals (case B), or may consist of ions containing chlorines from both reactants, the isotopes being distributed

$$RCl^{+*} + RCl \rightarrow RCl^{+*} + RCl \quad (A)$$

$$RCl^{+*} + RCl \rightarrow RCl^{+} + RCl^{*} \quad (B)$$

$$RCl^{+*} + RCl \rightarrow [R_2ClCl^{+*}] \rightarrow RCl^{+}(RCl^{+*}) + RCl^{*}(RCl) \quad (C)$$

in a purely random fashion (case C). The latter distribution is anticipated if the ion–molecule reaction under consideration involved the formation of an intermediate collision complex which is sufficiently long-lived to permit scrambling of the chlorine isotopes. The calculated distribution of isotopic chlorine in the product ions which would be expected for each of these three cases is shown for both ^{35}Cl and ^{37}Cl reactant ions in Table I. The experimentally observed distributions are shown in Table II for reactions of both isotopic species of two different ions.

Table I: Calculated Distribution of Isotopic Chlorine Products for Reactions of Ions with Vinyl Chloride

Isotope in reactant ion	Isotopic distribution of product ions — Mechanism — A: ^{35}Cl	A: ^{37}Cl	B: ^{35}Cl	B: ^{37}Cl	C: ^{35}Cl	C: ^{37}Cl
^{35}Cl	1.0	0	0.75	0.25	0.88	0.12
^{37}Cl	0	1.0	0.75	0.25	0.38	0.62

Table II: Observed Distribution of Isotopic Chlorines in Selected Product Ions for Reactions of Various Ions with Vinyl Chloride

Reactant ion	Product ions, % — $C_2H_3Cl^+$ ^{35}Cl	$C_2H_3Cl^+$ ^{37}Cl	$C_4H_6Cl^+$ ^{35}Cl	$C_4H_6Cl^+$ ^{37}Cl	$C_4H_6Cl^+$ ^{35}Cl	$C_4H_6Cl^+$ ^{37}Cl
$C_2H_3{}^{35}Cl^+$	86.6	13.4	82.8	17.2	87.6	12.4
$C_2H_3{}^{37}Cl^+$	38.8	61.2	...	...	39.8	60.2
$C_2H_4{}^{35}Cl^+$	NR	NR	NR	NR	87.4	12.6
$C_2H_4{}^{37}Cl^+$	NR	NR	NR	NR	37.9	62.1

A comparison of the calculated and experimental data of Tables I and II clearly indicates a randomized chlorine distribution in the product ions and strongly suggests that the reactions of $C_2H_3Cl^+$ and $C_2H_4Cl^+$ proceed through $[C_4H_6Cl_2{}^{+*}]$ and $[C_4H_7Cl_2{}^{+*}]$ intermediates, respectively. Although observing the chlorine distribution alone could lead to incorrect conclusions about chlorine randomization,[16] the deuterated vinyl chloride results shown in Table III support this mechanism.

Table III: Total Reaction Cross Sections for Ions with Vinyl Chloride

Ion	Cross section, Å²
$C_2H_2^+$	102
$C_2H_3^+$	71
$C_2H_3Cl^+$	37
$C_2H_4Cl^+$	38

Higher order ion–molecule reactions in vinyl chloride are also of interest. Except in unusually favorable cases, pressure limitations on the tandem spectrometer make it impossible to obtain secondary ionic species from the first stage in sufficient abundance to use as reactant ions. Consequently, sequential reactions were investigated by using source molecules which produce by primary fragmentation ions of the same empirical formula as the secondary, tertiary, etc., ions formed in vinyl chloride. For the ions of interest here, $C_2H_4Cl^+$ was obtained from 1,2-dichloropropane, $C_3H_4Cl^+$ from 1,2,3-trichloropropane, and $C_4H_5^+$ from 1,2-butadiene.

(16) In a study of ion–molecule reactions in methyl and ethyl chlorides in our laboratory, chlorine randomization was suggested by the chlorine isotope distribution observed in the protonated alkyl chloride product. When the corresponding reactions were studied using the deuterated parent ions, it was clear that a combination of hydrogen transfer from the neutral molecule and deuteron transfer from the reacting ion was actually occurring. It appears that the protonated alkyl chloride ion is not formed through a randomized intermediate complex but rather that it is produced by simple hydrogen atom and proton-transfer reactions.

The products from these ions are shown in reactions 7a through 9.

$$C_2H_4Cl^+ + C_2H_3Cl \rightarrow C_4H_6Cl^+ + HCl \quad 0.50 \quad (7a)$$

$$C_2H_4Cl^{+*} + C_2H_3Cl \rightarrow C_2H_4Cl^+ + C_2H_3Cl^* \quad 0.50 \quad (7b)$$

$$C_3H_4Cl^+ + C_2H_3Cl \rightarrow C_5H_6Cl^+ + HCl \quad (8)$$

$$C_4H_5^+ + C_2H_3Cl \xrightarrow{M} C_6H_7^+ + HCl \quad (9)$$

Again, the product distributions shown in Table II suggest that reaction 7 goes through an intermediate complex in which chlorine randomization occurs. Similar results were observed from the product from reaction 8. Reaction 7b is apparently a simple proton transfer from the protonated vinyl chlorinde to a vinyl chloride molecule. Reaction 9 could only be observed at high collision chamber pressures (40 μ) and apparently requires collision with a third body for it to occur. A note of caution should be injected in attributing reactions 7 through 9 to the actual reactions of secondary ions in the vinyl chloride system. There may well be differences in both internal energy and structure between secondary ions derived from ion–molecule reactions and those derived from primary fragmentation.

Experiments at Elevated Pressures. Vinyl chloride was also studied at pressures up to 200 μ in a modified time-of-flight mass spectrometer. Figures 1 and 2 illustrate the observed pressure dependences of the intensities of the various ions in the reaction sequence. Figure 1 shows the variation with pressure of vinyl ions and those products which were identified in the tandem

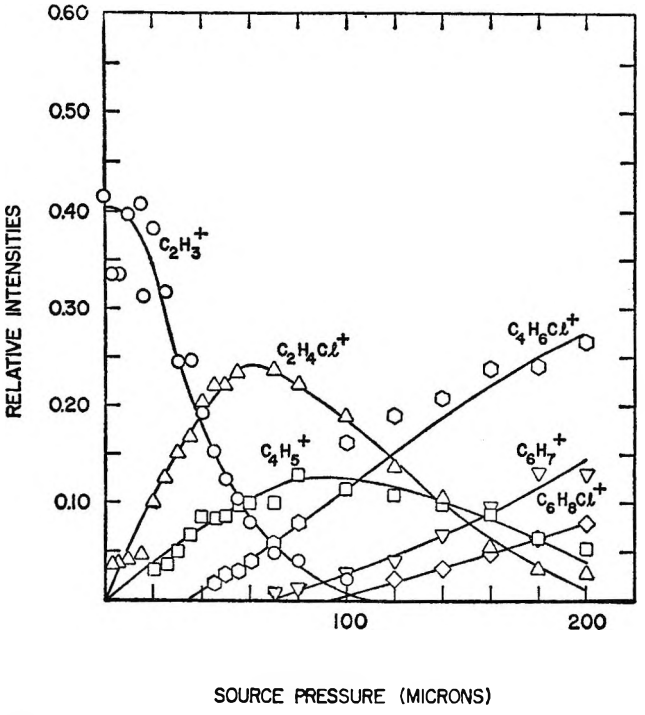


Figure 1. Pressure dependence of vinyl ion and the ionic products ultimately derived from it.

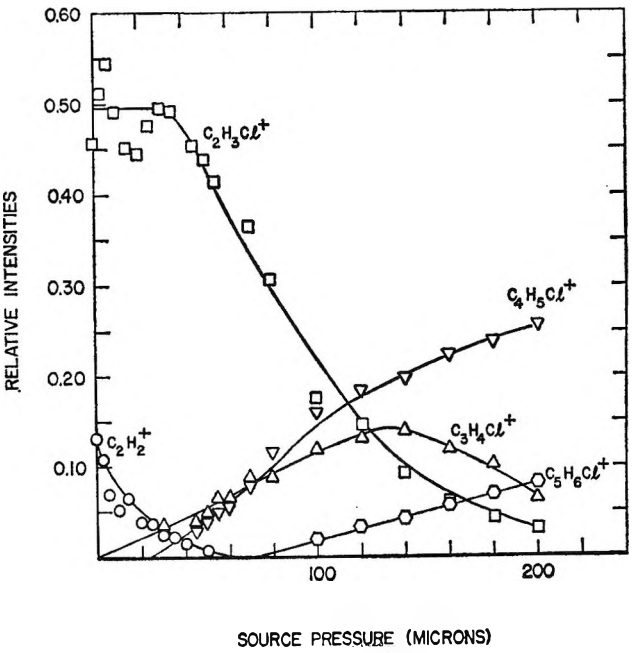


Figure 2. Pressure dependence of vinyl chloride and acetylene ions and products ultimately derived from their reactions.

experiments as having the vinyl ion as a precursor. The observed pressure dependence of relative ion intensities is in accord with the reaction sequence deduced. Similarly, Figure 2 shows the pressure variation of the parent ion and products ultimately derived from its reactions. The apparent "induction" period before parent ion is noted is attributed to the production of vinyl chloride molecular ions *via* the charge exchange reaction of acetylene ion with vinyl chloride (reaction 1). Once acetylene ion has been removed by reaction, the relative intensity of parent ion declines monotonically with pressure.

From semilogarithmic plots of the pressure data, total reaction cross sections were derived for the three major primary ions and for the protonated parent ion (Figure 3). These cross-section data are listed in Table IV. It is apparent that the cross section for the charge-transfer reaction of acetylene ion with vinyl chloride is quite large, and it is to be expected that a substantial fraction of the parent ion will be produced by this path as well as by direct electron impact. Also since the charge transfer of the parent ion with vinyl chloride was indicated by the tandem mass spectrometer study to be some 30 times as important as the other ion–molecule reactions, it is probable that most of the parent ions produced from electron impact undergo charge transfer before a change-of-identity reaction occurs. Further evidence supporting this assertion will be presented subsequently. The lower cross sections measured for the other three ions listed in Table III are understandable in view of the results of the isotopic experiments already cited. The latter experiments showed that all three of these ions have prominent back-reaction channels. In normal experi-

Table IV: Reactions of $C_2H_3Cl^+$, $C_2D_3Cl^+$, $C_2H_2^+$, and $C_2D_2^+$ with C_2H_3Cl at Various Collision Chamber Pressures in the Tandem Mass Spectrometer at a Temperature of 25°

Impacting ion	Pressure, μ	$C_2H_3Cl^+$	$C_3H_4Cl^+$	$C_3H_3DCl^+$	$C_3H_2D_2Cl^+$	$C_3HD_3Cl^+$	$C_4H_5Cl^+$	$C_4H_6Cl^+$	$C_4H_3D_2Cl^+$	$C_4H_2D_3Cl^+$	$C_4H_3D_3Cl^+$
$C_2H_3Cl^+$	5	48,600	1130	0	0	0	194	290	0	0	0
	25	100,000	4540	0	0	0	2430	1610	0	0	0
$C_2D_3Cl^+$	5	39,000	0	291	209	348	26	24	48	82	179
	25	100,000	1880	855	530	1137	1610	1030	267	482	749
$C_2H_2^+$	5	46,500	0	0	0	0	0	0	0	0	0
	25	100,000	1640	0	0	0	1070	700	0	0	0
$C_2D_2^+$	5	50,000	0	0	0	0	0	0	0	0	0
	25	100,000	1520	0	0	0	844	535	0	0	0

ments these reaction modes are not detected since they yield ionic products of the same mass as the reactant. Thus it is not surprising that the observed cross sections for the ions in question are somewhat lower than typically expected.

Additional information regarding the mechanism of the ionic processes involved can be obtained from the high-pressure data by the determination of the orders of formation of the individual ionic species. Since the intensity of a product ion of order, n, is proportional to the nth power of pressure, the reaction order for a particular ion will be given by the slope of a plot of the logarithm of ion intensity as a function of log (vinyl chloride) pressure. Figures 4 and 5 show such plots for various product ions. In these figures the true order of formation of a particular ion will actually be one order higher than that indicated directly by the slope because relative ion intensities (normalized to the total ionization summation) have been used instead of absolute values.

In these figures solid straight lines have been drawn with the appropriate slopes of 1, 2, or 3, for comparison with actual experimental points represented by the various symbols. It is observed that the data fit these lines quite accurately in most cases. Hence we conclude that the ions $C_4H_5^+$ and $C_2H_4Cl^+$ are second-order products, the ions $C_3H_4Cl^+$, $C_4H_5Cl^+$, and $C_5H_6Cl^+$ are

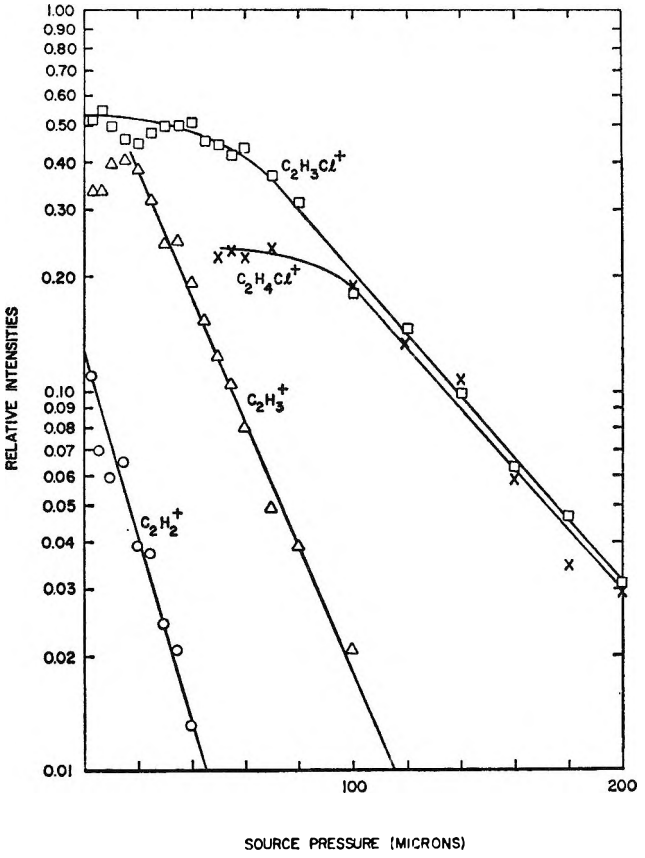


Figure 3. Semilogarithmic plots of relative intensities *vs.* source pressure for the primary ions and protonated vinyl chloride.

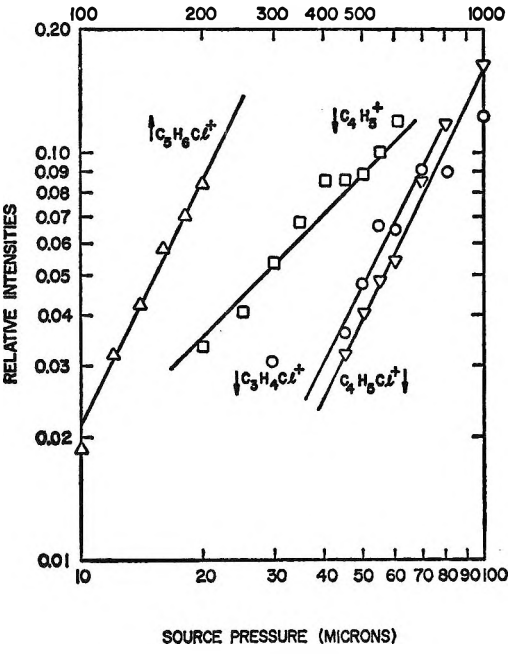


Figure 4. Logarithmic plots of relative intensities *vs.* source pressure for ion products in vinyl chloride.

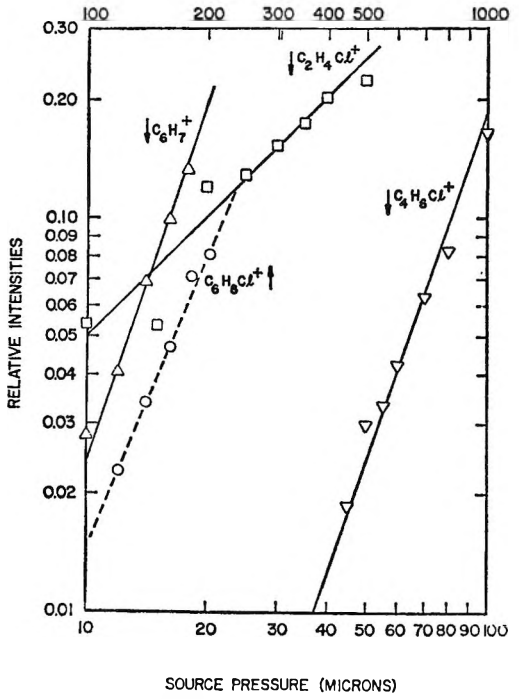


Figure 5. Logarithmic plots of relative intensities *vs.* source pressure for ion products in vinyl chloride.

third order, and the $C_6H_7^+$ and $C_4H_6Cl^+$ products are fourth-order ions. The dashed line drawn through the experimental points for the $C_6H_8Cl^+$ ion is of a non-integral slope suggesting that this ion is of mixed order (third and fourth).

With the exception of the $C_4H_5Cl^+$ and $C_4H_6Cl^+$, the orders determined for these products are in agreement with those predicted by the reaction sequence established by the tandem mass spectrometric results. However, the $C_4H_5Cl^+$ and $C_4H_6Cl^+$ products are one reaction order higher than expected. Here the tandem spectrometer sequence indicates that $C_4H_5Cl^+$ is formed by reaction 3b while $C_4H_6Cl^+$ must result mainly from reaction 7a. The tandem data and the single source data are also in disagreement as to the relative amounts of the $C_3H_4Cl^+$ and $C_4H_5Cl^+$ products. The ratio of products $C_3H_4Cl^+/C_4H_5Cl^+ = 0.80/0.06$ was found in the tandem experiments while the ratio is 0.06/0.05 at 30 μ in the single-stage instrument,

Reactivity of the Parent Ion. It is clear that there are significant discrepancies between the single source and the tandem mass spectrometric results for higher order ionic products in vinyl chloride. Since the over-all reaction sequence appears consistent in both types of experiments, the question of reactant identity does not appear to be the problem. However, there are two notable differences in the properties of primary reactant ions which are formed in these two instruments. In the first place, with the repeller potential employed, the reactant ions in the time-of-flight source have kinetic energies ranging from 0 to 3 eV, while ions in the primary beam of the tandem spectrometer have both a very low kinetic energy and only a small energy spread (0–0.3 eV ion energy) for the experiments under consideration. Secondly, the pressure in the time-of-flight ion source is greater than that in the collision chamber of the tandem, typically by a factor of 10 or more. This means that reactant ions in the former case can undergo multiple collisions whereas a collision chamber pressure of 5 μ for the tandem ensures single-collision conditions. Consequently, there may be substantial differences in the reactivity of the same ion under the two types of experimental conditions. Moreover, the isotopic studies carried out with the tandem spectrometer show that the production of parent ions by charge transfer from both the acetylene ion and the molecule ion is an important process. The parent ions produced by charge transfer may be expected to differ considerably in internal energy content from those produced directly by electron impact. It is therefore likely that the two types of parent ions react quite differently with regard to the production of higher order products.

In order to explore this possibility, the product distributions from impact of $C_2H_2^+$, $C_2D_2^+$, $C_2H_3Cl^+$, and $C_2D_3Cl^+$ ions on vinyl chloride were determined in the tandem mass spectrometer as a function of collision chamber pressure. At low collision chamber pressure, (5 μ), further reactions of the parent ions produced by charge transfer are negligible. Further, for the experiments with impacting $C_2D_3Cl^+$ ions, the isotopically mixed products, $C_3X_4Cl^+$, $C_4X_5Cl^+$, and $C_4X_6^+$ (X = H or D), are a measure of secondary ions derived directly from the impacting parent ions. At a collision chamber pressure of 25 μ, however, the $C_2H_3Cl^+$ ions produced by charge transfer suffer subsequent collisions with neutral vinyl chloride molecules. These ions can therefore react further and contribute to higher order products at this pressure. Since the products derived from the charge-transfer sequence contain no deuterium, the reaction products from the two types of precursor $C_2H_3Cl^+$ ions can be distinguished by such experiments.

Table IV shows the results of impacting these several ions on C_2H_3Cl at various collision chamber pressures. When the impacting ion is $C_2H_3Cl^+$, no distinction can be made between the condensation products formed from $C_2H_3Cl^+$ produced by primary ionization and charge exchange. However, a comparison of the 5- and 25-μ product distributions is quite instructive. The ratio of products $C_3H_4Cl^+:C_4H_5Cl^+:C_4H_6Cl^+$ of 0.70:0.12:0.18 at 5 μ is altered to 0.53:0.28:0.19 at 25 μ. As outlined above, interpretation of the vinyl chloride ion reactions is further clarified by impacting $C_2D_3Cl^+$ on C_2H_3Cl, since the products formed from the impacting ion contain deuterium and those derived from reaction of the charge-exchange product contain no deuterium. At 5 μ the data of Table IV show that no $C_3H_4Cl^+$ and only trace quantities of $C_4H_5Cl^+$ and $C_4H_6Cl^+$ are produced. At 25 μ increased amounts of $C_2H_3Cl^+$ produced by charge exchange and the sub-

Table V: Ratios of Higher Order Products Produced by Various Reactant Ions as a Function of Collision Chamber Pressure at a Temperature of 25°

Impacting ion	C_2H_3Cl pressure, μ	$C_3X_4Cl_{total}^+:C_4X_5Cl_{total}^+:C_4X_6Cl_{total}^+$	$C_3H_4Cl^+:C_4H_5Cl^+:C_4H_6Cl^+$	$C_3D_{n+1}H_{3-n}Cl^+:C_4D_{n+2}H_{3-n}Cl^+:C_4D_3H_3Cl^+$
$C_2H_3Cl^+$	5	0.70:0.12:0.18	0.70:0.12:0.18	...
	25	0.53:0.28:0.19	0.53:0.28:0.19	...
$C_2D_3Cl^+$	5	0.70:0.13:0.17	...	0.73:0.11:0.15
	25	0.52:0.28:0.21	0.42:0.36:0.23	0.63:0.19:0.19
$C_2H_2^+$	5	...	...	...
	25	0.48:0.31:0.20	0.48:0.31:0.20	...
$C_2D_2^+$	5	...	...	...
	25	0.52:0.29:0.18	0.52:0.29:0.18	...

sequent reaction products $C_3H_4Cl^+$, $C_4H_5Cl^+$, and $C_4H_6Cl^+$ are observed.

Two significant facts are apparent from the data. First, if the amount of totally hydrogenated products is compared with the mixed products, it appears that the charge-transfer molecular ion is somewhat more reactive than the molecular ion beam which is produced directly by electron impact. Also, since there is a change in product distribution observed for reaction of $C_2H_3Cl^+$ with vinyl chloride at elevated pressure, it is interesting to note the variation of the C_3 and C_4 product distribution as a function of chamber pressure. Table V shows the relative distributions for the three higher order products for the reaction sequence initiated by the various ions. The first column represents the ratio of the total amounts of these products formed. The second column shows only the ratio of these products which contain no deuterium—that is, the distribution resulting from the charge-transfer ion except for the case of $C_2H_3Cl^+$ reactant. The third column gives the ratio for the mixed products from reaction of $C_2D_3Cl^+$ with C_2H_3Cl and therefore shows the product distribution for the primary ion produced directly by electron impact. It can be seen that the total C_3 and C_4 product distributions observed for the $C_2H_3Cl^+$ and $C_2D_3Cl^+$ reactions with vinyl chloride (shown in column 1) are identical. However, a comparison of the product distribution derived from the parent ion formed by charge exchange with that produced by primary parent ion shows that the two are distinctly different. Moreover, there is a slight change in the product distribution formed directly from the $C_2D_3Cl^+$ primary ion with increasing pressure, as shown in column 3. This is possibly due to collisional degradation of the energy of either the $C_4X_6Cl_2^{+*}$ complex or of the primary ion itself prior to reaction. The latter is possible since a substantial number of "nonreactive" collisions occur in this system.

The product distributions for the vinyl chloride parent ion produced by charge exchange from $C_2H_2^+$ and $C_2D_2^+$ are also reported in Table V. Since the intensity of the acetylene ion from vinyl chloride is rather small, the reactions reported are for acetylene ions derived from acetylene and acetylene-d_2. In one experiment $C_2D_2^+$ from vinyl chloride-d_3 was impacted on vinyl chloride at 25 μ and the observed distribution of products was identical with that reported in Table V within experimental error. The small differences in the product distributions resulting from the two different acetylene ions and from the $C_2D_3Cl^+$ ion at 25 μ which are shown in column 2 are probably indicative of the reproducibility of these measurements.

The extreme sensitivity of the product distribution to the internal energy of the reaction complex prompted several additional experiments. In one series, the distribution of the products derived solely from the charge-transfer ion was studied as a function of collision chamber temperature. Table VI shows these results for charge-transfer parent ions produced from $C_2D_3Cl^+$. By normalizing all the product distributions to the same charge-exchange intensity, the relative rates of reaction to form each product can be compared. A considerably larger fraction of the total reaction leads to condensation products at the lower temperatures than at the higher. Further, the relative yields show that there is an increase in the extent of fragmentation of the complex at higher temperatures; that is, there is an increase in $C_3H_4Cl^+$ at the expense of $C_4H_5Cl^+$. Somewhat surprisingly, the $C_4H_6Cl^+$ relative intensity is a comparatively constant fraction of the condensation products over the entire temperature range, suggesting that it may be formed through a different complex.

A similar but less pronounced temperature effect is seen in Table VII which shows the effect of collision chamber temperature upon the product distribution from reaction of the parent vinyl chloride ion produced directly by electron impact. Again, at higher temperatures, the C_3 product is more important than in the room temperature reaction, although the $C_3H_4Cl^+$ fragment already constitutes a very large fraction of the

Table VI: Effect of Collision Chamber Temperature on the Higher Order Product Distribution and on the Relative Rate for Reaction of $C_2H_3Cl^+$ Produced by Charge Transfer

Collision chamber temp, °C	$C_2H_3Cl^+$	$C_3H_4Cl^+$	$C_4H_5Cl^+$	$C_4H_6Cl^+$	Relative yields $C_3H_4Cl^+:C_4H_5Cl^+:C_4H_6Cl^+$
200	100,000	557	184	213	0.58:0.19:0.22
160	100,000	878	398	406	0.52:0.24:0.24
130	100,000	995	482	436	0.52:0.25:0.23
100	100,000	1330	690	500	0.53:0.27:0.20
90	100,000	1200	712	610	0.48:0.28:0.24
25	100,000	1780	1540	930	0.42:0.36:0.21

Table VII: Effect of Collision Chamber Temperature on Higher Order Product Distribution from Reaction of $C_2H_3Cl^+$ Produced Directly by Electron Impact

Collision chamber temp, °C	Relative yields $C_3H_4Cl^+:C_4H_5Cl^+:C_4H_6Cl^+$
185	0.81:0.06:0.13
135	0.79:0.06:0.15
110	0.78:0.06:0.15
25	0.75:0.08:0.17

total products even at room temperature. Thus it appears that for this system the internal energy of the reacting ion is a major factor in determining the fragmentation channels of the reaction complex. An examination of the data in Table V further suggests that the parent molecule ion produced by electron impact must have considerably more internal excitation than the parent molecule ion formed by charge transfer.

In another series of experiments, the effect of reactant ion translational energy on the relative product distribution was examined. The reaction of the parent ion produced by electron impact was investigated over a rather narrow energy range. It was not possible to study the reaction at higher energies owing to the rapid decrease in reaction cross section with consequent reduction in product ion signal as the energy was raised. Table VIII shows that decreasing the primary ion energy by 0.2 eV results in a slight change in the $C_3H_4Cl^+:C_4H_5Cl^+:C_4H_6Cl^+$ distribution from 0.72:0.10:0.18 to 0.65:0.16:0.18. Essentially the same effect was observed for the distribution produced by secondary parent ions. Table IX shows the reactivity and the product distribution for these as a function of primary ion energy. From the latter table it can be seen that there is an over-all decrease in reactivity of about 50% when the translational energy increases from 0.3 to 1.05 eV. The relative product distribution also changes in the direction of increased fragmentation to $C_3H_4Cl^+$. From 1.05 to 9.05 eV, there is effectively no change in the relative rates of reaction or in the product distribution. Thus it appears that while a small amount of the reactant ion translational energy is converted to internal energy of the complex, there is a limit to the efficiency of this conversion. These observations are consistent with the interpretation of a dual mechanism for charge transfer, one portion of this reaction resulting from a long-range electron jump process largely independent of relative velocity, and the other an orbiting complex component which is significant only at low relative velocity. On the whole, the reaction is relatively independent of reactant ion velocity and certainly this parameter is less significant than internal energy of the reactants for the case under consideration.

Table VIII: Effect of Translational Energy of the $C_2H_3Cl^+$ Reactant on the Product Distribution when $C_2H_3Cl^+$ Is Produced by Electron Impact. Collision Chamber at 25°

Corr ion energy, eV	$C_3H_4Cl^+:C_4H_5Cl^+:C_4H_6Cl^+$
0.50	0.72:0.10:0.18
0.40	0.70:0.12:0.18
0.30	0.65:0.16:0.18

In view of the sensitivity of the parent ion reaction with vinyl chloride to internal energy of the reactants, it seemed appropriate to search for an effect of ionizing electron energy on the higher order product distribution. It was expected that this might provide evidence for the participation of excited states of the reactant $C_2H_3Cl^+$ ions analogous to that obtained in a previous study of the acetylene system.[17] Accordingly, ionization efficiency curves for both primary ions and product ions in vinyl chloride were determined in a single-source instrument, using a C.E.C. 21-103C mass spectrometer at elevated pressures. Figure 6 presents these curves for the three most important primary ions in vinyl chloride along with that of Ar^+ which was used as a reference ion. Taking a value of 15.76 eV for the appearance potential of Ar^+, the following ionization potential and appearance potentials were calculated.

$$IP(C_2H_3Cl^+) = 9.7 \pm 0.3 \text{ eV}$$

$$AP(C_2H_3^+) = 12.8 \pm 0.3 \text{ eV}$$

$$AP(C_2H_2^+) = 13.8 \pm 0.3 \text{ eV}$$

(17) A. D. Walsh, *Trans. Faraday Soc.*, 41, 35 (1945).

Table IX: Effect of Translational Energy of the $C_2H_3Cl^+$ Reactant on the Higher Order Product Distribution when $C_2H_3Cl^+$ Is Produced by Charge Transfer. Collision Chamber at 25°

Corr ion energy, eV	$C_2H_3Cl^+$	$C_3H_4Cl^+$	$C_4H_5Cl^+$	$C_4H_6Cl^+$	$C_3H_4Cl^+$:$C_4H_5Cl^+$:$C_4H_6Cl^+$
0.30	100,000	2220	1850	1200	0.42:0.35:0.20
0.55	100,000	1570	1040	722	0.47:0.31:0.22
1.05	100,000	1180	806	459	0.48:0.33:0.19
1.55	100,000	1110	727	451	0.49:0.32:0.20
2.05	100,000	1050	700	448	0.48:0.32:0.20
3.05	100,000	1100	625	471	0.50:0.28:0.21
4.05	100,000	1090	711	506	0.47:0.31:0.22
6.05	100,000	1100	823	561	0.44:0.33:0.23
9.05	100,000	1110	749	528	0.47:0.31:0.22

These values can be compared with previously reported observations of $IP(C_2H_3Cl^+) = 10.0$[17] and $AP(C_2H_3^+) = 12.8$.[18] Since the appearance potentials of the primary ions are quite widely separated, possible contributions to the higher order products can be readily assessed. Figure 7 shows the $C_3H_4Cl^+$, $C_4H_5Cl^+$, and $C_4H_6Cl^+$ product ion intensities along with the $C_2H_3Cl^+$ and $C_2H_2^+$ primary ion intensities as functions of electron energy. The top three curves are displaced to simplify the figure. The parent ion was identified as the source of the C_3 and C_4 products in the tandem spectrometer and, indeed, the onset of these products corresponds to the appearance potential of the $C_2H_3Cl^+$ ion. However, the product ion curves do not track the parent ion ionization efficiency curve. Instead the product curves exhibit much sharper initial slopes than that of the parent ion. Further, although the primary ion intensity doubles between about 12.0 and 17.0 V, on the uncorrected electron energy scale, there is no additional production of the secondary products. At about 17.0 V there is a striking increase in the C_3 and C_4 product intensities which corresponds closely to the appearance potential of $C_2H_2^+$ ion. This demonstrates clearly the occurrence of reaction 1 when $C_2H_2^+$ ion is formed by primary fragmentation of vinyl chloride and once again establishes that there are two types of reactant parent ions which contribute to the higher order products.

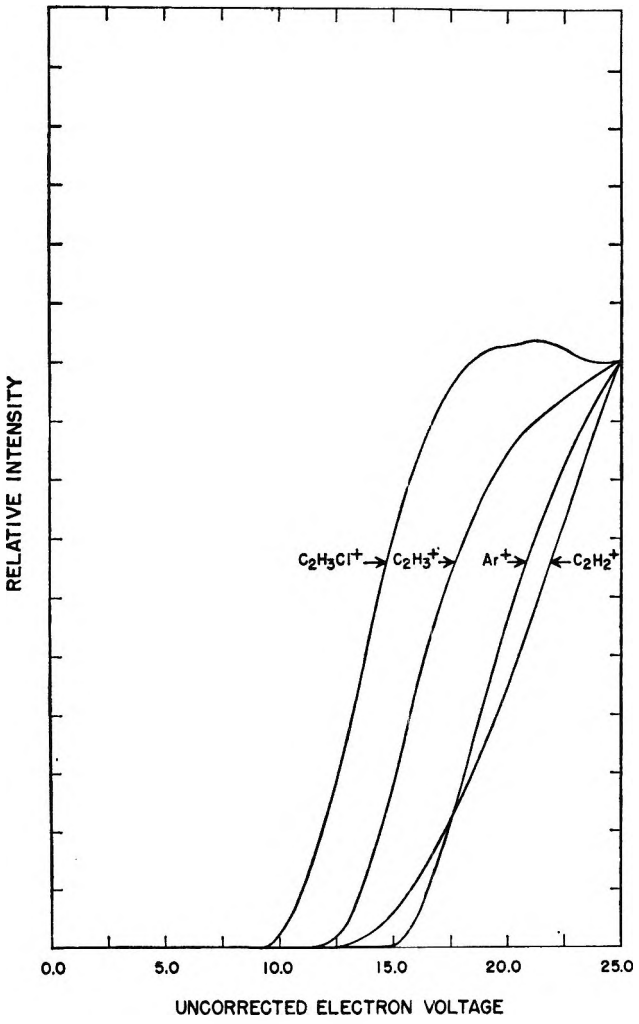


Figure 6. Appearance potential curves for the primary fragment ions of vinyl chloride.

In Figure 8, ionization efficiency curves for the primary ions are again shown along with those for $C_4H_5^+$ and m/e 63. As already noted, the tandem mass spectrometric studies show that $C_4H_5^+$ and $C_2H_4Cl^+$ are formed by reactions of the $C_2H_3^+$ ion. In agreement with this, the $C_4H_5^+$ product is observed to have the same appearance potential as the $C_2H_3^+$ primary. On the other hand, m/e 63 has a much less pronounced onset than does the $C_4H_5^+$ product. This may be explained by the fact that at energies below the appearance potential of $C_2H_3^+$, the m/e 63 product consists of $^{13}C^{12}CH_3Cl^+$ rather than the protonated molecule ion.

It is appropriate to compare our results on ion–molecule reactions in vinyl chloride with the observations for this system from recent experiments conducted by Harrison.[19] The latter investigator has detected both second- and third-order components in the products from reaction of parent ion. He has determined the second-order product distribution to be in the ratio $C_3H_4Cl^+$:$C_4H_5Cl^+$:$C_4H_6Cl^+$ = 0.68:0.16:0.16 at

(18) F. H. Field, *J. Chem. Phys.*, 21, 1506 (1953).
(19) A. G. Harrison, private communication.

Table X: Ratio of $C_3H_4Cl^+$:$C_4H_5Cl^+$:$C_4H_6Cl^+$ Product Distribution from Reactions of Parent Ions with Vinyl Chloride as Observed by Different Experimental Techniques

Source of $C_2H_3Cl^+$ reactant	Primary ionization	Charge transfer from $C_2D_3Cl^+$	Charge transfer from $C_2H_2^+$	High-pressure mass spectrometry (60 μ)
Product distribution from present work	0.80:0.06:0.14	0.42:0.36:0.23	0.48:0.31:0.20	0.40:0.34:0.26
Second-order product distribution from ref 19 (Harrison)	0.70:0.15:0.15			
Third-order product distribution from ref 19 (Harrison)		0.36:0.49:0.15		
Ion cyclotron resonance product distribution from ref 24 (Beauchamp)		0.31:0.58:0.11		

15 eV ionizing electron energy. This can be compared with the corresponding product distribution 0.70:0.12:0.18 observed in the present study for the reaction of parent ion with vinyl chloride at 25° and 5-μ collision chamber pressure in the tandem spectrometer. Harrison found the third-order product distribution to be 0.37:0.48:0.15, which again compares favorably with our distribution produced by charge-transfer parent ions of 0.42:0.36:0.23. These results are summarized in Table X.

Since Harrison's study involved only single-source experiments, he was unable to detect the charge-transfer reaction of the parent ion directly. He has, however, made two significant observations which point to the occurrence of such a process. First, he has noted that the second-order rate constant for reaction of parent ions with vinyl chloride is lower by a factor of 100 than those typically observed for such bimolecular ion–molecule reactions. This would certainly be the case if charge transfer, which Harrison cannot take into account in his rate measurements, were the dominant mode of reaction for this ion. Moreover from our data in Table IV for the reaction of $C_2D_3Cl^+$ ions with vinyl

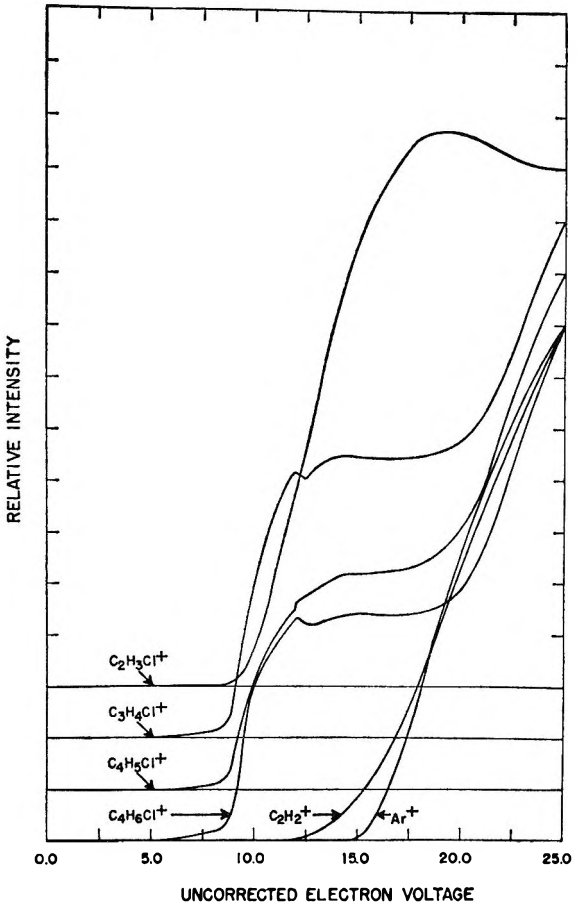


Figure 7. Appearance potential curves for the $C_2H_3Cl^+$ and $C_2H_2^+$ primary ions and for the C_3 and C_4 ionic secondary products.

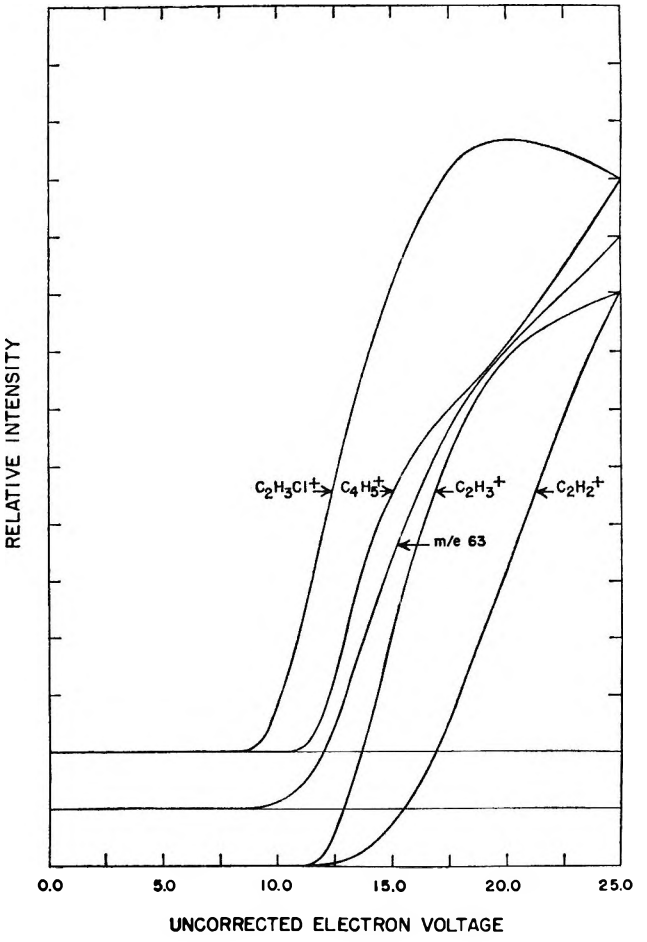


Figure 8. Appearance potential curves for the primary ions in vinyl chloride and the $C_4H_5^+$ and m/e 63 secondary products.

chloride, it can be seen that approximately equal amounts of condensation products are derived from the impacting ion and from the parent ion produced by charge transfer. It can be deduced from this that the rate constant for production of condensation products by the parent ion formed by charge transfer is about 100 times that for the primary parent ion since the intensity of the impacting ion beam is about 10^2 that of the charge-transfer product. Harrison's second observation which supports the charge-transfer sequence is his finding that at elevated source pressures, the withdrawal times for $C_2H_3Cl^+$ ions become very long. This suggests that these ions have been retarded in their passage out of the source, which is readily accounted for as resulting from the predominant charge-transfer reactions.

Comparison of Ion Cyclotron Resonance Spectroscopy with Conventional Mass Spectrometric Techniques. In a recent study of ionic reactions in vinyl chloride, Beauchamp, Anders, and Baldeschwieler[10] deduced the various ion–molecule reaction products using ion cyclotron resonance (icr) spectroscopy. In general their qualitative data are in good agreement with data obtained by conventional mass spectrometric techniques. Notable exceptions are the reported observation of $C_5H_5^+$ and $C_7H_7^+$ using icr while these ions were not detected in the present study However, icr spectroscopy appears to be very sensitive to residual impurities in the system so that the *m/e* 65 and 91 may be due to impurities. Beauchamp, *et al.*, also observed chlorine randomization in reactions 3a–3c, 7a, and 8, as we have discussed in an earlier section of this paper. However, in view of the complicated rection sequence which our study has revealed, the significance of the latter observations is somewhat questionable. Higher reaction sequences were observed by icr spectroscopy using the double-resonance technique. Again these sequences are in general agreement with those which we observe using the combined tandem and high-pressure mass spectrometric techniques. However, the detailed behavior of the parent vinyl chloride ion which was observed in the present study and also to some degree in the single source study by Harrison[19] could not be elaborated in the icr study. Moreover, the data of Beauchamp, *et al.*, give no indication of the overwhelming predominance of charge transfer as the reaction mode for the parent vinyl chloride ion although this reaction was explicitly considered.

It is interesting to compare the relative distributions of secondary products from the parent ion reaction in vinyl chloride as determined by several different methods. Table X shows results reported by Beauchamp[20] using icr, along with the data obtained by Harrison in single-source measurements (to which we have already referred), and the relative yields observed in the ARL tandem mass spectrometer. The column headings give the conditions under which the vinyl chloride parent ion was produced in our experiments. As noted above, Harrison's second-order product distribution has been included under the results for reaction of vinyl chloride parent ion produced directly by primary ionization, while his third-order product distribution is included under the distribution produced by reaction of parent vinyl chloride ion from charge transfer. It is somewhat more difficult to assign the icr data of Beauchamp since he reported neither isotopic studies nor measurements of reaction order. The best quantitative comparison, however, is obtained if the latter distribution is considered to result from the charge-transfer parent ion reactant. This implies that in the icr experiment essentially all of the reactant parent ions are produced by charge transfer, or the complex produced by the primary parent ions is degraded in energy to the extent that it decomposes in the same fashion as the complex formed by the secondary parent ions. As we have already mentioned, the product distributions from the two types of reactants appear to approach the same values with increasing numbers of collisions. The agreement between the distributions shown in Table X under the column labeled, "charge transfer from $C_2D_3Cl^+$," is quite remarkable in view of the demonstrated sensitivity of the reaction to such parameters as temperature, translational energy, and excitation energy of the impacting ion, since these obviously vary rather widely in the several experiments considered. As we have seen, however, the product distribution resulting from secondary parent ions is much less affected by these parameters than is the primary parent distribution. Again, this suggests that charge transfer is much more important for the vinyl chloride system in the cyclotron resonance experiment than has been previously realized.

Summary

The totality of the data obtained for vinyl chloride in the present study is best explained by the following reaction sequence for formation of the higher order condensation products.

$$C_2H_3Cl + e^- \rightarrow C_2H_3Cl^{+*} \quad (10a)$$

$$\rightarrow C_2H_2^+ + HCl \quad (10b)$$

$$C_2H_3Cl^{+*} + C_2H_3Cl \rightarrow C_2H_3Cl^{+\prime} + C_2H_3Cl \quad (11a)$$

$$\rightarrow [C_4H_6Cl_2^+]^* \rightarrow C_3 \text{ and } C_4 \text{ products} \quad (11b)$$

$$C_2H_3Cl^{+\prime} + C_2H_3Cl \rightarrow [C_4H_6Cl_2^+]' \rightarrow C_3 \text{ and } C_4 \text{ products} \quad (12)$$

$$C_2H_2^+ + C_2H_3Cl \rightarrow C_2H_3Cl^{+\prime\prime} + C_2H_2 \quad (13)$$

$$C_2H_3Cl^{+\prime\prime} + C_2H_3Cl \rightarrow [C_4H_6Cl_2^+]'' \rightarrow C_3 \text{ and } C_4 \text{ products} \quad (14)$$

From the appearance potential curves reported in

(20) J. L. Beauchamp, Doctoral Dissertation, Harvard University, 1968.

Figure 7, it can be deduced that the parent ion formed by electron impact in reaction 11a has in excess of 2.0 eV internal energy, probably in the form of vibrational energy. As already shown (reaction 6), charge transfer is more probable for this ion by a factor of 30 than an ion–molecule reaction resulting in a change of identity. Thus only a small fraction of the total reaction of this ion leads to the higher mass condensation products. Probably, in this case, any intermediate complex formed by an intimate collision is sufficiently excited that it fragments almost entirely to the original reactants. The parent ion produced by charge transfer in reaction 12a, however, is expected to differ considerably in internal energy from that produced by direct electron impact and it is apparent that ion–molecule reactions leading to condensation products (by way of an intermediate complex having less excitation energy) are much more favorable for this ion. It seems clear from the data presented in Tables IV and V that the collision complexes produced in reactions 11b, 12, and 14 must have different amounts of internal energy. It also appears that with increasing pressure, the complexes formed in all these processes fragment similarly, since the product distributions all approach the same ratios at higher pressures. This presumably indicates that, at some pressure, all the complexes are reduced to the same level of internal excitation by collisional deactivation. Our results clearly establish that excitation energy of the reactants can dramatically affect the internal energy of the reaction complex. For the vinyl chloride system, however, the translational energy of the reacting ion appears to be much less important than internal energy.

There remains to be explained the fourth-order dependence observed for the $C_4H_6Cl^+$ ion in the high-pressure study. This is possibly explained on the basis of an extra reaction step which would logically involve reaction 7b. That is, two protonation sequences would precede the production of $C_4H_6Cl^+$, and this is perhaps understandable if the $C_2H_4Cl^+$ precursor is highly excited. This additional reaction step would further isolate the $C_4H_6Cl^+$ yield with respect to the influence of the various reaction parameters discussed in this work, and, indeed, the relative yield of this product seems to be very little affected by these factors.

Acknowledgment. The authors express their gratitude to Professor A. G. Harrison for access to his data prior to publication and also for stimulating discussions of ion–molecule reaction problems. They are also indebted to Dr. J. L. Beauchamp for permission to cite unpublished results from his doctoral thesis.

Chemical Effects of Charge-Transfer Absorption. I. The Photoinduced Chain Reaction between Thallium(I) and Thallium(III)

by D. R. Stranks and J. K. Yandell

Department of Physical and Inorganic Chemistry, The University of Adelaide, Adelaide, South Australia 5001 *(Received July 16, 1968)*

Ultraviolet irradiation of ^{204}Tl-labeled thallium(I)–thallium(III) solutions induces rapid exchange with quantum yields ranging from 2 to 30 or higher. Initiation is due to charge-transfer absorption in Tl_{aq}^{3+} and $TlOH^{2+}$ producing a thallium(II) chain carrier. Rate constants for the propagation reactions of thallium(II) with thallium(I) and thallium(III) are derived. Chain termination is largely quadratic disproportionation of thallium(II), but at low light intensities, a linear termination reaction is more important. The relevance of these observations to the thermal mechanism for thallium(I)–thallium(III) exchange is discussed.

Introduction

The high-intensity absorption band of metal complexes, which normally occurs in the 2500–3200-Å region, is often described as a charge-transfer band.[1–3] An alternative molecular orbital description[4] is one of electronic excitation from a bonding orbital to a nonbonding or antibonding orbital. Whereas the charge-transfer microsymmetry is linear suggesting that the excitation involves only a single ligand and the central

(1) R. S. Mulliken, *J. Am. Chem. Soc.*, **74**, 811 (1952).
(2) J. N. Murrell, *Quart. Rev.* (London), **15**, 191 (1961).
(3) F. S. Dainton, Special Publication No. 1, The Chemical Society, London, 1954, p 18.
(4) C. K. Jørgensen, "Absorption Spectra and Chemical Bonding in Complexes," Addison-Wesley Publishing Co., Reading, Mass., 1962.

metal, the molecular orbital description suggests that all ligands are involved. The two descriptions are however very similar in that they both represent a transfer of charge from ligand to metal occurring with a large transition moment, as reflected in a high molar extinction coefficient.

In accord with these interpretations, the absorption of light in the charge-transfer bands of transition metal, lanthanide, and actinide complexes is known to initiate a variety of oxidation–reduction reactions.[5] A basic mechanism for these photochemical reactions may be envisaged as the homolytic dissociation of an excited state into a reduced metal ion and either an oxidized ligand or an oxidized associated anion. In the presence of suitable scavengers or in the event that the initial products are mutually stable, a reduced metal ion is observed as a product. Since dissociation of the excited state is in competition with other energy loss processes operating within a solvent cage, such as fluorescence, internal conversion, intersystem crossing, and energy transfer, the primary quantum efficiency for homolytic dissociation is often significantly less than unity. Additional recombination of dissociative fragments outside the solvent cage will further reduce the quantum yield observed for net product formation.

The known photochemistry of metal cations other than those of the transition elements, lanthanides, or actinides, is very sparse since only a single well-defined oxidation state of main-group elements usually exists in aqueous solution. However in perchloric acid media the +1 and +3 oxidation states of thallium can coexist and in the ultraviolet spectra both of these oxidation states exhibit high-intensity bands which may be assigned to charge-transfer transitions. At 2537 Å, the principal absorbing species in 1 *M* perchloric acid is the hydrolyzed thallium(III) species $TlOH^{2+}$ and a minor absorption occurs owing to the aquated species Tl_{aq}^{3+}. Absorption by Tl_{aq}^{+} only becomes significant at wavelengths shorter than 2537 Å. Absorption of 2537-Å quanta by thallium(III) solutions would be expected to induce the reactions

$$TlOH^{2+} + h\nu \rightarrow Tl^{2+} + OH$$

$$Tl_{aq}^{3+} + h\nu \rightarrow Tl^{2+} + OH + H^{+}$$

In the presence of added Tl_{aq}^{+}, scavenging of all hydroxyl radicals which escape primary and secondary recombination reactions would occur.[6]

$$Tl_{aq}^{+} + OH \rightarrow Tl^{2+} + OH^{-}$$

The 2537-Å photolysis of a thallium(III)–thallium(I) mixture should therefore result in the over-all initiation reaction

$$TlOH^{2+} + Tl_{aq}^{+} + h\nu \xrightarrow{\phi_1} 2Tl^{2+} + OH^{-} \qquad (I)$$

with a quantum yield ϕ_1, together with a minor contributory reaction

$$Tl_{aq}^{3+} + Tl_{aq}^{+} \rightarrow 2Tl_{aq}^{2+} \qquad (Ia)$$

The present study has sought evidence for the photolytic formation of the unstable intermediate oxidation state thallium(II) by investigating the photocatalysis of the thallium(I)–thallium(III) homonuclear electron-exchange reaction

$$*Tl^{III} + Tl^{I} \rightleftarrows *Tl^{I} + Tl^{III}$$

detected by isotopic labeling with ^{204}Tl. If reaction I accurately represents the initiation reaction induced by 2537-Å photolysis of a thallium(I)–thallium(III) mixture, then this could be followed by chain-propagation reactions involving a Tl^{2+} chain carrier

$$*Tl^{3+} + Tl^{2+} \rightleftarrows *Tl^{2+} + Tl^{3+} \qquad (k_{III})$$

$$*Tl^{2+} + Tl^{+} \rightleftarrows *Tl^{+} + Tl^{2+} \qquad (k_{I})$$

and a quadratic chain-termination reaction.

$$Tl^{2+} + Tl^{2+} \rightarrow Tl^{+} + Tl^{3+} \qquad (k_t)$$

Our generalized treatment of photoinduced chain reactions[7] suggests that, for this anticipated mechanism, the quantum yield for the over-all electron-exchange reaction is

$$\phi_{ex} = \phi_1 \left\{ \frac{k_I[Tl^I]k_{III}[Tl^{III}]}{k_I[Tl^I] + k_{III}[Tl^{III}] + 2(k_t I_{abs}\phi_1)^{1/2}} \times \left(\frac{1}{k_t I_{abs}\phi_1}\right)^{1/2} + \frac{k_I[Tl^I] + k_{III}[Tl^{III}] + (k_t I_{abs}\phi_1)^{1/2}}{k_I[Tl^I] + k_{III}[Tl^{III}] + 2(k_t I_{abs}\phi_1)^{1/2}} \right\} \qquad (1)$$

where ϕ_{ex} is the observed rate of electron exchange per absorbed light intensity, *i.e.*, R_{ex}/I_{abs}. The second term of eq 1 represents the contribution to electron exchange from the termination reaction in the absence of any propagation reaction. Alternatively, if the Tl^{2+} chain carrier were to undergo linear termination by reactions with a trace impurity or at the vessel walls, both proceeding at the same rate, as in

$$Tl^{2+} - S' \rightarrow Tl^{I} \quad \text{and} \quad Tl^{2+} + S'' \rightarrow Tl^{III} \qquad (k_t')$$

then ϕ_{ex} would be independent of light intensity.

$$\phi_{ex} = \phi_1 \left\{ \frac{k_I[Tl^I]k_{III}[Tl^{III}]}{k_I[Tl^I] + k_{III}[Tl^{III}] + 2k_t'} \left(\frac{1}{k_t'}\right) + \frac{k_I[Tl^I] + k_{III}[Tl^{III}] + k_t'}{k_I[Tl^I] + k_{III}[Tl^{III}] + 2k_t'} \right\} \qquad (2)$$

This study has therefore aimed at a quantitative

(5) A. W. Adamson, W. L. Waltz, E. Zinato, D. W. Watts, P. D. Fleischauer, and R. D. Lindholm, *Chem. Rev.*, **68**, 541 (1968).

(6) M. Anbar and P. Neta, *Intern. J. Appl. Radiation Isotopes*, **16**, 277 (1965).

(7) D. R. Stranks and J. K. Yandell, "Exchange Reactions" IAEA, Vienna, 1965.

evaluation of the catalytic effect of thallium(II) on the Tl(I)–Tl(III) exchange reaction. The findings are relevant to the general question of whether this thermal exchange reaction proceeds by a concerted transfer of two electrons or by a one-electron transfer to form thallium(II) followed by rapid disproportionation to thallium(I) and thallium(III); the latter reaction is the quadratic termination reaction described by k_t.

Experimental Section

Thallous perchlorate solutions were prepared by dissolving BDH thallous carbonate in dilute perchloric acid. Thallic perchlorate solutions were prepared either by dissolving BDH thallium(III) oxide in 5 *M* perchloric acid or by the anodic oxidation of thallous perchlorate solutions. Water which was twice distilled from $KMnO_4$ and K_2CrO_7 was used for all purposes. The use of vacuum-distilled perchloric acid, instead of AR grade perchloric acid, made no observable difference to measured quantum yields. The ^{204}Tl tracer was prepared in both oxidation states by treatment of thallous carbonate irradiated in the HIFAR reactor, Sydney, Australia.

Photolyses were performed in a cylindrical silica reaction vessel (2.5-cm diameter, 1-cm length) located in a constant-temperature water bath. Solutions in this vessel could be stirred and deaerated, but as these parameters did not affect quantum yields, these procedures were not followed in most photolyses.

The 2537-Å line, isolated from the output of a Hanovia low-pressure spiral mercury arc, was used as the principal light source. The arc was aligned with the reaction vessel on an optical bench. Light from the arc passed through 3 cm of water before it impinged on the reaction vessel thereby completely filtering out the 1849-Å radiation from the arc. Incident light intensities were determined by the ferrioxalate method of Hatchard and Parker.[8] A correction of 10% was necessary for light of wavelengths greater than 2537 Å which is photoactive in the ferrioxalate system but is not absorbed by the thallium solutions.

An Osram 400-W xenon arc coupled to a Bausch and Lomb high-intensity grating monochromator was used as a light source for measurement of quantum yields as a function of wavelength. The slits used with the monochromator were claimed by the manufacturer to give 90% emission within ±50 Å of the dialed wavelength. A 1-cm path length silica spectrophotometric cell, located in front of the exit slit such that all the reactant solution was illuminated, was used as a reaction vessel.

The intensity of the light absorbed by each thallium species was calculated from the measured incident light intensity and individual extinction coefficients either reported by Waind and Rogers[9] or determined experimentally.

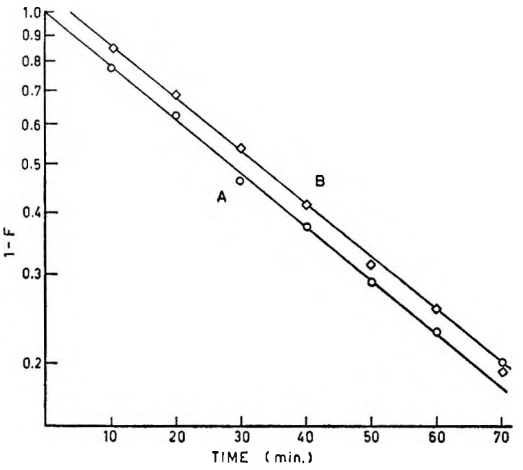


Figure 1. Typical rate plots: (A) preirradiated, [Tl(III)] = 0.005 *M*, [Tl(I)] = 0.0051 *M*, Tl(I) labeled; (B) not preirradiated, [Tl(III)] = 0.0051 *M*, [Tl(I)] = 0.005 *M*, Tl(III) labeled.

Fractions of exchange were determined by a separation scheme[10] based on thallium(I) chromate precipitation which in thermal exchanges gave less than 2% zero-time exchange. Both oxidation states were subjected to radioactive assay in a conventional GM liquid counting assembly. Rates of exchange were then determined from the customary log $(1 - F)$ *vs.* time plots. Initial rate experiments with carefully purified reagents gave excellent linear plots but small induction periods of a few minutes were observed; *i.e.*, extrapolation of log $(1 - F)$ to $F = 0$ gave positive time intercepts. These small induction periods evidently arose from traces of impurities, probably organic in nature. The induction periods were completely removed by preirradiating reactant solutions at 2537 Å for 1 hr prior to the addition of 2 or 3 drops of the ^{204}Tl tracer. The observed half-times for exchange were identical for preirradiated solutions and for solutions exhibiting small induction periods (Figure 1). Quantum yields quoted below all refer to freshly prepared reagents subjected to this preirradiation treatment.

Results

Half-times for the thermal thallium(I)–thallium(III) electron exchange at 25° range from 20 to 100 hr, depending on the reactant concentrations. When irradiated at 2537 Å, half-times for the electron-exchange system fell within the range 4–120 min. Consequently, no significant correction for the thermal-exchange rate was necessary.

Uncertainties in observed quantum yields, ϕ_{ex}, are

(8) C. G. Hatchard and C. A. Parker, *Proc. Roy. Soc.* (London), A235, 518 (1956).

(9) G. M. Waind and T. E. Rogers, *Trans. Faraday Soc.*, 57, 1360 (1961).

(10) I. R. Jonasson and D. R. Stranks, *Electrochim. Acta*, 13, 1147 (1968).

Table I: Dependence of ϕ_{ex} on Thallium(I) Concentration at 25°, 0.005 *M* Tl(III), and 1.1 *M* $HClO_4$

10^2[Tl(I)], *M*	$t_{1/2}$, min	$10^6 I_{abs}$, einsteins $l.^{-1}$ min^{-1}	ϕ_{ex}[b]	ϕ^1_{ex}[c]	ϕ^2_{ex}[d]
0.11	32 ± 4	12.9	1.51	1.55	1.88
0.26	31 ± 3	11.9	3.12	3.10	3.75
0.50	29, 30	12.1	4.90	4.90	5.95
0.51	33, 33, 31, 31, 29	11.8	4.65	4.62	5.62
1.00	42	12.0	4.61	4.61	5.61
	28	12.0	6.94	6.9	8.43
2.00	28	11.9	10.0	9.47	12.1
5.00	23	11.3	12.1	12.1	14.7
7.50	11	37.7	7.90	11.8	14.3
10.0	20,[a] 22[a]	11.4	13.6	13.4	16.3
15.0	11	34.3	8.75	12.7	15.4

[a] This thallium(III) solution was prepared from dissolution of Tl_2O_3; all other solutions were from dissolution of Tl_2CO_3 and anodic oxidation. [b] $\phi_{ex} = R_{ex}/I_{abs}$. [c] ϕ_{ex}^1 is the quantum yield for absorption by both Tl_{aq}^{3+} and $TlOH^{2+}$, corrected to $I_{abs} = 12.0 \times 10^{-6}$ einsteins $l.^{-1}$ min^{-1}. [d] ϕ_{ex}^2 is the quantum yield for absorption only by $TlOH^{2+}$, corrected to $I_{abs} = 12.0 \times 10^{-6}$ einsteins $l.^{-1}$ min^{-1}.

compounded from errors in both I_{abs} and R_{ex}. Errors in I_{abs} arise from both the experimental measurement of I_0 and the estimate, made from measured extinction coefficients, of the fraction absorbed of the incident light intensity. A total random error of ±3% and a systematic error up to ±9% is estimated in I_{abs}. The latter error is dependent on the magnitude of I_{abs}/I_0. Rates of exchange, as evaluated from log $(1 - F)$ *vs.* time plots, were subject to variations not exceeding ±5% for thermal rate measurements, but a variation of ±10% arose for photochemical rates. At a constant incident light intensity, the random error in ϕ_{ex} will be ±10%, but, at different light intensities, a random error of ±12% applies. It may be shown that even for solutions of high optical absorbances, the correction to ϕ_{ex} for nonuniform light absorption lies within the error limits and no correction for this effect was applied. The errors quoted above are expressed at the 90% confidence limit.

Under all conditions of reactant concentrations, light intensities, and temperature, the observed quantum yields for exchange exceeded unity and typically fell in the range 2–30. The general chain characteristics of the photochemically induced exchange are thereby established. Quantum yields were unaffected by the presence or absence of dissolved oxygen or by mechanical stirring. The photochemical exchange was extraordinarily sensitive to traces of Fe^{2+} and Fe^{3+} and the reaction could be virtually stopped at concentrations exceeding 10 μM.

Dependence of ϕ_{ex} on Thallium(I) Concentration. Table I summarizes the variation of ϕ_{ex} with thallium(I) concentration. The observed value of ϕ_{ex} $(= R_{ex}/I_{abs})$ is calculated from the absorbed light intensity due to Tl_{aq}^{+}, Tl_{aq}^{3+}, and $TlOH^{2+}$. The quantity ϕ^1_{ex} refers to quantum yields calculated on the basis of absorption by both Tl_{aq}^{3+} and $TlOH^{2+}$ and treating Tl_{aq}^{+} as an inactive absorbing species. Similarly ϕ^2_{ex} refers to quantum yields based on absorption by $TlOH^{2+}$ as the only active chromophore. Both ϕ^1_{ex} and ϕ^2_{ex} values have been normalized to a constant absorbed light intensity using the experimental intensity exponents summarized below.

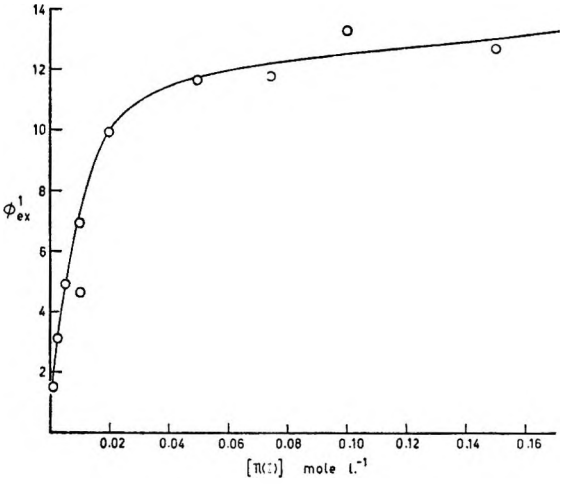


Figure 2. [Tl(I)] dependence.

Figure 2 shows that, at constant $[Tl^{III}]$, values of ϕ^1_{ex} (and also ϕ_{ex} and ϕ^2_{ex}) are approximately linear at low $[Tl^{I}]$ and approach a limiting "plateau" value at high $[Tl^{I}]$. This functional behavior is consistent with eq 1 for the important condition

$$k_I[Tl^I] + k^{III}[Tl^{III}] \gg 2(k_t I_{abs}\phi_1)^{1/2}$$

such that eq 1 simplifies to the form

$$\phi_{ex} = \phi_1 \left\{ \frac{k_I[Tl^I]k_{III}[Tl^{III}]}{k_I[Tl^I] + k_{III}[Tl^{III}]} \frac{1}{(k_t I_{abs}\phi_1)^{1/2}} + 1 \right\} \quad (3)$$

A convenient form of (3) to test the experimental results is

$$\frac{1}{\phi_{ex} - \phi_1} = \left\{ \frac{k_t I_{abs}}{\phi_1} \right\}^{1/2} \left\{ \frac{1}{k_{III}[Tl^{III}]} + \frac{1}{k_I[Tl^I]} \right\} \quad (4)$$

Figure 3 illustrates a plot of $1/\phi_{ex}$ *vs.* $1/[Tl^I]$, and the

Table II: Intensity Exponents of Photocatalyzed Exchange at 25°; 1.1 *M* $HClO_4$

10^2[T(I)], *M*	10^2[T(III)], *M*	Number of measurements	Range of $10^6 I_{abs}$, einsteins $l.^{-1}$ min^{-1}	*n* ($\phi_1 \simeq 0$)	*n* ($\phi_1 = 0.5$)
10.0	0.51	7	0.90–36.2	-0.27 ± 0.05	-0.28 ± 0.05
5.0	0.50	10	0.96–73.8	-0.34 ± 0.02	-0.35 ± 0.02
0.51	4.0	5	2.24–32.3	-0.37 ± 0.05	-0.40 ± 0.05
0.32	4.1	5	3.08–130	-0.44 ± 0.03	-0.51 ± 0.05

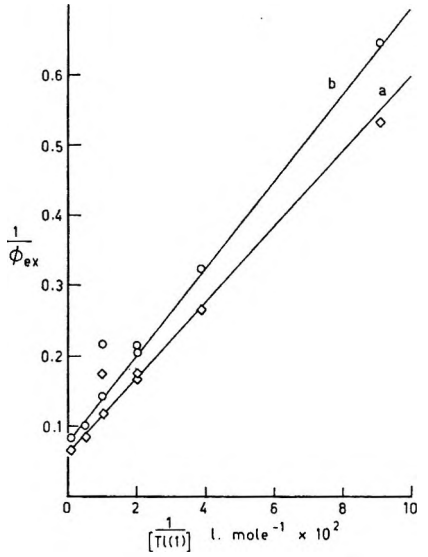


Figure 3. [Tl(I)] dependence. $a = 1/\phi^1_{ex}$; $b = 1/\phi^2_{ex}$.

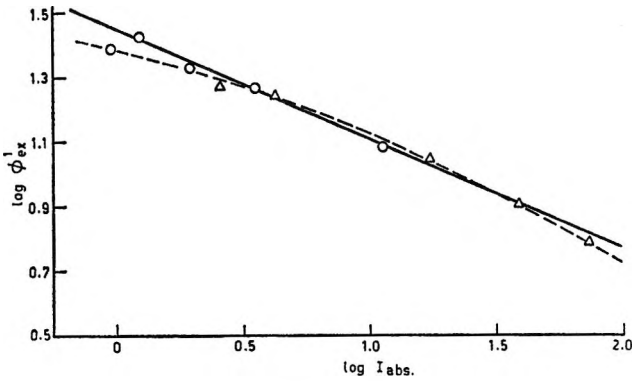


Figure 4. I_{abs} dependence. [Tl(I)] = 0.050 *M*; [Tl(III)] = 0.0051 *M*.

linearity of the plot, within the experimental errors, suggests that $\phi_{ex} \gg \phi_1$ under the experimental conditions. A value of $k_{III}/k_I = 1.6 \pm 0.5$ is derived from the ratio of slope to intercept of this plot. Equation 4 appears to be applicable over a 150-fold variation in $[Tl^I]$. An expression analogous to (4) would also apply to the linear termination mechanism described by eq 2. The applicability of these alternatives is decided by the intensity dependence of ϕ_{ex}.

Equation 3 predicts that at vanishingly low $[Tl^I]$ ϕ_{ex} tends to ϕ_1. Extrapolation of ϕ_{ex} at $[Tl^I] \leq 0.005$ *M* yields a value of $\phi_1 = 0.5 \pm 0.3$; the relatively large systematic and random errors in ϕ_{ex}, together with difficulties of working at low concentrations, preclude a really satisfactory estimate of ϕ_1.

Intensity Dependence of ϕ_{ex}. A chain mechanism terminated by a quadratic or mutual reaction requires an intensity exponent of −0.50 (eq 3) while a linear termination reaction would require ϕ_{ex} to be independent of I_{abs} (eq 2). Four series of measurements were undertaken; each series was conducted at constant $[Tl^I]$ and $[Tl^{III}]$ and over as wide a variation of light intensity as possible. One such series is illustrated in Figure 4 wherein the intensity exponent *n* in the equation

$$\phi_{ex} - \phi_1 = (\text{constant})(I_{abs})^n$$

is deduced from a graphical plot of log ϕ_{ex} *vs.* log I_{abs}.

In this instance $n = -0.34$, assuming $\phi_1 \simeq 0$, and $n = -0.36$, assuming the approximate value deduced above, namely, $\phi_1 = 0.5$. Intensity exponents deduced in this manner are summarized in Table II where it is seen that the −0.5 exponent required by a quadratically terminated chain mechanism is approached at higher light intensities. In each series, plots of ϕ_{ex} *vs.* $I_{abs}^{-1/2}$ were linear at high values of I_{abs} but deviations from linearity occurred at low light intensities. It is suggested that quadratic chain termination is the predominating contributor to the over-all mechanism of the chain reaction. However some linear termination accounts for the lower intensity exponent under some experimental conditions.

In the case where termination is partly quadratic and partly linear, our generalized treatment of chain-exchange reactions[7] yields an explicit solution for the dependence of ϕ_{ex} on reactant concentrations and I_{abs} which cannot be cast in a form against which the experimental data can be tested graphically. However, the relative rates of the quadratic to the linear termination reactions, $k_t[Tl^{2+}]/k_t'$, can be deduced numerically by the method described in the Appendix. The dashed curve in Figure 4 is based on this procedure and the curve reproduces the experimental points within the experimental error. This numerical analysis shows that the ratio of the rate of the quadratic termination reaction to that of the linear termination reaction varies from 0.26 at the lowest light intensities employed to 5.0 at the highest light intensities. Thus at the highest light intensities some 10% of all Tl(II) is being scavenged by the linear termination reaction(s). This analysis shows that under these conditions an

Table III: Variation of ϕ_{ex} with Thallium(III) Concentration at 25°, 0.050 M Tl(I), and 1.1 M $HClO_4$

10^2[Tl(III)], M	$t_{1/2}$, min	I_{abs}/I_0	$10^6 I_{abs}^1$, einsteins l.$^{-1}$ min^{-1}	ϕ^1_{ex}	$10^6 I_{abs}^2$, einsteins l.$^{-1}$ min^{-1}	ϕ^2_{ex}
1.1	49	0.336	2.86	5.18	2.35	6.30
2.1	47	0.333	5.14	5.54	4.21	6.73
5.1	23	0.330	11.3	12.1	9.28	14.8
10.1	20	0.550	18.4	15.6	15.1	19.0
	17	0.550	18.4	18.4	15.1	22.4
15.1	17	0.691	23.2	20.1	19.1	24.4
20.1	17	0.785	26.3	20.7	21.6	25.2
42.4	21	0.940	31.5	24.2	25.8	29.2

intensity exponent of −0.44 would be exhibited by the chain reaction at the high range of light intensities while this would fall to −0.15 at the lowest range of light intensities.

The numerical analysis also confirms that the plateau dependence of ϕ_{ex} on [Tl^I] (Figure 2) could not arise from the increased importance of a linear termination reaction at high [Tl^I]. Any reduction in ϕ_{ex} from this source is within the experimental uncertainty in ϕ_{ex}. This plateau must arise from the balancing effect of the two propagating reactions described by k_{III} and k_I.

Attempts were made to determine the rate constant for the quadratic termination reaction k_t by rotating-sector techniques. Flashing times down to 5 msec were employed but the reduction in ϕ_{ex} from the value for uninterrupted illumination was only of the order of 10%. It was concluded that k_t was of the order of diffusion-controlled rate constants (10^{10} M^{-1} sec^{-1}). The difficulties of achieving significantly shorter flashing times and of entirely eliminating linear termination reactions precluded further work in this direction.

Dependence of ϕ_{ex} on Thallium(III) Concentration. The variation of ϕ_{ex} with thallium(III) concentrations ranging from 0.0011 to 0.0424 M was investigated at a constant thallium(I) concentration of 0.050 M. Since thallium(III) is the principal light-absorbing species, variation of [Tl^{III}] involves simultaneous variation of a reactant and absorbed light intensity. Table III shows that ϕ^1_{ex} and ϕ^2_{ex} (referring to total thallium(III) and $TlOH^{2+}$ absorption, respectively) increase with increasing [Tl^{III}] and approach a limiting plateau value at high [Tl^{III}]. Equation 4, based on a purely quadratic termination chain mechanism, requires that at constant [Tl^I], $1/(\phi_{ex} - \phi_1)I_{abs}^{1/2}$ should be linear in $1/$[Tl^{III}]; this is tested in Figure 5 with the reasonable assumption that $\phi_1 \ll \phi_{ex}$. The deviation of the low-intensity points at high values of $1/$[Tl^{III}] may be accounted for by the error in the assumption that $\phi_{ex} \propto I_{abs}^{-1/2}$. The ratio of the slope to intercept of this plot yields a value of $k_{III}/k_I = 1.9 \pm 0.5$, in good agreement with the value obtained from the independent series of ϕ_{ex} measurements at variable thallium(I) concentrations.

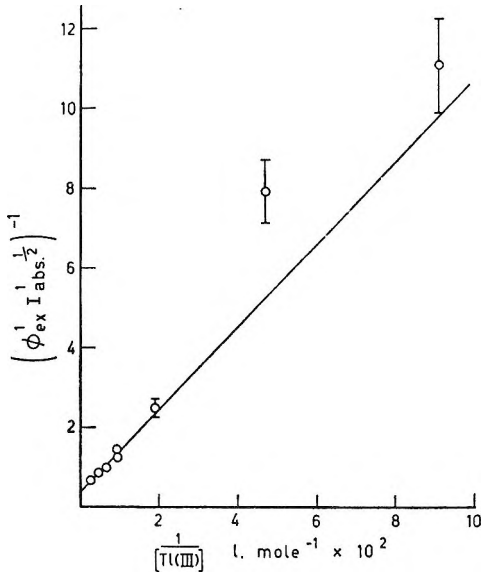


Figure 5. [Tl(III)] dependence and [Tl(III)] absorption.

Variation of ϕ_{ex} with Temperature. At constant reactant concentrations [Tl^I] = [Tl^{III}] = 0.005 M, ϕ^1_{ex} varies from 4.19 at 15.2° to 6.55 at 48.0° (Table IV). In this temperature range, the extinction coefficients of Tl_{aq}^{3+} and $TlOH^{2+}$ together with the formation constant of $TlOH^{2+}$ all increase significantly. Consequently at constant incident light intensity, there is a significant variation in I_{abs} with temperature. To deduce an apparent activation energy, it is necessary to use the light-intensity-independent quantity

Table IV: Variation of Quantum Yields with Temperature where [Tl(I)] = [Tl(III)] = 0.005 M, [HClO] = 1.1 M, and $I_0 = 3.35 \times 10^{-6}$ einsteins l.$^{-1}$ min^{-1}

Temp, °C	$t_{1/2}$ min	I_{abs}/I_0	ϕ^1_{ex}
15.2	48	0.258	4.19
20.1	47	0.298	3.70
25.0	31	0.344	4.84
29.1	26	0.374	5.32
35.0	23	0.454	4.95
	20.5	0.454	5.57
41.4	17	0.505	6.02
48.0	13.5	0.583	6.55

Table V: Variation of Quantum Yield[a] with Wavelength of Initiating Radiation at 25°, 0.0224 *M* Tl(I), 0.0214 *M* Tl(III), and 1.1 *M* $HClO_4$

	Wavelength, mμ				
	230	240	250	260	270
$t_{1/2}$, min	440,400	275,200	130,130	100,120	130,110
$10^6 \times$ total I_{abs}, einsteins $l.^{-1}$ min^{-1}	1.96	2.84	4.25	2.90	2.92
ϕ_{ex}	9.2	10.8	13.2	23.8	21.6
ϕ_{ex} (cor)	9	11	19	29	26
% light-abs Tl(III)	23.2	52	93	99	99.4
ϕ^1_{ex} (cor)	19	18	20	29	26
% light-abs $TlOH^{2+}$	6.3	33.0	74	81	74
ϕ^2_{ex} (cor)	36	19	22	32	30
% light-abs Tl_{aq}^{3+}	16.9	19	19	18	25
ϕ^3_{ex} (cor)	22	25	44	68	52

[a] Values of ϕ_{ex}, ϕ^1_{ex}, ϕ^2_{ex}, and ϕ^3_{ex} all corrected to $I_{abs} = 2.0 \times 10^{-6}$ einsteins $l.^{-1}$ min^{-1}.

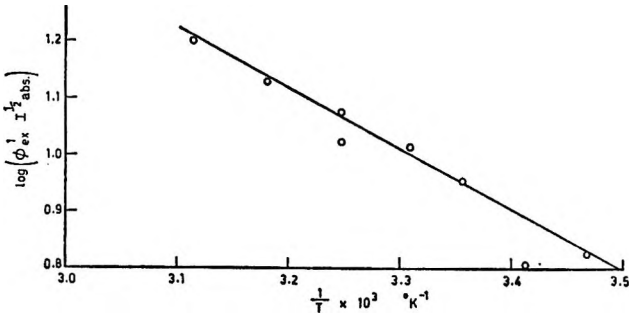


Figure 6. Temperature dependence. [Tl(III)] = 0.005 *M*; [Tl(I)] = 0.0051 *M*.

$\phi^1_{ex} I_{abs}^{1/2}$. Figure 6 is a plot of log $(\phi^1_{ex} I_{abs}^{1/2})$ *vs.* $1/T$, from which an apparent activation energy of 5.0 ± 1.0 kcal mol^{-1} is deduced.

Variation of ϕ_{ex} with Wavelength. Table V summarizes quantum yields measured at different incident wavelengths using the xenon arc–monochromator assembly. Because of the low light intensities and the small area of the emergent light beam, it was necessary to irradiate 2 ml of reactant solution and to sample the entire contents for "one-point" determinations of half-times. Table V shows that half-times and rates of exchange are subject to random errors of ±20%. The emergent radiation flux from the monochromator probably did not peak at the wavelength dialed on the monochromator since the intensity of the xenon arc falls rapidly with decreasing wavelength. A compensating effect is the steep rise in optical absorbance of the reactant solutions with decreasing wavelength. Absorbed light intensities were calculated at the dialed wavelengths and derived ϕ_{ex} values could be subject to a systematic uncertainty of ±15%; these systematic errors would differ at different incident wavelengths. Flicker in the xenon arc source caused random errors in actinometry of ±10%. Thus the over-all error in ϕ_{ex} values, listed in Table V, is approximately ±45%.

The value of the over-all quantum yields ϕ_{ex}, corrected to a constant absorbed light intensity, *falls* by a factor of 3 from 2700 to 2300 Å. At 2400 Å 48% of all light absorption is by Tl_{aq}^{+} and at 2300 Å this rises to 76.8%. The onset of significant Tl_{aq}^{+} absorption is accompanied by a sharp fall in ϕ_{ex}. It is concluded that Tl_{aq}^{+} is inactive photochemically and that this species acts as an "inner-filter." The mean value of ϕ^1_{ex}, calculated on the basis of light absorption by both Tl_{aq}^{3+} and $TlOH^{2+}$, is 22 ± 4 (mean deviation) over a wavelength range in which the ratio of the light absorbed by Tl_{aq}^{3+} to that by $TlOH^{2+}$ varies ninefold. The mean value of ϕ^2_{ex}, calculated for $TlOH^{2+}$ light absorption alone, is 28 ± 6. However, the value of ϕ^3_{ex}, calculated for Tl_{aq}^{3+} absorption alone, varies threefold and Tl_{aq}^{3+} cannot be the only photoactive species. The deviations in ϕ^1_{ex} are well within the estimated random and systematic errors in ϕ_{ex} value of ±45%. It is concluded that $TlOH^{2+}$ and probably Tl_{aq}^{3+} are photoactive and that the quantum yields for photoinitiation of the exchange reaction by these species are independent of wavelength.

Net Oxidation and Reduction during Photolysis. The extent of net oxidation or reduction of reactants during photolysis was assessed by irradiating ^{204}Tl-labeled solutions of thallium(I) and thallium(III) for periods well in excess of 10 exchange half-times. At 2537 Å, the infinite-time ^{204}Tl specific activities were constant to within 1% and upper limits may be set to the quantum yield for net oxidation of Tl^{+} of 0.02 and 0.001 for the net reduction of Tl^{3+}. The absence of measurable net oxidation and reduction is a stoichiometric restraint upon possible mechanisms for the chain reaction.

Effect of Added Anions. The optical absorbance of thallium(III) solutions is enhanced significantly by the presence of either 0.005 *M* chloride or sulfate anions due to the generation of $TlCl^{2+}$ and $TlSO_4^{+}$. However the presence of these concentrations of anions did not alter significantly observed quantum yields for exchange. These exploratory experiments suggest that a number of mixed thallium(III) complexes would initiate the thallium(I)–thallium(III) exchange.

It was also established that minor variations in acid concentration would have no measurable effect upon ϕ_{ex} values already quoted.

Discussion

The consistent observation of quantum yields well in excess of unity is compelling evidence for the photogeneration of a thallium(II) species. The quantitative treatment of possible exchange mechanisms requires that the chain carrier be capable of one-electron exchange with both thallium(III) and thallium(I). A thallium(II) species seems to be the only conceivable possibility.

Photoinitiation Processes. The initiation step of the mechanism arises from photochemical reactions of thallium(III) species. Light absorption by Tl_{aq}^{+} does not lead to significant initiation as judged by measurements at 2400 and 2300 Å (where Tl_{aq}^{+} is a major absorber) and by plateau quantum yields at Tl^{+} concentrations ranging from 0.05 to 0.15 M. The strong absorption due to Tl_{aq}^{+} below 2500 Å could be interpreted as involving charge transfer to solvent

$$Tl_{aq}^{+} + h\nu \rightarrow [Tl^{2+} \cdot e_{aq}^{-}] \rightarrow Tl^{2+} + H$$

but an alternative interpretation[4] is that this absorption is a d–s transition on the metal cation. This may account for the relative ineffectiveness of the absorption.

Initiation by thallium(III) absorbing species is consistent with the proposed charge-transfer assignment. Thus the first excited state for $TlOH^{2+}$ is expected to have a charge distribution shifted from that represented by $Tl^{3+} \cdot OH^{-}$ toward $Tl^{2+} \cdot OH$. The value of $\phi_1 \simeq 0.5$, for the generation of geminate radicals which have escaped primary and secondary recombination, is significantly less than 1. This situation may be represented as the generation of an excited species in a solvent cage followed by deexcitation and diffusion apart of geminate radicals, thus

$$Tl^{3+} \cdot OH^{-} + h\nu \rightleftarrows [Tl^{2+} \cdot OH] \overset{\phi}{\rightleftarrows} Tl_{aq}^{2+} + OH$$

and likewise for Tl_{aq}^{3+} absorption.

$$Tl_{aq}^{3+} + h\nu \rightleftarrows [Tl_{aq}^{2+}OH_2^{+}] \overset{\phi}{\rightleftarrows} Tl_{aq}^{2+} + OH + H^{+}$$

It is interesting that within the wavelength range 2700–2300 Å there is no significant evidence for a rise in quantum yields even though an additional 18.5 kcal mol^{-1} is delivered with the 2300-Å quanta. The simplified Noyes treatment[11] of diffusive recombination of geminate radical pairs predicts a strong wavelength dependence. Although the scavenging reaction

$$OH + Tl^{+} \rightarrow OH^{-} + Tl^{2+}$$

proceeds[6] at almost diffusion-controlled rates ($k = 9 \times 10^{9}\ M^{-1}\ sec^{-1}$) and, by the Noyes theory, would give an enhanced scavenging efficiency of up to 0.2, the recombination of two Tl^{2+}, as discussed below, also has a rate constant of a similar magnitude. Thus the effect of the kinetic energy of geminate radicals may well be removed by this unusual kinetic aspect of the scavenging reactions. Moreover there is unlikely to be any significant effect upon primary quantum yields due to possible competition of Tl^{+} for second recombination of Tl^{2+} and OH.

The effectiveness of halogeno- and sulfatothallium(III) species would suggest, in analogy to $TlOH^{2+}$, net reactions

$$TlX^{2+} + h\nu \rightarrow Tl^{2+} + X\cdot$$

followed by scavenging of the radical X by added Tl^{+}.

$$Tl^{+} + X\cdot \rightarrow Tl^{2+} + X$$

Propagation and Termination Reactions. The one-electron propagation reactions of thallium(II) with thallium(III) probably involves both Tl_{aq}^{3+} and $TlOH^{2+}$. For the thermal thallium(I)–thallium(III) electron exchange, the rate constants at 30° are[12]

$$k(Tl_{aq}^{3+}\text{–}Tl_{aq}^{+}) = 0.45\ M^{-1}\ hr^{-1}$$

and

$$k(TlOH^{2+}\text{–}Tl_{aq}^{+}) = 0.21\ M^{-1}\ hr^{-1}$$

The lack of any marked dependence of quantum yields on acid concentration is consistent with propagation reactions proceeding through reactions of Tl_{aq}^{3+} and $TlOH^{2+}$ with very similar rate constants.

The rotating-sector measurements suggest that the quadratic termination reaction proceeds with a rate constant characteristic of diffusion-controlled reactions. The disproportionation of Tl^{II}, generated in substantial concentrations by pulse radiolysis, has been shown[13] to exhibit a rate constant of $2.3 \pm 0.8 \times 10^{9}\ M^{-1}\ sec^{-1}$ and this is consistent with the photochemical evidence. The less important linear termination reactions probably arise from the same impurities responsible for the small induction periods. Extensive attempts were made to remove and identify these impurities without success although experience with micromolar concentrations of iron salts suggests that less than micromolar concentrations of impurities may be involved.

Deduction of Rate Constants. Our proposed exchange mechanism is as follows.

initiation

$$TlOH^{2+} + Tl_{aq}^{+} + h\nu \rightarrow 2Tl^{2+} + OH^{-}$$

$$Tl_{aq}^{3+} + Tl_{aq}^{+} + h\nu \rightarrow 2Tl^{2+}$$

propagation

$$*Tl^{III} + Tl^{II} \rightleftarrows *Tl^{II} + Tl^{III} \qquad (k_{III})$$

$$*Tl^{II} + Tl^{I} \rightleftarrows *Tl^{I} + Tl^{II} \qquad (k_{I})$$

(11) R. M. Noyes, *J. Am. Chem. Soc.*, **77**, 2042 (1955).

(12) R. W. Dodson and E. Roig *J. Phys. Chem.*, **45**, 2175 (1964).

(13) B. Cercek, M. Ebert, and A. J. Swallow, *J. Chem. Soc., A*, 612 (1966).

Table VI: Predicted Outer-Sphere Electron-Transfer Rate Parameters[a]

Reaction	$r(Tl_{aq}^{2+})$, Å	σ, Å	kcal/mol $\Delta G^{\ddagger}_{rep}$	$\Delta G_{SR}^{\ddagger}$	$\Delta G^{\ddagger}_{IR}$	$\Delta G^{\ddagger}$	$k(25°)$,[b] M^{-1} sec^{-1}
$Tl_{aq}^{3+} + Tl_{aq}^{2+}$	4.13	7.81	3.25	5.75	4.34	13.3	17
$Tl_{aq}^{3+} + Tl_{aq}^{2+}$	3.88	7.56	3.35	5.94	4.80	14.1	9
$TlOH^{2+} + Tl_{aq}^{2+}$	3.88	7.56	2.23	5.94	5.86	14.0	9
$Tl_{aq}^{+} + Tl_{aq}^{2+}$	4.13	8.33	1.02	5.41	6.45	12.9	37
$Tl_{aq}^{+} + Tl_{aq}^{2+}$	3.88	9.08	1.05	5.57	6.90	13.5	13
$Tl_{aq}^{3+} + Tl_{aq}^{2+}$	4.13	9.81	2.57	4.57	4.34	11.5	390
$Tl_{aq}^{3+} + Tl_{aq}^{2+}$	3.88	9.56	2.66	4.70	4.80	12.2	126
$Tl_{aq}^{+} + Tl_{aq}^{2+}$	4.13	10.33	0.82	4.35	6.45	11.6	296
$Tl_{aq}^{+} + Tl_{aq}^{2+}$	3.88	10.08	0.79	4.47	6.90	12.2	126

[a] $r(Tl_{aq}^{+}) = 4.20$ Å; $r(Tl_{aq}^{3+}) = 3.68$ Å. Hydration numbers of 6 are assumed in all cases. [b] Calculated for frequency factor of 10^{11} M^{-1} sec^{-1}.

termination

$$Tl^{II} + Tl^{II} \rightarrow Tl^{I} + Tl^{III} \qquad (k_t)$$

$$\left.\begin{aligned} Tl^{II} + S' &\rightarrow Tl^{I} \\ Tl^{II} + S'' &\rightarrow Tl^{III} \end{aligned}\right\} \text{minor} \qquad (k_t')$$

The analysis of the concentration dependence of ϕ_{ex} has shown that $k_{III}/k_I = 1.6 \pm 0.5$ (Tl^{+}) and $k_{III}/k_I = 1.9 \pm 0.5$ (Tl^{3+}). From the intercept of Figure 3, $k_{III}[Tl^{III}]\phi_1^{1/2}/(k_t I_{abs})^{1/2} = 17 \pm 3$ and assuming the published value for k_t, $k_{III} = (1.6 \pm 0.5) \times 10^7 \phi_1^{-1/2}$. If $\phi_1 \simeq 0.5$, then $k_{III} = 1.0 \times 10^6$ M^{-1} sec^{-1} at 25°; an uncertainty of a factor of 2 arises from ϕ_1. Thus $k_I = 5 \times 10^4$ M^{-1} sec^{-1} at 25°. Substitution of these derived values confirms that under all experimental conditions

$$k_I[Tl^{I}] + k_{III}[Tl^{III}] \geq 10(k_t I_{abs}\phi_1)^{1/2}$$

thus justifying the simplification of eq 1 to eq 3.

The observed activation energy for photochemical exchange arises from a complex contribution from k_I, k_{III}, and k_t (eq 3). The contribution from the diffusion-controlled reaction k_t will be $\frac{1}{2}(E_t) \simeq 2$ kcal mol^{-1}. Either one or both of k_I and k_{III} must exhibit activation energies less than 7 kcal mol^{-1} provided also that ϕ_1 is temperature independent. If ϕ_1 increases with temperature, then the activation energies for k_I and k_{III} will be closer to 5 kcal mol^{-1}.

Comparison of Observed and Predicted Rate Constants. It is of interest to compare the experimental estimates for k_I and k_{III} with the predictions of the Marcus[14] and Hush[15] treatments for adiabatic electron transfer *via* outer-sphere transition states. Table VI summarizes these predictions based on two values for the radius of the aquated Tl^{2+} ion; the value of 3.88 Å is that predicted by the Hush treatment while the value of 4.13 Å is chosen to illustrate the effect of a much larger ionic radius on the predictions. The rate constants are based on a frequency factor of 10^{11} M^{-1} sec^{-1} which is equivalent[16] to a free-energy contribution of 2.8 kcal mol^{-1} from the translational and rotational entropy loss in forming the transition states from the reactants. Calculations of the internal-rearrangement free energy $\Delta G^{\ddagger}_{IR}$ by means of Sutin's method[16] of calculating stretching force constants yields values of $\Delta G^{\ddagger}_{IR}$ considerably in excess of the Hush predictions, and the former predictions are therefore not listed.

The first five entries in Table VI are based on encounter distances (σ) derived from the sum of the two radii of the aquated cations; this is the customary "close-contact" model. Predicted rate constants are about 10^4 times smaller than the observed values. The final four entries in Table VI are based on encounter distances 2 Å greater than the close-contact distance. This assumption reduces the coulombic repulsive ($\Delta G^{\ddagger}_{rep}$) and solvent-rearrangement ($\Delta G^{\ddagger}_{SR}$) free energies, raises the predicted rate constants substantially, and also approximates to the observed relation $k_{III} = 1.7k_I$. The rationale for this assumption is that the unusual outer-electronic $6s^1$ configuration of thallium(II) may enable electron transfer to proceed over greater encounter distances. Nevertheless, the Hush predictions are still some 10^2 times too low. The assumption of hydration numbers larger than 6 with four primary aquo ligands subject to rearrangement and a larger number (say eight) at a somewhat greater distance not subject to rearrangement enhances the predicted rate constants by a further factor of 10. It is unlikely that specific anion catalysis by perchlorate anions would account for the remaining discrepancy. Electron transfer *via* inner-sphere transition states could however account for the unusually large rate constants and the failure of the outer-sphere calculations. This mechanism is readily available to the very labile aquated thallium ions.

The Thermal Tl(I)–Tl(III) Mechanism. The unusually high reactivity of thallium(II) carries implications for the mechanism of the thermal thallium(I)–thallium(III) electron exchange. Previously we had

(14) R. A. Marcus, *Discussions Faraday Soc.*, **29**, 21 (1960).
(15) N. S. Hush, *Trans. Faraday Soc.*, **59**, 557 (1961).
(16) N. Sutin, *Ann. Rev. Nucl. Sci.*, **12**, 285 (1962).

argued[7] that the extreme sensitivity of the photochemically induced exchange, in contrast to the insensitivity of the thermal exchange, was evidence against the thermal exchange proceeding *via* a Tl^{2+} intermediate. This reasoning may be logically invalid. A Tl^{2+} intermediate in the thermal exchange will only be susceptible to scavenging if the two geminate Tl^{2+} ions exist long enough to diffuse apart. Since, however, the disproportionation of two Tl^{2+} ions proceeds at diffusion-controlled rates, disproportionation by a second electron transfer will probably occur within the original solvent cage. Therefore the thermal Tl^{I}–Tl^{III} electron exchange could proceed by two successive one-electron transfers; the second electron transfer could occur in a time scale which is short in comparison to the time for diffusion of geminate Tl^{2+} ions from a solvent cage and these Tl^{2+} ions would not be detectable by chemical scavenging techniques. In the present photochemical system, the geminate Tl^{2+} ions separate with substantial kinetic energy at all wavelengths used. Chemical evidence for Tl(II) in the Tl(III) + Fe(II) reaction presumably arises because Tl(II) species are not generated in geminate pairs in this instance and efficient scavenging by Fe(III) is possible.[17]

Acknowledgment. This work was supported by an initial financial grant from the Chemical Society of London and later by the Australian Institute for Nuclear Science and Engineering. Grateful acknowledgment is made to both bodies for their support.

Appendix

Calculation of the Relative Rates of Linear and Quadratic Termination. Assuming one linear (k_t') and one quadratic (k_t) termination reaction, the steady-state concentration of the Tl^{2+} chain carrier is given by

$$2I_{abs}\phi_1 = 2k_t[Tl^{2+}]^2 + k_t'[Tl^{2+}] \qquad (A1)$$

It has been shown above, for the condition $\phi_{ex} \gg \phi_1$, that

$$\phi_{ex} = F[Tl^{2+}]$$

where the constant F is given by

$$F = \phi_1 k_I[Tl^I]k_{III}[Tl^{III}]/(k_I[Tl^I] + k_{III}[Tl^{III}])$$

Equation A1 may then be rearranged to the form

$$I_{abs} = A\phi_{ex}^2 + B\phi_{ex} \qquad (A2)$$

where $A = k_t/\phi_1 F^2$ and $B = k_t'/2\phi_1 F$.

The experimental data have been approximated by the empirical expression (*e.g.*, Figure 4)

$$\log \phi_{ex} = n \log I_{abs} + \text{constant} \qquad (A3)$$

so that the intensity exponent n is deduced from the relation

$$n = (\log \phi_{ex_1} - \log \phi_{ex_2})/(\log I_{abs_1} - \log I_{abs_2}) \qquad (A4)$$

where ϕ_{ex_1} and ϕ_{ex_2} are the limit values of ϕ_{ex} and the corresponding values of I_{abs} are I_{abs_1} and I_{abs_2}. Substitution by means of (A2) in (A3) yields

$$n - 1 = \left[\log\left(\frac{A\phi_{ex_1} + B}{A\phi_{ex_2} + B}\right)\right]\frac{\phi_{ex_2}}{\phi_{ex_1}}$$

Hence

$$\frac{A}{B} = \frac{p - 1}{\phi_{ex_1} - p\phi_{ex_2}} \qquad (A5)$$

where

$$p = \frac{\phi_{ex_1}}{\phi_{ex_2}} 10^{n-1}$$

The ratio of the rates of the quadratic termination reaction to the linear termination reaction is then

$$\frac{2k_t[Tl^{II}]}{k_t'} = \frac{p - 1}{\phi_{ex_1} - p\phi_{ex_2}}\phi_{ex} \qquad (A6)$$

Equation A6 may then be curve fitted to the experimental values using known values of ϕ_{ex} and with the ratio $2k_t[Tl^{II}]/k_t'$ as an adjustable parameter. Within the limits ϕ_{ex_1} to ϕ_{ex_2} a particular intensity exponent will therefore be derived for an assumed ratio of the rates of quadratic to linear termination.

(17) K. G. Ashurst and W. C. E. Higginson, *J. Chem. Soc.*, 3044 (1953).

The Use of Tritiated H_2S as a Radical Scavenger in the γ Radiolysis of Organic Liquids[1]

by William A. Pryor and Umberto Tonellato[2]

Department of Chemistry, Louisiana State University, Baton Rouge, Louisiana 70803 *(Received July 19, 1968)*

We here report the use of tritiated hydrogen sulfide as a scavenger in the γ radiation of benzene, cyclohexane, and toluene at 27°. The hydrocarbon solvents were recovered and purified, and their activity was determined. In separate experiments, the isotope effect k_H/k_T for the reaction of phenyl and cyclohexyl radicals with thiols has been measured. If it is assumed that labeling occurs primarily by radical reactions, then the yield of the tritiated hydrocarbon, G(RH-t), and the isotope effect can be combined to give a value for the yield of the parent-minus-hydrogen radical from these three solvents. (See eq 1 and 3.) The values so obtained agree quite well with literature values using iodine as a scavenger. The method has also been evaluated for producing tritium-labeled materials; it gives higher G values for the production of tritiated toluene than does the Wilzbach method and perhaps is somewhat more convenient.

The destruction of organic solvents by radiolysis occurs largely by free-radical and excited-molecule reactions.[3,4] Several scavenger methods[4,5] have been developed for quantitatively identifying the radicals which occur in these reactions, since these data can be used in attempts to elucidate the mechanisms of radiodestruction. Some time ago, in connection with another project, we examined tritiated hydrogen sulfide as a scavenger in the γ radiolysis of organic liquids. Our studies indicate that H_2S-t is a useful scavenger which gives data comparable with that obtained using other, more well-known scavengers such as iodine. During the course of our work, Ausloos and Lias reported the use of H_2S as a radical scavenger in the gas-phase radiolysis of propane,[6] Reisz, White, and Kon reported the use of H_2S-t in the solid-phase radiolysis of proteins,[7] and Ausloos, Scala, and Lias[8] reported some results using H_2S in the liquid phase.[9,10]

We had originally hoped that H_2S-t would prove to be a suitable reagent for a modified Wilzbach[11] method of synthesizing labeled organic materials. In the Wilzbach technique, tritiated hydrogen gas is mixed with an organic material, and self-radiolysis leads to tritiation of the organic substance. Since Wilzbach's orginal discovery, various "accelerated" methods[12] have been suggested. We initially felt that γ irradiation of organic materials in the presence of H_2S-t might have some advantages. However, since H_2S-t usually incorporates only one tritium per primary radical, the G values for incorporation of tritium into the substrate are not much larger than those obtained in the Wilzbach procedure. Nevertheless, our method may offer some convenience since H_2S-t can readily be prepared from H_2O-t and is easier to handle than is tritiated hydrogen gas. It is also possible that the labeled compounds prepared by this method may have lower levels of contamination from radioimpurities or that the chemical nature of these impurities could be more easily predicted. The occurrence of radioimpurities is the greatest drawback of the Wilzbach method.[11,12]

It has recently been shown[13] that HCl undergoes a chain reaction in which labeled atoms are incorporated with a G value for exchange of about 10^4; this system might be superior for Wilzbach-type labeling work and it should be studied from this viewpoint. Clearly, however, it could not be used as an index of radiodestruction.

Experimental Section

The H_2S-t was prepared by hydrolyzing Al_2S_3 with tritiated water in the absence of air,[14] was purified by two vacuum distillations, and was transferred to a calibrated bulb equipped with a manometer. A known volume of the H_2S was then transferred to an ampoule containing 1–2 ml of the substrate held at liquid nitro-

(1) Supported in part by the U. S. Air Force Office of Scientific Research, AFOSR(SRC)-OAR, under Grant No. 540-66, 1965–1967; and by the U. S. Public Health Service, National Institutes of Health, Grant GM-11908-03, 1967–1968.

(2) A Postdoctoral Fellow supported by the AFOSR, 1965–1967.

(3) For a general review, see J. W. T. Spinks and R. J. Woods, "Introduction to Radiation Chemistry," John Wiley & Sons, Inc., New York, N. Y., 1964, Chapter 6.

(4) (a) F. S. Dainton, *Pure Appl. Chem.*, **10**, 395 (1965); (b) R. A. Holroyd in "Aspects of Hydrocarbon Radiolysis," T. Gaümann and J. Hoigné, Ed., Academic Press, New York, N. Y., 1968, pp 1–32; (c) R. H. Schuler and R. W. Fessenden in "Radiation Research," North Holland Publishing Co., Amsterdam, 1967, pp 99–112; (d) P. Ausloos, *Ann. Rev. Phys. Chem.*, **17**, 205 (1966).

(5) A method which employs a somewhat different approach is the "radical sampling technique" in which isotopically labeled C_2H_4 or CH_3I is used. See R. A. Holroyd and G. W. Klein, *Int. J. Appl. Radiat. Isotopes*, **13**, 493 (1962); *J. Amer. Chem. Soc.*, **84**, 4000 (1962); *J. Phys. Chem.*, **69**, 194 (1965).

(6) P. Ausloos and S. G. Lias, *J. Chem. Phys.*, **44**, 521 (1966).

(7) (a) P. Riesz, F. H. White, and H. Kon, *J. Amer. Chem. Soc.*, **88**, 872 (1966); (b) F. H. White, P. Riesz, and H. Kon, *Radiat. Res.*, **32**, 744 (1967).

(8) P. Ausloos, A. A. Scala, and S. C. Lias, *J. Amer. Chem. Soc.*, **89**, 3677 (1967).

$$G(\text{RH-}t) = \frac{(\text{H or T atoms from } H_2S\text{-}t \text{ incorporated into recovered RH-}t)}{(100 \text{ eV absorbed})} \quad (1)$$

$$= \frac{(\text{total activity recovered in RH, } \mu\text{Ci})}{0.5(H_2S \text{ specific activity, } \mu\text{Ci/mol})} \frac{6.023 \times 10^{23}}{(100 \text{ eV absorbed})}$$

gen temperature. The ampoule was constructed so the organic liquid occupied about 95% of its volume. The specific activity of the H_2S was measured directly by absorption into a concentrated KOH solution which was counted in a Packard Model 3365 liquid scintillation counter. Corrections for quenching were made using a series of standard solutions purchased from Packard and the automatic external standardization mode of the counter. The irradiation source was a 11,000-Ci cobalt-60 pool reactor. The ampoules were rigidly held in a large evacuated glass cylinder which was placed in a diving bell. The temperature in the bell during irradiation was $27 \pm 2°$, and the dose rate was 1010 rad/min (Fricke dosimetry). After irradiation any gaseous products were removed, and the solvent was washed with KOH solutions and water and was then dried. A reverse isotope dilution technique using repeated distillations with an efficient column and large dilution factors was used to purify the substrate to constant specific activity. Clearly, this type of study could also give yields of products other than the recovered substrate; we did not attempt this type of analysis because we did not have access to a gas chromatograph–flow counter system.

Results

Hydrogen sulfide is an excellent candidate as a radical scavenger.[6-8,10] It reacts with radicals with a very large rate constant,[15] but the HS· which is produced does not abstract hydrogens from any but the most activated CH bonds.[6-8,16] Thus when tritiated H_2S is used not more than one tritium label should be introduced into the products for each primary radical formed for most organic substrates. If the isotope effect for the reaction of radicals with H_2S is determined, the yield of radioactive products can be related to the total yield of primary radicals.

Table I gives the data. We have expressed the amount of exchange in terms of G(RH-t), the yield, in molecules per 100 eV absorbed, of recovered labeled substrate. This G value is corrected for the specific activity of the H_2S-t used but not for any possible isotope effect[19] (see eq 1).

The activity of the H_2S-t was kept low so that any possible destruction caused by self-radiolysis would be small. (See run 7, Table I.) Runs 1–6 show that increasing the H_2S-t concentration in cyclohexane from 1.1 to 5.6% does not affect G(RH-t). Therefore, these concentrations of H_2S are sufficient to scavenge all the free cyclohexyl radicals.[20] Run 8 shows the effect of a larger absorbed dose. Although the accuracy of the data may not be sufficient, it would appear that G(RH-t) may decrease at higher doses.

(9) A number of related references can be cited, some of which have been reviewed by W. A. Pryor in "Annual Reports on the Mechanisms of Reactions of Sulfur Compounds," Vol. 2, N. Kharasch, B. S. Thyagarajan, and A. I. Khodair, Ed., Intra-Science Research Foundation, Santa Monica, Calif., 1967. Some of the more pertinent references are given: (a) Meissner and Henglein used D_2S to scavenge hydrogen atoms produced in the radiolysis of liquid hexane (G. Meissner and A. Henglein, *Ber. Bunsenges. Phys. Chem.*, **69**, 264 (1965)); (b) these workers also studied the radiolysis of solid, liquid, and gaseous H_2S (G. Meissner and A. Henglein, *Z. Naturforsch.*, **20b**, 1005 (1965)); (c) McNaughton has reported the radiolysis of H_2S in the liquid phase (G. S. McNaughton, *Trans. Faraday Soc.*, **62**, 1812 (1966)); (d) Myron and Johnsen reported the radiolysis of liquid ethanethiol (J. J. J. Myron and R. H. Johnsen, *J. Phys. Chem.*, **70**, 2951 (1963)); (e) it has long been known that H_2S adds to olefins under radiolytic conditions; see ref 10 and for a recent reference see K. Sugiomoto, W. Ando, and S. Oae, *Bull. Chem. Soc. Jap.*, **38**, 221 (1965); (f) Lunde and Hentz have studied the radiolysis of thiophene (G. Lunde and R. R. Hentz, *J. Phys. Chem.*, **71**, 863 (1967)); (g) Bergdolt and Schulte-Frohlinde have reported the yields of hydrogen in the radiation of solutions of thiophenol-d_1 in cyclohexane (A. Bergdolt and D. Schulte-Frohlinde, *Z. Naturforsch.*, **22b**, 270 (1967)); (h) Karmann, Meissner, and Henglein have reported the pulse radiolysis of aqueous solutions of H_2S (W. Karmann, G. Meissner, and A. Henglein, *Z. Naturforsch.*, **22b**, 273 (1967)); (i) Kroh and Hankiewicz have reported the radiation of benzene and toluene in the presence of H_2O-t (J. Kroh and E. Hankiewicz, *Chem. Phys. Lett.*, **1**, 542 (1968)) and concluded that labeling occurs primarily *via* excited molecule reactions.

(10) W. A. Pryor, "Free Radicals," McGraw-Hill Book Co., Inc., New York, N. Y., 1966.

(11) (a) K. E. Wilzbach, *J. Amer. Chem. Soc.*, **79**, 1013 (1957); (b) K. E. Wilzbach, *Advan. Tracer Methodol.*, **1**, 4, 28 (1963); (c) P. Reisz and K. E. Wilzbach, *J. Phys. Chem.*, **62**, 6 (1958).

(12) This has been reviewed: (a) J. R. Jones, *Lab. Pract.*, **14**, 433 (1965); (b) A. P. Wolf, Proceedings of the Second International Conference on Methods of Preparation and Storage of Labeled Compounds, Euratom Publishing Co., 1966; (c) H. L. Bradlow, D. K. Fukushima, and T. F. Gallagher, *Atomlight*, 2 (1959); (d) M. L. Whisman and B. H. Eccleston, *Nucleonics*, **20**, 98 (1962); (e) M. Wenzel and P. E. Schulze, "Tritium Markierung Darstellung, Messung und Anwendung nach Wilzbach Markierter Verbindungen in Medinzin, Chemie, Landwirtschaft Industrie," Walter de Gruyter and Co., Berlin, 1962.

(13) (a) J. W. Fletcher and G. R. Freeman, *Can. J. Chem.*, **44**, 2645 (1966); (b) this result could have been predicted from the studies of H. L. Benson and J. E. Willard, *J. Amer. Chem. Soc.*, **83**, 4672 (1961), **88**, 5689 (1966), and those of R. H. Wiley, W. Miller, C. H. Jarboe, J. R. Harrell, and D. J. Parish, *Radiat. Res.*, **13**, 479 (1960); see also P. J. Horner and A. J. Swallow, *J. Phys. Chem.*, **65**, 953 (1961).

(14) This technique is similar to that used to prepare D_2S by A. Kruis and K. Clusius, *Z. Phys. Chem.* (Leipzig), **B38**, 158 (1938).

(15) The following data can be cited: (a) the rate constant for the reaction of pentyl radicals with pentanethiol at 25° is 7×10^4 M^{-1} sec^{-1} (R. D. Burkhart, *J. Amer. Chem. Soc.*, **90**, 273 (1968)); the rate constant for the reaction of CF_3· with H_2S is 4.5×10^8 $\exp(-3900/RT)$ M^{-1} sec^{-1} (J. C. Amphlett and E. Whittle, *Trans. Faraday Soc.*, **63**, 2695 (1967)); the activation energy for this reaction has also been reported to be 3.9 kcal/mol by N. L. Arthur and T. N. Bell, *Can. J. Chem.*, **44**, 1445 (1966); (c) the rate constant for the reaction of methyl radicals with H_2S is 2.5×10^8 $\exp(-2600/RT)$ M^{-1} sec^{-1} (N. Imai and O. Tcyama, *Bull. Chem. Soc. Jap.*, **33**, 652 (1960)); (d) the rate constant for the reaction of OH· with H_2S in aqueous solution is 1.1×10^{10} M^{-1} sec^{-1};[9b] (e) the rate constant for the reaction H· + $H_2S \rightarrow H_2$ + HS· is 10^9 M^{-1} sec^{-1} in aqueous solution (G. Meissner and A. Henglein, *Ber. Bunsenges. Phys. Chem.*, **69**, 3 (1965)).

Table I: γ Radiation of Organic Liquids in the Presence of H_2S-*t*

Run	Substrate	Wt, g	Mol % of H_2S-*t*	Activity in H_2S-*t*, μCi	$10^{-20} \times$ absorbed dose, eV	Tritium incorp, μCi: In nonvolatile products	Tritium incorp, μCi: In purified substrate	G(RH-*t*)[a]
1	Cyclohexane	1.408	1.07	41.1	1.16	0.180	0.159	0.70
2	Cyclohexane	0.949	1.74	48.4	1.00	...	0.132	0.65
3	Cyclohexane	1.511	2.27	95.0	1.11	...	0.213	0.75
4	Cyclohexane	1.377	2.40	120.2	1.32	0.288	0.239	0.71
5	Cyclohexane	0.889	3.17	83.0	0.94	...	0.127	0.66[d]
6	Cyclohexane	0.721	5.61	116.6	0.76	0.135	0.104	0.67
7	Cyclohexane	1.506	4.30	235.5	0.014[b]	...	$<5 \times 10^{-4}$	...
8	Cyclohexane	1.206	4.82	211.3	2.32	0.448	0.359	0.61
9	Toluene	1.072	2.12	50.3	0.84	0.060	0.036[c]	0.22
10	Benzene	1.553	0.93	22.1	1.21	~0.04	0.022	0.094

[a] Not corrected for any isotope effect; see eq 1 and the discussion in the text. G(RH-*t*) = [(RH total activity, μCi)/0.5 (H_2S specific activity, μCi/mol)](6.023 $\times$ 10^{23}/100 eV absorbed). [b] Self-radiation experiment; not exposed to ^{60}Co. [c] Oxidation to benzoic acid by alkaline $KMnO_4$ and counting the benzoic acid showed that 78% of the activity was in the ring; in a second experiment, 80% ring activity was obtained. [d] Using D_2S, Fletcher and Freeman[13] obtained $G < 1.5$ for formation of $C_6H_{11}D$. [e] The average of runs 1–5 is $G = 0.69$.

Run 9 gives data using toluene as the substrate. Oxidation of the toluene to benzoic acid showed that 79% of the activity is incorporated in the ring. This can be compared with 92% from the Wilzbach labeling,[11a] 45% from Wilzbach modified with microwave irradiation,[21] 80% from Wilzbach modified with ultraviolet irradiation,[21] and 78% from recoil labeling.[22] The high fraction of the activity in the ring demonstrates that a radical-chain process is not responsible for the incorporation of the bulk of the activity; a radical chain would involve benzylic radicals and produce side-chain-labeled toluene almost exclusively.

Discussion

The difficulty with scavenger methods for identifying mechanisms of radiodestruction is that more than one mode of reaction with the scavenger is often possible.[3,4b-d] Iodine and HI, for example, are known to capture electrons as well as to react with radicals.[4b] The radical-sampling technique of Holroyd[5] may be free of this difficulty; apparently it gives data on radicals present without other complications. Calibration from this method suggests that in the liquid phase, where neutralization is rapid, iodine mainly scavenges radicals.[3,4]

It is known that H_2S reacts with ionic species as well as with radicals produced by radiolysis. For example, it undergoes hydride transfer with carbonium ions in the gas phase[6] and charge transfer in solution.[9a] However, it is probable that the most important mechanism for incorporation of tritium into the substrate RH in these liquid-phase radiolyses is by atom transfer from H_2S-*t* to the parent-minus-hydrogen radical,[8,9a] and we shall base the calculations below on this assumption.[23]

If all radicals are scavenged by the H_2S and if the chief mode of incorporation of tritium is by a radical mechanism, then G(RH-*t*) is equal to the yield of the parent-minus-hydrogen radical, G(R·), corrected for the isotope effect for the reaction of the R· free radical with H_2S-*t*.[24]

$$\begin{aligned} \mathrm{R}\cdot + \mathrm{H_2S} &\xrightarrow{k_H} \mathrm{RH} + \mathrm{HS}\cdot \\ \mathrm{R}\cdot + \mathrm{HST} &\xrightarrow{k_T} \mathrm{RT} + \mathrm{HS}\cdot \qquad (2) \\ G(\mathrm{RH}\text{-}t) &= G(\mathrm{R}\cdot)(k_T/k_H) \end{aligned}$$

In connection with another project,[25] we have measured

(16) (a) The abstraction of a benzylic hydrogen from toluene by the HS· radical should be exothermic by 4 kcal/mol (D($PhCH_2$–H) = 85 (see ref 17) and D(HS–H) = 89 (see ref 18)). Thus it is possible that for substrates like toluene more than one tritium is incorporated per parent-minus-hydrogen radical. However, as will be discussed below, the distribution of activity in toluene suggests that this is not an important mechanism for production of RH-*t*.

(17) A. S. Rodgers, D. M. Golden, and S. W. Benson, *J. Amer. Chem. Soc.*, 89, 4578 (1967).

(18) The dissociation energies for HS–H, CH_3S–H, and C_2H_5S–H are all 89 kcal/mol; see W. A. Pryor, "Mechanisms of Sulfur Reactions," McGraw–Hill Book Co., New York, N. Y., 1962, pp 17, 89.

(19) G(RH-*t*) is the yield of RH-*t* which would have been produced had pure T_2S been used instead of H_2S-*t* and assuming that there is no isotope effect. Alternatively, G(RH-*t*) can be viewed as the total yield of RH which has been chemically converted to either RH or RT, again assuming no isotope effect. The factor of 0.5 in eq 1 corrects for the two hydrogen atoms in H_2S.

(20) Ausloss and Lias,[8] found that 2.5% H_2S was sufficient to scavenge all the radicals in the gas-phase radiolysis of propane-d_8. Ausloos, Scala, and Lias[8] used 5% H_2S in the liquid-phase radiolysis of cycloalkanes.

(21) A. Thiemann, *Ber. Kernforsch. Julich*, 27, 73 (1961).

(22) M. Zifferero, *Energia Nucleare* (Milan). 4, 479 (1957).

(23) Clearly, this assumption is the weak point in our argument. However, the data appear to justify it. It is interesting, however, that H_2O-*t* appears to label compounds through a mechanism involving excited species (see ref 9i).

(24) The isotope effect is written as k_T/k_H since *less* activity than the statistical expectation is incorporated into the recovered RH because of the isotope effect.

(25) These isotope effects for radical reactions appear to spread radicals into an interesting and useful spectrum of selectivity and reactivity, and we plan to report a number of them at a future time.

Table II: Labeling of Toluene by Different Techniques

Tolune used, g	Tritium used, Ci	Method	10^{-20} absorbed dose, eV	Irradiation time	Activity in toluene, mCi	$10^2 \times G$(RH-t)	Ref
0.86	7.5	Wilzbach	~3	3 days	19	<10	*a*
0.86	0.3	Wilzbach	3	60 days	5.3	3.5	*b*
0.45	0.5	Wilzbach	0.5	5.5 days	0.32	1.3	*c*
0.05	1.0	Tesla coil	~0.3	0.5 min	43	350	*c*
0.006	0.5	Uv	~100	1.2 days	22.0	0.46	*c*
0.01	0.5	Microwave	~100	5 min	0.05	0.001	*c*
1.07	5.0×10^{-5}	H_2S-t	0.8	1 day	3.6×10^{-5}	22	*d*

[a] Reference 11a. [b] B. Aliprandi, F. Cacace, and L. Cieri, *Ric. Sci. Riv.*, **30**, 1 (1960). [c] Reference 21. [d] This work.

the isotope effect for the reaction of the cyclohexyl and phenyl radicals with tritiated propanethiol; the values of k_H/k_T are 6.9 and 2.4, respectively.[26,27] If we make the reasonable assumption[18] that the value of k_H/k_T will be similar for the reaction of radicals with H_2S-t and C_3H_7SH-t, then a value of $G(R\cdot)$ can be obtained.

$$G(R\cdot) = G(\text{RH-}t)\frac{k_H}{k_T} \qquad (3)$$

Taking the values of 0.69 and 0.094, respectively, for G(RH-t) for cyclohexane and benzene from Table I, we can calculate $G(R\cdot)$ to be 4.7 for the cyclohexyl radical and 0.23 for the phenyl.

The most useful comparison of these data is to data obtained using iodine as a scavenger. The G value for the yield of cyclohexyl iodide from cyclohexane[28] is approximately 4.0, and the value of G for phenyl iodide[29,30] is 0.2. Both of these results are in excellent agreement with our data. This supports the hypothesis that the main mechanism for tritiation of RH from H_2S-t is by a radical mechanism.

The calculation of the yield of radicals from toluene is more complex since four isomeric parent-minus-hydrogen radicals are possible and several isotope effects could occur. However, we can make an approximate calculation in the following way. From the distribution of activity, the structure of 79% of the radicals is CH_3–$C_6H_4\cdot$ and that of 21% is $\cdot CH_2$–C_6H_5. We can use the isotope effect found for phenyl radicals, namely, 2, for the reaction of the former radicals with H_2S, and we can take the polystyrene radical as a model for the latter radical and use an isotope effect of 7.[31] Then we obtain

G(toluene-minus-hydrogen radical) =

$$(0.79)(0.22)(2) + (0.21)(0.22)(7) = 0.7$$

This value would appear to be high. The total radical yield from toluene has been reported as 0.5,[29] and the parent-minus-hydrogen yield could be at most half of that.[16]

Table II compares this method for preparing labeled toluene with the normal and several modified Wilzbach methods. The value of G(RH-t) using H_2S compares well with all methods except the Tesla coil accelerated Wilzbach.[32]

(26) The value of k_H/k_T for the cyclohexyl radical at 27 ± 2° is obtained by extrapolating values at 100 and 130° measured by Mr. Kenneth Kneipp using C_6H_{11}–CO_3Bu-t as the radical source.

(27) The value of k_H/k_T for phenyl was measured at 60 and 80° using phenylazotriphenylmethane as the radical source by Mr. Kneipp. The extrapolated value at 27° is 2.4.

(28) These values have been reported: (a) G = 2.9 at 5 mM I_2 (J. Dauphin, *J. Chim. Phys.*, **59**, 1207 (1962)); (b) 3.4 at 3 mM I_2 (G. A. Muccini and R. H. Schuler, *J. Phys. Chem.*, **64**, 1435 (1960)); (c) 3.9 at 6 mM I_2 (S. Z. Toma and W. H. Hamill, *J. Amer. Chem. Soc.*, **86**, 1478 (1964)); (d) 4.0 at 40 mM I_2 (H. A. Dewhurst, *J. Phys. Chem.*, **62**, 15 (1958)); see also R. Blackburn and A. Charlesby, *Proc. Roy. Soc.*, **A293**, 51 (1966).

(29) (a) A. MacLachlan and R. L. McCarthy, *J. Amer. Chem. Soc.*, **84**, 2519 (1962); (b) J. A. Ward and W. H. Hamill, *ibid.*, **89**, 5116 (1967), gave the yield of phenyl iodide as 0.27 for 0.05 M iodine in benzene; they also cited unpublished work from their laboratory giving 4.0 as the yield of cyclohexyl iodide.

(30) The total yield of radicals from benzene has been measured as 0.7 by T. J. Hardwick, *J. Phys. Chem.*, **66**, 1611 (1962) as 0.6 by A. Henglein, H. Url, and W. Hoffmeister, *Z. Phys. Chem.* (Frankfurt am Main), **18**, 26 (1958), as 0.75 by V. A. Krongauz and Kh. S. Bagdasaryan, *Proc. Acad. Sci. USSR, Phys. Chem. Sect.*, **114**, 367 (1957), as 0.75 by R. B. Cundall and P. A. Griffith, *J. Phys. Chem.*, **69**, 1866 (1965), and as 0.78 by E. A. Cherniak, E. Collinson, F. S. Dainton, and G. M. Meaburn, *Proc. Chem. Soc.*, 54 (1958). The yield of phenyl radicals could be half as large as these values.

(31) A value of k_H/k_T for the benzyl radical at 60° can be calculated from the value of 3.9 for k_H/k_D for the reaction of the polystyryl radical with butanethiol-d_1 measured by L. A. Wall and D. W. Brown, *J. Polym. Sci.*, **14**, 513 (1954); the Swain equation then gives k_H/k_T = 7.1.

(32) Table I also lists high yields of nonvolatile, labeled substances. These are water-insoluble, high-boiling materials of unidentified structures. Clearly, it is important to remove radioimpurities such as, for example, cyclohexene-t from cyclohexane, and our purification was designed with this in mind. We believe that the high yields of these nonvolatile products do not influence the measured yields of recovered substrate, RH-t, the only quantity measured here.

A Molecular Orbital Description of TcH_9^{2-}

by Harold Basch[1] and A. P. Ginsberg

Bell Telephone Laboratories, Inc., Murray Hill, New Jersey *(Received July 22, 1968)*

A ground-state molecular orbital wave function has been calculated for the TcH_9^{2-} ion within the full, nonempirical Hartree–Fock–Roothaan formalism in a large gaussian orbital basis. The computed MO's are used to calculate net charges on the atoms, the absolute magnetic shielding at the protons, and the anisotropy in the strictly diamagnetic part of the bulk susceptibility. The calculated shielding is in satisfactory agreement with the experimental value. It is concluded that the hydrogens in TcH_9^{2-} are almost identical in regard to their electronic environment. The lowest lying band positions, polarizations, and intensities in the electronic absorption spectrum are estimated.

A hydrogen atom bonded directly to a transition metal atom or ion is noted for its high-field proton magnetic shielding constant.[2] We have used this experimental information to test the feasibility of obtaining a molecular orbital description of a metal hydride within the framework of the nonempirical molecular orbital theory, by calculating the ground and also certain excited electronic states and structural properties of the formally d^0 TcH_9^{2-} ion. The Roothaan SCF–MO formalism[3a] in a contracted (single-ζ for the core and double-ζ for the valence shell AO's) gaussian orbital basis[3b] was used. It should be noted that the calculational procedure contains no adjustable parameters, includes all electrons, and requires the evaluation of all (in this case ~20 million) integrals. Integral evaluation time was about 4 hr on a GE 645 computer.

For a closed-shell electronic configuration the computational procedure is perfectly straightforward, requiring only the choice of basis set and geometry. K_2TcH_9 is isostructural with K_2ReH_9 and has a unit cell volume only 1.7% greater than that of K_2ReH_9.[4] We have therefore assumed that the TcH_9^{2-} ion has the same structure as has been found for ReH_9^{2-} (point group D_{3h} symmetry) by a neutron diffraction study.[5] The structure is shown in Figure 1; a uniform Tc–H bond distance of 1.70 Å, slightly larger than the value of 1.69 Å found for ReH_9^{2-}, was used. The angle between hydrogens in the same vertical mirror plane was taken as 93.6°, the same as in ReH_9^{2-}.

The Tc basis set was obtained by first optimizing[6] all exponents in a $11^s8^p7^d$ gaussian primitive-orbital basis[7] for a Tc^{2+} $4d^5$ configuration. The resulting coefficients and exponents were then used to construct the contracted basis set shown in Table I. The 5s and 5p atomic orbitals were obtained by scaling the Slater orbital basis atomic SCF calculation for molybdenum of Roothaan and Synek.[8] For the H atoms a 4^s fit[9] to a Slater 1s exponent of ~0.9 was split into three-term and one-term sets of basis functions designated 1s and 1s′ in Table I. Note that the 4d AO has also been split into a 4d and a 4d′ orbital to allow greater variational freedom in the calculation away from the arbitrary choice of charge and configuration in the basis set and in an effort to minimize the basis set dependence of the computed results.

The computed ground-state MO's have been used to calculate net charges on the atoms *via* a Mulliken population analysis, the absolute magnetic shielding at the protons, and the anisotropy in the strictly diamagnetic part of the bulk susceptibility. Also, the positions of the lowest excited electronic states in the optical spectrum and their polarizations and intensities have been estimated.

The isotropic values for the absolute shielding at the protons were calculated from

$$\sigma_H = 3^{-1}c^{-2}[\langle\Psi_0 \mid r_H^{-1} \mid \Psi_0\rangle - \sum_q R_q\langle\Psi_0 \mid q_H/r_H^3 \mid \Psi_0\rangle] \quad (1)$$

where $3^{-1}c^{-2} = 17.7497 \times 10^{-6}$, $q = x, y, z$, Ψ_0 is the computed ground-state wave function, the integrals are in atomic units, and the proton is at a distance $R = \sqrt{\sum_q R_q^2} = 1.70$ Å from the Tc atom. This formula has been discussed elsewhere[10–13] and is considered fully applicable to the proton shielding in TcH_9^{2-}. The results of this investigation offer further evidence for the validity of (1) in these situations.[14]

(1) Ford Scientific Laboratory, Dearborn, Mich. 48121.

(2) For recent reviews see A. P. Ginsberg, *Transition Metal Chem.*, **1**, 111 (1965); M. L. H. Green and D. J. Jones, *Advan. Inorg. Chem. Radiochem.*, **7**, 115 (1965).

(3) (a) C. C. J. Roothaan, *Rev. Mod. Phys.*, **23**, 69 (1951); (b) H. Basch, C. Hollister, and J. W. Moskowitz, Abstracts, 154th National Meeting of the American Chemical Society, Chicago, Ill. 1967, No. O81.

(4) A. P. Ginsberg, *Inorg. Chem.*, **3**, 567 (1964).

(5) S. C. Abrahams, A. P. Ginsberg, and K. Knox, *ibid.*, **3**, 558 (1964).

(6) The atomic SCF computer program was kindly supplied by Dr. C. J. Hornback.

(7) $11^s = 11$ s-type gaussian primitive orbitals [radial dependence $\sim\exp(-\alpha r^2)$], etc. For a discussion of primitive *vs.* contracted functions, see J. M. Schulman, J. W. Moskowitz, and C. Hollister, *J. Chem. Phys.*, **46**, 2759 (1967).

(8) C. C. J. Roothaan and M. Synek, *Phys. Rev.*, **133**, A1263 (1964).

(9) S. Huzinaga, *J. Chem. Phys.*, **42**, 1293 (1965).

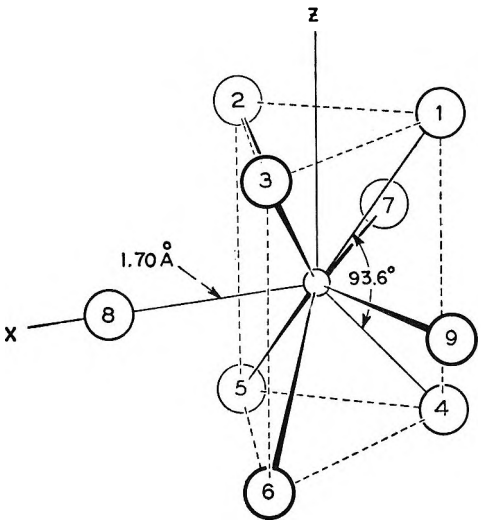


Figure 1. Perspective arrangement of hydrogen atoms in TcH_9^{2-}, based on the known structure of ReH_9^{2-}.

The first term in (1) is the average diamagnetic part of the shielding constant and for one of the equatorial protons amounts to $+295.2 \times 10^{-6}$. The second term is part of the ordinary paramagnetic shielding term, extracted from the usual sum over excited states[14] by a coordinate transformation on the angular momentum operator. For the same proton this second term contributes -251.5×10^{-6} for a net absolute shielding of 43.7×10^{-6}. For a proton at one of the apices of the trigonal prism the corresponding values are $(+295.6 - 250.9) \times 10^{-6} = 44.7 \times 10^{-6}$. Experimentally,[4] TcH_9^{2-} in solution shows only a single proton nmr absorption at τ 18.4 ppm which corresponds to an experimental absolute shielding of 39.0×10^{-6}.[15] Thus the high-field proton magnetic shielding constant is satisfactorily obtained from the computed MO's.

Table II presents a population analysis breakdown of the valence shell MO's and the individual MO contributions to the σ_H values quoted above. The core (Tc 1s, 2s, 2p, 3s, 3p, 3d, 4s, 4p) electrons contribute nothing to the shielding as can be predicted from eq 1 by considering the core functions as point charges; r_H^{-1} goes to R^{-1} and $R_q q_H / r_H^3$ also goes to R^{-1}. Previous authors[11,14] have tried to pinpoint the origin of, or largest contributions to, the chemical shift, but the very mixed metal + ligand character of these MO's precludes such an analysis here. Interestingly enough, a total population analysis predicts that each equatorial proton carries only a rather small excessive negative charge (−0.139). The corresponding value in the apical positions is −0.203. As expected, the slightly larger negative charge correlates with the slightly larger shielding constant. Previous investigators[16] have found that charges roughly twice as large as those obtained here were also able to explain the analogous high-field chemical shift in ReH_9^{2-}, which is only 0.7 ppm greater than in TcH_9^{2-}.

The average value of the diamagnetic contribution to the bulk magnetic susceptibility can be obtained from[12]

$$\chi^d = \frac{e^2 a_0^2 N}{6mc^2} \langle \Psi_0 | \sum_q q^2 | \Psi_0 \rangle \qquad (2)$$

where the prefactor is evaluated as 0.791998×10^{-6} cgs/g-atom, the integral is in atomic units, and the origin of q is taken at the center of mass or center of electronic charge,[12] which happen to coincide at the

Table I: Gaussian Orbital Basis Set[a]

AO	Basis function[b]
	Tc
1s	0.006461 (59,660) + 0.046997 (8920) + 0.213133 (2049) + 0.508622 (562.4) + 0.351552 (197.5)
2s	0.729331 (45.73) + 0.409957 (18.82)
3s	0.782913 (7.168) + 0.530820 (3.570)
4s	0.723624 (1.50) + 0.630291 (0.5250)
5s	0.534250 (0.1035) + 0.599810 (0.03242)
2p[c]	0.029791 (1113) + 0.190172 (266.4) + 0.496210 (84.56) + 0.404304 (31.96)
3p[c]	0.492456 (12.11) + 0.578946 (4.990)
4p[c]	0.4400 (2.066) + 0.781378 (0.6768)
5p[c]	0.534250 (0.1885) + 0.599810 (0.05901)
3d[d]	0.091822 (85.41) + 0.362753 (24.86) + 0.549056 (8.625) + 0.250134 (2.967)
4d[d]	0.077886 (2.967) + 0.423549 (1.271) + 0.448769 (0.5299)
4d′[d]	1.000000 (0.2078)
	H
1s	0.019060 (10.69) + 0.134240 (1.611) + 0.474490 (0.3630)
1s′	1.000000 (0.09865)

[a] The contracted Tc atom basis set is comparable to a minimal Slater orbital basis except for the d's which are probably somewhat better. [b] The functions are tabulated in the form $C_1(\alpha_1) + C_2(\alpha_2) + \ldots$, where the C's are the coefficients and the α's are the gaussian exponents. [c] Each of type x, y, and z, with radial dependence $\sim r \exp(-\alpha r^2)$. [d] Each of type xy, xz, yz, $x^2 - y^2$, and $2z^2 - x^2 - y^2$, with radial dependence $\sim r^2 \exp(-\alpha r^2)$.

(10) C. W. Kern and W. N. Lipscomb, *J. Chem. Phys.*, **37**, 260 (1962).
(11) R. M. Stevens, C. W. Kern, and W. N. Lipscomb, *ibid.*, **37**, 279 (1962).
(12) S. I. Chan and T. P. Das, *ibid.*, **37**, 1527 (1962).
(13) A. D. Buckingham and P. J. Stephens, *J. Chem. Soc.*, 2747 (1964).
(14) W. N. Lipscomb, *Advan. Magn. Resonance*, **2**, 137 (1967).
(15) From W. H. Flygare, J. M. Pochan, G. I. Kerley, T. Caves, M. Karplus, S. Aung, R. M. Pitzer, and S. I. Chan, *J. Chem. Phys.*, **45**, 2793 (1966); $\sigma_{TMS} - \sigma_{H_2O(g)} = +0.6 \times 10^{-6}$, $\sigma_{H_2O(g)} - \sigma_{H_2} = 3.4 \times 10^{-6}$, and $\sigma_{H_2} = 26.6 \times 10^{-6}$, yielding $\sigma_{TMS} = 30.6 \times 10^{-6}$. Therefore $\sigma_{TcH_9^{2-}} = 30.6 \times 10^{-6} + 8.4 \times 10^{-6} = 39.0 \times 10^{-6}$.
(16) L. L. Lohr, Jr., and W. N. Lipscomb, *Inorg. Chem.*, **3**, 22 (1964). These authors quote experimental σ values that are consistently $\sim 4.0 \times 10^{-6}$ higher than what would be derived using $\sigma_{TMS} = 30.6 \times 10^{-6}$ [15] and the experimental chemical shifts on the τ scale.[2]

Table II: Valence Shell MO's in TcH_9^{2-}

Symmetry[a]	Population analysis[b] H (1s)[e]	Tc (4d)[f]	Tc (5s)	Tc (5p)	Magnetic shielding[g] σ_H[c]	σ_H[d]
$6a_1'$	0.775		0.225		6.1	6.1
$2e''$ (xz)	0.47	0.53			2.3	5.7
$2e''$ (yz)	0.47	0.53			3.4	2.6
$5e'$ $(x^2 - y^2)$	0.54	0.42		0.04 (x)	11.8	2.5
$5e'$ (xy)	0.54	0.42		0.04 (y)	2.1	3.6
$7a_1'$ $(2z^2 - x^2 - y^2)$	0.38	0.62			4.5	2.6
$4a_2''$	0.83			0.17 (z)	4.3	8.1
$6e'$ $(x^2 - y^2)$	0.72	0.16		0.12 (x)	4.9	10.0
$6e'$ (xy)	0.72	0.16		0.12 (y)	4.3	3.5
$8a_1'$ $(2z^2 - x^2 - y^2)$	0.70	0.30				
$7e'$ $(x^2 - y^2, xy)$	0.695	0.305				
$3e''$ (xz, yz)	0.52	0.48				

[a] $1 \rightarrow 5a'$, $1 \rightarrow 3a_2''$, $1 \rightarrow 4e'$, and $1e''$ constitute the core. $8a'$, $7e'$, and $3e''$ are not occupied. The MO's are listed in order of increasing orbital energy. [b] Normalized to one electron per MO. [c] Absolute shielding for H(8) in Figure 1 using eq 1. [d] Absolute shielding for H(1) in Figure 1 using eq 1. [e] Sum of 1s and 1s' populations. [f] Sum of 4d and 4d' populations. [g] In ppm.

Table III: Lowest Lying Allowed Electronic Transitions in TcH_9^{2-}

Upper state (polarization)	One-electron excitation	$\Delta\epsilon$[a]	$-ER$[b]	Excitation energy[c]	Oscillator strength[d]
$^1E'$ (x, y)	$6e' \rightarrow 8a_1'$	0.51591	−0.25013	7.23	0.008
$^1E'$ (x, y)	$7a_1' \rightarrow 7e'$	0.55005	−0.25549	8.01	0.413
$^1E'$ (x, y)	$6e' \rightarrow 7e'$	0.52194	−0.17060	9.56	0.482
$^1A_2''$ (z)	$4a_2'' \rightarrow 8a_1'$	0.54098	−0.21019	9.00	0.470

[a] Orbital energy difference (in au). [b] Sum of electron repulsion energy terms (In au). [c] In eV. [d] See text.

Tc atom in TcH_9^{2-}. Since we are not able to obtain the paramagnetic only part of the susceptibility, of greater interest is the anisotropy in χ^d defined as $(\chi^d_{zz} - \chi^d_{xx})/\chi^d_{zz}$. We compute $\chi^d_{zz} = -57.86 \times 10^{-6}$ cgsu and χ^d_{xx} $(= \chi^d_{yy}) = -54.49 \times 10^{-6}$ cgsu, for a rather small anisotropy of about 6%. A population analysis of the metal valence shell orbitals yields the electronic distribution $4d^{5.698}5s^{0.632}5p^{1.275}$ with the 4d electrons rather uniformly distributed among the 5 orthogonal d orbitals, and the p electrons equally allotted to the $5p_x$, $5p_y$, and $5p_z$ orbitals. These data, combined with the previous information that both the net charges and proton chemical shifts are very similar for the equatorial and apical protons, support the assertion[5] that the hydrogens in TcH_9^{2-} are nearly equivalent with regard to their electronic environment. Thus in the solid, where rapid interchange of the protons does not take place, these calculations predict that the two proton nmr absorptions expected for TcH_9^{2-} will be very close to each other.

In the virtual orbital approximation and neglecting spin–orbit coupling effects, vertical electronic excitation energies can be obtained from the computed occupied and unoccupied MO's shown in Table II. There is no direct experimental evidence on the electronic absorption spectrum of TcH_9^{2-}, but the isostructural ReH_9^{2-} ion in solution shows a single maximum below 50,000 cm^{-1} at 5.9 eV ($f \approx 0.03$) which has been assigned as an $e' \rightarrow a_1'$ transition.[5] In going from Re to Tc in the same oxidation state we would expect the excitation energy to red-shift slightly.

The four lowest lying spin and electric dipole allowed excited states corresponding to one-electron excitations from occupied to unoccupied MO's in Table II and their oscillator strengths are shown in Table III. The formulas for deriving the excitation energies are obtained in the standard way[3a] and each involves an orbital energy difference ($\Delta\epsilon$) plus electron repulsion energy terms ($-ER$), individually tabulated in Table III. Oscillator strengths have been calculated from a mixed dipole velocity–dipole length expression which eliminates the excitation energy from appearing explicitly in the intensity calculation.[17]

From Table III it is clear that the lowest lying allowed transition is of x, y polarization, corresponding to the excitation of an electron from the $6e'$ to the $8a_1'$ MO. Although the computed excitation energy is apparently too high (by ~1.5 eV) and the intensity is too low, configuration mixing with the other nearby $^1E'$ states which have large oscillator strengths is sure to improve both the computed position and the intensity (especially the latter) of the first allowed tran-

(17) A. E. Hansen, *Mol. Phys.*, 13, 425 (1967).

sition. The first z-polarized transition ($^1A_2''$) is expected to be well separated from the first $^1E'$. This is a reasonably good accounting of the expected electronic absorption spectrum of TcH_9^{2-}, its predicted onset at rather high energies correlating with the observed spectrum of ReH_9^{2-}.

Acknowledgments. The authors wish to thank Dr. David B. Neumann for many interesting and informative discussions on properties, Dr. Charles Hornback for the use of his atomic SCF program, and Dr. M. B. Robin for clarifying discussions on ligand field spectra.

Proton Magnetic Resonance Study of Water–Ammonia Proton Exchange in Water–Ammonia Solutions Containing Added Potassium Hydroxide[1]

by Mohammed Alei, Jr., and Alan E. Florin

University of California, Los Alamos Scientific Laboratory, Los Alamos, New Mexico 87544 *(Received July 29, 1968)*

The exchange of protons between H_2O and NH_3 in solutions of H_2O in liquid NH_3 at 29.6 ± 0.2° is accelerated by addition of OH^-. The overall kinetics for H_2O concentrations from 1 to 12 M and added $[OH^-]$ from zero to $\sim 2 \times 10^{-3}$ M is well represented by rate = $k_1[OH^-] + k_2[OH^-][H_2O]^2 + k_3[NH_4^+][H_2O] + k_4[H_2O]^4$ with $k_1 = 7.4 \times 10^4$ sec^{-1}, $k_2 = 0.84 \times 10^4$ sec^{-1} M^{-2}, $k_3 = 3.48 \times 10^6$ sec^{-1} M^{-1}, and $k_4 = 0.058$ sec^{-1} M^{-3}. At the highest H_2O concentrations, the effect of the third term in the above rate expression allows one to place rather narrow limits on the ionization of H_2O in liquid NH_3. Thus at 12.2 M H_2O, $K_{ion} = [NH_4^+][OH^-]/[H_2O] = (3.9 \pm 0.3) \times 10^{-11}$ and at 9.05 M H_2O, $K_{ion} = (1.1 \pm 0.1) \times 10^{-11}$. The remaining terms in the rate expression suggest possible species in these systems.

Introduction

In a previous publication,[2] we pointed out that well-defined, separate nmr peaks are observed for H_2O and NH_3 protons at room temperature in H_2O–NH_3 solutions containing roughly 30 mol % or less H_2O. Thus the exchange of protons between H_2O and NH_3 is slow in the nmr sense under these conditions. We further demonstrated that this exchange could be markedly accelerated by addition of NH_4^+, and we reported on the results of a study of the kinetics of H_2O–NH_3 proton exchange accelerated by NH_4^+.

In this paper we report results of a study of H_2O–NH_3 proton exchange accelerated by hydroxide. This process is slower than the process involving NH_4^+ and is dependent on H_2O concentration in a way that suggests more than one H_2O species in the H_2O–NH_3 liquid system at room temperature. Moreover, under certain experimental conditions, the NH_4^+ arising from the ionization of H_2O can be detected and rather narrow limits can be placed on the ionization constant for H_2O at certain concentrations in liquid NH_3.

Experimental Section

Proton line width data were obtained using the Varian DA-60 instrument. All measurements were made at the equilibrium temperature in the nmr probe which was found to be very stable at 29.6 ± 0.2°.

A given H_2O–NH_3–KOH solution was prepared by mixing a measured amount of an appropriate dilute aqueous KOH solution with a measured quantity of anhydrous liquid NH_3. The samples were prepared and examined in the special plastic-valve, glass nmr cell shown in Figure 1. Because of its small size, light weight, and axial symmetry, the cell can be spun and a resolution of 0.3 Hz at 60 MHz can be obtained. The glass section is standard 1-mm wall × 5-mm o.d. Pyrex glass tubing, selected from several lengths of commercial stock for roundness and precise o.d. A slightly enlarged section near the open end of the glass tube permits firm attachment of a plastic valve. The stem-inlet of this valve is machined to the standard-taper angle to fit a ground joint on a glass vacuum system. The stem was removed completely for introduction of the aqueous KOH solution with a calibrated micropipet. The reassembled cell was then placed on a vacuum system, and the glass tube was cooled in liquid N_2 and evacuated. NH_3 was then added from a calibrated volume filled to a

(1) Work done under the auspices of the U. S. Atomic Energy Commission.

(2) M. Alei and A. E. Florin, *J. Phys. Chem.*, **72**, 550 (1968).

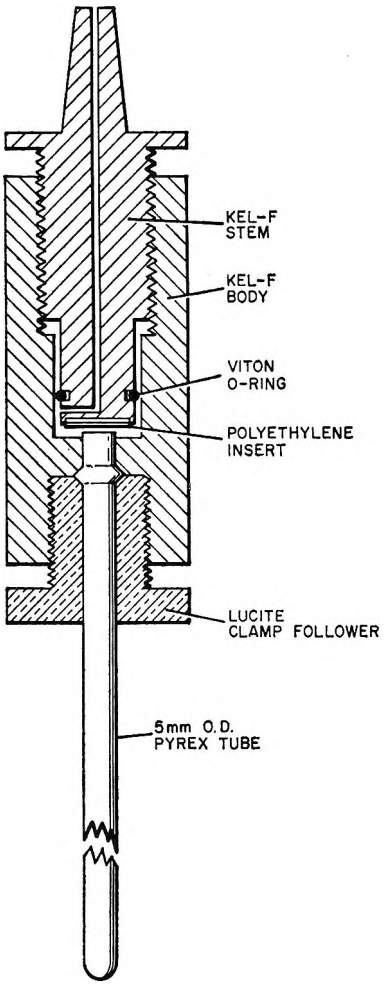


Figure 1. Plastic-valve, glass nmr cell.

measured pressure with NH_3 gas. The cell was calibrated for volume as a function of height of liquid in the cell so that final molarities could be calculated. The cell could easily withstand the ~150 psi equilibrium pressure over pure liquid NH_3 at room temperature. In fact, it survived testing at pressures in excess of 300 psi.

To obtain reproducible proton line widths in the NH_3–H_2O–KOH solutions, it was necessary to rinse the cell two or three times with a given solution. These rinses were especially important for solutions low in H_2O and KOH. It appeared that the glass tube was capable of consuming approximately the equivalent of a monolayer of KOH either by absorption or by neutralization of acidic constituents in the glass surface. The design of the cell made rinsing quite simple. After shaking a given liquid sample in the cell, simply inverting the cell and opening the valve allowed the NH_3 pressure to force the liquid out of the cell.

In an attempt to eliminate consumption of KOH by glass surfaces, two cells similar to the one shown in Figure 1 were constructed, one entirely of Teflon and one entirely of Kel-F (except for the Viton O-ring).

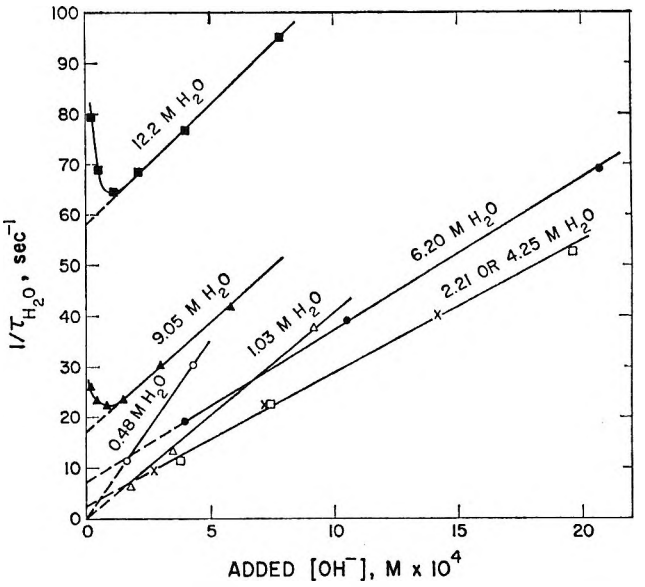


Figure 2. H_2O–NH_3 proton exchange accelerated by added [OH^-]: ○, 0.48 *M* H_2O; △, 1.03 *M* H_2O; □, 2.21 *M* H_2O; ×, 4.25 *M* H_2O; ●, 6.20 *M* H_2O; ▲, 9.05 *M* H_2O, ■, 12.2 *M* H_2O.

We found, however, that consumption of KOH was even more pronounced in these cells than it was in the glass–plastic cell. Whether this was due to leaching of acidic constituents from the plastic or diffusion of atmospheric CO_2 through the thin plastic walls is not certain. In any case, the all-plastic cells were of little use in this work. They might, however, be extremely useful for nmr studies in media highly corrosive to glass, and they can be made to withstand up to an internal pressure of ~10 atm.

Results

The analysis of the proton-exchange kinetics was based upon measurement of the width at half-height of the separate resonance for the water protons in the system. The width is related to the residence time for a proton in the H_2O environment[3] by the relationship

$$1/\tau_{H_2O} = (1/T_2') - (1/T_2) = \pi\Delta\nu_{H_2O} \qquad (1)$$

where τ_{H_2O} is the average time which a proton spends in the H_2O environment before returning to an NH_3 molecule and $\Delta\nu_{H_2O}$ is the half-height broadening in Hertz due to exchange. Figure 2 is a plot of $1/\tau_{H_2O}$ *vs.* added [OH^-] at several fixed concentrations of H_2O in liquid NH_3 at room temperature. At low [H_2O], the highest added [OH^-] which could be studied was generally limited by the point at which

(3) We should emphasize that the term "H_2O environment" implies nothing concerning the state of the water in these systems. The only justification for using this term is the observation that the area under the nmr peak representing the protons in this environment corresponds to the number of protons introduced as H_2O in making up the solution. Thus the H_2O environment could represent a single H_2O species or any number of H_2O species with rapid averaging of water protons among them. We also use the term "H_2O proton" to refer to the average proton in the H_2O environment.

further addition of KOH produced a solid residue and adding still more KOH produced more solid and no further increase in the width of the H_2O–proton resonance. If we assume that this limit represents the saturation solubility of KOH in the final solution, we find this solubility increases linearly with H_2O concentration in the region between 0 and 1.03 M H_2O. Thus at 0.48 M H_2O in liquid NH_3, the solubility of KOH is 6.3×10^{-4} M, while at 1.03 M H_2O, it is 12.8×10^{-4} M. At higher $[H_2O]$, the solubility of KOH increased much more rapidly with increasing $[H_2O]$.

Although KOH was used as the source of added $[OH^-]$ in all the data reported here, several experiments using NaOH or tetrapropylammonium hydroxide instead of KOH demonstrated that the broadening produced did not depend on the particular source of hydroxide. Addition of large amounts of KCl, on the other hand, produced no significant additional broadening in H_2O–NH_3 solutions containing small amounts of KOH. We therefore conclude that the observed increased broadening of the H_2O proton resonance with increasing addition of KOH is due to an exchange process involving a hydroxide ion species. We also observe that the width of the NH_3 proton peak increases with increasing added $[OH^-]$ and, in H_2O–NH_3 solutions with sufficient solubility for KOH, a single averaged peak for all protons can be produced by simply adding sufficient KOH at constant H_2O. It seems to us that the only conclusion consistent with these observations is that H_2O–NH_3 proton exchange is accelerated by a hydroxide ion species. The width of the H_2O–proton resonance provides a convenient and sensitive quantitative measure of the rate of this exchange since no other processes contribute significantly to the width of this resonance. In principle, the width of the NH_3 proton resonance should also reflect changes in the rate of NH_3–H_2O proton exchange and, with proper consideration of the relative abundances of the NH_3 and H_2O proton environments, one might expect to derive the same kinetic results from an analysis of the NH_3 proton line widths as from an analysis of the H_2O proton line widths. In practice, however, the NH_3 proton line widths are much less amenable to quantitative study of H_2O–NH_3 proton exchange for two reasons. First, one can easily show that for a given change in the rate of exchange between protons in an H_2O environment and protons in an NH_3 environment, the absolute change in hertz in the width of the H_2O proton resonance is p_{NH_3}/p_{H_2O} times as great as the corresponding change in the width of the NH_3 proton resonance, where p_{NH_3} and p_{H_2O} are the fractions of total protons in each environment. At 12 M H_2O in NH_3, the ratio of p_{NH_3}/p_{H_2O} is $\sim$4 and at 1 M H_2O in NH_3 it is $\sim$30. Thus the H_2O proton line width is a much more sensitive indicator of changes in the H_2O–NH_3 exchange rate under the experimental conditions employed in this work. The second and more serious limitation in attempting to use the NH_3 proton line width for quantitative study of H_2O–NH_3 proton exchange is the fact that processes other than H_2O–NH_3 proton exchange can make significant contributions to the NH_3 proton line width. In particular, since over nearly the entire compositional range of this study the NH_3 proton resonance is a triplet due to ^{14}N–H spin–spin coupling, the NH_3 proton spectrum can be influenced by changes in the rate of ^{14}N quadrupolar relaxation and the rate of NH_3–NH_3 proton exchange. The latter process can become especially important at the higher H_2O concentrations and low added $[OH^-]$ where NH_4^+ arising from the ionization of H_2O in liquid NH_3 can accelerate NH_3–NH_3 proton exchange to a much greater degree than it does NH_3–H_2O proton exchange. Thus Clutter and Swift[4] have demonstrated that this process proceeds at a rate of 6.9×10^9 sec^{-1} which is at least two orders of magnitude faster than the rate of H_2O–NH_3 proton exchange in the presence of NH_4^+. For these reasons and the fact that the primary purpose of this work was to examine the H_2O–NH_3 proton-exchange process, we have not attempted to analyze the NH_3 proton line widths in detail.

Discussion

The data plotted in Figure 2 give direct insight into the form of the rate expression for H_2O–NH_3 proton exchange in the presence of added $[OH^-]$. If we define rate as being equal to the number of moles of H_2O per liter which exchange a single proton with NH_3 each second, then τ_{H_2O}, the average residence time for a proton in the H_2O environment, is related to to rate by the expression

$$1/\tau_{H_2O} = \text{rate}/2[H_2O] \qquad (2)$$

where $[H_2O]$ is the molar concentration of H_2O in the system. Thus from a knowledge of the dependence of $1/\tau_{H_2O}$ on various parameters, one can readily deduce the dependence of rate upon these parameters.

The most readily apparent feature of the data plotted in Figure 2 is the linear increase in $1/\tau_{H_2O}$ with increasing added $[OH^-]$, at constant $[H_2O]$, over nearly the entire range of the data. The only experimentally significant departure from this linear dependence occurs at 9.05 and 12.2 M H_2O at very low values of added $[OH^-]$. Under these conditions, we observe a minimum in the plot of $1/\tau_{H_2O}$ *vs.* added $[OH^-]$ so that, at very low added $[OH^-]$, $1/\tau_{H_2O}$ increases rather sharply with *decreasing* added $[OH^-]$. Moreover, at 12.2 M H_2O, even in the region where $1/\tau_{H_2O}$ increases with increasing added $[OH^-]$, we have observed that the resonance for the NH_3 protons becomes a better-resolved triplet as the H_2O proton resonance

(4) D. R. Clutter and T. J. Swift, *J. Amer. Chem. Soc.*, **90**, 601 (1968).

becomes broader. If we assume that NH_4^+ is considerably more effective than OH^- in accelerating H_2O–NH_3 proton exchange and that it accelerates NH_3–NH_3 proton exchange to an even greater degree, then the above observations are consistent with the presence of significant equilibrium concentrations of NH_4^+ arising from ionization of H_2O at high concentrations of H_2O in liquid NH_3. Returning to the general features of the data in Figure 2, we note that the slopes of the straight lines decrease with increasing $[H_2O]$ at low $[H_2O]$ and increase with increasing $[H_2O]$ at higher $[H_2O]$. Moreover, at constant [KOH], the dependence of $1/\tau_{H_2O}$ on $[H_2O]$ proceeds from an inverse dependence at low $[H_2O]$ to a direct dependence at high $[H_2O]$. Finally, we note that at higher $[H_2O]$, the straight lines in Figure 2 extrapolate to positive values of $1/\tau_{H_2O}$ at zero added $[OH^-]$ and the extrapolated value increases very markedly with increasing $[H_2O]$.

To interpret the above observations, we propose an expression of the form

$$1/\tau_{H_2O} = k_1[OH^-]/[H_2O]^m + k_2[OH^-][H_2O]^n + k_3[NH_4^+] + k_4[H_2O]^p \quad (3)$$

where the bracketed quantities are meant to denote equilibrium molar concentrations. Thus $[OH^-]$ is not strictly equal to added $[OH^-]$, the abscissa in Figure 2, but is essentially indistinguishable from it except at high $[H_2O]$ and low added $[OH^-]$ where the ionization of H_2O contributes significantly to the equilibrium $[OH^-]$. At the lowest H_2O concentrations, dominance of the first term in eq 3 produces the direct dependence on $[OH^-]$ and inverse dependence on $[H_2O]$ as observed. With increasing $[H_2O]$, the second and fourth terms become increasingly important so that, at H_2O concentrations above ~3 or 4 M, $1/\tau_{H_2O}$ becomes directly dependent on $[H_2O]$ as well as $[OH^-]$ and a significant and increasingly large intercept at zero $[OH^-]$ is produced. We tentatively assume that the dependence of this intercept on $[H_2O]$ is given by $k_4[H_2O]^p$. As mentioned earlier, the third term in eq 3 becomes experimentally apparent only at higher H_2O concentrations. As added $[OH^-]$ is reduced to very low values, the equilibrium concentration of NH_4^+ produced by the ionization $H_2O + NH_3 \rightleftarrows NH_4^+ + OH^-$ becomes large enough to make a very significant contribution to H_2O–NH_3 proton exchange. As we have shown in a previous publication,[2] the acceleration of this exchange by NH_4^+ contributes $1.74 \times 10^6[NH_4^+]$ to $1/\tau_{H_2O}$. Thus k_3 in eq 3 is 1.74×10^6.

To evaluate k_1, k_2, m, and n in eq 3 we note that the slope of a given plot of $1/\tau_{H_2O}$ *vs.* added $[OH^-]$ at fixed $[H_2O]$ is determined by the first two terms and given by

$$\text{slope} = k_1/[H_2O]^m + k_2[H_2O]^n \quad (4)$$

Thus

$$[H_2O]^m \cdot \text{slope} = k_1 + k_2[H_2O]^{m+n} \quad (5)$$

which requires that a plot of $[H_2O]^m \cdot$ slope *vs.* $[H_2O]^{m+n}$ be linear. Table I lists the slope of the $1/\tau_{H_2O}$ *vs.* added $[OH^-]$ plot for each H_2O concentration studied (*cf.* Figure 2). By trial and error we find that the best fit of the data is obtained by assuming $m = n = 1$; *i.e.*, the best line is obtained by plotting $[H_2O] \cdot$ slope *vs.* $[H_2O]^2$. The pertinent calculated values for testing this best fit are also included in Table I. The quality of the fit is demonstrated by the constancy of k_2 in the last column of the table. For H_2O concentrations between 1.03 and 9.05 M, the constancy of k_2 is quite good. The average of the four values of k_2 in this region is 0.42×10^4 sec^{-1} M^{-2} with a standard deviation of $\pm 0.03 \times 10^4$ sec^{-1} M^{-2}. Attempts to fit the data with other values of m and n demonstrate that deviations from linearity especially at higher H_2O concentrations become very large for values of n other than 1. For values of m other than 1 a significant deviation occurs at lower H_2O concentrations (between 1.03 and 2.21 M $[H_2O]$). Using $k_2 = 0.42 \times 10^4$ and the expression (eq 5 above with $m = n = 1$) $k_1 = [H_2O] \cdot \text{slope} - k_2[H_2O]^2$, we may calculate values of k_1 for H_2O concentrations of 1.03 to 9.05 M. The average of five values for k_1 is 3.7×10^4 sec^{-1} with a standard deviation of $\pm 0.4 \times 10^4$ sec^{-1}. Significant deviations from the above fit occur at 0.48 and 12.2 M H_2O where the slope of the $1/\tau_{H_2O}$ *vs.* added $[OH^-]$ plot is, in each case, somewhat less than required. The deviation at 0.48 M H_2O is not understood but could be due to a systematic loss of KOH to the glass walls of the nmr cell. The deviation at 12.2 M H_2O, on the other hand, is in the direction expected if the ionization of H_2O produces concentrations of OH^-

Table I: Test of Parameters in Eq 5

$[H_2O]$, M	Slope $\times 10^{-4}$, sec^{-1} M^{-1}	$[H_2O] \cdot$ slope $\times 10^{-4}$, sec^{-1}	$[H_2O]^2$, M^2	$k_2 = \frac{\Delta([H_2O] \cdot \text{slope})}{\Delta([H_2O]^2)}$ $\times 10^{-4}$, sec^{-1} M^{-2}
0.48	7.00	3.36	0.23	
				1.01
1.03	4.08	4.20	1.06	
				0.42
2.21	2.62	5.79	4.88	
				0.40
4.25	2.62	11.13	18.1	
				0.37
6.20	3.02	18.72	38.4	
				0.47
9.05	4.32	39.1	81.9	
				0.27
12.2	4.70	57.3	149	

significant in comparison with the added $[OH^-]$. With values for k_1, k_2, m, n, and k_3, we may utilize eq 3 and the data at 9.05 and 12.2 M H_2O to place rather narrow limits on the extent of ionization of H_2O at these concentrations in liquid NH_3 at room temperature. Thus, by substituting appropriate values, eq 3 becomes

$$1/\tau_{H_2O} = (3.7 \times 10^4[OH^-])/[H_2O] + 0.42 \times 10^4[OH^-][H_2O] + 1.74 \times 10^6[NH_4^+] + k_4[H_2O]^p \quad (6)$$

We now define K_{ion} so that

$$[NH_4^+] = [H_2O]\cdot K_{ion}/[OH^-] \quad (7)$$

Substituting eq 7 in 6 and combining terms

$$1/\tau_{H_2O} = [OH^-] \times [(3.7 \times 10^4)/[H_2O] + 0.42 \times 10^4[H_2O]] + [(1.74 \times 10^6[H_2O]\cdot K_{ion})/[OH^-]] + k_4[H_2O]^p \quad (8)$$

where $[OH^-]$, the equilibrium hydroxide ion concentration, is given by

$$[OH^-] = A + X - [(B - (B^2 - 4C)^{1/2})/2] \quad (9)$$

where $A = ([H_2O]\cdot K_{ion})^{1/2}$, X = added $[OH^-]$, $B = 2A + X$, $C = X\cdot A$.

By combining eq 8 and 9 we may obtain an expression for $1/\tau_{H_2O}$ as a function of added $[OH^-]$, $[H_2O]$, K_{ion}, and $k_4[H_2O]^p$. Thus, assuming arbitrary values for K_{ion} and $k_4[H_2O]^p$ we may calculate curves for $1/\tau_{H_2O}$ *vs.* added $[OH^-]$ at a given $[H_2O]$ and compare these with the experimental data. Actually, a nonlinear least-squares program written for the CDC 6600 computer was used to find values for K_{ion} and $k_4[H_2O]^p$ which gave the best agreement between calculated and experimental curves at a given H_2O concentration. For the 12.2 M data these values were $K_{ion} = (3.9 \pm 0.3) \times 10^{-11}$, $k_4[H_2O]^p = 52.1 \pm 0.7$ sec^{-1} and for the 9.05 M data, $K_{ion} = (1.1 \pm 0.1) \times 10^{-11}$, $k_4[H_2O]^p = 16.8 \pm 0.4$ sec^{-1}. With regard to the values of K_{ion} we note that they are increasing with increasing $[H_2O]$ and are both higher than the value of 3×10^{-12} reported by Clutter and Swift[3] for K_{ion} in liquid NH_3 containing up to ~0.5 M H_2O. In view of the expected increase in dielectric constant with increasing H_2O in this system, one would certainly also expect K_{ion} to increase. However, even with accurate knowledge of the dielectric constant as a function of composition it would be difficult to predict the exact variation in K_{ion} with any reliability.

With regard to the values of $k_4[H_2O]^p$ we note that the value of 52.1 at 12.2 M H_2O is somewhat smaller than the value (~58) which would have been obtained by extrapolation of the essentially linear portion of the experimental $1/\tau_{H_2O}$ *vs.* added $[OH^-]$ at 12.2 M H_2O. This is consistent with the fact that a plot of $1/\tau_{H_2O}$ *vs.* equilibrium $[OH^-]$ would have produced a steeper line with a smaller intercept. The value of $k_4[H_2O]^p = 16.8$ at 9.05 M H_2O is indistinguishable from the value obtained by extrapolation of the linear portion of the experimental data at 9.05 M H_2O. At lower $[H_2O]$, therefore, one expects the value of $k_4[H_2O]^p$ to be given quite accurately by extrapolating the experimental lines to zero added $[OH^-]$. Values of $k_4[H_2O]^p$ obtained by extrapolation at 6.20 and 4.25 M H_2O are 7 and 2, respectively.

As mentioned earlier, we have thus far only assumed the mathematical form, $k_4[H_2O]^p$. If this assumption is valid, $\log (k_4[H_2O]^p) = \log k_4 + p \log [H_2O]$ and a log–log plot of $k_4[H_2O]^p$ *vs.* $[H_2O]$ should produce a straight line with slope = p. Such a plot is shown in Figure 3 where the data are fit very well by a line

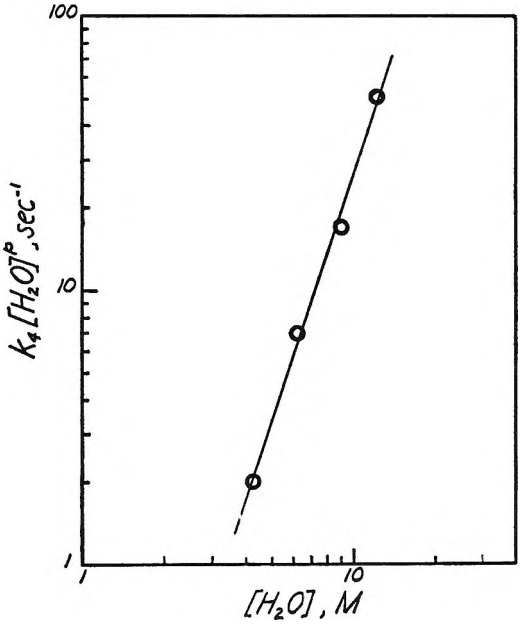


Figure 3. Ion-independent H_2O–NH_3 proton exchange.

with slope = 3. Thus, the ion-independent contribution to $1/\tau_{H_2O}$ is given by $k_4[H_2O]^3$. From any pair of values of $k_4[H_2O]^p$ and $[H_2O]$ we may then calculate $k_4 = 0.029$.

We may now write the complete expression for $1/\tau_{H_2O}$ (*cf.* eq 3) in the following form

$$1/\tau_{H_2O} = k_1[OH^-]/[H_2O] + k_2[OH^-][H_2O] + k_3[NH_4^+] + k_4[H_2O]^3 \quad (10)$$

Combining eq 10 with eq 2

$$\text{rate} = k_1'[OH^-] + k_2'[OH^-][H_2O]^2 + k_3'[NH_4^+][H_2O] + k_4'[H_2O]^4 \quad (11)$$

where $k_1' = 2k_1 = 7.4 \times 10^4$ sec^{-1}, $k_2' = 2k_2 = 0.84 \times 10^4$ sec^{-1} M^{-2}, $k_3' = 3.48 \times 10^6$ sec^{-1} M^{-1}, and $k_4' = 0.058$ sec^{-1} M^{-3}.

Equation 11 represents the simplest rate expression which adequately describes H_2O–NH_3 proton exchange in the region from 1 to 12 M H_2O in liquid NH_3 solutions with added hydroxide. As written, this expression implies no dependence upon the concentration of NH_3 in any of the rate-determining steps. However, we should emphasize that the NH_3 concentration changes by only ~15% (from ~35 to ~30 M) over the entire range of this study. In view of the experimental uncertainties, it would therefore be difficult for this work to positively establish whether or not an $[NH_3]$ dependence is involved in kinetics. In spite of this shortcoming, however, the dependences upon $[H_2O]$, $[OH^-]$, and $[NH_4^+]$ are quite clear and the terms in eq 11 can still provide valuable insight into possible species and mechanisms involved in the rate-determining processes. Thus the first term in eq 11 suggests exchange between a hydrated OH^- ion and NH_3. The existence of a hydrated OH^- in this system is consistent with the observation that the saturation solubility of KOH in H_2O–NH_3 solutions is directly proportional to the H_2O concentration at the lowest H_2O concentrations used in this study. It is also consistent with the conclusion by Jolly[5] that hydroxide ion is strongly solvated by H_2O and poorly solvated by NH_3. Because H_2O is always in large excess relative to OH^- in the systems studied here and because at low $[H_2O]$ the change in NH_3 concentration with change in $[H_2O]$ is negligible, proton exchange between NH_3 and a species $(H_2O)_n \cdot OH^-$ might be well represented by the first term in eq 11.

The second and fourth terms in eq 11 suggest the possibility that a dimeric H_2O species may exist in the H_2O–NH_3 liquid system. Thus the second term could represent an exchange process involving a dimeric water species, whose equilibrium concentration would be proportional to $[H_2O]^2$, and hydrated OH^-. Whether or not a separate NH_3 species were also involved would depend on the nature of the dimeric H_2O species. If the dimeric H_2O species were also associated with NH_3 (the species $NH_3 \cdot 2H_2O$, for example), then an encounter between the dimeric H_2O species and hydrated OH^- might suffice to produce NH_3–H_2O proton exchange whose kinetics could be expressed by the second term in eq 11. Likewise, the fourth term in eq 11 could represent an exchange process involving a collision between two H_2O dimers or an exchange process involving a tetrameric H_2O species. Thus, although other interpretations are possible, the kinetic data would be at least consistent with the existence of dimeric and monomeric forms of H_2O in equilibrium in the H_2O–NH_3 liquid system.

Acknowledgment. The authors are indebted to Dr. T. W. Newton of this laboratory for assistance with the nonlinear least-squares computer program used in some of the calculations.

(5) W. L. Jolly, *J. Chem. Educ.*, 44, 304 (1967).

The Nature of Water Species in Water–Ammonia Solutions as Inferred from Proton and Oxygen-17 Nuclear Magnetic Resonance Observations[1]

by Mohammed Alei, Jr., and Alan E. Florin

University of California, Los Alamos Scientific Laboratory, Los Alamos, New Mexico 87544 *(Received July 29, 1968)*

H_2O proton shifts as a function of H_2O concentration in liquid NH_3 at 29.6 ± 0.2° are well interpreted in terms of an equilibrium between monomeric and dimeric forms of H_2O. The intrinsic shift for the average H_2O proton in the monomeric species is −268.2 ± 0.2 Hz relative to TMS while for the dimeric species it is −416 ± 12 Hz. The equilibrium constant for formation of dimer is $K_2 = (1.26 \pm 0.15) \times 10^{-2}$. ^{17}O shifts in $H_2{}^{17}O$–NH_3 liquid mixtures at room temperature when compared with ^{17}O shifts in $H_2{}^{17}O$–acetone and $H_2{}^{17}O$–$(CH_3)_3N$ suggest that the shielding at the ^{17}O nucleus may be principally determined by the degree to which oxygen lone-pair electrons act as donors to solvent protons in hydrogen bond formation. Such interactions may be more important than heretofore considered. The temperature coefficient of the H_2O proton shift in very dilute solutions of H_2O in liquid NH_3 is 13.5×10^{-3} ppm/deg and appears to be a property of a proton in the N---H–O hydrogen bond in this system. The temperature coefficient for the proton shift in liquid NH_3 is 2.7×10^{-3} ppm/deg.

Introduction

In a recent study[2] of H_2O–NH_3 proton exchange in H_2O–NH_3 solutions containing OH^-, the kinetic data were well fit by an expression which suggested the possibility of more than one H_2O species in the systems studied. In particular, it was pointed out that the rate expression would be consistent with an equilibrium between monomeric and dimeric forms of H_2O.

In this paper we report results of a study at 29.6 ± 0.2° of the shift, as a function of H_2O concentration, of the nmr peak due to H_2O protons in H_2O–NH_3 solutions up to 14 *M* in H_2O. The data are well interpreted in terms of an equilibrium between monomeric and dimeric forms of H_2O. In an effort to better understand the types of interactions in which the various species might be involved, we have also studied the ^{17}O shift as a function of composition in H_2O–NH_3 liquid system at 29.6 ± 0.2°. When compared with similar measurements in the H_2O–acetone and H_2O–$(CH_3)_3N$ systems, the ^{17}O shifts suggest that the water oxygen may act as an electron-pair donor to solvent protons. Finally, measured temperature dependences of the nmr shift of H_2O protons and NH_3 protons in the H_2O–NH_3 liquid system at low H_2O concentrations support the proposal by Muller and Reiter[3] that the temperature dependence of shift may be a characteristic property of a proton in a given type of hydrogen bond rather than mainly a reflection of changes in relative amounts of various hydrogen-bonded species in equilibrium.

Experimental Section

Proton and ^{17}O shift data were obtained with the Varian DA-60 instrument. All measurements were made at the equilibrium temperature in the nmr probe which was found to be very stable at 29.6 ± 0.2°.

Proton shifts were measured against tetramethylsilane (TMS) or tetramethylmethane (TMM) as internal references. TMM was a convenient reference in H_2O–NH_3 solutions ~2 *M* in H_2O where the TMS spectral position was matched (and hence the reference obscured) by the upfield member of the ^{14}N-split, NH_3 proton triplet. The position of the TMM resonance is 54.3 Hz downfield of the TMS resonance, and this separation is independent of H_2O molarity over the range studied. All shifts could, therefore, be easily referred to TMS and could be determined to ±0.5 Hz.

^{17}O shifts were measured with a magnetometer making use of the control probe and associated electronics which normally supply a proton reference signal for nmr field-lock in the "external reference" version of the Varian field-synchronized recorder. The magnetometer protons were located less than 1 in. from the nuclei under study hence varying field gradients did not introduce appreciable error. A variable radiofrequency oscillator, a frequency counter, and an amplifier for the modulation-frequency phase detector completed the magnetometer. With this technique ^{17}O shifts could be measured with an accuracy of ±1 ppm.

Water enriched to ~3% in ^{17}O was used for measurement of the ^{17}O shifts at high mol % H_2O while at low percentages, H_2O enriched to ~30% in ^{17}O was used. The NH_3 was Matheson anhydrous material, acetone was Baker Analyzed reagent, and trimethylamine was Eastman White Label. Samples were prepared and examined in a plastic-valve, glass nmr cell described elsewhere.[2] Water and acetone were pipetted into the

(1) Work done under the auspices of the U. S. Atomic Energy Commission.

(2) M. Alei, Jr., and A. E. Florin, *J. Phys. Chem.*, **73**, 857 (1969).

(3) N. Muller and R. C. Reiter *J. Chem. Phys.*, **42**, 3265 (1965).

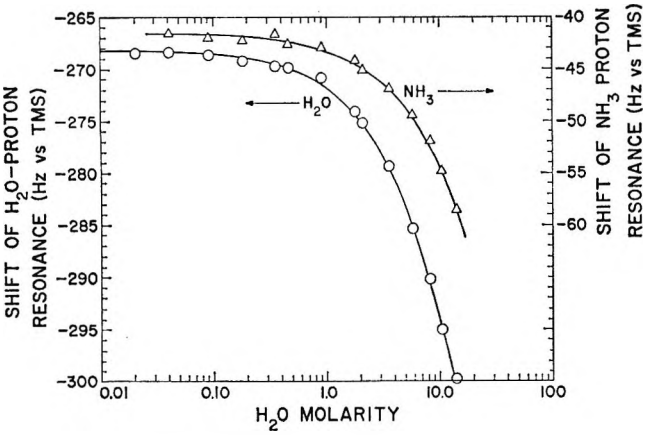


Figure 1. H_2O and NH_3 proton shifts in H_2O–NH_3 solutions.

cell, and NH_3 and $(CH_3)_3N$ were added by condensation of the gas from calibrated volumes on a vacuum system.

Results

The shift of the nmr peak for H_2O protons is shown in Figure 1 where it is plotted against H_2O molarity in liquid NH_3 at 29.6 ± 0.2°. The H_2O molarity is arbitrarily plotted on a logarithmic scale so that all the data, covering nearly three orders of magnitude variation in H_2O molarity, can be legibly displayed on a single plot. The shift of the center component of the NH_3 proton triplet is also shown in Figure 1. The highest concentration of 14 *M* H_2O represents a practical limit beyond which increasingly rapid averaging of H_2O and NH_3 protons begins to significantly distort and shift the individual proton resonances. Under these circumstances, accurate shifts cannot be measured without resorting to a detailed analysis of line shapes.

^{17}O nmr shifts in the H_2O–NH_3 liquid system over the entire range of composition at 29.6 ± 0.2° are shown in Figure 2. Measured ^{17}O shifts in the H_2O–acetone and H_2O–trimethylamine systems are also shown. A fact not apparent in these data is that the ^{17}O resonance is a rather sharp singlet at H_2O concentrations greater than ~30 mol % and a well-defined triplet with splitting of ~80 Hz at H_2O concentrations below ~10 mol %. It thus appears that there is no rapid, direct proton exchange between H_2O species under conditions where H_2O–NH_3 proton exchange is slow.

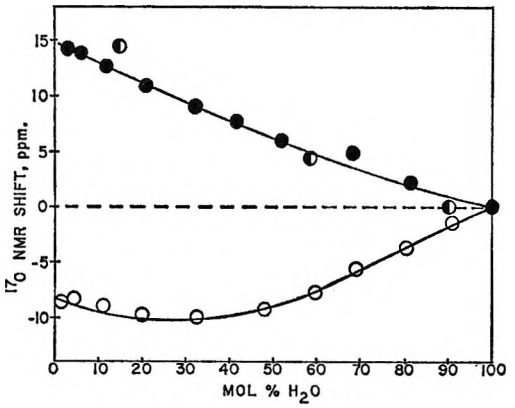


Figure 2. $H_2{}^{17}O$ shifts in mixed liquid systems: ○, H_2O–NH_3; ●, H_2O–acetone; ◐, H_2O–$(CH_3)_3N$.

Because the shift of the H_2O proton resonance in Figure 1 approaches a limiting value at low H_2O concentrations, we were afforded an opportunity to observe the effect of temperature on the shift of this resonance over a range of H_2O concentrations in which changes in H_2O concentration produced a negligible effect on the shift at room temperature. The results of the temperature study are shown in Figure 3 where

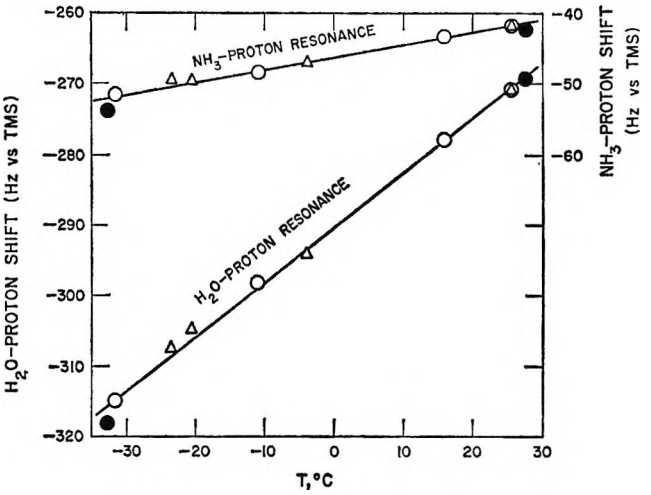


Figure 3. Temperature dependences of proton nmr shifts: ●, 0.048 mol % H_2O; ○, 0.074 mol % H_2O; △, 0.44 mol % H_2O.

the shift of the H_2O proton resonance is plotted *vs.* temperature at three different H_2O concentrations. The shift of the center component of the NH_3 proton triplet over the same temperature interval is also shown.

Discussion

The shift of the resonance for the water protons with H_2O concentration (Figure 1) provides definite indication of at least two H_2O species in this system. Thus, if we assume that in very dilute solutions of H_2O in liquid NH_3, the water is present as a monomeric species (probably associated with one or more NH_3 molecules through N - - - H–O hydrogen bonds as the extrapolated shift of −268 Hz at infinite dilution is far downfield of the proton shift in gaseous H_2O), the dependence of shift on H_2O concentration could be explained in terms of an equilibrium between this monomer and at least one other H_2O species. If we assume only one other species in equilibrium with monomer, the linear dependence of the shift on water concentration at low $[H_2O]$ suggests a monomer–dimer equilibrium. Following the treatment of Saunders and

Hyne,[4] the pertinent equations would then be

$$\nu = (\nu_1 M_1 + 2\nu_2 K_2 M_1^2)/(M_1 + 2K_2 M_1^2) \quad (1)$$

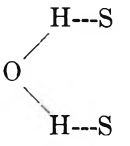
and

$$C = M_1 + 2K_2 M_1^2 \quad (2)$$

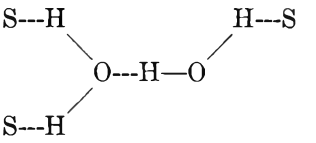
where ν = observed shift, ν_1 = average shift for water protons in monomeric H_2O species, ν_2 = average shift for water protons in dimeric H_2O species, K_2 = equilibrium constant for formation of dimeric H_2O species, M_1 = concentration of monomeric H_2O species, and C = total H_2O concentration, $[H_2O]$.

If a monomer–dimer equilibrium is to adequately interpret our observed shift data, we must be able to find values of the parameters ν_1, ν_2, and K_2 which, when substituted in the above equations, will produce calculated shifts in agreement with the observed values. For this purpose, we utilized a nonlinear least-squares program written for the CDC 6600 computer to select parameter values which minimized the sum of the squares of the deviations of calculated from experimental shifts. On the basis of the 14 experimental shifts, best values for the parameters were found to be: $\nu_1 = -268.2 \pm 0.2$ Hz; $\nu_2 = -416 \pm 12$ Hz, and $K_2 = (1.26 \pm 0.15) \times 10^{-2}$ where the error limits in all cases represent standard deviations. With these values, the unweighted sum of the squares of the deviations of the 14 observed shifts from the 14 calculated shifts was 1.5 Hz^2 and in no case did an experimental shift differ from a calculated shift by more than 0.6 Hz. Thus the experimental data are fit extremely well by a monomer–dimer equilibrium. The data were tested in similar fashion against a model assuming an equilibrium between a monomeric and a trimeric water species. For the best fit in this case, the unweighted sum of the squares of the deviations was 5.7 Hz^2, and several experimental points differed from calculated points by 0.8 to 1.0 Hz which lies clearly outside our experimental uncertainty of ± 0.5 Hz. It thus appears that the assumption of an equilibrium between a monomeric and dimeric H_2O species is the simplest hypothesis which adequately accounts for the observed shift of the water proton resonance in liquid NH_3 solutions up to 14 M in H_2O. As noted earlier, such an equilibrium would also be consistent with the observed kinetics for proton exchange in H_2O–NH_3 solutions containing added $[OH^-]$.

Though the foregoing discussion makes it seem plausible that water exists primarily in the form of monomeric and dimeric species when dissolved in liquid NH_3 at room temperature, the proton nmr shift data, per se, give little insight into the specific structures of these species. It seems clear that there must be at least two different environments for water protons but the exact nature of these environments is not revealed by our experiments. Holmes, Kivelson, and Drinkard[5] in their study of dilute solutions of water in a number of organic solvents have assumed a water monomer complexed to solvent through hydrogen bonding between water protons and basic solvent sites, *i.e.*



where S represents a solvent molecule. They interpret their nmr shift data in terms of an equilibrium between this monomeric H_2O species and a dimeric species with structure



These seem to us to be reasonable structures insofar as they indicate likely environments for water protons. Such species could, moreover, certainly account for our reported shifts for the water proton in the H_2O–NH_3 system. On the other hand, the above structures suggest that solvent protons should experience an upfield shift due to some breaking of solvent structure by the H_2O molecules. In fact (*cf.* Figure 1) the NH_3 proton resonance experiences a very significant downfield shift on addition of increasing amounts of H_2O to liquid NH_3. Moreover, the proposed structures imply no interaction between water oxygen and solvent protons. In calculating the energy of a single water–solvent hydrogen bond from heat of mixing data, Holmes, Kivelson, and Drinkard do in fact ignore possible hydrogen bonds involving water oxygen as an electron donor and a solvent proton as acceptor. In a more recent publication dealing with water species in organic solvents, Johnson, Christian, and Affsprung[6] also assume that amines and ketones are unable to interact favorably with the oxygen of the water molecule.

The ^{17}O nmr shift data in Figure 2 seem to us to indicate a significant interaction between water oxygen and solvent protons in the systems under discussion. In a recent publication,[7] we showed that ^{17}O nmr shifts in liquid and gaseous water are consistent with a decrease in diamagnetic shielding at the oxygen atom with increasing hydrogen bonding. Whether oxygen lone-pair donation or O–H bond elongation or both are important in determining the shielding at the oxygen was not evident from the work cited. However, if we examine the data in Figure 2 with the assumption that the observed shifts are due to differences in hydrogen

(4) M. Saunders and J. B. Hyne, *J. Chem. Phys.*, **29**, 1319 (1958).

(5) J. R. Holmes, D. Kivelson, and W. C. Drinkard, *J. Amer. Chem. Soc.*, **84**, 4677 (1962).

(6) J. R. Johnson, S. D. Christian, and H. E. Affsprung, *J. Chem. Soc., A*, 1924 (1967).

(7) A. E. Florin and M. Alei, Jr., *J. Chem. Phys.*, **47**, 4268 (1967).

bonding experienced by a water molecule in going from pure liquid H_2O to a solution of water in a given solvent, some interesting inferences may be drawn. In the first place, the downfield shift of ^{17}O resonance for H_2O in liquid NH_3 would indicate generally stronger hydrogen bonding between H_2O and NH_3 than between water molecules in pure liquid H_2O. If the principal factor determining the shielding at the ^{17}O nucleus in a water molecule is the length of the O–H bond and the degree to which it is altered by hydrogen bonds involving the H_2O proton as an acceptor for a pair of electrons from a solvent donor atom, then one would expect the ^{17}O shift in a dilute solution of H_2O in trimethylamine to be comparable with that for a dilute solution of H_2O in NH_3 since in both cases the solvent donor is an amine nitrogen. If, on the other hand, the shielding at the water oxygen is largely determined by the degree to which the oxygen lone-pair electrons participate in hydrogen bond formation with solvent protons as acceptors, then one might expect the shift of the ^{17}O resonance for a dilute solution of water in $(CH_3)_3N$ to be more comparable with that for a dilute solution of water in acetone since both solvents offer similar types of protons as acceptors for lone-pair electrons of the water oxygen. The fact that the ^{17}O shift for water in $(CH_3)_3N$ is observed to be comparable with that for water in acetone suggests that the shielding at the oxygen nucleus of the water molecule is primarily determined by the degree to which oxygen lone-pair electrons are involved in hydrogen bond formation. Thus the downfield shift, relative to pure liquid water, of the ^{17}O resonance in dilute solutions of water in NH_3 suggests that a water oxygen donates electrons better to protons in liquid NH_3 than it does, on the average, to protons in liquid water. Whether or not this further implies that the O - - - H–N hydrogen bond is stronger than the O - - - H–O hydrogen bond in liquid water depends on the degree to which pure liquid water is considered to be hydrogen bonded. On the other hand, in acetone or $(CH_3)_3N$ as solvent, the upfield shift of the ^{17}O resonance would indicate an O - - - H–C hydrogen bond weaker than the O - - - H–O hydrogen bond in liquid water. What is most significant, however, is the fact that even in dilute solutions in acetone or $(CH_3)_3N$ the ^{17}O resonance of the water molecule is still some 21 ppm downfield of its position in gaseous water.[7] If our proposed model is correct, the O - - - H–C hydrogen bond could thus conceivably be of the order of $\frac{21}{36}$ or ~0.6 as strong as the O - - H–O hydrogen bond in liquid H_2O assuming complete hydrogen bonding in pure liquid H_2O and a linear relationship between hydrogen bond strength and ^{17}O shifts for the water molecules in these systems. Of course the uncertainties in these assumptions preclude any reliable quantitative assignment of relative bond strengths. However, in view of the quite large downfield shift relative to $H_2{}^{17}O$ vapor of the $H_2{}^{17}O$ resonance for dilute solutions of water in acetone it seems highly unlikely that there is no significant interaction between the oxygen of the water molecule and the protons of acetone. We therefore suggest that ignoring possible interaction between water oxygen and solvent protons in dilute solutions of water in organic solvents may not be generally valid.

One other aspect of the $H_2{}^{17}O$ shift data which should be pointed out is the qualitative agreement between the ^{17}O shifts and water proton shifts in the H_2O–NH_3 system. Though the minimum in the $H_2{}^{17}O$ shift at ~30 mol % (~12 *M*) H_2O is not very pronounced, it appears to be real and would be consistent with the presence of at least two water species in dilute solutions of H_2O in NH_3. In view of the preceding discussion, it seems likely that the species are monomeric and dimeric forms of H_2O associated with solvent NH_3 not only *via* hydrogen bonds involving water protons and NH_3 nitrogen, but also through bonding of NH_3 protons by water oxygen. If this is so and if as we have suggested earlier the O - - - H–N hydrogen bond is a rather strong one, one should expect addition of H_2O to NH_3 to produce a downfield shift of the resonance for the average NH_3 proton. As pointed out earlier this is indeed observed (*cf.* Figure 3).

The temperature dependence of the nmr shift of the H_2O proton in very dilute solutions of H_2O in NH_3 (Figure 3) seems clearly to be a property of the H_2O proton in the monomeric H_2O species. As is evident in Figure 3, the temperature coefficient of 0.81 Hz/deg or 13.5×10^{-3} ppm/deg does not vary by more than ~5%, if at all, over an approximately tenfold variation in H_2O concentration between 0.176 and 0.019 *M*. Over this same concentration range, the change in shift with varying H_2O concentration is not experimentally detectable indicating negligible concentrations of dimeric H_2O species at room temperature. Under these conditions, if the large observed temperature coefficient of shift were due to changes with temperature in the equilibrium constant for formation of dimeric from monomeric H_2O species, one would expect the temperature coefficient to be rather strongly dependent on total H_2O concentration. Since this is clearly not so, the change in shift with temperature is probably related to changes in properties of hydrogen bonds involving water protons in monomeric H_2O species. Muller and Reiter[3] have proposed that variations with temperature of nmr chemical shifts for protons involved in hydrogen bonds may be attributed to changes in the degree of excitation of the hydrogen bond stretching vibrational mode in a given hydrogen-bonded species. These authors suggest that the temperature coefficient of 9.5×10^{-3} ppm/deg[8] for the proton shift in pure liquid water between 25 and 110° may be substantially due to such distortion rather than

(8) W. G. Schneider, H. J. Bernstein, and J. A. Pople, *J. Chem. Phys.*, **28**, 601 (1958).

rupture of hydrogen bonds. If we accept this interpretation, our observed temperature dependence for the shift of water protons in very dilute solutions of H_2O in NH_3 could be due to changes in the degree of excitation of the stretching mode of N - - - H–O hydrogen bonds involving both water protons hydrogen bonded by NH_3 nitrogens in a single, monomeric H_2O species. It is interesting to compare the observed coefficient of 13.5×10^{-3} ppm/deg for a proton in such an environment with the value of 9.5×10^{-3} ppm/deg for the proton resonance in liquid H_2O and 2.7×10^{-3} ppm/deg for the proton resonance in liquid NH_3 (*cf.* Figure 3). If we assume that the shift of nonhydrogen-bonded protons is temperature independent, and that liquid H_2O and liquid NH_3 are as completely hydrogen bonded as possible, then we might consider that the temperature coefficient characteristic of an N - - - H–N proton is $3 \times 2.7 \times 10^{-3} = 8.1 \times 10^{-3}$ ppm/deg compared with 9.5×10^{-3} ppm/deg for an O - - - H–O proton and 13.5×10^{-3} ppm/deg for an N - - - H–O proton. The magnitudes of the temperature coefficients of proton shift would thus seem to fall in the order one might expect for the energies of the hydrogen bonds involving the protons in question. Whether the temperature coefficient for proton shift might be generally useful in assigning relative hydrogen bond strengths seems, however, highly questionable. Even assuming the temperature coefficient to be entirely determined by excitation of the hydrogen bond stretching vibration, the magnitude of the temperature coefficient would depend on the anharmonicity of the vibration as well as upon the bond strength. Moreover, Hindman, *et al.*,[9] have demonstrated that dispersion interactions can account for rather large temperature coefficients for proton shifts in liquid H_2S, H_2Se, and H_2Te. Although such interactions might be expected to be less important in liquid H_2O or liquid NH_3, they cannot, in general, be ignored.

Acknowledgment. The authors are indebted to Dr. B. B. McInteer and Mr. R. M. Potter of this laboratory for the preparation of the enriched ^{17}O used in this study. We are also indebted to Dr. T. W. Newton of this laboratory for assistance with the nonlinear least-squares computer program used in some of the calculations.

(9) J. C. Hindman, A. Svirmickas, and W. B. Dixon, *J. Chem. Phys.*, 47, 4658 (1967).

Aqueous Chemistry of Inorganic Free Radicals.[1] VI. The Effect of Oxygen on the Rate of Photolysis of Hydrogen Peroxide in Aqueous Solutions Containing Carbon Monoxide

by F. P. Laming, George Buxton, and W. K. Wilmarth

Department of Chemistry, University of Southern California, Los Angeles, California 90007 *(Received July 29, 1968)*

When aqueous H_2O_2 is photolyzed in solutions containing both CO and O_2, the rate of photolysis is decreased to a value less than that observed in the absence of CO. In the interpretation presented for these results, the conclusion is reached that in their reactions with the OH radical, the rate constant for CO is 72 ± 3.6 times larger than that of H_2O_2. To supplement our earlier kinetic studies in the O_2-free system, tracer studies using ^{14}CO in the photolysis have been made in an effort to identify the free radical reactive intermediate involved in chain termination at low H_2O_2 concentrations.

Introduction

An earlier paper in this series deals with the use of CO as a scavenger for the OH radicals generated by the photolysis of H_2O_2.[2] Most of the studies were carried out in solutions in which the O_2 concentration was thought to be low enough not to influence the kinetic results. One of the objectives of these experiments was the evaluation of the relative scavenger efficiencies of CO and H_2O_2 in their reactions with the OH radical.

In the present studies, the photolysis of aqueous H_2O_2 has been carried out in solutions containing both CO and O_2. The work was carried out because the results provide an alternate method of evaluating the relative scavenger efficiencies mentioned above. The present evaluation of the scavenger efficiencies leads to the conclusion that in their reactions with the hy-

(1) This work was supported by the U. S. Atomic Energy Commission.
(2) G. Buxton and W. K. Wilmarth, *J. Phys. Chem.*, 67, 2835 (1963).

droxyl radical, the rate constant for CO is 72 ± 3.6 times larger than that of H_2O_2. This ratio of rate constants is somewhat larger than that reported earlier. Possible reasons for this discrepancy are discussed below.

In addition to the work under consideration we report below tracer studies of the photolysis of H_2O_2 in O_2-free solutions using ^{14}CO. The results, while incomplete, lead to reconsideration of the mechanism proposed earlier for the O_2-free system. In particular, consideration is given to the possibility that chain carrying and, under some conditions, chain termination involves reactions of the CHO radical, generated by reaction of CO_2H and CO. Since our earlier work was completed, ^{60}Co irradiation studies using CO as a scavenger have elucidated some aspects of the chemical behavior of the CHO radical.[3,4]

Experimental Section

Reagents. Ordinary distilled water was purified by distillation from dilute peroxydisulfate solution, the steam being transported by an O_2 carrier gas through a Vycor tube enclosed in a furnace maintained at 800–900°. The water from any given distillation was used within a few days since it has been found that longer standing sometimes leads to erratic kinetic behavior.

In most experiments, Baker Analyzed 30% H_2O_2, free from inhibitors, was used without further purification, since our earlier studies indicated that this procedure was satisfactory.[2] However, in further support of this assumption, it was shown that there was no change in kinetic behavior if the H_2O_2 was purified by vacuum distillation at 70° in an all-glass apparatus.

Matheson Co. CP grade CO and Airco U.S.P. O_2 were purified before use. In part, the purification procedure involved condensing the gas in a glass trap cooled with liquid N_2 and using a middle fraction of the boiling liquid as a source of purified gas. In addition, before condensation, the O_2 and perhaps other impurities in the CO were removed by passing the CO over CuO supported on asbestos and maintained at 360°.

Apparatus. The radiation source was a 4-W G.E. germicidal lamp, catalog No. G4T4/1, equipped with a 58 G 827 ballast. Almost all of the ultraviolet radiation emitted by the lamp[5] is of wavelength 2537 Å. In our experiments only the 2537-Å radiation is of importance, since shorter wavelengths are not transmitted by the 7910 Vycor reaction cells, and the longer wavelengths are not appreciably absorbed by the H_2O_2. Oscilloscope measurements showed that the lamp did not require an appreciable "warm-up" time. Periodic tests showed that there was no detectable change in intensity of the lamp during the course of the experiments.

When the lamp described above was operated in the conventional fashion using a 110-V ac power supply, oscilloscope measurements showed that the intensity of the lamp oscillated with a 60-cycle frequency. However, in a few experiments the lamp was operated using a 163 dc power supply and electronic circuitry which produced an almost constant intensity, except for a slight ripple with a frequency of 2.5×10^3 cps.

The cylindrical cells were made of 7910 Vycor glass. In a kinetic experiment, the pure O_2 and CO being evolved from the boiling liquids passed through separate flow meters to determine the relative volumes, then through an efficient mixing chamber, and finally into the reaction cells through a side arm near the base of each cell. In each cell the gas bubbled through the solution at a rate of approximately 17 cc/min.

The photolysis experiments were usually run in duplicate to provide a check on reproducibility. During photolysis, two identical cells were placed on either side and equidistant from the lamp at a distance of approximately 5 cm, a distance great enough so that cell positioning could be accurately reproduced in successive experiments.

Kinetic Procedure. On rare occasions the cells were cleaned with acidic permanganate solutions,[6] but generally they were merely rinsed several times with purified water after each kinetic experiment. When the permanganate cleaning procedure was used, it was followed by careful rinsing of the cells with purified water containing H_2O_2, purified water alone, and finally by 15 min steaming, with the partially condensed steam rinsing the walls of the inverted cells.

At the beginning of a given experiment the cells were each rinsed four times with aliquots of the solution to be photolyzed. Fifteen cubic centimeters of the solution to be photolyzed was then added to each cell, and the cell was capped with an ungreased ground joint attached to a capillary tube which provided an exit for the mixed gases and prevented the solution from coming in contact with air. Before introducing the mixed gases, the H_2O_2 solutions were preirradiated for 1 hr to remove any traces of oxidizable impurities which may have been present. The "initial" H_2O_2 concentration was then determined by iodometric analysis[7] of a 1.0-cc aliquot.

Before irradiation the solution was saturated by bubbling the mixed gases through the solution for 40 min, a period which preliminary experiments indicated was more than adequate. Calculations indicated that if the period of continuous irradiation was limited to a time of 30 sec, in a typical experiment the concentration of CO would have decreased only about 15%, even if no CO had dissolved from the gas which was bubbling

(3) Y. Raef and A. J. Swallow, *Trans. Faraday Soc.*, 59, 1631 (1963).
(4) T. Balkas, F. S. Dainton, J. K. Dishman, and D. Smithies, *ibid.*, 59, 81 (1963).
(5) J. P. Hunt and H. Taube, *J. Amer. Chem. Soc.*, 74, 5999 (1952).
(6) G. V. Buxton, S. P. Wilford, and R. J. Williams, *J. Chem. Soc.*, 4957 (1962).
(7) A. O. Allen, C. J. Hochanadel, J. A. Gormley, and T. W. Davis, *J. Phys. Chem.* 56, 575 (1952).

through the solution. To avoid possible changes of CO during irradiation because of the questionable efficiency in maintaining saturation by bubbling the gas through the solution, irradiation times were limited to periods of 30-sec duration, with 10 min bubbling to maintain saturation between irradiation times. Total irradiation times between H_2O_2 analyses were therefore of necessity rather short, usually of the order of 10–15 min. In the 10–15 minute period, the change in H_2O_2 concentrations fell in the range of 5–10%, a factor which limited the accuracy of the experiments to perhaps ±10%.

^{14}CO Tracer Studies in O_2-Free Solutions. Photolysis experiments were carried out in a closed system with the ^{14}CO being handled by high-vacuum techniques. The experiments were limited to the range of H_2O_2 concentration below 10^{-4} *M* where previous kinetic studies suggested that the chain reaction was terminated by bimolecular reaction of CO_2H (in our revised mechanism presented below by reaction of organic radicals derived from CHO). At the time it was felt that termination by CO_2H would yield either oxalate ion or CO_2 plus formate ion. In actual fact none of these products was produced in significant amounts.

In initial work, our method of analysis was designed to separate and identify only $C_2O_4^{2-}$ and HCO_2H. Our procedure for determination of $C_2O_4^{2-}$ involved measurement of the change in activity of the solution upon precipitation of BaC_2O_4 with excess barium ion from solutions containing added $C_2O_4^{2-}$ and HCO_2H carrier. After removal of $C_2O_4^{2-}$, the identification of labeled HCO_2H involved a comparison of the distribution coefficient between ether and water of the residual activity with that of the added HCO_2H carrier. Distribution experiments were carried out over a range of pH in an effort to show that the radioactive species had the same p*K* as the added formic acid.

Product analysis in the manner indicated was used in five experiments, all carried out in aqueous solution without added acid or base. Time of irradiation was 10 min, except in one experiment where irradiation time was reduced to 4.0 min without apparent change in the product distribution—an indication that photolysis of primary products was perhaps not of importance. Total activity in the solution after irradiation was found to be approximately that calculated from the kinetic parameters. In all of these experiments 64 ± 4% of the activity was found to follow the $C_2O_4^{2-}$ carrier when it was precipitated as BaC_2O_4. Unfortunately, as we shall see below, later work indicated that the labeled product was not $C_2O_4^{2-}$. Presumably the activity was present in an ion which forms a poorly soluble barium salt and follows the $C_2O_4^{2-}$ carrier in the precipitation. When the remaining 35–40% of the activity was distributed between acidic aqueous solution and ether, the observed distribution coefficient was 4.0, whereas the added HCO_2H had a distribution coefficient of 1.8, a value consistent with that in the literature. Distribution coefficients carried out over a range of pH suggested that only part of the product was a weak acid, with an ionization constant in the range of that of the stronger carboxylic acids. In the last two of the five experiments H_2CO tracer was added after precipitation of BaC_2O_4 and a dimedone derivative of the H_2CO was formed and removed from the solution. The dimedone derivative carried 17 ± 3% of the total initial activity. Since later experiments using the chromatographic technique did not confirm the presence of H_2CO, it can only be concluded that the solution contained a labeled substance (or substances) that follows the precipitation of the aldehyde derivative.

In the remaining time available for the work, an effort was made to develop a less ambiguous analytical procedure based upon the technique of paper chromatographic separation of the reaction products as their 2,4-dinitrophenylhydrazine derivatives. The initial step in this procedure required concentration of the 50.0 cc of irradiated solution to a volume of approximately 0.1 cc by vacuum distillation at 25°. Before concentration the excess H_2O_2 was catalytically decomposed by adding a minute trace of catalase to the solution. In the concentration procedure, HCO_2H and other volatile materials were found to constitute only 5–10% of the total activity.

The major effort was devoted to experiments in in neutral solution, since the salts formed in neutralization of 1.0 *M* $HClO_4$ complicated the concentration and analysis of these acidic solutions. In all, a total of four experiments were carried out in neutral solution. After concentration, a portion of the solution was analyzed using 80% phenol as a solvent in the chromatographic separation. The remainder of the solution was treated with 2,4-dinitrophenylhydrazine, the hydrazones were extracted with $CHCl_3$, and the chromatographic analysis performed using butanol–methanol–NH_3 as a solvent.

In preliminary tests, the R_f values of $H_2C_2O_4$, $HCO \cdot CO_2H$, $(OC)(CO_2H)_2$, $(CH_2OH)_2(CO_2H)_2$, and $CH_2OH \cdot CO_2H$ were measured in 80% phenol, a solvent which cleanly separated all of the above acids. When the concentrated irradiated solution was chromatographed in 80% phenol, it was found 70% of the activity did not move away from the initial spot, a behavior unlike that of any of the substances listed above. A second product, consisting of about 10% of the activity, was found to have an R_f value which was also different from any of the predicted products. The remaining 20% of the activity was divided about equally among three substances,[8] two of which remain unidentified and one which was tentatively identified, perhaps incorrectly, as $CH_2OH \cdot CO_2H$.

(8) It is possible that some or all of the minor products arise from secondary photolysis or thermal degradation of the major product.

When the labeled products in the concentrated irradiated solutions were converted to hydrazone derivatives before being chromatographed, approximately 65% of the activity was converted from a $CHCl_3$ insoluble to a $CHCl_3$ soluble material, presumably because of hydrazone formation. Studies using known hydrazine derivatives indicate that separation of products could be achieved using a butanol–methanol–NH_3 solvent, but again the chromatographs did not lead to a positive identification of a reaction product. There was some indication that activity was being lost through volatilization during the separation, perhaps by decarbonylation of an unstable compound. It may be noted that carboxylic acids would be present as nonvolatile ammonium salts in the ammoniacal medium.

In two experiments the irradiation was carried out in 1.0 M $HClO_4$, but only qualitative conclusions may be drawn from the results, since the neutralization of the acid and removal of the salts may have introduced further uncertainties in the analytical procedures. However, it did appear that the total activity in the solution was substantially less than that formed in pure water. Further, the distribution of products appeared to be different, either because the initial products were different or because degradation of products occurred before it was possible to reduce the acidity of the medium.

Results

The experiments in which the photolysis of aqueous H_2O_2 was studied in the presence of both CO and O_2 are summarized in Table I. All experiments were carried out at 21 ± 1°, the temperature of the laboratory. Except for the last two experiments of Table I, the incident light intensity was 5.3×10^{-9} einstein cm^{-2} sec^{-1}. In the last two experiments, in which the lamp was operated with a dc power source, the incident light intensity was 7.4×10^{-9} einstein cm^{-2} sec^{-1}.

Table I: Photolysis of Aqueous H_2O_2 in Solutions Containing CO and O_2

$10^2(CO)/(H_2O_2)$	$10^3(H_2O_2)$, M	$\frac{(O_2)}{(H_2O_2)}$	2×10^6 φI_a	$\frac{2\varphi I_a}{-d(H_2O_2)/dt}$
0.76	6.5	0.18	1.15	1.7
2.0	2.7	0.42	0.53	2.2
2.3	3.6	0.17	0.71	2.8
2.6	6.2	0.16	1.11	2.8
3.0	3.7	0.30	0.73	3.7
3.2	4.6	0.22	0.87	4.1
4.1	3.9	0.26	0.76	3.8
4.5	4.2	0.24	0.81	3.8
5.6	6.7	0.11	1.17	4.2
5.6	3.3	0.30	0.65	4.2
5.7	3.8	0.26	0.75	4.7
5.7	6.6	0.12	1.16	4.8
7.0	5.4	0.14	0.99	5.9

In all experiments values of $-d(H_2O_2)/dt$ were obtained from a graphical evaluation of the slope of a plot of H_2O_2 concentration *vs.* time of irradiation. When the photolysis is carried out in the absence of CO, $-d(H_2O_2)/dt$ equals $2\varphi I_a$, where φ represents the primary of the absorbed light, measured in the units of einsteins absorbed $liter^{-1}$ sec^{-1}. At room temperature, φ has the numerical value of 0.5.

As we have indicated in the Introduction, the results obtained in the present experiments using mixtures of CO and O_2 lead to somewhat different conclusions than drawn from the earlier experiments by Buxton[2] in which an attempt was made to study the scavenger action of CO in the absence of oxygen. Consequently, some of the earlier experiments were repeated in an effort to discover the source of the discrepancy. In the present work the H_2O_2 concentration covers the range above 2.65×10^{-3} M. In this region, it was concluded earlier that the photolytically induced chain reaction had as a termination step the bimolecular reaction of two HO_2 radicals to produce H_2O_2 and O_2. Since O_2 is an efficient inhibitor for the chain reaction, there was the possibility that O_2 accumulated during a period of irradiation to the point where it was producing inhibition. Earlier, it had been concluded that such inhibition was not occurring to an appreciable extent, the evidence being that the rate of photolysis decreased by only 10%, an amount approaching the limit of error, when the irradiation time was increased from a 1-min to a 10-min irradiation period. These experiments were repeated with the same results being obtained in the present work. In addition, an experiment was carried out using a 5-sec period of continuous irradiation, with a 6-min period of bubbling of the pure CO between successive periods of irradiation. This procedure increased the reaction rate 15%, an amount believed to be approximately the error in reproducibility. However, the 15% increase in rate was not nearly large enough to resolve the discrepancy under discussion. In view of the sensitivity of the chain reaction to O_2, it is possible that even these precautions were not adequate, but a further reduction in irradiation time was impractical using the present apparatus.[9]

In view of the inconclusive nature of these results, a few experiments were repeated using the dc power supply, since there was the faint possibility that the 60-cps ripple was producing anomalous results.[10] Again, the present results were found to be in good agreement with those obtained earlier over the entire range in H_2O_2 concentration of $(2–34) \times 10^{-4}$ M.

(9) There is some doubt that the 6-min period interval between irradiation periods was adequate, but a longer interval was not feasible using the available apparatus.

(10) In the present experiments, where efficient radical scavengers are present at relatively large concentrations, it is not to be expected that the results would depend on the power supply, because the average lifetime of the radicals is very short compared to the oscillation of the light.

Discussion

The results obtained for the photolysis of H_2O_2 in the presence of CO and O_2 will be discussed initially in terms of the mechanism

$$H_2O_2 \xrightarrow{h\nu} 2OH \quad (A)$$

$$OH + CO \xrightarrow{k_1} CO_2H \quad (1)$$

$$CO_2H + O_2 \longrightarrow CO_2 + HO_2 \quad (2)$$

$$OH + H_2O_2 \xrightarrow{k_3} H_2O + HO_2 \quad (3)$$

$$2HO_2 \longrightarrow O_2 + H_2O_2 \quad (4)$$

In the absence of CO and other scavengers the photolysis of H_2O_2 is a nonchain reaction at the light intensity and H_2O_2 concentrations covered in this work.[5,10a] Under these conditions it is generally agreed that the photolysis[2] occurs by reactions A, 3, and 4. When CO and O_2 are added to the solution, the CO and H_2O_2 compete for the OH radicals in reactions 1 and 3. At large values of $(CO)/(H_2O_2)$, where reaction 3 may be neglected, the sequence of reactions A, 1, 2, and 4 should cause $-d(H_2O_2)/dt$ to approach zero. An experimental verification of this prediction was presented in our earlier paper.[2] This observation provides strong evidence of the limiting form of the mechanism under consideration.

To obtain an experimental value of k_1/k_3, the objective of the present work, it was necessary to work at values of $(CO)/(H_2O_2)$ where an appreciable fraction of the OH radicals disappeared both by reaction 1 and 3. Under these conditions the above mechanism and the steady-state approximation leads to the prediction that $-d(H_2O_2)/dt$ should be given by eq 5.

$$-\frac{d(H_2O_2)}{dt} = \frac{2\varphi I_a}{1 + [k_1(CO)/k_3(H_2O_2)]} \quad (5)$$

The best least-squares value of $k_1/k_3 = 72 \pm 3.6$ was obtained in a computer calculation using the experimental values of $-d(H_2O_2)/dt$ and $2\varphi I_a$, and the concentrations of CO and H_2O_2 listed in Table I. In this computation each data point was weighted by a factor directly proportional to the per cent change in H_2O_2 in the individual experiments, since this was thought to be the principal factor limiting the accuracy of the measurements. The mean deviation of 11% indicates that the experiments were of a rather low accuracy. As we have indicated above, this arose primarily from the low quantum yield for H_2O_2 photolysis carried out under the present experimental conditions and the correspondingly small changes in H_2O_2 concentration observable in a given experiment.

Equation 5 may be rearranged to give eq 6, a form more conducive for graphical presentation of the results.

$$\frac{2\varphi I_a}{-d(H_2O_2)/dt} = \frac{k_1(CO)}{k_3(H_2O_2)} + 1 \quad (6)$$

A plot of the left side of eq 6 *vs.* $(CO)/(H_2O_2)$ is presented in Figure 1, with the straight line drawn with the predicted intercept of unity and the value of $k_1/k_3 = 72 \pm 3.6$ listed above.

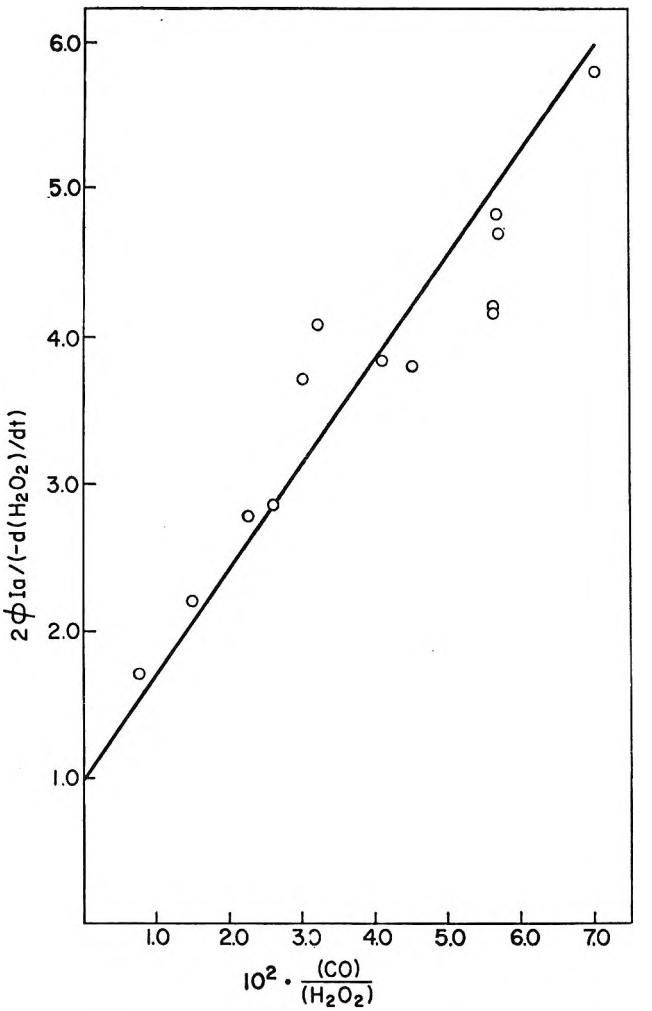


Figure 1. A graphical evaluation of the validity of eq 6.

Before discussing the discrepancy between this value of k_1/k_3 and our earlier result of 13.0, it is necessary to reconsider the mechanism originally proposed[2] for the O_2-free solutions. The necessity for reconsideration arises from the results of the ^{14}CO tracer studies presented above. In reevaluation of the mechanism, it will be useful to discuss the kinetic data obtained in two ranges of H_2O_2 concentration where limiting forms of the rate law were observed. Let us first turn our attention to studies at H_2O_2 concentrations less than 10^{-4} M,

(10a) F. S. Dainton and J. Rowbottom, *Trans. Faraday Soc.*, 49, 1160 (1953).

since this is the concentration range employed in the ^{14}CO work. In doing so, it may be useful to note that the evaluation of k_1/k_3 did not involve kinetic data at these H_2O_2 concentrations.

At H_2O_2 concentrations less than 10^{-4} M, the rate law was found to be three-halves order in H_2O_2, a result compatible with a mechanism based on reactions A, 1, 7, and 8.

$$CO_2H + H_2O_2 \longrightarrow CO_2 + H_2O + OH \quad (7)$$

$$2CO_2H \longrightarrow \text{products} \quad (8)$$

At the time, it was felt that the products formed in chain termination by reaction 8 would be either $C_2O_4^{2-}$ or HCO_2H and CO_2, but the tracer results reveal that these are not produced in significant quantities. In view of this it is necessary to consider the possibility the CO_2H reacts with CO to produce CHO, despite some rather complex evidence[3] from ^{60}Co irradiation studies that this reaction does not occur. If CHO is formed in reaction 9, it might be expected to react with H_2O_2 in reaction 10, the two reactions replacing reaction 7 as a chain carrying step.

$$CO_2H + CO \longrightarrow CO_2 + CHO \quad (9)$$

$$CHO + H_2O_2 \longrightarrow CO + H_2O + OH \quad (10)$$

The revised mechanism would then be A, 1, 9, 10, and 11, the latter being responsible for chain termination.

$$2CHO \longrightarrow \text{products} \quad (11)$$

As we shall see in the following discussion, eq 11 and perhaps 9 and 10 as well are probably oversimplified, since the tracer evidence suggests CHO is bonded to either CO_2 or one or more CO molecules.

If eq 11 correctly represented chain termination it would seem that products would be $(CHO)_2$ or CO_2 plus formaldehyde, species which are definitely not formed in significant amounts.

To account for the rather large yield of products which precipitate with $BaSO_4$, it might be assumed that reaction 9 produced $CO \cdot CO_2H$ which on bimolecular termination would yield the dihydrate of $(COCO_2H)_2$, the species[11] $(CHOH)_2(CO_2H)_2$. Again the tracer studies show that $(CHOH)_2(CO_2H)_2$ is not an important reaction product. In addition, it is claimed[3] that the ^{60}Co irradiation products imply that reaction 9 does not yield $CO \cdot CO_2H$ (or CHO).

Finally there is the possibility that the species COH adds one or two CO molecules to form $(CO)_2COH$. This third mechanism would predict that termination would lead to the formation of ions having the general formula $(CO)_n^{2-}$, with $n = 4$, 5, or 6. The assumption that such ions might be formed is based largely on the observation that $C_6O_6^{2-}$ is a major product in the reduction of CO by Na in liquid ammonia.[12] Formation of the cyclic $(CO)_n^{2-}$ ions would probably be a thermodynamically favorable process, since the ions constitute a recently recognized family of resonance stabilized aromatic substances.[13] Positive identification of the ions would be of considerable interest, since it is known that CO does not normally undergo free radical polymerization in the absence of a comonomer. Unfortunately, time limitations prevented us from attempting to identify these species as reaction products.

Let us now consider our former kinetic studies in the range of H_2O_2 above 2×10^{-3} M H_2O_2, the region labeled 13 in Figure 1 of our earlier paper. Under these limiting conditions the rate was found to be approximately zero order in H_2O_2, a rate law which suggested a chain mechanism based on reactions A, 1, 7, and 4. It was data obtained in this region which were used in our evaluation of k_1/k_3. It is possible that our original mechanism should be retained here since at these higher H_2O_2 concentrations reaction 7 would compete more favorably with reaction 9 or any of the alternatives to reaction 9 discussed above. To simplify the following discussion we will refer to eq 9 and 10 despite the likelihood that this is an oversimplification. The point of importance is that reaction 7 might be replaced by reactions 9 and 10 without invalidating our earlier evaluation of k_1/k_3. This situation arises because when reaction 4 is responsible for chain termination the rate constant for reaction 7 or alternately for reactions 9 and 10 does not appear in the rate law.

Apart from our work, there has been no other direct measurement of the ratio k_1/k_3. However, the ratios of the rate constants for reactions of many pairs of scavengers with the OH radical have been obtained from ^{60}Co irradiation studies. Other rate-constant ratios have been derived from studies of the Fenton reagent, but these values depend upon the questioned assumption[14] that the Fenton reaction produces OH radicals instead of Fe(IV) ions. Neither source of data provides a direct determination of k_1/k_3, but an approximate value of 23 ± 9 may be obtained by combining the three rate-constant ratios. The indicated uncertainty

$$k_{OH+CO}/k_{OH+Fe^{2+}} = 2.6^{15} \text{ or } 3.79^{16}$$

$$k_{OH+Fe^{2+}}/k_{OH+H_2} = 5.7^{15}, 4.5\text{–}7.1^{17}$$

$$k_{OH+H_2}/k_{OH+H_2O_2} = 1.20^{18}$$

(11) $(COCO_2H)_2$ is known only in the form of its dihydrate. Like many other dibasic acids the barium salt is poorly soluble.

(12) A. F. Scott, *Science*, **115**, 118 (1952). Various considerations suggest that the CO_2H radical must be a reducing agent comparable in strength to sodium in ammonia.

(13) For a recent review, see papers by R. West and coworkers, *J. Amer. Chem. Soc.* **85**, 2577 (1963).

(14) A. E. Cahill and H. Taube, *ibid.*, **74**, 2312 (1952).

(15) F. S. Dainton and T. J. Hardwick, *Trans. Faraday Soc.*, **53**, 333 (1957).

(16) T. J. Hardwick, *Can. J. Chem.*, **35**, 437 (1957).

(17) W. G. Rothschild and A. O. Allen, *Radiation Res.*, **8**, 101 (1958), obtained the pH dependent value 4.7–7.1 in the pH range 1.59–2.18.

(18) C. J. Hochanadel, *ibid.*, **17**, 286 (1962).

in the figure 23 ± 9 is calculated merely from the spread of reported values for the given scavenger ratios.[19]

Since our earlier publication, the application of the pulsed-radiolysis technique has yielded absolute values for the rate constants of reaction of OH and various substrates which are considered more accurate than the relative values based on the combination of several series of scavenger experiments, such as those discussed above.[20] If we assume a rate constant ratio $k_{OH+CO}/k_{OH+Fe^{2+}} = 3.2$, the average of the two values cited above, the generally accepted value[21] of $k_{OH+Fe^{2+}} = 2.5 \times 10^8\ M^{-1}\ sec^{-1}$ and the two reported[22,23] pulsed-radiolysis values of $k_{OH+H_2O_2} = 1.2 \times 10^7\ M^{-1}\ sec^{-1}$ and $2.3 \times 10^7\ M^{-1}\ sec^{-1}$, we calculate the values $k_{OH+CO}/k_{OH+H_2O_2}$ of 67 and 35, respectively. Thus, the case of the recent pulsed-radiolysis rate constants yields results in reasonable agreement with our data for the relative reactivity of CO and H_2O_2 with OH.

(19) The value 23 ± 9 differs from the figure 11.7 ± 7.6 presented in the earlier paper, the discrepancy arising from an arithmetic error made in the original calculation.

(20) For a summary of available data, see M. Anbar and P. Neta, *Int. J. Appl. Radiat. Isotopes*, 18, 493 (1967).

(21) H. A. Schwarz, *J. Phys. Chem.*, 66, 255 (1962).

(22) H. Fricke and T. J. K. Thomas, *Radiation Res. Suppl.*, 4, 35 (1964).

(23) J. K. Thomas, *Trans. Faraday Soc.*, 61, 702 (1965).

A Mass Spectrometric Investigation of the Low-Pressure Pyrolysis of Borane Carbonyl. The Bond Dissociation Energy of Diborane

by T. P. Fehlner and G. W. Mappes

Department of Chemistry, University of Notre Dame, Notre Dame, Indiana 46556 *(Received August 5, 1968)*

The thermal decomposition of borane carbonyl, BH_3CO, has been examined in a low-pressure glass flow reactor over the temperature range of 400–560°K. The loss of BH_3CO and the formation of CO, B_2H_6, BH_3, and H_2 were measured. The rate of the reaction, $BH_3CO \rightarrow BH_3 + CO$, was observed near the low-pressure limit. The probability of reaction per collision has been examined over a range of average number of gas and wall collisions. The wall collisions are about 10 times more effective than gas-phase collisions. The homogeneous reaction exhibits a statistical-weight inverse secondary kinetic isotope effect of 0.38 ± 0.05 at 450°K while the wall reaction exhibits a normal isotope effect of 1.2 ± 0.3. The rate constant and the kinetic isotope effect at the low-pressure limit have been calculated as a function of the critical energy using the vibrational frequencies of BH_3CO and BD_3CO. The critical energy that fits the data is used to fix $D(H_3B–BH_3)$ at 36 ± 3 kcal. Evidence for an interesting role of the surface in the heterogeneous reaction is presented.

In 1937 Burg and Schlesinger[1] showed that heating diborane in an excess of carbon monoxide produced a simple adduct of BH_3, borane carbonyl (BH_3CO). This compound has been and still is of considerable interest. Our interest stems from several sources: the decomposition *via* B–C bond cleavage occurs readily, yet the compound is easily prepared and stored; this molecule is a convenient source of BH_3; and the energetics of the reactions of BH_3CO can serve to distinguish between the variety of values presented for the symmetrical dissociation energy of diborane, $D(H_3B–BH_3)$.

The overall thermal decomposition of this compound has been studied and discussed by several groups.[2] Previously, one author (TF)[3] reported on a mass spectrometric study of the low-pressure pyrolysis of BH_3CO in a tubular flow reactor. It was found that at low conversions $BH_3CO \rightarrow BH_3 + CO$ is the major reaction. On the basis of negative evidence it was assumed that the homogeneous reaction was being observed (*i.e.*, the wall was acting as a simple collider) and the $D(H_3B–CO)$ bond energy was estimated from the observed rate constant. After considerably more work on this type of system, it became apparent that this early study had several major weaknesses. Studies of other hydrides definitely showed an active role for the surface[4] and considerably undermined the assumption of homogeneity. The reactor used did not have a well defined temperature or reaction time[5] and the fact was not considered that if the reaction was homogeneous it

(1) A. B. Burg and H. I. Schlesinger, *J. Amer. Chem. Soc.*, 59, 780 (1937).

(2) (a) A. B. Burg, *ibid.*, 74, 3482 (1952); (b) S. H. Bauer, *ibid.*, 78, 5775 (1956); (c) Y. C. Fu and G. R. Hill, *ibid.*, 84, 353, (1962); (d) M. E. Garabedian and S. W. Benson, *ibid.*, 86, 176 (1964).

(3) T. P. Fehlner and W. S. Koski, *ibid.*, 87, 409 (1965).

(4) T. P. Fehlner, *ibid.*, 89, 6477 (1967); 90, 4817 (1968).

(5) A. Pentenero and P. LeGoff in "Mass Spectrometry," R. I. Reed, Ed., Academic Press, New York, N. Y., 1965, pp 305–346.

was probably in the fall-off region.[6] On the instrumental side, a conventional mass spectrometric system was used and thus the formation of the product CO could not be measured quantitatively. We now present a reexamination of this reaction in which these points are unambiguously resolved. In addition, kinetic isotope effects are measured and some interesting information concerning the actual role of the wall is presented.

Experimental Section

The characteristics of the reactor used in these studies have been previously described in detail[4] and only pertinent differences are described here. As lower reactor temperatures were used here, there were fewer temperature gradients and more of the reactor surface was active. At a reactor temperature of 450°K the difference between thermocouples 2 and 3 was negligible,[7] while thermocouple 4 read 440°K. The reactant gas entered through a 0.4-mm diameter water-cooled capillary leak and in one reactor, hereafter called F1, exited through a 0.35-mm diameter thin-walled orifice and in the other reactor, hereafter called F2, through a 0.12-mm diameter thin-walled orifice. Except for the different exit orifices the two reactors were identical. In both cases, the reactor walls were coated with boron. The pressure drop across the capillary, calculated from measured conductances, was a factor of 9.5 in F1 and 1.9 in F2. The average number of wall collisions, ν_w, was 2.5×10^4 in F1 and 1.6×10^5 in F2.[8] At room temperature a nitrogen molecule spends an average time of 0.50 sec in F1 and 3.0 sec in F2. Back diffusion through the capillary is negligible in both reactors.

As before, a modulated molecular beam sampling technique was used, and the details have been presented earlier.[4] This technique allows a high degree of discrimination between sample beam molecules and other interfering molecules such as background molecules, scattered beam molecules, and products of pyrolysis in the source.[9] For molecular flow through the reactor exit orifice, as was the case in this work, it gives assurance of unambiguous quantitative sampling. It was particularly helpful in this study where one of the products, CO, has the same mass as a large background peak, m/e 28, and is also a product of source decomposition.

The observed ion spectrum allows the neutral product composition in the ion source of the mass spectrometer to be determined. From this composition, the composition in the chemical reactor must be deduced. In these experiments the beam composition is representative of the reactor composition, and as the beam molecules are labeled with a particular frequency and phase, there is a well-established relationship between the observed ion signals and the composition in the reactor. To identify the products of the thermal decomposition, borane carbonyl was introduced into the reactor at a given flow rate and the mass spectrum was obtained. The temperature of the reactor was first increased and then decreased in a stepwise fashion, and the mass spectrum was obtained at each temperature after allowing sufficient time for temperature equilibration. Changes in the ion intensities at the following masses were observed: 42, 41, 40, 39, 28, 27, 26, 25, 14, 13, 2.

In several experiments the flow of the BH_3CO into the reactor was varied at constant reactor temperature. These experiments were used to determine the effect of the number of collisions on the probability of reaction per collision. The isotope effect was measured similarly except that the variation in the flow of BH_3CO and BD_3CO was made in the same experiment so that the reactor temperature variations were minimized.

During one experiment variable partial pressures of CO were added independently to the inlet of the reactor. The addition of CO with the reactor at room temperature decreased the partial pressure of BH_3CO in the reactor and thus decreased the m/e 41 ion signal. This decrease in ion signal was measured as a function of the partial pressure of CO added. The room temperature experiment could then be used to correct the decomposition experiment for the decrease in the partial pressure of BH_3CO in the reactor due to flow changes. Because of this correction the efficiency of CO is not accurately known.

Borane carbonyl was prepared by the reaction of diborane with a large excess of carbon monoxide in a stainless steel cylinder at 90° and several atmospheres pressure.[1] The crude borane carbonyl was then purified by trap-to-trap distillation in a grease-free vacuum system and stored at 77°K until used. During each experiment the purified product was kept at a constant low temperature (143°K), and the vapor in equilibrium with liquid borane carbonyl was admitted to the reactor through a variable leak. The leak was used to adjust the pressure in the reactor while the vapor–liquid equilibrium served to keep the reactor pressure constant. The presence or absence of the m/e 27 or m/e 26 ion peak as well as the magnitude of the m/e 28 ion peak was used as a measure of the purity of the borane carbonyl. The initial purity was better than 95% and the purity after a 6-hr run was better than 95%. Sensitivity calibrations for diborane, carbon monoxide, and borane carbonyl were made by measuring the m/e 26, m/e 28, and m/e 40 ion intensities, respectively, at a given pressure. The pressures were measured with a thermocouple gauge which was

(6) This point was called to our attention by G. N. Spokes and S. W. Benson, whom we thank, in a private communication.

(7) See Figure 1 of ref 4.

(8) $\nu_w = S/A$ where S is the surface area of the reactor and A is the area of the exit orifice.

(9) S. N. Foner in "Advances in Atomic and Molecular Physics," D. R. Bates, Ed., Academic Press, Inc., New York, N. Y., 1966, p 385.

continually calibrated against a McLeod gauge for each of the gases. The pressures are known absolutely to ±10%. BD_3CO was prepared in the same manner as borane carbonyl, except that B_2D_6 was used in the preparation. The isotopic purity of the BD_3CO was about 85% as determined from the mass spectrum. Since the *m/e* 41 ion peak was used to follow the loss of BD_3CO the effective isotopic purity was about 90%.

Results and Discussion

Identification of Products. The variations of selected ion intensities with reactor temperature and average number of collisions (time) are shown in Figures 1, 2, and 3. Figure 1 illustrates the loss of borane carbonyl and the formation of carbon monoxide for the two different reaction times. The *m/e* 28 ion intensity has been corrected for the contribution due to fragmentation of BH_3CO. The initial decrease in the *m/e* 40 ion peak is not due to decomposition but rather to the dependence of the ion intensity on the beam velocity. The origin of the CO^+ ion signal was confirmed by observing the relative phase of the *m/e* 28 signal as a function of reactor temperature.[4] This varied from a value characteristic of BH_3CO to one characteristic of CO as the reactor temperature was increased. Figure 2 illustrates the changes in *m/e* 26 and *m/e* 13 for the reactor F1 (short time). Assignment of the change in the *m/e* 26 ion peak to the formation of diborane is straightforward as one sees the appearance of the characteristic fragmentation pattern of diborane. The *m/e* 13 curve has been corrected for the contributions due to fragmentation of borane carbonyl and diborane and consequently, as the residual intensity is very low, the precision is poor. As noted further below, this change is attributed to borane. Figure 3 shows the changes in *m/e* 2 and *m/e* 14 for the reactor F2. The change in *m/e* 14 has been corrected for the contribution due to the fragmentation of borane carbonyl and diborane and again is attributed to borane. Support for this assignment is obtained by the observation of a shift to lower energies of the appearance potentials of both the *m/e* 14 and 13 ion peaks at elevated reactor temperatures. The change in *m/e* 2 is assigned to the formation of hydrogen. The poor precision here is due to the presence of a large background ion signal and the low molecular weight of this product. In short, carbon monoxide, diborane, hydrogen, and borane were observed as products. Higher hydrides of boron are not present at levels greater than 2%. Even though the conditions of the previous study[3] were considerably different, the same products should have been observed. As B_2H_6 and H_2 were not observed, the previous results are suspect in this regard also.

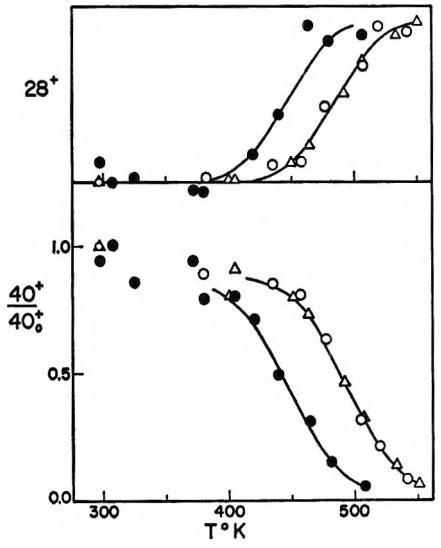


Figure 1. Variation in the *m/e* 40 ion intensity and the *m/e* 28 ion intensity with reactor temperature. The open circles and triangles refer to data taken in reactor F1 at a pressure of 12 mTorr. The closed circles refer to data in reactor F2 at 104 mTorr. The intensity scale for *m/e* 28 is arbitrary and is different for the F1 and F2 data.

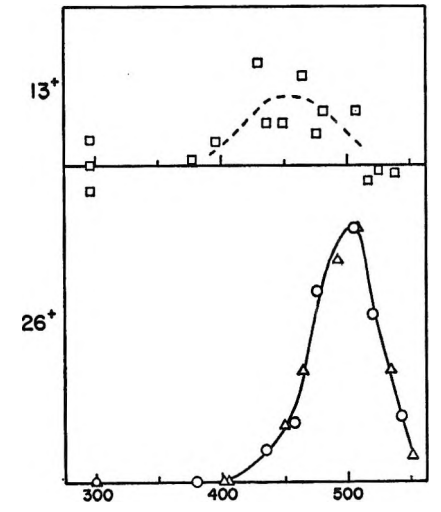


Figure 2. Variation in the *m/e* 13 and 26 ion intensities with the temperature of reactor F1. The data on *m/e* 13 were taken at 10 mTorr and the data on *m/e* 26 at 23 mTorr.

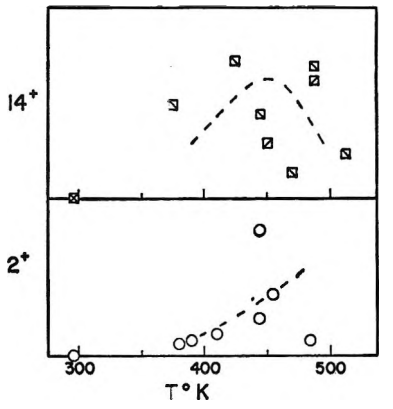


Figure 3. Variation in the *m/e* 15 and 2 ion intensities with the temperature of reactor F2. The data on *m/e* 14 were taken at 125 mTorr and the data on *m/e* 2 at 140 mTorr.

Stoichiometry. Calibrations were made directly for carbon monoxide, diborane, and hydrogen. A sensitivity for borane, m/e 13 and 14, was estimated by assuming that the total cross section for ionization of BH_3CO is the same as that for BH_3 and using the fragmentation pattern of borane.[10] It was found that 0.98 ± 0.17 mol of CO was formed per mole of borane carbonyl decomposed. The data on diborane are illustrated in Figure 4 where the ratio of diborane to

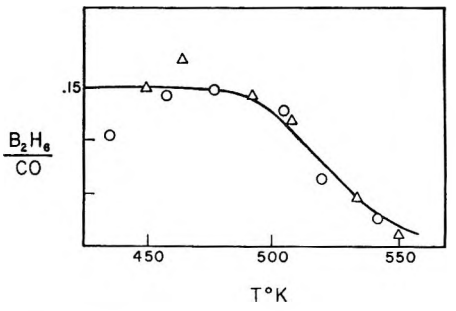


Figure 4. The data points are the ratio of the yield B_2H_6 to CO for reactor F1 at a pressure of 12 mTorr. The solid curve is a normalized empirical decomposition curve for B_2H_6 in reactor F1 at 5 mTorr.

carbon monoxide is given as a function of temperature for reactor F1. This ratio decreases above 480°K indicating the loss of B_2H_6. That this loss is identical with the simple pyrolysis of B_2H_6 is shown by the agreement of the data points with the solid line which is a normalized plot of the fractional decomposition of pure diborane in the same reactor. The B_2H_6/CO ratio is always less than the maximum value of 0.5 and at temperatures less than the decomposition point of diborane this ratio *does not increase* with increasing reactor time, *i.e.*, with increasing the number of collisions. For example, at 450°K, $B_2H_6/CO = 0.15$ for F1 but 0.12 for F2. The data on borane are rather crude but are important for mechanistic reasons (see below). At 450°K the ratio of borane formed to borane carbonyl lost is 0.05 ± 0.02 for F1 and 0.008 ± 0.006 for F2. The determination of hydrogen gas permits the mass balance for hydrogen to be complete, but the data are too scattered to be meaningful.[11] For example, for F2 the mass balance with respect to hydrogen is 51 ± 60% with 80% of the probable error being due to the hydrogen determination. The boron mass balance was not determined as solid boron deposits out in the reactor. The results are summarized in the following diagram.

$$BH_3CO \xrightarrow{0\text{-}5\%} BH_3 + CO$$

$$BH_3CO \xrightarrow{70\text{-}100\%} B + \tfrac{3}{2}H_2 + CO$$

$$BH_3CO \xrightarrow{0\text{-}30\%} \tfrac{1}{2}B_2H_6 + CO$$

The Mechanism. It has been shown in detail previously that this reactor can be treated as a type of flow reactor.[3,4,10,12,13] The data are fitted with an order, n, and a function of temperature, $h(T)$.[14] For a first-order reaction, $h(T)$ is equal to the probability of reaction per collision, b (which is the same as the first-order rate constant divided by the collision frequency) and one can use these kinetic parameters to establish a mechanism in the usual manner.

The extent of reaction was followed by measuring the loss of reactant and the formation of CO, B_2H_6, BH_3, and H_2, the last two rather crudely. The loss of borane carbonyl gave an order n of slightly greater than one (1.1) and $\log b = 5.3 - 4890/T$.[15] The formation of CO paralleled the loss of BH_3CO over the range of these experiments. This suggests that the initial reaction, $BH_3CO \rightarrow BH_3 + CO$, is being observed. However, the next most abundant product is diborane, a fact which at first sight is unsettling. Now either diborane is formed directly from borane carbonyl or it is formed in a subsequent step from borane. If diborane is formed directly from borane carbonyl and if this is the exclusive decomposition path, then at temperatures below the observed decomposition point of diborane the ratio of diborane formed to borane carbonyl lost should be 0.5. Values more than a factor of 2 less than this are observed. If borane carbonyl is lost by two paths, only one of which produces diborane, then the ratio could be less than 0.5, but the probability of formation of B_2H_6 from BH_3CO per collision[16] at a temperature below the decomposition point of diborane would be independent of the number of collisions. This probability is in fact a factor of 8 different for the two reactors. The final alternative is that diborane is formed from borane. If so, then the probability of formation of B_2H_6 from BH_3 per collision[17] should be independent of the number of collisions. At 450°K values of $b = 2.1 \times 10^{-4}$ and 1.8×10^{-4} are obtained from F1 and F2, respectively. It seems quite clear that diborane results from the recombination of borane, probably by a Rideal mechanism. It is interesting to compare this value for the recombination of BH_3 with a measured value for the recombination of

(10) A. B. Baylis, G. A. Pressley, Jr., and F. E. Stafford, *J. Amer. Chem. Soc.*, **88**, 2428 (1966).

(11) In this case, the presence of a large background peak, the low molecular weight of H_2, and the presence of a fragment ion peak from BH_3CO combine to increase the noise level.

(12) P. LeGoff, *J. Chim. Phys.*, **53**, 359 (1956); **53**, 369 (1956); **53**, 380 (1956).

(13) S. W. Benson and G. N. Spokes, *J. Amer. Chem. Soc.*, **89**, 2525 (1967).

(14) The order is obtained from the slope of a plot of $\log BP_0$ *vs.* $\log (1 - B)P_0$ at constant temperature, where B is the fraction of BH_3CO which has reacted, *i.e.*, the fractional reactor yield, and P_0 is the initial reactant pressure. $h(T)$ is obtained by examining $B/(1 - B)^n$ as a function of temperature at constant P_0.

(15) Figures 5 and 7 implicitly show these results, and consequently the data are not plotted in different form here.

(16) $B(B_2H_6)/[1 - B(BH_3CO)]\nu_w$ where $B(B_2H_6)$ is the yield of diborane.

(17) $B(B_2H_6)/[B(BH_3)\nu_w]$.

methyl radicals on a surface.[18] A value of $b = 2 \times 10^{-4}$ between 290 and 770°K was obtained and is attributed to a Rideal mechanism. The similarity of these rates suggests a similarity of reactivity.

With the origin of B_2H_6 established, a net b for the reaction of borane can be calculated from the observed yield of borane and the yield of CO, *i.e.*, the amount of borane expected if none decomposed. In this case values of $b = 6.8 \times 10^{-4}$ and 7.3×10^{-4} are obtained at 450°K for the low and high collision number reactors, respectively. The difference in the net reaction probability of borane and the reaction probability of borane to form diborane must be due to a parallel decomposition path. This parallel path undoubtedly results in the production of boron and hydrogen, but, unfortunately, the data on hydrogen production are not good enough to confirm this.

The reaction mechanism below the decomposition temperature of B_2H_6 is

$$BH_3CO \xrightarrow{a} BH_3 + CO$$

$$BH_3 + BH_3(w) \xrightarrow{b} B_2H_6$$

$$BH_3 \xrightarrow{c} B(s) + \tfrac{3}{2}H_2$$

where reaction a is grossly first order in borane carbonyl. As we are working in a pressure region where the number of gas collisions is nearly equal in magnitude to the number of wall collisions, the expressions we have been using above should really be refined to take this into account. By doing so it will be seen that valuable information on the nature of reaction a is obtained.

One may take the gas-phase collisions into account by writing the fractional yield of the reactor

$$B = \frac{\nu_w b_w + \nu'_g b'_g}{1 + \nu_w b_w + \nu'_g b'_g} \quad (1)$$

where ν_w is the number of wall collisions, ν'_g is the total number of gas-phase collisions, b_w is the probability of reaction per wall collision, and b'_g is some weighted average probability of reaction per gas collision. Considering only the major species, this may be rewritten as

$$B/(1 - B) = \nu_w b_w + b_g(BH_3CO)\nu_g(BH_3CO) + b_g(CO)\nu_g(CO) \quad (2)$$

where $b_g(X)$ is the probability of reaction per collision with species X and $\nu_g(X)$ is the average number of X collisions. Finally, this may be reduced to

$$B/(1 - B) = \nu_w b_w + b_g \nu_g^0[1 - B(cK - 1)] \quad (3)$$

where K is the relative efficiency of CO as a collider compared to BH_3CO, ν_g^0 is the initial number of BH_3CO collisions, and c is the square root of the ratio of the molecular weights of CO and BH_3CO. K is empirically measured as is pointed out below. For low yields (and/or small K) a good approximation to the last equation is

$$B/(1 - B) \approx \nu_w b_w + b_g(BH_3CO)\nu_g(BH_3CO) \quad (4)$$

This is equivalent to neglecting the CO collisions in eq 2. Consequently, a plot of $B/(1 - B)$ *vs.* $\nu_g(BH_3CO)$ should yield an approximately straight line with a slope of b_g and an intercept of $\nu_w b_w$. Figures 5 and 7 show

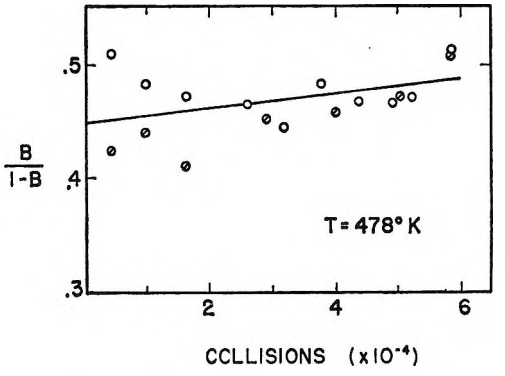


Figure 5. $B/(1 - B)$ as a function of the number of borane carbonyl collisions in reactor F1. The open circles refer to loss of reactant and the others to formation of CO.

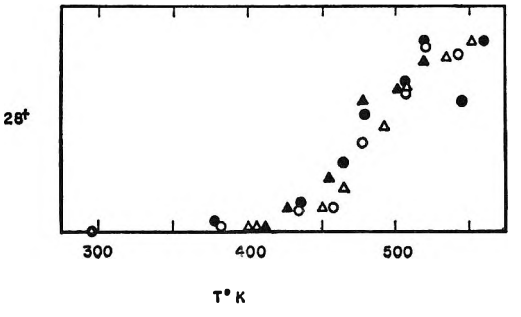


Figure 6. Variation in the m/e 28 ion intensity for BH_3CO (open circles and triangles) and for BD_3CO (closed circles and triangles) as a function of temperature for reactor F1 at pressure of 13 mTorr. These experiments were carried out on different days.

examples of this plot for data from F1 and F2, respectively.[19,20] The data points are from both the loss of reactant and the formation of CO and the straight line is the least-squares fit of the data. A most important piece of information to be derived from these curves is that b_g is better than 10 times less than b_w. Thus the wall is acting in an essentially different fashion from a simple collider.

This is also shown in a most striking fashion by examining the relative rates of BH_3CO and BD_3CO.

(18) P. LeGoff, A. Cassuto, and A. Pentenero, *Ind. Chim. Belge.*, 29, 342 (1964).

(19) The fact that the slope is not zero shows up in the previously mentioned order curves where the slope was slightly greater than 1.

(20) The number of gas kinetic collisions was calculated from the pressure using a collision diameter of 5 Å for BH_3CO.

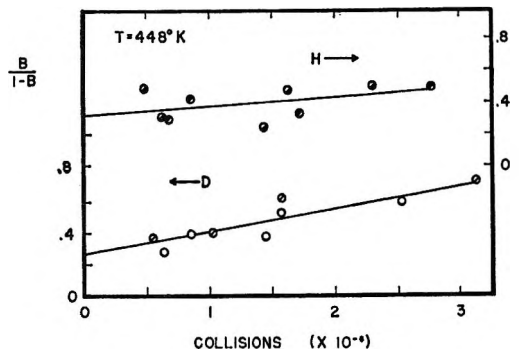


Figure 7. $B/(1 - B)$ as a function of the number of borane carbonyl collisions in reactor F2. The shaded circles refer to BH_3CO and the open circles to BD_3CO. The lines are least-squares fits of the data. BH_3CO and BD_3CO were run on the same day under identical reactor conditions.

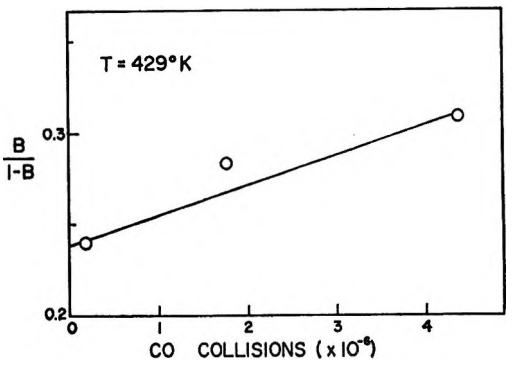


Figure 8. $B/(1 - B)$ as a function of the number of carbon monoxide collisions at a constant borane carbonyl pressure of 17 mTorr in F2.

Figure 6 shows the overall production of CO in F1 for BH_3CO and BD_3CO. In Figure 7 we separate the wall reaction and gas-phase reaction.[20] In this example b_H/b_D for the gas-phase reaction is 0.39 while for the wall reaction it is 1.3. A number of similar determinations yields $b_H/b_D = 0.38 \pm 0.05$ for the gas-phase reaction and $= 1.2 \pm 0.3$ for the wall reaction.[21] It is clear that the isotope effect for the gas-phase reaction is different from that for the wall reaction, the former being large and inverse and the latter being small and normal. As the wall and gas-phase reactions are essentially different, we now divide the discussion into two parts, one dealing with the gas-phase reaction and one with the wall reaction.

The Homogeneous Decomposition. As has been pointed out by Bunker, the theory of unimolecular reactions is probably good enough to calculate absolute rates within a factor of 2.[22] If the gas-phase reaction here is a unimolecular reaction, then we should be able to calculate a threshold energy both from the absolute values of the reaction constants and from their temperature dependence. First, however, it is necessary to show that a simple unimolecular reaction, uncomplicated by the back reaction, is being observed and that the reaction is homogeneous. It is necessary to determine in what part of the "fall-off" region we are operating and to show that there are sufficient collisions to achieve temperature equilibrium. The following empirical evidence relates to these points.

If the back reaction is effective, then increasing the CO concentration should decrease the overall yield. On the other hand, if the simple unimolecular process $BH_3CO \rightarrow BH_3 + CO$ is being observed, eq 2 predicts that increasing CO will increase the net yield. In Figure 8 we show the effect of increasing the number of CO collisions at a constant number of BH_3CO collisions. This figure confirms the latter hypothesis and allows us to calculate a value for K, the relative efficiency of CO with respect to BH_3CO, of 0.4.

An effective way to show where we are operating in the "fall-off" region is to compare BH_3CO with CH_3NC. The unimolecular isomerization of the latter compound has been extensively studied from the low-pressure limit to the high-pressure limit.[23,24] Now the characteristics of the fall-off curve are determined by the number of atoms, the vibrational frequencies of the molecule, and E_0/T (E_0 is the critical energy). BH_3CO and CH_3NC have the same number of atoms, both are symmetrical tops[23,25] and have similar frequency patterns,[23,25] and we are operating at low E_0/T.[26] In addition, the A factor for $BH_3CO \rightarrow BH_3 + CO$ is at least as large as that for $CH_3NC \rightarrow CH_3CN$.[2d,23] It is clear from Figure 1 of ref 23 that at the pressures we are using CH_3NC is reacting at or very near the low-pressure limit. Therefore, the assumption that BH_3CO is decomposing at the low-pressure limit is a good one. Further confirmation results from the observed large inverse secondary isotope effect. For unimolecular reactions proceeding near the low-pressure limit, large statistical-weight inverse secondary kinetic isotope effects are expected.[24] For CH_3NC a value of $k_H/k_D = 0.28$ was observed at 503.6°K and 10^{-2} Torr.[24] Here a value of 0.38 is observed at 488°K and a mean pressure of 4×10^{-2} Torr.

Reaction homogeneity is strongly suggested by the observation of b_g, *i.e.*, increased yield with increasing numbers of gas-phase collisions. Once again confirmation results from the large inverse isotope effect. If the wall were involved in producing the increased yield with increasing density, then one might well expect little or no isotope effect as an absorbed species would un-

(21) The deviations given here are average deviations from the mean. The standard deviation of the slope of an individual experiment is obviously much higher. Although there is considerable scatter in the absolute values of b_g taken on different days, the relative values of b_H and b_D taken on the same day were much better.

(22) D. Bunker, "Theory of Elementary Gas Reactions," Pergamon Press, Ltd., Oxford, England, 1966, p 73.

(23) F. W. Schneider and B. S. Rabinovitch, *J. Amer. Chem. Soc.*, **84**, 4215 (1962).

(24) F. W. Schneider and B. S. Rabinovitch, *ibid.*, **85**, 2365 (1963).

(25) R. C. Taylor, *J. Chem. Phys.*, **26**, 1131 (1957).

(26) Lower E_0/T shifts the fall-off curve up the pressure scale. In this case the shift is *ca.* 0.3 log unit.

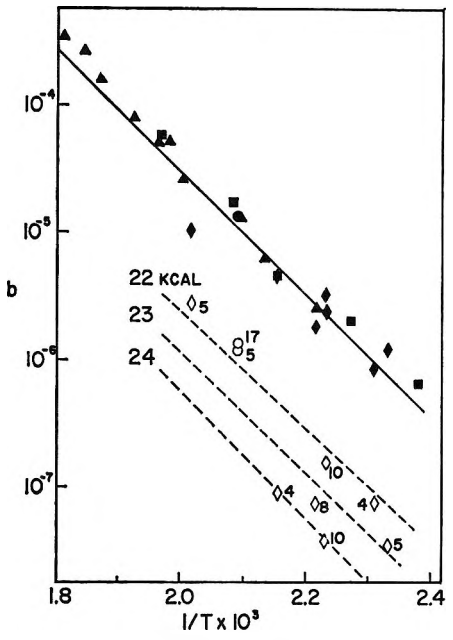


Figure 9. The probability of reaction per collision, b, as a function of the reciprocal temperature for the gas-phase reaction (open points) and the surface reaction (closed points). ○, ●, ▲ refer to reactor F1 and ◇, ◆, ■, refer to reactor F2. The solid line is a least-squares fit of the surface points and the dashed curves are calculated b_g as a function of temperature for the indicated critical energies in kcal. The numbers alongside the b_g data refer to the number of points used in each measurement.

doubtedly be involved. The observed b_g, then, is taken to result from the homogeneous reaction.

The measured values of b_g for both F1 and F2 are given in Figure 9 along with the b_w. The average number of gas collisions in F2 is about 50 times that in F1. From Figure 9 it may be seen that b_g in F2 is not larger than b_g in F1. Apparently, complete temperature equilibrium has been achieved in the reactor.[27] We conclude that the simple unimolecular reaction, $BH_3CO \rightarrow BH_3 + CO$, is being observed at the low-pressure limit and thus we can apply the theory of unimolecular reactions. We may simply relate our b_g to the limiting value of the second-order constant, k_{bi}, as[28]

$$k_{bi} = k/c$$

where k is the first order constant and c is the concentration. This may be rewritten as

$$k_{bi} = zk/\omega$$

as $\omega = zc$ where ω is the collision frequency and z is the collision number. One the other hand

$$k = \omega b_g$$

thus $b_g = k_{bi}/z$.

Now the limiting second-order rate constant is

$$k_{bi} = z\Lambda$$

where

$$\Lambda = Q_v^{-1} \int_{E_0}^{\infty} N(E) \exp(-E/RT) dE$$

and Q_v is the vibrational partition function, and $N(E)$ is the density of vibrational energy levels of the molecule.[29,30] b_g then is simply Λ, and Λ can be evaluated as a function of E_0. Λ was calculated for various E_0's and temperatures in the following manner. Q_v was calculated in the normal manner. $N(E)$ was evaluated as a function of energy using the method of Whitten and Rabinovitch[31,32] and the measured vibrational frequencies of BH_3CO.[25] The integral was then graphically evaluated for various E_0's. The results are shown in Figure 9 as a function of temperature for three values of E_0. Comparison with the data points yields an average value of $E_0 = 22.8$ kcal with an average deviation of 0.4 kcal. The expected isotope effect can also be easily evaluated utilizing the measured frequencies of BD_3CO.[25] For a threshold of 22.8 kcal a calculated value of $b_H/b_D = 0.36$ is obtained compared to a measured value of 0.38.

There is another factor which will affect the magnitude of E_0. Although the rotations are nearly excluded from participation in intermolecular energy transfer, they do influence the critical energy for dissociation.[33] If a decomposing molecule has a nonzero angular momentum then the critical energy will be less than the value for a molecule decomposing with zero angular momentum. The difference for a symmetric top is given by

$$\Delta E = J(J+1)(h^2/8\pi^2)[(1/I) - (1/I^+)]$$

where J is the quantum number and I and I^+ are the moments of inertia of the molecule and activated complex, respectively.[33] To estimate this rotational effect we made the following calculations. A model of the activated complex with a B–C bond order of 0.1 was chosen and the BC bond length in the activated complex was estimated using Pauling's rule.[34] The thermal distribution of rotational levels was then calculated for $T = 0$ and 450°K. The distribution was then divided into 10 rotational level sections and a ΔE was

(27) It has been shown previously (ref 4) that translational temperature equilibrium was reached in F1. This is a necessary, but not sufficient, condition that vibrational equilibrium be achieved.

(28) N. B. Slater, "Theory of Unimolecular Reactions," Cornell University Press, Ithaca, N. Y., 1959, p 138.

(29) O. K. Rice, "Statistical Mechanics, Thermodynamics and Kinetics," W. H. Freeman and Co., San Francisco, Calif., 1967, p 560.

(30) In arriving at this result strong collisions and random lifetimes are assumed. All molecules with energies greater than the critical energy can react, the molecular rotations are assumed inactive, and vibrational anharmonicity is neglected. Rotational effects are also neglected here.

(31) G. Z. Whitten and B. S. Rabinovitch, *J. Chem. Phys.*, **38**, 2466 (1963); **41**, 1883 (1964).

(32) D. C. Tardy, B. S. Rabinovitch, and G. Z. Whitten, *ibid.*, **48**, 1427 (1968).

(33) W. Forst, *ibid.*, **48**, 3665 (1968).

(34) L. Pauling, *J. Amer. Chem. Soc.*, **69**, 542 (1947).

calculated for the mean J of each section. By weighting each ΔE according to the area of its section, a mean $\Delta E = 0.42$ kcal was calculated. E_0 then becomes 23.2 kcal.

Although the critical energy determined here does not depend on the activated complex, E_0 is not exactly equal to the high-pressure activation energy, E_a. E_a does depend slightly on the model chosen for the activated complex.[23] It is sufficient for our purposes to assume that the vibrational frequencies of the activated complex are identical with those of the molecule with the exception of the B–C stretch which is taken to correspond to the reaction coordinate. With this model, E_a is 24.0 kcal.

Strictly for purposes of comparison, a Slater n value of 6 and an effective number of oscillators of 3.5 may be calculated from the data.[23,24,28] These values are of the same order of magnitude as those obtained for the isomerization of CH_3NC.[23]

The Surface Reaction. The b_w for the surface reaction are shown at the top of Figure 9 for both F1 and F2. The agreement between the points from F1 and those from F2 is good and the straight line is the least-squares fit of the data. The first-order rate constant is given by $\log k_w = \log \omega b_w = 10.1 - 4890/T$. A comparison between b_w found here and that obtained previously is shown in Figure 10.[35] b_H/b_D for the surface reaction is 1.2 ± 0.3 as was given above. There are two important facts to explain. First, the activation energy is nearly the same as that for the gas-phase reaction (22.4 compared to 24.0 kcal) but the frequency factor is $10^{4.3}$ less than the high-pressure limit[2d] and $10^{1.4}$ greater than the gas-phase value at 450°K and 4×10^{-2} Torr. Second, there is a small normal isotope effect as compared to a large inverse isotope effect. We now consider several hypotheses for the low-pressure surface reaction to explain these observations.

A natural hypothesis is that b_w describes a true heterogeneous reaction involving strong interactions between surface sites and the reactants and/or products. This type of interaction results in a much lower frequency factor for the surface reaction than for the homogeneous reaction, and surface reactions generally predominate only when they involve significantly lower activation energies. Here the activation energies are nearly the same while the frequency factor is only $10^{4.3}$ times smaller. For a typical unimolecular surface reaction with an activation energy equal to the value for the homogeneous reaction, one would expect the rate to be more like 10^{12} times smaller than that for the homogeneous reaction.[36] Therefore, we must eliminate this hypothesis.

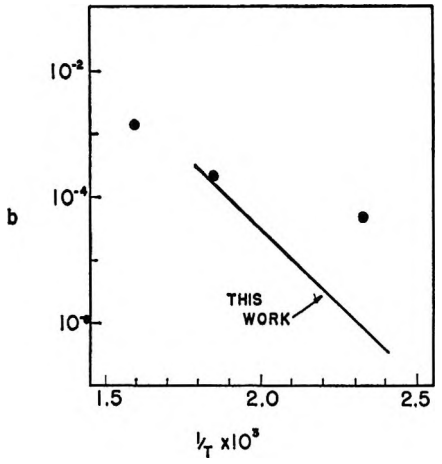


Figure 10. A comparison of b_w for this study (solid curve) with the data of ref 3 (solid points).

Another hypothesis is that the wall is acting as a more efficient collider than the reactant molecules. This would explain the equal activation energies and also why b_w is greater than b_g at a given temperature. However, if this is correct, then an inverse isotope effect of about the same magnitude as that for the gas-phase reaction should be observed. It is not; therefore, this hypothesis must be discarded also.

A third hypothesis visualizes a special role for the surface and might be called the "sticky-collision" hypothesis. We postulate that the reactant molecule is physically adsorbed (weakly bound) on the surface for times long compared to the vibrational period but short compared to the residence time in the reactor. During its encounter[37] with the wall the molecule undergoes many "collisions" and may become excited to an energy greater than the reaction threshold. We postulate that this activated species has a lifetime due to the weak interaction with the wall and consequently it may either be desorbed in the activated state or deactivated before it is desorbed. If the activated species is desorbed then it decomposes before it collides with either the wall or another gas molecule as we are working at a collision frequency such that every free molecule that picks up energy greater than the threshold will decompose. One may write this mechanism as

$$AB + S \rightleftarrows {}^*AB\text{–}S \rightarrow \text{products}$$

where AB refers to the reactant and S to the surface. The similarity to the Lindeman mechanism is clear but there is one big difference in that it is the probability of desorption that controls the decomposition. We now postulate that the adsorbed species resides on the surface for a time which is long compared to the lifetime of the activated species on the surface. If so then the

(35) The temperatures of the points from ref 3 have been empirically corrected. The temperatures were measured previously with a thermocouple centered in the reactor. Later unpublished work with an identical reactor showed that temperatures measured in this fashion were much lower than the wall temperature. Later work also showed that the reactor temperature profile was peaked and increased in sharpness with increasing temperature.

(36) K. J. Laidler, "Chemical Kinetics," McGraw-Hill Book Co., New York, N. Y., 1965, pp 286–296.

(37) The similarity of this terminology to that for encounters in solution is intended.

probability of deactivation is much larger than the probability of desorption and thus we have, in a sense, a unimolecular reaction proceeding at the high-pressure limit. The rate constant may be written simply as

$$k_w = C_s(kT/h)(Z_w^+/Z_sZ_g)\exp(-E/RT)$$

where Z_w^+, Z_s, and Z_g are partition functions for the activated complex, surface site, and an AB molecule, respectively, and C_s is the number of surface sites per cm². As there is little interaction between the adsorbed species and the wall, this model allows the activation energy for the surface reaction to equal that for the gas-phase reaction. One can now write the ratio of the rate of the surface reaction to that of the homogeneous reaction as

$$R_w/R_g = c_sZ_w^+/Z_sZ_g^+ \approx 10^{-12}Z_w^+$$

For a completely bound surface activated complex $R_w/R_g \approx 10^{-12}$ as in the first hypothesis. For a completely mobile complex on the surface $R_w/R_g \approx 10^4$. R_w/R_g observed is $10^{-4.3}$, and thus a partially mobile complex on the surface is postulated. This fits in with the idea of a weakly adsorbed species. The third hypothesis then can explain the observed data on the surface reaction in a satisfactory manner.

This rather interesting role that the surface plays in this reaction may have more generality for the following reason. We have clearly shown above that these surface data do not fit the model of $BH_3CO \rightarrow BH_3 + CO$ proceeding at the low pressure limit with the wall acting as a simple collider. In studies very similar to ours, Benson and Spokes have reported data (b_w's) on isopropyl iodide[13] and *t*-butyl hydroperoxide.[38] Besides

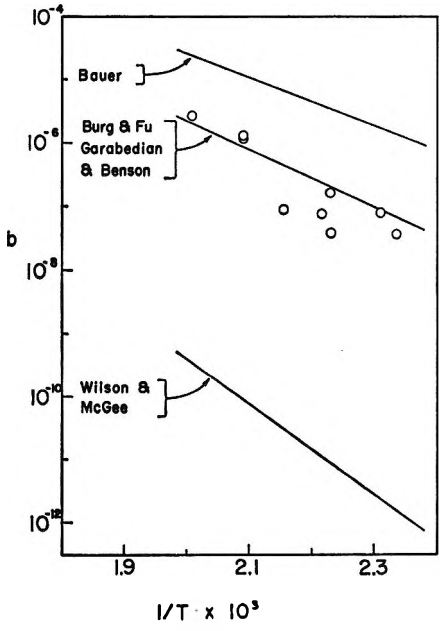


Figure 11. A plot of b_g as a function of the reciprocal temperature. The solid curves are calculated for critical energies of 18.75, 22.05, and 34.05 kcal reading from top to bottom. The data points are b_g from this work.

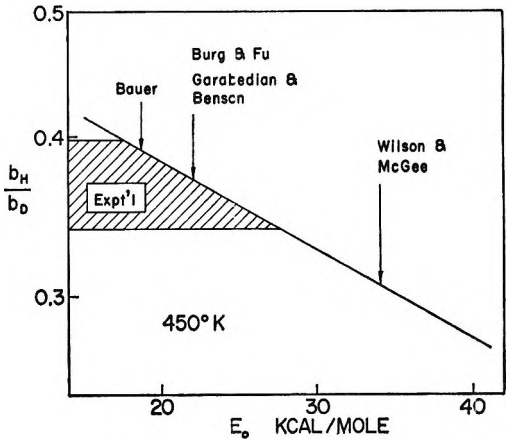


Figure 12. A plot of the isotope effect as a function of the critical energy. The shaded area refers to the range of experimental values from this work.

the interesting mechanistic conclusions presented, they have fitted their data with the classical RRK theory using an effective number of oscillators equal to about $s/2 + 1$ where s is the total number of oscillators. Our *surface* data can be fitted with seven effective oscillators which is also $s/2 + 1$ (This fit is for comparative purposes only and does not imply that the surface reaction is a unimolecular reaction at the low-pressure limit.) The fact that $s/2 + 1$ oscillators fits the surface data here and in these other studies may be merely coincidental, and more evidence is required to postulate any more generality.[39,40] It does point out, however, that the properties of a simple gas-phase collider cannot be attributed to a surface without some experimental support. The isotope effect is a convenient test of the surface interaction.

The Symmetrical Dissociation Energy of Diborane. The reported values for the symmetrical dissociation energy of diborane, $D(H_3B\text{–}BH_3)$, are 28.4 ± 2 kcal,[41] 35 ± 3 kcal,[2d] 35.0 ± 0.5[4] kcal,[42] 59.0 kcal.[43] We believe that the data reported here are good enough to provide an independent determination of this bond energy and we proceed as follows. From the equilibrium constant data of Burg,[2a] $D(H_3B\text{–}BH_3) = 2D(H_3B\text{–}CO) - 9.1$ kcal. Therefore a determintion of $D(H_3B\text{–}CO)$ serves to determine $D(H_3B\text{–}BH_3)$. Now $D(H_3B\text{–}CO) = E_a^f - E_a^r$, where E_a^f is the activation energy for the dissociation reaction and E_a^r is the activation energy for the reaction of BH_3 and CO. While we do not know the value of E_a^r, it is reasonable to assume

(38) S. W. Benson and G. N. Spokes, *J. Phys. Chem.*, **72**, 1182 (1968).

(39) It appears (ref 40) that there should not be a universal number of effective oscillators for the gas-phase reaction. With our mechanism it is not impossible for the surface data to appear to yield such a universal number.

(40) D. W. Placzek, B. S. Rabinovitch, and G. Z. Whitten, *J. Chem. Phys.*, **43**, 4071 (1965).

(41) S. H. Bauer, *J. Amer. Chem. Soc.*, **78**, 5775 (1956).

(42) A. B. Burg and Y. Fu, *ibid.*, **88**, 1147 (1966).

(43) J. H. Wilson and H. A. McGee, *J. Chem. Phys.*, **46**, 1444 (1967).

it is small. If $E_a^r = 0$, then $D(H_3B-BH_3) = 38.5$ kcal and will be reduced by $2E_a^r$ if $E_a^r \neq 0$. It is reasonable to assume $0 \leq E_a^r \leq 2$ kcal and thus $34 \leq D(H_3B-BH_3) \leq 38$ kcal. To place this determination in perspective, Figure 11 shows the values of b_g expected for critical energies corresponding to $D(H_3B-BH_3)$ values of 28.4, 35.0, and 59.0 kcal. Our data for the homogeneous reaction are also shown. Additional support for our value of the diborane bond energy is obtained by noting that the magnitude of the inverse isotope effect expected for the homogeneous reaction depends on the critical energy. Figure 12 shows this dependence, and we have indicated the expected isotope effects corresponding to values of $D(H_3B-BH_3)$ of 28.4, 35.0, and 59.0 kcal. Although the measured isotope effect suffers from considerable scatter, it appears good enough to exclude the high value for $D(H_3B-BH_3)$.

If one accepts the hypothesis concerning the surface reaction, a value for $D(H_3B-BH_3)$ can also be calculated from these data. The activation energy for this reaction is a "high-pressure" value and is slightly lower than the true value due to the weak surface interaction. Once again making the approximation that the reverse reaction has negligible activation energy, a value of $D(H_3B-BH_3)$ of 36 kcal/mol is obtained.

Besides the assumption concerning E_a^r above there are a number of other sources of error which we have estimated as follows. By comparison with the CH_3NC study,[23] the estimated error in the calculation of the absolute rate is about a factor of 2 in the rate or 1 kcal in E_a^f. The measurement of the area of the reactor exit orifice is probably good to 20% or 0.5 kcal in E_a^f. The uncertainty in temperature gives an error of 0.6 kcal in E_a^f and the random error in the measurement of b_g yields an error of 0.4 kcal in E_a^f. We conclude that $D(H_3B-BH_3)$ is 36 ± 3 kcal.

Acknowledgments. This work was supported by National Science Foundation Grant, NSF-GP-6820. G. M. acknowledges his support as a National Science Foundation Predoctoral Fellow since 1965. The discussions with B. S. Rabinovitch are gratefully acknowledged.

Positronium Interactions in Aqueous Oxyacids and Hydrogen Compounds[1]

by S. J. Tao and J. H. Green

New England Institute for Medical Research, Ridgefield, Connecticut *(Received August 12, 1968)*

The lifetimes of positrons in the oxyacid–water systems, H_3PO_4, H_2SO_4, $HClO_4$, HNO_3, and water, and in the hydrogen compound–water systems, HCl, HF, NH_3, H_2O_2, and water, were determined. The short lifetime component (τ_1), the long lifetime component (τ_2), and the intensity (I_2) of the long lifetime component were derived from the composite lifetime data. The connection between changes in I_2, the solution composition, and hot radical reactions is discussed. Data are discussed in terms of a proposed oxidation of positronium (Ps) by H^+ and of possible chemical reactions leading to compounds of Ps and some estimates of bond energies are made: PsO (2.2 ± 0.5 eV), PsOH (<1.5 eV), PsF (2.9 ± 0.5 eV), and PsCl (2.0 ± 0.5 eV). The unknown bond strength of O–Cl in ClO_4^- is estimated as 3.3 ± 0.5 eV.

1. Introduction

The formation and existence of positronium atoms in most condensed media has stimulated a great deal of interest.[2] Since positronium is "stable" in a chemical sense and its structure is similar to a hydrogen atom, it is expected that it should resemble the hydrogen atom in its reactivity. Therefore it should be possible to study the chemistry of positronium, particularly in aqueous media

Trumpy[3] had reached the conclusion that the oxidation potential of positronium is very near to zero, possibly slightly positive, after a detailed study of the angular correlation of γ-quantum emission from the annihilation of positrons in different materials. However, he also raised some fundamental questions such as: "When $SbCl_3$ is not paramagnetic, why do lifetime experiments on solutions of this substance and $NaNO_3$ give fundamentally different results? Would lifetime

(1) Research conducted in the Department of Nuclear and Radiation Chemistry, University of New South Wales, Sydney, Australia, and at the New England Institute for Medical Research.

(2) (a) J. Green and J. Lee, "Positronium Chemistry," Academic Press, New York, N. Y., 1964; (b) A. T. Stewart and L. O. Roellig, Ed., "Positron Annihilation," Academic Press, New York, N. Y., 1967.

(3) G. Trumpy, *Phys. Rev.*, **118**, 668 (1960).

measurements on other oxidizing substances give quenching of τ_2 as by $SbCl_3$ or quenching of I_2 as by $NaNO_3$?"

A similar problem was also studied by McGervey, *et al.*,[4] using lifetime technique, and a block diagram of possible processes involved in positron and positronium annihilation was also given. Later their studies were further extended[5,6] and the temperature dependence of I_2 and τ_2 for positrons in certain solutions was explained.[6]

Another similar problem has been studied by Goldanskii, *et al.*,[7] and tunneling of the electron through the potential barrier from positronium to the acceptor was suggested to explain certain anomalous phenomena in positronium annihilation. Recently, this problem was attacked again by Bertolaccini, *et al.*[8] Extensive reviews can also be found elsewhere.[2b]

However, the questions raised by Trumpy[3] were still not fully answered in the works mentioned. Recently, a new basis was suggested for discussing chemical reactions between positronium and ionic or neutral species in liquids.[9] This had been described earlier in a report by Tao and Green and discussed by McGervey in ref 2b. It was shown that the positronium formation fraction in pure liquids depends not only on the dissociation energy of the medium (Ore-gap theory) but also on the threshold, $I_A - I_p$, where I_A and I_p are the ionization potentials of the liquid and positronium. The energy regions in which positronium reactions may occur are defined in terms of ionization potentials and bond strengths of the constituents of the liquid and of positronium. Attention is paid to likely positronium reactions, *e.g.*, compound formation, double decomposition, oxidation, and reduction, and their effects on the parameters involved in positron annihilation lifetime spectra.

Here we would like to apply this theory to the extensive measurements made on positronium in aqueous solutions of oxyacids and hydrogen compounds. It is understood that such an interpretation may be quite tentative. However, we hope such a discussion will induce more study and more discussion which eventually will benefit our understanding of positronium chemistry.

2. Experimental Methods

There are four principal methods available: the measurement of positron mean lifetimes and intensities and their variations; the study of the angular correlation of annihilation radiation to give data on electron momenta; the measurement of annihilation from the triplet state by triple-coincidence photon detection; and the determination of the spectrum of annihilation radiation by the methods of nuclear pulse spectroscopy.

Lifetime and intensity determinations provide the most useful information particularly now that we have time-to-amplitude converters, multichannel analyzers, and digital computer analysis of the experimental data. Details of the equipment, which was constructed for this research, are described elsewhere.[10-13] When the apparatus was used in this study it had a time resolution of 0.70 nsec (full width at half-height) and a logarithmic slope on the prompt peak (^{60}Co source) of 0.12 nsec. For a ^{22}Na source on a polished copper or aluminum surface, the logarithmic slopes were 0.20 and 0.22, respectively. The precisely linear part of the time range was 30 nsec and this was not only sufficient for the lifetime determination but the apparatus also gave a flat background on the short-time side of the lifetime distribution.

The ^{22}Na source (about 3 μCi) was homogeneously distributed through the sample as nearly carrier-free sodium chloride in a total volume of 0.5–2.0 ml. Each lifetime measurement required about 1000 min to give a statistically reliable number of coincidence counts. Two examples of the measured lifetime spectra, for pure water and for 0.18 mole fraction hydrogen peroxide in

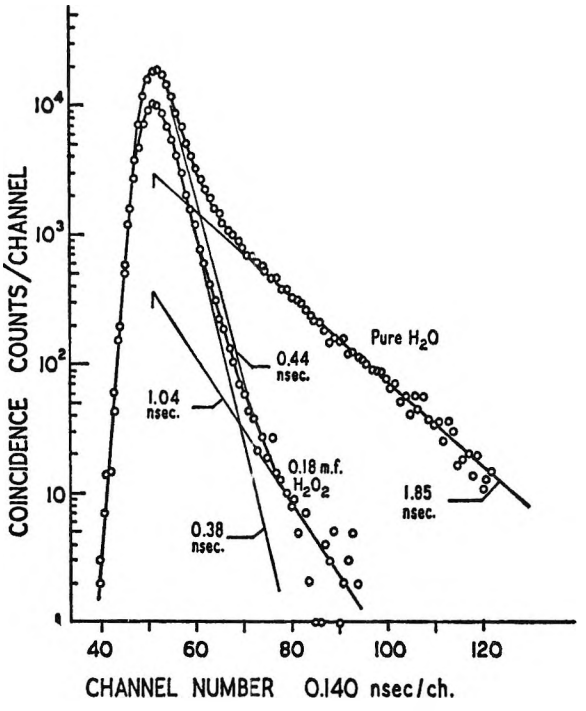


Figure 1. Delayed coincidence (lifetime) diagrams for water and 0.18 mf H_2O_2.

(4) J. D. McGervey, H. Horstman, and S. DeBenedetti, *Phys. Rev.*, **124**, 1113 (1961).

(5) J. E. Jackson and J. D. McGervey, *J. Chem. Phys.*, **38**, 300 (1963).

(6) H. Horstman, *J. Inorg. Nucl. Chem.*, **27**, 1191 (1965).

(7) V. I. Goldanskii, V. G. Firsov, and V. P. Shantarovich, *Dokl. Akad. Nauk SSSR*, **155**, 636 (1964).

(8) M. Bertolaccini, A. Bisi, and L. Zappa, *Nuovo Cimento*, **46**, 237 (1966).

(9) S. J. Tao and J. H. Green, *J. Chem. Soc.*, 408 (1968).

(10) J. Bell, S. J. Tao, and J. H. Green, *Nucl. Instr. Methods*, **35**, 213 (1965).

(11) J. Bell, G. J. Celitans, S. J. Tao, and J. H. Green, *ibid.*, **37**, 51 (1965b).

(12) J. Bell, S. J. Tao, and J. H. Green, *ibid.*, **35**, 320 (1965c).

(13) S. J. Tao, J. Bell, and J. H. Green, *ibid.*, **35**, 222 (1965).

water, are shown in Figure 1. The experimental curves were resolved into their two-exponential lifetime components as illustrated and the best least-squares fit was found in each case. It will be seen that the very important value of I_2, the fraction of all positrons which annihilate with the longest lifetime (*i.e.*, from orthopositronium) could be determined with quite good accuracy (to $\pm 5\%$ of I_2).

A detailed summary of methods of data reduction is given elsewhere.[14] For the sake of simplicity, the results from 2-exponential component analysis are adopted here.

3. Results

The positron annihilation lifetime spectra were obtained for a wide range of compositions in four oxyacid–water systems. The concentrations of the H_3PO_4–H_2O system extended over the whole range from 0.00 mf (mole fractions) to 1.00 mf H_3PO_4 and to the H_3PO_4–P_2O_5 system containing 0.74 mf P_2O_5. Values of τ_1 (mean life of the short component), τ_2 (mean life of the long component), and I_2 (the intensity, or percentage of all positrons, corresponding to τ_2) are given in Table I. The concentrations of the H_2SO_4–H_2O system also extended over the whole range and to the H_2SO_4–SO_3 system containing 0.09 mf SO_3. Results for these systems are given in Table II. The concentrations of $HClO_4$–H_2O mixtures were limited to the range from 0.00 to 0.3 mf $HClO_4$. Results are given in Table III.

Table I: The Annihilation Lifetimes and Intensities of the Long Component for Positron Annihilation in H_3PO_4–H_2O and H_3PO_4–P_2O_5 Systems

Mole fraction	τ_1, nsec	τ_2, nsec	I_2, %
	H_3PO_4–H_2O System		
0.074 H_3PO_4	0.44 ± 0.02	1.84 ± 0.09	18.0 ± 1.0
0.161	0.44 ± 0.02	1.96 ± 0.10	19.4 ± 1.0
0.189	0.40 ± 0.02	1.76 ± 0.09	20.2 ± 1.0
0.308	0.44 ± 0.02	1.95 ± 0.10	21.4 ± 1.0
0.445	0.42 ± 0.02	2.09 ± 0.10	20.3 ± 1.0
0.465	0.42 ± 0.02	2.06 ± 0.10	27.4 ± 1.0
0.622	0.45 ± 0.02	2.28 ± 0.10	23.8 ± 1.0
0.82	0.46 ± 0.02	2.54 ± 0.12	18.5 ± 1.0
0.98	0.47 ± 0.02	2.75 ± 0.14	19.8 ± 1.0
	H_3PO_4–P_2O_5 System		
0.005 P_2O_5	0.48 ± 0.02	2.52 ± 0.13	17.7 ± 1.0
0.053	0.48 ± 0.02	2.44 ± p.12	17.8 ± 1.0
0.15	0.47 ± 0.02	1.90 ± 0.12	15.2 ± 1.0
0.74	0.35 ± 0.02	1.21 ± 0.12	14.8 ± 1.0

Table II: The Annihilation Lifetimes and Intensities of the Long Component for Positron Annihilation in H_2SO_4–H_2O and H_2SO_4–SO_3 Systems

Mole fraction	τ_1, nsec	τ_2, nsec	I_2, %
	H_2SO_4–H_2O System		
0.060 H_2SO_4	0.43 ± 0.02	1.82 ± 0.09	17.3 ± 1.0
0.100	0.48 ± 0.02	1.97 ± 0.10	18.2 ± 0.8
0.162	0.41 ± 0.02	1.87 ± 0.09	18.6 ± 0.8
0.216	0.44 ± 0.02	2.09 ± 0.10	18.4 ± 0.8
0.310	0.40 ± 0.02	2.14 ± 0.11	20.2 ± 1.0
0.398	0.42 ± 0.02	2.22 ± 0.11	19.0 ± 0.8
0.545	0.43 ± 0.02	2.38 ± 0.12	18.5 ± 0.8
0.646	0.46 ± 0.02	2.58 ± 0.12	18.5 ± 0.8
0.777	0.42 ± 0.02	2.64 ± 0.12	17.3 ± 0.8
0.85	0.46 ± 0.02	2.90 ± 0.12	15.4 ± 1.0
1.00	0.45 ± 0.02	3.00 ± 0.13	12.6 ± 1.0
	H_2SO_4–SO_3 System		
0.01 SO_3	0.46 ± 0.02	2.88 ± 0.13	13.4 ± 1.0
0.04	0.43 ± 0.02	2.69 ± 0.15	9.9 ± 1.0
0.09	0.44 ± 0.02	2.58 ± 0.20	7.2 ± 1.0

Table III: The Annihilation Lifetimes and Intensities of the Long Component for Positron Annihilation in $HClO_4$–H_2O and HNO_3–H_2O Systems

Mole fraction	τ_1, nsec	τ_2, nsec	I_2, %
	$HClO_4$–H_2O System		
0.050 $HClO_4$	0.41 ± 0.02	1.85 ± 0.10	15.4 ± 1.0
0.100	0.47 ± 0.02	1.91 ± 0.10	13.3 ± 1.0
0.190	0.44 ± 0.02	1.97 ± 0.10	13.3 ± 1.0
0.295	0.45 ± 0.02	2.06 ± 0.10	12.6 ± 1.0
	HNO_3–H_2O		
0.004 HNO_3	0.39 ± 0.01	1.67 ± 0.01	13.1 ± 0.3
0.01	0.39 ± 0.01	1.60 ± 0.02	8.6 ± 0.3 (10 ± 2)[a]
0.015	0.39 ± 0.01	1.59 ± 0.03	6.6 ± 0.5
0.02	...	...	(7 ± 2)[a]
0.03	0.38 ± 0.01	1.51 ± 0.03	3.8 ± 0.3
0.06	0.37 ± 0.01	1.25 ± 0.10	1.6 ± 0.4
0.10	0.37 ± 0.01	1.24 ± 0.14	0.8 ± 0.4 (5 ± 2)[a]
0.17	0.37 ± 0.01	0.95 ± 0.10	1.5 ± 0.6
0.37	0.39 ± 0.01	1.05 ± 0.10	1.5 ± 0.6
0.72	0.42 ± 0.01	1.10 ± 6.20	1.4 ± 0.9

[a] Green and Bell.[8]

In the HNO_3–H_2O system, the concentration range was from 0.004 to 0.72 mf HNO_3. Collected results for this system are also given in Table III.

Positron annihilation spectra were measured in aqueous hydrogen peroxide solutions with the expectation that the instability of H_2O_2 (the HO–OH bond strength is only 1.5 eV) would have a marked quenching effect on positronium. The results found for solutions in the concentration range up to 0.2 mf H_2O_2 are given in Table IV.

Positron lifetimes in a series of hydrogen compounds would provide useful data, but because of the experimental difficulties in handling the pure compounds, a series of aqueous solutions of the compounds were studied instead. Results of lifetime measurements on aqueous solutions of ammonia, hydrogen fluoride, and hydrogen chloride are listed in Table V.

(14) S. J. Tao, *IEEE Nucl. Sci.*, 15, 175 (1968).

Table IV: The Annihilation Lifetimes and Intensities of the Long Component for Positron Annihilation in H_2O_2–H_2O Systems

H_2O_2, mf	τ_1, nsec	τ_2, nsec	I_2, %
Pure water	0.42 ± 0.02	1.83 ± 0.05	23.0 ± 0.8
0.010	0.45 ± 0.02	1.83 ± 0.10	13.9 ± 1.0
0.021	0.45 ± 0.02	1.71 ± 0.10	9.0 ± 1.0
0.042	0.41 ± 0.02	1.47 ± 0.10	7.0 ± 1.0
0.084	0.40 ± 0.02	1.28 ± 0.10	3.7 ± 0.8
0.176	0.38 ± 0.01	1.04 ± 0.10	3.6 ± 0.8

Table V: The Annihilation Lifetimes and Intensities of the Long Component for Positron Annihilation in NH_3–H_2O, HF–H_2O, and HCl–H_2O Systems

Mole fraction	τ_1, nsec	τ_2, nsec	I_2, %
	NH_3–H_2O System		
0.093 NH_3	0.40 ± 0.02	1.82 ± 0.08	25.8 ± 1.0
0.157	0.39 ± 0.02	1.87 ± 0.08	26.0 ± 1.0
0.295	0.44 ± 0.02	1.88 ± 0.08	24.0 ± 1.0
	HF–H_2O System		
0.070 HF	0.41 ± 0.02	1.82 ± 0.09	21.2 ± 1.0
0.156	0.46 ± 0.02	2.02 ± 0.09	19.2 ± 1.0
0.281	0.46 ± 0.02	2.12 ± 0.10	16.5 ± 1.0
0.473	0.46 ± 0.02	2.19 ± 0.10	17.9 ± 1.0
	HCl–H_2O System		
0.030 HCl	0.42 ± 0.02	1.83 ± 0.09	18.2 ± 1.0
0.058	0.42 ± 0.02	1.78 ± 0.09	19.9 ± 1.0
0.114	0.43 ± 0.02	1.86 ± 0.09	19.1 ± 1.0
0.184	0.44 ± 0.02	1.89 ± 0.09	20.6 ± 1.0

Positron lifetime spectra in a few media at some specific concentrations have been measured by some other workers.[15] For such cases their results agree quite well with ours. We shall discuss the results by separating them into the different categories of probable chemical reactions suggested by us earlier.[9]

4. Discussion

4.1. The Effect of H^+. The plots of the intensities of the second component for oxyacid and hydrogen compound aqueous solutions *vs.* mole fraction of the compound are drawn in Figure 2. The first surprising feature is that the linear extrapolations of these curves for the stronger acids, H_3PO_4, H_2SO_4, $HClO_4$, and HNO_3, all converge to an intensity of $\simeq$17% instead of 23% for pure water. This suggests that a common mechanism among all the strong acids is responsible for the change of I_2 at low acid concentrations. Naturally, the intervention of H^+ is suspected. According to our theory[9] a "hot" reaction between H^+ and either positrons or positronium is the most likely one to be responsible for such a phenomenon. Inclusion of an oxyacid in water causes an overlapping of the positronium formation gaps which, at least for a minor quantity of

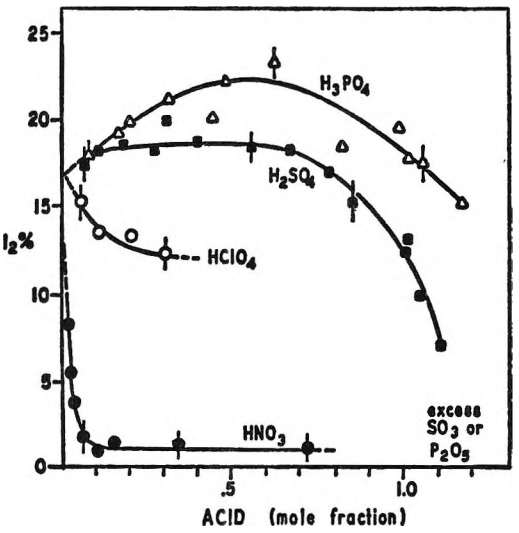


Figure 2. Intensities of the second component in lifetime spectra for positron annihilation in some oxyacid–water systems.

acids, in general increases the positronium formation fraction. Therefore, a reduction of the positronium formation fraction is unlikely to be the principal cause of a decrease in I_2. This leaves oxidation of positronium by simple electron transfer the more reasonable explanation

$$Ps + H^+(aq) \longrightarrow Ps^+ + H(aq)$$

If the excitation energy is negligible, the threshold of this reaction is $I_p - I_H$, where I_H is the ionization potential of H(aq) and I_p is the ionization potential of positronium. The reduction in I_2 is 6%, which is about one-fourth of 23%; this indicates that one-fourth of the Ps atoms are oxidized. Thus it appears that there is a narrow energy range in which oxidation of Ps can occur. This would be the case if I_p were much greater than I_H, since the Ps atom is oxidized when its kinetic energy is at least equal to $I_p - I_H$. In addition, the rate of this reaction must clearly be very fast ($\geq 10^{10}$ sec^{-1} M^{-1}). This can be attributed to the great mobility of the electron hole H^+ in water. It is also implied that the rate for this reaction is faster in more dilute H^+ solutions.

4.2. Formation of PsO. Another interesting feature appears in the variation of I_2 with mole fraction of the oxyacids: the values of I_2 are nearly constant at acid mole fractions between 0.3 and 0.7. These constant values of I_2 are 22, 18.5, and 1% for H_3PO_4–H_2O, H_2SO_4–H_2O, and HNO_3–H_2O systems, respectively. For the $HClO_4$–H_2O system, though there are no available data on I_2 for acid concentrations higher than 0.35 mf, it seems that (although I_2 decreases very quickly at low concentrations) the I_2 curve levels off to a flat region in the acid concentration range about 0.5 mf. If the flat portion does exist, the constant values of I_2 should be 12% for the $HClO_4$–H_2O system.

(15) For example: HNO_3, ref 16; HCl, ref 6.

These values of I_2 follow a systematic pattern which must have an explanation. A change in positronium formation gap is ruled out as a common cause since it cannot explain the great reduction of I_2 for $HClO_4$–H_2O and HNO_3–H_2O systems. Green and Bell[16] offered the formation of $Ps^+NO_3^-$, which competes strongly with the positronium formation reaction, as an explanation for the decrease of I_2 in NO_3^- solutions. However, by analogy with hydrogen compounds, the formation of $Ps^+ClO_4^-$, $Ps^+HSO_4^-$, and $Ps^+H_2PO_4^-$ should be more favored than the formation of $Ps^+NO_3^-$, since HNO_3 is the most highly dissociated acid among their corresponding hydrogen counterparts. A more reasonable explanation is offered here. At these moderate acid concentrations, most of the acid molecules appear in the first dissociated form, $H_2PO_4^-$, HSO_4^-, ClO_4^-, or NO_3^-, and Ps may react with them to form PsO by the reactions

$$Ps + H_2PO_4^- \longrightarrow PsO + H_2PO_3^-$$

$$Ps + HSO_4^- \longrightarrow PsO + HSO_3^-$$

$$Ps + ClO_4^- \longrightarrow PsO + ClO_3^-$$

$$Ps + NO_3^- \longrightarrow PsO + NO_2^-$$

If the value of the reaction threshold is greater than zero, *i.e.*, $D_{AB} - D_{PA} > 0$, the intensity of the second component will be reduced according to the value of the threshold if the reaction rate is fast.[9] The lower the threshold the more the intensity of the second component is reduced. Such reactions can occur in a solution when Ps is hot, *i.e.*, with more energy than the threshold, since the excess energy can be easily carried away by a third body.

This is just the case observed here, where there is not much change in τ_2 in the range concerned. The values of D_{AB} for $(H_2PO_3\text{–}O)^-$, $(HSO_3\text{–}O)^-$, and $(NO_2\text{–}O)^-$ are known,[17] but the value of D_{PA} for PsO is unknown. However, we can estimate the bond strength of PsO approximately by the following empirical method. The values of D_A are plotted against the corresponding values of I_2 in the flat region of the curve (Figure 2) as shown in Figure 3. It is found, as I_2 approaches zero, that the extrapolated value of D_A is 2.2 eV, which is just the value of D_{PA} for PsO if the activation energy is neglected. The bond energy of Ps–O is, therefore, estimated to be $\leq$2.2 eV. From Figure 3 the unknown thermochemical bond energy of $(ClO_3\text{–}O)^-$ may also be found; it is about 3.3 eV, taking the value of I_2 in the flat portion as 12%. One of the important factors neglected here is the formation fraction of Ps for these oxyacid ions, which is determined mainly by their ionization potentials. Unfortunately, these values are unknown, and the error involved may be of the magnitude of 1 eV until the ionization potentials can be found.

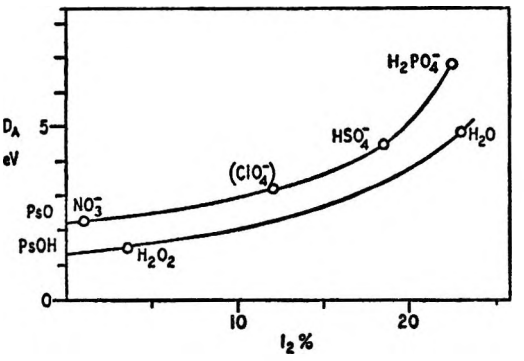


Figure 3. Empirical relationship between the values of D_{AB} and I_2.

4.3. The Formation of PsOH. Hydrogen peroxide is an oxidizing agent and is very unstable, its HO–OH bond strength being only 1.5 eV. It is therefore surprising to find that its quenching effect on Ps is not as great as expected. The values of λ_2 and I_2 of positrons in the H_2O_2–H_2O system with H_2O_2 concentrations up to 0.2 mf are plotted against mole fractions in Figure 4.

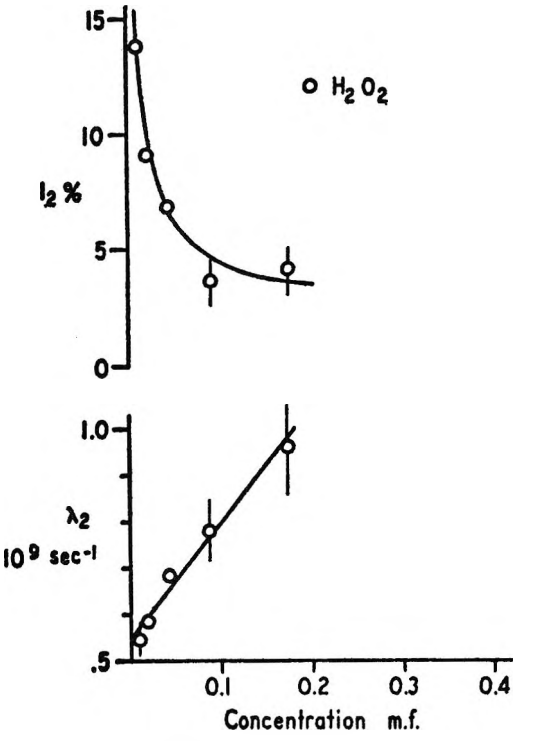


Figure 4. Lifetime and intensity of the second component in lifetime spectra for positron annihilation in H_2O_2–H_2O.

The intensity levels off at a value of 3.5% at an H_2O_2 concentration of 0.2 mf.

This may be explained if the bond strength of Ps–OH is less than 1.5 eV, the reaction

$$Ps + H_2O_2 \longrightarrow PsOH + OH$$

(16) R. E. Green and R. E. Bell, *Can. J. Phys.*, 35, 398 (1957).

(17) These values have been taken from the best estimates of thermochemical bond energies (E) given by T. L. Cottrell, "The Strengths of Chemical Bonds," Butterworth and Co. Ltd., London, 1958, rather than the bond dissociation energies, and a compilation is listed elsewhere.[9] The P–O, S–O, and N–O bond energies are $\simeq$156, 104, and 53 kcal/mol, respectively.

is responsible for the reduction of I_2, and the pick-off or conversion quenching rate of positronium in pure H_2O_2 is greater than that in pure H_2O.

Referring to Figure 3, a rough extrapolation from the values of D_{AB} and I_2 for H_2O and H_2O_2, gives the value of the bond strength of Ps–OH as 1.3 eV. This is much lower than the value of 4.8 eV for H–OH. If the greater quenching effect on the annihilation lifetime τ_2 is considered to be wholly due to pick-off, the pick-off quenching cross section of H_2O_2 is estimated to be 1.0×10^{-20} cm^2.

The decrease of I_2, as the acid concentration increases beyond 0.7 mf for both H_3PO_4–H_2O and the H_2SO_4–H_2O systems, can be also partly attributed to the formation of PsOH by such reactions as

$$Ps + HO\text{–}PO_3H_2 \longrightarrow PsOH + PO_3H_2$$

In mixtures of such high acid concentrations most of the acid exists as free acid rather than ions. The bond strength between the HO radical and the center atom of the free acid is expected to be weaker than the bond strength of the O atom and the center atom of the ions of the corresponding acid, which in turn reduces the threshold energy of the double-decomposition reaction. The positronium formation fraction may also be reduced because the ionization potentials of these acids are expected to be higher.

4.4. Hydrogen Compounds. The Ps formation gaps and the Ps compound formation gaps for simple hydrogen compounds of carbon (CH_4), nitrogen (NH_3), oxygen (H_2O), fluorine (HF), and chlorine (HCl) are shown in Figure 5, where the values of 2.9 and 2.0 eV are adopted as the bond strengths of PsF and PsCl.

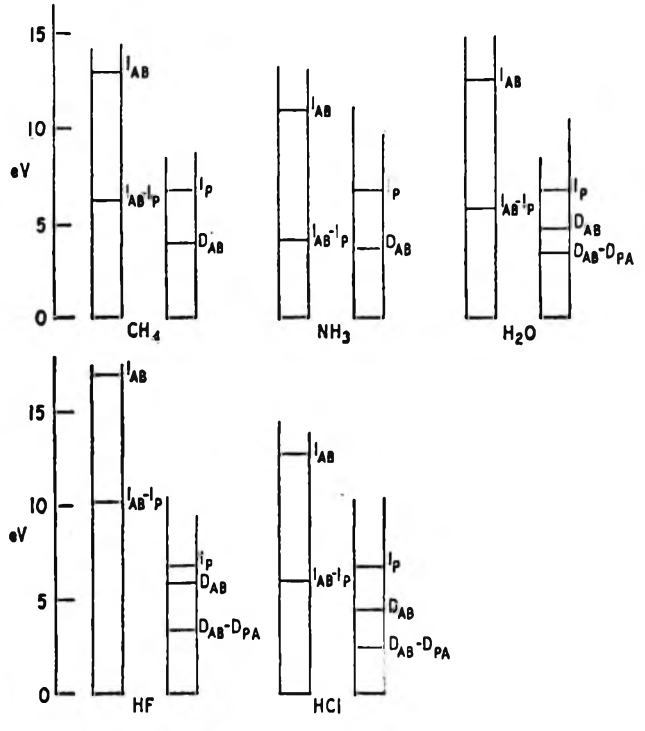


Figure 5. Ps compound formation gap for CH_4, NH_3, H_2O, HF, and HCl.

The estimate for PsCl depends primarily on the observations of Tao[18] on annihilation rates of positrons in Cl_2 and Ar–Cl_2 gas mixtures. The resonance annihilation of Ps was attributed to the reaction $Ps + Cl_2 \rightarrow PsCl + Cl$. This reaction occurs only when Ps has energies above thermal. This is in agreement with the fact that from the concentration of Cl_2 in the Ar–Cl_2 mixture in which the second shoulder just appears, the resonance annihilation energy was estimated reasonably as 0.5 eV, not far above thermal energies. The dissociation energy of Cl_2 is 2.5 eV and the bond strength of PsCl is then about 2.0 eV. This estimate is supported by the theoretical value, 1.55 eV, calculated by Simons.[19]

An estimate of the bond strength in PsF is obtained by noting that, when a hydrogen atom in benzene is replaced by fluorine, the value of I_2 is reduced from 40 to 27%.[20] Since the ionization potential of benzene is close to that of fluorobenzene, the reduction in I_2 is most probably due to the formation of PsF by the reaction $C_6H_5F + Ps \rightarrow PsF + C_6H_5$. From the shape of the empirical curves (Figure 2) the relation between threshold energy for Ps compound formation and the value of I_2 can be roughly determined. The threshold energy for formation of PsF by the above reaction is thus estimated as 3.0 eV. The dissociation energy of HF is 5.9 eV and therefore 2.9 eV is a fair estimate of the bond strength of PsF.

The error in the bond strengths so far estimated should be about 1 eV. Bond strengths of H_3C–Ps or H_2N–Ps should approach zero.

From the above data, the intensities of the second component for the pure compounds should decrease in the order CH_4, NH_3, H_2O, and HCl provided that the positronium formation fractions are approximately the same. The positron annihilation lifetimes and the intensity of the long component in condensed methane, CH_4, are not known but the values for *n*-pentane and *n*-hexane have been measured[20] to be $\tau_2 = 4.0$ and 3.8 nsec, and $I_2 = 39$ and 40% respectively. The high values of I_2 are due to the lower ionization potentials, *e.g.*, 10.9 eV for *n*-hexane, and essentially to the negligible Ps compound formation gap. The positron annihilation lifetime τ_2 and the intensity I_2 of the long component in pure condensed NH_3, HF, and HCl at room temperature are not available. If their values in dilute water solutions can be used as an indication (Table V), the intensities, I_2, for C_5H_{12}, NH_3, H_2O, HF, and HCl just follow a decreasing order. (The particularly low value of I_2 in HF–H_2O systems of higher HF concentrations may be due to the high ionization

(18) S. J. Tao, *Phys. Rev. Lett.*, 14, 935 (1965).
(19) L. Simons, *Phys. Rev.*, 90, 165 (1953).
(20) S. J. Tao and J. W. Lee, unpublished data.

potential of HF and the stable associated HF system, which in turn considerably reduce the positronium formation fraction.)

4.5. Pick-off Quenching and τ_2. In the oxyacids, except HNO_3, positrons have a longer lifetime τ_2 than in water. (However, even in highly concentrated HNO_3 the value of τ_2 is still about 1 nsec.) This indicates that the effect of oxidation on Ps is negligible after Ps has slowed down below the threshold energy and become thermalized. Only pick-off still remains effective at thermal energies. The longer lifetime of τ_2, or lower pick-off quenching rate, for oxyacids is mainly due to their low molar density. For instance, the pick-off quenching cross section for H_2SO_4 was calculated to be 4.0×10^{-21} cm^2 which is greater rather than smaller than that of water, 2.3×10^{-21} cm^2. The low quenching rates of hydrocarbons are also due to their low molar densities, *e.g.*, 0.00767 M/cm^3 for *n*-hexane, compared with that of water 0.0556 M/cm^3. Only the low quenching rate of HF can be attributed to a lower pick-off quenching cross section instead of low molar density. Since HF has a very high ionization potential, its low Ps pick-off quenching cross section is expected.[21]

The values of τ_2 for oxyacid mixtures agrees well with the formula[9]

$$\lambda_{pq} = \frac{\rho}{\rho_A}\lambda_{pqA}\frac{1 + [(W_B\rho_A\lambda_{pqB} - 1)/W_A\rho_B\lambda_{pqA}]\chi}{1 + [(W_B/W_A) - 1]\chi}$$

where λ_{pq} is the pick-off quenching rate of the mixture; the densities of A, B, and their mixture are ρ_A, ρ_B, and ρ, respectively; the molecular weights are W_A and W_B; pick-off quenching rates of pure A and B are λ_{pqA} and λ_{pqB} and χ is the mole fraction.

A plot for the H_2SO_4–H_2O system, where pick-off quenching rates of 0.556×10^9 sec^{-1} (τ_2 = 1.8 nsec) and 0.333×10^9 sec^{-1} (τ_2 = 3.0 nsec) are used for pure H_2O and H_2SO_4 is shown in Figure 6, as an example. This relationship fits the experimental data better than a simpler relationship based on density variations. (Also see Figure 7.)

4.6. Formation of $PsSO_3$. In the H_2SO_4–SO_3 system, excess SO_3 both strongly quenches I_2 and slightly increases the annihilation rate, τ_2 (Table II). The bond strength O–SO_2 in SO_3 is about 3.5 eV, not small enough to be supposed to lead to quenching of Ps by formation of PsO. Therefore, an alternative explanation is required. It seems more reasonable to attribute the change in I_2 and τ_2 to formation of $PsSO_3$ by the reactions Ps + SO_3 → $PsSO_3$ which may occur at thermal energies.

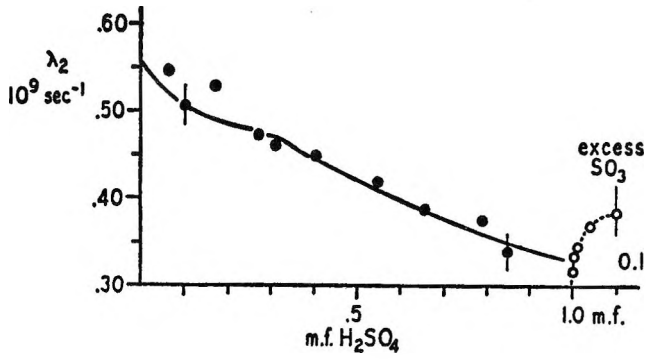


Figure 6. The values of λ_2 for H_2SO_4–H_2O system. The solid line represents the theoretical curve for two pick-off quenching agents.

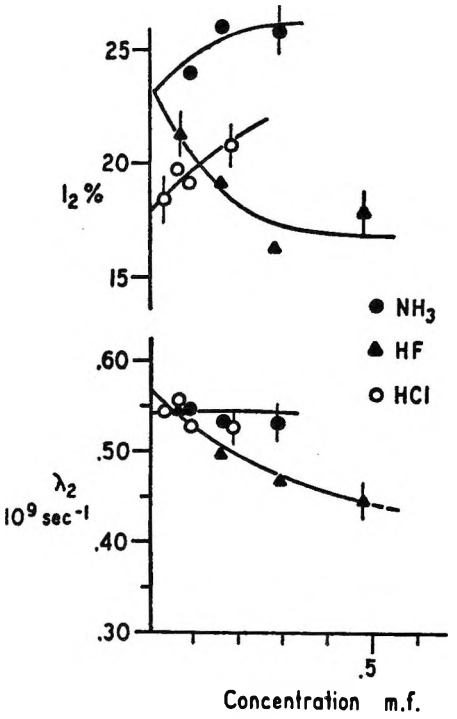


Figure 7. Values of λ_2 and I_2 for NH_3–H_2O, HF–H_2O, and HCl–H_2O systems.

However, in the H_3PO_4–P_2O_5 system (Table I) the annihilation rate increases considerably with increasing P_2O_5 concentration, while I_2 remains quite high (τ_2 is more than halved at 0.74 mf P_2O_5 while I_2 falls only from 18 to 15%). This is interpreted to mean that P_2O_5 quenches Ps mainly by pick-off rather than by oxidation or compound formation. This is in agreement with the general chemical behavior of SO_3 and P_2O_5.

5. Conclusion

Here we would like to point out once more that the explanations given in the previous sections are tentative. However, no matter how tentative these explanations are, the experimental results strongly support two important aspects in the theory of positronium annihilation. First, a considerable part of the Ps atoms annihilate before thermalization, and the average energy at their annihilation may be of the magnitude of 1 eV. Second, since Ps annihilates during slowing down, it undergoes many hot radical reactions with the medium.

(21) D. C. Liu and W. K. Roberts, *Phys. Rev.*, 130, 2322 (1963).

Some of the possible reactions may become the dominant ones and most of these reactions do possess a threshold energy. Therefore, the resultant annihilation lifetime spectrum may not necessarily fit a simple multiexponential decay scheme.

If we apply the "free volume" theory proposed by Brandt, *et al.*,[22] to molecular liquids and aqueous solutions, we shall find that the distortion of the electronic wave function of the positronium atom is small, about a few per cent.[23] This implies that thermalized positronium occupies a cavity of relatively large size. Consequently, positronium is expected to behave as an atom in liquids. However, the penetration of the total positronium wave function into the barrier of the cavity is sufficiently large to alter the lifetime of positronium significantly. This is the contribution of the "pick-off" quenching. The deep penetration of positronium wave functions into neighboring molecules implies that activation energy for most of the positronium reactions is negligible. This also explains why the rates of the positronium reactions are very fast provided energy conservation is satisfied. This, in turn, further supports our theory that the change of intensity I_2 is mainly due to a chemical reaction. From such an elementary theory we are able to give reasonable explanations for some hot Ps reactions in certain aqueous solutions and obtain valuable estimates of some Ps bond strengths.

A recent investigation by Hsu and Wu[24] has indicated a method of measuring kinetic energy involved in positronium annihilation. This will enable us to measure an important unknown parameter involved in positronium reactions, the energy possessed by positronium when it annihilates. It is hoped that these measurements and this report will serve as a stimulant for further understanding of positronium chemistry.

Acknowledgments. Research sponsored by the Air Force Office of Scientific Research, Office of Aerospace Research, United States Air Force, under AFOSR Grants No. 62-398, 961-65, and 1195-67, and by the U. S. Atomic Energy Commission, Grant No. AT(30-1)3661. We are grateful to J. Bell for technical assistance.

(22) W. Brandt, S. Berko, and W. W. Walker, *Phys. Rev.*, **120**, 1289 (1960).

(23) S. J. Tao, unpublished data.

(24) F. H. Hsu and C. S. Wu, *Phys. Rev. Lett.*, **18**, 889 (1967).

Absolute Intensity of Thin-Film C_6H_6(s) from Reflectance and Transmittance near 680 Cm^{-1}

by Donald E. Glover and J. Leland Hollenberg

Department of Chemistry, University of Redlands, Redlands, California 92373 *(Received August 13, 1968)*

The infrared reflectance and transmittance spectra of the ν_{11} (a_{2u}) fundamental of C_6H_6(s) for thin films have been measured. Optical expressions for the reflectance and transmittance of thin films have been used to calculate the refractive index n and the absorption index k. Integration of k over the band gives an absolute intensity $\Gamma = 11.7 \pm 1.3$ cm^2 mmol^{-1}, which is about 36% lower than the apparent absorption intensity of 15.9. Comparison to results of other workers is made.

In a preliminary report,[1] we have described the observation of very significant reflection from a thin-film sample of crystalline benzene. Because reflection losses from thin films have previously been ignored, or their importance indicated theoretically,[2] the need for direct experimental data is apparent. Moreover, the influence of intermolecular coupling and medium effects on intensities in condensed phases cannot be determined until accuracy of measurement is improved. With the purpose of obtaining the absolute intensity free from possible reflection errors, the reflectance and transmittance spectra of the ν_{11} (a_{2u}) fundamental of C_6H_6 in the solid phase near 680 cm^{-1} were analyzed. Both the experimental procedures and calculations are described here in detail.

Experimental Procedure

Reagent grade benzene which had repeatedly been frozen and pumped under high vacuum was stored over molecular sieve in a glass sample tube attached to the line. A cross section of the conventional dewar cold cell used to form the sample is shown in Figure 1. The copper frame holding the AgCl substrate makes good thermal contact with a coolant chamber above. Temperatures were measured with copper–constantan thermocouples. Although other workers have reported

(1) J. L. Hollenberg and D. E. Glover, *J. Phys. Chem.*, **71**, 1544 (1967)

(2) S. Maeda and P. N. Schatz, *J. Chem. Phys.*, **35**, 1617 (1961); S. Maeda, G. Thyagarajan, and P. N. Schatz, *ibid.*, **39**, 3474 (1963); K. Kozima, W. Suetaka, and P. N. Schatz, *J. Opt. Soc. Amer.*, **56**, 181 (1966).

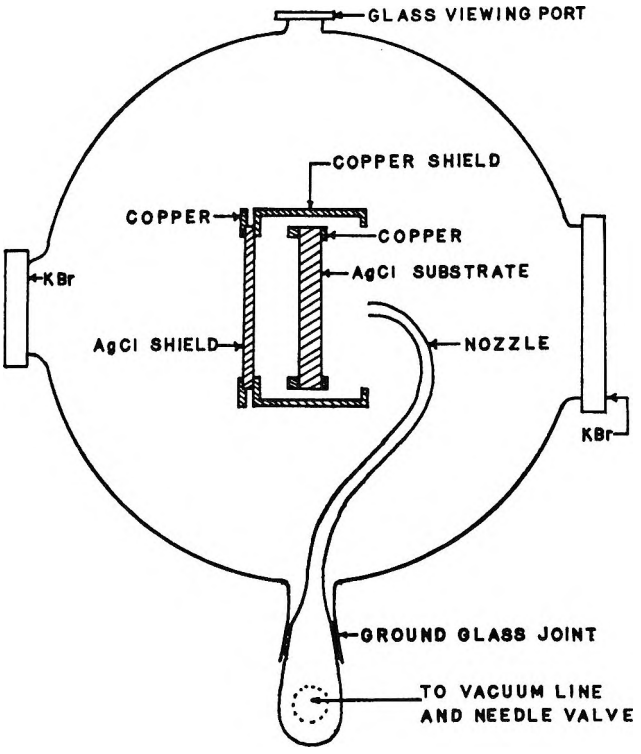


Figure 1. Cross section perpendicular to axis of cold cell. Optical path is from right to left.

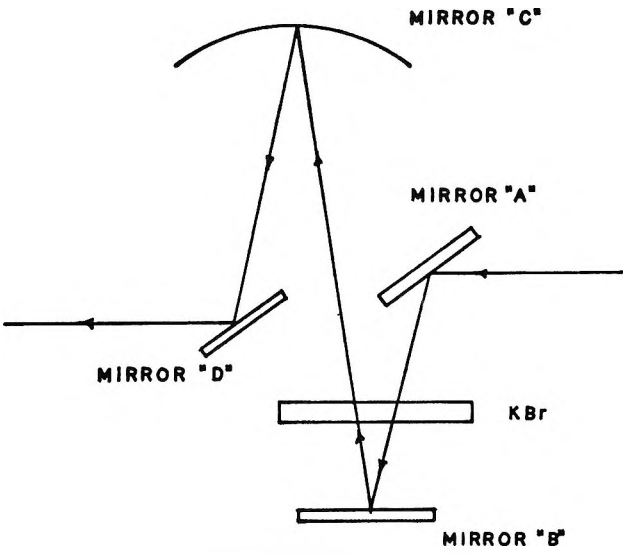


Figure 2. Mirror system placed in the Beckman IR-12 sample compartment for reflectance studies.

there is no evidence of sample deposition on the back side of the substrate,[3] this possibility was minimized by mounting a 1 mm thick window of AgCl over the rear opening in the copper radiation shield (see Figure 1). The shield is in thermal contact with a separate outer coolant chamber, but since no liquid nitrogen was used in this chamber, the sample could not condense on the extra AgCl window. Our experience indicates that ice formation is not serious under the conditions of the experiments.

The thin-film sample was formed by depositing benzene vapor in about 5 min onto the AgCl substrate, which was maintained near 155°K during this time to form an annealed polycrystalline film. The film thickness was determined by the transmission fringe method of Hollenberg and Dows,[4] using a Cary 14 spectrophotometer. Several films were studied before all the factors required for a careful determination of intensity were recognized. In this paper experimental results and calculations are based on work with the final two films, with thicknesses 1.26 and 1.46 μ. Each film was cooled to 100 ± 2°K after deposition.

The procedure used to obtain the necessary data will now be described. The single-beam transmission spectrum was recorded with a Beckman IR-12 spectrophotometer, with slit width about 0.84 cm^{-1}. The cell was then removed and the mirror system shown in Figure 2 was installed. All mirrors are front surface aluminized and uncoated. The single-beam reference reflection spectrum R_0 was recorded. To obtain the correct R_0 an extra KBr window identical with that on the cold cell was mounted as shown. The distance of this KBr window from the reference mirror B in Figure 2 matched the corresponding distance in the cold cell. Mirror B was at a focal plane in the optical system. In this work it was assumed that 100% of the light incident on reference mirror B was reflected, although the work of Bennett, *et al.*,[5] shows that 98–99% might be expected.

Mirror B and the extra KBr window were next removed and the cold cell placed so that the AgCl substrate, with the film on its front surface, occupied the same position as mirror B. Considerable care had to be taken to adjust the cell position to achieve maximum signal, but this is not a serious limitation on the method. The single-beam reflection spectrum R of the film was recorded, with slit width about 0.9 cm^{-1}, which is far less than the band half-width of 10 cm^{-1}. After warming the cell to remove the sample the empty cell transmittance was obtained.

The aluminized mirrors will have a tendency to polarize light reflected from them because the angle of incidence is 10° from the normal. However, we assume that the solid benzene sample is polycrystalline and therefore isotropic in nature. Thus R and R_0 should be affected in an equivalent manner by polarization. Moreover, even if the film were anisotropic, Bennett and Koehler[6] reported calculations that the reflectances for the two states of polarization differ typically by less than 0.001 for angles as much as 10° off normal incidence.

(3) H. Yamada and W. B. Person, *J. Chem. Phys.*, **38**, 1253 (1963).
(4) J. L. Hollenberg and D. A. Dows, *ibid.*, **37**, 1300 (1962).
(5) H. E. Bennett, J. M. Bennett, and E. J. Ashley, *J. Opt. Soc. Amer.*, **52**, 1245 (1962).
(6) H. E. Bennett and W. F. Koehler, *ibid.*, **50**, 1 (1960).

Because atmospheric CO_2 absorbs strongly in the 680-cm^{-1} region, it was necessary to remove CO_2 as completely as possible. This was accomplished by adding to the air-drying apparatus a 3-in. pipe about 3 ft long containing Linde 13X molecular sieve. This system reduced the Q-branch absorption of CO_2 to less than 5–10% for about 90 min. The pipe was heated overnight with dry air moving through to regenerate the sieve.

In order to determine the effect of the extra AgCl window and the rear KBr window on the experimental reflectance, mirror B was moved back to the positions occupied by these windows. No signal could be detected so it was presumed that these reflecting surfaces are too far from the focal point to contribute light to the detector.

Experimental Results

The reflectance and transmittance spectra of a 1.26 μ thick film of solid C_6H_6 at 100°K are shown in Figure 3. The spectra of a 1.46-μ film are shown in Figure 4. We did not attempt a systematic study of R *vs.* sample thickness but selected for calculations those spectra which showed large reflectance. It can be seen from these spectra that as much as 50% of the incident light may be reflected. A similar experiment by Besette and Cabana[7] on solid CF_4 shows about 70% reflectance. Thus it is clearly evident that quantitative corrections for reflectance must be made if thin film transmittance spectra are used to determine absolute intensities of strong absorbers.

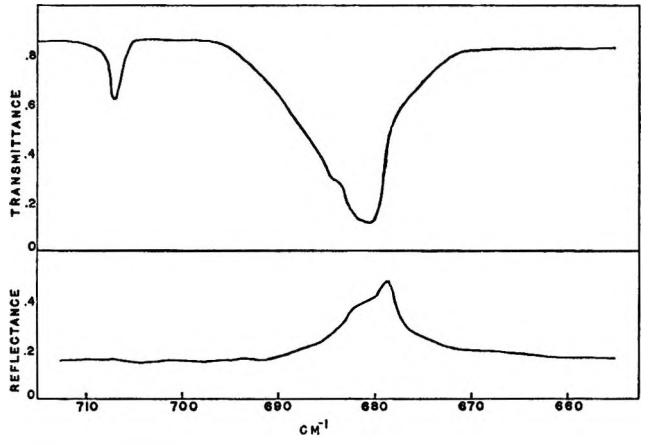


Figure 3. Reflectance and transmittance spectra of 1.26-μ film of C_6H_6(s) at 100°K. Slit width 0.8 cm^{-1}.

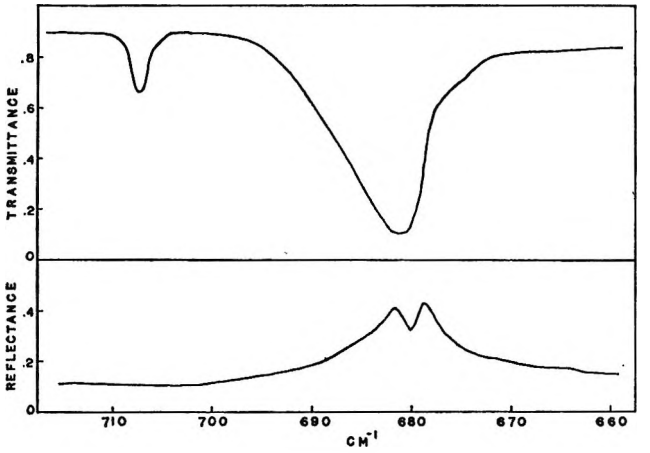


Figure 4. Reflectance and transmittance spectra of 1.46-μ film of C_6H_6(s) at 100°K. Slit width 0.8 cm^{-1}.

Calculations

Equations given by Heavens[8] for the reflectance R and transmittance T of a thin absorbing film on an infinitely thick transparent substrate were used as the basis for calculating the refractive index n and the absorption index k. Because this reference is out of print, and because various authors continue to cite Heavens, the equations are given in the Appendix. These equations are of the form

$$R_H = f_1(n, k, d, \lambda) \quad (1)$$

$$T_H = f_2(n, k, d, \lambda) \quad (2)$$

where d is film thickness and λ is wavelength. In principle, the experiments provide enough data so that there are two equations in the two unknowns n and k. However, these equations cannot be solved explicitly for n and k, so that an iterative procedure with a computer was necessary.

In order to begin calculations the experimental data must be altered to the appropriate form. First we consider that the total incident light intensity I is

$$I = R + T + S + A \quad (3)$$

where S is scattered light and A is absorbed light. In this work it was assumed that S is negligible. We have some evidence for setting $S = 0$. During the sample deposition, the transmitted energy at 7140 cm^{-1} decreased by 3.5%, undoubtedly due to scattering. Since Rayleigh scattering is proportional to ν^4, it is clearly negligible at 680 cm^{-1}. We are assuming that Mie scattering is also unimportant.

In the wings of the transmittance band, A is zero so that in this special circumstance eq 3 reduces to

$$I = R_E + T_E \quad (4)$$

Here $R_E = R/R_0$, *i.e.*, the reflection signal from the film divided by the reflection signal from the reference mirror B. $T_E = T/T_0$, where T is the transmission signal read from the spectrum, and T_0 is the new "base line" calculated such that $R_E + T_E = 1.00$. The empty cell transmission can now be fitted to the observed T_0 value in the wings of the band so that T_E can be readily calculated where $A \neq 0$.

(7) F. Bessette and A. Cabana, *Spectrochim. Acta*, in press.

(8) O. S. Heavens, "Optical Properties of Thin Solid Films," Butterworth and Co. Ltd., London, 1955, pp 76, 77.

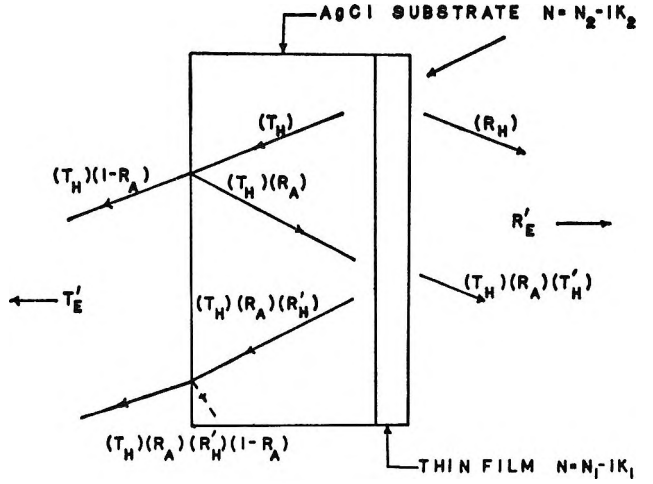


Figure 5. Reflected and transmitted energy relations for light incident from a vacuum on a thin film supported on a relatively thick substrate.

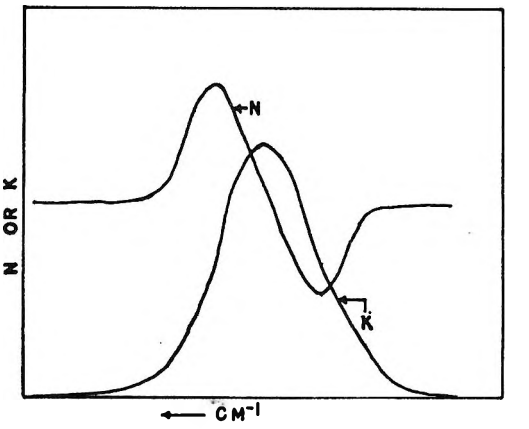


Figure 6. Theoretical behavior of refractive index and absorption index in the region of a fundamental vibration.

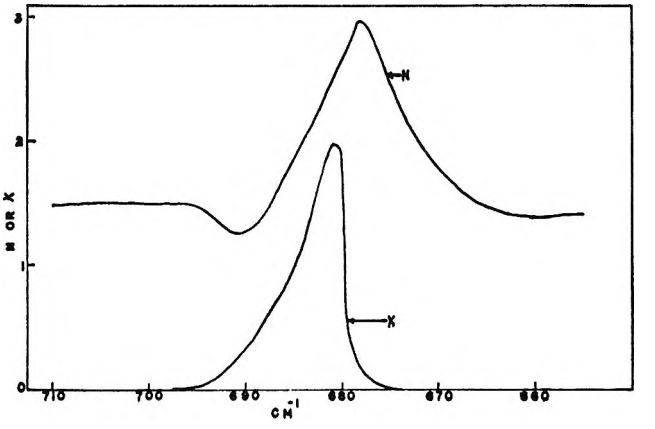


Figure 7. Plot of calculated n and k through the ν_{11} (a_{2u}) fundamental region of C_6H_6(s) at 100°K.

The reflection and transmission of light by the thin film on the relatively thick substrate is represented in Figure 5. The incident light at the upper right gives rise to reflectance R_H which is expressed by the Heavens equations in the Appendix. Reflectance from the back surface of the substrate R_A causes additional light to be detected. R_A is defined by the relation[9]

$$R_A = (n - 1)^2/(n + 1)^2 \qquad (5)$$

where n is the refractive index of the AgCl. T_H is the transmitted light as given by the Heavens equations. Hence, $T_H R_A$ is the amount of light approaching the film in the reverse direction. By changing the appropriate refractive indices the fraction transmitted is T_H' so that additional light reflected is $T_H R_A T_H'$. Calculations showed that additional reflections from the back surface of the AgCl contribute a negligible amount. The theoretical reflectance R_E' is thus

$$R_E' = R_H + T_H R_A T_H' \qquad (6)$$

In a similar manner the theoretical transmittance T_E' is

$$T_E' = (T_H + T_H R_A R_H')(1 - R_A) \qquad (7)$$

The computer calculations were made by determining R_E' and T_E' with the Heavens equations and eq 5–7 for n and k incremented 0.1 at a time. Whenever the calculated R_E' and T_E' agreed with the experimentally determined R_E and T_E to within 0.02, the values of n and k were printed. The procedure was repeated for each data point corresponding to a given part of the spectrum.

In many cases there were several values of n and k which corresponded to the criterion for agreement of calculation and experiment. One reason for this is that the functions are sometimes double valued. Another reason is that in some regions, large changes in n and k produce relatively small changes in R_E' and T_E'. When the functions are double valued, n and k are selected to maintain smooth and continuous curves similar to the theoretical behavior described by Jenkins and White[10] which is represented in Figure 6.

If the experimental uncertainty in R_E and T_E were made lower than the estimated 0.02, the uncertainties in n and k would be smaller. However, this problem can be overcome to considerable degree by measuring R_E and T_E for more than one film. This is due to the fact that the wavelength regions at which n and k are indeterminate change as film thickness changes. To obtain satisfactory n and k values for a few values of λ for a given film, it was necessary to use data from another film.

The results of the above calculations for n and k are shown in Figure 7. Data points were obtained at about 2-cm^{-1} intervals except in regions where n and k appeared to be changing rapidly. In such regions 1- or even 0.5-cm^{-1} intervals were used. The typical uncertainty in n is about ± 0.25 and in k is about ± 0.15. Drawing a smooth curve through adjacent data points usually reduced this uncertainty.

(9) F. A. Jenkins and H. W. White, "Fundamentals of Optics," McGraw-Hill Book Co., Inc., New York, N. Y., 1950, p 563.
(10) Reference 9, p 473.

The Heavens equations were derived for light incident normal to the surface of the sample. In our reflectance experiments light approaches at an average angle 10° from the normal, but according to Bennett and Koehler,[6] and Jenkins and White,[11] the error caused by assuming normal incidence is small enough to be neglected.

Intensity Results

The absolute intensity Γ is related to k by

$$\Gamma = \frac{4\pi}{C}\int k\,d\nu \qquad (8)$$

where C is sample concentration in mmol cm^{-3}, the complex refractive index $\mathbf{n} = n - ik$ defines k, and ν is in cm^{-1}. By integrating the k curve in Figure 7 and using eq 8, the value of Γ was found to be 11.7 ± 1.3 cm^2 mmol^{-1}. The uncertainty given was estimated from the fact that an error of ±0.02 in R_E and T_E shifts k about 0.1–0.3. This estimate may be a poor indication of the precision of the method because a separate determination of Γ for a different film thickness gave agreement within 3%. This estimated error probably represents an upper limit.

Results obtained by various workers for the intensity of ν_{11} are given in Table I. From one of the transmittance spectra we computed by the method of Hollenberg and Dows[4] an apparent intensity of 15.9. This value is clearly too high by about 36%, although previous values reported in the literature are not as high as this. The reasons for variation in apparent absorption intensities may include the use of different instruments and somewhat different operating conditions.

The present value for Γ of 11.7 agrees well with our earlier estimate[1] of 12.3. This estimate was obtained from an apparent absorption intensity measurement of 16.0 using the approximate correction described by Jenkins and White,[12] which lowers T_0 by $(R - R_w)$, where R_w is the reflectance in the wings of the band. A partial correction of this nature is already commonly made for the nonabsorbing portion of a band by "fitting down in the wings" when apparent intensities are calculated. It will be interesting to see if this approximate correction works well in other cases, because the present reflection method is certainly more cumbersome than the apparent absorption intensity method.

Table I: Intensity Results for ν_{11} (a_{2u}) Fundamental of C_6H_6(s)

	Γ, cm^2 mmol^{-1}	Method
Hollenberg and Dows[a]	13.2 ± 1.7	Apparent absorption of thin film
Anderson and Person[b]	13.5 ± 3.4	Reflectance of bulk
Yamada and Person[c]	13.5 ± 2	Apparent absorption of thin film
Andermann and Chance[d]	22.3	Reflectance of bulk
Hollenberg and Glover[e]	12.3	Apparent absorption of thin film
This work	11.7 ± 1.3	Reflectance and transmittance of thin film

[a] Reference 4. [b] G. R. Anderson and W. B. Person, *J. Chem. Phys.*, 36, 62 (1962). [c] H. Yamada and W. B. Person, *ibid.*, 38, 1253 (1963). [d] Calculated by G. Andermann and K. Chance using a Kramers Kronig dispersion method with data of ref *b* (unpublished work). [e] Derived from apparent absorption intensity of 16.0 in ref 1.

Acknowledgment. Acknowledgment is made to the donors of the Petroleum Research Fund, administered by the American Chemical Society, for partial support of this research. D. E. G. wishes to thank the National Science Foundation and the California Foundation for Biochemical Research for fellowships.

Appendix

If

$$g_1 = \frac{n_0^2 - n_1^2 - k_1^2}{(n_0 + n_1)^2 + k_1^2}$$

$$h_1 = \frac{2n_0k_1}{(n_0 + n_1)^2 + k_1^2}$$

$$g_2 = \frac{n_1^2 - n_2^2 + k_1^2 - k_2^2}{(n_1 + n_2)^2 + (k_1 + k_2)^2}$$

$$h_2 = \frac{2(n_1k_2 - n_2k_1)}{(n_1 + n_2)^2 + (k_1 + k_2)^2}$$

$$A = 2(g_1g_2 + h_1h_2)$$

$$B = 2(g_1h_2 - g_2h_1)$$

$$C = 2(g_1g_2 - h_1h_2)$$

$$D = 2(g_1h_2 + g_2h_1)$$

$$\alpha_1 = 2\pi k_1d_1/\lambda$$

$$\gamma_1 = 2\pi n_1d_1/\lambda$$

where d_1 = film thickness, λ = wavelength, and n_0, n_1, k_1, n_2, and k_2 are defined by the diagram

n_0	vacuum
$n_1 - ik_1$	film
$n_2 - ik_2$	substrate

then

$$R_1 = \frac{(g_1^2 + h_1^2)\exp(2\alpha_1) + (g_2^2 + h_2^2)\exp(-2\alpha_1) + A\cos 2\gamma_1 + B\sin 2\gamma_1}{\exp(2\alpha_1) + (g_1^2 + h_1^2)(g_2^2 + h_2^2)\exp(-2\alpha_1) + C\cos 2\gamma_1 + D\sin 2\gamma_1}$$

(11) Reference 9, p 561.
(12) Reference 9, p 197.

is the reflectance of the film with light incident from the vacuum side.

$$R'_1 = \frac{(g_2^2 + h_2^2)\exp(2\alpha_1) + (g_1^2 + h_1^2)\exp(-2\alpha_1) + A\cos 2\gamma_1 + B\sin 2\gamma_1}{\exp(2\alpha_1) + (g_1^2 + h_1^2)(g_2^2 + h_2^2)\exp(-2\alpha_1) + C\cos 2\gamma_1 + D\sin 2\gamma_1}$$

is the reflectance when light is incident from the substrate side.

$$T_1 = \frac{n_2}{n_0}\frac{[(1 + g_1)^2 + h_1^2][(1 + g_2)^2 + h_2^2]}{\exp(2\alpha_1) + (g_1^2 + h_1^2)(g_2^2 + h_2^2)\exp(-2\alpha_1) + C\cos 2\gamma_1 + D\sin 2\gamma_1}$$

is the transmittance of the film for light incident from either side.

The Orthohydrogen–Parahydrogen Conversion and Hydrogen–Deuterium Equilibration on Sodium Tungsten Bronzes[1]

by F. T. Jones[2] and E. M. Loebl

Department of Chemistry, Polytechnic Institute of Brooklyn, Brooklyn, New York *(Received August 14, 1968)*

The parahydrogen conversion and H_2–D_2 equilibration were studied as a function of temperature and pressure on sodium tungsten bronzes of composition between $Na_{0.30}WO_3$ and $Na_{0.98}WO_3$. Conversion but not H_2–D_2 equilibration was observed at 77°K, indicating that conversion at low temperatures occurs by a magnetic mechanism. Both conversion and equilibration were observed at temperatures above 273°K. The results are best explained by a dissociative-adsorption mechanism over the pressure range 15–370 Torr. The pressure dependence of the rate constants, together with the equilibrium exchange of deuterium with a hydrogenated surface, indicate that the reaction occurs on sparsely separated regions of high local activity. In the region 273–473°K, $E_a = 6.8 \pm 0.2$ kcal/mol for the conversion on all of the cubic bronzes, but the Arrhenius preexponential factor shows a maximum at $Na_{0.7}WO_3$ similar to the maximum observed in the electrical conductivity for randomly selected crystals.

Introduction

The sodium tungsten bronzes are nonstoichiometric tungstates of sodium which can be represented by the formula Na_xWO_3, where $0 < x < 1$. The tungstate lattice is cubic with the perovskite structure at compositions above $x \approx 0.4$ and tetragonal below $x \approx 0.4$. In the cubic region the lattice constant increases uniformly with sodium content[3] obeying the equation $a(\text{Å}) = 0.0819x + 3.7846$, thus increasing by only 0.045 Å over the whole range. However, at the same time, the electronic properties depend markedly on composition.

Brown and Banks[4] and Gardner and Danielson[5] reported that the electrical resistivity decreases as the sodium content is increased up to the composition $Na_{0.70}WO_3$, but then increases again at higher sodium concentrations. The minimum at $x \approx 0.7$ was explained on the basis of a superlattice of ordered sodium ions at this composition. However, recent measurements made on crystals carefully selected for their homogeneity[6] with respect to resistivity indicate that the resistivity decreases continuously between $x = 0.4$ and 1.0 suggesting that the minimum at $x \approx 0.7$ was due, in part, to heterogeneous regions of high resistivity at high sodium concentrations. The Hall coefficient decreases and the number of conduction electrons increases, with increasing sodium content, but an anomalous inflection point[7] in the R_H *vs.* x and ρ *vs.* x curves suggests that (1) ordering may still be important and (2) the charge carriers cannot be treated by the free-electron model.

The present work was carried out in an attempt to correlate electrical properties of the sodium tungsten bronzes with their catalytic activity, using samples which had been prepared by methods which lead to a

(1) This work was supported in part by the Office of Naval Research under Contract No. NONR 839 (24) NR 051-405. Submitted in partial fulfillment of the degree Doctor of Philosophy at Polytechnic Institute of Brooklyn.

(2) Department of Chemistry, Stevens Institute of Technology Hoboken, N. J. 07030.

(3) B. W. Brown and E. Banks, *J. Am. Chem. Soc.*, **76**, 963 (1954).

(4) B. W. Brown and E. Banks, *Phys. Rev.*, **84**, 609 (1951).

(5) W. R. Gardner and G. C. Danielson, *ibid.*, **93**, 46 (1954).

(6) L. D. Ellerbeck, H. R. Shanks, P. H. Sidles, and G. C. Danielson, *J. Chem. Phys.*, **35**, 298 (1961).

(7) L. D. Muhlestein and G. C. Danielson, *Phys. Rev.*, **158**, 825 (1967).

minimum in the resistivity at $x \approx 0.7$. The parahydrogen conversion and H_2–D_2 equilibration were used since they are the simplest types of chemical reaction possible in a heterogeneous system.

Experimental Section

Materials. Electrolytic grade hydrogen (Airco, Inc.) and deuterium (99.5%, A. D. Mackay, Inc.) were purified by first passing through a liquid nitrogen trap to remove water vapor and then by diffusion through palladium thimbles at 300°. Krypton and helium for surface area determinations were assayed reagent grade (Airco, Inc.) and mass spectrometric analysis showed no detectable impurities. The bronze powders had been prepared in the laboratory of Professor E. Banks at this institute from mixtures of stoichiometric amounts of Na_2WO_4, WO_3, and tungsten by reaction in the solid state at 500–700° and the compositions were checked by chemical analysis and X-ray diffraction analysis.

Parahydrogen was prepared from normal hydrogen by adsorbing on degassed coconut charcoal at 77°K and cooling to 50°K by pumping on the liquid nitrogen bath. This temperature corresponds to an equilibrium concentration of 76% parahydrogen. The hydrogen was desorbed without significant decrease in the parahydrogen content by rapidly raising the temperature.

Apparatus. In some experiments the catalyst was degassed under ultrahigh vacuum. However, rapid parahydrogen conversion occurred on the metal bakeout valves and ionization gauge, so these components were dispensed with and conventional low pressures of 10^{-7} Torr were used. The quartz reaction cell (~25 cm^3) was connected *via* a graded seal and liquid nitrogen U trap to a Toepler gauge, thermistor gauge, and gas storage bulbs. The Toepler gauge was used to measure the pressure in the catalysis experiments and for the H_2 and Kr adsorption isotherms. Hydrogen adsorption was also studied on the bronzes with a thermistor gauge similar to that described by Rosenberg.[8]

In the catalysis experiments gas samples were periodically extracted from the reaction cell and analyzed by the Farkas thermal conductivity micromethod.[9] About 0.1 μmol of gas was sufficient for each analysis, so the change in total pressure during a run was insignificant over the pressure range used in the work. The thermal conductivity gauge was calibrated against normal hydrogen in the conversion experiments and against an H_2–D_2–HD mixture having the same H_2:D_2 ratio as the reactant gas but which had been equilibrated by passing over a hot nichrome spiral.

Results

Surface Areas. The surface areas of the catalysts were determined by krypton adsorption at 77°K, using helium to measure the dead volume of the reaction cell. The adsorption isotherm data conform to the BET equation up to relative pressures of at least $P/P_0 = 0.3$, and surface areas calculated by this method and the point B method[10] agree to within 4%. Assuming the cross-sectional area of an adsorbed krypton molecule[8] to be 19.4 $Å^2$, the surface areas of samples used in this work were within the range 0.10–0.18 m^2, corresponding to specific surface areas of 0.20–0.40 m^2/g.

Activation of the Catalyst. At constant temperature and total pressure the parahydrogen conversion and H_2–D_2 exchange invariably showed a logarithmic decay of the reactant concentration with time. This first-order behavior is always observed since both reactions are equivalent to simple isotopic exchange reactions.[11]

After degassing under vacuum, the bronzes showed a small but measurable activity which increased while in contact with hydrogen: at 423°K this activation process was very slow, at 448°K it lasted 5 days, and at 473°K it lasted about 3 days. The increase in activity at 448°K is shown in Figure 1 where the first-order rate

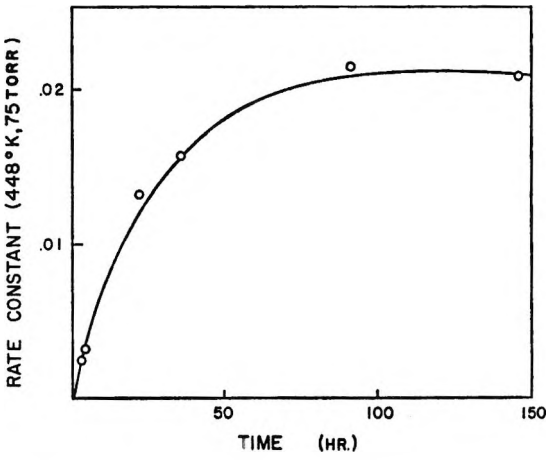


Figure 1. Activation of sodium tungsten bronze in H_2 at 448°K.

constant is plotted as a function of the total time in hydrogen. After activation the catalyst was stable for many weeks provided subsequent treatment did not poison the surface. An activated bronze could be partially deactivated merely by pumping for several hours, but the activity was again restored on standing in hydrogen. Intentional poisoning by air resulted in permanent deactivation, and a surface thus poisoned could not be reactivated by pumping or standing in hydrogen.

Temperature Dependence. Above 273°K the rate constants for the parahydrogen conversion increase with increasing temperature, obeying the Arrhenius equation over the range 273–473°K, within experimental error, as seen in Figure 2. The activation energies for most of the cubic bronzes in Table I lie

(8) A. J. Rosenberg, *J. Amer. Chem. Soc.*, **78**, 2929 (1956).
(9) A. Farkas, *Z. Physik. Chem.*, **B22**, 344 (1933).
(10) P. D. Emmett in "Catalysis," Vol. I, Reinhold Publishing Corp., New York, N. Y., 1954, Chapter 2.
(11) R. A. Marcus, *J. Chem. Phys.*, **23**, 1107 (1955).

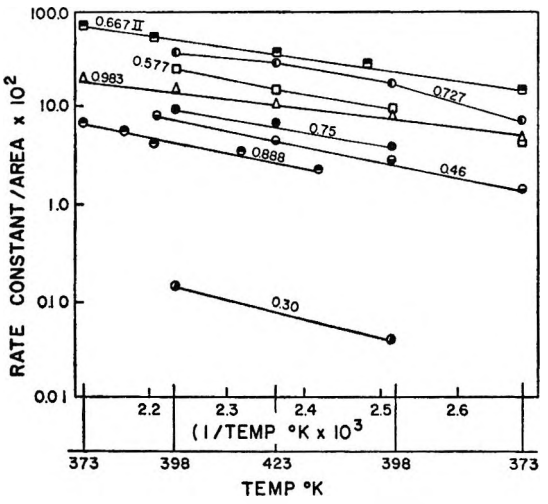


Figure 2. Temperature dependence of bronzes for high-temperature parahydrogen conversion at 80 Torr. Bronze compositions (x) are as indicated.

close to an average value of 6.8 ± 0.2 kcal/mol, with no discernible dependence on the sodium content of the bronze. In a few cases, however, much lower activation energies were obtained, and analysis of these samples by X-ray diffraction disclosed the presence of unreacted tungsten. The activation energy for the tetragonal bronze of composition $x = 0.30$, however, is anomalously high (9.2 kcal/mol).

Below 273°K the rate for parahydrogen conversion increases with decreasing temperature, thus showing a small negative apparent activation energy. This is shown in Figure 3 for the bronze of composition $Na_{0.58}WO_3$. Although the activity at 77°K is still several orders of magnitude below that in the high-temperature region, the minimum around 273°K is unmistakable.

In the high-temperature region the H_2–D_2 equilibration parallels the parahydrogen conversion, with rate constants roughly half as large as those for conversion.

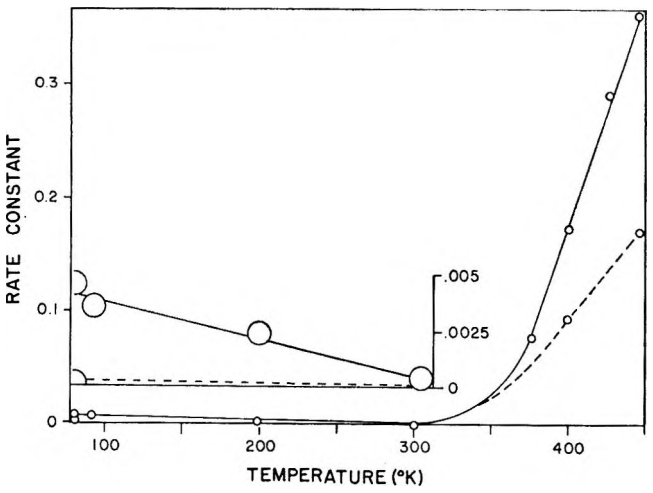


Figure 3. Temperature dependence of conversion (solid line) and equilibration (broken line) at 80 Torr for $Na_{0.58}WO_3$.

Table I: Dependence of b and E_a on Bronze Composition

x	b at 448°K, Torr	E_a, kcal/mol
0.300 (tetragonal)	...	9.2
0.460	130	6.9
0.577	206	7.2
0.584	1190	...
0.667	1450	7.1
0.727	...	6.1
0.750	395	6.7
0.888	...	6.7
0.983	...	4.3

However, equilibration is not detectable below 273°K and remains below the limits of detection down to at least 77°K.

Pressure Dependence. The parahydrogen conversion rate was measured as a function of pressure at several temperatures. In some cases the results fit an equation of the form $k = aP^{n-1}$, where a is a constant and n, the apparent order, is constant over the pressure range studied. For these bronzes the values of n were close to 0.5 ± 0.1. In many cases, however, the apparent order was not constant and decreased with increasing pressure. The H_2–D_2 equilibration showed the same pressure dependence as the parahydrogen conversion and yielded the same values of n.

Hydrogen Adsorption. Many attempts were made to determine hydrogen adsorption isotherms at temperatures between 77 and 473°K and covering a pressure range of 10^{-4}–400 Torr. At low pressures (up to 0.5 Torr) a thermistor gauge was used and at higher pressures the conventional Toepler gauge was used. It was not possible to detect hydrogen adsorption under any conditions for the 0.5-g samples used in this work. Attempts were made to measure adsorption isotherms both on freshly degassed "virgin" samples and on samples previously activated in hydrogen, with similar results. The accuracy of the pressure measurements was such that an uncertainty of 1% in the pressure (as an upper limit) at 0.5 Torr introduced an uncertainty of 0.03 in the fractional coverage of the geometrical surface area. Therefore, 0.03 represents the maximum coverage which could be involved in hydrogen adsorption.

Further attempts were made to determine the extent of hydrogen adsorption by following the exchange of deuterium in the gas phase with hydrogen adsorbed on the surface. A bronze which had been in contact with H_2 for several weeks at 448°K was pumped on for about 45 min to remove the weakly adsorbed hydrogen, and then a low pressure of D_2 (~3 Torr) was introduced. A slow first-order reaction occurred, producing measurable amounts of H_2 or HD. Under these conditions, however, the thermal conductivity method is not able to identify which of these products is formed. It was possible to calculate the equilibrium concentration from

the kinetic data and the equation[12]

$$kt + \ln (C - C') = \ln [(C_0 - C_\infty)(1 - e^{-k\Delta})]$$

where C and C' are the concentrations at times t and $t + \Delta$, respectively, and C_0 and C_∞ are the initial and equilibrium concentrations, respectively. The calculated value of C_∞ agreed with the value measured after 20 hr. If H_2 is produced by exchange of D_2 with adsorbed hydrogen atoms, the results indicate a fractional coverage of 0.017; on the other hand, if HD is produced, the fractional coverage is 0.034. The same results were obtained when the reaction was carried out in the reverse direction, *i.e.*, exchange of H_2 with adsorbed deuterium. These results are consistent with the conclusion of the previous paragraph.

Deactivation of the Catalyst. Measured amounts of air were mixed with the parahydrogen to determine the effect of intentionally poisoning the surface. With a pressure of 5×10^{-3} Torr of air in 75 Torr of H_2, no effect was noticed, but at 22×10^{-3} Torr the activity at 448°K was reduced by 50% in less than 10 min. This quantity of air was sufficient to cover about 10% of the surface area if completely adsorbed. Larger amounts of air and longer contact times caused more extensive deactivation. This type of deactivation was irreversible, for the original activity could not be recovered by contact with hydrogen or degassing at temperatures as high as 640°K followed by the usual hydrogen activation treatment. The activity at 77°K was reduced by the same amount as the activity at high temperatures, and it is therefore concluded that the low-temperature parahydrogen conversion is not due to adsorbed molecular oxygen but is associated with paramagnetic sites on the surface of the bronze.

Discussion

Kinetics of the Reaction. The rate of change of reactant concentration in a heterogeneous reaction depends on both the surface area and the number of reactant molecules in the system. If the experimental rate constant, k_e, is determined from the change in concentration of the gas volume above the catalyst, $k_e = (1/t) \ln (C_0/C)$ for a first-order reaction. A rate constant for the surface reaction, k_s, can be defined by the relationship

$$k_e = (A/N)k_s \qquad (1)$$

where A is the surface area of the catalyst and N is the total number of moles of H_2 in the system. Since the amount of adsorbed hydrogen is very small in comparison with the gas phase and was below the limits of detection in this work, N can be taken to be the number of moles in the gas phase: $N = PV/RT$.

The rates for parahydrogen conversion and H_2–D_2 equilibration are similar at high temperatures, indicating that the reaction proceeds through adsorbed hydrogen atoms. The constancy of the Arrhenius activation energy suggests that the surface is energetically homogeneous and that a simple Langmuir adsorption mechanism may apply. For dissociative adsorption of H_2 at a surface site S

$$H_2 + 2S \underset{k_{-1}}{\overset{k_1}{\rightleftharpoons}} 2SH \qquad (2)$$

the fraction of the sites which are covered by hydrogen atoms, θ, is given by

$$\theta = \frac{\sqrt{P}}{\sqrt{P} + \sqrt{b}} \qquad (3)$$

where b is the desorption:adsorption rate constant ratio, k_{-1}/k_1. If eq 2 also describes the mechanism for parahydrogen conversion and deuterium exchange (Bonhoeffer–Farkas mechanism) and if adsorption is the rate-determining step, $k_s = kP(1 - \theta)^2$ for an immobile layer. Therefore

$$\frac{1}{\sqrt{k_e/A}} = \frac{\sqrt{P}}{\sqrt{bk'}} + \frac{1}{\sqrt{k'}}$$

where $k' = (RT/V)k$. Alternatively, if desorption is the rate-determining step, $k_s = k\theta^2$ and

$$\frac{1}{\sqrt{k_e/A}} = \frac{\sqrt{P}}{\sqrt{k'}} + \frac{\sqrt{b}}{\sqrt{k'}}$$

Both cases lead to an equation of the form

$$\frac{1}{\sqrt{k_e/A}} = M\sqrt{P} + N \qquad (4)$$

which predicts that $1/\sqrt{k_e/A}$ should be a linear function of $\sqrt{P}$ and that $\sqrt{b} = N/M$. Figures 4 and 5 show that the linear relationship is obeyed within experimental error. Values of b are given in Table I for the cubic bronzes.

When k_s can be described by both a Langmuir-type dissociative-adsorption isotherm and an empirical Freundlich isotherm $k_s = kP^n$, then $d \ln k_s/dP$ should be the same in both cases and it can be shown that $\theta = 1 - n$. Accepting $n = 0.5$ from the kinetic results, $\theta = 0.5$. This is clearly in disagreement with the adsorption experiments which led to the conclusion that only ~1–3% of the geometrical surface area is active in adsorption but may be reconciled by assuming that parahydrogen conversion can occur only on these adsorbing areas. Thus, using the limits quoted above, the fraction of the surface taking part in catalysis lies between 0.005 and 0.01.

It is not possible to determine whether adsorption or

(12) A. A. Frost and R. G. Pearson, "Kinetics and Mechanism," 2nd ed, John Wiley & Sons, Inc., New York, N. Y., 1965, p 45.

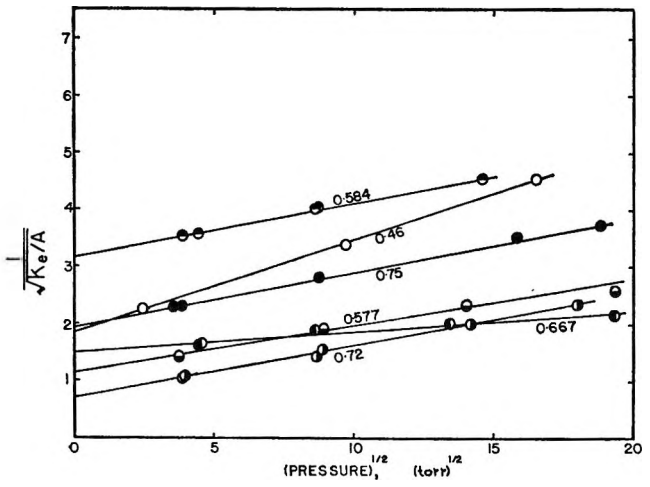


Figure 4. Test of eq 4 for parahydrogen conversion at 448°K. Bronze compositions (x) are as indicated.

desorption is the rate-determining step, since both cases lead to an equation of the form given by (4). Indeed, from the values of $b = k_{-1}/k_1$ in Table I, it can be shown that at a pressure of 400 Torr desorption may be rate determining ($b/P < 1$) for bronzes of composition x = 0.46, 0.577, and 0.75, but adsorption may be rate determining ($b/P > 1$) for x = 0.584 and 0.667. Alternatively, for x = 0.46, 0.577, and 0.75, adsorption may be the slow step at the low-pressure limit of the present work (15 Torr) but desorption is the slow step at 400 Torr. Nevertheless, when dissociative adsorption of hydrogen is rate determining, k_s should be given by the expression[13]

$$k_s = Z\alpha F(1 - \theta)^2 e^{-E/RT} \qquad (5)$$

where $Z = P/\sqrt{2\pi mkT}$ is the number of molecules colliding with the surface cm^{-2} sec^{-1}, α is the sticking probability, E can be equated to the experimental activation energy, and F is the fraction of the geometrical surface area which is catalytically active. Assuming $\alpha = 0.1$, $\theta = 0.5$, and $E = 6.8$ kcal/mol, k_e/A calculated from (5) and (1) is in agreement with the values in Figures 3–5 if $F \approx 3 \times 10^{-3}$, consistent with the conclusions of the previous paragraph that the active surface area is a very small fraction of the geometrical area.

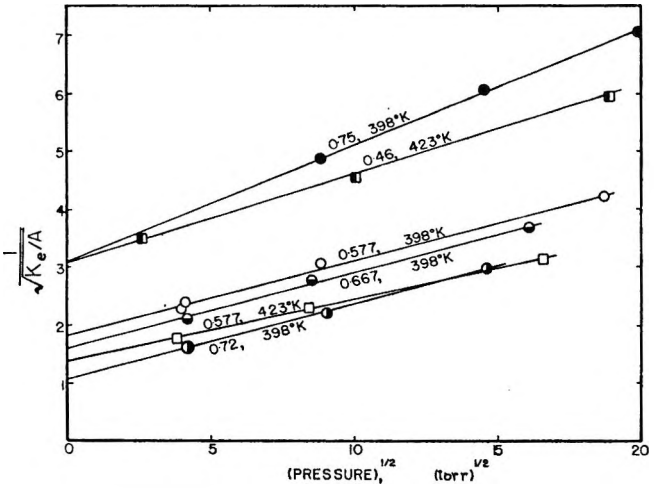


Figure 5. Test of eq 4 for parahydrogen conversion at 398 and 423°K. Bronze compositions and temperatures are as indicated.

The heat of adsorption, ΔH_a, can be calculated[14] from the temperature dependence of b. The data in Figures 4 and 5 indicate that b is practically independent of temperature in most cases, implying $\Delta H_a \approx 0$. Therefore the apparent activation energies in Table I are close to the true activation energies for the surface reaction. The small values of ΔH_a and of the apparent order n suggest that the reaction is occurring on fairly saturated regions of the surface. However the small values for total coverage require that these active regions be few in number.

The rate constants for conversion and equilibration at low pressures (<10 Torr) on metallic surfaces have been found to obey an equation of the form[15]

$$1/k_e = MP + N \qquad (6)$$

which would be expected if the reaction proceeded through a three-body complex between adsorbed hydrogen atoms and H_2 molecules in the second layer (Eley–Rideal mechanism). The results of the present work obey eq 4 at least over the pressure range 15–370 Torr but not eq 6.

Dependence on Catalyst Composition. Catalytic activity of surfaces can often be correlated with electronic properties of the solid. The increase in activation energy in Pd–Au[16] and Ni–Cu[17] alloy systems as the concentration of transition element is increased has been ascribed to a reduction of charge carriers as the d orbitals are filled. In many cases a compensation effect is observed between the activation energy and the preexponential factor when both E_a and A are found to change.

The activation energy for the parahydrogen conversion on sodium tungsten bronzes is independent of composition for the cubic bronzes and is close to the gas-phase value of 6 kcal/mol. However, the rate constant and hence the preexponential factor show a marked dependence on composition, passing through a maximum at $Na_{0.7}WO_3$. This behavior closely parallels the maximum in electrical conductivity which has been reported for these samples,[4] as shown in Figure 6 where

(13) D. R. Ashmead, D. D. Eley, and R. Rudham, *Trans. Faraday Soc.*, **59**, 207 (1963).

(14) G. C. Bond, "Catalysis by Metals," Academic Press, London, 1962, p 70.

(15) S. J. Holden and D. R. Rossington, *J. Phys. Chem.*, **68**, 1061 (1964).

(16) A. Couper and D. D. Eley, *Discussions Faraday Soc.*, **8**, 172 (1950).

(17) D. A. Dowden and P. W. Reynolds, *ibid.*, **8**, 184 (1950).

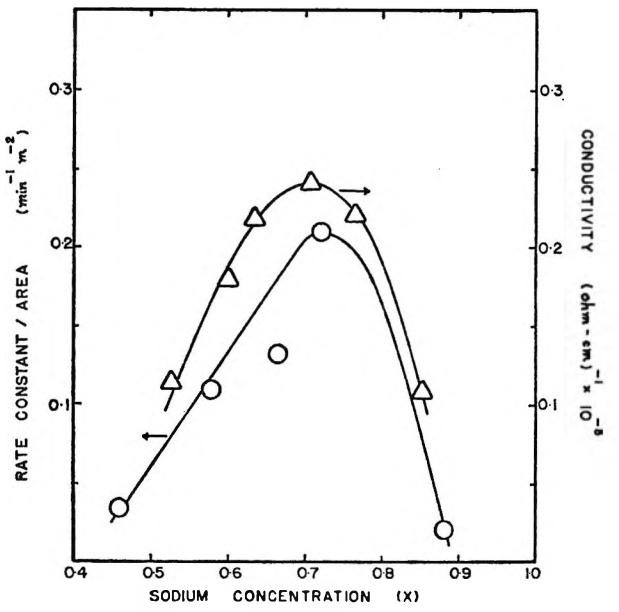


Figure 6. Dependence of catalytic activity for conversion (○) and electrical conductivity (△) on bronze composition. Conductivities calculated from data of Brown and Banks.

both rate constant per area and conductivity are plotted as a function of bronze composition.

An increase in either the extent of hydrogen adsorption or the rate of desorption could lead to an increase in catalytic activity. Although an increase in the extent of adsorption (F in eq 5) cannot be ruled out, Table I clearly shows that the desorption:adsorption rate constant ratio, b, is largely responsible for the maximum in catalytic activity at $x = 0.7$. If hydrogen is present on the surface as adsorbed ions and neutralization is necessary before desorption can occur, then the enhanced desorption rate can be interpreted as an enhanced accessibility of conduction electrons from the solid. Alternatively, if the diffusion of hydrogen atoms along the surface prior to desorption is rate determining, enhanced electrical conductivity should lead to greater mobility of adsorbed atoms and an increased rate of desorption.

Oxide catalysts usually require an adaptation period in the presence of the reactant gas before reproducible results can be obtained. Stone[18] has explained this activation process as a gradual enrichment of the surface layers with interstitial metal cations. Such a process would appear to be too permanent to explain the rapid reversible deactivation which occurs when hydrogen is removed from the sodium tungsten bronzes or the irreversible poisoning when oxygen is admitted to an activated surface. A more tenable explanation is that the activation process consists of diffusion of hydrogen into the lattice to alter the electronic properties of the surface and several adjacent layers. The rapid para-hydrogen conversion must still occur predominantly on the surface, however, since diffusion of hydrogen out of the lattice would be a slow process. Irreversible oxygen poisoning could then result if oxygen atoms are allowed to diffuse into the hydrogenated lattice to form H_2O or OH trapped in interstitial positions.

Acknowledgment. The authors are grateful to Professor E. Banks for supplying the bronze samples and for many helpful discussions, to Dr. I. Sarfati for suggesting improvements in the manuscript, and to the E. I. du Pont Educational Fund for a grant-in-aid.

(18) F. S. Stone in "Chemistry of the Solid State," W. E. Garner, Ed., Butterworth and Co. Ltd., London, 1955, p 400.

Relation between Local Structure and Thermodynamic Properties in Aqueous Fluids

by Frank H. Stillinger, Jr., and Arieh Ben-Naim

Bell Telephone Laboratories, Incorporated, Murray Hill, New Jersey *(Received August 26, 1968)*

Using the conventional statistical-mechanical theory of concentration fluctuations, we examine the nature of local molecular structure in water and aqueous solutions. In particular, we evaluate Δ_H, the excess number of water-molecule protons in the region surrounding (but exterior to) a fixed water molecule. By comparing the temperature dependence of Δ_H with its analogs for alcohols and liquid methane, the anomalous nature of liquid water is affirmed. In the case of a few aqueous solutions for which both isothermal compressibilities and partial molar volumes at infinite dilution are available, the initial composition dependence of Δ_H has been obtained. The sign and magnitude of this solute effect on local water-molecule order constitutes a new way to classify these solutes as "structure formers" or "structure breakers."

I. Introduction

The invention and development of powerful theoretical techniques in recent years has produced significant progress in understanding the liquid state,[1,2] but it is fair to say that this progress has been confined largely to "simple fluids," that is, substances such as the noble gases whose constituent particles are actually (or nearly) spherical. Of incomparably greater importance in physical chemistry though are liquids composed of polyatomic molecules whose noncentral interactions produce characteristic chemical distinctions.

Foremost among the polyatomic liquids of course is water. There is ample experimental evidence that water is an anomalous substance both in pure form and as a solvent.[3] In the quest for a satisfactory quantitative description of the enormous range of chemical and biological reactions that occur in aqueous media, it surely will be necessary to devise a deductive theory first that predicts the anomalous behavior of water itself from fundamental principles.

The goal in this paper, however, is not the development of a first-principles theory of liquid water and aqueous solutions. Instead, our more modest aim is to produce a quantitative measure of hydrogen-bond order in aqueous fluids. As is the case with all other techniques that have been applied to this problem, whether spectroscopic, thermodynamic, or kinetic, the result is far less than a complete characterization of molecular order. However, we believe that addition of yet another measure of structure in water, and one which is independent of others currently available, will hasten the construction of the desperately needed fundamental statistical-mechanical theory of water.

The next section provides our line of reasoning for pure water. We show that experimental density and isothermal compressibility data, supplemented by some elementary knowledge of molecular structure, lead to a numerical measure, Δ_H, of local hydrogen-bond order in the liquid. Specifically, Δ_H equals the average proton excess in the proximity of (but exterior to) a fixed water molecule. Both pressure and temperature effects on Δ_H are exhibited.

The third section broadens our analysis to include other hydrogenic liquids. To provide suitable contrasts for water, both methane (essentially a "simple fluid") and the aliphatic alcohols are examined. Even allowing for hydrogen bonding, water behaves anomalously.

Aqueous solutions are the object of attention in the fourth section. Partial molar volume measurements, along with isothermal compressibilities, for varying composition permits computation of the solute effect on Δ_H. The sign and magnitude of this effect comprises a convenient criterion for dividing substances into "structure-making" and "structure-breaking."[4]

The final discussion section provides a few comments on our method and tentative interpretation of our computations. Also we stress in that section the need for broader and more accurate solution data.

II. Pure Water

The key relation in our consideration of pure water is the rigorous fluctuation–compressibility theorem[5] which links the isothermal compressibility κ_T with the fluid's pair correlation function $g^{(2)}(r)$

$$kT\kappa_T = c^{-1} + \int [g^{(2)}(r) - 1]\mathrm{d}\mathbf{r} \qquad (1)$$

Here k is the Boltzmann constant, T is the absolute temperature, c is the number density, and $g^{(2)}(r)$ must be regarded as the infinite-system limit function with asymptote unity so that the integral can span all space.

(1) H. L. Frisch and J. L. Lebowitz, "The Equilibrium Theory of Classical Fluids," W. A. Benjamin, Inc., New York, N. Y., 1964.

(2) S. A. Rice and P. Gray, "The Statistical Mechanics of Simple Liquids," Interscience Publishers, New York, N. Y., 1965.

(3) J. L. Kavanau, "Water and Solute-Water Interactions," Holden-Day, Inc., San Francisco, Calif., 1964.

(4) H. S. Frank and W.-Y. Wen, *Discussions Faraday Soc.*, **24**, 133 (1957).

(5) T. L. Hill, "Statistical Mechanics," McGraw-Hill Book Co., Inc., New York, N. Y., 1956, p 236.

For simple fluids consisting of spherically symmetric molecules it is natural to reckon the "position" of any given molecule as coincident with its geometric center, *i.e.*, its centroid. In fact, though, the fluctuation–compressibility theorem (1) is invariant to a shift of "position" of molecules relative to their centroids, for $g^{(2)}(r)$ is then modified merely by double convolution with a unit-integral kernel, and this operation leaves the integral in the right member of eq 1 unchanged.[6]

A similar observation is valid in the case of water. We thus have the option of supposing that the position of any given water molecule is precisely the position of its oxygen nucleus. With this convention, eq 1 for water may be written

$$kT\kappa_T = c^{-1} + \int [g_{OO}^{(2)}(r) - 1]d\mathbf{r} \qquad (2)$$

to stress the specific use of the pair correlation function for oxygen nuclei. A point of conceptual interest in eq 2 is that it has the outward appearance of a fluctuation–compressibility relation for an assembly of oxygen atoms; the protons play merely the passive (but extremely important!) role of providing the correct potential function for the set of oxygens as they move about.

One also has the freedom to take the reverse point of view, namely that the protons are the "important" particles upon which to focus attention, with the oxygens merely present to produce the correct potential function for those protons as they move about. The relation entirely analogous to eq 2 that applies to this alternative point of view is

$$kT\kappa_T = (2c)^{-1} + \int [g_{HH}^{(2)}(r) - 1]d\mathbf{r} \qquad (3)$$

We use here an obvious notation for the pair correlation function for the protons, and it has been recognized that their number density is twice that of the oxygens.

A further transformation is possible that stems from the view of liquid water as an electrolyte, albeit an extremely weak one. Thus water may be regarded as a stoichiometric mixture of doubly charged anions (the oxygens) and singly charged cations (the protons), and since this electrolyte has a nonvanishing conductivity, it is subject to microscopic electroneutrality conditions. In terms of $g_{OO}^{(2)}$, $g_{HH}^{(2)}$, and the cross-correlation function $g_{OH}^{(2)}$, these conditions are[7]

$$1 = c\int [g_{OH}^{(2)}(r) - g_{OO}^{(2)}(r)]d\mathbf{r} \qquad (4)$$

$$1 = 2c\int [g_{OH}^{(2)}(r) - g_{HH}^{(2)}(r)]d\mathbf{r} \qquad (5)$$

The first of these two conditions affirms that the net average charge in the vicinity of any oxygen anion is precisely equal in magnitude but opposite in sign to the anion's charge. The second, eq 5, provides the equivalent statement for average charge surrounding any proton.

Equation 4 may next be used to eliminate $g_{OO}^{(2)}$ from eq 2. The result is the same as one obtains by using eq 5 to eliminate $g_{HH}^{(2)}$ from eq 3

$$kT\kappa_T = \int [g_{OH}^{(2)}(r) - 1]d\mathbf{r} \qquad (6)$$

It is this last form of the fluctuation–compressibility relation that is most useful in assessing intermolecular structure in water.

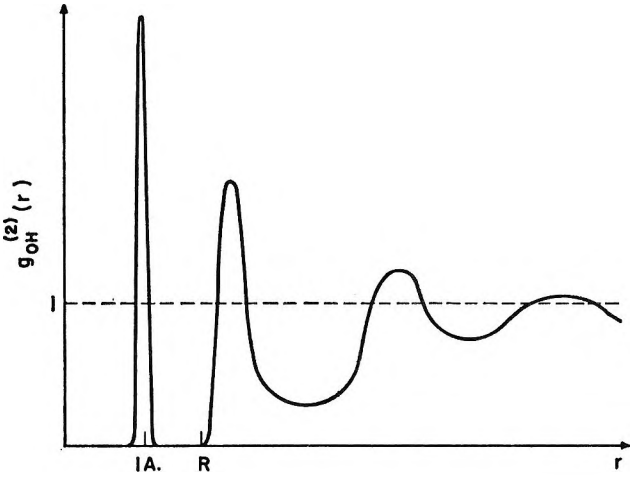


Figure 1. Schematic diagram of the cross-correlation function $g_{OH}^{(2)}(r)$ for liquid water. The sharp peak around 1 Å is the contribution of the intramolecular O–H covalent bonds. The distance R is a lower bound to all intermolecular O···H pair distances, the smallest group of which represent direct hydrogen bonds between pairs of water molecules. $g_{OH}^{(2)}(r)$ for sufficiently large r approaches the limit unity.

Figure 1 provides a schematic plot of the cross-correlation function $g_{OH}^{(2)}$. As a distance r increases from zero, $g_{OH}^{(2)}$ at first is zero, but in the neighborhood of 1 Å, this function will have a high and narrow peak corresponding to the intramolecular covalent O–H bond distance. Although thermal motion and inherent positional indeterminacy of quantum-mechanical origin conspire to give this first peak a natural width, it should nevertheless be virtually isolated. The remaining oxygen–hydrogen distances will equal or exceed the distance of closest approach in hydrogen bonding. From the distances measured in ice (2.76 Å between neighboring oxygen atoms)[8] we conclude that

$$R = 1.75 \text{ Å} \qquad (7)$$

(6) The integrand of course does change under this process.

(7) Local electroneutrality conditions of this sort are basic in standard electrochemical theory. They provide for instance a means of determining one of the integration constants in the Debye–Hückel theory of ion atmospheres; see, for instance, R. A. Robinson and R. H. Stokes, "Electrolyte Solutions," Butterworth and Co. Ltd., London, 1955, p 78.

(8) Reference 3, p 1.

is a suitable greatest lower bond on intermolecular O···H distances. Figure 1 indicates the position R will be well to the large-r side of the isolated intramolecular peak.

We now split the integral in eq 6 into two parts

$$kT\kappa_T = 4\pi \int_0^R [g_{OH}^{(2)}(r) - 1]r^2dr + 4\pi \int_R^\infty [g_{OH}^{(2)}(r) - 1]r^2dr \quad (8)$$

Were it not for the intramolecular isolated peak in the range $0 \leq r \leq R$, the integrand of the first integral in (8) would be simply -1, and the integral would be trivial to perform. However, the intramolecular peak provides an additional contribution to the integral which, for precisely two protons per water molecule,[9] is easily seen to yield

$$4\pi \int_0^R [g_{OH}^{(2)}(r) - 1]r^2dr = -(4\pi R^3/3) + (1/c) \quad (9)$$

This reduction allows eq 8 to be rewritten thus

$$kT\kappa_T = -(4\pi R^3/3) + (1/c) + 4\pi \int_R^\infty [g_{OH}^{(2)}(r) - 1]r^2dr \quad (10)$$

The average proton density at radial distance r from any oxygen atom is by definition $2cg_{OH}^{(2)}(r)$. Therefore, the quantity

$$\Delta_H = 2c \int_R^\infty [g_{OH}^{(2)}(r) - 1] \times 4\pi r^2dr \quad (11)$$

equals the local average excess number of protons outside a radius-R sphere surrounding an oxygen atom in water, compared to the overall proton density $2c$. By multiplying eq 10 through by $2c$ and transposing terms, we obtain an expression for the microscopic quantity Δ_H in terms of macroscopic observables

$$\Delta_H = 2kTc\kappa_T - 2 + (8\pi R^3c/3) \quad (12)$$

If the protons outside the R sphere were completely disordered, and thus uniformly distributed with density $2c$, the quantity Δ_H would vanish identically. Of course, the protons are not uniformly distributed in this exterior region as a result of the various forces operative. Principal among these is hydrogen bonding, and the first peak for $r > R$ in Figure 1 represents protons directly hydrogen bonded to the central oxygen. Presuming some suitable choice of maximum permissible distance for definition of hydrogen bonding, one could obtain the number of hydrogen bonds in liquid water directly from a curve such as Figure 1. Successive peaks and valleys of $g_{OH}^{(2)}(r)$ beyond $r = R$ contain contributions of longer and longer chains of hydrogen bonds. It is thus clear that Δ_H provides an overall measure of local hydrogen-bond order in water.

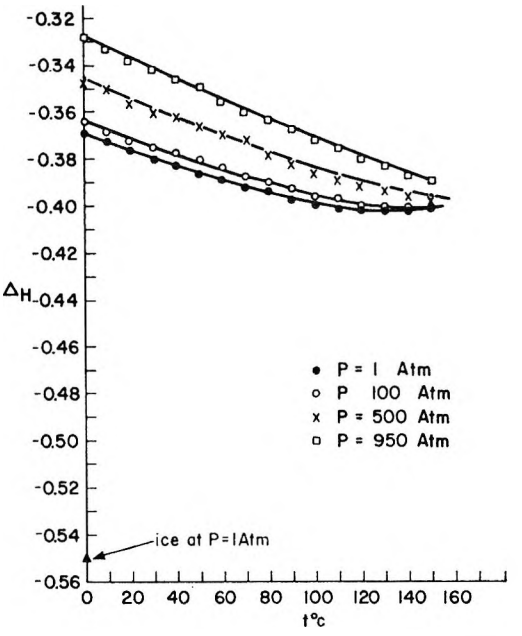


Figure 2. Local proton excess Δ_H for liquid water at various pressures, in the temperature range 0–150°. The value for ice at 1 atm and 0° has been included for comparison and differs very little from the value for ice at absolute zero. Above 100°, the $P = 1$ curve uses c and κ_T values extrapolated from higher pressures.

With the specific choice for R shown in eq 7, Δ_H has been evaluated from eq 12 for pure water. Figure 2 presents Δ_H in the temperature range 0–150° for several pressures. The required density and compressibility data for the calculations were obtained from the measurements of Kell and Whalley.[10] For comparison, Δ_H has also been computed for ice at 0° and 1 atm,[11] using the compressibility reported by Jona and Scherrer.[12] The fact that the "excess" Δ_H turns out to be negative merely indicates a local deficit of protons outside the R sphere in the temperature range considered.

A more extended temperature range for Δ_H is shown in Figure 3 (0–360°), but all confined to 325 atm. The necessary density and compressibility data were taken from Dorsey's compilation.[13] The obvious point of interest is the fact that the negative Δ_H for low temperature passes through a minimum and then increases to relatively large positive values. We defer comment on this phenomenon until the final discussion section.

(9) We disregard now the very small fraction ($\leq 10^{-7}$) of dissociated molecules.

(10) G. S. Kell and E. Whalley, *Phil. Trans. Roy. Soc. London*, **285**, 565 (1965).

(11) For ice it is necessary to interpret the correlation functions in their translationally and orientationally averaged sense. Otherwise the fluctuation–compressibility theorem takes a more elaborate form involving the solid's elastic constants; see F. H. Stillinger, Jr., *Phys. Rev.*, **142**, 237 (1966).

(12) F. Jona and P. Scherrer, *Helv. Phys. Acta*, **25**, 35 (1952).

(13) N. E. Dorsey, "Properties of Ordinary Water-Substance," Reinhold Publishing Corp., New York, N. Y., 1940.

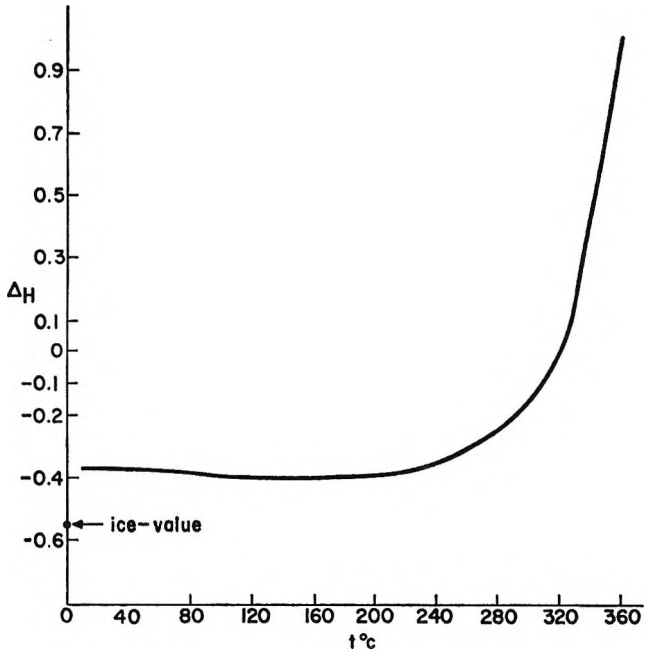


Figure 3. Variation of Δ_H for water with temperature up to about the critical temperature. The pressure is fixed at 325 atm.

III. Comparison with Other Pure Fluids

Unless equivalent structural information is available for other substances, the Δ_H values just exhibited for pure water are difficult to appreciate or interpret. For that reason we now extend our procedure to cover other liquids. Most commentary is reserved for the final section.

A. Methane. As a first example we consider methane, principally because it should typify the behavior of nonhydrogen-bonded fluids of compact molecules. The two obvious forms of the fluctuation–compressibility theorem, analogous to previous eq 2 and 3 for water, are

$$kT\kappa_T = c^{-1} + \int [g_{CC}^{(2)}(r) - 1]d\mathbf{r} \qquad (13)$$

and

$$kT\kappa_T = (4c)^{-1} + \int [g_{HH}^{(2)}(r) - 1]d\mathbf{r} \qquad (14)$$

Liquid methane under ordinary circumstances exhibits no detectable ionization, but still one formally has local electroneutrality conditions connecting the carbon–carbon and proton–proton correlation functions $g_{CC}^{(2)}$ and $g_{HH}^{(2)}$ to the carbon–proton cross-correlation function $g_{CH}^{(2)}$ [14]

$$1 = c\int [g_{CH}^{(2)}(r) - g_{CC}^{(2)}(r)]d\mathbf{r} \qquad (15)$$

$$1 = 4c\int [g_{CH}^{(2)}(r) - g_{HH}^{(2)}(r)]d\mathbf{r} \qquad (16)$$

These last relations may be used to convert either eq 13 or eq 14 to the analog of eq 6 for water

$$kT\kappa_T = \int [g_{CH}^{(2)}(r) - 1]d\mathbf{r} \qquad (17)$$

The cross-correlation function $g_{CH}^{(2)}$ for liquid methane should behave qualitatively in very much the same way as shown in Figure 1 for its water analog. The major quantitative differences are that the isolated intramolecular peak should correspond to four protons (*vs.* two in water) and should occur at about 1.095 Å;[15] also the fact that the lattice spacing in solid methane is 4.16 Å[16] means that virtually no intermolecular C···H pairs can occur below a greatest lower bound of

$$R = 3.06 \text{ Å} \qquad (18)$$

In the same manner as before, we split the radial integration in eq 17 into two ranges, 0 to R and R to ∞. Then the former may be carried out explicitly, and the latter interpreted as a local proton excess for methane. We again denote this excess by Δ_H. One finally obtains the expression

$$\Delta_H = 4kTc\kappa_T - 4 + (16\pi R^3 c/3) \qquad (19)$$

where for methane

$$\Delta_H = 4c\int_R^\infty [g_{CH}^{(2)}(r) - 1] \times 4\pi r^2 dr \qquad (20)$$

Figure 4 displays the methane Δ_H, evaluated in the liquid phase at the vapor pressure, from 100–160°K.[17]

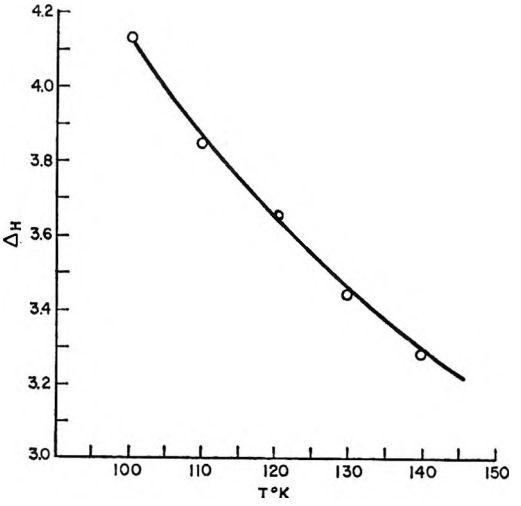


Figure 4. Local proton excess Δ_H for liquid methane in coexistence with its vapor.

(14) In deriving these relations, methane is formally regarded as a mixture of quadruply charged anions (the carbon atoms) and singly charged cations (the hydrogens).

(15) L. Pauling, "The Nature of the Chemical Bond," Cornell University Press, Ithaca, N. Y., 1960, p 226.

(16) H. W. Schamp, Jr., E. A. Mason, A. C. B. Richardson, and A. Altman, *Phys. Fluids*, 1, 329 (1958).

(17) For comparison, note that methane's triplet-point temperature is 90.6°K, and its critical temperature is 190.16°K.

The requisite density and compressibility data were taken from the recent paper by Grigor and Steele.[18] The results are in marked contrast to those for water; they are large and positive and seem to decline in magnitude smoothly as T increases.

B. Alcohols. The alcohols constitute an interesting class of liquids in the present context because, like water, they are strongly associated by hydrogen bonding. Nevertheless, their physical, chemical, and biological properties are sufficiently different from those of water to lead one to expect rather different local structure.

One conceptual complication now intrudes. The alcohols contain protons not only as part of the hydroxyl groups, but also in the alkyl groups as well. However, under ordinary conditions the exchange rate between these two classes of protons will be negligible, so they may be regarded as distinguishable. Since the hydroxyl protons are the ones directly involved in the structure-forming hydrogen bonding, they are the only ones we shall consider. The alkyl-group protons will be disregarded.

Derivation of the alcohol Δ_H follows the same pattern as before. In the case of monohydroxy alcohols, with one oxygen atom and one relevant proton per molecule, the local excess of these relevant hydroxyl protons outside a fixed oxygen-centered R sphere is found to be

$$\Delta_H = kTc\kappa_T - 1 + (4\pi R^3 c/3) \qquad (21)$$

where the correlation-function definition of the local excess is

$$\Delta_H = c\int_R^\infty [g_{OH}^{(2)}(r) - 1] \times 4\pi r^2 dr \qquad (22)$$

There is evidence that alcohols are able to form slightly shorter hydrogen bonds than water. A study[19] of the methanol crystal shows for example that nearest-neighbor hydrogen-bonded oxygen atoms are separated by only 2.66 Å, or about 0.10 Å less than in water. Furthermore, the first peak of the radical distribution functions measured for liquid methanol and ethanol[20] indicates that this shrinkage relative to water applies also after melting. However, it is also known that the covalent O–H bond length at least for methanol is somewhat smaller than for water.[21] Therefore, we feel justified in using the same R value for alcohols that was shown in eq 7 for water.

Figure 5 shows Δ_H for methanol and ethanol at 1 atm in the temperature range 0–60°.[22] Regrettably, simultaneous density and compressibility data for the higher alcohols are available only at 0°,[23] so these substances are represented only by single points on the graph. The notable features are that Δ_H is negative just as for water (but unlike methane), but in contrast to water the slopes of at least the two curves shown are positive. In the limit of very long aliphatic chain length for the homologous series of normal alcohols, eq 21 indicates

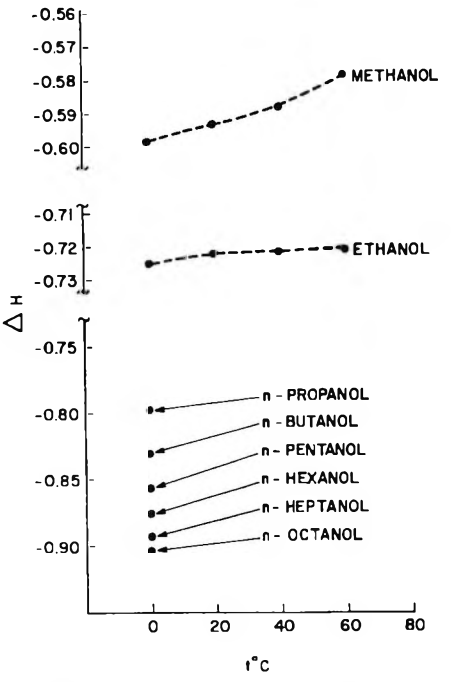


Figure 5. Δ_H values for some normal aliphatic alcohols. The pressure is 1 atm.

that Δ_H should formally converge to the temperature-independent constant -1.

IV. Binary Aqueous Solutions

The variations of Δ_H for pure water with changing temperature and pressure reflect the way that these externally controlled parameters affect local molecular structure. Another sort of perturbation that is available to the experimenter is addition of solutes to the water. In view of the large current interest in this solute effect on water structure, especially with regard to the so-called "hydrophobic bond,"[24,25] we now show that Δ_H can also serve as a useful probe for structure in aqueous solutions.

We restrict attention solely to binary aqueous solutions. The general Kirkwood–Buff solution theory[26] provides the necessary starting point in the form of an expression for the integral of the water–water pair correlation function. If we let subscript 1 refer to

(18) A. F. Grigor and W. A. Steele, *J. Chem. Phys.*, **48**, 1032 (1968).
(19) K. J. Tauer and W. N. Lipscomb, *Acta Cryst.*, **5**, 606 (1952).
(20) D. L. Wertz and R. K. Kruh, *J. Chem. Phys.*, **47**, 388 (1967).
(21) G. Herzberg, "Molecular Spectra and Molecular Structure," D. Van Nostrand, Inc., New York, N. Y., 1945, p 498.
(22) Compressibilities were taken from "Handbook of Chemistry and Physics," 47th ed, The Chemical Rubber Co., Cleveland, Ohio, 1966, p F-10; densities were obtained from "International Critical Tables," Vol. III, McGraw-Hill Book Co., New York, N. Y., 1928, p 27.
(23) W. P. McKinney, G. F. Skinner, and L. A. K. Staveley, *J. Chem. Soc.*, 2415 (1959).
(24) W. Kauzmann, *Advan. Protein Chem.*, **14**, 1 (1959).
(25) G. Némethy, *Angew. Chem.*, **6**, 195 (1967).
(26) J. G. Kirkwood and F. P. Buff, *J. Chem. Phys.*, **19**, 774 (1951).

water and 2 to the solute, the analysis in ref 26 leads to the identity

$$\int [g_{OO}^{(2)}(r) - 1]\mathrm{d}\mathbf{r} = \frac{kT(\partial\mu_2/\partial N_2)_{T,V,N_1}}{Vc_1^2\{(\partial\mu_1/\partial N_1)_{T,V,N_2}(\partial\mu_2/\partial N_2)_{T,V,N_1} - (\partial\mu_1/\partial N_2)_{T,V,N_1}(\partial\mu_2/\partial N_1)_{T,V,N_2}\}} - \frac{1}{c_1} \quad (23)$$

Here V is the system volume, and N_1 and N_2 are the numbers of water and solute molecules in V, respectively, and the chemical potentials are equal to μ_1 and μ_2. Also in eq 23 we have exercised the option as before to utilize the oxygen nuclei as "positions" of the water molecules.

The electroneutrality condition shown in eq 4 is still valid (with c_1 in place of c), so eq 23 may be rewritten in terms of the cross-correlation function,[27]

$$c_1 \int [g_{OH}^{(2)}(r) - 1]\mathrm{d}\mathbf{r} = \frac{kT(\partial\mu_2/\partial N_2)_{T,V,N_1}}{Vc_1\{(\partial\mu_1/\partial N_1)_{T,V,N_2}(\partial\mu_2/\partial N_2)_{T,V,N_1} - (\partial\mu_1/\partial N_2)_{T,V,N_1}(\partial\mu_2/\partial N_1)_{T,V,N_2}\}} \quad (24)$$

The constant-volume partial derivatives in this last relation may be eliminated in favor of the experimentally more direct constant-pressure derivatives *via* the formula ($\alpha, \beta = 1, 2; \gamma \neq \beta$)

$$\left(\frac{\partial\mu_\alpha}{\partial N_\beta}\right)_{T,V,N_\gamma} = \left(\frac{\partial\mu_\alpha}{\partial N_\beta}\right)_{T,p,N_\gamma} + \frac{\bar{v}_\alpha\bar{v}_\beta}{\kappa_T V} \quad (25)$$

Here we have introduced the partial molecular volumes

$$\bar{v}_\beta = \left(\frac{\partial V}{\partial N_\beta}\right)_{T,p,N_\gamma} \quad (26)$$

and the constant-composition isothermal compressibility

$$\kappa_T = -\frac{1}{V}\left(\frac{\partial V}{\partial p}\right)_{T,N_1,N_2} \quad (27)$$

Also, the Gibbs–Duhem equation permits elimination of cross derivatives in eq 24. One thus obtains

$$c_1 \int [g_{OH}^{(2)}(r) - 1]\mathrm{d}\mathbf{r} = \frac{(kT\kappa_T/c_1)[(\partial\mu_2/\partial N_2)_{T,p,N_1} + (\bar{v}_2^2/\kappa_T V)]}{\{(\partial\mu_1/\partial N_1)_{T,p,N_2}[\bar{v}_2^2 + (c_1\bar{v}_1\bar{v}_2/c_2)] + (\partial\mu_2/\partial N_2)_{T,p,N_1}[\bar{v}_1^2 + (c_2\bar{v}_1\bar{v}_2/c_1)]\}} \quad (28)$$

Further considerable simplification results from use of the formula

$$\left(\frac{\partial\mu_1}{\partial N_1}\right)_{T,p,N_2} = \left(\frac{N_2}{N_1}\right)^2\left(\frac{\partial\mu_2}{\partial N_2}\right)_{T,p,N_1} \quad (29)$$

whence

$$c_1 \int [g_{OH}^{(2)}(r) - 1]\mathrm{d}\mathbf{r} = kTc_1\left\{\kappa_T + \frac{\bar{v}_2^2}{V(\partial\mu_2/\partial N_2)_{T,p,N_1}}\right\} \quad (30)$$

The left member of eq 30 next may be treated in exactly the same way as for pure water. The generalized expression for the local proton excess thereupon becomes

$$\Delta_H = 2kTc_1\left\{\kappa_T + \frac{\bar{v}_2^2}{V(\partial\mu_2/\partial N_2)_{T,p,N_1}}\right\} - 2 + \frac{8\pi R^3 c_1}{3} \quad (31)$$

In the limit of infinite solute dilution, the divergence of the partial derivative $(\partial\mu_2/\partial N_2)$ allows one to recover eq 12 for pure water.

Our main interest in eq 31 is evaluation of the initial trend of Δ_H as a small amount of solute is added to pure water. If we use superscript zero to denote pure water, then in the dilute solution regime we may write

$$\Delta_H = \Delta_H^{(0)} + \Delta_H' c_2 + \dots \quad (32)$$

also one has

$$c_1 = c_1^{(0)} - c_1^{(0)}\bar{v}_2^{(0)}c_2 + \dots \qquad \kappa_T = \kappa_T^{(0)} + Ac_2 + \dots \quad (33)$$

The succeeding terms not explicitly shown in eq 32 and 33 will be proportional to c_2^2 for nonelectrolytes, and to $c_2^{3/2}$ for electrolytes. In order to obtain an expression for the desired coefficient Δ_H' from eq 31, it necessary only to use in addition the low-concentration form of the chemical potential derivative

$$\left(\frac{\partial\mu_2}{\partial N_2}\right)_{T,p,N_1} \approx \frac{kT}{c_2 V} \quad (34)$$

Hence we obtain

$$\Delta_H' = 2kTc_1^{(0)}A + \bar{v}_2^{(0)}c_1^{(0)} \times [2\bar{v}_2^{(0)} - (8\pi R^3/3) - 2kT\kappa_T^{(0)}] \quad (35)$$
$$= 2kTc_1^{(0)}A + \bar{v}_2^{(0)}(2c_1^{(0)}\bar{v}_2^{(0)} - \Delta_H^{(0)} - 2)$$

The coefficient A for initial composition dependence of solution compressibility has been listed by Harned

(27) The solute molecules might contain hydrogens, but we take the point of view (analogous to that for the alcohols) that the water protons can be distinguished. The correlation function $g_{OH}^{(2)}(r)$ refers only to water protons.

and Owen for a few simple electrolytes.[28] For others, A may be obtained in principal from pressure dependence of $\bar{v}_2^{(0)}$, for if we denote

$$\varphi_K^{(0)} = \left(\frac{\partial \bar{v}_2^{(0)}}{\partial p}\right)_{T,N_1,N_2} \tag{36}$$

then it is easy to show that

$$A = \varphi_K^{(0)} - \kappa_T^{(0)}\bar{v}_2^{(0)} \tag{37}$$

Table I presents Δ_H' results for several salts at 25°. The required $\bar{v}_2^{(0)}$ values for the inorganic salts are listed in ref 28 [Table (8-5-1), p 361]. For the alkylammonium salts $\bar{v}_2^{(0)}$ measurements were taken from Verrall and Conway[29] for the chlorides, from Wen and Saito for the bromides,[30] and from Conway, Verrall, and Desnoyers for the iodides.[31] The direct A values for lithium, sodium, and potassium chlorides are located by footnote 28. For the other inorganic salts, eq 37 was used to compute A from $\varphi_K^{(0)}$'s listed by Owen and Brinkley,[32] and $\bar{v}_2^{(0)}$'s in ref 28. The isothermal quantities $\varphi_K^{(0)}$ appear not to be available for the alkylammonium salts, so in their place the corresponding adiabatic quantities[33]

$$\varphi_{K,\mathrm{ad}}^{(0)} = \left(\frac{\partial \bar{v}_2^{(0)}}{\partial p}\right)_{S,N_1,N_2} \tag{38}$$

were used; this replacement is justified first because our experience shows that the contribution of the A term to Δ_H' is relatively small for organic salts, and second because isothermal and adiabatic aqueous compressibilities differ by so little.[34]

Consistent with the procedure in section III, we have disregarded the alkyl group hydrogens in the substituted ammonium salts, and have allowed only the water-molecule hydrogens to be counted in Δ_H'.

Table I: Coefficient of Initial Solute Dependence for Local Proton Defect in Aqueous Solutions of Various Electrolytes at 25°

Salt	Δ_H'
LiCl	−15.3
NaCl	−21.8
KCl	31.9
NaBr	14.3
KBr	96.0
CsBr	247
LiI	121
KI	239
Na_2CO_3	−50.3
K_2CrO_4	82.6
Na_2SO_4	−79.3
K_2SO_4	34.7
$(CH_3)NH_3Cl$	367
$(CH_3)_2NH_2Cl$	747
$(CH_3)_3NHCl$	1,240
$(CH_3)_4NCl$	1,800
$(CH_3)_4NBr$	2,090
$(C_2H_5)_4NBr$	5,140
$(n\text{-}C_3H_7)_4NBr$	9,970
$(n\text{-}C_4H_9)_4NBr$	16,000
$(CH_3)_4NI$	2,550
$(C_2H_5)_4NI$	5,790
$(n\text{-}C_3H_7)_4NI$	10,900
$(n\text{-}C_4H_9)_4NI$	17,000

V. Discussion

(1) Of the pure liquids examined by our Δ_H technique, water alone exhibits a minimum as temperature is varied. This apparently anomalous behavior immediately brings to mind the analogous behavior of water's molar volume, which among liquids uniquely has a minimum. This latter fact is often mentioned in connection with discussions of the extent of hydrogen-bond order in liquid water at various temperatures, and we feel that the Δ_H behavior is no less relevant in this regard. As temperature is lowered through 0°, the water molar volume curve extrapolated into the supercooled region approaches the molar volume of ice, and this single fact by itself would seem to indicate that the local order in water is literally icelike (*i.e.*, pieces of the ice I lattice). However, we see from Figures 2 and 3 that the opposite is true for the independent quantity Δ_H. It seems most likely, therefore, that the structural order forming as liquid water is cooled is bulky, like ice I, but has rather different structure. The most reasonable assumption is that this structure is a random network composed of polygons of varying numbers of sides and conformations, with significant bridging, free chain ends, and innumerable random polyhedra. These various structures would be present in concentrations varying with temperature and pressure.

(2) As a result of steric hindrance by the alkyl chains and the fact that their hydroxyl groups can participate in only two hydrogen bonds at most, the range of possible structures in the alcohols is far narrower than in water. Very probably chains of various lengths predominate. Rise in temperature simply would reduce the mean chain length, and Δ_H rises monotonically to reflect this simple degradation. By contrast, the nonmonotonic Δ_H in liquid water presumably results partly from similar reduction in total amount of hydrogen bonding, but of at least equal importance is temperature-induced shift in *type* of order. It is not hard to imagine that Δ_H for water results from a delicate interplay among the geometrically distinct ways of linking together groups of water

(28) H. S. Harned and B. B. Owen, "The Physical Chemistry of Electrolytic Solutions," 3rd ed, Reinhold Publishing Corp., New York, N. Y., 1958, p 378.

(29) R. E. Verrall and B. E. Conway, *J. Phys. Chem.*, **70**, 3961 (1966).

(30) W.-Y. Wen and S. Saito, *ibid.*, **68**, 2639 (1964).

(31) B. E. Conway, R. E. Verrall, and J. E. Desnoyers, *Trans. Faraday Soc.*, **62**, 1 (1966).

(32) B. B. Owen and S. R. Brinkley, Jr., *Chem. Rev.*, **29**, 461 (1941).

(33) B. E. Conway and R. E. Verrall, *J. Phys. Chem.*, **70**, 3952 (1966).

(34) Reference 28, p 386.

molecules by hydrogen bonding, with some of these structures giving positive Δ_H contributions and other negative Δ_H contributions.

(3) That the water Δ_H and apparently those for the alcohols as well become large and positive near the critical point is relatively easy to understand. At this high temperature (374° for water), the fluid is far less dense than the ordinary liquid and may be well viewed merely as a somewhat compressed gas. The very strong attraction between water molecules then acts to produce an average increase in molecular density, surrounding a given molecule, that exceeds the low macroscopic density in the fluid. This shell of attracted neighbors (each with two protons) provides a strong positive contribution to Δ_H.

(4) On the basis of the very sketchy evidence we have so far been able to accumulate, negative Δ_H's seem to be characteristic of hydrogen-bonded molecular arrangements, *i.e.*, molecules strongly and closely bound to a *small* number of nearest neighbors to produce a rather open overall structure. Methane with positive Δ_H must be representative of liquids with higher numbers of nearest neighbors and tighter overall packing. Indeed, if we assume that methane molecules are arranged as rigid spheres, with diameter a, we may use the scaled-particle theory of the rigid-sphere equation of state[35] to convert eq 19 to

$$\Delta_H = 4\left[\frac{(1-y)^4}{(1+2y)^2} - 1 + \frac{4\pi cR^3}{3}\right] \qquad (39)$$

$$y = \frac{\pi ca^3}{6}$$

by introduction of an explicit form for the isothermal compressibility. For liquid methane $y \cong 1$ if a is chosen to be the crystal nearest-neighbor distance. The first term in the right member of eq 39 then is virtually zero and Δ_H is dominated strongly by the last term. The decrease of the positive methane Δ_H as temperature increases along the vapor pressure curve is therefore almost exclusively due to reduction in c in that last term by thermal expansion.

(5) Figures 2 and 3 show that in the temperature range for which the salt effects in Table I apply (25°), Δ_H decreases with increasing temperature for pure water. Those salts with negative Δ_H', therefore, may tentatively be considered as perturbing water in the same way as increasing temperature, and those with positive Δ_H' as equivalent to temperature reduction. Thus the former class may be called "structure breakers," and the latter class "structure formers," though these identifications should always be augmented by the understanding that solute structural shifts are certainly more subtle and variegated than just the single temperature-shift type. Nevertheless, the strong effect exhibited in Table I toward more positive Δ_H's among the substituted ammonium salts, as the size and number of alkyl groups increase, is in full accord with the ideas underlying the hydrophobic bond concept for hydrocarbon substituents in aqueous media.[24,25] Aside from the possibly anomalous character of Li^+, it can also seen from Table I that increase in size of spherical inorganic ions tends to produce an increase in Δ_H, that is, more overall structure.

(6) Unfortunately, we are prevented from studying the solute effect on water of dissociating protonic acids (such as HCl) or hydroxides (such as NaOH). The reason is simply that they would introduce a new effect which would obscure comparison with the other solutes, namely, a change in stoichiometry of the oxygen–hydrogen framework. By suitable combination of Δ_H results on several precisely measured systems with common ions, it may eventually be possible to isolate and evaluate this framework composition effect.

(7) Finally, we must remark on the desirability of measuring those thermodynamic properties for a wide variety of liquids that would permit a comprehensive extension of the few Δ_H computations presented here. As examples of pure substances, special interest attaches to HF, HCN, and NH_3 liquids, and we urge their densities and isothermal compressibilities be precisely and simultaneously determined over a wide range of temperatures and pressures. Liquid carboxylic acids, which seem to have a marked propensity for ring formation as dimers, would also be interesting. So far as solutions are concerned, it would first be advisable to study the effect of simple dissolved gases (*e.g.*, Xe, N_2, CO, CH_4) by making the required κ_T and $\bar{v}_2$ measurements in dilute solution and then to compare those results with the behavior of more complicated substances like butane, urea, sucrose, and dimethyl sulfoxide. Furthermore, extension of the considerations in section IV to order c_2^2 for hydrocarbon solutions should provide additional information on the mechanism of hydrophobic bonding analogous to that provided by other solution data recently analyzed in great detail by Kozak, Knight, and Kauzmann.[36]

Acknowledgment. The authors are grateful to Professor H. C. Longuet-Higgins for comments on the subject material of this paper, especially his suggestion that methane would provide an illuminating contrast for water.

(35) H. Reiss, H. L. Frisch, and J. L. Lebowitz, *J. Chem. Phys.*, 31, 369 (1959).

(36) J. J. Kozak, W. S. Knight, and W. Kauzmann, *ibid.*, 48, 678 (1968).

Infrared Spectra of the Surface Species Produced by Reactions of Ammonia with Germania Gel

by M. J. D. Low and Kun-ichi Matsushita

Department of Chemistry, New York University, New York, New York 10453 *(Received August 29, 1968)*

Infrared spectra were recorded from 4000 to 500 cm^{-1} of ammonia sorbed on dehydroxylated germania gel. Extensive dissociation of ammonia occurred, with the formation of Ge–OH groups. The spectra showed that beside physisorbed ammonia, which gave rise to absorptions at 3600–2500, 3420, 3312, and 1610 cm^{-1} as well as a previously unreported one near 1260 cm^{-1}, at least four other surface species were formed. Bands at 3363, 3267, 1600, 1210, and 700 cm^{-1} were attributed to ammonia weakly coordinated to surface germanium atoms. Bands at 3467, 3393, and 1535 cm^{-1} were attributed to a more strongly bonded primary amine which might be the precursor of a secondary amine giving rise to a band at 3397 cm^{-1}. A minor band near 2195 cm^{-1} was attributed to Ge–H structure.

Introduction

Although germanium-containing devices are widely used and "real" germanium surfaces have been studied extensively, relatively little is known about the nature of the surface species formed when gases become adsorbed on germanium or germanium oxide surfaces. However, infrared spectroscopic techniques are useful for the study of such reactions and, using germania gel as analog of real germanium, the formation of some surface groupings has recently been described. The formation of hydroxyls[1] and Ge–H groups[2] was observed, and some surface structures resulting from the reactions of germania with acetic and propionic acids[3] as well as with methanol, formaldehyde, and formic acid[4] have been described. Those studies have now been extended to the reaction of ammonia with germania gel surfaces.

Experimental Section

The preparation of the germania gel and many other experimental procedures have been described elsewhere.[2] Prior to exposure to ammonia, a fresh pellet was degassed at 500° for 5 hr, heated for 5 hr in 300 Torr of oxygen at 500°, and then degassed for 5 hr at 550°. Ammonia of 99.99% purity was purchased from Matheson Co. and was vacuum distilled and subjected to freeze–pump–thaw cycles. Spectra were recorded with a Perkin-Elmer Model 621 spectrophotometer. As the transmittances of the samples were below 20%, screens were extensively used in the reference beam and ordinate scale expansions were used as required.

Results and Discussion

Trace A of Figure 1 is a typical "background" spectrum of well-degassed germania gel and shows a weak band near 3670 cm^{-1} (hereafter termed the Ge–OH band) attributed[1,2] to isolated surface Ge–OH groups; there are also very strong absorptions of the germania below 1600 cm^{-1} with "windows" near 1300–1100 and 700–500 cm^{-1}. When such a specimen was exposed to ammonia at 25° at low pressure (spectrum B, Figure 1), the Ge–OH band increased in intensity, a broad band attributed[1,2] to hydrogen-bonded hydroxyls formed near 3570 cm^{-1} (*e.g.*, spectrum C, Figure 1), and other absorptions were observed over the entire spectral range which was examined. The intensity of the Ge–OH band declined with increasing ammonia pressure (spectra A, B, Figure 2) but increased when sorbed ammonia was removed. On degassing, the Ge–OH and 3570-cm^{-1} bands exhibited behavior very much like that observed[2] when hydroxylated germania was degassed. Many of the absorptions, especially those in the N–H region, broadened and were obscured when the amount of sorbed ammonia was increased. A very broad absorption formed at higher ammonia pressures in the 3600–2500-cm^{-1} range (spectrum B, Figure 2) and, as in the case of ammonia sorption on porous glass[5] or silica,[6] is attributed to physically adsorbed ammonia.

Although the spectra were complex, it was possible to use observations on changes in band intensities and position, band shapes, and the like, to separate the numerous bands into several groups. Three major groups are given in Table I. Other, minor bands will be considered later.

All bands of groups A, B, and C could be observed at low ammonia pressure. With increasing pressure, group A bands grew more than group B bands; group C bands did not seem to be affected, but it was difficult to be certain of this because the group A bands obscured the others. Although all of these bands could be diminished by pumping at low temperature, the group C bands were diminished more slowly than others and

(1) M. J. D. Low and P. Ramamurthy, *Chem. Commun.*, 733 (1966).
(2) M. J. D. Low, N. Madison, and P. Ramamurthy, *Surface Sci.*, in press.
(3) J. C. McManus and M. J. D. Low, *J. Phys. Chem.*, **72**, 2378 (1968).
(4) J. C. McManus, K-I. Matsushita, and M. J. D. Low, *Can. J. Chem.*, in press.
(5) M. J. D. Low, N. Ramasabramanian, and V. V. Subba Rao, *J. Phys. Chem.*, **71**, 1726 (1967).
(6) N. W. Cant and L. H. Little, *Can. J. Chem.*, **43**, 1252 (1965).

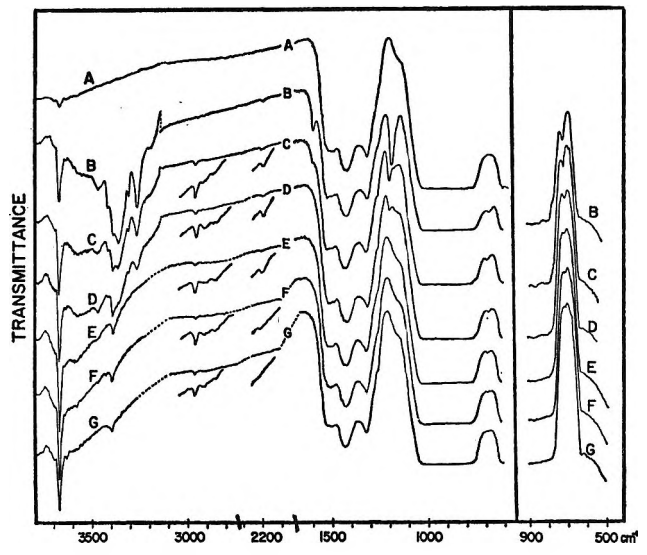


Figure 1. Ammonia sorption—low pressure. A well-degassed germania specimen (spectrum A) was exposed to 0.5 Torr of NH_3 for 1 hr at 25° and degassed for 30 min at 25° (spectrum B). The sample was then degassed at 25° for 10 hr (spectrum C) and for 30 min at 100° (D), 215° (E), 335° (F), and 410° (G). The ordinates are displaced to avoid overlapping. The segments of spectra C to G near 3000 and near 2200 cm^{-1}, as well as those of the insert showing the 900–200-cm^{-1} range, were recorded at 5 times the ordinate expansion.

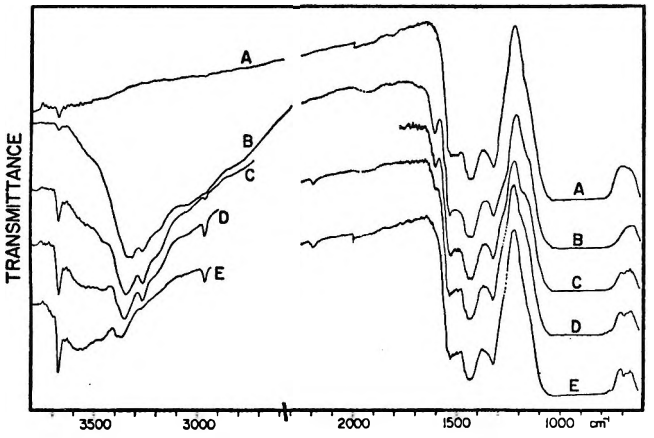


Figure 2. Ammonia sorption—high pressure. A well-degassed germania specimen (spectrum A) was exposed to 26 Torr of ammonia at 25° for 12 hr (spectrum B) and was then degassed for 5 min at 25° (C), 16 hr at 25° (D), and 30 min at 110° (E). The ordinates are displaced.

were removed by pumping above 100°. Group A bands declined somewhat more rapidly than group B bands and were almost completely removed by pumping at 25° for 0.5 day. Group B bands were retained after pumping at 25° for several days. However, differences in rates were difficult to discern in the N–H region. Also, a band increased and shifted from 1603 to 1610 cm^{-1} when the ammonia sorption increased, declined, and shifted to 1603 cm^{-1} when much of the weakly held ammonia was removed, and then declined further and shifted to 1600 cm^{-1} on further degassing near 100°. The decline and shift from 1610 cm^{-1}

Table I: Major Bands of Adsorbed Ammonia

Group A cm^{-1}	Group B cm^{-1}	Group C cm^{-1}	
	H H H \ | / N ••	H H \ / N |	
Physisorbed ammonia	Ge	Ge	Assignment
3420	3363	3467	ν_a (N–H)
3312	3267	3393	ν_s (N–H)
1610	1600		δ_d (NH_3)
		~1535	δ (NH_2)
~1260	1210		δ_s (NH_3)
	700		ρ_r (NH_3)

paralleled the decline of the very broad band of physically adsorbed ammonia and of an absorption near 1260 cm^{-1} (the latter appears as a broad shoulder in spectrum B, Figure 2). Such effects suggested that the same weakly held species responsible for the 3600–2500-, 3420-, 3312-, and 1260-cm^{-1} absorptions caused much of the absorptions near 1610 cm^{-1}, while a second weakly but somewhat more tightly held species brought about the absorption at 1600 cm^{-1} and other group B bands. A third species was responsible for group C.

The position and behavior of the 3420-, 3312-, and 1610-cm^{-1} bands and the broad 3600–2500-cm^{-1} absorption are very similar to those found when ammonia was physically adsorbed on a variety of solids. The effects were reviewed by Little.[7] There is consequently little doubt that the group A bands were caused by physically adsorbed ammonia. The band assignments are given in Table I and are like those reported previously,[7] with the exception of that at 1260 cm^{-1}. Such an absorption has not been observed before because adsorbents such as silicas or aluminas used in earlier studies absorb very strongly in the region where the low-frequency ammonia deformation band would be expected. The 1260-cm^{-1} absorption exhibits a fairly large shift from the positions of the deformation bands of gaseous (968, 932 cm^{-1}) and crystalline[8] (1060 cm^{-1}) ammonia, but the shift is in the direction expected for a strongly hydrogen-bonded system.[7,9] Unfortunately, the occurrence of the absorption as a broad shoulder causes uncertainty about its position, so that these considerations must remain qualitative.

The five bands termed group B show good correspondence with those of typical amine complexes. These have been reviewed by Nakamoto.[10] Also, the

(7) L. H. Little, "Infrared Spectra of Adsorbed Species," Academic Press, New York, N. Y., 1966.

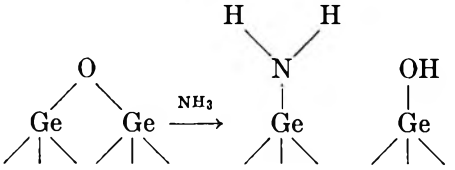
(8) M. E. Jacox and D. E. Milligan, *Spectrochim. Acta*, **19**, 1173 (1963).

(9) V. N. Abramov, A. V. Kiselev, and V. I. Lygin, *Russ. J. Phys. Chem.*, **38**, 1020 (1964).

(10) K. Nakamoto, "Infrared Spectra of Inorganic and Coordination Compounds," John Wiley and Sons, Inc., New York, N. Y., 1963, p 143 ff.

two bands in the N–H stretching region are similar to bands attributed to ammonia coordinated to surface boron atoms on porous glass and boria-impregnated silica,[5] and the stretching bands and the two bending bands are similar to bands attributed to ammonia coordinated to surface aluminum atoms. The various bands observed on chemisorption of ammonia on aluminas and silica–aluminas were reviewed by Little.[7] In view of these similarities, the group B bands are attributed to a weakly bound surface complex consisting of ammonia coordinated to a germanium atom. The assignments given in Table I are based on earlier ones.[5,7,10] The 700-cm^{-1} rocking band has not been previously reported, because it falls in a region in which previously used adsorbents absorb very strongly. A Ge–N stretching band, which would be expected in the 300–400-cm^{-1} range,[10] was not observed because the germania was opaque below about 500 cm^{-1}.

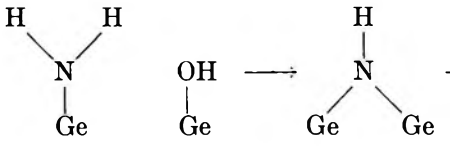
The two bands at 3467 and 3393 cm^{-1} of group C fall in the N–H stretching region, closely fit Bellamy and Williams' equation relating the frequencies of asymmetric and symmetric stretching fundamentals of primary amines[11] and also are similar to those of $-NH_2$ species formed on porous glass,[5,7] silicas, and aluminas.[7] The 1535-cm^{-1} band was superimposed on an intense band of the germania, and consequently was weak and indistinct. However, spectra of amido complexes suggest that an $-NH_2$ deformation band[10] would occur near 1500–1600 cm^{-1}, and bands assigned to such a mode of dissociatedly adsorbed ammonia were observed at 1555 cm^{-1} with silica[12] and at 1560 and 1510 cm^{-1} with alumina.[13] It is consequently not unreasonable to assign the group C bands to a primary surface amine formed by a reaction



(1)

which will also lead to the formation of the bands of isolated and perturbed hydroxyl groups.

One stretching band of the primary amine was observed near 3467 cm^{-1} at relatively high stages of coverage, declined, and shifted to near 3470 cm^{-1} on degassing at 100°, and along with the 1535-cm^{-1} band, disappeared above 100°. The second stretching band was originally observed near 3390 cm^{-1}, declined, and shifted to near 3393 cm^{-1} on mild pumping, but then shifted to 3397 cm^{-1} and declined only slowly with increasing severity of degassing conditions. The 3397-cm^{-1} band was removed at 500°. The effects suggest that some of the weakly bound material was converted to a relatively strongly bound species. The interpretation is difficult and somewhat uncertain, because only one band is available. However, the single 3397-cm^{-1} band falls in the region of N–H stretching fundamentals where a single band due to a secondary amine would be expected. In view of this and the manner of formation of the band, the 3397-cm^{-1} band is assigned to a surface secondary amine formed by a reaction such as



(2)

The water formed could remain adsorbed or react with the germania to produce hydroxyls, either of which would contribute to the broad 3570-cm^{-1} band, or be desorbed at the higher temperatures.

A small band was formed near 2966 cm^{-1}, increased slightly when weakly bound material was desorbed (spectra B–D, Figure 2), but declined only slightly at higher temperatures. Two smaller bands could be observed near 2920 and 2870 cm^{-1} by means of scale expansion (Figure 1). The three bands appeared to be largely independent of the change of other bands, and persisted even after degassing at 500°. The 2966-cm^{-1} band (and also the two other less intense bands) falls in the range expected for a stretching fundamental of NH_4^+, on the basis of earlier work on surface NH_4^+ reviewed by Little.[7] Bands attributable to an NH_4^+ deformation were not observed, but these, if present, would be superimposed on the intense absorption of the germania in the 1300–1600-cm^{-1} region, so that detection would be difficult. The small bands might be caused by NH_4^+ formed by a reaction of ammonia with hydroxyls, but the assignment is speculative. An alternate explanation is that the bands were caused by a carbonaceous contaminant.

A very small band whose behavior was independent of that of other bands was detected near 2195 cm^{-1}. It began to decline on pumping near 200° and exhibited behavior much like that of bands formed by the reaction of water or hydrogen with germania.[2] The 2195-cm^{-1} band is consequently attributed to surface Ge–H groups. These could be formed directly through the dissociation of ammonia or from the water[2] formed in reaction 2. The mechanism is uncertain. However, the Ge–H band was not significantly changed when the amount of sorbed ammonia was increased, suggesting that the reaction leading to the formation of the Ge–H species could not occur extensively because one of the reactants—possibly a portion of the surface which consisted of Ge or GeO—was present to a limited extent.

Acknowledgment. Support by means of a grant from the National Center for Air Pollution Control is gratefully acknowledged.

(11) L. J. Bellamy and R. L. Williams, *Spectrochim. Acta*, **9**, 341 (1957).
(12) J. B. Peri, *J. Phys. Chem.*, **70**, 2937 (1966).
(13) J. B. Peri, *ibid.*, **69**, 231 (1965).

Infrared Studies of the Reactions between Silica and Trimethylaluminum

by D. J. C. Yates, G. W. Dembinski, W. R. Kroll, and J. J. Elliott

Corporate Research Laboratories, Esso Research and Engineering Company, Linden, New Jersey
(Received September 9, 1968)

We have studied spectroscopically the reaction between trimethylaluminum and silica. The reaction is shown to involve mostly the "free" hydroxyl groups of the silica rather than the "hydrogen bonded" hydroxyl groups. A rearrangement of the aluminum alkyl takes place, the final products being methyl groups bound to silicon atoms, and silicon–hydrogen groups. Confirmatory evidence for such a rearrangement was obtained by examining the spectra of the reaction products of silica with methanol and chlorinated methyl silanes. A possible mechanism for the reaction is suggested.

Introduction

It is well known that aluminum alkyls are unstable in the presence of oxygen[1] or water,[2,3] decomposing very rapidly to hydrated alumina and hydrocarbons if excess water is used. Little is known of their reaction paths when limited amounts of water are present.[4] Such circumstances can be found on the surface of finely divided stable oxides, which commonly contain OH groups even when all molecular water has been removed at high temperature.

Surface hydroxyl groups can be reacted in various ways; they can be exchanged with deuterium,[5,6] replaced with methoxy groups,[7] or reacted with molecules such as silanes,[8,9] boron trichloride,[10] or diborane.[11] Silica hydroxyl groups have also been found to react with organometallic compounds such as alkyllithium and alkylmagnesium iodide,[12] and also with aluminum alkyls.[13–15] In many of these investigations, no spectroscopic experiments have been carried out, or when they have, only the OH region has been examined.

In the case of aluminum alkyls, no spectroscopic investigations have been reported; the only information known is the type and amount of hydrocarbon formed as a result of the reaction. We have determined, by infrared studies, that predominantly one type of hydroxyl group on silicas reacts with aluminum alkyls. In addition, a very striking rearrangement of the alkyl molecule takes place, as chemisorbed silicon–methyl groups are formed on the surface, rather than aluminum–methyl groups which others have postulated,[13] and might indeed have been expected to form.

Experimental Section

a. Materials. Three forms of silica were used: Cabosil, Davison silica gel, and porous glass. Most of the work was done with the Cabosil, Grade HS5, surface area about 300 m^2/g, obtained from the Cabot Co., Boston, Mass. The silica gel, Code No. 951, has a surface area of 600 m^2/g and was obtained from the W. R. Grace Co., Davison Chemical Division, Baltimore, Md. The porous glass used was in the form of a plate, 0.25 mm thick, similar to that used earlier.[7]

Trimethylaluminum was obtained from the Ethyl Corp., New York, N. Y., of purity 99.9%. Reagent grade methanol was used. Tetramethylsilane, of purity 99%, was obtained from N.M.R. Specialties, New Kensington, Pa. Hexamethyldisiloxane was obtained from K and K Laboratories, Plainview, N. Y. Trimethylchlorosilane and trichloromethylsilane were obtained from the Dow Chemical Corp., Midland, Mich.

b. Apparatus. Because of the extreme chemical reactivity of trimethylaluminum, initial experiments were performed using a simple silica cell similar to that described elsewhere.[7] Later, it was found that the trimethylaluminum did not significantly attack either the vacuum grease, glyptal cement, or barium fluoride, and our usual rotatable dual cells[16] were used. Details of the vacuum system have been given[16] earlier. A Beckman IR7 grating spectrometer was used, with an external mirror system providing an accessible focus. Details of the resolution achieved are given in the legends of the figures.

(1) K. Ziegler, F. Krupp, and K. Zosel, *Lieb. Ann. Chem.*, **629**, 241 (1960).
(2) K. Ziegler in "Organoaluminum Compounds," H. Zeiss, Ed., Reinhold Publishing Corp., New York, N. Y., 1960, p 206.
(3) G. E. Coates in "Organo-metallic Compounds," Methuen and Co., Ltd., London, 1956, p 75.
(4) G. B. Sakharoskaya, N. N. Korneev, A. F. Popov, E. I. Larikov, and A. F. Zhigach, *Zh. Obshch. Khim.*, **34**, 3435 (1964).
(5) M. P. Boehm, *Advan. Catal.*, **16**, 179 (1966).
(6) J. L. Carter, P. J. Lucchesi, P. Corneil, D. J. C. Yates, and J. H. Sinfelt, *J. Phys. Chem.*, **69**, 3070 (1965).
(7) M. Folman and D. J. C. Yates, *Proc. Roy. Soc.*, **A246**, 32 (1958).
(8) T. E. White, Proceedings of the Society of Plastics Industry, 20th Annual Meeting, Chicago, Ill., 1965, Reinforced Plastics Division, Section 3B, p 1.
(9) L. R. Snyder and J. W. Ward, *J. Phys. Chem.*, **70**, 3941 (1966).
(10) F. H. Hambleton and J. A. Hockey, *Trans. Faraday Soc.*, **62**, 1694 (1966).
(11) H. G. Weiss, J. A. Knight, and I. Shapiro, *J. Amer. Chem. Soc.*, **81**, 1823 (1959).
(12) J. J. Fripiat and J. Uytterhoeven, *J. Phys. Chem.*, **66**, 800 (1962).
(13) M. Liefländer and W. Stöber, *Z. Naturforsch.* **15B**, 411 (1960).
(14) M. Sato, T. Kanbayashi, N. Kobayashi, and Y. Shima, *J. Catal.*, **7**, 362 (1967).
(15) H. Jenkner, *Z. Naturforsch.*, **14B**, 133 (1959).
(16) D. J. C. Yates and P. J. Lucchesi, *J. Chem. Phys.*, **35**, 243 (1961).

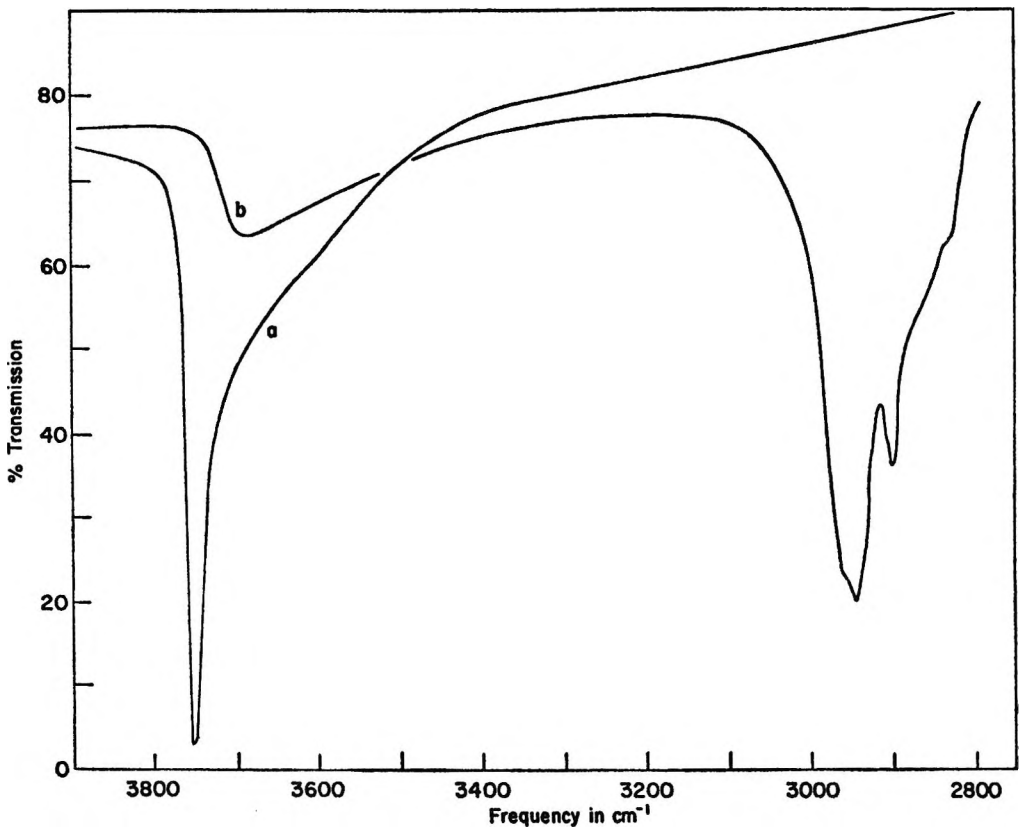


Figure 1. Interaction of trimethylaluminum with thin (about 15 mg/cm²) silica (Cabosil): a, spectrum after evacuation at 500°; b, after treatment at room temperature with $Al(CH_3)_3$ vapor, and removal of excess vapor at room temperature. Resolution at 2800, 2900, and 3000 cm^{-1} is 3.8, 3.0, and 2.3 cm^{-1}, respectively.

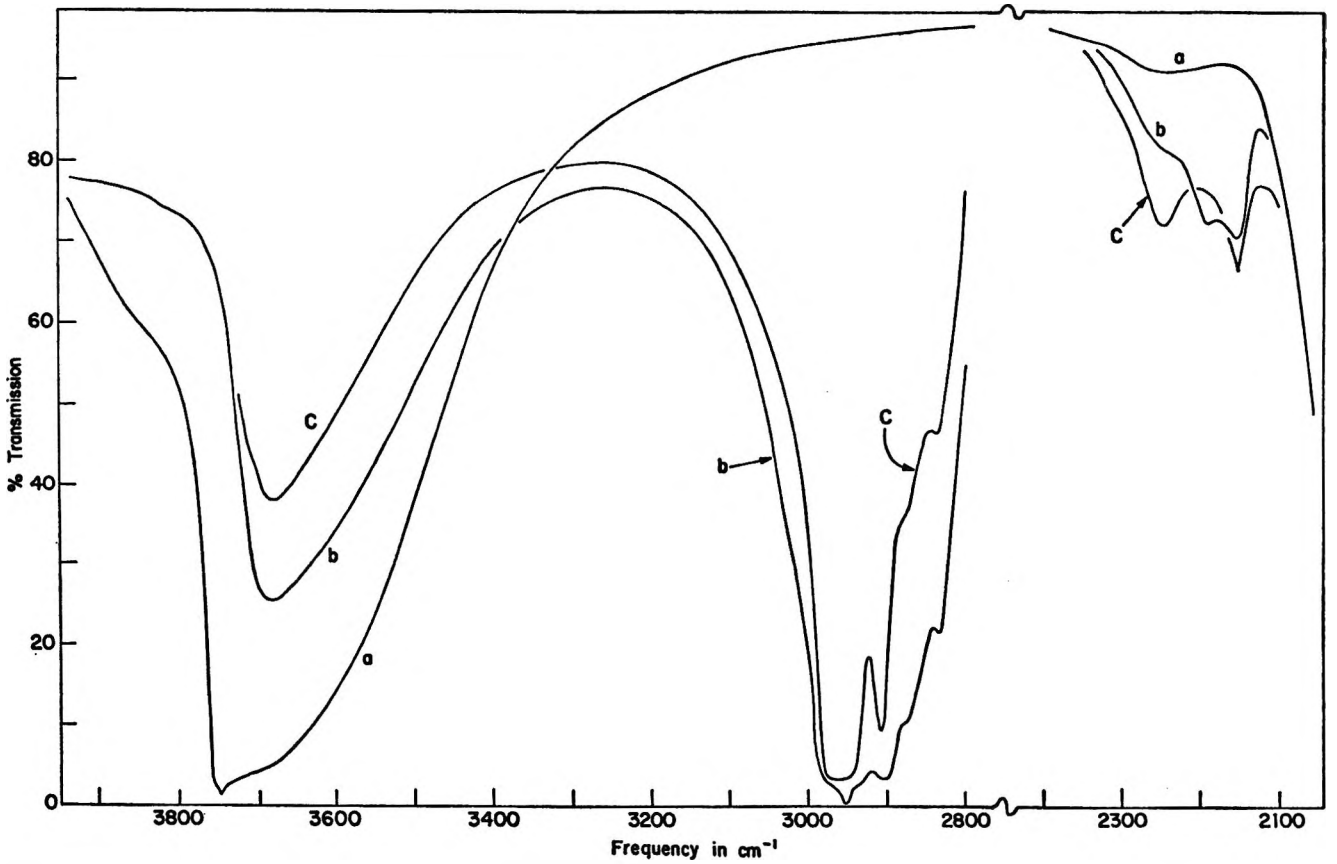


Figure 2. Interaction of trimethyl aluminum with thick (about 60 mg/cm²) Cabosil: a, after initial evacuation at 400°; b, after treatment with $Al(CH_3)_3$ vapor at room temperature, and evacuation at room temperature for 10 min; c, after evacuation at 300° for 10 min. Resolution at 2200, 2800, 2900, and 3000 cm^{-1} is 2.4, 4.5, 3.5, and 2.7 cm^{-1}, respectively.

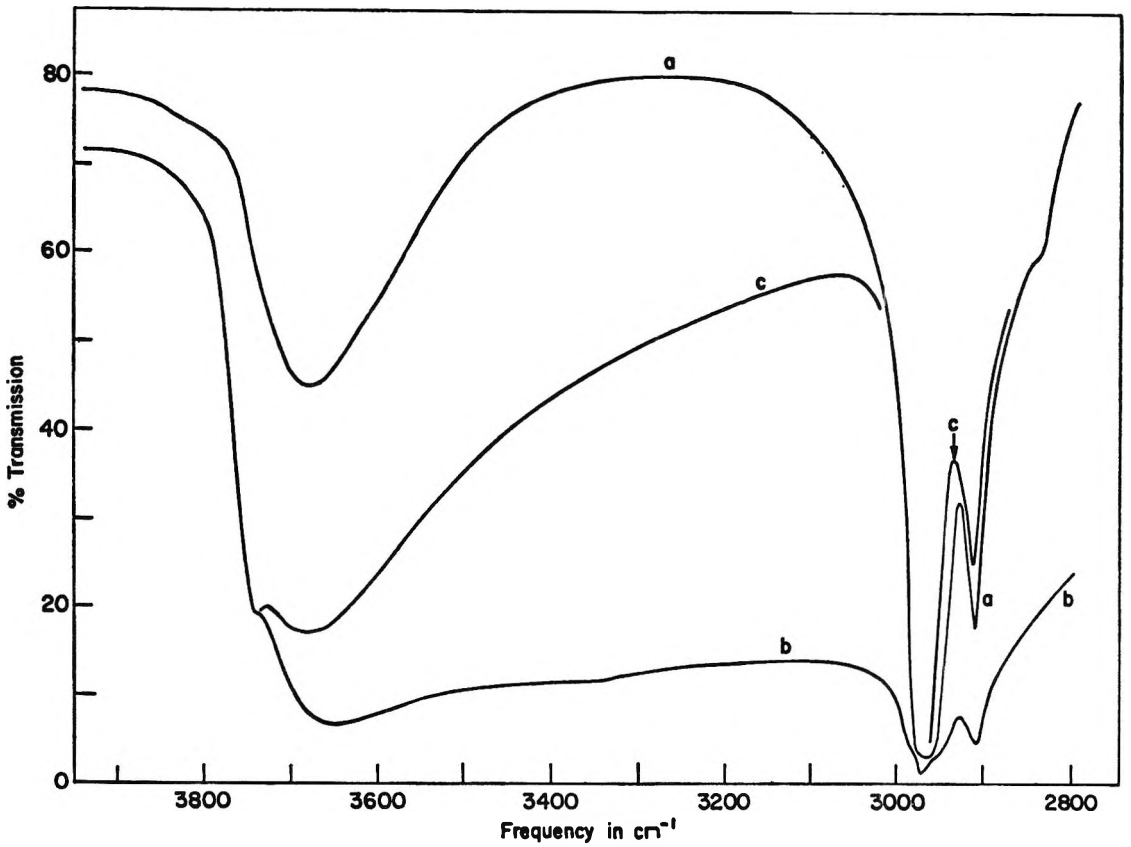


Figure 3. Addition of water to methyl groups adsorbed on silica: a, sample as in Figure 2c, but evacuated an additional 15 min at 400°; b, spectrum run 40 min after adding 4 mm of water vapor; c, spectrum run after evacuating at room temperature for 3 min, 100° for 15 min, and finally at 200° for 20 min. Resolution identical with that used in Figure 2.

c. Procedure. After initial evacuation of the samples at elevated temperature to remove adsorbed water, their spectra were recorded over the whole accessible region (about 1400 to 4000 cm^{-1}). The trimethylaluminum was usually added as an excess of vapor at room temperature, but it was sometimes distilled over as a liquid by cooling the end of the cell containing the sample. After a few minutes, the unreacted compound, together with any methane formed, was removed by evacuation. If desired, a further dose was added using the same procedure. The trimethylaluminum was always purified immediately before use by freezing it at 77°K, evacuating until vacua in the region of 10^{-5} Torr were obtained, and then warming to room temperature. A similar procedure was followed with the silanes and methanol, except that they were always added as vapor, in excess.

Results

Data obtained with thin Cabosil samples are shown in Figure 1. It will be seen that a very extensive reaction has occurred, with a striking decrease in the intensity of the OH groups. Similar data were obtained with a thicker sample of silica (Figure 2), but the resulting CH stretching bands of the adsorbed methyl groups were much more intense. This sample was used to study the stability of these methyl groups by evacuating at high temperatures (Figures 2 and 3), by adding water (Figure 3), and by deuterium exchange (Figure 4). The experiments with Davison silica gel and porous glass were with relatively thick samples, and the spectra obtained were similar to those shown in Figure 2. However, no studies were made of the effects of water addition or deuterium exchange with these particular samples.

To show that the adsorbed species formed by the reaction of trimethylaluminum were not methoxy groups, studies were made of the chemical reaction between methanol and the OH groups. Some of the data obtained are shown in Figure 5. Companion deuterium exchange studies were also made with the methoxylated silica (Figure 6).

To obtain data on known types of chemisorbed methyl groups, exchanges were performed between silica and tetramethylsilane (Figure 7) and trichloromethylsilane (TCMS) (Figure 8). Although there are some data on adsorbed species obtained from TCMS,[8] no high-resolution spectra have been published and no high-resolution spectra have been given of adsorbed silicon methyl groups obtained from trimethylchlorosilane (TMCS).[8,17] The frequencies of the various adsorbed species are given in Table I.

There seem to be very few published data in the CH stretching region on the infrared spectra with high

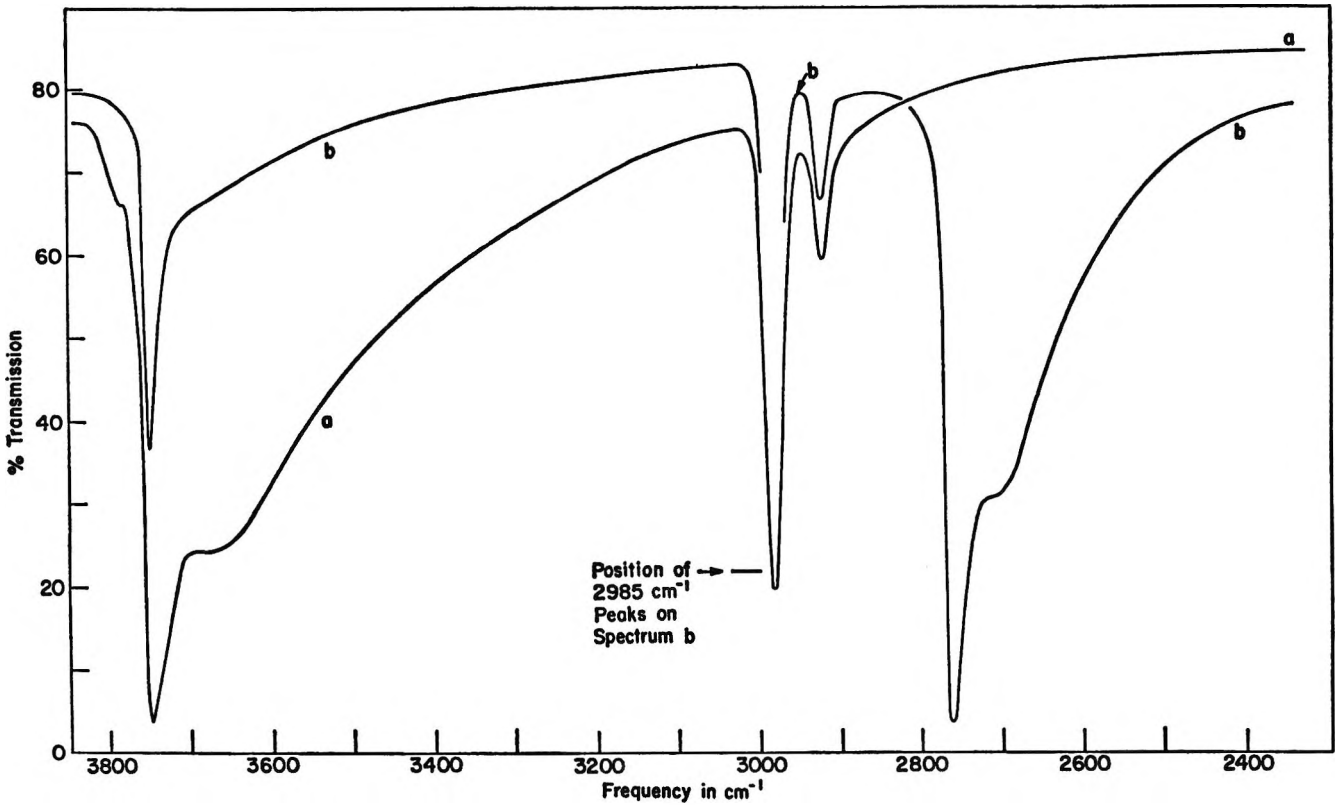


Figure 4. Deuterium exchange of silica with adsorbed methyl groups: a, sample as in Figure 3c, but evacuated at 400° for 70 min; b, after heating in deuterium (12 cm pressure) for 15 min at 400°. Resolution identical with that used in Figure 2.

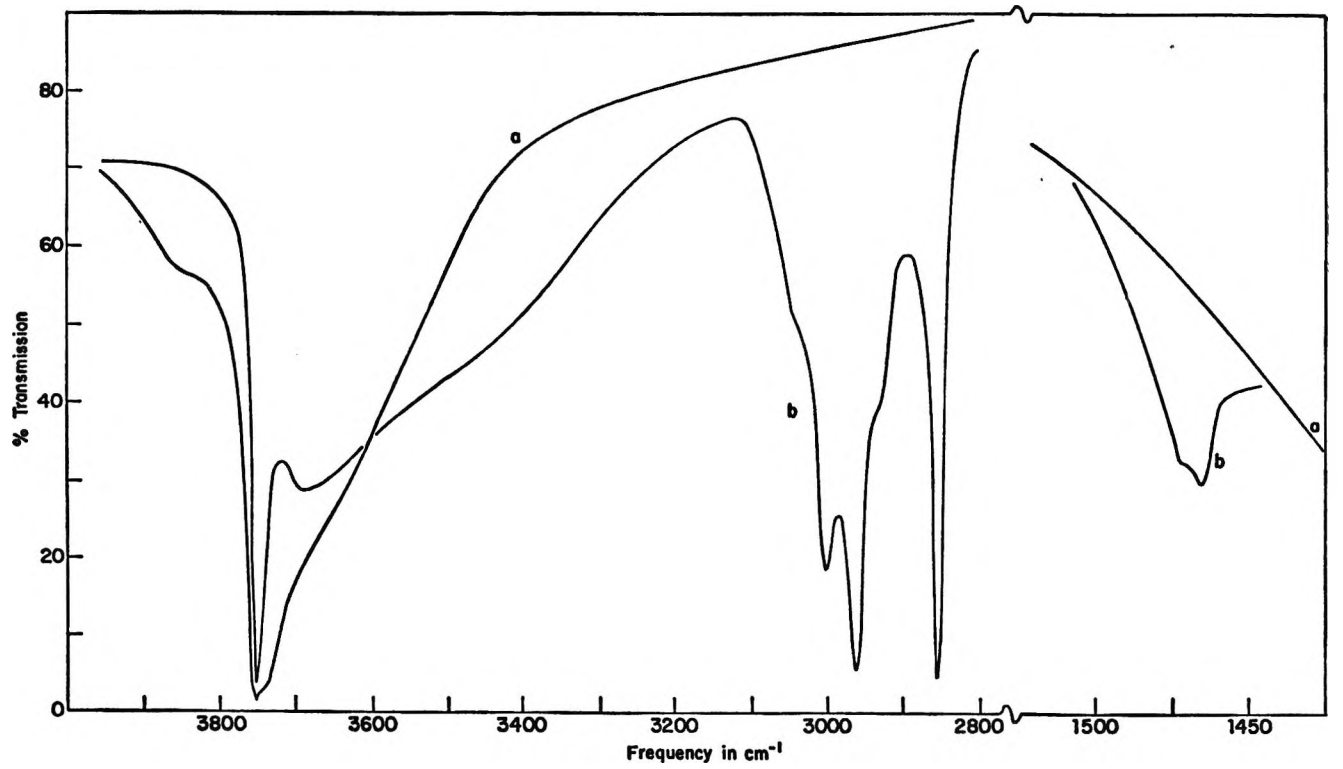


Figure 5. Reaction between methanol and Cabosil (thickness about 40 mg/cm²): a, spectrum after evacuation at 500° for 2 hr; b, methanol (13 cm pressure) added at room temperature, then heated to 350° in 10 min, and methanol changed. Kept at 350° for 45 min, then evacuated for 15 min at 350°, and cooled to room temperature, then the spectrum recorded. Resolution at 1475, 2800, 2900, and 3000 cm^{-1} is 3.6, 4.2, 3.2, and 2.6 cm^{-1}, respectively.

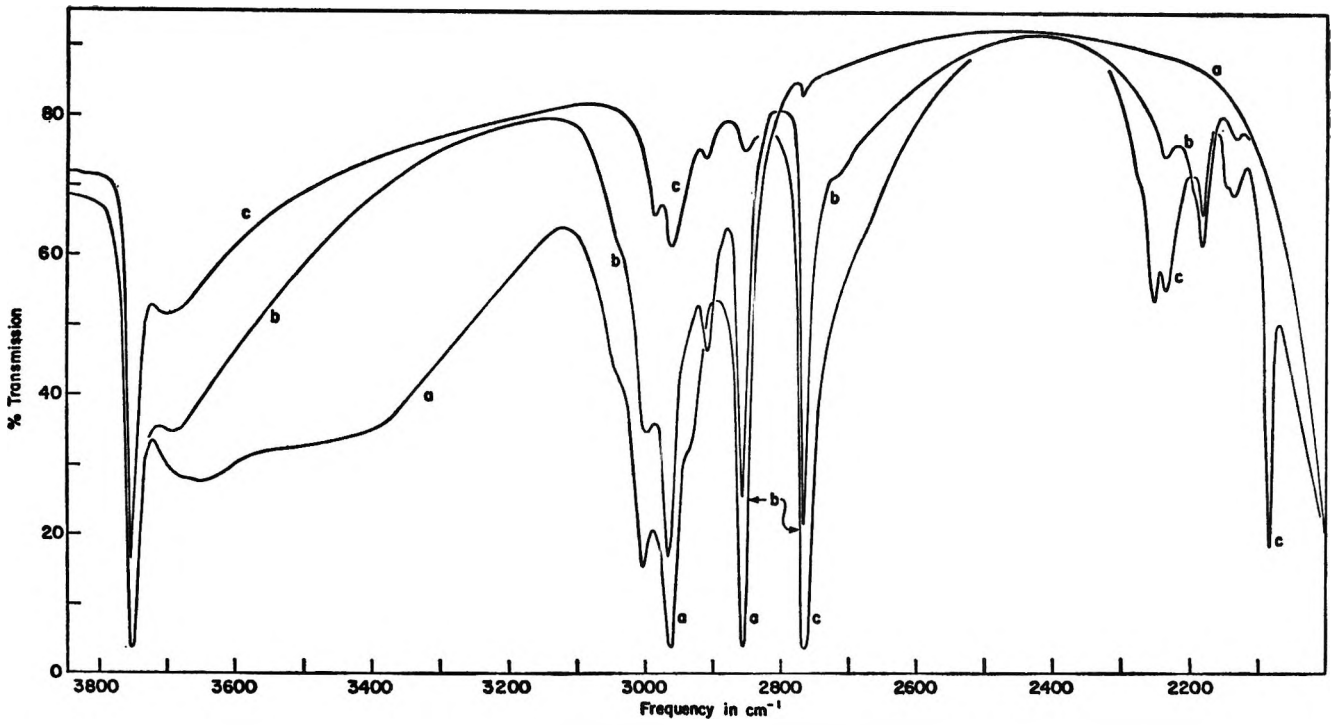


Figure 6. Deuterium exchange on silica with methoxy groups: a, sample as in Figure 5b, but after treatment with 10.0 cm of D_2 at 350° for 10 min; b, after treatment with 27.6 cm of D_2 at 500° for 15 min; c, after treatment with 63.7 cm of D_2 at 550° for 25 min. Resolution identical with Figure 5.

resolution of compounds containing aluminum–methyl groups and silicon–methyl groups, so we have presented some data on these compounds in Figure 9 and Table II.

Discussion

Reaction between Trimethylaluminum and Silica. When trimethylaluminum (TMA) reacts with silica, it is known[13,14] that methane is formed. This reaction is presumed to go by the abstraction of a hydrogen atom (from an OH group) from the solid which combines with the methyl groups to form methane. This idea is shown to be correct, in a general sense, by the spectra shown in Figures 1 and 2. In Figure 1, it will be seen that the hydroxyl band remaining in the silica is asymmetric. This is because the band is a composite of a sharp, narrow band at 3750 cm^{-1} caused by the isolated OH groups,[17–20] and a broader, weaker band extending from about 3750 cm^{-1} to 3500 cm^{-1}. The latter band shows the presence of hydroxyl groups hydrogen-bonded to each other (see Figure 16 of ref 20). If sufficiently high temperatures are used during the evacuation of the sample, the broad band can be removed on most forms of silica, leaving only the sharp band of the isolated hydroxyl groups.[20]

Figure 1 shows that a very striking difference in reactivity exists between these two types of hydroxyl groups. The 3750-cm^{-1} band had a peak optical density of 1.45 before adding the TMA, but only about 0.05 afterward, showing that essentially all of these OH groups had been removed from the surface. There is no well-defined maximum in the broad band of the hydrogen-bonded hydroxyl groups, but the band at 3700 cm^{-1} was reduced to 41% of its original intensity. The hydrogen-bonded hydroxyl groups seem much less reactive than the isolated ones. This is most surprising, as TMA is so very reactive with water—so much so, that the amount of methane produced from the reaction of oxides with trimethylaluminum has been proposed as a method for determining the total hydroxyl content of such solids.[14] Clearly this is not correct, and one should not assume that because a given organometallic compound is very reactive with water it will necessarily provide an excellent way of measuring the total surface hydroxyl content of solids. No definite cause can yet be suggested for the nonremoval of the hydrogen-bonded OH groups. It may partly be due to molecular size effects, as shown by the surface reactions with

Table I: Frequencies of Adsorbed Methyl Groups on Silica

Starting compd	CH stretching frequencies, cm^{-1}	Difference in cm^{-1}
$Al(CH_3)_3$	2955, 2902	53
$Si(CH_3)_4$	2970, 2915	55
$SiCl(CH_3)_3$	2968, 2910	58
$SiCl_3CH_3$	2992, 2925	67
CH_3OH	3000, 2962, 2856	38, 106

(17) V. Ya. Davydov, A. V. Kiselev, and L. T. Zhuralev, *Trans. Faraday Soc.*, 60, 2254 (1964).
(18) R. S. McDonald, *J. Amer. Chem. Soc.*, 79, 850 (1957).
(19) R. S. McDonald, *J. Phys. Chem.*, 62, 1168 (1958).
(20) D. J. C. Yates, *Advan. Catal.*, 12, 265 (1960).

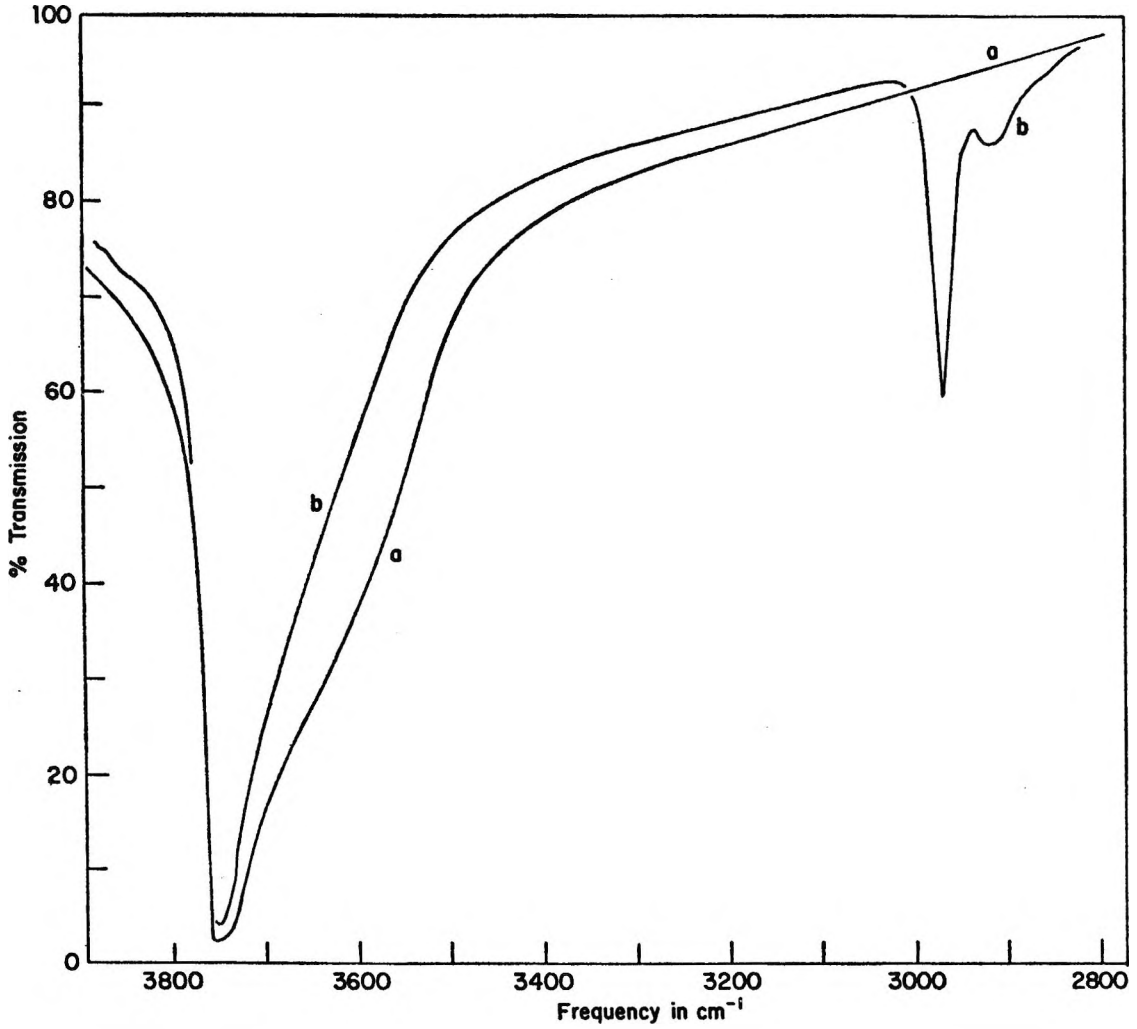


Figure 7. Reaction between silicon tetramethyl and Cabosil (thickness about 50 mg/cm²): a, background spectrum after evacuation at 500° for 1 hr; b, after adding 19.6 cm pressure of $Si(CH_3)_4$ at room temperature, heating rapidly to 500° for 30 min, then cooling to room temperature and evacuating for 2 min. Resolution at 2800, 2900, and 3000 cm^{-1} is 3.2, 2.5, and 2.0 cm^{-1}, respectively.

Table II: Frequencies of Methyl Groups in Pure Compounds Containing Aluminum–Methyl or Silicon–Methyl Groups

Compound	State, thickness in cm	CH stretching frequencies, cm^{-1}	Difference in cm^{-1}	CH deformation frequencies, cm^{-1}
$Al(CH_3)_3$	Pure, 0.0024	2940, 2898	42	1250, 1205
$Si(CH_3)_4$	Solution (0.1%) in CCl_4, 1.0	2960, 2895	65	...
$SiCl(CH_3)_3$	Pure, 0.0023	2968, 2908	60	1255
$SiCl_3CH_3$	Solution (0.1%) in CCl_4, 1.0	2985, 2918	67	...
$O[Si(CH_3)_3]_2$	Solution (0.01%) in CCl_4, 1.0	2965, 2910	55	...
Silicone grease	Smear on NaCl Plate	2968, 2910	58	1262

methanol. In this contrasting reaction, the smaller methanol molecule mainly reacts with the hydrogen-bonded OH groups, leaving the free hydroxyl groups essentially unaffected (Figure 5).

Even though the TMA is much larger than methanol, this cannot, of itself, be the only reason for lack of removal of some of OH groups. For example, that fraction of the hydrogen-bonded OH groups that are on what may be considered to be "flat" portions of the surface should react with TMA. However, those OH groups which are in narrow crevices will be beyond the radius of action of the TMA. It is known that Cabosil consists essentially of nonporous spheres and it is probable that the only crevices and pores that exist which are inaccessible to TMA are those formed as a result of pressing the powdered material into self-supporting disks.

The absorption in the 2800–3000-cm^{-1} region (Figure 1) shows that the species formed during the displacement reaction of the hydroxyl group contains a hydro-

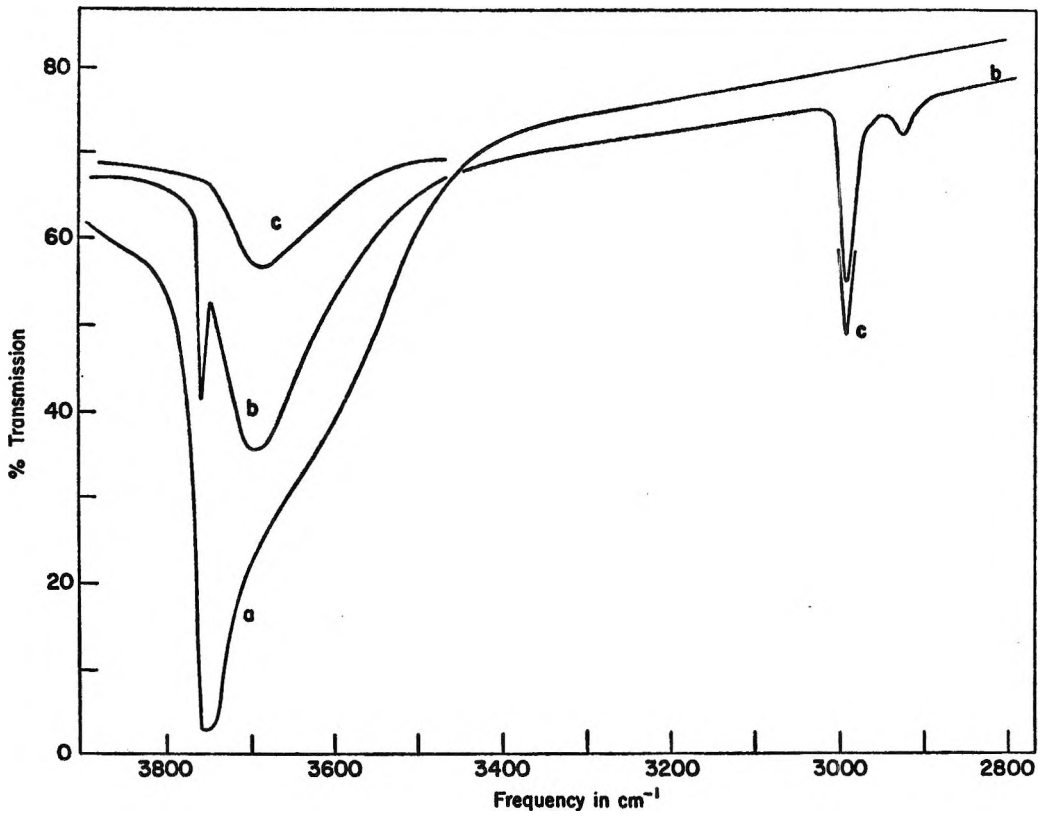


Figure 8. Reaction between trichloromethylsilane and Cabosil (thickness about 35 mg/cm²): a, background spectrum after evacuation at 500° for 2 hr; b, after treatment with TCMS vapor (about 10 cm pressure) at 400° for 15 min, and evacuation at 400° for 5 min; c, as for b, but treatment at 500°. Resolution at 2800, 2900, and 3000 cm^{-1} is 4.0, 3.1, and 2.4 cm^{-1}, respectively.

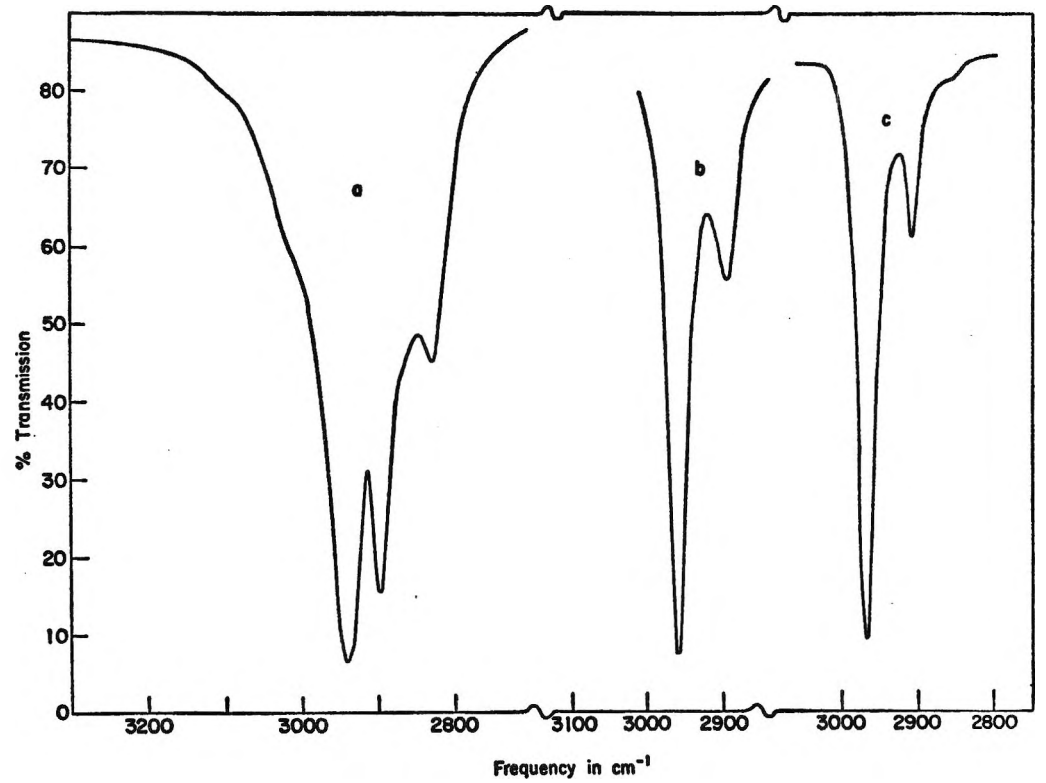
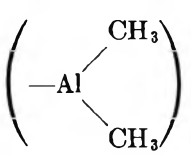


Figure 9. Spectra in the CH stretching region of compounds containing aluminum–methyl groups and silicon–methyl groups. Details of the state of the samples, and thicknesses, are identical with those given in Table II. Pure $Al(CH_3)_3$, a; solution of $Si(CH_3)_4$, b; and silicone grease, c. Resolution at 2800, 2900, and 3000 cm^{-1}: a, 1.6, 1.2, and 1.0 cm^{-1}; b, 2.8, 2.2, and 1.7 cm^{-1}; and 3.2, 2.5, and 2.0 cm^{-1}.

carbon. It will be seen that there are predominantly two bands, at 2955 and 2902 cm^{-1}, although weaker bands can be seen at 2965 and 2835 cm^{-1} (see Table I also). Similar bands are seen with the thicker sample (Figure 2) but now the band near 2960 cm^{-1} is too intense to be precisely located. This hydrocarbon was not thought to be a methoxy group, because of the simplicity of the spectrum. Methoxy groups (Figure 5) show three strong bands in this region of the spectrum (see next section) in contrast to the species made from TMA, which has only two. With compounds containing a methoxy group, the methyl deformation is found close to 1450 cm^{-1}, both for methyl alcohol and dimethyl ether, as well as with surface methoxy groups. The presence of a band at 1450 cm^{-1} permits[21,22] interaction by Fermi resonance between the first vibrational overtone and a fundamental carbon–hydrogen stretching vibration, with a resulting increase in the number of observed bands in the spectrum in the 2800–3000-cm^{-1} region. When methyl groups are attached to a silicon atom, as with silicone oils and greases, or in halogenated methylsilanes, the methyl deformation band is found close to 1260 cm^{-1}. Consequently, the frequency of the first overtone would be in a region where interaction with the carbon–hydrogen stretching vibration cannot occur. A similar argument holds for a methyl group attached to an aluminum atom, as in dimethyl aluminum chloride, where the deformation vibration is found[23] near 1200 cm^{-1}. As shown in Figure 5, we found two overlapping bands near 1470 cm^{-1} when methanol was reacted with silica, whereas no bands were found in that region when trimethylaluminum or chloromethyl silanes were reacted with silica.

For both samples, additional bands were seen in the 2100–2400 cm^{-1} region after reaction with TMA, although only shown for the thicker sample. The most intense bands (and the only ones seen with the thin sample) are at 2160 and 2195 cm^{-1}. A shoulder at 2255 cm^{-1} is seen in Figure 2. It seems very unlikely that these bands are those of adsorbed hydrocarbons, as the only vibrations in such molecules which occur anywhere in this region are those of the triple bonds in acetylenic molecules.[24] It is, of course, most improbable that such entities would be formed under our reaction conditions. These bands are probably those of SiH groups, as they usually absorb[24] in the 2100 to 2200 cm^{-1} region. Such groups have been found[25] on adding atomic hydrogen to silicon, at 2100 cm^{-1}. It is unlikely they are due to Al–H vibrations, as these usually occur[26] between 1700 and 1800 cm^{-1}.

It was suggested by Liefländer and Stöber[13] that aluminum–methyl groups



would be left on the surface of silica after treatment with TMA. If this is so, in view of the violent reaction between TMA and water or oxygen, we might expect that such methyl groups would readily react with other adsorbed molecules, such as water or oxygen. Figure 3 shows that these reactions did not occur. When water was added, large amounts were adsorbed, giving the typical very broad band characteristic of hydrogen-bonded systems.[27] This broad band made it difficult to determine the intensity of the CH bands, although it was obvious that they were only but little affected by the adsorbed water. The water was removed by a series of evacuations at increasing temperatures, and the final treatment, after evacuation at 200°, gave spectrum c (Figure 3). The CH band near 2960 cm^{-1} was not noticeably changed in intensity, while the band near 2900 cm^{-1} is a little weaker.

The very stable configuration of these methyl groups is shown also by other experiments. On several occasions at the end of the experiment, dried air was added to the cell and the spectrum was rerun. No effect was ever detected on the adsorbed species. Finally, these methyl groups show an entirely remarkable and unexpected resistance to deuterium exchange. From Figure 4, it will be seen that after adding water and evacuating at 400°, the sharp 3750-cm^{-1} band is again present, together with a broad band of hydrogen-bonded hydroxyl groups. Some of the methyl groups had been removed by the addition of water and subsequent high-temperature evacuation (compare Figure 2b and 4a). The first deuteration lasted 15 min at 400°, and it will be seen that both types of OH groups are converted into OD groups but that no decrease in the CH bands took place, and no CD groups could be detected. A further deuteration (not shown in the figure) was done (with a fresh dose of D_2) at 400° for 2.25 hr, but although further OH–OD exchange occurred, no CH–CD exchange took place. The sample was then evacuated at 500° for 0.5 hr, and the spectrum was rerun. This spectrum is not shown, but the CH bands became slightly weaker after this treatment. A third deuteration was then done at 500° for 3 hr. After this, nearly all of the OH groups were converted into OD groups but there was still no effect on the CH groups, and no CD groups could be detected. This is very surprising indeed, as it is quite probable that the mechanism of exchange between deuterium and surface

(21) G. Herzberg, "Infrared and Raman Spectra of Polyatomic Molecules," D. Van Nostrand, Inc., Princeton, N. J., 1945.
(22) M. Falk and E. Whalley, *J. Chem. Phys.*, 34, 1554 (1961).
(23) E. Hoffmann, *Z. Elektrochem.*, 64, 616 (1960).
(24) L. J. Bellamy, "The Infrared Spectra of Complex Molecules," 2nd ed, John Wiley and Sons, Inc., New York, N. Y., 1958.
(25) G. E. Becker and G. W. Gobeli, *J. Chem. Phys.*, 38, 2942 (1963).
(26) E. G. Hoffman and G. Schomburg, "Advances in Molecular Spectroscopy," Pergamon Press, London, 1962.
(27) G. C. Pimentel and A. L. McClellan, "The Hydrogen Bond," W. H. Freeman and Co., San Francisco, Calif., 1960.

OH groups is by the deuterium initially being dissociated; such deuterium atoms would then readily exchange with any hydrogen present. This may occur on pure silica (such as Cabosil) as shown by our data with a surface covered with methoxy groups (Figures 5 and 6, and next section). Both the CH and OH groups are then rapidly exchanged with D_2 at 500° and the simplest mechanism of exchange would seem to be that which involves atomic deuterium as an intermediate.

The lack of reactivity would seem to make it unlikely that the groups left after treating silica with TMA contain Al–C linkages, but that they might be Si–C groups. The presence of bands in the Si–H stretching region also leads to the same conclusion. Unless some oxygen were removed from the surface by a strong reducing agent (such as TMA) it is very difficult to account for the presence of these Si–H bands. This whole question will be discussed in more detail later.

Reaction between Methanol and Silica. We wished to study surface methoxy groups at comparable resolutions to that used in our TMA work, in order to determine the differences in the spectra. Methanol was reacted with Cabosil at 350° for 1 hr, and the results are shown in Figure 5. It will be seen that three sharp CH bands are present: at 3000, 2962, and 2856 cm^{-1}. In addition, shoulders are present at 3040 and 2935 cm^{-1}. It is of interest to note that the 2856-cm^{-1} band is very narrow, with half-width 11 cm^{-1}. Our spectrum is quite similar to that given by McDonald,[19] but his samples of Cabosil were much thinner, and the bands consequently weaker. In addition, we have found two overlapping CH deformation bands near 1470 cm^{-1} (Figure 5), which is further evidence that we have formed surface methoxy groups. No results in this region were given in the earlier work. It is well established[24] that the deformation frequencies of $-OCH_3$ groups occur close to 1460 cm^{-1}. We note that $C-CH_3$ groups have a deformation band[24] at 1450 ± 20 cm^{-1}, but it is difficult to see how such groups could have been formed from methanol on silica.

In contrast to the reaction with TMA, it will be seen that the isolated OH groups at 3750 cm^{-1} are but little affected by this reaction, as their peak intensity after the methanol treatment is 80% of their intensity after the initial evacuation of the sample. Those OH groups mainly affected seem to be hydrogen bonded OH groups of frequency close to 3720 cm^{-1}. At this frequency, the OH band after methanol treatment is only 43% of its initial value. However, it should be noted that the methanol treatment, in addition to removing OH groups, forms new OH groups, or possibly rearranges the existing OH groups. This is shown by the fact that curves a and b of Figure 5 cross at 3600 cm^{-1}, and at frequencies below this the OH band on spectrum b is more intense than that of a. The processes taking place during high-temperature reaction of methyl alcohol with silica are clearly most complex, and will need considerable further study before they are understood in any degree of detail. Deuteration of the methoxy groups has also been studied (Figure 6). After the initial deuteration at 350°, only a very small band at 2768 cm^{-1}, of OD groups, and no CD groups, could be detected. However, after deuteration at 500°, both OD and CD groups could be seen. Further exchange at 550° removed most of the CH-containing species, while leaving quite a strong OH band at 3750 cm^{-1}. Thus, in very marked contrast to the results with the surface methyl groups derived from trimethylaluminum, the methoxy groups exchange very readily with D_2. In fact, the data of Figure 6 indicate that all of the CH groups will be converted into CD groups before all of the OH groups are exchanged.

After the deuteration experiments shown in Figure 6, the sample was remethylated with CH_3OH. This was done initially at 350° for 15 min and the CH bands were restored to their original intensity, as seen in Figure 6a. The OD band was nearly all removed, but the CD bands remained quite strong. On further methylation, at 600° for 20 min, all of the OD and CD groups were removed, but surface OH groups remained. It was noticed that after this methylation at 600°, the sample was still as white as it was initially. This observation should be contrasted with earlier work on porous glass,[7] where 360° was used for methylation. At that time, in an attempt to remove all of the OH groups, higher temperatures than 360° were used, but the samples went brown and black, as the methyl alcohol was decomposed by the surface. This relative reactivity of porous glass may be due to the sodium impurity it contains, as shown by work on the effect of γ radiation[28] on this material.

Formation of Silicon–Methyl Groups on Silica. In another approach to show that the methyl groups formed from TMA and silica are silicon–methyl groups, we have studied the properties of surface silicon–methyl groups, made from a series of silicon compounds and silica.

The first compound used was tetramethylsilane, which is very stable and easy to handle. Figure 7 shows that, as might be expected, the reaction does not take place readily, as temperatures of 500° had to be used. While there is some reduction in the intensity of the 3750-cm^{-1} band, the main effect is on the hydrogen-bonded band between 3750 and 3500 cm^{-1}. The adsorbed species, most probably in the trimethyl form, $-Si(CH_3)_3$, have CH stretching bands at 2970 and 2915 cm^{-1}.

We have also studied the reaction between trimethylchlorosilane (TMCS) and Cabosil, but have not given the spectra as they are similar to those published

(28) D. J. C. Yates and P. J. Luccesi, *J. Amer. Chem. Soc.*, **86**, 4258 (1964).

earlier.[17] The effects in the OH region are quite pronounced, and we found them to be similar to those reported elsewhere,[17] in that mainly the free OH groups react with TMCS (presumably with the formation of HCl). It has also been shown[8] with dimethyldichlorosilane that mostly the free OH groups are removed at 400°. It should, however, be noted that when a wide range of silicas is used with varying pore sizes and surface areas, the situation becomes very complex.[9] In addition, as mentioned by Snyder and Ward,[9] we agree that there is really no clear-cut differentiation of hydroxyl groups into "free" and "hydrogen-bonded" types. The fact that the band caused by the hydrogen-bonded species extends continuously from 3750 cm^{-1} to lower frequencies demonstrates this.

The spectra of the methyl groups which remain on the surface after TMCS treatment have been given by only one group of workers,[17] and no CH frequencies were given. For our samples, the bands were found at 2968 and 2910 cm^{-1} (see Table I). These bands are at almost the same frequency as those surface groups put on silica from silicon tetramethyl, and this agreement substantiates the idea that both treatments give adsorbed silicon trimethyl groups. In the case of these groups formed from TMCS, we have performed deuterium exchange experiments. The initial deuteration was at 400° for 15 min, while the next was at 500° for the same time. In agreement with the idea that silicon–methyl groups are formed in the trimethylaluminum experiments (Figure 4) none of the methyl groups from TMCS exchanged into CD groups, while quite extensive OH–OD exchange took place.

As no information seems available on adsorbed silicon–methyl species containing one methyl group, we have briefly studied the reaction of trichloromethylsilane (TCMS) with silica. Figure 8 shows that extensive removal of the surface OH groups took place, with predominantly the free OH groups being removed, as with TMCS. However, some support for an intermediate frequency OH group being most reactive[9] is given by spectrum b. At this intermediate stage, it will be seen that the OH band at 3740 cm^{-1} is weaker than the band at 3750 cm^{-1} (the "free" hydroxyl band) while initially (spectrum a) they were of very similar intensity. Finally after the 500° treatment (c), both these bands have gone, leaving a weak, broad band due to hydrogen-bonded hydroxyl groups with a peak at 3680 cm^{-1}. Clearly the reactions between these chlorinated silanes and silica are very complex.

The CH stretching frequencies of these monomethyl silane groups are at 2992 and 2925 cm^{-1}, which is significantly higher in frequency than the corresponding trimethylsilane species.

Finally, it should be noted that the difference in the two CH stretching frequencies of the silicon–methyl groups put on the surface from tri- and tetramethylsilanes are essentially the same as are found in the methyl groups put on the surface by reaction with TMA (see Table I). This reinforces our view that silicon–methyl groups are found on silica after reaction with TMA under our conditions.

Conclusions

The stability to water, air, and deuterium of the surface species obtained when trimethylaluminum reacts with silica, together with the close similarity of the spectra of the product with that of silica known to contain silicon–methyl groups, strongly suggests that the surface species formed from TMA and silica contains silicon–methyl groups rather than aluminum–methyl groups.

Unexpected though this is, it is not inconsistent with the energies required to make and break the various bonds involved in such a rearrangement. The heat of formation of fused silica,[29] $\Delta H(SiO_2)$ is −198 kcal/mol, giving −49.5 kcal/mol of Si–O bonds. The heat of formation of alumina,[29] $\Delta H(Al_2O_3)$ is −390 kcal/mol, giving a value of −65 kcal/mol per Al–O bond. This indicates that the Al–O bond is more stable than the Si–O bond by some 15 kcal/mol. Cottrell gives[30] the bond energy of the C–Al bond in $Al(CH_3)_3$ as 61 kcal/mol and the energy of the C–Si bond in $Si(CH_3)_4$ as 72 kcal/mol, so the latter is 11 kcal/mol more stable than the former. It follows that a combination of Al–O and Si–C bonds in the surface structure would be more stable than a combination of Al–C and Si–O bonds, providing a thermodynamic driving force for the proposed rearrangement.

A mechanism for the reaction can be suggested. From the observed loss of free (nonhydrogen bonded) hydroxyl groups of the silica, it is reasonable to suppose that the initial interaction between the trimethylaluminum and the surface takes place *via* these particular hydroxyl groups, liberating methane. For these isolated hydroxyl groups, the lone pairs of electrons on their oxygen atoms are readily available to interact with molecules having electron acceptor properties which come close to the surface. The oxygen atoms in the hydrogen-bonded hydroxyl groups, in contrast, have their lone-pair electrons participating in the hydrogen bond. Such oxygen atoms will necessarily be less reactive toward electron-acceptor molecules, which can explain the lack of reaction between trimethylaluminum and hydrogen-bonded hydroxyls.

The above reaction, if the only one occurring, might well leave a dimethylaluminum species on the surface, as suggested by Liefländer and Stöber.[13] On the contrary, we find silicon–methyl groups (and some silicon–hydrogen groups) to be the final product of the reaction.

(29) "Handbook of Chemistry and Physics," 44th ed, The Chemical Rubber Co., Cleveland, Ohio, 1963.

(30) T. L. Cottrell, "The Strength of Chemical Bonds," 2nd ed, Butterworth and Co. Ltd., London, 1958, p 275.

It seems very likely that, after the initial loss of one methyl group from the trimethylalumnium, the aluminum atom reacts further with nearby oxygen atoms of the silica, through a concerted 4-center reaction involving the unfilled fourth-coordinate position of the aluminum atom. This results in the breaking of two silicon–oxygen linkages and the formation of two silicon–methyl bonds, giving the observed adsorbed species. This assumption is also supported by the observed[15] reactions in the liquid state between trialkylaluminums and octamethylcyclotetrasiloxane in which the Si–O–Si bond can be cleaved. In these reactions, the trialkylaluminum acts as an alkylation agent by transfer of one alkyl group to the silicon moiety. The alkylation action of trialkylaluminums has been well established.[31]

(31) H. Jenkner, *Chem. Z.*, **86**, 527 (1962).

Ultrasonic Absorption in Hydrated Melts. I. Systems of $Ca(NO_3)_2 \cdot 4H_2O$ and Its Mixtures with Water

by G. S. Darbari and S. Petrucci

Polytechnic Institute of Brooklyn, Brooklyn, New York 11201 *(Received September 16, 1968)*

Results of ultrasonic absorption measurements of $Ca(NO_3)_2 \cdot 4H_2O$ melts and of 1:4.3, 1:4.7, and 1:5.0 $Ca(NO_3)_2$–H_2O mixtures are presented. The temperature range 25–75° and the frequency range of 3–195 MHz have been investigated. A relaxation process at 20 ± 5 MHz for $Ca(NO_3)_2 \cdot 4H_2O$, shifting to higher frequencies by addition of water, is reported. This relaxation tends to disappear by increasing the temperature. The volume viscosities are calculated in the frequency region below and above the observed relaxation region. The conclusion is drawn that two overlapping sources of the volume viscosities exist. At frequencies below the relaxation region, structural and nonstructural molecular rearrangements contribute to the excess sound absorption over the classical Stokes value. The energy barrier of this over-all process is larger than the one for shear viscous flow as indicated by the decrease of the ratio η_v/η_s with temperature. At frequencies larger than the observed relaxation region only the structural contributions to the sound absorption remain. The barrier of energy for the compression volume viscosity η_v' is the same as the one for the shear viscosity η_s. This indicates that all of the possible translation molecular rearrangements have been frozen out after the relaxation except the ones with a barrier of translational energy equal to the viscous flow.

Introduction

Theories of equilibrium and mass transport properties of diluted electrolytic solutions are based on the classical Debye–Hückel model. Transport theories start at infinite dilution and dissect a transport property like electrical conductance into the ionic components and calculate the ionic interactions at nonzero concentration. The Fuoss–Onsager[1] and other similar theories, with all of the complexity of the mathematical derivation and sophistication in predicting the various interionic effects, are rarely valid at $C \geq 10^{-2}$–10^{-1} M for a 1:1 electrolyte in water at room temperature. For concentrated solution the situation for transport theories has begun to improve in the past few years.

As predicted a long time ago by Fuoss,[2] the most promising development seems to be derived from the fused-salt end of the concentration scale. Angell[3] has applied the free-volume theory of Cohen and Turnbull[4] with remarkable success to transport theories of fused salts and glass-forming mixtures like the system $Ca(NO_3)_2$–KNO_3,[3] to other fused salts,[5] to highly concentrated glass-forming electrolyte solutions like $Ca(NO_3)_2 \cdot 4H_2O$ and $Mg(NO_3)_2 \cdot nH_2O$ (n variable from 3 to 6), and to mixtures of $Ca(NO_3)_2 \cdot 4H_2O$–KNO_3.[6,7] According to the Cohen and Turnbull theory as well as to similar ones,[8] liquids that show a glass transition have an apparent energy of activation for shear flow that changes rapidly with temperature and

(1) R. M. Fuoss and F. Accascina, "Electrolytic Conductance," Interscience Publishers, Inc., New York, N. Y., 1959; R. M. Fuoss and K.-L. Hsia, *Proc. Natl. Acad. Sci. U. S.*, **57**, 1550 (1967).

(2) R. M. Fuoss, *Chem. Rev.*, **17**, 27 (1935).

(3) C. A. Angell, *J. Phys. Chem.*, **68**, 218 (1964); **68**, 1917 (1964).

(4) M. H. Cohen and D. Turnbull, *J. Chem. Phys.*, **31**, 1164 (1959).

(5) C. A. Angell, *J. Phys. Chem.*, **69**, 399 (1965).

(6) C. A. Angell, *ibid.*, **69**, 2137 (1965).

(7) C. A. Angell, *J. Electrochem. Soc.*, **112**, 1224 (1965).

(8) A. Doolittle, *J. Appl. Phys.*, **22**, 1471 (1951); **23**, 238 (1951); M. Williams, R. Landel, and J. Ferry, *J. Am. Chem. Soc.*, **77**, 3701 (1955); J. Beuche, *J. Chem. Phys.*, **30**, 748 (1959).

becomes infinity at a temperature T_0. At this temperature the liquid assumes the characteristics of an amorphous solid or a glass. Generally $T_0 > 0°K$ while for $T_0 = 0°K$ the non-Arrhenius character of the liquid disappears and the temperature dependence of the transport property resembles the one of an Arrhenius liquid.

T_0 was therefore defined as an ideal glass temperature where all of the translational movements disappear and the free-volume parameter goes to zero.[4] It is also clear that in terms of the transport properties of the glass-forming liquid it is the difference $(T - T_0)$ that is characteristic of the ability of the liquid to sustain mass transport. For normal liquids T is the corresponding value $(T_0 = 0)$. An alternate treatment relating T_0 to the temperature where the configurational entropy vanishes has been proposed.[9] The following is not invalidated by this alternate thermodynamic approach.

The general idea proposed by the Cohen–Turnbull theory[4] is that "*any liquid in principle would go through a glass transition if sufficiently undercooled and if crystallization did not occur.* The implication of the use of the Cohen and Turnbull theory to electrolyte solutions by Angell is to have tested a theoretical tool to explain the temperature and concentration dependence[10] of transport properties, a problem unsolved by classical approaches in concentrated solutions.

The major limitation to the general applicability of the above theory is the limited number of systems showing glass-forming properties, and therefore the limited possibility of verifying the generality of the above findings in all ionic liquids. Indeed to observe a glass transition temperature, it is necessary to cool a liquid to a temperature where the time scale of the experiment and the time scale of the mass transport molecular rearrangements become comparable. For ordinary mass transport experiments, therefore, one must cool the liquid close to T_0 for glass-forming liquids. In general, many liquids crystallize before showing even a non-Arrhenius behavior, thus limiting the possibility of applying the above theory.

This limitation can, in principle, be removed if one could study the glasslike properties of a liquid at temperatures higher than the glass transition temperatures. This can be achieved if the time scale of the experiment is so reduced that the time necessary for the molecular rearrangements becomes of the same order as the time necessary to respond to the applied stress.

These times ($<10^{-6}$ sec) are far beyond the range of classical transport experiments but are within the range of ultrasonic techniques (where the applied stress corresponds to a high-frequency adiabatic compression). By using ultrasonic waves, a pseudo-glass transition may, in principle, be caused in normal liquids at temperatures above their freezing temperatures.[11]

Litovitz applied ultrasonic absorption techniques to fused alkali nitrates and demonstrated the existence of a volume viscosity η_v with ratios $\eta_v/\eta_s \approx 5$–20.[12] For the case of fused $ZnCl_2$[13] it was possible to measure the actual relaxation time and attribute it to a structural relaxation.

The hydrated melt $Ca(NO_3)_2 \cdot 4H_2O$, that, as stated above, is a glass-forming liquid, had been investigated in this laboratory in a pilot research.[14] A relaxation appeared to exist.

In this paper a more extensive and precise series of measurements in a wider range of temperatures varying the salt–water composition is presented.

A phenomenological interpretation of the sound absorption at frequencies below and above the relaxation region is proposed in terms of the volume viscosities. It is contended that if this interpretation is correct, ultrasonic absorption may become a tool for the study of mass transport properties of electrolyte solutions and fused salts. The enormous potentiality of this method is in its ability to "freeze out" progressively all of the possible translational molecular rearrangements by varying the frequency of the compressional wave.

Experimental Section

Fisher reagent $Ca(NO_3)_2 \cdot 4H_2O$ was used without further purification. It was melted in a closed bottle without loss of water. This was checked by subsequent analysis by cation-exchange technique and acid titration by Tham.[14a] Addition of water by weight to $Ca(NO_3)_2 \cdot 4H_2O$ and subsequent analysis of the melt was performed in order to prepare the various mixtures investigated.

The thermostat with a proportional Bailey thermoregulator was used and thus the temperature was maintained constant within 0.05°.

A new ultrasonic stainless steel cell of improved design especially suitable for moderately high temperatures (below the Curie point of quartz) was used. It consists of a twin-crystal interferometric system. The upper crystal (sender) is a 1-in. diameter X-cut quartz crystal mounted on the top of a 7 in. long, 1-in. diameter fused-quartz delay line.

The lower crystal (receiver), also a 1-in. diameter X-cut quartz crystal, is mounted on a circular stainless steel plate suspended from a stainless steel block by means of three rods placed 120° apart. The metal block also holds the delay line. The metal plate holding

(9) G. Adam and J. H. Gibbs, *J. Chem. Phys.*, **43**, 139 (1965).
(10) C. A. Angell, *J. Phys. Chem.*, **70**, 3988 (1966).
(11) T. A. Litovitz in "Physical Acoustics," Vol. 2, Part A, W. P. Mason, Ed., Academic Press, 1965.
(12) R. W. Higgs and T. A. Litovitz, *J. Acoust. Soc. Am.*, **32**, 1108 (1964).
(13) G. T. Gruber and T. A. Litovitz, *J. Chem. Phys.*, **40**, 13 (1964).
(14) S. Petrucci and F. Fittipaldi, *J. Acoust. Soc. Am.*, **42**, 517 (1967).
(14a) L. Meites, "Handbook of Analytical Chemistry," McGraw-Hill Book Co., Inc., New York, N. Y., 1963, p 334.

the lower crystal can be oriented with respect to the lower face of the delay line by means of the micrometers driving the three 120° apart rods holding the lower plate.

The upper crystal and the attached delay line can be moved vertically with respect to the lower metal plate and crystal by means of a micrometer that could read up to 5×10^{-4} in. The assembly incorporates coaxial electrical connectors for the two crystals, the electrical line connecting the lower crystal (receiver) being insulated from contact with the liquid by a stainless steel tubing.

The entire assembly is dipped in a Pyrex cell containing the melt so that only the lower plate and the crystal and part of the delay line are immersed in the melt. An O-ring seal between the Pyrex cell and the metal assembly keeps the melt completely sealed.

The advantage of this "dip" cell is that the melt can be purified if necessary (by vacuum, dry N_2, filtration) before using the ultrasonic cell directly in the Pyrex cell. In such cases a Pyrex apparatus with O-ring vacuum connections and stopcocks is connected to the Pyrex cell. All of the drying procedure precedes the melting of the salt, and then the upper glass apparatus is removed and substituted with the ultrasonic cell. The ultrasonic cell compartment above the melt can also be blanketed by dry nitrogen when necessary.

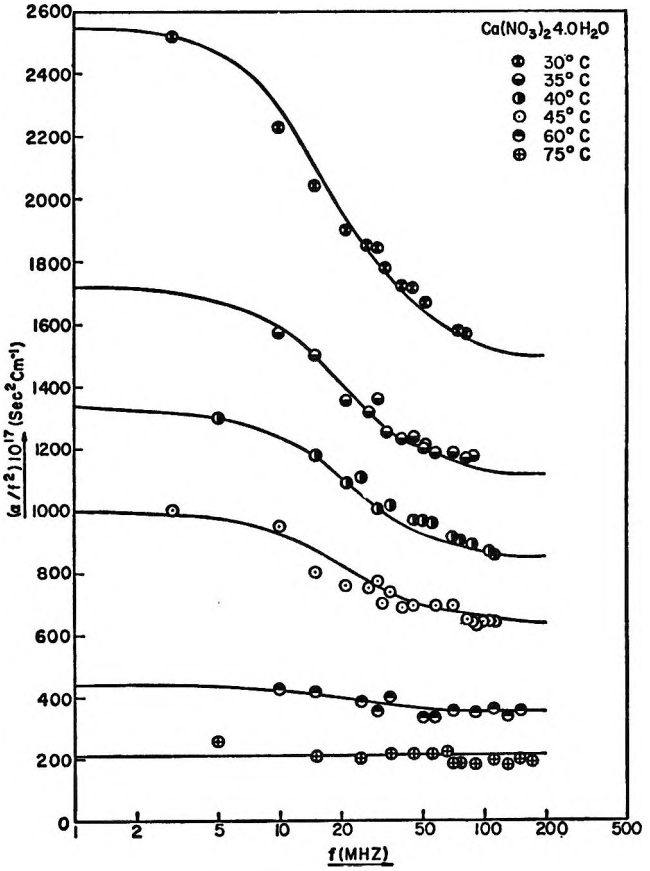


Figure 1. Plot of α/f^2 (cm^{-1} sec^2) *vs.* the frequency (MHz) for $Ca(NO_3)_2 \cdot 4H_2O$ at various temperatures.

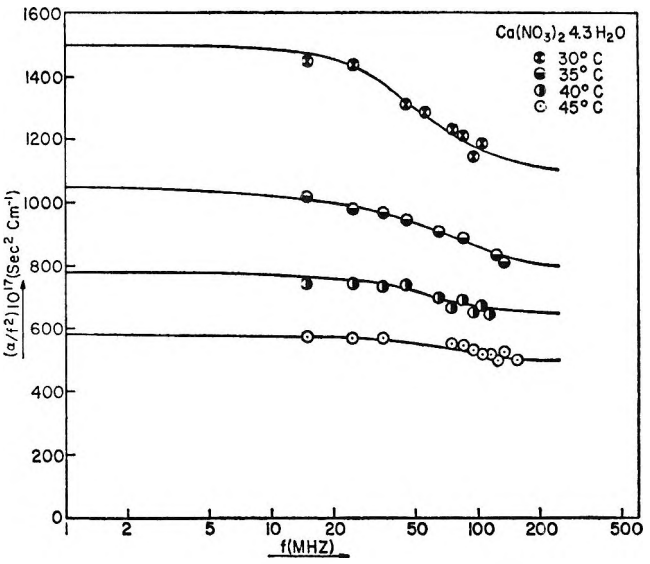


Figure 2. Plot of α/f^2 (cm^{-1} sec^2) *vs.* the frequency (MHz) for $Ca(NO_3)_2 \cdot 4.3H_2O$ at various temperatures.

The above assures the flexibility for working in anhydrous fused salts.

X-cut quartz crystals of 3, 5, and 10 MHz (fundamental) were used. The electronic equipment consisted of a Chesapeake U-100 pulser (frequency range 1–210 MHz), an Arenberg WA-600-E receiver (frequency range 3–65 MHz), and a Matec 560 receiver (frequency range 5–320 MHz). A 608A Hewlett-Packard standard signal generator and a Tektronix 535 scope completed the assembly. The mounting of this instrumentation and its detailed use have been discussed elsewhere.[15]

Results

In Table I the results for the absorption coefficient α (cm^{-1}) as α/f^2 (cm^{-1} sec^2) at various frequencies f (MHz) and temperatures (°C) are reported for the compositions investigated. The sound velocities measured at 10 MHz are also reported. No definite trend within the sensitivity of the method (±20 m/sec) was observed in the case of $Ca(NO_3)_2 \cdot 4.7H_2O$ and $Ca(NO_3)_2 \cdot 5H_2O$. In Figures 1–4 the quantities $10^{17}(\alpha/f^2)$ are reported *vs.* the frequency f. For $Ca(NO_3)_2 \cdot 4H_2O$ at 75° a straight line indicates the absence of a relaxation (within the sensitivity of the data) in the frequency range investigated.

For the other temperatures and compositions, the data have been fitted to the function for a single relaxation

$$\frac{\alpha}{f^2} = \frac{A}{1 + (f/f_r)^2} + B \qquad (1)$$

where B is the high-frequency value of α/f^2, A is a

(15) S. Petrucci, *J. Phys. Chem.*, 71, 1174 (1967); S. Petrucci and M. Battistini, *ibid.*, 71, 1181 (1967).

Table I: Data of Sound Absorption α/f^2 and Frequency f for Various Temperatures and Compositions Investigated

$Ca(NO_3)_2 \cdot 4H_2O$

$t = 30°$		$t = 35°$		$t = 40°$		$t = 45°$		$t = 60°$		$t = 75°$	
f, MHz	$10^{17}(\alpha/f^2)$, cm^{-1} sec^2	f, MHz	$10^{17}(\alpha/f^2)$, cm^{-1} sec^2	f, MHz	$10^{17}(\alpha/f^2)$, cm^{-1} sec^2	f, MHz	$10^{17}(\alpha/f^2)$, cm^{-1} sec^2	f, MHz	$10^{17}(\alpha/f^2)$, cm^{-1} sec^2	f, MHz	$10^{17}(\alpha/f^2)$, cm^{-1} sec^2
3	2522	10	1573	5	1300	3	1000	10	424	5	259
10	2225	15	1500	15	1180	10	956	15	410	15	200
15	2040	21	1349	21	1095	15	800	25	380	25	200
21	1900	27	1313	25	1110	21	760	30	352	35	218
27	1850	30	1360	30	1010	27	755	35	395	45	210
30	1840	33	1254	35	1020	30	775	50	331	55	214
33	1780	39	1232	45	970	33	700	57	335	65	221
39	1720	45	1236	50	968	35	737	70	355	75	181
45	1720	50	1200	55	960	39	690	90	340	90	180
51	1670	51	1207	69	915	45	695	110	364	110	196
75	1580	57	1181	75	902	57	690	130	334	130	179
81	1570	70	1183	87	890	69	695	150	353	150	192
$u = 1915 \pm 20$ m/sec		81	1174	105	868	81	642	$u = 1830 \pm 20$ m/sec		170	189
		87	1179	110	857	87	640			$u = 1820 \pm 20$ m/sec	
		$u = 1905 \pm 20$ m/sec		$u = 1888 \pm 20$ m/sec		90	638				
						99	645				
						105	645				
						110	640				
						$u = 1848 \pm 20$ m/sec					

$Ca(NO_3)_2 \cdot 4.3H_2O$

$t = 30°$		$t = 35°$		$t = 40°$		$t = 45°$	
f, MHz	$10^{17}(\alpha/f^2)$, cm^{-1} sec^2	f, MHz	$10^{17}(\alpha/f^2)$, cm^{-1} sec^2	f, MHz	$10^{17}(\alpha/f^2)$, cm^{-1} sec^2	f, MHz	$10^{17}(\alpha/f^2)$, cm^{-1} sec^2
15	1450	15	1020	15	750	15	575
25	1440	25	980	25	748	25	565
45	1310	35	965	35	740	35	565
55	1290	45	948	45	738	75	555
75	1235	65	910	65	700	85	545
85	1210	85	888	75	673	95	538
95	1150	125	838	85	695	105	520
105	1190	135	815	95	658	115	520
$u = 1874 \pm 20$ m/sec		$u = 1862 \pm 20$ m/sec		105	675	135	527
				115	655	155	500
				$u = 1860 \pm 20$ m/sec		$u = 1854 \pm 20$ m/sec	

$Ca(NO_3)_2 \cdot 4.7H_2O$, $u = 1856 \pm 20$ m/sec

$t = 25°$		$t = 30°$		$t = 35°$		$t = 40°$		$t = 45°$	
f, MHz	$10^{17}(\alpha/f^2)$, cm^{-1} sec^2	f, MHz	$10^{17}(\alpha/f^2)$, cm^{-1} sec^2	f, MHz	$10^{17}(\alpha/f^2)$, cm^{-1} sec^2	f, MHz	$10^{17}(\alpha/f^2)$, cm^{-1} sec^2	f, MHz	$10^{17}(\alpha/f^2)$, cm^{-1} sec^2
15	945	15	650	15	470	5	415	15	275
25	885	35	625	25	480	15	395	25	275
33	868	45	615	35	475	25	390	35	285
39	880	65	600	45	478	35	385	45	295
45	835	75	580	55	475	45	370	55	295
55	825	85	575	75	468	65	378	65	285
65	795	95	575	85	468	75	348	75	285
95	795	105	565	95	470	85	348	85	280
125	750	115	560	105	458	95	355	95	280
135	740	125	550	115	460	125	340	105	280
				125	460	135	345	115	275
				135	455	145	330	125	265
				145	445			135	265
				155	435				

Table I (*Continued*)

$Ca(NO_3)_2 \cdot 5H_2O$, $u = 1847 \pm 20$ m/sec

$t = 25°$		$t = 30°$		$t = 35°$		$t = 40°$		$t = 45°$	
f, MHz	$10^{17}(\alpha/f^2)$, cm^{-1} sec^2	f, MHz	$10^{17}(\alpha/f^2)$, cm^{-1} sec^2	f, MHz	$10^{17}(\alpha/f^2)$, cm^{-1} sec^2	f, MHz	$10^{17}(\alpha/f^2)$, cm^{-1} sec^2	f, MHz	$10^{17}(\alpha/f^2)$, cm^{-1} sec^2
15	660	15	505	15	385	15	304	15	255
25	643	25	495	25	378	25	300	25	230
45	653	35	478	35	365	35	290	35	225
55	643	45	485	45	370	45	292	45	240
75	600	55	475	55	368	55	305	55	238
85	600	75	478	65	342	75	295	65	245
95	575	85	473	85	348	85	288	75	240
105	550	90	455	95	348	95	280	85	240
115	560	105	428	115	328	105	285	95	222
135	540	115	435	135	325	125	275	105	225
		125	418	165	305	135	280	115	230
		135	408			145	280	125	228
		165	410			155	275	135	235
						165	270	165	218
						175	265		
						195	250		

constant, and f_r is the relaxation frequency. Equation 1 has been fitted to the data as a three-parameter equation in A, B, and f_r. The solid lines in Figures 1–4 represent eq 1, except for the melt $Ca(NO_3)_2 \cdot 4H_2O$ at 75° where the best estimate of the value of α/f^2 is $10^{-17}(200 \pm 10)$ cm^{-1} sec^2. The results of the above calculations are given in Table II. The A and B values are precise within $\pm 10\%$.

Discussion

According to Litovitz[11] and Lamb,[16] the ratio α/f^2 exceeds the classical Stokes value for most liquids, the excess being due to a volume viscosity contribution to the energy loss. The total loss is

$$\frac{\alpha}{f^2} = \frac{2\pi^2}{\rho u^3}\left[\frac{4}{3}\eta_s + \eta_v + (\gamma - 1)\frac{x}{c_p}\right] \qquad (2)$$

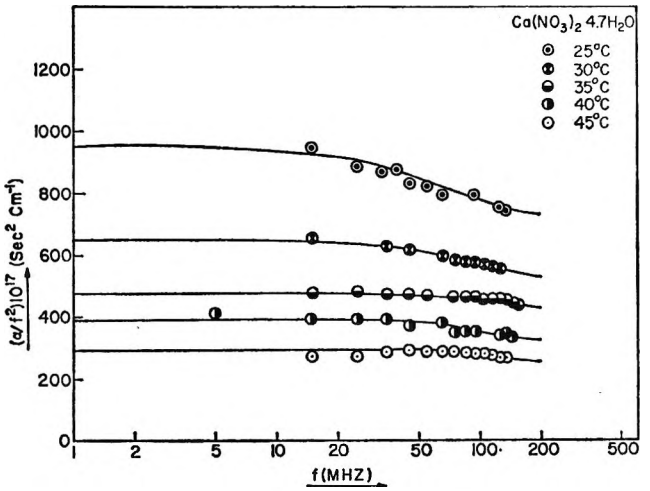


Figure 3. Plot of α/f^2 (cm^{-1} sec^2) *vs.* the frequency (MHz) for $Ca(NO_3)_2 \cdot 4.7H_2O$ at various temperatures.

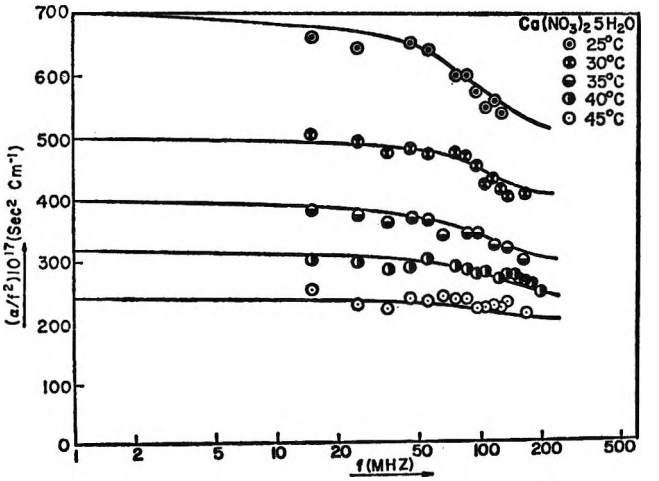


Figure 4. Plot of α/f^2 (cm^{-1} sec^2) *vs.* the frequency (MHz) for $Ca(NO_3)_2 \cdot 5H_2O$ at various temperatures.

with u the sound velocity, ρ the density (g/cm^3), $\gamma = c_p/c_v$, c_p and c_v the specific heats at constant pressure and volume, respectively, x the coefficient of thermal conductivity, η_s the shear viscosity coefficient, and η_v the volume viscosity coefficient.

The classical Stokes expression on the other hand is

$$\frac{\alpha_{class}}{f^2} = \frac{2\pi^2}{\rho u^3}\left[\frac{4}{3}\eta_s + (\gamma - 1)\frac{x}{c_p}\right] \qquad (3)$$

For almost all liquids (except liquid metals and liquid helium) the term due to the thermal conductivity is small[11,16] compared with the term due to shear viscosity.

For the present data the α_{class}/f^2 (calculated on the basis of eq 3 omitting the thermal conductivity term) is lower than the B value in eq 1 as it can be seen from

(16) J. Lamb, ref 11, pp 203–209.

Table II: Densities, Shear Viscosities, A, B, and f_r Parameters (α_{class}/f^2) and Ratios η_v/η_s and η_v'/η_s for the Various Temperatures and Compositions Investigated

Temp, °C	ρ, g/cm³	η_s, P	10^{17} A, cm⁻¹ sec²	10^{17} B, cm⁻¹ sec²	f_r, MHz	$10^{17}(\alpha_{Stokes}/f^2)$, cm⁻¹ sec²	η_v/η_s	$\eta_v'/\eta_s = R$
				$Ca(NO_3)_2 \cdot 4H_2O$				
30	1.743	2.014	1050	1500	18 ± 3	433	6.5	3.3
35	1.738	1.392	620	1100	20 ± 3	304	6.2	3.5
40	1.734	1.062	480	850	20 ± 3	239	6.1	3.4
45	1.730	0.835	350	650	20 ± 3	201	5.3	3.0
60	1.717	0.427	90	350	20 ± 5	107	4.1	3.0
75	1.704	0.234	...	200	...	60	3.2	3.1
				$Ca(NO_3)_2 \cdot 4.3H_2O$				
30	1.721	1.175	400	1100	45 ± 5	272	6.0	4.0
35	1.717	0.832	250	800	50 ± 5	197	5.8	4.1
40	1.712	0.661	140	640	60 ± 10	157	5.3	4.1
45	1.710	0.501	80	500	70 ± 10	121	5.0	4.2
				$Ca(NO_3)_2 \cdot 4.7H_2O$				
25	1.694	1.123	250	720	60 ± 10	272	3.3	2.2
30	1.690	0.832	130	520	70 ± 10	202	3.0	2.2
35	1.688	0.589	60	400	100 ± 10	143	3.1	2.4
40	1.681	0.468	70	320	100 ± 20	114	3.2	2.4
45	1.678	0.363	50	240	120 ± 20	89	3.0	2.3
				$Ca(NO_3)_2 \cdot 5.0H_2O$				
25	1.673	0.813	200	500	80 ± 10	201	3.3	2.0
30	1.672	0.602	140	380	90 ± 10	151	3.2	2.0
35	1.671	0.468	110	290	90 ± 10	110	3.5	2.2
40	1.663	0.355	100	220	100 ± 10	89	3.4	2.0
45	1.657	0.279	50	190	120 ± 20	70	3.2	2.3

Table II. This suggests that contributions to η_v from other relaxation processes with relaxation frequency higher than the one observed exist. The ratio η_v/η_s can be calculated rearranging eq 2 and 3 (dropping the thermal conductivity terms) into

$$\frac{\eta_v}{\eta_s} = \frac{4}{3}\left(\frac{\alpha}{\alpha_{class}} - 1\right) \tag{4}$$

The value of α in eq 4 can be considered either below the observed relaxation frequency region or above it. In both cases the ratio α/f^2 is constant with frequency. From eq 1 for $f \ll f_r$

$$\left(\frac{\alpha}{f^2}\right)_{f \ll f_r} = A + B \tag{5}$$

The value of α can therefore be calculated for $f \ll f_r$. In Table II the ratio η_v/η_s is reported. For $Ca(NO_3)_2 \cdot 4H_2O$ this ratio is not constant as it should be, in principle, for a purely structural relaxation.[11,16] In fact, the ratio η_v/η_s decreases with temperature. For higher water content than $4.3H_2O$ this trend, if existing, is not visible within precision of the data.

Further from eq 1, for $f \gg f_r$

$$\left(\frac{\alpha}{f^2}\right)_{f \ll f_r} = B$$

The value of $\eta_v'/\eta_s = R$ is reported in Table II as calculated from the above relation. η_v' is the contribution to η_v at frequencies larger than the observed relaxation frequencies. It can be seen that the ratio η_v'/η_s changes with composition of the liquid but for each composition does not show any systematic change with temperature within the precision of the determination of B. It is now postulated as in the case of fused alkali nitrates[12] that the source of η_v' is structural or in other words that the sources of η_v' are due to energy losses caused by the finite time of structural rearrangements in the melt under the passage of the ultrasonic wave. η_v' is therefore a compressional viscosity that corresponds physically to the shear resistance to a closer molecular packing (and *vice versa*) under the influence of the sinusoidal sound wave.

The term structural is used[11] to mean molecular rearrangements that have a barrier of energy equal to the ones for translational viscous flow, all of the other types of translational rearrangements (rupture and formation of chemical bonds, exchange of ligands, etc.) having been frozen out at the frequencies in question or, in other terms, having relaxed to the perturbation.

Interpretation of η_v' in Terms of the Free-Volume Theory. It has been suggested[11] that η_v' and η_s are due to similar processes. If one then accepts the inter-

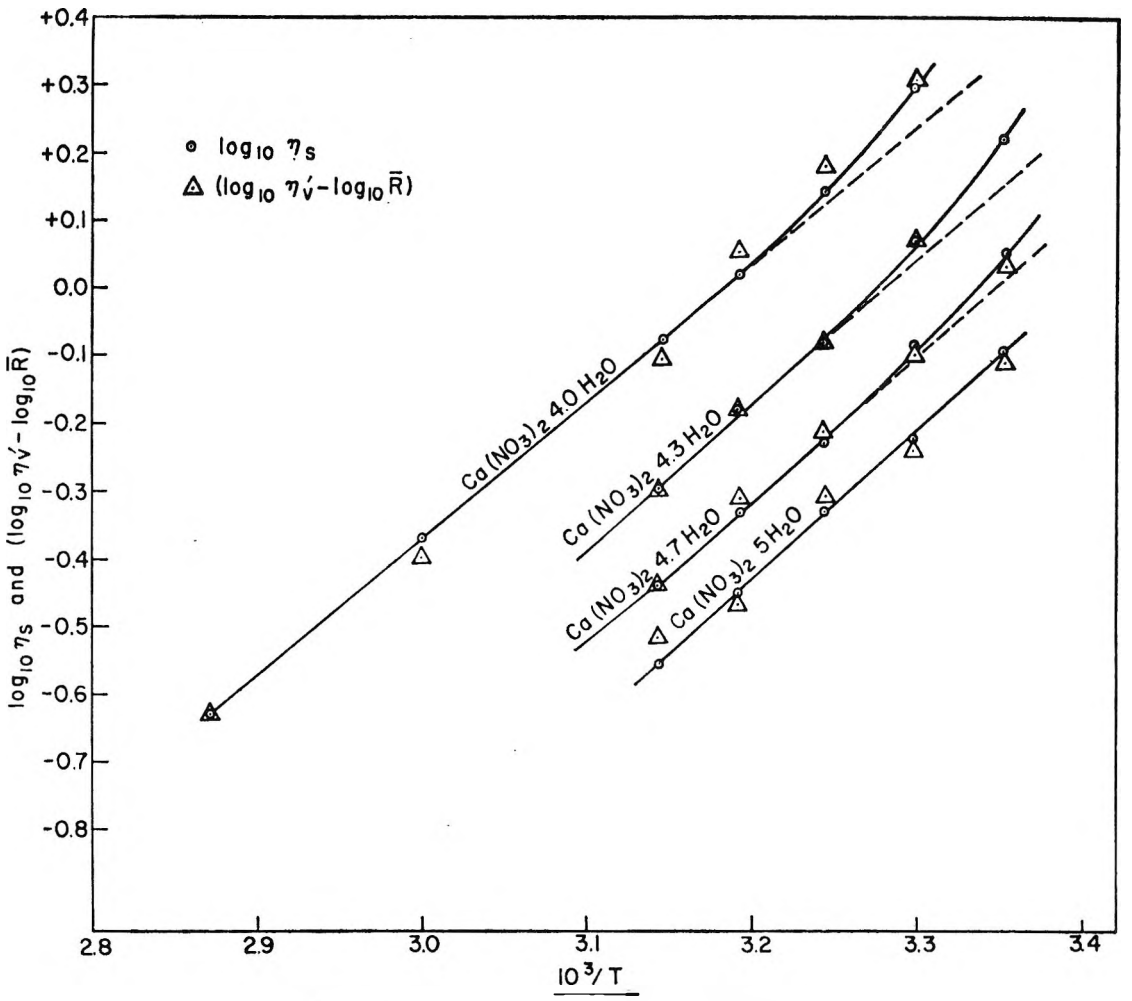


Figure 5. Plot of $\log \eta_s$ and $(\log \eta_v' - \log \bar{R})$ *vs.* $1/T$ for $Ca(NO_3)_2 \cdot 4H_2O$, $Ca(NO_3)_2 \cdot 4.3H_2O$, $Ca(NO_3)_2 \cdot 4.7H_2O$, and $Ca(NO_3)_2 \cdot 5H_2O$.

pretation of Moynihan[17] for the shear viscosities of $Ca(NO_3)_2 \cdot 4H_2O$ in terms of the Cohen–Turnbull theory, then

$$\eta_s = BT^{1/2} \exp\left(\frac{k(\eta_s)}{T - T_0}\right) \quad (6)$$

From Table II given η_v'/η_s = constant, one can assume the relation

$$\eta_v' = B'T^{1/2} \exp\left(\frac{k(\eta_v)}{T - T_0}\right) \quad (7)$$

For $Ca(NO_3)_2 \cdot 4H_2O$ Moynihan has reported from shear viscosity data and eq 6 $T_0 = 205°K$, $k(\eta_s) = 676°K$, and $B = 0.01192$. In Figure 5 the data of Moynihan for shear viscosity are plotted as $\log \eta_s$ *vs.* $1/T$ for $Ca(NO_3)_2 \cdot 4H_2O$. For the other compositions the data from other sources of literature[18] are also plotted in Figure 5.

On the same graph the calculated η_v' from the experimental individual ratios R and η_s are reported as $(\log \eta_v' - \log \bar{R})$ *vs.* $1/T$. $\bar{R}$ is the average value of the ratio η_v'/η_s for a particular liquid composition.

It may be seen that the two functions $\log \eta_s$ and $(\log \eta_v' - \log \bar{R})$ are identical, as expected, indicating that for functions 6 and 7 $B' = BR$, $k(\eta_s) = k(\eta_v)$ while the T_0 values also seem identical within the temperature range investigated and the precision of the method.

The present result focuses on the ultrasonic method as a novel way to study transport properties of electrolytes. Since η_v can be measured only by ultrasonics, a unique role is assigned to this technique.

Nature of the Relaxation. Some comment on the nature of the relaxation must also be made. The fact that the relaxation process tends to disappear by increasing temperature suggests that the relaxation is of thermal nature,[16] namely, is ruled by the ΔH and not the ΔV of the relaxing process. It is possible that a thermolabile complex is destroyed by increasing the temperature.

The shift of the relaxation frequency by addition of water may indicate a bimolecular second-order process with water entering into the mechanism of reaction. Alternatively the addition of water may shift the

(17) C. T. Moynihan, *J. Phys. Chem.*, **70**, 3399 (1966).

(18) J. Timmermanns, "Physical Chemical Constants of Binary Systems," Vol. 3, Interscience Publishers, Inc., New York, N. Y., 1960, p 782.

relaxation frequency decreasing the viscosity of the medium if the molecular rearrangements are partially viscosity controlled.

It is interesting to notice that assuming a process of the type $A \rightleftarrows B$ the relaxation frequency is given[19] by $f_r = (1/2\pi)(k_f + k_R)$ with k_f and k_R the two rate constants. Taking $k_f \approx k_R \approx 10^8\ sec^{-1}$ as determined by Eigen[20] (for substitution of water around Ca^{2+} in dilute solutions) $f_r \simeq 32$ MHz which is the right order of magnitude. Raman[21] and infrared spectra indicate the presence of contact and/or solvated ion pairs in $Ca(NO_3)_2 \cdot 4H_2O$, although no clear-cut evidence has appeared as yet as to which of the two species is present.

Too little information is available for these systems to give an unambiguous molecular interpretation of the observed relaxation. The phenomenological approach developed above seems the only attack feasible at the present time.

Acknowledgment. This work was sponsored by the Air Force Office of Scientific Research, Grant 1185-67.

(19) M. Eigen and L. DeMaeyer in "Investigations of Rates and Mechanism of Reaction," S. L. Friers, E. S. Lewis, and A. Weissberger, Ed., Interscience Publishers, Inc., New York, N. Y., 1963, Part II, p 903.

(20) M. Eigen and G. Maass, *Z. Physik. Chem.*, **49**, 163 (1966).

(21) R. E. Hester and K. Krishnan, *J. Chem. Phys.*, **46**, 3405 (1967).

Thermodynamics of Aqueous Mixtures of Electrolytes and Nonelectrolytes. VII. Enthalpies of Transfer of Perchloric and Hydrochloric Acids from Pure Water to Aqueous Ethylene Glycol and Aqueous Acetic Acid at 25°

by J. H. Stern and J. M. Nobilione

Department of Chemistry, California State College at Long Beach, Long Beach, California 90801 *(Received September 20, 1968)*

The enthalpies of transfer of perchloric acid from pure water to aqueous ethylene glycol and to aqueous acetic acid have been determined calorimetrically across the entire mixed-solvent spans and are compared with analogous enthalpies of transfer of hydrochloric acid. The differences in aqueous ethylene glycol and in that composition region of aqueous acetic acid where both solutes remain predominantly ionized are discussed in terms of the relative effects of perchlorate and chloride as net structure-breaking ions. Enthalpies in glycol-rich solutions indicate anion-independent changes in the solvation sphere of the proton, while in acetic acid rich solution the results suggest important differences in the extensively ion-paired solutes.

Introduction

Previous papers[1,2] described the thermodynamics of transfer of HCl at low molalities from water to aqueous acetic acid[1] and to ethylene glycol,[2] respectively, over the mixed solvent (ms) range from pure water to the pure nonelectrolyte (ne). This contribution reports on the enthalpies of transfer ($\overline{\Delta H}_2$) of $HClO_4$ from water to these two mixed solvent media, and contrasts the remarkable differences in behavior of the two solutes as the "leveling effect" of water gradually gives way to specific ion–ne and other interactions. Individual differences begin appearing as the interionic forces increase with decreasing dielectric constant of the ms. It is of interest to compare these effects in two varied hydroxylic ms for ions of such differing dimensions as chloride and perchlorate. Enthalpies of transfer (and entropies) reflect the complicated solvent structure changes, while the free energy ($\overline{\Delta F}_2$) of transfer is frequently linear or changes monotonically over the entire ms range.[1,2] In many systems $\overline{\Delta F}_2$ is very difficult to obtain and is thus frequently not available, as for $HClO_4$, and in such cases $\overline{\Delta H}_2$ is most useful.

Both chloride and perchlorate are recognized to be net structure-breaking ions; *i.e.*, their presence in aqueous solution tends to shift the dynamic equilibrium between clusters or "icebergs" and simpler forms of water in favor of the latter.[3] Perchlorate ion is generally considered as the most effective inorganic univalent anion net structure breaker while the much smaller chloride ion is relatively weak in this respect.[3]

(1) J. H. Stern and J. M. Nobilione, *J. Phys. Chem.*, **72**, 1064 (1968).

(2) J. H. Stern and J. M. Nobilione, *ibid.*, **72**, 3937 (1968).

(3) J. L. Kavanau, "Water and Solute-Water Interactions," Holden-Day, Inc., San Francisco, Calif., 1964, p 52.

Experimental Section

Calorimetric Procedure. The determination of $\overline{\Delta H}_2$ at 25° *via* the enthalpy of dilution method[1] and the calorimeter[4] have been described previously.

Materials. Concentrated perchloric acid was AR grade. All other materials and preparation of solutions have been described previously.[1,2]

Results and Discussion

Values of the enthalpies of transfer of $HClO_4$ in ethylene glycol–water and acetic acid–water together with estimates of the over-all experimental error at experimental ne mole fractions (X_3) are shown in Tables I and II. Analogous values for HCl have been published elsewhere.[1,2] A total of 50 runs were carried out within a final acid concentration range from 0.001 to 0.004 *m*.

Table I: Enthalpies of Transfer of Perchloric Acid From Water to Aqueous Ethylene Glycol

X_3	$\overline{\Delta H}_2$, kcal/mol
0.102	0.33 ± 0.02
0.278	−0.98 ± 0.03
0.490	−3.08 ± 0.03
0.690	−4.58 ± 0.07
0.807	−5.05 ± 0.10
0.896	−4.72 ± 0.05
0.997	−2.09 ± 0.04

Table II: Enthalpies of Transfer of Perchloric Acid from Water to Aqueous Acetic Acid

X_3	$\overline{\Delta H}_2$, kcal/mol
0.099	−0.13 ± 0.05
0.245	−0.97 ± 0.06
0.333	−1.07 ± 0.05
0.504	−1.12 ± 0.07
0.642	−1.64 ± 0.06
0.743	−1.66 ± 0.07
0.884	−0.53 ± 0.10
0.997	1.57 ± 0.07

Figure 1 shows $\overline{\Delta H}_2$ for HCl and $HClO_4$ in aqueous ethylene glycol. The dielectric constant of the ms remains sufficiently high[5] even in glycol-rich solutions (38 in pure glycol) so that $\overline{\Delta H}_2$ represents primarily ion–ne interactions across the entire ms range. The two similar "s" shaped curves indicate complex structural changes. In the water-rich region both curves show small enthalpy maxima, with that of $HClO_4$ somewhat narrower. This region has earlier been interpreted as one of enhanced "structuredness" relative to water.[2,6] The difference in curves here is too small for comparison.

In the second region of decreasing enthalpies, the

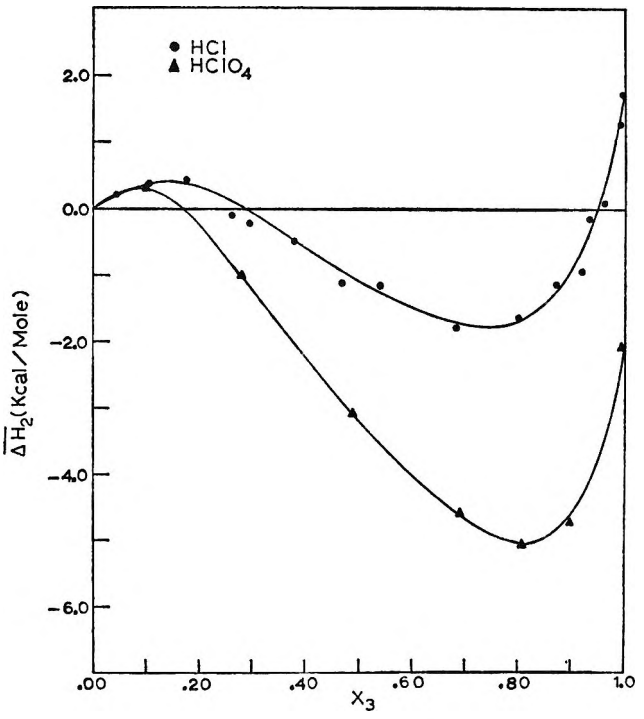


Figure 1. Enthalpies of transfer of HCl and $HClO_4$ from water to aqueous ethylene glycol.

behavior of the two solutes becomes more specific with increasing X_3. The difference in enthalpies of transfer, $\Delta(\overline{\Delta H}_2) = \overline{\Delta H}_2(HClO_4) - \overline{\Delta H}_2(HCl)$ is equal to the differences of the sums of coulombic and structural contributions, $\Delta(\overline{\Delta H}_2)_c$ and $\Delta(\overline{\Delta H}_2)_s$, respectively, and $\Delta(\overline{\Delta H}_2) = \Delta(\overline{\Delta H}_2)_c + \Delta(\overline{\Delta H}_2)_s$.

The difference in enthalpies of transfer is negative. The sign of $\Delta(\overline{\Delta H}_2)_c$ may be obtained from the Born enthalpies of transfer[7] which predict that the ratio of coulombic enthalpies should be inversely proportional to ionic radii. Since perchlorate ion is larger than chloride ion, $\Delta(\overline{\Delta H}_2)_c$ is negative. Thus $\Delta(\overline{\Delta H}_2)$ may be either positive or negative, on this basis alone. However, this ms region is less ordered[2,6] than the partially three-dimensional hydrogen-bonded structure of pure water, and thus the transferred ions break or "melt" less net structure. Consequently their structural enthalpies are lowered; *i.e.*, $(\overline{\Delta H}_2)_s$ is negative. This loss of structural enthalpy should vary with structure-breaking efficiency of the ions; hence $\Delta(\overline{\Delta H}_2)_s$ is also negative.[7]

In the glycol-rich regicn the enthalpies rise sharply. Now however, the increases in $\overline{\Delta H}_2$ from the minima at *ca.* $X_3 = 0.8$ to $X_3 = 1.0$ are nearly the same for both acids, *ca.* 3 kcal/mol, and this rise thus appears to be independent of the anion. The glycol-rich region

(4) J. H. Stern and C. W. Anderson, *J. Phys. Chem.*, **68**, 2528 (1964).
(5) U. Sen, K. K. Kundu, and M. N. Das, *ibid.*, **71**, 3665 (1967).
(6) F. Franks and D. J. G. Ives, *Quart. Rev.* (London), **20**, 1 (1966).
(7) For a detailed treatment of the thermodynamics of transfer, see D. Feakins, B. C. Smith, and L. Thakur, *J. Chem. Soc.*, *A*, 714 (1966).

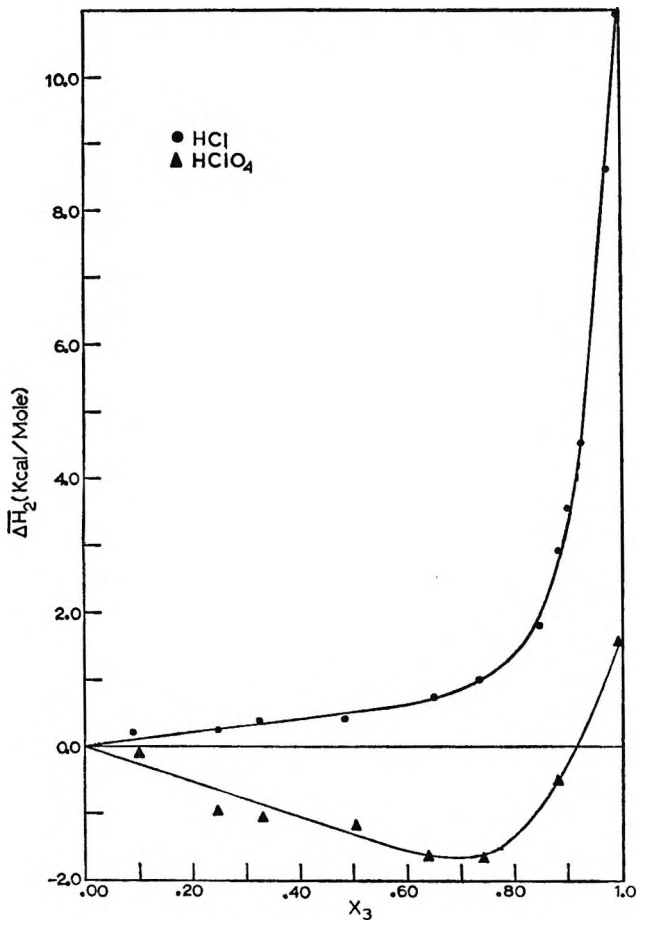
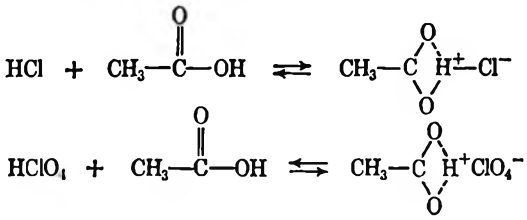


Figure 2. Enthalpies of transfer of HCl and $HClO_4$ from water to aqueous acetic acid.

may be interpreted as one in which the nonelectrolyte begins penetrating the inner hydration structure of the ions with complete exchange of solvating species between ms at the observed minimum and pure glycol. The nonspecific anion dependence suggests that these changes occur primarily in the solvation sphere of the proton.

In Figure 2, $\overline{\Delta H_2}$ for $HClO_4$ in HOAc–H_2O is plotted *vs.* X_3 together with the analogous plot of HCl[1] for comparison. It may be observed that both curves have the same general two-part form. The left-hand side corresponds to transfer from pure water to ms where both HCl[1] and $HClO_4$ remain predominantly ionized, with the latter transfer proceeding at lower enthalpies. If it is assumed that in the HOAc–H_2O system the negative $\Delta(\overline{\Delta H_2})$ reflect changes in $\Delta(\overline{\Delta H_2})_s$, then this ms appears to be less ordered than pure water, just as in the analogous second region of the glycol–water system. It is recognized that this conclusion is somewhat speculative, since the structural and coulombic contributions to the free energy and entropy of transfer for both chloride and perchlorate ions should also be known. The structural picture is further complicated by perchlorate ion hydrogen bonding differences in pure water and in the mixed solvent. For example, X-ray evidence shows hydrogen bonding between perchlorate ion and pure water and between several ions by water bridges.[8] The extent of this effect in the ms, where three-way hydrogen bonding is possible between all components of the solution, is not known.

Past *ca.* $X_3 = 0.75$, HOAc lowers the dielectric constant to such an extent (ϵ 6 in pure HOAc) that attraction between the proton and the anion may result in extensive ion-pair formation. In the case of HCl with a pK of dissociation of 8.55 [9] in pure HOAc there are very few ions, and ion–ne effects may be neglected. Perchloric acid, however, is the strongest acid known in pure HOAc with a pK for association of 4.87 [9] and thus remains partially dissociated.[10] The increase in the enthalpy of transfer in this region for HCl is about three times that of $HClO_4$. This mainly may be a reflection of the relative order of acid strengths in HOAc and the difference of solvated association complexes.



Further studies on the transfer of HCl and $HClO_4$ to aqueous glycerol are in progress.

Acknowledgment. The financial assistance of the National Science Foundation is gratefully acknowledged.

(8) S. H. Bauer and P. Andersen, *Ann. Rev. Phys. Chem.*, **4**, 233 (1953).

(9) S. Bruckenstein and I. M. Kolthoff, *J. Amer. Chem. Soc.*, **78**, 2974 (1956).

(10) In dioxane-rich aqueous solution (ϵ 10) lithium perchlorate remains dissociated, while lithium chloride and lithium chlorate are each associated. For a discussion of these differences, which may be due to much greater solvation of the perchlorate ion than of the other two anions, see F. Accascina, A. D'Aprano, and R. Triolo, *J. Phys. Chem.*, **71**, 3469 (1967).

Electron Scavenging in the Radiolysis of Cyclohexane Solutions of Alkyl Halides[1]

by John M. Warman, K.-D. Asmus, and Robert H. Schuler

Radiation Research Laboratories, Mellon Institute, Carnegie-Mellon University, Pittsburgh, Pennsylvania 15213
(Received September 20, 1968)

The formation of alkyl radicals in irradiated solutions of CH_3Cl, CH_3Br, and C_2H_5Br in cyclohexane has been investigated at concentrations from 10^{-4} to 0.5 M. Experiments with added ethylene and cyclopropane show that the radicals do not result from reactions of either hydrogen atoms or positive ions. From this it appears that radical formation results exclusively from electron capture. The observed concentration dependence can be very well described by the expression

$$G(R_S) = G_{fi} + G_{gi}\frac{\{\alpha_s[S]\}^{1/2}}{1 + \{\alpha_s[S]\}^{1/2}}$$

The low concentration limit (G_{fi}) is identified with the free-ion yield and is found to be ~0.1. It is believed that the high concentration limit ($G_{fi} + G_{gi}$), which is found to be 3.9 ± 0.1, can be identified with the total yield of electrons available for reaction with solutes. The above expression has been used to treat competitive electron capture by two alkyl halides. Deviations from ideality observed in the CH_3Cl–C_2H_5Br system are interpreted in terms of electron transfer from a CH_3Cl anion to the bromide. It is shown that such secondary ionic reactions can be described quantitatively.

In recent years there has been considerable interest in the role of electron-scavenging processes in the radiolysis of hydrocarbon solutions. A fair number of studies on this subject have now been carried out, and the current status of knowledge has been summarized in an article which appears elsewhere.[2] The first attempt to examine the importance of electron capture in the radiolysis of hydrocarbon solutions was made in 1954 by Williams and Hamill[3] when they studied the radical yields produced from solutions of alkyl halides. They found that appreciable yields of radicals were produced from the solute (G's > 1) at concentrations above 10^{-2} M and attributed these yields for the most part to dissociative electron-capture processes. It has, however, always been difficult to rule out other possible mechanisms which might also result in formation of radicals from alkyl halides. Interest in details of the chemical effects of the electron-capture process has been renewed by the finding of Scholes and Simic[4] that large yields of nitrogen are formed in the radiolysis of solutions of nitrous oxide in cyclohexane. Because this solute has been used as a specific electron scavenger in aqueous systems[5] with considerable success by numerous workers and is known to give nitrogen as a result of electron-capture processes in the radiolysis of gaseous mixtures,[6] the qualitative conclusion of Scholes and Simic that nitrogen results from electron capture in the nitrous oxide–cyclohexane solutions seems very likely to be valid. However, the nitrogen yields observed are very high and indicate that some additional effects which involve secondary processes are also present.

The primary aim of the present research was to reinvestigate the radical yields from alkyl halide solutions in order to examine as critically as possible the extent to which electron capture contributes to them and to determine the concentration dependence of electron scavenging over as wide a concentration range as possible. The latter is of particular interest in view of recent theoretical treatments of the subject. A knowledge of the concentration dependence is also necessary for the quantitative treatment of competitive scavenging in systems containing more than one solute. Attention has been focused here on the alkyl bromides and chlorides. It is known that in the case of methyl iodide solutions considerable methane is formed.[7,8] Because of this and other complications due to hydrogen atom and positive-ion attack on the iodides, these solutes will be treated separately.[9]

Experimental Section

Cyclohexane (Phillips research grade) was chromatographed through a silica gel column to remove polar and olefinic impurities. Matheson methyl chloride, methyl bromide, and ethylene were distilled (at −80°) and then stored on a vacuum line. Ethyl

(1) Supported in part by the U. S. Atomic Energy Commission.

(2) J. M. Warman, K.-D. Asmus, and R. H. Schuler, Advances in Chemistry Series, No. 82, American Chemical Society, Washington, D. C., 1968, p 25.

(3) R. R. Williams and W. H. Hamill, *Radiat. Res.*, **1**, 158 (1954).

(4) G. Scholes and M. Simic, *Nature*, **202**, 895 (1964).

(5) F. S. Dainton and D. B. Peterson, *ibid.*, **186**, 878 (1960); *Proc. Roy. Soc.*, **A267**, 443 (1962).

(6) G. R. A. Johnson and J. M. Warman, *Nature*, **203**, 73 (1964); *Trans. Faraday Soc.*, **61**, 1709 (1965).

(7) R. H. Schuler, *J. Phys. Chem.*, **61**, 1472 (1957).

(8) P. R. Geissler and J. E. Willard, *J. Amer. Chem. Soc.*, **84**, 4627 (1962).

(9) R. H. Schuler and J. L. McCrumb, to be published.

bromide was purified gas chromatographically and then outgassed and stored on the vacuum line. Radioiodine ($^{131}I_2$) was prepared as described previously.[10]

A measured pressure-volume of the solute vapor was added to 5 ml of an outgassed solution of cyclohexane containing radioiodine of known specific activity. Vapor volumes above the sample were ~0.5 cc so that essentially all of the solute was in the liquid phase. Initial experiments indicated that for solute concentrations less than 10^{-3} M the yields from samples prepared in the conventional way were possibly too low because of the failure to remove CO_2 during the outgassing procedure. Therefore for solute concentrations below 10^{-3} M cyclohexane was dried over sodium and pumped a number of times on the vacuum line at room temperature to remove CO_2. Radioiodine of known specific activity and the desired amount of alkyl halide were then added on the vacuum line without further exposure of the sample to air. The iodine concentration in this case was determined optically after the irradiation. Preparation of the samples in this way considerably increased the yields at concentrations of ~10^{-4} M but had little or no effect at concentrations above 10^{-3} M. In general, iodine concentrations were ~0.4 mM or higher except for experiments at the lowest solute concentrations where the iodine concentration was always lower than that of the solute. Comparison experiments at different iodine concentrations showed that the iodine affected the observed radical yields only when present at a concentration higher than those of the other solutes. The samples were irradiated with ^{60}Co γ rays at an absorbed dose rate of 5×10^{18} eV cc^{-1} hr^{-1} in cyclohexane. Total doses were 4×10^{17} eV cc^{-1} except where low iodine concentrations required more limited irradiations. At the doses used only 10–20% of the iodine reacted during the irradiation.

Alkyl radicals produced from the alkyl halides during irradiation were measured as the alkyl iodide produced by the reaction

$$R\cdot + {}^{131}I_2 \longrightarrow R^{131}I + I\cdot$$

From the results on methyl-radical scavenging in 2,2,4-trimethylpentane[7] (where 50% of the methyl radicals react with iodine at 6×10^{-7} M) scavenging should be quantitative (>99%) at the iodine concentration employed. Several experiments intercomparing results at 10^{-4} and 10^{-3} M iodine confirmed this expectation. Alkyl iodides were separated gas chromatographically, and their yields were measured as described previously.[10] The yields of $CH_3\cdot$ and $C_2H_5\cdot$ radicals from cyclohexane in the absence of alkyl halides were found to be <0.02. Methane and hydrogen yields were determined by conventional vacuum line methods with mass spectrometric analysis of the fraction volatile at liquid nitrogen temperature.

In certain experiments ethylene or tetramethylethylene was used to scavenge hydrogen atoms. For ethylene the scavenging efficiency was calculated from the relative rate constants for the scavenging and abstraction reactions (1:0.0034).[11,12] From competitive studies between ethylene and tetramethylethylene the hydrogen atom scavenging efficiency of the latter is estimated to be approximately equal to that of the former.

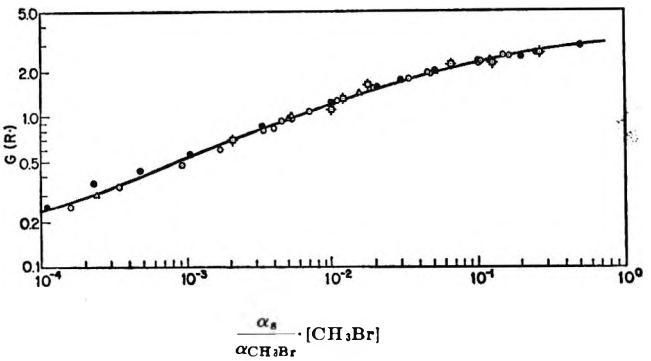


Figure 1. Radical yields from various electron scavengers as a function of solute concentration: ●, CH_3Br, ○; CH_3Cl ($\alpha_{CH_3Cl} = 0.334\alpha_{CH_3Br}$); △, C_2H_5Br ($\alpha_{C_2H_5Br} = 0.483\alpha_{CH_3Br}$). Also included are the results of Hagemann and Schwarz (ref 30) on benzyl chloride, -⊡-, for which α_s is taken equal to α_{CH_3Br}. The solid line is that calculated using eq II with $G_{fi} = 0.12$, $G_{si} = 3.8$, and $\alpha_{CH_3Br} = 16.2$.

Results and Discussion

The yields of methyl radicals from CH_3Br and CH_3Cl solutions and ethyl radicals from C_2H_5Br solutions in cyclohexane have been determined over the concentration range 10^{-4} to 0.5 M and are reported in Figure 1. At the highest concentrations yields of between 2 and 3 are observed in agreement with previous studies[3,8] where it had been suggested that dissociative electron capture

$$e^- + RX \longrightarrow R\cdot + X^- \qquad (1)$$

was responsible for the high yields observed. In several auxiliary experiments the yields of methyl radicals due to electron capture by CH_3F (0.1 M) were found to be less than 0.05. For this solute reaction 1 is expected to have negligible importance because of its high endothermicity (1.6 eV). The first part of the following discussion is an attempt to determine to what extent, if any, other reactions contribute to the radical yields; the second part is a discussion of the quantitative aspects of the concentration dependence observed in Figure 1; and the third involves the application of the description of this observed dependence to competitive situations.

Specificity of Electron Scavenging. One of the major problems is to distinguish between radical formation

(10) R. H. Schuler and P. R. Kuntz, *J. Phys. Chem.*, **67**, 1004 (1963).
(11) R. A. Holroyd, *ibid.*, **70**, 1341 (1966).
(12) J. L. McCrumb and R. H. Schuler, *ibid.*, **71**, 1953 (1967).

resulting from dissociative attachment (reaction 1) and that produced by hydrogen atom attack.

$$H\cdot + RX \longrightarrow R\cdot + HX \qquad (2)$$

Ethylene has been used as a hydrogen atom scavenger in cyclohexane radiolysis and the yield of ethyl radicals formed by

$$H\cdot + C_2H_4 \longrightarrow C_2H_5\cdot \qquad (3)$$

has been determined. Because hydrogen atoms also abstract from the solute

$$H\cdot + C_6H_{12} \longrightarrow H_2 + C_6H_{11}\cdot \qquad (4)$$

it has been necessary to extrapolate the observed yields to infinite ethylene concentration to determine the hydrogen atom yield. The yield so obtained is ~ 1.5.[11,12] This yield is considerably lower than the radical yields observed in alkyl halide solutions so that reaction 2 cannot, therefore, completely account for radical formation from the solute. There is, however, the possibility that radical formation is in part due to reaction 2. If hydrogen atom attack does occur, then the addition of ethylene should result in a decrease in $G(R)$ owing to the competing reaction of hydrogen atoms with the ethylene. Data obtained on CH_3Cl–C_2H_4 solutions in cyclohexane are given in Table I and demonstrate that the ethylene has no observable effect on the methyl radical yield even where $[C_2H_3]/[CH_3Cl]$ is 8 and the ethylene scavenges 75% of the hydrogen atoms. (The remaining 25% abstract from the solvent.) Methyl chloride does reduce the ethyl radical yield slightly. The effect is comparable to that produced by the solutes SF_6 and N_2O and therefore is attributed to a decrease in that part of the hydrogen atom yield which results from ion recombination. This decrease is parallel to the known reduction in the yield of molecular hydrogen by these electron scavengers.[13] From the above there is no indication that reaction 2 is responsible for any of the methyl radicals observed in the methyl chloride system. Similar data on CH_3Br–C_2H_4 solutions are given in Table II. Primarily it is important to note that there is no decrease in the methyl radical yield upon the addition of C_2H_4 to the CH_3Br solutions. This is true even for the 0.01 M CH_3Br solution containing a tenfold excess of C_2H_4 where again 75% of the hydrogen atoms react with the ethylene. At the higher methyl bromide concentrations an increase in the methyl radical yield is observed, and the ethyl radical yield appears to be correspondingly low. This effect is at the moment anomalous and appears to be specific to ethylene since tetramethylethylene, which is as efficient a hydrogen atom scavenger as ethylene, has little effect on the methyl radical yield (see footnote *a* in Table II). Thus, while it does not appear that hydrogen atoms react with CH_3Br in cyclohexane, because of the above-mentioned anomaly this conclusion is not as clear-cut as in the case of methyl chloride. For a 0.1 M solution of C_2H_5Br the addition of 0.1 M tetramethylethylene does not cause a decrease in $G(C_2H_5)$ indicating that for this solute hydrogen atom attack can also be ruled out as a source of alkyl radicals.

Recent studies have shown that certain solutes are capable of reacting with positive ions in hydrocarbon radiolysis.[14,15] Experiments have therefore been carried

Table I: Methyl and Ethyl Radical Yields from Methyl Chloride and Ethylene Solutions in Cyclohexane

$[CH_3Cl]$	$[C_2H_4]$	$G(CH_3)$	$G(C_2H_5)$
...	0.108	...	0.99
0.0131	...	0.93	...
0.0131	0.109	0.91	0.96
0.138	...	1.90	...
0.138	0.109	1.90	0.92
0.440	...	2.43	...
0.440	0.107	2.57	0.87
...	0.0106	...	0.34
0.100	...	1.75	...
0.100	0.0104	1.75	0.29
0.410	...	2.43[a]	...
0.410	0.0107	2.46	0.33

[a] Interpolated from experimental results.

Table II: Methyl and Ethyl Radical Yields from Methyl Bromide and Ethylene Solutions in Cyclohexane

$[CH_3Br]$	$[C_2H_4]$	$G(CH_3)$	$G(C_2H_5)$
...	0.108	...	0.99
0.0104	...	1.24	...
0.0104	0.103	1.29	0.85
0.102	...	2.34[a]	...
0.102	0.101	2.54	0.61
0.219	...	2.62[b]	...
0.219	0.102	3.12	0.52
0.316	...	2.78[b]	...
0.316	0.102	3.25	0.45

[a] A solution containing 0.1 M CH_3Br and 0.1 M tetramethylethylene gives a methyl yield of 2.37; a solution containing 0.5 M CH_3Br and 0.1 M tetramethylethylene gives a methyl yield of 3.06 which may be compared to 2.96 in the absence of the tetramethylethylene. [b] Interpolated.

(13) K.-D. Asmus, J. M. Warman, and R. H. Schuler, to be published.

(14) J. W. Buchanan and F. Williams, *J. Chem. Phys.*, **44**, 4377 (1966).

(15) P. Ausloos, A. A. Scala, and S. G. Lias, *J. Amer. Chem. Soc.*, **88**, 1583 (1966); **88**, 5701 (1966).

Table III: The Effect of Cyclopropane on the Alkyl Radical Yields from Cyclohexane Solutions of Alkyl Halides

RX	[RX]	[c-C_3H_6]	G(R)
CH_3Cl	0.0110	...	0.81
	0.01	0.08	0.80
	0.01	0.40	0.81
CH_3Br	0.0099	...	1.23
	0.0102	0.209	1.34
C_2H_5Br	0.0102	...	0.96
	0.0102	0.212	1.06

out to examine for possible formation of alkyl radicals due to positive-ion scavenging. As is shown in Table III, the addition of a 20-fold excess of cyclopropane, a known specific positive-ion scavenger, has no effect on the methyl radical yield from CH_3Cl solutions and even slightly increases the methyl and ethyl radical yields from methyl and ethyl bromide solutions. This latter effect may be related to the increase observed in the CH_3Br–C_2H_4 solutions because ethylene is also known to be a positive-ion scavenger. In addition, CH_3Cl and CH_3Br increase the yield of products produced from cyclopropane, as do other electron scavengers which convert the electrons into less mobile negative ions.[15,16] Positive-ion reactions, if they occur, do not appear to result in the formation of alkyl radicals.

Of the possible alternate causes of dissociation of the solute, the most difficult to argue against is transfer of electronic excitation energy from the solvent. Holroyd[17] has suggested that energy transfer occurs in the radiolysis of N_2O–cyclohexane solutions and is responsible for the high nitrogen yields observed. Hentz and Knight[18] and Yoshida and Sato,[19] however, have shown that the localization of energy in scintillator solutions results from trapping of electrons and/or positive ions by the scintillator molecule rather than by energy transfer. In relation to the present study photolytic dissociation of alkyl halides occurs quite readily and energy transfer might well be advanced to explain radical formation. To check this as a general possibility perfluoroazomethane and perfluoroacetone (0.1 M) were irradiated in cyclohexane solution. In the respective experiments neither nitrogen nor carbon monoxide was found, though these products are readily formed in the photolysis. It is argued from this that energy is not available in a form in which it is necessarily transferred to produce dissociation of the solutes.

Assuming that the alkyl halides are electron scavengers, one must of course ask if the alkyl radical yield is a quantitative measure of the products resulting from the electron-capture process. Recent experiments[20] exploring the use of $^{14}CH_3Br$ as an electron scavenger show that the only radioactive products formed in detectable amounts are $^{14}CH_4$ and $^{14}CH_3C_6H_{11}$ and that the latter represents only ~3% of the total

Table IV: Methane Yields in the Absence and Presence of Iodine Scavenger[a]

	$[I_2]$, M	$G(CH_4)_0$	$G(CH_4)_{I_2}$
CH_3I[b]		16.0	0.61[c]
CH_3Br	1.8×10^{-3}	2.18[d]	0.05
CH_3Cl	1.8×10^{-3}	1.34	0.03

[a] At 0.1 M alkyl halide. [b] Data from ref 7; the high methane yield in the absence of iodine is due to a chain reaction involving reaction of cyclohexyl radicals with methyl iodide to form methyl radicals followed by hydrogen abstraction by the latter. [c] Independent of iodine concentration from 3×10^{-5} to 10^{-3} M. [d] Rzad and Warman (ref 20) have demonstrated that 97% of the methyl radicals produced from 0.1 M $^{14}CH_3Br$ abstract hydrogen from the solvent to give methane.

yield. The total yields of these products are, in fact, found to be identical with the methyl radical yields determined in the present work. Complex reactions resulting from the electron-capture process can, therefore, be ruled out. In the case of methyl iodide solutions it is known[7] that a considerable yield of molecular methane, which does not disappear upon the addition of iodine, is produced. Similar experiments on methyl bromide and methyl chloride solutions containing added iodine show no significant yield of molecular methane. The pertinent data are reported in Table IV. It seems likely, as has been suggested several times,[21,22] that the molecular methane observed in the case of the methyl iodide solutions is due to diffusion-controlled recombination of methyl radicals with the hydrogen iodide formed by abstraction of iodine by hydrogen atoms, *i.e.*

$$H\cdot + CH_3I \longrightarrow [CH_3\cdot + HI] \longrightarrow CH_4 + I\cdot \quad (5)$$

The lack of formation of molecular methane in the cases of methyl bromide and chloride solutions is in accord with the absence of hydrogen atom attack on the halogen.

Concentration Dependence of Electron Scavenging. From the above it would appear that electron capture is the exclusive source of radicals produced from the alkyl chlorides and bromides, and in what follows we will assume that contributions from other sources are negligible. Conductivity experiments[23–25] have shown

(16) S. J. Rzad and R. H. Schuler, *J. Chem. Phys.*, in press.
(17) R. A. Holroyd, *J. Phys. Chem.*, 72, 759 (1968); Advances in Chemistry Series, No. 82, American Chemical Society, Washington, D. C., 1968, p 488.
(18) R. R. Hentz and R. J. Knight, *J. Phys. Chem.*, 72, 1783 (1968).
(19) T. Yoshida and S. Sato, *Bull. Chem. Soc. Jap.*, 40, 2217 (1967).
(20) S. J. Rzad and J. M. Warman, *J. Chem. Phys.*, 49, 2861 (1968).
(21) J. Roberts and W. H. Hamill, *J. Phys. Chem.*, 67, 2446 (1963).
(22) R. A. Holroyd and G. W. Klein, *Int. J. Appl. Radiat. Isotopes*, 15, 633 (1964).
(23) A. O. Allen and A. Hummel, *Discussions Faraday Soc.*, 36, 95 (1963); A. Hummel, A. O. Allen, and F. H. Watson, Jr., *J. Chem. Phys.*, 44, 3431 (1966).
(24) G. R. Freeman, *ibid.*, 38, 1022 (1963); G. R. Freeman and J. M. Fayadh, *ibid.*, 43, 86 (1965).
(25) W. F. Schmidt, *Z. Naturforsch.*, 23b, 126 (1968).

that only a small fraction of the ion pairs produced in irradiated hydrocarbons (~3% in cyclohexane) become distributed homogeneously in the solution and recombine in second-order processes. At the intensities commonly employed in γ-ray experiments, these free ions have mean lifetimes of the order of seconds and will therefore be readily scavenged at low solute concentrations. The observed radical yields (see Figure 1) are considerably greater than the yield of free ions, $G_{fi} \cong 0.1$, measured in the conductivity experiments. Reaction with ion pairs which undergo geminate recombination and have a very short lifetime ($\sim 10^{-10}$ sec) is therefore indicated.

At low solute concentrations the yield of product, $G(P)$, from positive ion scavenging studies has been found to be approximately proportional to the square root of the solute concentration,[14,15] and recently[26] it has been found to be quite well described by an expression of the form given by the theoretical treatment of Hummel.[27]

$$G(P) = G_{fi} + K\{k_s[S]\}^{1/2} \qquad (I)$$

In eq I, K is a constant which involves geometrical parameters and the diffusion coefficients of the ionic entities, and k_s is the rate constant for reaction of the ion with the solute. The methyl radical yields from CO_2-free solutions of CH_3Br are plotted against $[CH_3Br]^{1/2}$ in Figure 2 together with the results from experiments[20] in which the radioactive products from solutions of $^{13}CH_3Br$ were examined. The two sets of results are in excellent agreement and again show that at its low concentration the iodine acts only as a radical scavenger and does not interfere with electron scavenging by solute alkyl halide. The required presence of iodine does, however, present a low concentration limitation to the present studies, and it is valuable to have the results from the studies with $^{14}CH_3Br$ which do not have this limitation and can be carried out at somewhat lower concentrations. As can be seen in Figure 2 a linear dependence of yield upon $[S]^{1/2}$ is found, in accord with eq I. The intercept corresponds to $G_{fi} = 0.12$ and is in agreement with conductivity measurements of this quantity[23-25] and with the recent value of 0.15 determined by the clearing field method.[28] It also agrees with the extrapolated low concentration limit of 0.11 obtained from a study of positive-ion scavenging by cyclopropane.[26]

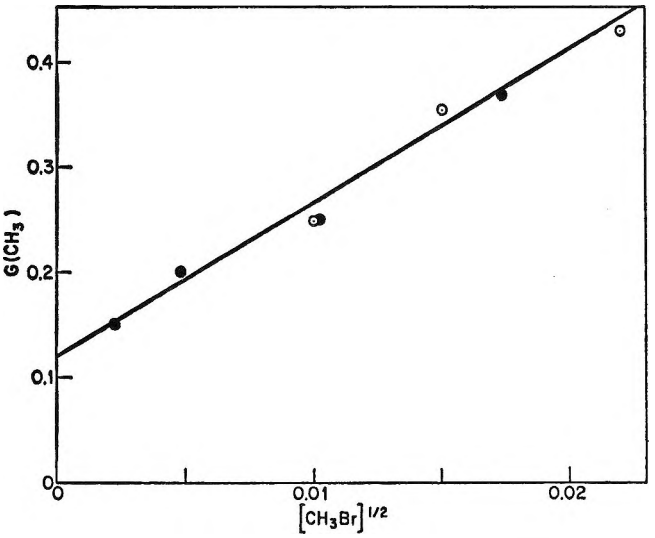


Figure 2. Dependence of the methyl radical yield on $[CH_3Br]^{1/2}$ observed in this study, ○; in the work reported in ref 20, ●.

Because the total yield of ion pairs formed is limited ($G_i \cong 4$ if gas phase W values are applicable) a deviation from eq I must necessarily occur at higher scavenger concentrations. As can be seen in Figure 1, above 10^{-3} M solute the slope of the concentration dependence continuously decreases. However, even at the highest concentrations used there is no indication that a limiting value has been reached and such a limit must be in excess of the value of 3.0 observed at 0.5 M CH_3Br. In the high-concentration region the functional dependence of the scavenging efficiency upon solute concentration is not given explicitly by existing theories. It is useful therefore to attempt to describe the results empirically. The dependence observed at low concentrations corresponds to that which would result from a hypothetical reaction scheme in which competition occurs homogeneously between ion recombination and processes which are kinetically proportional to the square root of the solute concentration. For such a scheme the overall concentration dependence is given by

$$G(P) = G_{fi} + G_{gi}\frac{\sqrt{\alpha_s[S]}}{1 + \sqrt{\alpha_s[S]}} \qquad (II)$$

where G_{gi} is the yield of ion pairs which undergo geminate recombination in the case of the pure hydrocarbon but which are available for reaction with the solute. At low concentrations eq II becomes

$$G(P) = G_{fi} + G_{gi}\sqrt{\alpha_s[S]} \qquad (III)$$

so that $G_{gi}\sqrt{\alpha_s}$ can be identified with $K\sqrt{k_s}$ in Hummel's expression. From this, α_s is seen to be directly proportional to the rate constant for reaction of the electron with the solute and will be called here the solute reactivity. Rearrangement of eq II gives

$$\frac{1}{G(P) - G_{fi}} = \frac{1}{G_{gi}} + \frac{1}{G_{gi}\alpha_s^{1/2}}\frac{1}{[S]^{1/2}} \qquad (IV)$$

and accordingly a plot of $[G(P) - G_{fi}]^{-1}$ *vs.* $[S]^{-1/2}$ should be linear. The data on the three solutes examined correspond very well to the predicted dependence (Figure 3). A common intercept which

(26) S. J. Rzad and R. H. Schuler, *J. Phys. Chem.*, **72**, 228 (1968).
(27) A. Hummel, *J. Chem. Phys.*, **48**, 3268 (1968).
(28) W. F. Schmidt and A. O. Allen, *Science*, **160**, 301 (1968).

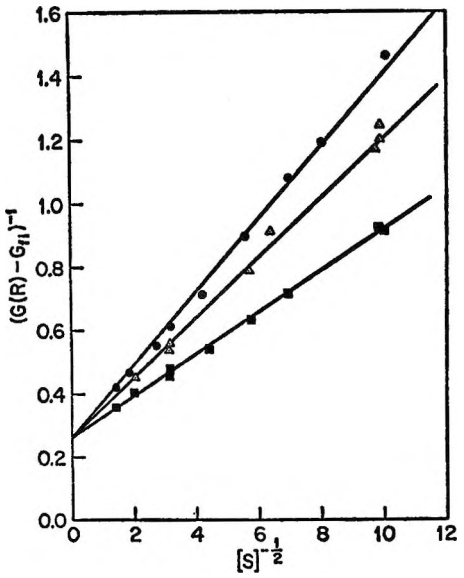


Figure 3. Plot of the alkyl radical yields from ●, CH_3Cl; △, C_2H_5Br; and ■, CH_3Br solutions in cyclohexane according to eq IV with G_{fi} taken as 0.12. The common intercept corresponds to $G_{gi} = 3.8$.

corresponds to $G_{gi} = 3.8 \pm 0.1$ is observed.[29] The fact that a common intercept is observed does, of course, give considerable credence to the concept that the solutes are detecting the geminate ions with an efficiency $\sqrt{\alpha_s[S]}/(1 + \sqrt{\alpha_s[S]})$ determined by the relative probability of the ion-scavenging and recombination processes. With this model the total yield of ion pairs, $G_{fi} + G_{gi}$, is 3.9. This suggests that the assumption frequently made, that gas phase W values are applicable to the liquid, is valid.

While the values for α_s can be determined from the slopes and intercepts of the individual curves of Figure 3, the relative values so obtained will reflect the square of small differences in the intercept. As an alternative approach the entire set of data for each solute was treated by assuming common values of 0.12 and 3.8 for G_{fi} and G_{gi}, respectively, and then varying α_s to minimize the standard deviation between the observed and calculated results. If the assumption of a common limiting value at infinite scavenger concentration is correct, this approach should give a more consistent set of values of α_s. The values obtained were 16.2, 7.82, and 5.41 M^{-1}, respectively, for methyl bromide, ethyl bromide, and methyl chloride. The standard deviations between the calculated and observed yields using these values of α_s were, for the three individual sets of data, 0.040, 0.032, and 0.035. The data of Rzad and Warman on the methane yield similarly treated gave $\alpha_{CH_3Br} = 15.4$. The reciprocals of α_s are of some interest because, according to this model, they represent the concentrations at which a particular solute scavenges one-half of the electrons. These concentrations are 0.062, 0.128, and 0.185 M for CH_3Br, C_2H_5Br, and CH_3Cl, respectively. The factors used in Figure 1 to normalize the concentration scales for CH_3Cl and C_2H_5Br to that of CH_3Br are in fact the ratios of the appropriate values of α_s; 5.41/16.2 = 0.334 for CH_3Cl and 7.82/16.2 = 0.483 for C_2H_5Br. The solid curve is that calculated from eq II with $G_{fi} = 0.12$, $G_{gi} = 3.8$, and $\alpha_s = \alpha_{CH_3Br} = 16.2\ M^{-1}$. The independent data of Hagemann and Schwarz,[30] where benzyl chloride was used as the solute and the yield of benzyl radicals determined from the optical absorption in pulse radiolysis experiments, is also shown in Figure 1. The concentration dependence of the latter is certainly very similar to that reported for the solutes studied here, and the quantitative agreement is amazingly good if one makes the reasonable assumption that the reactivity of the benzyl chloride is nearly the same as that of methyl bromide.

One might at first be surprised by the factor of 3 difference in the reactivities of methyl bromide and chloride and perhaps even more so by the factor of 2 difference between methyl and ethyl bromide. A few experiments were also carried out on ethyl chloride solutions where the ethyl radical yields observed (0.68, 1.06, and 1.40 at 0.1, 0.2, and 0.5 M, respectively) were considerably lower than for methyl chloride. Interpreted according to eq II, these yields correspond to a value for $\alpha_{C_2H_5Cl}$ of 0.5 or only one-tenth that of the reactivity of methyl chloride. Effects of structure and of the electron affinity of particular groups thus appear to have pronounced effects on the reactivity of the individual solutes in the electron-capture process. A survey of electron-scavenging effects observed in various systems[2] indicates no value of α_s much larger than $\sim 20\ M^{-1}$, and it is believed that this value represents the maximum possible and presumably is governed by limiting rates for diffusion.

Competitive Experiments. When two or more solutes are simultaneously present, the term $\alpha_s[S]$ in eq II must be replaced by the sum of the individual values of this term. For two solutes

$$G(\text{total scavenging}) = G_{fi} + G_{gi}\frac{\{\alpha_1[S_1] + \alpha_2[S_2]\}^{1/2}}{1 + \{\alpha_1[S_1] + \alpha_2[S_2]\}^{1/2}} \quad \text{(V)}$$

Studies of systems containing both CH_3Br and C_2H_5Br (Table V) and CH_3Cl and C_2H_5Br (Table VI) show total yields which agree very well with those yields calculated using eq V and the values of α_s for each solute taken as those determined in the single solute systems.

(29) Weighted least-mean-squares treatments of the data above 0.01 M give intercepts corresponding to $G_{gi} = 3.76$, 3.84, and 4.01 for the data on methyl bromide, ethyl bromide, and methyl chloride. In treating the data no correction has been made for the direct effect on the solute so that extrapolated limits may be high by 0.1–0.2 units. Similar data of Rzad and Warman (ref 20) on the ^{14}C products produced from $^{14}CH_3Br$ solutions give $G_{gi} = 3.79$.

(30) R. J. Hagemann and H. A. Schwarz, *J. Phys. Chem.*, **71**, 2694 (1967).

Table V: Radical Yields from Competitive Studies between Methyl and Ethyl Bromides

[CH_3Br]	[C_2H_5Br]	$G(CH_3)$ Obsd	$G(CH_3)$ Calcd[a]	$G(C_2H_6)$ Obsd	$G(C_2H_6)$ Calcd[a]	$G(C_2H_6)/[C_2H_5Br]$ / $G(CH_3)/[CH_3Br]$	$G(CH_3 + C_2H_6)$ Obsd	$G(CH_3 + C_2H_6)$ Calcd[a]
0.099	0.501	0.70	0.81	2.09	1.98	0.59	2.79	2.78
0.102	0.211	1.23	1.29	1.43	1.28	0.56	2.66	2.57
0.102	0.103	1.55	1.64	0.89	0.80	0.57	2.44	2.44
0.102	0.0290	1.95	2.04	0.36	0.28	0.65	2.31	2.32
0.0104	0.107	0.33	0.34	1.81	1.68	0.53	2.14	2.02
0.0103	0.0508	0.51	0.52	1.29	1.23	0.51	1.80	1.75
0.0103	0.0205	0.74	0.77	0.85	0.74	0.58	1.59	1.51
0.0097	0.0098	0.91	0.91	0.51	0.45	0.55	1.42	1.36
0.0104	0.0054	1.05	1.05	0.32	0.27	0.59	1.37	1.32
0.0010	0.0020	0.31	0.35	0.41	0.34	0.66	0.72	0.69
0.0010	0.0010	0.33	0.43	0.23	0.21	0.67	0.56	0.63

[a] Values calculated using eq V and VI and $G_{fi} = 0.12$, $G_{gi} = 3.8$, $\alpha_{CH_3Br} = 16.2$, and $\alpha_{C_2H_5Br} = 7.82$.

In the absence of complicating factors when two electron scavengers react competitively

$$e^- + S_1 \xrightarrow{k_{s_1}} P \qquad (6)$$

$$e^- + S_2 \xrightarrow{k_{s_2}} Q \qquad (7)$$

the total yield of electrons scavenged should be distributed between reactions 6 and 7 such that a fraction $\alpha_1[S_1]/(\alpha_1[S_1] + \alpha_2[S_2])$, reacts with S_1 to form P. Multiplying eq V by this fraction leads to the expression

$$G(P)_{S_2} = \left[G_{fi} + G_{gi}\frac{\{\alpha_1[S_1] + \alpha_2[S_2]\}^{1/2}}{1 + \{\alpha_1[S_1] + \alpha_2[S_2]\}^{1/2}}\right] \times \frac{\alpha_1[S_1]}{\alpha_1[S_1] + \alpha_2[S_2]} \qquad (VI)$$

which describes the expected yield of product P in the presence of the second solute. It will be noted that this expression directly takes into account the increased yield of scavenged electrons when a second solute is added to the system. Previously Hagemann and Schwarz[30] used a graphical method to accomplish this, but most other workers that have carried out competitive studies have merely assumed that the total yield does not change when the second solute is added. This latter assumption necessarily leads to too low an estimate of the relative rate constant.

The data given in Table V for the CH_3Br–C_2H_5Br solutions show that eq VI and its analog for $G(Q)_{S_1}$ describe the distribution of the electron reaction between the two solutes reasonably well though the methyl radical yields tend to be slightly low and the ethyl radical yields slightly high. From eq VI and the analogous one for the yield from the second solute

$$\frac{G(Q_2)_{S_1}/[S_2]}{G(P_1)_{S_2}/[S_1]} = \frac{\alpha_2}{\alpha_1} \qquad (VII)$$

The values of the quantities on the left side of eq VII from the competitive experiments average to 0.58. This value is somewhat higher than the ratio $\alpha_{C_2H_5Br}/\alpha_{CH_3Br} = 0.48$ obtained from the measurements on the individual solutes. This slight discrepancy and that between the individual observed and calculated yields can, at this point, be considered to involve experimental uncertainties in the determination of the individual parameters.

Similar data on the individual product yields from the CH_3Cl–C_2H_5Br mixed solute system given in Table VI illustrate a gross departure from the predictions of eq VI given parenthetically in the table. It is seen that the experimental ethyl radical yields are consistently higher and the methyl radical yields consistently lower than the predicted values. The observed values of the ratio

$$(G(C_2H_5)/[C_2H_5Br])/(G(CH_3)/[CH_3Cl])$$

are considerably higher than the ratio of α's given in the previous section ($\alpha_{C_2H_5Br}/\alpha_{CH_3Cl} = 1.45$) and vary from experiment to experiment. Since the total yield is as expected, it is quite clear that some secondary reaction increases the ethyl radical yield at the expense of a decreased decomposition of the methyl chloride. It seems likely that this is a secondary ionic reaction. The fact that the measured methyl radical yields are appreciably lower than predicted by eq VI cannot be explained if electron capture occurs dissociatively. From this it would appear that, at least in the case of methyl chloride, the molecular anion is the product of electron capture and that the observed methyl radicals are produced in the neutralization process. Assuming this to be the case electron transfer between an initially formed and stabilized methyl chloride anion and ethyl bromide seems to be a likely explanation for the disagreement between calculation and experiment.

$$CH_3Cl^- + C_2H_5Br \longrightarrow CH_3Cl + [C_2H_5Br]^- \longrightarrow CH_3Cl + C_2H_5\cdot + Br^- \qquad (8)$$

In any event the quantitative evaluation of the

Table VI: Radical Yields from Competitive Studies between Methyl Chloride and Ethyl Bromide

[CH_3Cl]	[C_2H_5Br]	$G(CH_3)$ Obsd	$G(CH_3)$ Calcd[a,b]	$G(C_2H_6)$ Obsd	$G(C_2H_6)$ Calcd[a,b]	$\frac{G(C_2H_5Br)/[C_2H_5Br]}{G(CH_3)/[CH_3Cl]}$ Obsd	$\frac{G(C_2H_5Br)/[C_2H_5Br]}{G(CH_3)/[CH_3Cl]}$ Calcd[c]	$G(CH_3 + C_2H_6)$ Obsd	$G(CH_3 + C_2H_6)$ Calcd[a,b]
0.203	0.101	1.00	(1.35)[a] 0.97[b]	1.29	(0.97) 1.35	2.6	2.8	2.29	2.32
0.102	0.104	0.63	(0.88) 0.63	1.50	(1.29) 1.54	2.3	2.4	2.13	2.17
0.0485	0.103	0.34	(0.50) 0.36	1.71	(1.55) 1.69	2.4	2.2	2.05	2.05
0.0209	0.103	0.18	(0.25) 0.17	1.68	(1.74) 1.80	1.9	2.1	1.86	1.98
0.201	0.202	0.68	(1.01) 0.65	1.77	(1.45) 1.82	2.6	2.8	2.45	2.48
0.103	0.202	0.38	(0.62) 0.38	1.92	(1.76) 1.98	2.6	2.5	2.30	2.37
0.103	0.491	0.17	(0.34) 0.18	2.47	(2.35) 2.51	3.0	2.9	2.64	2.69
0.100	0.049	0.93	(1.17) 0.92	1.03	(0.81) 1.06	2.3	2.4	1.96	1.98
0.107	0.0103	1.40	(1.60) 1.42	0.37	(0.22) 0.40	2.7	2.9	1.77	1.82
0.0098	0.0100	0.38	(0.46) 0.41	0.72	(0.67) 0.72	1.9	1.7	1.11	1.13

[a] Values in parentheses calculated using eq V and VI and $G_{fi} = 0.12$, $G_{ai} = 3.8$, $\alpha_{CH_3Cl} = 5.41$, and $\alpha_{C_2H_5Br} = 7.82$. [b] Values not in parentheses calculated by applying the correction term $(1 + \beta[S_2]^{1/2})^{-1}$ to the parenthetical values with β taken as 1.5 M^{-1} (see eq XI). [c] Calculated from eq XII with $\alpha_1 = \alpha_{CH_3Cl} = 5.41\ M^{-1}$, $\alpha_2 = \alpha_{C_2H_5Br} = 7.82\ M^{-1}$, and $\beta = 1.5\ M^{-1}$.

methyl and ethyl radical yields cannot be made with eq VI alone. An additional solute interaction term, which in general can be written as $f([S_1], [S_2])$, must be included to take into account the possibility of a reaction such as 8. The yield $G^*(P)_{S_2}$ under these circumstances can then be expressed in terms of the yield of product which would be formed in the absence of a secondary reaction, $G(P)_{S_2}$, as calculated from eq VI and this solute interaction term.

$$G^*(P)_{S_2} = G(P)_{S_2} \cdot f([S_1], [S_2]) \qquad \text{(VIII)}$$

If the secondary reaction involves an electron-transfer process which proceeds in only one direction, as is suggested in writing reaction 8, an approximate description of $f([S_1], [S_2])$ can be derived. Electron capture by a solute can be assumed to result in the formation of a negative-ion positive-ion spatial distribution similar to the original electron positive ion distribution. This assumption is supported by the fact found in pulse radiolysis[31,32] studies, where the negative ions were directly examined, that the yield of long-lived (and homogeneously distributed) negative ions is not substantially different from the free-ion yield measured in the pure hydrocarbons. One must, indeed, go to observation periods much shorter than microseconds to directly observe appreciable yields of these negative ions.[33] A competition will therefore occur between secondary reactions and ion recombination in much the same way as between electron capture and ion recombination. The concentration dependence for the secondary reactions of negative ions will in the first approximation be of the same form as that for electron scavenging. Neglecting the free-ion component, the yield which should normally appear as product P (from S_1) and is not converted into

(31) G. Scholes, M. Simic, G. E. Adams, J. W. Boag, and B. D. Michael, *Nature*, **204**, 1187 (1964).

(32) J. P. Keene, E. J. Land, and A. J. Swallow, *J. Amer. Chem. Soc.*, **87**, 5284 (1965).

(33) J. K. Thomas, K. Johnson, T. Klippert, and R. Lowers, to be published. A yield of ~1 of negative ions was observed in a 0.1 *M* diphenyl solution in cyclohexane. These negative ions decayed on the time scale of ~50 nsec.

product Q (from S_2) will be given by

$$G(\text{secondary reaction of } S_1^-) = G(P)_{S_2} \frac{\{\beta[S_2]\}^{1/2}}{1 + \{\beta[S_2]\}^{1/2}} \quad (IX)$$

where β is a constant, similar to α, describing the reactivity of S_2 towards the negative ion formed from S_1. The total yield of product from S_1 is then decreased by this amount giving

$$G^*(P)_{S_2} = G(P)_{S_2}\left(1 - \frac{\{\beta[S_2]\}^{1/2}}{1 + \{\beta[S_2]\}^{1/2}}\right) \quad (X)$$

$$= G(P)_{S_2}\left(\frac{1}{1 + \{\beta[S_2]\}^{1/2}}\right) \quad (XI)$$

For this case $f([S_1], [S_2])$ is explicitly given by the term in the brackets and is seen to be independent of the concentration of S_1. Such an independence in fact is found in the CH_3Cl–C_2H_5Br system. For the four runs at 0.1 M C_2H_5Br but with various concentrations of CH_3Cl, the ratios of the observed yield of methyl radicals to those calculated from eq VI are 0.74, 0.72, 0.68, and 0.72. Using an average ratio of 0.72 the reactivity β is evaluated from eq XI as 1.5 M^{-1}. With this value of β and the α's determined from the individual solutes, the yields of $CH_3\cdot$ and $C_2H_5\cdot$ can be predicted for the remaining experiments. As can be seen in Table VI the experimental data are well described by these predictions.

From the complete expressions for the yields of products from the individual solutes in the presence of a second competing solute, one can show that

$$\frac{G^*(Q)_{S_1}/[S_2]}{G^*(P)_{S_2}/[S_1]} = \frac{\alpha_2}{\alpha_1} + \left(\frac{[S_1]}{[S_2]} + \frac{\alpha_2}{\alpha_1}\right)\{\beta[S_2]\}^{1/2} \quad (XII)$$

The deviations in the measured quantity

$$(G(C_2H_5)/[C_2H_5Br])/(G(CH_3)/[CH_3Cl])$$

from the ratio $\alpha_{C_2H_5Br}/\alpha_{CH_3Cl} = 1.45$ are completely accounted for by the correction term on the right of eq XII as is seen in a comparison of columns 7 and 8 of Table VI. The apparently wild variations between experiments in the measured ratios are also accounted for because, as is seen in eq XII, the correction term is strongly dependent on $[S_1]/[S_2]$ particularly at high values of this concentration ratio. For example, the high value of the ratio observed in the experiment with 0.107 M CH_3Cl and 0.0103 M C_2H_5Br, which one might at first think to be relatively unaffected by secondary effects because of the low concentration of the second solute (so that $\beta[S_2]$ is small), is actually profoundly affected because of the high ratio of $[CH_3Cl]:[C_2H_5Br]$. Because of the significant contribution of the correction term in eq XII at concentrations where it is possible to measure the quantity given by the left side accurately, α_2/α_1 cannot be determined from measurements of this latter quantity.

One might briefly comment again, at this point, on the data from the CH_3Br–C_2H_5Br system. By analogy with the above, the data can be accounted for in detail if one assumes electron transfer from CH_3Br^- to C_2H_5Br with $\beta \cong 0.03$. This explanation, however, requires that the methyl bromide anion is sufficiently long-lived that it can react before it dissociates, a situation which seems much less likely than in the case of methyl chloride. It is also difficult to see why electron transfer should occur selectively from what appears to be the more to the less reactive solute. Because the deviations from ideality are not great, the complications appear to be quite minor.

The occurrence of secondary ionic reactions obviously presents a very serious problem which vitiates most attempts to determine the reactivity of solutes from competitive studies. In certain cases reasonable limits can be assigned to the reactivity where measurements have been carried out over wide ranges in the concentrations of both solutes. Perhaps the best such example is the system SF_6–CH_3Br in cyclohexane where the system is very nearly ideal and α_{SF_6} is estimated to be 18 M^{-1}.[34] In other cases, solutes known to be good electron scavengers exhibit little competitive effect (*e.g.*, CO_2 which appears to be as good an electron scavenger as methyl chloride[2] has little effect on the $CH_3\cdot$ yield from CH_3Br),[34] and normal interpretation of competitive experiments leads to grossly incorrect conclusions. In all of these cases it is useful to be able to treat the data analytically and eq II and VI, and the other equations derived from them are of great assistance in such treatments.

Acknowledgment. The authors wish to thank Mr. P. Wood of Oxford University for assistance with some of the measurements during a summer stay in these laboratories.

(34) P. P. Infelta and R. H. Schuler, to be published.

The Behavior of Entropy at Low Temperatures

by Alan J. Brainard

Department of Chemical and Petroleum Engineering, University of Pittsburgh, Pittsburgh, Pennsylvania 15213 *(Received September 24, 1968)*

The behavior of entropy as $T \rightarrow 0$ is investigated. In particular, the question of whether the $(\partial^2 S/\partial T^2)_v$ is >0 or <0 in this limit is discussed. Various models which represent specific heat phenomena are introduced and all lead to the conclusion that $(\partial^2 S/\partial T^2)_v > 0$ as $T \rightarrow 0$.

Introduction

The study of the behavior of the entropy of a body as its temperature is reduced to zero is of interest. The Nernst postulate, often called the third law of thermodynamics, is a guiding rule in this domain. This postulate tells us that the entropy must be independent of all thermodynamic parameters as $T \rightarrow 0$. Figure 1 represents this feature of the Nernst postulate where the two curves are drawn for different values of an additional parameter, say the volume of the system.

The behavior shown in Figure 1 is in agreement with the behavior presented in ref 1 and 2. The low-temperature behavior of the entropy of a body has also been described[3] as shown in Figure 2.

It is the purpose of this paper to consider the two possibilities shown in Figures 1 and 2 and to see which more closely represents the known behavior of pure substances. This paper will be limited to positive temperature systems. See ref 4 for an account of negative temperature systems. In addition, we shall not concern ourselves with the limiting entropy value as $T \rightarrow 0$. Whether this limiting value is in fact zero will not change the treatment given here. That problem is discussed in ref 5 and 6.

Thermodynamic Stability

The curves shown in Figures 1 and 2 are understood to connect equilibrium states. Thermodynamic stability considerations are now presented to establish criteria for variations about these equilibrium states. Consider a fixed amount of a homogeneous pure single substance. In the initial equilibrium state the system has an entropy, S, a volume, V, and an internal energy, U.

Since the energy of a system maintained at constant volume and entropy is a minimum for states of stable equilibrium, we have

$$\left(\frac{\partial^2 U}{\partial S^2}\right)_v > 0 \tag{1}$$

Now since

$$\left(\frac{\partial U}{\partial S}\right)_v = T \tag{2}$$

we obtain immediately

$$\left(\frac{\partial^2 U}{\partial S^2}\right)_v = \left(\frac{\partial T}{\partial S}\right)_v = \frac{T}{nC_v} > 0 \tag{3}$$

Thus stability considerations have shown us that the specific heat at constant volume, $C_v > 0$, for $T > 0$.[7,8] We make use of this fact by noting that the slope of the curves given in Figures 1 and 2 is given by $(\partial S/\partial T)_v$ and must therefore be >0. Figures 1 and 2 both satisfy this requirement.

The magnitude of $(\partial^2 T/\partial S^2)_v$ will be of direct concern to us in the subsequent development. Since

$$\left(\frac{\partial^3 U}{\partial S^3}\right)_v = \left(\frac{\partial^2 T}{\partial S^2}\right)_v \tag{4}$$

one might hope that thermodynamic stability would enable us to establish the limiting behavior of $(\partial^2 S/\partial T^2)_v$. Unfortunately, the third-order term (as do all odd order terms) drops out of the stability development, and thus thermodynamics is silent on this point.

Limiting Behavior as $T \rightarrow 0$

Inspection of Figures 1 and 2 reveals that they require that the entropy exhibit quite different behavior in the limit as $T \rightarrow 0$. Figure 1 would indicate that

$$\lim_{T \rightarrow 0} \left(\frac{\partial S}{\partial T}\right)_v = 0 \tag{5}$$

(1) M. J. Klein, "The Laws of Thermodynamics," in Scuola internazionale di fisica, Proceedings Course X, Figure 4, Varenna, Italy, 1960, pp 1–22.

(2) J. Wilks, "The Third Law of Thermodynamics," Oxford University Press, 1961, Figure 34(b).

(3) G. N. Hatsopoulos and J. H. Keenan, "Principles of General Thermodynamics," John Wiley & Sons, New York, N. Y., 1965, Figure 46-1.

(4) N. F. Ramsey, *Phys. Rev.*, **103**, 20 (1956).

(5) J. Wilks, ref 2, p 32.

(6) L. Tisza, "Generalized Thermodynamics," MIT Press, Cambridge, Mass., 1966, pp 119, 120.

(7) E. A. Guggenheim, "Thermodynamics," 4th ed, North-Holland Publishing Co., Amsterdam, 1959, Chapter 4, pp 96–102.

(8) J. G. Kirkwood and I. Oppenheim, "Chemical Thermodynamics," McGraw-Hill, Book Co., Inc., New York, N. Y., 1961, Chapter 6, pp 59–67.

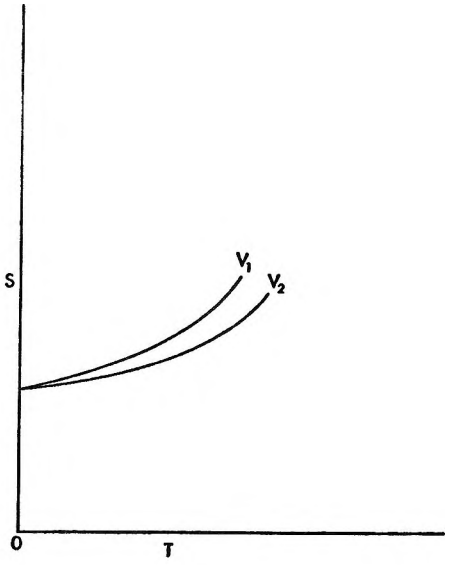


Figure 1.

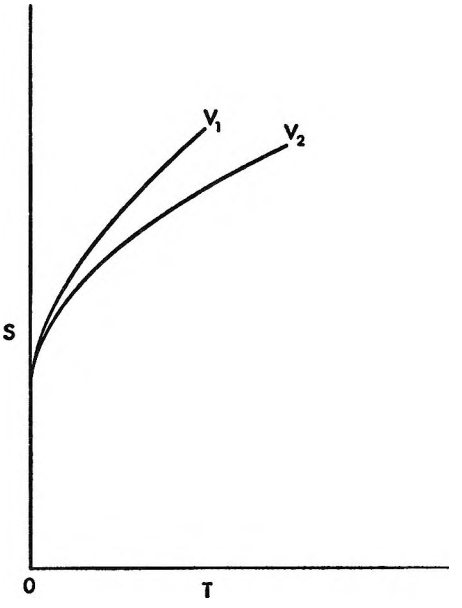


Figure 2.

or a small positive value, while Figure 2 gives

$$\lim_{T\to 0}\left(\frac{\partial S}{\partial T}\right)_v > 0 \tag{6}$$

In addition, we see that while Figure 1 indicates

$$\left(\frac{\partial^2 S}{\partial T^2}\right)_v > 0 \tag{7}$$

in contrast Figure 2 gives

$$\left(\frac{\partial^2 S}{\partial T^2}\right)_v < 0 \tag{8}$$

Thus the question reduces to determining whether eq 7 or eq 8 is more consistent with the behavior of pure substances.

The Nernst postulate tells us that

$$\lim_{T\to 0} C_v = 0 \tag{9}$$

Rewriting eq 3 and taking the limit, we have

$$\lim_{T\to 0}\left(\frac{\partial S}{\partial T}\right)_v = \lim_{T\to 0}\frac{nC_v}{T} \tag{10}$$

Thus it is only necessary that $C_v \to 0$ faster than $T \to 0$ in order to establish eq 5. There are three possibilities for the case

$$\lim_{T\to 0}\left(\frac{\partial S}{\partial T}\right)_v = 0 \tag{11}$$

and they are shown as curves A, B, and C in Figure 3.

Curves B and C can be ruled out as they do not satisfy eq 3. Thus whenever $C_v \to 0$ faster than $T \to 0$, we can establish the behavior shown in Figure 1.

Models Used to Represent Specific Heat

We shall consider the following models representing specific heat phenomena: a, contributions to the specific heat due to the thermal vibrations of the atoms in a lattice, represented by the Debye model; b, contributions to the specific heat due to the electrons in metals (good conductors of electricity); c, Schottky, or noncooperative specific heat; d, cooperative or λ-type specific heat, represented by the Bragg–Williams model.

a. The Debye model gives the following relation for the specific heat of a crystalline solid at low temperatures

$$C_v = a\left(\frac{T}{\theta_D}\right)^3 \tag{12}$$

where $a > 0$, and θ_D is the characteristic temperature known as the Debye temperature. For a solid obey-

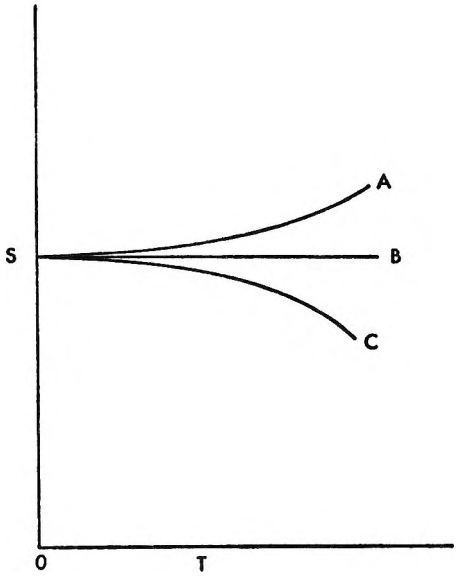


Figure 3.

ing the Debye model

$$\lim_{T\to 0} \frac{nC_v}{T} = \lim_{T\to 0} \frac{naT^2}{\theta_D{}^3} = 0 \qquad (13)$$

which is in agreement with eq 5. Furthermore

$$\left(\frac{\partial^2 S}{\partial T^2}\right)_v = \frac{2anT}{\theta_D{}^3} > 0 \quad (T > 0) \qquad (14)$$

for a Debye solid. We see that a Debye solid follows the behavior shown in Figure 1.

b. The Debye model is limited to insulators. When we consider metals, we find that the electrons in metals contribute an additional term to the specific heat which is proportional to the absolute temperature.[9] As a result, the total specific heat for these substances is given by

$$(C_v)_m = bT^3 + cT \qquad (15)$$

where the first term accounts for the lattice contributions and the second term for the electron contributions. For these substances we have

$$\lim_{T\to 0} \frac{(C_v)_m}{T} = c \qquad (16)$$

and

$$\left(\frac{\partial^2 S}{\partial T^2}\right)_v = 2bT \qquad (17)$$

As both b and c are >0,[10] we find that while the limiting value of $(\partial S/\partial T)_v$ as $T \to 0$ does not go to zero for metals, that eq 7 is satisfied, and thus they follow the general behavior shown in Figure 1.

c. The specific heat of a substance showing a Schottky "anomaly" is given by[11]

$$(C_v)_s = R\left(\frac{\Delta E}{kT}\right)\frac{\exp(\Delta E/kT)}{[1 + \exp(\Delta E/kT)]^2} \qquad (18)$$

where R is the gas constant, k is Boltzmann's constant, and ΔE represents the difference in energy between the first excited state and the ground state. From eq 18 we have

$$\lim_{T\to 0} \frac{(C_v)_s}{T} = \lim_{T\to 0} \left\{R\left(\frac{\Delta E}{kT^2}\right)\frac{\exp(\Delta E/kT)}{[1 + \exp(\Delta E/kT)]^2}\right\} \qquad (19)$$

Now the right-hand side of eq 19 can be written as

$$R\left(\frac{\Delta E}{kT^2}\right)\left[\frac{1}{\exp(\Delta E/kT) + 2 + \exp(-\Delta E/kT)}\right]$$

Because of the presence of the exponential term, $\exp(\Delta E/kT)$, the right-hand side clearly approaches 0 as $T \to 0$. We find that

$$\lim_{T\to 0} \frac{(C_v)_s}{T} = 0 \qquad (20)$$

Thus materials which exhibit a Schottky specific heat "anomaly" also follow the behavior shown in Figure 1.

d. The Bragg–Williams model gives the following relation for the ferromagnetic contribution to the specific heat[12]

$$(C_v)_{B-W} = \frac{Rs^2(1 - s^2)}{(T/T_c)^2 \times [1 - (T_c/T)(1 - s^2)]} \qquad (21)$$

where s is a measure of the degree of order and T_c is the transition temperature. From eq 21 we have

$$\lim_{T\to 0} \frac{(C_v)_{B-W}}{T} = \lim_{T\to 0} \frac{Rs^2(1 - s^2)}{(T^3/T_c^2)[1 - (T_c/T)(1 - s^2)]} \qquad (22)$$

Clearly it is only necessary that $(1 - s^2) \to 0$, faster than $T^3 \to 0$ as $T \to 0$ in order to satisfy

$$\lim_{T\to 0} \frac{(C_v)_{B-W}}{T} = 0 \qquad (23)$$

The degree of order, s, is given by

$$s = \tanh\left(\frac{sT_c}{T}\right) \qquad (24)$$

thus

$$(1 - s^2) = \frac{1}{\cosh^2(sT_c/T)} = \frac{4}{\exp(2sT_c/T) + 2 + \exp(-2sT_c/T)} \qquad (25)$$

Since by definition, $s \to 1$ as $T \to 0$, we see from eq 25 that due to the presence of the exponential term, $(1 - s^2) \to 0$ faster than $T^3 \to 0$ as $T \to 0$.

Using the Bragg–Williams model to represent the λ-type behavior of ferromagnetic materials in zero external magnetic fields, we find that the behavior shown in Figure 1 results. Thus we see that the behavior shown in Figure 1 is more in keeping with the predictions of all models considered.

In conclusion, we should note, however, that consideration of the behavior of pure substances at higher temperatures reveals that $(\partial^2 S/\partial T^2)_v$ can have positive, negative, and zero values.[13] It is only in the limiting case where $T \to 0$ that it seems that eq 7 alone is valid.

(9) A. H. Wilson, "Thermodynamics and Statistical Mechanics," Cambridge University Press, Cambridge, 1966, pp 169–172.

(10) J. Wilks, ref 2, p 35.

(11) R. G. Schurlock, "Low Temperature Behavior of Solids: An Introduction," Dover Publications, New York, N. Y., 1966, p 35.

(12) E. A. Moelwyn-Hughes, "Physical Chemistry," 2nd ed, Pergamon Press, Oxford, 1964, p 685.

(13) E. A. Guggenheim, "Applications of Statistical Mechanics," Clarendon Press, Oxford, 1966, p 42.

A Parametric Study of Bimolecular Exchange Reactions

by Don L. Bunker and Tiang-Shing Chang

Department of Chemistry, University of California, Irvine, California *(Received September 25, 1968)*

For the reaction $A + BC \rightarrow AB + C$, we have constructed a treatment in which the degree of adiabaticity or statisticality of the process may be parametrically varied. Reaction probabilities and product energy distributions have been calculated for $K + Cl_2$, $Cs + CH_3I$, $H + Cl_2$, $K + HBr$, and $H + H_2$. The form of the theory that best describes these reactions is a semistatistical one, somewhat more closely allied to the statistical treatment of Light than to the adiabatic model of Marcus.

Introduction: Why a Parametric Treatment?

The theory of bimolecular exchange reactions can be divided into sectors. The basis of the division is the degree of coupling between reactant and product states.

At one extreme we have the adiabatic-type theory advanced by Marcus[1] for the treatment of reaction cross sections. In this it is proposed that certain dynamical degrees of freedom not directly involved in the reaction event shall remain in the same quantum state (or shall conserve action) while the reaction occurs. This theory is the logical successor to the transition-state treatment. It requires a separation of the reaction coordinate from all the others and thus endows the reaction products with the best possible "memory" for the initial condition of the reactants.

There is a middle ground, populated by usually rather formal theories of the connection of each initial to many final states,[2] beyond which there occurs the fully statistical approach advocated by Light.[3] Here the products have no memory whatever for initial states, beyond that imposed by conservation laws. Different possible detailed results of a reaction event are probable in simple proportion to the number of states that correspond to them.

The two opposite theories have been tested, the statistical more thoroughly than the adiabatic, with mixed results for each. As is entirely reasonable from a theoretician's viewpoint, the tests have emphasized the truth or falsity of the individual theories. There have as yet been no comparisons of two treatments of the same reaction or attempts to encompass large numbers of laboratory results.

It is also possible to organize an inquiry around reactions rather than theoretical models. Are most reactions adiabatic, statistical, or in between? The material we present here is a possible first step toward a treatment that facilitates answering this question. Such a treatment must contain at least one empirical parameter in terms of which laboratory reactions may be meaningfully classified. In our formulation there are two such parameters—the adiabaticity or statisticality of the various degrees of freedom and the range of reaction coordinate over which this prescription operates. Others are possible, but we believe the present experimental evidence is not extensive enough to justify more than two.

We have constructed our calculation around a limited three-dimensional mechanical model of a reaction involving three atoms, this being the least complicated situation for which we believe our treatment makes sense. At its most adiabatic, our procedure exceeds the intent of Marcus' work, since we calculate product energy distributions for many reactions in which some kind of failure of adiabaticity is clearly inevitable. Conversely, at its most statistical, it stops somewhat short of Light's method; it should be considered a semistatistical model. (The distinction between statistical and semistatistical will be elaborated in the discussion that follows.) On the whole, however, the range of adaptability of our procedure is not too far out of register with that delimited by the landmarks erected by Marcus and Light.

Notation

Symbolically, the reaction is $A + BC \rightarrow AB + C$. Boldface **A** or **S**, with subscripts and superscripts, represent particular parameterizations of the theory. The superscript f measures, on a scale of 0–1, the range of reaction coordinate to which the description applies. The conventions associated with this are illustrated in Figure 1 for reactions without and with a potential barrier (the symmetrical case of the latter is shown, for

(1) The key papers are: R. A. Marcus, *J. Chem. Phys.*, **45**, 2138, 2630, 4493, 4500 (1966), and *Discussions Faraday Soc.*, **44**, 7 (1967). For application to $H + H_2$, see R. A. Marcus, *J. Chem. Phys.*, **46**, 959 (1967), and M. S. Child, *Discussions Faraday Soc.*, **44**, 68 (1967). A similar treatment of $K + HI$ has been given by M. S. Child, *Proc. Roy. Soc.* (London), **A292**, 272 (1966).

(2) Examples: C. A. Coulson and R. D. Levine, *J. Chem. Phys.*, **47**, 1235 (1967); F. T. Smith, *ibid.*, **36**, 248 (1952); D. A. Micha, *Arkiv Fysik*, **30**, 411, 425, 437 (1965); L. Hofacker, *Z. Naturforsch.*, **18a**, 607 (1963).

(3) J. C. Light, *Discussions Faraday Soc.*, **44**, 14 (1967), and P. Pechukas, J. C. Light, and C. Rankin, *J. Chem. Phys.*, **44**, 794 (1966), may be used as key references. Alternate theoretical routes have been provided by B. C. Eu and J. Ross, *ibid.*, **44**, 2467 (1966); J. Keck, "Variational Theory of Reaction Rates," Fluid Mechanics Laboratory, Massachusetts Institute of Technology, Cambridge, Mass., 1966; and E. E. Nikitin, *Teor. i Eksperim. Khim., Akad. Nauk Ukr. SSR*, **1**, 135 (1965).

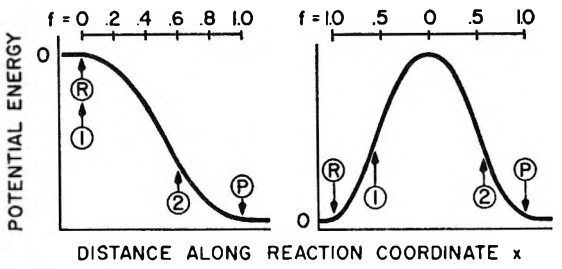


Figure 1. Labeling conventions for the reaction coordinate, shown with $f = 0.6$.

simplicity). The figure has been drawn with $f = 0.6$. The range described by f is between points 1 and 2. The measurement is unidirectional if there is no barrier and bidirectional if there is. Outside the range the reaction is strictly adiabatic. The possible parameterizations are: S^f, semistatistical; A_s^f, adiabaticity of the BC vibration → ABC stretch → AB vibration only; A_b^f, adiabaticity of the BC rotation → ABC bend → AB rotation only; **A**, full adiabaticity, for which f is irrelevant.

The circled symbols in Figure 1 are used as subscripts to designate different points on the reaction path. Reactants and products, each viewed as an atom plus a diatom, are denoted by R and P, respectively. The beginning and end of the f region, inside which the system is treated as a triatomic molecule ABC, are represented by 1 and 2. Quantities to which these subscripts may be applied include: J, rotational quantum number; v, vibrational quantum number; I, moment of inertia of a diatom; ν, vibrational frequency of a diatom; ϵ, translational energy; μ, reduced mass of a diatom; ϕ, potential energy on reaction coordinate, measured from zero indicated in Figure 1; x, the reaction coordinate; σ, maximum *geometric* cross section for the reaction or its reverse.

Theory

We formulate the reaction probability per collision $P(L, \epsilon_R)$ as a function of total angular momentum L and initial relative translational energy, with the intention of later summing over distributions of these

$$P(L, \epsilon_R) = \sum_{J_R, v_R} \alpha P(J_R, v_R) / \sum_{J_R, v_R} P(J_R, v_R) \quad (1)$$

where the summed P's are the distributions of reactant internal states. The quantity α has a very complicated dependence on many things. Its value is 0 or 1; it will be 1 only if all the following conditions are met.

(1) There is enough energy for the reaction to get adiabatically from point R to point 1 (applies only to reactions with a barrier)

$$\epsilon_R - \phi(x) + h(v_R + \tfrac{1}{2})[\nu_R - \nu(x)] + \tfrac{1}{2}\hbar^2 J_R(J_R + 1)[I_R^{-1} - I(x)^{-1}] \geq 0 \quad (2)$$

for all $x_R \leq x \leq x_1$. Here $I(x)$ and $\nu(x)$ refer to the diatom BC. All quantities with an x dependence are to be evaluated along the reaction path, the shape of which will eventually have to be specified.

(2) There is enough energy for the adiabaticity of those triatomic vibrations that are so treated between points 1 and 2. Let $b = 1$ for adiabatic bending (**A** and A_b^f), 0 otherwise; and let $s = 1$ for adiabatic stretching (**A** and A_s^f), 0 otherwise. Then

$$\epsilon_R - \phi(x) + h(v_R + \tfrac{1}{2})[\nu_R - s\nu_s(x)] + [\tfrac{1}{2}\hbar^2 J_R(J_R + 1)/I_R] - bJ_R h\nu_b(x) - [L^2/2I_C(x)] \geq 0 \quad (3)$$

for all $x_1 \leq x \leq x_2$. Symbols which refer to the triatom ABC are the bend and stretch frequencies ν_b and ν_s and the moment of inertia I_C.

(3) At point 2, there exists a set of (L_2, J_2, χ, v_2) for which it is possible to satisfy the list of conditions (A) through (G). The angle χ is between vectors representing L_2, the AB–C orbital angular momentum, and $J_2\hbar$, the AB rotational angular momentum. We apply a geometric approximation at this point—that ABC passes through a linear configuration so that the problem of composition of angular momentum is simplified. The rotational kinetic energy of such an object can be found by simple vectorial arguments; it is

$$T = (L_2^2/2I_C) + [J_2(J_2 + 1)\hbar^2/2I_2] - L_2[J_2(J_2 + 1)]^{1/2}\hbar(\cos\chi)/I_C \quad (4)$$

(A) If $s = 1$, as in **A** and A_s^f, then $v_2 = v_R$.

(B) If $b = 1$, as in **A** and A_b^f, then[4] $J_2 = J_R$.

(C) The AB–C orbital angular momentum L_2 is not too large for a reasonable exit cross section σ_P. Since

$$\epsilon_2 = \epsilon_R - \phi_2 + h[(v_R + \tfrac{1}{2})\nu_R - (v_2 + \tfrac{1}{2})\nu_2] + \tfrac{1}{2}\hbar^2[\{J_R(J_R + 1)/I_R\} - \{J_2(J_2 + 1)/I_2\}] \quad (5)$$

we require

$$L_2 \leq (2\sigma_P \mu\epsilon_2/\pi)^{1/2} \quad (6)$$

in which μ is the reduced mass of AB and C. This follows from the definition of angular momentum in terms of velocity and impact parameter. Test (C) is extended to the rest of the reaction path in (F), below.

(D) Energy is conserved at point 2. From eq 4

$$\epsilon_2 = T - [J_2(J_2 + 1)\hbar^2/2I_2] \quad (7)$$

(E) Angular momentum is conserved at point 2. This means that L_2 and $J_2\hbar$, added vectorially at angle χ, must yield a vector of magnitude L.

(4) This statement is a fairly low approximation to the actual adiabaticity requirement, but it is tolerable because the parameterizations of most interest did not turn out to rely heavily on it. For a description of how this should have been done, see R. A. Marcus, *J. Chem. Phys.*, 49, 2617 (1968). Equation 100 of this is the one of interest.

(F) There is not too much orbital angular momentum for the adiabatic motion from point 2 to point P

$$L_2 \leq L + J_R\hbar \tag{8}$$

a requirement the consequences of which we will discuss later, and

$$L_2 \leq [2\sigma_P\mu\epsilon(x)/\pi]^{1/2} \tag{9}$$

for all $x_2 \leq x \leq x_P$, where

$$\epsilon(x) = \epsilon_R - \phi(x) + h(v_2 + \tfrac{1}{2})[\nu_2 - \nu(x)] + \tfrac{1}{2}\hbar^2 J_2(J_2 + 1)[I_2^{-1} - I(x)^{-1}] \tag{10}$$

(G) There is enough energy for this adiabatic process; $\epsilon(x)$ is positive over the range of eq 9.

If $f = 1$, (F) and (G) may be omitted. The quantum numbers v_2 and v_P are identical, and so are J_2 and J_P. The distributions of J_P and v_P, symbolically and without normalization, are

$$P(v_P, J_P) = \sum_{J_R, v_R} P(v_R, J_R) \sum_{L_2, \chi} (2J_2 + 1)(2L_2 + 1)\alpha \tag{11}$$

Computational Tactics

This theory, unlike others,[1,3] accepts a limited amount of information about the shape of the potential surface. In the present calculation we supply an 11-entry table of values of $\phi(x)$, $\nu_s(x)$, and $\nu_b(x)$; f is restricted to multiples of 0.1. The reaction path is assumed to have the shape shown in Figure 2. The curved part is a quarter-circle,[5] and tabulation is at intervals of 9° from θ = 0–90°. All tests involved in establishing the value of α are made at these points.

Summation over J_R, v_R and all subsidiary variables is done by random sampling. For fixed ϵ_R and L, J_R and v_R are chosen from distributions corresponding to a prescribed temperature, with attention to nuclear spin statistical effects if they are important. If tests (1) and (2) are passed, J_2 is sampled from a $(2J_2 + 1)$-weighted distribution if $b = 0$, and if $s = 0$, v_2 is randomly chosen.[6] The maximum value L_{max} of L_2 consistent with requirement (3C) and with eq 8 is next calculated, and L_2 is sampled in the range 0 to L_{max} with weight[7] $2L_2 + 1$. The χ corresponding to (3D) and (3E) are next calculated and compared. If they match within a small $\Delta\chi$, $\alpha = 1$; otherwise new v_2, J_2, and L_2 are selected. For $\Delta\chi = 15°$, 1800 repetitions of this cycle are sufficient, as shown by exponential decline of the distribution of number of trials for J_R and v_R that have $\alpha = 1$. Ordinarily many fewer trials suffice.

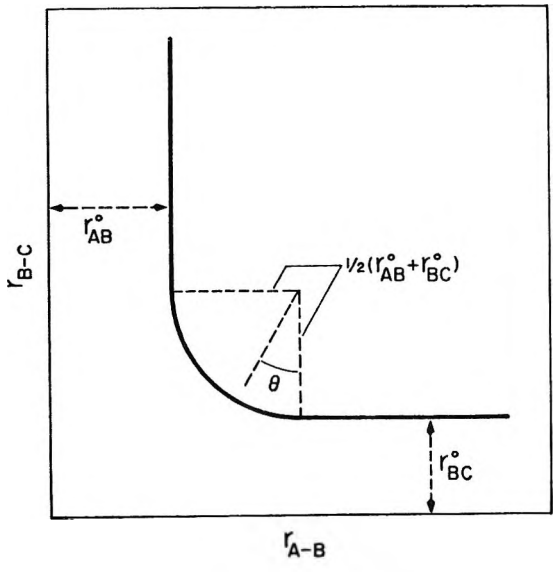


Figure 2. Shape conventions for the reaction path.

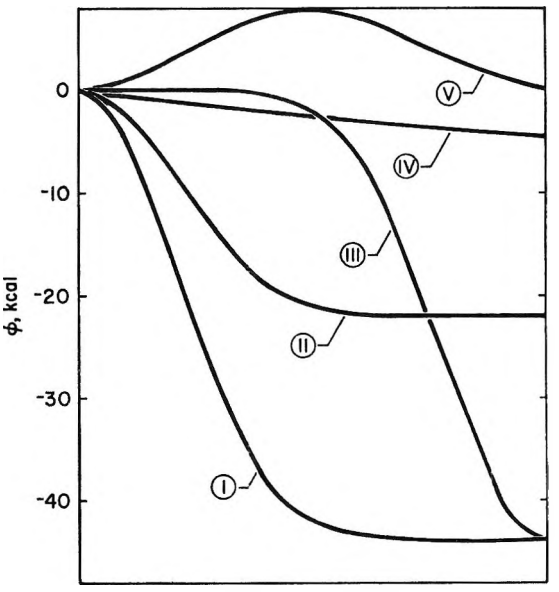


Figure 3. Reaction path profiles: standard case, I; heavy-atom case, II; light-atom attractive case I and repulsive case, III; K + HBr, IV; H + H_2, V. The energetics are correct but the shapes are arbitrary.

The Standard Case: Equal Masses, Attractive Surface

All of the reaction path profiles used in this study are shown in Figure 3. In all nonbarrier cases $\nu_s(x)$ was distributed linearly between ν_R and ν_P, $\nu_b(x)$ was 100 cm^{-1} all along the reaction path, σ_P was 100 $Å^2$, and the temperature corresponded to that of the relevant laboratory experiments. All bond lengths were derived from the known properties of diatoms.

The standard case involves atoms of equal mass, 40 amu (approximately, K + Cl_2), with $\epsilon_R = 10^{-13}$ erg, ν_R = 560 cm^{-1}, and ν_P = 280 cm^{-1}. As is expected for

(5) This is a simplified form of the artificial potential proposed by F. T. Wall and R. N. Porter, *J. Chem. Phys.*, 36, 3256 (1962).

(6) It would be easy to make s and b into continuous variables if the amount of experimental data warranted it. For example, the probability of v_2 could be made proportional to $\exp[-s'(v_R - v_2)^2]$, with $0 \leq s' \leq \infty$ and s' an appropriate function of s.

(7) It is debatable whether $2L_2 + 1$ or uniform weighting is more consistent with our geometrically restricted mechanical model. Fortunately, tests show that the effect on the results is not very important.

reactions of high exothermicity, there is nearly zero reaction probability for A_s^1 and A_b^1. A_s^1 fails because so little energy can be accomodated as product vibration, and A_b^1 fails because the combination of $\nu_b(x)$ and large J_R usually requires more energy than there is. The best fit, in terms of the known[8] properties of these reactions, is S^1. Smoothed distributions of v_P and J_P for four values of L are shown in Figures 4 and 5, along with over-all results obtained by summation over

$$P(L) = \pi L/\sigma_R \mu' \epsilon_R, \qquad (12)$$

with $\sigma_R = 100$ Å^2 and μ' the reduced mass of A and BC. The J_P distribution corresponds roughly to a temperature in the range 1000–2000°K. Reaction probability was 1.00, 1.00, 0.82, and 0.48 for the descending series of L.

The effect of decreasing f is shown in Figures 6 and 7. The J_P distribution is less drastically affected than that for v_P, which shifts rapidly to small values when f becomes small. This is a very useful way for this parameter to behave.

A Heavy-Atom Case: Cs + CH_3I

The A, B, and C masses were 133, 127, and 15; $\nu_R = 560$ cm^{-1}; $\nu_P = 280$ cm^{-1}; largest $L = 2.6 \times 10^{-25}$ cgsu. Otherwise, this was similar to the standard case. Tests were made for S^0, S^1, A_s^1, and A_b^1, with results quite similar to those described above.

The point of this is that Entemann and Herschbach[9] have recently discovered that this reaction produces products having unusually little CsI internal excitation. Since this did not appear for S^1, *either* an unusual parameterization of the theory is required or (as Entemann and Herschbach suggest) an unusual potential surface is involved. In our calculations the shape of the potential surface would be most important for $f \cong 0.5$.

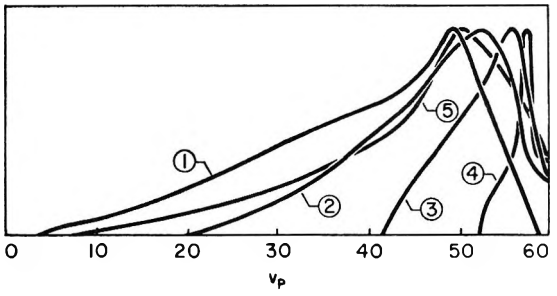


Figure 4. Distributions of v_P for standard case S^1: 1, $L = 1.6 \times 10^{-25}$; 2, $L = 1.2 \times 10^{-25}$; 3, $L = 0.8 \times 10^{-25}$; 4, $L = 0.4 \times 10^{-25}$; 5, summed over L. The ordinate has arbitrary units.

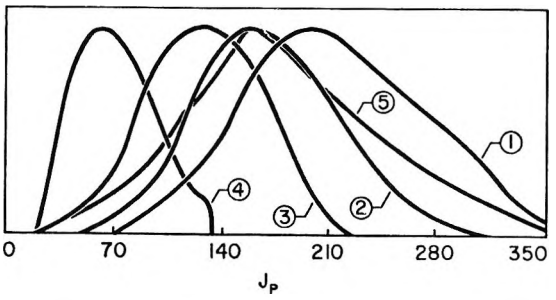


Figure 5. Distributions of J_P for the standard case S^1. Labels are the same as for[a] Figure 4.

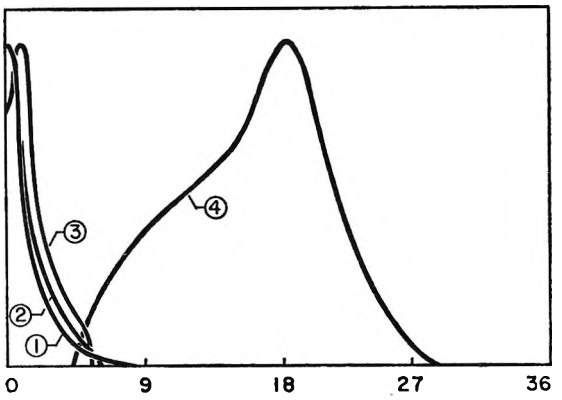


Figure 6. Distributions of v_P for the standard case S^0 and $S^{0.3}$: 1, $L = 1.6 \times 10^{-25}$; 2, $L = 1.2 \times 10^{-25}$; 3, $L = 0.8 \times 10^{-25}$, all for S^0; 4, $L = 1.6 \times 10^{-25}$ for $S^{0.3}$. The ordinate has arbitrary units.

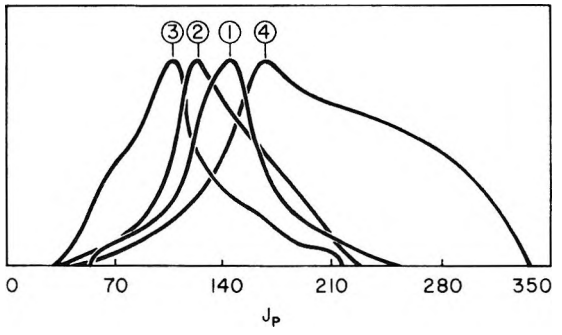


Figure 7. Distributions of J_P for the standard case S^0 and $S^{0.3}$. Labels are the same as for Figure 6.

A Light-Atom Case: H + Cl_2

Masses 1, 36, and 36, $\nu_R = 560$ cm^{-1}, $\nu_P = 3000$ cm^{-1}, $\epsilon_R = 4 \times 10^{-14}$ erg, and $L = 2 \times 10^{-26}$ were used. This is another reaction which does not produce the largest possible v_P, and for which a "repulsive" potential surface has been proposed.[10] We studied it with attractive and repulsive reaction path contours (both are shown in Figure 3).

The reaction is definitely subject to some constraints not present in the other cases. S^1 and S^0 are unsuccessful on both surfaces—the reaction probability, though not zero, is too small (a few per cent) to permit v_P and J_P distributions to be accumulated. There is no

(8) R. Grice and P. B. Empedocles, *J. Chem. Phys.*, 48, 5352 (1968).

(9) E. A. Entemann and D. R. Herschbach, *Discussions Faraday Soc.*, 44, 289 (1967).

(10) The key reference is now K. G. Anlauf, P. J. Kuntz, D. H. Maylotte, P. D. Pacey, and J. C. Polanyi, *ibid.*, 44, 183 (1967).

single simple reason for this behavior, which involves the interaction of eq 4–8. Simultaneous satisfaction of these when L is small requires special values of v_R and J_R; most of the successful points were for $v_R = 1$. There is, however, an intermediate range of f for which the reaction has normal properties. At $S^{0.5}$ on the attractive surface, the probability of reaction is 0.81. Switching to the repulsive surface shifts the reaction to $S^{0.7}$, with probability 0.25. The v_P distributions are shown in Figure 8. It is the attractive surface that agrees best with the experiments for v_P. The J_P distributions are mildly non-Boltzmann, peaked at $J_P = 35$ (attractive) and $J_P = 25$ (repulsive). The experimentally observed bump at low J_P has been attributed to rotational relaxation.

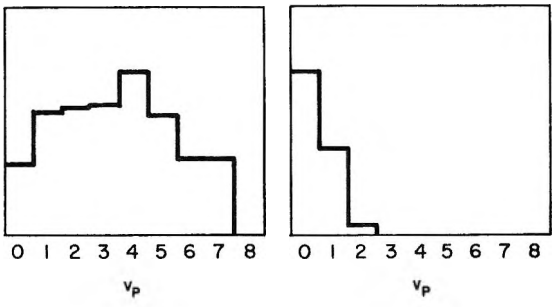


Figure 8. Distributions of v_P for the light-atom case; $S^{0.5}$ with attractive surface and $S^{0.7}$ for repulsive surface.

We do not believe that our test tells very much about the character of the reaction path contour. Rather, it contributes another item to the evidence that this reaction is kinematically something of a special case.

K + HBr

In some ways this has been an easy reaction to interpret theoretically. The combination of small exothermicity with a large quantity of conserved angular momentum places severe constraints on the outcome of the reaction; J_P must be as large as possible. All other aspects of the reaction are subordinate to this. The high J_P feature is found experimentally,[11] in Light's theory,[3] and in trajectory studies.[12] It also appears in the present theory (masses 39, 80, 1; v_R = 2650, v_P = 230; $\epsilon_R = 1.3 \times 10^{-13}$, $L = 1.9 \times 10^{-25}$). The reaction may be either S^0 or S^1 with unit probability. There also exists a probability of 0.25 per collision for the A_s^1 parameterization, but A_b^1 is unsuccessful.

H + H_2

We tested this reaction only for probability of occurrence, since the product states are not experimentally available. The parameters[13] were 1 amu for masses, $\sigma_R = 15$ Å^2, $\nu_b = 950$, $\epsilon_R = 3.8 \times 10^{-12}$ (for which a high probability of reaction would be expected), and $L = 3 \times 10^{-26}$. The intermediate stretching frequency increased linearly from 2200 cm^{-1} at the barrier to 4400 cm^{-1} at the ends of the curved part of the reaction path.

We found that S^1 and A_s^1 had unit probability and that A_b^1 had none. In S^1, about half the time $v_P = v_R$; otherwise $v_P - v_R = 1$. These results are both roughly compatible with the conclusions reached by Karplus[14] from trajectory studies.

Discussion

The tendency of this far from exhaustive first set of tests is to suggest that the best over-all parameterization is S^1, or perhaps S with f somewhere between 0.5 and 1. Since this is at one extreme of our parameterization range, we have to inquire into the relation between our fully semistatistical case, S^1, and Light's fully statistical treatment (for which, in effect, f is also 1).

There are three differences, aside from those of model sophistication. Our calculation is not reversible—we neglect the possibility that the intermediate (ABC) will reform A + BC, whereas Light assigned this full statistical weight. We impose the constraint expressed by eq 8, thus rejecting states accepted by Light in which final orbital and rotational angular momenta have opposite senses and unusually high values. Finally, we incorporate information about the geometry of (ABC), and other theories do not.

Light has commented on the fact that his theory does not produce inverted product vibrational distributions. Our procedure does not suffer from this difficulty. It would be pleasant if the explanation turned out to lie in the first two differences noted above. A revised Light-type theory could then, in principle, be constructed, and it would require knowledge only of reactant and product properties.

That this is probably a vain hope can be seen from the following construction, based on our mechanical model of the reaction in the S^1 modification. Figure 9 shows the semiclassical v, J^2 plane for this reaction. (A subsidiary illustration for the infrequent angular-momentum-limited case, *e.g.*, K + HBr, is also provided.) All symbols refer to products; E is total energy. The diagonal dashed line arises from energy conservation

$$E \geq vhv + (J^2\hbar^2/2I) \qquad (13)$$

The vertical solid line is our constraint of eq 8, $J\hbar \leq L$. The final orbital angular momentum will be

$$L' = b[2\mu(E - vhv - J^2\hbar^2/2I)]^{1/2} \qquad (14)$$

(11) C. Maltz and D. R. Herschbach, *ibid.*, 44, 176 (1937); see also A. E. Grosser and R. B. Bernstein, *J. Chem. Phys.*, 43, 1140 (1965).

(12) D. L. Bunker, unpublished results.

(13) Based on the potential surface of R. N. Porter and M. Karplus, *J. Chem. Phys.*, 40, 1105 (1964).

(14) M. Karplus, *Discussions Faraday Soc.* 44, 78 (1967); see also R. A. Marcus, *ibid.*, 44, 87 (1967).

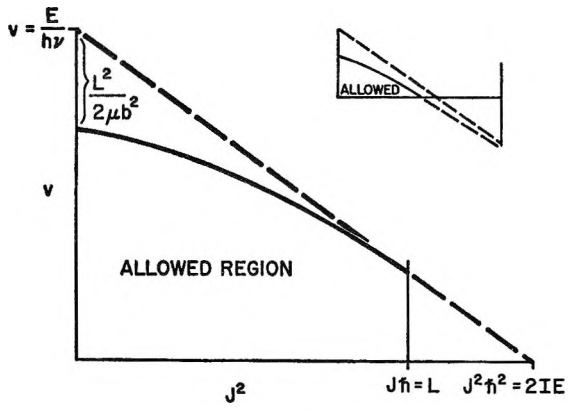


Figure 9. Plane of final v, J^2 permitted by S^1 parameterization. The smaller diagram is for the angular-momentum-limited case.

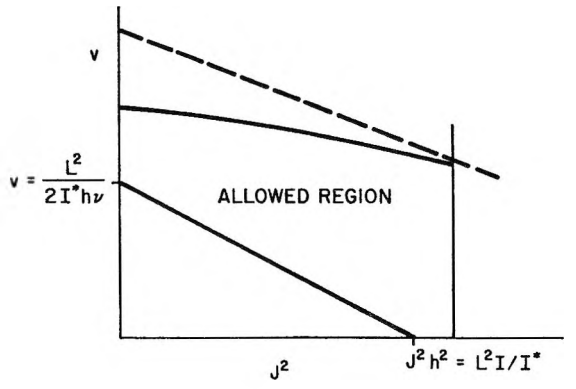


Figure 10. Figure 9 revised to include a product translational limitation.

with b the exit impact parameter and μ the AB − C reduced mass. The over-all angular momentum cannot be composed unless $J\hbar \geq L - L'$. This leads to

$$vh\nu \leq E - (J^2\hbar^2/2I) - [(L - J\hbar)^2/2\mu b^2] \quad (15)$$

which generates the curved line shown in the figure.

It is very clear that low v will dominate the final energy pattern, since the largest number of J states will always be associated with them. No amount of manipulation of the partitioning of angular momentum between $J\hbar$ and L' will relieve this condition. Only a remodeling which weighs against large amounts of product translational energy would help.

Such a feature is present in our treatment because of conditions (3D) and (3E). In making these tests at point 2 on the reaction coordinate, we effectively limit the product translational energy to

$$L_2^2/2I_C - L_2[J_2(J_2 + 1)]^{1/2}\hbar \cos\chi/I_C \quad (16)$$

that which is associated with the over-all rotation of (ABC). In reconstructing Figure 9, then, we might in an approximate way require that

$$vh\nu + (J^2\hbar^2/2I) \geq L^2/2I^* \quad (17)$$

in which I^* is an ABC final moment of inertia that might be prescribed in a number of ways, *e.g.*, from Figure 2 and its conventions. We would obtain the kind of situation depicted in Figure 10 (one of three possible configurations is shown). The product vibrational energy distribution for this figure would rise at low v, attain a flat maximum, and then decrease rapidly. This corresponds with what is observed, and positively identifies condition (3D) as the key feature in our treatment. A theory of product excitation based on Figure 10 and all of its ramifications, however, is only a little less bulky than the main calculation with which we established S^1 as the most significant parameterization.

There are many other ways in which this study might have been carried out. Adopting $f = 1$, $b = 0$, and variable[6] s might lead to results nearly as good as those we have achieved and so might a number of other ways of tampering with Light's prescription[3] for the relative probabilities of final states. The **A** alternatives might better be defined in terms of maximum persistence of quantum numbers consistent with conservation laws, rather than in the absolute form we have used. All of these things are clear by hindsight, but it is by no means certain that we would thereby evade the situation that has developed in our study—the predominance of (ABC) properties over those of AB and C.

We therefore reach the following tentative conclusion. To make a satisfactory model of A + BC → AB + C, *it will probably be necessary to include structural information about the intermediate state ABC.* We have done this in a minimal way in the preceding paragraphs, *via* the single quantity I^*. Our calculation as a whole provides another alternative. Both of these, in crude form, appear to be somewhat successful, and we believe that future exploration along this line will be fruitful.

Acknowledgments. The work was supported by the Army Research Office, Durham, N. C., under Contract DAHCO4-67-C-0054. Most of the calculations involved purchase of computer time from the North Node of the Campus Computing Network, UCLA. This arrangement would not have been feasible without the spirited cooperation of Mr. Kenneth Tom and Mrs. Dorothy Parkin, whom we thank.

Bonding in C_1 and C_2 Fluorides

by Thomas C. Ehlert

Department of Chemistry, Marquette University, Milwaukee, Wisconsin 53233 *(Received September 25, 1968)*

A Farlow-type reaction involving manganese trifluoride and graphite has been used to generate the gaseous species $(CF_2)_{n=1,2,3...}$, CF_3, and C_2F_2 under equilibrium conditions. By mass spectrometric methods it has been found that $\Delta H_f°_{298}$ for $CF_2(g)$, $CF_3(g)$, and $C_2F_2(g)$ are -41.1 ± 2, -102.5 ± 3, and -45 ± 6 kcal mol^{-1}, respectively. These and other data show that $D°_{298}(CF_3\text{-F})$, $-(CF_2\text{-F})$, $-(CF\text{-F})$, and $-(C\text{-F})$ are 139.4, 80.2, 123.7, and 126.0 (all ± 3) kcal mol^{-1}, respectively. The C≡C bond in difluoroacetylene is found to be 60 kcal weaker than that in acetylene.

Introduction

Complete bond dissociation energy data are available for very few molecules having more than three atoms. In this paper the existing data on C_1 fluorides are reviewed and new experimental data are presented which permit evaluation of $D(CF_3\text{-F})$, $D(CF_2\text{-F})$, $D(CF\text{-F})$, and $D(C\text{-F})$. Values for the carbon–carbon triple bond and the carbon–carbon double bond in C_2 fluorides are reported.

An accurate value for the total bond energy in CF_4 may be calculated from $\Delta H_f°_{298}[CF_4(g)]$ recently reported to be -223.04 ± 0.18 kcal mol^{-1}.[1] Using the sublimation enthalpy of carbon and the dissociation energy of fluorine,[2] one finds $\Delta H°_{atom}[CF_4(g)] = 469.4 \pm 2.3$ kcal mol^{-1}. For $CF_3(g)$ $\Delta H_f°_{298} = -94.8$ kcal mol^{-1} may be obtained by combining the ionization potential (I.P.) of CF_3, 9.25 ± 0.04 eV;[3] the appearance potential (A.P.) of CF_3^+ from CHF_3, 14.53 ± 0.05 eV,[4] with enthalpy of formation data for $CHF_3(g)$ and $H(g)$.[2] However, $\Delta H_f°_{298} = -110.8 \pm 2.1$ kcal mol^{-1} is obtained using $D(CF_3\text{-H}) = 106.4 \pm 0.5$ kcal mol^{-1} from the kinetics of chlorinating CHF_3.[5] The possibility of excited product formation in the dissociative ionization of CHF_3 requires that 94.5 kcal be considered a lower limit to $-\Delta H_f°[CF_3(g)]$ while the latter value should be an upper limit since it is based upon the activation energy for the reaction $Cl + CHF_3 \rightarrow HCl + CF_3$. It is apparent that an independent check on this value would be very desirable. The standard enthalpy of formation of $CF_2(g)$ seems to be close to -41 kcal mol^{-1} at 298°K since a large number of diverse methods give values within a few kilocalories of this.[2] Evidently then $D°(CF\text{-F}) + D°(C\text{-F}) = 249.6 \pm 3.3$ kcal mol^{-1} at 298°K. $D°_0(C\text{-F})$ has been reported as 114 kcal mol^{-1} (4.96 eV),[6] but it was recently found[7] that inclusion of the second anharmonicity constant in the Birge–Sponer extrapolation raised $D°_e$ to 126.8 kcal mol^{-1} (5.50 ± 0.10 eV) and $D°_{298}$ to 126.0 ± 2.3 kcal mol^{-1}.

If one defines the strength of the double bond in C_2F_4 as ΔH for the reaction

$$C_2F_4(g) \longrightarrow 2CF_2(g) \qquad (1)$$

then available data give 73 ± 6 kcal mol^{-1} at 298°K.[2] While the true value of ΔH_{298} for reaction 1 almost certainly lies within the limits given, an attempt to reduce the uncertainty seemed worthwhile. The situation with regard to the triple bond in FC≡CF is far less satisfactory since there are no experimental data on the stability of C_2F_2. If such were available it would be possible to calculate the "triple" bond strength in this molecule and thereby improve our understanding of the effect of fluorine substitution on the bonding ability of carbon.

Experimental Section

The apparatus, consisting of an effusion molecular beam source and a quadrupole mass spectrometer for studying the species produced in the beam source, has been described previously.[8] To improve the quality of the appearance potential measurements the energy spread in the ionizing beam was reduced by narrowing the ionizer entrance and exit slits. Also, trap current regulation of the ionizing electron beam was used instead of emission current regulation. A cylindrical effusion cell, machined from spectrographic grade graphite to have a 90° conical orifice 1.1 mm in diameter at the smaller (lower) end, was degassed by heating under vacuum before loading with 0.5 g of 99.5% MnF_3. The MnF_3 was used as received[9] without further purification. Precautions were taken to minimize contact with moisture. To help assure the attainment of equilibrium inside the cell, the quantity of sample used was such as to provide a sample surface at least 100 times larger than the orifice area while

(1) E. Greenberg and W. Hubbard, *J. Phys. Chem.*, **72**, 222 (1968).
(2) "JANAF Thermochemical Tables," The Dow Chemical Co., Midland, Mich.
(3) C. Lifshitz and W. Chupka, *J. Chem. Phys.*, **47**, 3439 (1967).
(4) J. Farmer, I. Henderson, F. Lossing, and D. Marsden, *ibid.*, **24**, 348 (1956).
(5) J. Coomber and E. Whittle, *Trans. Faraday Soc.*, **62**, 2183 (1966).
(6) E. Andrews and R. Barrow *Proc. Phys. Soc.*, **64A**, 481 (1951).
(7) T. Porter, D. Mann, and N. Acquista, *J. Mol. Spectry.*, **16**, 228 (1965).
(8) T. C. Ehlert, R. M. Hilmer, and Sr. E. A. Beauchamp, *J. Inorg. Nucl. Chem.*, **30**, 3112 (1968).
(9) Research Inorganic Chemical Co., Sun Valley, Calif.

sample pressure at no time exceeded 10^{-5} atm within the cell.

The sample temperature was monitored with chromel–alumel thermocouples, one inserted in the cell top and another in the base. Thermocouple junction potentials, measured with a Honeywell 2732 potentiometer, were reproducible to 0.01 mV (0.25°). A third thermocouple, located in the cell base, provided an error signal to operate the beam source temperature control, maintaining the temperature of the sample cell constant within 1°. To minimize temperature errors (a) the thermocouple wires were continuous from sample to potentiometer or cold junction, (b) the wires were air-annealed at a red heat after installation, (c) the cold junctions were immersed at least 7 in. in separate distilled water–ice mixtures, and (d) the cell top was made 10 to 15° hotter than the base. Junction potentials were converted to temperature using the manufacturer's calibration[10] after these corrections were verified, ±0.05 mV, in a separate experiment. Sample temperatures were taken as an average of the top and bottom temperatures weighted by the distance of the sample from the top and bottom thermocouples.

Getter ion pumps maintained the pressure at less than 10^{-6} mm in the beam source region and considerably lower in the quadrupole region even at the highest sample temperatures.

Owing to the linear mass dispersion of the quadrupole analyzer, the determination of ion mass-to-charge ratios (m/e) was straightforward. Ions derived from neutral species originating in the effusion cell were identified by their abrupt disappearance upon closing the slit through which the sample vapors pass in order to reach the ionizer. Ionization efficiency curves[11] were obtained by varying the electron energy in 0.1- or 0.2-eV steps while maintaining the sample temperature and the electron beam current constant. The electron energy scale was calibrated by comparison of the observed A.P. of O_2^+, 13.06 ± 0.1 eV, with I.P. of O_2 = 12.063 ± 0.001 eV.[12] Both the "initial break" method[11] and a recently described deconvolution method[13] were used to determine A.P.'s. Agreement between the two methods was within experimental error in all cases. Identification of the neutral precursor of ionic species was based upon temperature dependence studies, the A.P., and isotopic abundance in addition to the m/e value of the ion.

Results and Discussion

An extremely complex mass spectrum resulted when 70-V electrons were used for ionization of the sample vapors. At least 100 peaks were produced, extending to above m/e 400. Reducing the electron energy to 15 V still gave detectable signals for the monopositive ionic species CF, C_2F, CF_2, C_3F, C_2F_2, CF_3, C_3F_2, C_2F_3, C_3F_3, C_2F_4, C_3F_4, C_2F_5, C_3F_6, C_4F_6, C_3F_7, C_5F_7, C_4F_8, C_6F_9, C_6F_{10}, and C_7F_{10}. Since the mass analyzer would not resolve the 0.06 amu mass difference between $^{55}MnF_x$ and $^{12}C_3F_{x+1}$, the possibility of contribution by MnF_x to these species was given careful consideration. As discussed in the following text only the $x = 0$ species, m/e 55, was satisfactorily identified—as due to simple ionization of Mn(g) at low electron energies. Considering this plus the low intensity of the heavier ions, identification efforts were limited to the species listed in Table I. The ion with m/e 31, certainly CF^+, could arise from numerous fragmentation processes,[14] but not from simple ionization of CF as evidenced by the high A.P. Interpretation of the m/e 43 ionization efficiency curve was not attempted.

Table I: AP's and Precursors in the MnF_3—Graphite Reaction

Ion m/e	A.P., eV	Precursor
31	13.3 ± 0.3	?
50	11.7 ± 0.2	CF_2
55	7.4 ± 0.1	Mn
62	11.4 ± 0.5	C_2F_2
69	9.8 ± 0.2	CF_3
74	13.9 ± 0.5	?
93	12.4 ± 0.3	?
100	9.8 ± 0.3	C_2F_4
112	12.0 ± 0.2	?
150	10.8 ± 0.2	C_4F_6?

The agreement of the observed A.P. of m/e 50 with the I.P. reported for CF_2, 11.7 eV[15] suggests that CF_2 is the precursor of this ion at least to the first upward inflection at 14.0 ± 0.4 eV. The process beginning at 14.0 was not determined but it is not CF_2^+ from C_2F_4 since this requires 15.1 eV.[16] Additional evidence that m/e 50 is a C_1 species came from measurement of the relative currents of m/e 50 and m/e 51 ions. With 70-V electrons m/e 51 was 1.2 ± 0.2% of m/e 50. The expected abundance of $^{13}CF_2$ relative to $^{12}CF_2$ is 1.1%.

There is little doubt that the low energy ion current of m/e 55 derives from the simple ionization of Mn(g). Using the observed A.P. of O_2^+, 13.06 ± 0.1 eV, to calibrate the electron energy scale, A.P. m/e 55 was found to be 7.4 ± 0.1 eV, in excellent agreement with

(10) Hoskins Manufacturing Co., Detroit, Mich.

(11) R. W. Kiser, "Introduction to Mass Spectrometry and Its Applications," Prentice-Hall, Inc., Englewood Cliffs, N. J., 1965, p 163.

(12) J. Sampson and R. Cairns, *J. Opt. Soc. Amer.*, **56**, 769 (1966).

(13) R. Winters, J. Collins, and W. Courchene, *J. Chem. Phys.*, **45**, 1931 (1966).

(14) American Petroleum Institute Research Project 44, "Mass Spectral Data," Chemical and Petroleum Research Laboratory, Carnegie Institute of Technology, Pittsburgh, Pa.

(15) I. Fisher, F. Lossing, and J. Homer, *J. Amer. Chem. Soc.*, **87**, 957 (1965).

(16) C. Lifshitz and F. Long, *J. Phys. Chem.*, **67**, 2463 (1963).

the spectroscopic I.P. of Mn, 7.43 eV.[17] Furthermore, an upward inflection found at 9.2 ± 0.1 eV agrees with the appearance of Mn^+ in the lowest of the closely spaced ^5D states, 1.77 to 1.86 eV above the ground state of Mn^+.[17] In its other features the observed ionization efficiency curve closely resembles that reported in an earlier study of the MnF_2–Mn reaction.[18] All parts of the *m/e* 55 curve were found to have a temperature dependence essentially equivalent to the heat of sublimation of α-manganese.[19] The ion current of *m/e* 56 was less than 0.1% of the *m/e* 55 current compared to about 3% expected if *m/e* 55 is C_3F^+ and *m/e* 56 is $^{13}C^{12}C_2F^+$. Whereas these findings strongly support the electron energy scale correction applied and suggest the presence of Mn(c) in the reaction mixture, reaction heats involving Mn species were not evaluated because no other Mn species could be unequivocally identified.

The I.P. of C_2F_2 has not been reported previously. The similar molecules, acetylene and propyne, have I.P. = 11.41 and 10.36 eV, respectively.[11] The observed A.P., 11.4 ± 0.5 eV, thus suggests that *m/e* 62 arises from simple ionization of C_2F_2, at least to the first upward break at 13.8 ± 0.3 eV. The *m/e* 63 ion current was found to be 2.0 ± 0.2% of the *m/e* 62 current compared to 2.0% expected for a C_2 species. No attempt was made to identify the higher energy process.

Although CF_3^+ is also a common fragment in fluorocarbon mass spectra the very low A.P. found here for *m/e* 69, 9.8 ± 0.2 eV, is convincing evidence of the presence of $CF_3(g)$. It should be noted that the electron impact I.P. of CF_3, 10.10 ± 0.05 eV,[4] differs from the photon impact I.P., 9.25 ± 0.04 eV, because of the structural difference between CF_3 and CF_3^+.[3] The presence of a 1% satellite at *m/e* 70 supports the identification of *m/e* 69 as CF_3^+. Since the A.P.'s of CF_3^+ from C_2F_4 and CF_4, the most abundant products in Farlow type reactions,[20,21] are 13.5 and 15.4 eV, respectively,[22] the thermodynamic studies were performed using 13.5-V electrons. There was evidence for the presence of both C_3 and Mn species at *m/e* 74, 93, and 112, but despite considerable efforts we were unable to identify the precursors of any of these ions in the threshold region. Certainly *m/e* 74 cannot be due to simple ionization of MnF, a process which requires only 8.7 eV, while the observed A.P. of *m/e* 93 is too high to reconcile with the I.P. of MnF_2, 11.5 ± 0.3 eV, but too low to be MnF_2^+ from MnF_3, a process which requires 13.7 ± 0.3 eV.[18,23] Each peak was found to have a small satellite (3%, 1%, and 1% of the main peak, respectively) at the next higher mass number. Sensitivity considerations alone indicate that ions derived from subliming MnF_2 or MnF_3 should have been undetectable in the threshold region at the temperature of the ionization efficiency studies. As a consequence, reactions involving MnF_x and C_3F_{x+1} were excluded from the thermodynamic studies. C_2F_4 is interpreted to be the precursor to $C_2F_4^+$ because the observed A.P. agrees with both previously reported values for I.P. C_2F_4, 10.12[16] and 9.3 ± 0.2 eV,[24] and is too low to be due to a fragmentation process. Again, this interpretation is substantiated by the presence of a 2% isotope peak at *m/e* 101. Lastly, the low A.P. of $C_3F_6^+$ at *m/e* 150 indicates the ion is not a fragment and by its similarity to the I.P.'s of olefins and acetylenic molecules supports the conclusion that C_3F_6 is the precursor.

After having determined the precursors to the various ions formed by low-energy electron impact ionization, the ion currents for CF_2^+, CF_3^+, $C_2F_2^+$, and $C_2F_4^+$ were measured at each of a series of temperature ranging from 874 to 944°K in run 1 and from 867 to 963°K in run 2 using 13.5-V electrons to assure that the only parent ion currents were measured. From these data equilibrium constants for the equilibria

$$2CF_2(g) \longrightarrow C_2F_4(g) \quad (2)$$

$$3C_2F_4(g) \longrightarrow 4CF_3(g) + 2C(s) \quad (3)$$

and

$$2C(s) + C_2F_4(g) \longrightarrow 2C_2F_2(g) \quad (4)$$

were found using the $P = kI^+T$,[25] which relates the partial pressure of a species in the effusion cell to the absolute temperature of the sample and the measured positive ion current through the proportionality constant *k*. In order to do this it was first necessary to evaluate *k* for each species in the equilibria. A calibration experiment was performed wherein cadmium was vaporized from the same effusion cell and the total Cd^+ current produced at a known temperature was measured from which k_{Cd} was calculated using the vapor

Table II: Values of $k = P/I^+T$ for C–F Species, Atm A^{-1} $°K^{-1}$

Ion	Run 1	Run 2
$C_2F_2^+$	4.81	5.47
$C_2F_4^+$	0.816	0.927
CF_2^+	5.27	5.99
CF_3^+	0.679	0.772

(17) C. E. Moore, "Atomic Energy Levels," National Bureau of Standards Circular 467 (I, 1949; II, 1952; III, 1958).

(18) R. Kent, T. Ehlert, and J. Margrave, *J. Amer. Chem. Soc.*, 86, 5090 (1964).

(19) T. Ehlert, Marquette University, submitted for publication.

(20) M. Farlow, U. S. Patent No. 2,709,192.

(21) M. Farlow and E. Muetterties, U. S. Patent No. 2,709,191.

(22) J. Warren and J. Craggs, "Mass Spectrometry," Institute of Petroleum, London, 1952.

(23) K. Zmbov and J. Margrave, *J. Inorg. Nucl. Chem.*, 29, 673 (1967).

(24) J. Margrave, *J. Chem. Phys.*, 31, 1432 (1959).

(25) W. Chupka and M. Inghram, *ibid.*, 21, 371 (1963).

Table III: Equilibrium Constant Equation Parameters and Reaction Enthalpies with Standard Deviations

Reaction	Run	A, kcal mol^{-1} °K^{-1}	B, cal °K^{-1} mol^{-1}	$\Delta H°_{298}$, kcal mol^{-1} Second law	$\Delta H°_{298}$, kcal mol^{-1} Third law
2	1	66.98 ± 0.7	−36.50 ± 0.8	−68.2 ± 0.4	−72.6
	2	67.72 ± 3	−36.99 ± 3	−69.0 ± 3	−72.9
3	1	−50.23 ± 4	16.87 ± 4	52.7 ± 4	66.9
	2	−54.70 ± 4	24.05 ± 4	57.1 ± 4	64.8
4	1	−75.43 ± 4	31.55 ± 6	74.9 ± 5	79.9
	2	−57.08 ± 4	11.49 ± 4	56.5 ± 4	79.6

pressure of cadmium.[26] It is easily shown that, in the presence of mass discrimination *in the mass analyzer*

$$\frac{k_j}{k_i} = \frac{G_i\sigma(E)_i A_i \tau_i}{G_j\sigma(E)_j A_j \tau_j} \qquad (5)$$

where multiplier gains G convert detector output (electrons) to the equivalent positive ion input, $\sigma(E)$ is the relative cross section for ionization by electrons of energy E, A is the isotopic abundance, and τ is the ion transmission efficiency, *i.e.*, the discrimination of the quadrupole analyzer. Gains were experimentally determined except for the low intensity $C_2F_2^+$ ion which was estimated with little loss in accuracy.[27] $\sigma(E)$ values were calculated by making the usual assumptions that $\sigma(E) \propto (\sigma_{max})(E - \text{A.P.})$, where Mann's σ_{max} values were used,[28] and that molecular cross sections are sums of atomic cross sections. The latter assumption holds well for hydrocarbons[29] and might therefore apply to fluorocarbons. The τ values were found as follows. Prior to this experiment the 70-eV fragmentation patterns of a large number of organic substances were obtained and compared to published[14] spectra obtained with relatively nondiscriminating analyzers. From these data a τ *vs.* mass curve was synthesized which indicated $\tau \propto (m/e)^{-1.1}$, the factor used here to get relative τ values. The resulting k values, summarized in Table II, are within 25% of a second set calculated using the measured Mn^+ current and assuming unit activity α-manganese to be present as a product of the reaction.[30] Cross section and other uncertainties remain, however, to cause as much as a factor of 2 uncertainty in these quantities. The derived equilibrium constants and reaction enthalpies found using JANAF thermodynamic functions are reported in the form

$$R \ln K_p = (A/T) + B$$

in Table III. A second-law heat of reaction at the median temperature, $\Delta H°_{913}$, was calculated from A of each equation and converted to $\Delta H°_{298}$ using available data.[2] Such second-law values are independent of pressure calibrations but suffer from rather large random deviations, presented in Table III as standard deviations from the least-squares line. In addition, cumulative systematic errors, chiefly a ±4° temperature uncertainty, contribute another ±1 kcal mol^{-1}. A single third-law $\Delta H°_{298}$ was found for each equation through the use of free-energy functions.[2] A factor of 2 uncertainty in each pressure leads to an uncertainty of about 1 kcal per such term in the equilibrium constant.

The data in Table III and supplementary information from the JANAF tables are used in the following discussion. The dissociation enthalpy, *i.e.*, the strength of the double bond, in C_2F_4 at 298°K is 68.6 ± 3 kcal mol^{-1} by the second law and 72.8 ± 2 kcal mol^{-1} by the third law. The third-law value should be more reliable in this case because the molecular parameters are rather well known. The value is in sharp contrast with $D(CH_2=CH_2)$, 160 kcal mol^{-1}. The $\Delta H_f°_{298}[CF_2(g)]$ is −41.1 ± 2 kcal mol^{-1}, in very close agreement with previous values. Average second- and third-law results for $\Delta H_f°_{298}[CF_3(g)]$ are −102.5 ± 3 and −99.8 ± 3 kcal mol^{-1}, respectively. Since the free-energy functions for CF_3 are based on estimated properties, the second-law value is preferred. The stepwise removal of fluorine atoms from $CF_4(g)$ therefore requires 139.4, 80.2, 123.7, and 126.0 kcal mol^{-1} at 298°K, all ± about 3 kcal mol^{-1}. The significant points in these data are the near equivalence of the p electrons and the large (60 kcal) expenditure of energy required, presumably as promotion energy, to add a fluorine to CF_2. Data for other fluorides[31,32] also show that direct involvement of the s electrons in bonding is energetically costly, *e.g.*, $D(AlF_2\text{–}F)$ = 156, $D(AlF\text{–}F)$ = 106, $D(Al\text{–}F)$ = 159, $D(BF_2\text{–}F)$ = 181, $D(BF\text{–}F)$ = 123, and $D(B\text{–}F)$ = 159 kcal mol^{-1}. For $C_2F_2(g)$ $\Delta H_f°_{298}$ = −44.6 ± 6 and −37.6 ± 4 kcal mol^{-1} are the respective average second- and third-law results. Although these agree within experimental error, it must be noted that the electronic states of C_2F_2

(26) An. N. Nesmeyanov, "Vapor Pressure of the Elements," Academic Press, New York, N. Y., 1963.

(27) W. Ploch and W. Walcher, *Rev. Sci. Instrum.*, **22**, 1028 (1951).

(28) J. Mann, *J. Chem. Phys.*, **46**, 1646 (1967).

(29) J. Otvos and D. Stevenson, *J. Amer. Chem. Soc.*, **78**, 547 (1956).

(30) Elemental Mn was not detectable in the reaction residue by X-ray crystallography so the absolute pressure calibration was based on the cadmium experiment even though several per cent Mn could have been present but escaped detection.

(31) T. Ehlert and J. Margrave, *J. Amer. Chem. Soc.*, **86**, 3901 (1964).

(32) D. Hildenbrand and E. Murad, *J. Chem. Phys.*, **43**, 1400 (1965).

are unknown and only the ν_3 vibrational frequency has been measured.[33] The second-law $\Delta H_f°_{298}[C_2F_2(g)]$, -45 ± 6 kcal mol^{-1}, plus $\Delta H_f°_{298}[CF(g)]$ found from $D°_{298}$ give 171 kcal for $D(CF{\equiv}CF)$ which is about 60 kcal *weaker* than the triple bond in acetylene. While the reason for this effect is not obvious, it is apparent that the fluorine is charge-withdrawing, not charge-donating as is sometimes postulated, in the CF_2 and CF molecules.

Acknowledgments. This work has been supported by the Research Corporation and the National Science Foundation.

(33) J. Heicklen and V. Knight, *J. Phys. Chem.*, 69, 2494 (1965).

Catalytic Polarographic Current of a Metal Complex.[1] VI. Correlation of the Nickel(II)–*o*-Phenylenediamine Prewave Height with the Surface Concentration of the Ligand[2]

by Lowell R. McCoy and Harry B. Mark, Jr.

Department of Chemistry, University of Michigan, Ann Arbor, Michigan 48104 *(Received September 30, 1968)*

The surface concentration, Γ, of *o*-phenylenediamine on mercury has been determined by differential capacitance measurements as a function of both the ligand volume concentration and the electrode potential in several different electrolyte systems. The Γ values obtained at relatively high bulk ligand concentrations (10^{-3}–10^{-1} *M*) have been extrapolated to the concentration range (2×10^{-5}–4×10^{-4} *M*) employed in previous polarographic measurements of the nickel(II)–*o*-phenylenediamine prewave. The rate of attainment of near-equilibrium surface coverage at these low bulk concentrations has been examined through a study of the dependence of the prewave height on the time of current measurement. The experimental results are in accord with those predicted by a simplified mathematical treatment based on a surface-controlled catalytic mechanism assuming fast adsorption when the ligand concentration is in excess of 10^{-4} *M* in 0.1 *M* electrolytes. The dependence of the prewave height on the ligand surface concentration is also correctly predicted by the theoretical treatment. A previously reported examination of the effect of the electrode double layer on the prewave height had indicated that the electroactive species possessed a charge of +1 rather than the charge of +2 expected for a complex formed by Ni(II) and an uncharged ligand. In this study it was found that correction for differing ψ^0 potentials in 0.1 and 0.5 *M* potassium chloride also indicated that an effective charge of +1 is involved in the rate-determining step.

It was shown in a previous paper[2d] that the structure of the electrode double layer has a pronounced effect on the height of the polarographic prewave obtained with Ni(II) in the presence of *o*-phenylenediamine. The results of that study were qualitatively consistent with a previous suggestion that the prewave reaction mechanism involves a rate-limiting chemical reaction between the hexaaquonickel ion and the adsorbed ligand which is cyclically regenerated by reduction of the electroactive adsorbed complex.[2a,b] The simplified mathematical treatment of the reaction mechanism presented on that basis, however, incorporated unsubstantiated assumptions concerning the adsorption behavior of the ligand and produced an unexpected result with respect to the charge of the electroactive species.

This paper presents the results of the determination of the surface concentration of the ligand on mercury as a function of volume concentration and electrode potential in several electrolytes. The theoretical dependence of the prewave height on the ligand surface concentration is further examined using these experimental values.

Experimental Section

The methods used in making the polarographic measurements generally followed routine procedures and have been described in a previous paper.[2d] Surface concentrations of *o*-phenylenediamine were calculated from differential capacitance measurements. The impedance bridge and polarizing circuits used in making

(1) This research was supported in part by grants from the National Science Foundation (NSF GP-4620 and GP-6425) and the U. S. Army Office of Research, Durham, N. C. (No. DA-31-124-ARO-D-284).

(2) For other papers of this series see: (a) H. B. Mark, Jr., and C. N. Reilley, *J. Electroanal. Chem.*, 4, 189 (1962); (b) H. B. Mark, Jr., *ibid.*, 7, 276 (1964); (c) H. B. Mark, Jr., L. R. McCoy, E. Kirowa-Eisner and H. C. MacDonald, Jr., *J. Phys. Chem.*, 72, 1083 (1968). (d) L. R. McCoy, H. B. Mark, Jr., and L. Gierst, *ibid.*, 72, 4637 (1968).

these measurements are similar in construction to those described by Delahay and Trachtenburg.[3] A 10-mV signal, peak to peak, was provided by an oscillator with a frequency range from 133 to 1036 Hz. As in the case of the polarographic measurements, the mercury drop was dislodged at any desired period using an electromagnetic hammer. Bridge balance settings of the variable resistor and capacitor were monitored using a Tektronix 564 storage oscilloscope equipped with a Type 3A1 dual-trace amplifier and a Type 3B3 delayed-time base triggered by the large bridge output transient at the fall of the drop.

Capillary tubes for the dropping mercury electrode were prepared by drawing 0.5-mm capillary tubing to a long, slender point. These were broken to a length which gave a flow of 0.4–0.6 mg/sec at a height of 100 cm. The capillaries were cleaned with alcoholic potassium hydroxide, rinsed repeatedly with triply distilled water, and dried. They were then made water repellant by drawing the vapors of General Electric SC 87, a silane derivative, through the bore for a brief time. A small portion of the tip was broken off prior to final calibration and use to ensure wetting by the electrolyte. The capillary tip was centered within a counterelectrode consisting of a length of platinum wire wound in the shape of a sphere approximately 2 cm in diameter.

The mercury drop was polarized through a saturated calomel electrode (sce) whose tip was immersed in a small reservoir. Electrical contact between the reservoir and the cell solution was made through a KCl bridge consisting of a length of $\frac{1}{8}$-in. diameter polyethylene tubing. A Vycor "thirsty glass" plug was inserted into the end of the tube entering the cell to retard diffusion of KCl into the cell during the capacitance measurements. The tubing and plug were replaced after each set of measurements to avoid contamination of the next solution.

Electrolyte solutions were prepared from triply distilled water and analytical grade reagents, further purified where necessary. These were thoroughly deaerated with purified nitrogen prior to addition of weighed quantities of *o*-phenylenediamine to avoid air oxidation of the ligand. The *o*-phenylenediamine was used in the form of the free base, purified from the technical grade by repeated recrystallization from dichloromethane. The capacitance measurements, like the polarographic measurements, were made in a thermostated 50-ml cell maintained at 25 ± 0.1°. The pH of the electrolyte solution was adjusted initially to 7.0 ± 0.05 by the addition of small quantities of the acid or base of the electrolyte as required. No pH adjustment was made after additions of *o*-phenylenediamine.

Surface Concentration Calculations

As some evidence existed that *o*-phenylenediamine was adsorbed rapidly at a mercury surface,[2d] differential capacitance measurements were made with a dropping mercury electrode using an ac bridge. These experiments were made in several electrolytes. Potassium chloride was chosen as one of these because accurate ψ^0 values had been calculated for this electrolyte over a wide concentration range.[4] Lithium perchlorate was chosen as another because of the considerable body of data already accumulated with regard to the nickel(II)–*o*-phenylenediamine prewave using solutions of this salt.[2d] Potassium acetate was selected as the third salt as the behavior of the prewave had also been studied earlier in this electrolyte[2b] and because the prewave in this electrolyte presented some unusual features not found with the other supporting electrolytes.[2d]

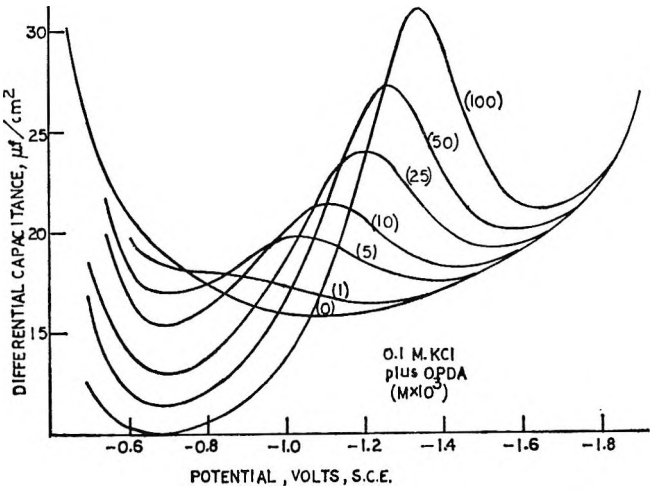


Figure 1. Differential capacitance curves for *o*-phenylenediamine in 0.1 *M* KCl.

As a rapid approach to equilibrium coverage is an essential requirement for the use of a dropping mercury electrode in adsorption studies, the effect of the time of bridge balance upon the capacitance per unit area for a given system was determined. No time dependence was found within a range of 0.1–5.0 sec at concentrations of ligand equal to or in excess of 10^{-2} *M* in 0.1 *M* supporting electrolytes. No experiments of this type were made at lower concentrations of *o*-phenylenediamine because of the small displacement of the capacitance curve for the ligand from that of electrolyte alone in such cases. In view of the above results, however, it was felt that a close approach to equilibrium coverage was being obtained at the lowest concentration included in the differential capacitance measurements, 10^{-3} *M*, at the 3-sec bridge balance time used thereafter.

No measurable frequency dependence was found for the capacitance values over the range of the oscillator (133–1036 Hz) either with the supporting electrolyte

(3) P. Delahay and I. Trachtenberg, *J. Am. Chem. Soc.*, **79**, 2355 (1957).

(4) D. C. Grahame, unpublished data supplied by R. Parsons.

alone or upon the inclusion of the ligand. While none should be expected in the former instance, the lack of a frequency dependence at various potentials in the presence of several different concentrations of ligand was surprising. Damaskin, *et al.*,[5] have, however, reported a similar lack of frequency response in the case of aniline. All further measurements were therefore made at a frequency of 1036 Hz where the precision of the bridge was highest.

The results of capacitance measurements for various concentrations of *o*-phenylenediamine in 0.1 *M* potassium chloride are shown in Figure 1. The curves obtained in the other electrolytes were similar in appearance.[6]

In the case of an uncharged substance, the surface concentration, Γ, can be calculated with the aid of the following expression derived from the Gibbs adsorption isotherm[7]

$$\left(\frac{\partial q}{\partial \mu}\right)_E = \left(\frac{\partial \Gamma}{\partial E}\right)_\mu = \frac{1}{RT}\left(\frac{\partial q}{\partial \log a}\right)_E \qquad (1)$$

where q is the charge on the electrode at the electrode potential, E, μ is the chemical potential, and a is the activity of the adsorbate in the solution.[8] Provided that the activity coefficient does not change with the bulk concentration of the adsorbed substance, the activity may be replaced by the concentration in eq 1. The electrode charge, q, at any electrode potential can be obtained by integration of the differential capacitance curves from the potential of the electrocapillary maximum where $q = 0$. Alternatively, integration can be carried out from some potential, E_0, where desorption is complete at all concentrations of interest. The charge on the electrode is, therefore, a constant at this potential and is independent of the concentration of (in this case) *o*-phenylenediamine. The second course was chosen here. Designating the charge value obtained in this manner as q^* to distinguish it from the true electrode charge

$$q^* = \int_{E_0}^{E} C\,dE = q + q^0 \qquad (2)$$

where q^0 is the true electrode charge at E_0 and C is the differential capacitance. As the constant, q^0, is eliminated in differentiation, eq 1 then becomes

$$\frac{1}{2.3RT}\left(\frac{\partial q^*}{\partial \log c}\right)_E = \left(\frac{\partial \Gamma}{\partial E}\right)_c \qquad (3)$$

where c is the concentration of *o*-phenylenediamine. Equation 3 may then be solved for Γ yielding

$$\Gamma = \frac{1}{2.3RT}\int_{E_0}^{E}\left(\frac{\partial q^*}{\partial \log c}\right)_E dE \qquad (4)$$

Values of q^* and the differential $(\partial q^*/\partial \log c)_E$ were calculated graphically. The potential E_0 was set at

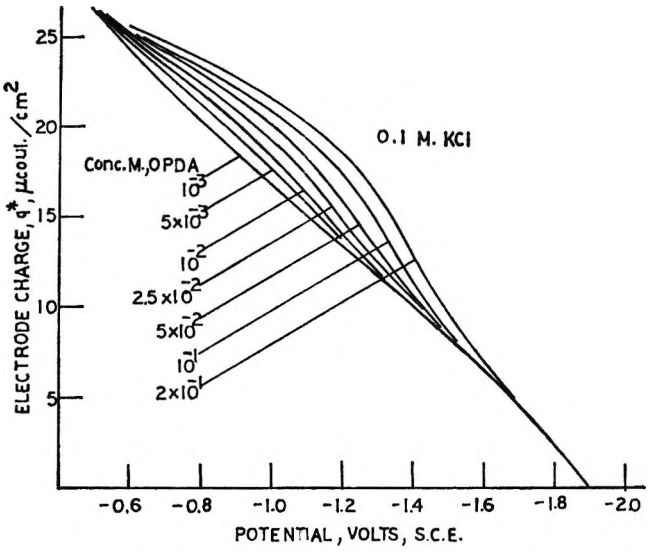


Figure 2. Integrated capacitance curves, q^* *vs.* electrode potential.

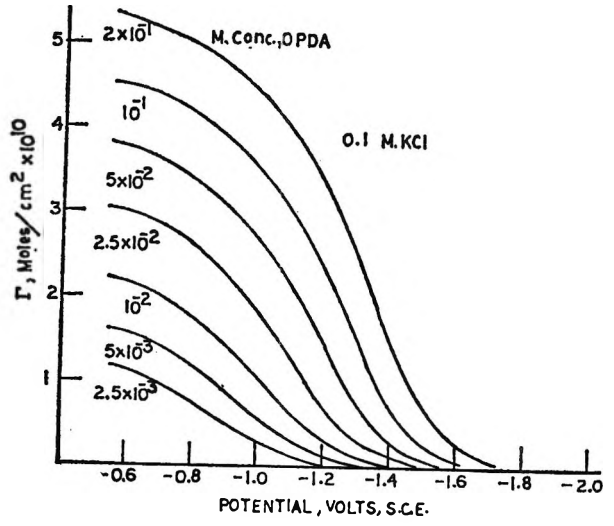


Figure 3. Surface concentrations of *o*-phenylenediamine as a function of electrode potential and ligand concentration.

−1.900 V *vs.* sce. While the integrations may be carried out in this manner with adequate precision, graphical differentiation inspires less confidence. The curves obtained from the differential values exhibited some scatter and these were smoothed prior to the second integration yielding Γ. Values of q^* and Γ obtained as a function of bulk concentration and electrode potential in 0.1 *M* potassium chloride appear in Figures 2 and 3.

The surface concentrations of *o*-phenylenediamine obtained by the methods described above correspond

(5) B. B. Damaskin, I. P. Mishutushkina, V. M. Gerovich, and R. I. Kaganovich, *Russ. J. Phys. Chem.*, 38, 976 (1964).

(6) L. R. McCoy, Ph.D. Thesis, University of Michigan, Ann Arbor, Mich., 1967.

(7) P. Delahay, "Double Layer and Electrode Kinetics," Interscience Publishers, Inc., New York, N. Y., 1965, p 28.

(8) While Γ is more properly termed the surface excess, the usual practice of equating this value to the actual surface concentration will be followed here.

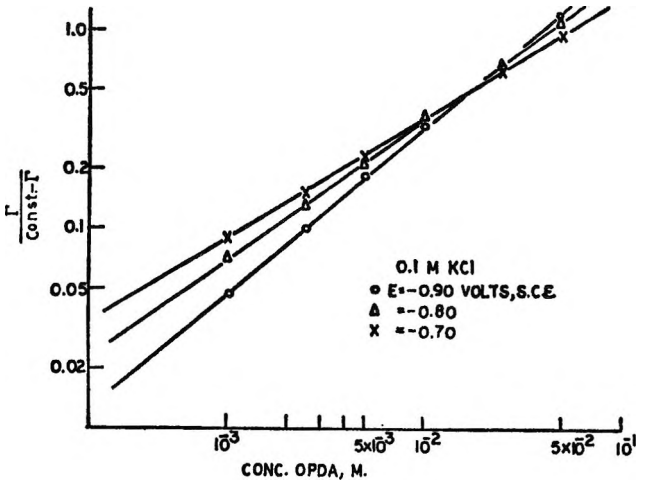


Figure 4. Extrapolation of experimental surface concentrations.

to bulk concentrations one to two orders of magnitude greater than those used in polarographic measurements of prewave heights. It is evident by inspection of Figure 1 that 10^{-3} M represents about the lowest concentration of this substance that can be investigated by differential capacitance measurements within the limits of precision or, more particularly, reproducibility of the bridge settings. Values of Γ for lesser concentrations were therefore calculated by extrapolation of the experimental data. This was done for each electrode potential by plotting $\log [\Gamma/(\text{constant} - \Gamma)]$ against the logarithm of the volume concentration as shown in Figure 4. The linearity of the experimental data achieved by this expedient was quite satisfactory.

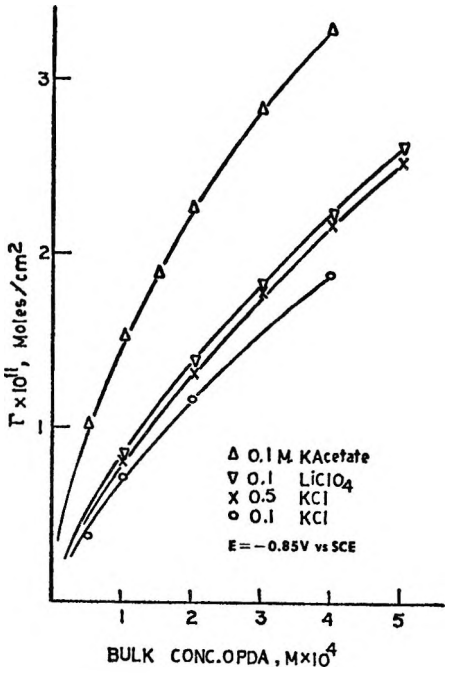


Figure 5. Extrapolated surface concentrations of *o*-phenylenediamine as a function of volume concentration in various electrolytes

While the functional form of this relationship is that of the Langmuir isotherm, the value of the "constant" required for linearization of the data varies with the electrode potential. While the significance of this variation will be discussed in a subsequent paper with regard to the probable orientation of the adsorbed substance, the extrapolation procedure may be regarded for present purposes as wholly empirical. Surface concentrations obtained by extrapolation appear in Figure 5. The propriety of using these extrapolated values in prewave calculations is examined below.

Theoretical Dependence of Prewave Height on the Ligand Surface Concentration

In a previous paper[2d] it was shown that the height of the prewave (assuming the cyclic mechanism described above) could be related to the experimental variables by

$$\lambda = \frac{k_f[\mathrm{L}]_{ads}\sqrt{t}}{\sqrt{D}} \exp\left(-\frac{zF}{RT}\psi^0\right) \qquad (5)$$

where λ is the rate parameter derived from the ratio of the prewave height to the diffusion-limiting wave height of the hexaaquonickel ion by using a form of Koutecky's[9] relationship for a heterogeneous electrochemical reaction, $[\mathrm{L}]_{ads}$ is the surface concentration of the ligand, k_f is the forward chemical rate constant for the complex-forming reaction, t is the time of current measurement, D is the diffusion coefficient of the hexaaquonickel ion, ψ^0 is the potential of the outer Helmholtz plane, z is the charge of the electroactive complex, and F, R, and T have their usual meaning. As this relationship is now derived for the chemical rate-limiting case, the prewave height must be measured at a potential where the electrochemical rate exceeds the chemical rate, *i.e.*, at an electrode potential corresponding to the prewave "plateau." In deriving eq 5, it was assumed that $[\mathrm{L}]_{ads}$ is a time-invarient quantity and, hence, that near-equilibrium coverage is attained early in the drop life (4 sec in the polarographic measurements). In this context, this term may be equated to Γ. It was assumed that the fractional surface coverage by the ligand was small enough to have little effect on the value of ψ^0 as determined for the supporting electrolyte alone. As the data in Figure 5 indicate, the second assumption may be accepted without great difficulty as the surface concentrations at the bulk concentrations employed in the polarographic measurements do not exceed a few per cent of the saturation surface coverage. The first assumption is more difficult to justify. While some assurance was obtained that at least near-equilibrium values of Γ were present at concentrations of 10^{-2} M, no direct evidence existed that a similarly fast approach to equilibrium coverage is attained at polarographic concentrations ranging from

(9) J. Koutecky, *Collection Czech. Chem. Commun.*, 18, 597 (1953).

10^{-5} to 10^{-3} M. As noted, differential capacitance measurements do not have adequate sensitivity to permit direct experimental determination of surface concentrations at these lower concentrations of the ligand.

The degree of approach to equilibrium surface coverage at the drop time used in the polarographic measurements can be estimated by considering the dependence of λ on the time current measurement. If λ is determined at some suitable electrode potential as a function of time in any given electrolyte and Γ is equated with $[L]_{ads}$, eq 5 is reduced to

$$\frac{\lambda}{\Gamma} = (\text{constant})\sqrt{t} \qquad (6)$$

If the equilibrium surface coverage of the ligand is approached slowly, eq 6 is clearly invalid as $[L]_{ads}$ was treated as a time-invariant quantity. If, however, adsorption proceeds rapidly, the experimental data will conform closely to eq 6. Thus, a plot of λ/Γ *vs.* $\sqrt{t}$ permits some estimate of the rate at which equilibrium coverage is approached at various ligand concentrations. The work of Delahay and Fike[10] suggests that this rate will become slower as the ligand concentration is decreased.

In making these calculations for the nickel(II)–*o*-phenylenediamine prewave, the extrapolated values of Γ were used. As these were derived from equilibrium surface concentrations, these extrapolated values should also represent the equilibrium values of Γ pertaining to the lower polarographic range of ligand concentrations. The time dependence of λ/Γ found for a range of volume concentrations of this ligand is shown in Figure 6. While the scatter of the data is somewhat greater than desirable, a clear deviation both from linearity and the rest of the data occurs only at 2×10^{-5} M. At higher concentrations, the data are grouped quite closely and exhibit reasonable compliance with the theoretical time dependence. At the concentrations of *o*-phenylenediamine employed in most of the polarographic measurements, 1.6×10^{-4} M, there is, therefore, a good probability that equilibrium coverage is approached rapidly enough to justify the use of eq 5 and 6 despite their approximate nature.

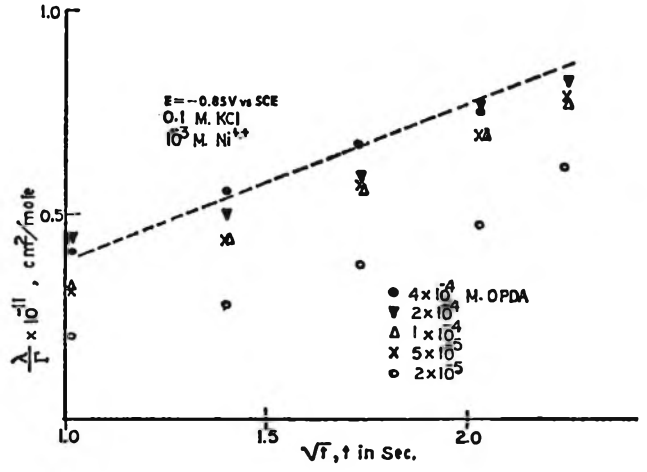


Figure 6. Dependence of the rate parameter λ on time of current measurement.

Equation 5 expresses λ as a function of the surface concentration of the ligand. With these surface concentrations now available, a direct comparison of experimental results with theoretical predictions is now possible. If the ions of the supporting electrolyte are not specifically adsorbed, the exponential term of eq 5 may be regarded as a constant when comparing data taken in 1:1 electrolytes at the same concentration. It has been shown by Grahame and Soderberg[11] and Wroblowa, *et al.*,[12] that adsorption of the chloride, acetate, and perchlorate anions in the potential range of the prewave is too small to affect significantly the values of the ψ^0 potential for an electrolyte concentration of 0.1 M considered here. In dilute electrolytes, the diffusion coefficient, D, may also be considered as a constant. At a fixed time of current measurement, t, a linear relationship is, therefore, expected between λ and the ligand surface concentration.[13]

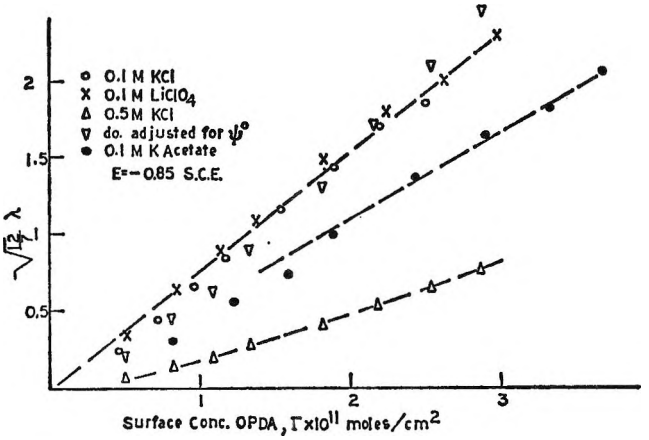


Figure 7. Dependence of the rate parameter λ on ligand surface concentration.

Values of λ (shown here as the equivalent of Koutecky's χ^{2d}) obtained from prewave height measurements at an electrode potential of −0.85 V *vs.* the sce are shown as a function of the extrapolated values of Γ in Figure 7. Several interesting points are raised by these results. The data obtained in 0.1 M solutions of potassium chloride and lithium perchlorate are quite

(10) P. Delahay and C. T. Fike, *J. Am. Chem. Soc.*, 80, 2628 (1958).

(11) D. C. Grahame and B. A. Soderberg, Technical Report No. 14 to the Office of Naval Research, Amherst College, Amherst, Mass., Feb 18, 1954.

(12) H. Wroblowa, Z. Kovac, and J. O'M Bockris, *Trans. Faraday Soc.*, 61, 1523 (1965).

(13) This statement assumes that a 1:1 complex is formed between the hexaaquonickel ion and the ligand. This was found to be the case as previously reported.[2d]

linear (except at the lower surface concentrations where slow adsorption is to be expected) and are virtually coincident. The data obtained with 0.1 M potassium acetate are also quite linear but differ significantly from those of the other electrolytes at the same concentration. This discrepancy largely reflects the different surface–volume concentration relationship found for the ligand in this solution (see Figure 5). As it does not appear possible to explain this difference on the basis of either activity or electrolyte anion adsorption effects at this time, some other factor is believed to be involved (see also ref 2d for other observations on this point). This unusual behavior of the acetate supporting electrolyte has also been observed in the study of the effect of the *p*-phenylenediamine–nickel(II) system.[14] Further investigation of this effect is in progress.

Referring again to Figure 7, the differences obtained in 0.1 and 0.5 M solutions measured at an applied potential of −0.85 V may be properly attributed to the differing ψ^0 potentials of these solutions. The 0.5 M data may be "normalized" to permit a direct comparison with that obtained in the 0.1 M solution by the relationship derived from eq 5

$$[\lambda_{0.1}]_{t,D,T} = [\lambda_{0.5}] \exp\left[-\frac{zF}{RT}(\psi_{0.1}^0 - \psi_{0.5}^0)\right] \quad (7)$$

Using ψ^0 values calculated by Grahame,[4] the 0.5 M data adjusted on this basis show fair agreement with those observed in 0.1 M potassium chloride. To obtain this agreement between the data for these two solutions, however, it was necessary to assign a value of +1 to z. As noted in a previous paper,[2d] other ψ^0 potential correlations also yielded this charge value for the electroactive species rather than the value of +2 expected for a complex formed between Ni(II) and an uncharged ligand.

A slight deviation from linearity is also evident in the data for 0.5 M potassium chloride. It is felt that there was an appreciable reduction in the value of the diffusion coefficient for the ligand in the more concentrated electrolyte which leads to a slower approach to equilibrium coverage. This point is also under investigation.

The experimental results presented above are in general accord with the predictions of a simplified mathematical treatment of a prewave mechanism involving the formation of an electroactive complex between Ni(II) and adsorbed *o*-phenylenediamine. The assumption of rapid attainment of near-equilibrium surface coverage is tenable at the ligand concentrations employed for polarographic studies of the prewave.[2d] As stated above, the charge of the electroactive species is not, however, in accord with the expected charge for such a complex. Information of interest to this point may be found in an examination of the adsorption characteristics of the ligand. This aspect of the problem will be discussed in a subsequent paper.

(14) E. Kirowa-Eisner, H. C. MacDonald, Jr., and H. B. Mark, Jr., unpublished results.

Photolysis of Ketene. Mechanism of Hydrogen Production and the Reaction of Methylene with Methane[1]

by A. H. Laufer

National Bureau of Standards, Washington, D. C. 20234 *(Received October 4, 1968)*

The photolysis of ketene has been investigated at photon energies from 3.96 (3130 Å) to 8.43 eV (1470 Å). Hydrogen is produced at all wavelengths. Based upon the photolysis of CD_2CO–CH_2CO mixtures the reaction $CH_2CO \rightarrow H_2 + C_2O$ is suggested as a primary process. The sequence of reactions 1 and 2 has also been examined.

$$CH_2 + CH_4 \rightarrow C_2H_6^* \quad (1)$$

$$C_2H_6^* \rightarrow H_2 + C_2H_4 \quad (2)$$

It is concluded that of the decomposition paths available to $C_2H_6^*$ fewer than 6% proceed *via* reaction 2 over a wide energy range. The significance of this finding with respect to the photodecomposition of methane is discussed.

Introduction

The chemical properties of methylene, generated by the photolysis of ketene, diazomethane, or diazirine, have been studied by many investigators, and a number of reviews have been published recently.[2] The formation of methylene has also been proposed as a result of mass spectrometric analysis of the isotopic ethanes produced in the vacuum ultraviolet photolysis of a scavenged mixture of CH_4–CD_4.[3] The maximum excess energy which is available to the methylene fragment from the photolysis of methane at 1236 Å is about 5.5 eV assuming a primary split into CH_2 and H_2. Very little is known regarding the partition of energy between photolytic fragments so that the final energy available to the CH_2 prior to reaction is not clear. It has been suggested, however, that the insertion reaction of "energetic" CH_2 with CH_4 results in an excited ethane which may decompose into C_2H_4 and H_2.[3,4]

$$CH_2 + CH_4 \rightarrow C_2H_6^* \quad (1)$$

$$C_2H_6^* \rightarrow H_2 + C_2H_4 \quad (2)$$

Photolysis of a CH_4–CD_4 mixture results in an enhanced yield of H_2 as compared to that of D_2.[5] The reaction sequence 1 and 2 plus a consideration of the deuterium isotope effect on reaction 2 would suggest such an enrichment. The present work is designed to investigate this possibility.

Vanpee and Grard[6] photolyzed ketene with light of 2500–3800 Å in the presence of methane but did not report the formation of H_2. The maximum energy available to the separating fragments in these experiments was 34.3 kcal/mol based on $\Delta H_f°(CH_2) = 91.9$ kcal/mol,[7] $\Delta H_f°(CH_2CO) = -14.6$ kcal/mol, and $\Delta H_f°(CO) = -26.4$ kcal/mol.[8] Chanmugam and Burton[9] performed similar experiments with CH_2 from ketene in the presence of CD_4, the maximum energy available to the fragments being 56 kcal/mol. Here again neither H_2 nor D_2 was reported.

Bell and Kistiakowsky[10] investigated the photolysis of diazomethane with methane at wavelengths greater than 3100 Å. In all probability the most prominent photochemical lines absorbed by CH_2N_2 were those appearing at 3660, 4047, and 4358 Å.[11] If we now accept a value of $\Delta H_f°(CH_2N_2)$ to be 67 kcal/mol.[2b] then the maximum energy to be partitioned among the fragments is 55 kcal/mol. Frey[12] has shown that methylene from diazomethane photolyzed at 3660 Å may possess as much as 15 kcal/mol more energy than the CH_2 from ketene photolyzed at 3130 Å when it

(1) This work was supported in part by the U. S. Atomic Energy Commission.

(2) (a) H. M. Frey, "The Reactions of Methylene and Some Simple Carbenes," in "Progress in Reaction Kinetics," Vol. 2, G. Porter, Ed., Pergamon Press, New York, N. Y., 1964, pp 131–164; (b) J. A. Bell, "The Properties and Reactivity of Methylene," in "Progress in Physical Organic Chemistry," Vol. 2, S. G. Cohen, A. Streitwieser, Jr., and R. W. Taft, Ed., Interscience Publishers, New York, N. Y., 1964, pp 1–61; (c) W. B. DeMore and S. W. Benson, "Preparation, Properties, and Reactivity of Methylene" in "Advances in Photochemistry," Vol. 2, W. A. Noyes, Jr., G. S. Hammond, and J. N. Pitts, Jr., Ed., Interscience Publishers, Now York, N. Y., 1964, pp 219–261.

(3) P. Ausloos, R. Gorden, Jr., and S. Lias, *J. Chem. Phys.*, **40**, 1854 (1964).

(4) J. E. Manton and A. W. Tickner, *Can. J. Chem.*, **38**, 858 (1960).

(5) A. H. Laufer and J. R. McNesby, *J. Chem. Phys.*, **49**, 2272 (1968).

(6) M. Vanpee and F. Grard, *Bull. Soc. Chim. Belg.*, **60**, 208 (1951).

(7) W. A. Chupka and C. Lifshitz, *J. Chem. Phys.*, **48**, 1109 (1968).

(8) "Selected Values of Chemical Theromodynamic Properties," NBS Technical Note 270-3, U. S. Government Printing Office, Washington, D. C., 1968, Tables 23–27.

(9) J. Chanmugam and M. Burton, *J. Amer. Chem. Soc.*, **78**, 509 (1956).

(10) J. A. Bell and G. B. Kistiakowsky, *ibid.*, **84**, 3417 (1962).

(11) R. K. Brinton and D. H. Volman, *J. Chem. Phys.*, **19**, 1394 (1951).

(12) H. M. Frey, *Trans. Faraday Soc.*, **56**, 1201 (1960).

reacts. Even under such conditions H_2 was not reported.

Ketene has three distinctly different electronic absorption regions. Absorption is fairly weak in the region from 3900 to 2400 Å with a broad maximum near 3150 Å ($\epsilon = 1$ atm^{-1} cm^{-1} where ϵ is defined by the expression $I = I_0 \exp[-\epsilon pl]$). At higher energies (2200–1900 Å), the spectrum consists of four diffuse bands whose maximum extinction coefficient is about 360 atm^{-1} cm^{-1} at 2130 Å.[13,14] A number of discrete bands begins at 1830 Å and continues into the vacuum ultraviolet to the onset of ionization, 1300 Å.[15]

Except for a few studies all the photochemical work with ketene has used radiation in the 3100-Å region. Knox, *et al.*,[14] have found H_2 and C_2H_2 to be the major products in the high-intensity flash photolysis of ketene (2000–4000 Å) although very high temperatures due to adiabatic heating may have been responsible. Hydrogen was reported as a product in a single experiment using a zinc resonance lamp at 2139 Å[16] suggesting the possibility of another primary process at higher energies. Walter[17] has recently completed a study of the photolysis of ketene at 2139 Å attributing the formation of hydrogen to the overall sequence

$$CH_2 + CH_2CO \rightarrow H_2 + C_2H_2 + CO \qquad (3)$$

without specifying the nature of the intermediate.

The major difference in reactivity between the singlet CH_2 which has been produced from ketene and the methylene from methane, also in a singlet state,[18] is the available energy. At 1470 Å, for example, the maximum energy available to the methylene from ketene is 4.97 eV, a value comparable to that of the same fragment from the 1236-Å photolysis of CH_4. Photolysis of ketene–methane mixtures at high energies presents the problem of distinguishing hydrogen formed from ketene itself from that formed from reactions 1 and 2. The approach used in the present work was to photolyze CD_2CO in a large excess of CH_4. In this case the hydrogens arising from the two mechanisms are isotopically quite different so that the importance of the insertion followed by decomposition [(1) and (2)] could be ascertained.

Experimental Section[19]

The mercury-free vacuum system was of the conventional type with metal valves equipped with polyfluorocarbon O-rings or borosilicate glass with Viton-A seats. The gas mixtures did not come into contact with grease at any time. Pressures were measured with a diaphragm gauge accurate to ±0.5 mm. Experiments in the vacuum ultraviolet region were done with a xenon lamp ring-sealed into a reaction vessel. The 1295-Å line was eliminated by a sapphire window on the lamp. A gas-circulating pump was included in the system.[20]

The reaction vessel for all other wavelengths was a cylindrical quartz cell 10 cm long with a 2.8-cm Suprasil window. The light sources were (a) a low-pressure Hg resonance lamp which emitted 2537 and 1849 Å in the ratio of 7:3 and (b) a medium-pressure mercury arc from which 3130 Å was isolated by an interference filter whose transmission at 2537 Å was eliminated by means of a Corning 7740 filter which absorbs all light below 2800 Å. The 2537-Å radiation was isolated by an interference filter. The 1849 Å was isolated by two filters in series, each with a transmission ratio of 30:1 for 1849:2537. In all cases the volume between reaction vessel and lamp was continuously flushed with He. Stray radiation was eliminated as determined by control "dark" experiments in which no products could be detected.

The purification of the CH_4 has been described previously.[5] CH_2CO was prepared by the pyrolysis of acetic anhydride.[21] After the walls were thoroughly deuterated by D_2O, CD_2CO was prepared by pyrolysis of acetic anhydride-d_6 (Merck Sharp and Dohme Ltd. of Canada). Mass spectral analysis indicated that the maximum CHDCO impurity was 3.51%. Both ketenes were stored separately at liquid nitrogen temperatures.

Gas pressures were measured, and the material was condensed in a trap attached to the reaction vessel with either liquid N_2 or H_2. The ketene pressure varied from 7 to 10 mm. As the rate of reaction of methylene with methane is only 0.183 times that of the reaction with ketene,[6] mixtures were made in the ratio of at least 7 (CH_4/CD_2CO) so that a minimum of 50% of the CH_2 produced reacted with CH_4. Product hydrogen was determined by cooling the reaction mixture with liquid hydrogen and analyzing the residual gas (H_2, HD, and D_2) by mass spectrometry. It was determined experimentally that mixtures of H_2 and D_2 were not fractionated by this procedure. In the photolysis of pure CD_2CO the material was condensed at −196°, and the CO and D_2 were analyzed as previously described.[5] With the ratio of D_2/CO from CD_2CO known at all wavelengths, the measurement of D_2 in the CD_2CO–CH_4 mixture served as an internal actinometer.

Total hydrocarbon product analysis was performed

(13) K. H. Sauer, Ph.D. Thesis, Harvard University, 1957.

(14) K. Knox, R. G. W. Norrish, and G. Porter, *J. Chem. Soc.*, 1477 (1952).

(15) W. C. Price, J. P. Teegan, and A. D. Walsh, *ibid.*, 920 (1951).

(16) H. Gesser and E. W. R. Steacie, *Can. J. Chem.*, 34, 113 (1956).

(17) T. A. Walter, Ph.D. Thesis, Harvard University, 1967.

(18) G. Herzberg, "Electronic Spectra of Polyatomic Molecules," D. Van Nostrand Co., Inc., New York, N. Y., 1966, p 528.

(19) Certain commercial instruments and materials are identified in this paper in order adequately to specify the experimental procedure. In no case does such identification imply recommendation or endorsement by the National Bureau of Standards, nor does it imply that the instruments or materials identified are necessarily the best available for the purpose.

(20) J. S. Watson, *Can. J. Technol.*, 34, 373 (1956).

(21) G. J. Fischer, A. F. McLean, and A. W. Schnizer, *J. Org. Chem.*, 18, 1005 (1953).

with a gas chromatograph equipped with a flame-ionization detector. The column used was 23 ft long packed with 30% squalane on Chromosorb P.

Results

Deuterium was produced from the photolysis of CD_2CO at all wavelengths studied: 1470, 1849, 2537, and 3130 Å. The D_2/CO ratio decreases with a reduction in the incident photon energy as shown in Figure 1. Only at 1849 and 1470 Å, where the hydrogen yield is relatively large, could a reliable isotopic composition of the hydrogens produced in the photolysis of a 1:1 mixture of CH_2CO/CD_2CO be obtained. The values are presented in Table I.

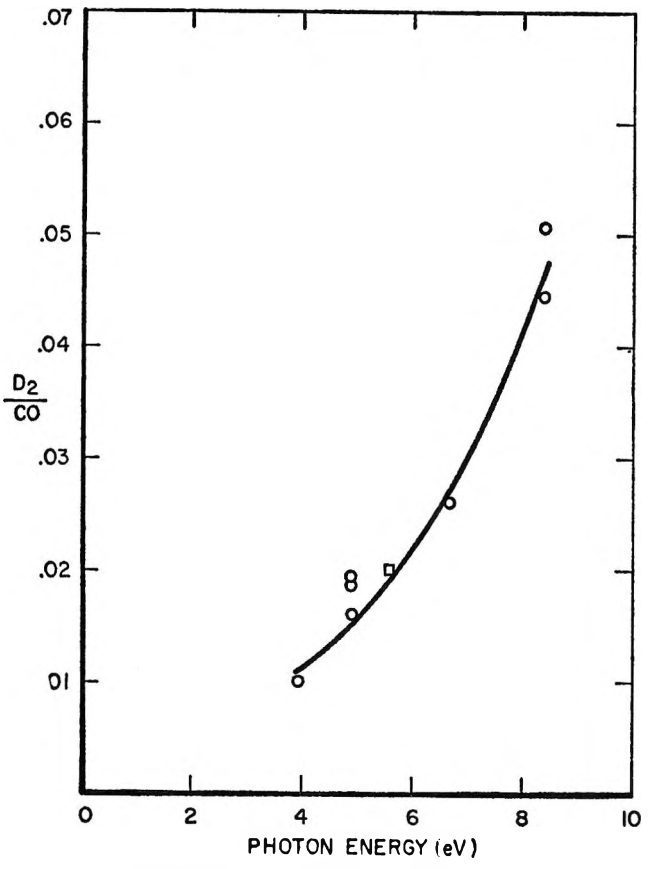


Figure 1. D_2/CO ratio from photolysis of CD_2CO as a function of energy: O, this work; □, ref 17.

The H_2/D_2 ratio at 1470 Å is not in agreement with values of the extinction coefficients at this wavelength which were measured using a 0.5-m Seya-Namioka vacuum monochromator and a xenon resonance lamp as the light source. Although the spectrum of ketene is sharply structured in the 1470-Å region,[15] the absorption is most probably continuous for a few angstroms on either side of 1470 Å. Because the width of the resonance line is less than 1 Å, it would fall entirely within the continuum, and the extinction coefficients are probably correct. The results are

Table I: Per Cent Isotopic Hydrogen Produced in Photolysis of 1:1 Mixtures of CH_2CO and CD_2CO

λ, Å	H_2	HD	D_2
1849	49.4	7.4	43.3
1470	54.3	12.5	33.2

$\epsilon_{CH_2CO} = 360 \pm 20$ atm^{-1} cm^{-1} and $\epsilon_{CD_2CO} = 310 \pm 15$ atm^{-1} cm^{-1} in the pressure range of 0.3–2.5 mm.

Based on a wavelength independent quantum yield of CO equal to 2.0, the conversion was always less than 0.05%. Ethylene accounts for about 80% of all the hydrocarbon products. In the region of interest, the maximum extinction coefficient of C_2D_4 is at 1470 Å where the value is about 400 atm^{-1} cm^{-1}.[22] At the concentrations of ethylene present in the systems at such low conversions all the D_2 measured arises from decomposition of CD_2CO.

The photolysis of CD_2CO, at all wavelengths, yielded nonreproducible quantities of HD in excess of that anticipated from the photolysis of the small CHDCO impurity. It was determined that the isotopic integrity of CD_2CO was not severely affected by contact with the walls of the reaction vessel for a time which closely approximated a photolysis run. Hence exchange of CD_2CO to CHDCO could not account for the HD. Deuterating the walls with D_2O followed by photolysis of CD_2CO reduced the HD/D_2 ratio but did not completely eliminate HD formation. Similar results were obtained in the presence of large quantities of CO_2. Finally, to remove any H atoms, a mixture of 3.85% C_2D_4 in CD_2CO was photolyzed at 2537 Å. The HD yield was thereby reduced to its lowest value relative to D_2. Photolysis, to about 1% conversion, of CH_2CO with the low-pressure Hg resonance lamp (both 2537 and 1849 Å) resulted in the following hydrocarbon products: C_2H_4, 80.5%; C_2H_6, 7.2%; C_2H_2, 5.9%; C_3H_8, 2.1%; butene-1, 1.4%; C_3H_6, 1.3%; CH_4, 1.2%; and C_3H_4 (allene), 0.4%.

At all wavelengths except 1470 Å, in those experiments involving mixtures of CD_2CO and CH_4, the insertion of CD_2 into CH_4 and subsequent decomposition of the excited ethane ($C_2H_4D_2$*) into H_2 was not observed. Since HD is formed from the "direct" photolysis of CD_2CO, the decomposition of $C_2H_4D_2$* into HD could not be ascertained. Upper limits of the H_2 produced from decomposition of $C_2H_4D_2$* are shown in Table II.

Discussion

A. Decomposition of Ketene. The presence of D_2 as a product of the direct photolysis of ketene-d_2 suggests the occurrence of several possible mechanisms. Because the hydrogen yield in the photolysis of CD_2CO–

(22) M. C. Sauer, Jr., and L. M. Dorfman, *J. Chem. Phys.*, **35**, 497 (1961).

Table II: H_2 Production from the Reaction of CD_2 and CH_4

λ, Å	Ketene/methane	D_2[a]	H_2[a]
3130	0.137	26	<3
2537	0.110	4	<1.5
1849	0.115	4	<1.5
1470	0.101	135	3

[a] Arbitrary units.

CH_2CO mixtures at 1849 and 1470 Å (Table I) is mainly H_2 and D_2, molecular detachment of hydrogen is operative.

A primary process which can produce unmixed hydrogens is

$$CH_2CO \rightarrow CH_2 + CO \quad \Delta H = 80.1 \text{ kcal/mol (3.47 eV)} \tag{4a}$$

$$CH_2 \rightarrow H_2 + C \quad \Delta H = 79.4 \text{ kcal/mol (3.44 eV)} \tag{4b}$$

This sequence requires in excess of 6.9 eV. As shown in Figure 1, H_2 is produced at lower energies than the threshold for the process which indicates that reaction 4a followed by 4b cannot be the sole hydrogen-producing reaction.

Another source of unmixed hydrogen is

$$CH_2CO \rightarrow C_2O + H_2 \tag{5}$$

A value of $\Delta H_f^\circ(C_2O) = 68.5 \pm 15$ kcal/mol [23] leads to a ΔH of reaction 5 of 83.1 ± 15 kcal/mol (3.60 eV). However, there is considerable uncertainty in $\Delta H_f^\circ(C_2O)$, and if the value is 93 ± 5 kcal/mol, as suggested by Bayes,[24] then reaction 5 could not proceed at wavelengths greater than 2650 Å. If, as suggested by Figure 1, a single reaction can account for the production of H_2, then (5) represents between 2 and 8% of the total primary processes in the photolysis of ketene.

The fate of the C_2O radical formed in (5) is not clear. Decomposition into carbon and CO is only possible at incident energies greater than 6.9 eV (~1800 Å) so that in all probability the C_2O retains its integrity throughout the photolysis. Bayes and coworkers[24] have examined the chemistry of the C_2O radical and its reaction with olefins. Without specifying the multiplicity of C_2O, the insertion reaction

$$C_2O + C_nH_{2n} = C_{n+1}H_{2n} + CO \tag{6}$$

predominates with simple olefins at low pressures. Reaction 6 (where $C_nH_{2n} = C_2H_4$) could then account for the small amount of allene observed in the ketene photolysis (see Results). The other possible mode of formation of allene is the reaction of CH_2 with C_2H_2. This reaction, however, produces approximately an equal amount of methylacetylene[25] which is absent in our experiments as well as in those of others.[17]

Another model leading to hydrogen in CH_2CO photolysis is represented by reaction 3 which is an exothermic process. The unstable intermediate in the reaction sequence is either C_2H_4* or C_2H_4CO*. Assuming CH_2 adds across the carbon–carbon double bond in ketene-d_2, the resulting ethylene would be CD_2CH_2. To obtain either H_2 or D_2 to the almost total exclusion of HD from such an intermediate requires an exclusive detachment from one of the carbon atoms.

Many workers have examined the isomerization and decomposition of deuterated ethylenes over a wide range of conditions and energies. Even at energies where decomposition into C_2H_2 and H_2 is small, H atom scrambling is observed.[26] Decomposition of CH_2CD_2 at all wavelengths from 2537 Å (mercury photosensitization)[27] through the direct photolysis at 1849, 1470, and 1236 Å[28] indicates that large quantities of HD are present in the hydrogen fractions. If CH_2 inserts into the C–H bond of ketene, the resulting ethylene will be less symmetrical than CH_2CD_2 and similar arguments prevail. These results appear to eliminate reaction 3 as the major source of hydrogen in the ketene system.

The presence of HD in the hydrogen fraction from CD_2CO photolysis is an enigma. The reduction in HD by partial deuteration of the wall clearly indicates the importance of the wall. It is difficult to conceive of a D atom formed in the center of the reaction vessel freely diffusing to the wall without reaction since it is estimated that H atoms react with ketene

$$H + CH_2CO = CH_3 + CO$$

only 6.5 times slower than with ethylene[29] or 1 effective collision in 5000.

B. H_2 Production from $CD_2 + CH_4$. The yield of D_2 from CD_2CO serves as a convenient "handle" to assay the importance of reactions 1 and 2. H_2, the only monitored product from the decomposition of $C_2H_4D_2$*, represents but a fraction of the total hydrogen expected depending on the model chosen. If each H or D atom in $C_2H_4D_2$* is equally accessible, then the expected ratio, on a purely statistical basis, of $H_2/HD/D_2$ is 6:8:1. This is a minimum relative value of H_2 since an isotope effect in favor of H_2 would, no doubt, be operative. To estimate the isotope effect, two models are chosen.

1. *Molecular Hydrogen from the Photodecomposition of CH_2D_2 at* 1236 Å. Here, presumably, all the atoms

(23) JANAF Thermochemical Tables (2nd Addendum), The Dow Chemical Co., Midland, Mich., Aug 1967.

(24) C. Willis and K. D. Bayes, *J. Phys. Chem.*, **71**, 3367 (1967).

(25) J. Terao, N. Sakai, and S. Shida, *J. Amer. Chem. Soc.*, **85**, 3919 (1963).

(26) S. Tsunashima, S. Hirokami, and S. Sato, *Can. J. Chem.*, **46**, 995 (1968).

(27) A. B. Callear and R. J. Cvetanović, *J. Chem. Phys.*, **24**, 873 (1956).

(28) H. Okabe and J. R. McNesby, *ibid.*, **36**, 601 (1962).

(29) H. E. Avery and R. J. Cvetanović, *ibid.*, **48**, 380 (1968).

are equally accessible, and the statistical ratio expected of $H_2/HD/D_2$ is 1:4:1. Experimentally we find 3:6:1[30] which results in a specific probability of formation of 3:1.5:1. If we assume a similar isotope effect in conjunction with the statistical expectation from $C_2H_4D_2^*$, the hydrogen from the latter would be in the per cent ratio 58:39:3.

2. *Molecular Hydrogen from Photolysis of CH_3CD_3.* Another model may be based on the decomposition of CH_3CD_3 at 1470 Å (8.4 eV).[31] To obtain the correct isotopic distribution of $H_2/HD/D_2$ equal to 58:17:25, an isotope effect of 2:1.5:1 and a geometrical factor of 0.12 is required. The geometrical factor represents the hydrogen arising from both carbon atoms as compared to that from one of the atoms. Applying the results to $C_2H_4D_2^*$ suggests that the isotopic hydrogen would be in the ratio 56:35:9.

To calculate the maximum fraction of $C_2H_4D_2^*$ which decomposes into hydrogen and ethylene, we assume (1) the $H_2/HD/D_2$ ratio expected from $C_2H_4D_2^*$ is 57:37:6 (the average of the two model calculations above) and (2) the relative rate of reaction of CD_2 with CD_2CO and CH_4 is energy independent. The following reactions are required.

$$CD_2CO \rightarrow CD_2 + CO \quad (7)$$

$$CD_2CO \rightarrow D_2 + C_2O \quad (8)$$

$$CD_2 + CD_2CO \rightarrow C_2D_4 + CO \quad (9)$$

$$CD_2 + CH_4 \rightarrow C_2H_4D_2^* \quad (10)$$

$$C_2H_4D_2^* \rightarrow CD_2H + CH_3 \quad (11)$$

$$C_2H_4D_2^* \rightarrow \text{hydrogen} + \text{ethylene} \quad (12)$$

The fraction of excited ethane decomposing into hydrogen and ethylene is defined as

$$F = k_{12}(E^*)/[k_{11}(E^*) + k_{12}(E^*)] = 1/(1 + k_{11}/k_{12}) \quad (I)$$

where $E^* = C_2H_4D_2^*$. The measured quantity is

$$H_2/D_2 = k_{12}(E^*)f_{H_2}/[k_{12}(E^*)f_{D_2} + \Phi_2 I_a] \quad (II)$$

where $f_{H_2} = 0.57$ and $f_{D_2} = 0.06$ as discussed above and Φ_2 is the quantum yield of reaction 8. The usual steady-state approximations lead to

$$\frac{H_2}{D_2} = \frac{\Phi_1[(1/1 + k_9K/k_{10}M)][(1/1 + k_{11}/k_{12})]\, f_{H_2}}{\Phi_1[(1/1 + k_9K/k_{10}M)][(1/1 + k_{11}/k_{12})]f_{D_2} + \Phi_2} \quad (III)$$

where K/M is the ratio of CD_2CO/CH_4 in the original mixture and k_9/k_{10} is the ratio of relative rate constants of reactions 9 and 10 and has been determined to be 5.47.[6] Φ_1 is the quantum yield of reaction 7. In the absence of CH_4 only reactions 7, 8, and 9 occur and

$$\left(\frac{D_2}{CO}\right)_0 = \frac{\Phi_2 I_a}{2\Phi_1 I_a}$$

Substitution into eq III results in

$$\frac{H_2}{D_2} = \frac{[(1/k_9K/k_{10}M + 1)]f_{H_2}}{2(D_2/CO_0[1 + k_{11}/k_{12}] + f_{D_2}[(1/k_9K/k_{10}M + 1)]} \quad (IV)$$

The calculated values of F using the data in Table II, Figure 1, and eq IV are shown in Table III. The most meaningful result is that at 1470 Å, since H_2 was not observed at any other wavelength. It may be concluded that the decomposition of excited ethane by reaction 12 is unimportant.

Table III: Fraction (F) of Excited $C_2H_4D_2^*$ Decomposing into Hydrogen + Ethylene

λ, Å	E, eV[a]	F
3130	0.49	<0.0093
2537	1.42	<0.035
1849	3.24	<0.058
1470	4.97	0.0057

[a] Maximum energy available to the CD_2 prior to reaction with CH_4.

To relate these results to the methane photolysis at 1236 Å, it may be argued that the CH_2 obtained from CH_4 possesses significantly more energy than the CH_2 from ketene. In the flash photolysis of CH_4, however, Braun[32] has observed H_2 vibrationally excited to $v = 5$ or 6, *ca.* 2.5 eV. Since the flash lamp is not monochromatic, the maximum energy retained by the resulting CH_2 can vary from 1.5 to 3.2 eV. These energies are clearly in the range covered by photolysis of ketene in which H_2 is not produced from decomposition of the excited ethane.

Acknowledgment. The author expresses his appreciation to R. F. Hampson, Jr., for helpful discussions and to J. R. McNesby for critical evaluation of this manuscript.

(30) A. H. Laufer, unpublished data.
(31) H. Okabe and J. R. McNesby, *J. Chem. Phys.*, 34, 638 (1961).
(32) W. Braun, private communication.

A Theoretical Study of Alkane Positive Ions in γ-Irradiated Organic Solids

by K. Narita and K. Funabashi

Department of Chemistry and the Radiation Laboratory,[1]
University of Notre Dame, Notre Dame, Indiana 46556 *(Received October 4, 1968)*

The nature of optical transitions and the decay of absorption spectra of alkane positive ions in γ-irradiated organic solvents at 77°K are studied theoretically. Absorption maxima for C_7 to C_{16} alkanes are calculated assuming that the optical absorption involves excitation of C–C bonding electrons. Positive charge migration is treated as a phonon-assisted tunneling process and the effective mass of the hole is estimated.

I. Introduction

Positive ions in γ-irradiated solid alkanes have been studied extensively by Louwrier and Hamill.[2] Characteristically broad spectra have their peaks in the range 500–1000 nm for C_7 to C_{16} alkanes and the spectral intensities decay with half-lives of the order of hours at 77°K. In this work we consider the nature of the electronic states involved in the optical absorption of alkanes and the mechanism of positive charge migration leading to charge neutralization.

It is not self-evident that the positively charged species under consideration are the parent (unconverted) ions rather than some product ions. However, the fact that the positive charge decays in solid media[2] suggests positive charge migration between identical molecules. It will be assumed throughout the paper that we are dealing with the parent ions. Furthermore the electronic transition associated with the optical absorption experiment is assumed to be intramolecular. The possibility that some intermolecular charge-transfer transition might be involved can be ruled out by the fact that absorption spectra of alkanes are nearly identical for the two different solvents, carbon tetrachloride and 2-methyldecane.

Electronic excited states of alkane positive ions have been calculated by Fueki[3] and Lorquet.[4] The lowest excited states of these ions, which have the maximum transition dipole moment, were calculated to be the range of 2500 to 5000 nm above the ground ionic state. Although the difference in equilibrium configuration of neutral ground-state molecules and their ions could modify the excitation energies somewhat and the accuracies of these calculations are not too great for the excited states, the discrepancy seems too much to ascribe the observed optical transitions to the excited states which were calculated by Fueki and Lorquet.

Our model for the optical transition is essentially the same as the one that has been studied by Raymonda and Simpson[5] for neutral alkanes, except for the obvious difference that one of the bonds is ionized in a zeroth-order description. It is shown in the next section that the model of independent-systems theory with reasonable choice of parameters leads to fair agreement with experiment.

The absorption spectrum of 3-methylpentane positive ion decays slowly (half-life of the order of hours) in the solid matrix of 2-methyldecane at 77°K whereas the decay rate of the same ion in the solid matrix of carbon tetrachloride is so small that the intensity of the absorption spectrum is practically unchanged for hours at the same temperature. It is conjectured that the positive charge transfer (hole migration) takes place essentially through the overlap of the hole wave function at two adjacent solute sites (phonon-assisted tunneling) rather than hopping through the solvent molecules and retrapping at a neighboring solute molecule. A reason for this physical model comes from the concentration dependence of the decay rate.[2] A simple calculation is presented to test whether the observed decay rates can be understood as functions of concentration and temperature.

II. Excited States of Alkane Ions

In this section we describe a simple model for electronic excitation of alkane ions. We are interested in the positions of absorption maxima and their red shift with respect to the number of carbon atoms in linear alkanes. The experimental absorption maxima are shown in Table I together with the computed values. In the case of branched alkanes the absorption maximum moves toward "blue" as the position of branch goes to the center of the molecule.

For description of the excited states of alkane ions, we consider only those states which arise from excitation and ionization of C–C bonds. Effects of mixing C–H bonds are ignored. A possibility that the optical transitions of our interest might involve excitation of

(1) The Radiation Laboratory of the University of Notre Dame is operated under contract with the U. S. Atomic Energy Commission. This is AEC Document No. C00-38-633.

(2) P. W. F. Louwrier and W. H. Hamill, *J. Phys. Chem.*, in press.

(3) K. Fueki, *ibid.*, **68**, 2656 (1964).

(4) J. C. Lorquet, *Mol. Phys.*, **9**, 101 (1965).

(5) J. W. Raymonda and W. T. Simpson, *J. Chem. Phys.*, **47**, 430 (1967).

Table I: Absorption Maxima of Alkane Ions

	Exptl.,[2] eV	Theoret, eV
Normal C_7	2.21	2.10
C_8	1.90	1.90
C_9	1.77	1.78
C_{10}	1.66	1.69
C_{11}	1.59	1.62
C_{12}	1.48	1.57
C_{13}	1.46	1.54
C_{14}	...	1.51
C_{15}	1.35	1.49
C_{16}	1.33	1.47
2-Methyl C_9	1.65[a]	1.56
3-Methyl C_9	1.77[a]	1.58
4-Methyl C_9	1.84[a]	1.59

[a] Absorption maxima for the branched alkanes are measured in 3MP solvent, while those of normal alkanes are measured in carbon tetrachloride solvent (ref 2).

C–H bonds directly has been considered and has been ruled out on the ground that the model did not give the red shift of absorption maxima with respect to the number of carbon atoms. Following the Raymonda–Simpson scheme,[5] the Hamiltonian for a group of C–C bonds is written as

$$H = \sum_i H_i + \sum_{i>j} V_{ij} \tag{1}$$

where H_i is the Hamiltonian for bond i and V_{ij} is the interaction between bonds i and j. The zeroth-order ground-state wave function for the ion is given by a linear combination of wave functions such as

$$\Phi_i = \phi_i' \prod_{i \neq j} \phi_j \tag{2}$$

where ϕ_j is the normalized ground-state wave function for neutral bond j and satisfies

$$H_j\phi_j = \alpha_0\phi_j \tag{3}$$

and ϕ_i' is the normalized ground-state wave function for ionized bond i and satisfies

$$H_i\phi_i' = 0 \tag{4}$$

Linear combinations of wave functions (2) generate correct zeroth-order wave functions and the first-order energies. The corresponding states include the ground ionic-state and $(n-1)$ excited ionic states (n: the number of C–C bonds). These are essentially the same excited ionic states as those calculated by Fueki[3] and Lorquet.[4]

For the excited ionic states of our interest, we use a basic function of the type

$$\Phi_i^{\dagger} = \psi_i \prod_{j \neq i;\, j \neq i+1} \phi_j \tag{5}$$

where ψ_i is the normalized wave function where bond i is in the first excited state and bond $(i+1)$ is ionized or vice versa, and satisfies

$$(H_i + H_{i+1} + V_{i,i+1})\psi_i = \alpha_1'\psi_i \tag{6}$$

We shall not attempt to calculate α_1' in (6), but the excitation energy, $(\alpha_1' - \alpha_0)$, of such a two-bond system can be estimated as follows. The excitation energy in an isolated C–C bond (ethane) is known to be about 9 eV from the work of Raymonda and Simpson.[5] If the excited C–C bond is approximated as a particle in a box, addition of ionized C–C bond would cut down the excitation energy to one-fourth of 9 eV. On the other hand, the excited electron in the two-bond system feels a core-attraction potential of twice the strength of the core potential in a single bond. The latter effect will bring the excitation energy back to the initial value of 9 eV or a little less. In the following calculation, the excitation energy is parameterized and the best fit with experiment is obtained when the excitation energy in the two-bond system is about 7 eV.

The wave function of type (5) is $(n-1)$-fold degenerate. With the techniques of degenerate-perturbation theory the first-order energies for the excited states can be calculated. Taking the nearest-neighbor approximation, the off-diagonal elements in the secular determinant, $\langle \Phi_i^{+} \mid H \mid \Phi_{i+1} \rangle \equiv \beta_{ij}$, have the same value β in our model.

With the choice of $\beta = 2.8$ eV and the zeroth-order excitation energy, $\alpha_1' - \alpha_0$, equal to 6.95 eV, the lowest eigenvalues of the secular determinants are given for linear alkanes, C_7 to C_{16} and a few branched alkanes in Table I.

It is not possible to estimate the magnitude for β and give a reasonable account for our particular choice at this time, but our β is expected to be somewhat greater than that of Raymonda and Simpson (0.74 eV)[5] or that of Fueki (~1.7 eV),[3] simply because our zeroth-order states of two-bond systems overlap to a greater extent between adjacent zeroth-order states.

III. Transition Rate for Positive Charge Transfer

In this section we consider the rate for positive charge transfer from one solute site to another. Specifically the solvent molecule is 3-methylpentane (3MP) and the solute is 2-methyldecane (2MD). Their ionization potentials are about 10.3 eV for 3MP and 10.2 eV for 2MD. In order to get some feeling on the relative magnitudes of various factors contributing to the positive charge (hole) transfer, we approximate the hole wave function for $(2MD)^+$ by that of a particle in a square well whose size is equal to the molecular dimension, and also the solvent molecules are considered to form a continuum. The depth of the square-well potential for a relaxed ion is the sum of the difference in ionization potentials between 3MP and 2MD, ϵ, and the relaxation energy, Δ. The latter contains the intramolecular and intermolecular contributions. In

order for the hole to move from one site to another the energy difference, Δ, between the two sites must be supplied from molecular vibrations (phonons). This situation is similar to the hopping mechanism of impurity conduction for low-impurity concentrations in semiconductors. In the latter case, however, the energy difference Δ comes from fluctuation in Coulomb potentials due to charged centers. Miller and Abrahams[6] obtained an expression for the transition rate of electron hopping, U_{if}, between site i and site f, using the deformation potential approximation

$$U_{if} = \left(\frac{E_1^2 \mid \Delta \mid}{\pi\rho_0 s^5 \hbar^4}\right) W^2 n_q \tag{7}$$

where E_1 is the deformation-potential constant and is defined by

$$\Delta \equiv E_1(\delta V/V) \tag{8}$$

where δV is the volume change due to relaxation, ρ_0 is the density of the medium, s is the velocity of longitudinal sound in the medium, and n_q is the number of phonons having the energy Δ

$$n_q \sim \exp(-\Delta/kT) \tag{9}$$

and W is the resonance energy and is defined by

$$W = L - SJ \tag{10}$$

$$L = -(\psi_i V_i \psi_j) \tag{11}$$

$$J = -(\psi_i V_j \psi_i) \tag{12}$$

$$S = (\psi_i \psi_j) \tag{13}$$

In (11), (12), and (13), ψ_i is the localized hole wave functions at sites i and V_j is the trap potential at site j.

The wave function for the hole in a square-well potential can be written as

$$\psi(r) = \frac{A \sin \alpha r}{r};$$

$$\alpha = \left[\frac{2\kappa m(V_0 - \mid \epsilon \mid)}{\hbar^2}\right]^{1/2} \quad (r < a)$$

$$\psi(r) = \frac{Ce^{-\beta r}}{r};$$

$$\beta = \left[\frac{2\kappa m \mid \epsilon \mid}{\hbar^2}\right]^{1/2} \quad (r > a) \tag{14}$$

where a is the radius of the square-well potential and κ is the ratio of the effective mass of the hole to the electron mass

$$\kappa = m^*/m \tag{15}$$

The condition that $[1/\psi(r)][\partial\psi(r)/\partial r]$ must be continuous at $r = a$ gives the relation between α and β

$$\eta = -\xi \cot \xi \tag{16}$$

where $\eta = \beta a$, and $\xi = \alpha a$. Thus the conditions of continuity at $r = a$ and normalization of $\psi(r)$ determine the complete wave function and the potential depth V_0 for each given value of κ and $\mid \epsilon \mid$.

Calculation of L, S, and J using the wave function (14) gives

$$L = -V_0 \frac{4\pi AC}{l\beta^2} (\cosh \eta - 1)e^{-\beta l}$$

$$S = \frac{4\pi AC}{l\beta^2} (\cosh \eta - 1)e^{-\beta l}$$

$$J = -V_0 \frac{\pi C^2}{2l^2\beta^2} [2a \cosh 2\eta - (1/\beta)2\eta]e^{-\beta l} \tag{17}$$

where l is the average nearest-neighbor distance of 2MD molecules. In calculating (17) we used $1 \ll \beta l$, because the numerical estimation shows that the value of βl is about one order of magnitude larger than 1 even in the highest 2MD concentration in the experiment of Louwrier and Hamill.

The numerical values of the hole transition rates for 0.5 mol % of 2MD at temperature 77°K are given in Table II, taking the trap depth ϵ and the effective mass ratio κ as parameters. In the calculation we used the following values for other constants: l = 40 Å; a = 3.7 Å; ρ_0 = 0.676 g/cm³; $s = 5 \times 10^5$ cm/sec; Δ = 0.14 eV; and E_1 = 0.64 eV. The average distance, l, and the radius of potential, a, are estimated from the concentration of 2MD and the molecular volume of 3MP. ρ_0 is the density of 3MP. For the sound velocity, s, we use the average value for glassy materials. The activation energy obtained from the experiment 0.14 eV is used for Δ. The deformation potential constant E_1 is estimated using Δ and polarizability of 3MP to be 17×10^{-24} cm³.

It can be seen from Table II that the transition rate for hole transfer is a sensitive function of the product $\kappa\epsilon$. If ϵ = 0.1 eV, the correct order of magnitude for the hole transition is obtained for κ = 3 or 4. Another important factor in determining the order of magnitude

Table II: Transition Rates for 0.5 Mole % of 2MD in 3MP

κ ϵ	W^2, eV²	U_{ij}, sec⁻¹
0.1	0.93×10^{-8}	4.7×10^{1}
0.2	0.43×10^{-10}	2.2×10^{-1}
0.3	0.70×10^{-12}	3.5×10^{-3}
0.4	2.2×10^{-14}	1.1×10^{-4}
0.5	1.0×10^{-15}	5.1×10^{-6}

(6) A. Miller and E. Abrahams, *Phys. Rev.*, **120**, 745 (1960).

of U_{ij} is the temperature factor contained in n_q of (9). When the effect of the negative charge, *i.e.*, trapped electron is considered, Δ in (9) must be replaced by $(\Delta - \epsilon_c)$, where ϵ_c is the difference in the Coulomb potentials at sites i and j due to the negative charge. It is clear that the transition rate becomes very large when $\Delta \lesssim \epsilon_c$.

IV. Decay of Optical Absorption

The discussion in the preceding section shows that the transition rate from one 2MD site to another becomes quite large when the hole is near the negative charge with which the hole recombines. The motion of a charge may be considered as of diffusion or non-diffusion type according to the condition

$$\epsilon_c \lesssim kT$$

where ϵ_c is the difference in Coulomb potentials between adjacent hopping sites. Thus it is convenient to consider a sphere of radius r_c, outside which the motion of a hole can be considered as diffusion type and inside which recombination is practically instantaneous.

The length that a hole can move within the time interval t can be written

$$R_D^2(t) = Utl^2 \tag{18}$$

where l is the average distance a hole can move in one hop, *i.e.*, the average nearest-neighbor distance of 2MD, and U is the hopping frequency (essentially the same as U_{ij} in the preceding section).

The recombination time τ is practically equal to the time required for a hole to contact a sphere of radius r_c by diffusion motion. Thus

$$R_D(\tau) = R(n) - r_c \tag{19}$$

where $R(n)$ is the average nearest-neighbor distance between negative and positive charges, and is proportional to the inverse cube root of positive charge concentration n

$$R(n) \equiv a_1 n^{-1/3} \tag{20}$$

From eq 18, 19, and 20 we get

$$\frac{1}{\tau} = \frac{Ul^2 n^{2/3}}{(a_1 - r_c n^{1/3})}$$

The differential equation for decay of charge density n is

$$-\frac{dn}{dt} = \frac{n}{\tau} = \frac{Ul^2 n^{5/3}}{(a_1 - r_c n^{1/3})} \tag{21}$$

Integration of this equation gives

$$-\tfrac{3}{2}a_1^2(n^{-2/3} - n_0^{-2/3}) + 6a_1 r_c(n^{-1/3} - n_0^{-1/3}) + r_c^2 \log(n/n_0) = -Ul^2 t \tag{22}$$

where n_0 is the charge concentration n at time $t = 0$.

Equation 22 can be rewritten in a more compact form with the reduced charge density n_1 and reduced lengths, l_1, R_1

$$-\tfrac{3}{2}R_1^2(n_1^{-2/3} - 1) + 6R_1(n_1^{-1/3} - 1) + \log n_1 = -Ul_1^2 t \tag{23}$$

where

$$n_1 \equiv n/n_0$$
$$l_1 \equiv l/r_c$$
$$R_1 \equiv R(n_0)/r_c$$

Equation 23 gives the change in the carrier concentration with time. We can determine the constants involved in the eq 23 by fitting it to the experimental decay curve for 1 mol % 2MD at 77°K. Experiment shows[2]

$$n_1 = 0.7 \quad (t = 40 \times 60 \text{ sec})$$
$$n_1 = 0.5 \quad (t = 152 \times 60 \text{ sec}) \tag{24}$$

Putting (24) into (23) we can get

$$R_1 = 1.14 \tag{25}$$

and

$$Ul_1^2 = 6.58 \times 10^{-6} \tag{26}$$

Using these constants, we can fit the theoretical curve closely to the experimental one as shown in Figure 1.

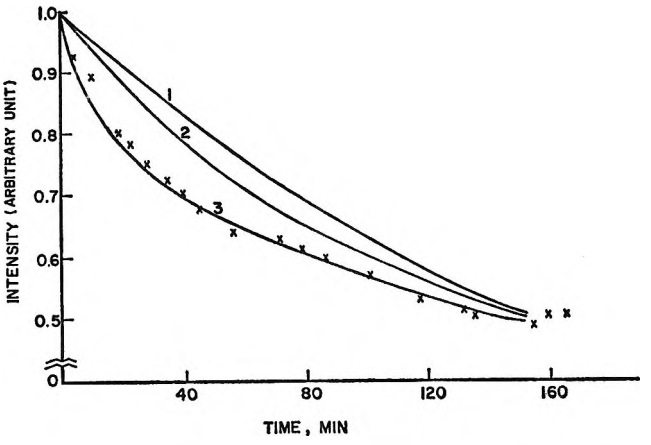


Figure 1. Decay of optical absorption. Curves 1 and 2 refer to the decay schemes $dn/dt \sim n$ and $dn/dt \sim n^2$, respectively. Curve 3 is the result of our kinetic scheme, and × indicates experimental points.

The critical radius r_c may be determined by the condition

$$(\epsilon_c)_{r=r_c} = [(\partial/\partial r)(e^2/\kappa r)]_{r=r_c} \sim kT \tag{27}$$

which gives the value of $r_c \sim 200$ Å for the experimental condition. If we make a rough estimation for $r(n_0)$ by

$$R(n_0) = (3/4\pi n_0)^{1/3} \tag{28}$$

Equations 27 and 28 together with eq 25 and 26 give

$$n_0 = 2.26 \times 10^{16}\ \text{cc}^{-1}$$
$$U = 2.1 \times 10^{-4}\ \text{sec}^{-1} \quad (29)$$

Our theory can also account for the reduced optical density for lower 2MD concentration at lower temperatures, because the value of r_c determined by (27) will increase with decreasing temperature, resulting in a reduced n_0. Because of the crudeness of our theory, the numerical values given in (29) should not be taken too seriously. However, the physical features of our model seem to be consistent with the experimental situation.

V. Discussion

Hole migration is quite common in inorganic crystals and not unusual in aromatic hydrocarbon solids. It is not, however, too obvious that aliphatic hydrocarbons should have the same effect, because the intramolecular relaxation caused by removal of a σ-bonding electron upon ionization is expected to be appreciable and consequently the positive charge is likely to be trapped in the neighborhood of the site of initial ionization. If the electron removed upon ionization of a paraffin hydrocarbon comes from a single bond and the positive charge is completely localized at the bond, bond elongation is rather substantial (one-electron C–C bond length is about 2 Å [7]). On the other hand, bond elongation is expected to be small if the positive charge is delocalized over all the C–C bonds for large paraffins. It is not possible to predict the degree of positive charge delocalization from a theoretical approach alone. A study of hyperfine structure of esr signals for the ion radicals might reveal some information on this problem.

Positive charge migration in γ-irradiated organic solids could take place more efficiently before the ion relaxes vibrationally or electronically. Such a mechanism involving excited positive ions[8] can be important for a short period ($\sim 10^{-13}$ sec) after ionization. In the system that we studied, 2MD in 3MP, most of the ionizations occur in 3MP initially and are transferred to 2MD molecules. This transfer might involve excited positive ions. Positive charge transfer among 2MD molecules, however, seems to involve only the relaxed 2MD positive ion. We tentatively come to the conclusion that the intramolecular relaxation energy of an alkane ion is small (≥ 0.1 eV), and the positive charge in the ion is delocalized.

The definition of the critical radius r_c in the problem of charge neutralization is by no means unique. In fact, the motion of positive charge outside the sphere of radius r_c should be treated as that of a diffusion in Coulomb field. The latter problem has no simple solution at this time except for a treatment such as the prescribed diffusion model[9] which has been used for a study of charge neutralization of an isolated pair of charges. In the γ-irradiated organic solids with the total dose of 10^{19} eV/g or more, a positive charge feels not only a Coulomb field due to one negative charge but also a fluctuating Coulomb field due to all other charges present in the system. The fluctuating field partially cancels the Coulomb field due to one negative charge. Our definition of r_c is significant only in this sense.

Acknowledgments. The authors express their gratitude to Professor J. L. Magee, Professor W. H. Hamill, and Dr. P. W. F. Louwrier for stimulating and informative discussions.

(7) J. L. Franklin and F. W. Lampe, *Trans. Faraday Soc.*, **57**, 1449 (1961).
(8) T. Miyazaki, *J. Phys. Chem.*, **71**, 4282 (1967).
(9) A. Mozumder, *J. Chem. Phys.*, **48**, 1659 (1968).

Argon-Ethylene Layer Formation on Graphitized Carbon Black[1a]

by Carl F. Prenzlow,[1b] H. Richard Beard, and Robert S. Brundage

National Bureau of Standards, Gaithersberg, Maryland, and California State College at Fullerton, Fullerton, California
(Received December 18, 1967)

Argon isotherms have been measured on various coverages of ethylene on graphitized carbon black in the range 64–78°K. The molecular area of ethylene at 77°K was estimated to be 17.8–18.8 Å^2. This value corresponds best with a model of ethylene molecules rocking to and fro on the carbon surface. The prefrozen layer methods of Halsey have been extended to a system in which capillarity is a complication. The maximum thickness of the ethylene film was found to be 2 layers. Argon V_m lowering on ethylene was observed and attributed to loose packing of argon rather than to ethylene capillarity or surface roughness of carbon. A two-dimensional phase transition, presumably of the liquid → solid type, has been observed for the first time on a prefrozen layer system.

Introduction

The preadsorbed layer technique has been introduced into physical adsorption studies by Halsey and Singleton,[2] who studied argon adsorption on xenon, and by Steele and Aston,[3] who studied helium adsorption on argon.

To measure argon isotherms on xenon films with varying characteristics, Halsey deposited xenon by a process of slow cooling onto three widely different underlying surfaces: anatase, silver iodide, and graphitized carbon black. His results show that in general prefrozen layers do not grow indefinitely thick, but rather form layers of definite thickness, and that the maximum finite thickness of a prefrozen film of a particular adsorbate (in this case xenon) varies from adsorbent to adsorbent.

The argon–xenon-graphitized carbon system is of particular interest because graphitized carbon is believed to present a uniform potential to both xenon and argon. Studies of this system showed that a single prefrozen layer of xenon is quite uniform, that a film composed of two or more layers is somewhat jumbled, and that the maximum thickness of the xenon film is about six layers.

For comparison with the xenon system, we have undertaken similar studies of argon adsorption on ethylene layers on graphitized carbon. Ethylene was chosen because of its close similarity in vapor pressure data with xenon and because of its molecular simplicity.

Experimental Section

Vacuum System. Adsorption measurements were made in a conventional BET constant-volume apparatus. Gas pressures were read with a cathetometer graduated to 0.05 mm and measured in mercury manometers 14 mm in diameter.

Gases. Helium, argon, and xenon gases of better than 99.9% purity were obtained in sealed glass bulbs from Air Reductions Sales Co. Ethylene was Matheson scientific grade, which was pumped upon at liquid nitrogen temperatures in successive freeze–thaw cycles until it showed a negligible vapor pressure. A mass spectrometric analysis revealed the gas to be 99.5% pure with 0.33% C_4 and C_5 unsaturated hydrocarbons, 0.09% C_4 and C_5 saturated hydrocarbons, and 0.09% C_2 and C_4 alcohols.

Adsorbent. A sample of graphitized carbon black designated Sterling FT (2700) was kindly supplied to us by Dr. W. R. Smith of Godfrey L. Cabot, Inc., Cambridge, Mass. This sample is stated to be equivalent to P-33 (2700), a graphitized carbon which was used by Halsey in previous experiments on xenon layers.[4]

To check the identity of these two carbons, an argon isotherm was measured on bare surface FT (2700) at 73.9°K and compared with a previously measured isotherm on bare surface P-33 (2700) at 73.5°K. The two isotherms were virtually identical. Furthermore, an argon isotherm at 77.1°K on one xenon layer on Sterling FT (2700) was identical with an argon isotherm on one xenon layer on P-33 (2700) measured by Prenzlow and Halsey.[4] Samples of Sterling FT (2700) were packed in the adsorption tube to a density of 0.59 g/cc.

The dead space for each sample at a particular ethylene coverage was measured with reagent helium at each liquid nitrogen temperature used. A styrofoam float gauge was used to measure the level of liquid nitrogen in the cyrostat so that dead spaces could be corrected for bath level variations.

Outgassing Procedure. Sterling FT (2700) was out-

(1) (a) Presented at the 146th National Meeting of the American Chemical Society, Denver, Colo., January 1964; (b) to whom correspondence should be addressed at California State College at Fullerton, Chemistry Department, Fullerton, Calif.

(2) J. H. Singleton and G. D. Halsey, Jr., *J. Phys. Chem.*, **58**, 330 (1954).

(3) (a) W. A. Steele and J. G. Aston, *J. Chem. Phys.*, **23**, 1547 (1955); (b) W. A. Steele and J. G. Aston, *J. Amer. Chem. Soc.*, **79**, 2393 (1957).

(4) C. F. Prenzlow and G. D. Halsey, Jr., *J. Phys. Chem.*, **61**, 1158 (1957).

gassed for 12 hr at 400° after evacuation to 10^{-4} mm or less prior to each set of adsorption measurements. Argon could be removed from surfaces fractionally covered with ethylene by evacuating for 12 hr at liquid nitrogen temperatures, and it could be removed from one or more layers of ethylene by evacuating for 10 min at liquid nitrogen temperatures. No change was detected in the argon isotherms on ethylene systems after outgassing.

Measurement of Temperature. Most of the temperatures in the adsorption vessel were measured with an argon vapor pressure thermometer using the data for solid argon of Clark, Din, and Robb.[5] A few temperatures for isotherms measured at 52–54 cm, which are just above the argon triple point of 83.78°K, were obtained from liquid vapor pressure data of Clark, Din, and Robb.[5] Temperatures of nitrogen isotherms were measured using a nitrogen vapor pressure thermometer and the liquid vapor pressure data of Giauque and Clayton.[6] Temperatures of ethylene isotherms were measured from ethylene vapor pressures using the liquid vapor pressure data of Egan and Kemp.[7] Temperatures were controlled and measured to within 0.02°K by pumping the liquid nitrogen cryostat in a manner previously described.[4]

Deposition of Ethylene Layers. The adsorption vessel and its silvered dewar for layer deposition have been previously described.[2] Measured gas volumes of ethylene (STP) were prefrozen onto the carbon by controlled cooling[2] using a methane vapor thermometer to follow the process. Cooling periods of at least 4 hr were allowed for ethylene depositions up to one layer from a temperature of 106°K to 85°K. At least 16 hr was allowed for deposition of ethylene doses of two or more layers. Several millimeters of reagent helium was added to the ethylene to ensure heat transfer during all depositions.

Results

The monolayer volume of ethylene on one gram of Sterling FT (2700) was determined by the surface titration method of Singleton and Halsey.[2] Increasing doses of ethylene were prefrozen onto the carbon surface, the argon isotherm at each ethylene dosage was measured, and the argon point B was determined for each of these isotherms. The monolayer volume of ethylene was taken to be 2.44 ± 0.01 cc/g since at this coverage the first hump in an argon isotherm (and the point B) disappears, as shown by the 1.00 ethylene layer isotherm in Figure 1. This precise V_m value could be used to indicate the packing and orientation of ethylene molecules on the carbon black surface provided that the true specific area of Sterling FT (2700) were accurately known. Such a specific area can be calculated from reliable V_m values for argon, krypton, and xenon on P-33 (2700), which were obtained by "step height" and "surface titration" methods by Halsey and co-workers.[2,4] Rare gas data seem ideal for calculating the true specific area of Sterling FT (2700) because the carbon surface is believed to present no potential energy barriers to prevent hexagonal close packing of rare gas atoms[8] and because simple spherical particles can present no surface orientation problems.

The main problem which arises is in determining the correct area occupied per rare gas atom on the carbon surface.[4] This is usually taken to be the area per atom in the hexagonally packed (111) plane of the solid rare gas crystal. In this case the specific area of carbon may be calculated from rare gas bulk solid density data by means of the formula

$$S = 0.4110(M/\rho)^{2/3}V_m \quad (1)$$

in which S is the area in square meters per gram of carbon black, M is the gram atomic weight of the rare gas, and ρ is the density of the rare gas solid at the temperature of V_m measurement. Density data for solid argon, krypton, and xenon, which are suitable for making these calculations, have recently been published by Eatwell and Smith.[9] Estimates of the specific area, calculated in this fashion, have been listed in Table I.

Table I: Estimated Specific Areas of P-33 (2700) from Rare Gas Density Data[a]

Adsorbate	Temp, °K	Solid density	V_m	Calcd area, m²/g
Argon	64.5	1.679	3.66	12.45
Krypton	78	2.932	3.15	12.11
Xenon	78	3.647	2.76	12.30

[a] The true specific area, averaged from these estimates, is taken to be 12.3 ± 0.2 m²/g.

On the other hand, Lander and Morrison[10] recently have published low-energy election diffraction (LEED) data for xenon adsorbed on the basal plane of graphite. Their data indicate that xenon is hexagonally close packed and has a surprisingly low area per atom of 15.7 Å². Using this value and the xenon V_m value 2.76 cc/g,[4] one estimates the specific area of Sterling FT (2700) to be 11.6 m²/g.

By its very nature, LEED should provide a more direct and exact measurement of atomic areas than density measurements and hence a better estimate of the absolute carbon black surface area. However, because LEED data for argon and krypton on the basal

(5) Clark, Din, and Robb; Michels, Wasseraar, and Zweitering, *Physica's Grav.*, 17, 880 (1951).

(6) W. F. Giauque and J. O. Clayton, *J. Amer. Chem. Soc.*, 55, 4879 (1933).

(7) C. J. Egan and J. D. Kemp, *ibid.*, 59, 1264 (1937).

(8) A. D. Crowell and D. M. Young, *Trans. Faraday Soc.*, 49, 1080 (1953).

(9) A. J. Eatwell and B. L. Smith, *Phil. Mag.*, 5, 463 (1960).

(10) J. Lander and J. Morrison, *Surface Sci.*, 5, 163 (1966).

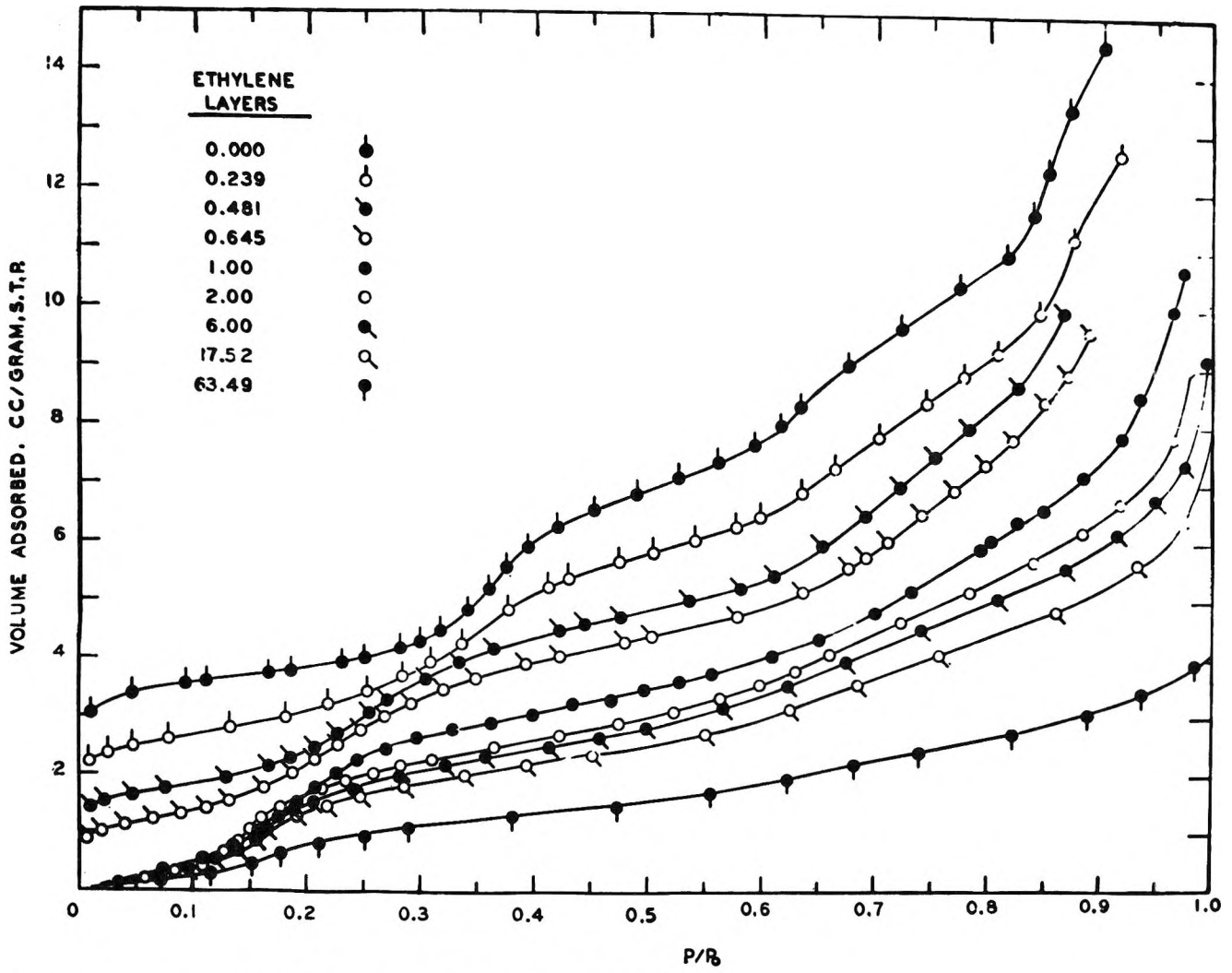


Figure 1. Argon adsorption on various coverages of ethylene at 77.5°K.

plane of graphite have so far not been published, we are unable to cross check the 11.6 m^2/g value. Consequently, for the present we cautiously assign the true specific area of Sterling FT (2700) within the range 11.6 to 12.5 m^2/g.

Using a specific area of Sterling FT (2700) in this range and 2.44 cc/g as the monolayer volume of ethylene, we assign the area 17.8–18.8 $Å^2$ to each preadsorbed ethylene molecule. This range of area does not correspond with any of the areas calculated for localized adsorption at periodically spaced lattice sites on the graphitic carbon surface, such as the center of alternate hexagons of carbon atoms (20.8 $Å^2$).

Furthermore, this range of area is significantly lower than the molecular area of ethylene assigned by Kiselev[11] from BET measurements (21 $Å^2$) and even lower than the value he calculated for close packed ethylene molecules lying flat on the carbon black surface (19.5 $Å^2$).

Table II shows the results of our molecular area calculations for closest packed ethylene in several possible fixed orientations with respect to the carbon black surface. In addition to calculations for flat, vertical, and sidewise ethylene orientation, we have made calculations for a tilted ethylene molecule because potential energy calculations, which are summarized in Tables III and IV and which allow for the anisotropy of the ethylene molecule, indicate that the most stable orientation for an individual ethylene molecule occurs when the molecular plane is tilted at about 35° and the carbon–

Table II: Area per Ethylene Molecule in Various Orientations with Hexagonal Closest Packing

Fixed orientation	Area, $Å^2$
Flat	19.2
Vertical	12.3
Sidewise	15.2
Tilted at 35°	16.4
Free rotating molecule	20.6

(11) A. G. Bezus, V. P. Dreving, and A. V. Kislev, *Russ. J. Phys. Chem.*, **38**, 59 (1964).

Table III: Orientation *vs.* Potential Energy of Adsorbed Ethylene Molecules

Orientation	$C \times 10^{58}$, erg cm^6	Z, Å	E, cal/mol
Flat, molecular plane ‖ to surface; C=C bond ‖ to surface	1.55	3.70	−2590
Sidewise, molecular plane ⊥, C=C bond ‖ to surface	1.59	3.97	−2170
Vertical, molecular plane ⊥, C=C bond ⊥ to surface	1.63	4.29	−1760
Tilted, molecular plane 35° C=C bond ‖ to surface	1.68	3.55	−3180

Table IV: Parameters for Calculating Kirkwood–Mueller Constants

	cm^{-3} × 10^{25}	cm^{-3} × 10^{25}
Ethylene		
Vertical orientation	52.5	3.19
Sidewise orientation	39.0	3.46
Flat orientation	33.8	3.66
35° tilt	35.8	3.59
Random orientation	42.6[a]	3.12[b]
Argon	16.2	3.24
Graphite	10.2	13.5[c]

[a] J. Hirchfelder, C. Curtiss, and R. Bird, "Molecular Theory of Gases and Liquids," John Wiley & Sons, New York, N. Y., 1954, p 950. [b] C. Barton, R. G. Meisenheimer, and D. P. Stevenson, *J. Phys. Chem.*, **64**, 1312 (1960). [c] H. T. Pinkick *Phys. Rev.*, **94**, 319 (1954).

carbon bond is parallel to the carbon black surface. An end view of this orientation is shown in Figure 2.

These potential energy calculations were made using the equation

$$E = -N\pi C/6Z^3 \qquad (2)$$

in which N is the number of carbon atoms per cc of carbon black, C is the Kirkwood–Mueller constant, and Z is the distance of closest approach of the ethylene molecule to the carbon black surface. The distance Z was taken to be the distance from the center of the ethylene molecule in a particular orientation to the outermost plane of graphitic carbon black atoms. In these calculations the C=C bond distance of ethylene was taken to be 1.33 Å, the C–H distance 1.09 Å, the $=C<^{H}_{H}$ angle 116.6°,[12] the π-bond radius 1.85 Å, and the van der Waals radius of hydrogen to be 1.20 Å. The van der Waals radius for graphitic carbon atoms was taken to be 1.85 Å.

The Kirkwood–Mueller constant C was evaluated by means of the eq 3 in which m is the mass of the electron, c is the velocity of light, α_1 is the polarizability of

$$C = 6mc^2\left(\frac{\alpha_1\alpha_2}{(\alpha_1/\chi_1) + (\alpha_2/\chi_2)}\right) \qquad (3)$$

the ethylene molecule in a direction perpendicular to the carbon black surface, χ_1 is the magnetic susceptibility of the ethylene molecule perpendicular to the carbon black surface, α_2 is the polarizability of graphitized carbon black, and χ_2 is the magnetic susceptibility of graphitized carbon black. Polarizabilities of ethylene in various orientations were calculated using the bond polarizabilities of Denbigh.[13] Magnetic susceptabilities of ethylene in the same orientations were calculated using the bond susceptibilities of Guy and Tillieu.[14] Parameters for calculating Kirkwood–Mueller constants are listed in Table IV.

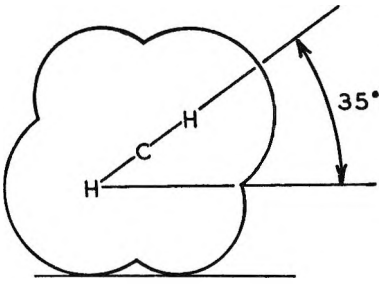


Figure 2. End view of an ethylene molecule in its lowest energy orientation.

The areas in Table II were calculated after first determining the closest packing arrangement of ethylene molecules with a two-dimensional coordination of 6, using the graphical method of Zorkii and Porai-Koshits.[15] Their method was extended to the tilted ethylene molecules by using three-dimensional models in place of two-dimensional patterns.

Table II also shows the results of a molecular area calculation for an ethylene molecule freely rotating about its longest axis, using the method of Bezus, Dreving, and Kiselev.[16] With the ethylene dimensions quoted below eq 2 we obtain a value of 20.6 Å^2 as the area of a freely rotating ethylene molecule in a 6 coordination. We note that this value is in agreement with Kiselev's area (21 Å^2), measured at 173°K, but that 20.6 Å^2 is decidedly higher than our experimental molecular area (17.5–18.8 Å^2) measured at 77°K.

Furthermore, we note that the areas calculated for flat, vertical, sidewise, and tilted fixed orientations of ethylene in closest 6 packing are in poor agreement with our experimental range of areas. In particular, we note that the area for closest packed ethylene in the tilted orientation is only 16.4 Å^2.

This is disturbing because we expect tilted ethylene in closest packing to be the preferred surface state of ethylene at low temperatures. An experimental value of 17.5–18.8 Å^2 implies either that the ethylene is pack-

(12) K. Kuchitzu, *J. Chem. Phys.*, **44**, 906 (1966).
(13) K. G. Denbigh, *Trans. Faraday Soc.*, **36**, 936 (1940).
(14) J. Guy and J. Tillieu, *J. Chem. Phys.*, **24**, 1117 (1956).
(15) P. M. Zorkii and M. A. Porai-Koshits, *Kristallografiya*, **6**, 655 (1961).
(16) A. G. Bezus, V. P. Dreving, and A. V. Kiselev, *Russ. Colloid J.*, **23**, 328 (1961).

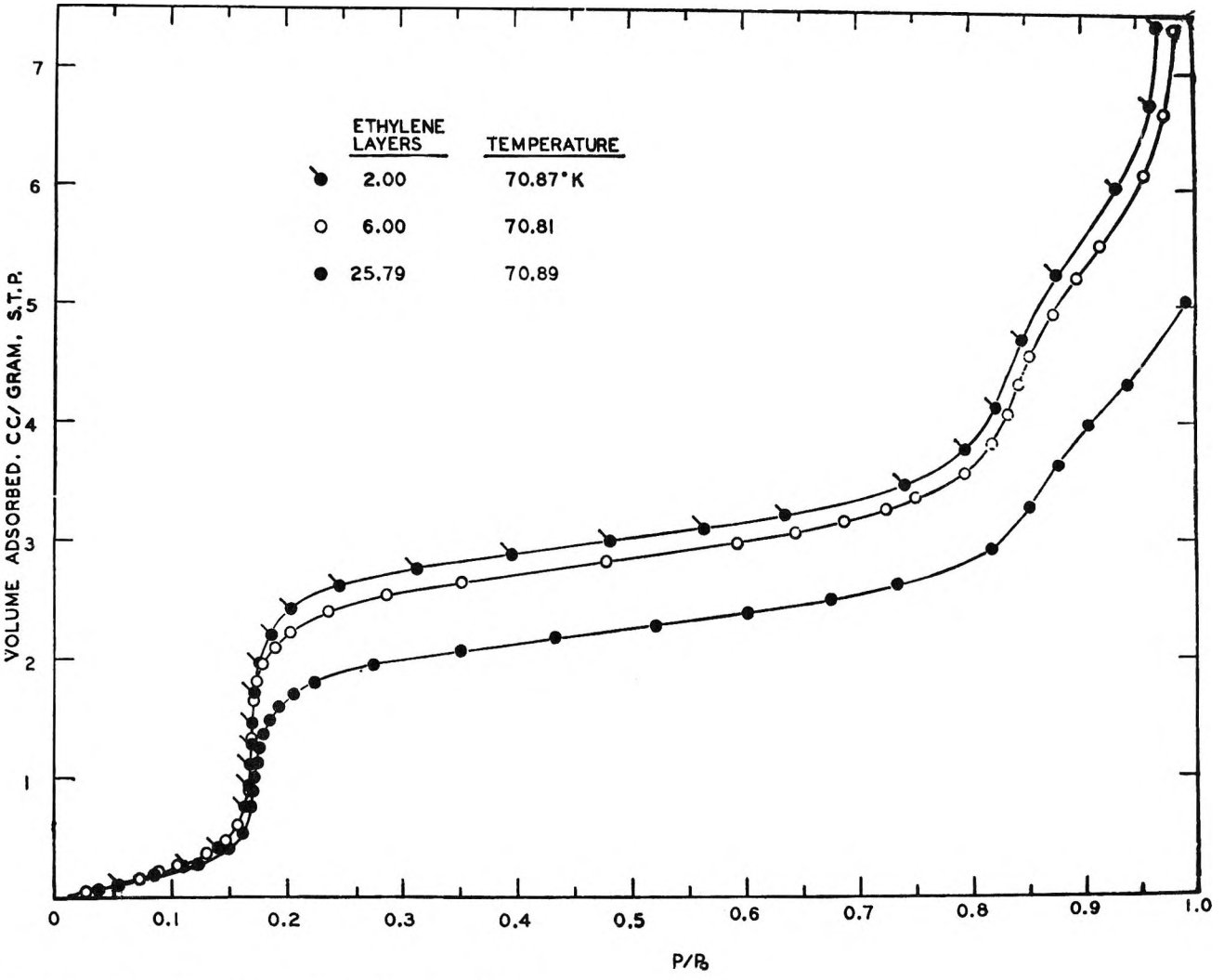


Figure 3. Argon adsorption on ethylene layers at 70.8°K.

ing with a coordination less than 6 or that there is still enough thermal motion at 77°K to cause the effective area per molecule to be greater than 16.4 Å².

We favor the latter explanation. It seems quite reasonable for ethylene to undergo large oscillations or hindered rotations on the carbon surface at 77°K. Neglecting lateral interactions, the potential energy difference between a flat ethylene molecule and a tilted ethylene molecule, whose energies are listed in Table III, is small enough to indicate that oscillation between these positions is probable at 77°K. Furthermore, a λ-type anomaly in the heat capacity of bulk solid ethylene, which most reasonably could be attributed to a gradual increase in molecular rotation, has been observed in the temperature range 53–90°K.[7,17]

The Film Thickness of Preadsorbed Ethylene. One of the distinctive features of the study by Singleton and Halsey on xenon layers was the observation of limiting isotherms.[2] In the argon–xenon–P-33 (2700) system, for instance, the argon isotherm on six layers of xenon was virtually indistinguishable from isotherms on 9.7 and 19.4 xenon layers at 78°K.

Halsey accounted for this behavior in two ways. First he demonstrated that a potential theory of adsorption, which specifies an inverse cube law potential, adequately represents the data for all xenon coverages and predicts limiting argon isotherm behavior for six or more xenon layers. Second, he has proposed that a large dose of xenon, after forming a surface film at least six layers thick on the carbon, does not fill the remaining pore space between the large nonporous carbon black particles, but instead forms bulk crystals of negligible area elsewhere in the tube, maintaining a constant area xenon surface with a limiting argon isotherm behavior.[2]

Our attempts to apply this procedure to ethylene layers were hampered at large ethylene doses (two or more nominal layers) by the relatively low vapor pressure of ethylene near its bulk triple point (104°K, 1 mm). At ethylene vapor pressures adequate to ensure rapid distribution of ethylene throughout the carbon sample, ethylene is a liquid which will fill pores

(17) M. E. Jacox, *J. Chem. Phys.*, **36**, 140 (1962).

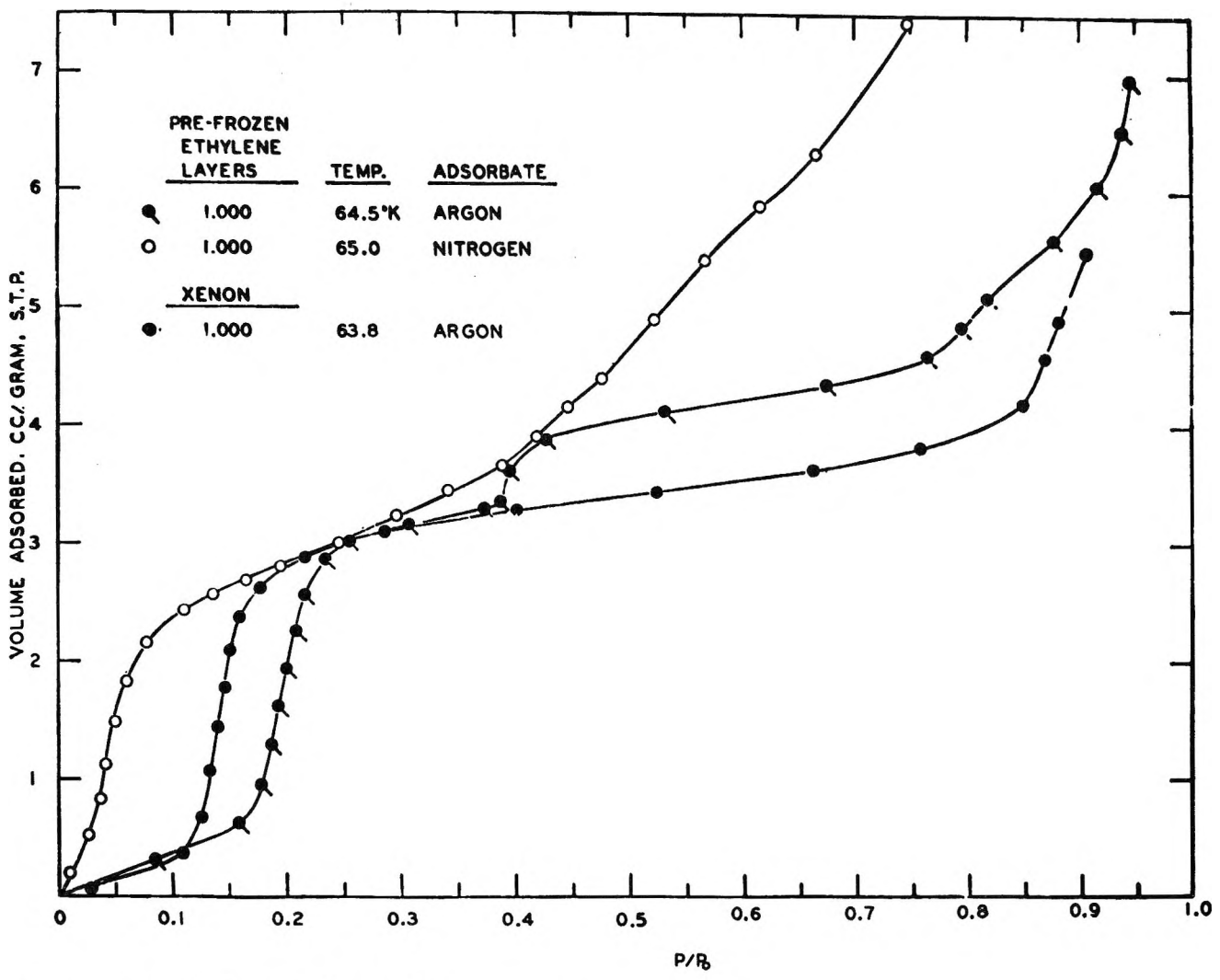


Figure 4. Argon and nitrogen isotherms at low temperatures.

by capillary attraction, provided the ethylene dose is large enough to cover the carbon with a surface film first. On the other hand, at low temperatures where ethylene is solid and capillarity is presumably no problem, we found that mass transport of ethylene was inconveniently slow. For instance, when ethylene was frozen into the adsorption bulb stem at 90°K and then was allowed to contact the carbon sample only at 90°K or lower, small, but definite, changes were noted in each succeeding argon isotherm which was used to monitor the ethylene layer growth, even after 14 days. No conclusions about ethylene film thickness could be drawn from such measurements.

Fortunately, in spite of capillarity, we were able to determine the prefrozen ethylene film thickness by analyzing low-temperature argon isotherms on ethylene layers which were deposited by the conventional slow cooling method. In these experiments ethylene was first allowed to equilibrate with carbon black at 1 cm vapor pressure at 106°K, in order to ensure complete formation of a surface film. Then the sample was slowly cooled over a period of 16 or more hours to liquid nitrogen temperatures. Naturally, at 106°K one would expect the smallest capillary pores of the carbon powder to be filled with *any excess* liquid ethylene above that needed to form the adsorbed film. Slow cooling would eventually freeze this ethylene in the filled pores, thereby diminishing the surface area available for argon adsorption. As a consequence, one would not expect overlapping argon isotherms with increased ethylene doses. Rather one might expect the behavior we observed in Figure 1, which shows that the argon isotherms at 77.5°K on 2, 6, 17.5, and 63.5 ethylene layers are distinctly different and do not permit simple analysis for layer thickness.

However, as shown in Figure 3, the argon isotherms for ethylene coverages of two or more layers at 70.8°K show nearly vertical risers. Halsey has developed equations for calculating the positions of these risers, which are drastically affected by the number and nature of underlying adsorbate layers. As a consequence, we were able to analyze our data with the following difference equation, which is easily obtained from Halsey's eq 2,[18] if one assumes a constant compatibility factor g

and if one assumes that the potential energy between an argon atom and the carbon black varies inversely with the cube of the distance from the carbon surface and that the potential energy between an argon atom and each ethylene layer varies inversely with the fourth power of the distance from that layer.

$$kT \ln (P/P_0)_{n+1} - kT \ln (P/P_0)_n = E_n - E_{n+1}$$
$$= N_2C_2\pi\{[d + (n-1)d_0 + d_1]^3\}^{-1} - \tfrac{1}{6}(N_2C_2\pi)$$
$$\times \{[d + nd_0 + d_1]^3\}^{-1} - \tfrac{1}{2}(N_1C_1\pi)\{(d + nd_0)^4\}^{-1} \quad (4)$$

In this equation $(P/P_0)_n$ is the riser position for argon adsorption on n prefrozen ethylene layers, E_n is the energy of interaction between an argon atom and an adsorbent composed of n ethylene layers and the underlying graphitized carbon. N_2 is the number of carbon atoms per cc in graphitized carbon, N_1 is the number of ethylene molecules per cm² in an ethylene layer; d is the distance of closest approach for argon to the outermost ethylene layer, taken to be the sum of the atomic radius of argon and half of the distance between ethylene planes; d_0 is the distance between planes of ethylene parallel to the graphitized surface of carbon; and d_1 is the distance of closest approach for ethylene to the graphitized carbon surface, taken to be the sum of half the distance between ethylene planes and half the distance between graphite planes.

C_2 and C_1 are Kirkwood–Mueller constants for argon–graphite and argon–ethylene interactions, respectively, calculated in the conventional fashion using eq 3 and using the parameters for randomly oriented ethylene in Table IV.

As Figure 3 shows, the experimental value for the riser of argon on two ethylene layers is $P/P_0 = 0.171 \pm 0.001$, as determined at the midpoint of the riser. After inserting this value, as well as $N_2 = 1.13 \times 10^{23}$ atoms/cm³, $N_1 = 5.33 \times 10^{14}$ atoms/cm², $d = 3.65$ Å, $d_0 = 3.49$ Å, $d_1 = 3.44$ Å, $C_2 = 1.055 \times 10^{-58}$, and $C_1 = 1.817 \times 10^{-58}$, into the difference equation, we were able to successively calculate theoretical riser positions for the ethylene coverages listed in Table V. The results of these calculations show that a third-layer riser should occur no lower than 0.206. The riser, if it existed, could have been easily distinguished with our apparatus from the second layer riser at $P/P_0 = 0.171 \pm 0.001$. However, as Figure 3 further shows, no riser value other than 0.171 was observed for larger ethylene doses, even 25 nominal ethylene layers; hence we conclude that the maximum thickness of the prefrozen ethylene is two layers.

Table V: Calculated Argon Riser Positions on Various Ethylene Coverages

Layers of ethylene	P/P_0
2	0.171 (from expt)
3	0.206
4	0.222
5	0.230
6	0.233

Lowered V_m's on Prefrozen Layers. In Figure 4, low-temperature argon and nitrogen isotherms on one layer of ethylene are shown. The V_m values which were estimated from these isotherms, as well as V_m values estimated from isotherms shown in Figures 1 and 3, from several isotherms which are not shown, and from previous work by Prenzlow and Halsey,[4] have been summarized in Table VI.

One notes that the V_m's measured on one or more layers of ethylene are distinctly lower than the V_m measured on bare carbon. Further, one notes that the argon V_m falls drastically until two ethylene layers have been deposited, then it undergoes a more gradual decrease with larger doses of ethylene. This effect is most easily seen in column 8 of Table VI.

Gradual lowering of the argon V_m is to be expected because, as we have previously pointed out, large ethylene doses fill the carbon pores by liquid capillarity; however, the drastic falloff in argon V_m at 1 and 2 ethylene layers is not expected, particularly since no second-layer V_m lowering was observed when argon adsorbed on bare carbon.[4] In this case the second-layer V_m and the first-layer V_m both had the same value, 3.66 cc/g.

V_m lowering on prefrozen layers has been noted previously for argon adsorption on one xenon layer on P-33 (2700) at 64–78°K,[4,19] where xenon capillarity is presumably nonexistent. More recently, it has been observed for nitrogen adsorption on water layers on silica[20] and for nitrogen adsorption on benzene and methanol layers on carbon black.[21]

Prenzlow[19] and Steele and Kebbekus[22] have ascribed the lowering of the argon V_m on one layer of xenon on highly graphitized carbon to a looser two-dimensional argon packing on xenon than on bare carbon. Wade[20] has ascribed the lowering of nitrogen V_m on water layers on silica to capillary condensation by water in the pores between silica particles. Dubinin[21] has ascribed the lowering of nitrogen V_m's on benzene and methanol layers to surface roughness of carbon.

Surface roughness seems unlikely as a possible cause of this argon V_m lowering because prior work on graphitized carbon blacks indicates little, if any, heterogeneity.[23,24]

(18) J. H. Singleton and G. D. Halsey, Jr., *Can. J. Chem.*, **33**, 184 (1955).
(19) C. F. Prenzlow, Ph.D. Thesis, University of Washington 1957, University Microfilms, Ann Arbor, Mich.
(20) W. Wade, *J. Chem. Phys.*, **68**, 1029 (1964).
(21) A. I. Saraklov, M. M. Dubinin, and Lu. F. Berezkina, *Izv. Akad. Nauk SSSR Chem. Ser.* **7**, 1165 (1963).
(22) W. A. Steele and E. Kebbekus, *J. Chem. Phys.*, **43**, 292 (1965).
(23) M. H. Polley, W. D. Schaffer, and W. R. Smith, *J. Phys. Chem.*, **67**, 469 (1953).
(24) D. Graham, *ibid.*, **61**, 1310 (1957).

Table VI: V_m and Surface Area Estimates on Various Dosages of Prefrozen Ethylene

Nominal layers of ethylene	Ethylene gas volume, cc/g (STP)	V, condensed volume of ethylene cc/g[f]	Temp, °K	V_m, cc/g	Method of V_m determination	Estimated area, m²/g	$-\Delta V_m/\Delta V$	Ref to previous work
			Argon Adsorption					
Bare carbon			64.5	3.66	*a*	12.5		4
Ethylene								
1.00	2.44	0.00427	64.5	3.06	*d*	10.4	141	
			64.5	4.00	*e*			
2.00	4.88	0.00854	70.9	2.94	*a*	10.0	28	
6.00	14.64	0.0256	70.8	2.80	*c*	9.5	8.2	
17.52	42.75	0.0748	70.8	2.44	*c*	8.3	7.3	
25.79	62.93	0.1101	70.9	2.22	*c*	7.5	6.2	
63.49	154.92	0.2711	77.5	1.49	*c*	5.1	4.5	
Xenon								
1.00	2.76	0.0060	63.8	3.06	*b*	10.4		
			Nitrogen Adsorption					
Bare carbon			64.5	2.94	*a*	12.3		4
Ethylene								
1.00	2.44	0.00427	65.0	2.45	*b*	10.3	117	

[a] The flattest point on an isotherm tread. [b] The point B. [c] Ratios of similar shaped curves, using the 2 ethylene layer isotherm as a reference. [d] Point B of the initial tread prior to the hump in Figure 4. [e] Point B of the hump above $P/P_0 = 0.4$ for 1 ethylene layer in Figure 4. [f] Ethylene in the condensed state was assumed to be solid with a density of 0.715 g/cc.

Likewise, capillary filling of pores between carbon particles seems improbable as a cause of argon V_m lowering on one layer of ethylene. Using the Kelvin equation

$$\ln P/P_0 = -2\gamma V \cos\theta/rRT \qquad (5)$$

we may calculate the minimum value of P/P_0 at which ethylene capillary pore filling can occur in the smallest pores of Sterling FT (2700). To make this calculation, we assume the surface tension of ethylene at 104°K to be $\gamma = 31.1$ dyn/cm, the molecular volume of ethylene to be $V = 48.2$ cm³, and the contact angle between ethylene and graphite to be 0°. Mercury porosimeter measurements[25] further indicate that Sterling FT (2700) has a negligible volume of pores with radii less than 100 Å; hence, we may set r equal to 100 Å as a minimum. Using these values we calculate the minimum P/P_0 at which pore filling can occur to be 0.71. On the other hand, the ethylene isotherm measured on Sterling FT (2700) at 133.8°K, which is shown in Figure 5, indicates that the first ethylene layer is deposited at a P/P_0 value less than 0.02; consequently, the low argon V_m for one ethylene layer, as compared to the argon V_m on bare carbon, cannot be due to ethylene pore filling by capillarity.[26,27]

We regard the lowered argon V_m on one ethylene layer as being due to looser argon packing on ethylene than on bare carbon black. Unfortunately, we are unable to specify the exact nature of this looser packing. The looser packing could be more or less random and nonlocalized as in a two-dimensional liquid, or it could be highly ordered and localized as in Langmuir adsorption. Possibly, potential energy calculations similar to those of Kebbekus and Steele[22] or direct LEED measurements of the argon–ethylene–graphite system may resolve the question of packing.

A Peculiar Isotherm Hump. The argon isotherms at 64°K on one ethylene layer and on one xenon layer, which are exhibited in Figure 4, tend to overlap in the region $P/P_0 = 0.25$ to 0.35 and both appear to have a point B of about 3.06 cc/g (STP). However, at $P/P_0 = 0.35$ the isotherm for argon on one ethylene layer shows an abrupt break and differs by about 0.70 cc/g (STP) from the isotherms for argon on one xenon layer in the region beyond the hump.

Conceivably, this could be an example of a transition investigated theoretically by Stebbins and Halsey.[28]

(25) H. R. Rootare and C. F. Prenzlow, *J. Phys. Chem.*, 71, 2733 (1967).

(26) Conclusions for two ethylene layers are similar. In this case we must assume that a monolayer of ethylene is deposited in all of the pores before any capillary pore filling can begin; hence the minimum radius is lowered by the thickness of the ethylene layer to about 95 Å and a P/P_0 value calculated to be 0.69. However, as shown in Figure 5, the second layer hump in the ethylene isotherm at 133.8°K occurs at $P/P_0 = 0.45$. Hence, we may conclude that ethylene capillarity is not responsible for argon V_m lowering on two prefrozen ethylene layers.

(27) The same arguments may be used to demonstrate that ethylene capillarity did not affect the ethylene V_m measured earlier to be 2.44 cc/g. Potential energy calculations and the ethylene isotherms in Figure 5 both indicate that ethylene doses up to a monolayer are deposited at P/P_0 values near 0.02, which corresponds to a low chemical potential. On the other hand the Kelvin equation calculations above indicate that P/P_0 must exceed 0.71 before any capillary condensation can occur at a much higher chemical potential. Hence we may conclude that a monolayer of ethylene was deposited and measured without complications due to capillarity.

(28) J. P. Stebbins and G. D. Halsey, Jr., *J. Phys. Chem.*, 68, 3863 (1964).

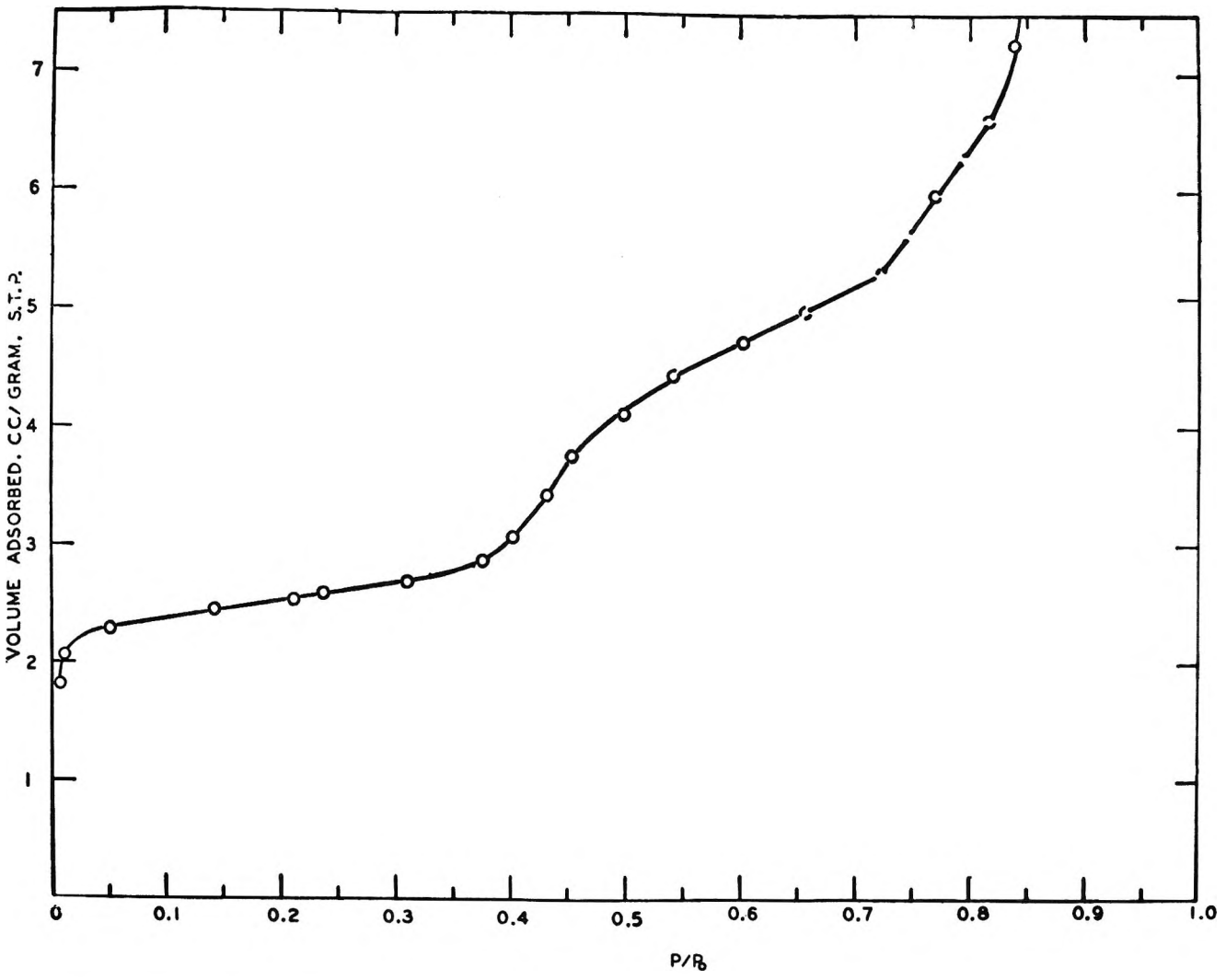


Figure 5. Adsorption of ethylene.

These workers have predicted that rare gases, such as neon and argon, adsorbed on surfaces with no potential energy wells to restrict two-dimensional movement, undergo, at sufficiently low temperatures, a transition from a two-dimensional liquid with loose packing to a two-dimensional, hexagonal close-packed solid.

They further predict that the transition should occur near a coverage of $\theta = 1$ and that the range of coverage for such a transition should be no greater than $\Delta\theta = 0.2$.

Equally conceivable at this point is the possibility that argon is undergoing a transition from a loose, localized two-dimensional solid to a close-packed two-dimensional solid. We intend to investigate transitions of this sort further.

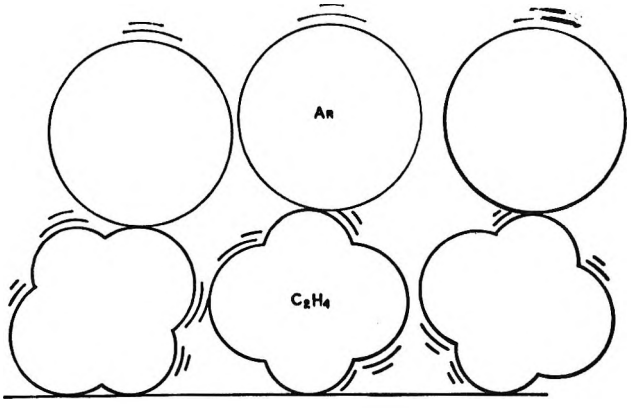


Figure 6. Argon adsorption on one ethylene layer prior to the hump at $P/P_0 = 0.4$.

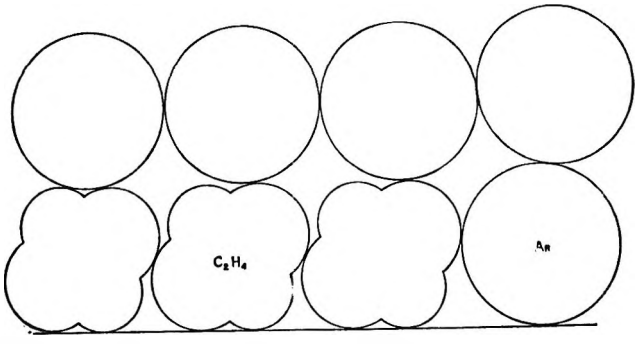


Figure 7. Argon adsorption on one ethylene layer after the hump.

Finally, there is a possibility that the argon hump is due to a phase change in the underlying ethylene layer. At argon pressures prior to the hump in Figure 4, ethylene may be oscillating to and fro about its longest axis and argon atoms may adsorb on top of these oscillating molecules as depicted in Figure 6. The V_m for such atoms may be 3.06 cc/g (STP).

At the hump the argon pressure may be adequate to cause the ethylene monolayer to contract to a close packing of tilted fixed ethylene molecules, with a molecular area of 16.4 Å^2. This contraction would free as much as 1.5 m^2/g of carbon surface on which argon could further adsorb in close packing and would increase the apparent V_m of argon to 3.96 cc/g, which is close to the observed point B beyond the hump (4.00 cc/g (STP). This situation is depicted in Figure 7 (which, however, for simplicity, does not correctly show the side view of ethylene molecules in hexagonal packing).

We have collected other data on the argon–ethylene–graphitized carbon black system which we hope to publish in the near future.

The Electrical Conductances of Some Alkali Metal Halides in Aqueous Solutions from 0 to 800° and at Pressures to 4000 Bars[1]

by Arvin S. Quist and William L. Marshall

Reactor Chemistry Division, Oak Ridge National Laboratory, Oak Ridge, Tennessee 37830 *(Received May 27, 1968)*

The electrical conductances of 0.01 *m* aqueous solutions of LiCl, NaI, KCl, KBr, KI, RbF, RbCl, RbBr, RbI, CsCl, CsBr, and CsI were measured from 0 to 800° and at pressures to 4000 bars. Evaluation of these results, together with those from previous measurements on NaCl and NaBr, indicate that in general all of these electrolytes exhibit the same type of conductance behavior at elevated temperatures and pressures. Thus at high temperatures where most of the long-range structure of water appears to be destroyed, the relative order of the specific conductances of these electrolytes remains constant—except for some instances at the highest temperatures when association effects appear to change this order. At temperatures below 100°, comparative changes in the specific conductances of these electrolytes both with temperature and pressure can be correlated with the apparent disruption of the structure of water by the ions, by pressure, and by temperature. Thus, the present measurements indicate that the simpler behavior observed quantitatively in previous extensive measurements on several electrolytes at high temperatures and pressures probably can be extended to include all of the alkali metal halides.

The properties of electrolyte solutions have been the subject of investigations by physical chemists for many years. One of the most convenient and direct methods that has been used for obtaining information about the existence and behavior of ions in these solutions has been the measurement of the electrical conductance of these solutions. The results of these measurements have provided a significant portion of the current knowledge about the behavior of ions in solution and have permitted the testing of theoretical equations that accurately describe ion–ion interactions in dilute solutions.[2] However, very little quantitative information is available concerning ion–solvent interactions in electrolyte solutions. This is particularly true about the interactions between ions and water. Water is by far the most important of the ionizing solvents, but unfortunately it is also the most complex of these liquids, probably because of the existence of tetrahedrally coordinated water molecules that form some type of structure[3] in the liquid state. This structure appears to be modified by the presence of ions in solution. Therefore, a complete description of the behavior of aqueous solutions must include the effects of (1) ion–ion interactions, (2) ion–solvent interactions, and (3) modification of the water structure by ions. Much of the effect of (3) may be eliminated when studies on aqueous solutions are carried out at high temperatures and pressures. Because water appears to become less

(1) Research sponsored by the U. S. Atomic Energy Commission under contract with the Union Carbide Corp.

(2) R. M. Fuoss, L. Onsager, and J. F. Skinner, *J. Phys. Chem.*, **69**, 2581 (1965).

(3) H. S. Frank and W.-Y. Wen, *Discussions Faraday Soc.*, **24**, 133 (1957).

structured as its temperature is raised,[4-6] at high temperature the behavior of electrolytes will be dominated by (1) and (2) with little added complications due to (3). Near room temperature, some of the water structure may also be destroyed by increasing the pressure and thus an increase in pressure will also decrease the effect of (3). Therefore, it appears that the study of aqueous solutions at high pressures at both low and high temperatures is a promising area of research that may lead to a better understanding of ion–solvent interactions in electrolyte solutions.

Much of our knowledge of the properties of aqueous solutions above 100°, and in particular in the supercritical region above 374°, has been obtained from electrical conductance studies. The first accurate studies at temperatures much above 100° were carried out by Noyes and coworkers[7] who measured the conductances of several electrolytes to 306° at saturation vapor pressure. Fifty years later, Fogo, Benson, and Copeland[8] extended precise conductance measurements into the supercritical region. In 1956, Franck reported the results of measurements to 750° and 2500 bars.[9] In recent years we have measured the conductances of aqueous solutions of K_2SO_4,[10a] $KHSO_4$,[10b] H_2SO_4,[10c] NaCl,[10d] NaBr,[10e] HBr,[10f] and NH_3[10g] to 800° and 4000 bars. Each of these electrolytes was studied at several molalities in order to calculate limiting equivalent conductances and ionization constants from the data. From these results it appears that aqueous solutions exhibit simpler behavior at elevated temperatures and pressures than at room temperature. For example, the limiting equivalent conductance in the temperature range 400–800° appears to be a linear function of density only, independent of temperature.[10b,d-g] Although the slope of the line of Λ_0 *vs.* density has approximately the same value for all the salts, it is significantly different for acids and bases. However, our results indicate that the extrapolated intercept at zero solvent density is nearly the same for all uni-univalent electrolytes. As all of these electrolytes are only partially ionized at high temperatures and pressures, we were able to calculate ionization constants at zero ionic strength in the temperature region 400–800°. When the molar concentration of water was included as a variable in the ionization constant, values of the constants were obtained that were independent of solvent density (pressure) at constant temperature. Success of this principle for the high-temperature aqueous solutions led to its wide application to equilibrium constants in mixed solvents at 25°, and a questioning of the validity of conventional plots of log K *vs.* the reciprocal of the dielectric constant.[11,12] This recent approach gave reasonable estimates for the net change in hydration number when two ions react to form an ion pair and, with additional data on solubilities at high temperatures and pressures, provided an estimate for the sum of the primary waters of hydration for the two ions.[10d]

In a further extension of the investigation of aqueous solutions at high temperatures and pressures, we present in this paper a comparison of the conductances of 0.01 *m* solutions of most of the alkali metal halides. This summary includes data on LiCl, NaCl, NaBr, NaI, KCl, KBr, KI, RbF, RbCl, RbBr, RbI, CsCl, CsBr, and CsI to 800° and 4000 bars. With the exception of KCl,[9a] NaCl,[8,10d] and NaBr,[10e] to our knowledge these conductances are the first experimental measurements that have been reported for these salts at supercritical temperatures and pressures. However, estimates of ionization constants for the alkali metal chlorides under these conditions have been published, based on measurements of 0.01 *m* solutions from 450 to 750°.[9]

Experimental Section

A complete description of the equipment and procedures used for these measurements is contained in an earlier paper.[10d] A conductance cell having no pressure seals in the high-temperature region was used for all experiments. Solutions of KCl, KBr, KI, CsBr, and CsI were prepared from single crystals (Harshaw Chemical Co., Cleveland, Ohio) and conductivity water. Solutions of CsCl, RbF, RbCl, RbBr, and RbI were prepared from 99.9% pure (or better) salts (K & K Laboratories, Plainview, N. Y.). The solution of NaI was prepared from reagent grade salt (Mallinckrodt Chemical Works, St. Louis, Mo.). With the exception of the single-crystal materials, all of the salts were dried at 110–120° prior to use. A stock solution of approximately 1.0 *m* LiCl was prepared from the hydrated, purified salt (less than 0.03 wt % of the other alkalis and alkaline earths). From this stock solution, a 0.01 *m* LiCl solution was prepared, and its conductivity was accurately measured in a glass conductance cell at 25.00 ± 0.01°. By comparison with literature values,[13] the molality of this solution was accurately determined, and a suitable dilution was made so that the final solution had a molality of 0.01000 *m*. Several different

(4) E. Fishman and P. Saumagne, *J. Phys. Chem.*, **69**, 3671 (1965).

(5) E. U. Franck and K. Roth, *Discussions Faraday Soc.*, **43**, 108 (1967).

(6) G. E. Walrafen, *J. Chem. Phys.*, **47**, 114 (1967).

(7) A. A. Noyes, *et al.*, "The Electrical Conductivity of Aqueous Solutions," Publication No. 63, Carnegie Institution of Washington, Washington, D. C., 1907.

(8) J. K. Fogo, S. W. Benson, and C. S. Copeland, *J. Chem. Phys.*, **22**, 212 (1954).

(9) E. U. Franck, (a) *Z. Phys. Chem.* (Frankfurt am Main), **8**, 92, 107, 192 (1956); (b) *Angew. Chem.*, **73**, 309 (1961).

(10) (a) A. S. Quist, *et al.*, *J. Phys. Chem.*, **67**, 2453 (1963); (b) *ibid.*, **70**, 3714 (1966); (c) *ibid.*, **69**, 2726 (1965); (d) *ibid.*, **72**, 684 (1968); (e) *ibid.*, **72**, 2100 (1968); (f) *ibid.*, **72**, 1545 (1968); (g) *ibid.*, **72**, 3122 (1968).

(11) W. L. Marshall and A. S. Quist, *Proc. Nat. Acad. Sci. U. S.*, **58**, 901 (1967).

(12) A. S. Quist and W. L. Marshall, *J. Phys. Chem.*, **72**, 1536 (1968).

(13) H. S. Harned and B. B. Owen, "The Physical Chemistry of Electrolytic Solutions," Reinhold Publishing Corp., New York, N. Y., 1958, p 697; K. A. Kreiger and M. Kilpatrick, *J. Amer. Chem. Soc.*, **59**, 1878 (1937); T. Shedlovsky, *ibid.*, **54**, 1411 (1932).

inner electrodes were used for these measurements. Their cell constants, as determined with 0.01000 demal KCl solutions at 25.00 ± 0.01°, ranged from 1.96 to 0.489 cm^{-1}.

The precision (reproducibility) of the high-temperature (200–800°), high-pressure measurements for each experimental run was about ±0.7% at the lowest temperatures to ±1–2% at 800°, with an estimated overall accuracy of ±2% or better. The precision of the measurements for each run at 0–120° was better than ±0.5%; however, the accuracy may not be better than ±1–2%. Therefore, for comparison at intersection points of these values with more accurate values obtained by refined techniques, a normalization or adjustment of the present values can be made to obtain greater accuracy.

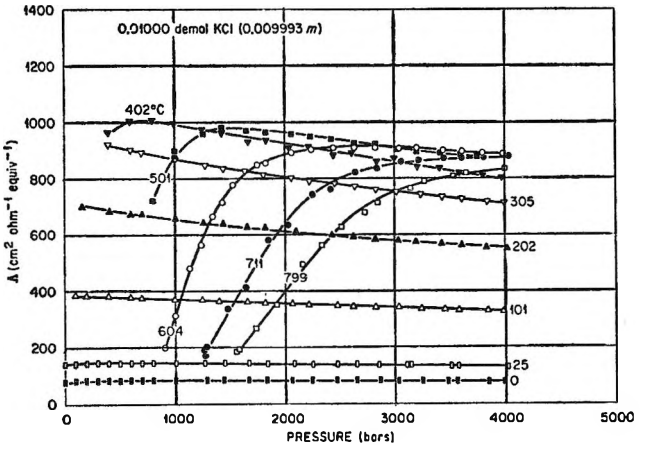


Figure 2. Equivalent conductances of 0.01000 demal (0.009993 *m*) KCl solutions as a function of pressure at several temperatures.

Results

The experimental conductances were converted into specific conductances by the methods described earlier.[10d] A graphical example of a complete set of these specific conductances, each curve corresponding to a constant temperature and plotted as a function of pressure, is shown in Figure 1 for 0.01000 demal (0.745263 g of KCl/1000 g of solution) KCl solutions. Corresponding curves for 0.01000 *m* solutions of the other 1–1 salts conform closely to those shown in Figure 1, as do those presented previously for NaCl and NaBr.[10d,e] The curves for the different salts therefore show only quantitative differences in specific conductances. Approximately the same number of experimental points (an average of 22, with extremes of 15 and 30) at each temperature were obtained for each 0.01000 *m* salt solution with no difference in precision of measurement. The values of specific conductances for the 12 salts studied, smoothed with respect to pressure but not with temperature, are presented in Table I and represent the data within the precision and qualifications stated in the Experimental Section. They therefore can be treated as equivalent to the "raw" data. Included also in Table I are those similarly smoothed values for 0.01000 *m* NaCl and NaBr presented elsewhere in graphical form.[10d,e]

Specific conductances were selected as the basis for intercomparison of these electrolytes. However, the behavior observed when equivalent conductances are plotted as a function of pressure and density is shown in Figures 2 and 3 for 0.01 demal KCl solutions. Figure 4 compares specific conductances *vs.* density for the same solution. The corresponding graphs for the other uni-univalent salts are similar to those for KCl.

Discussion

Comparisons of the isobaric specific conductances of most of the alkali metal halides, grouped according to

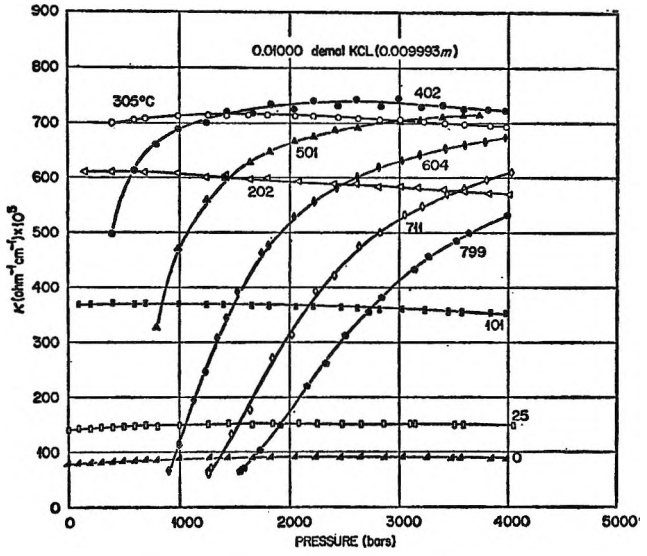


Figure 1. Specific conductances of 0.01000 demal (0.009993 *m*) KCl solutions as a function of pressure at several temperatures.

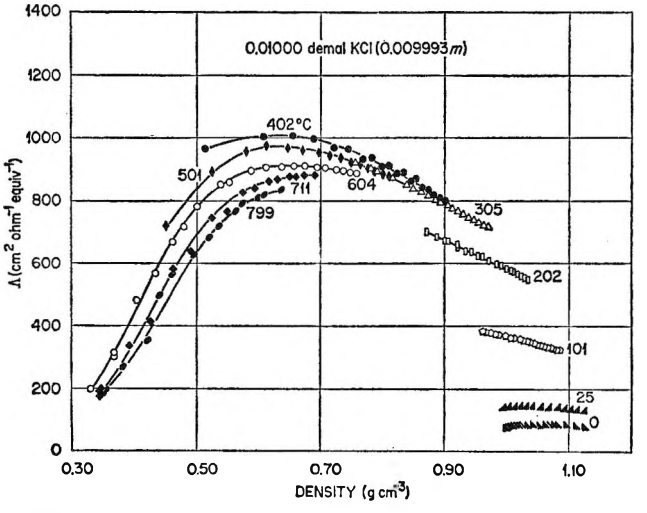


Figure 3. Equivalent conductances of 0.01000 demal (0.009993 *m*) KCl solutions as a function of density at several temperatures.

Table I: Specific Conductances (ohm^{-1} cm^{-1}) × 10^5 of 0.01000 *m* Alkali Metal Halide Solutions from 0 to 800° and at Pressures to 4000 Bars[a]

Salt	Temp., °C	Pressure, Bars 1	500	1000	1500	2000	2500	3000	3500	4000
	0	54.0	59.0	62.5	64.9	66.0	66.5	66.0	65.5	64.5
	25	107.7	112.5	115.4	117.4	118.2	118.5	118.3	117.5	116.5
	102	(300)	300	300	300	300	297	295	293	291
	207	(518)	516	512	509	504	500	493	489	483
LiCl	301	(585)	605	610	610	608	605	600	595	587
	401	-	528	618	643	652	652	648	645	640
	442	-	280	568	620	645	650	655	657	657
	494	-	-	420	542	595	622	635	646	650
	547	-	-	230	450	545	590	615	628	638
	594	-	-	88	325	470	540	580	605	622
	692	-	-	-	100	260	390	470	525	560
	795	-	-	-	23	95	205	308	390	450
	0	69.5	71.1	74.8	77.0	78.1	78.1	77.5	76.3	74.9
	25	121.2	126.0	129.1	131.0	131.7	131.5	130.7	129.3	127.5
	106,108	(341)	341	340	338	336	333	330	327	323
	203	(556)	551	544	538	533	528	523	518	513
	309	(622)	651	660	664	664	662	659	653	648
	318	(617)	655	670	675	676	675	673	669	664
NaCl	404,405	-	512	632	670	682	688	690	690	690
	455,458	-	145	540	620	655	677	685	690	695
	506,507	-	-	395	553	615	655	665	675	685
	515	-	-	350	518	585	620	640	655	665
	554,555	-	-	210	445	542	595	628	650	665
	594	-	-	100	355	490	565	610	640	655
	606	-	-	80	320	468	545	590	620	635
	708,710	-	-	15	108	263	395	480	540	575
	812	-	-	-	30	110	222	327	415	477
	0	65.5	69.8	72.5	73.8	73.9	73.2	72.0	70.2	68.5
	25	120.6	124.1	126.2	127.0	126.6	125.5	124.0	122.0	119.8
	100	339	340	338	337	332	328	324	321	317
	205	(540)	537	533	528	522	516	510	503	497
	300	(620)	637	641	641	638	634	628	622	616
NaBr	399	-	550	643	667	675	680	678	677	675
	441	-	325	585	637	660	670	675	677	677
	501	-	-	445	575	622	645	655	657	660
	557	-	-	240	470	565	605	632	645	655
	600	-	-	132	390	515	582	620	640	653
	698	-	-	20	153	325	440	510	555	585
	809	-	-	-	40	135	258	360	435	487
	0	63.8	67.5	69.5	70.0	69.4	68.2	66.7	64.7	62.5
	25	118.0	121.0	121.7	121.4	120.1	118.0	115.9	113.4	110.6
	101	(320)	318	315	310	305	300	296	291	287
	207	(552)	548	541	533	524	517	508	500	493
	306	(610)	624	625	623	622	619	614	610	603
NaI	406	-	540	623	646	650	652	650	648	640
	457	-	235	573	625	643	650	653	653	652
	508	-	-	460	570	612	632	640	645	647
	605	-	-	152	412	527	580	605	626	633
	702	-	-	22	190	368	472	530	568	590
	796	-	-	-	68	208	338	425	485	522
	0	78.2	84.4	88.4	90.7	91.7	91.6	90.9	89.5	87.7
	25	141.5	147.0	150.3	152.0	152.6	152.4	151.5	149.9	147.6
	101	(369)	369	368	367	365	362	358	354	349
	202	(610)	609	606	602	596	590	583	577	572
KCl	305	(684)	703	714	715	714	711	706	700	693
	402	-	575	687	720	733	737	737	733	725
	501	-	-	470	612	665	690	705	713	715
	604	-	-	115	385	518	590	630	657	675
	711	-	-	-	135	312	442	522	575	610
	799	-	-	-	52	170	308	410	485	532
	0	79.0	85.3	89.0	90.8	91.6	91.2	90.0	88.3	86.2
	25	143.0	147.6	150.8	152.2	152.2	151.3	149.6	147.4	144.6
	110	(397)	396	394	392	387	382	377	372	367
	211	(612)	611	606	600	594	587	580	572	564
	310	-	690	694	695	695	694	692	689	682
KBr	402	-	560	662	690	700	703	705	705	703
	447	-	300	597	648	673	688	698	700	700
	503	-	-	455	590	642	667	683	692	695
	596	-	-	150	405	525	577	617	636	648
	692	-	-	24	185	360	467	528	567	595
	798	-	-	-	62	195	328	420	485	530
	0	80.0	85.0	88.2	89.2	89.4	88.4	87.0	85.0	82.5
	25	143.2	146.8	148.7	149.0	148.3	146.7	144.5	142.2	139.2
	110	(399)	398	396	390	383	377	372	366	357
	210	(600)	596	589	581	573	565	557	548	540
	308	(660)	685	690	686	681	673	666	660	651
	404	-	565	652	690	683	686	685	682	677
KI	446	-	325	595	645	663	670	673	673	670
	503	-	-	472	590	627	646	660	670	672
	543	-	-	360	537	600	628	643	650	655
	647	-	-	78	315	463	535	575	600	615
	711	-	-	25	192	355	465	527	568	595
	744	-	-	-	145	317	432	497	542	568
	803	-	-	-	80	225	355	440	500	543

Salt	Temp., °C	Pressure, Bars 1	500	1000	1500	2000	2500	3000	3500	4000
	0	67.4	72.4	75.4	77.4	78.2	78.3	78.0	77.2	75.8
	25	125.0	128.5	131.2	132.8	133.5	133.4	132.8	132.0	130.4
	100	332	330	328	325	323	321	318	316	315
	203	(570)	568	566	562	560	555	551	545	540
	303	(605)	623	636	642	645	647	647	643	638
	356	-	585	620	633	645	650	655	656	655
RbF	400	-	515	603	635	650	655	660	663	657
	460	-	156	507	580	615	630	642	650	655
	502	-	-	403	523	570	597	610	620	630
	606	-	-	110	333	455	520	555	580	600
	718	-	-	-	136	287	398	467	510	537
	801	-	-	-	58	175	295	380	437	475
	0	80.5	86.8	90.8	92.7	93.3	93.0	92.2	90.6	88.6
	25	145.0	150.0	153.0	154.6	154.7	154.5	153.2	151.0	148.4
	102	(369)	370	368	367	363	360	357	353	348
	201	(628)	620	613	608	602	595	590	583	577
	302	(687)	709	717	717	715	713	709	706	702
RbCl	350	(585)	680	710	720	722	720	718	715	707
	409	-	525	660	695	712	715	722	720	718
	448	-	290	600	665	695	716	725	730	730
	547	-	-	290	507	595	640	665	677	683
	602	-	-	135	392	520	592	635	660	678
	697	-	-	17	161	336	450	517	558	585
	793	-	-	-	62	187	327	425	490	530
	0	81.8	87.6	91.0	92.7	93.0	92.2	91.0	89.0	86.5
	25	146.0	150.5	153.0	154.0	154.0	152.6	151.0	148.4	145.5
	102	(374)	372	370	367	362	357	352	348	342
	202	(617)	613	608	601	594	586	578	570	562
	302	(690)	713	720	718	713	708	702	697	690
	352	(562)	645	674	682	682	682	680	675	670
RbBr	401	-	566	675	709	718	722	725	720	715
	454	-	265	600	663	690	707	715	720	720
	494	-	-	500	610	655	675	685	690	692
	546	-	-	310	515	594	630	650	660	665
	617	-	-	115	367	503	575	617	640	650
	650	-	-	60	290	440	527	575	607	625
	709	-	-	30	175	345	460	528	570	595
	742	-	-	-	120	285	405	485	533	572
	809	-	-	-	67	198	320	415	480	520
	0	81.2	86.2	88.4	89.3	88.7	87.5	85.7	83.5	80.8
	25	145.0	148.2	149.5	149.3	148.0	146.0	143.4	140.2	137.0
	100	357	357	353	349	343	337	331	325	318
	199	(590)	583	576	567	558	550	540	530	522
	300	(656)	674	675	672	668	665	658	652	642
	348	(610)	660	682	688	688	682	675	667	662
RbI	401	-	570	657	676	684	682	680	675	670
	447	-	300	597	645	665	670	672	673	672
	503	-	-	500	615	650	665	670	674	675
	547	-	-	360	543	610	640	655	665	668
	598	-	-	183	435	538	588	613	630	638
	641	-	-	105	355	495	565	600	622	632
	700	-	-	-	230	410	510	566	605	620
	802	-	-	-	95	245	380	465	518	552
	0	80.8	86.7	90.1	91.9	92.0	91.6	90.6	88.6	86.3
	25	144.5	149.3	151.7	152.5	152.5	151.4	149.5	147.4	144.5
	102	(363)	362	360	357	353	350	346	340	334
	201	(615)	612	607	600	593	583	577	569	560
	303	(664)	687	692	690	685	681	675	669	660
CsCl	400	-	585	680	703	710	710	710	706	703
	447	-	305	600	665	692	705	707	707	707
	512	-	-	445	600	656	685	700	703	705
	599	-	-	140	400	525	587	620	643	655
	648	-	-	50	275	440	525	575	605	623
	700	-	-	25	180	370	485	553	592	618
	796	-	-	-	70	205	335	425	485	525
	0	81.7	87.5	90.8	92.5	92.6	91.6	90.0	88.0	85.5
	25	144.5	148.3	150.6	151.2	150.6	148.6	146.3	143.5	140.5
	120	(420)	417	412	407	401	395	388	382	375
	220	(625)	622	614	605	597	587	577	568	558
	314	(660)	685	692	688	683	677	670	665	650
CsBr	414	-	515	645	675	690	690	690	615	680
	462	-	175	575	640	668	680	682	6 11	680
	509	-	20	450	587	640	665	675	6 0	680
	632	-	-	95	340	482	550	593	6.7	630
	712	-	-	25	177	350	460	523	570	592
	813	-	-	-	72	203	330	425	492	535
	0	80.0	84.5	86.7	87.0	86.4	85.0	83.0	80.5	77.8
	25	142.5	145.3	146.0	145.4	144.0	141.1	138.5	135.0	131.6
	105	(397)	392	387	380	373	366	358	351	343
	206	(610)	600	590	578	568	558	547	536	525
	303	(684)	697	695	687	678	669	658	649	638
CsI	401	-	580	660	675	680	680	675	665	655
	448	-	323	595	657	675	680	680	677	672
	503	-	-	480	600	633	650	658	662	665
	607	-	-	160	418	532	588	618	632	638
	661	-	-	70	300	450	530	574	600	613
	708	-	-	35	200	370	470	530	565	584
	762	-	-	15	135	300	413	488	535	565
	798	-	-	-	100	250	370	450	503	543

[a] Values in parentheses are those extrapolated to saturation vapor pressure.

anion, are given in Figure 5 where specific conductance is plotted against temperature at a pressure of 4000 bars. This behavior is characteristic of salts of strong acids and bases and can be explained in terms of the effect of temperature upon the viscosity and density of water and upon the degree of dissociation of the salts. As the temperature increases from 0 to 800° the viscosity of water decreases very rapidly initially,[14,15] resulting in a sharp increase in the mobilities of the ions. Above approximately 300° the rate of decrease of viscosity with increasing temperature diminishes considerably,[16] and therefore the ionic mobilities do not increase as rapidly as at lower temperatures. The curves in Figure 5 reach maxima near 400° and then decrease with increasing temperature, indicating that factors other

(14) R. A. Robinson and R. H. Stokes, "Electrolyte Solutions," 2nd ed (revised), Butterworth and Co. Ltd., London, 1965, p 457.

(15) K. E. Bett and J. B. Cappi, *Nature*, 207, 620 (1965).

(16) K. H. Dudziak and E. U. Franck, *Ber. Bunsenges. Phys. Chem.*, 70, 1120 (1966).

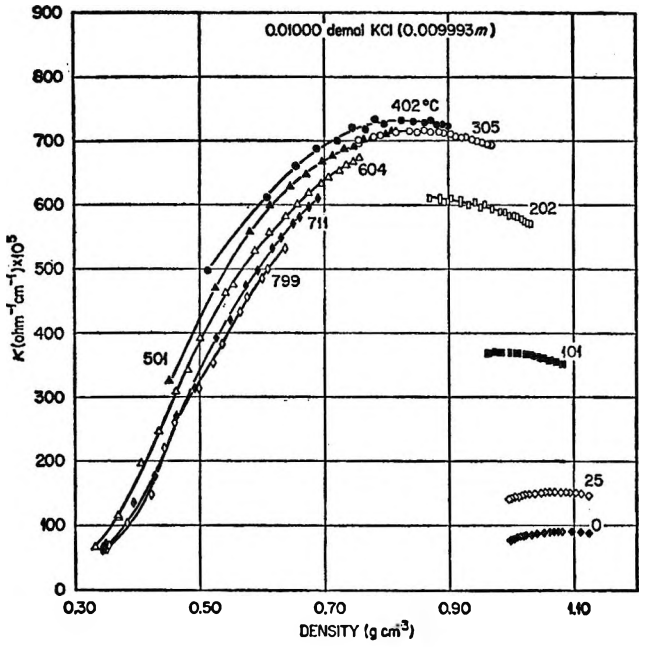


Figure 4. Specific conductances of 0.01000 demal (0.009993 m) KCl solutions as a function of density at several temperatures.

than viscosity must be considered at higher temperatures. Because the isobaric density of water decreases with increasing temperature,[17,18] this effect will reduce the number of ions per unit volume for a solution of constant molality and therefore will cause a decrease in specific conductance. It has also been found[9,10] that ionic association increases with increasing temperature; consequently, this effect will also reduce the number of ions per unit volume and, accordingly, the specific conductance. The maximum in isobaric specific conductance results when the increase in ionic mobility due to the viscosity effect is offset by a decrease in ionic concentration due to density and association effects.

The three sets of curves given in Figure 5 show a nearly consistent behavior, where at all temperatures the order of conductance is Rb^+, $K^+ > Cs^+ > Na^+ > Li^+$. As seen from these curves, the conductances of the rubidium and potassium ions are almost the same in these 0.01 m solutions. Below 200° there is practically no difference in the conductances of these two ions. Above 200° the rubidium ion appears to be more mobile in iodide and bromide solutions, but the potassium ion has the higher conductance in chloride solutions. However, at present we cannot find any significance in this change in relative behavior of these two ions since the variations are small and nearly within the limits of the experimental accuracy. Figure 6 compares the specific conductances of the alkali metal chlorides at a pressure of 1000 bars. The general features of this graph are similar to those observed at 4000 bars. Although not shown, the relative behavior at 1000 bars of the bromide and iodide solutions are the same as for the chloride solutions.

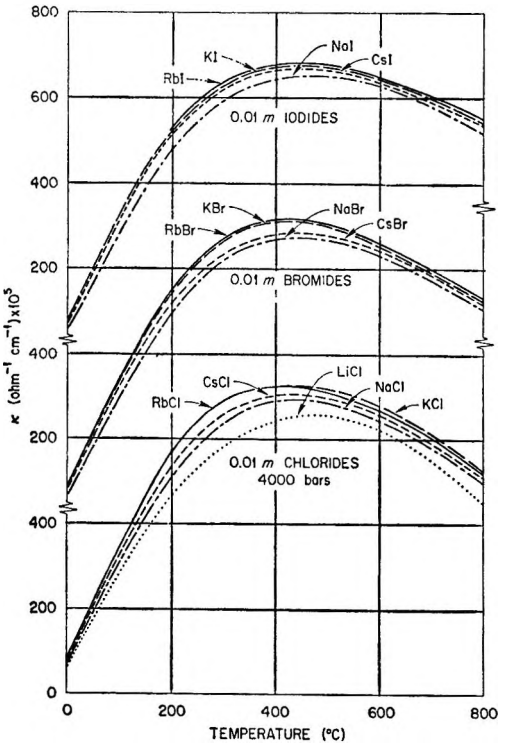


Figure 5. Isobaric specific conductances of 0.01000 m aqueous solutions of some alkali metal halides as a function of temperature; pressure = 4000 bars.

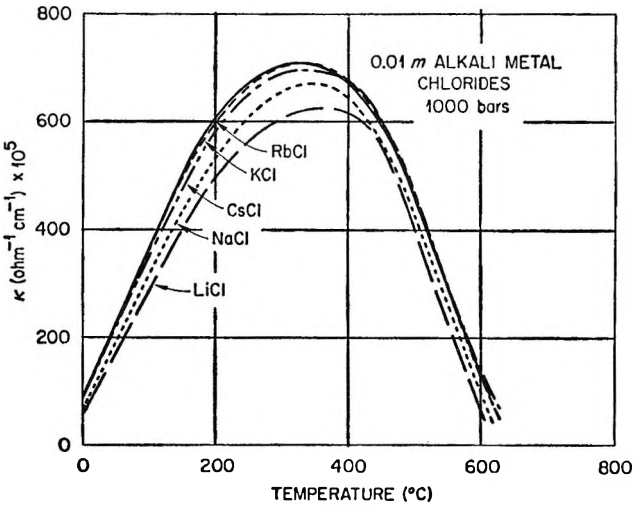


Figure 6. Isobaric specific conductances of 0.01000 m aqueous solutions of the alkali metal chlorides as a function of temperature; pressure = 1000 bars.

It is of interest to compare the relative conductances of the alkali metal ions as shown in Figure 5 at high temperatures and pressures with their corresponding behavior at room temperature and atmospheric pres-

(17) W. E. Sharp, "The Thermodynamic Functions for Water in the Range −10 to 1000° and 1 to 250,000 Bars," University of California Radiation Laboratory Report UCRL-7118, 1962.

(18) S. Maier and E. U. Franck, *Ber. Bunsenges. Phys. Chem.*, **70**, 639 (1966).

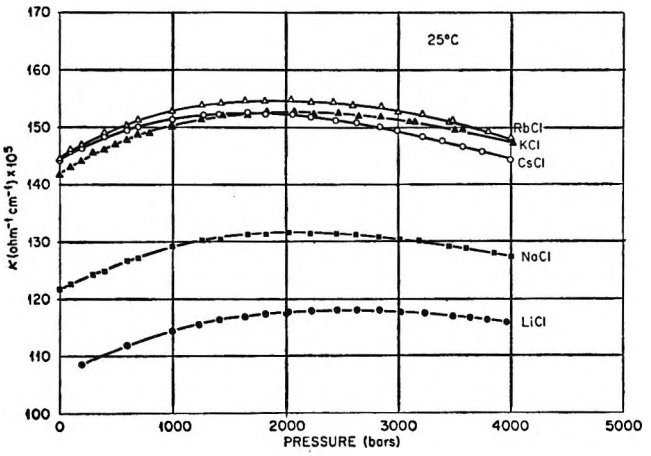


Figure 7. Isothermal specific conductances of 0.01000 *m* alkali metal chloride solutions as a function of pressure at 25°.

sure. At 25° and 1 atm, the *limiting* equivalent conductances of these ions are given by Robinson and Stokes[19] in the order Rb^+ (77.81) > Cs^+ (77.26) > K^+ (73.50) > Na^+ (50.10) > Li^+ (38.68). At 0° and 1 atm, the order is the same except that the conductances of the cesium ion and the rubidium ion are essentially equal. Figure 7 illustrates the effect of pressure on the conductances of the alkali metal chlorides at 25°.[20] This graph shows that the relative order of the conductances of the alkali metal ions changes as the pressure is increased from 1 to 4000 bars. Thus the cesium ion is more mobile than the potassium ion at 1 bar, but is less mobile at 4000 bars. Also, the difference between the mobility of the rubidium ion and the potassium ion decreases with increasing pressure. One approach to explain the change in order of conductances of the alkali metal ions with increasing temperature and pressure might be a correlation with their relative effects on the structure of water. In a discussion of ionic *B* coefficients (obtained from the Jones–Dole equation that describes the viscosity of electrolyte solutions as a function of electrolyte concentration), Stokes and Mills[21] described the cesium ion as having a large, disruptive effect on the structure of water in the immediate vicinity of the ion. This structure-breaking effect leads to a reduction in viscosity in the neighborhood of the ion and thus gives the cesium ion a greater mobility than it might be expected to have on the basis of ion size. Since increasing the pressure tends to break up the structure present in liquid water, the cesium ion will have less structure to break at high pressures and so its "excess" mobility will be diminished. The potassium ion has only a small effect on the structure of water and therefore the change in its conductance with increasing pressure is close to "normal." Consequently, when the pressure is increased, the conductance of the cesium ion near room temperature will decrease relative to that of the potassium ion. This behavior is observed in Figure 7. The rubidium ion is slightly structure breaking (a *B* coefficient midway between K^+ and Cs^+),

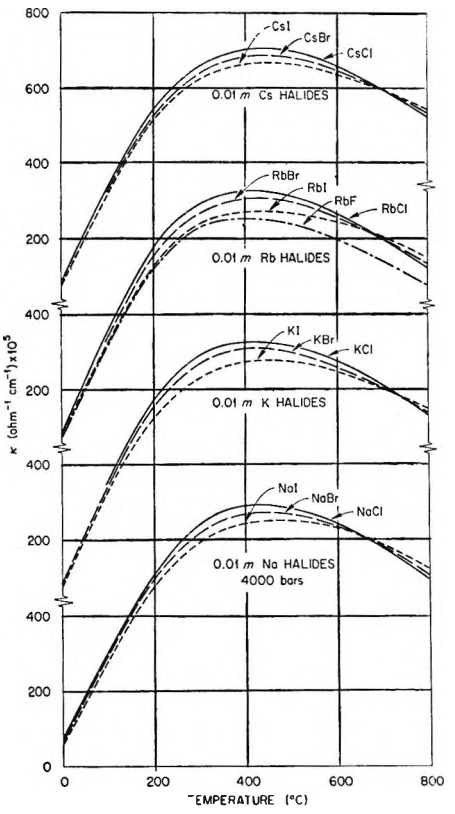


Figure 8. Isobaric specific conductances of 0.01000 *m* aqueous solutions of some alkali metal halides as a function of temperature; pressure = 4000 bars.

and therefore it also loses some of its excess mobility with increasing pressure. As seen in Figure 7, the conductance of the rubidium ion relative to that of the potassium ion has decreased until they are nearly the same at 4000 bars. A similar type of explanation can be used to describe the relative behavior of these ions with increasing temperature as the structure of water appears also to be broken down at elevated temperatures.[4-6] The much lower conductances of LiCl and NaCl in Figures 5–7 probably reflect chiefly a stronger hydration of Li^+ and Na^+ compared to K^+, Rb^+, and Cs^+, with Li^+ being the more hydrated of the two ions.[21]

Another comparison is given in Figure 8 where the alkali metal halides are grouped according to cation, and conductances are plotted as a function of temperature at a constant pressure of 4000 bars. Again, consistent behavior is observed for the four groups of curves. Below 600°, the order of conductance is Cl^- > Br^- > I^- > F^-. However, near 700°, there is a crossover, and the order is then I^- > Br^- > Cl^- > F^-. This type of behavior is also observed at lower pressures as shown in Figure 9 for the rubidium halides at 1000

(19) See ref 14, p 465.

(20) The effect of pressure on the conductance of a 0.01 *m* KCl solution at 25° agrees well with the results of W. A. Zisman, *Phys. Rev.*, 39, 151 (1932); A. J. Ellis, *J. Chem. Soc.*, 3689 (1959); and F. H. Fisher, *J. Phys. Chem.*, 66, 1607 (1962).

(21) R. H. Stokes and R. Mills, "Viscosity of Electrolytes and Related Properties," Pergamon Press, Oxford, 1965.

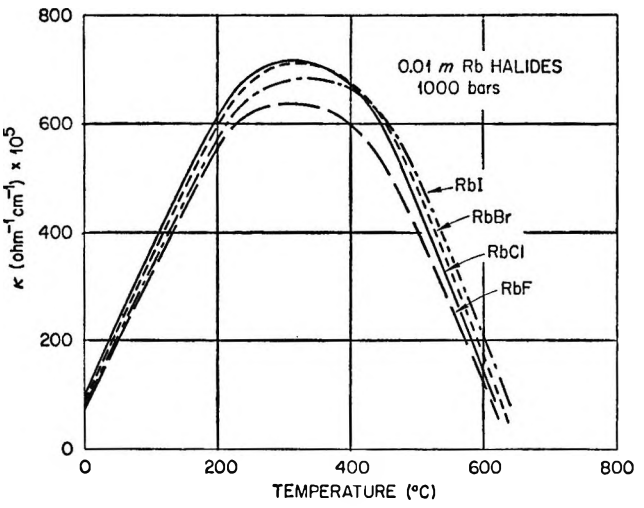


Figure 9. Isobaric specific conductances of 0.01000 *m* aqueous solutions of the rubidium halides as a function of temperature; pressure = 1000 bars.

bars. The change in order of conductance does not appear to be connected with any relative effects of the ions on the structure of water since most of the structure is probably destroyed before temperatures near 700° are reached. A reasonable explanation may relate to the differences in degree of association of these salts at high temperatures. Thus, as the salts become more associated with rising temperature,[10d,e] the different but increasing quantities of ions lost in the formation of the ion pairs will cause a proportionally greater difference in the respective conductances. This explanation requires that the 0.01 *m* chloride solutions contain more associated species than the corresponding bromide or iodide solutions. Sodium chloride is observed to be a weaker electrolyte than NaBr or NaI in the temperature range 400–800°.[10d,e,22] This behavior is also in agreement with the results of conductance studies on rubidium halides in water–dioxane mixtures, which indicate that the order of association is $Cl^- > Br^- > I^-$.[23] Therefore it is possible that, although the limiting conductance of the chloride ion may be larger than that of the bromide or iodide ion at 800° and 4000 bars, association effects may cause the conductance of 0.01 *m* chloride solutions to be less than the corresponding bromide or iodide solutions. Since crossovers were not observed (except for the questionable case of K^+ and Rb^+) when isobaric specific conductances *vs.* temperature plots were grouped according to anion (Figure 5), the behavior shown in Figure 8 may indicate that ionic association is more dependent on the anion than on the cation.

The relative conductances of the halide anions at elevated temperatures and pressures may be compared with their relative values near room temperature and atmospheric pressure. Aside from the crossovers near 700° (at 4000 bars) and 450° (at 1000 bars) discussed above, the order of conductance of the halide ions at elevated temperatures and pressures is $Cl^- > Br^- > I^- > F^-$. The order at 25° and 1 atm is[19] Br^- (78.14) > I^- (76.84) > Cl^- (76.35) > F^- (55.4), but at 55° it has changed to[19] Br^- (127.86) > Cl^- (126.40) > I^- (125.44) > F^-. Let us assume that the "normal" order, without regard to any influence of the ions on the structure of water, is given by the high-temperature results. Then the order found near 25° may be explained, as was the behavior of the cesium and rubidium ions, in relation to the effect of the bromide and iodide ions on the structure of water. Both of these halide ions have negative *B* coefficients, with that of the iodide ion being more negative than that of the bromide ion.[21] Thus both of these ions reduce the viscosity in their vicinity, leading to an excess mobility for these ions. The *B* coefficients become more positive with increasing temperature, indicating the diminution of this effect at higher temperatures and an approach to more "normal" behavior. As mentioned earlier, this approach to "normality" occurs because the structure of water is destroyed by increasing temperature, and consequently these ions have less or very little structure to break. Thus the iodide ion, with the larger excess mobility, has reached its normal position in the ranking of the halide ions when a temperature of 55° has been attained, but higher temperatures (and greater disruption of the water structure) are required in order that the mobility of the chloride ion exceeds that of the bromide ion.

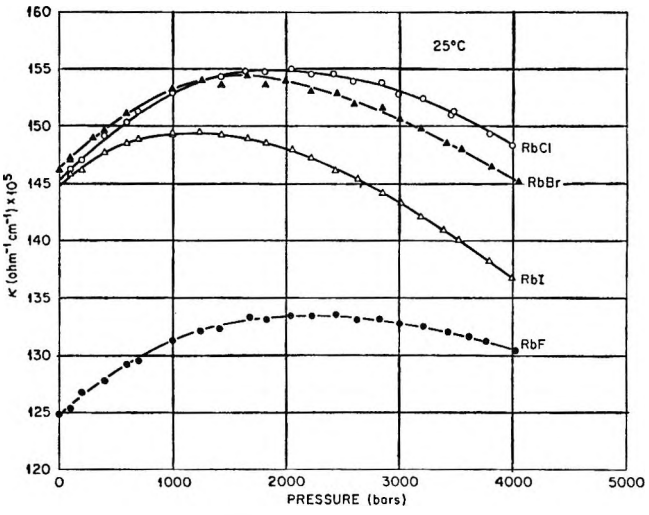


Figure 10. Isothermal specific conductances of 0.01000 *m* aqueous rubidium halide solutions as a function of pressure at 25°.

Figure 10 shows the effect of pressure on the specific conductances of the rubidium halides at 25°. Although the relative values for the conductances of the chloride and iodide ions at 1 bar are slightly different from literature values,[19] these differences are within the

(22) L. A. Dunn and W. L. Marshall, *J. Phys. Chem.*, **73**, 723 (1969).
(23) T. L. Fabry and R. M. Fuoss, *ibid.*, **68**, 974 (1964).

expected accuracy of our measurements. The relative behavior of the halide ions given in Figure 10 is consistent with predictions from a knowledge of the ionic B coefficients. Since increasing the pressure on water at 25° destroys its structure, at high pressures the structure-breaking ions, with little structure to break, will lose their excess mobility and become normal in behavior. Thus at high pressures at 25° the relative conductances of the halide ions change to the order that is observed at high temperatures. By analogy with the behavior of Li^+ and Na^+ (Figure 7), the much lower specific conductances of RbF probably reflect chiefly a stronger hydration of F^-, compared to the other anions, and thus a lower ionic mobility. The effect of pressure on the conductance of aqueous RbF, as shown in Figure 10, is consistent with the structure-making behavior of the fluoride ion as observed from viscosity studies.[24] Increasing pressure destroys the solvent structure, counteracting the solvent-ordering properties of the fluoride ion, and, consequently, increasing its conductance relative to the other ions. The relative behavior of LiCl at 25° (Figure 7) can be explained in a similar manner, since solvated Li^+ is considered to be a structure-making ion.

Summary

By comparing the effect of pressure on alkali metal halide conductances at 0 and 25°, it appears that most of the long-range structure of water has been destroyed by the time pressures of 4000 bars have been reached. These pressure effects at 0 and 25°, as well as the relative changes in conductance with increasing temperature, appear to be consistent with previously postulated structure-making and structure-breaking effects of ions as deduced from their viscosity B coefficients near room temperature and atmospheric pressure. However, this correlation is not all-restrictive, and other explanations may be found of equal or better plausibility.

At elevated temperatures, where there no longer appears to be any significant long-range water structure, the relative behavior of these ions remains constant—under all conditions when cation behavior is compared, and until appreciable but slightly different extents of association occur in the case of anions. Earlier quantitative results on NaCl[10d] and NaBr[10e] and recent results on NaI[22] indicated that the hydration numbers of these ions were unaffected by pressure and temperature from 400 to 800° and to 4000 bars. Therefore, the present measurements indicate that, for all of the alkali metal halides presently studied, the ion–solvent interactions remain constant in the temperature region 400–800°.

From the relative values of the conductances of these 0.01 m alkali metal halides at high temperatures and pressures, it should be possible to make good estimates of limiting equivalent conductances of these electrolytes based on the reported values for NaCl,[10d] NaBr,[10e] and NaI.[22] With these estimated values for Λ_0 and the conductances of the 0.01 m solutions presented in this paper, it is possible to estimate the degree of dissociation of each electrolyte at these supercritical temperatures and pressures.[9a] Although it is of interest to make Walden product comparisons for these electrolytes under supercritical conditions, the available viscosity data for water extend only to 560° and 3500 bars, and are reliable only to ±5%.[16] Previous work[10d] has indicated that correlation of the Walden product at high temperatures as a function of density is not as simple nor as useful as the correlation of Λ_0 *vs.* density.

Acknowledgment. It is a pleasure to acknowledge the technical assistance of Wiley Jennings in making most of the conductance measurements. We would also like to thank Dr. Fred Vaslow for supplying the sample of LiCl. One of the authors (A. S. Q.) would like to express thanks to Professor E. U. Franck, Institut für Physikalische Chemie, der Universität Karlsruhe, Germany, for his hospitality during the time this manuscript was completed.

(24) E. R. Nightingale and R. F. Benck, *J. Phys. Chem.*, 63, 1777 (1959).

Apparent Molal Heat Capacities of Aqueous Solutions of Alkali Halides and Alkylammonium Salts

by H. Rüterjans, F. Schreiner, U. Sage, and Th. Ackermann[1]

Institut für Physikalische Chemie der Universität Münster, Münster (Westfalen), Schlossplatz 4, Germany *(Received May 27, 1968)*

Specific heats of aqueous solutions of various alkali halides (LiCl, KCl, KF, CsCl, and CsI) and alkylammonium salts (CH_3NH_3Cl, $C_2H_5NH_3Cl$, and $(n\text{-}C_4H_9)_4NBr$) have been measured in the temperature range of 30–130° with an adiabatic calorimeter. The apparent molal heat capacities ${}^{\Phi}C_p$ evaluated from the heat capacity data are negative in the case of the investigated alkali halides and positive in the case of the alkylammonium salts. The temperature dependence of ${}^{\Phi}C_p$ reveals a maximum at about 50–90° for all cases except $(n\text{-}C_4H_9)_4NBr$. Approximate values for the partial molal heat capacities $\bar{C}_{p2}^{\circ}$ can be obtained by extrapolation of ${}^{\Phi}C_p$ to infinite dilution. The influence of the dissolved salts on the solvent structure and the contribution of the solvent–solute interaction to the partial molal heat capacities are discussed.

Introduction

Within the past several years there has been an increasing interest in the structure of water and especially the structure of water around polar and nonpolar groups.[2] From various theoretical models, thermodynamic properties of water and of aqueous solutions have been calculated.[3–6] Usually the standard-state functions, *i.e.*, at infinite dilution, have been evaluated; therefore the experimentally determined partial molal heat capacities $\bar{C}_{p2}^{\circ}$ at infinite dilution and as a function of temperature are of considerable importance. The known thermodynamic functions at 25° can be extended to higher temperatures by use of partial molal heat capacities over the desired temperature range.

There are several methods proposed and used for obtaining values of $\bar{C}_{p2}^{\circ}$. For aqueous solutions of electrolytes, various authors[7,8] have obtained values for the apparent molal heat capacities, ${}^{\Phi}C_p$, from accurate heat capacity measurements. This quantity is related to $\bar{C}_{p2}$ by the expressions

$$\bar{C}_{p2} = {}^{\Phi}C_p + n_2 \frac{\partial {}^{\Phi}C_p}{\partial n_2}$$

$$\bar{C}_{p2} = {}^{\Phi}C_p + \tfrac{1}{2} m^{1/2} \frac{\partial {}^{\Phi}C_p}{\partial m^{1/2}}$$

where n_2 is the number of moles of solute and m is the molality of the solution. Hence,[7] at infinite dilution

$$\bar{C}_{p2}^{\circ} = {}^{\Phi}C_p^{\circ}$$

It is a convenient experimental fact that for most substances ${}^{\Phi}C_p$ varies linearly with $m^{1/2}$ over a wide concentration range (0.05–3.0 m).[7,9] Although the experimental slopes in this concentration range may differ considerably from the predicted theoretical slopes of the Debye–Hückel theory, extrapolations are made to infinite dilution thus obtaining approximate values of $\bar{C}_{p2}^{\circ}$. For a large number of electrolytes, values of $\bar{C}_{p2}^{\circ}$ at 25° have been determined in this way.[7]

Only a few precise calorimetric studies of heat capacities as a function of temperature have been reported. Eigen and Wicke[8] first obtained values of $\bar{C}_{p2}^{\circ}$ for NaCl, LiBr, and $MgCl_2$ over a wide range of temperatures from heat capacity data. In addition, for HCl,[10] NaOH,[11] some carboxylic acids, and their sodium salts,[12] values of $\bar{C}_{p2}^{\circ}$ have been determined as a function of temperature from accurate heat capacity measurements.

Criss and Cobble[13] used another method for obtaining standard-state partial molal heat capacities of electrolytes as a function of temperature. This method employs heats of solution measurements. Integral heats of solution are determined at a series of concentrations and temperatures. From the extrapolated

(1) To whom correspondence should be addressed.

(2) E. Wicke, *Angew. Chem., Int. Ed.*, **5**, 106 (1966); *Angew. Chem.*, **78**, 1 (1966).

(3) G. Nemethy and H. A. Scheraga, *J. Chem. Phys.*, **36**, 3382 (1962).

(4) A. Eucken, *Nachr. Akad. Wiss. Göttingen, Math.-Phys. Kl., IIa. Math.-Phys. Chem. Abt.*, 38 (1946); *Z. Elektrochem.*, **52**, 255 (1948); **53**, 102 (1949).

(5) (a) R. P. Marchi and H. Eyring, *J. Phys. Chem.*, **68**, 221 (1964); (b) C. M. Davis and T. A. Litovitz, *J. Chem. Phys.*, **42**, 2563 (1965).

(6) K. Buijs and G. R. Choppin, *ibid.*, **40**, 3120 (1964).

(7) H. S. Harned and B. B. Owen, "The Physical Chemistry of Electrolytic Solutions," 3rd ed, Reinhold Publishing Corp., New York, N. Y., 1958, pp 78, 349.

(8) M. Eigen and E. Wicke, *Z. Elektrochem.*, **55**, 354 (1951).

(9) F. T. Gucker, Jr., *Ann. N. Y. Acad. Sci.*, **51**, 680 (1949).

(10) E. Wicke, M. Eigen, and Th. Ackermann, *Z. Phys. Chem.* (Frankfurt), **1**, 340 (1954).

(11) Th. Ackermann, *Z. Elektrochem.*, **62**, 411 (1958).

(12) Th. Ackermann and F. Schreiner, *ibid.*, **62**, 1143 (1958).

(13) C. M. Criss and J. W. Cobble, *J. Amer. Chem. Soc.*, **83**, 3223 (1961); R. E. Mitchell and J. W. Cobble, *ibid.*, **86**, 5401 (1964); J. C. Ahluwalia and J. W. Cobble, *ibid.*, **86**, 5377 (1964); E. C. Jekel, C. M. Criss, and J. W. Cobble, *ibid.*, **86**, 5404 (1964).

values of the heat of solution at infinite dilution, values of $\bar{C}_{p2}^{\circ}$ as a function of temperature have been calculated for $BaCl_2$, NaCl, CsI, $NaReO_4$, $HReO_4$, and $GaCl_3$.[13] Since the values of $\bar{C}_{p2}^{\circ}$ obtained by the two methods are derived in entirely different ways, it is a good confirmation of the validity of the data that the temperature dependence of the values of $\bar{C}_{p2}^{\circ}$ for NaCl found by either method is in good agreement.[8,13]

In the present paper we report additional heat capacity measurements with an adiabatic calorimeter. The partial molal heat capacities of LiCl, KCl, KF, CsCl, CsI, CH_3NH_3Cl, and $C_2H_5NH_3Cl$ at infinite dilution and as a function of temperature are evaluated from the calorimetric data.

Experimental Section

Apparatus. The heat capacity measurements were carried out with recording adiabatic calorimeters. For a detailed description of the apparatus and experimental procedure, the reader is referred to the literature.[14–16]

Materials and Filling Procedure. For preparing the solutions, doubly distilled water was used throughout. The electrolytes were purchased from E. Merck A.G., Darmstadt (KCl, LiCl, CsCl, CsI, CH_3NH_3Cl, and $C_2H_5NH_3Cl$), Riedel-DeHaen, Seelze (KF), and Fluka A.G., Buchs, Switzerland [$(n\text{-}C_4H_9)_4NBr$]. They were reported to be of highest purity and were used without further purification. Three or four solutions of different molality were prepared for each electrolyte by dissolving an accurately weighed amount of electrolyte in the corresponding amount of water. After each experiment the molality of the solution was found to be unchanged from the original values.

Approximately 275 ml of the solutions was put into the calorimeter vessel[16] thus allowing the solution to expand into a space of 20–30 ml when heated. To remove all dissolved gases, the calorimeter vessel was quickly evacuated and then sealed under the liquid's own vapor pressure. Because of the small vapor space of 20–30 ml, the measured heat capacity should be corrected to obtain the desired heat capacity C_p, *i.e.*, under constant pressure.

The measured quantity

$$C_{p_{sat}} = \left(\frac{dq}{dT}\right)_{sat}$$

includes as well the heat capacity of the vapor and also an amount which is attributed to the vaporization of a small fraction of the liquid. If we denote q_{vap} as the heat of vaporization and x as the fraction of vapor, we obtain for the measured heat capacity

$$C_{p_{sat}} = \left(\frac{dq}{dT}\right)_{sat} = (1 - x)C_{p_{sat\ liq}} + xC_{p_{sat\ vap}} + q_{vap}\frac{dx}{dT}$$

In this equation the second term on the right-hand side is extremely small and can be neglected. The first term is equal to $C_{p_{sat\ liq}}$, whereas the third term may be large.

The conversion of the heat capacity under vapor pressure $C_{p_{sat}}$ to the heat capacity under constant pressure C_p can be achieved with the formula[17]

$$C_p - C_{p_{sat}} = T\left(\frac{\partial v}{\partial T}\right)_p\left(\frac{\partial p}{\partial T}\right)_{sat}$$

For the difference, $C_p - C_{p_{sat}}$, the data for water yield a value of 0.0046 cal/deg mol at 373°K, or about 0.03% of the total heat capacity.

These corrections can be neglected here because in a blank experiment with pure water we determine the heat capacity of the calorimeter vessel applying the correct values of C_p of Osborne, Stimson, and Ginnings.[14–16] Thus all corrections which have to be made are implicit in the heat capacity of the calorimeter vessel.

Results

The measured specific heat values of the solutions are converted to the apparent molal heat capacities according to the formula

$$^{\Phi}C_p = \frac{c_{p_{sol}}(1000 + mM_2) - 1000c_{p_{H_2O}}}{m}$$

where m is the molality of the solute of molecular weight M_2 and $c_{p_{sol}}$ and $c_{p_{H_2O}}$ are the specific heats of the solution and pure solvent, respectively.

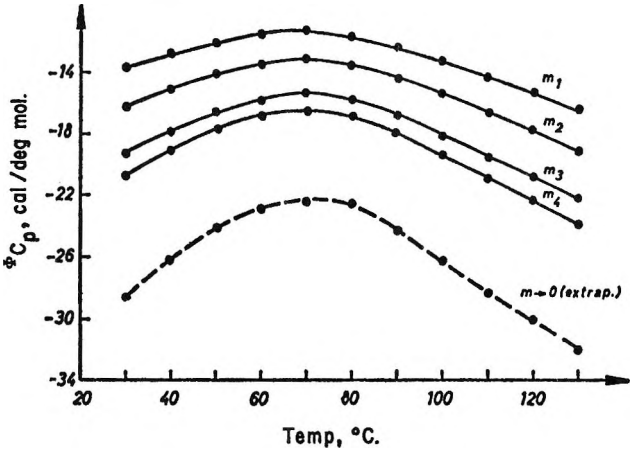


Figure 1. Apparent molal heat capacities of KCl plotted against temperature: $m_1 = 1.804$; $m_2 = 1.250$; $m_3 = 0.717$; $m_4 = 0.509$ (m = mol/kg of H_2O).

(14) A. J. B. Cruickshank, P. A. Giguere, and Th. Ackermann, "Experimental Thermodynamics," Vol. 1, J. P. McCullough and D. W. Scott, Ed., Butterworth and Co. Ltd., London, 1968, Chapter 12.

(15) Th. Ackermann, *Z. Elektrochem.*, **62**, 411 (1958).

(16) Th. Ackermann and H. Rüterjans, *ibid.*, **68**, 850 (1964).

(17) G. N. Lewis and M. Randall, "Thermodynamics," 2nd ed, revised by K. S. Pitzer and L. Brewer, McGraw-Hill Book Co., Inc., New York, N. Y., 1961, p 65.

Table I: Apparent Molal Heat Capacities of Alkali Halides and Alkylammonium Salts in Aqueous Solutions[a]

CsCl

Temp, °C	Concn, mol/kg of H_2O 1.606	1.084	0.498	Extrap
30	−22.7	−24.8	−27.1	−32.6
40	−20.3	−22.3	−24.3	−29.4
50	−18.3	−20.2	−22.1	−26.8
60	−17.0	−18.7	−20.6	−25.2
70	−16.2	−17.9	−19.8	−24.4
80	−15.6	−17.3	−19.2	−23.8
90	−15.4	−17.2	−19.2	−24.0
100	−15.6	−17.5	−19.6	−24.6
110	−15.9	−17.9	−20.3	−25.7
120	−16.2	−18.5	−21.1	−27.0
130	−16.7	−19.2	−22.0	−28.6

CsI

Temp, °C	Concn, mol/kg of H_2O 1.652	1.066	0.517	Extrap
30	−17.8	−21.0	−25.1	−34.3
40	−16.7	−19.5	−23.0	−31.0
50	−15.7	−18.2	−21.3	−28.5
60	−15.0	−17.3	−20.2	−26.8
70	−14.6	−16.7	−19.4	−25.5
80	−14.6	−16.6	−19.3	−25.3
90	−14.8	−16.9	−19.6	−25.7
100	−15.0	−17.2	−19.9	−26.0
110	−15.4	−17.5	−20.2	−26.4
120	−15.6	−17.8	−20.6	−26.9
130	−16.0	−18.2	−21.0	−27.3

LiCl

Temp, °C	Concn, mol/kg of H_2O 1.755	0.969	0.497	Extrap
30	−8.3	−10.0	−11.4	−14.8
40	−7.2	−8.7	−10.0	−13.0
50	−6.2	−7.6	−8.7	−11.5
60	−5.7	−7.0	−8.0	−10.6
70	−5.6	−6.7	−7.7	−10.0
80	−5.7	−6.9	−8.0	−10.6
90	−6.2	−7.5	−8.7	−11.5
100	−6.8	−8.3	−9.5	−12.5
110	−7.6	−9.1	−10.4	−13.4
120	−8.5	−10.1	−11.3	−14.6
130	−9.4	−11.1	−12.5	−15.9

KCl

Temp, °C	Concn, mol/kg of H_2O 1.804	1.250	0.717	0.509	Extrap
30	−13.7	−16.3	−19.3	−20.7	−28.7
40	−12.8	−15.1	−17.8	−19.1	−26.2
50	−12.1	−14.1	−16.5	−17.7	−24.1
60	−11.5	−13.4	−15.8	−16.8	−22.8
70	−11.3	−13.2	−15.4	−16.4	−22.3
80	−11.7	−13.5	−15.7	−16.7	−22.5
90	−12.4	−14.4	−16.8	−17.9	−24.3
100	−13.2	−15.4	−18.1	−19.3	−26.2
110	−14.2	−16.5	−19.5	−20.8	−28.3
120	−15.3	−17.7	−20.7	−22.2	−30.0
130	−16.3	−19.1	−22.1	−23.7	−32.1

KF

Temp, °C	Concn, mol/kg of H_2O 1.576	1.048	0.800	0.497	Extrap
30	−12.0	−14.5	−16.0	−18.0	−25.4
40	−10.1	−12.7	−14.0	−15.9	−22.6
50	−9.0	−11.4	−12.6	−14.3	−20.8
60	−8.3	−10.4	−11.5	−13.0	−19.3
70	−8.0	−9.9	−10.9	−12.3	−18.2
80	−8.1	−9.9	−10.8	−12.3	−18.1
90	−8.5	−10.5	−11.5	−12.9	−18.9
100	−8.8	−11.1	−12.1	−13.7	−20.3
110	−9.3	−12.1	−13.4	−15.2	−23.6
120	−10.0	−13.4	−15.4	−18.2	−27.0
130	−11.0	−17.5	−18.0	−21.2	−34.1

CH_3NH_3Cl

Temp, °C	Concn, mol/kg of H_2O 2.010	1.300	0.745	Extrap
0	−0.5	−2.5	−3.6	−9.6
10	2.7	0.3	−0.5	−6.4
20	4.9	2.9	2.3	−3.2
30	6.7	5.1	4.5	−0.4
40	8.6	7.1	6.6	2.0
50	10.1	8.6	8.1	3.4
60	11.3	10.1	9.2	4.5
70	12.0	10.9	9.9	5.5
80	12.5	11.5	10.4	6.0
90	12.6	11.7	10.6	5.8
100	12.7	11.2	10.2	4.3
110	12.2	10.1	9.0	1.5
120	11.5	8.2	7.1	−3.0

$C_2H_5NH_3Cl$

Temp, °C	Concn, mol/kg of H_2O 2.000	1.250	0.749	Extrap
0	...	...	...	(1.8)
10	21.5	17.6	15.3	8.1
20	23.8	20.7	19.2	12.5
30	26.1	24.0	22.8	16.8
40	28.0	26.4	25.1	19.9
50	29.5	28.1	29.0	22.4
60	30.4	29.2	28.3	24.4
70	30.9	29.7	29.0	25.6
80	30.6	29.4	28.8	25.5
90	29.8	28.5	28.0	24.8

$(n\text{-}C_4H_9)_4NBr$

Temp, °C	Concn, mol/kg of H_2O 0.688	0.476	0.327
10	288.5	292.0	288.3
20	279.7	284.7	276.4
30	270.9	276.6	270.0
40	263.1	268.9	265.3
50	256.0	262.8	260.7
60	250.4	257.0	256.6
70	245.3	251.8	253.3
80	240.7	247.0	250.1
90	236.0	241.9	246.7
100	231.4	236.9	243.5
110	226.4	230.9	239.8
120	221.0	225.1	234.6
130	215.1	218.9	228.0

[a] All values of ${}^{\Phi}C_{p2}$ have the dimensions cal/mol deg.

Values of ${}^{\Phi}C_p$ obtained in this way are listed in Table I and are shown graphically for three or four different concentrations of KCl, CH_3NH_3Cl, and $(n\text{-}C_4H_9)_4NBr$ in Figures 1–3.

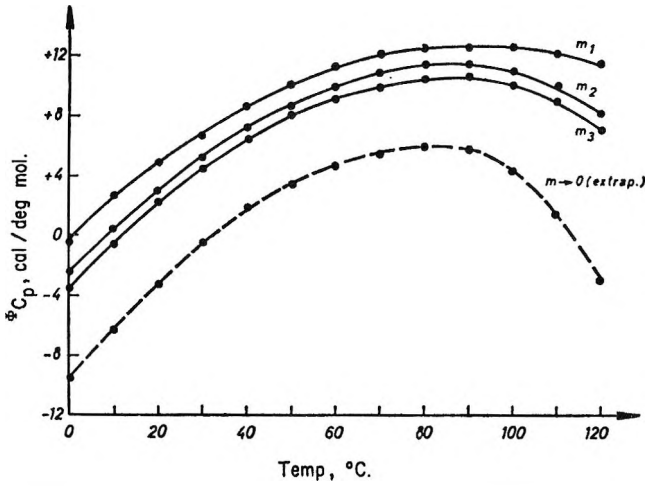


Figure 2. Apparent molal heat capacities of CH_3NH_3Cl plotted against temperature: $m_1 = 2.010$; $m_2 = 1.300$; $m_3 = 0.745$ (m = mol/kg of H_2O).

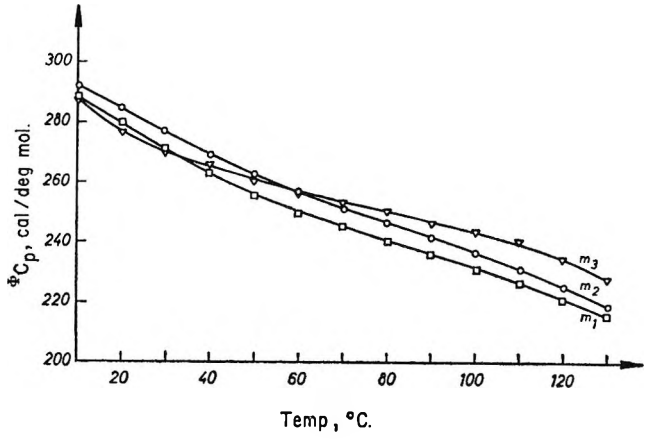


Figure 3. Apparent molal heat capacities of $(n\text{-}C_4H_9)_4NBr$ plotted against temperature: $m_1 = 0.688$; $m_2 = 0.476$; $m_3 = 0.327$ (m = mol/kg of H_2O).

Since the apparent molal heat capacities at infinite dilution are equal to the partial molal heat capacities, the concentrations are chosen such that the values of ${}^{\Phi}C_p$ may be extrapolated to infinite dilution. With the exception of tetra-*n*-butylammonium bromide, all investigated electrolytes display a linear dependence of ${}^{\Phi}C_p$ *vs.* $m^{1/2}$ at all temperatures examined. As an example, the data for KCl are plotted in this way in Figure 4.

The slope A of the relationship ${}^{\Phi}C_p$ *vs.* $m^{1/2}$ according to

$$ {}^{\Phi}C_p = {}^{\Phi}C_p^{\circ} + A\sqrt{m} $$

$$ ({}^{\Phi}C_p^{\circ} = \bar{C}_{p2}^{\circ}) $$

is not the same as the slope calculated from the Debye–Hückel theory,[7] but from very accurate heat capacity

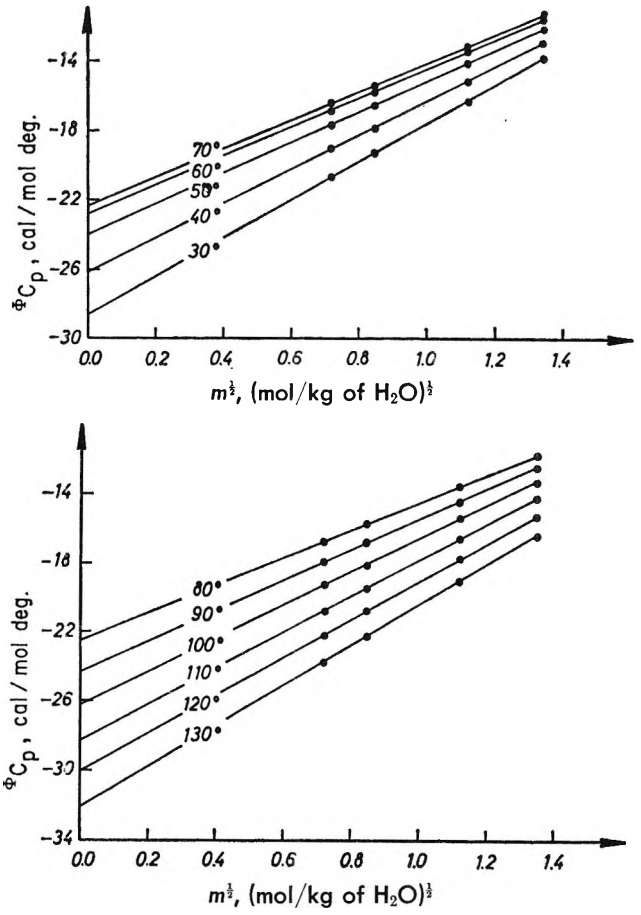


Figure 4. Apparent molal heat capacities of KCl plotted against the square root of molality for different temperatures.

measurements of Gucker[9] it can be shown that the empirical relationship between ${}^{\Phi}C_p$ and $m^{1/2}$ is valid at least to a concentration of 0.05 mol/1000 g of H_2O. The difference between the empirically found slope A and the theoretically calculated slope should only give a small correction to the extrapolated value of ${}^{\Phi}C_p^{\circ}$ or $\bar{C}_{p2}^{\circ}$, since, although there might be a considerable difference between the numerical values of the slopes, the correction of $\bar{C}_{p2}^{\circ}$ or ${}^{\Phi}C_p^{\circ}$ should not exceed ± 0.5 cal/mol deg. On the other hand, the theoretically calculated slopes of ${}^{\Phi}C_p$ *vs.* $m^{1/2}$ at infinite dilution depend strongly on the first and second temperature derivative of the dielectric constant of water, and the slopes themselves therefore are uncertain to about 50%.[7]

The linearly extrapolated values of ${}^{\Phi}C_p^{\circ}$ or $\bar{C}_{p2}^{\circ}$ are also listed in Table I and are indicated by the dashed lines in Figures 1 and 2 for KCl and CH_3NH_3Cl. For tetra-*n*-butylammonium bromide, a linear dependence between ${}^{\Phi}C_p$ and $m^{1/2}$ is not found (Figure 5), and hence extrapolated values of $\bar{C}_{p2}^{\circ}$ are not obtained.

Values of $\bar{C}_{p2}^{\circ}$ at 25° are known for several alkali halides.[18] We have not measured $\bar{C}_{p2}^{\circ}$ at 25° for these

(18) V. B. Parker, "Thermal Properties of Aqueous Univalent Electrolytes," National Standard Reference Data Series, National Bureau of Standards 2, Category B, Washington, D. C., 1965.

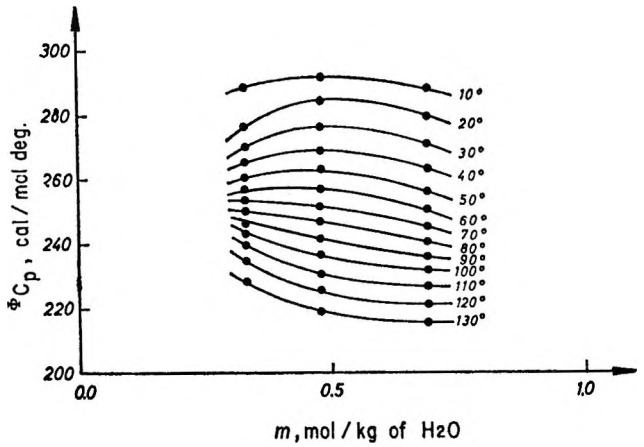


Figure 5. Apparent molal heat capacities of $(n\text{-}C_4H_9)_4NBr$ plotted against molality for different temperatures.

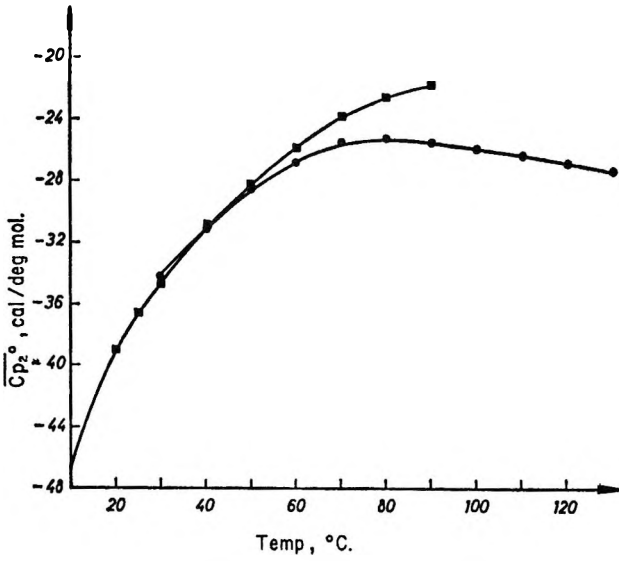


Figure 6. Comparison of values for the partial molal heat capacities C_{p2}° of aqueous cesium iodide obtained by the "integral heat" method (■) and by heat capacity measurements (●).

electrolytes. However, an extrapolation of our data to 25° reveals values which are in most cases not much different from those obtained previously at 25°. As for the temperature dependence of $\bar{C}_{p2}^{\circ}$, Mitchell and Cobble[13] published data for CsI between 0 and 100°. These data, which were obtained by the "integral heat" method are in very good agreement with our data (Figure 6).

Discussion

a. Alkali Halide Solutions. The partial molal heat capacities $\bar{C}_{p2}^{\circ}$ of all investigated alkali halides are negative and display a maximum in the temperature dependence. With increasing molecular weight or with increasing ionic radius the values of $\bar{C}_{p2}^{\circ}$ become more negative in the range of 30–70°, whereas above 70° this order seems to be reversed.

The essential features of the results shown in Figures 7 and 8 may be explained by using recent theoretical models of water structure.[3-6] Using a concept of Frank and Wen,[19] Nemethy and Scheraga[3] developed a model of water structure in which water consists of clusters of tetrahedrally coordinated water molecules. These clusters contain about 90 to 25 water molecules depending on temperature. Between these clusters, they assume that the water molecules are unbonded or only slightly bonded.

Generally the hydration[20] of ions is described in terms of two concentric shells. In the inner shell the water molecules are oriented by the field of the ion. This region is about one water molecule thick. In the second layer the field of the ionic charge does not have a dominant influence on the arrangement of the water molecules but the normal water structure, *i.e.*, containing clusters, is disrupted because of the geometrical arrangements of the ions with the first hydration layer. Beyond the second layer, water has essentially its normal structure. The number of water molecules in the second layer and the thickness of the shell are subject to question. In general there will be a varying number of water molecules in this layer depending on the amount of water in the first shell and on the size and the charge of the ion. The discussion of the partial molal heat capacities will deal mainly with this second hydration shell, since one would expect that this second layer, and of course the difference of the thermodynamic behavior of water in this layer with respect to undisturbed water, contributes the main part of the differences in the standard state partial molal heat capacities of the various electrolytes.

The magnitudes of the partial molal heat capacities $\bar{C}_{p2}^{\circ}$ at various temperatures will essentially depend upon the sum of the following two main contributions.

1. When the temperature of the solution is raised, an increasing amount of energy is required for the dissociation of water molecules from the hydration shells around the ion. This contribution to the partial molal heat capacity, $\bar{C}_{p2}^{\circ}$, is positive and may amount to several hundred cal/mol deg. This effect depends strongly on temperature and may decrease at higher temperatures, since we assume that below 130° only water molecules from the second hydration layer are dissociating, whereas the water molecules of the first hydration shell, which are bound by strong ion–dipole interaction are essentially unaffected. If this assumption proves correct, a second maximum in $\bar{C}_{p2}^{\circ}$, should be expected above 130°, due to the dissociation of the first hydration shell.

2. Since a considerable amount of water is bound to the ions, the structure of normal water is no longer maintained in these solutions. The clusters are de-

(19) H. S. Frank and W. Y. Wen, *Discussions Faraday Soc.*, 24, 133 (1957).

(20) (a) H. S. Frank and M. J. Evans, *J. Chem. Phys.*, 13, 507 (1945); (b) H. S. Frank, *Proc. Roy. Soc.*, A247, 481 (1958).

composed to smaller aggregates also because of the geometrical requirements, which make the existence of large clusters between the hydrated ions unlikely. For this reason, less energy is needed to decompose the remaining clusters than in normal water. This effect implies a large but negative contribution to $\bar{C}_{p2}^{\circ}$. With increasing temperature the difference between the water structure in the electrolyte solution and in pure water decreases and the "pure solvent" contribution to $\bar{C}_{p2}^{\circ}$ becomes less negative.

Compared to these two main contributions to $\bar{C}_{p2}^{\circ}$ the contribution of the ions themselves is small, namely, about 12 cal/mol deg, and is assumed to be independent of temperature. Of course this holds only for small ions, which only have three translational degrees of freedom. For larger ions such as ReO_4^- the partial molal heat capacity is positive due to their rotational and vibrational degrees of freedom.[13] If there were no influence on the water structure by the ions this part would of course be the main contribution to the partial molal heat capacity at infinite dilution. With the above-mentioned concepts of the contributions to the partial molal heat capacities, the results in Figures 7 and 8 may easily be interpreted.

1. All alkali halides listed in Figures 7 and 8 display negative values of $\bar{C}_{p2}^{\circ}$ over the entire temperature range of 30–120° in accordance with the fact that the structure of normal water is disrupted. However, this does not mean that all alkali halides are mainly "structure breaking."[2,19] Since various ions have different degrees of hydration, the net amount of structure (*i.e.*, hydrogen bond formation, in the tetrahedral form or in the nontetrahedral form) may be larger or smaller than in normal water.

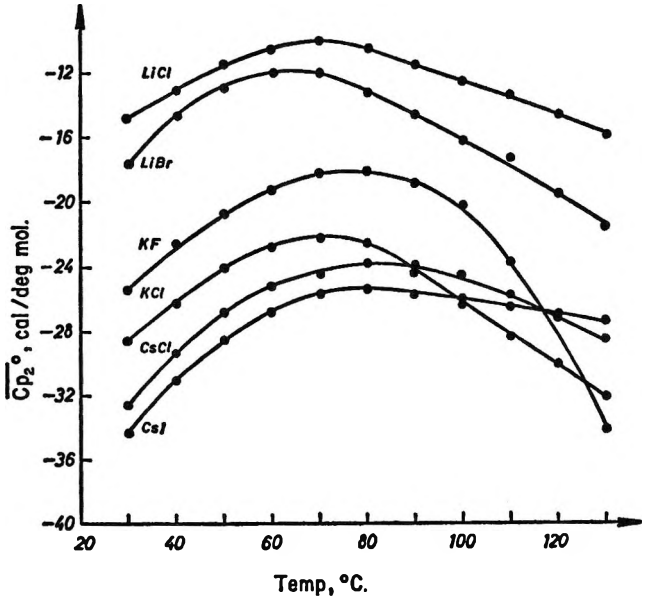


Figure 7. Partial molal heat capacities C_{p2}° of alkali halides plotted against temperature (LiCl, KF, KCl, CsCl, and CsI from this work; LiBr from Eigen and Wicke[8]).

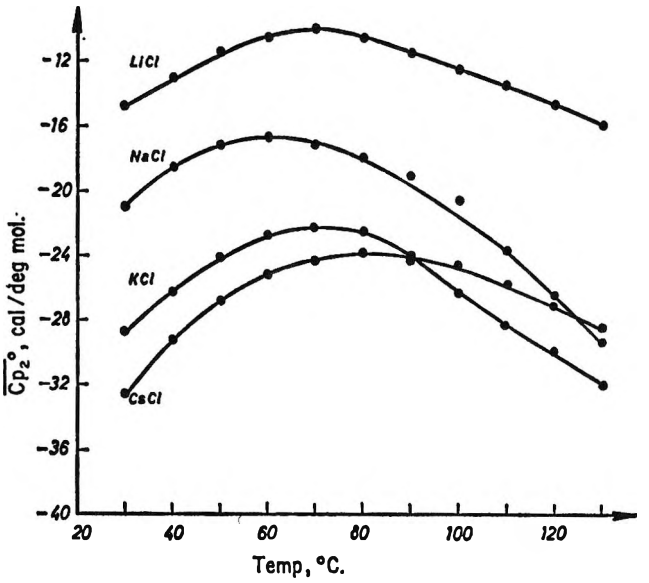


Figure 8. Partial molal heat capacities C_{p2}° of alkali chlorides plotted against temperature (LiCl, KCl, and CsCl from this work; NaCl from Eigen and Wicke[8]).

2. A maximum in the partial molal heat capacity at elevated temperatures can only be explained by the degradation of a hydration shell, which is bound with not too much energy to the ions. This degradation process starts at room temperature and is completed in most cases at 130°. It makes for, as already discussed, a positive contribution to the partial molal heat capacity.

3. Between room temperature and the temperature of the maximum (60–80°) the partial molal heat capacities are more negative with increasing size of the ions. If we assume that at room temperature all ions are equally hydrated. *i.e.*, that there are two intact hydration shells around the ions, but with the difference that with increasing ionic radius these hydration shells contain more water molecules and hence require a larger volume, then less space and fewer water molecules are left to form the normal water structure. Therefore less energy is required to disrupt the bulk water structure, and the partial molal heat capacities become more negative. This is consistent with other experimental evidence that ions of large size are mainly "structure breaking."

4. At higher temperatures (100–130°) all partial molal heat capacities are decreasing. Most electrolytes display a more negative value at 130° than at 30°. This should justify the assumption that the first hydration layer is essentially still unaffected at 130°. If the first layer were to be decomposed at 120°, the partial molal heat capacity would not have such negative values. It is also remarkable that in the series KF, KCl, CsCl, CsI the partial molal heat capacity at 130° becomes more *positive* with increasing ionic radius. This can be interpreted in the following way. At 130° the second hydration layer is decomposed, and in the case of KF

and KCl, the first hydration layer is still unaffected. As for CsI and possibly also for CsCl (due to the contribution of the cesium ion), the decomposition of the first layer seems to begin around 100°. Thus the partial molal heat capacity of CsI only decreases slightly from the point of the maximum up to 130°due to the positive contribution of the beginning of the decomposition of the first hydration layer. The relatively high value of $\bar{C}_{p2}°$ for LiCl at 130° can be explained by the incomplete decomposition of the second hydration layer of the lithium ion which still needs considerable energy for the disruption of the structure of that shell at this temperature. So far nothing has been said about the respective contributions of the cation and anion to the extrapolated values of $\bar{C}_{p2}°$. At the present time this can be done only with some arbitrariness because of the uncertainties of the physical properties of single ions in solution. Such a division has been attempted by Eigen and Wicke[8] for NaCl, LiBr, and $MgCl_2$ for the temperature range of 0–130°.[21] They used a concept of Eucken based on the structure of pure water and of water in ionic solutions. The difference in the ionic radii of the cations and anions are taken into account by assuming a relatively small energy change for anions and a large energy change for cations for the dissociation process of the second hydration layer.

The result of their calculation is that the small cations Li^+, Na^+, and Mg^{2+} display positive contributions to the partial molal heat capacity, which decrease with increasing temperature, whereas the large anions Cl^- and Br^- yield negative contributions, which become less negative with increasing temperature. This means that the anions Cl^- and Br^- are structure breaking and the cations Li^+, Na^+, and Mg^{2+} are structure making. The authors report a calculated value of $\bar{C}_{p2}°$ for the chloride ion of -41 cal/mol deg at 30°. From the experimentally determined partial molal heat capacity of KCl (Table I), it follows that the contribution of the potassium ion to the value of $\bar{C}_{p2}°$ of KCl is 12 cal/mol deg. This again yields a value of $\bar{C}_{p2}°$ of -37 cal/mol deg for the fluoride ion. Thus at 30° there is a difference of 49 cal/mol deg between the ionic contributions of K^+ and F^- in the partial molal heat capacity of KF. At higher temperatures this difference is remarkably large also.

In discussing this large difference it is striking that the ionic radii of both ions are nearly equal (1.33 Å for K^+ and 1.36 Å for F^-).[22] The hydration energy of the F^- ion is larger (119 cal/mol) than that of the K^+ ion (79 cal/mol).[23] Moreover, the limiting ionic mobility is smaller for the F^- ion (54.4 cm^2 ohm^{-1}) than for the K^+ ion (73.5 cm^2 ohm^{-1}).[24] All of these values indicate that the F^- ion should be hydrated at least as much as the potassium ion. Hence the large difference in the partial molal heat capacities of the two ions does not seem to be justified. However, the partial molal heat capacities are certainly a good starting point for a theoretical consideration of the ion–water interaction.

b. Alkyl ammonium Salt Solutions. In order to get some information about the influence of nonpolar solutes on the structure of water, it would be desirable to know values of $\bar{C}_{p2}°$ of hydrocarbons as the corresponding model compounds for this class of substances. However, because of the slight solubility of hydrocarbons in water it is not possible to determine the partial molal heat capacity of these nonpolar solutes by heat capacity measurements of the kind described in the present work. Instead, we have utilized alkylammonium salts in which the nonpolar alkyl chain is connected with a polar group to increase the solubility. The difficulty arises as to how the values of $\bar{C}_{p2}°$ can be divided into the contribution of the alkyl chain and the positive ammonium group. Also the partial molal heat capacity of the Cl^- ion is not known as has been discussed above. This difficulty can be overcome in measuring $\bar{C}_{p2}°$ of a homologous series of compounds in which the alkyl chain is increased by a CH_2 group in going from one member to the next higher one. The difference in $\bar{C}_{p2}°$ of the two alkylammonium salts can then be attributed to the CH_2 group, and we shall denote this difference as the partial molal heat capacity of a CH_2 group ($C_{p(-CH_2-)}°$).

As already mentioned, the apparent molal heat capacities of NH_3CH_3Cl and $C_2H_5NH_3Cl$ display a linear dependence on the square root of concentration; hence the partial molal heat capacity $\bar{C}_{p2}°$ can be obtained by extrapolation. The temperature dependence of $\bar{C}_{p2}°$ is similar to that of the other electrolytes (Figure 9). A maximum is observed in both cases at 70–90°. The partial molal heat capacity of methylammonium chloride increases from a value of -2 cal/mol deg at 25° to a maximum value of about 6 cal/mol deg and decreases again at higher temperatures. The partial molal heat capacity of $C_2H_5NH_3Cl$ displays a very similar temperature dependence, except that its value is about 18–20 cal/mol deg larger than the value of $\bar{C}_{p2}°$ of CH_3HN_3Cl. Hence, the partial molal heat capacity of a CH_2 group is about 18–20 cal/mol deg over the whole temperature range studied.

In contrast to the behavior of all previously investigated electrolytes, the apparent molal heat capacity of tetra-*n*-butylammonium bromide does not vary linearly with the square root of concentration, as is

(21) C. M. Criss and J. W. Cobble, *J. Amer. Chem. Soc.*, 86, 5390 (1964), reported average heat capacities for ions up to 200°. Qualitatively these are in agreement with the division made by Eigen and Wicke in that cations exhibited positive values while the anions had negative values. However, the cations become more positive and the anions more negative with increasing temperature, in contrast to the argument put forth by Eigen and Wicke.

(22) L. Pauling, "The Nature of the Chemical Bond," 3rd ed, Cornell University Press, Ithaca, N. Y., 1959, p 514.

(23) A. Eucken, "Lehrbuch der chemischen Physik," Vol. 2, Leipzig, 1943.

(24) Landolt-Börnstein, "Zahlenwerte und Funktionen," Vol. II, 6th ed, Part 7, p 259.

Table II: Data for the Evaluation of Molal Heat Capacities for a CH_2 Group in either Pure or Dissolved State at 25° (All Data Have the Dimensions cal/mol deg)

Molecule	Partial molal heat capacity C_{p2}°	Partial molal heat capacity $C_{p(-CH_2-)}^\circ$	Molecule	Molal heat capacity C_p	Molal heat capacity $C_{p(-CH_2-)}$
HCOOH	21.5[a]		HCOOH(l)	23.7[c]	
		20.5			5.8
CH_3COOH	42.0[a]		CH_3COOH(l)	29.5[c]	
		16.8			8.6
C_2H_5COOH	58.8[a]		C_2H_5COOH(l)	38.1[d]	
		16.7			7.2
n-C_3H_7COOH	75.5[b]		n-C_3H_7COOH(l)	45.3[e]	
HCOONa	−5.5[a]		HCOOH(g)	11.6[f]	
		15.0			5.8
CH_3COONa	9.5[a]		CH_3COOH(g)	17.4[g]	
		31.2			
C_2H_5COONa	40.7[a]				
			CH_4	8.5[h]	
					4.1
CH_3NH_3Cl	−2.0		C_2H_6	12.6[h]	
		16.6			5.0
$C_2H_5NH_3Cl$	14.6		C_3H_8	17.6[h]	

[a] Ackermann and Schreiner.[12] [b] C. R. Bury and D. G. Davies, *J. Chem. Soc.*, 2413 (1932) (15°). [c] F. D. Rossini, "Selected Values of Chemical Thermodynamic Properties," U. S. Government Printing Office, Washington, D. C., 1952. [d] Landolt-Börnstein, "Physikalische-Chemische Tabellen," Part 3, Berlin, 1936. [e] C. D. Hodgman, Ed., "Handbook of Chemistry and Physics," 40th ed, Chemical Rubber Publishing Co., Cleveland, Ohio, 1958. [f] W. Waring, *Chem. Rev.*, 51, 171 (1952). [g] J. O. Halford, *J. Chem. Phys.*, 10, 582 (1942). [h] F. D. Rossini, *et al.*, "Selected Values of Properties of Hydrocarbons," U. S. Government Printing Office, Washington, D. C., 1947.

demonstrated in Figure 5. There are at least two possible reasons for this behavior. On the one hand, tetra-*n*-butylammonium bromide may not be completely dissociated in the solution so that contributions to ${}^\Phi C_{p2}$ may arise from the dissociation process, which may vary with concentration. On the other hand, the big cation requires such a large space that in concentrated solutions the average distance between two molecules may be only equivalent to one water molecule. In this case the structure of the solvent cannot be considered as being homogeneous, and the apparent molal heat capacity may depend on the concentration of the solute in quite another way than is observed for the other electrolytes. However, the strong temperature dependence of ${}^\Phi C_{p2}$ (decreasing values of ${}^\Phi C_p$ with increasing temperature) at all investigated concentrations indicates that the water structure in these solutions is reduced when the temperature of the solution is increased. Because of the unknown dependence on concentration, an extrapolation of ${}^\Phi C_{p2}$ to infinite dilution was not attempted.

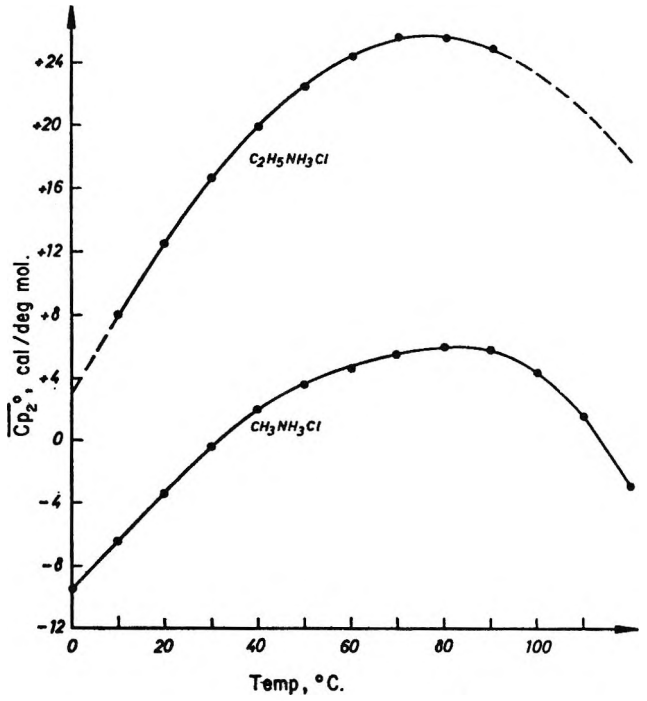


Figure 9. Partial molal heat capacities C_{p2}° of alkylammonium salts plotted against temperature.

A previous determination of $\bar{C}_{p(-CH_2-)}^\circ$ for a CH_2 group has been carried out by Ackermann and Schreiner for the series formic acid, acetic acid, and propionic acid.[12] By measuring $\bar{C}_{p2}^\circ$ of the sodium salts of these carboxylic acids, they also obtained values of $\bar{C}_{p2}^\circ$ for the CH_2 group. All of these data, together with the results of the alkylammonium salts (Figure 9), are listed in Table II for 25°. It is striking that in most cases the partial molal heat capacity for a CH_2 group is about 15–20 cal/mol deg, although the polar groups, which are nearest to the alkyl chains, are different and therefore might be differently hydrated. It seems that the polar group with its hydration spheres does not have a large influence upon the contribution of the nonpolar part of the molecule to $\bar{C}_{p2}^\circ$.

It is interesting to compare the differences in the

heat capacities of the pure carboxylic acids with $C_{p(-CH_2-)}°$. In Table II, the values of C_p are presented for the whole series in the liquid state and for monomeric HCOOH and CH_3COOH, in both the liquid and gaseous states, from which the differences $C_{p(-CH_2-)}$ are readily evaluated. For comparison, the values of C_p of the gaseous hydrocarbons CH_4, C_2H_6, and C_3H_8 are listed also in Table II.

All data for the pure fatty acid series (either in the liquid or in the gaseous state) as well as for the hydrocarbons display values of $C_{p(-CH_2-)}$ of 4–9 cal/mol deg.

This implies that the partial molal heat capacity of a CH_2 group in aqueous solution exhibits an additional contribution of 7–11 cal/mol deg, which can be attributed to the interaction of the nonpolar CH_2 group with the solvent.

According to the concepts of water structure,[2-6] the explanation of this additional *positive* contribution to $\bar{C}_{p2}°$ can only be that the degree of structural order of water around a nonpolar alkyl chain is increased. When the temperature of the solution is raised, more energy than in normal water is required to melt the regions of increased hydrogen bonding around the nonpolar group; hence, this additional part of $\bar{C}_{p2}°$ is positive.

This type of water structure in the surroundings of a nonpolar solute, the so-called hydration of the second kind,[25] gives an explanation for the fact that hydrocarbons dissolve in water with negative heat of solution. However, nonpolar solutes are only slightly soluble in water. The positive free energy of solution arises from a large negative entropy of solution. Frank and Evans introduced the concept of "iceberg formation" around nonpolar solutes.[20a] Some authors have interpreted this by assuming an increased amount of *tetrahedral* hydrogen bonding.[26] In contradiction to this assumption, however, there is some experimental evidence from chemical shift measurements of the water protons in such solutions.[27,28] This latter evidence has led Wicke[2] to propose the existence of nontetrahedral hydrogen bonds in the environment of the nonpolar group. It seems that at the present time there are not enough experimental data available to settle the question of what sort of hydrogen bonds are present in water and in such aqueous solutions.[28] In view of both our measurements and other experimental results it can only be said that the introduction of a nonpolar hydrocarbon molecule into water leads to an increase in the degree of ordering of the water and the extent of hydrogen bonding.

With increasing temperature one would expect that the structural regions around the nonpolar group are being decomposed, and, in fact, the positive additional contribution to $\bar{C}_{p2}°$ for a CH_2 group justifies this assumption. It is interesting to observe that in all investigated homologous series $\bar{C}_{p(-CH_2-)}°$ remains constant for the whole temperature range considered. A possible reason for this result would be that the contribution to $\bar{C}_{p2}°$ from the CH_2 group itself may become larger due to the activation of vibrational degrees of freedom, whereas the part of $\bar{C}_{p(-CH_2-)}°$ which arises from the interaction of the nonpolar solute with water may decrease because of the preceding decomposition of the regions of higher order of the water.

From Figure 3 it is seen that the apparent molal heat capacities of tetra-*n*-butylammonium bromide strongly decrease with increasing temperature. Although this quantity contains contributions from the mutual interactions of the dissolved molecules, this strong decrease in ${}^{\Phi}C_{p2}$ with temperature should arise from the diminishing contribution of the decomposition process for the regions, which have more structure than normal water.

Acknowledgment. We wish to thank the Deutsche Forschungsgemeinschaft for a grant.

(25) H. G. Hertz, *Ber. Bunsenges. Phys. Chem.*, **68**, 907 (1964).
(26) G. Nemethy and H. A. Scheraga, *J. Chem. Phys.*, **36**, 3401 (1962).
(27) H. G. Hertz and W. Spalthoff, *Z. Elektrochem.*, **63**, 1096 (1959).
(28) H. H. Rüterjans and H. A. Scheraga, *J. Chem. Phys.*, **45**, 3296 (1966).

Spectrofluorometric Studies. IV. Some New Aspects of the Photochemistry of Monofluorobenzene

by M. E. MacBeath, G. P. Semeluk, and I. Unger

Department of Chemistry, University of New Brunswick, Fredericton, New Brunswick, Canada *(Received June 20, 1968)*

The photochemistry of monofluorobenzene in the vapor phase has been examined over a range of wavelengths extending from 2350 to 2710 Å. The sensitized emission of biacetyl was used to determine triplet-state yields for exciting wavelength of 2470, 2550, 2590, and 2670 Å. The effect of cyclohexane on the fluorescence yield and on the sensitized emission yield has been examined. $\Phi_{singlet} + \Phi_{triplet} = 0.67$ at $\lambda_{ex} = 2470$ Å; this sum is 0.75 at $\lambda_{ex} = 2550$ Å, 0.93 at $\lambda_{ex} = 2590$ Å, and 0.82 at $\lambda_{ex} = 2670$ Å. A mechanism consistent with the experimental observations is presented.

Introduction

Monofluorobenzene (FB) lends itself very well to photochemical investigation for several reasons: the molecule does not dissociate when irradiated in the 2500-Å spectral region;[1] its absorption in this region is relatively strong;[2] it exhibits fluorescent emission very similar to, and in the same region as, that of benzene;[3] its triplet state lies very close to that of benzene;[4] it has four distinct absorption maxima between 2400 and 2700 Å,[2] which makes it possible to examine differences in photochemical behavior due to transition into four relatively closely spaced vibrational levels; and the presence of a heavy atom has a tendency to increase the lifetime of the excited state.[5] Unger[3] applied the sensitized emission of biacetyl (BiA) technique[6,7] to FB excited at 2537 Å and reported a triplet yield of about 0.90 while the sum of triplet plus singlet yield was given as 1.13. The fact that the total quantum yield exceeded unity combined with a possible error due to the "around the corner effect"[8] prompted Phillips[9] to reexamine the photochemistry of FB using the Cundall technique[10,11] as a diagnostic for the triplet state. The total quantum yield of singlet and triplet was given as 1.05 ± 0.09 by Phillips, still distressingly higher than unity. We felt that it was of interest systematically to investigate the photochemical behavior of FB as a function of exciting wavelength and to try to resolve some of the anomalies reported in the two previous investigations.[3,9]

Experimental Section

Materials. The monofluorobenzene used was obtained from the Aldrich Chemical Co. Vpc analysis showed this material to be essentially pure. The biacetyl was also obtained from Aldrich, stored in a dark bulb, and purified just prior to use by bulb-to-bulb distillation *"in vacuo."* The benzene was fluorometric grade obtained from Hartman-Leddon Co. and used without further purification. The cyclohexane, obtained from the same company, was also fluorometric grade.

The high-vacuum line employed in this study was a grease- and mercury-free line using Hoke packless diaphragm metal valves exclusively. Pressure measurements were performed by means of a spiral gauge constructed at the National Research Council in Ottawa. Pressures below 3 Torr were measured by allowing a relatively large pressure into the gauge and then expanding into the previously calibrated line containing the cell and mixing pump, and also into a large calibrated flask when necessary. A flow-through cell, cuvette type, 1 × 1 × 4.5 cm high and polished on four sides, was used. Mixing was accomplished by means of an all-glass circulating pump constructed at the National Research Council in Ottawa.

Emission measurements were performed on a modified[12] Aminco-Bowman spectrophotofluorometer (SPF), obtained from the American Instrument Co. Inc. The entrance slit of the excitation monochromator was set at 0.5 mm and the exit slits were set at 1.0, 0.5, and 1.0 mm. This combination of slits allowed a band pass of approximately 70 Å which, although fairly large, was necessary in order to obtain sufficient light intensity. Two entrance slits were used on the emission monochromator, both set at 1.0 mm and the exit slit on this monochromator was also 1.0 mm. These slit arrangements were

(1) O. P. Semenova and G. S. Tsikunov, *Zh. Fiz. Khim.*, **18**, 311 (1944).

(2) W. F. Forbes, *Can. J. Chem.*, **37**, 1977 (1959); S. H. Wollman, *J. Chem. Phys.*, **14**, 123 (1946).

(3) I. Unger, *J. Phys. Chem.*, **69**, 4284 (1965).

(4) D. F. Evans, *J. Chem. Soc.*, 2753 (1959).

(5) E. C. Wu and O. K. Rice, *J. Phys. Chem.*, **72**, 542 (1968).

(6) H. Ishikawa and W. A. Noyes, Jr., *J. Amer. Chem. Soc.*, **84**, 1502 (1962).

(7) H. Ishikawa and W. A. Noyes, Jr., *J. Chem. Phys.*, **37**, 583 (1962).

(8) W. A. Noyes, Jr., and C. S. Burton, International Conference on Photochemistry, Munich, Sept 6–9, 1967.

(9) D. Phillips, *J. Phys. Chem.*, **71**, 1839 (1967).

(10) R. B. Cundall, F. G. Fletcher, and D. G. Milne, *Trans. Faraday Soc.*, **60**, 1146 (1964).

(11) R. B. Cundall and A. S. Davis, *ibid.*, **62**, 1151 (1966).

(12) F. W. Ayer, F. Grein, G. P. Semeluk, and I. Unger, *Ber. Bunsenges. Physik. Chem.*, **72**, 282 (1968).

found to give a minimum of scattered light as well as good reproducibility. Experimental details concerning the light source, emission, and absorption measurements have been given previously.[12]

To obtain the quantum yields of fluorescence of FB and the sensitized emission of BiA from the data obtained in our system, a relative method was used and has been described elsewhere.[3] To use this method it is necessary to calibrate the instrument with a reference material whose quantum yield of fluorescence has been accurately determined and whose spectral range is close to that of FB. Benzene satisfied both of these requirements very well. Thus all fluorescent yields reported in this paper are based on a fluorescent quantum yield of benzene being 0.183[13] and all triplet yields are based on a triplet yield of benzene of 0.63.[14]

The extinction coefficient for FB varies from 8 to 700 over the wavelength range in this study. At the higher values, even in the small cell used in this study, there is a possibility of error due to the "around the corner effect." In view of this, Beer's law was used to calculate the light absorbed in the central portion of the cell from which emission was viewed.[15] Since the extinction coefficient also varies with pressure, it was determined at every pressure used.

The phosphorescent emission from biacetyl falls in the same region as the second-order light from the fluorescence of FB and, unless compensated for, could lead to artificially high sensitized emission yields. Blank runs were carried out with FB and the percentage of fluorescence transmitted as second order was determined. Then using the figure obtained above, for any mixture of FB and BiA, this second-order contribution was calculated and subtracted from the total emission.

Results

Fluorescence Measurements. The variation of fluorescent quantum yield of FB as a function of exciting wavelength is shown graphically in Figure 1. The yield is

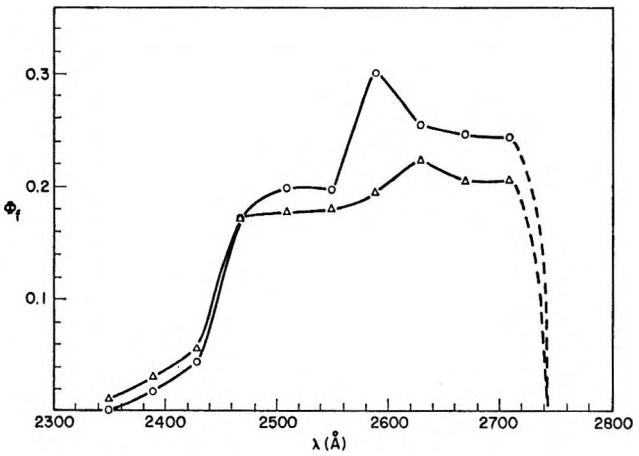


Figure 1. Variation of fluorescence quantum yield as a function of exciting wavelength: ○, 5 Torr of FB; △, 40 Torr of FB.

Table I: Variation of Φ_f and $1/\Phi_f$ as a Function of FB Concentration at Various Exciting Wavelengths

$\lambda_{excitation}$, Å	Equation of line	Press. range of FB, Torr
2390	$\Phi_f = 0.015 + 0.011 \times 10^3$[FB] ±28.3%, max 33.2%	5.5–48
2430	$\Phi_f = 0.043 + 0.008 \times 10^3$[FB] ±6.45%, max 12.8%	3.5–49
2470	$1/\Phi_f = 5.84 + 0.004 \times 10^3$[FB] ±3.02%, max 10.4%	3.6–49
2510	$1/\Phi_f = 5.05 + 0.261 \times 10^3$[FB] ±2.18%, max 5.6%	3.6–48
2550	$1/\Phi_f = 5.10 + 0.298 \times 10^3$[FB] ±1.54%, max 2.78%	3.4–48
2590	$1/\Phi_f = 2.96 + 0.988 \times 10^3$[FB] ±1.02%, max 2.09%	3.4–48
2630	$1/\Phi_f = 3.87 + 0.298 \times 10^3$[FB] ±0.64, max 1.86%	3.0–48
2670	$1/\Phi_f = 3.93 + 0.447 \times 10^3$[FB] ±0.87%, max 2.80%	3.0–48
2710	$1/\Phi_f = 3.89 + 0.429 \times 10^3$[FB] ±3.12%, max 3.56%	2.7–48

≃0 at 2350 Å, it rises to a value of about 0.20 at 2500 Å (depending on pressure), and it varies little from this point until 2710 Å. Several other features are worth noting. At 2470 Å the fluorescence yield is pressure independent; below this wavelength plots of Φ_f *vs.* [FB] are linear with positive slope; see Table I. Above 2470 Å plots of $1/\Phi_f$ *vs.* [FB] are linear and exhibit a positive slope; see Table I. (The errors reported in the tables are for any individual run; day to day reproducibility is of the order of 15%.) At low pressure a maximum in fluorescent yield occurs at 2590 Å. It should be emphasized here that the self-quenching shown above 2470 Å is not an artifact since only the light absorbed in that portion of the cell being viewed by the emission monochromator was considered in calculating fluorescent yields.

The fluorescence of FB is quenched more strongly by BiA than by itself; these data are summarized in Table II. In all cases plots of $1/\Phi_f$ *vs.* [BiA], at constant [FB], are linear. Addition of cyclohexane to FB increases the fluorescent yield when λ_{ex} is 2470 Å but does not affect this yield for any of the other exciting wavelengths

(13) W. A. Noyes, Jr., W. A. Mulac, and D. A. Harter, *J. Chem. Phys.*, **44**, 2100 (1966).
(14) W. A. Noyes, Jr., and D. A. Harter, *ibid.*, **46**, 674 (1967).
(15) J. L. Durham, G. P. Semeluk, and I. Unger, *Can. J. Chem.*, **46**, 3177 (1968).

Table II: Variation of $1/\Phi_f$ as a Function of BiA Concentration, at Constant FB Concentration, for Various Exciting Wavelengths

$\lambda_{excitation}$, Å	Equation of line[a]	Press. range of BiA, Torr
2470	$1/\Phi_f = 6.02 + 7.72 \times 10^3$[BiA] ±2.38%, max 6.20%	0.1–29
2550	$1/\Phi_f = 5.49 + 7.74 \times 10^3$[BiA] ±1.39%, max 5.8%	0.1–20
2590	$1/\Phi_f = 2.49 + 4.51 \times 10^3$[BiA] ±2.53%, max 6.72%	0.1–20
2670	$1/\Phi_f = 3.64 + 7.33 \times 10^3$[BiA] ±1.45%, max 2.85%	0.1–20

[a] FB pressure constant at 5 Torr.

examined; typical data obtained are shown in Figure 2 and in Table III.

Sensitized Emission Measurements. The triplet yield of FB excited at 2470, 2550, 2590, and 2670 Å was determined using the sensitized emission of biacetyl technique. Three types of experiments were performed at the four wavelengths mentioned above. (a) The FB pressure was held constant at 5 Torr and the BiA pressure was varied. Plots of $1/\Phi_p$ *vs.* [BiA] go through a minimum at about 10 Torr of BiA and then become linear. The data are summarized graphically in Figure 3. (b) The BiA pressure was held constant at 5 Torr

Table III: Effect of Cyclohexane on the Fluorescence Yield and Sensitized Emission Yield of FB in BiA–BF Mixtures for Various Exciting Wavelengths

$\lambda_{excitation}$, Å	Φ_f	Φ_p	Pressure, Torr: CH	FB	BiA
2470	0.108	0.23	0.0	10.0	5.0
	0.117	0.28	5.14	10.0	5.0
	0.127	0.24	10.28	10.0	5.0
	0.127	0.32	20.56	10.0	5.0
	0.127	0.33	30.07	10.0	5.0
2550	0.118	0.37	5.42	10.0	5.0
	0.120	0.36	10.42	10.0	5.0
	0.116	0.38	20.49	10.0	5.0
	0.122	0.40	30.49	10.0	5.0
2590	0.237	0.44	4.72	10.0	5.0
	0.239	0.46	9.79	10.0	5.0
	0.237	0.46	19.79	10.0	5.0
	0.241	0.44	29.93	10.0	5.0
2670	0.178	0.40	0.0	9.93	5.0
	0.179	0.39	5.21	9.93	5.0
	0.178	0.42	10.21	9.93	5.0
	0.176	0.39	20.07	9.93	5.0
	0.181	0.40	30.07	9.93	5.0

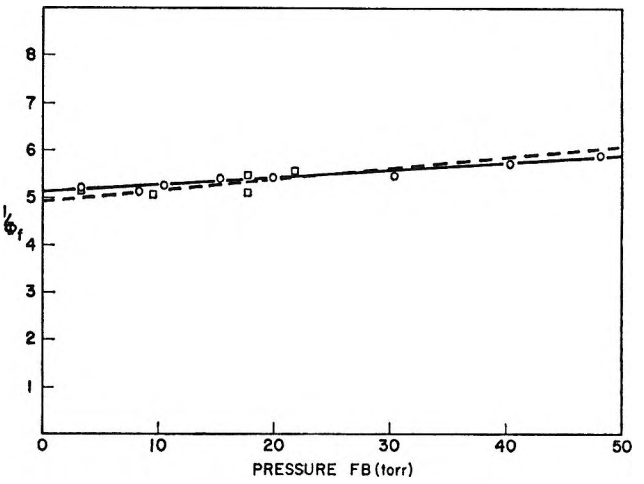


Figure 2. Variation of fluorescence yield of FB as a function of FB concentration, ○, and as a function of FB concentration in the presence of 50 Torr of cyclohexane, □; $\lambda_{excitation}$ = 2550 Å.

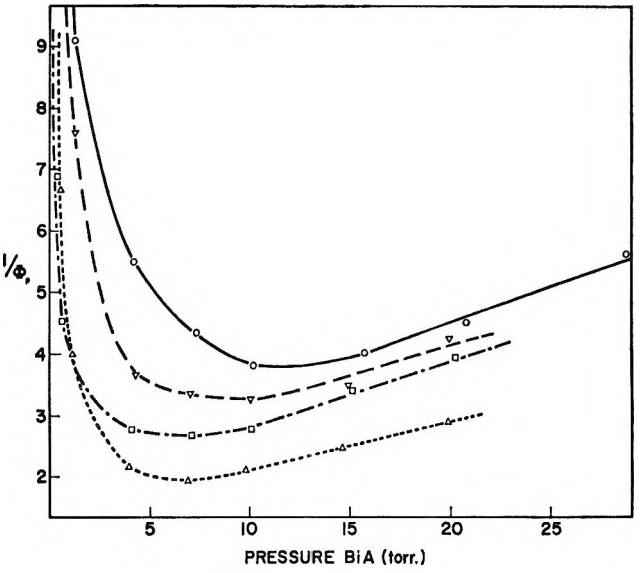


Figure 3. Variation of $1/\Phi_p$ *vs.* BiA pressure; FB pressure constant at 5 Torr: ○, 2470 A; ◑, 2550 Å; △, 2590 A; □, 2670 A.

and the FB pressure varied. Plots of $1/\Phi_p$ *vs.* pressure of FB go through a minimum at about 10 Torr of FB and then become linear; see Table IV. (c) The FB pressure was held constant at 10 Torr, the BiA pressure was held constant at 5 Torr, and the sensitized emission yield was measured as a function of increasing cyclohexane (CH) pressure; Φ_p increases with increasing CH pressure at λ_{ex} = 2470 Å but is not affected by CH at the other exciting wavelengths; see Table III.

Discussion

Our experimental observations combined with the known photochemical behavior of biacetyl[16] lead us to

(16) W. A. Noyes, Jr., and I. Unger, *Advan. Photochem.*, **4**, 49 (1966), and references therein.

postulate the following mechanism, for exciting wavelength greater than 2470 Å.

$$FB + h\nu \longrightarrow {}^1FB^I \quad (1)$$

$${}^1FB^I \longrightarrow FB + h\nu \quad (2)$$

$${}^1FB^I(+M) \longrightarrow {}^3FB^I(+M) \quad (3)$$

$${}^1FB^I + FB \longrightarrow 2FB \quad (4)$$

$${}^1FB^I \longrightarrow \text{isomerization} \quad (5)$$

$${}^3FB^I(+M) \longrightarrow FB(+M) \quad (6)$$

$${}^1FB^I + BiA \longrightarrow {}^1BiA^{II} + FB \quad (7)$$

$${}^3FB^I + BiA \longrightarrow {}^3BiA^{I*} + FB \quad (8)$$

$${}^3BiA^{I*} \longrightarrow \text{dissociation} \quad (8a)$$

$${}^3BiA^{I*} + M \longrightarrow {}^3BiA^I + M \quad (8b)$$

$${}^1BiA^{II} \longrightarrow \text{dissociation} \quad (9)$$

$${}^1BiA^{II} + M \longrightarrow {}^1BiA^I + M \quad (10)$$

$${}^1BiA^I \longrightarrow {}^3BiA^I \quad (11)$$

$${}^1BiA^I \longrightarrow BiA + h\nu_f \quad (12)$$

$${}^3BiA^I \longrightarrow BiA + h\nu_p \quad (13)$$

$${}^3BiA^I \longrightarrow BiA \quad (14)$$

$${}^3FB^I \longrightarrow \text{isomerization} \quad (15)$$

In the above mechanism FB and BiA represent ground-state monofluorobenzene and biacetyl molecules, respectively. The Arabic numerals represent spin multiplicities and the Roman numerals are used to indicate first or second excited states. M represents any quenching molecule, and the asterisk denotes a vibrationally excited molecule. Reactions 3 and 6 are shown as possibly being bimolecular; it is difficult to conceive of these reactions occurring without collisions. However, at the pressures used here collisions may not be rate determining. Reactions 5 and 15 are included since it has been established that benzene and benzene derivatives may undergo phototransposition of ring carbon atoms when excited in the neighborhood of 2500 Å.[17-19] Reaction 10 very likely does not occur.[20] For simplicity only one mechanism is given for wavelengths above 2470 Å, but the various rate constants will have values dependent on wavelength and some rate constants may have negligible values at some exciting wavelengths. Since at shorter wavelengths the possibility of dissociation must be taken into account, the following steps and reactions 2, 3, and 5 describe the situation below 2470 Å.

$$FB + h\nu \longrightarrow {}^1FB^{I*} \quad (16)$$

$${}^1FB^{I*}(+M) \longrightarrow {}^3FB^{I*}(+M) \quad (17)$$

$${}^1FB^{I*} + FB \longrightarrow {}^1FB^I + FB \quad (18)$$

$${}^1FB^{I*} \longrightarrow \text{dissociation} \quad (19)$$

$${}^1FB^{I*} \longrightarrow \text{isomerization} \quad (20)$$

$${}^1FB^{I*} \longrightarrow h\nu + FB \quad (21)$$

Here the asterisk is used to indicate a molecule that is very highly vibrationally excited. In our mechanism we have allowed only for two vibrational levels of the first singlet to be taking part in the various reactions. In reality, a great many vibrational levels must be involved, each with its own rate constant. A detailed treatment would give much more complex expressions. We do not feel that our data warrant such a detailed treatment. The fluorescent quantum yield for exciting wavelengths below 2470 Å would be given by

$$\Phi_f = \frac{k_2k_{18}[FB] + k_{21}(k_2 + k_3 + k_4[FB] + k_5)}{(k_2 + k_3 + k_4[FB] + k_5)(k_{17} + k_{18}[FB] + k_{19} + k_{20} + k_{21})} \quad (22)$$

If $k_4 < (k_2 + k_3 + k_5)$ and $k_{18} < (k_{19} + k_{20})$, then eq 22 reduces to

$$\Phi_f = \frac{k_2k_{18}[FB] + k_{21}(k_2 + k_3 + k_5)}{(k_{17} + k_{19} + k_{20} + k_{21})(k_2 + k_3 + k_5)} \quad (23)$$

Equation 23 predicts that plots of Φ_f *vs.* [FB] should be linear and have a positive slope and is consistent with experimental observation; see Table I.

Returning now to the case above 2470 Å, steady-state

Table IV: Variation of $1/\Phi_p$ as a Function of Pressure of FB, at Constant Pressure of BiA, for Various Exciting Wavelengths

$\lambda_{excitation}$, Å	Equation of line[a]	Pressure range of FB, Torr
2470	$1/\Phi_p = 3.97 - 0.149 \times 10^3[FB]$ ±1.75%, max 2.92%	17–46.4
2550	$1/\Phi_p = 2.62 + 0.112 \times 10^3[FB]$ ±2.80%, max 4.12%	20–50
2590	$1/\Phi_p = 1.77 + 0.261 \times 10^3[FB]$ ±3.05%, max 4.88%	10–49
2670	$1/\Phi_p = 2.11 + 0.242 \times 10^3[FB]$ ±2.68%, max 5.46%	12–52

[a] BiA pressure constant at 5 Torr.

(17) K. E. Wilzbach, A. L. Harkness, and L. Kaplan, *J. Amer. Chem. Soc.*, **90**, 1116 (1968), and references therein.
(18) H. R. Ward and J. S. Wishnok, *ibid.*, **90**, 1085 (1968).
(19) D. Bryce-Smith and H. C. Longuet-Higgins, *Chem. Commun.*, 593 (1966).
(20) J. Lemaire, *J. Phys. Chem.*, **71**, 2653 (1967).

Table V: Values of Rate Constants and Quenching Cross Sections at Various Exciting Wavelengths

$\lambda_{excitation}$, Å	K_2, sec^{-1}	K_3, sec^{-1}	K_4, mol^{-1} l. sec^{-1}	σ^2 of FB, Å^2	K_7, mol^{-1} l. sec^{-1}	σ^2 of BiA, Å^2
2470	5.10×10^7	2.47×10^8	2.04×10^8	0.03	3.94×10^{11}	55.7
2510	4.41×10^7	1.79×10^8	1.15×10^{10}	1.67		
2550	4.48×10^7	1.84×10^8	1.36×10^{10}	1.98	3.47×10^{11}	49.0
2590	2.9×10^7	5.68×10^7	2.87×10^{10}	4.17	1.31×10^{11}	18.7
2630	3.44×10^7	9.87×10^7	1.02×10^{10}	1.48		
2670	3.54×10^7	1.04×10^8	1.58×10^{10}	2.29	2.59×10^{11}	36.6
2710	3.61×10^7	1.04×10^8	1.55×10^{10}	2.25		

treatments yields

$$1/\Phi_f = \frac{k_2 + k_3 + k_5}{k_2} + \frac{k_4[\mathrm{FB}]}{k_2} + \frac{k_7[\mathrm{BiA}]}{k_2} \quad (24)$$

Equation 24 predicts that plots of $1/\Phi_f$ *vs.* [FB] at zero [BiA] should be linear with intercept $= (k_2 + k_3 + k_5)/k_2$ and slope $= k_4/k_2$ while plots of $1/\Phi_f$ *vs.* [BiA] at constant [FB] should be linear with slope $= k_7/k_2$. These predictions are confirmed experimentally. Using the integrated molar absorptivity for FB given in the literature,[21] the radiative lifetime τ_0 can be determined. Fluorescent yields can now be used to obtain the mean radiation lifetime τ,[22] and hence k_2 at the various exciting wavelengths. Making now the reasonable assumption that k_5 is either zero or negligible,[23] k_3, k_4, k_7, and quenching cross sections can be evaluated, which are summarized in Table V. Assuming (10) and (11) to be unimportant, the steady-state treatment for sensitized emission gives

$$\Phi_p^{-1} = \frac{(k_{13} + k_{14})(k_{8a} + k_{8b}[\mathrm{M}])(k_6 + k_{15} + k_8[\mathrm{BiA}]/(k_2 + k_3 + k_4[\mathrm{FB}] + k_5 + k_7[\mathrm{BiA}])}{k_{13}k_{8b}k_8k_3[\mathrm{M}][\mathrm{BiA}]} \quad (25)$$

at moderate [BiA], $k_8[\mathrm{BiA}] > (k_5 + k_{15})$ and eq 25 reduces to

$$\Phi_p^{-1} = \frac{(k_{13} + k_{14})(k_{8a} + k_{8b}[\mathrm{M}])(k_2 + k_3 + k_7[\mathrm{FB}] + k_5 + k_7[\mathrm{BiA}])}{k_{13}k_{8b}k_3[\mathrm{M}]} \quad (26)$$

Again at moderate pressures of either FB or BiA, and particularly in the presence of CH, $k_{8b}[\mathrm{M}] > k_{8a}$ and eq 26 becomes

$$\Phi_p^{-1} = \frac{(k_{13} + k_{14})(k_2 + k_3 + k_4[\mathrm{FB}] + k_5 + k_7[\mathrm{BiA}])}{k_{13}k_3} \quad (27)$$

Equation 27 predicts that at constant [FB] plots of $1/\Phi_p$ *vs.* [BiA] should be linear with a positive slope; similarly at constant [BiA], plots of $1/\Phi_p$ *vs.* [FB] should be linear and have a positive slope. This is indeed found to be the case experimentally. Equation 27 also predicts that CH should have no effect on the sensitized emission yield. This prediction is confirmed for λ_{ex} of 2550, 2590, and 2670 Å. However, at 2470 Å the sensitized emission yield does increase with addition of CH, which is probably due to quenching of very highly vibrationally excited FB molecules, from dissociating levels. Table III, which summarizes these results, shows that at lower pressures of CH, for $\lambda_{ex} = 2470$ Å the per cent increase in Φ_p is seen to be approximately the same as the per cent increase in Φ_f.

The sum of $\Phi_{singlet} + \Phi_{triplet}$ is found to be 0.67 for $\lambda_{ex} = 2470$ Å, 0.75 for $\lambda_{ex} = 2550$ Å, 0.93 for $\lambda_{ex} = 2590$ Å, and 0.82 for $\lambda_{ex} = 2670$ Å. These figures were arrived at by adding the unquenched fluorescence yield to the triplet yield. The true triplet yield is equal to the triplet yield determined experimentally multiplied by the ratio Φ_f (unquenched)/Φ_f (quenched). The reason for this has been eloquently stated by Phillips[9] and is simply based on the fact that in determining triplet yields by the biacetyl technique some of the singlet, and thus the triplet, is quenched. It is very difficult to estimate the errors associated with the values given above. In Tables I, II, and IV the reproducibility of the data is given. One would have to add to this the error in Almy and Gillette's[24] work ($\simeq \pm 12\%$) on which our data are based, to obtain an estimate of the error in our work. Finally, it should be pointed out that the use of truly monochromatic light is necessary if one is to reach any firm conclusions in studies of this type. In the present instance the band pass was approximately 70 Å; this is much too large and absorption may occur into different vibrational levels of the first electronic state. Each of these has a different extinction coefficient, different fluorescent rate, intersystem crossover rate, etc. Simultaneous excitation into two or more vibrational levels will tend to obscure any distinct reactions occurring

(21) M. Ballester, J. Palau, and J. Riera, *J. Quant. Spectry. Radiative Transfer*, 4, 819 (1964).

(22) J. G. Calvert and J. N. Pitts, Jr., "Photochemistry," John Wiley and Sons, Inc., New York, N. Y., 1966, p 174.

(23) K. E. Wilzbach, A. L. Harkness, and L. Kaplan, International Conference on Photochemistry, Munich, Sept 6–9, 1967.

(24) G. M. Almy and P. R. Gillette, *J. Chem. Phys.*, 11, 188 (1943).

from a specific level and errors due to the "around the corner" effect may be introduced if the extinction coefficient for one vibrational level is much larger than that of its neighbors. The relatively large band pass used here was the best that our instrumentation could provide.

Acknowledgments. The authors gratefully acknowledge a grant from the Associated Alumni of the University of New Brunswick toward the purchase of the instrumentation used in this study and other financial assistance from the National Research Council of Canada.

Mass Spectrometric Investigation of the High-Temperature Reaction of Hydrogen with Boron Carbide[1]

by Sara J. Steck,[2] George A. Pressley, Jr., and Fred E. Stafford

Department of Chemistry and the Materials Research Center, Northwestern University, Evanston, Illinois 60201 *(Received June 24, 1968)*

The boron-containing gaseous molecules BH, BH_3, HBC_2, and $BH_2C_xH_{2x+1}$ ($x = 1$ and 2) have been identified as products of a high-temperature reaction of hydrogen with boron carbide; higher molecular weight boron–carbon–hydrogen molecules may have been present, but they could not be observed because of interference from hydrocarbons formed in the reaction. Evidence for BH_2 was not found. Concentrations of BH_3 and the two alkylboranes far exceeded the predicted equilibrium quantities. This phenomenon is thought to result from a steady-state reaction in the crucible, and a mechanism is suggested. The other molecules, BH and HBC_2, appeared to be present in near-equilibrium concentrations. Values for $D°(BH–H)$ and $D°(BH_2–H)$ are discussed; revisions are suggested. Secondary electron multiplier gains determined for H, H_2, and ^{11}B are in the ratio 1:3.5:19.2 for 6.5-kV ions. $D(H–BC_2)$ is determined to be 100 ± 10 kcal/mol.

Introduction

Tabulated thermodynamic data[3] suggest that the high-temperature reaction of hydrogen with boron carbide should yield such relatively simple molecules as BH, BH_2, and BH_3. All three of these species have been identified as transient intermediates, and various properties have been reported: for BH, both the uv[4] and vacuum uv[5] spectra have been subject to rotational analyses and the ionization potential was evaluated;[5] for BH_2, an electron impact ionization potential[6] has been obtained, and rotational analysis of the electronic spectrum has indicated a bent geometry in the ground state;[7] and for BH_3, the ionization potential[6–8] and the mass spectrum[9] have been measured. Because of the small number of electrons in these molecules, data for these species are particularly valuable for comparison with results of theoretical calculations.[10–14] Some discrepancies appear to exist between the limited experimental data and various theoretical treatments; for instance, the available thermodynamic data[3] for these hydrides do not agree with arguments used to explain the boron fluoride bond dissociation energies.[15]

Especially since the carboranes show greater thermal stability than do the boron hydrides, the high-temperature reaction of boron carbide with hydrogen might be expected also to yield boron–carbon–hydrogen species. In particular, the molecules BC_2 and B_2C

(1) Supported by the Advanced Research Projects Agency through the Materials Research Center at Northwestern University and by the U. S. Atomic Energy Commission, Document No. C00-1147-27. The acquisition and maintenance of the mass spectrometer facility have been made possible by support from the Materials Research Center, the Atomic Energy Commission, and the university.

(2) Recipient of Public Health Service Fellowships 1-F1-GM-29, 815-01A1, and 5-F1-GM-29, 815-02 from the National Institute of General Medical Sciences. 1966–1968.

(3) D. R. Stull, Ed., "JANAF Thermochemical Tables," Clearinghouse for Federal Scientific and Technical Information, Springfield, Va., April 1968, Document No. PB-168,370.

(4) J. W. C. Johns, F. A. Grimm, and R. F. Porter, *J. Mol. Spectrosc.*, 22, 435 (1967).

(5) S. H. Bauer, G. Herzberg, and J. W. C. Johns, *ibid.*, 13, 256 (1964).

(6) T. P. Fehlner and W. S. Koski, *J. Amer. Chem. Soc.*, 86, 2733 (1964).

(7) G. Herzberg and J. W. C. Johns, *Proc. Roy. Soc.*, A298, 142 (1967).

(8) J. H. Wilson and H. A. McGee, Jr., *J. Chem. Phys.*, 46, 1444 (1967).

(9) A. B. Baylis, G. A. Pressley, Jr., and F. E. Stafford, *J. Amer. Chem. Soc.*, 88, 2428 (1966).

(10) P. C. H. Jordan and H. C. Longuet-Higgins, *Mol. Phys.*, 5, 121 (1962).

(11) W. C. Price, T. R. Passmore, and D. M. Roessler, *Discussions Faraday Soc.*, 35, 201 (1963).

(12) A. C. Hurley, *Proc. Roy. Soc.*, A261, 237 (1961).

(13) F. O. Ellison, *J. Chem. Phys.*, 43, 3654 (1965).

observed by Verhaegen, *et al.*,[16] might react with hydrogen to form BC_2H and B_2CH which are isoelectronic with C_3 and BC_2, respectively. Higher hydrogen content species analogous to the $BX_2Si_nX_{2n+1}$ compounds (X = F, n = 1, 2, 3[17,18] and X = Cl, n = 1[19]), which have been synthesized using high-temperature molecules, would correspond to dissociated alkylborane dimers.

Identifications of boron–hydrogen and boron–hydrogen–carbon species formed in the high-temperature reaction of hydrogen with boron carbide, together with postulated mechanisms of formation and/or thermodynamic data and implications, are reported in this paper. An extensive high-temperature, high-molecular-weight carbon–hydrogen system extending to m/e 140 and beyond also was observed and will be reported elsewhere.[20]

Experimental Section

Spectra were obtained with a Nuclide Analysis Associates 12-in. radius, 60° sector Inghram-type high-temperature mass spectrometer.[21,22] Hydrogen (Matheson prepurified grade) was admitted to the spectrometer through a cylinder pressure regulator, a vacuum regulator (J. T. Baker Chemical Co.), a glass vacuum line with a ballast bulb and manometer, a Granville-Phillips (Boulder, Colo.) variable leak, and an Andonian Associates (Waltham, Mass.) leak. This line is then attached to the inlet into the spectrometer (Figure 1 in ref 9).

A tilting McLeod gauge, which was attached to the stainless steel tube leading into the instrument (Figure 1[9]), was used to measure the absolute hydrogen pressure. A boron nitride (Norton Co., Worcester, Mass.) tube served as an electrical insulator between the steel tube and the stem of the ATJ graphite (National Carbon Co.) reactor. Pressure of the hydrogen in the crucible was calculated using the McLeod gauge readings and conductance corrections[23] for the inlet system; four-mesh "high boron content" boron carbide from the Norton Co. was loosely packed over the bottom inlet into the reactor and three-quarters of the way up the crucible. Electron bombardment from two tungsten filaments heated the 15.9-mm i.d. reactor; the crucible assembly and heating filaments were surrounded by a set of tantalum shields to diminish heat radiation. A power-regulated high-voltage supply based on an Argonne National Laboratories design[24] greatly facilitated the experiments. Temperature was determined with a Leeds and Northrup disappearing-filament optical pyrometer which could be sighted on black-body radiation holes at the top and bottom of the graphite reactor; an emissivity correction of 0.84 was made for grayness of the hole and for attenuation by the intervening window. Products of the reaction effused through a 0.37-mm diameter orifice in the reactor cap.

To accommodate relatively high hydrogen pressures in the reactor, a 1-in. Edwards Speedivac mercury-diffusion booster pump was placed between the forepump and the three mercury-diffusion pumps of the differential pumping system.[9,22] This booster pump effectively lowers the backing pressure while it increases the forepump throughput.

A movable beam defining slit located between the crucible assembly and the ion source region was used to differentiate species arising from the crucible orifice from those which had collided with the instrument walls and the ion source assembly and from those which arose from the crucible lip or the tantalum radiation shields.

In the ion source region, a beam of ionizing electrons intersected the molecular beam arising from the crucible orifice. The ion source was normally operated with an ionizing electron voltage of 70 eV, with a total emission current of 1.2 mA, which corresponds to a trap current of about 10^{-5} A and with an ion-accelerating voltage of 4 kV. Appearance potentials were calibrated to the appearance potential of boron and were evaluated using the vanishing-current method.[25]

After mass analysis, ions were detected by both a 50% transmission grid collector and a secondary electron multiplier so that relative multiplier gains could be determined for intense peaks. The 16-stage multiplier used in the early experiments was normally operated with 3.9 kV across the dynode resistor string but the 20-stage multiplier used in later experiments was operated at 2.5 kV. Typical multiplier gains for the latter were: H^+, 1.25×10^4; H_2^+, 4.4×10^4; and B^+, 2.40×10^5. Other ions observed had gains of the order of 10^5.

Direct digital acquisition and computer treatment of data[26] were used in most experiments.

(14) S. Peyerimhoff, R. J. Buenker, and L. C. Allen, *J. Chem. Phys.*, **45**, 734 (1966); L. C. Allen and J. D. Russell, *ibid.*, **46**, 1029 (1967).

(15) D. L. Hildenbrand in "Advances in High Temperature Chemistry," Vol. I, L. Eyring, Ed., Academic Press, New York, N. Y., 1967, pp 193–219.

(16) G. Verhaegen, F. E. Stafford, and J. Drowart, *J. Chem. Phys.*, **40**, 1622 (1964).

(17) P. L. Timms, T. C. Ehlert, J. L. Margrave, F. E. Brinckman, T. C. Farrar, and T. D. Coyle, *J. Amer. Chem. Soc.*, **87**, 3819 (1965).

(18) P. L. Timms, *ibid.*, **89**, 1629 (1967).

(19) P. L. Timms, *Inorg. Chem.*, **7**, 387 (1968).

(20) S. J. Steck, G. A. Pressley, Jr., S. -S. Lin, and F. E. Stafford, *J. Chem. Phys.*, in press.

(21) W. A. Chupka and M. G. Inghram, *J. Phys. Chem.*, **59**, 100 (1955); M. G. Inghram and J. Drowart in "High Temperature Technology," McGraw-Hill Book Co., Inc., New York, N. Y., 1960, pp 219–240.

(22) F. E. Stafford, G. A. Pressley, Jr., and A. B. Baylis, "Mass Spectrometry in Inorganic Chemistry," Advances in Chemistry Series, No. 72, American Chemical Society, Washington, D. C., 1968, pp 137–152.

(23) S. Dushman, "Scientific Foundations of Vacuum Technique," J. M. Lafferty, Ed., John Wiley & Sons, Inc., New York, N. Y. 1962, pp 80–117.

(24) E. Johannsen, personal communication, Argonne National Laboratories, 1967.

(25) F. H. Field and J. L. Franklin, "Electron Impact Phenomena," Academic Press, New York, N. Y., 1957, pp 28–30.

(26) R. J. Loyd and F. E. Stafford, "Mass Spectrometry in Inorganic Chemistry," Advances in Chemistry Series, No. 72, American Chemical Society, Washington, D. C., pp 127–136.

Data

Ions observed in the mass spectra were identified on the basis of isotope ratios, shutter percentages,[27] and mass defect. Figure 2 in ref 22 shows the resolution of ion peaks at the same nominal mass in the monoborane ion group; Figure 1 shows the resolution of HCl^+, C_3^+, and HBC_2^+, all at m/e 36. Species containing one boron and three or more carbons cannot be so resolved. Spectra were generally measured at 70 eV because of the small ion intensities found for many of the species.

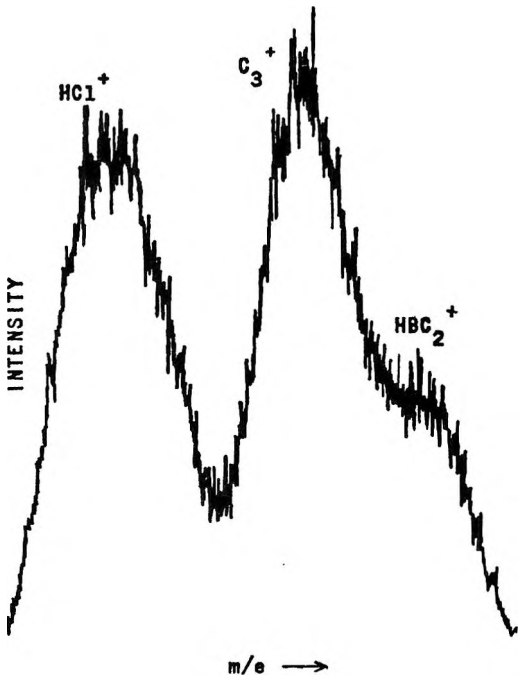


Figure 1. Mass peak 36; well-defined peaks are HCl^+ and C_3^+; the shoulder on the right-hand side is HBC_2^+.

Large percentage shutter effects[27] were observed for ions corresponding to the neutral species C_3, BC_2, B_2C, and B before hydrogen was admitted to the reactor; all of these species have been reported previously.[16,21] Ions from the species BC, which also has been reported,[16] were not clearly resolved in these experiments because of interference at m/e 22 and 23.

A mass spectrum of the boron-containing ions observed after hydrogen was introduced into the crucible is given in Table I. Although no positive mass defect (*i.e.*, boron-containing) ions could be resolved at ion peaks at $m/e \sim 50$, the shutter percentages[27] on the high-mass side (positive mass defect) of the hydrocarbon peaks were generally greater than that observed at the top of the hydrocarbon peak. This behavior suggests that higher molecular weight boron-containing species were present but not clearly observable with the resolution available.

Both hydrogen pressure and temperature dependence studies were made of the ions given in Table I. For law of mass action studies, ion intensities were measured

Table I: Mass Spectrum of Boron-Containing Species Formed in the Reaction of 0.19 Torr of Hydrogen with High-Boron-Content Boron Carbide at 2427°K[a]

m/e	Species	Relative intensity
11	$^{11}B^+$	100
12	$^{11}BH^+$	4.6
13	$^{11}BH_2^+$	14.6
14	$^{11}BH_3^+$	4.6
22[b]	$^{10}BC^+$	0.04
24	$^{10}BCH_2^+$, $^{11}BCH^+$	0.29
25	$^{11}BCH_2^+$, etc.	0.52
26	$^{10}BCH_4^+$	1.6
27	$^{11}BCH_4^+$	6.0
28	$^{11}BCH_5^+$	0.26
29[c]	$^{11}BCH_6^+$?	0.06
33	$^{10}B_2C^+$	0.50
34	$^{11}B_2C^+$, $^{10}BC_2^+$, $^{10}B_2CH^+$	3.6
35	$^{11}BC_2^+$, $^{11}B_2CH^+$, $^{10}BC_2H^+$	11.6
36[d]	C_3	10.9
36[d]	$^{11}BC_2H^+$, etc.	6.8
37[e]	$^{11}BC_2H_2^+$	0.49
38	$^{10}BC_2H_4^+$	0.10
39	$^{11}BC_2H_4^+$	0.41
40	$^{11}BC_2H_5^+$	0.30
41[c]	$^{11}BC_2H_6^+$?	0.06

[a] Run 671211-33 taken at 70 eV and not corrected for secondary electron multiplier gain. [b] A large interfering photo-ion effect[21] is observed at m/e 23. [c] Shutter percentages[27] of these mass peaks are half those of the preceding peaks. [d] See Figure 1. [e] The ion intensity of this mass peak in this particular spectrum seems anomalously large if compared to other spectra.

at three hydrogen pressures (*ca.* 0.008, 0.06, and 0.19 Torr in the reactor) at each of six temperatures between 2100 and 2400°K. Ion intensities, except those of B^+ and C_3^+, normally showed a hydrogen pressure dependence of approximately $P(H_2)^{1/2}$; between the two higher pressures, BH_3^+, BH_2^+, and BH^+ ion intensities did show a hydrogen dependence between $P(H_2)^{2/2}$ and $P(H_2)^{3/2}$ at two of the temperatures investigated. Difficulties in measuring the small ion intensities, possible saturation of the secondary electron multiplier, and length of time required for measurements cannot account for such large deviations from the law of mass action as are indicated for ions (and therefore the neutral progenitors) that contain three to six hydrogen atoms. Because of temperature gradients as large as 100–200° between the radiation holes at the top and bottom of the reactor, temperature dependence of the ion intensities is not as well defined as desired. Changes of the ion intensities with temperature, however, roughly divided them into the following groups: m/e 41–37, m/e 36–33, m/e 28–22, and m/e 14–10.

(27) "Shutter percentage" is the ratio of the molecular beam intensity to the total ion intensity at a given mass peak. Argon, for example would show about a 4% shutter effect at these temperatures. Ions from a reactive species, one that is rapidly pumped by collisions with the vacuum chamber walls, would have a 100% shutter effect.

Interpretation of Data

Identification of Neutral Progenitors. Formation of the ions listed in Table I by ion–molecule reactions in the source region or by collisions of molecules in the molecular beam is ruled out by the low source pressures (3×10^{-6} Torr), molecular flow conditions at all but the highest pressures studied, and the one-half power hydrogen pressure dependence of many species. Any ion–molecule or molecular beam reaction mechanism requires a first, second, or third power dependence, which was not observed.

Boron-containing ions that were clearly resolved from the hydrocarbon ions at the same nominal masses can be discussed in three separate groups. The first of these groups includes those peaks at *m/e* 41–33. Ions at *m/e* 33–35 were observed before hydrogen was introduced into the reactor and arose from B_2C and BC_2. Isotope distributions[28] (Table I) suggest that the ions at *m/e* 36–41 contain only one boron atom, *i.e.*, $BC_2H_x^+$. The logical neutral progenitor of these ions is an alkylborane such as $BH_2C_2H_5$ or $BH(CH_3)_2$. Two alkylboranes, *asym*-dimethyldiborane and ethyldiborane, are among the best model compounds from which to infer fragmentation patterns for the proposed progenitors; other model compounds are the BX_3 molecules (X = H, F, Cl, Br, and I) and $BF_2Si_2F_5$. Accordingly, relative ion intensities for selected peaks in the $BC_2H_x^+$ and BCH_x^+ ion groups of *asym*-dimethyldiborane[28] and ethyldiborane[28] are listed in Table II. The large relative intensity at *m/e* 41 in the *asym*-dimethyldiborane spectrum (line 1) suggests that the probable fragmentation pathway of $BH(CH_3)_2$ would be loss of hydrogen, a fragmentation pattern that would be expected for a BX_2Y molecule in which the B–CH_3 bond is stronger than the B–H bond.[29] The ethyldiborane ion peaks (line 2) suggest that the principal fragmentation pathway for $BH_2C_2H_5$ would be loss of a methyl group to give the most intense peaks in the BCH_x^+ ion group; this fragmentation pattern would be predicted for a molecule in which the B–C and B–H bonds are stronger than the C–C bonds. This type of spectrum is observed[17] for $BF_2Si_2F_5$, a molecule in which the Si–Si bond is the weakest. The observed spectrum (line 3) shows smaller ion intensity at *m/e* 41 than at *m/e* 40 and 39. This behavior is not that of a B–H bond being most easily cleaved (*asym*-dimethyldiborane) and corresponds more closely to that shown by ethyldiborane. Accordingly, ethylborane $BH_2C_2H_5$ is inferred to be the species present; the analogous molecule $BF_2Si_2F_5$ has been formed (at low temperatures) from high-temperature species by Timms, *et al.*[17]

Table II: Comparison of the Relative Intensities of Ion Peaks from *asym*-Dimethyldiborane and Ethyldiborane with Those Observed in the High-Temperature Reaction of Hydrogen with Boron Carbide

m/e	41	40	39	27	26
asym-Dimethyldiborane[a]	100	58	35	30	15
Ethyldiborane[a]	9	18	15	100	59
Observed spectrum	1	5	7	100	27

[a] See ref 28.

The most intense boron–carbon–hydrogen ion peak was resolved on the high-mass side of the C_3^+ ion peak as shown in Figure 1. This ion was resolved only above 2300°K and at the higher hydrogen pressures used. Assignment of this ion is logically HBC_2^+ from neutral HBC_2, a molecule that is isoelectronic with C_3. A half-power hydrogen pressure dependence supports this assignment.

Difficulty encountered in stripping the boron isotope ion contributions from *m/e* 33 through 36 gives some evidence for the molecule HB_2C, which is isoelectronic with BC_2, or possibly H_2B_2C, which is isoelectronic with C_3.

The second ion group in which ions with positive mass defects relative to the hydrocarbon background were resolved is *m/e* 29–22. None of these ions, with the possible exception of BC^+, was observed until after hydrogen was introduced into the reactor. Comparison of the ratio $I(27^+)/I(26^+)$ to the known isotopic distribution of boron[28] shows that the ions are members of the BCH_x^+ rather than the $B_2H_x^+$ series. Table II, line 2, shows that appreciable contributions to the intensities of these peaks would be expected from fragmentation of ethylborane, the proposed progenitor of the higher molecular weight boron–carbon–hydrogen ions. The relative intensities in the mass spectrum of ethyldiborane,[28] however, suggest that ethylborane probably does not account for all the BCH_x^+ ion intensity; this argument suggests that BH_2CH_3 also is present. Timms[19] has reported the synthesis of the analogous compound BCl_2CCl_3 by two different high-temperature reactions.

The presence of HBC, a molecule isoelectronic with C_2, need not be invoked to explain the ion intensity at *m/e* 24.

Mass peaks 14–10 represent the last group of boron-containing ions. Since all of these ions may be formed by a fragmentation process, rough appearance potentials (AP's) were obtained and used to help determine the progenitors. Resolution of these peaks from the adjacent ones due to hydrocarbon ions[22] permitted measurement of appearance potentials.

The observed appearance potential for BH_3^+ is 11.5 ± 0.5 eV (uncertainties quoted are average deviations). That this ion is formed from neutral

(28) I. Shapiro, C. O. Wilson, J. F. Ditter, and W. J. Lehmann, "Borax to Boranes," Advances in Chemistry Series, No. 32, American Chemical Society, Washington, D. C., 1961, pp 127–138.

(29) F. W. McLafferty, "Interpretation of Mass Spectra," W. A. Benjamin, Inc., New York, N. Y., 1966.

BH_3 is suggested by the agreement with the two reported electron impact values of the ionization potential, 11.4 ± 0.2[6] and 12.32 ± 0.1[8] eV. This ion, moreover, is not usually seen in boron hydride or alkylborane mass spectra.[28] Temperature and hydrogen pressure dependence experiments also suggest that it is not formed from higher molecular weight boron-containing ions.

An AP of 12.3 ± 0.5 eV was found for BH_2^+; this is considerably greater than the reported ionization potential of 9.8 ± 0.2 eV[6] and more nearly approaches the value 12.95 ± 0.05 eV[8] for the AP of BH_2^+ from BH_3. The AP for the formation of BH_2^+ from either BH_2CH_3 or $BH_2C_2H_5$ should be about the same or higher; large contributions from these alkylboranes to the BH_2^+ ion intensity, however, are not expected by analogy with alkyldiborane spectra.[29] That no more than 5–10% of the observed BH_2 intensity could be due to neutral BH_2 is indicated by (1) the high appearance potential, (2) the agreement of the present experimental ratio for $I(BH_3^+)/I(BH_2^+)$ with that previously observed[9] for BH_3 formed from diborane, and (3) the constancy of the ratio $I(BH_3^+)/I(BH_2^+)$ with changes in temperature and hydrogen pressure. This limit does not preclude the presence of BH_2 if it undergoes extensive fragmentation upon ionization.

A break in the BH^+ ionization efficiency curve suggests that this ion is formed both by ionization of neutral BH and by decomposition of another ion such as BH_3^+. Spectroscopic measurements give an ionization potential of 9.77 eV[5] for BH; the present electron impact value is 9.8 ± 0.5 eV. A break in the ionization efficiency curve gives an appearance potential of 13.7 ± 1.0 eV for the second process; this is close to the value 13.66 ± 0.02 eV[8] observed for the formation of BH^+ from BH_3.

Molecules deduced to be present when hydrogen is treated with boron carbide at high temperatures are therefore, BH, BH_3, HBC_2, BC_2H_7, and probably BCH_5. Some evidence for $BC_3H_x^+$ ions was found, but these and higher molecular weight species could not be resolved from the hydrocarbons formed.[20] Contributions from the free-radical BH_2 to BH_2^+, if any, were masked by fragmentation.

Partial Pressures. Observed ion currents were reduced to partial pressures and compared with values calculated from tabulated[3] equilibrium constants. The relationship between observed ion intensity and partial pressure $P(X)$ is

$$P(X) = [I^+(X)\,T]/[\gamma(X_i)\sigma(X)\,S]. \quad (1)$$

$I^+(X)$ is the sum of all ion intensities due to X. Lack of knowledge of the fragmentation pattern of the molecule can introduce error into the calculation; even for a small molecule such as BH_3, the total ion intensity with 70-eV ionizing electrons is about four times that of the parent ion.[9] T is the temperature of the reactor.

Table III: Multiplier Gains and Ionization Cross Sections Used to Calculate Partial Pressures

Species	Multiplier gain, γ	Cross section, σ
H	1.25×10^4	0.76[a]
H_2	4.4×10^4	1.1[b]
B	2.40×10^5	3.2[a]
BH	2.4×10^5	3.96[c]
BH_2	2.4×10^5	4.72[c]
BH_3	2.4×10^5	5.58[c]
HBC_2	1.8×10^5	9.8[c]
BH_2CH_3	1.8×10^5	9.9[c]

[a] See ref. 30 and 31. [b] Experimental valueas cited in ref 31. [c] Cross section is found by summing the cross sections of the atoms in the molecule; difficult to determine multiplier gains for species such as HBC_2 are assumed to be the same as for a related species such as BC_2.

$\gamma(X_i)$ is the secondary electron multiplier gain for a given ion. It was measured for a number of ions for which it is then known within 10%; for ions of low intensity or for ions at mass peaks where interference occurred, it was estimated by analogy and is probably correct to within 50%. $\sigma(X)$ is the cross section for ionization of X. Few experimental results are available for absolute cross sections and most of them are estimated in one of several ways.[30,31] Error in these numbers could be a factor of 2, especially for molecules where the cross section is assumed to be the sum of the atomic cross sections. The values of γ and σ used in the calculations are tabulated in Table III. S is the instrument sensitivity. Three means used to estimate it were comparison of: (1) the boron ion intensities to tabulated partial pressures of boron,[3] (2) the hydrogen atom to hydrogen molecule ion intensity ratios to equilibrium constants[3] for the re-

Table IV: Instrument Sensitivities Calculated from Boron Ion Intensity, Hydrogen Atom/Hydrogen Molecule Intensity Ratio, and Hydrogen Pressure Measurement[a]

Hydrogen pressure	I	II	III
B[b] sensitivity	9.7×10^{-8}	1.1×10^{-7}	7.6×10^{-8}
$\frac{H}{H_2}$[c] sensitivity	8.5×10^{-8}	1.6×10^{-7}	1.9×10^{-7}
H_2[d] sensitivity	1.4×10^{-6}	1.1×10^{-6}	8.5×10^{-7}

[a] Run 671209. See Table V for the hydrogen pressures, T = 2280°K. [b] Calculated using eq 1 with the partial pressure from JANAF[3] and the observed boron ion intensity. [c] Calculated using eq 1 for the ratio of the intensities of H to H_2 and the appropriate equilibrium constant. [d] Calculated using eq 1 and the pressure of hydrogen read from the McLeod gauge, corrected for conductance effects and dissociation of the hydrogen.

(30) F. E. Stafford, "Mass Spectrometry in Inorganic Chemistry," Advances in Chemistry Series, No. 72, American Chemical Society, Washington, D. C., 1968, pp 115–126.

(31) S.-S. Lin and F. E. Stafford, *J. Chem. Phys.*, 48, 3885 (1968).

Table V: Comparison of Observed and Calculated[a] Partial Pressures (atm) for Some Species Formed in the High-Temperature Reaction of Hydrogen with Boron Carbide at 2280°K[b]

	I		II		III	
	Obsd	Calcd	Obsd	Calcd	Obsd	Calcd
H_2	7.6×10^{-5}		2.3×10^{-4}		4.8×10^{-4}	
BH[c]	2.6×10^{-8}	7.2×10^{-8}	5.8×10^{-8}	1.2×10^{-7}	4.6×10^{-8}	1.8×10^{-7}
BH_2[d]	$<1.3 \times 10^{-8}$	1.5×10^{-7}	$<3.5 \times 10^{-8}$	4.4×10^{-7}	$<1.6 \times 10^{-8}$	9.2×10^{-7}
BH_3[e]	1.4×10^{-7}	4.6×10^{-11}	3.2×10^{-7}	2.3×10^{-10}	1.8×10^{-7}	7.3×10^{-10}
HBC_2[f]	5.0×10^{-8}		7.7×10^{-8}		5.9×10^{-8}	
BH_2CH_3[g]			7×10^{-8}	1×10^{-13}		

[a] Calculated using equilibrium constants from ref 3; See text. [b] Run 671209. [c] Observed intensity of ion is assumed to be one-half that at $^{11}BH^+$ multiplied by 1.25. [d] Observed intensity is assumed to be less than one-tenth that at $^{11}BH_2^+$ multiplied by 1.25. [e] Observed intensity of ion is assumed to be five times that observed at $^{11}BH_3^+$. [f] Observed intensity is assumed to be intensity at $^{11}BC_2H^+$ multiplied by 1.25. [g] From run 671211 with an average temperature of 2342°K and with a hydrogen pressure approximately equal to pressure II. Observed intensity is assumed to be one-half intensity at m/e 27$^+$ ($^{11}BH_2CH_2^+$). Calculated pressure is estimated as discussed in text at eq 2.

action $H_2(g) \rightarrow 2H(g)$, and (3) the hydrogen molecule ion intensities to the hydrogen pressures read from the McLeod gauge and corrected for the inlet tube conductance[23] and the dissociation of the hydrogen molecule. Three sets of sensitivities so calculated for one temperature are tabulated in Table IV. The first two methods give sensitivities that agree within a factor of 2, but the third method differs from the other two by about a factor of 10. The sensitivities calculated by each method were essentially constant with changes in temperature but varied with changes in hydrogen pressure (Table IV).

Several problems were responsible for the difficulties encountered in calculating the instrument sensitivity. The boron sensitivity varied because at constant temperature, the boron ion intensity fluctuated by as much as 50% with hydrogen pressure; the intensity change may have resulted from depletion of boron on the surface of the sample. The H/H_2 ratio sensitivity suffered from difficulty in measuring the H_2 molecular beam ion intensity which was only 3% of the total. This sensitivity also seemed to reflect some saturation of the secondary electron multiplier. The hydrogen pressure sensitivity contains error from the uncertainty in the McLeod gauge pressure readings and from the ill-defined conductance effect corrections for the loosely packed reactor.

The H/H_2 ratio sensitivity was used to calculate the observed pressures in Table V. For the particular data used to construct Tables IV and V, the intensities of the boron ion and the boron-containing ions were smaller at the highest hydrogen pressure than at the intermediate pressure. Consequently, use of the H/H_2 ratio sensitivities suggests lower partial pressures for all of these species at the highest hydrogen pressure whereas, use of the boron sensitivities gives highest pressures for all species at the highest hydrogen pressure.

On the basis of these considerations, especially that of uncertainty in S, the most probable error in the absolute pressures is estimated to be a factor of 20. The "literature" pressures given in Table V are calculated from tabulated[3] equilibrium constants but depend on hydrogen pressures calculated using S. Some of the error in S, therefore, cancels in the ratio of observed to literature pressures; expected uncertainty in this ratio is a factor of 5–6.

Comparison of the calculated and observed pressures in Table V suggests that the BH molecule is, within a factor of 3, present in the predicted[3] equilibrium concentrations. The upper limit for the partial pressures of BH_2 is low by a factor of 10; this difference by itself, particularly if BH_2 fragments extensively, does not exclude the possibility that neutral BH_2 is present in the reactor. Observed partial pressures for BH_3, surprisingly, are several orders of magnitude larger than the calculated equilibrium amounts. A comparison for HBC_2 is not available.

To estimate the thermodynamic concentration of the alkylboranes BH_2R (R = CH_3, C_2H_5) at these temperatures and pressures, the following calculations were made. $D(BH_2\text{–}H)$ and $D(BH_2\text{–}R)$ were assumed to be equal, which makes $\Delta H°$ for the reaction

$$BH_3 + R \rightarrow BH_2R + H \qquad (2)$$

equal to zero. Also, the differences in the free-energy functions, Δfef, where

$$fef = \frac{G°_T - H°_{298}}{T}$$

are estimated to be 7 eu by analogy to that[3,32] for the reaction

$$CH_4 + CH_3 \rightarrow C_2H_6 + H \qquad (3)$$

The difference is assumed to be independent of temperature. Use of this estimate in the relation

$$\Delta H°_{298} = -RT \ln K - T\Delta fef \qquad (4)$$

together with concentrations of BH_3, CH_3, and H

(32) G. N. Lewis and M. Randall, "Thermodynamics," revised by K. S. Pitzer and L. Brewer, McGraw-Hill Book Co., Inc., New York, N. Y., 1961, p 682.

Table VI: Observed Reaction Enthalpies, Heats of Formation, and Atomization Energies (kcal/mol)[a]

Molecule	Chemical equilibrium	ΔH°_{298}	$\Delta H_f\,^\circ_{298}$	$\Delta H_{at}\,^\circ_{298}$
B	$0.25B_4C(s) \rightleftarrows B(g) + 0.25C(s)$	133 ± 5	130	
BH	$B(s, B_4C) + H(g) \rightleftarrows BH(g)$	56 ± 5	108	77
	$B(g) + H_2(g) \rightleftarrows BH(g) + H(g)$	26 ± 5	107	
HBC_2	$BC_2(g) + H_2(g) \rightleftarrows HBC_2(g) + H(g)$	4 ± 5	130	397

[a] Third-law calculations for 23 separate points representing 11 different temperatures were made to obtain each ΔH°_{298} recorded. The uncertainties are accuracies; standard deviations were ± 1 to ± 3 kcal/mol. All data used in the cycle to calculate $\Delta H_f\,^\circ_{298}$ and $\Delta H_{at}\,^\circ_{298}$ come from ref 3.

calculated from the observed hydrogen pressure and tabulated[3] equilibrium constants, gives a calculated $P(BH_2CH_3)$ equal to 1×10^{-13} atm, the observed pressure (Table V) is 7×10^{-8} atm. The C_2H_5 partial pressure should be much lower than that of CH_3; consequently, the difference between the calculated and observed partial pressures is expected to be even larger than for BH_2CH_3. This discrepancy is greater than any reasonable experimental error. To account for it, $D(BH_2\text{–}CH_3)$ or $D(BH_2\text{–}C_2H_5)$ must be 50–60 kcal/mol larger than $D(BH_2\text{–}H)$ and/or the Δfef must be in error by 25 eu; this is unlikely.

Table V gives only a small fraction of the data points measured; however, the formalism of third-law calculations[21] with eq 4 can be utilized to summarize all of the measurements. Apparent equilibrium constants were calculated using eq 1. Free-energy functions for $B_4C(s)$, C(s), B(g), BH(g), $BH_2(g)$, $BH_3(g)$, $H_2(g)$, and H(g) were taken from the JANAF compilation;[3] the difference in *fef* between $BC_2(g)$ and $HBC_2(g)$ was estimated to be equal to that between $C_2(g)$ and $C_2H(g)$.[3] In this formalism, a factor of 10 in a partial pressure or in the equilibrium constant at these temperatures results in a 10-kcal/mol difference in the calculated ΔH°, *i.e.*, $RT \ln 10 \approx 10$ kcal/mol.

The heat of sublimation for boron estimated by this method (130 ± 5 kcal/mol, Table VI) is within experimental error of that presently accepted by JANAF[3] (132.8 ± 4 kcal/mol); values at the lowest hydrogen pressures were about 4 kcal/mol more exothermic than those for the highest pressures; a trend with changing temperature was not observed. The calculated heat of formation for BH (107 ± 5 kcal/mol) is only slightly more endothermic than that (105.8 ± 2.0 kcal/mol) derived from the spectroscopic value of $D(B\text{–}H) = 3.39$ eV;[3,12] no systematic trends with changing temperature or hydrogen pressure were noted for either of the two reactions used in calculating the values given in Table VI. Agreement of results for the above two species with other experimental work suggests that the thermodynamic properties given in Table VI for the new molecule HBC_2 are accurate within ± 10 kcal/mol since HBC_2, as well as BH, is observed to obey the law of mass action.

For BH_3, enthalpies of reaction were calculated for the four isomolecular reactions

$$B(s) + 2H_2(g) \rightarrow BH_3(g) + H(g)$$
$$2B(s) + 2H_2(g) \rightarrow BH_3(g) + BH(g)$$
$$B(g) + 3H_2(g) \rightarrow BH_3(g) + 3H(g)$$
$$BH(g) + 2H_2(g) \rightarrow BH_3(g) + 2H(g)$$

As expected from the failure of $I(BH_3^+)$ to vary with hydrogen pressure according to the law of mass action, values of the heat of formation of BH_3 calculated from the heats of reaction for the above four equations and from tabulated[3] data varied systematically with pressure; trends in the values were observed also for temperature and the reaction calculated. In all cases, the ΔH_f° so calculated were 20–40 kcal/mol more exothermic than the accepted value[3] of 25.5 ± 10 kcal/mol. This means that averaged over all sets of measurements made, BH_3 is present in quantities 10^2–10^4 greater than that expected for equilibrium conditions; this difference is at least a factor of 10 beyond experimental error.

Measurements[33] similar to these on $CH_2(g)$ led to a heat of formation that is 13.5 kcal/mol more exothermic than that deduced from recent, reliable photoionization work;[34] in this case also, the CH_2 thus appears to be present in 10- to 30-fold excess over the equilibrium quantity.

Formation of the Gaseous Molecules. That the observed partial pressures for borane and the alkylboranes are so much larger than those calculated from established thermodynamic data is unexpected in two ways. First, because of the way the boron carbide is packed in the reactor, molecules are expected to undergo 10^4 wall collisions. Second, these complicated molecules that are present in greater than equilibrium quantities have been formed from the elements.

The most reasonable explanation of the present results seems to be the steady-state formation of radicals and other reactive intermediates in larger than equilibrium quantities; this effect is perhaps aided by

(33) W. A. Chupka, J. Berkowitz, D. J. Meschi, and H. A. Tasman in "Advances in Mass Spectrometry," Vol. II, R. M. Elliott, Ed., The Macmillan Co., New York, N. Y. 1963, pp 99–109.

(34) W. A. Chupka and C. Lifshitz, *J. Chem. Phys.*, 48, 1109 (1968).

the temperature and pressure gradients in the cell, or those between the cell and the hydrogen inlet tube. Analogous work with the carbon–hydrogen systems[20,33] indicates such a kinetically controlled reaction. The one-half power hydrogen pressure dependences of $P(BH_3)$ and $P(BII_2CH_3)$ suggest that BH, which seems to be in equilibrium with the hydrogen, is involved in the formation mechanism of these molecules. Observed reactions[35,36] of the isoelectronic species C suggest the following insertion reactions[37] $BH + H_2 \rightarrow BH_3$ and $BH + CH_4 \rightarrow BH_2CH_3$ as steps in the mechanism. Both reactions are expected to be exothermic by 80–100 kcal/mol and, therefore, are energetically favorable. The reaction $BH + H_2 \rightarrow BH_2 + H$ almost certainly is endothermic (see below) and is not expected to occur; this is in agreement with the fact that BH_2 is not observed.

That these molecules, once formed, do not come into equilibrium with the condensed phase rapidly is, in retrospect, not surprising. This phenomenon has been observed also for $BC_2(g)$ in contact with solid boron carbide–graphite mixtures.[16] A kinetic barrier to the decomposition of hydrocarbons on hot graphite surfaces also is known.[20,33,38,39]

Discussion

Although no directly comparable work on the high-temperature boron–carbon–hydrogen and boron–hydrogen systems has been done, related studies exist. Work by Verhaegen, *et al.*,[16] showed small amounts of BC, B_2C, and BC_2 in the gas phase above boron carbide at ~2000°K; hydrogen-containing derivatives of these molecules that are likely to be formed are those isoelectronic with C_2, BC_2, and C_3. Of these proposed molecules, definite experimental evidence was found only for HBC_2. Thermodynamic estimates made for this molecule suggest a heat of atomization of 397 ± 10 kcal/mol. Adding $D°_0(C_2)$ = 143 kcal/mol,[3] $D°_0(BC)$ = 106 kcal/mol,[3] and $D°_0(BH)$ = 78 kcal/mol[3] and dividing the sum into the atomization energy for HBC_2 leads to a calculated resonance stabilization of 1.2; this value can be compared to 1.12 estimated for C_3 and 1.18 estimated for BC_2.[16] (The stabilization of HBC_2 would be the same even if the hydrogen is assumed to be bonded to carbon instead of boron because $D°_0(CH)$ = 81 kcal/mol.[3] Even if the atomization energy were only 377 kcal/mol [*i.e.*, $D(H–BC_2)$ = 80 kcal/mol instead of 100 kcal/mol], the calculated resonance stabilization would be 1.15.

Other resolved boron–carbon–hydrogen ions have been assigned to alkylborane progenitors. Although ethyl- and methylboranes are known as dimers at low temperature, reasonable thermodynamic estimates indicate that they should not be observable under the present conditions. An analogous molecule BCl_2SiCl_3 also has been formed in high-temperature flow system reactions;[19] molecules corresponding to the formulas $BF_2Si_xF_{2x+1}$ (x = 1, 2, and 3)[17,18] have been synthesized at low temperatures by cocondensation of the high-temperature species BF and SiF_2 with SiF_4 and BF_3.

Table VII: Bond Dissociation Energies (kcal/mol) of Borane

Bond	JANAF[a]	Wilson and McGee[b]	Jordan and Longuet-Higgins[c]
B–H	78	84	76
BH–H	110	90	66
BH_2–H	75	83	102
$\Sigma = A$(B–3H)	263	257	244

[a] Reference 3. [b] Reference 8. [c] Reference 10.

Experimental evidence for BH and BH_3, but not for BH_2, is contrary to predictions made with the successive bond dissociation energies calculated from electron impact data for borane.[3,8] Thermodynamic results selected by JANAF[3] (column 1 of Table VII) include electron impact values for D(BH–H) and $D(BH_2–H)$; D(B–H) is spectroscopically determined; and A(B–3H), the atomization energy of borane, is established by the heat of vaporization of boron (132.8 ± 4 kcal/mol), the dissociation energy of hydrogen (104.200 ± 0.001 kcal/mol), and the heat of formation and the dissociation energy of diborane (9.8 ± 4.0, 40 ± 10 kcal/mol). Thus, if D(B–H) is accepted as correct, the sum $[D(BH–H) + D(BH_2–H)]$ must be equal to 185 kcal/mol. Electron impact data of Wilson and McGee[8] (column 2 in Table VII) are constrained to fit a slightly different atomization energy for BH_3; this second study gives a result for D(BH–H) different by about 1 eV. This divergence of electron impact data, the lack of evidence for BH_2 in this experiment, and theoretical treatments suggest that further revision of the accepted bond dissociation energies is necessary. Jordan and Longuet-Higgins,[10] using an extrapolation of N–H and C–H parameters, obtained the values given in column 3 in Table V; their treatment does not depend on the recently corrected D(CH–H) and $D(CH_2–H)$[34,40] and, in fact, correctly predicts the newly determined values. Their calculations for the B–H bond energies, in contrast to the above values, suggest that $D(BH_2–H)$ is the largest of the three, but they also predict a linear structure for BH_2, which is in disagreement with experi-

(35) C. MacKay, J. Nicholas, and R. Wolfgang, *J. Amer. Chem. Soc.*, **89**, 5758 (1967).

(36) C. MacKay and R. Wolfgang, *ibid.*, **83**, 2399 (1961).

(37) For instance, J. Hine, "Physical Organic Chemistry," McGraw-Hill Book Co., Inc., New York, N. Y., 1962.

(38) T. B. Reed in "Advances in High Temperature Chemistry," Vol. I, L. Eyring, Ed., Academic Press, New York, N. Y., 1967, pp 260–316.

(39) For instance, H. B. Palmer, J. Lahaye, and K. C. Hou, *J. Phys. Chem.*, **72**, 348 (1968).

(40) W. A. Chupka, *J. Chem. Phys.*, **48**, 2337 (1968).

ment.[7] Price, Passmore, and Roessler,[11] using isoelectronic comparisons, interpolated bond energies for all the first-row hydrides and their singly charged ions; this work gave values sensibly identical with those of JANAF[3] (Table VII, column 1). This treatment, however, is drastically affected by a number of more recently determined bond energies. In particular, the newly revised values for $D(CH-H)$ and $D(CH_2-H)$ of 101 and 108 kcal/mol[34,40] also change the corresponding bond dissociation energies of CH_2^+ and CH_3^+, the ions that are isoelectronic with BH_2 and BH_3. These and other new dissociation energies no longer lead to graphs with nearly parallel lines as drawn by Price, *et al.* The new curves, however, suggest that $D(BH_2-H)$ is approximately equal to or greater than $D(BH-H)$. The new interpolation is, therefore, in qualitative agreement with the Jordan and Longuet-Higgins treatment which suggests that $D(BH_2-H)$ is larger than $D(BH-H)$. An sp^2 hybridization argument used to explain the successive bond dissociation energies of BF_3 ($D(BF_2-F) = 161$ and $D(BF-F) = 122$ kcal/mol)[15] also suggests this ordering. To form BX_2, an s electron of BX must be promoted to a p orbital forming an sp^2 hybrid, but to form BX_3, no promotional energy is needed; this difference results in a larger BX_2–X bond energy. For BH_2, sp^2 hybridization is indicated by the bent ground state.[7] In view of these arguments and since the sum $[D(BH_2-H) + D(BH-H)] = [A(B-3H) - D(B-H)]$ is reasonably well known (Table VII, column I[3]), approximate values for the two bond dissociation energies can be deduced.[41]

Acknowledgments. The authors wish to thank the men of the Chemistry Shop, the Materials Science Shop, and the Chemistry Electronics Shop and especially Mr. Edward Falkenberg, who made special efforts to keep our temperamental experimental set-up running. We would also like to acknowledge helpful discussion with Professor John L. Margrave.

(41) NOTE ADDED IN PROOF. New results [E. S. Domalski and G. T. Armstrong, *J. Res. Nat. Bur. Stand.*, 72, 133 (1968)] for ΔH_f ($B_{4.222}C$) do not affect the present calculations significantly.

The Electronic Density Distributions in Carbon Monoxide, Carbonyl Sulfide, and Carbon Dioxide

by Mark J. Hazelrigg, Jr., and Peter Politzer

Department of Chemistry, Louisiana State University in New Orleans, New Orleans, Louisiana 70122 *(Received July 8, 1968)*

Plots of electronic density distributions are presented for CO, SCO, and CO_2. These are found to vary gradually in the order CO, SCO, CO_2, as expected. The validity of the transferability of bond properties concept is examined for the C–O bond in SCO and CO_2, and it is found to be only roughly valid in this case.

The carbon–oxygen bond represents one of the most important and widely found chemical linkages, one which occurs prominently in all branches of chemistry. It would be useful, therefore, to have a better understanding of the electronic structure of this bond and of the manner in which this structure (and hence the properties of the bond) is affected by the presence of various substituents on the carbon atom.

At least a start toward the achievement of this kind of understanding is now possible, through the availability of good wave functions for molecules containing the carbon–oxygen bond. The present work has involved the study of three such molecules: carbon monoxide, which has a pure C–O bond unaffected by the presence of any other atom; carbon dioxide, in which the effect of a second oxygen atom can be seen; and carbonyl sulfide, in which this second oxygen has been replaced by a sulfur atom, so that the relative effects of oxygen and sulfur atom substituents upon the C–O bond can be examined.[1]

The molecular wave functions used in this work were the self-consistent-field functions of McLean and Yoshimine.[2] They are believed to be close to the Hartree–Fock limit, which means that they should give

(1) Extended-basis-set self-consistent-field wave functions, believed to be good approximations to Hartree–Fock functions, have been calculated for carbon monoxide by R. K. Nesbet, *J. Chem. Phys.*, 40, 3619 (1964), and W. M. Huo, *ibid.*, 43, 624 (1965). In both cases, the functions were analyzed in considerable detail, in terms of the expectation values of various molecular properties. An interpretative study of the electrostatic forces within the molecule has also been carried out by P. Politzer, *J. Phys. Chem.*, 69, 2132 (1965).

(2) A. D. McLean and M. Yoshimine, "Tables of Linear Molecule Wave Functions," International Business Machines Corp., San Jose, Calif., 1967.

good results, of first-order accuracy, for one-electron properties, such as the electronic density distributions.[3,4]

For each molecule, the total electronic density and the density difference function were calculated. The total density at any point $\mathbf{r}$ is given by

$$\rho(\mathbf{r}) = \sum_i N_i \phi_i^*(\mathbf{r}) \phi_i(\mathbf{r})$$

where N_i is the number of electrons in molecular orbital ϕ_i. The density difference function, originally introduced by Roux and coworkers,[5,6] is defined as

$$\Delta\rho(\mathbf{r}) = \rho(\mathbf{r}) - \sum_j \rho_j(\mathbf{r})$$

The second term represents the sum of the electronic densities of the atoms which constitute the molecule, these being placed at the same positions as they occupy in the molecule but assumed to have undergone no interactions with each other and to have remained undistorted, as in the free state. The density difference function is interpreted as indicating the overall rearrangement of charge density which occurs when the atoms come together to form the molecule.

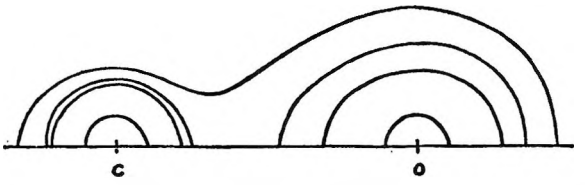


Figure 1. Total electronic density distribution in carbon monoxide. The contours correspond to the values 10.0, 1.0, 0.7, and 0.4, moving outward from each nucleus.

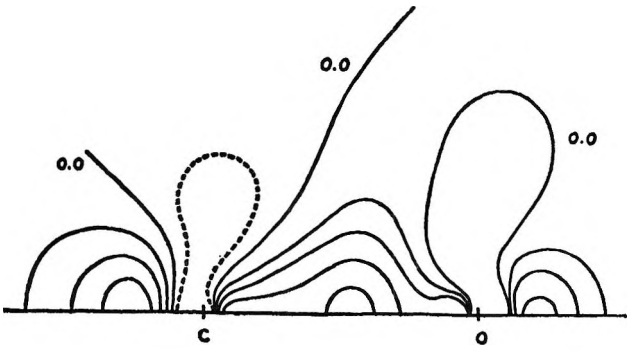


Figure 2. Density difference function for carbon monoxide. The contours come at intervals of 0.04, starting from the 0.0 lines; dotted lines correspond to negative values.

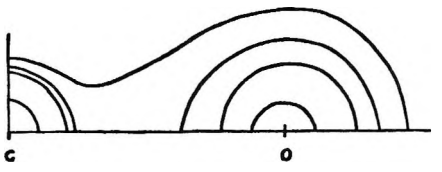


Figure 3. Total electronic density distribution in carbon dioxide. The contours correspond to the values 10.0, 1.0, 0.7, and 0.4, moving outward from each nucleus.

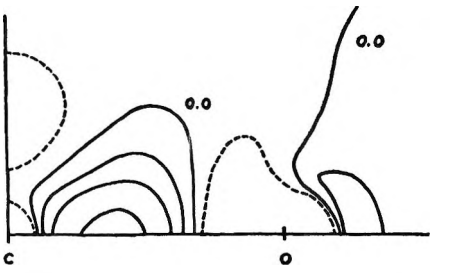


Figure 4. Density difference function for carbon dioxide. The contours come at intervals of 0.04, starting from the 0.0 lines; dotted lines correspond to negative values.

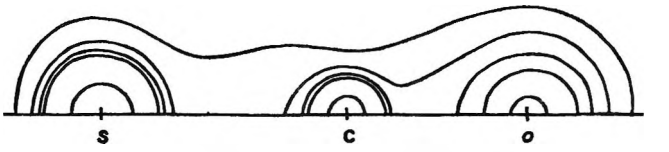


Figure 5. Total electronic density distribution in carbonyl sulfide. The contours correspond to the values 10.0, 1.0, 0.7, 0.4, and 0.15, moving outward from each nucleus.

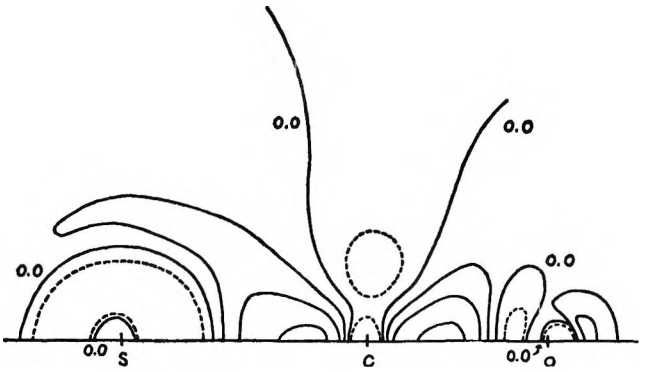


Figure 6. Density difference function for carbonyl sulfide. The contours come at intervals of 0.04, starting from the 0.0 lines; dotted lines correspond to negative values.

The density distributions of the atoms were computed from the self-consistent-field atomic wave functions of Clementi,[7] which again are close to the Hartree–Fock limit and therefore consistent in accuracy with the molecular functions. In calculating the atomic densities, the p-electron distributions were averaged over all spatial directions.

The total electronic density distributions and the density difference functions are presented in Figures 1–6. These diagrams show the distribution of the electrons in each of these molecules and the manner in which this distribution differs from that of the free atoms. A certain amount of caution is necessary in interpreting these diagrams. For example, an initial

(3) L. Brillouin, *Actualites Sci. Ind.*, No. 71 (1933); No. 159 (1934).
(4) M. Cohen and A. Dalgarno, *Proc. Phys. Soc.* (London), **77**, 748 (1961).
(5) M. Roux, S. Besnainou, and R. Daudel, *J. Chim. Phys.*, **53**, 218, 939 (1956).
(6) M. Roux, *ibid.*, **55**, 754 (1958).
(7) E. Clementi, "Tables of Atomic Wave Functions," International Business Machines Corp., San Jose, Calif., 1965.

examination of Figure 1 might suggest that carbon monoxide is made up of a nearly unperturbed carbon atom and a strongly polarized oxygen atom. The density difference plot (Figure 2) shows, however, that the carbon does in fact undergo much rearrangement; there is considerable movement of charge from the regions above and below the nucleus (that is, perpendicular to the bond) to positions along the molecular axis. It turns out that the symmetrical total density contours around the carbon nucleus in Figure 1 are essentially identical with those of the 1s electrons in a free carbon atom; the valence electrons have, for the most part, shifted into the regions to the left or right of the nucleus. Thus the unsymmetrical total density contours around the oxygen nucleus in Figure 1 probably include sizable contributions from the valence electrons of the carbon.

The density difference function for carbon monoxide brings out clearly the important features of the molecule: the large buildup of electronic density in the internuclear region, and the localized concentrations of charge near each nucleus (the "lone pairs"). It is in these features that the characteristic properties of carbon monoxide originate—its very strong bond, which has a higher dissociation energy than that in any other diatomic molecule, and its ability to act as an electron-pair donor, which involves a sharing of the carbon lone pair (the highest-energy electrons in the molecule) with some acceptor.

In examining the electronic structures of carbon dioxide and carbonyl sulfide, it is helpful to view these in terms of the series CO–SCO–CO_2, which presumably reflects increasing perturbation of the pure carbon-oxygen bond of carbon monoxide. Chemical intuition suggests that a sulfur atom should have a lesser perturbing effect upon the original carbon–oxygen entity than an oxygen, so that the electronic structural change should be less in going from CO to SCO than in going from CO to CO_2. These expectations are confirmed by the electronic density diagrams, particularly by the density difference plots (Figures 4 and 6). The addition of a sulfur atom has a significant effect upon the charge distribution around the oxygen nucleus of carbon monoxide; there is now a region of negative $\Delta\rho$ to the left of the oxygen, instead of the charge buildup which was there previously, and the oxygen lone pair has been very distinctly reduced. In carbon dioxide these trends are carried further; the region of negative $\Delta\rho$ has grown, while the lone pair has diminished yet further.

In both of these latter species, the concentration of electronic density along the C–O bond is much less than it is in carbon monoxide, which is consistent with experimental data (to be cited) showing the strength of this bond to be considerably less in SCO and CO_2 than in CO. It is interesting and useful to compare the carbon–oxygen bond in carbonyl sulfide and in carbon dioxide, since such a comparison is very relevant to the important question of the transferability of bond properties. The approximation is commonly made that a given type of bond (that is, single, double, or triple) between some two particular atoms will have nearly the same properties in a variety of different molecules in which it is found. Thus there are tables of bond energies, bond moments, and bond lengths, which give supposedly good approximations to the actual values of these properties in the various molecules in which the given bond occurs. A comparison of the charge distribution in the C–O bond of SCO and CO_2, two different but basically very similar molecules, provides an opportunity to examine the validity of the transferability of bond properties concept, at least for one particular bond, in a fundamental manner, in terms of the electronic structure of the bond.

Qualitatively, the C–O bonds in CO_2 and SCO are certainly very similar, as can be seen from Figures 4 and 6. There are differences in detail, however, which seem to be fairly significant. The decrease in electronic density to the left of the oxygen nucleus is considerably greater in CO_2, while the oxygen lone pair is greatly reduced. It is difficult to estimate the effects of such variations,[8] but it would seem that they are bound to have some influence upon the bond properties, and that these will be only roughly transferable from one molecule to the other.

One such property of the C–O bond in CO_2 and SCO for which an approximate quantitative comparison can be made is the bond energy. The energy required for the process $CO_2 \rightarrow C + O + O$ is 388 kcal/mol,[9] which means that a value of 194 kcal/mol can be taken as the strength of each C–O bond. To break up SCO, $SCO \rightarrow S + C + O$, the energy required is 332 kcal/mol,[9] but here it is not clear how to divide this between the S–C and C–O bonds. It is possible, however, to make an estimate of these two separate bond energies, in the following manner. For the process $CS_2 \rightarrow C + S + S$, the energy requirement is 256 kcal/mol,[10] indicating an energy of 128 kcal/mol for each C–S bond. Thus, if the C–O and C–S bonds in SCO were the same as in CO_2 and CS_2, the total bond energy would be 128 + 194 = 322 kcal/mol—which is 10 kcal/mol less than is actually observed. It has already been pointed out, however, that in terms of electronic structure, the C–O bond in SCO seems to occupy an intermediate position between those in CO and CO_2. This suggests that its bond energy should be greater than that of the corresponding bond in CO_2. By a similar sort of reasoning, the C–S bond would be ex-

(8) In fact, they may partially cancel each other as far as affecting the strength of the C–O bond is concerned, since the presence of a lone pair, as well as the absence of electrons in the internuclear region, can weaken a bond (see, for example, Politzer, ref 1).

(9) Cited in M. Yoshimine and A. D. McLean, *Intern. J. Quantum Chem., Symp. No.* 1, 313 (1967).

(10) T. L. Cottrell, "The Strengths of Chemical Bonds," 2nd ed, Butterworth and Co. Ltd., London, 1958.

pected to be weaker in SCO than in CS_2, since it would presumably be affected more by a neighboring oxygen than by a sulfur atom. These inferences are supported by the facts that the C–O bond length is slightly less in SCO than in CO_2, 1.157 Å compared to 1.162 Å, while the C–S distance is greater in SCO than in CS_2, 1.560 *vs.* 1.55 Å.[10,11] On the basis of these arguments, the value 128 kcal/mol would be an upper bound to the energy of the C–S bond in SCO, and the C–O bond would therefore have a lower bound of 204 kcal/mol. The actual value for the C–S bond would presumably be somewhat less than 128 kcal/mol, and that for the C–O correspondingly more than 204 kcal/mol.

Thus it would appear that the carbon–oxygen bond in SCO will be stronger than that in CO_2 by perhaps 15–20 kcal/mol, which is consistent with the conclusion, based on a comparison of electronic structures, that the properties of the bond in the two cases will be only approximately similar.[12]

A final point of interest is brought out by the density difference diagram for carbonyl sulfide. Rather surprisingly, Figure 6 shows no localized buildup of charge on the outer side of the sulfur nucleus. The sulfur does not appear to have a lone pair, in contrast to the oxygens in the three molecules studied.

Acknowledgments. The authors are grateful to the Kayser-Roth Foundation for partial support of this work. They also appreciate financial assistance from the L.S.U.N.O. Computer Research Center (NSF Grant No. GP-2964).

(11) Y. Morino and C. Matsumura, *Bull. Chem. Soc. Jap.*, **40**, 1095 (1967).

(12) The dissociation energy of the C–O bond in carbon monoxide is 256 kcal/mol (ref 10); as pointed out earlier, it is considerably stronger in CO than in either SCO or CO_2.

Primary Processes in the Acetone Photochemical System

by H. Edward O'Neal[1]

Department of Chemistry, San Diego State College, San Diego, California 92115

and Carl W. Larson

Department of Chemistry, University of Washington, Seattle, Washington *(Received August 14, 1968)*

A revised mechanism which quantitatively correlates the data for the principal emission (phosphorescence) and the dissociation primary processes in the acetone photochemical system is presented. Two decomposition processes are proposed, a spontaneous decomposition from upper vibrational levels of hot triplets formed isoergotically after light absorption, and a decomposition of thermalized triplets which is a unimolecular pressure-dependent process. Quite consistent high- and low-pressure Arrhenius parameters for the thermal decomposition are determined from several data sources and place the critical barrier to triplet decomposition at about $E_a \simeq 10 \pm 1$ kcal/mol. When treated in accordance with the proposed mechanism, a quantitative correlation of the emission and the decomposition data in terms of their temperature, pressure, and wavelength dependencies is demonstrated. The zero-point level of the acetone triplet is placed at about 80 kcal/mol above the acetone ground state.

Introduction

In a prior communication, we reported the results of the effect of hydrogen bromide on the photolysis of acetone using light in the 3150-Å region.[2] Decomposition quantum yields (ϕ_d) were shown to be strongly quenched by hydrogen bromide, and from studies of ϕ_d as a function of temperature and hydrogen bromide pressure it was concluded that two kinds of primary decomposition processes were operative. The first involved spontaneous decomposition from vibrationally excited triplet-state molecules formed isoergotically after absorption; the decomposition was essentially unaffected by hydrogen bromide. The second involved a pressure-dependent decomposition of triplet-state molecules in thermal equilibrium with their environment; this process could be strongly quenched by hydrogen bromide. The qualitative and quantitative conclusions of the former study with regard to the primary processes in acetone are summarized in the simplified reaction coordinate diagram of Figure 1 and in Mechanism A.

(1) Author to whom reprint requests should be sent.

(2) C. W. Larson and H. E. O'Neal, *J. Phys. Chem.*, **70**, 2475 (1966).

Mechanism A

$$CH_3COCH_3(A) \xrightarrow{h\nu} \text{(in one step or a sequence of steps)} \longrightarrow {}^3(CH_3COCH_3)^* \text{ or } {}^3A_n^*$$

$${}^3A_n^* \xrightarrow{k'(\epsilon)^*} CH_3\cdot + CH_3CO \qquad k'(\epsilon)^* = A\left(\frac{E - {}^3E_c}{E}\right)^{s-1} \qquad A = 10^{15.1}\ \text{sec}^{-1},\ s = 18,\ E_c = 17\ \text{kcal}$$

$${}^3A_n^* + M \xrightarrow{Z} {}^3A_0 + M^* \qquad Z = \text{collision frequency bimolecular rate constant}$$

$${}^3A_0 + M \xrightarrow{{}^3k_d} CH_3\cdot + CH_3CO + M \qquad {}^3k_d = 10^{12.25-9.96/\theta}\ \text{l./mol-sec}$$

$${}^3A_0 \xrightarrow{k_p} {}^1A_n + h\nu\ \text{(phosphorescence)}$$

$${}^3A + HBr \xrightarrow{k_T} CH_3C(OH)CH_3 + Br \qquad k_T = 10^{9.6-1.1/\theta}\ \text{l./mol-sec}$$

Although the decomposition quantum yield data leave little doubt that both a spontaneous decomposition and a pressure-dependent thermal decomposition of the acetone triplet are involved in the mechanism, some of the quantitative conclusions of the earlier paper concerning these processes were not very satisfactory. The first was that the Rice–Ramsperger–Kassel (RRK) form for the spontaneous decomposition rate constant, $k'(\epsilon)^*$, required an $s = 18$, which was close to the maximum number of vibrational degrees of freedom in acetone (*i.e.*, 24). At the experimental temperatures employed this is an unreasonably high value. The second was that an activation energy for thermal decomposition of the acetone triplet of ${}^3E_c = 17$ kcal/mol was needed to fit the spontaneous decomposition data. Since the experimental activation energy for this process at 200 Torr total pressure seemed to be about 10 kcal/mol,[3a] it was necessary to postulate that the observed decomposition was a unimolecular process in its low-pressure region. However, since it was also shown that the spontaneous decomposition process was competitive with, but slower than, collisional deactivation at $P_{total} \simeq 75$ Torr, one would expect the thermal decomposition under similar conditions to be in the fall-off region *and not near* the limiting low-pressure region.

Several very careful and thorough studies of the fluorescence and phosphorescence of acetone as functions of total pressure, temperature, and exciting wavelength have been reported.[3-7] These emission processes are competitive with decomposition; thus a correlation between emission and decomposition quantum yield data must exist. In this paper the emission and decomposition quantum yield data for the acetone photolysis have been quantitatively reexamined in terms of a slightly revised primary process scheme. It is shown that the revised mechanism is consistent with all of the primary process data, that it avoids the unsatisfactory aspects of the former study, and that it resolves many of the perplexing problems originally posed by the emission data.

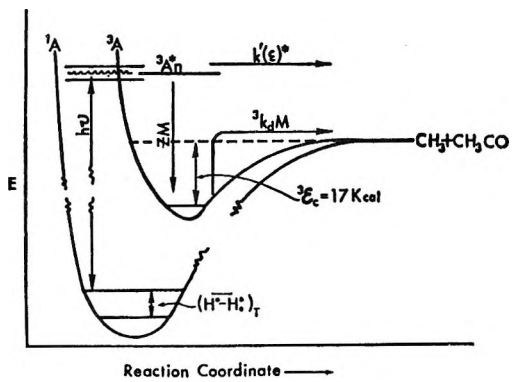


Figure 1. Original primary process mechanism proposed by Larson and O'Neal.[2]

Discussion

The revised mechanism for the primary processes in the acetone photolysis (Figure 2 and Mechanism B) incorporates an upper triplet state which is not "tied" to the acetone ground state. Decomposition, both spontaneous and thermal, occurs *via* an electronic state crossing to some type of an unstable, repulsive state (presumably a singlet). Perhaps the most significant revision of the mechanism is that the thermal decomposition of the acetone triplet is treated as a unimolecular reaction in its pressure fall-off region.

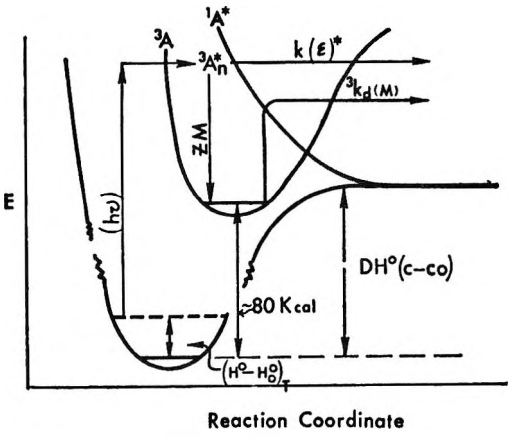


Figure 2. Reaction coordinate representation of the primary processes in the acetone photochemical system.

(3) (a) H. J. Groh, G. W. Luckey, and W. A. Noyes, Jr., *J. Chem. Phys.*, 21, 115 (1953); (b) R. E. Hunt and W. A. Noyes, Jr., *J. Amer. Chem. Soc.*, 70, 467 (1948).

(4) G. W. Luckey, A. B. F. Duncan, and W. A. Noyes, Jr., *J. Chem. Phys.*, 16, 407 (1948).

(5) G. W. Luckey and W. A. Noyes, Jr., *ibid.*, 19, 227 (1951).

(6) J. Heicklen, *J. Amer. Chem. Soc.*, 81, 3863 (1959).

(7) W. E. Kaskan and A. B. F. Duncan, *J. Chem. Phys.*, 18, 427 (1950).

Mechanism B. Decomposition and Phosphorescence

$$^3A_m^* \xrightarrow{k(\epsilon)^*} CH_3\cdot + CH_3CO \quad \text{(spontaneous decomposition)} \quad \begin{cases} A_\infty^* = 10^{11.1}\ \text{sec}^{-1} \text{ where } k(\epsilon)^* = A_\infty^*\left(\dfrac{E-E_0}{E}\right)^{s-1} \\ {}^3E_c = 9.1\text{–}10.3\ \text{kcal/mol}; \qquad s = 5.7\text{–}7.2\ \text{(thermal)} \end{cases}$$

$$^3A_m^* + M \xrightarrow{Z} {}^3A_0 + M^* \quad \text{(collisional deactivation)}$$

$$\left.\begin{aligned} {}^3A + M &\underset{Z}{\overset{k_0}{\rightleftharpoons}} {}^3A_m + M \\ {}^3A_n &\xrightarrow{k(\epsilon)} CH_3\cdot + CH_3\dot{C}O \end{aligned}\right\} \quad \text{(thermal decomposition)} \quad \begin{cases} {}^3k_d = \dfrac{k_0 k(\epsilon) M}{ZM + k(\epsilon)} \\ k_0 = 10^{9.81-5.95/\theta}\ \text{l./mol-sec} \end{cases}$$

$$^3A_0 \xrightarrow{k_p} {}^1A_{n'} + h\nu \ \text{(phosphorescence)} \quad \begin{cases} k_\infty = \left(\dfrac{k_0 k(\epsilon)}{Z}\right) = 10^{10.14-9.6/\theta}\ \text{sec}^{-1} \end{cases}$$

$$^3A_0 \xrightarrow{k_{ic}} A_{m'} \quad \text{(internal conversion)} \quad k_{ic} \simeq 10^{4.96-1.84/\theta}\ \text{sec}^{-1}$$

$$^3A + HBr \xrightarrow{k_T} \text{quench} \quad \text{(triplet trapping)} \quad k_T = 10^{9.6-1.1/\theta}\ \text{l./mol-sec.}$$

I. Kaskan and Duncan (K & D)

The phosphorescence lifetime study by K & D has been most influential to the quantitative features of the revised mechanism. K & D found that acetone emission lifetimes (phosphorescence) were strongly pressure dependent (see Figure 3). The usual Stern–Volmer (SV) plots of τ^{-1} *vs.* P were not linear but the data could be fit by an equation of the form

$$\tau^{-1} = k_1 + k_2P/(1 + k_3P) \qquad \text{(I)}$$

An interesting aspect of the lifetime curves is their similarity to unimolecular rate constant fall-off curves. One would expect that a pressure-dependent decomposition in competition with phosphorescence would produce just the kind of behavior observed. Thus steady-state treatment of mechanism B gives the following relations

$$^3k_{d(uni)} = \frac{k_0 M}{1 + [ZM/k(\epsilon)]} \qquad \text{(II)}$$

$$^3\tau^{-1} = k_p + k_{ic} + {}^3k_{d(uni)}$$

$$= \frac{(k_p + k_{ic}) + \{(k_p + k_{ic})[Z/k(\epsilon)] + k_0\}M}{1 + [ZM/k(\epsilon)]} \qquad \text{(III)}$$

Equation II is the simple Hinshelwood–Lindemann relation for the pressure dependence of a unimolecular rate constant with k_0, Z, and $k(\epsilon)$ being the specific rate constants for second-order collisional activation, for collisional deactivation of energized molecules, and for spontaneous decomposition of collisionally energized molecules, respectively. It is apparent that eq I and III are identical in form when $k_1 = (k_p + k_{ic})$; $k_3 = Z/k(\epsilon)$ and $k_2 = [(k_1 \times k_3) + k_0]$. We therefore propose that the curvatures of the SV plots, Figure 3, result almost entirely from the pressure dependence of the decomposition of triplet-state acetone molecules.

A reviewer has suggested that the curvatures in the K & D lifetime plots could be a result of acetone triplet quenching by the product biacetyl. Indeed our first interpretation of the K & D data invoked this effect. However, the efficiency of biacetyl as a triplet quencher is known[8] and the amount of biacetyl product produced in the flash of a K & D lifetime run can be calculated.

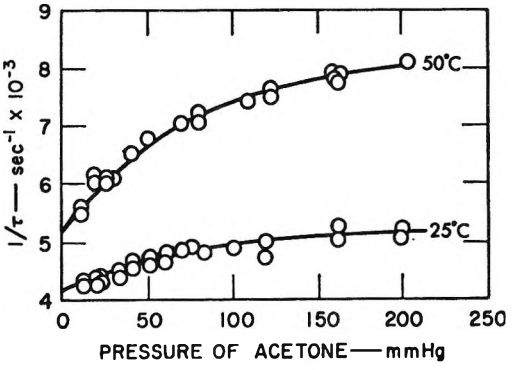


Figure 3. Variation of the "phosphorescence" lifetime of acetone with pressure—Kaskan and Duncan.

At the relatively low intensities employed by K & D to obtain the lifetime data of Figure 3, it can be shown that triplet quenching by biacetyl was negligible. Note also that the degree of curvature in the τ plots increases with increasing temperature. This is incompatible with triplet quenching by biacetyl since biacetyl quantum yields decrease rapidly with increasing temperature as a result of the acetyl radical decomposition. At much higher intensities, K & D did observe a lifetime-intensity dependence (*i.e.*, 10% decrease in τ with a 50-fold I_0 increase). This latter effect can be quan-

(8) J. Heicklen and W. A. Noyes, Jr., *J. Amer. Chem. Soc.*, 81, 3858 (1959).

titatively correlated with the biacetyl product formation.

The Arrhenius parameters for the pertinent rate constants of eq III can be calculated from the K & D lifetime data. One obtains for the triplet decomposition rate constant in the low-pressure limit, $k_0 = 10^{5.31-5.30/\theta}$ mm^{-1} sec^{-1}; for the triplet decomposition rate constant in the high-pressure limit, $k_\infty = k_0 k(\epsilon)/Z = 10^{9.81-9.07/\theta}$ sec^{-1}; and for the ratio of spontaneous decomposition to collisional deactivation rate constants (*i.e.*, the $M_{1/2}$ pressure when $k_{uni} = \frac{1}{2}k_\infty$), $M_{1/2} = 10^{4.51-3.77/\theta}$ mm (see also Table II). Note that the *A* factors for the low- and high-pressure decompositions are considerably lower than allowed for "normal" simple bond fissions in unimolecular rate theory. Low *A* factors, however, would be expected for decompositions involving forbidden electronic state crossings. Thus it is reasonable in terms of photochemistry and unimolecular rate theory to propose decomposition *via* an upper repulsive singlet as shown in Figure 2.

Additional support for the pressure dependence of the triplet decomposition comes from several other studies, all concerned with the acetone phosphorescence quantum yields (Q_p). The pertinent equations from the steady state are

$$Q_p = \left(\frac{ZM}{k(\epsilon)^* + ZM}\right)\left(\frac{k_p}{k_p + k_{ic} + {}^3k_{d(uni)}}\right) \quad \text{(IV)}$$

Equation IV rearranges to give

$$Q_p^{-1}F_M^{-1} = \left(\frac{k_{ic} + k_p}{k_p}\right) + \frac{k_0}{k_p}\left(\frac{M}{X_M}\right) \quad \text{(V)}$$

where

$$F_M = \left(1 + \frac{k(\epsilon)^*}{ZM}\right); \qquad X_M = \left(1 + \frac{M}{M(\frac{1}{2})}\right)$$

The function F_M, being dependent on the rate constant for spontaneous decomposition of hot triplets formed as a consequence of the absorption act ($k(\epsilon)^*$), is strongly wavelength dependent. For studies in the 3130-Å region, employing standard mercury arcs and filter combinations, reasonable F_M values can be evaluated at various pressures and temperatures from the spontaneous decomposition quantum yield data of O'Neal, *et al.* (Table II). The function X_M can also be calculated at various pressures and temperatures from the results of the present interpretation of the K + D data (Table I).

In the following sections, we apply eq V to the phosphorescence data of ref 2, 5, and 6.

II. Luckey and Noyes (L & N)

L & N measured the total emission efficiencies (Q) of acetone when excited by light in the 3130-Å region (*i.e.*, light sources and filters similar to those employed by L & O), over a range of temperatures (25–300°), as a function of acetone pressure (25–200 Torr), and as a function of various additives (O_2, NO, H_2, and N_2). The data are reproduced in the first two columns of Table IIIA and in Table IIIB. With O_2 and NO the emission efficiencies were strongly quenched and approached constant values at any particular temperature. H_2 and N_2 did not affect the emissions. This is consistent with the interpretation that the phosphorescence (Q_p) was quenched by O_2 and NO and that the emission remaining (Q_f) originated either from a prior state (*e.g.*, first excited singlet) or from a vibrationally excited, short-lived, triplet. These alternatives will be discussed in a future communication.

Fluorescence quantum yields for acetone are very small (*e.g.*, less than 0.3% of all excited acetone molecules return to the ground state by fluorescence); therefore errors in their measurement are undoubtedly large. Defining the emission from acetone in the presence of O_2 and NO as a fluorescence, one observes that

Table I: Kaskan and Duncan Lifetime Data Related to Mechanism B[a]

K & D constants	Units	25°	50°
$k_1 = (k_D + k_{ic})$	sec^{-1}	4.1×10^3	5.25×10^3
$k_2 = (k_1 \times k_3 + k_0)$	sec^{-1} mm^{-1}	1.0×10^2	1.1×10^2
$k_0 = \frac{Z}{k(\epsilon)} = \frac{k_0}{k_\infty}$	mm^{-1}	1.8×10^{-2}	1.1×10^{-2}
$M(\frac{1}{2}) = \frac{k(\epsilon)}{Z} = \frac{k_\infty}{k_0}$	mm	55.6	90.8
k_0	mm^{-1} sec^{-1}	26	52
k_∞	sec^{-1}	1445	4720

[a] k_0 is the Hinshelwood–Lindemann (H-L) low-pressure limiting rate constant for acetone decomposition. k_∞ is the H-L high pressure limiting rate constant for ^{3}A decomposition. $M(\frac{1}{2})$ is the RRK pressure at which $^3k_{d(uni)} = \frac{1}{2}k_\infty$. Z is the rate constant for collisional deactivation of excited triplets (in mm^{-1} sec^{-1}). $k_0 = 10^{5.31-5.30/\theta}$ mm^{-1} sec^{-1}. $k_0 = 10^{10.06-5.95/\theta}$ l./mol-sec. $k_\infty = 10^{9.81-9.07/\theta}$ sec^{-1}. $M(\frac{1}{2}) = k(\epsilon)/Z = k_\infty/k_0 = 10^{4.51-3.77/\theta}$ mm. $(k_{ic} + k_D) = 10^{4.96-1.84/\theta}$ sec^{-1}.

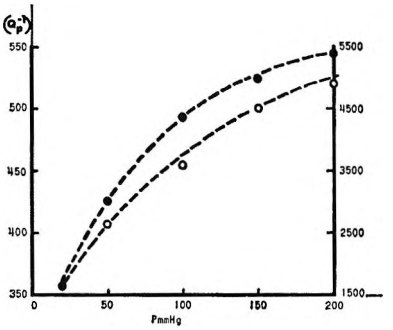


Figure 4. Stern–Volmer plot of phosphorescence quantum yields—Luckey and Noyes. Data for 25° (○), left-hand ordinates. Data for 120° (●), right-hand ordinates. The degree of curvature *increases* with increasing temperature.

Table II: Summary of Decomposition Quantum Yields of Acetone Determined by O'Neal, *et al.* (3140 Å)

		Obsd		Calcd			
T, °C	$\bar{M}$, mm	$\phi_d{}^{*a}$	$\phi_d\bar{M}^b$	$\phi_d(M)^c$	$\phi_d''\bar{M}^d$	$[k(\epsilon)^*/ZM]$	$[k(\epsilon)^*/Z]$
25	75	0.044	...	0.18	(0.18)	0.046	3.45
44	65	0.080	0.28	0.31	(0.34)	0.085	5.5
96	70	0.18	0.88	0.68	(0.76)	0.22	15.4
126	77	0.25	0.92	0.76	(0.85)	0.33	25.4
150	75	0.32	1.00	0.83	(0.89)	0.47	35.3

[a] $\phi_d{}^*$ is the acetone decomposition quantum yield obtained in excess hydrogen bromide. The hydrogen bromide eliminated all decomposition normally occurring *via* thermalized triplet-state molecules. $\phi_d{}^* = k(\epsilon)^*/(k(\epsilon)^* + ZM)$. [b] ϕ_d is the total acetone decomposition quantum yield (pure acetone) observed. [c] ϕ_d' values were calculated from ${}^3k_d$, $(k_{ic} + k_p)$ and $M_{1/2}$ values of K and D (Table I) and $\phi_d{}^*$ values of L and O (above) using the relation: $\phi_d(\text{total}) = [{}^3k_d(1 - \phi_d{}^*)/({}^3k_d + k_{ic} + k_p)] + \phi_d{}^*$. [d] The ϕ_d'' values in parenthesis were obtained as in c with the exception that the ${}^3k_d$ values of G L and N were employed (see discussion on GL & N results).

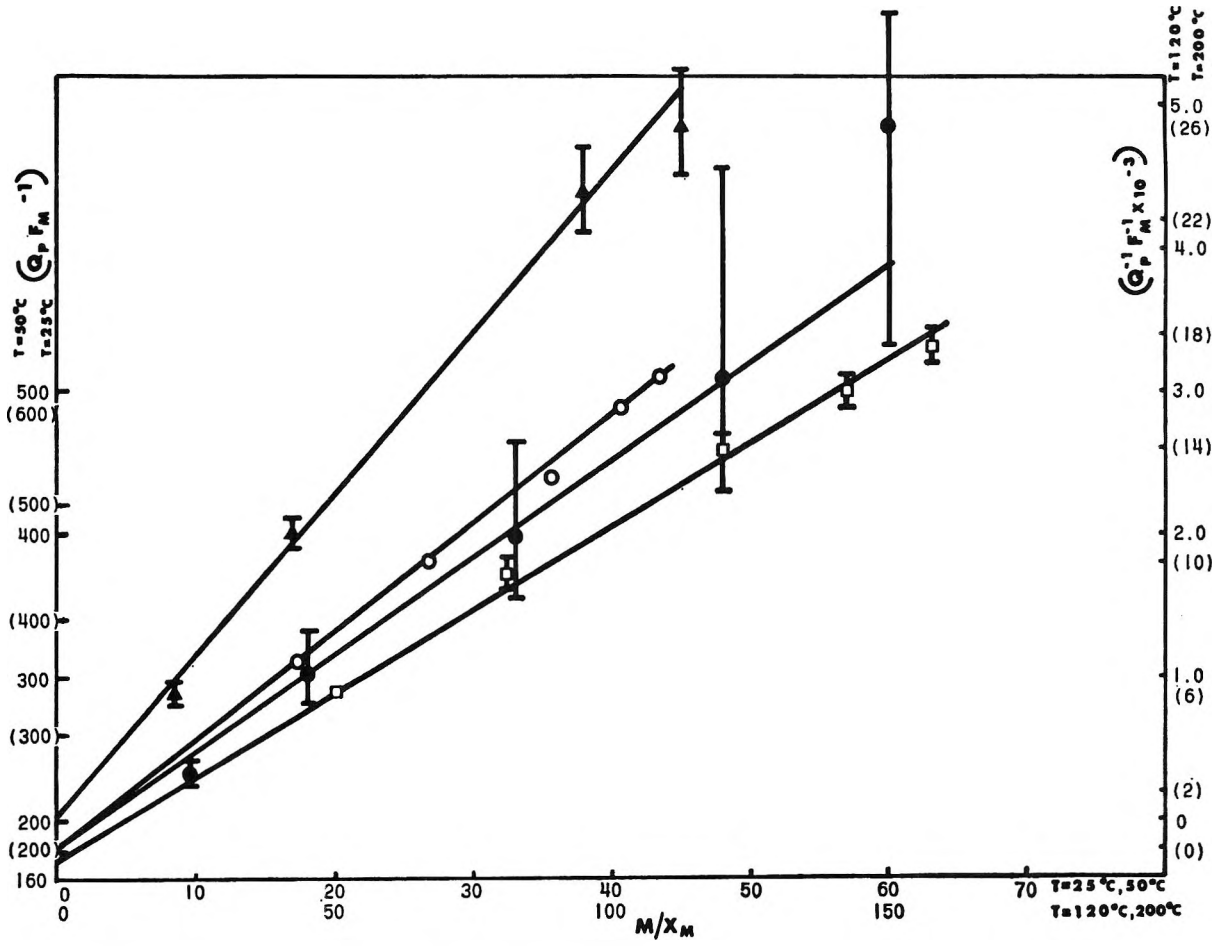


Figure 5. "Corrected" phosphorescence quantum yields variation with pressure and temperature (eq V) by Luckey and Noyes. $(Q_pF_M)^{-1}$: I, estimated error limits in $(Q_pF_M)^{-1}$; 25° (○), values on left from 160 to 500; 50° (□), values on left (parenthesis) from 200 to 600; 120° (▲), values on right from 0 to 5 × 10^3; 200° (●), values on right (parenthesis) from 0 to 26 × 10^3; (M/X_M): 25 and 50°, upper bottom from 0 to 70; 120 and 200°, lower bottom from 0 to 150.

the Q_f yields of L & N (Table IIIB) show a slight systematic decrease with increasing pressure. This behavior is very likely spurious since the more recent and probably more reliable fluorescence data obtained by Heicklen (Table V) show just the opposite effect. Therefore we have calculated average fluorescence quantum yields at each temperature and subtracted these averages from the total emissions to obtain the phosphorescence Q_p values required in eq V. An apparent negative energy dependence for fluorescence seems real and this effect is discussed later.

Calculated values of $Q_p{}^{-1}$, $(Q_p \times F_M)^{-1}$, and (M/X_M) are shown in columns 5, 6, 8, 9 of Table IIIA. Plots of the data according to eq V for the temperatures 25, 50,

Table III: A. Data[a] of Luckey and Noyes as Applied to Eq V

T = 25°	$M(\frac{1}{2})$ = 55.6 mm			$[k(\epsilon)^*/Z]$ = 3.46 mm, 3140 Å		$Q_f \times 10^4 = 56 \pm 3$, $Q_f^{-1} = 179 \pm 9$	
P, mm	Q^{-1} [a]	$Q \times 10^4$	$Q_D \times 10^4$	(Q_D^{-1})	$(Q_D^{-1} \times 15)$	F_M	$(Q_D F_M)^{-1}$	(M/X_M)
25	21	475	419	23.8	357 ± 3	1.138	313	17.2
50	23.5	425	369	27.1	407 ± 3	1.069	381	26.3
100	26	384	328	30.3	455 ± 5	1.035	440	35.7
150	28	356	300	33.3	500 ± 5	1.023	488	40.7
200	29	345	289	34.6	520 ± 8	1.017	512	43.6
T = 50°	$M(\frac{1}{2})$ = 91 mm			$[k(\epsilon)^*/Z]$ = 6.30 mm, 3140 Å		$Q_f \times 10^4 = 54 \pm 3$, $Q_f^{-1} = 186 \pm 8$	
P, mm	Q^{-1}	$Q \times 10^4$	$Q_D \times 10^4$	(Q_D^{-1})	$(Q_D^{-1} \times 15)$	F_M	$(Q_D F_M)^{-1}$	(M/X_M)
25	24	417	363	27.5	413	1.250	331	19.7
50	27.5	363	309	32.3	485	1.126	432	32.3
100	32	312	258	38.7	581	1.063	547	47.6
150	34	294	240	41.7	626	1.042	600	56.7
200	35	285	231	43.3	650	1.032	630	62.8
T = 120°	$M(\frac{1}{2})$ = 260 mm			$[k(\epsilon)^*/Z]$ = 22.9 mm, 3140 Å		$Q_f \times 10^4 = 49 \pm 1.5$, $Q_f^{-1} = 205 \pm 5$	
P, mm	Q^{-1}	$Q \times 10^4$	$Q_D \times 10^4$	(Q_D^{-1})	$(Q_D^{-1} \times 15)$	F_M	$(Q_D F_M)^{-1}$	(M/X_M)
25	72	139	90	111	1,660	1.915	868	22.8
50	100	100	51	196	2,940	1.458	2,020	41.9
100	120	83.3	34.3	292	4,380	1.229	3,560	72.2
150	127	78.8	29.7	337	5,050	1.152	4,380	95.2
200	130	76.8	27.8	360	5,400	1.114	4,830	112.5
T = 200°	$M(\frac{1}{2})$ = 595 mm			$[k(\epsilon)^*/Z]$ = 61.7; 3140 Å		$Q_f \times 10^4 = 45.5 \pm 2$, $Q_f^{-1} = 220 \pm 10$	
P, mm	Q^{-1}	$Q \times 10^4$	$Q_D \times 10^4$	(Q_D^{-1})	$(Q_D^{-1} \times 15)$	F_M	$(Q_D F_M^{-1})$	(M/X_M)
25	160	62.3	16.8	595	8,930	3.46	2,580	24
50	177	56.3	10.8	926	13,900	2.23	6,230	45.2
100	185	54.0	8.5	1,178	17,700	1.62	10,900	85.5
150	192	52.0	6.5	1,540	23,200	1.41	16,450	120
200	200	50.0	4.5	2,220	33,800	1.31	25,400	150

B. Fluorescence of Acetone (*i.e.*, Emission with Added O_2 and NO)[a,b]

T = 50°			
P, mm	NO	O_2	Q^{-1}*
150	5		167
150	7		200
T = 200°			
160	16		220
T = 300°			
50			227
100			238
150			252
200			265

T = 140°			
P, mm	O_2	NO	Q^{-1}
	150	5	210
	150	10	215
	150	20	215
	50	5	177
	50	10	182
	50	20	183
	150	7.5	208
	150	25	211

[a] The emission data of L & N were reported in arbitrary intensity units. To obtain absolute intensities Q^{-1} must be multiplied by 15 (note column 6 of Table IIIA). [b] Data pertinent to Figure 4.

120, and 200° are shown in Figure 4. The errors limits indicated for $(Q_D F_M)^{-1}$ are those arising from the uncertainty in the fluorescence quantum yields and are probably minimum values. Note that the extreme curvatures obtained by plots of the phosphorescence data in the usual Stern–Volmer form (see Figure 5) have been entirely removed within experimental error by the F_M and X_M corrections. The slopes and intercepts of the lines give (k_0/k_p) and $(k_{ic} + k_p)/k_p$, respectively. Intercepts seem to decrease somewhat with tempera-

Table IV: Groh, Luckey, and Noyes-Kaskan and Duncan Lifetime Data Related to the Acetone Triplet Decomposition (200 Torr Pressure)

All $\times 10^{-3}$ sec^{-1}	25°	32°	50°	75°	Source
$I \times 10^{-3}$ [a]		6.6	9.2	20.5	G L & N
$I \times 10^{-3}$	5.2				K & D
$(k_{ic} + k_p) \times 10^{-3}$	4.1	4.4	5.2	6.4	K & D
$^3k_{d(uni,\ 200\ Torr)} \times 10^{-3}$ [b]	1.1	2.2	4.0	14.1	G L & N
$^3k_{d(uni,\ 200\ Torr)} \times 10^{-3}$ [c]	1.13	1.62	3.25	9.87	K & D

[a] $I = (^3k_d + k_p + k_{ic})$ at $P_T = 200$ Torr. [b] ^3k_d (G L & N) $= I - (k_{ic} + k_p)$. [c] ^3k_d(K & D) $= k_0M/(1 + M/M_{1/2})$; values of k_0 and $M_{1/2}$ from Table I.

ture, although the errors are too great to be certain of this. For the slopes, one obtains $(k_0/k_p)_{mm^{-1}} = 7.4$ (25°), 7.3 (50°), 45.3 (120°), and 135 (200°), which give an activation energy difference of $(E_0 - E_p) \simeq 5.6 \pm 1.0$ kcal/mol. This is in very good agreement with the activation energy obtained from the K & D data for the same processes. Although the apparent errors in the phosphorescence quantum yields are smallest at the low temperatures, the real errors may in fact be largest there. The reason for this is that the product biacetyl is an extremely efficient quencher of the acetone emission.[8] Since quantum yields of biacetyl decrease rapidly with temperature (a result of the acetyl radical decomposition), triplet quenching by biacetyl would be expected to be most important at 25°. From the results of Heicklen and Noyes,[8] it can be shown that such quenching should be important at 25° in the L & N system. This could account for the nearly identical slopes (k_0/k_p) at 25 and 50°. Similar calculations show that the higher temperature phosphorescence data cannot be much in error as a result of biacetyl–acetone triplet quenching processes.

III. "High Pressure" Triplet Decomposition Kinetics—Groh, Luckey, and Noyes (GL & N)

GL & N studied the lifetime of the acetone emission as a function of added oxygen. Quite well behaved Stern–Volmer plots of τ^{-1} *vs.* O_2 were obtained at 32, 50, and 75° for constant acetone concentrations (6.34×10^{18} molecules/cc $\simeq$ 200 Torr). According to mechanism B, the equation of the (SV) lines should be

$$\tau^{-1} = k_p + k_{ic} + {}^3k_{d(200)} + k_r{}^1(O_2) \qquad \text{(VI)}$$

Intercepts should therefore equal

$$I = \tau^{-1}\ (\text{pure acetone 200 Torr}) = {}^3k_{d(200)} + k_{ic} + k_p \qquad \text{(VII)}$$

Subtracting $(k_{ic} + k_p)$, K & D data, Table I, from the GL & N intercepts gives values for the triplet decomposition rate constant at 200 Torr pressure (Table IV). From an Arrhenius plot of these values one obtains $\log {}^3k_{d(200\ Torr)} = 10.46 - 10.15/\theta$. Considering the probable errors in the decomposition rate constants obtained in this manner, this is in good agreement with the parameters calculated at the same total pressure from the K & D data (*i.e.*, $\log {}^3k_{d(200)} = 9.58 - 8.9/\theta$).

Decomposition Quantum Yields for Acetone (3130 Å). According to the revised mechanism, quantum yields for acetone decomposition should be given by

$$\phi_d = \{{}^3k_d(1 - \phi_d{}^*)/[{}^3k_d + k_{ic} + k_p]\} + \phi_d{}^* \qquad \text{(VIII)}$$

where

$$\phi_d{}^* = k(\epsilon)^*/[k(\epsilon)^* + ZM] \qquad \text{(IX)}$$

and

$${}^3k_d = \frac{k_0M}{(1 + M/M_{1/2})} \qquad \text{(X)}$$

Since ^3k_d and $\phi_d{}^*$ are T and P dependent, the decomposition quantum yields (ϕ_d) should also vary with pressure and temperature. If the $\phi_d{}^*$ values of L & O (Table II) are used, along with the various triplet rate constant data of Table IV, one can calculate from eq VIII acetone decomposition quantum yields under various conditions. Results at 25 and 75° are summarized in the curves of Figure 6. By way of comparison, experimental decomposition quantum yields of Herr

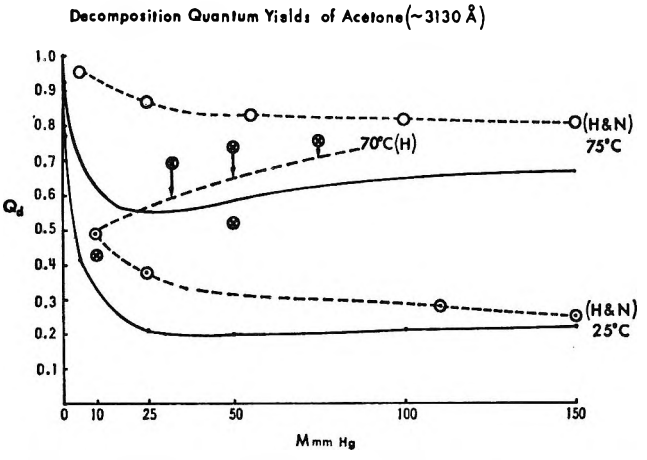


Figure 6. Theoretical decomposition quantum yields variation with pressure (3130 Å): O, Herr and Noyes, λ = 3130 Å; ⊗, Heicklen and Noyes, λ = 3130 Å, T 70°; (———), lines are theoretical ϕ_d curves; (- - - -), experimental ϕ_d curves.

Table V: Emission Efficiencies of Acetone Vapor—Heicklen

Acetone pressure, M, mm	$Q_{Total} \times 100 = (Q_f + Q_p) \times 100$, $T = 40°$, 2800 Å	2890 Å	2970 A	3020 Å	3130 A	$T = 63°$, 3130 A	M, mm
24.8	0.194	0.323	0.691	1.25	2.06	1.55	30
48.5	0.273	0.502	0.938	1.33	2.08	1.48	55
77	0.386	0.700	1.09	1.44	1.71	1.31	113
100	0.543	0.893	1.34	1.67	1.96	1.16	170
148	0.665	1.07	1.48	1.62	1.94	1.26	217
203	0.855	1.22	1.52	1.67	1.78		
			Oxygen Present: $Q_f \times 100$; $T = 40°$				
24.8	0.194	0.206	0.199	0.189	...		
48.5	0.159	0.153	0.180	0.178	...		
77	0.155	0.169	0.182	...	0.203		
100	0.169	0.194	0.208	0.210	0.208		
148	0.169	0.203	0.187	(0.237)	0.213		
203	0.176	0.206	0.201	0.219	0.205		
Q_f: (data)	0.170	0.189	0.193	0.199	0.207	Q_f(error) $\simeq \pm 0.03$	
Q_f: (Figure 7)	0.154	0.159	0.165	0.172	0.207		

and Noyes[9] and Heicklen and Noyes[8] are also shown. Considering the size of the probable errors inherent in the decomposition data, the agreement between calculated and observed values is acceptable.

It is interesting to note that the calculated curves show a minimum in ϕ_d at around 25 Torr. It can be shown that the minimum becomes more pronounced at longer wavelengths. An experimental verification of this effect would be interesting.

Calculated decomposition quantum yields may also be compared with those determined experimentally by L & O at 44, 96, and 126° (see Table II). Here the agreement is quite good if the ^3k_d values of GL & N are used in the calculations. Decomposition quantum yields are quite dependent on ϕ_d* yields and these, in turn, vary significantly with wavelength. Since the incident radiation used by L & O was estimated to have an average around 3150 Å, the calculated curves of Figure 6 may be low for 3130-Å yields by as much as 0.1 unit. Because of the extreme sensitivity of quantum yields in general to wavelength, it is clear that future photochemical primary process studies should give more attention to the precise determinations of the effective wavelengths of absorbed light than has been exercised in the past.

IV. Heicklen (H)

Heicklen studied the emission efficiencies[10] of acetone at 40° as a function of pressure and wavelength (selected by a monochromator) with and without added O_2. In addition, emission efficiencies resulting from 3130-Å absorbed radiation were studied at two temperatures, 40 and 63°. The data are given in Table V.

1. Fluorescence Quantum Yields. Defining the emission from acetone in the presence of O_2 as fluorescence, it is clear from Heicklen's data that the fluorescence is not much changed by variations in wavelength or pressure. Although there appears to be a small systematic increase in fluorescence with increasing pressure (behavior just opposite to that observed by L & N), the apparent increase in Q_f at 24.8 Torr and at all λ suggests that this variation could easily be a result of experimental error. On the other hand, inspection of the Q_f values and their averages at each λ indicates a small but real increase in emission with increasing wavelength. This correlates with the decrease in Q_f observed by L & N with increasing temperature. It is possible to compare semiquantitatively the two sets of fluorescence data (H and L & N) if one assumes that fluorescence quantum yields depend only on the energy of the states formed in the absorption process. Thus, for example, fluorescence resulting from the absorption of 3020-Å light (94.68 kcal/mol), at 40° $(H° - H_0°)_{vib} = 1.69$ kcal/mol[11]) giving an energy state 96.37 kcal/mol above the ground state, should be very comparable to that obtained by the absorption of 3140-Å light (91.07 kcal/mol) at an effective temperature of 549°K where $(H° - H°_0)_{vib} = 5.30$ kcal/mol. Thus $E_{3020} + (H° - H°_0)_{40°} = E_{3140} + (H° - H°_0)_{T(effective)}$.

Other "effective" temperatures at 3140 Å[12] for the wavelengths employed by Heicklen are: 3130 Å, T = 337°K; 2970 Å, T = 625°K; 2890 Å, T = 737°K;

(9) D. S. Herr and W. A. Noyes, Jr., *J. Amer. Chem. Soc.*, 62, 2052 (1940).

(10) Note that the emission efficiencies of (H) are a factor of 4–5 higher than those of (L & N) and probably more reliable. Light emissions in acetone are all extremely low and errors in absolute measurements can be quite large. Relative variations, however, should be reliable.

(11) R. E. Pennington and K. A. Kobe, *J. Amer. Chem. Soc.*, 79, 300 (1957); thermodynamic properties of acetone.

(12) We have assumed λ = 3140 Å for both L & N and L & O. This is a compromise between the measured incident average λ of 3150 Å and the known decrease in extinction coefficient with increasing λ.

Table VI

T = 40°, 3130 Å, $[k(\epsilon)^*/Z] \simeq$ 8.3 Torr					T = 63°, 3130 Å, $k(\epsilon)^*/Z$ = 12.6 Torr				
M_{Torr}	Q_D	F_M	$(Q_D F_M)^{-1}$	(M/X_M)	M_{Torr}	Q_D	F_M	$(Q_D F_M)^{-1}$	(M/X_M)
24.8	1.85	1.34	40.3	18.8	30	1.34	1.42	52.5	22.0
48.0	1.87	1.17	45.7	29.7	55	1.27	1.23	63.9	36.5
77	(1.50)	1.11	(59.8)	38.5	113	1.10	1.11	81.8	57.5
100	1.75	1.08	52.8	43.5	170	0.95	1.07	98.5	69.0
150	1.73	1.06	54.5	50.8	217	1.05	1.06	90.0	75.0
200	1.57	1.04	61.2	55.8					

and 2800 Å, T = 856°K. A type of Arrhenius plot of the collective fluorescence data is shown in Figure 7. Although the fluoresence emissions of L & N show a slightly stronger energy dependence than do those of H, the two sets of data agree within the errors. The line drawn through the experimental data points represents a reasonable "best fit" compromise and gives a small negative activation energy of $E_f \simeq -0.54$ kcal/mol. The last two rows of Table V reemphasize that the differences between the observed average fluorescence yields and those predicted from the best line in Figure 7 are not outside experimental error.

2. Phosphorescence Quantum Yields (H). Phosphorescence quantum yields obtained from the differences between total and fluorescence emissions (Table V) are shown as a function of wavelength and pressure in Figure 8. The sizes of the circles are twice the size of the random scatter in the fluorescence yields and represent fair minimum estimates of the errors in the phosphorescence yields.[13]

The shapes of these curves are very interesting and provide strong support for the proposed primary process mechanism. Thus at the short wavelengths (*i.e.*, high absorbed energy), spontaneous decomposition of highly excited triplet-state molecules must be appreciably faster than collisional deactivation. Increasing the pressure should therefore principally deactivate hot molecules to phosphorescing states and increase phosphorescence yields. Note that at 2800 Å the increase in Q_p is almost linear with increasing M. At the long wavelengths, particularly 3130 Å, most of the hot triplets (even at the lowest experimental pressure of 24.8 Torr) are collisionally deactivated to phosphorescing states. Increasing the pressure under these conditions enhances the pressure-dependent decomposition of the thermalized triplets and can decrease phosphorescence yields. According to the mechanism, at sufficiently high pressures all the Q_p *vs.* M curves must go through a maximum similar to the 3130 Å results. The pressure at the maximum then represents the condition at which collisional deactivation of hot triplets ($^3A^*$) is exactly balanced by the unimolecular decomposition of thermalized triplets ($^3A_0$).

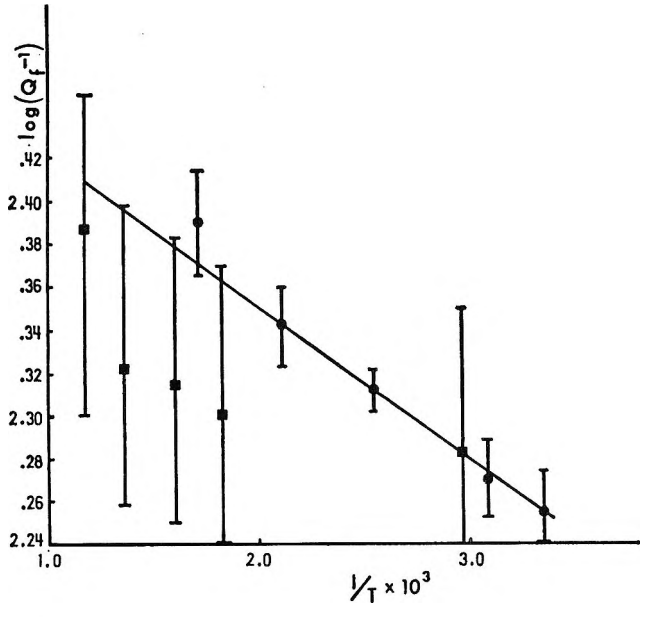


Figure 7. Temperature dependence of fluorescence quantum yields of acetone (3140 Å): ●, data of Luckey and Noyes; ■, data of Heicklen where various wavelength excitations have been converted into effective temperatures at 3140 Å (see text).

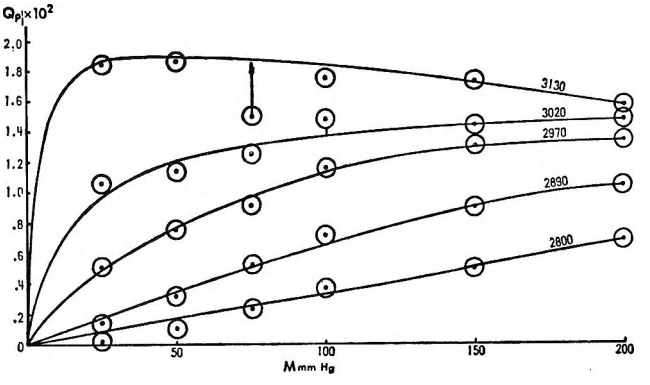


Figure 8. Acetone phosphorescence quantum yields at various wavelengths as a function of pressure—Heicklen.

3. Phosphorescence Quantum Yields (3130 Å) Variation with M. The phosphorescence data of H (3130 Å) has been examined relative to eq V in the same manner as were the corresponding data of L & N. The pertinent functions are given in Table VI and plots of

(13) Since only two points lie well off the smoothed curves, these error estimates seem reasonable.

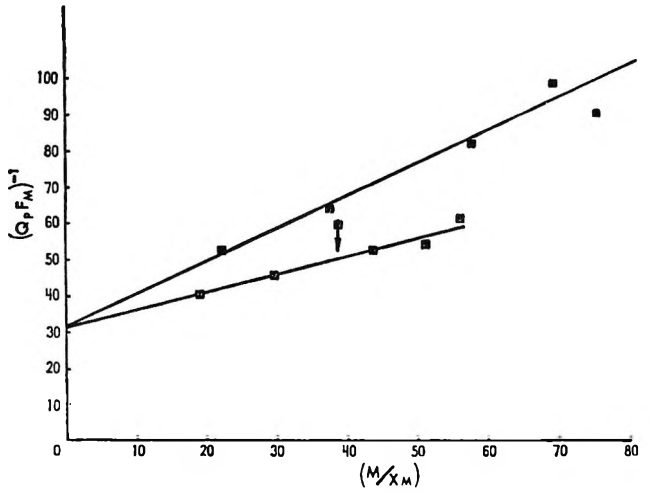


Figure 9. "Corrected" phosphorescence quantum yields variation with pressure and temperature (eq V)—Heicklen: $F_M = (1 + k(\epsilon)^*/Z_M)$; $X_M = M/(1 + M/M_{1/2})$: ⊡, (40°) results; ■, (63°) results; slope = (k_0/k_p).

$(Q_pF_M)^{-1}$ *vs.* (X_M/M) are shown in Figure 9. Rate constant ratios calculated from the slopes are k_0/k_p = 0.508 (40°) and k_0/k_p = 0.882 (63°). These give $(E_0 - E_p) \simeq 4.9$ kcal/mol based on the pressure standard state which is in excellent agreement with the K & D and L & N values.

4. Phosphorescence Dependence on Wavelength and Pressure. Rearrangement of eq V gives

$$Q_pF_M = k_p/(k_{ic} + k_p + {}^3k_{d(uni)}) \qquad (XI)$$

At any constant pressure the right-hand side of eq XI is constant; thus phosphorescence data at all wavelengths can be compared to those at 3130 Å, and one obtains

$$(Q_pF_M)_\lambda = (Q_pF_M)_{3130} = S \qquad (XII)$$

F_M for 3130 Å is known from the thermal data; therefore $(Q_pF_M)_{3130} = S$ is also known. Equation XII rearranges to give

$$(S)/Q_p(\lambda) = 1 + (k(\epsilon)_\lambda^*/Z)(M^{-1}) \qquad (XIII)$$

The pertinent quantities for testing eq XIII have been calculated from Heicklen's data and are shown in Table VII. Plots of (S/Q_p) *vs.* $1/M$ (Figure 10) should have intercepts of unity and slopes equal to $(k(\epsilon)^*/Z)$. The predicted behavior is obtained for the longest wavelength (3020 Å) although decided curvature is apparent at the other three wavelengths. It is possible to give a very interesting explanation of this curvature within the context of the present mechanism. Thus far we have tacitly assumed a strong collision model (*i.e.*, a single collision) for deactivation of the hot triplets. At very high vibrational energy contents for $^3A^*$, one collision may not be sufficient to reduce the energy of the triplets below their critical value. Subsequently, we will show that the average vibrational energy contents above the critical energy for decomposition of hot triplets formed by absorption of 3130- and 3020-Å radiation (40°) are about 2.84 and 6.17 kcal/mol, respectively. These triplets are not excessively hot; therefore a single collision is probably sufficient for deactivation.[14] The energies above the critical value for triplets formed at shorter wavelengths are all appreciably larger than 6 kcal (*e.g.*, $(E - E_0) \simeq 7.76$, 10.47, and 13.61 kcal/mol at 2970, 2890, and 2800 Å, respectively); thus at least two collisions may be required for deactivation. One can readily show that for a two-collision deactivation process, eq XIII should be revised to

$$\frac{(Q_pF_M)_{3130}}{Q_{p(\lambda)}} = 1 + \frac{k(\epsilon)^* + k'(\epsilon)^*}{ZM} + \frac{k(\epsilon)^*k'(\epsilon)^*}{Z^2M^2} \qquad (XIV)$$

where $k'(\epsilon)^*$ is the average spontaneous decomposition rate constant of the active triplet at the average energy state produced by the first collision.

It is clear that eq XIV predicts curvature at low pressures. The limiting slope as $(1/M) \rightarrow 0$ should give $(k(\epsilon)^* + k'(\epsilon)^*)/Z$ and the deviations of points from the limiting high-pressure line should provide a rough measure of $(k'(\epsilon)^*/Z.)$ Although the errors are large, we estimate that at 2800 Å, $(k(\epsilon)^*/Z) \simeq 320$ and $(k'(\epsilon)^*/Z) \simeq 31$; at 2890 Å, $(k(\epsilon)^*/Z) \simeq 110$ and $(k'(\epsilon)^*/Z) \simeq 35$; at 2970 Å $(k(\epsilon)^*/Z) \simeq 44$ and $(k'(\epsilon)^*/Z) \simeq 18$; and at 3020 Å, $(k(\epsilon)^*/Z) \simeq 37$. These numbers correspond to a removal of about 6.8, 4.2, and 3.3 kcal/

Table VII: Phosphorescence Wavelength Dependence Data (Heicklen)[a]

		2800		2890	
M_{Torr}	$(Q_pF_M)_{3130}$[b]	Q_p	(S/Q_p)	Q_p	(S/Q_p)
24.8	2.47	0.08	30.9	0.17	14.5
50	2.20	0.17	13.0	0.34	6.48
77	2.00	0.24	8.35	0.51	3.93
100	1.90	0.33	5.77	0.66	2.88
150	1.78	0.48	3.71	0.90	1.98
200	1.67	0.68	2.69	1.04	1.61

		2970		3020	
M_{Torr}	$M^{-1} \times 10^2$	Q_p	(S/Q_p)	Q_p	(S/Q_p)
24.8	4.03	0.05	4.93	0.98	2.52
50	2.02	0.79	2.79	1.21	1.82
77	1.30	0.98	2.04	1.31	1.53
100	1.00	1.14	1.67	1.37	1.39
150	0.676	1.30	1.37	1.44	1.24
200	0.493	1.34	1.25	1.48	1.13

[a] Taken from Table V and Figures 8 and 9. [b] $S = (Q_pF_M)_{3130}$ Å.

(14) B. S. Rabinovitch, *et al.*, have shown in a number of systems that strong collisions remove from 6–10 kcal/mol collision of excess vibrational energy. J. W. Simons, B. S. Rabinovitch, and D. W. Setzer, *J. Chem. Phys.*, **41**, 800 (1964); **40**, 1751 (1964); *Bull. Soc. Chim. Belges*, **71**, 662 (1962).

Table VIII: Summary of Results[b]

A. Thermal Decomposition of Acetone Triplet (^{3}A)

Source	Log $^3A_0$	$^3E_0$	Log$^3A_\infty$	$^3E_\infty$	s
Kaskan and Duncan	10.05	5.95	9.81	9.07	5.7
Luckey and Noyes		6.2			
Groh, Luckey, and Noyes[a]			10.46	10.15	7.5
Heicklen		5.5			

B. Spontaneous Decomposition of Acetone Triplet (^{3}A*)[e]

Source	λ, Å	T	$(E - E_0)$	$[k(\epsilon)^*/Z]$	$[k^1(\epsilon)^*/Z]$[d]	s
Larson and O'Neal	3140	44	2.6	5.5		6.7[c]
Larson and O'Neal	3140	96	3.2	15.4		6.7
Larson and O'Neal	3140	126	3.1	24.4		6.7
Larson and Steorie	3140	150	4.0	35.3		6.7
Heicklen	3130	40	2.8	8.3		6.6
	3020	40	6.2	37.5		8.1
	2970	40	7.8	44	18	9.1
	2890	40	10.4	110	35	9.8
	2800	40	13.6	320	30	9.7

[a] P_{total} = 200 Torr. Slightly higher parameters would apply to k_∞. [b] Units are A_0 (l./mol-sec); A_∞ (sec^{-1}), E_∞ and E_0 (kcal/mol), s = number of effective oscillators (RRK theory). [c] The s = 6.7 values have been assumed to be constant in the thermal studies in order to calculate ϵ_{00} (see text). Some slight increase, however, is more realistic. [d] Decomposition to stabilization ratios assuming a two-step collisional deactivation process (see text). [e] $k(\epsilon)^* = A_\infty^*(E - E_3/E)^{s-1}$; $\epsilon_{00} \simeq$ 80.5 kcal/mol; $A_\infty^* \simeq 10^{11.1}$ sec^{-1}.

mol by the first collisions at 2800, 2890, and 2970 Å, respectively. It would appear that if the accuracy in the acetone emission data could be improved, the acetone photochemical system could provide a convenient vehicle for studies of the mechanism of collisional energy exchange. A more sophisticated treatment of the data *via* RRKM calculations would then be warranted.

V. Estimation of the RRK s Values and ϵ_{00} (the Zero Point Energy Difference between the Acetone Triplet and the Acetone Ground State). According to the RRK theory, the number of effective oscillators contributing to the thermal decomposition of a uimolecular reaction reaction can be estimated from the limiting high- and low-pressure activation energies using the relation

$$E_\infty - E_0 = (s - \tfrac{3}{2})RT \qquad \text{(XV)}$$

The K & D results give $s \simeq 5.7$, whereas using the G L & N, $E_\infty \simeq 10.3$ kcal/mol and the average $E_0 \simeq 5.9$ kcal/mol, one obtains $s \simeq 7.5$. Effective s can also be estimated from the triplet vibrational heat capacity since each classical oscillator contributes R to $C_p°$. Assuming that the vibrational frequencies of the acetone triplet are not significantly different from those of the acetone ground state one finds $C_{vib}°(60°)$ = 11.3 cal/mol °K and an $s \simeq 5.7$. A value for s between 5.7 and 7.5 therefore seems quite reasonable for the thermal decomposition.

The RRK theory relation for a spontaneous decomposition rate constant is

$$k(\epsilon)^* = A_\infty^* \left(\frac{E - E_0}{E}\right)^{s-1} \qquad \text{(XVI)}$$

If we assume that s for the thermal triplet decomposition is the same as the s for the triplet spontaneous decomposition sensitized by 3140-Å light, then the L & O spontaneous decomposition quantum yields as a function of temperature (Table II) can be used to obtain a

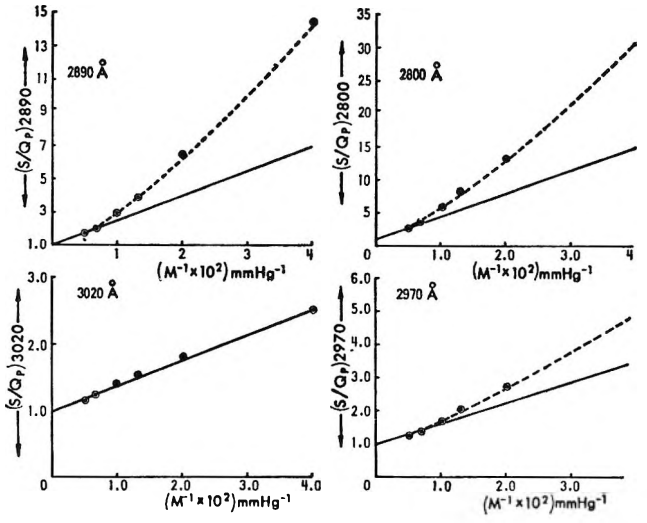


Figure 10. Determination of decomposition/stabilization ratios of hot triplets, variation with pressure and wavelength (eq XIII).

value for ϵ_{00}.[15] From (XVI) one then calculates (using $(k(\epsilon)^*/Z)$ data of Table II) that $\epsilon_{00} = 79.6$ for $s = 7.5$ and $E_\infty = 10.3$; $\epsilon_{00} = 80.6$ for $s = 6.7$ and $E_\infty = 9.7$; or $\epsilon_{00} = 81.5$ for $s = 5.7$ and $E_\infty = 9.15$ (ϵ_{00} and E_∞ in kcal/mol). Thus an $\epsilon_{00} = 80.5 \pm 1$ kcal/mol fits the L & O data quite well. If $s = 6.7$, $E_\infty = 9.7$ kcal/mol and $\epsilon_{00} = 80.5$ kcal/mol are adopted, along with $k(\epsilon)^*/Z = 5.0$ Torr (40°), one also obtains (A_∞^*/Z) (40°) $= 10^{4.54}$ Torr. This gives an $A_\infty^* = 10^{11.1}$ sec^{-1} ($Z \simeq 10^{6.6}$ mm^{-1} for $\sigma = 4.4$ Å) which is about a factor of 5 larger than the G L & N value at 200 Torr. The fact that A_∞^* from the spontaneous decomposition data is very nearly the same (within experimental error) as the thermal decomposition A factor for the triplet decomposition is strong evidence for attributing the spontaneous decomposition to the decomposition of vibrationally excited triplet-state molecules rather than to the decomposition of some other species (*e.g.*, excited singlets).

It is possible to compare the thermal and wavelength spontaneous decomposition results by calculating the RRK s at the various wavelengths employed by Heicklen. Since s must be energy dependent, one would expect a gradual increase in s with decreasing wavelength. From (XVI), with $\epsilon_{00} = 80.5$, $E_\infty = 9.7$, and $(A_\infty^*/Z) = 10^{4.54}$ Torr, the results are: $s = 6.6$ (3130 Å), $s = 8.1$ (3020 Å), $s = 9.1$ (2970 Å), $s = 9.8$ (2890 Å), and $s = 9.7$ (2800 Å). The expected behavior is obtained.

The results relative to the revised mechanism for all studies are summarized in Tables VIIIA and VIIIB.

The temperature dependencies of the fluorescence and the phosphorescence (see Figure 7 and $k(\epsilon)^*/Z$ values of Table VIIIB) appear to be stronger than the corresponding wavelength dependencies. The present mechanism requires identical behavior for hot triplets formed by either mode of excitation as long as the hot triplets are in the same energy range. A possible explanation for the "apparent" discrepancies between thermal and wavelength results may reside in the different energy distributions of the hot triplets around their average energy state. Hot triplets produced thermally (by irradiation at 3140 Å) will have a much broader Boltzmann distribution than those produced by irradiation at low temperatures (40°). Thus a slightly stronger energy dependence for spontaneous decomposition would be expected. Detailed RRKM calculations are in progress to see if these variations are real or are only apparent.

The acetone photochemical system is complex and as always there are questions which remain unresolved. However, the main features of mechanism B seem to be qualitatively and quantitatively consistent with the emission and decomposition data. Future studies of this system must necessarily recognize the complex relations between the emission processes, the spontaneous decomposition process, and the pressure-dependent triplet decomposition process. In a future communication we plan to discuss some of the intriguing kinetic restrictions placed on the acetone fluorescence by the present mechanism for decomposition and fluorescence.

Acknowledgment. The authors wish to express their gratitude to the National Science Foundation for its financial support of this work.

(15) In this case, $E - E_0 - (H^\circ - H^\circ_0)_{vib}(T) + h\nu + E_\infty - \epsilon_{00}$ and $E = (H^\circ - H^\circ_0)_{vib}(T) + h\nu - \epsilon_{00}$. In addition, $h\nu = 91.07$ (3140 Å), 91.35 (3130 Å), 94.68 (3020 Å), 96.27 (2970 Å), 98.94 (2890 Å) and 102.12 (2800 Å) all in kcal/mol, and $(H^\circ - H^\circ_0)_{vib} = 1.69$ (40°), 1.73 (44°), 2.36 (96°), 2.72 (126°), and 3.10 (150°), also in kcal/mol.

The Effect of Normal Aliphatic Alcohols on Electrode Kinetics

by Katsumi Kanzaki Niki[1] and Norman Hackerman

Department of Chemistry, The University of Texas, Austin, Texas 78712 *(Received August 19, 1968)*

The applicability of a potential-step method for measuring the current–time variation in the electrode reaction of the V(II)–V(III) couple on the hanging mercury drop electrode in 1 *N* H_2SO_4 was verified both in the absence and in the presence of alcohols. The effective electrode area did not change significantly with the alcohols adsorbed on the surface. This indicated mobility of the adsorbed molecules. The polarographic limiting current was attained before the desorption potential of the alcohols was reached, and it remained constant even in the presence of the adsorbate. This is explained by the formation of a uniform barrier on the electrode. The rate constants of the electrode reaction decreased with increasing alcohol concentration, but the dependence of reaction rate on coverage was not linear. Traube's rule was found to be applicable, with a factor of one-fourth. The effect of coverage on the reaction rates by alcohols is explained in terms of the orientation of the alcohols.

It is known that surface-active substances often have a marked effect on electrode processes. In spite of numerous studies on adsorption of surface-active substances on electrodes, there is still no adequate theory of the effect of adsorbed molecules on electrode processes. Early works in polarography on the effect of surface-active substances were carried out extensively by Russian and Czech investigators.[2] They assumed that the adsorbed layer of surface-active substances merely influenced the electrochemical process at the electrode surface.[2b] Diffusion of reactants to positions next to the adsorbed layer on the electrode was not taken into account. There are several papers[3–7] on electrode kinetics in the presence of neutral surface-active substances, and a linear relationship between rate constant and fractional coverage was demonstrated in most cases.

This work uses a potential-step method to study the effect of neutral organic substances on electrode kinetics. The method permits elucidation of the mode of diffusion of the reacting species to the electrode. In addition to the potential-step procedure, polarography, capillary electrometry, and cyclic voltammetry were used. To simplify the study, the V(II)–V(III) couple was selected because the reaction rate constant[8,9] at the standard potential is well within the range of the application of a potential-step method. Also, vanadium ions are said not to adsorb specifically on a mercury electrode,[10] and the standard potential of this system is close to the potential of the electrocapillary maximum for mercury in the absence of specific adsorption, so that the coverage by the adsorbed molecules hardly varies around the standard potential.

Experimental Section

Solutions. The clear blue solution of $VOSO_4$ was prepared according to the method of Johns and Colvin.[11] The concentration of $VOSO_4$ was determined with $KMnO_4$, using a Jones reductor in the usual analytical method.[12] All solutions were prepared from twice-distilled water and were purified by activated charcoal.[13] For each experiment $VOSO_4$ was reduced with stirring on the mercury pool cathode to V(III) and then to V(II). The concentrations of both V(III) and V(II) were determined by polarography, and the equilibrium potentials were measured by the hanging mercury drop electrode as an indicator electrode. The vanadic–vanadous solution was maintained under nitrogen. Nitrogen was purified by bubbling through a concentrated vanadous sulfate solution, then through a solution identical with that being studied, then to the electrolytic cell. This minimized vapor losses of water and alcohols from the electrolytic cell. Measurements were made at 25.5 ± 1.0°.

Alcohols. Certified *n*-butyl alcohol and *n*-amyl alco-

(1) Sumitomo Chemical Co., Minato-ku, Nagoya, Japan.

(2) For instance: (a) For a review in polarography: C. N. Reilley and W. Stumm, "Progress in Polarography," Vol. I, P. Zuman, Ed., Interscience, New York, N. Y., 1962, pp 81–121; (b) A. N. Frumkin, *Dokl. Akad. Nauk SSSR*, **85**, 373 (1952); *Proc. Intern. Congr. Surface Activity, 2nd, London, 1957*, 58 (1957); (c) J. Heyrovský, F. Sorm, and J. Forjt, *Collect. Czech. Chem. Commun.*, **12**, 11 (1947); (d) M. Matyas, *ibid.*, **16**, 496 (1951).

(3) P. Delahay and I. Trachtenberg, *J. Amer. Chem. Soc.*, **80**, 2094 (1958).

(4) W. Lorenz and W. Müller, *Z. Phys. Chem.*, (Frankfurt am Main) **18**, 141 (1958).

(5) L. Gierst, "Advances in Electrochemistry and Electrochemical Engineering," Vol. I, P. Delahay, Ed., Interscience, New York, N. Y., 1960, pp 55, 94.

(6) W. Müller and W. Lorenz, *Z. Phys. Chem.* (Frankfurt am Main) **27**, 23 (1961).

(7) A. Aramata and P. Delahay, *J. Phys. Chem.*, **68**, 880 (1964).

(8) J. E. B. Randles, *Can. J. Chem.*, **37**, 238 (1959).

(9) J. E. B. Randles, "Progress in Polarography," Vol. I, P. Zuman and I. M. Kolthoff, Ed., Interscience, New York, N. Y., 1962, p 123.

(10) K. M. Joshi, W. Mehl, and P. Parsons, *Trans. Symp. Electrode Processes, Philadelphia, Pa., 1959*, 249 (1961).

(11) G. Johns and J. N. Colvin, *J. Amer. Chem. Soc.*, **66**, 1563 (1944).

(12) For example: G. H. Ayres, "Quantitative Chemical Analysis," Harper & Brothers, New York, N. Y., 1958, p 451.

(13) G. Baker, ref 10, p 251.

hol (Fisher Scientific Co.) were used without further purification, since impurities were hardly detectable by vapor phase chromatography. The *n*-hexyl alcohol was prepared from practical grade *n*-hexyl acetate; it was then purified by vapor phase chromatography. The concentrations of alcohols were chosen so that the same amount of each alcohol would be adsorbed at the mercury solution interface, according to Hansen and Craig.[14] The relative concentrations (C/C_s), rather than C, are used. C_s is the solubility of the alcohol in water, and the values of C_s were taken from Hansen, *et al.*,[15] and Seidell.[16]

Electrolytic Cell. The all-glass three compartment electrolytic cell was used for all experiments. Compartments were separated from one another by fine sintered-glass membranes. One compartment contained the hanging mercury drop electrode, the mercury pool, and the dropping mercury electrode. A compartment on one side contained the anode, and one on the other was a bridge to the Hg_1, Hg_2SO_4, 1 *N* H_2SO_4 reference electrode. The hanging mercury drop electrode made by Metrohm, Ltd., Switzerland, was used as the working electrode. The capillary of the hanging mercury drop electrode was silicladed. The mercury drop (maintained 10 sec in the solution) was renewed each time. Mercury was distilled twice under vacuum.

Potentiostat. A Wenking 61 RS electronic potentiostat with an external reference potential source was used. The working electrode was negatively polarized in all experiments by applying a 10-mV step over the equilibrium potential.

Polarography and Cyclic Voltammetry. The linear scanning potentiostat for polarography and the cyclic triangular wave generator for cyclic voltammetry used a Philbrick Research Model 6009 operational amplifier. The scan rate for polarography was about 46 mV/min, and the mercury drop life was about 7 sec. The sweep rate of the cyclic voltammetry was varied from 67 mV/sec to 150 V/sec.

Capillary Electrometer. The capillary electrometer was constructed according to the method described by Hansen, Kelsh, and Granthan.[17] Measurements were made in 1 *N* H_2SO_4 solution and with several concentrations of alcohols in 1 *N* H_2SO_4 solution in the absence of the vanadium ions to achieve more nearly the conditions corresponding to an ideally polarized electrode. The radius of the capillary at the null point was determined by standardization against a solution of known surface tension.[18] All these measurements were also made at 25.5 ± 1.0°.

Results

Polarographic Studies. The V(II)–V(III) couple showed a quasi-reversible polarographic wave and gave simple reduction and oxidation waves in 1 *N* H_2SO_4. With increasing alcohol concentration, the polarographic wave became more irreversible. However, the diffusion currents observed were more positive than the displacement potential of the alcohol, and there was no visible effect on the diffusion current on addition of *n*-amyl and *n*-hexyl alcohols but *n*-butyl alcohol lowered it up to 4% at higher concentrations.

The diffusion coefficients of V(II) and V(III), determined polarographically by using the Ilkovic equation, were for 8.0×10^{-6} and 6.5×10^{-6} cm²/sec, respectively. The standard potential of the V(II)–V(III) couple was -0.953 ± 0.001 V. None of these alcohols had any effect on the equilibrium potential. The standard electrochemical reaction rate constant, calculated from polarographic data as done by Randles,[8] was $(1.04 \pm 0.03) \times 10^{-3}$ cm/sec, and the transfer coefficient, α, was 0.52. At higher alcohol concentra-

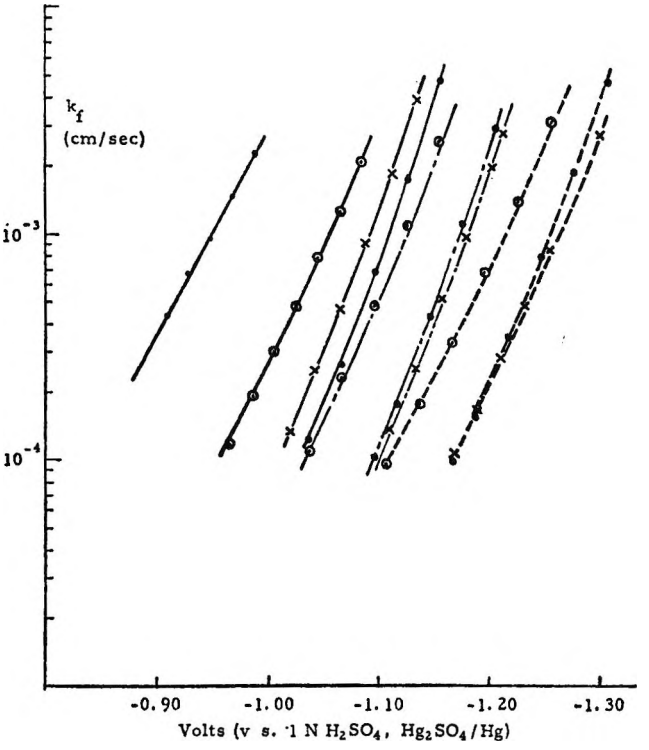


Figure 1. Effect of alcohols on the charge-transfer rate constant of the V(III) + e → V(II) in 1 *N* H_2SO_4 obtained from polarography: —·—, without alcohol; -⊙-⊙-, 34.4 m*M* ($C/C_s = 3.5 \times 10^{-2}$) *n*-butyl alcohol; -⊙---⊙-, 68.8 m*M* ($C/C_s = 7.0 \times 10^{-2}$) *n*-butyl alcohol; -⊙---⊙-, 172 m*M* ($C/C_s = 17.5 \times 10^{-2}$) *n*-butyl alcohol; -×—×-, 10 m*M* ($C/C_s = 3.5 \times 10^{-2}$) *n*-amyl alcohol; -×-·-×-, 20 m*M* ($C/C_s = 7.0 \times 10^{-2}$) *n*-amyl alcohol; -×—×-, 50 m*M* ($C/C_s = 17.5 \times 10^{-2}$) *n*-amyl alcohol; -●—●-, 2.18 m*M* ($C/C_s = 3.5 \times 10^{-2}$) *n*-hexyl alcohol; -●-·-●-, 4.36 m*M* ($C/C_s = 7.0 \times 10^{-2}$) *n*-hexyl alcohol; -●- -●-, 10.9 m*M* ($C/C_s = 17.5 \times 10^{-2}$) *n*-hexyl alcohol.

(14) R. S. Hansen and R. P. Craig, *J. Phys. Chem.*, **58**, 211 (1954).
(15) R. S. Hansen, Y. Fu, and F. B. Bartell, *ibid.*, **53**, 769 (1949).
(16) A. Seidell, "Solubilities of Organic Compounds," D. Van Nostrand Co., Princeton, N. J., 1941.
(17) R. S. Hansen, D. J. Kelsh, and D. H. Granthan, *J. Phys. Chem.*, **67**, 2316 (1963).
(18) C. A. Smolders and E. M. Duyvis, *Rec. Trav. Chim.*, **80**, 635 (1961).

tions, the V(II)–V(III) system may be considered to be totally irreversible. Thus the reaction rate constant can be calculated in the usual manner.[19] The results are shown in Figure 1.

Potential-Step Method: the Electrode Kinetic Parameter of the V(II)–V(III) Couple. The current–time relationship for the V(II)–V(III) oxidation–reduction couple for mass transfer controlled by semi-infinite linear diffusion given by

$$I_t = AF[k_f C^*_{V(III)} - k_b C^*_{V(II)}] \exp(Q^2 t) \operatorname{erfc}(Qt^{1/2}) \quad (1)$$

$$Q = [k_f/D^{1/2}_{V(III)} + k_b/D^{1/2}_{V(II)}]$$

where I_t is the current at the time, t, elapsed from electrolysis beginning; F, the Faraday; A, the electrode area; k_f and k_b, the reaction rate constants for the cathodic and the anodic reactions, respectively; $C^*_{V(III)}$ and $C^*_{V(II)}$, the bulk concentrations of V(III) and V(II), respectively; and $D_{V(III)}$ and $D_{V(II)}$, the diffusion coefficients. When $Qt^{1/2} \ll 1$, eq 1 becomes

$$I_t = I_{t=0}\{1 - 2(Qt^{1/2}/\pi^{1/2})\} \quad (2)$$

Accordingly, the rate constant was obtained from the short-time extrapolation to $t = 0$ assuming that the surface area of the electrode equals its geometrical area. The extrapolation was made in the interval $t = 5$ to 25 msec. The reaction rate constants calculated from $I_{t=0}$ were denoted by $k_f(I_{t=0})$ and the transfer coefficient, α, was calculated from the slope of log $k_f(I_{t=0})$ *vs.* potential. The results are shown in Figure 2. The standard rate constant $k^\circ(I_{t=0}) = (1.42 \pm 0.05) \times 10^{-3}$ cm/sec and $\alpha = 0.50$.

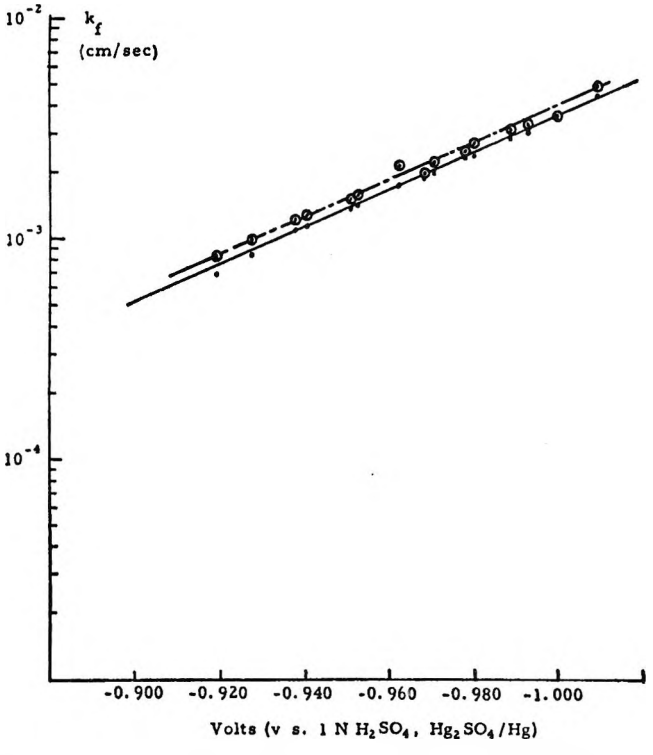


Figure 2. Charge-transfer rate constant for V(III) + e → V(II) in 1 *N* H_2SO_4 (calculated from potential-step method). Rate constant calculated from Q, – -⊙—⊙—⊙- –; rate constant calculated from $I_{t=0}$, -●-●-●-.

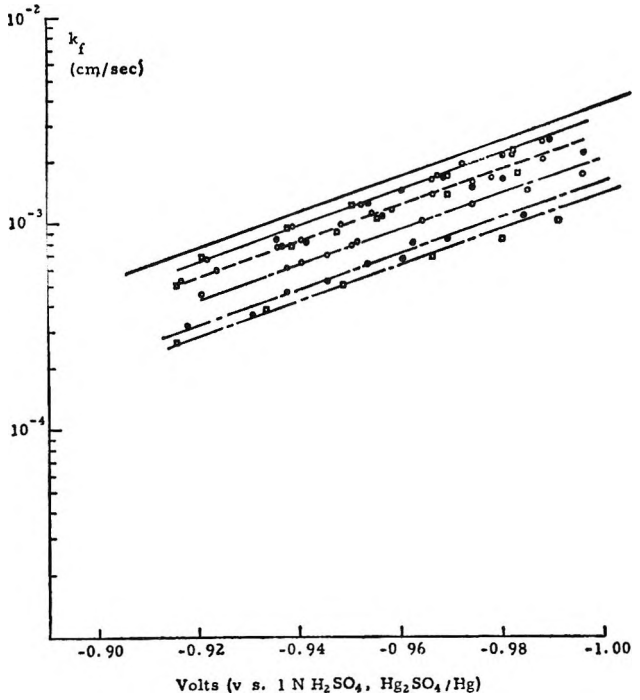


Figure 3. Charge-transfer reaction rate constant for V(III) + e → V(II) in 1 *N* H_2SO_4 in the presence of alcohols (calculated from $I_{t=0}$): without alcohol, ——; 3.44 m*M* *n*-butyl alcohol, -○—○-; 6.9 m*M* *n*-butyl alcohol, – -○--○- –; 13.8 m*M* *n*-butyl alcohol, -○— - —○-; 1.0 m*M* *n*-amyl alcohol, -●——●-; 2.0 m*M* *n*-amyl alcohol, – -●--●- –; 4.0 m*M* *n*-amyl alcohol, -●— - —●—; 0.213 m*M* *n*-hexyl alcohol, -□—□-; 0.43 m*M* *n*-hexyl alcohol, – -□--□- –; 0.85 m*M* *n*-hexyl alcohol, -□— - —□-.

On the other hand, by rearrangement of eq 1

$$I_t/I_{t=0} = \exp(Q^2 t) \operatorname{erfc}(Qt^{1/2}) \quad (3)$$

The true rate constant can be calculated from Q without knowing the surface area of the electrode, by comparing experimental values of $I_t/I_{t=0}$ with the values of $\exp(Q^2 t) \operatorname{erfc}(Qt^{1/2})$ at various Q and t. The rate constant $k_f(Q)$ is given by

$$k_f(Q) = \frac{Q}{\{(1/D^{1/2}_{V(III)}) + (1/D^{1/2}_{V(II)})(C^*_{V(III)}/C^*_{V(II)}) \exp(F\eta/RT)\}} \quad (4)$$

Calculation of $k_f(Q)$ is sometimes in error because of the inaccuracy of the measurements plus inaccuracy in $I_{t=0}$. The latter can be eliminated by repeating the calculation of $I_t/I_{t=0}$ by changing $I_{t=0}$ until the

(19) P. Delahay, "New Instrumental Methods in Electrochemistry," Interscience, New York, N. Y., 1954, pp 74–79.

minimum deviations in Q at various times t are obtained. Results are shown in Figure 2.

The effective electrode area for the charge-transfer reaction was calculated from the ratio $k_f(I_{t=0})/k_f(Q)$. The effective area of the hanging mercury drop was 90 ± 3% of its geometric area.

The Electrode Kinetic Parameters of the V(II)–V(III) Couple in the Presence of Alcohols. The reaction rate constants $k_f(I_{t=0})$ in the presence of alcohols were calculated in the same way and are shown in Figure 3. Standard rate constants are given in Table I. The effective area of the hanging mercury drop was also calculated in the same way, and was about 90%, since the model of the semi-infinite linear diffusion to the plane surface can also be applied to these cases. The reaction rate constants decreased with increasing alcohol concentration, but the transfer coefficient did not change significantly. The effective electrode area of the hanging mercury drop also did not show a significant change even in the presence of alcohol.

Table I: Standard Rate Constant of the Reaction of $V^{3+} + e \leftrightarrows V^{2+}$ in the Presence of Alcohol

Concn, mM	Standard rate constant, k°, cm/sec	Effective area of the electrode, %	
		X^a	σ^b
	Without Alcohol		
	1.42×10^{-3} ($\alpha = 0.50$)	91	3
	n-Butyl Alcohol		
3.44	1.25×10^{-3}	90	2
6.9	1.03×10^{-3}	88	4
13.8	8.0×10^{-4}	87	3
	n-Amyl Alcohol		
1.0	1.23×10^{-3}	92	2
2.0	9.9×10^{-4}	89	2
4.0	6.1×10^{-4}	90	4
	n-Hexyl Alcohol		
0.213	1.25×10^{-3}	91	2
0.43	1.00×10^{-4}	89	4
0.85	5.4×10^{-4}	87	3

[a] X, the ratio of the effective electrode area to its geometrical area. [b] σ, standard deviation.

It is interesting to note that in the presence of alcohols, the reaction rate of the V(II)–V(III) couple was markedly influenced by the time interval (0–20 min) between formation of a new mercury drop and application of the step function of potential at higher concentrations of V(II). The retarding effect was not only affected by the time interval, but also by stirring, and by V(II) concentration. It was only slightly dependent on concentration and type of alcohol. At high V(II) concentration and in the presence of alcohols, the value of $I_{t=0}$ dropped almost to zero, even though by alcohols surface coverage electrocapillary measurements showed less than 100%.

Cyclic Voltammetry. Voltammograms of the V(II)–V(III) couple at sweep rates from 67 mV/sec to about 150 V/sec showed a typical quasi-reversible wave but did not indicate intermediates either in the presence or absence of the alcohols. With increasing alcohol concentration, the voltammograms were distorted in both the cathodic and anodic direction. Although the peaks become sharper, a complete separation of anodic and cathodic processes was observed, as should be the case for an irreversible process. The cathodic peak potential shifted a little in the cathodic direction with increasing sweep rate, while the anodic peak potential did not change. Increasing the time interval between formation of a new mercury drop and initiation of the potential sweep makes the voltammograms more drawn out; that is, the system appeared to be more irreversible with increasing time.

Adsorption of the Alcohols on Mercury. Adsorption of organic compounds on the electrode can be studied thermodynamically by measuring interfacial tension changes of an ideally polarized electrode. From Gibbs' adsorption equation the surface coverages were calculated assuming the activity coefficients of the alcohols to be unity, and the adsorbed alcohols to be oriented perpendicular to the surface of the mercury and occupying 21 Å²/molecule (7.90×10^{-10} mol/cm² for monolayer adsorption).

Discussion

Charge-Transfer Reaction of the V(II)–V(III) Couple in 1 N H_2SO_4. The V(II)–V(III) couple showed a quasi-reversible polarographic wave in 1 N H_2SO_4 as had been observed by Randles.[9] Voltammograms also showed the quasi-reversible characteristics and no reaction intermediates. Israel and Meites[20] reported intermediates for the V(II)–V(III) couple in aqueous acidic sulfate solutions. Therefore, the reaction of the V(II)–V(III) oxidation–reduction couple is very likely a moderately rapid one-electron charge-transfer reaction in 1 N H_2SO_4 solution. The standard potential and the electrode kinetic parameters of the V(II)–V(III) couple in 1 N H_2SO_4 solution obtained in this work are in good agreement with previous works.[8,10,11]

Determination of the Effective Area of the Electrode. Bonnemay, *et al.*,[21] determined the effective area of the hanging amalgam electrode (Zn–Hg) from the intercept at $t = 0$, $I_{t=0}$, and the slope of the linear approximation of current–time results of potentiostatic polarization. It was found that this method did not give good results compared with the present work.

(20) Y. Israel and L. Meites, *J. Electroanal. Chem.*, 8, 99 (1964).
(21) M. Bonnemay, E. Levant, and E. P. d'Ange d'Orsay, *Compt. Rend.*, 260, 2493 (1965).

Values of Q calculated from their method contained an inevitable error, which can easily be shown by mathematical analysis of eq 3. Also, a small error in $I_{t=0}$ leads to a larger error in the determination of the values of Q. On the other hand, the determination of the effective area from the values of $I_t/I_{t=0}$ and $I_{t=0}$ gives a fairly accurate result whenever the error in the measurement of I_t is small.

Effect of the Alcohols on Kinetics of Charge-Transfer Reaction and the Effective Area of the Electrode. Delahay and Trachtenberg[3] and Müller and Lorenz[6] studied the effects of organic substances on electrode kinetics by assuming that the local reaction rate was negligible at a covered surface and that the reaction rate at an uncovered surface is unaffected. Later, Aramata and Delahay[7] considered the effect of *n*-amyl alcohol on the potential distribution in the electrical double layer. They observed the linear relationship between rate constant and surface coverage at low coverages of *n*-amyl alcohol.

In the present work the variation of the standard rate constant is not proportional to the surface coverages by the alcohols, even though the change of the potential distribution in double layer was taken into account. Although the reaction rate constant was markedly influenced by the alcohols, the transfer coefficient was not. This behavior is quite similar to the system Zn^{2+}–Zn amalgam in the presence of thymol and cyclohexanol.[22] Biegler and Laitinen[23] also observed nonlinear relationships between rate constant and fractional electrode coverage for reduction of both Cd^{2+} and $HPbO_2^-$ in the presence of *n*-butyl alcohol, thymol, and leucoriboflavin.

Since the model of semi-infinite linear diffusion to the electrode for the V(II)–V(III) couple was verified even in the presence of alcohols, the barrier formed by the adsorbed alcohol appears to be uniform even if the surface coverage is less than 100%. This means that the diffusion process of particles undergoing reduction was not affected by the alcohols. de Boer[24] has stated that in gas adsorption on solids the average residence time of the molecules on the surface is of the order of 10^{-7} sec, provided that the energy of adsorption is about 9 kcal/mol. The exchange rate of the adsorbed alcohol molecules[25] in a liquid film will probably be less than it is in a gaseous film.

Thus, there are two ways in which the adsorbed molecule may exhibit dynamic character. One is rapid movement of the adsorbed molecules on the surface, *i.e.*, a two-dimensional gas; the other is a high exchange rate at equilibrium. Because of the continuous rapid movement or exchange of the adsorbed molecules, the coverage may be purely statistical in nature and the measurement gives only an average which makes the barrier appear uniform. At any given instant, the electroactive particles probably have their easiest access to the electrode at an uncovered position on the surface and inhibitory effects are most pronounced at positions occupied by alcohol molecules. Thus, the current–time variations in the presence of adsorbed layers of alcohols may be expressed by the usual rate equation, such as eq 1. However, the reaction rate constants are expressed in the form of $f(\Gamma)k_f$ and $f(\Gamma)k_b$, respectively, where $f(\Gamma)$ is a function of the amount of adsorbed alcohol on the electrode, $f(\Gamma) = 1$ when $\Gamma = 0$ and $0 \leq f(\Gamma) \leq 1$ when $\Gamma > 0$.

For the V(II)–V(III) couple in the presence of alcohol, the apparent rate constant, $f(\Gamma)k_f$, is small. Thus, the polarographic wave becomes more irreversible with increasing alcohol concentration. As shown by polarographic measurements the limiting current is not affected by the alcohols, probably because the effective electrode area is unchanged by coverage. The slight change of limiting current at higher concentrations of *n*-butyl alcohol is likely due to change of bulk properties of the solution by the alcohol, since a much more concentrated solution of *n*-butyl alcohol is required to attain the same relative concentrations used for the other alcohols. If k° is very large, as in the reduction of Ag^+, even though $f(\Gamma)$ is very small, $f(\Gamma)k_f$ may still be large enough to be polarographically reversible, as was observed by Matyas.[2d] When organic molecules are strongly adsorbed on the electrode surface, the adsorbed molecule may become immobile; accordingly, the polargraphic wave becomes more irreversible and the limiting current becomes smaller.

Effect on Reaction Kinetics of the Time Interval between the Formation of a Mercury Drop and Initiation of the Step Function of the Potential. The reaction rate of the system V(II)–V(III) drops markedly at higher concentrations of the alcohols.[26] This is true also even at very low alcohol concentrations when the mercury drop is maintained at the equilibrium potential for a long time (5–20 min) before applying added voltage. Electrocapillary measurements in the system with the same concentration of alcohol, but without V(II) and V(III), show surface coverage of 10–20% and an almost instantaneous attainment of adsorption equilibrium. Since the inhibition effect is accelerated by increasing the concentration of V(II) and also by stirring the solution, the inhibition may be associated with V(II) ions, such as by preferential adsorption of the ions with the alcohol molecules or a reaction inter-

(22) G. Torsi and P. Delahay, "Double Layer and Electrode Kinetics," P. Delahay, Ed., Interscience, New York, N. Y., 1965, p 233.

(23) T. Biegler and H. A. Laitinen, *J. Electrochem. Soc.*, 113, 852 (1966).

(24) J. H. de Boer, "Physical Chemistry of Surfaces," A. W. Adamson, Ed., Interscience, New York, N. Y., 1960, p 461.

(25) According to E. Blomgren, J. O'M. Bockris, and C. Jesch, *J. Phys. Chem.*, 65, 2000 (1961), the heat of displacement of BuOH is 3.7 kcal/mol at $\theta = 0.25$.

(26) At a higher ratio of $C_{V(II)}/C_{V(III)}$ (especially greater than 1. When the ratio of $C_{V(II)}/C_{V(III)}$ is less than 1, this type of inhibition effect is quite small.)

Table II: Surface Excess of the Alcohols at Mercury–Solution Interfaces

n-Butyl alcohol		*n*-Amyl alcohol		*n*-Hexyl alcohol	
Concn, m*M*	10^{-10} mol/cm²	Concn, m*M*	10^{-10} mol/cm²	Concn, m*M*	10^{-10} mol/cm²
6.9	0.5	2.0	0.7	0.424	0.6
17.9	1.3	5.0	1.6	1.07	1.5
34.4	2.3	10	2.8	2.13	2.6
69	3.9	20	4.3	4.3	4.0

mediate on the electrode. The stirring effect suggests a diffusion-controlled step. Although the nature of these effects is still not clear, no further study has been made of this.

Cyclic Voltammetry. The shift of cathodic potential in the cathodic direction with increasing sweep rate in the presence of alcohol reflects the presence of adsorbed molecules on the electrode making the electrode reaction irreversible. On the other hand, adsorbed molecules may desorb completely from the electrode at the potential where anodic peak appeared. Hence, the anodic reaction rates are large enough to be reversible, and the anodic peak potential would not shift with increasing sweep rate.

Traube's Rule for the Adsorption of Alcohols and Reaction Kinetics. As others[27] observed, Traube's rule is applicable to adsorption of normal fatty acids (acetic to caproic) on mercury from 1 *N* Na_2SO_4. The present electrocapillary measurements also showed that adsorption of *n*-butyl, *n*-amyl, and *n*-hexyl alcohol from 1 *N* H_2SO_4 on mercury follows Traube's rule. The coefficient was about one-fourth as shown in Table II. The solubilities of these alcohols in water[15] decreased by one-quarter for each additional CH_2 group. Therefore, the concept of the relative concentration of the homologous series of normal fatty alcohols proposed by Hansen, Fu, and Bartell[15] as an extended Traube's rule may be equivalent to the original Traube's rule.

The model of two condensers in parallel is assumed as the double layer structure and the lateral interaction between adsorbed molecules and other particles on the electrode is neglected in order to simplify the discussion. When the adsorbed molecules lie flat on the electrode at lower concentrations of alcohols, the effective area of the electrode decreases regularly with increasing number of CH_2 group if the surface excess of the alcohols stays constant. This effect is observed experimentally as shown in Figure 4 and Table III. Here the ratio of the available electrode area, *S*, is assumed to be given by

$$S = \frac{k^\circ \text{ (with alcohol)}}{k^\circ \text{ (without alcohol)}} \times 100\% \qquad (5)$$

Hence the fractional coverage was $(100 - S)\%$.

In medium alcohol concentrations, the reaction rate does not change regularly with number of CH_2 groups at a given relative concentration of the alcohol, *i.e.*, at a given surface excess. With increasing alcohol concentration, the reaction rate constants of the V(II)–V(III) couple with different alcohols tend to be congruent with each other. The effect of the alcohols at higher concentrations may be explained in terms of the orientation of the alcohols. Oriented parallel to the surface, *n*-butyl alcohol exhibits the smallest area and *n*-hexyl alcohol the highest. The inhibition effects on the rate constant should follow this order for a

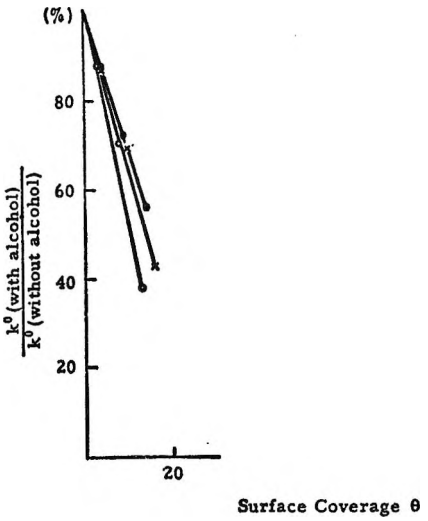


Figure 4. Influence of coverage on rate constant: ●—●, *n*-butyl alcohol; ×—×, *n*-amyl alcohol; ○—○, *n*-hexyl alcohol.

Table III: Apparent Fractional Coverages[a] of the Electrode in the Presence of Alcohols

	S, %	(100 − *S'*), %	*S'*, %
Without alcohol	100	0	100
13.5 m*M* *n*-butyl alcohol	56	44	56
3.5 m*M* *n*-amyl alcohol	47	50	50
0.85 m*M* *n*-hexyl alcohol	38	56	44

[a] Assumed that the apparent fractional coverage by *n*-butyl alcohol is 44% and the alcohol molecule lies flat on the electrode.

$$\text{Apparent fractional coverage } (100 - S')\% = \frac{\text{projected area of normal aliphatic alcohol}}{\text{projected area of } n\text{-butyl alcohol}} \times 44\%$$

(27) R. I. Kaganovich, V. M. Gerovich, and T. G. Osotova, *Dokl. Akad. Nauk SSSR*, 155, 893 (1964).

given amount of adsorbed alcohols on the mercury electrode. In more nearly perpendicular orientation, the projected area of normal aliphatic alcohols on the mercury electrode is about the same. Thus, the inhibition effect in this orientation is proportional to the amount of adsorbed alcohols on the mercury and not on the alcohol itself. The deviation of the inhibition effect from regularity in the medium concentration range is explained by some perpendicular orientation and some parallel. With increasing alcohol concentration, it is reasonable that perpendicular orientation predominates; therefore, the rate constants in the presence of the different alcohols become superimposable on each other at a given relative concentration of the alcohol.

Acknowledgment. We deeply appreciate support of this work by The Robert A. Welch Foundation of Houston, Texas, and by the Office of Naval Research, Contract NONR375(15). The authors also express their thanks to Dr. Allen J. Bard and Mr. David Jones for their extensive discussion and reading, and to many others for their helpful discussion. One of the authors (K. K. N.) also thanks Sumitomo Chemical Company of Japan for the leave of absence which permitted him to undertake this work.

Far-Ultraviolet Spectra of Hydrogen and Hydroxyl Radicals from Pulse Radiolysis of Aqueous Solutions. Direct Measurement of the Rate of H + H[1]

by P. Pagsberg, H. Christensen,[2a] J. Rabani,[2b] G. Nilsson,[2a] J. Fenger, and S. O. Nielsen

Danish Atomic Energy Commission Research Establishment, Risø, Denmark, and Aktiebolaget Atomenergi, Studsvik, Nyköping, Sweden *(Received August 22, 1968)*

Pulse radiolytic absorption transients have been observed in aqueous solutions between 200 and 300 nm using an 11-MeV Linac and an optical detection system that allowed accurate measurements (a) down to 200 nm and (b) 0.2 μsec after the electron pulse. With 10^{-3} *M* $HClO_4$ + 0.027 *M* H_2 ($p(H_2)$ = 35 atm) transients with second-order decay were observed which had amplitudes that decayed monotonically in the region from 200 to 240 nm. Assigning these transients to free H atoms, the molar decadic absorptivities ϵ at 200, 210, and 240 nm of H were found to be 900, 560, and 0 M^{-1} cm^{-1}, respectively, and $2k_{H+H} = (1.55 \pm 0.10) \times 10^{10}$ M^{-1} sec^{-1} from measurements at 200 and 210 nm. The transients could be completely quenched by addition of O_2 resulting in a species with the absorption spectrum of HO_2. Furthermore, the transient at 210 nm was not affected when $HClO_4$ was left out of the H_2-saturated solution and N_2O ($> 2 \times 10^{-3}$ *M*) was added instead. The apparent OH transient in 2×10^{-3} *M* N_2O (no H_2) decayed according to second-order kinetics with a calculated rate constant that after correction for the reaction of H with OH was found to be $(1.04 \pm 0.10) \times 10^{10}$ M^{-1} sec^{-1} independent of the wavelength used. The calculated ϵ for OH showed, after correction for the absorbance of H_2O_2, H, and OH^-, one broad absorption maximum near 230 nm with ϵ 530 M^{-1} cm^{-1} and one below 200 nm. The measurements at 200 nm had to be corrected for a substantial contribution from OH^- to the observed optical absorption. The calculated values of ϵ_H and ϵ_{OH} account quantitatively at all wavelengths used for the initial absorption of the transients in 10^{-3} *M* $HClO_4$ (no H_2) if it is assumed that H_3O, if formed, decomposes to yield H + H_2O after no longer than 0.2 μsec. The light absorption of aqueous solutions of H and to some extent of OH at 200 nm is attributed to a red shift of the water absorption continuum beginning at 186 nm, caused by a partial electron transfer from the first excited singlet state of water to a neighboring H or OH free radical in analogy with the optical transition associated with the β bands in alkali halide crystals.

Introduction

Free hydrogen atoms in the gas phase do not absorb light in the ground state at longer wavelengths than 121.57 nm,[3] and it has, in general, been assumed that solutions of free hydrogen atoms in water do not absorb light in the far-ultraviolet spectral region (>200 nm). It is the purpose of this report to demonstrate that solutions of free hydrogen atoms in water, produced by pulsed radiolysis in solutions saturated with pressurized H_2, do in fact absorb light appreciably at 200 nm and to suggest the type of optical transition involved.

(1) Presented at the Symposium on Photochemistry and Radiation Chemistry at Natick, Mass., April 22–24, 1968. A preliminary communication has appeared: S. O. Nielson, P. Pagsberg, J. Rabani, H. Christensen, and G. Nilsson, *Chem. Commun.*, 1523 (1968).

(2) (a) Aktiebolaget Atomenergi, Studsvik, Nyköping, Sweden; (b) Department of Physical Chemistry, The Hebrew University, Jerusalem, Israel.

(3) G. Herzberg, "Atomic Spectra and Atomic Structure," 2nd revised ed, Dover Publications, New York, N. Y., 1944, p 25.

Assuming that the optical absorption transients (that are measured with an improved pulse radiolysis technique) are caused by free hydrogen atoms, a direct determination of the rate constant $2k_{H+H}$ is possible. The value found at room temperature is $2k_{H+H} = (1.55 \pm 0.10) \times 10^{10}\ M^{-1}\ sec^{-1}$. This value should be compared with the values in the literature[4-9] based on indirect methods and ranging from 1.2×10^{10} to $3.2 \times 10^{10}\ M^{-1}\ sec^{-1}$.

The absorption spectrum above 200 nm of the OH radical in aqueous solution has been determined by pulse radiolysis of $2 \times 10^{-3}\ M$ N_2O solutions since it can be compared with the OH spectrum reported by Thomas, *et al.*[10] It is shown in the present investigation that the reported[10] apparent difference between the OH spectrum at pH 7 and pH 3 can be understood when the light absorption of H and OH^- is taken into account. From the pulse radiolytic absorption transients above 210 nm in $2 \times 10^{-3}\ M$ N_2O $2k_{OH+OH}$ can be calculated directly with good accuracy. The value found is $2k_{OH+OH} = (1.04 \pm 0.10) \times 10^{10}\ M^{-1}\ sec^{-1}$, which agrees with the value reported by Thomas, *et al.*,[10] using a similar method. Other values of $2k_{OH+OH}$ in the literature[6,11-13] are based on indirect methods and range from 0.8×10^{10} to $1.26 \times 10^{10}\ M^{-1}\ sec^{-1}$.

Experimental Section

Pulse Irradiation. Electron pulses 0.7–1.5 μsec long with an average electron energy of 10–11 MeV were obtained from the Risø Linac. The 250-mA beam was not monoenergetic, and attention had to be paid to the fact that the average electron energy and the ratio dose/(average pulse current × pulse width) varied somewhat with pulse width. The front and the back of the pulse had a rise time (corresponding to a change between 10 and 90% of full beam current) of *ca.* 0.2 μsec. Two irradiation cells were used. One consisted of a Suprasil quartz cylinder (length 2.55 cm, 1.5 cm i.d.) with 1.25-mm thick, optically flat end windows. The cell was irradiated in air along its axis at a position where the diameter of the electron beam (measured between half-intensity points) had increased to *ca.* 2 cm. The dose averaged over the cell with a 1-μsec pulse was *ca.* 3×10^{20} eV/l. The analyzing light beam entered the cell approximately parallel to but in opposite direction to the electron beam and was reflected by a 3 × 4 mm aluminum mirror coated directly on the outer surface of the cell window facing the Linac. The optical path length was $2 \times 2.55 = 5.1$ cm. To prevent light which was reflected by the first cell window in the light path without entering the cell from reaching the photomultiplier, the two cell windows were mounted so that they formed an angle of a few degrees with each other.

The other irradiation cell (Figure 1) was used for irradiations under an atmosphere of 35 atm of hydrogen. It consisted of a heavy-walled Pyrex tube (length 7.1 cm, 1.2 cm i.d.) equipped with 6-mm thick optical windows of Suprasil quartz that also served as the pressure tight ends (with O-ring seal) in an outer cylinder made of 1.5-mm thick stainless steel that contained the 35 atm of hydrogen. The Pyrex body could be filled through a hole in the Pyrex tube and a corresponding hole with side arm in the stainless steel body. The cell was irradiated from the side in a position where the electron beam after passing a quadrupole magnetic field had a cross section that approximately fitted the inner Pyrex body of the cell. The dose averaged over the cell with a 1-μsec pulse was *ca.* 10^{20} eV/l. The analyzing light beam traversed the cell perpendicularly to the electron beam with an optical path length of 7.1 cm.

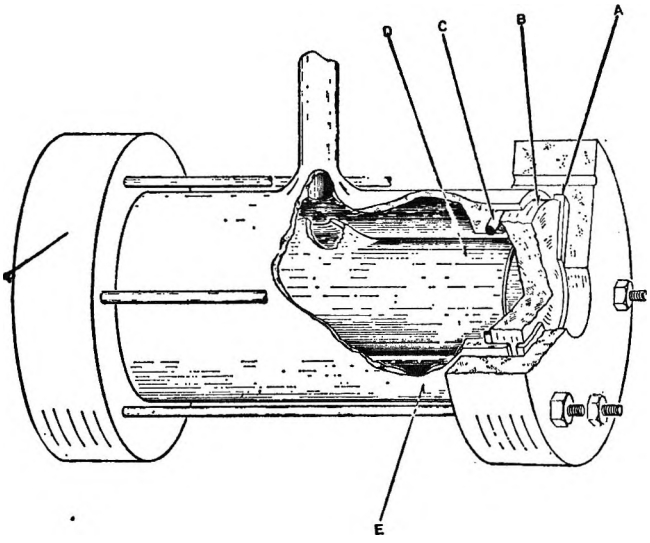


Figure 1. Pressure cell. Valves and manometer are not shown. (A) Teflon gasket; (B) quartz window; (C) O-ring; (D) Pyrex cell; (E) stainless steel pressure containment.

The timing, shape, and current intensity of every single pulse was monitored by photographing the oscillogram of the output of a toroidal coil wound around the window of the Linac. It was proved by a series of dosimeter runs that the dose absorbed in the cells could be monitored to better than 3% in a short series of runs by measuring the area under the pulse in the oscillogram. In some of the runs the dose given by a single pulse was also monitored by a transmission

(4) J. K. Thomas, *J. Phys. Chem.*, 67, 2593 (1963).
(5) H. A. Schwarz, *ibid.*, 67, 2827 (1963).
(6) H. Fricke and J. K. Thomas, *Radiat. Res., Suppl.*, 4, 35 (1964).
(7) H. A. Schwarz, *ibid.*, 4, 89 (1964).
(8) J. P. Sweet and J. K. Thomas, *J. Phys. Chem.*, 68, 1363 (1964).
(9) J. Rabani and D. Meyerstein, *ibid.*, 72, 1599 (1968).
(10) J. K. Thomas, J. Rabani, M. S. Matheson, E. J. Hart, and S. Gordon, *ibid.*, 70, 2409 (1966).
(11) H. A. Schwarz, *ibid.*, 66, 255 (1962).
(12) M. Anbar and P. Neta, *Int. J. Appl. Radiat. Isotopes*, 18, 493 (1967).
(13) J. Rabani and M. S. Matheson, *J. Phys. Chem.*, 70, 761 (1966).

monitor of Taimuty type.[14] In most of the runs reported here the timing of the electron pulse relative to an advanced trigger pulse was accurate to better than 0.1 μsec, and the dose was reproducible to better than 4%.

Optical Detection. The analyzing light used to monitor the pulse radiolytic optical absorption transients was taken from an Osram xenon lamp XBO 450 with Suprasil quartz bulb. The lamp had a continuous emission spectrum down to below 200 nm. The transmission of the optical system and in particular the brightness of the Xe arc at 200 nm was found to be so low that not enough light reached the photomultiplier cathode at this wavelength (overall effective relative aperture f/9.9) to permit accurate measurements of the rather weak optical transients of H and OH. The normal Xe lamp current of 28 A, supplied by a current-regulated power supply (Lambda, Model LE 104), was, therefore, increased to *ca.* 180 A *ca.* 300 μsec before the Linac was fired. The current increment of *ca.* 150 A was delivered from a 0.04 F capacitor bank of electrolytic capacitors charged to 35 V that were discharged through a transistorized switch and adjustable series regulator.[15] By the time the Linac was fired the brightness of the Xe arc had increased 25–30 times over the normal level and remained either at this level or changed slowly and linearly with time with a deviation of less than 0.5% (see Figure 1) for at least 300 μsec after the electron pulse. The reproducibility of consecutive light pulses fired at more than 5-sec intervals was excellent and allowed a scale expansion of as much as 25 times to be used in the optical detection channel. Pulsing the lamp in this way with 180-A current pulses of 800 μsec duration increased the brightness of the Xe arc 25–30 times not only at 200 nm (where it is most needed) but also at longer wavelengths over most of the ultraviolet spectral region. Between 5000 and 10,000 light pulses have been obtained from one Xe lamp before the reproducibility of the light pulses deteriorated and the cathode showed marked corrosion.

Via a system of three lenses made of Suprasil quartz and six vacuum-evaporated aluminum mirrors with a reflectivity of more than 82% each at 200 nm the light beam from the Xe lamp passed through the irradiation cell and subsequently through a Zeiss MM 12 double quartz prism monochromator to an EMI 9558Q photomultiplier operated with 5 or 6 dynodes.[16] The monochromator and photomultiplier were placed behind a 10-cm lead shield. When the lenses were properly set at 200 nm so that light of this wavelength was focused on the entrance slit of the monochromator the level of scattered light at 200 nm was so low that it could not be detected. At the maximum slit width of 2.0 mm the band width of the monochromator at 200 nm was 0.95 nm. The anode resistance of the photomultiplier was 1 kΩ which gave a signal of 0.4 V at the maximum allowed anode current[16] and a response time of the optical detection channel of 80 nsec. The electrical signal went directly to a fast, cascaded, emitter follower *via* a protective transistor limiter that limited the signal to 0.7 V. The emitter follower drove the signal undistorted through 15 m of 75-Ω coaxial cable to two Tektronix 555 oscilloscopes with type W plug-in units. To protect the vertical amplifiers in the oscilloscopes at high gain from overloading and subsequent slow recovery due to the strong signal from the Cerenkov radiation, a clamping circuit[17] with a fast electronic switch was placed in the input to the oscilloscopes. A fraction of 1 μsec before the electron pulse started, this clamping circuit was adjusted to switch the inputs of the oscilloscopes over to some arbitrary signal that, however, was visible on the oscilloscope screens. The input of the oscilloscopes was again switched back to the transmission line from the photomultiplier, 0.2 μsec after the electron pulse and the Cerenkov radiation had faded away. The clamping signal and the fast response of the system is visible in Figure 2. The overall system was shown to be linear in its response to changing light intensity.

Dosimetry. The absorbed dose was measured by filling the cells with 10^{-3} *M* $K_4Fe(CN)_6$ dissolved in triply distilled water saturated with N_2O and subsequently shaken less than 5 min before irradiation with 5 ml of air per 100 ml of solution in the syringe. The oxygen in the air acted as an H atom scavenger, preventing their reaction with $Fe(CN)_6^{3-}$.[13] $G(Fe(CN)_6^{3-})$ was equated with $G_{OH} + G_e = 2.65 + 2.6 = 5.25$,[18] and the molar decadic absorptivity ϵ of $Fe(CN)_6^{3-}$ was taken as 1000 at 420 nm.[13] Dosimeter runs calibrated the electron pulse monitor so that the dose for every electron pulse could be calculated from the monitor reading. A Jena WG 6 light filter that cuts out wavelengths shorter than 300 nm minimized the photochemical oxidation of $Fe(CN)_6^{4-}$. N_2O was purified as in ref 13. The variation of dose with the distance from the accelerator in the 2.55-cm two-pass cell was measured with what amounted essentially to a cell with five 5-mm long compartments that could be filled individually one after the other with dosimeter solution while the other compartments contained water. The dose in the rear 5 mm of the cell as seen from the Linac was found to be *ca.* 40% of the highest dose measured in the front 5 mm of the cell. The dose increased almost linearly through the cell. The relative dose variation within the 7.1-cm pressure cell was not measured but it was estimated to be less marked than the corresponding variation in the 2.55-cm cell.

(14) S. I. Taimuty and B. S. Deaver, Jr., *Rev. Sci. Instrum.*, 32, 1098 (1961).
(15) T. Hviid and S. O. Nielsen, in preparation.
(16) J. P. Keene, *J. Sci. Instrum.*, 41, 493 (1964); *Rev. Sci. Instrum.*, 34, 1220 (1963).
(17) H. Christensen, G. Nilsson, P. Pagsberg, and S. O. Nielsen, *ibid.*, in press.

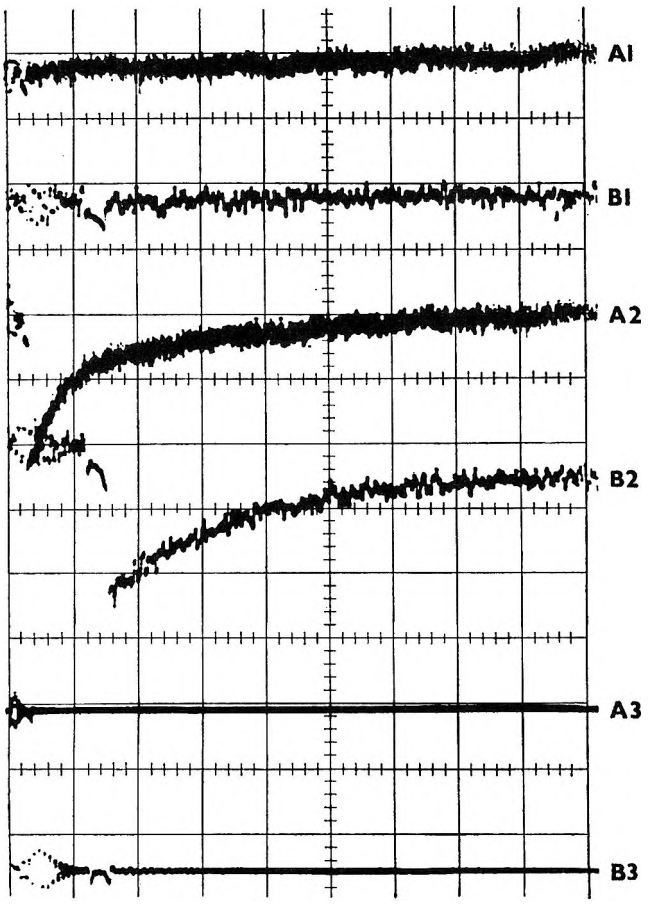


Figure 2. Oscilloscope traces of light intensity *vs.* time: $\lambda = 200$ nm, slit = 2.0 mm, and response time *ca.* 80 nsec. One large ordinate division corresponds to 5.37% transmission and one large abscissa division to 20 μsec for A traces and 5 μsec for B traces. Traces with the same number were triggered simultaneously. A2 and B2: light transmission of 7.1 cm of 10^{-3} *M* $HClO_4$ + 0.027 *M* H_2 after irradiation with a 1.2-μsec electron pulse that had just faded away 7.7 μsec after start of the two oscilloscope traces. A3 and B3: Cerenkov light intensity recorded under conditions identical with those used in A2 and B2 but with no analyzing light. The oscillations before the electron pulse were due to electrical noise pick-up. A1 and B1: light intensity from pulsed Xe lamp (100% transmission) recorded under conditions identical with those used in A2 and B2 but with no electron pulse. The arbitrary signal level to which the oscilloscope inputs were clamped during the duration of the electron pulse is visible in all the traces from 6 to 7.7 μsec after sweep start.

Materials and Methods. The general techniques of pulse radiolysis have been treated in detail.[18-20] We used the "syringe" technique[21] with 100-ml Summit syringes made of Pyrex; they were baked at 470°. The filling and emptying of the two-pass cell under 1 atm of He was remote-controlled.[17] The following chemicals were used: triply distilled water; N_2O purified by bubbling through NaOH–pyragallol;[13] $HClO_4$, 60%, Merck analytical grade; Ar purified by distillation; and H_2 purified carefully by passing it through 2 m of molecular sieve at −196° and subsequently through a dust filter. Solutions were stored for up to 30 hr in syringes which, in turn, were kept in a moistened plastic bag. Before filling the pressure cell it was flushed carefully with H_2, and while still being flushed it was then filled with the deaerated and Ar-saturated solution and rapidly connected to a combined vacuum–pressure line that supplied the pressurized H_2, and N_2O and O_2 when used. The cell was taken through several cycles of evacuation to 0.5 atm and pressurization with H_2 to 35 atm. The cell had a volume ratio of gas/liquid of *ca.* 4:1, and the inner Pyrex body of the cell with quartz windows had room for a 0.3-ml gas bubble without interfering with the light path through the cell (Figure 1). This gas bubble was in good contact with both the liquid and the gas inside the cell while the cell was being shaken. Measurements at 250 nm of the OH absorption transient in 10^{-3} *M* $HClO_4$ indicated that complete gas equilibration was established after 30 min of gentle shaking. All irradiations were done at 23–25°.

Results

The performance of the optical detection channel is shown in Figure 2. At 200 nm and with a response time of 80 nsec, the peak-to-peak noise on the 100% light level corresponded to less than 2% of light transmission. The strong Cerenkov signal was almost completely suppressed by the clamping circuit which also allowed apparently true measurements to begin 0.2 μsec after the electron pulse had faded away. As seen from trace B3 of Figure 2, long-lived luminescence from the cell windows and satellite pulses from the photomultiplier were practically absent. This was not true at the much lower intensities obtained with an unpulsed Xe lamp.

ϵ_H and $2k_{H+H}$. When the 7.1-cm pressure cell was filled with 10^{-3} *M* $HClO_4$ + 0.027 *M* H_2 (p_{H_2} = 35 atm) and irradiated with 1.2-μsec electron pulses, optical absorption transients were observed (Figure 2) from 200 to 240 nm that appeared to be independent of (a) the number (at least 10) of electron pulses previously given to the same solution and (b) the particular stock solution of $HClO_4$ used. To calculate the absorbance of the transients they were first corrected for the small slope of the 100% transmission level (see Figure 2, B1). The optical transmission scale (see Figure 2) was then calibrated from the oscilloscope gain and an oscillogram with gain one showing both the 100% and 0% transmission levels. Finally, the absorbance of the transients as a function of time after the

(18) L. M. Dorfman and M. S. Matheson in "Progress in Reaction Kinetics," Vol. III, G. Porter, Ed., Pergamon Press, Oxford, 1965, Chapter 6.

(19) J. W. Boag in "Actions Chimiques et Biologiques des Radiations," M. Haissinsky, Ed., Masson et Cie, Paris, 1963, Series VI, Chapter 1.

(20) J. P. Keene in "Pulse Radiolysis," M. Ebert, J. P. Keene, A. J. Swallow, and J. H. Baxendale, Ed., Academic Press, Inc., New York, N. Y., 1956, p 1.

(21) E. J. Hart, S. Gordon, and J. K. Thomas, *J. Phys. Chem.*, 68, 1271 (1964).

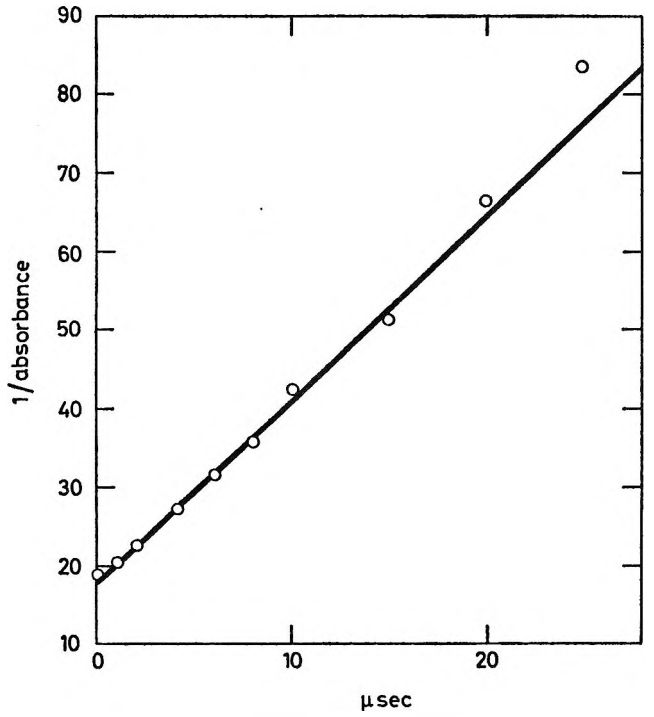


Figure 3. Second-order plot of the decay of the pulse radiolytic transient B2 in Figure 2. Absorbance is true decadic absorbance minus decadic "asymptotic" absorbance read 160 μsec after the electron pulse. The time is microseconds after the end of the electron pulse.

end of the electron pulse was calculated and corrected by subtracting the "asymptotic" absorbance read at 160 μsec after the electron pulse from all the values. The reciprocal of this corrected absorbance was then plotted against time (see Figure 3). The decay of the transients was found to agree well with second-order kinetics at 200 and 210 nm. At higher wavelengths the transients were too weak to warrant kinetic analysis.

In the pressure cell hydrated electrons, e_{aq}^-, and OH are rapidly removed by reactions with H_3O^+ and H_2, respectively. If we assume (as will be supported in the following) that both reactions result in the formation of H, the observed optical transients may be provisionally assigned to H. The half-times of e_{aq}^- and OH are 0.03 and 0.5 μsec, respectively, under our conditions[11,22a–c] compared with the *ca.* 8 μsec half-time of the optical transients (see Figure 3). Only a small error in the calculation of the apparent molar decadic absorptivity, ϵ_H, and of the rate constant $2k_{H+H}$ is introduced by assuming that only H is present at the end of the electron pulse. In extrapolating (absorbance)$^{-1}$ to time zero the reactions during the first microsecond of the optical transients are disregarded. Taking $G_e = 2.6$, $G_{OH} = 2.65$, and $G_H = 0.55$ [18] and applying a 5% correction for recombination during the electron pulse, c_H at time zero immediately after the electron pulse is calculated to be 8.43×10^{-6} M in the experiment treated in Figure 3. This value, together with the absorbance at time zero (obtained from extrapolation along the straight line in Figure 3) and the light path 7.1-cm, give $\epsilon_H = 915$ M^{-1} cm^{-1} at 200 nm. A value of $2k_{H+H} = 1.53 \times 10^{10}$ M^{-1} sec^{-1} is obtained from the slope of the line by multiplication with 7.1×915. The results of other runs on two different days were treated in a similar way and are summarized in Table I. At 210 nm ϵ_H has dropped to 563, but practically the same value (1.51×10^{10} M^{-1} sec^{-1}) was found for $2k_{H+H}$. Although the optical transients observed at wavelengths above 210 nm were not treated kinetically, absorbances at time zero were derived from them by extrapolation and ϵ_H was calculated. The results are given in Figure 4.

Table I: ϵ_H and $2k_{H+H}$ in 10^{-3} M $HClO_4$ + 0.027 M H_2[a]

Expt	Wavelength, nm	ϵ_H, M^{-1} cm^{-1}	$2k_{H+H} \times 10^{-10}$,[d] M^{-1} sec^{-1}
1	210.0	563	1.51
1	200.0	915	1.53
1	200.0	918	1.44
1	200.0	915	1.99
2	200.0	971	1.25
2	200.0	785	1.57
		Av[b] 900 ± 30[c]	Av 1.55 ± 0.10[c]

[a] At 23–25°. [b] Average of values at 200 nm only. [c] Standard deviation. [d] In the calculation of $2k_{H+H}$ the corresponding values of ϵ_H were used.

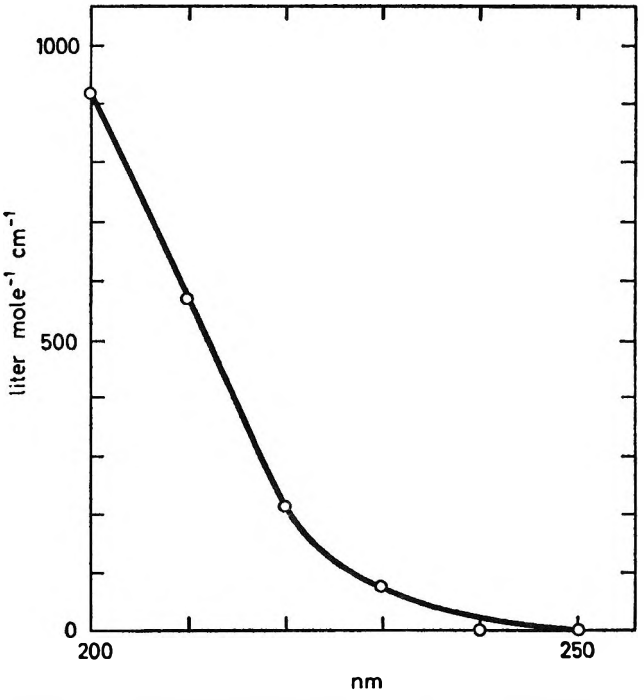


Figure 4. Absorption spectrum of the pulse radiolytic transient observed in 10^{-3} M $HClO_4$ + 0.027 M H_2 at 23–25° calculated as molar decadic absorptivity of free hydrogen atoms.

(22) (a) J. P. Keene, *Radiat. Res.*, **22**, 1 (1964); (b) L. M. Dorfman and I. A. Taub, *J. Amer. Chem. Soc.*, **85**, 237 (1963); (c) S. Gordon, E. J. Hart, M. S. Matheson, J. Rabani, and J. K. Thomas, *ibid.*, **85**, 1375 (1963).

In agreement with the assumption made that the optical transients are due to H, it was found that the optical transient observed at 210 nm was unaffected by substitution of N_2O for 10^{-3} M $HClO_4$. N_2O, which was difficult to add in known concentrations to the pressure cell, was present in a concentration estimated as 10^{-2} $M > c(N_2O) > 2 \times 10^{-3}$ M. Good measurements at 200 nm of the pulse radiolytic transients in the presence of high concentrations of N_2O are difficult because of the N_2O light absorption.

The absorption spectrum of OH is needed to obtain the absorption spectrum of H, independently, from the measurements in the two-pass cell (no H_2). The following subsection describes the measurements on OH.

ϵ_{OH} and $2k_{OH+OH}$. When the two-pass cell was filled with 2×10^{-3} M N_2O and irradiated with 1.1-μsec electron pulses, optical transients with half-times less than 10 μsec were observed from 200 nm to well above 300 nm. The oscillograms of the transients were treated in the same way as described above for the transients in the pressure cell in order to calculate absorbance as a function of time. The decay of the absorbance followed second-order kinetics to a good approximation at all wavelengths investigated as shown by second-order plots of (absorbance)$^{-1}$ *vs.* time (see Figure 5). Kinetic data were collected from solutions that were irradiated only once. Doubling the N_2O concentration did not appear to affect the pulse radiolytic transients.

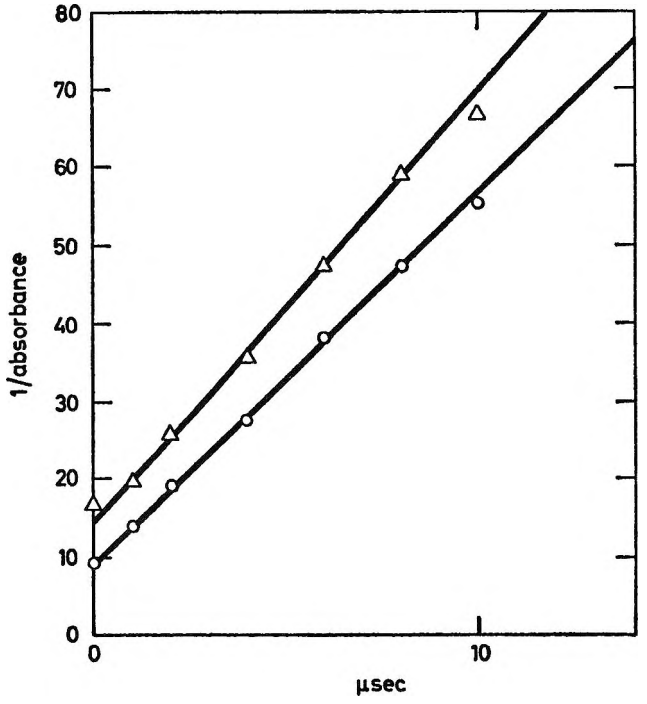


Figure 5. Second-order plot of the decay of the pulse radiolytic transient in 2×10^{-3} M N_2O at 200 nm. Absorbance is true decadic absorbance minus decadic "asymptotic" absorbance read 160 μsec after the 1.1-μsec electron pulse. The time is microseconds after the end of the electron pulse. Lower curve: uncorrected for OH^- light absorption; upper curve: corrected for OH^- light absorption.

Estimates were made of the error in the second-order rate constant produced by the nonhomogeneity of the radiation field. Computation showed that the error in the second-order rate constant calculated from the second-order plot deviated less than 2% from the true second-order rate constant. Similar results have recently been reported by Sauer[23] and by Boag.[24]

The pulse radiolytic transients in N_2O solutions have been assigned to OH radicals.[10,25,26] To calculate the molar decadic absorptivity of free OH, ϵ_{OH}, and the rate constant $2k_{OH+OH}$, we must first introduce a correction for the reaction of the primary yield of H atoms ($G_H = 0.55$) with the large excess of OH radicals present at time zero immediately after the electron pulse ($G(OH) = G_e + G_{OH} = 5.25$). Noting that $2k_{OH+OH}$ is of the order of 1.0×10^{10} M^{-1} sec^{-1} [6,10-13] and that the value of k_{H+OH} may be taken as 1.2×10^{10} M^{-1} sec^{-1},[4] this correction was introduced by defining an effective molar decadic absorptivity ϵ' for the sum of H and OH (H and OH maintain approximately the same ratio H/OH throughout the decay of the transient because $2k_{OH+OH} \approx k_{H+OH}$). ϵ' is related to the absorbance calculated from the transients as described above by eq 1 and to ϵ_H, ϵ_{OH}, and the yield of H_2O_2 after total decay of the transient, $G(H_2O_2)$, by eq 2.

$$\text{absorbance} = 5.1(c_H + c_{OH})\epsilon' \quad (1)$$

$$(G_{OH} + G_e + G_H)\epsilon' = (G_{OH} + G_e)\epsilon_{OH} + G_H\epsilon_H - (G(H_2O_2) - G_{H_2O_2})\epsilon_{H_2O_2} \quad (2)$$

$$G(H_2O_2) - G_{H_2O_2} = 0.5(G_{OH} + G_e)^2(G_{OH} + G_e + G_H)^{-1} \quad (3)$$

Equation 3 is easily derived by statistical reasoning under the assumption that H and OH are kinetically equivalent. This assumption is also necessary for eq 1-3 to be exact. For H and OH to be kinetically equivalent $2k_{H+H}$ would have to equal $2k_{OH+OH} = k_{H+OH}$. However, due to the large excess of OH over H the value of $2k_{H+H}$ is not critical.

From the readings of the electron pulse monitor that was calibrated with the ferrocyanide dosimeter the value of the sum $c_{OH} + c_H$ at time zero was calculated after correcting for a small recombination (*ca.* 10%) during the 1.1-μsec electron pulse. $c_{OH} + c_H$ was found to be *ca.* 3×10^{-5} M in most of the experiments. ϵ' was then calculated from eq 1 using the absorbance at time zero as obtained from extrapolation along the best-fitting straight line in the second-order plot (see

(23) M. C. Sauer, Jr., ANL-7327, May 1967.
(24) J. W. Boag, *Trans. Faraday Soc.*, 64, 677 (1968).
(25) J. K. Thomas, *ibid.*, 61, 702 (1965).
(26) D. M. Brown, F. S. Dainton, and D. C. Walker in "Pulse Radiolysis," M. Ebert, J. P. Keene, A. J. Swallow, and J. H. Baxendale, Ed., Academic Press, Inc., New York, N. Y., 1965, p 221.

Table II: ϵ_{OH} and $2k_{OH+OH}$ in 2×10^{-3} M N_2O[a]

Wavelength, nm	ϵ', M^{-1} cm^{-1}	ϵ_{OH}, M^{-1} cm^{-1}	$2k_{OH+OH} \times 10^{-10}$,[f] M^{-1} sec^{-1}
200.0	695[b]		1.74[b]
200.0	433[c]		1.20[c]
200.0	463[d]	509[d]	1.16[d]
210.0	387[d]	447	0.95[d]
210.0	411		0.91
220.0	455	523	1.20
230.0	470	543	1.10
240.0	432	494	0.98
250.0	411	463	0.91
250.0	413		0.97
		Av[e]	1.04 ± 0.04[f]

[a] At 23-25°. [b] Uncorrected for OH^- light absorption. [c] Corrected for OH^- light absorption. [d] In 2×10^{-3} M N_2O + 4×10^{-5} M $HClO_4$. [e] Excluding value uncorrected for OH^- light absorption. [f] Standard deviation. [g] Corrected for the reaction H + OH.

Figure 5). ϵ' and ϵ_{OH} as calculated from eq 2 and 3 substituting the values of G_e, G_{OH}, and G_H already used, ϵ_H from Figure 3, and $\epsilon_{H_2O_2}$ from ref 27, are given in Table II. In applying the correction for light absorption by H atoms we anticipate the final conclusion (see Discussion) that all results obtained are consistent with an assignment of the spectrum in Figure 4 to H atoms. Some values of ϵ_{OH} are plotted in Figure 6. Owing to the approximate kinetic equivalency of H and OH, $2k_{OH+OH}$ may be calculated with good accuracy from the slope of the second-order plot by multiplication with the corresponding value of ϵ' and with the length of the light path, 5.1 cm. The resulting values of $2k_{OH+OH}$ are given in Table II.

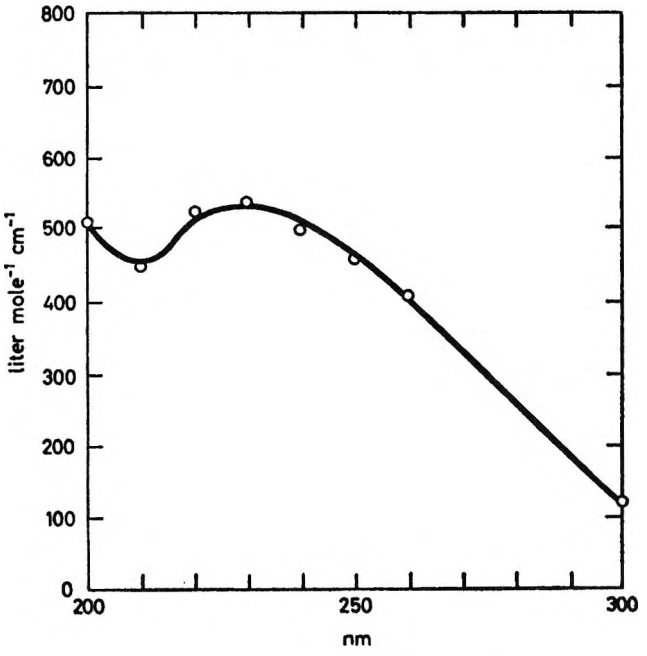


Figure 6. Absorption spectrum of the pulse radiolytic transient observed in 2×10^{-3} M N_2O calculated as molar decadic absorptivity of free OH radicals after correction for the light absorption of H_2O_2, H, and OH^-.

If k_{H+OH} is approximately equal to $2k_{OH+CH}$ as assumed above, the present treatment using ϵ' is better than the kinetic treatment where the presence of H is completely neglected. Such a treatment leads to a value of $2k_{OH+OH}$ that is overestimated by *ca.* 10%.

The values found for $2k_{OH+OH}$ in Table II in the region from 210 to 250 nm all fall between 0.91×10^{10} and 1.20×10^{10} M^{-1} sec^{-1}. The value found at 200 nm, however, using the same method of making a second-order plot (Figure 5, lower curve) and calculating ϵ' and $2k_{OH+OH}$, leads to $2k_{OH+OH} = 1.74 \times 10^{10}$ (Table II). We believe that this is caused by the neglect of OH^- ions formed by reaction 4. OH^- absorbs light at 200 nm with $\epsilon_{OH^-} = 1000$.[27] The absorptivity is almost an order of magnitude smaller at 210

$$N_2O + e_{aq}^- \longrightarrow N_2 + OH^- + OH \qquad (4)$$

nm, and the contribution of OH^- to the pulse radiolytic optical transients can be neglected at this wavelength and above. At 200 nm, on the other hand, light absorption by OH^- makes an appreciable contribution to the observed optical transients as shown by the difference between the upper and lower curves in Figure 5. OH^- formed by reaction 4 and possibly by other reactions (making the initial yield $G_{OH^-} > 0$) in the neutral solution decays by reacting with an equivalent amount of H_3O^+ with a rate constant $k(OH^- + H_3O^+) = 1.4 \times 10^{11}$ M^{-1} sec^{-1},[28] and it is easy to calculate c_{OH^-} at any given time t (in seconds) after the end of the electron pulse from eq 5

$$(c_{OH^-})^{-1} = (c^\circ_{OH^-})^{-1} + 1.4 \times 10^{11} \times t \quad \text{(liters/mole)} \qquad (5)$$

where $c^\circ_{OH^-}$ is the concentration of OH^- immediately after the electron pulse. As there is extensive recombination of OH^- and H_3O^+ during the 1.1-μsec electron pulse, $c^\circ_{OH^-}$ does not depend very much on the value chosen for G_{OH^-}. For the run shown in Figure 5 $c^\circ_{OH^-}$ was calculated to be *ca.* 1.0×10^{-5} M.

When the upper second-order plot in Figure 5 that is corrected for the OH^- light absorption is used to determine ϵ' and $2k_{OH+OH}$, a value of $2k_{OH+OH} = 1.20 \times 10^{10}$ M^{-1} sec^{-1} is found, in good agreement with the values determined at the other wavelengths. It is, furthermore, in agreement with the suggestion that OH^- makes an appreciable contribution to the pulse

(27) Landolt-Börnstein Tables, 6th ed, "Atomic and Molecular Physics," Vol. I "Molecules II," part 3, Springer-Verlag, Berlin, 1951, p 231.

(28) M. Eigen and L. DeMayer, *Z. Elektrochem.*, **59**, 986 (1955).

radiolytic transients at 200 nm in 2×10^{-3} M N_2O that the pulse radiolytic transients in 2×10^{-3} M N_2O + 4×10^{-5} M $HClO_4$ was found to give "normal" values of $2k_{OH+OH}$ at 210 and 200 nm (0.95×10^{10} and 1.16×10^{10}, respectively) without any correction for OH^- light absorption (Table II). In the acidified solution OH^- disappears in a pseudo-first-order reaction with H_3O^+ with a decay time of less than 0.2 μsec. The average of all the values of $2k_{OH+OH}$ in Table II that either have been corrected for OH^- light absorption or do not need this correction is 1.04×10^{10} with a standard deviation of 0.04×10^{10}. Owing to the small systematic errors introduced by the data treatment, we give $2k_{OH+OH}$ as $(1.04 \pm 0.10) \times 10^{10}$ M^{-1} sec^{-1}.

Pulse Radiolytic Transients in 10^{-3} M $HClO_4$. When the two-pass cell was filled with 10^{-3} M $HClO_4$ and irradiated with 1.2-μsec electron pulses, optical transients were observed from 200 nm to well above 300 nm. As will be further described in a future report, the initial absorbance of these transients could, after a small correction for recombination during the electron pulse, be quantitatively accounted for by the initial yields already used[18] of OH, H, and e_{aq}^- (that was assumed immediately to be transformed into H) supplemented with $G_{H_2O_2} = 0.7$ [18] and the absorption spectra of H, OH, and H_2O_2 given in Figures 4 and 6 and in ref 27, respectively.

Quenching of the "H-Transient" by O_2. The pressure cell was filled with 10^{-3} M $HClO_4$ + 0.027 M H_2 + *ca.* 10^{-3} M O_2 (it was difficult to add O_2 in known concentration to the pressure cell) and irradiated with a 1.2-μsec electron pulse. A radiation induced absorbance was observed 0.2 μsec after the end of the electron pulse in the region investigated from 200 to 250 nm. In this wavelength region the absorbance did not appear to decrease during the first 100 μsec after the pulse which indicates that the "H-transient" that is observed in the absence of O_2 between 200 and 240 nm (Figure 4) is completely quenched by O_2. The species resulting from the quenching has an absorption spectrum given in Figure 7 which is based on the absorbance measured 0.2 μsec after the electron pulse and on the assumption that the G value of the resulting species is equal to $G_{OH} + G_e + G_H = G(HO_2)$. A comparison of Figure 7 with the reported[29] spectrum of HO_2 leads to the conclusion that the "H-transient" is quenched by oxygen to give HO_2 radicals and no other uv-absorbing species. The small discrepancy between the HO_2 spectrum in Figure 7 and the reported[29] HO_2 spectrum in the region above 210 nm where they are both known should not be stressed because our experiments with oxygen added are not as accurate as the other experiments reported in this paper. Thus for unknown reasons not investigated further the absorbance after the pulse in the presence of O_2 increased very slightly with time at some of the wavelengths investigated.

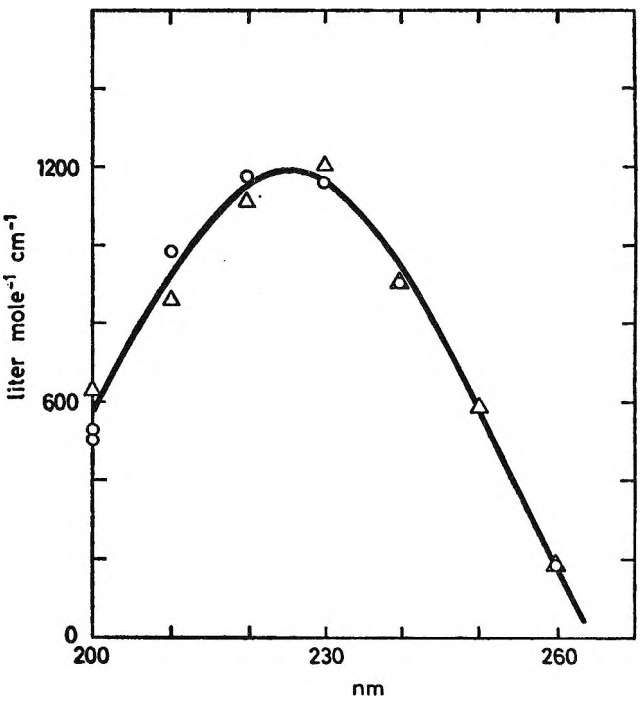


Figure 7. Absorption spectrum of HO_2 calculated approximately (see text) from the initial absorbance of the pulse radiolytic transients produced by 1.2-μsec electron pulses in: ○, 10^{-3} M $HClO_4$ + 2.6×10^{-4} M O_2 in the two-pass cell; △, 10^{-3} M $HClO_4$ + 0.027 M H_2 + *ca.* 10^{-3} M O_2 in the pressure cell.

O_2-quenching experiments were also performed in the two-pass cell filled with 10^{-3} M $HClO_4$ + 2.6×10^{-4} M O_2 (air saturation). Again, it was found that the "H-transient" appeared to have been very nearly completely quenched when absorbance measurements were started a few tenths of 1 μsec after the electron pulse with the formation of HO_2 as the only product. The spectrum of HO_2 found that together with the absorbance of OH accounts for the data after making a rough estimate of recombination during the electron pulse is given in Figure 7. The spectra of HO_2 found with the two-pass cell and with the pressure cell are not significantly different.

An estimate of the rate of quenching of the "H-transient" by O_2 was provided by pulse radiolysis of 10^{-3} M $HClO_4$ + 2.6×10^{-5} M O_2 in the two-pass cell. The initial absorbance of the transients observed at 240 nm indicated a degree of scavenging of H atoms of *ca.* 25%. Likewise, the initial absorbance at 200 nm was found to be consistent with a degree of quenching of the species responsible for the "H-transient" of somewhere between 20 and 40%. The experiments are difficult at this wavelength and are not very accurate because $G \times \epsilon$ values of only $0.3(G_H + G_e)(\epsilon_{H}^{200\text{ nm}} - \epsilon_{HO_2}^{200\text{ nm}}) \approx 300$ are involved. Taking the degree of quenching observed 0.2 μsec after the end of the electron pulse (*i.e.*, *ca.* 0.3 μsec after the pulse current had decreased to half of

(29) G. Czapski and L. M. Dorfman, *J. Phys. Chem.*, 68, 1169 (1964).

its maximal value) as 25% and noting that the width of the electron pulse was 1.2 μsec, we may calculate $k(H + O_2)$ and the second-order rate constant k of quenching of the "H-transient" by O_2.

$$k(H + O_2) \approx k$$
$$\approx 0.25[2.6 \times 10^{-5} \times (0.3 + 0.6) \times 10^{-6}]^{-1}$$
$$\approx 10^{10}\ M^{-1}\ \text{sec}^{-1} \quad (6)$$

Discussion

The value of $\epsilon_{OH}^{260} = 405\ M^{-1}\ \text{cm}^{-1}$ found in the present investigation at 260 nm (see Figure 6) agrees well with $\epsilon_{OH}^{260} = 410\ M^{-1}\ \text{cm}^{-1}$ reported by Rabani.[30] In addition, our value of $2k_{OH+OH} = (1.04 \pm 0.10) \times 10^{10}\ M^{-1}\ \text{sec}^{-1}$ based on measurements between 200 and 250 nm agrees well with the value of $2k_{OH+OH} = 1.05 \times 10^{10}\ M^{-1}\ \text{sec}^{-1}$ reported from pulse radiolysis of $10^{-3}\ M$ N_2O at 260 nm by Thomas, *et al.*[10] They used $\epsilon_{OH}^{260} = 370\ M^{-1}\ \text{sec}^{-1}$ [25] to calculate $2k_{OH+OH}$ from the slope of the second-order plot of the pulse radiolytic transient apparently without correcting for the presence of H. As seen above this procedure leads to an *ca.* 10% overestimate of $2k_{OH+OH}$ which, however, in their case was compensated by the use of a value of ϵ_{OH} that is *ca.* 10% lower than ours. Thus the good agreement between our value of $2k_{OH+OH}$ and that of Thomas, *et al.*,[10] may serve as a check on the pulse-radiolysis techniques employed.

The main advantage of the type of pressure cell used in the present investigation is that it can be filled with pure H_2 so that the first single-pulse electron irradiation gives meaningful results. It was found and verified by calculation that up to 10 electron pulses could be given to the same solution of $10^{-3}\ M$ $HClO_4$ + 0.027 M H_2 without producing significant changes in the optical transients observed.

With the dose per pulse employed of 10^{20} eV/l. or more, it is a good approximation to assume that the transients have decayed to a constant level 160 μsec after the electron pulse. Thus the measured absorbance of the transients at $t = 160$ μsec can be used to correct the absorbances of the same transient measured at shorter times with the extrapolated absorbance at $t = \infty$.

Assignment of the "H-Transient." The pulse radiolytic transient that has been referred to above as the "H-transient" is observed in "pure" form by irradiating the pressure cell filled with $10^{-3}\ M$ $HClO_4$ + 0.027 M H_2. It has a spectrum shown in Figure 4 where its molar decadic absorptivity has been calculated on the assumption that the transient is due to free H atoms. The same decay kinetics observed at both 200 and 210 nm shows that it is the same species which is absorbing at both wavelengths. We now actually propose to assign the "H-transient" to the presence of dissolved free H atoms. The reason for this assignment is that the transient in every respect tested behaves as an optical absorption transient due to free H atoms. Thus, (a) the "pure" transient decays following second-order kinetics (Figure 3). (b) The value calculated for $2k_{H+H} = (1.55 \pm 0.10) \times 10^{10}\ M^{-1}\ \text{sec}^{-1}$ under the assumption that the "H-transient" is due to H falls within the range of values of $2k_{H+H}$ found by indirect methods.[4-9] (c) The "H-transient" as observed in $10^{-3}\ M$ $HClO_4$ + 0.027 M H_2 at 210 nm is independent of whether H is formed by reactions 7 or 8

$$H_2 + OH \longrightarrow H + H_2O \quad (7)$$

$$e_{aq}^- + H_3O^+ \longrightarrow H + H_2O \quad (8)$$

thus also providing evidence that H_3O, if formed as an intermediate in reaction 8, has a lifetime that does not exceed a few tenths of 1 μsec. (d) The initial absorbance of the pulse radiolytic transient in $10^{-3}\ M$ $HClO_4$ can be accounted for at all wavelengths investigated by the commonly accepted initial radiolytic yields[18] and by the absorption spectra of H and OH (Figures 4 and 6), and by that of H_2O_2. This indicates that the "H-transient" is observed in $10^{-3}\ M$ $HClO_4$ as well (further supported by the analysis of the decay kinetics as will be shown in a future report) with a strength relative to that observed in $10^{-3}\ M$ $HClO_4$ + 0.027 M H_2 that is proportional to the concentration of free H atoms. (e) The "H-transient" appears to be completely quenchable by O_2 with a calculated rate constant $k(H + O_2) \approx 10^{10}\ M^{-1}\ \text{sec}^{-1}$ assuming the "H-transient" to be due to H. The only product of the quenching reaction with O_2 appears to be HO_2.

It should also be noted that the observed second-order decay of the "H-transient" in conjunction with the calculated, nearly diffusion-controlled second-order rate constant $2k_{H+H} = 1.6 \times 10^{10}\ M^{-1}\ \text{sec}^{-1}$ (assuming the "H-transient" to be due to H with $G(H) = G_{OH} + G_e + G_H = 5.8$) make it difficult to assign the "H-transient" to a radiation produced species with $G < 0.6$. Such an assignment would mean that the species in question would have a second-order decay constant larger than $k(H^+ + OH^-) = 1.4 \times 10^{11}\ M^{-1}\ \text{sec}^{-1}$. The "H-transient" must, therefore, either be due to free dissolved H atoms or to some other radiation-produced species with $G > 0.6$ and a lifetime that under our conditions is several microseconds. It has so far not been necessary to postulate the existence of such a species in the radiation chemistry of water, and we prefer to assign the "H-transient" to H atoms.

Nature of the Far-Ultraviolet Spectrum of H. The absorption spectrum of H given in Figure 4 is surprising in view of the fact that free hydrogen atoms in the gas phase do not absorb light in the ground state at longer wavelengths than 121.57 nm.[3] A solvent red shift of the absorption spectrum of H of more than

(30) J. Rabani in "Radiation Chemistry of Aqueous Systems," G. Stein, Ed., Interscience, New York, N. Y., 1968, p 229.

70 nm (30,000 cm^{-1}) is hardly conceivable. We tentatively interpret, therefore, the absorption spectrum of aqueous solutions of H (Figure 4) as a comparatively small red shift of the first water absorption continuum beginning at 186 nm.[31] The water molecules contributing to the red shift must be those in direct contact with the dissolved H atoms. In view of evidence from esr measurements of essentially free H atoms in aqueous phases (see *e.g.*, ref 32a), this red shift must be due to a perturbation of the corresponding excited state only of H_2O leaving the ground state essentially unperturbed. Whereas a dissolved H atom does not interact with more than thermal energies with any H_2O solvent molecule in its ground state, it can interact much more strongly with a neighboring, electronically excited water molecule H_2O^* *via* a partial, negative charge transfer from H_2O^* to H. The energetic conditions for this charge transfer to take place from the first excited (continuous) singlet state of H_2O (ionization potential $\leq$ 12.6 − 6.7 = 5.9 eV[32b]), associated with the first absorption continuum from 186 to 145 nm, to H (electron affinity 0.77 eV[33]) is comparable to the conditions for charge transfer in many well-known charge-transfer complexes.[34] Due to the compensating coulomb attraction the distance over which the charge transfer is to occur is critical for the extent of the charge transfer and hence for the perturbation (red shift) of the water continuum band beginning at 186 nm. A qualitative explanation along this line may be offered for the apparent absence of the solvent perturbation band in aqueous solutions of HO_2 (Figure 7). The absorption spectrum of aqueous solutions of OH (Figure 6) appears, on the other hand, to show the beginning of a solvent perturbation band at 200 nm. It may be tentatively interpreted along similar lines as the absorption spectrum of H shown in Figure 4. Our spectrum of OH (Figure 6) differs somewhat from that of Thomas, *et al.*,[10] below 220 nm. These authors, however, stated certain reservations concerning their measured spectra below 220 nm, and we believe our OH spectrum to be the more correct.

A semiquantitative treatment of the far-ultraviolet absorption spectra of aqueous solutions of H and of OH is under way and will be presented in a future report. The optical transition proposed above to account for these spectra is analogous to the transition believed to be responsible for the β bands in alkali halides.[35]

Acknowledgments. We thank the staff of the Accelerator Division, Risø, for careful Linac operation, K. B. Hansen, E. Mose Christiansen, and K. E. Neisig of the Electronics Department for help with circuitry, K. Søe Højberg and Tove Rosendahl Hansen for computer calculations, and Farukh Said and C.-G. Blixen-Finecke for aid in the experimental work. The special help of Dr. E. J. Hart, Argonne National Laboratory, with pressure cell irradiations is gratefully acknowledged.

(31) G. Herzberg, "Electronic Spectra and Electronic Structure of Polyatomic Molecules," D. Van Nostrand Co., Princeton, N. J., 1966, p 585.

(32) (a) P. W. Atkins and M. C. R. Symons, "The Structure of Inorganic Radicals," Elsevier Publishing Co., Amsterdam, 1967, p 84. (b) The ionization potential of water in the gas phase is 12.6 eV. The quantum associated with the 186-nm absorption edge is 6.7 eV.

(33) J. D. Weisner and B. H. Armstrong, *Proc. Phys. Soc.*, 83, 31 (1964).

(34) L. J. Oosterhoff in "Modern Quantum Chemistry," O. Sinanoglu, Ed., Academic Press, Inc., New York, N. Y., 1965, Part I, p 137.

(35) J. J. Markham, *Solid State Phys., Suppl.*, 8, 1 (1966).

Enthalpy of Hydrolysis of Rhenium Trichloride. Enthalpy and Free Energy of Formation of Rhenium Sesquioxide[1]

by R. H. Busey, E. D. Sprague, and R. B. Bevan, Jr.

Chemistry Division, Oak Ridge National Laboratory, Oak Ridge, Tennessee 37830 *(Received September 3, 1968)*

The standard enthalpy of hydrolysis of rhenium trichloride in alkaline solution to form hydrated rhenium sesquioxide has been observed to be -54.29 ± 0.14 kcal (gfw of $ReCl_3$)$^{-1}$ at 25°. This result combined with other available thermal data gives for the enthalpy of formation $\Delta H_f°(Re_2O_3) = -119.2$ kcal mol^{-1}. The entropy of Re_2O_3 is estimated to be 32 cal deg^{-1} mol^{-1} which leads to $\Delta F_f°(Re_2O_3) = -101.6 \pm 0.6$ kcal mol^{-1} for the free energy of formation at 25°. The electrode potentials of the half-reactions $2Re + 6OH^- = Re_2O_3 + 3H_2O + 6e^-$ and $Re_2O_3 + 2OH^- + 3H_2O = 2ReO_2 \cdot 2H_2O + 2e^-$ are computed to be 0.333 ± 0.004 and 1.25 ± 0.01 V, respectively.

Introduction

The enthalpy,[2] entropy, and free energy[3] of formation of $ReCl_3(c)$ are known. The trichloride is readily hydrolyzed to hydrated Re_2O_3 in alkaline solution in the absence of oxygen.[4] The sesquioxide in the presence of oxygen is rapidly oxidized to the dioxide, and it reduces water with evolution of hydrogen at 100°.[4] A determination of the enthalpy of hydrolysis of $ReCl_3$ to the hydrated Re_2O_3 should be possible provided the oxide is kinetically stable in the alkaline solution for a period of time sufficient to carry out the observation. Such a measurement gives the enthalpy of formation of the sesquioxide based upon that of $ReCl_3$.

We have observed that rhenium sesquioxide is indeed sufficiently stable in dilute alkaline solution to permit a calorimetric determination of the enthalpy of hydrolysis of rhenium trichloride. These results together with an estimate of the entropy of Re_2O_3 give a value for the free energy of formation. These data thus extend our knowledge of the redox potentials of rhenium in alkaline solution to the trivalent state. No previous thermochemical data on hydrated rhenium sesquioxide are reported in the literature.

Experimental Section

Materials. The anhydrous $ReCl_3$ used was the same material employed and described in the low-temperature heat capacity measurements.[3] To determine if any degradation in purity had occurred in subsequent handling of the hygroscopic $ReCl_3$, a Mohr volumetric chloride determination was made during the course of this investigation which indicated a purity of 100.04%.

A 0.2 *N* NaClO solution was prepared by dilution of ~5% Fisher reagent NaClO and standardized and frequently checked iodometrically using Fisher standard reagent 0.1000 *N* in $Na_2S_2O_3$. The titer of the latter reagent was checked against primary standard $K_2Cr_2O_7$. The standardized ClO^- reagent was used to determine the average oxidation state of the rhenium in the calorimetric solution following a hydrolysis run.

Sodium hydroxide solutions were prepared by diluting 1 *N* NaOH stock solution and determining the final concentration by titrating aliquots with Fisher standard reagent 0.1000 *N* in HCl.

Calorimeter. The solution calorimeter previously employed[5] has been modified by introducing a 100-ohm thermistor in place of the combination resistance thermometer–heater and employing a specially constructed 450-ml dewar with a very thin inner wall (0.2 mm).[6] The top 3 cm of the straight-wall, round-bottom dewar is not silvered to reduce heat conduction from the bath to the contents of the flask. These modifications of the calorimeter dewar as advocated by others[7] have resulted in a calorimeter which reaches equilibrium following an electrical energy input in less than 2 min. The performance of the calorimeter was tested by measurements on THAM (tris(hydroxymethyl)aminomethane).[8]

Procedure. All handling of the $ReCl_3$ was done in a vacuum-type drybox filled with argon and equipped

(1) This research was sponsored by the U. S. Atomic Energy Commission under contract with Union Carbide Corp.

(2) J. P. King and J. W. Cobble, *J. Amer. Chem. Soc.*, 82, 2111 (1960).

(3) R. B. Bevan, Jr., R. A. Gilbert, and R. H. Busey, *J. Phys. Chem.*, 70, 147 (1966).

(4) W. Geilmann and F. W. Wrigge, *Z. Anorg. Allgem. Chem.*, 214, 239 (1933).

(5) (a) R. H. Busey, K. H. Gayer, R. A. Gilbert, and R. B. Bevan, Jr., *J. Phys. Chem.*, 70, 2609 (1966); (b) R. H. Busey, H. H. Dearman, and R. B. Bevan, Jr., *ibid.*, 66, 82 (1962).

(6) The inner portion of the dewar was fabricated on a glass lathe starting with a 22-mm o.d. Pyrex glass tube with a 1.5-mm wall and expanding to give a tube with ~0.2-mm wall and 60-mm o.d. The authors wish to express their appreciation to members of the Chemistry Division Glass shop under R. W. Poole for their patience in fabricating these dewars.

(7) W. P. Hutchinson and A. G. White, *J. Sci. Instr.*, 32, 309 (1955); J. J. Christensen, R. M. Izatt, and L. D. Hansen, *ibid.*, 36, 779 (1965).

(8) S. R. Gunn, *J. Phys. Chem.*, 69, 2902 (1965); R. J. Irving and I. Wadsö, *Acta Chem. Scand.*, 18, 195 (1964).

with an analytical balance. Trays of P_2O_5 within the drybox ensured an anhydrous atmosphere. The calorimetric samples of $ReCl_3$ were contained in a Teflon sample holder with gold foil lids paraffined onto each end. Within the calorimeter paraffined threads were used to remove the lids to initiate the reaction and to prevent the lids from falling to the bottom of the calorimeter.

The NaOH solutions were boiled and purged with nitrogen or argon to remove dissolved oxygen before adding to the calorimeter. After the solution was cooled, sufficient boiled water was added to bring the concentration to its original value and an aliquot was taken for hydroxide concentration determination. A predetermined volume of this solution (325 ml) was placed in the calorimeter dewar and the air above the solution removed by purging for 15–20 min with the dewar in position in the calorimetric apparatus. To ensure anaerobic conditions, the dewar was then lowered slightly and a weighed amount (50–75 mg) of $ReCl_3$ was added to the solution to serve as a getter for any trace of oxygen remaining in the solution. The calorimeter was then reassembled and purging continued for another 10 min.

Immediately after a determination of the temperature rise caused by the hydrolysis reaction, the calorimeter was cooled by pumping on 1 ml of water introduced into a cooling bulb within the calorimeter. The calorimeter was allowed to equilibrate for 1 hr before two to four heat capacity determinations were made. The average oxidation state of the rhenium was then determined by adding a 50-ml aliquot of 0.2 N standardized NaClO solution directly to the dewar. When the solution became water clear, it was transferred to a flask and the excess ClO^- was determined iodometrically.

Experimental Results

Seven determinations of the heat of solution of THAM in 0.100 N HCl to give a solution of concentration 5 g/l. were made to check the performance of the calorimeter. The THAM employed was Fisher primary standard for acidimetry, not the calorimetric standard which is now available from the National Bureau of Standards. The average of the seven determinations was $\Delta H = -7120$ cal mol^{-1} at 25° with an average deviation of ±3 cal mol^{-1}. This result is 0.2% more exothermic than the results of the authors given in ref 8. Unfortunately, this difference cannot be evaluated critically because of possible sample differences. We used Fisher THAM straight out of a fresh bottle with no further purification or drying. These determinations indicate that our solution calorimeter as presently designed may yield enthalpies with a systematic error of ~0.2%.

Table I gives the data for the enthalpy of hydrolysis of $ReCl_3$ expressed in terms of the defined thermochemical kilocalorie equal to 4.184 absolute kilojoules. The hydrolysis reaction is[9]

$$ReCl_3(c) + 3OH^- = \tfrac{1}{2}Re_2O_3(c) + \tfrac{3}{2}H_2O + 3Cl^- \quad (1)$$

It is the hydrated sesquioxide which is precipitated. The isolated "dry" precipitate has been observed to correspond closely to $Re_2O_3 \cdot 3H_2O$.[10] Since its composition in contact with aqueous solution is uncertain, all thermodynamic data given in this paper refer to Re_2O_3 ignoring its hydration water as is customary in such cases.

Table I: Enthalpy of Hydrolysis of $ReCl_3(c)$ by NaOH Solution at 25°

Run no.	[OH⁻], N	$ReCl_3(c)$, g	$-\Delta H$, kcal × (gfw of $ReCl_3$)$^{-1}$
4	0.151	0.5498	54.54
5	0.146	0.5225	54.24
6	0.146	0.3266	54.45
7	0.145	0.3406	54.40
8	0.0512	0.2967	54.37
11	0.290	0.3176	54.91[a]
12	0.295	0.3248	54.17
13	0.0992	0.3198	54.23
14	0.0978	0.3269	54.63
15	0.102	0.3017	54.34
			$\Delta H_1° = -54.29 \pm 0.14$

[a] Rejected by Chauvenet's criterion.

The average result of the determinations of the average oxidation state of the rhenium following an hydrolysis run was 3.12 ± 0.02. These determinations were made, of necessity, 2–3 hr after the hydrolysis reaction was initiated in the calorimeter. These results suggest that a significant amount of Re(IV) develops in this time, but this interpretation is not consistent with the results of two determinations of the oxidation state of the rhenium in $ReCl_3(c)$ made directly on the crystals. In the latter determinations the sample of $ReCl_3(c)$ was added directly to the alkaline ClO^- solution. The direct titrations also gave 3.12 ± 0.02, which in turn does not agree with the purity determined by the much more accurate chloride analyses. In all of the above determinations the ClO^- was in twofold excess above that required to oxidize the Re(III) to ReO_4^- which might not have been sufficient.[11] The

(9) Anhydrous rhenium trichloride is in reality Re_3Cl_9; F. A. Cotton and J. T. Mague, *Inorg. Chem.*, 3, 1402 (1964). For simplicity, results are given in terms of the gram formula weight: gfw of $ReCl_3$ = 292.56 g.

(10) F. Hurst, P. Gibart, and K. Traore, *Compt. Rend.*, 263C, 97 (1966).

(11) (a) King and Cobble[2] in their calorimetric observations on the oxidation of $ReCl_3(c)$ by alkaline ClO^- used 3–7-fold excess ClO^- and stated that the correct stoichiometry was proven by determination of the final ClO^- concentration. It is interesting, however, that in their analyses of their $ReCl_3(c)$ for the oxidation state using slightly basic hydrogen peroxide they obtained 3.09 ± 0.03. Since they stated that their procedure minimizes but does not completely prevent the catalytic decomposition of the peroxide, this figure may be low. (b) F. Hurst, *et al.*,[10] obtained by Ce^{4+} titration an average oxidation state ranging from 3.08 to 3.14 for the rhenium in hydrated Re_2O_3 formed from hydrolysis of $ReCl_3$.

agreement of the oxidation state determinations between the $ReCl_3(c)$ and the rhenium in the calorimeter following hydrolysis is interpreted to mean that little or no change in oxidation state occurred when the trichloride was hydrolyzed. A kinetics experiment described below corroborates this interpretation.

A kinetics experiment was performed to determine the rate at which Re_2O_3 is oxidized by water to give the dioxide and hydrogen

$$Re_2O_3 + 5H_2O = 2ReO_2 \cdot 2H_2O + H_2$$

From data given below it may be calculated that for this side reaction $\Delta F^\circ = -19.8$ kcal. A weighed sample of $ReCl_3(c)$ contained in a thin-wall glass bulb was hydrolyzed by breaking the bulb beneath a thoroughly degassed 0.15 N NaOH solution. The solution was contained in a known, constant volume system equipped with a mercury manometer. The rate of hydrogen evolution, which is a measure of the reaction rate, was determined from pressure *vs.* time observations. The kinetics of the oxidation of Re_2O_3 was observed to be complex. For the first 4 hr the reaction appeared to be first order following the rate law $-dx/dt = 0.012x$, where x represents the fraction of Re_2O_3 remaining after t hours.[12] For 1 hr after initiating the reaction (*e.g.*, after initiating the hydrolysis reaction in the calorimeter), the rate of oxidation of Re_2O_3 by water is constant to $\sim 1\%$ since in this time only 1.2% has been oxidized. The rate of heat evolution from this oxidation is thus constant and is superimposed upon the normal temperature after-drift of the calorimeter. This additional heat rate represented only 1% of the normal heat leak. (The enthalpy of the oxidation of Re_2O_3 by H_2O may be calculated from the data given below to be -22.5 kcal mol^{-1}.) The calculation of the temperature rise from the fore- and after-drift automatically corrects for this slow side reaction.

There is an additional side reaction to the one above, namely: $Re_2O_3 + 3H_2O = \frac{1}{2}Re + \frac{3}{2}ReO_2 \cdot 2H_2O$. This reaction is also thermodynamically possible with $\Delta F^\circ = -31.9$ kcal. The extent to which this side reaction occurs cannot be detected by the ClO^- titration for the average oxidation state since this reagent would oxidize the rhenium metal to ReO_4^-. Hurst, *et al.*,[10] present an X-ray diffraction pattern on their isolated $Re_2O_3 \cdot 3H_2O$ as well as other X-ray patterns of products obtained from heat treatment. The heat-treated samples exhibit X-ray diffraction lines due to Re and ReO_2 whereas the initial sample of $Re_2O_3 \cdot 3H_2O$ does not. Unfortunately, this is not positive proof that the initial sample does not contain Re and ReO_2 because these phases, formed at low temperatures, may not be crystalline and thus not give a distinct X-ray pattern. It is assumed that this second side reaction, like the first side reaction studied kinetically, is slow at 25° and that it is automatically corrected for in computing the temperature rise due to the hydrolysis reaction. If this assumption is erroneous and an initial rapid disproportionation occurs, the absolute value of ΔH_1° observed would be too large, resulting in a less exothermic free energy of formation. This in turn would mean that Re_2O_3 is more unstable toward disproportionation than indicated below.

Thermochemical Calculations

In the corrections required to convert the observed enthalpies (Table I) to the enthalpy at infinite dilution, the correction involving the relative partial molal enthalpy of water is entirely negligible. The enthalpies of dilution of NaOH and NaCl were taken from Harned and Owen.[13] The enthalpy of reaction 1 corrected to infinite dilution is $\Delta H_1^\circ = -54.29 \pm 0.14$ kcal (gfw of $ReCl_3)^{-1}$. The correction is small, the corrected enthalpy differing only 0.08 kcal from the simple average of the observed enthalpies. This result combined with the enthalpy of formation of $ReCl_3(c)$, -63.0[2] kcal (gfw of $ReCl_3)^{-1}$, and the enthalpies of formation of OH^-, Cl^-, and H_2O taken from Latimer[14] gives for the enthalpy of formation of the hydrated rhenium sesquioxide: $\Delta H_f^\circ(Re_2O_3) = -119.2$ kcal mol^{-1} at 25°.

The entropy of Re_2O_3 may be estimated from known entropies of other sesquioxides, correcting for the mass difference by

$$S(Re_2O_3) = S(M_2O_3) + \tfrac{3}{2}R \ln (\text{at. wt of Re})/(\text{at. wt of M})$$[15]

From the entropies given by Latimer[14] for La_2O_3, Bi_2O_3, and Sb_2O_3, the entropy of Re_2O_3 at 25° is calculated to be 31.6, 35.6, and 30.7 cal deg^{-1} mol^{-1}, respectively. From Latimer's[14] tables of estimated entropy contributions of ions in solids, the entropy of Re_2O_3 is 31.5. The average of all four is 32.3 ± 1.8; the entropy of Re_2O_3 is taken as 32 ± 2 cal deg^{-1} mol^{-1} at 25°.

In making this estimate no account has been taken of any magnetic entropy the compound may possess at room temperature. The gaseous Re^{3+} ion has the $(Xe)5d^4$ electronic structure, and the ground state is $5D_0$. There are no magnetic susceptibility measurements to indicate the ground state of the metal ion in

(12) Beyond 4 hr the reaction rate decreased more slowly than required by the first-order kinetics observed in the first 4 hr. The data from 2 to 8 hr could be fit to the rate law, $-dx/dt = 0.00030x/(1-x)$, but below 2 hr this rate law gave a reaction rate much greater than observed. The inverse proportionality of the rate to the fraction of dioxide formed, $(1-x)$, suggests that a protective film of dioxide is coating the Re_2O_3 particles and preventing or hindering their oxidation. Beyond 8 hr, however, the reaction rate again decreased more slowly than indicated by this rate law. The decrease continued until from 15 to 50 hr the rate appeared constant at 0.07%/hr.

(13) H. S. Harned and B. B. Owen, "The Physical Chemistry of Electrolytic Solutions," 2nd ed, Reinhold Publishing Corp., New York, N. Y., 1950.

(14) W. M. Latimer, "Oxidation Potentials," 2nd ed, Prentice-Hall, Inc., New York, N. Y., 1952.

(15) G. N. Lewis and M. Randall, "Thermodynamics," revised by K. S. Pitzer and L. Brewer, McGraw-Hill Book Co., Inc., New York, N. Y., 1961.

the oxide. In an octahedral environment neglecting spin–orbit coupling, the degenerate d orbitals of the gaseous Re^{3+} ion would be split to give a low-spin ground state with an electron spin of unity. A tetragonal distortion of the octahedral field, or a tetrahedral field, gives a diamagnetic ground state. Strong spin–orbit coupling, which is present in third transition series ions, would likewise lead to a diamagnetic ground state.[16] It is thus anticipated that hydrated Re_2O_3 will be either diamagnetic or only weakly paramagnetic at room temperature and will possess little or no magnetic entropy at this temperature.

The estimated entropy of Re_2O_3, 32 ± 2 cal deg^{-1} mol^{-1}, combined with the entropies of Re and O_2,[17] gives -59 ± 2 cal deg^{-1} mol^{-1} for the entropy of formation of Re_2O_3 at 25°. This estimate, together with the above enthalpy of formation, gives the free energy of formation of Re_2O_3 at 25°; $\Delta F_f^\circ(Re_2O_3) = \Delta H_f^\circ - T\Delta S_f^\circ = -101.6 \pm 0.8$ kcal mol^{-1}.

The potential of the $Re-Re_2O_3$ couple in alkaline solution is computed to be 0.333 ± 0.006 V and that of the Re_2O_3–$ReO_2 \cdot 2H_2O$ couple in alkaline solution to be 1.25 ± 0.01 V.[18] These potentials show that Re_2O_3 is quite unstable with respect to disproportionation into Re metal and $ReO_2 \cdot 2H_2O$(c) and that it is thermodynamically unstable in alkaline solution toward oxidation to $ReO_2 \cdot 2H_2O$ by water. The apparent stability observed in this research must be a kinetic stability. The oxidation of the sesquioxide by water to $ReO_2 \cdot 2H_2O$ is perhaps prevented by the formation of a thin, protective layer of the latter on the particles of the former.

Hurst, *et al.*,[10] have interpreted their thermogravimetric data obtained on $Re_2O_3 \cdot 3H_2O$ under a high vacuum at 500° as being due to the reaction: $Re_2O_3 \cdot 3H_2O = Re + ReO_2 + 3H_2O + \frac{1}{2}O_2$. This reaction, however, is not as thermodynamically favorable as the simple disproportionation reaction: $Re_2O_3 \cdot 3H_2O = \frac{1}{2}Re + \frac{3}{2}ReO_2 + 3H_2O$. It is readily seen that $\Delta F_2^\circ - \Delta F_1^\circ = \frac{1}{2}\Delta F_f^\circ(ReO_2)$ where the subscripts 1 and 2 refer to the first and second reaction, respectively. This difference is approximately -35 kcal at 500°.[19] This does not mean, however, that the first reaction with oxygen as a product cannot occur. The first reaction above may be divided into two equilibria: $Re_2O_3 \cdot 3H_2O = Re_2O_3 + 3H_2O$ and $Re_2O_3 = Re + ReO_2 + \frac{1}{2}O_2$.

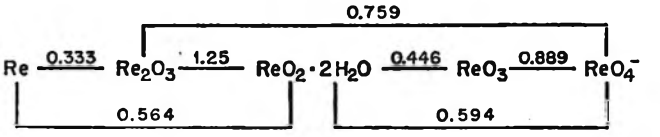


Figure 1. Redox scheme of rhenium in basic solution. Potential in volts.

If only the latter of these equilibria is considered, it may be calculated from our $\Delta F_f^\circ(Re_2O_3)$ and $\Delta F_f^\circ(ReO_2)$[19] that the partial pressure of oxygen at 25° is only $\sim 10^{-17}$ mm. If the entropy change of the reaction is approximately constant from 25 to 500°, the partial pressure of oxygen increases to a few millimeters at 500°, sufficient for the reaction to go to completion when carried out under a high vacuum. In view of the fact that the second reaction (no O_2 evolution) is much more thermodynamically favorable (ΔF° is approximately -32 kcal at 500° for the reaction $Re_2O_3 = \frac{1}{2}Re + \frac{3}{2}ReO_2$) than the reaction proposed by Hurst, *et al.*, confirmation or repudiation of their results is needed.[20]

The potential diagram of rhenium in alkaline solution including the data of this research and thermal data given by King and Cobble[21] is given in Figure 1.

(16) See, *e.g.*, C. J. Ballhausen, "Introduction to Ligand Field Theory," McGraw Hill Book Co., Inc., New York, N. Y., 1962.

(17) $S^\circ(Re) = 8.74$ cal deg^{-1} mol^{-1} from U. Piesbergen, *Z. Naturforsch.*, 19a, 1075 (1964); $S^\circ(O_2(g)) = 49.00$ cal deg^{-1} mol^{-1} from Latimer.[14]

(18) Auxiliary data from Latimer[14] and $\Delta F_f^\circ(ReO_2 \cdot 2H_2O) = -202.4$ kcal mol^{-1} from ref 5a.

(19) This datum is obtained from $\Delta F_f^\circ(ReO_2)$ and $\Delta S_f^\circ(ReO_2)$ at 25° with the assumption that the latter is independent of temperature between 25 and 500°. $\Delta F_f^\circ(ReO_2) = -89.0$ kcal mol^{-1} at 25° is computed from the potential of the ReO_2–ReO_4^- couple measured by Z Z. Hugus and cited by Latimer[14] using $\Delta F_f^\circ(ReO_4^-(aq)) = -167.1$ kcal mol^{-1} from G. E. Boyd, J. W. Cobble, and W. T. Smith, Jr., *J. Amer. Chem. Soc.*, 75, 5783 (1953). $\Delta S_f^\circ(ReO_2) = -40.7$ cal deg^{-1} mol^{-1} at 25° is based upon the entropy of Re,[17] O_2,[14] and ReO_2.[5a] That $\Delta S_f^\circ(ReO_2)$ is approximately independent of temperature may be demonstrated by assuming the entropy ncrease of Re and ReO_2 in the temperature range–500° corre-isponds to the observed increase, respectively, of W and IrO_2 tabulated by K. K. Kelley, U. S. Bureau of Mines Bulletin 584, U. S. Government Printing Office, Washington, D. C., 1960.

(20) In addition to the simple disproportionation reaction, another thermodynamically possible reaction is: $Re_2O_3 \cdot 3H_2O = 2ReO_2 + H_2 + 2H_2O$. The loss in weight of a sample of $Re_2O_3 \cdot 3H_2O$ *via* this reaction, however, would be considerably less than observed by Hurst, *et al.*[10]

(21) J. P. King and J. W. Cobble, *J. Amer. Chem. Soc.*, 79, 1559 (1957).

The Proton Magnetic Resonance Spectra of Five *ortho*-Substituted Phenols

by James L. Roark and William B. Smith

Chemistry Department, Texas Christian University, Fort Worth, Texas 76129 *(Received September 12, 1968)*

The proton magnetic resonance spectra of five *ortho*-substituted (methoxy-, chloro-, bromo-, iodo-, and nitro-) phenols have been determined in carbon tetrachloride and in dimethyl sulfoxide solutions. The spectra were completely determined for the first solvent and for the chemical shifts in the latter. The values of the chemical shifts are compared with results for other *ortho*-disubstituted benzenes.

Recently we have examined the proton magnetic resonance spectra for a large number of *ortho*-disubstituted benzenes,[1,2] and a summary of the various factors thought to influence aromatic proton chemical shifts has been given.[2] In particular, we have observed that substituent effects at the *ortho* position can be correlated with the parameter Q[1-3] and that empirical values for Q may be derived from chemical shifts for protons in known systems.[2]

Concurrently, Traynham and coworkers[4] have noted that the chemical shift for the phenolic proton in a series of phenols in dimethyl sulfoxide (DMSO) correlated with σ_p^- and that the relation held for *ortho*-substituted phenols. Thus, it has been possible for them to establish a σ_o^- scale which measures the electronic effects of the substituent at the phenolic proton and, presumably, the *ortho* carbon. The method employed suggests that no steric effects of the substituents were being measured. Because of these observations, it seemed of interest to determine the ring proton chemical shifts in the same system. It was hoped that a comparison of the H_3 chemical shift with Q and with the chemical shift of the phenolic proton might be instructive as to the mode of operation of substituent effects on proton chemical shifts at the *ortho* position.

Experimental Section

The various phenols were studied in both carbon tetrachloride and in DMSO solutions (10% v/v) with tetramethylsilane as an internal standard. All samples were thoroughly degassed before measurement. Spectra were determined on a Varian A-60A spectrometer at resolutions between 0.1 and 0.2 cps as measured by the width at half-height of the narrowest line in the spectrum. Spectra were recorded on the 50-cps chart width at a sweep speed of 0.02 cps. All spectra were calibrated by the usual audio-side-band technique, and measured line frequencies were the averages of four to six determinations.

The spectra in carbon tetrachloride were completely analyzed as before.[1,2,5] Lines for nonadjacent protons were assigned by application of the additivity rules of Martin and Dailey.[6] Substituent parameters for the phenol hydroxyl group were taken from the appropriate chemical shifts in phenol[7] as d_o, 0.55 ppm; d_m, 0.18 ppm; and d_p, 0.47 ppm. The chemical shifts for H_3 were assigned using the previously developed Q relationships.[2] The spectra changed only slightly in the solvent DMSO. The chemical shifts of the various protons could be estimated quite well (we feel to at least 0.01 ppm) by comparison with the completely analyzed spectra in carbon tetrachloride. The spectral parameters are given in Table I. The spectrum for 2-methoxyphenol is given in Figure 1 as an example of a tightly coupled unsymmetrical four-spin system.

In the spectrum of 2-nitrophenol in carbon tetrachloride the line assigned to H_5 appears as an octet of doublets due to a long-range splitting with the phenol proton (J = 0.42 cps). This has been noted previously.[8] In DMSO this coupling disappears, and the H_5 lines appear as a sharp octet.

Discussion

The chemical shifts of aromatic protons *ortho* to a varying group of substituents have been found to correlate well with the parameter Q.[1-3] This parameter has been defined by Schaefer and coworkers[3] as P/r^3I where P is the polarizability of the C–X bond, r is the bond length, and I is the ionization potential of the element X. The concept of Q arose from consideration of the paramagnetic term of the Ramsey shielding equation which contains an average excitation energy, here approximated as I^{-1}, and which arises from mixing of excited states of the substituent with the ground state

(1) W. B. Smith and G. M. Cole, *J. Phys. Chem.*, 69, 4413 (1965).

(2) W. B. Smith and J. L. Roark, *J. Amer. Chem. Soc.*, 89, 5018 (1967).

(3) (a) F. Hruska, H. M. Hutton, and T. Schaefer, *Can. J. Chem.*, 43, 2392 (1965); (b) T. Schaefer, F. Hruska, and H. M. Hutton, *ibid.*, 45, 3143 (1967).

(4) J. G. Traynham and G. A. Knesel, *J. Org. Chem.*, 31, 3350 (1966); J. G. Traynham and M. T. Tribble, private communication. We wish to thank Professor Traynham for purified samples of several of the phenols used in this study.

(5) W. B. Smith and J. L. Roark, *J. Chem. Eng. Data*, 12, 587 (1967).

(6) J. S. Martin and B. P. Dailey, *J. Chem. Phys.*, 39, 1722 (1963).

(7) S. Castellano, C. Sun, and R. Kostelnik, *Tetrahedron Lett.*, 51, 5205 (1967).

(8) S. Castellano and R. Kostelnik, *ibid.*, 51, 5211 (1967).

Table I: Parameters for the *ortho*-Substituted Phenols[a]

ortho-Substituent	τ_3	τ_4	τ_5	τ_6	J_{34}	J_{35}	J_{36}	J_{45}	J_{46}	J_{46}	Rms[b]
CH_3O	3.27	3.28	3.22	3.16	8.12	1.48	0.36	7.67	1.68	8.14	0.031
	3.15	3.15	3.11	3.11	...	...	...	...	...	...	...
Cl	2.75	3.21	2.89	3.03	8.11	1.59	0.35	7.50	1.52	8.25	0.019
	2.63	3.16	2.80	2.96	...	...	...	...	...	...	...
Br	2.60	3.27	2.85	3.03	8.10	1.56	0.30	7.40	1.55	8.22	0.027
	2.47	3.22	2.76	2.98	...	...	...	...	...	...	...
I	2.41	3.39	2.83	3.06	7.97	1.55	0.27	7.35	1.50	8.17	0.020
NO_2	1.92	3.05	2.45	2.88	8.64	1.71	0.40	7.16	1.31	8.48	0.029
	2.08	2.98	2.42	2.81	8.36	1.71	0.33	7.29	1.29	8.37	0.044

[a] Coupling constants are in cps. The first entry for each compound is for the carbon tetrachloride solvent; the second is for DMSO. [b] Root-mean-square error in fit.

of the electrons in the C–H bond. Suffice it to say, Q can only be calculated from the definition for hydrogen and the halogens. However, in our work we have noted that H_3 in a series of 2-X-halobenzenes followed Q_X very well with no dependence on the nature of the halogen.[2] Consequently, empirical values of Q for other functional groups were derived and applied to other systems from the parent halobenzene plot. Among these groups were methoxyl, cyano, and nitro.

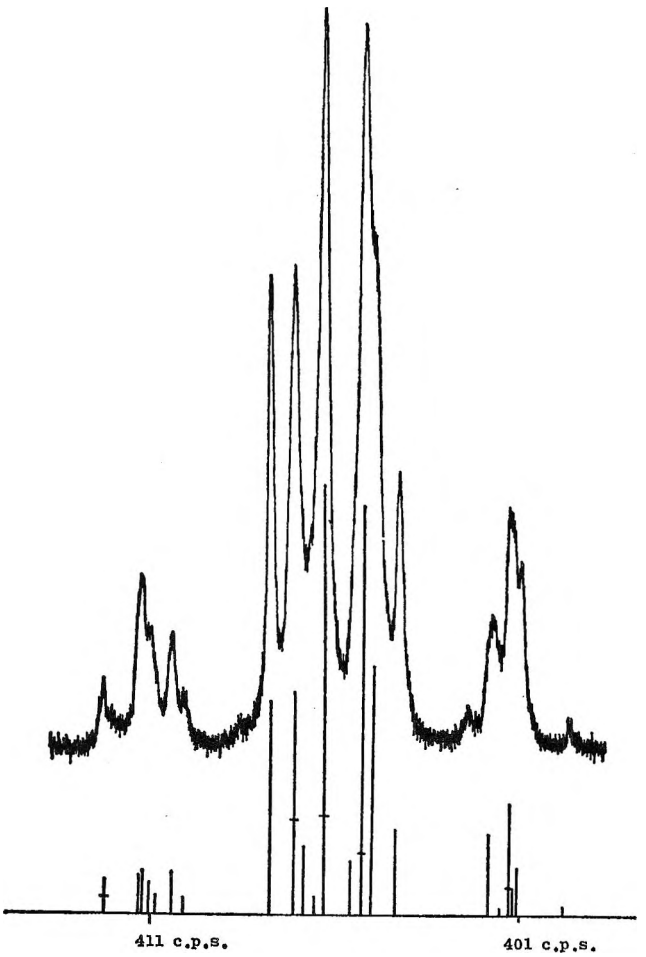


Figure 1. Experimental and calculated 60-Mcps spectra of 2-methoxyphenol.

In their original work, Schaefer and coworkers[3a] noted the correlation of the *ortho* protons in the halobenzenes (and benzene itself) with their calculated Q values. We have recently found that while the values for methoxyl and cyano fit this plot for their appropriate *ortho*-proton chemical shifts, the point for nitrobenzene is far off the plot if the Q derived from the *ortho*-disubstituted benzenes (4.00) is used.[9] The value of Q required for nitrobenzene itself is 6.33. Furthermore, the Q relation has been found to work very well for H_3 in a series of *para*-disubstituted benzenes where only the *para* substituent is varied, and Q_{NO_2} is 6.33 in this situation also. In future discussions we will refer to $Q(2)$ as the value obtained from the *ortho*-disubstituted benzenes and to $Q(1)$ as the value obtained when the substituent is flanked by hydrogens.[10]

The most reasonable explanation for the variation in Q_{NO_2} is the change in molecular geometry on going from nitrobenzene to an *ortho*-substituted nitrobenzene. In nitrobenzene the nitro group is presumed to be planar with the aromatic ring. With a large *ortho* substituent the nitro group is forced out of the ring plane.

In Figure 2 is shown the plot of the H_3 chemical shifts for the phenol series *vs.* the appropriate Q values. For *o*-nitrophenol in carbon tetrachloride the chelate ring structure ensures the planarity of the nitro group, and the $Q(1)$ value clearly applies. Evidence for the planar ring structure is given by the long-range coupling of the phenolic proton to H_5.[11] Polarized infrared studies by Francel[12] also indicate the planar structure of *o*-nitrophenol. In DMSO some intermediate value of Q_{NO_2} is required. Reasonably, DMSO competes with the nitro group for the phenolic proton. The

(9) Unpublished results.

(10) We have found that the amino and hydroxyl groups also show different Q values when flanked only by hydrogens on the benzene ring as opposed to when there is a large *ortho* substituent [$Q(1)$ = 0.67 and 0.38; $Q(2)$ = 0.11 and 1.19, respectively].

(11) Such couplings are well known in other, more highly substituted phenols and benzaldehydes. They are of maximum value when operating through the "straightest zig zag path;" see for instance S. Forsen and R. A. Hoffman, *J. Mol. Spectry.*, **20**, 168 (1966).

(12) R. J. Francel, *J. Amer. Chem. Soc.*, **74**, 1265 (1952).

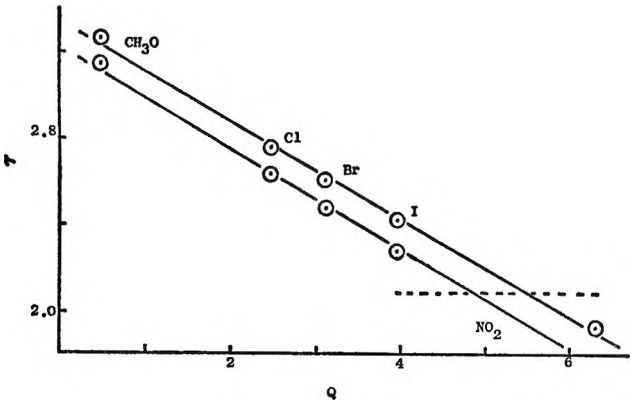


Figure 2. H_3 chemical shifts *vs.* Q for a series of 2-substituted phenols in carbon tetrachloride (upper) and DMSO (lower). Dashed line shows the chemical shift for H_3 for *o*-nitrophenol in DMSO over the range of values for Q_{NO_2}.

chelate ring structure is broken, and the nitro group is forced out of the plane of the ring. Presumably some time-averaged situation exists. In DMSO the long-range coupling of the phenolic proton to H_5 is no longer apparent.

As shown in Figure 3, there is a correlation of sorts between the H_3 chemical shifts and σ_o^- though the quality of the fit is indeterminant from the limited amount of data. It has been known for some time that *ortho*-proton chemical shifts roughly follow σ_p in the monosubstituted benzenes.[13] The halogens are anomalous in behavior, a fact that has been attributed to large magnetic anisotropy effects.[13] The Q relation provides a more satisfactory correlation for *ortho*-proton shifts, but it is not completely clear to us whether the definition of Q encompasses a mode of substituent interaction with the ring comparable with the resonance and inductive effects measured by σ or whether these electronic effects represent another term in the Q expression, imposed by the empirical way in which our Q's are determined; outside the original definition, *e.g.*, a plot of Q *vs.* σ_p gives a fair correlation with the halogens again off the plot. In any event, it is evident that for groups such as nitro there is a geometric dependence for the Q relation which may be useful in solving stereochemical problems. As shall be seen below, this does not seem to arise because of magnetic anisotropy.

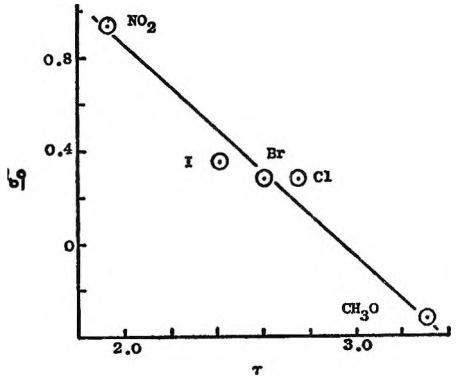


Figure 3. H_3 chemical shifts for the 2-substituted phenols *vs.* Traynham's σ_o^- values.[4]

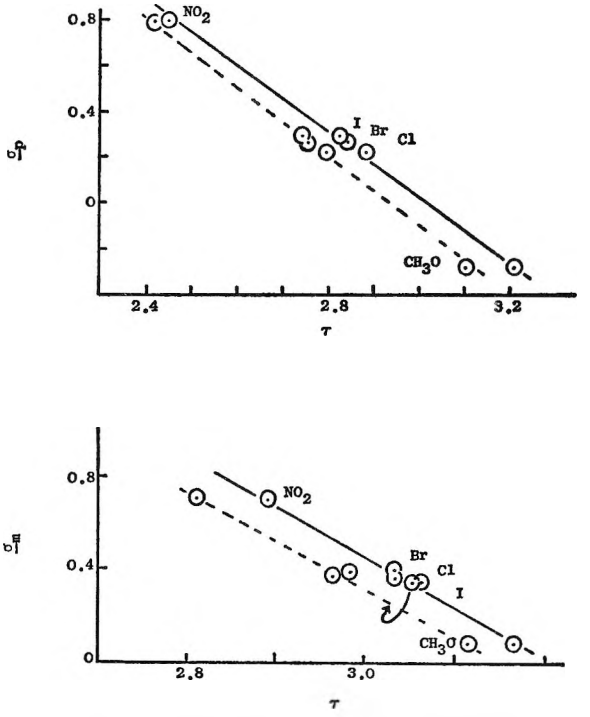
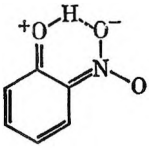


Figure 4. H_5 chemical shifts *vs.* σ_p (upper plot) and H_6 chemical shifts *vs.* σ_m (lower plot) for a series of 2-substituted phenols. Solid lines are for carbon tetrachloride solutions while dashed are for DMSO solutions.

It has been observed previously that the H_6 chemical shifts in a series of *ortho*-disubstituted benzenes vary with the alteration of the C-2 substituent as σ_m.[2] It may be seen in Figure 4 that the same relation holds for the phenols in both carbon tetrachloride and DMSO solution (the exception of *o*-iodophenol in DMSO is real and unaccounted for). Similarly, plots of the H_5 chemical shifts (Figure 3) are seen to follow σ_p very well indeed. The point of interest here is that the rotation of the nitro group from the plane of the benzene ring does not influence the electron density at H_5 or H_6 in any way different from the in-plane nitro group. Yet there is evidence that structures such as I are of more importance in carbon tetrachloride than in



I

DMSO by virtue of the enhanced values of J_{34} and J_{56} and the decreased value of J_{45} in the former as compared to the latter solvent.[14]

(13) H Spiesecke and W. G. Schneider, *J. Chem. Phys.*, 35, 731 (1961).

(14) The influence of resonance-contributing structures and π-bond orders on *ortho* coupling constants have been subjects of previous investigations: W. B. Smith, W. H. Watson, and S. Chiranjeevi, *J. Amer. Chem. Soc.*, 89, 1438 (1967); W. B. Smith and T. Kmet, *J. Phys. Chem.*, 70, 4034 (1966).

The change at H_3 on rotating the nitro group out of the plane of the ring is not due to magnetic anisotropy as might be supposed.[15] The change at H_6 on altering solvents still follows σ_m (Figure 4) for *o*-nitrophenol. There is a similar change at H_4. The slight change at H_5 is uninformative since H_5 is on the symmetry axis of the nitro group. If the alterration in chemical shifts at H_3 in *o*-nitrophenol on changing solvents were due to the magnetic anisotropy of the nitro group, one could reasonably expect the effect to appear also at H_4 and H_6.[6]

Acknowledgment. We wish to acknowledge the generous support of The Robert A. Welch Foundation.

(15) I. Yamaguchi, *Mol. Phys.*, 6, 106 (1963).

The Nuclear Magnetic Resonance Spectra of Six *ortho*-Substituted Fluorobenzenes

by James L. Roark and William B. Smith

Department of Chemistry, Texas Christian University, Fort Worth, Texas 76129 *(Received September 12, 1968)*

The proton and fluorine nuclear magnetic resonance parameters have been determined for six *ortho*-substituted fluorobenzenes. The chemical shifts for the protons adjacent to the *ortho* substituents were found to follow the Q parameter correlation quite well, and there was also a fair correlation of Q with the fluorine chemical shifts. The nitro group provides an exception in both series which is taken to indicate that the nitro group is somewhat out of the plane of the aromatic ring on the average of the nmr time scale for *o*-nitrofluorobenzene.

During the course of our studies of substituent effects on proton chemical shifts in aromatic systems, we have found that the chemical shifts of protons adjacent to the substituents on the ring are well correlated by the parameter Q.[1-3] This parameter, originally defined by Schaefer and coworkers,[4] is presumably a measure of the paramagnetic shielding induced by the mixing of excited states of the substituent with ground states of the electrons in the *ortho* C–H bond.[4] While the definition of Q is not restated here, it is true that the parameter may be calculated only for hydrogen and the halogens. Experimental methods for determining Q for other functional groups have been developed,[2,3] and it has been noted that groups without cylindrical symmetry along the C–X axis may show multiple Q values depending on the average orientation of X with respect to the ring.[3] Values of Q for groups coplanar with the ring are characterized by $Q(1)$ while "out of the plane" values are called $Q(2)$. Several sets of these have been given in the preceding paper,[3] and an argument was presented against magnetic anisotropy as an explanation of the effect.

We wish to report here the parameters for a series of *ortho*-substituted fluorobenzenes. This series was attractive in that it completed our earlier work with the halobenzenes[1,2] and it has been noted that *ortho* fluorines for the *ortho* fluorohalobenzenes also follow the Q relation.[4a] We wished to know if this was true for other substituent groups.

Experimental Section

The fluorobenzenes were all commercially available compounds. They were run in 10% v/v solutions and degassed as before. The general technique has been described.[1-3,5] Spectra were determined on a Varian A-60A instrument. The fluorine decoupled spectra were taken with the aid of a Nuclear Magnetic Resonance Specialties SD-60B heteronuclear decoupler operating through a modified A-60 probe. Fluorine spectra were taken on a Varian HA-100 operating at 94.1 Mcps. Chemical shifts were taken with reference to 1,1,2,2-tetrachloro-3,3,4,4-tetrafluorocyclobutane (TCTFB) as an internal standard. All spectra were calibrated by the usual audio-side-band technique.

The fluorine decoupled spectra were used to obtain a preliminary set of parameters for the ring protons. These were then used to fit the normal spectra. The fluorine decoupled, normal, and calculated spectra for *o*-cyanofluorobenzene are shown in Figure 1. The various chemical shifts are given in Table I and coupling constants in Table II. The values for 2-bromo- and 2-iodofluorobenzene have been determined in

(1) W. B. Smith and G. M. Cole, *J. Phys. Chem.*, 69, 4413 (1965).

(2) W. B. Smith and J. L. Roark, *J. Amer. Chem. Soc.*, 89, 5018 (1967).

(3) J. L. Roark and W. B. Smith, *J. Phys. Chem.*, 73, 1043 (1969).

(4) (a) F. Hruska, H. M. Hutton, and T. Schaefer, *Can. J. Chem.*, 43, 2392 (1965); (b) T. Schaefer, F. Hruska, H. M. Hutton, *ibid.*, 54, 3143 (1967).

(5) W. B. Smith and J. L. Roark, *J. Chem. Eng. Data*, 12, 587 (1967).

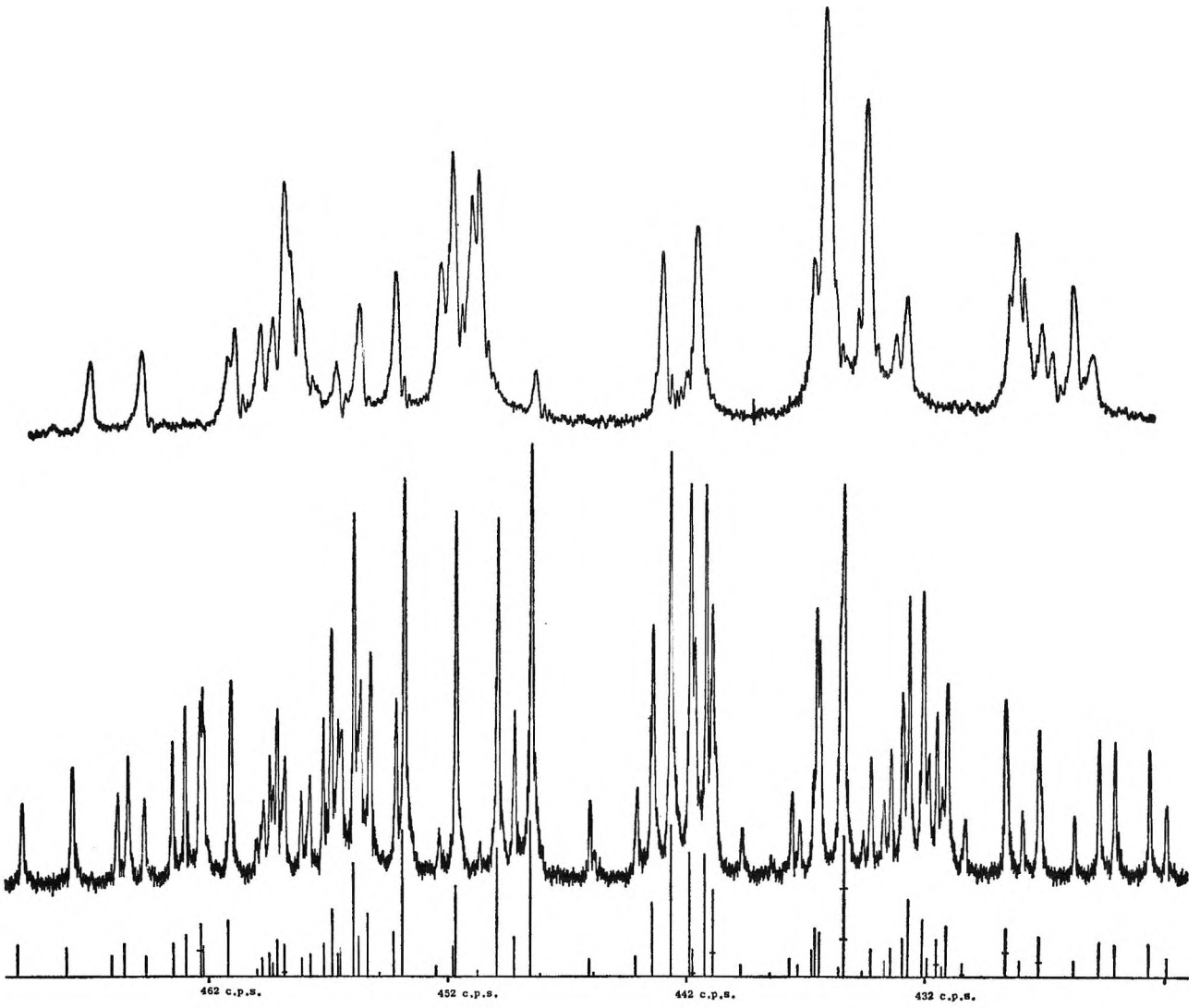


Figure 1. Fluorine decoupled (upper), normal (middle), and calculated spectra (lower) of *o*-cyanofluorobenzene.

Table I: Chemical Shifts for 2-Substituted Flurorbenzenes

2-X[a]	τ_3	τ_4	τ_5	τ_6	Rms[b]	δ_F[c]
F	2.93	2.93	2.93	2.93	...	23.91
	3.01	3.01	3.01	3.01	...	...
Cl	2.66	2.99	2.84	2.93	0.038	1.18
Br	2.50	3.03	2.78	2.94	0.032	−7.07
	2.56	3.12	2.87	3.03	0.031	...
I	2.30	3.16	2.75	3.00	0.030	−20.95
	2.34	3.24	2.83	3.08	0.047	...
CN	2.38	2.71	2.37	2.78	0.039	−6.82
NO_2	1.97	2.67	2.34	2.69	0.045	4.27

[a] The first entry is for carbon tetrachloride solutions. Where a second entry is given, the solvent is cyclohexane. [b] Root-mean-square error in fitting proton lines. [c] In ppm from TCTFB. Values for 2-X of methoxyl, hydroxyl, and methyl were 21.12, 26.80, 3.60 ppm, respectively.

carbon tetrachloride recently by Castellano and Kostelnik,[6] and our values agree very well indeed. These two compounds and 2-chlorofluorobenzene have been recently reported in tetramethylsilane solutions.[7] Our values and the signs of our coupling constants are in good accord.

The spectrum for *o*-difluorobenzene collapsed to one line on irradiation of the fluorine, and no further analysis was attempted.

The chemical shifts for the fluorines in this series were determined previously on neat samples.[8] These results agree with ours determined in dilute carbon tetrachloride solutions.

Discussion

The chemical shift data reported in Table I show many of the regularities exhibited by our previous studies of other *ortho*-substituted halobenzenes.[2] While not shown here, the plot of H_6 *vs.* σ_m for the substituent

(6) S. Castellano and R. Kostelnik, *Tetrahedron Lett.*, 51, 5211 (1967).

(7) J. E. Loemker, J. M. Read, Jr., and J. H. Goldstein, *J. Phys. Chem.*, 72, 991 (1968).

(8) H. S. Gutowsky, D. W. McCall, B. R. McGarvey, and L. H. Meyer, *J. Amer. Chem. Soc.*, 74, 4809 (1952).

Table II: Coupling Constants for 2-Substituted Fluorobenzenes

2-X[a]	J_{34}	J_{35}	J_{36}	J_{45}	J_{46}	J_{56}	J_{3F}	J_{4F}	J_{5F}	J_{6F}
Cl	8.01	1.70	0.31	7.47	1.46	8.29	7.33	−0.87	4.79	9.10
Br	7.96	1.66	0.26	7.40	1.47	8.21	6.80	−0.64	4.79	8.50
	7.96	1.67	0.27	7.38	1.44	8.17	6.83	−0.65	4.73	8.41
I	7.83	1.64	0.26	7.39	1.43	8.22	6.30	−0.24	5.03	7.94
	7.92	1.66	0.28	7.46	1.45	8.27	6.17	−0.27	5.00	7.97
CN	7.82	1.78	0.40	7.61	1.04	8.55	6.43	−0.24	5.43	9.01
NO_2	8.18	1.75	0.31	7.40	1.27	8.30	7.59	−0.93	4.35	10.68

[a] The first entry is for carbon tetrachloride solutions. Where a second entry is given, the solvent is cyclohexane.

at the 2-position is quite linear. Similarly, the shifts for H_5 follow σ_p of these substituents. Moreover, the substituent chemical shifts at H_4 behave in the same fashion as the *meta*-proton values in the monosubstituted benzenes.[2]

Differences from our previous halobenzene series, however, appear in the Q correlation plot. In Figure 2 are shown the plots of Q for the various *ortho* substituents against the proton chemical shifts at H_3 and the fluorine chemical shifts, respectively. In our previous studies,[2,3] we have found that one of two Q values for the nitro group is required. When the nitro group is flanked by a large bulky *ortho* substituent at C-1, the H_3 shift correlation requires the $Q(2)$ value 4.00. If the nitro group is coplanar with the ring (as when flanked on both sides by hydrogens or when constrained by a hydrogen bond as in *o*-nitrophenol[3]) the $Q(1)$ value of 6.33 is applied. Clearly neither of these extreme values for Q_{NO_2} applies to *o*-nitrofluorobenzene. Figure 2 shows that an intermediate value would be required, a situation very much like that encountered previously for *o*-nitrophenol in dimethyl sulfoxide.

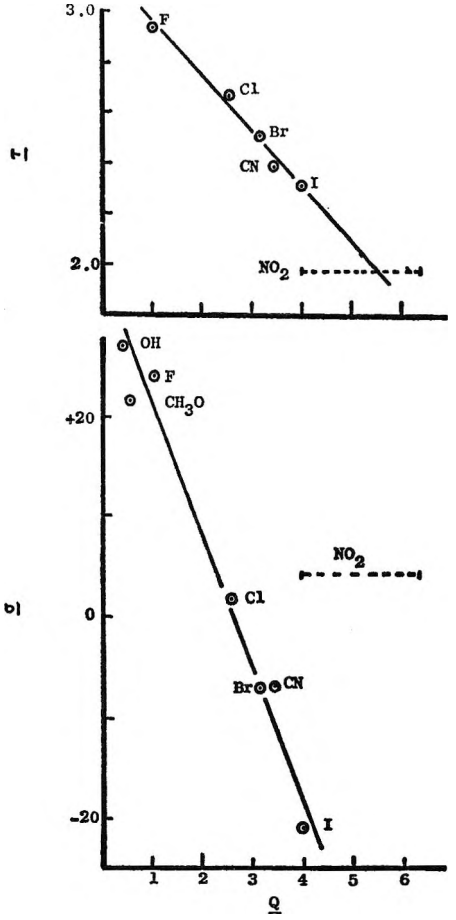


Figure 2. Chemical shifts of H_3 (upper) *vs.* Q and fluorine chemical shifts (lower) *vs.* Q for a series of 2-X-fluorobenzenes. The dotted lines are the appropriate shifts for the nitro compound over the range of Q_{NO_2}.

Nitrobenzene has been shown to be planar by X-ray measurements.[9] Infrared studies have been used to show *o*-bromonitrobenzene to have the nitro group out of the ring plane, and the same is most likely true for *o*-chloronitrobenzene.[10] It has been conjectured that *o*-nitrofluorobenzene is planar.[11] However, the results from these nmr measurements suggest that on the nmr time scale the nitro group in the latter compound is slightly out of the ring plane. Conclusions quite similar to these have been derived from solvent effect studies by Rae.[12]

The Q plot for the fluorine chemical shifts (Figure 2) shows fairly good agreement for the various calculated and experimental values of Q. However, the point for *o*-nitrofluorobenzene is well off the plot to the high-field side. Clearly resonance contributing structures of the *o*-quinoid type involving the fluorine and nitro group are not the explanation here since these would tend to deshield the fluorine. Such a structure seems to be important in *o*-nitrophenol as shown previously.[3] Magnetic anisotropy also does not offer an explanation since the proton and fluorine have roughly the same geometrical relation to the nitro group, and it may be presumed that anisotropy effects should be approximately the same at both positions. This is not confirmed by the data.

(9) J. Trotter, *Acta Cryst.*, **12**, 884 (1959).
(10) R. J. Francel, *J. Amer. Chem. Soc.*, **74**, 1265 (1952).
(11) J. Hamer, L. Placek, and M. Ahmad, *Tetrahedron, Suppl.*, **20**, 395 (1964).
(12) I. D. Rae, *Aust. J. Chem.*, **20**, 2381 (1967).

According to Schaefer, *et al.*,[4] the Q parameter is a measure of paramagnetic shielding effects resulting from the mixing of the ground state of the proton or fluorine with excited states of the substituent under the aegis of the angular momentum operator. This effect should be different in magnitude for fluorine as opposed to hydrogen and, presumably, geometry dependent. The theoretical aspects of the Q parameter have not yet been completely delineated. The parameter, however, does provide many empirical correlations of nmr data and seems to provide some useful insights into the geometrical arrangements within these molecules.

Acknowledgment. The generous support of The Robert A. Welch Foundation is hereby gratefully acknowledged.

The Proton Magnetic Resonance Spectra of Several 2-Substituted Pyridines

by William B. Smith and James L. Roark

Department of Chemistry, Texas Christian University, Fort Worth, Texas 76129 *(Received September 12, 1968)*

The nmr parameters for nine 2-substituted pyridines are reported both as the free bases in carbon tetrachloride solution and as the cations in 1:1 trifluoroacetic acid-acetic acid. The chemical shifts in these systems are compared with those previously derived for a series of *ortho*-disubstituted benzenes. The shifts for H_3 in both solvents correlate with the parameter Q. H_5 correlates with σ_p. Behavior at H_4 and H_6 is more complex.

Recently, we have examined the nmr parameters for a large number of *ortho*-disubstituted benzenes.[1] The results of these studies may be summarized as follows for a series of 1-X-2-Y-benzenes in which X is held constant and Y varied through a range of substituents: (1) protons adjacent to Y follow the parameter Q_Y with certain reservation regarding the steric requirements of X and Y; (2) the chemical shift of H_5 follows the σ_p of Y while H_6 follows σ_m; and (3) the chemical shift of H_4 behaves just as the *meta* proton in the monosubstituted benzenes.

As an extension of this work,[1] we have now examined the spectra for a series of 2-substituted pyridines and their cations. This series was of interest for several reasons. Dewar and Marchand[2] have discussed the effects of the nitrogen in γ-picoline on the proton chemical shifts in that substance as those due to a substituent operating by a pure inductive effect. According to this viewpoint, the 2-substituted pyridines might be considered as *ortho*-disubstituted benzenes in which the one substituent operates solely by the inductive effect.

In our original work,[1b] the observation that H_6 followed σ_m was interpreted as suggesting that the substituent at C-1 insulated H_6 from the "field effect" of the substituent at C-2. During the course of discussions with colleagues, it was pointed out that all of our C-1 substituents contained p electrons and should be highly polarizable by Y. Thus, the field effect of Y might be actually enhanced by transmission through X. If so, the unshared pair of electrons on the pyridine nitrogen should behave as a polarizable substituent and H_6 should follow σ_m.

The parameters for several 2-substituted pyridines have been reported previously.[3] Since these were carried out on either neat liquids or on solutions in dimethyl sulfoxide, the chemical shifts were of little utility for our purposes. Here, we have used dilute solutions in carbon tetrachloride. In addition, we have determined the chemical shifts of the related cations.

Experimental Section

The pyridines in this study were commercially available except for 2-iodopyridine and 2-nitropyridine. The former was prepared by the method of Baker and McEvoy[4] and the latter by the method of Kirpal and Bohm.[5] Solutions (10% v/v) were made up in carbon tetrachloride, and tetramethylsilane was added as an internal standard. Several pyridines were not suffi-

(1) (a) W. B. Smith and G. M. Cole, *J. Phys. Chem.*, **69**, 4413 (1965); (b) W. B. Smith and J. L. Roark, *J. Amer. Chem. Soc.*, **89**, 5018 (1967); (c) J. L. Roark and W. B. Smith, *J. Phys. Chem.*, **73**, 1043 (1969); (d) J. L. Roark and W. B. Smith, *ibid.*, **73**, 1046 (1969).

(2) M. J. S. Dewar and A. P. Marchand, *J. Amer. Chem. Soc.*, **88**, 354 (1966).

(3) (a) W. Brugel, *Z. Elektrochem.*, **66**, 259 (1962); (b) V. J. Kowalewski and D. G. de Kowalewski, *J. Chem. Phys.*, **37**, 2603 (1962).

(4) B. R. Baker and F. J. McEvoy, *J. Org. Chem.*, **30**, 128 (1955).

(5) A. Kirpal and W. Bohm, *Ber.*, **65**, 680 (1932).

Table I: Parameters for 2-Substituted Pyridines[a]

2-X	J_{34}	J_{35}	J_{36}	J_{45}	J_{46}	J_{56}	τ_3	τ_4	τ_5	τ_6	Rms[b]
NH_2	8.37	1.01	0.98	7.17	1.97	5.05	3.65	2.74	3.53	2.06	0.020
CH_3O	8.35	0.98	0.81	7.09	2.06	5.08	3.38	2.57	3.27	1.94	0.032
CH_3	7.71	1.17	0.93	7.50	1.89	4.88	2.99	2.58	3.04	1.63	0.048
F	8.23	0.91	0.78	7.23	2.10	4.95	3.12	2.23	2.85	1.81	0.030
Cl	8.08	0.98	0.80	7.41	2.06	4.86	2.76	2.42	2.85	1.69	0.029
Br	8.03	0.94	0.79	7.39	2.09	4.81	2.60	2.54	2.83	1.69	0.013
I	7.75	1.25	0.82	7.45	2.06	4.82	2.35	2.73	2.80	1.72	0.031
CN	7.80	1.19	0.96	7.85	1.74	4.84	2.30	2.12	2.45	1.31	0.041
NO_2	8.26	1.05	0.86	7.38	1.86	4.62	1.84	1.94	2.32	1.41	0.029

[a] Dilute solutions in carbon tetrachloride. Coupling constants in cps. [b] Root-mean-square error in line positions.

ciently soluble in carbon tetrachloride and were studied in mixtures of carbon tetrachloride and acetone. These results were extrapolated to pure carbon tetrachloride. Studies on several soluble pyridines indicated results obtained in this fashion to be quite good.

In general, techniques and analyses were carried out as previously described.[1] The exact analysis of H_6 in these compounds was facilitated by the use of nitrogen decoupling provided by a Nuclear Magnetic Resonance Specialities Model SD-60 B heteronuclear decoupler. The spectrum of 2-methylpyridine was obtained at 100 Mcps (Varian HA-100) with the methyl group decoupled. Couplings to the methyl group were taken from a first-order analysis of the Varian A-60A spectrum as $J_{3CH_3} = \pm 0.50$ cps, $J_{4CH_3} = \pm 0.25$ cps, $J_{5CH_3} = \pm 0.60$ cps, and $J_{6CH_3} = \pm 0.20$ cps, respectively. The spectrum of 2-fluoropyridine was analyzed *in toto*. The values for the couplings to fluorine were $J_{3F} = -2.85$ cps, $J_{4F} = 8.18$ cps, and $J_{5F} = 2.49$ cps.[6] The coupling J_{6F} could not be resolved and was assigned as zero in the computer analysis. All other spectral parameters for the pyridines are given in Table I.

The various cations were studied in dilute solutions (10% v/v) of 1:1 trifluoroacetic and acetic acids. Spectra were recorded on a Varian HA-100 using the acetic acid methyl protons as the internal lock. Chemical shifts are referenced to these protons. These spectra were usually nearly first order, and chemical shifts could be readily ascertained by comparison with the spectra of the free bases. It is estimated that these shifts are good to 0.01 ppm. (See Table II.)

Table II: Chemical Shifts for Protonated 2-Substituted Pyridines[a]

2-X	δ_3	δ_4	δ_5	δ_6
NH_2	4.94	5.72	4.77	5.79
CH_3O	5.38	6.38	5.39	6.20
CH_3	5.76	6.39	5.67	6.49
F	5.35	6.26	5.55	6.37
Cl	5.92	6.45	5.89	6.64
Br	6.03	6.30	5.89	6.69
I	6.32	6.13	5.92	6.69
CN	6.14	6.44	6.05	6.8
NO_2	6.29	6.16	5.76	6.67

[a] Solutions (10% v/v) in 1:1 trifluoroacetic acid–acetic acid. Chemical shifts are in ppm from the acetic acid methyl protons which served as an internal reference.

Discussion

The proton chemical shifts in the 2-substituted pyridines show some of the same patterns observed in the monosubstituted benzenes. The shifts at H_5 (Table I) follow σ_p quite well as do *para*-proton chemical shifts in the benzenes.[7] Since it has been recently shown that carbon-13 shifts at C-5 follow σ_p just as the *para* carbons in the monosubstituted benzenes, it would seem that π-electron density effects produced by substituents at C-2 are reflected by both types of chemical shifts.[8] While not shown, the correlation of H_5 in the protonated pyridines with σ_p is fairly good though the points for the cyano and nitro group are unaccountably off the plot.

The behaviors of H_4 and H_6 in both series are quite different though both are *meta* to the substituent. The chemical shifts of H_4 correlate well with *meta*-proton shifts in the monosubstituted benzenes. In the protonated series, the plot is somewhat cruder. Since substituent effects at this position are not well understood, these observations are passed without further comment.

In contrast, the chemical shifts of H_6 in the pyridines follow σ_m quite well (Figure 1), the methyl and cyano groups being exceptions in this case. In the protonated pyridines, also shown in Figure 1, there appears to be at best only an extremely rough correlation. Indeed, comparison with the *meta*-proton chemical shifts *vs.* σ_m for the monosubstituted benzenes shows about the same quality of fit.

(6) These values are in reasonably good agreement with the earlier reported values of Brugel.[3a] The sign of J_{3F} was assumed to be negative on the basis of the reported work of R. H. Cox and A. A. Bothner-By, *J. Phys. Chem.*, 72, 1646 (1968), and J. C. Deck, Thesis, University of Illinois, 1966.

(7) H. Spiesecke and W. G. Schneider, *J. Chem. Phys.*, 35, 731 (1961).

(8) H. L. Retcofsky and R. A. Friedel, *J. Phys. Chem.*, 72, 2619 (1968).

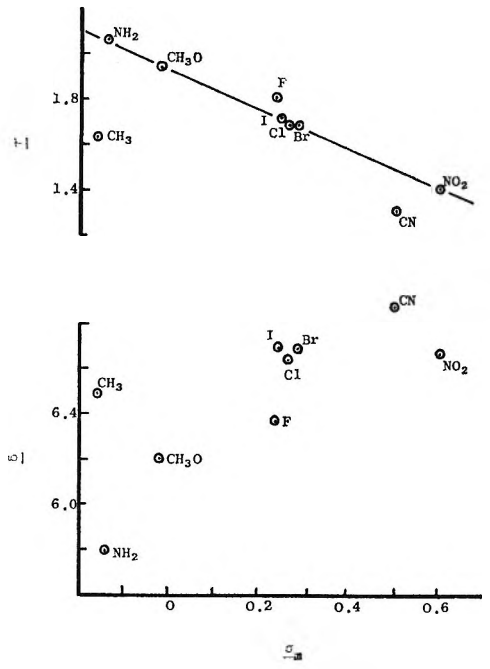


Figure 1. The relationship of the chemical shifts of H_6 in the 2-substituted pyridines (upper) and pyridinium cations (lower) with σ_m.

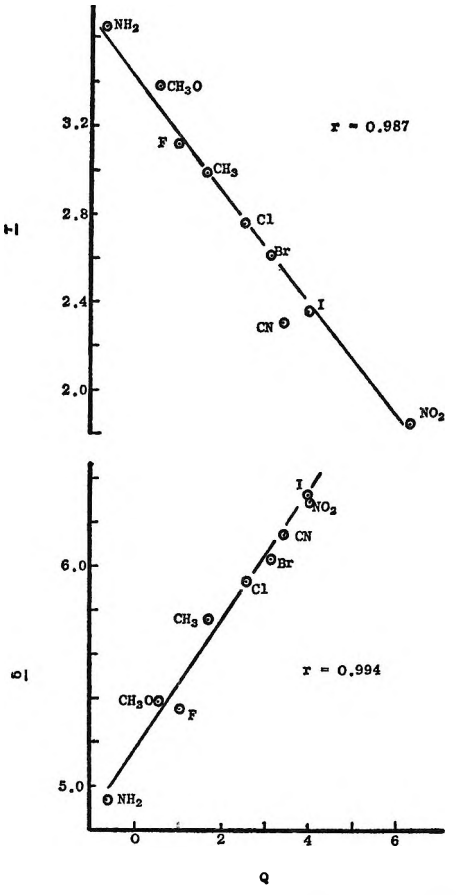


Figure 2. The correlation of H_3 in the 2-substituted pyridines (upper) and their respective cations (lower) with Q. The least-squares correlation coefficient for each is given.

These results tend to confirm the speculation that substituent effects on proton chemical shift *meta* to the substituent consist, in part, of a field effect measured by σ_m which may be relayed by an intervening polarizable substituent. From our various studies, the chemical shift change in going from a methoxyl group to a nitro group is as follows with the indicated intervening groups: methyl, 0.18 ppm; chloro, 0.28 ppm; bromo, 0.27 ppm; iodo, 0.30 ppm; and the nitrogen lone pair, 0.53 ppm.

The chemical shifts for H_3 *vs.* the parameter Q for the free bases and the pyridinium ions are shown in Figure 2. The definition and presumed meanings of Q have been given a number of times.[1,9] Suffice it to say here we have found that two values of Q are required for groups such as the nitro group which may be either normally in the plane [$Q_{NO_2}(1)$] or out of the plane [$Q_{NO_2}(2)$] when flanked by a large group.[1c] In some situations where the nitro group is only slightly out of the ring plane on the average of the nmr time scale, intermediate values of Q are required.[1c,d] For the pyridines, it is evident that the $Q_{NO_2}(1)$ value of 6.33 was needed; *i.e.*, the nitro group is in the plane of the ring just as in nitrobenzene itself. However, when protonated, the electronic interaction between the nitro group and the ring must be reduced, and the nitro appears to be out of the ring plane [the $Q_{NO_2}(2)$ value is required]. A rather similar situation occurs in the vinyl compounds. The *cis* vinyl hydrogens follow the Q relation.[10] For nitroethylene the $Q_{NO_2}(2)$ value is found to fit best. Here, too, electronic interactions must be sufficiently small as to produce no appreciable barrier to rotation about the C–N bond.

Finally, it may be noted that the normal $Q_{NH_2}(1)$ value of -0.67[1c] was used for both the free-base plot and for the protonated pyridine plot in Figure 2. Clearly, the 2-amino group is not protonated in the acid mixture used here. No doubt a much different value of Q would be needed for the ammonium group.

Acknowledgment. The generous financial support of The Robert A. Welch Foundation is hereby gratefully acknowledged. The Varian HA-100 used in this research was made available by virtue of a grant from the National Science Foundation.

(9) (a) F. Hruska, H. M. Hutton, and T. Schaefer, *Can. J. Chem.*, 43, 2392 (1965); (b) T. Schaefer, F. Hurska, and H. M. Hutton, *ibid.*, 45, 3143 (1967).

(10) See ref 1b, Figure 4.

A Contribution to the Theory of Dielectric Dispersion of Colloidal Particles

by Robert S. Alwitt

Research and Development Laboratories, Sprague Electric Company, North Adams, Massachusetts 01247
(Received September 13, 1968)

The Schwarz theory for the low-frequency dielectric dispersion of colloidal suspensions has been extended by introduction of a relaxation spectrum of ionic mobilities derived from properties of the diffuse double layer. The dispersion and absorption equations provide a reasonable fit for the experimental results of Schwan, Schwarz, Maczuk, and Pauly without the introduction of arbitrary parameters. A limitation of this theory is its failure to predict the observed frequency dependence of the dielectric increment at large $\omega\tau$.

I. Introduction

A theory to explain the low-frequency dielectric dispersion of colloidal suspensions has been proposed by Schwarz.[1] This theory accounts for most of the unique dielectric characteristics of these suspensions, such as a dielectric constant several orders of magnitude greater than the high-frequency limit, the low-frequency range in which these high dielectric constants are observed, and the dependence upon particle size and volume fraction. However, the basic theory predicts a simple Debye-type dispersion rather than the broader dispersion that is always observed. Although he noted that a theoretical treatment of the diffusion process in the counterion atmosphere may result in a relaxation spectrum, Schwarz did not pursue that approach but instead introduced an arbitrary rectangular distribution of activation energies for diffusion in the counterion atmosphere. Very good agreement was obtained between this theory and the experimental results of Schwan, *et al.*,[2] by choice of a reasonable value for the range of activation energies.

In the present paper it is shown that a modest extension of the Schwarz theory, utilizing a relaxation spectrum of ionic mobilities derived from properties of the classical diffuse double layer, results in dispersion and absorption curves very similar to those presented by Schwarz. The equations for these curves do not contain any arbitrary parameters, but only experimentally accessible terms.

II. Theory

Consider a plane solid–solution interface with a charge density σ (esu/cm^2) uniformly distributed over the solid surface and a charge of like magnitude but opposite sign distributed throughout the diffuse double layer in the solution adjacent to the surface. (This model holds for curved surfaces as long as $1/\kappa \ll$ radius of curvature.) The charge density ρ at a point in the solution is given by Poisson's equation

$$\rho(x) = -\frac{D}{4\pi}\frac{\mathrm{d}^2\varphi}{\mathrm{d}x^2} \tag{1}$$

where φ is the potential in the solution at a distance x from the surface and D is the dielectric constant. An electric field E impressed parallel to the surface will cause ionic motion such that the viscous force will be equal but opposite to the electric force. Equating these forces leads to an expression for ionic mobility as a function of potential in the diffuse double layer, as shown by Cole.[3] Thus, the force on a differential volume of solution is

$$F = E\rho = \eta\frac{\mathrm{d}^2v}{\mathrm{d}x^2} \tag{2}$$

where v is the net ionic velocity and η is viscosity. Substituting eq 1 into eq 2 and integrating yields

$$v = \frac{DE}{4\pi\eta}(\zeta - \varphi) \tag{3a}$$

where ζ is the potential at $x = 0$. The mechanical mobility u (*i.e.*, ionic velocity per unit mechanical force) is then

$$u = \frac{D}{4\pi\eta e_0}(\zeta - \varphi) \tag{3b}$$

Considering now the relaxation processes in the diffuse double layer, the contribution of a single relaxation time τ to the complex dielectric increment is

$$\Delta\epsilon^* = \frac{\Delta\epsilon_0}{1 + i\omega\tau} \tag{4}$$

where $\Delta\epsilon_0$ is the static dielectric increment and ω is the angular frequency. The total $\Delta\epsilon^*$ is obtained by integrating over the distribution of relaxation times contained within the diffuse double layer

$$\Delta\epsilon^* = \frac{\Delta\epsilon_0}{-\sigma}\int_0^\infty \frac{\rho\,\mathrm{d}x}{1 + i\omega\tau} \tag{5}$$

(1) G. Schwarz, *J. Phys. Chem.*, **66**, 2636 (1962).
(2) H. P. Schwan, G. Schwarz, J. Maczuk, and H. Pauly, *ibid.*, **66**, 2626 (1962).
(3) K. S. Cole, *Cold Spring Harbor Symp. Quant. Biol.*, **1**, 23 (1933).

where τ is given by Schwarz's eq 28

$$\tau = R^2/2ukT \tag{6}$$

with u defined by eq 3b and R being the radius of a spherical particle.

Case 1. Small Values of ζ ($|\zeta| \ll 2RT/F$). For this case

$$\zeta \cong \frac{4\pi\sigma}{D\kappa} \tag{7}$$

and the Debye approximation of an exponential potential distribution in the double layer holds[3,4]

$$\varphi = \zeta e^{-\kappa x} \tag{8}$$

where κ is the reciprocal Debye length. Under these conditions, solution of eq 1 gives

$$\rho = -\sigma\kappa e^{-\kappa x} \tag{9}$$

Substitution of eq 7 and 8 into eq 3b yields for the mechanical mobility

$$u = \frac{\sigma}{e_0\kappa\eta}(1 - e^{-\kappa x}) \tag{10}$$

Upon substitution of eq 9 and 10, eq 5 can be integrated in a straightforward manner to give for the real and imaginary parts of the dielectric increment

$$\Delta\epsilon' = \Delta\epsilon_0[1 - \omega\tau_0 \arctan(1/\omega\tau_0)] \tag{11}$$

$$\Delta\epsilon'' = \frac{\Delta\epsilon_0}{2}\omega\tau_0 \ln\frac{1 + \omega^2\tau_0^2}{\omega^2\tau_0^2} \tag{12}$$

where

$$\tau_0 = R^2\kappa\eta/2\sigma_0 kT \tag{13}$$

The surface charge density σ_0 is in units of charges per square centimeter, *i.e.*, $\sigma_0 = \sigma/e_0$. Equations 11 and 12 are shown in Figure 1 as the curves labeled $z = 0$. The dispersion and absorption curves for a Debye distribution of a single relaxation time are shown for comparison.

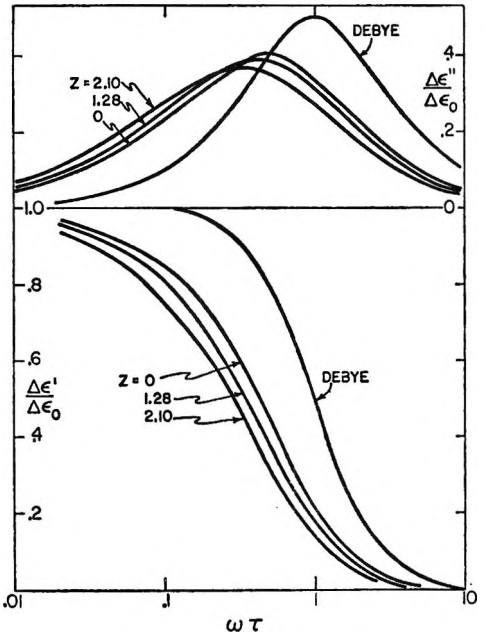


Figure 1. Dispersion and absorption curves from eq 20 and 21

Table I: Dielectric Dispersion from Eq 20 and 21[a]

$\omega\tau$	$\Delta\epsilon'/\Delta\epsilon_0$	$\Delta\epsilon''/\Delta\epsilon_0$	$\Delta\epsilon'/\Delta\epsilon_0$	$\Delta\epsilon''/\Delta\epsilon_0$
	$z = 0.02$		$z = 0.32$	
0.010	0.9844	0.0461	0.9839	0.0469
0.020	0.9690	0.0782	0.9681	0.0794
0.040	0.9388	0.1288	0.9371	0.1304
0.080	0.8807	0.2023	0.8780	0.2040
0.160	0.7740	0.2952	0.7702	0.2963
0.320	0.5964	0.3802	0.5920	0.3798
0.387		0.3944		0.3936
0.469		0.4017		0.4004
0.567		0.4007		0.3990
0.640	0.3590	0.3955	0.3556	0.3936
1.280	0.1511	0.3049	0.1494	0.3027
2.560	0.0467	0.1818	0.0461	0.1803
5.120	0.0124	0.0958	0.0123	0.0950
10.240	0.0032	0.0486	0.0031	0.0482
20.480		0.0244		0.0242
	$z = 0.64$		$z = 1.28$	
0.010	0.9825	0.0492	0.9773	0.0577
0.020	0.9654	0.0829	0.9558	0.0952
0.040	0.9324	0.1349	0.9154	0.1512
0.080	0.8702	0.2087	0.8424	0.2254
0.160	0.7590	0.2994	0.7195	0.3100
0.320	0.5793	0.3788	0.5348	0.3744
0.387		0.3911		0.3819
0.469		0.3966		0.3828
0.567		0.3940		0.3763
0.640	0.3456	0.3880	0.3111	0.3682
1.280	0.1446	0.2964	0.1281	0.2744
2.560	0.0446	0.1761	0.0392	0.1613
5.120	0.0119	0.0927	0.0104	0.0847
10.240	0.0030	0.0470	0.0026	0.0429
20.480		0.0236		0.0216
	$z = 2.10$		$z = 2.56$	
0.010	0.9679	0.0727	0.9620	0.0817
0.020	0.9384	0.1167	0.9276	0.1295
0.040	0.8849	0.1789	0.8662	0.1951
0.080	0.7936	0.2528	0.7644	0.2679
0.160	0.6517	0.3260	0.6122	0.3337
0.320	0.4604	0.3651	0.4185	0.3583
0.366		0.3654		0.3554
0.443		0.3607		0.3467
0.536		0.3499		0.3324
0.640	0.2546	0.3343	0.2238	0.3146
1.280	0.1014	0.2378	0.0871	0.2175
2.560	0.0306	0.1372	0.0261	0.1239
5.120	0.0081	0.0716	0.0069	0.0644
10.240	0.0021	0.0362	0.0017	0.0326
20.480		0.0183		0.0162

[a] Accuracy significant to last digit.

(4) H. Müller, *Cold Spring Harbor Symp. Quant. Biol.*, **1**, 1 (1933).

(5) R. Parsons in "Modern Aspects of Electrochemistry," No. 1, J. O'M. Bockris, Ed., Academic Press, New York, N. Y., 1954, pp 103–179.

Case 2. General Solution for All Values of ζ. The simplest way to proceed is to consider ρ, τ, and x in eq 5 as functions of potential φ. Parsons[5] has shown that

$$\frac{d\varphi}{dx} = -B\kappa \sinh(\varphi/B) \tag{14}$$

where $B = 2kT/ze_0$ for a z:z valent electrolyte. Differentiating eq 14 and combining with eq 1 gives

$$\rho(\varphi) = -\frac{DB\kappa^2}{4\pi} \sinh(\varphi/B) \cosh(\varphi/B) \tag{15}$$

The ionic mobility is now given by eq 3b without further assumptions. Substituting eq 14, 15, 6, and 3b into eq 5 gives

$$-\frac{\Delta\epsilon_0}{\sigma}\int_0^\infty \frac{\rho\, dx}{1+i\omega\tau} = -\frac{D\kappa\Delta\epsilon_0}{4\pi\sigma}\int_\zeta^0 \frac{\cosh(\varphi/B)\, d\varphi}{1+[i\omega G/(\zeta-\varphi)]} \tag{16}$$

where $G = 4\pi\eta R^2/2kTD$. Equating the real and imaginary parts of the right-hand side of eq 16 with the real and imaginary parts of $\Delta\epsilon^* = \Delta\epsilon' - i\Delta\epsilon''$ gives

$$\frac{\Delta\epsilon'}{\Delta\epsilon_0} = -\frac{D\kappa}{4\pi\sigma_0}\int_\zeta^0 \frac{(\zeta-\varphi)^2 \cosh(\varphi/B)\, d\varphi}{(\zeta-\varphi)^2+\omega^2G^2} \tag{17}$$

$$\frac{\Delta\epsilon''}{\Delta\epsilon_0} = -\frac{\omega GD\kappa}{4\pi\sigma_0}\int_\zeta^0 \frac{(\zeta-\varphi)\cosh(\varphi/B)\, d\varphi}{(\zeta-\varphi)^2+\omega^2G^2} \tag{18}$$

The integration of these equations is aided by the transformation $\gamma = (\zeta-\varphi)/\zeta$. Noting that[5]

$$\sigma_0 = \frac{D\kappa B}{4\pi}\sinh\frac{\zeta}{B} \tag{19}$$

integration by parts yields

$$\frac{\Delta\epsilon'}{\Delta\epsilon_0} = 1 - \frac{\omega\tau z}{\sinh z}\arctan\frac{1}{\omega\tau} + \frac{\omega\tau z^2}{2\sinh z}\left[e^{-z}\int_0^1 e^{z\gamma}\arctan\frac{\gamma}{\omega\tau}\,d\gamma - e^{z}\int_0^1 e^{-z\gamma}\arctan\frac{\gamma}{\omega\tau}\,d\gamma\right] \tag{20}$$

$$\frac{\Delta\epsilon''}{\Delta\epsilon_0} = \frac{\omega\tau z}{2\sinh z}\left[\ln(\omega^2\tau^2+1) - \cosh z\ln(\omega^2\tau^2) - z\cosh z\int_0^1 \sinh z\gamma\ln(\omega^2\tau^2+\gamma^2)\,d\gamma + z\sinh z\int_0^1 \cosh z\gamma\ln(\omega^2\tau^2+\gamma^2)\,d\gamma\right] \tag{21}$$

where

$$z = \zeta/B \tag{22}$$

$$\tau = \frac{\tau_0 \sinh z}{z}$$

The integrals in eq 20 and 21 could not be solved in closed form but were computed for several values of z and $\omega\tau$. Values of $\Delta\epsilon'/\Delta\epsilon_0$ and $\Delta\epsilon''/\Delta\epsilon_0$ are listed in Table I. For small z eq 20 and 21 reduce to eq 11 and 12, as required.

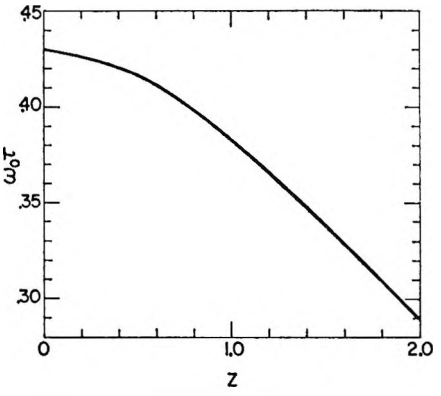


Figure 2. Dependence of characteristic frequency on $z = \zeta/B$.

Dispersion and absorption curves calculated from eq 20 and 21 for several values of z are shown in Figure 1. The shift of the characteristic frequency ω_0 with z is shown in Figure 2. The maximum in the dielectric loss occurs at a value of $\omega\tau$ larger than $\omega_0\tau$, as seen by examination of Figure 2 and Table I. These relations would be represented by a skewed arc locus in a Cole–Cole plot, reflecting the asymmetry of the relaxation spectrum.[6]

III. Comparison with Experimental Results

A thorough test of this extension of the Schwarz theory requires experimental measurement of both dielectric dispersion and surface charge density and/or ζ potential. No sufficiently complete set of data was found in the literature. The best results available for this purpose are the dielectric dispersion data on polystyrene latex suspensions of Schwan, *et al.*,[2] since an estimate of the maximum surface charge density can be obtained from the work of Sieglaff and Mazur[7] on a similar system.

Sufficient data were presented by these authors to generate internally consistent dispersion curves for two experimental runs and to compare these with the experimental data. The matter of consistency arose because it was necessary to choose a value of z in the absence of measurements of ζ or σ_0. The procedure

(6) R. H. Cole in "Progress in Dielectrics," Vol. 3, J. B. Birks, Ed., John Wiley & Sons, Inc., New York, N. Y., 1961, pp 47–100.
(7) C. L. Sieglaff and J. Mazur, *J. Colloid Sci.*, 15, 437 (1960).

used was to pick a value for z, determine $\omega_0\tau$ from Figure 2, use the experimentally determined critical frequency to calculate τ, get τ_0 from eq 22, calculate σ_0 from eq 13, and finally determine z from eq 19. This procedure was repeated until the final and initial values of z agreed to within 1%. The dispersion and absorption curves corresponding to this z were then compared with the experimental points.

Two such comparisons are shown in Figures 3 and 4. The data for Figure 3 were taken from Figure 3 in ref 1 and those for Figure 4 came from Figure 4 and accompanying tables in ref 2. Parameters of these systems and calculated values of τ, ζ, and σ_0 are given in Table II.

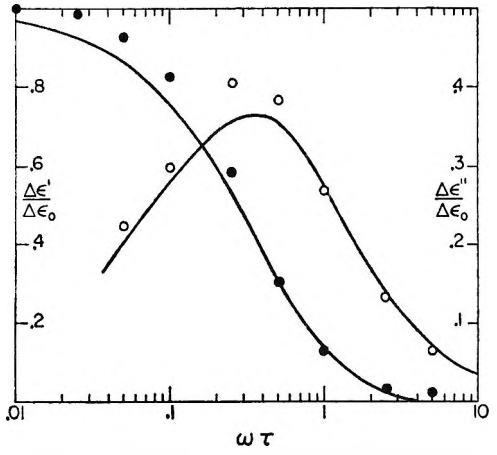


Figure 3. Comparison of experimental points with theoretical curves: ●, $\Delta\epsilon'/\Delta\epsilon_0$; ○, $\Delta\epsilon''/\Delta\epsilon_0$. See text and Table II for details.

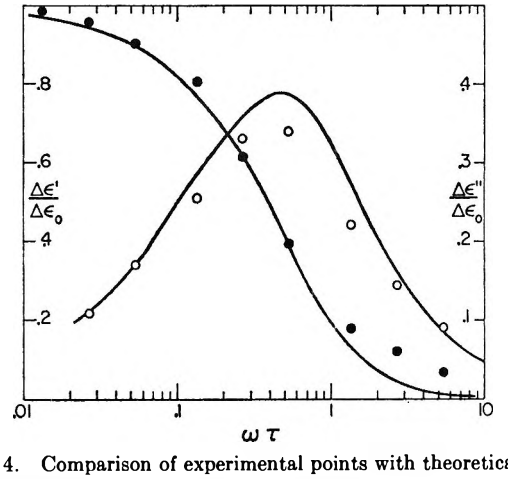


Figure 4. Comparison of experimental points with theoretical curves; same symbols as Figure 3. See text and Table II for details.

In neither case did the predicted curves provide an exact fit of the data but the differences were not large. At low $\omega\tau$ the misfit in $\Delta\epsilon'/\Delta\epsilon_0$ was less than 10% and in the vicinity of the loss peak the difference between observed and predicted values of $\Delta\epsilon''/\Delta\epsilon_0$ was ±15%.

Perhaps a more fundamental limitation is indicated by the misfit in $\Delta\epsilon'/\Delta\epsilon_0$ at large $\omega\tau$, as in Figure 4. Schwarz[1] has shown that these particular data can be approximated by a circular arc locus in a Cole–Cole plot. The dispersion equation for such a relaxation spectrum requires that at large $\omega\tau$ the slope of $\log(\Delta\epsilon'/\Delta\epsilon_0)$ *vs.* $\log\omega\tau$ is negative with an absolute value less than 2.[6,8] However eq 11 and 20 predict a slope of −2. (The distribution proposed by Schwarz[1] has this same limitation.) A slope of less than −2 seems to be characteristic of colloidal systems,[9] and any dispersion equation should predict this behavior. It might be noted that such broadening of the dispersion has been observed in many dielectric systems other than colloids.[8]

Table II: Data for Figures 3 and 4

Source	Figure 3 Figure 3 of ref 1	Figure 4 Figure 4 of ref 2
Exptl		
Vol fraction (p)	0.22	0.30
Particle radius (R), cm	5.85×10^{-5}	9.4×10^{-6}
KCl concn, N	5.7×10^{-3}	3.2×10^{-2}
Temp, °K	298	296
ω_0, sec^{-1}	3.52×10^{3}	9×10^{4}
$\Delta\epsilon_0$	3.7×10^{4}	2.42×10^{3}
ϵ_∞		44
Calcd		
τ_0, sec	4.15×10^{-5}	3.56×10^{-6}
z	2.10	1.04
$\lvert\zeta\rvert$, mV	108	53
σ_0, cm^{-2}	2.3×10^{13}	1.6×10^{13}
σ_0 (from $\Delta\epsilon_0$), cm^{-2}	2.2×10^{13}	0.72×10^{13}

Another test of this theory is provided by a comparison between σ_0 obtained from the calculation of z with that calculated from $\Delta\epsilon_0$ (eq 46 of Schwarz). These results are listed in Table II. The agreement for Figure 3 is excellent whereas for Figure 4 the agreement is less satisfactory though still within a factor of 3. In the latter case the volume fraction of suspended matter was 0.30 and at such a high concentration we may not be justified in using Schwarz's eq 46. For solids contents less than 15% Schwarz[1] calculated for two cases that σ_0 was 1.5×10^{13} and 2.0×10^{13} cm^{-2}, about the same range as given by our present theory. These results are consistent with the electrophoretic measurements made by Sieglaff and Mazur on a similar polystyrene latex system, from which an adsorption site density of about 2×10^{13} cm^{-2} was calculated.[6]

IV. Conclusions

A simplified treatment of the distribution of ionic mobilities within the diffuse double layer leads to dispersion and absorption curves for colloidal suspensions that are broader and flatter than Debye-type curves

(8) K. S. Cole and R. H. Cole, *J. Chem. Phys.*, **9**, 341 (1941).
(9) H. Fricke and H. J. Curtis, *J. Phys. Chem.*, **41**, 729 (1937).

and are a function of ζ potential. Internally consistent application of these relations accounts reasonably well for the experimental results of Schwan, Schwarz, Maczuk, and Pauly[2] without the introduction of arbitrary parameters.

More complete experimental results must be obtained in order to test rigorously both this theory and the basic Schwarz theory. A limitation of this theory is that it does not predict the observed frequency dependence of $\Delta\epsilon'$ at large values of $\omega\tau$.

The Dielectric Dispersion of Paper Impregnated with a Glycol Electrolyte

by Robert S. Alwitt

Research and Development Laboratories, Sprague Electric Company, North Adams, Massachusetts 01247
(Received September 13, 1968)

Paper impregnated with an electrolyte of sodium salicylate in ethylene glycol displayed a dielectric dispersion very similar to those observed for colloidal suspensions, except that $\Delta\epsilon'$ was several orders of magnitude greater than previously reported values. The results were interpreted using the Schwarz theory for the dielectric dispersion of colloidal particles, modified by a relaxation spectrum derived from properties of the diffuse double layer. The large $\Delta\epsilon'$ was apparently due to a high surface charge density, for which the temperature and concentration dependences were estimated. From the agreement of calculated and observed fiber diameters it was apparent that the processes responsible for dielectric dispersion occurred on the surfaces of the macroscopic fibers rather than on interior surfaces of the swollen fiber.

I. Introduction

During the course of an investigation of the electrical properties of paper in nonaqueous electrolytes it was found that the impregnated paper exhibited a very broad low-frequency dielectric dispersion, similar to that observed by Fricke and Curtis[1,2] for aqueous suspensions of cellulose and other colloidal systems. Our interest in this property was with regard to its effect on the electrical behavior of electrolytic capacitors,[3] in which electrolyte-soaked paper serves as an electrode spacer. Because of the diverse uses for paper it was thought that the results would be of general interest, particularly since no information has apparently been published on the dielectric properties of paper sheet in electrolyte solutions. The results are interpreted using a theory developed by Schwarz[4] for the low-frequency dielectric dispersion of colloidal particles in electrolyte solutions, modified by introduction of a relaxation spectrum derived from properties of the diffuse double layer.

II. Theory

It has long been recognized that the dielectric properties of colloidal suspensions arise from the motion of ions, under the influence of an external electric field, within the electric double layer at the solid–solution interface. Schwan, *et al.*,[5] have shown that a tangential surface conductance is insufficient to account for either the magnitude of the dielectric dispersion or the low-frequency range in which it is found. Indeed, Fricke and Curtis[2] had previously shown that a surface capacitance must also be operative. Schwarz[4] introduced the idea of a surface diffusion flux acting counter to that produced by the impressed field. This results in a phase shift between current and field on the surface such that a surface capacitance results. This capacitance can occur at low frequencies and results in an apparent dielectric constant for the suspension that may be several orders of magnitude greater than that calculated from Maxwell–Wagner relations.

Schwarz has shown that the relaxation time for counterion motion along a sphere of radius R is $\tau = R^2/2ukT$, where u is the ionic surface mobility. In general, there will be a distribution of surface mobilities giving rise to a relaxation spectrum. A set of equations describing the dielectric dispersion has recently been derived using the mobility distribution predicted by diffuse double layer theory.[6] For small values of the ζ potential ($|\zeta| < 25$ mV) these expressions are, for the dielectric increment

$$\epsilon' - \epsilon_\infty = \Delta\epsilon' = \Delta\epsilon_0[1 - \omega\tau_0 \arctan(1/\omega\tau_0)] \quad (1)$$

(1) H. Fricke and H. J. Curtis, *Phys. Rev.*, **47**, 974 (1935).
(2) H. Fricke and H. J. Curtis, *J. Phys. Chem.*, **41**, 729 (1937).
(3) R. S. Alwitt, *J. Electrochem. Soc.*, to be published.
(4) G. Schwarz, *J. Phys. Chem.*, **66**, 2636 (1962).
(5) H. P. Schwan, G. Schwarz, J. Maczuk, and H. Pauly, *ibid.*, **66**, 2626 (1962).
(6) R. S. Alwitt, *ibid.*, **73**, 1052 (1969).

and for the increment of dielectric loss

$$\epsilon'' - \epsilon_\infty = \Delta\epsilon'' = (\Delta\epsilon_0/2)\omega\tau_0 \ln [(1 + \omega^2\tau_0^2)/\omega^2\tau_0^2] \quad (2)$$

where

$$\tau_0 = R^2\kappa\eta/2\sigma_0 kT \quad (3)$$

For larger values of the ζ potential the dielectric increment and dielectric loss are functions of ζ. For the purposes of examining our experimental results and estimating the magnitude of some physical properties, use of eq 1 and 2 will be sufficient.

The paper sheet can be considered to be an array of cylinders (rods, fibers) aligned with their long axis in the plane of the sheet. Hydrogen bonding between fibers maintains the properties of a sheet. Although interactions between particles in such an array would be greater than in a suspension, it might be expected that the Schwarz theory would still describe the essential features of the dielectric dispersion properties of such material. Of course, some of the equations would have to be modified for a suspension of cylinders instead of spheres.

Equations 1 and 2 are independent of particle geometry. Equation 3 is valid for a cylinder aligned with its long axis perpendicular to the impressed field. This is because symmetry in the axial direction permits reduction to the same two-dimensional problem as for a sphere. Although solution of Laplace's equation for the potential in the electrolyte and inside the cylinder must be developed in terms of Bessel functions rather than Legendre polynomials, this has no effect on the final relation between surface charge density and surface potential.

The static dielectric increment ($\Delta\epsilon_0$) for an array of cylinders aligned with their long axis perpendicular to the field (*e.g.*, a paper sheet between two flat electrodes) differs in two regards from $\Delta\epsilon_0$ for a suspension of spheres. (See eq 36 of ref 4.) First, the additional dielectric constant due to the presence of a counterion layer is for a cylinder only half that for a sphere. This follows from the analysis by O'Konski[7] of the effect of particle shape and orientation on surface conductivity. Second, the functional dependence of $\Delta\epsilon_0$ on volume fraction (p) of particles is different for spheres and cylinders. Fricke[8] has presented a general expression for $\Delta\epsilon_0$ of a suspension of ellipsoids (his eq 28). With the conditions that the conductivity of the electrolyte is much greater than that of the particles and the permittivity of the particles plus counterion layer is much greater than that of the electrolyte, it follows that for spheres

$$\Delta\epsilon_0 = \frac{9}{4}\frac{p}{[1 + (p/2)]^2}\epsilon_2$$

and for cylinders aligned perpendicular to the field

$$\Delta\epsilon_0 = \frac{4p}{(1 + p)^2}\epsilon_2$$

where ϵ_2 is the permittivity of a particle with its counterion layer. From these relationships and $\Delta\epsilon_0$ for a colloidal suspension of spheres (eq 46 in ref 4), it follows that for a colloidal suspension of cylinders aligned perpendicular to the impressed field

$$\Delta\epsilon_0 = \frac{2p}{(1 + p)^2}\frac{e_0^2 R\sigma_0}{\epsilon_r kT} \quad (4)$$

When $\omega\tau_0 > 1$, eq 1 reduces to

$$\Delta\epsilon' \cong \Delta\epsilon_0/3(\omega\tau_0)^2 \quad (5)$$

For the special case of a 1:1 electrolyte, for which the Debye length is

$$1/\kappa = (DkT/8\pi ne_0^2)^{1/2} \quad (6)$$

substitution of eq 3, 4, and 6 into eq 5 yields

$$\Delta\epsilon' = \frac{1}{3\pi}\frac{p}{(1 + p)^2}\frac{D(kT)^2\sigma_0^3}{\epsilon_r n\eta^2 R^3}\omega^{-2} \quad (7)$$

It has been found experimentally for colloidal suspensions that at large values of $\omega\tau$ the slope of log $\Delta\epsilon'$ *vs.* log ω often has an absolute value less than 2.[6] The ramifications of this observation need not be considered in this present work since eq 7 is only used to estimate the temperature and concentration dependence of σ_0, and the observed average slope of $-\frac{7}{4}$ was not so different from -2 as to affect significantly these estimates.

III. Experimental Procedure

Two types of paper commonly used as electrode spacers in electrolytic capacitors were examined. (The author is indebted for the information in this paragraph to W. A. Selke, Schweitzer Division, Kimberly-Clark Corp., Lee, Mass. 01238.) One, commonly known as Manila paper, is made from the fibers of the abaca plant (*musa textilus*). These fibers range in diameter from about 16 to 32 μ. The pulp receives only a very light beating so these fiber dimensions are retained in the finished sheet, which is quite porous. The particular material used here had a dry thickness of about 60 μ and a void fraction of 0.79. The other paper is commonly known as Benares paper and is made from the fibers of the sunn plant (*crotaleria juncea*). The plant fibers are about 15–40 μ in diameter, but this pulp is more heavily beaten so that in the paper sheet most of the fibers have been broken down to fibrils of about 3–5 μ diameter. The Benares paper is more dense than the Manila, and in these experiments had a

(7) C. T. O'Konski, *J. Phys. Chem.*, **64**, 605 (1960).
(8) H. Fricke, *ibid.*, **57**, 934 (1953).

void fraction of 0.65 and a thickness of about 25 μ. Other properties of these papers have been reported elsewhere.[9]

The parallel capacitance and resistance of electrolyte-impregnated paper was determined at temperatures from -24 to $+80°$ and at frequencies from 60 to 1000 Hz. Solutions of sodium salicylate in ethylene glycol, 0.015–0.500 M, were used as electrolytes. (Sodium salicylate is soluble in a number of organic solvents and was chosen in anticipation of extending this work to electrolytes made with other solvents.) Both papers swelled during immersion in glycol electrolytes. After prolonged immersion the Manila paper was 76 μ thick and the Benares paper was 32 μ thick.[9]

In order to bring the measured capacitance and resistance within the range of available bridges, the paper was measured in series with an external capacitor, as indicated in Figure 1a. The bridge measured the equivalent series combination, as in Figure 1b. Values of C_p and R_p were calculated from the expressions

$$C_{eq} = C_{ext}\frac{1 + (\omega R_p C_p)^2}{1 + (\omega R_p C_p)^2 + \omega^2 R_p^2 C_p C_{ext}} \quad (8)$$

$$R_{eq} = R_{ext} + [R_p/(1 + \omega^2 R_p^2 C_p^2)] \quad (9)$$

by means of a trial and error method using a digital computer.

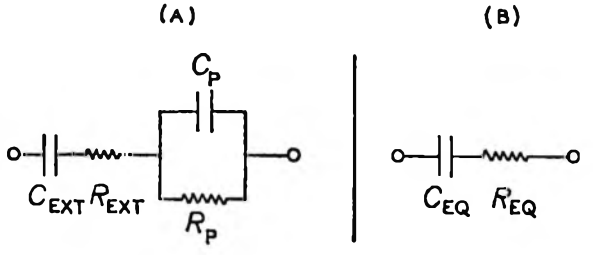


Figure 1. (A) Experimental circuit of paper (C_p, R_p) in series with capacitor (C_{ext}, R_{ext}). (B) Circuit measured by bridge.

The impregnated paper was placed between platinized foil electrodes which were connected in series to the external capacitor (1600 μF) and the measuring bridge. The area of an electrode was about 20 cm^2. The electrode–paper assembly was placed between glass slides and kept in intimate contact with spring clips. The pressure was not sufficient to prevent swelling of the paper to its equilibrium thickness.[9] Care was taken to exclude air from the sandwich. The papers were immersed in the electrolyte overnight at 25° prior to use.

The parallel capacitance and resistance was related to the real and imaginary parts of the complex dielectric constant by the expressions

$$\text{dielectric constant} = \epsilon' = (d/A\epsilon_r)C_p \quad (10)$$

$$\text{dielectric loss} = \epsilon'' = (d/A\epsilon_r)(\omega R_p)^{-1} \quad (11)$$

The paper thickness was taken as the equilibrium swollen thickness in glycol. Most of the results reported were obtained with a single sheet of paper between the electrodes. Some measurements made with a stack of three sheets of paper yielded the same values for ϵ' as with a single sheet, indicating that electrode polarization did not significantly affect results.

The high-frequency limit of the dielectric constant, ϵ_∞, was estimated from Maxwell–Wagner dispersion relations to be about 25 for Benares–glycol and 30 for Manila–glycol.

IV. Results

Some dielectric dispersion curves, typical of those obtained over the range of experimental conditions, are shown in Figure 2. The important features of these data follow.

(1) There are exceedingly large dielectric increments for both papers. The maximum values close to 10^7 obtained in this work compare with values for $\Delta\epsilon'$ of 10^4–10^5 observed in previous studies of colloidal

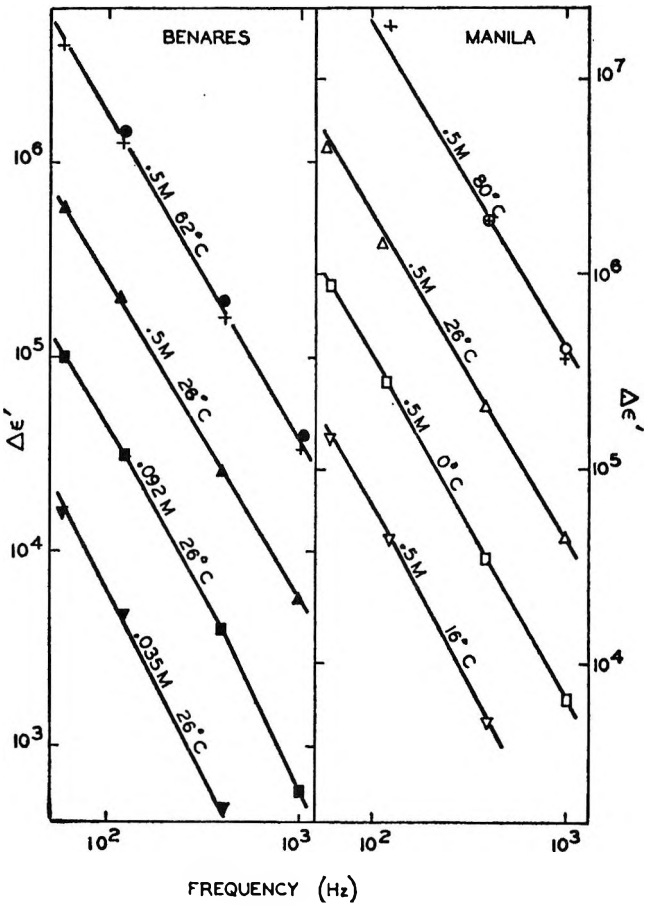


Figure 2. Frequency dependence of dielectric increment. Concentrations and temperatures as indicated. All data for single sheets, except those indicated by +, show results with three sheets of paper.

(9) R. S. Alwitt, *Electrochem. Technol.*, **6**, 172 (1968).

suspensions.[2,5] It was not possible to measure higher values of $\Delta\epsilon'$ accurately.

(2) A linear logarithmic relationship exists between the dielectric increment and frequency. Fricke and Curtis[1,2] found this dependency for a number of colloidal suspensions over a similar frequency range.

(3) At all concentrations and temperatures the characteristic frequency, f_0, was less than the lowest frequency measured. (By definition, $f = f_0$ when $\Delta\epsilon' = \Delta\epsilon_0/2$.) This follows from some general characteristics of dielectric dispersion curves which are that the maximum curvature of log $\Delta\epsilon'$ *vs.* log f occurs in the vicinity of f_0 and approximations to linear log relationships, extending over several decades of $\Delta\epsilon'$, can only be obtained at higher frequencies. Stated differently, the data in Figure 2 were all obtained at conditions such that $\omega\tau > 1$.

(4) The slopes of these lines ranged from -1.64 to -1.90, varying in a random fashion. This is less than the value of -2 predicted by eq 5.

(5) Both papers exhibited the same dielectric behavior, with $\Delta\epsilon'$ for Manila paper always about 7 times that for Benares paper.

The temperature dependence of $\Delta\epsilon'$ was examined using eq 7. No reliable data could be found on the viscosity of glycol below 20°. Since it is well established that the resistivity and viscosity of dilute electrolytes exhibit the same temperature dependence,[10] the change of resistivity with temperature was used as a measure of viscosity. The agreement with available viscosity data at higher temperatures was excellent. The term DT is almost temperature independent and need not be considered. To compare results at several concentrations and with the two papers, the ratio of $\Delta\epsilon'$ at two temperatures was evaluated.

$$\Delta\epsilon'_1/\Delta\epsilon'_2 = (T_1/T_2)(\rho_1/\rho_2)^2(\sigma_{01}/\sigma_{02})^3 \qquad (12)$$

No information was available on the temperature dependence of surface charge density. In Figure 3, the ratio of dielectric increments at a frequency of 100 Hz is plotted against the temperature and resistivity ratios of eq 12, using 25° as the reference temperature. If surface charge was independent of temperature, the data would be described by a line of unity slope passing through the reference point. The deviations of the data from this line are not great, but suggest a slight temperature dependence for surface charge density. For example, the deviation could be accounted for if the surface charge decreased by about a factor of 2 as the temperature increased from -25 to $+80$°.

In Figure 4 $\Delta\epsilon'$ at 100 Hz for Benares paper is shown as a function of solute concentration. The dielectric increment is obviously not inversely proportional to concentration as predicted by eq 7. Again, the deviation from the predicted behavior could be accounted for

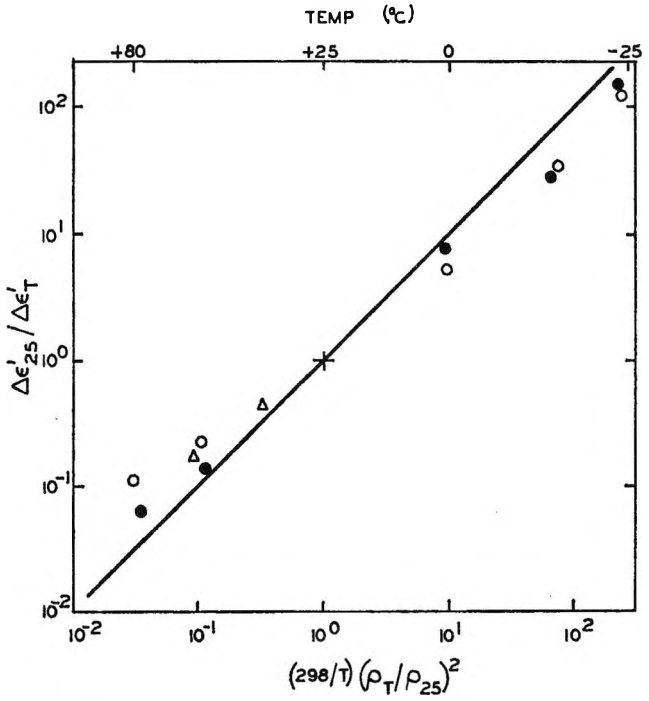


Figure 3. Temperature dependence of $\Delta\epsilon'$ at 100 Hz: ○, Manila, 0.5 *M*; △, Manila, 0.092 *M*; ●, Benares, 0.5 *M*.

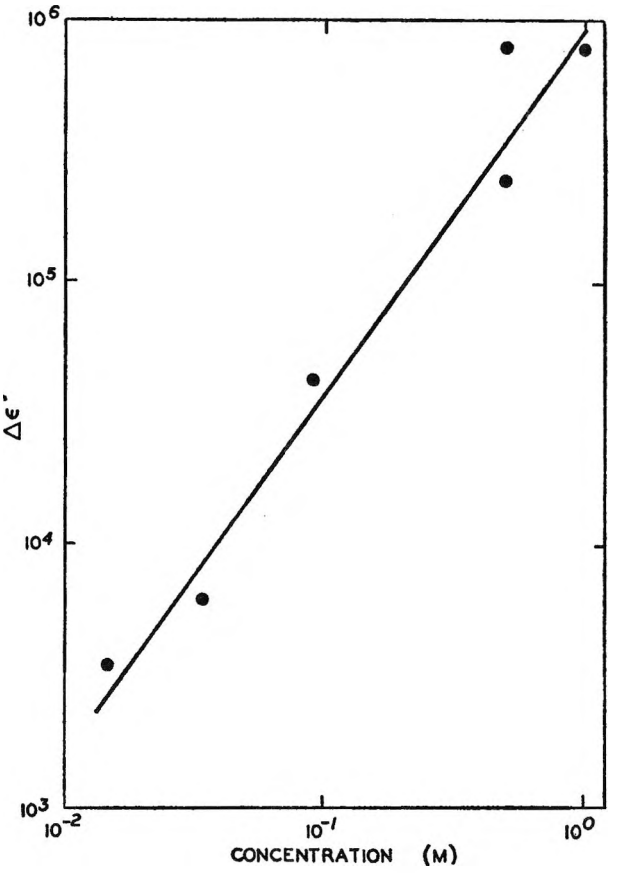


Figure 4. Concentration dependence of $\Delta\epsilon'$ for Benares paper at 26° and 100 Hz.

(10) H. C. Jones, "Conductivity and Viscosity in Mixed Solvents," Publication No. 80, Carnegie Institution of Washington, Washington, D. C., 1907.

if surface charge increased with increasing concentration according to $\sigma_0 \propto n^{0.8}$, assuming the magnitude of ζ remained small. The results with Manila paper showed a similar concentration dependence.

The total resistance of a colloidal suspension is made up of two parts, a frequency-independent resistance of bulk electrolyte and a frequency-dependent surface resistance.[2,4,5] In general, the first is much larger than the second. The resistance of the electrolyte-impregnated papers that we studied had this same characteristic. Thus, the total resistance was proportional to electrolyte resistivity, over a wide range of concentrations and temperatures, but superposed on this was a small frequency dependence. Some typical results are shown in Figure 5. A similar low-frequency dispersion of electrical resistance was observed by Mason, *et al.*,[11] for paper pulp in dilute aqueous KCl solutions. The surface resistance decreased with increasing frequency to a constant value at high frequencies.

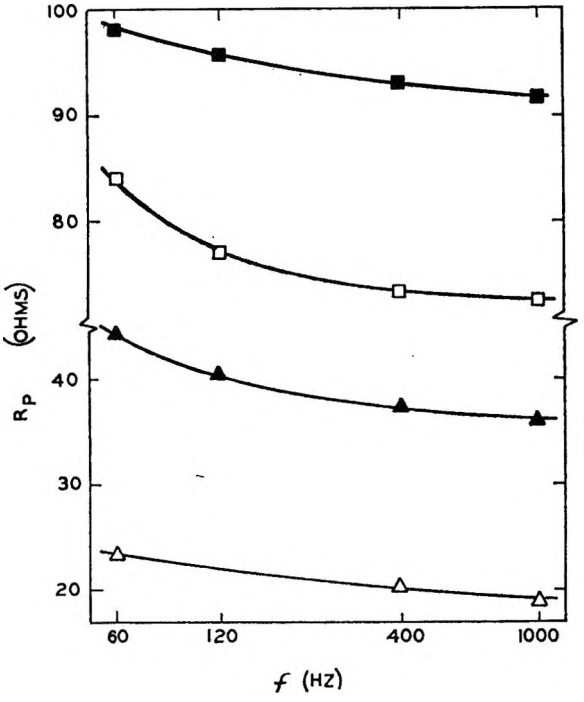


Figure 5. Frequency dependence of resistance of the paper sheet, 1 cm² in area. Symbols are the same as in Figure 2.

The dielectric loss in eq 2 is a property of the surface process only, and the $\Delta\epsilon''$ for the surface must be calculated from the bulk resistance and the total measured resistance. Reliable values for bulk resistance were not available and the surface dielectric loss of these papers was not of primary interest to us, so this line of experimentation was not pursued.

V. Discussion

An evaluation can be made to see if the very large values of $\Delta\epsilon'$ and small values of f_0 reported here are consistent with the known physical properties of the systems. Considering first the Manila paper, the largest $\Delta\epsilon'$ was 2×10^7 ($\Delta\epsilon'_{max}$) obtained at conditions of 80°, 0.50 M concentration, and 120 Hz. As we have shown, at these conditions $f_0 < 120$ Hz so $\Delta\epsilon_0 > 2\Delta\epsilon'_{max}$ and $\Delta\epsilon_0/\omega_0 > 5.3 \times 10^4$. From eq 1 it is easily determined that

$$\omega_0 = 0.43/\tau_0 \tag{13}$$

Combining eq 3, 4, and 13 leads to the expression

$$\frac{\Delta\epsilon_0}{\omega_0} = \frac{p}{0.43(1+p)^2} \frac{e_0^2 \eta R^3}{\epsilon_r (1/\kappa)(kT)^2} \tag{14}$$

which is independent of surface charge density. Inserting the right-hand side of eq 14 into the inequality for Manila paper leads to the result $R > 5\ \mu$. This is consistent with the observation that the fibers of this paper have a diameter of 16–32 μ in the dry state and somewhat greater when swollen. This calculation for Benares under similar conditions leads to $R > 3\ \mu$. This is slightly greater than expected for a system of fibrils of 3–5-μ diameter (dry), but may be due to the presence of some larger diameter fibrils because of incomplete beating of the pulp. In any event, for both papers the magnitude of $\Delta\epsilon'$ at these frequencies and experimental conditions is consistent with the known physical properties of the paper.

By choosing suitable values for R it is possible to estimate a lower limit for σ from eq 4 and an upper limit from eq 3 and 13. With $R = 10\ \mu$ for Manila and $R = 4\ \mu$ for Benares paper, these limits indicate that the magnitude of σ_0 is 10^{16} cm^{-2} for Manila paper and 10^{15} cm^{-2} for Benares paper. Previously reported values for several aqueous dispersions have been in the range 10^{12}–10^{13} cm^{-2}.[4,12] Thus, it appears that the large values of $\Delta\epsilon'$ with these papers were due to a very high surface charge density.

It was thought that the large σ_0 might be the result of strong specific adsorption of salicylate anions. However, measurements made with KCl substituted for sodium salicylate gave the same high values of $\Delta\epsilon'$ and showed the same concentration dependence of $\Delta\epsilon'$. Thus, the magnitude of σ_0 was not due to unique adsorptive properties of the anion.

It might be noted in passing that the magnitude of $\Delta\epsilon'$, according to eq 7, depends strongly upon the ratio σ_0/R. This ratio is estimated to be larger for Manila than for Benares paper, which probably accounts for the higher values of $\Delta\epsilon'$ obtained with Manila paper.

Schwan, *et al.*,[5] found that the dielectric data for a suspension of polystyrene spheres fell on a circular arc locus in a Cole–Cole plot. Cole[13] has shown that

(11) D. A. Goring, G. J. Biefer, and S. G. Mason, *Can. J. Res.*, **28B**, 339 (1950).

(12) S. M. Neale and R. H. Peters, *Trans. Faraday Soc.*, **41**, 478 (1946).

(13) K. S. Cole, *J. Chem. Phys.*, **9**, 341 (1941).

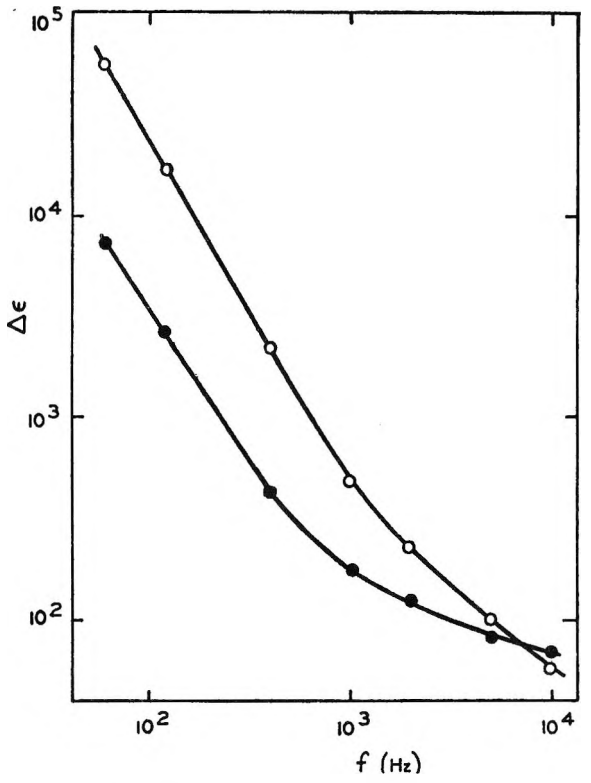


Figure 6. Dielectric dispersion in 0.015 *M* solution 26°: ○, Manila; ●, Benares.

this behavior is typical of many real dielectrics. The formula derived by Cole[13] for the complex dielectric constant of such systems

$$\epsilon^* = \epsilon_\infty + (\epsilon_0 - \epsilon_\infty)/[1 + (i\omega\tau)^{1-\alpha}]$$

has the characteristic that at intermediate values of $\omega\tau$ ($1 < \omega\tau < 100$) a plot of log $\Delta\epsilon'$ *vs.* log $\omega\tau$ has a linear portion with a negative slope with an absolute value less than 2, the value of the slope depending upon α ($0 < \alpha < 1$). At still higher values of $\omega\tau$ the slope approaches the value of $\alpha - 1$. For example, if $\alpha = 0.02$ the slope changes from -1.68 to -0.98.

To see if the paper might show this change in slope, some measurements were made at conditions designed to give very high values of $\omega\tau$. The results are shown in Figure 6. A change in slope was observed but it was greater than predicted from the Cole theory. With Manila paper the slope changed from -1.70 to -0.74 and with Benares paper a still smaller slope was obtained at the highest frequencies.

It is of interest that the results obtained in these experiments indicate that the effective particle diameters are those of the macroscopic fibers or fibrils. Cellulose swells in electrolyte solutions made with suitable solvents,[9] the imbibed electrolyte causing a separation between adjacent microscopic strands of cellulose by rupture of hydrogen bonds.[14] *A priori* it seemed possible that the dielectric properties of impregnated paper were due to the subfiber structure surrounded by imbibed electrolyte in the pores and channels of the fiber. If this had been the case, the effective particle diameter would have appeared to be several orders of magnitude smaller than was found. It is possible that effects due to this substructure are superposed on those of the macroscopic fibers. For example, the higher than expected values of $\Delta\epsilon'$ obtained at higher frequencies (Figure 6) could be due to a dispersion involving the fiber substructure.

VI. Summary

Paper impregnated with a glycol electrolyte displayed a dielectric dispersion very similar to those observed for colloidal suspensions, except that $\Delta\epsilon'$ was several orders of magnitude greater than previously reported values. Estimates of σ_0 suggested that a high surface charge density accounted for the large $\Delta\epsilon'$. Using a distribution of relaxation times based upon ionic mobility in the electric double layer, it was estimated that σ_0 decreased slightly with increasing temperature and increased with solute concentration. The calculated particle diameters were consistent with the picture that the processes responsible for the dielectric dispersion occurred on the surfaces of the macroscopic fibers rather than on interior surfaces of the swollen fiber.

Acknowledgment. The author is grateful to Mrs. E. Vigna for obtaining the laboratory results reported here.

VII. Appendix. List of Symbols

A	Paper area, cm^2
d	Paper thickness, cm
e_0	Electronic charge
D	Dielectric constant
f	Frequency, Hz
k	Boltzmann constant
n	Concentration = cations/cm^3 for a 1:1 electrolyte
p	Volume fraction of particles
R	Particle radius, cm
T	Temperature, °K
u	Ionic surface mobility
ϵ', ϵ''	Real and imaginary part of complex dielectric constant
ϵ^*	Complex dielectric constant
ϵ_0, ϵ_∞	Low- and high-frequency limits of dielectric constant
$\Delta\epsilon_0$	Static dielectric increment = $\epsilon_0 - \epsilon_\infty$
ϵ_r	Permittivity of free space = 8.85×10^{-14} F/cm and 7.97×10^{-2} esu/cm
η	Viscosity, P
κ	Reciprocal Debye length of ionic atmosphere, cm^{-1}
ρ	Resistivity, ohm-cm
σ_0	Surface charge density, charges/cm^2
τ	Relaxation time, sec
ω	Angular frequency, sec^{-1}

(14) P. H. Hermans, "Physics and Chemistry of Cellulose Fibers," Elsevier Publishing Co., New York, N. Y., 1949.

The Secondary Electroviscous Effect. Paths of Approach of Two Charged Spheres in a Viscous Medium

by J. Blachford,[1] F. S. Chan, and D. A. I. Goring

Department of Chemistry, McGill University, and Physical Chemistry Division, Pulp and Paper Research Institute of Canada, Montreal, Quebec, Canada *(Received September 17, 1968)*

Using Verwey and Overbeek's theory and Stokes' law the paths of two charged particles undergoing interaction have been calculated. Brownian motion and inertial effects are assumed to be negligible; the particles are spherical and nonswelling and the flow is laminar. From the calculated paths and the collision frequency the concentration dependence of the viscosity has been theoretically derived for a suspension of spherical, charged, nonswelling particles. At high ionic strength the theory agrees well with previously described experiments on sulfonated polystyrene latex, but at low ionic strength the theory overestimates the Huggins coefficient, k', particularly at low shear rates.

Introduction

The concentration dependence of the reduced viscosity for polyelectrolytes increases with a reduction in the ionic strength. This phenomenon has been referred to as the "secondary electroviscous effect" to distinguish it from the "primary electroviscous effect" which refers to the increase in the intrinsic viscosity with a reduction in ionic strength.[2]

The secondary electroviscous effect can be explained in terms of a balance of the electrostatic repulsive force between the particles and the hydrodynamic compressive force on each particle. Because of the repulsive force, two particles on approaching one another in a shear gradient are slowed and forced to deviate from their original paths. As a result, a velocity difference develops between each particle and the adjacent liquid, and this, in turn, creates a hydrodynamic force on the particle which opposes the electrostatic force. Because of the velocity difference, frictional energy is expended which contributes to the viscosity.

On the basis of this explanation for the secondary electroviscous effect, we have developed in a previous paper[3] a quantitative theory which involves the assumption that the particles move in a circular path during interaction and that the angle θ remains constant during interaction. In the present paper the exact path is calculated by solving with a computer the differential equation of motion.

Theoretical Section

As in the previous treatment,[3] Brownian motion and inertial effects are assumed to be negligible; the particles are spherical and nonswelling, and the flow is laminar. Perhaps the most important assumption is that the particles repel one another to such an extent that the flow lines around them never interact significantly. The van der Waals force of attraction is ignored since it is only significant when the particles are very close together.

Paths of Interacting Particles. Figure 1 shows the coordinate system for describing the interaction of a pair of spheres of equal radius, a, undergoing laminar motion. The origin is midway between the two particles, and the distance between particle centers, $2r$, depends on the angles of approach, the shear rate, the ionic strength, and the radius and charge of the particles. The liquid flows with a velocity of Gy in the x direction.

The exact paths of approach and recession of the two interacting charged particles can be calculated from an equation expressing the balance between the electrostatic repulsive force and the hydrodynamic compressive force. Differentiation of Verwey and Overbeek's expression[4] for the electrostatic potential energy of repulsion between the particles gives

$$F_E = \frac{-\epsilon a^2 \zeta^2 e^{2\kappa a}}{4\gamma^2} \frac{2\kappa r + 1}{r^2 e^{2\kappa r}} \qquad (1)$$

The ζ potential, ζ, is used here rather than the surface potential because the hydrodynamic radius, a, is used. The importance of the Hoskin correction factor,[5] γ, for ζ is discussed in a previous paper.[6] At the large distances of separation that interest us the factor β included by Verwey and Overbeek equals unity.

The hydrodynamic force on a particle, F_H, is given by Stokes' law

$$F_H = 6\pi\eta_0 a \Delta v \qquad (2)$$

(1) H. L. Blachford, Limited, Montreal 3, Quebec, Canada.

(2) B. E. Conway and A. Dobry-Duclaux in "Rheology," F. Eirich, Ed., Vol. 3, Academic Press, New York, N. Y., 1960, Chapter 3.

(3) F. S. Chan, J. Blachford, and D. A. I. Goring, *J. Colloid Interfac. Sci.*, 22, 378 (1966).

(4) E.J. W. Verwey and J. Th. G. Overbeek, "Theory of the Stability of Lyophobic Colloids," Elsevier, Amsterdam, 1948.

(5) N. E. Hoskin, *Trans. Faraday Soc.*, 49, 147 (1953).

(6) J. Blachford, *J. Colloid Interfac. Sci.*, in press.

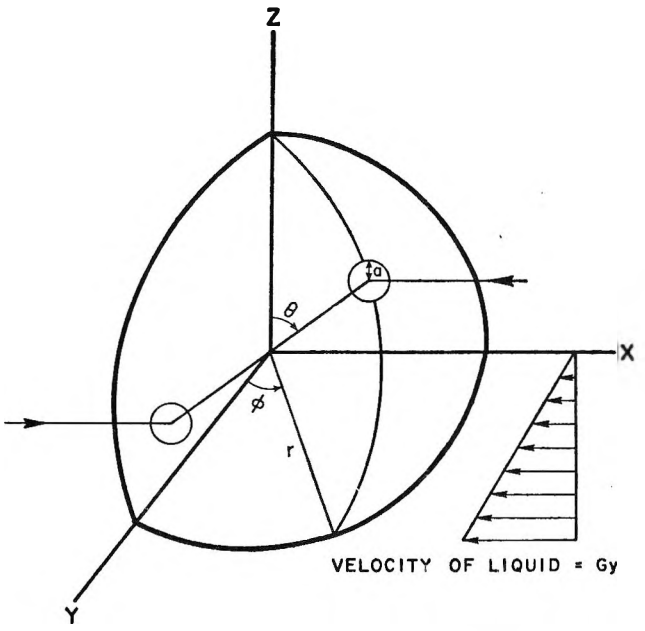


Figure 1. Representation in a spherical coordinate system of the collision between two charged spheres.

If dr/dt is the velocity of the particle in the r direction, then

$$\Delta v = -Gr \sin^2\theta \cos\phi \sin\phi - \frac{dr}{dt} \tag{3}$$

Since inertial effects are negligible, the hydrodynamic force must equal the electrostatic force, thus

$$6\pi\eta_0 a\left(Gr \sin^2\theta \cos\phi \sin\phi + \frac{dr}{dt}\right) = \frac{\epsilon a^2\Psi^2 e^{2\kappa a}}{4\gamma^2}\frac{2\kappa r + 1}{r^2 e^{2\kappa r}} \tag{4}$$

The next step is to reduce the number of variables in eq 4. The electrostatic repulsive force acts only in the r direction; therefore, the θ and ϕ coordinates of the particle change at the same rate as do those of the liquid. Hence

$$\frac{d\theta}{dt} = -G \cos\theta \sin\theta \sin\phi \cos\phi \tag{5}$$

$$\frac{d\phi}{dt} = -G \cos^2\phi \tag{6}$$

Solving eq 5 and 6 leads to $\tan\theta = B/\cos\phi$ and $dt = -d(\tan\phi)/G$. Substituting these two relations and $Y = 2\kappa r$ into eq 4 gives

$$\frac{dY}{d\tan\phi} = Y\frac{\tan\phi}{1 + (1/B^2) + \tan^2\phi} + BH\frac{Y+1}{Y^2e^Y} \tag{7}$$

For given values of H, θ_0, and ϕ_0, eq 7 can be solved by the Runge–Kutta method using a computer, provided the initial value of Y, denoted Y_0, is known.

The value of Y_0 should be such that the electrostatic force between the particles at $r = Y_0/2\kappa$ results in a negligible contribution to the viscosity. A trial and error procedure shows that the interaction is negligible when the hydrodynamic force on the particle, calculated assuming the particle is stationary (*i.e.*, $dr/dt = 0$) is 10,000 times the electrostatic force. Therefore, Y_0 is obtained by solving

$$Y_0\frac{\tan\phi_0}{1 + (1/B^2) + \tan^2\phi_0} = 10{,}000H\frac{Y_0 + 1}{Y_0^2 e^{Y_0}} \tag{8}$$

Equations 7 and 8 were solved for H values of 10^4 to 10^{12}, and for θ_0 and ϕ_0 values of 0.1 to 89.9°. Figure 2 gives the particle path as Y *vs.* ϕ for $H = 10^6$, $\phi_0 = 85°$, and $\theta_0 = 85°$. At these angles the collision is almost "head on." For comparison the paths are also given for no interaction and according to the previous theory.

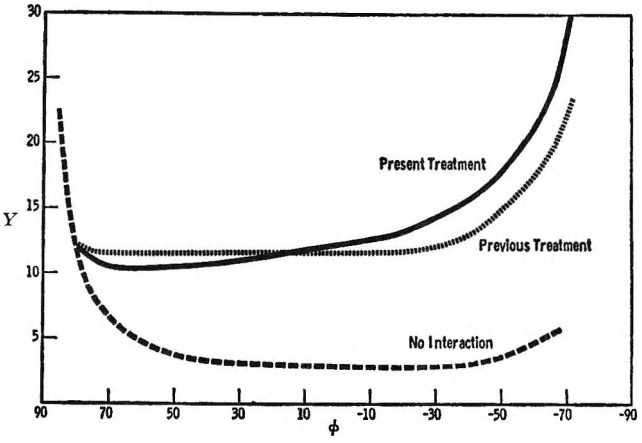


Figure 2. Theoretical paths during interaction of two particles when $H = 10^6$, $\theta_0 = 85°$, and $\phi_0 = 85°$.

The path is somewhat different from that given by the previous treatment. It is not circular, and at values of ϕ less than zero there is interaction, while the previous theory assumes no interaction. The greatest difference between the theories is that previously θ was assumed to remain constant during interaction, while according to the present treatment $\tan\theta = B/\cos\phi$, and so if θ_0 and ϕ_0 equal 85° then at ϕ equal to zero θ equals 45°.

One of the assumptions common to both theories is that the flow lines around the particles never interact significantly. It is valuable, therefore, to calculate the minimum distance separating the particles during a collision. As θ_0 and ϕ_0 approach 90° this minimum distance decreases, since the collision approaches "head on." For θ_0 and ϕ_0 equal to 89.9° and when H lies between 10^4 and 10^9 the minimum value of Y, denoted Y_{min}, is given by

$$Y_{min} = 9 \log H - 1.4 \tag{9}$$

The distance of separation is then calculated from $Y_{min} = 2\kappa r_{min}$. If the surfaces of the particles are separated by less than a particle diameter, it is likely that the flow lines around the particles interact significantly. Since the collision frequency is small at high values of

θ_0 and ϕ_0, and since the minimum distance of separation increases rapidly as θ_0 and ϕ_0 decrease, it is probable that if r_{min} is only slightly smaller than $2a$ the theory is still applicable.

Calculation of Huggins Coefficient. As previously shown, when two particles approach one another sufficiently closely the electrostatic repulsive force hinders the motion of the particles, and therefore causes a velocity difference between the particles and the surrounding liquid. Frictional energy is thereby dissipated as heat, and so the viscosity is increased.

Combining eq 3 and 4, and substituting $Y = 2\kappa r$ and the expression for H leads to

$$\Delta v = \frac{HG}{2\kappa}\frac{Y+1}{Y^2e^Y} \tag{10}$$

The energy dissipated per particle per collision is

$$E = 6\pi\eta_0 a\int_0^t (\Delta v)^2\,dt \tag{11}$$

Substituting eq 9 into eq 10 and using $dt = -d(\tan\phi)/G$ gives

$$E = \frac{3\pi\eta_0 aH^2G}{2\kappa^2}\int_{\tan\phi_0}^{\tan\phi_n}\frac{Y+1}{Y^2e^Y}\,d(\tan\phi) \tag{12}$$

where ϕ_n is the value of ϕ beyond which the contribution to the energy dissipated is negligible. The value of ϕ_n is found by trial and error.

We must now calculate the energy dissipated per unit time, but to do so we must first calculate the collision frequency. A collision between two spheres will be considered to occur when the distance between the centers of the spheres is such that the particles interact significantly. This distance is denoted as $2r_0$ and is equal to Y_0/κ. If a collision surface which is at a distance of $2r_0$ from the origin is described about a reference particle placed at the origin, all particles whose centers are carried to this surface will "collide" with the reference particle.

Let dA be the area projected on the yz plane of the surface element contained in the interval $d\theta_0$, $d\phi_0$ at θ_0, ϕ_0 on the collision surface. The number of particles whose centers pass through this area in unit time equals

$$nGz\,dA = nGz\,dy\,dz \tag{13}$$

On transforming to spherical polar coordinates

$$z = 2r_0\cos\theta_0 = \frac{Y_0}{\kappa}\cos\theta_0 \tag{14}$$

$$y = 2r_0\sin\theta_0\cos\phi_0 = \frac{Y_0}{\kappa}\sin\theta_0\cos\phi_0 \tag{15}$$

Differentiation of the first of these expressions with respect to θ_0 leads to

$$dz = \frac{1}{\kappa}\left(\cos\theta_0\frac{dY_0}{d\theta_0} - Y_0\sin\theta_0\right)d\theta_0 \tag{16}$$

When eq 8 is differentiated with respect to θ_0

$$\frac{dY_0}{d\theta_0} = \frac{-Y_0\cos 2\theta_0\sin\phi_0}{T} \tag{17}$$

Equation 17 is substituted into eq 16 and the result is substituted into eq 13. In an analogous manner an expression for dy is obtained and substituted into eq 13. These two substitutions give

$$n\,dz\,dy\,Gz = -\frac{nGY_0^3}{\kappa^3}\times\left(\frac{2\sin\phi_0\cos^4\theta_0 - \sin\phi_0\cos^2\theta_0}{T} + \sin\theta_0\cos\theta_0\right)\times\left(\frac{\sin^2\theta_0\cos\theta_0\cos^2\phi_0}{T} + \sin\theta_0\sin\phi_0\right)d\theta_0\,d\phi_0 \tag{18}$$

Having calculated the collision frequency and the energy dissipated per collision, the total energy dissipated and the Huggins coefficient can be obtained. The increment in solution viscosity caused by particle interaction is

$$\Delta\eta = \frac{E_t}{G^2} \tag{19}$$

where E_t is the total energy dissipated per unit volume per unit time

$$E_t = 4nEnGz\,dy\,dz \tag{20}$$

If the concentration is sufficiently low that three-body and higher collisions are negligible, then by definition

$$\frac{\eta_{sp}}{c} = [\eta] + \frac{\Delta\eta/\eta_0}{c} \tag{21}$$

For "isoionic" dilution Huggins equation[7] applies

$$\frac{\eta_{sp}}{c} = [\eta] + k'[\eta]^2c \tag{22}$$

On combining eq 18, 19, and 20 along with $n = Nc/100M$ and substituting the result into eq 21 and 22, we find that

$$k' = 6.83\times 10^{44}\frac{a}{M^2\kappa^5[\eta]^2}(H^2J) \tag{23}$$

where

$$J = \int_{\theta_0=0.1^\circ}^{\theta_0=89.9^\circ}\int_{\phi_0=0.1^\circ}^{\phi_0=89.9^\circ} EY_0^3\times\left(\frac{2\sin\phi_0\cos^4\theta_0 - \sin\phi_0\cos^2\theta_0}{T} - \sin\theta_0\cos\theta_0\right)\times\left(\frac{\sin^2\theta_0\cos\theta_0\cos^2\phi_0}{T} - \sin\theta_0\sin\phi_0\right)d\theta_0\,d\phi_0 \tag{24}$$

(7) M. L. Huggins, *J. Amer. Chem. Soc.*, 64, 2716 (1942).

In calculating J no significant error is introduced by not integrating from 0° to 90°. Fortunately, an almost linear relation exists between ln (H^2J) and ln H.

$$\ln (H^2J) = 1.351 + 0.617 \ln H - 0.00808 (\ln H)^2 \quad (25)$$

Therefore

$$k' = 6.83 \times 10^{44} \frac{a}{M^2\kappa^5[\eta]^2} \times \exp [1.351 + 0.617 \ln H - 0.00808 (\ln H)^2] \quad (26)$$

Theoretical values of k' can be calculated directly from eq 26.

Comparison with Experiment. The theory can be tested using previously obtained experimental results for monodisperse sulfonated latex particles of 380-Å radius.[3] Because these particles are monodisperse, spherical, and nonswelling they are very suitable. The method of Stigter and Mysels[8] was used to calculate the ζ potential from the electrophoretic mobility. As explained in a previous paper[6] the ζ potentials are so high Hoskin's correction[5] must be applied. Table I shows the corrected values of the ζ potential along with the corresponding values of the ionic strength, I_E.

Our theory is applicable only if the minimum distance of separation of the particles is sufficiently great. Substitution into eq 9 indicates that the centers of the particles are always separated by a distance of at least 3.3 times the radius of a particle. We have assumed that an insignificant amount of interaction of the flow lines occurs at this distance. It is interesting to note that a particle separation of 3.3 radii in a stationary suspension corresponds to a volume fraction of 0.16 which must therefore represent an upper concentration limit of validity. However, the data used to test the theory are well below this limit, being derived from suspensions of volume fraction of 0.01 or less.

Table I: Theoretical and Experimental Values of k' for Several Values of Shear Rate, G, and Ionic Strength, I_E

G, sec^{-1}	$I_E \times 10^4$, M	$\zeta \times 10^4$, esu	k', previous treatment	k', present treatment	k', exptl
650	1.0	3.57	22.4	23.8	11.9
650	1.8	2.78	12.5	15.5	8.68
650	4.0	2.38	5.60	6.56	6.67
650	10.0	1.95	2.49	2.93	4.55
9,000	1.0	3.57	9.15	11.0	8.76
9,000	1.8	2.78	5.41	6.46	6.99
9,000	4.0	2.38	2.58	2.63	4.42
9,000	10.0	1.95	1.29	1.32	2.19
16,000	1.0	3.57	6.25	7.95	6.41
16,000	1.8	2.78	3.87	4.92	5.37
16,000	4.0	2.38	2.11	2.13	3.84
16,000	10.0	1.95	1.10	1.14	1.56

Table I gives the theoretical and experimental values of k'. The present treatment gives values which are not significantly different from those given by the previous treatment.[3] Apparently the differences between the two derivations which lead to different paths do not affect the calculated values of k'.

The results show that the experimental values of k' are generally lower than the values calculated by the theory. The greatest disagreement between theory and experiment occurs at low ionic strengths and shear rates. It is under these conditions that the assumption of no interaction of flow lines is most reasonable, and so the explanation of the disagreement must lie elsewhere. Among the assumptions of the previous theory are a circular path, constancy of θ, and no interaction beyond ϕ equal to zero. Since these assumptions are not included in the present theory they cannot be cited as possible reasons for the disagreement between theory and experiment. One of the achievements, therefore, of the present paper is that the number of possible reasons for disagreement has been reduced.

Acknowledgments. The authors are greatly indebted to Mr. Emil Koller for performing the extensive computer calculations.

Appendix. Nomenclature

a	Particle radius
B	$\tan \theta_0 \cos \phi_0$
c	Concentration
E	Energy dissipated per particle per collision
F_E	Electrostatic repulsive force
F_H	Hydrodynamic compressive force
G	Shear rate
H	$= \frac{\epsilon a^2 \Psi_0^2 e^{2\kappa a} \kappa^3}{3\pi\eta_0 a G}$
I_E	Ionic strength
J	Dimensionless variable, calculated from H
k'	Huggins coefficient
M	Molecular weight
N	Avogadro's number
n	Concentration in number of particles per cm^3
r	Half the distance between two particles
T	$= 10^4 H \frac{2 + 2Y_0 + Y_0^2}{Y_0^3 e^{Y_0}} - \sin \theta_0 \cos \theta_0 \sin \phi_0$
Δv	Relative velocity between particle and liquid
Y	$2\kappa r$
ϵ	Dielectric constant of medium
ζ	ζ potential
η_0	Viscosity of water
$\Delta\eta$	Viscosity increment caused by particles
$[\eta]$	Intrinsic viscosity
κ	Reciprocal of the Debye double layer thickness

Subscripts with θ, ϕ, r, and Y refer to values at which computer calculations were started.

(8) P. Stigter and K. G. Mysels, *J. Phys. Chem.*, **59**, 45 (1955).

Interpretation of Chlorophyll Electron Spin Resonance Spectra[1]

by M. Garcia-Morin,[2a] R. A. Uphaus, J. R. Norris,[2b] and J. J. Katz

Chemistry Division, Argonne National Laboratory, Argonne, Illinois 60439 *(Received September 25, 1968)*

Dry, oxygen-free chlorophyll systems possess no intrinsic dark esr signal, nor can a photo-esr signal be induced in such systems by irradiation with red light. Chlorophyll–water micelles, which form in aliphatic hydrocarbon solvents, yield a narrow, reversible, photo-induced esr signal on irradiation with red light. Oxygen in either dry or water-containing systems causes extensive photodecomposition. In benzene solution, a solvent in which micelle formation is not favored, photooxidation is much more rapid than in dodecane. The line shape and isotope effects on the narrow, reversible, photo-induced esr signal are consistent with a delocalization of an electron into a large micelle. A new model for the primary light conversion act in photosynthesis is suggested in which light absorption by a chlorophyll–water micelle results in the formation of chlorophyll radical cation and anions (Chl^- and Chl^+), which furnish the reducing and oxidizing power for the reactions of photosynthesis.

Introduction

Electron spin resonance (esr) signals have been observed in photosynthesizing algae and bacteria,[3] chloroplast and chromatophore preparations,[4] and in solid or dissolved chlorophyll.[5] A bewildering variety of narrow, broad, light, dark, reversible, and irreversible signals have been reported, but even in the case of chlorophyll itself, no consistent interpretation of the signals has emerged. In a general way it was recognized that water and oxygen were somehow implicated in the esr observations. However, some of the earlier experiments were carried out with solid chlorophyll, where removal or equilibration with water and oxygen is slow and incomplete, and in still other experiments exclusion of water or oxygen could not be certain. Thus, no definite conclusions about the role of water or oxygen could be drawn. The experiments described here, we believe, go far to provide an unequivocal interpretation for the genesis of esr photo signals in chlorophyll solutions.

In earlier work, we have shown that magnesium in chlorophyll always has a coordination number larger than 4, and that unless ligand groups are present in the axial position(s), the magnesium is coordinatively unsaturated. As a result of the strong tendency of magnesium to coordinate ligands in the 5th and 6th axial positions, chlorophyll in nonpolar solvents exists as dimers or oligomers held together by the interaction of the ketone oxygen function of one molecule with the central magnesium atom of another: C=O - - - Mg.[6] Electron-donor (nucleophile) molecules in nonpolar solvents can compete for coordination to magnesium, and sufficiently strong electron donor molecules disaggregate the dimers or oligomers to form monomeric chlorophyll·solvate species.[7] We have recently shown that water is a unique nucleophile for chlorophyll because of its ability to donate electrons and to form hydrogen bonds simultaneously. The consequences of water–chlorophyll interaction are observed to be strongly solvent dependent.[8] In benzene solutions (chlorophyll concentration $< 10^{-3}$ M) water forms the dimer hydrate $Chl_2 \cdot H_2O$ and partially disaggregates the chlorophyll dimers to form monomeric $Chl \cdot H_2O$. In dodecane, to the contrary, chlorophyll–water interactions result in the formation of ordered aggregates of colloidal dimensions, as established by ultracentrifugation and X-ray diffraction. The absorption spectrum of these micelles is strongly shifted to the red. We have found that these aggregates yield very narrow, reversible esr photo signals with red light.[9] Water was shown to be necessary for that signal, but the role of the micelle, of oxygen, and of the solvent remained to be elucidated. We have now studied the effects of

(1) Based on work performed under the auspices of the U. S. Atomic Energy Commission.

(2) (a) Resident Research Associate from the University of Puerto Rico, 1966–1968; (b) Resident Research Associate, 1968.

(3) B. Commoner, J. J. Heise, B. B. Lippincott, R. E. Norberg, J. V. Passonneau, and J. Townsend, *Science*, **126**, 57 (1957); M. B. Allen, L. H. Piette, and J. C. Murchio, *Biochem. Biophys. Acta*, **60**, 539 (1962); B. Kok and H. Beinert, *Biochem. Biophys. Res. Commun.*, **9**, 349 (1962); E. C. Weaver, *Photochem. Photobiol.*, **7**, 93 (1968); P. B. Sogo, G. N. Pon, and M. Calvin, *Proc. Nat. Acad. Sci.*, **43**, 387 (1957).

(4) W. H. Storey, C. M. Monita, and D. G. Cadena, *Nature*, **195**, 963 (1962); J. A. Lippincott and B. B. Lippincott, *Arch. Biochem. Biophys.*, **105**, 359 (1964); G. M. Androes, M. F. Singleton, and M. Calvin, *Proc. Nat. Acad. Sci.*, **48**, 1022 (1962); H. Beinert and B. Kok, *Biochim. Biophys. Acta*, **88**, 278 (1964); H. Schleyer, *Biochim. Biophys. Acta*, **153**, 427 (1968).

(5) S. S. Brody, G. Newell, and T. Gastner, *J. Chem. Phys.*, **64**, 544 (1960); V. Holmgorov, and A. Terenin, *Naturwissenschaften*, **48**, 158 (1961); A. F. H. Anderson and M. Calvin, *Nature*, **199**, 241 (1963); B. Smaller, "Free Radicals in Biological Systems," M. S Blois, Ed., Academic Press, New York, N. Y., 1961, p 315; G. Sherman and E. Fujimor, *Nature*, **219**, 375 (1968).

(6) J. J. Katz, L. J. Boucher, R. C. Dougherty in "The Chlorophylls," L. P. Vernon and G. R. Seely, Ed., Academic Press, New York, N. Y., 1966, Chapter 7, pp 185–251.

(7) J. J. Katz, H. H. Strain, D. L. Leussing, and R. C. Dougherty, *J. Amer. Chem. Soc.*, **90**, 784 (1968).

(8) J. J. Katz and K. Ballschmiter, *Angew. Chem.*, **80**, 283 (1968).

(9) J. J. Katz, K. Ballschmiter, M. Garcia-Morin, H. H. Strain, and R. A. Uphaus, *Proc. Nat. Acad. Sci.*, **60**, 100 (1968).

adding water, oxygen, or both, on the esr signals of chlorophyll. We have used benzene and dodecane as solvents representing extremes of behavior with respect to the products of the chlorophyll–water interaction.

Experimental Section

Materials. Chlorophyll a, pyrochlorophyll a, and pheophytin a were prepared by standard procedures.[10] It is essential that very pure chlorophyll, free of oxidation products, be used for the esr experiments. We verified in advance that the chlorophyll samples we used gave no esr signal in the absence of air and water. Solvents were the best commercial grade. Dodecane was treated with concentrated sulfuric acid, washed with aqueous bicarbonate, and then with water. Dodecane and benzene were dried over silica gel. By a vapor phase chromatographic procedure, the benzene was shown to have a water content of 18–20 μg/ml and the dodecane to contain 5–10 μg/ml of water. Vpc showed the solvents to be free of impurities and the water content of the solvents was checked also by Karl Fischer titration. In all of our experiments, where a chlorophyll–water micelle is referred to, the chlorophyll/water ratio in the solution was shown by vpc analysis to be sensibly 1:1.

Preparation of Esr Samples. All of the chlorophyll systems studied were conveniently prepared in quartz vessels shown in Figure 1. A carbon tetrachloride solution of chlorophyll was placed in the sample tube and the system was attached to the vacuum line. After thorough degassing, the carbon tetrachloride was distilled away. Completely dry samples were prepared by redissolving the chlorophyll in a quantity of fresh, dried carbon tetrachloride and subsequent solvent distillation. After complete removal of the solvent, the chlorophyll was heated to 60° under a high vacuum, after which the vessel was sealed off from the vacuum line. Hydration of the chlorophyll film was effected by opening the proper break-seal and exposing the chlorophyll film to water vapor for at least 2 days. By proper placement of black paper and/or aluminum foil it was possible to produce a slight temperature gradient which ensured that no liquid phase water actually condensed onto the chlorophyll. After the hydration process was concluded, all visible droplets of water were distilled back into the water tube and the tube quickly sealed off. This procedure did not remove appreciable water from the chlorophyll–water film. This hydration procedure was shown by direct analysis to yield chlorophyll monohydrate. The tube containing the desired solvent was then broken, the solvent distilled over by moderate heating, and the solution constituted by sonication. A chlorophyll concentration of 10^{-3} *M* was used in all experiments.

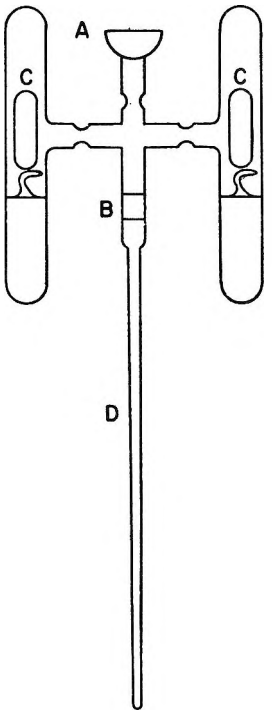


Figure 1. The sample vessel is attached to a vacuum line by means of the O-ring joint A; B, Pyrex-to-quartz graded seal, attached to a 5-mm standard quartz esr tube D. The side arms were filled with solvent, degassed water, or purified oxygen, and sealed off. At the appropriate time the breaker seals could be broken by the magnetic stirring bars C. If dry oxygen was needed a quantity of degassed, activated silica gel was sealed into the oxygen ampoule.

Spectra. All spectra were taken with a 12-in. Varian V-4502 spectrometer system. The *g* values were calculated from the value of the microwave frequency as determined with a 5245L Hewlett-Packard counter and the value of the magnetic field determined as measured with a Varian FH-20 gaussmeter. The FH-20 gaussmeter, in turn, was calibrated by a Perkin-Elmer M-2 proton magnetometer. Spectra were collected at 100-kc modulation frequency at appropriate modulation amplitudes and microwave power levels, using conventional criteria for selection of spectrometer parameters.

Irradiation. A 200-W xenon lamp was used for irradiation. Cut-off filters isolated the spectral region 600–900 nm.

Results

Water-Free, Oxygen-Free Systems. Chlorophyll a solutions in benzene or dodecane prepared with rigorous exclusion of water and oxygen have no dark signal, and no photo-esr signals are generated with red light. As far as we know, these are the first experiments reported with chlorophyll in which neither light nor dark esr signals were detected.

Water-Containing, Oxygen-Free Systems. Oxygen-free hydrated systems were prepared in evacuated esr

(10) H. H. Strain and W. A. Svec in ref 6, Chapter 2, pp 21–66.

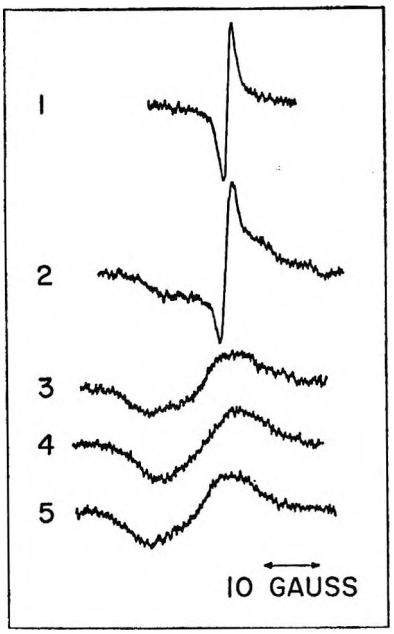


Figure 2. Esr signals generated from hydrated chlorophyll a in dodecane solution. All the measurements were made on the same oxygen-free system. The chlorophyll concentration was approximately 10^{-3} *M*. Red light (600–900 nm) was used for irradiation. Curve 1, photo-induced signal in the freshly made up system, wherein only a narrow line is present; curve 2, after 17 hr of red light irradiation, a broad signal appears superimposed on the photo signal; curve 3, at termination of irradiation the narrow photo signal decays, leaving a permanent dark signal; curve 4, the system of curve 3 after removal of all water by freezing; curve 5, the now water-free system under irradiation. No narrow signal is observed after water removal.

sample tubes and the esr spectra recorded. Hydrated dodecane systems showed no initial esr dark signal. Upon irradiation with red light, a photo-induced esr signal was observed (Figure 2, curve 1), with a peak-to-peak line width of about 1 G (g = 2.0025), as previously reported.[9] This signal grew or decayed ($1/t$) in about 4 sec; it vanished completely after the end of illumination. Long-continued irradiation (~17 hr) of the oxygen-free dodecane–chlorophyll–water system resulted in a broad signal (12–14 G, g = 2.0040), upon which the narrow photo signal was superimposed (Figure 2, curve 2). This signal persisted after termination of irradiation (Figure 2, curve 3), but the narrow signal decayed. Removal of water from the system (by freezing it back into the side arm) resulted in disappearance of the narrow signal, leaving only the broad signal, which neither decayed in the dark (Figure 2, curve 4) nor grew upon further irradiation (Figure 2, curve 5). Prolonged illumination of these hydrated systems always resulted in the eventual formation of a dark precipitate showing no esr signal; absorption spectra in the visible indicate that it is pheophytin. Similar, oxygen-free, hydrated chlorophyll a systems in benzene gave, before irradiation, a broad (12–14 G, g = 2.0016) dark signal of low intensity. Irradiation of hydrated solutions of chlorophyll a in benzene with red light generated a very intense but short-lived esr signal; the photoreaction giving rise to the signal was over in about 1 sec. This solution after irradiation showed a large permanent dark signal that appeared to be identical in g value with that present before irradiation. Illumination of wet benzene solutions for 48 hr resulted in an even more intense esr dark signal (again of unchanged width and g value); spectroscopic examination indicated that considerable pheophytin had formed.

Water-Free, Oxygen-Containing Systems. Chlorophyll systems in which water was rigorously excluded but which contained oxygen at 1 atm pressure showed greatly different behavior. In dodecane solution, exposure of the chlorophyll to dry oxygen did not produce a dark signal prior to the illumination. Irradiation then produced a broad (10–12 G) signal which did not decay in the dark. Oxygen in dry benzene solutions produced a small dark signal, which grew rapidly upon irradiation and persisted on storage in the dark. This signal resembled that found in dodecane, but was of much higher intensity. After 65 hr of irradiation a red precipitate formed, leaving a completely colorless supernatant solution. No esr signal could be detected in the precipitate. This photooxidation product was not further investigated; it appears to be similar to other chlorophyll oxidation products reported in the literature.[11]

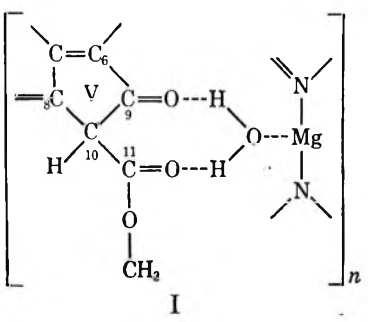
Systems Containing Both Oxygen and Water. Benzene or dodecane chlorophyll solutions in which both water and oxygen are present show an intense esr signal immediately after illumination, decaying completely in a few seconds, and too short-lived for us to record. After this initial burst, a stable signal appears; this is the usual broad signal of about 12 G width. In dodecane, the photo-induced signal appears more slowly; the signal that forms is at most only a few gauss wide. Although the transient signal in benzene was too brief for us to record, the dodecane and benzene chlorophyll solutions containing water and oxygen appear to be qualitatively similar, and appear to differ mainly in the rate of reaction of the chlorophyll.

Discussion

Two esr signals, one photoinduced, narrow, reversible, and short-lived, the other dark, broad, irreversible, and long-lived, must be accounted for. Aliphatic solvents such as dodecane favor the formation of large chlorophyll–water micelles in which chlorophyll molecules are held together by hydrogen bonds formed between the water coordinated to the magnesium of one chlorophyll molecule and the ketone carbonyl and carbomethoxy ester carbonyl groups of ring V of a

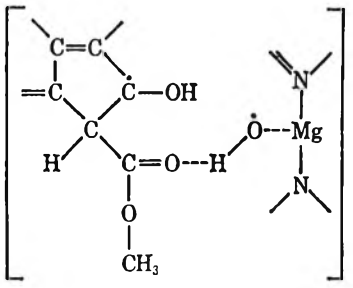
(11) G. R. Seely in ref 6, Chapter 17, p 550.

second chlorophyll molecule[9]



I

We believe the experimental data favor the hypothesis that the micelle as a whole is involved in the formation of the narrow photo signal. We assume that absorption of red light leads to electronic transitions involving the hydrogen-bonded carbonyl groups in structure I. Photo-induced reduction by hydrogen abstraction is known to take place in many aromatic ketones and carbon-containing molecules.[12] Such a process would generate free radicals of the type



II

Fast electron and proton exchange must take place between the odd electron sites in this structure; we would also expect the odd electron at carbon 9 would be delocalized into the conjugated system of the macrocycle, and thus into the chlorophyll–water array itself. A signal produced in this way should be narrow because of rapid exchange of spins in the micelle, as discussed below. In benzene solution, where the principal species are chlorophyll dimer monohydrate and chlorophyll monomer monohydrate, and no significant concentration of micelles occurs, the formation of free radicals by light absorption is rapidly followed by chemical decomposition. All this implies that a micelle of a minimum size is required for the reversible, narrow photo signal.

We have observed the narrowest esr photo signal thus far reported for chlorophyll systems. The line narrowing produced by deuterium substitution[9] strongly suggests that the unpaired electron must be delocalized to a significant extent. Moreover, because of the extreme narrowness of the signal, we believe that the electron spin (or spins) is migrating throughout the chlorophyll–water micelle. Delocalization into only one chlorophyll molecule seems unable to account for the extreme narrowness of this chlorophyll esr signal. Conceivably, the electron can be delocalized over the entire micelle, or, as we consider more probable, spin migration occurs from chlorophyll to chlorophyll molecule in the micelle. The line shape will then be determined by the rate and nature of the migration.

We discuss two possible limiting cases, considering only electron–proton interactions. In one extreme, a spin could be delocalized into the entire micelle containing a large number, N, of equivalent protons, resulting in a narrow Gaussian line. If this were the only mechanism contributing to the line shape, the width of such a Gaussian line is proportional to $1/(N)^{1/2}$.

A Lorentzian line shape would be produced under the following quite different conditions. A spin delocalized in a circumscribed region of a large micelle has a certain, relatively broad line width expressible as a frequency Δ. If the region of the spin delocalization is migrating at a rate large compared to Δ, then the resulting line shape is narrow and Lorentzian.

Thus, migration of a spin throughout the micelle could result in two extremes of delocalization, yielding either a Gaussian or a Lorentzian shape. Furthermore, if the rate of spin migration is not sufficiently rapid, then the line shape cannot be predicted from such simple considerations as above. Interaction with other nuclei and spin-lattice relaxation superimposed could yield line shapes that are neither Gaussian nor Lorentzian.

We have thus indicated why the measurement of the line shape alone is not sufficient to establish the mechanism of the narrowness of the esr signal. We have examined the line shape of the sharp signal very closely, and it appears to be Lorentzian. For the reasons just given, however, we can only say that the Lorentzian line shape is consistent with, but does not necessarily prove, our proposed delocalization mechanism for the narrowing of the signal.

That the micelle, or at least an appreciable portion of it, is involved in the narrow photo signal receives support from experiments with pyrochlorophyll a.[13] This substance differs from chlorophyll a only in the absence of the carbomethoxy group at position 10. Pyrochlorophyll, too, interacts with water in dodecane solution, but ir evidence indicates the micelles that form have a very different structure. We have been unable to produce narrow reversible photo signals from pyrochlorophyll a–water aggregates under conditions similar to those used for chlorophyll a–water. A broad, irreversible signal, however, was observed on long-continued irradiation. These observations we take to confirm the importance of specific structural relationships. The size of the chlorophyll–water aggregates

(12) G. S. Hammond and N. J. Turro, *Science*, 142, 1541 (1963).

(13) F. C. Pennington, H. H. Strain, W. A. Svec, and J. J. Katz, *J. Amer. Chem. Soc.*, 86, 1418 (1964).

also appears critical. Chlorophyll–water micelles in cyclohexane, a solvent in which the micellar size is much smaller than in dodecane as judged from centrifugation data, yield much weaker photo signals. In general, we find that conditions which fragment or destroy the micelle make the narrow, reversible photo signal diminish or vanish.

The delocalized electron and the electron deficient oxygen atom (structure II) must eventually result in chemical modification of the chlorophyll, leading to various oxidized or reduced chlorophyll reaction products, which are presumed to be the source of the broad, dark signal. As the micelle becomes fragmented by chemical attack, fewer opportunities for spin exchange remain, and the signal becomes broad. In dry, oxygen-free systems no hydrogen abstraction is possible with red light. Addition of oxygen does not produce narrow signals or intense transients, and only irreversible broad signals are obtained. The experiment on an oxygen-free system in which we have generated a broad, dark signal by prolonged illumination that is very similar to the signal obtained in oxygen-containing systems suggests that the chlorophyll has been oxidized by reaction with water with energy supplied by light.

The interpretation advanced here for the genesis of the photo-esr signal is directed to the case of chlorophyll–water micelles, where the chlorophyll and water are in the ratio 1:1. These micelles have an absorption maximum at 740 nm, whereas the longest wavelength form of chlorophyll in nature is reported to absorb light at 700–710 nm. It thus appears unlikely that the micelles we have discussed here occur in significant concentration in the plant. However, a chlorophyll–chlorophyll micelle (held together by C=O - - - Mg interactions) into which an occasional water molecule is inserted to form the entity shown in structure I appears to be a reasonable possibility. Such micelles would need a highly hydrophobic environment in which to exist, but the lipids and aliphatic hydrocarbons[14] known to occur in chloroplasts could provide the required millieu. Structure II is then a possible first product of the light conversion act in photosynthesis. The first result of light absorption would be to form free radicals of the type II in places where water is present between two chlorophyll molecules. The free electron transferred into the micelle and the HO· radical coordinated to magnesium thus become the ultimate sources of the reducing and oxidizing power for the dark reactions of photosynthesis. As the electron-deficient oxygen atom is a powerful oxidant, an electron may be extracted from the adjacent chlorophyll molecule. Delocalization of the electron at position 9 forms the radical anion Chl^-, and electron abstraction by the electron deficient oxygen atom would form the radical cation Chl^+. Structure II may thus be viewed as the precursor of Chl^- and Chl^+. The experiments reported here indicate that chlorophyll incorporated into chlorophyll–water micelles survives internal oxidation–reduction much better than does monomeric chlorophyll. The very small turnover of chlorophyll in nature argues against the presence of reactive monomeric chlorophyll in the chloroplast. Rapid transport of electrons (and of the balancing protons) in and out of the micelle may be the mechanism whereby chemical damage to chlorophyll *in vivo* is prevented, and the means whereby the oxidizing and reducing power implicit in Chl^+ and Chl^- are made available for the oxidation of water and the reduction of carbon dioxide. The addition and removal of electrons from the micelle would presumably be carried out by the quinones, cytochromes, ferridoxin, and other intermediates generally assumed to be involved in electron transport. The role of chlorophyll b, the carotenoids, and the plant lipids and the relation of the model proposed here to the widely accepted two-photochemical reaction scheme for photosynthesis remain for further consideration.

(14) K. Stransky, M. Streibl, and F. Sôrm, *Coll. Czech. Chem. Commun.*, **33**, 416 (1968); P. Gulz, *Phytochem.*, **7**, 1009 (1968); E. Gelpi, J. Oro, N. J. Schneider, and E. O. Bennett, *Science*, **161**, 701 (1968).

Foreign Gas Quenching of Sulfur Dioxide Vapor Emission

by H. D. Mettee[1]

Department of Chemistry, The University of Texas at Austin, Austin, Texas *(Received October 16, 1968)*

Quenching probabilities per gas kinetic collision for 15 common collision partners with electronically excited SO_2 are presented and compared to those found independently for electronically excited I_2, NO_2, and OH. In each of the latter cases, and for excited singlet SO_2, the quenching process is efficient, usually requiring from only one to ten collisions. The single parameter which best correlates most of the data is the polarizability of the quencher.

Introduction

Callear's recent reviews[2] summarize the fragmented character of the theoretical and experimental states of knowledge of electronic energy quenching processes. Most of the present information deals with excited atoms, and their usually great reactivity precludes a meaningful physical description if the collision partner is a polyatomic molecule. The situation is even less clear for the case of quenching the excited states of simple molecules by either atoms or other simple molecules.

The iodine and NO_2 systems have been studied with a fairly wide variety of collision partners. Steinfeld and Klemperer[3] and Brown and Klemperer[4] found a quenching dependence which varied with the product of the reduced mass of the collision complex and the polarizability of the partner. Apparently no contribution arose from a permanent dipole. This finding confirmed an earlier expectation of Rössler.[5]

On the other hand, Myers, Silver, and Kaufman's study of the quenching of NO_2 fluorescence[6] showed an increased quenching cross section for those collision partners with a dipole moment and "molecular complexity." In both of these systems the quenching cross sections were of the order of the gas kinetic cross sections or slightly less. This situation may be contrasted with the general immunity to fluorescence quenching of many carbonyl and aromatic vapors using the relatively simple collision partners under consideration.

The present study extends these quenching studies to the singlet, and in less detail to the triplet, systems of SO_2. It is found empirically that a linear relation exists between the probability of fluorescence quenching per gas kinetic collision ($1/Z_{QF}$) and the polarizability of the collision partner for most partners. The data for I_2, NO_2, and that for OH measured and collected by Tanaka, *et al.*,[7] are satisfactorily presented in a similar way. For OH and I_2 the quenching mechanisms are probably collision-induced predissociation, while for NO_2 and SO_2 the processes of collision-induced internal conversion and/or intersystem crossing are likely channels.

Experimental Section

The apparatus is the same as previously described.[8] All of the commercially available gases were checked for purity by use of a Consolidated Engineering Model 21-401 mass spectrometer and were found to be at least 99% pure, except D_2O (Stohler Isotope) which was not analyzed, and D_2 (Union Carbide) which was *ca.* 6% HD. Because the gases do not vary over orders of magnitudes in their quenching efficiencies (except for NO quenching the phosphorescence), even impurity levels of a few per cent were tolerable.

The thermocouple and Magnevac gauges were calibrated when necessary by the known-volume-ratio expansion method and a Wallace and Tierman 0–50-mm circular diaphragm gauge was used as a reference.

A typical experiment consisted of condensing 200 μ of SO_2 in the right-angle emission cell cold finger with liquid N_2 and adding the selected pressure of quencher gas followed by allowing the SO_2 to vaporize and refill the cell. For those foreign gases condensed by liquid N_2, a technique which measured their partial pressures after the experiment by known-volume expansion was employed. The emission intensities were measured at 3400 (I_f) and 4152 Å (I_p), as described,[8] using in most cases four exciting wavelengths, namely 2750, 2850, 2960, and 3020 Å.

The data were plotted in the usual Stern–Volmer form, $(I_E^\circ/I_E)_\lambda$ *vs.* quencher pressure, where I_E° is an emission intensity of 200 μ of SO_2 and I_E is the same in the presence of a quencher using an exciting wave-

(1) Chemistry Department, Youngstown State University, Youngstown, Ohio 44503.

(2) (a) A. B. Callear, "Photochemistry and Reaction Kinetics," P. G. Ashmore, F. S. Dainton, and T. M. Sugden, Ed., Cambridge University Press, Cambridge, 1967, p 133; (b) A. B. Callear, *Appl. Opt.*, **2**, 145 (1965).

(3) (a) J. I. Steinfeld and W. Klemperer, *J. Chem. Phys.*, **42**, 3475 (1965); (b) J. I. Steinfeld, *ibid.*, **44**, 2740 (1966).

(4) R. L. Brown and W. Klemperer, *ibid.*, **41**, 3072 (1964).

(5) F. Rössler, *Z. Phys.*, **96**, 251 (1935).

(6) G. H. Myers, D. M. Silver, and F. Kaufman, *J. Chem. Phys.*, **44**, 718 (1966).

(7) M. Kaneko, Y. Mori, and I. Tanaka, *ibid.*, **48**, 4468 (1968).

(8) H. D. Mettee, *ibid.*, **49**, 1784 (1968).

Table I: SO_2 Emission Quenching Data Compared with Selected Other Data

Collision partner	σ, Å[a]	$\alpha \times 10^{24}$, cm³[b]	SO_2 $1/Z_{QF}$	SO_2 $1/Z_{QP}$[c]	I_2[d] $1/Z_{v'=18}$	I_2[d] $1/Z_{v'=26}$	NO_2[e] $1/Z_{QF}$	OH[f] $1/Z_{QF}$	$\lvert\Delta\epsilon\rvert$,[g] eV
^3He	2.16	0.204	...	...	...	0.072	...	...	16.9
^4He	2.16	0.204	0.079	0.0041	0.018	0.105	0.04	0.085	16.9
Ne	2.54	0.392	0.14	0.0040	0.056	0.32	...	...	13.1
Ar	3.60	1.63	0.21	0.0053	0.20	0.49	0.08	0.69	8.1
Kr	4.12	2.47	0.26	0.0060	0.45	0.79	...	...	6.9
Xe	4.80	4.01	...		0.98	1.51	...	...	...
H_2	2.83	0.79	0.12	0.0063	0.054	0.078	0.06	0.26	7.7
D_2	2.83	0.79	0.13	0.0057	0.071		...	0.26	7.7
N_2	3.86	1.76	0.28	0.0074	0.22		0.10	0.32	4.9
O_2	3.69	1.60	0.27	0.010	0.27	0.79	0.13	0.54	2.0
NO	3.78	1.70[+]	0.59	1.73	0.73		0.20	...	1.8
CO	3.44	1.95	0.35	0.0082			...	2.3	4.4
CO_2	4.94	2.65	0.63(1.1)[h]	0.0085		2.0	0.27	0.94	2.0
CH_4	4.27	2.60	0.34	0.0068			0.16		4.8
CH_3Cl	...	4.56	...	...		1.5	...		...
CF_4	4.70	4.0[+]	0.53	0.0089			0.39		8.1
H_2O	5.36	1.40[+]	...	...			0.48	2.6	3.0
D_2O	5.36	1.40	1.2	0.028			...		3.0
SF_6	6.08	6.0[+]	0.68	0.016			0.35		2.0
NH_3	...	2.26	...	...		0.90	...		...
SO_2	4.34	3.72	1.0	0.027		1.07	...		0.0
NO_2	4.20	3.[‡]	...	...	...	...	0.24		...
I_2	...	9.3[+]	...	...	4.6	3.4	...		...

[a] Most collision diameters are root-mean square values tabulated in ref *i*. Others from various sources. [b] Polarizabilities are taken directly from ref *j*, except for noble gases and those marked (+). The latter were estimated from an empirical plot of polarizability *vs.* polarization, whose latter values are given in ref *j*. (‡) NO_2 value used was that of N_2O. Noble gas values are given in ref *k*. [c] Involves the assumption that all those $^1SO_2$ molecules which do not fluoresce reach the $^3S_0$ level, the parent level for phosphorescence. [d] Reference 3. [e] Reference 6. [f] Reference 7. The gas kinetic collision diameter of OH* used was 4.0 Å. The gas kinetic collision cross sections were calculated using the accepted expression $(\sigma_{EM})^2 = [\frac{1}{2}(\sigma_E + \sigma_M)]^2$. [g] The absolute value of the electronic energy difference between $^1S_0$ (vibrationally relaxed) and the closest electronic level of the quencher of the same multiplicity if choice was possible. [h] Calculated from data of Greenough and Duncan,[13] using the present collision diameters. [i] W. Kauzmann, "Kinetic Theory of Gases," W. A. Benjamin Co., New York, N. Y., 1966, p 209. [j] Landolt-Bornstein, "Zahlenwerte und Funktionen," Vol. I, Part 3, Springer-Verlag, Berlin, 1951, p 510. [k] W. Edgell, "Argon, Helium and Rare Gases," Vol. I, Ed., G. A. Cook, Interscience, New York, N. Y., 1961, p 151.

length λ. The 90% confidence limits of the slopes showed error limits of *ca.* ±15% for fluorescence quenching and *ca.* ±25% for phosphorescence quenching. The quenching rate constants, k_q, were divided by the calculated gas kinetic collision number to estimate the probability of quenching per collision. This number is effectively the ratio of the quenching cross section to the gas kinetic cross sections.

Results

The basic characteristics of the SO_2 vapor absorption and emission spectra have been outlined elsewhere.[8] The measured emission intensities at 3400 and 4152 Å were taken to correspond to the total fluorescence and phosphorescence intensities, respectively. (About 20% of the intensity at 3400 Å was contributed as fluorescence to the intensity measured at 4152 Å, so that the phosphorescence intensity was corrected accordingly.)

Using a fixed exciting wavelength, fluorescence emission measurements were also made at 3200 and 3650 Å. For the cases of pure SO_2 added in small pressure increments at low pressures (5–50 μ) and of N_2 quenching experiments, the fractional changes in the emission intensities measured at these additional wavelengths were the same as those measured at 3400 Å, for a given pressure change. Thus both the foreign gas and self-quenching of fluorescence data were demonstrated to be independent of the emission wavelength selected.

For the relatively high pressures of SO_2 used here (200 μ) the quenching rate constants were also found to be independent of exciting wavelength. Two experiments using 50 μ of SO_2 with Ar and He showed slightly steeper Stern–Volmer plots for the longer wavelengths of excitation. When proper account of the lifetime differences[8] was taken, however, the same quenching constant was found for all exciting wavelengths.[9]

(9) No exactly analogous experiment was performed for the phosphorescence quenching. It was observed that the relative band intensities showed no dramatic pressure dependence, which is anticipated if the parent levels are vibrationally equilibrated as assigned.

Discussion

The following mechanism is a useful framework for discussion.

$$S_0 + h\nu_n = {}^1S_n \qquad I_a$$

$${}^1S_n = S + h\nu_f \qquad k_1[{}^1S_n] = I_f \quad (1)$$

$${}^1S_n = S \qquad k_{1a}[{}^1S_n] \quad (1a)$$

$${}^1S_n = {}^3S_m \qquad k_{1b}[{}^1S_n] \quad (1b)$$

$${}^1S_n + S = 2S \qquad k_{2a}[{}^1S_n][S] \quad (2a)$$

$${}^1S_n + S = {}^3S_m \qquad k_{2b}[{}^1S_n][S] \quad (2b)$$

$${}^3S_m = S \qquad k_3[{}^3S_m] \quad (3)$$

$${}^3S_m + S = 2S \qquad k_{4a}[{}^3S_m][S] \quad (4a)$$

$${}^3S_m + S = {}^3S_o \qquad k_{4b}[{}^3S_m][S] \quad (4b)$$

$${}^3S_o = S \qquad k_5[{}^3S_o] \quad (5)$$

$${}^3S_o = S + h\nu_p \qquad k_6[{}^3S_o] \quad (6)$$

$${}^3S_o + S = 2S \qquad k_7[{}^3S_o][S] \quad (7)$$

In this mechanism any bimolecular process involving S might equally well involve a quencher molecule M, and in the following these steps will be denoted by the corresponding rate constant primed.

Fluorescence Quenching and Vibrational Relaxation. The present author's earlier work[8] indicated that steps 1a and 1b are unimportant. The recent experiments of Rao, Collier, and Calvert[10] suggest that the relative importance of these unimolecular steps $k_1:k_{1a}:k_{1b}$ is 0.20:0.73:0.07. In neither case are the data compelling, and for the purpose of the present work the question may be put aside since these pathways are unimportant at the pressures used here, compared to steps 2a and 2b.

The standard steady-state treatment of fluorescence quenching gives the following expression.

$$(I_f^\circ/I_f) = 1 + \frac{(k_{2a}' + k_{2b}')}{k_1 + (k_{2a} + k_{2b})[S]}[M] \quad (8)$$

Combining $(k_{2a} + k_{2b}) = k_q$ and $(k_{2a}' + k_{2b}') = k_q'$ and recognizing that at the pressure of SO_2 used the bimolecular term dominates the denominator, it is is easily seen that k_q' may be estimated from the slope of the Stern–Volmer plot. The value of k_q was taken to be the gas kinetic collision number, $k_q = 2.63 \times 10^{-10}$ cm^3 molecules^{-1} sec^{-1}, as previously established.[8,11] The two low SO_2 pressure experiments would be expected to show the observed exciting wavelength dependence of the slope since k_1, the reciprocal fluorescence lifetime, likely decreases with increasing exciting wavelength.[8]

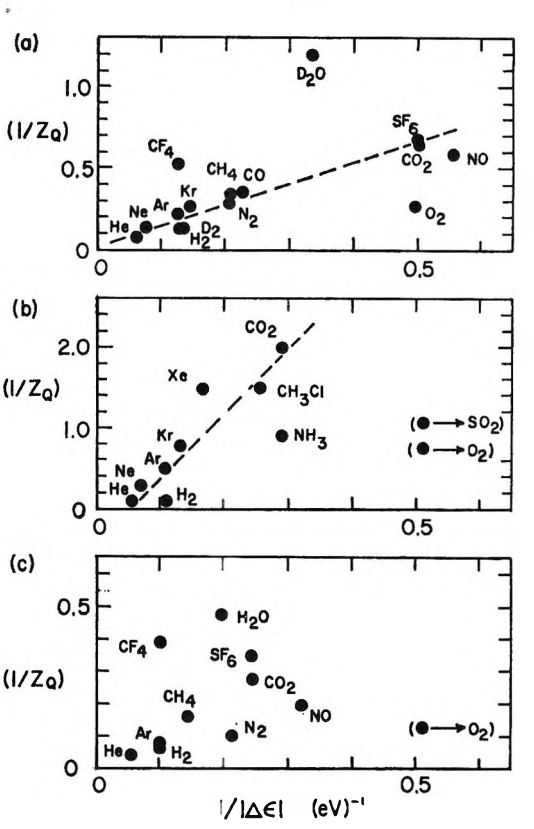


Figure 1. The fluorescence quenching efficiency of various collision partners plotted against the reciprocal absolute value of the smallest electronic energy defect $[\epsilon(\text{Emitter}^*) - \epsilon(M^*)]$ for three systems of fluorescence: (a) SO_2 ($\tilde{A}(^1B_1)$); (b) I_2 ($B\ ^3\Pi_{0u}^+$) ($v' = 25$); and (c) NO_2 ($\tilde{A}\ ^2B_1$).

The fact that k_q' is independent of exciting wavelength, and the values themselves are fairly close to the gas kinetic values, precluding extensive vibrational relaxation (if it occurs at all), suggests that the quenching cross section of $^1SO_2$ is independent of its vibrational energy content. This may be compared to the case of I_2 (Table I) where, even accounting for differences in the fluorescent lifetime[12] for $v' = 15$ or 25, it appears more probable to quench those excited states with more vibrational energy. Turner[13] reported this fact some years ago and Steinfeld[3b] has since documented it extensively.

Since the results indicated there was no observable dependence of the quenching constant k_q' on the fluorescence emission wavelength (for N_2 and for pure SO_2 and presumably the other partners), it is reasonable to conclude that little or no vibrational relaxation is occurring in $^1SO_2$ prior to emission. This is in accord

(10) N. Rao, S. Collier, and J. G. Calvert, *J. Amer. Chem. Soc.*, submitted for publication.

(11) K. F. Greenough and A. B. F. Duncan, *ibid.*, **83**, 555 (1961).

(12) Ref 3 and Chutjian, J. K. Link, and L. Brewer, *J. Chem. Phys.*, **46**, 2666 (1967), are not in complete accord on their actual values of the radiative lifetimes of I_2 ($B\ ^3\Pi_{0u}^+$) at various levels. These differences, however, are obscured by the pronounced exciting wavelength dependence of quencher efficiencies.

(13) L. A. Turner, *Phys. Rev.*, **41**, 627 (1932).

with the facts that the emission always begins at the exciting wavelength, independent of pressure, and that the k_q' values are close to the gas kinetic values. That some amount of vibrational relaxation is occurring with a fairly large cross section is suggested by the apparent requirement for parent levels other than those thought to be produced optically to explain the "resonance" bands.[8]

On the other hand, Myers, Silver, and Kaufman[6] observe for NO_2 that k_q' is apparently larger for fluorescent emission wavelengths near the exciting "line" than for those measured at longer wavelengths. That is, for the same amount of added quencher the shorter fluorescence wavelengths are apparently preferentially quenched. Using 4358-Å excitation, the difference amounts to a factor of 3 in going from an emission wavelength of 4680 to 6330 Å using either Ar or NO_2 itself. This "red shift" in the fluorescence intensity distribution with increased pressure plainly indicates vibrational relaxation is occurring prior to emission.[14]

It is interesting that the cross sections for fluorescent quenching of both NO_2 and SO_2 are quite similar and yet vibrational relaxation appears to be much more probable for NO_2. However, it should be borne in mind that the intensity wavelength distribution of fluorescence of SO_2 is relatively independent of exciting wavelength (excepting that portion on the short wavelength shoulder). It is therefore still possible that appreciable vibrational relaxation in $^1SO_2$ prior to emission might occur unnoticed. The earlier evidence suggests that it does occur but only slightly.

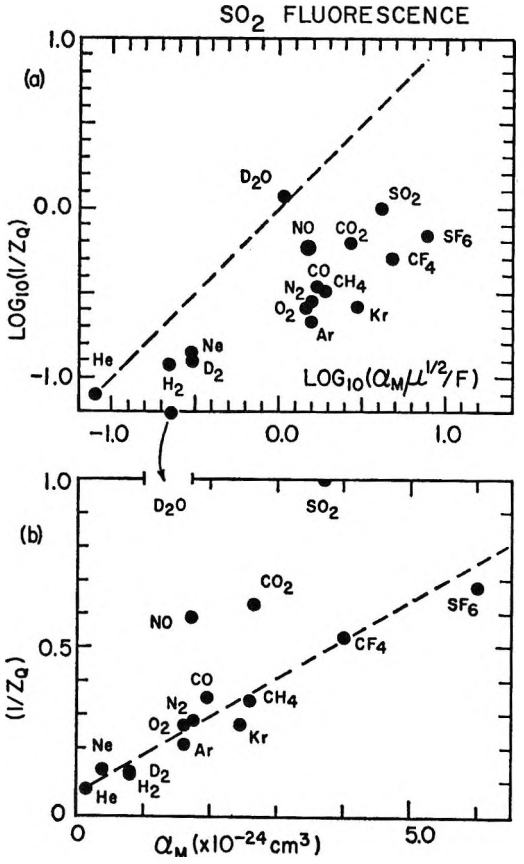


Figure 2. SKB plot (a) and polarizability plot (b) of the experimental quenching probability of various collision partners with SO_2 [$(\tilde{A}^1B_1)$].

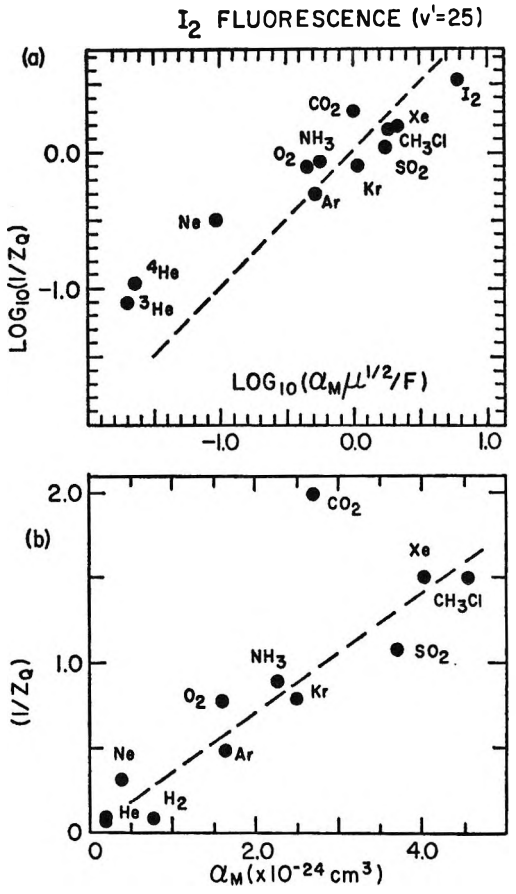


Figure 3. SKB plot (a) and polarizability plot (b) of the experimental quenching probability of various collision partners with I_2 ($B^3\Pi_{0u}^+$) ($v' = 25$).[3a]

Fluorescence Quenching Parameter. The values of $(1/Z_{QF})$ listed in Table I show the quenching efficiency of various collision partners for both SO_2 and NO_2 range over about one order of magnitude, except possibly for "chemically reactive" species such as H_2O or D_2O. It so happens that the products of the square root of the reduced mass of the collision complex and the polarizability of the collision partner extend over about two orders of magnitude. In these cases a Steinfeld–Klemperer–Brown[3,4] (SKB) type plot "overpredicts" the quenching efficiency, normalized to He, or shows large scatter if normalized to a more suitable base.

Various terms were selected to relate these quenching efficiencies and were found unsuccessful for SO_2 and other systems. Among these were the ionization po-

(14) This effect has been noted by S. E. Schwartz, private communication, whose additional finding of a shorter fluorescence lifetime of NO_2 with shorter exciting wavelengths parallels that suggested for SO_2.

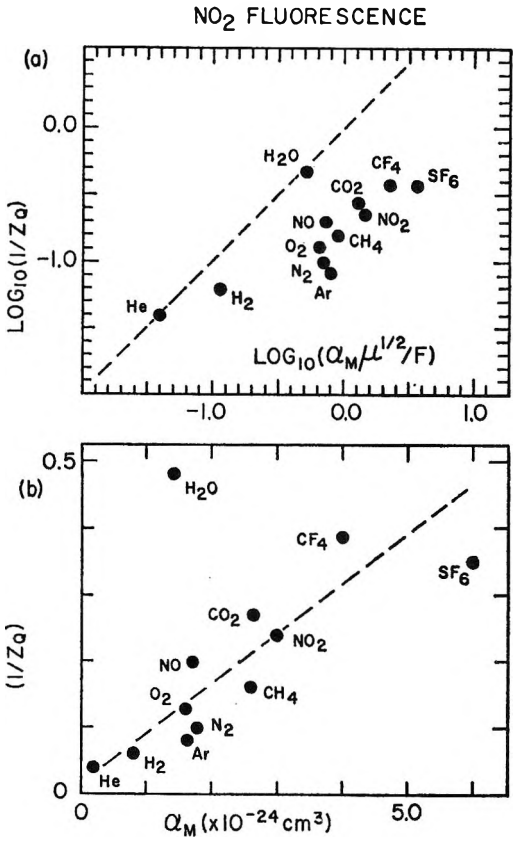


Figure 4. SKB plot (a) and polarizability plot (b) of the experimental quenching probability of various collision partners with NO_2 ($\tilde{A}\ ^2B_1$).[6]

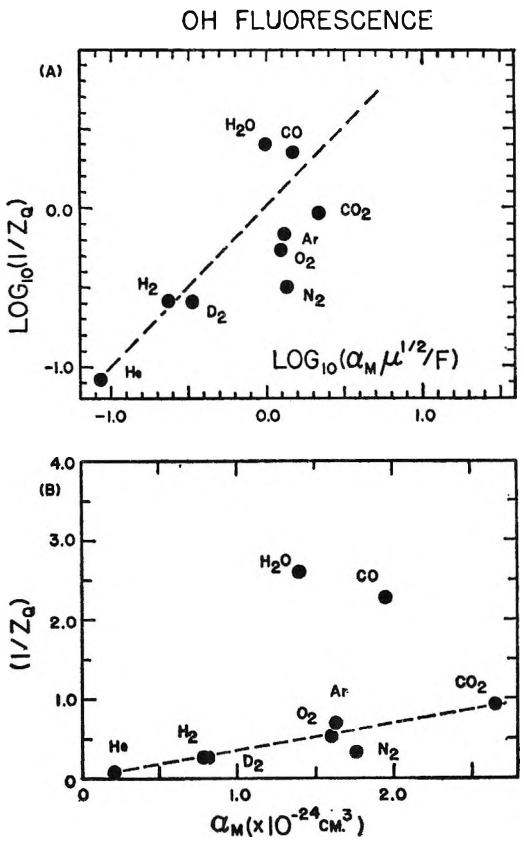


Figure 5. SKB plot (a) and polarizability plot (b) of the experimental quenching probability of various collision partners with OH ($A\ ^2\Sigma^+$).

tential of the quencher,[15] the number of electrons in the quencher molecule, and the spin-orbit parameter for the heaviest atom in the quencher molecule. The first of these failed because the ionization potential was not variable enough and the spin-orbit term was far too variable. The fourth, the reduced mass term, was tried alone and showed much scatter.

Because of the great attention focused on the "energy defect" (normally the residual energy converted into translation after a near-resonant transfer) in collisional relaxation phenomena,[2] a plot of $|\Delta\epsilon|^{-1}$, the reciprocal absolute electronic energy difference between the relaxed $^1SO_2$ and the nearest electronic level of the collision partner (of the same multiplicity if available), was attempted. Figure 1a shows such a plot to be reasonably successful for $^1SO_2$ although it is somewhat less successful for I_2, with a few anomalous points in each case which may be rationalized. Unfortunately such was not the case for NO_2 (Figure 1c). Figures 2–5 compare the SKB plots with those based solely on polarizability.

The points on the SKB plots may be shifted to the left or right, depending on the normalizing factor F, which was selected in each case to correctly predict ^4He. In all of these systems, however, the scatter is still appreciable (even on a log–log grid), and the experimental data do not generally show as wide a divergence as the predicted values. It may be noteworthy that for the polarizability plots those anomalously efficient quenchers are reactive, have dipoles, or have lower-lying electronic levels. (Unfortunately, some adequately predicted cases have similar characteristics.)

Phosphorescence Quenching. For the pure SO_2 system, the limit of the inverse phosphorescence yield at high pressure is

$$Q_p^{-1} = \text{constant} + \frac{(k_{2a} + k_{2b})(k_{4a} + k_{4b})k_7}{k_{2b}k_{4b}k_6} \quad (9)$$

If all of those $^1SO_2$ which do not fluoresce become ^3S_o, so that $k_{2a} = k_{4a} = 0$, then the Stern–Volmer slope is (k_7/k_6). Using Duncan and Caton's value[16] of the phosphorescent lifetime at low SO_2 pressure as $(k_6)^{-1}$, k_7 may be estimated as 7×10^{-12} cm^3 molecule^{-1} sec^{-1}. This corresponds to about 35 gas kinetic collisions, as a minimum, which are required to self-quench ^3S_o. Naturally if precursors to ^3S_o other than those ^1S_n which fluoresce (and ^3S_o molecules) are lost by other

(15) A. B. Callear, *Chem. Soc. Ann. Rep.*, 61, 48 (1964).

(16) R. B. Caton and A. B. F. Duncan, *J. Amer. Chem. Soc.*, 90, 1945 (1968).

channels k_7 would be reduced accordingly. The results of most other workers[10,16,17] indicate this is happening so that perhaps several hundred to several thousands of gas kinetic collisions are required to collisionally quench ^3S_o.

For the present purposes it is possible to estimate a limiting, high pressure slope for I_p°/I_p as

$$I_p^\circ/I_p = \text{constant} + \frac{k_7'(k_{4a}' + k_{4b}')(k_{2a}' + k_{2b}') \cdot k_{2b}k_{4b}}{k_7(k_{4a} + k_{4b})(k_{2a} + k_{2b}) \cdot k_{2b}'k_{4b}'[S]} \cdot [M] \quad (10)$$

If the same assumption is again made, then

$$I_p^\circ/I_p = \text{constant} + \frac{k_7'}{k_7 \cdot [S]} \cdot [M] \quad (11)$$

and values of k_7' may be estimated. Converting these values in the usual way into a quenching probability per gas kinetic collision, one finds a minimum of 100 to 200 collisions required for most partners except NO to remove ^3S_o. Because of the varying correctness of the major assumption with each M and its questionable validity to begin with, further comments are deferred.

Conclusion

The present collision quenching efficiencies for foreign gases with electronically excited $^1SO_2$, and those measured by others for I_2, NO_2, and OH, are found to be adequately predicted by use of only the polarizability of the quenching partner. It would thus appear that the dependence of quenching efficiency on the duration of the collision is unnecessary in these cases. If this relationship is physically meaningful then the collision quenching of fluorescence may involve an induced dipolar field of sufficient strength to enhance an intersystem crossing process.

Steinfeld's formal expression for quenching,[3a] which is based on conventional scattering theory that leads to a reduced mass term in the final expression, does not specify a quenching mechanism.[18] In spite of this the formalism may be used[3b] to treat the collision quenching of fluorescence, at least as for I_2 in the case of the breakdown of molecular symmetry caused by a van der Waals interaction. On this basis a polarizability relationship is not surprising but a satisfying quantum mechanical description of these collisions has yet to be achieved.

Acknowledgments. The author is extremely grateful to The Robert A. Welch Foundation for their support of this work and to Dr. W. Albert Noyes, Jr., for his continued interest. The author also thanks the many colleagues at the University of Texas with whom this work was discussed. Finally the cooperation of Drs. Rao, Collier, and Calvert for sending a preprint of their work is gratefully acknowledged.

(17) S. J. Strickler and D. B. Howell, *J. Chem. Phys.*, 49, 1947 (1968).

(18) It should be added that a reduced mass term may be correct, but that it might not always be detectable.

Aspects of the Pulse Radiolysis and γ Radiolysis of Alkyl Iodides and Their Mixtures[1]

by C. Capellos[2a] and A. J. Swallow[2b]

Nuclear Technology Laboratory, Department of Chemical Engineering and Chemical Technology, Imperial College, London, S.W.7, England, and the Paterson Laboratories, Christie Hospital and Holt Radium Institute, Manchester 20, England *(Received November 22, 1968)*

Liquid alkyl iodides have been subjected to pulse radiolysis and γ radiolysis. A 2-μsec electron pulse produces a broad transient absorption band with a peak near 400 nm, with $G\epsilon$ equal to 18,000, 26,000, and 34,000 for methyl, ethyl, and isopropyl iodides, respectively. This band disappears in a second-order reaction, and is considered to be mainly due to an iodine atom alkyl iodide charge-transfer complex. Its extinction coefficient at the maximum is 9000 l. mol^{-1} cm^{-1} for all three iodides. A weaker and more rapidly decaying absorption is seen in the region 650–750 nm attributable to a positively charged species. The band with the peak near 400 nm appears with the same intensity when dissolved oxygen is present, but the decay kinetics are different. In mixtures of methyl and isopropyl iodides its formation is a nonlinear function of composition. In solutions of isopropyl iodide in cyclohexane, the concentration dependence of the band suggests that the charge-transfer complex has its origin partly in an ion-recombination process. Initial yields of iodine and HI have been determined for the γ radiolysis of alkyl iodides. The yield of HI falls off rapidly with dose, reaching a plateau at high doses. In mixtures of liquid methyl and isopropyl iodides, the dependence of the iodine and HI yields on composition follows a similar curve to that of the band at 400 nm in the pulse radiolysis. The I_2 and HI yields vary with composition of mixture in quite a different way at −196°.

Alkyl iodides are relatively simple. The molecules have a high electron affinity and contain one bond (C–I) which is much weaker than the others. They can readily be obtained in the liquid, solid, and gas phases, and striking observations can be made when the materials are irradiated under appropriate conditions and examined by techniques like electron spin resonance spectroscopy, mass spectrometry, and ultraviolet absorption spectrophotometry. For these reasons their radiation and photochemistry has received extensive study, and the results have provided interesting information about the short-lived chemical species which can be derived from them. The literature on the radiation chemistry of the alkyl iodides up to mid-1958 has been exhaustively reviewed elsewhere.[3] Among the more recent studies may be mentioned some of those by Hamill and his school[4] and Willard and his school.[5] We now report further work on the radiation chemistry of the alkyl iodides, paying attention to the phenomena occurring when mixtures are irradiated. Among other techniques, we have used pulse radiolysis to examine transient species.

Experimental Section

Alkyl iodides were obtained from Hopkin and Williams or British Drug Houses and were purified in the dark by passing through a 60-cm column of silica gel to remove polar or unsaturated impurities, followed by vacuum distillation through a 60-cm fractionating column packed with glass rings, the middle cut being collected. The purified iodides contained no detectable iodine or hydrogen iodide. Potassium iodide, iodic acid, and carbon tetrachloride were all Analar, from Hopkin and Williams, and were used without further purification. Ethylene was supplied by Ethylene Plastique. Nitrous oxide was obtained from B.O.C.

For the pulse-radiolysis experiments, samples were deaerated by bubbling with argon, stated to contain less than 6 ppm of oxygen. The iodides were cooled with ice water during the degassing, to minimize evaporation. To prepare samples for γ irradiation, the alkyl iodide was placed together with phosphorus pentoxide in a deaeration flask on a vacuum line and deaerated by the freezing-pumping-thawing technique. When the irradiated sample was to be analyzed for iodine, the alkyl iodide (10 ml) was distilled into an irradiation vessel connected to a spectrophotometer cell and sealed off under vacuum. Spectrophotometric measurements could be made after interrupting the irradiation without exposing the sample to air. Where the sample was to be analyzed for hydrogen iodide, the alkyl iodide (5 ml) was distilled through a constriction into an ampoule which was subsequently sealed off.

(1) From the Ph.D. dissertation of C. Capellos, University of London, England. The work reported here has been sponsored in part by the Aeronautical Research Laboratory, O.A.R., through the European Office, Aerospace Research, U. S. Air Force, Contract AF.61(052)-456.

(2) (a) Department of Chemistry, Brookhaven National Laboratory, Upton, N. Y. 11973. (b) Paterson Laboratories, Christie Hospital and Holt Radium Institute, Manchester 20 England.

(3) A. J. Swallow, "Radiation Chemistry of Organic Compounds," Pergamon Press, Oxford, England, 1960.

(4) (a) R. F. Pottie, R. Barker, and W. H. Hamill, *Radiation Res.*, 10, 644 (1959); (b) H. A. Gillis, R. R. Williams, and W. H. Hamill, *J. Amer. Chem. Soc.*, 83, 17 (1961); (c) E. P. Bertin and W. H. Hamill, *ibid.*, 86, 1301 (1964); (d) S. Z. Toma and W. H. Hamill, *ibid.*, 86, 148 (1964); (e) J. P. Mittal and W. H. Hamill, *ibid.*, 89, 5749 (1967).

(5) (a) H. J. Arnikar and J. E. Willard, *Radiation Res.*, 30, 204 (1967); (b) R. F. C. Claridge and J. E. Willard, *J. Amer. Chem. Soc.*, 88, 2404 (1966); (c) R. F. C. Claridge and J. E. Willard, *ibid.*, 89, 510 (1967).

Pulse-radiolysis experiments were done with a 2-μsec pulse from the 4-MeV electron linear accelerator at AEI, Trafford Park, Manchester, using the equipment of Keene.[6] γ Irradiations were performed with a 700-Ci ^{60}Co source.[7] When the vessel containing the spectrophotometer cell was used, the cell was shielded with lead during irradiation.

The dose absorbed by the alkyl iodides was calculated on the basis of that absorbed by the Fricke dosimeter. For the electron irradiations, the modified Fricke dosimeter was used (oxygen-saturated 10^{-2} M $FeSO_4$ in 0.8 N H_2SO_4),[8] and the dose in the alkyl iodides was calculated on the basis of the relative electron densities of the iodide and the dosimeter solution. An additional correction, amounting to about 4%, was made to allow for the difference in depth–dose distribution between the iodide and the dosimeter, which caused the maximum in the depth–dose curve to shift out of the path of the light beam. For the γ irradiations the relative doses in the dosimeter solution and in the alkyl iodides was calculated from the relative mass absorption coefficients,[9] so taking into account absorption by the photoelectric effect, and a correction was made for a soft component in the γ irradiation.[10]

Iodine was determined spectrophotometrically at its absorption maximum at 480 nm. The molar extinction coefficient at this wavelength was found to be 1350 l. mol^{-1} cm^{-1} for solutions in all alkyl iodides used. At 360 nm the extinction coefficient was 2540 l. mol^{-1} cm^{-1} for iodine in methyl, ethyl, and isopropyl iodides. Hydrogen iodide was determined by freezing the irradiated sample with liquid nitrogen, then opening the ampoule and placing 10 ml of water on top of the frozen alkyl iodide. After melting, the HI was extracted into the water, which was then washed twice with carbon tetrachloride. The efficiency of the extractions was checked by means of pH measurements using 10^{-4} M HI. In the analysis of irradiated samples iodic acid was added to oxidize the HI to iodine, which was then extracted into cyclohexane, and from that into aqueous potassium iodide. The I_3^- complex so obtained was determined spectrophotometrically at 350 nm taking the molar extinction coefficient to be 26,400 l. mol^{-1} cm^{-1}.[11]

Results

Pulse radiolysis of deaerated alkyl iodides produced broad transient absorption spectra with peaks near 400 nm. The absorption spectra at various times after a ~5000-rad pulse are shown for ethyl iodide in Figure 1. Initial values of $G\epsilon_{400}$ (*i.e.*, the product of the number of molecules of the species formed per 100 eV and the molar extinction coefficient at 400 nm) were obtained by using pulses of 600 and 1000 rads in order to reduce the decay of the species during and immediately after the pulse to a negligible level. The values found were 18,000, 26,000, and 34,000 (molecules/100 eV) (l. mol^{-1} cm^{-1}) for methyl, ethyl, and isopropyl iodides, respectively. Taking all errors into account these values are considered to be accurate to about 10%. After the transient absorptions had disappeared, the residual permanent absorption spectra were indistinguishable from the spectra of solutions of iodine in alkyl iodides and corresponded to the same G values for iodine formation as found with γ radiation.

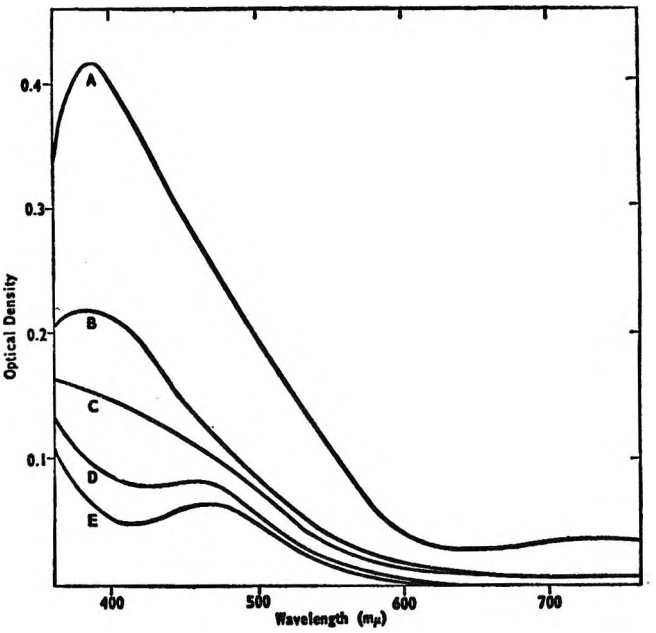


Figure 1. Absorption spectra of ethyl iodide at various times after a pulse of fast electrons (~5000 rads, optical path length 1.6 cm): A, immediately after pulse; B, 5 μsec later; C, 10 μsec; D, 20 μsec; E, 40 μsec.

The decay of the transient absorptions at 410 nm (where solutions of molecular iodine in alkyl iodides have a minimum in their absorption curve) followed second-order kinetics, independently of dose in the range 1000–5000 rads. Values of k/ϵ_{410} were 1.7×10^6, 7×10^5, and 1.1×10^6 cm sec^{-1} for methyl, ethyl, and isopropyl iodides, respectively, where k is the rate constant defined by $-d[R]/dt = k[R]^2$, and R is the species being observed. Gover and Porter had found $k/\epsilon_{410} = 8 \times 10^5$ cm sec^{-1} in the flash photolysis of iodine in ethyl iodide.[12]

Air-saturated solutions of alkyl iodides exhibited similar absorption spectra after the pulse to the air-free solutions. However, the pattern of decay was different. In the air-saturated solutions the absorption around 500 nm decreased rapidly over a microsecond or so and

(6) J. P. Keene, *J. Sci. Instrum.*, **41**, 493 (1964).
(7) G. R. Hall and M. Stroat, *J. Imp. Coll. Chem. Eng. Soc.*, **13**, 80 (1961).
(8) J. K. Thomas and E. J. Hart, *Radiation Res.*, **17**, 408 (1962).
(9) C. Capellos, Ph.D. Thesis, University of London, England, 1965.
(10) W. Bernstein and R. H. Schuler, *Nucleonics*, **13**, No. 11, 110 (1955).
(11) G. Meshitsuka and M. Burton, *Radiation Res.*, **10**, 499 (1959).
(12) T. A. Gover and G. Porter, *Proc. Roy. Soc.*, **A262**, 476 (1961).

then increased again, reaching a final level much higher than in the absence of oxygen. This observation is consistent with the higher yield of iodine in γ irradiations when oxygen is present.[13]

Mixtures of methyl and isopropyl iodides have been pulsed, and the initial absorption at 400 nm determined as a function of composition. The effect of composition expressed as volume percentage is shown in Figure 2. Energy partition may be nearly proportional to valence electron fraction.[14] The greatest deviation between volume percentage and valence electron percentage occurs near 50 vol %, which is 46.3 valence electron percentage methyl iodide, so that a plot of absorption at 400 nm against valence electron percentage would differ only slightly from Figure 2.

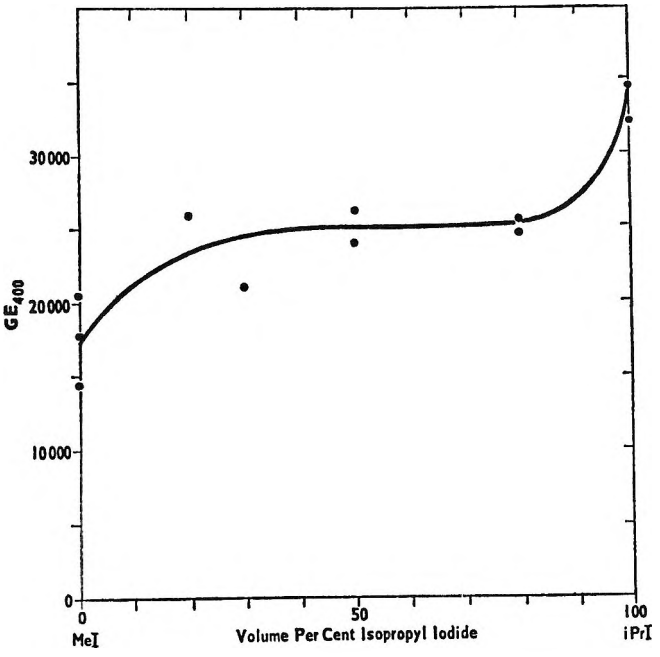


Figure 2. Product of G value and extinction coefficient at 400 nm for mixtures of alkyl iodides (~5000 rads).

Pulses of radiation, ~5000 rads, were given to solutions of isopropyl iodide in cyclohexane. Broad absorptions were seen as in pure alkyl iodides. The value of $G\epsilon_{410}$ was determined as a function of composition and the G value for transient was calculated on the basis of ϵ_{410} 8500 l. mol^{-1} cm^{-1} (see Discussion). The result is shown in Figure 3. Saturation with nitrous oxide produced no effect on the initial absorption at 410 nm.

The formation of iodine was measured for the γ irradiation of pure liquid alkyl iodides at doses of up to about 10^{19} eV/g. Initial yields (molecules I_2 per 100 eV absorbed) were calculated from the linear part of the yield–dose plot, and found to be G = 1.33 for methyl iodide, G = 2.01 for ethyl iodide, and G = 2.90 for isopropyl iodide, in good agreement with previous work.[15] Ethylene at a pressure of 254 mm had no

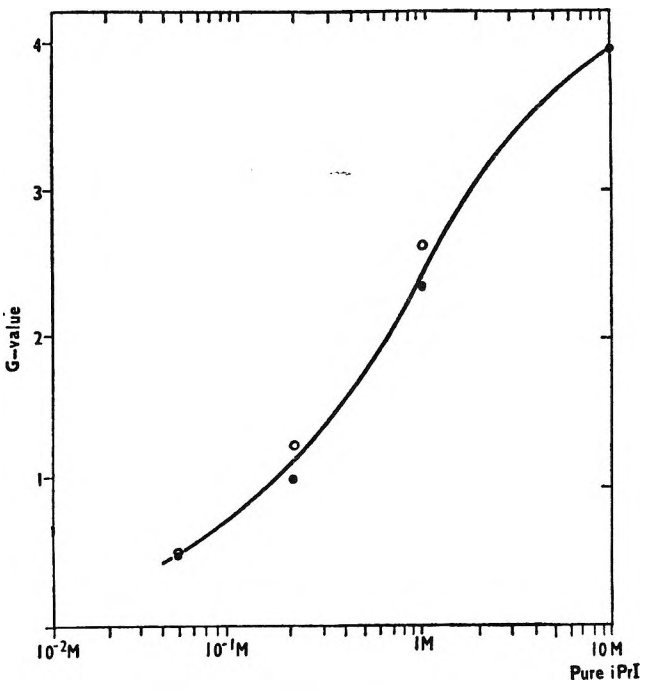


Figure 3. Yield of transient absorbing at 410 nm, in pulse radiolysis of solutions of isopropyl iodide in cyclohexane: ●, without N_2O; ○, N_2O (120 mM).

effect on the yield of iodine from ethyl iodide, but saturation of the liquid with air gave initial yields of G = 3.81 for methyl iodide and G = 4.03 for ethyl iodide. In the presence of oxygen at a pressure of 842 mm, the yield of iodine from methyl iodide was G = 4.92. At −196°, iodine formation from crystalline alkyl iodide was found to be linear with dose up to about 10^{19} eV/g. For methyl iodide the yield was G = 0.37 and for isopropyl iodide, G = 0.57 Hornig and Willard have reported G = 0.32 for methyl iodide, in agreement with our result, but found G = 0.325 for isopropyl iodide.[16] The discrepancy may be connected with the fact that alkyl iodides can exist at low temperatures in glassy as well as crystalline forms: for ethyl iodide, where a comparison could be made, the iodine yields in the glassy form were three times as great as in the crystalline form.[16]

The formation of hydrogen iodide in the γ irradiation of pure liquid alkyl iodides was linear with dose up to about 3×10^{17} eV/g but fell off at larger doses. G values were calculated from the linear part of the curve. The yields obtained for methyl, ethyl, isobutyl, and isopropyl iodides are plotted in Figure 4 as a function of the number of hydrogen atoms present in the β position in the molecule. The G values are higher than those reported previously,[4a,5a] presumably because of the

(13) Reference 3, p 100.

(14) A. J. Swallow, *Discussions Faraday Soc.*, 36, 273 (1963); A. MacLachlan, *J. Amer. Chem. Soc.*, 82, 3390 (1960).

(15) Reference 3, p 99.

(16) E. O. Hornig and J. E. Willard, *J. Amer. Chem. Soc.*, 79, 2429 (1967).

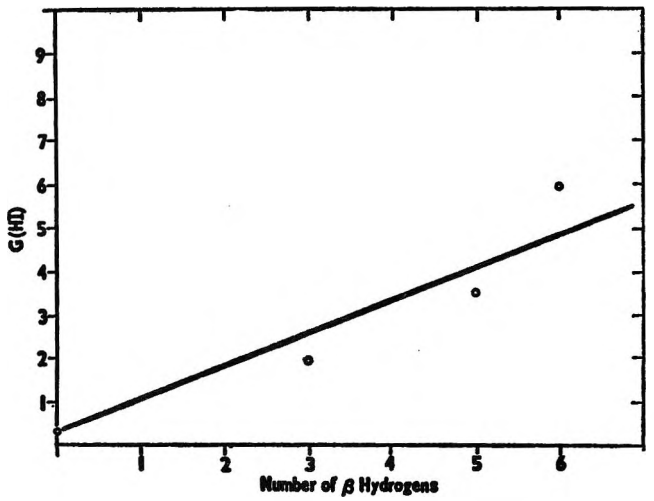


Figure 4. Initial yield of hydrogen iodide in the γ radiolysis of alkyl iodides as a function of the number of β-hydrogens atoms in the molecule.

lower doses used here. Using ethyl iodide, it was shown that ethylene at a pressure of 760 mm reduced the yield of hydrogen iodide to about half at a dose of 3.4×10^{20} eV/ml. At $-196°$ the initial yield of hydrogen iodide from pure crystalline methyl iodide was $G = 0.55$ and from pure crystalline isopropyl iodide $G = 7.00$.

Yield–dose curves for iodine formation in the γ irradiation of various mixtures of alkyl iodides were measured, and initial yields were calculated. The iodides chosen for these studies were methyl iodide and isopropyl iodide, since these show the lowest and highest yields, respectively, when the pure liquid is irradiated. The effect of composition on yield for irradiation in the liquid phase is shown in Figure 5, and for irradiation at $-196°$ in Figure 6. While preparing the frozen iodides for irradiation, it was noted that whereas outside the range 55–85% isopropyl iodide the frozen mixture was opaque, the mixtures within this range were more transparent (*i.e.*, tended to the glassy form) being most transparent at 70% isopropyl iodide. Yield–dose curves were also obtained for the formation of hydrogen iodide (Figure 7). For the mixtures as for the pure iodides the yields of hydrogen iodide began to fall off at much lower doses than the yields of iodine. The initial yields were estimated from curves like those in Figure 7. The effect of composition on yield is shown in Figure 5. Similar experiments were done at $-196°$. The effect of composition on initial hydrogen iodide yield at $-196°$, calculated from the linear portion of yield–dose curves, is shown in Figure 6.

Discussion

The absorption spectra seen in the alkyl iodides at 5 μsec after a radiation pulse, shown for ethyl iodide in Figure 1, resemble that already published for cyclohexyl

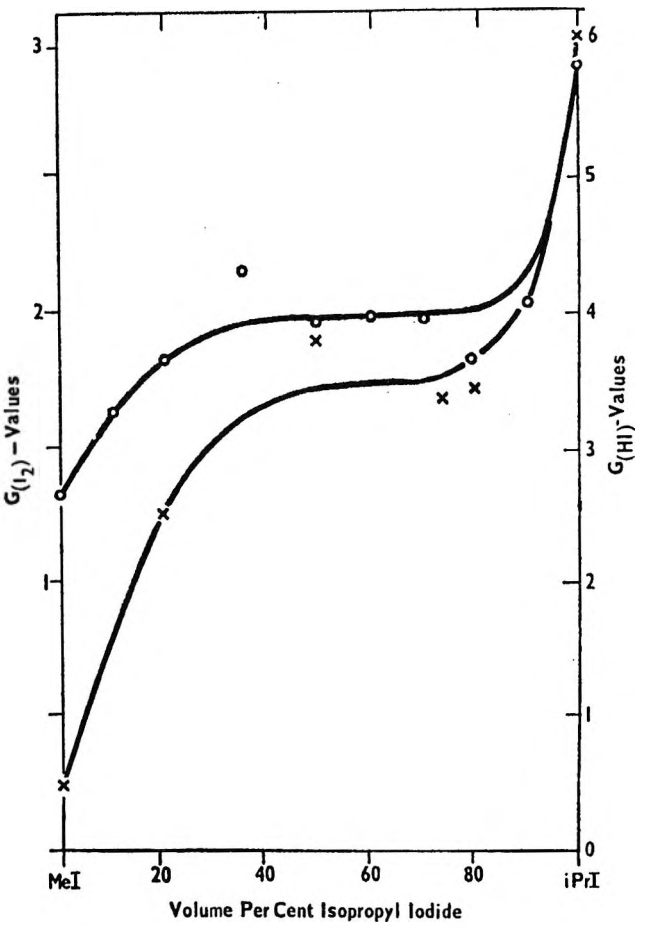


Figure 5. Yield of iodine and HI in γ radiolysis of mixtures of methyl and isopropyl iodide at room temperature: O, iodine; ×, HI.

iodide.[17] An additional broad absorption above ~620 nm is now seen, which decays almost to zero within 5 μsec. The main band with a peak near 390 nm is attributed to a charge-transfer complex between iodine atoms produced by the radiation and the parent alkyl iodide. Gover and Porter had previously seen a similar band in the flash photolysis of iodine in ethyl iodide, attributed to the iodine atom–ethyl iodide charge-transfer complex, but also saw a separate band at 490 nm.[12] Since no such band appears in pulse radiolysis, and since the use of flash photolysis could conceivably lead to photodecomposition of the solvent, it is suggested that the separate band near 490 nm in Gover and Porter's experiments may have been due to the presence of iodine molecules produced by the flash. It cannot be excluded that some molecular iodine would be produced directly by the pulse in the radiation case, but with an extinction coefficient of only 1350 l. mol^{-1} cm^{-1}, any molecular iodine could only account for a small fraction of the initial absorption in the neighborhood of 490 nm. After the transients produced by the radiation have decayed, the residual absorption spec-

(17) M. Ebert, J. P. Keene, E. J. Land, and A. J. Swallow, *Proc. Roy. Soc.*, A287, 1 (1965).

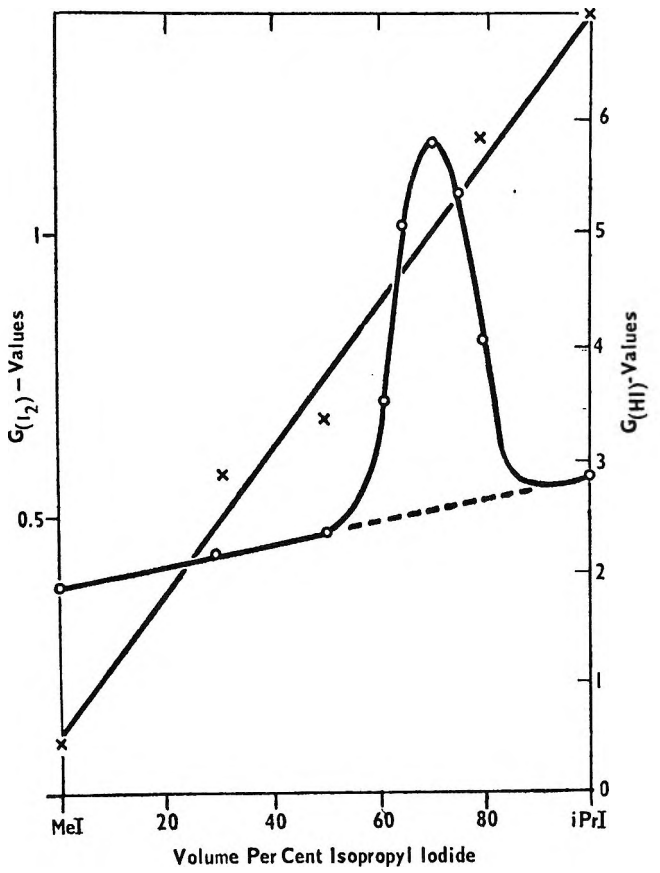


Figure 6. Yield of iodine and HI in γ radiolysis of mixtures of methyl and isopropyl iodide at −196°: ○, iodine; ×, HI.

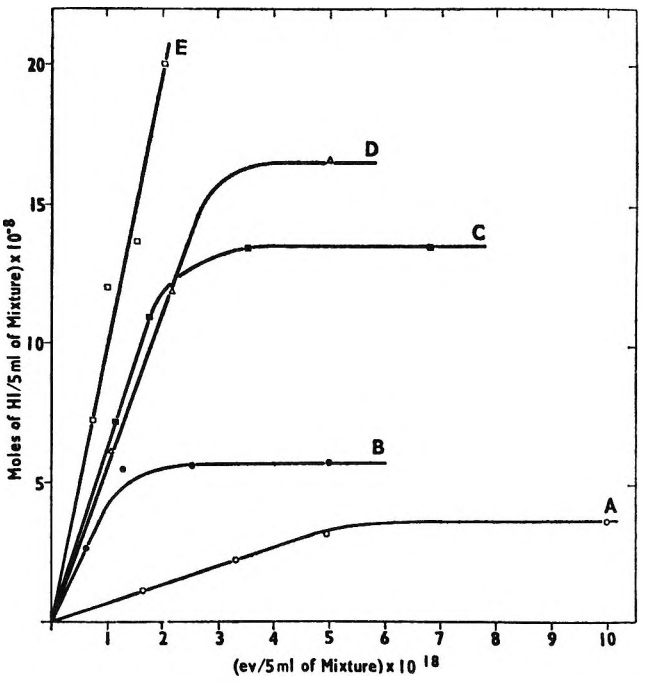


Figure 7. Production of HI as a function of dose in the γ radiolysis of mixtures of alkyl iodides at room temperature: A, pure methyl iodide; B, 20 vol % isopropyl iodide; C, 50 vol % isopropyl iodide; D, 75 vol % isopropyl iodide; E, 100% isopropyl iodide.

trum is, as might be expected, entirely attributable to molecular iodine together with its charge-transfer complex with the solvent.

The transient spectrum seen in pulse radiolysis may be compared with the spectra seen in the γ radiolysis of low-temperature glasses by Claridge and Willard[5b,c] and Hamill and colleagues.[4c,e] The low-temperature glasses, whether pure alkyl iodides or solutions of alkyl iodides in hydrocarbons, exhibit several overlapping absorption bands between the wavelength where the solvent ceases to absorb and 900 nm, the highest wavelength for which results are reported. Among the bands seen is a strong one with a peak at 760 nm which may be due to $(RI)_2^+$ or to R_2I^+ formed by the ion–molecule reaction.[4a]

$$RI^+ + RI \rightarrow R_2I^+ + I$$

It may be that the weak broad absorption with a peak above 700 nm shown in Figure 1 is due to this species. The disappearance of this band within 5 μsec suggests that most of the positive species have reacted with negative species well within 5 μsec. The reason that the pulse-radiolysis spectrum is simpler than the low-temperature glass spectrum may be that the charged species are essentially absent after a microsecond or so. If this is correct, the spectrum measured some nanoseconds after a short pulse of radiation may resemble the spectra seen in glasses rather than the spectrum of Figure 1.

It is possible to obtain an estimate for the extinction coefficient of the charge transfer complex from the present results. If it were to be assumed that the G value for the charge-transfer complex were twice that of the I_2 finally formed, the values of $G\epsilon_{400}$ would lead to extinction coefficients at 400 nm of 6800, 6500, and 6100 l. mol^{-1} cm^{-1} for methyl, ethyl, and isopropyl iodide, respectively. However, if some of the I_2 is formed without the intermediate formation of detectable charge-transfer complex the true extinction coefficients would be higher than this. A higher extinction would also result if some of the molecular iodine is formed through the reaction of aliphatic radicals with hydrogen iodide after the pulse. Consequently, the values given above may be lower limits. A value of ϵ_{490} of 13,000 l. mol^{-1} cm^{-1} was obtained for the ethyl iodide complex by Gover and Porter, from their flash photolysis experiments, based on the assumption that the bimolecular disappearance of transient at 410 nm was diffusion controlled. This assumption certainly appears to be valid for the cyclohexane–iodine atom complex, where the experimental rate constant for decay[17] is 1.06×10^{10} l. mol^{-1} sec^{-1}. From Gover and Porter's spectrum, the extinction coefficient at 400 nm would be almost identical with the extinction they give at 490 nm. The disappearance of absorption at 410

nm in the pulse radiolysis of ethyl iodide cannot be ascribed simply to the bimolecular reaction of the charge-transfer complex, because of the likely involvement of the reaction of alkyl radicals with HI. However, it is noted that our value of k/ϵ is very similar to Gover and Porter's, so that the reaction with HI may not greatly affect the observed decay kinetics. In the case of methyl iodide the kinetics will be even less affected by HI, because the G value for HI is so small. If the diffusion-controlled rate for methyl iodide is taken to be 1.5×10^{10} l. mol^{-1} sec^{-1}, the extinction coefficient at 400 nm calculated from our value of k/ϵ_{410} would be 10,000. Taking all these considerations into account we take our best value for the extinction coefficient at 400 nm to be 9000 ± 2000 l. mol^{-1} cm^{-1} (8500 at 410 nm). There is no reason to suppose that the extinction coefficients for the different iodides studies are significantly different from each other within the error quoted. This is in line with the behavior of the I_2 alkyl iodide charge transfer complexes: for these complexes the principal absorption maximum is very close to the solvent cutoff at ~350 nm, but at 360 nm where absorption due to the solvent is not important and yet the complex absorbs strongly, the extinction coefficient for methyl, ethyl, and isopropyl iodides is the same.

The apparently biphasic effect of composition on the value of $G\epsilon$ after the pulse, shown in Figure 2, seems likely to be due to changes in the G value for the charge-transfer complex. We assume that the primary processes in the radiolysis of the alkyl iodides are excitation to levels which lead to decomposition without ionization, and excitation to levels where the molecule becomes ionized. The ejected electrons would be captured dissociatively by different alkyl iodide molecules. It is proposed that excited and ionized alkyl iodide molecules are capable of transferring their excitation energy or charge to other alkyl iodide molecules before decomposition occurs. It is suggested that in the case of mixtures of methyl iodide and isopropyl iodide, transfer from excited molecules is in the opposite direction to charge transfer from ionized molecules

$$R_1I^+ + R_2I \rightarrow R_1I + R_2I^+$$

$$R_2I^* + R_1I \rightarrow R_2I + R_1I^*$$

Thus excitation energy may go from methyl iodide to isopropyl iodide and positive charge from isopropyl iodide to methyl iodide, or both transfers may be in the other direction. Excitation and ionization of methyl iodide both give rise to the charge-transfer complex in relatively low yield, and excitation and ionization of isopropyl iodide give rise to the complex in high yield, consistent with the relative weakness of the C–I bond in this molecule. When isopropyl iodide is present in a mixture containing mainly methyl iodide, one of the transfers can take place, so that the isopropyl iodide produces a more than proportionate rise in yield. When methyl iodide is present in a mixture containing mainly isopropyl iodide, the other transfer can occur, so that in this case methyl iodide produces a more than proportionate *drop* in yield. This explanation is of course by no means proved, and it is possible that other reactions, such as those associated with electron capture, may be involved in the nonproportionality.

The shape of the curve in Figure 3 would be qualitatively consistent with the formation of the charge-transfer complex by electron capture by the alkyl iodide, followed by charge neutralization to yield an iodine atom which then gives the complex. Nitrous oxide produces no effect even at 0.05 M isopropyl iodide, where there is twice as much N_2O as alkyl iodide. It could be that isopropyl iodide is much more efficient than N_2O at capturing electrons in this system. Another possibility is that at least some charge-transfer complex is formed through positive charge transfer from an ion derived from cyclohexane to alkyl iodide, followed by neutralization.[18] Charge-transfer complex formed in this way would be unaffected by N_2O. Still more complex may be formed[4c] by the action of hydrogen atoms derived from cyclohexane

$$H + i\text{-PrI} \rightarrow HI + i\text{-Pr}\cdot$$

$$R\cdot + HI \rightarrow RH + I$$

the iodine atom giving the complex. The concentrations of solute which are needed to produce appreciable yields of charge-transfer complex are higher by more than an order of magnitude than are needed to produce comparable yields of triplet states in the pulse radiolysis of solutions of aromatic compounds in cyclohexane.[19] This could be because of dissociation of the charge-transfer complex at the lower alkyl iodide concentrations. However, it is not possible to obtain an equilibrium constant from these data because of the large number of processes which may be contributing to the formation of the complex.

The effect of the number of β-hydrogen atoms on the yield of HI (Figure 4) resembles the effect on the yield of I_2 in both radiolysis[16,20] and photolysis[20] of alkyl iodides. It is consistent with the view that HI is formed in a "molecular" reaction following the excitation or ionization of alkyl iodide. A unimolecular decomposition of excited molecules has been proposed to account for the production of HI in the flash photolysis of ethyl iodide.[21] The high yield (G = 7.0)

(18) T. S. Croft and R. J. Hanrahan, *J. Phys. Chem.*, **66**, 2188 (1962); I. Mani and R. J. Hanrahan, *ibid.*, **71**, 3301 (1967).

(19) E. J. Land and A. J. Swallow, *Trans. Faraday Soc.*, **64**, 1247 (1968).

(20) E. L. Cochran, W. H. Hamill, and R. R. Williams, *J. Amer. Chem. Soc.*, **76**, 2145 (1954).

(21) B. A. Thrush, *Proc. Roy. Soc.*, **A243**, 555 (1957).

obtained from isopropyl iodides at −196° is also consistent with this view.

It is not easy to explain why the yield of HI should diminish at higher doses. Ethylene, when present in much larger quantity than the unsaturated hydrocarbons produced by the radiation, did not produce a sufficient drop in HI yield to enable a slow thermal reaction between HI and unsaturated double bonds to account for the result, unless other unsaturated hydrocarbons are greatly more reactive than ethylene. Alkyl radicals would be expected to react with HI, but the rate constant for the reaction is a little less than that for the reaction with I_2,[22] so that on this view the HI yield could not drop off while the iodine concentration continues to rise. The result is thus still unexplained.

In an attempt to account for the shape of the $G_{(I_2)}$ curve in Figure 5, we have considered the contribution which could be due to thermal alkyl radicals, which are produced from methyl iodide with $G = 4.79$, but from isopropyl iodide only with $G = 3.06$,[23] reacting with hydrogen iodide which is produced in low yield from methyl iodide but in high yield from isopropyl iodide. Such a mechanism would be expected to produce higher iodine yields from the mixtures than would be expected if species produced from the two iodides did not interact with each other. We have made a calculation based on the mechanism of Hanrahan and Willard, assuming that the rate constants for the reactions of alkyl radicals with iodine and HI are equal, and independent of the nature of the alkyl radical. The calculated curve for iodine production resembles Figure 5 between 0 and 40% isopropyl iodide, but above 40% it continues to rise smoothly toward the 100% axis instead of levelling off and then rising again as in Figure 5. Furthermore, this mechanism would be expected to lead to HI yields *lower* than would be obtained if there were no interaction between the species produced from the two components, and the HI curve of Figure 5 shows that this is not borne out experimentally. We have made a similar calculation based on the mechanism of Gillis *et al.*,[4b] and this fits the results even less well. We therefore believe that these interactions play a relatively minor part in the system, and that the explanation of the shapes of the curves of Figure 5 may be the same as already given above to account for Figure 2.

The mixtures at −196° (Figure 6) behave quite differently from the liquid mixtures, and we believe that the principal contribution to nonlinearity here is a change from the crystalline form of the solid to the glassy form in the range 15–45% methyl iodide. This effect masks any effect of the type occurring in the liquid phase.

Acknowledgments. The authors wish to thank Professor G. R. Hall and Drs. P. G. Clay, M. Ebert, and E. J. Land for helpful discussions and for their interest in this work.

(22) D. Perner and R. H. Schuler, *J. Phys. Chem.*, **70**, 2224 (1966); I. Mani and R. J. Hanrahan, *ibid.*, **70**, 2233 (1966).

(23) R. J. Hanrahan and J. E. Willard, *J. Amer. Chem. Soc.*, **79**, 2434 (1957).

Solubilities of Ammonia in Alkali Nitrate and Perchlorate Melts[1]

by S. Allulli

Laboratorio di Chimica delle Radiazioni e Chimica Nucleare del C.N.E.N., Istituto di Chimica Generale ed Inorganica, Università di Roma, Rome, Italy *(Received May 2, 1968)*

The solubility of ammonia at pressures between 5 and 50 mm in various (Li–K)NO_3 mixtures, in (Li–Na–K)NO_3 eutectic, and in (Li–K)ClO_4 eutectic at different temperatures has been determined. The solubility increases with increasing Li^+ ion concentration and decreases with increasing temperature. Henry's law constants (moles of solute/mm mole of solvent) are about 10^{-5} and 10^{-3} for (Li–K)NO_3 mixtures and (Li–K)ClO_4 eutectic, respectively. The influence of the composition of the solvent on the solubility of the ammonia and the mechanism of the dissolution process are discussed. To test the relationship between the absorption of polar gases and their dipole moments, solubility measurements of hydrogen sulfide, carbon monoxide, chloroform, and acetone in molten (Li–K)NO_3 eutectic at 160° were also attempted, but in all cases the solubilities were found to be too small ($<10^{-7}$ mol/mm mol of solvent) to be detected with our experimental technique.

Information concerning the solubility of gases in molten salts appears, at present, very scanty. Small values (10^{-7} to 10^{-8} mol/ml atm), are reported for the solubilities of nonpolar gases such as the noble gases in molten fluorides[2] and chlorine or carbon dioxide in fused chlorides.[3,4]

With respect to the behavior of polar gases, only the solubility of water in fused nitrates[5–7] and chlorides[8] has been extensively investigated; data are also available on the solubility of hydrogen fluoride in molten fluorides[9,10] and hydrogen chloride in molten chlorides.[11]

This paper presents an investigation of the solubilities of some polar gases in fused (Li–K)NO_3 eutectic at 160°. Additional information on the dissolution process of the polar gases has been obtained by measurements of the solubility of ammonia in the (Li–K)NO_3 system at various compositions, in (Li–Na–K)NO_3 eutectic, and in (Li–K)ClO_4 eutectic.

Experimental Section

Materials. Finely powdered $NaNO_3$ (ERBA RP), KNO_3 (ERBA RP) and $KClO_4$ (ERBA RP) were vacuum dried at 110° for 24 hr. $LiNO_3$ (ERBA RP) and $LiClO_4$ (RUDI PONT) were dehydrated at a lower temperature (70°) to avoid hydrolysis reactions. After the solubility measurements, the samples were dissolved in distilled water and their alkali ion concentrations were determined by an E.E.L. flame photometer. NH_3 (Matheson Co), H_2S (Rivoira 98% purity), CO (Gerling Holz & Co. Hamburg) were used without further purification; $CHCl_3$ (ERBA RP) and $(CH_3)_2CO$ (ERBA RP ACS) were distilled under vacuum before use. The purity of ammonia and carbon monoxide (>99.5%) was checked by mass spectrometry.

Solubility Measurements. The apparatus consisted of a vacuum line having four outlets. Attached to these were an Edwards high-vacuum pump in series with a mercury diffusion pump, a Pyrex cell containing the fused salt, and a globe of known volume (88.8 ml) provided with a mercury manometer and a gas reservoir. The whole apparatus, excluding pumps and cell, was thermostated with a water bath at 30 ± 0.1°; the absorption cell was dipped in a molten salt bath controlled at ±0.5° by an S.A.E. 136 thermoregulator. Before the absorption measurements, the salt (10 g) was vacuum degassed (10^{-4} mm) at 70° for 48 hr; the temperature was then slowly raised over a period of 6–7 hr to the required value. The cell was then left under vacuum for 12 hr at the operating temperature before starting solubility experiments. After the stopcock to the fused salt cell was closed, the gas was allowed to enter the system to the desired pressure. The stopcock to the molten salt was then opened and the pressure was measured at time intervals of several minutes over a period of 3–4 hr until no further pressure drop occurred. In some cases measurements were also performed up to 12 hr, but no further pressure drop was found. The attainment of the equilibrium being sufficiently fast, absorption measurements were performed without stirring.

(1) This work was supported by the Consiglio Nazionale delle Richerche.

(2) (a) W. R. Grimes, N. V. Smith, and G. M. Watson, *J. Phys. Chem.*, **62**, 862 (1958); (b) M. Blander, W. R. Grimes, N. V. Smith, and G. M. Watson *ibid.*, **63**, 1164 (1959).

(3) Yu. M. Ryabukhin, *Russ. J. Inorg. Chem.*, **7**, 565 (1962).

(4) D. Bratland, K. Grjotheim, C. Krohn, and K. Motzfeldt, *Acta Chem. Scand.*, **20**, 1811 (1966).

(5) (a) Bertozzi *Z. Naturforsch.*, **22a**, 1748 (1967); (b) G. Bertozzi *Quad. Ric. Sci.*, **35**, 40 (1965).

(6) J. P. Frame, E. Rhodes, and A. R. Ubbelohde, *Trans. Faraday Soc.*, **57**, 1075 (1961).

(7) F. R. Duke and A. S. Doan, Jr., *Iowa State Coll. J. Sci.*, **32**, 451 (1958).

(8) W. J. Burkhard and J. D. Corbett, *J. Amer. Chem. Soc.*, **79**, 6361 (1957).

(9) J. H. Shaffer, W. R. Grimes, and G. M. Watson, *J. Phys. Chem.*, **63**, 1999 (1959).

(10) P. E. Field and J. H. Shaffer, AEC Accession No. 36785 Rept. ORNL P 2202 (1966).

(11) T. L. Lukmanova and Ya. E. Vil'nyanskii, *Izv. Vysshikh Uchebn. Zavedenii, Khim. i Khim. Tekhnol.*, **7**, (3), 510 (1964).

To avoid errors due to the determination of the apparent volume of this system, the number of gaseous moles absorbed was calculated by the expression

$$\Delta m = \frac{P_{in}V_1}{RT_1}\left(1 - \frac{P_{eq}}{P_{ex}}\right) \quad (1)$$

where P_{in} is the initial pressure of gas, P_{eq} is the equilibrium pressure of gas, P_{ex} is the pressure of gas immediately after expansion to the cell, V_1 is the volume of the globe with the manometer, and T_1 is the temperature of the globe with the manometer. This equation can be derived as follows. The adsorption apparatus can be considered to consist of n volume elements at various temperatures ranging from 30° to the fused salt temperature, V_1 and T_1 being the volume and the temperature of the globe, and V_n the volume of the cell at the experimental temperature T_n. Therefore, the moles of gas before and after the absorption will be

$$m_{in} = m_{1ex} + m_{2ex} + \cdots m_{nex} \quad (2)$$

$$m_{eq} = m_{1eq} + m_{2eq} + \cdots m_{neq} \quad (3)$$

Subtraction of (3) from (2) yields

$$\Delta m = (m_{1ex} + m_{2ex} + \cdots + m_{nex}) - (m_{1eq} + m_{2eq} + \cdots m_{neq}) \quad (4)$$

From the ideal gas equation, it follows that

$$\Delta m = \frac{P_{ex}}{R}\left(\sum_{j=1}^{n}\frac{V_j}{T_j}\right) - \frac{P_{eq}}{R}\left(\sum_{j=1}^{n}\frac{V_j}{T_j}\right) \quad (5)$$

Equation 2 can be expressed as

$$\frac{P_{in}V_1}{RT_1} = \frac{P_e}{R}\left(\sum_{j=1}^{n}\frac{V_j}{T_j}\right) \quad (6)$$

By substituting (6) in (5), eq 1 is obtained. Δm is seen to depend only upon the values of P_{in}, P_{ex}, and P_{eq} which were measured to ±0.05 mm by a Gaertner 867 cathetometer, V_1 and T_1 being constant at all experimental conditions.

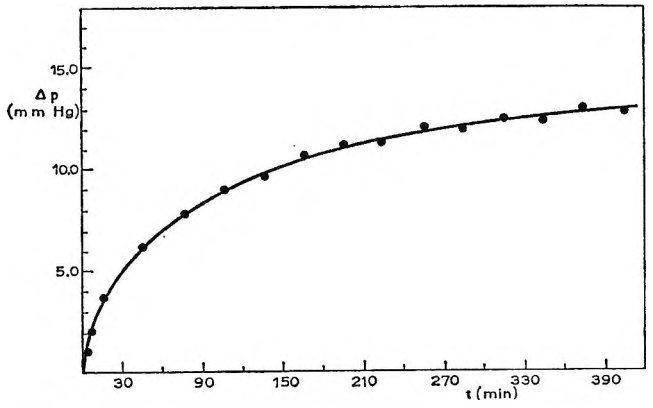


Figure 1. Absorption rate of ammonia in (Li–K)NO_3 eutectic at 160°; Δp = difference between the pressure obtained immediately after the expansion of the gas (P_{ex}) and the pressure at the time t.

It must be noted that eq 1 can be applied only for slow absorption rates if one is to read P_{ex} with sufficient precision. The kinetics of the absorption process (Figure 1) seems sufficiently slow compared with the time of reading (a few seconds) to ensure that errors due to the application of eq 1 are in the same range as the other experimental errors. On the other hand, the time of reading is sufficiently long to allow thermal equilibration of the gas, because measurements on the expansion of the gas in the cell without molten salts show that P_{ex} remains unchanged over a period of 1 hr. Prior determinations of the equilibrium constants were found to vary no more than 3% over all experimental conditions.

Results and Discussion

Linear dependence of ammonia solubility and the equilibrium pressure, in the range of temperatures and pressures investigated (up to 50 mm), was found for all the melts under study.

In Table I the values of the reciprocal Henry's law constant, K (moles of ammonia per mole of solvent per millimeter pressure), for the solubility of the ammonia in various molten media are reported. From this table one can see that the amount of ammonia dissolved decreases as the temperature of the melt increases. In Figure 2, the values of K are plotted against the reciprocal of the absolute temperature. From the slope of

Table I: Solubility of Ammonia (K = moles of NH_3/mm mole of solvent) in Various Ionic Melts

Solvent composition, mol %		T, °C	$K \times 10^5$
(Li–K)NO_3	43:57	160	4.1
		190	2.45
		210	1.7
		250	1.05
(Li–K)NO_3	75:25	242	4.2
		275	2.05
		292	1.5
		325	0.85
$LiNO_3$		260	12.5
		283	7.05
		303	4.1
		315	3.1
(Li–Na–K)NO_3	27:18:55	160	2.1
		185	1.5
		202	1.15
		250	0.7
(Li–K)ClO_4	76:24	234	128
		251	84
		266	61.5
		288	37
		311	23

Table II: Enthalpy and Entropy Changes of Solution of Ammonia, Water, and Argon in Various Fused Media

Solvent composition, mol %		Gas	ΔH, kcal/mol	$\Delta S_1 = \Delta H/T$, eu	$\Delta S_2 = R \ln Cs/Cd$, eu	ΔS_3, eu	T, °K
(Li–K)NO_3	43:57	NH_3	−7.0	−13.4	−3.9	−9.5	523
(Li–K)NO_3	75:25	NH_3	−11.8	−22.8	−6.6	−16.2	523
$LiNO_2$		NH_3	−16.5	−30.4	−8.7	−21.7	543
(Li–Na–K)	27:18:55	NH_3	−5.8	−11.1	−3.1	−8.0	523
(Li–K)ClO_4	76:24	NH_3	−13.8	−26.4	−12.4	−14.4	523
(Li–K)NO_3	50:50[a]	H_2O	−10.4	−20.0	−8.8	−11.2	523
(Li–Na–K)F	46, 5:11, 5:42[b]	Ar	12.4	12.4	12.5	−0.1	1000

[a] From ref 5a. [b] From ref 2b. Density data for (Li–K)NO_3 mixtures taken from I. G. Murgulescu and S. Zuca, *Electrochim. Acta*, **11**, 1383 (1966); for (Li–Na–K)NO_3 mixture, from M. Steinberg and N. H. Nacktrieb, *J. Amer. Chem. Soc.*, **72**, 3558 (1950). For (Li–K)ClO_4 eutectic, data are not available in literature; measurements performed in our laboratory gave an approximate value of 2.1 g/ml at 250°.

these curves the enthalpy change for the process

$$NH_{3,(g,Cg)} \rightleftarrows NH_{3,(d,Cd)} \qquad (7)$$

is calculated, subscripts g and d indicating gaseous and dissolved ammonia, respectively; C_d represents the concentration of the dissolved ammonia in equilbrium with ammonia at concentration C_g.

As pointed out by Grimes, *et al.*,[2a] equilibrium 7 can be divided into two stages (ideal isothermal expansion and transfer of ammonia from gaseous to liquid phase at the same concentration).

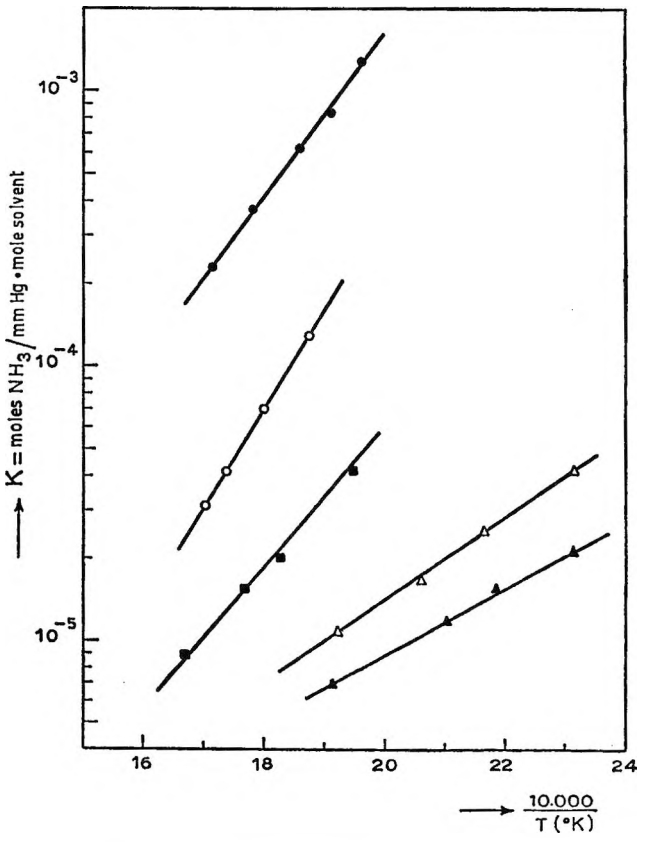


Figure 2. Temperature dependences of solubilities of ammonia in various molten mixtures: ○, pure $LiNO_3$, $\Delta H = -16.5$ kcal/mol; ■, (Li–K)NO_3, 75:25, $\Delta H = -11.8$ kcal/mol, △, (Li–K)NO_3, 43:57, $\Delta H = -7.0$ kcal/mol; ▲, (Li–Na–K)NO_3, 27:18:55, $\Delta H = -5.8$ kcal/mol; ●, (Li–K)ClO_4· 76:24, $\Delta H = -13.8$ kcal/mol.

For the latter process, the value of the entropy change ΔS_3 (or standard entropy of solution), which is a function only of the properties of the gas in the solvent,[2b] can be obtained. Table II reports the enthalpy and the entropy changes for the absorption of ammonia in molten nitrates and perchlorates and, for comparison, the data obtained by Bertozzi[5a,b] for the solubility of water in molten nitrates and by Grimes, *et al.*,[2a] for argon in molten fluorides.

From Table II the following observations are apparent. (a) The standard entropy of solution of ammonia is smaller than those of the noble gases in molten fluorides. (Lack of information about the solubility of inert gases in molten nitrates does not allow a direct comparison with our values, but it can be noted that the solubility of argon in molten sodium nitrate at 369°[12] is of the same order of magnitude as those found in other melts[2b] or for other inert gases.[4]) (b) The enthalpy of solution of the ammonia is negative while for the noble gases it is positive. (c) The enthalpy and the entropy of solution of the ammonia depend on the concentration of Li^+ ions in the melt.

Taking into account the strong polarizing power of Li^+ ions and the permanent dipole of the ammonia molecule, the dissolution process of ammonia in the melts investigated seems to be related to an ion–dipole interaction analogous to that reported for water in molten nitrates.[5]

Moreover, the ratio between values of standard entropy of solution of ammonia in (Li–K)NO_3 eutectic and water in (Li–K)NO_3 50:50 mixture agrees with the ratio of the values of the dipole moments of these gases (ammonia = 1.47 D, water = 1.84 D), thus suggesting a direct proportionality between the solubility of polar gases and the dipole strengths of the gaseous molecules.

To test this hypothesis, measurements with other

(12) J. L. Copeland and W. C. Zybko, *J. Phys. Chem.*, **69**, 3631 (1965).

polar gases such as carbon monoxide, hydrogen sulfide, chloroform, and acetone (whose dipole moments are 0.1, 0.92, 1.02, and 2.88 D, respectively) were performed. In all cases no detectable absorption ($<10^{-7}$ mol/mm mol of solvent) of these gases in (Li–K)NO_3 eutectic at 160° was found.

The slight solubility of carbon monoxide in fused salts can be due to an ion–dipole interaction which must be weak because of the low dipole moment of the CO molecule.

On the other hand, considerations based on the interstitial model of fused salts[2b] can explain only the low solubility values found for chloroform and acetone, but would not explain satisfactorily the behavior of hydrogen sulfide. In fact, this gas has a dipole moment and a molecular radius (calculated assuming molecules as centers of repulsive forces and not hard spheres[13]) very close to those of water and ammonia. Furthermore, all these radii are of the same order of magnitude as the radius of the holes present in the melt, as calculated with Furth's equation,[14] assuming $\gamma_{mic} = \gamma_{mac}$.

As another alternative, we might consider the acidic nature of the Li^+ ion; the large differences of solubility between hydrogen sulfide and ammonia in water could be considered to vary as a function of the different basic strengths of these gases, which are in the order $NH_3 > H_2O \gg H_2S$.

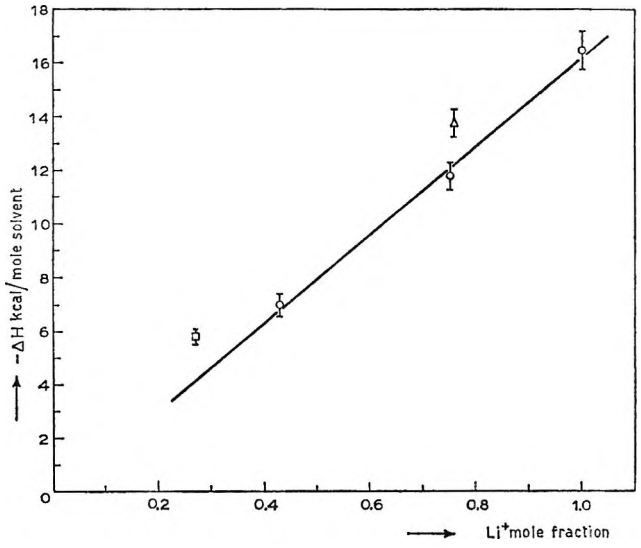


Figure 3. Enthalpy of solution of ammonia *vs.* Li^+ mole fraction: ⊖, (Li–K)NO_3 mixtures; ⊟, (Li–Na–K)NO_3 eutectic; △, (Li–K)ClO_4, eutectic.

The plot of the enthalpy of solution of ammonia *vs.* Li^+ mole fraction for the melts investigated (Figure 3) appears linear for (Li–K)NO_3 mixtures; a similar behavior was observed by Bertozzi[5a] for the solubility of water in molten alkali nitrates.

It is evident that the data obtained for the (Li–Na–K)NO_3 eutectic and (Li–K)ClO_4 eutectic do not fall on the curve. This is not surprising if, as suggested by other authors,[15,16] several kinds of association of the solvent ions take place in these melts depending upon crystal radius, electric charge, and temperature. Since the "activity" of lithium ions depends upon the anions and the cations present in the melt, the more negative value found for the (Li–K)ClO_4 eutectic is expected if one considers this system as more acidic than the corresponding (Li–K)NO_3 system. It is interesting to observe that the electrophoretic behavior of inorganic anions [Cl(I), CrO_4(II), NO_3(I) etc.] in molten (Li–K)ClO_4 eutectic agrees with this suggestion, since all the anions examined behave as cations or stay at the application point.[16] A similar explanation may hold for the (Li–Na–K)NO_3 eutectic since the substitution for potassium by smaller sodium ions raises the "activity" of lithium ions; nevertheless, in this case, sodium ions (owing to their small crystalline radius) can also contribute directly to the ammonia solubility.

Further investigations on the behavior of polar, molecular species added to these highly ionized melts seem to be of interest in order to contribute to the knowledge of the properties of extremely concentrated electrolyte solutions.

Acknowledgment. The author wishes to express his thanks to Professor G. Alberti for many helpful discussions.

(13) E. A. Moelwyn-Hughes, "Physical Chemistry," Pergamon Press, London 1957, p 597.
(14) R. Furth, *Proc. Cambridge Phil. Soc.*, **37**, 252 (1941).
(15) F. Lantelme and M. Chemla, *Electrochim. Acta*, **10**, 665 (1965).
(16) G. Alberti and S. Allulli *Chromatogr. Rev.*, **10**, 99 (1968).

The Distribution of Hydrogen Isotopes between $H_2PO_4^-$ and Water in Partially Deuterated Solutions[1a]

by Maurice M. Kreevoy, Richard A. Landholm,[1b] and Robert Eliason[1c]

School of Chemistry of the University of Minnesota, Minneapolis, Minnesota 55455 *(Received June 3, 1968)*

Using nmr, the distribution of hydrogen isotopes between water and diacid phosphate in partially deuterated aqueous solution has been determined. When coupled with the known isotopic ratios of acid dissociation constants of phosphoric acid and diacid phosphate, and certain assumptions, this permits the distribution to be evaluated for phosphoric acid and monoacid phosphate as well. The first two are reasonable and permit a reasonable approximation of the acid dissociation constant of phosphoric acid in isotopically mixed solvent. That for monoacid phosphate is unreasonable, and it is concluded that ΔF° of transfer of this species from H_2O to D_2O is probably not zero.

An essential prerequisite to the use of solvent hydrogen isotope effects for quantitative mechanistic studies is knowledge of the isotopic composition of reagents as a function of the isotopic composition of the solvent. Phosphoric acid is particularly interesting in this respect because it is a convenient acid for study in many acid-catalyzed reactions, and also because of its analogy with the acids related to water. That is, H_3PO_4 is analogous with H_3O^+, $H_2PO_4^-$ with H_2O, HPO_2^{2-} with OH^-, and PO_4^{3-} with O^{2-}.

To avoid complications arising from symmetry, it is convenient to consider these compositions in terms of fractionation factors,[2] symbolized by ϕ_{M_nX}, where M_nX is a molecule containing n exchangeable hydrogen atoms. (The symbol M is used throughout this paper to designate one of the isotopes of hydrogen, without specifying which; M_X is used for one H, D, or T in the molecule X.) The fractionation factor, ϕ_{M_nX}, is defined as the equilibrium constant for the redistribution reaction shown in eq 1.

$$D_{M_2O} + H_{M_nA} \overset{\phi_{M_nA}}{\rightleftharpoons} D_{M_nA} + H_{M_2O} \qquad (1)$$

The fractionation factor for M_3O^+ is l.[2]

The fractionation factor for a monobasic acid, ϕ_{MA}, is given by $K_{HA}l^3/K_{DA}$,[2] where K_{MA} is the acid dissociation constant of MA in M_2O, *if the solvated MA has only one site of exchangeable protons with an isotopic content different from that of the solvent and A^- has none.* This caveat is equivalent to the assumption that ΔF° of transfer of A^-, HA, or DA from H_2O to D_2O would be zero in the absence of exchange in the latter two cases. However, for a polyprotic acid the equivalent assumption still does not permit the evaluation of ϕ_{M_nA}, because $K_{H_nA}l^3/K_{D_nA}$ then gives $\phi_{M_nA}{}^n/\phi_{M_{n-1}A}{}^{n-1}$.[2] If all the ratios of dissociation constants in the series M_nA, $M_{n-1}A$, etc., were available it would be possible to deduce all the ϕ's, at each step making the assumption described above. For phosphoric acid the ratios are available, with high reliability, for the first and second dissociation, but not the third.[2,3] Instead $\phi_{M_3PO_4}$ and $\phi_{M_2PO_4^-}$ have been inferred from $K_{M_3PO_4}$ as a function of the deuterium content of the solvent.[2] Since $K_{M_3PO_4}$ is a relatively insensitive function of the ϕ's, this technique does not limit them very closely. An nmr technique has now been used to determine $\phi_{M_2PO_4^-}$ directly.[4,5] The resulting ϕ's are numerically somewhat different from the earlier values, but they are reasonably compatible with the isotopic variation of $K_{M_3PO_4}$. The derived value for $\phi_{MPO_4^{2-}}$ seems anomalous, and an explanation is offered.

Experimental Section

Nmr shifts were measured with a Varian Model A-60 spectrometer. A Hewlett-Packard Model 3300A function generator was used to generate side bands. Their frequency was determined with a Hewlett-Packard Model 373A electronic counter. The temperature of the probe was measured with an iron–constantan thermocouple during each series of measurements and was always 28 ± 1°.

The position of the combined H_2O–$H_2PO_4^-$ peak was measured relative to 0.05 M tetramethylammonium chloride (Eastman White Label) as an internal reference by plotting Δ (the chart position of the H_2O–$H_2PO_4^-$ side band less the chart position of the reference resonance) against the side-band frequency. When Δ

(1) (a) Supported, in part, by the National Science Foundation through GP-7915. (b) National Aeronautics and Space Administration Graduate Trainee, 1965–1968. National Science Foundation Summer Fellow (Graduate Teaching Assistant), 1965. (c) Hercules Corporation Summer Fellow, 1965; du Pont Company Summer Fellow, 1966; Ethyl Corporation Fellow, 1966–1967.

(2) P. Salomaa, L. L. Schaleger, and F. A. Long, *J. Amer. Chem. Soc.*, **86**, 1 (1964).

(3) R. Gary, R. G. Bates, and R. A. Robinson, *J. Phys. Chem.*, **68**, 3806 (1964).

(4) A. J. Kresge and A. L. Allred, *J. Amer. Chem. Soc.*, **85**, 1541 (1963).

(5) V. Gold, *Proc. Chem. Soc.*, 141 (1963).

is zero the side-band frequency is the separation between the reference and the parent H_2O–$H_2PO_4^-$ resonance. The position of the H_2O resonance in undeuterated water, $\delta_{TMAC}{}^{H_2O}$, was measured on two separate occasions and values of 1.602 and 1.605 ppm were obtained. The average of these, 1.603, was adopted for $\delta_{TMAC}{}^{H_2O}$, and all observed resonance positions, δ_{TMAC}, were assumed to be uncertain by ~0.002. The plots of Δ *vs.* the side-band frequency were accurately linear, and the apparent uncertainty of δ_{TMAC} was much less than this. Most of the scatter is thought to be due to small temperature changes. A change of 1° corresponds to a change of 0.005 ppm in δ_{TMAC}.[6]

Solutions were made up from demineralized water, D_2O (Bio-Rad Laboratories, 99.8 atom % D) and $NaH_2PO_4 \cdot H_2O$ (Mallinkrodt, Analytical Reagent) by weight. After each solution was made up and a sample removed for the nmr study the water was removed from the remainder by distillation and its H content determined from its near-ir spectrum.[7]

Results

Values of δ_{TMAC} for various solutions of NaM_2PO_4 in M_2O are shown in Table I.

Table I: δ_{TMAC} in Isotopically Mixed Aqueous Diacid Phosphate Solutions at 28°

(NaM_2PO_4), *M*	Atom % H	δ_{TMAC}, ppm	$\phi M_2PO_4^-$
0.0	100.0	1.603	...
1.5	100.0	1.747	...
2.0	100.0	1.815	...
3.0	100.0	1.940	...
4.0	100.0	2.082	...
5.5	100.0	2.323	...
2.0	59.3	1.818	0.85
4.0	54.8	2.118	0.74
5.5	53.1	2.378	0.82
5.5	28.1	2.413	0.81
2.0	28.0	1.823	0.84
4.0	23.2	2.145	0.76
0.0	1.0	1.574	...

If the shifts characteristic of $H_2PO_4^-$ and H_2O, $\delta_{TMAC}{}^{H_2PO_4^-}$, and $\delta_{TMAC}{}^{H_2O}$ are independent of the NaM_2PO_4 concentration, δ_{TMAC}, in the absence of deuterium, is governed by eq 2, where χ_{H_nA} is the fraction of hydrogen atoms present as H_nA. Figure 1 shows that eq 2 is accurately obeyed, within the

$$\delta_{TMAC} = \chi_{H_2O}\delta_{TMAC}{}^{H_2O} + \chi_{H_2PO_4^-}\delta_{TMAC}{}^{H_2PO_4^-} \quad (2)$$

uncertainty of the present measurements, and permits the evaluation of $\delta_{TMAC}{}^{H_2PO_4^-}$, 7.19 ± 0.03 ppm (50% confidence limits, evaluated by the method of least squares.[8])

Previous work on salts without exchangeable hydrogens has shown that they induce changes in δ^{H_2O}, the magnitude of which depend on the nature and concentration of the salt.[9] In 2, 4, and 5.5 *M* $NaNO_3$ $\delta_{TMAC}{}^{H_2O}$ has been remeasured, and the salt-induced shifts are in very good agreement with those previously reported.[9] They are in the opposite direction from those induced by NaH_2PO_4, and smaller by about a factor of 2. Similar results have been reported for $NaClO_4$.[9] If it is assumed that NaH_2PO_4 has a salt effect on $\delta_{TMAC}{}^{H_2O}$, of approximately the same magnitude as $NaNO_3$, in addition to the effect caused by its exchangeable hydrogens, the the $\delta_{TMAC}{}^{H_2O}$ to be used in eq 2 should be that measured in the presence of an appropriate concentration of $NaNO_3$, rather than that measured in pure water. Figure 1 also shows a test of eq 2 using such values of $\delta_{TMAC}{}^{H_2O}$. From this comparison it is clear that eq 2 fits the data far better with $\delta_{TMAC}{}^{H_2O}$ measured in water, and this has been used throughout the rest of this work.

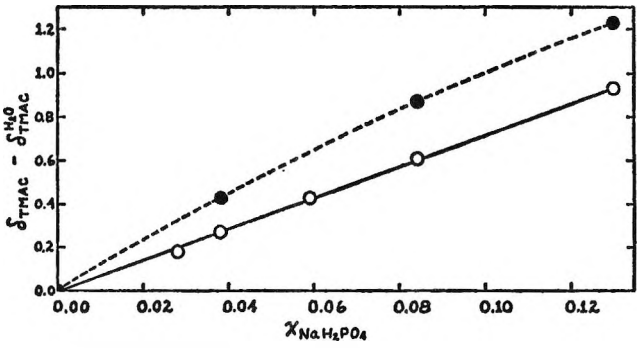


Figure 1. A test of eq 2 for H_2O–NaH_2PO_4 mixtures at 28 ± 1°. When $\delta_{TMAC}{}^{H_2O}$ is that measured in pure water the plot (open circles, solid line) shows no visible curvature, and the least-squares intercept is zero, as required by eq 2. The least-squares slope, 7.19 ± 0.03 ppm, is $\delta_{TMAC}{}^{H_2PO_4^-}$. When $\delta_{TMAC}{}^{H_2O}$ is that measured in $NaNO_3$ solutions whose concentration equals that of the NaH_2PO_4 the plot (closed circles, dashed curve) is systematically nonlinear and the best straight line forced through the points would not go through the origin. The origin is an experimental point in both series.

A small change in the position of the water resonance occurs when H is partially replaced with D. Equation 3 has been suggested for the corrected water resonance position, $\delta'_{TMAC}{}^{H_2O}$.[10]

$$\delta'_{TMAC}{}^{H_2O} = \delta_{TMAC}{}^{H_2O} - 0.019\chi(1 + 0.017T) \quad (3)$$

(The atom fraction D is χ; T is the centigrade temperature). A check of eq 1 with χ, 0.99, and T, 28° yielded a δ'_{TMAC} of 1.574 ppm while eq 3 requires 1.575 ppm.

(6) G. V. D. Tiers, *J. Chem. Phys.*, 62, 1151 (1958).

(7) M. M. Kreevoy and T. S. Straub, *Anal. Chem.*, 41, 214 (1969).

(8) C. A. Bennett and N. L. Franklin, "Statistical Analysis in Chemistry and the Chemical Industry," John Wiley and Sons, Inc., New York, N. Y., 1954, pp 36–40.

(9) J. A. Pople, W. G. Schneider, and H. J. Bernstein, "High Resolution Nuclear Magnetic Resonance," McGraw-Hill Book Co., New York, N. Y., 1959, p 449.

(10) A. Merbach, *J. Chem. Phys.*, 46, 3450 (1967).

By definition $\phi_{M_2PO_4^-}$ is given by eq 4. (The parentheses indicate atom fractions or mole fractions.) In isotopically mixed solvents δ_{TMAC}

$$\phi_{M_2PO_4^-} = \frac{(D_{M_2PO_4^-})(H_{M_2O})}{(H_{M_2PO_4^-})(D_{M_2O})} \quad (4)$$

is given by eq 5. It, together with the conservation conditions, eq 6–8, is sufficient to determine all the

$$\delta_{TMAC} = \frac{(H_{M_2O})\delta'_{TMAC}{}^{H_2O} + (H_{M_2PO_4^-})\delta_{TMAC}{}^{M_2PO_4^-}}{\{(H_{M_2O}) + (H_{M_2PO_4^-})\}} \quad (5)$$

atom fractions required in eq 4. Values of $\phi_{M_2PO_4^-}$ obtained using eq 4–8 are shown in Table I. The only

$$2(1 - \chi) = (H_{M_2O}) + (H_{M_2PO_4^-}) \quad (6)$$

$$2(M_2O) = (H_{M_2O}) + (D_{M_2O}) \quad (7)$$

$$2(M_2PO_4^-) = (H_{M_2PO_4^-}) + (D_{M_2PO_4^-}) \quad (8)$$

additional assumption involved in these calculations is that $\delta_{TMAC}{}^{H_2PO_4^-}$ is independent of χ. Table I shows no apparent trend in $\phi_{M_2PO_4^-}$ as a function of χ, supporting this assumption, which also seems intuitively attractive.

Cursory inspection of the calculations shows that most of the scatter in $\phi_{M_2PO_4^-}$ originates in error in the nmr measurements, rather than in (M_2O) and $(M_2PO_4^-)$. That being so, standard theory for the propogation of error[11] gives eq 9 for the uncertainty in $\phi_{M_2PO_4^-}$. (The uncertainty in x is indicated by $\Delta(x)$; C is a collection of constants). Since

$$\Delta(\phi_{M_2PO_4^-}) = C\Delta(\delta_{TMAC}{}^{H_2PO_4^-} - \delta_{TMAC})$$
$$\left\{\frac{1}{(H_{M_2O})} + \frac{1}{(D_{M_2O})} + \frac{1}{(H_{M_2PO_4^-})} + \frac{1}{(D_{M_2PO_4^-})}\right\}$$
$$\times (1 - x) \quad (9)$$

$\Delta(\delta_{TMAC}{}^{H_2PO_4^-} - \delta_{TMAC})$ is also approximately constant, the inverse of

$$\{1/(H_{M_2O}) + 1/(D_{M_2O}) + 1/(H_{M_2PO_4^-}) + 1/(D_{M_2PO_4^-})\}(1 - x)$$

was used as a weighting factor to get a weighted average value of $\phi_{M_2PO_4^-}$.[11] This is 0.80 with a probable error of ±0.01. The same values are obtained if an unweighted average is taken instead.

Discussion

From $\phi_{M_2PO_4^-}$, $\phi_{M_3PO_4}$ and $\phi_{MPO_4^{2-}}$ are readilty evaluated. The already mentioned assumption that ΔF° of transfer is zero was made, 1.603 was taken for $K_{H_3PO_4}/K_{D_3PO_4}$[2] and 3.79 for $K_{H_2PO_4^-}/K_{D_2PO_4^-}$.[3] The value of $\phi_{M_3PO_4}$ is 0.70 and that for $\phi_{MPO_4^{2-}}$ is 0.51.

The $\phi_{M_2PO_4^-}$ value is entirely reasonable, as is $\phi_{M_3PO_4}$. Based on a $K_{HSO_4^-}/K_{DSO_4^-}$ of 2.2,[12] bisulfate ion, which is similar in structure and acidity to H_3PO_4, gives a $\phi_{MSO_4^-}$ of 0.72. Values of ϕ_{MA} for carboxylic acids of about the strength of H_3PO_4 are similar to, though somewhat higher than $\phi_{M_3PO_4}$.[13] Many authors[13–17] have anticipated that, within a series of related acids, ϕ_{MA} (or K_{HA}/K_{DA}, which is proportional to ϕ_{MA} for monoprotic acids) should increase with decreasing K_{HA}, but that various series of acids should show quantitatively different behavior.[13,15,16] Using eq 10,[2] $K_{H_3PO_4}/K_{M_3PO_4}$ can be calculated for various H_2O–D_2O mixtures from $\phi_{M_3PO_4}$, $\phi_{M_2PO_4^-}$, and l.

$$K_{H_3PO_4}/K_{M_3PO_4} = \frac{(1 - \chi + \chi\phi_{M_3PO_4})^3}{(1 - \chi + \chi l)^3(1 - \chi + \chi\phi_{M_2PO_4^-})^2} \quad (10)$$

Figure 2 compares the calculated curve with the experimental values of Salomaa, Schaleger, and Long.[2] The fit is reasonable, about as good as the fit originally shown (Figure 1 of ref 2) and better than that produced with the original ϕ values and the present value of l.

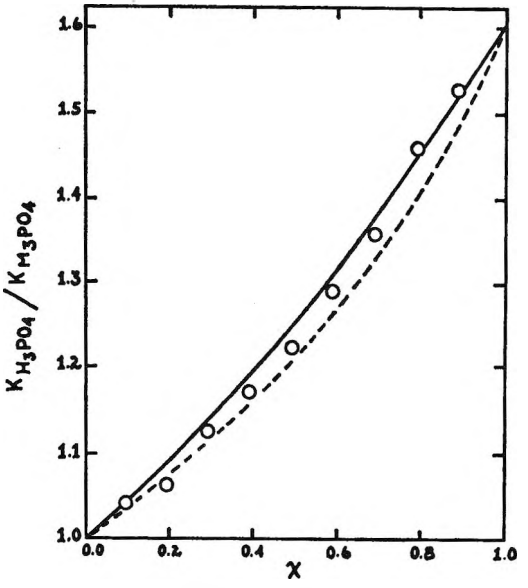


Figure 2. Comparison of theoretical curve produced by eq 10 with $\phi_{H_3PO_4}$, 0.80; and l, 0.69 (solid line) with the experimental values of Salomaa, Schaleger, and Long (circles). The dashed curve is that produced with $\phi_{H_3PO_4}$, 0.77; $\phi_{H_2PO_4^-}$, 0.98; and l, 0.69.

(11) J. Topping, "Errors of Observation and Their Treatment," 3rd ed, Chapman and Hall, Ltd., London, England, 1962, pp 82, 88, 89.

(12) M. H. Lietzke and R. W. Stoughton, *J. Phys. Chem.*, **67**, 652 (1963), report 2.27; a recent redetermination by Mr. John Melquist in this laboratory gave 2.18.

(13) R. P. Bell and A. T. Kuhn, *Trans. Faraday Soc.*, **59**, 1789 (1963).

(14) C. K. Rule and V. K. La Mer, *J. Amer. Chem. Soc.*, **60**, 1974 (1938).

(15) E. Høgfeldt and J. Bigeleisen, *ibid.*, **82**, 15 (1960).

(16) N. C. Li, P. Tang, and R. Mathur, *J. Phys. Chem.*, **65**, 1074 (1961).

(17) References to much earlier work are given in ref 13–16.

On the other hand, the value of $\phi_{MPO_4^{2-}}$ is unreasonable both in magnitude and its relation to $\phi_{M_2PO_4^-}$. Acids as weak as HPO_4^{2-} generally have ϕ values *well above* 1.0.[13] The values of $K_{H_2PO_4^-}/K_{D_2PO_4^-}$, with an l of 0.69, and the assumption that ΔF° of transfer is zero, requires that $\phi_{MPO_4^{2-}}$ be substantially *smaller* than $\phi_{M_2PO_4^-}$ regardless of the value assigned to the latter. The assumption of a zero ΔF° of transfer is the likely culprit. It has long been known and recently reemphasized that this is an inexact approximation.[18] Structurally an attractive hypothesis is that HPO_4^{2-}, which is a fairly strong base, hydrogen bonds to a number of solvent molecules more strongly than they hydrogen bond to each other. This would be likely to lead to a positive ΔF° of transfer from H_2O to D_2O,[19] and could account for the observed effect. Direct, experimental determination of $K_{HPO_4^{2-}}/K_{DPO_4^{2-}}$, and also $\phi_{MPO_4^{2-}}$ might help to clarify this situation.

(18) D. M. Goodall and F. A. Long, *J. Amer. Chem. Soc.*, **90**, 238 (1968).
(19) M. M. Kreevoy, *J. Chem. Educ.*, **41**, 636 (1964).

Reduction of Cobalt(III) Complexes by Monovalent Zinc, Cadmium, and Nickel Ions in Aqueous Solutions[1]

by D. Meyerstein[2] and W. A. Mulac

Chemistry Division, Argonne National Laboratory, Argonne, Illinois, and the Nuclear Research Centre, Negev, Israel *(Received June 26, 1968)*

The specific rates of reaction of Zn^+, Cd^+, Ni^+, and e_{aq}^- with a series of Co(III) complexes have been determined. The mechanisms of reduction and their dependence on the electronic structure of the monovalent cations are discussed.

The specific rates of reduction of a series of cobalt(III) complexes by different cations[3-8] and by hydrogen atoms,[9-11] have been recently measured. The results have been used as guides for the elucidation of the reaction mechanism. Several criteria based on the kinetic evidence have been suggested in order to differentiate between "outer-sphere" and "inner-sphere" reducing agents.[3-5,12]

Recent studies have shown that monovalent zinc, cadmium, and nickel ions, formed by the reduction of the corresponding bivalent ions by the hydrated electrons, are powerful reducing agents.[13,14] Many reactions of these cations have been measured.[14-17] It has been of interest therefore to measure their rates of reaction with a series of cobalt(III) complexes in order to obtain a better understanding of the mechanism of reduction by these cations.

The specific rates of reaction of Zn^+, Cd^+, and Ni^+ with a series of $Co(III)(NH_3)_5X$ and $Co(III)(En)_2XY$ complexes have been determined. The results suggest that Zn^+ is mainly an outer-sphere reducing agent, Ni^+ is mainly an inner-sphere reducing agent, and Cd^+ reacts *via* both mechanisms.

Experimental Section

Materials. The water has been triply distilled. $ZnSO_4$, $CdSO_4$, $NiSO_4$, and CH_3OH were Baker Analyzed

(1) Based on work performed under the auspices of the U. S. Atomic Energy Commission.
(2) Reprint requests to be sent to D. Meyerstein, Nuclear Research Centre, Negev, Israel.
(3) J. F. Endicott and H. Taube, *J. Amer. Chem. Soc.*, **86**, 1686 (1964).
(4) A. Zwickel and H. Taube, *ibid.*, **83**, 793 (1961).
(5) J. P. Candlin, J. Halpern, and D. L. Trimm, *ibid.*, **86**, 1019 (1964).
(6) J. P. Candlin and J. Halpern, *Inorg. Chem.*, **4**, 766 (1965).
(7) J. H. Espenson, *ibid.*, **4**, 121 (1965).
(8) J. P. Candlin, J. Halpern, and S. Nakamura, *J. Amer. Chem Soc.*, **85**, 2517 (1965).
(9) G. Navon and G. Stein, *J. Phys. Chem.*, **69**, 1391 (1965).
(10) M. Anbar and D. Meyerstein, *Nature*, **206**, 818 (1965).
(11) J. Halpern and J. Rabani, *J. Amer. Chem. Soc.*, **88**, 699 (1966).
(12) H. Diebler, P. H. Dodel, and H. Taube, *Inorg. Chem.*, **5**, 1688 (1966).
(13) J. H. Baxendale and R. S. Dixon, *Z. Physik. Chem.* (Frankfurt am Main), **43**, 161 (1964).
(14) D. Meyerstein and W. A. Mulac, *J. Phys. Chem.*, **72**, 784 (1968).
(15) J. H. Baxendale, J. P. Keene, and D. A. Stott in "Pulse Radiolysis," Academic Press, London, 1965, p 107.
(16) J. H. Baxendale, J. P. Keene, and D. A. Stott, *Chem. Commun.*, 715 (1966).
(17) G. V. Buxton, F. S. Dainton, and G. Thielens, *ibid.*, 201 (1967).

Reagents. The complexes $[Co(NH_3)_5H_2O](ClO_4)_3$, $[Co(NH_3)_5Cl](ClO_4)_2$, $[Co(NH_3)_5Br](ClO_4)_2$, $[Co(NH_3)_5N_3](ClO_4)_2$, $[Co(NH_3)_5CN](ClO_4)_2$, and $[Co(En)_2CO_3]Cl$ have been obtained from Professor H. Taube. The complexes $[Co(NH_3)_6](ClO_4)_3$, $[Co(NH_3)_5NCS]SO_4$, $[Co(En)_3]Cl_3$, *cis*-$[Co(En)_2Cl_2]ClO_4$, and *trans*-$[Co(En)_2Cl_2]Cl$ have been obtained from Professor F. Basolo. The complexes $[Co(NH_3)_5$ acetate$](ClO_4)_2$ and $[Co(NH_3)_5$ fumarate$](ClO_4)_2$ have been obtained from Professor J. Halpern. The complex $[Co(NH_3)_5F](ClO_4)_2$ has been obtained from Dr. G. Navon. The purity of the complexes has been checked by measuring the absorption spectra of their solutions and comparing them with the spectra reported in the literature.

Procedure. For the determination of the specific rate constants of the complexes with the hydrated electron, solutions containing 5×10^{-6} to 2×10^{-5} M of the complexes and 1×10^{-3} M methanol have been used. For the determination of the rate constants of M^+ (M = Zn, Cd, or Ni) with the complexes, solutions containing 2×10^{-2} M MSO_4, 1×10^{-3} M methanol, and the Co(III) complexes in the concentration range of 5×10^{-5} to 3×10^{-4} M have been used. The solutions were deaerated by shaking with argon gas in a syringe and then expelling the gas. This procedure was repeated four times leaving a residual concentration of oxygen less than 3×10^{-7} M. In order to minimize the extent of hydrolysis of the complexes, all solutions were prepared immediately before the irradiation. (At most 3 hr passed between dissolving the complex and the irradiation, the extent of hydrolysis, determined spectrophotometrically, being smaller than 10%.)

The pulse-radiolytic experiments were carried out using a 0.4-μsec, 15-MeV electron pulse from a linear accelerator yielding a dose of $0.6–6 \times 10^{19}$ eV $l.^{-1}$ per pulse (producing 0.3–3 μM reducing radicals). The decay of e_{aq}^- was followed spectrophotometrically at 5750 Å using a 4-cm double-path cell giving an 8-cm total light path. A 450-W xenon lamp was used as an analyzing light source, and a Bausch and Lomb monochromator followed by a IP28 photomultiplier and a Type 555 Tetronix oscilloscope fitted with a Polaroid camera was used for recording the absorption changes in the solution.

In order to minimize photochemical decomposition of the solutes which might be induced by the analyzing light, a Corning 7–54 glass filter was introduced between the xenon lamp and the cell when an absorption was followed at 5750 Å. This filter was replaced by the filters 0–53 and 3–68 when the absorption was followed at 3100 Å. Furthermore, a mechanical shutter was kept closed until shortly before the pulse and the solutions were kept in the dark.

The calculations were carried out using Chloe, an automatic photoelectronic scanner,[18] for reading the Polaroid pictures and transferring the data to a magnetic tape which was then used in a computer program for the analysis of the kinetics.[19] All traces were analyzed for first- and second-order decay and pseudo-first-order rates were calculated when a good first-order decay plot was obtained for at least three half-lives. A correction for the decay of M^+ in the absence of oxidants was included when needed; this correction was always smaller than 25%. For every rate constant at least ten traces were analyzed, which were obtained by pulse radiolyzing ten sample solutions, prepared by using at least two different stock solutions to dilute to several different concentrations. Some of the complexes have a relatively high absorption coefficient at 3100 Å, and their reactions with M^+ were followed therefore at 3300 Å. In some cases the light transmittance at the end of the reaction was slightly higher than before the pulse, due to the decomposition of the complex. In these cases one also has to correct partially for the reaction of hydrogen atoms and CH_2OH radicals with the complex. As the latter correction is not very accurate though always smaller than 10%, a larger error limit is given for these results.

Results and Discussion

The radiolysis of water may be described by

$$H_2O \rightarrow e_{aq}^-, H, OH, H_2, H_2O_2, H_3O_{aq}^+ \quad (1)$$

the yields of the products being $G_{e_{aq}^-} = 2.6$, $G_{OH} = 2.65$, $G_H = 0.6$, $G_{H_2} = 0.45$, and $G_{H_2O_2} = 0.75$. In solutions containing MSO_4 salts, Co(III) complexes, and methanol the following reactions are expected

$$e_{aq}^- + M^{2+} \rightarrow M^+ \quad (2)$$

$$e_{aq}^- + Co(III) \rightarrow Co(II) \quad (3)$$

$$H + CH_3OH \rightarrow CH_2OH + H_2 \quad (4)$$

$$H + Co(III) \rightarrow Co(II) + H^+ \quad (5)$$

$$OH + CH_3OH \rightarrow CH_2OH + H_2O \quad (6)$$

$$CH_2OH + Co(III) \rightarrow CH_2O + Co(II) \quad (7)$$

$$CH_2OH + CH_2OH \rightarrow HOCH_2CH_2OH \quad (8)$$

$$M^+ + Co(III) \rightarrow Co(II) + M^{2+} \quad (9)$$

$$M^+ + M^+ \rightarrow M^{2+} + M \quad (10)$$

$$M^+ + H_2O_2 \rightarrow M^{2+} + OH + OH^- \quad (11)$$

When the Co(III) complexes are added in concentrations low enough to avoid a major contribution of reaction 3 as compared to reaction 2, one can study

(18) The Chloe system was developed at the Argonne National Laboratory Applied Mathematics Division, by an Engineering group led by Donald Hodges. A detailed description of this machine is given in Technical Memorandum No. 61, by Donald Hodges, Applied Mathematics Division, Argonne National Laboratory, Nov 1963.

(19) M. C. Sauer, ANL-7146 Report (1966).

Table I: Specific Rates of Reduction of Co(III) Complexes[a]

	Zn^+	Cd^+	Ni^+	e_{aq}^-	H
$Co(NH_3)_6^{3+}$	8.4×10^8	1.72×10^8	$\leq 5 \times 10^6$	8.5×10^{10}	$\leq 1.6 \times 10^{6m,n,o}$
$Co(NH_3)_5H_2O^{3+}$	1.56×10^{9b}	6.2×10^{8b}	$\leq 5 \times 10^{6b}$	8.0×10^{10c}	$\leq 1 \times 10^{6m,o}$
$Co(NH_3)_5OH^{2+}$	1.10×10^{9d}	9.0×10^{8e}	1.3×10^{7f}	6.0×10^{10g}	2.5×10^{7n}
$Co(NH_3)_5F^{2+}$	8.2×10^8	5.4×10^8	$\leq 5 \times 10^6$	6.6×10^{10}	$\leq 1.2 \times 10^{6m,n,o}$
$Co(NH_3)_5Cl^{2+}$	2.2×10^9	2.2×10^9	6.5×10^8	7.8×10^{10}	0.73^n–16×10^{8o}
$Co(NH_3)_5Br^{2+}$	2.6×10^{9b}	2.5×10^{9b}	1.05×10^{9b}	8.0×10^{10}	0.46^m–14×10^{9o}
$Co(NH_3)_5N_3^{2+}$	1.49×10^{9i}	1.41×10^{9i}	$5.8 \times 10^{8i,j}$	7.2×10^{10}	3.9^n–11×10^{8o}
$Co(NH_3)_5CN^{2+}$	1.30×10^9	9.1×10^8	3.3×10^{8l}	7.4×10^{10}	3.7^n–6.1×10^{7o}
$Co(NH_3)_5NCS^{2+}$	1.65×10^{9i}	1.32×10^{9i}	$4.1 \times 10^{8i,j}$	7.3×10^{10}	6.3×10^{9o}
$Co(NH_3)_5OOCCH_3^{2+}$	5.0×10^8	9.0×10^7	$\leq 5 \times 10^6$	7.3×10^{10}	1.3×10^{6o}
$Co(NH_3)_5$fumarate$^+$	1.21×10^{9l}	8.3×10^{8l}	...	6.5×10^{10}	6.1×10^{9o}
$Co(En)_3^{3+}$	2.5×10^8	1.60×10^7	$\leq 5 \times 10^6$	8.5×10^{10}	...
cis-$Co(En)_2NH_3Cl^{2+}$	1.47×10^9	1.75×10^9	4.7×10^8	6.6×10^{10}	...
cis-$Co(En)_2NH_3NO_2^{2+}$	$2.7 \times 10^{9j,k}$	$2.8 \times 10^{9j,k}$	$3.3 \times 10^{8j,k}$	6.6×10^{10}	...
$Co(En)_2FH_2O^{2+}$	4.7×10^8	4.1×10^8	$\leq 5 \times 10^6$	6.3×10^{10}	...
$Co(En)_2CO_3^+$	4.7×10^8	6.7×10^8	$\leq 5 \times 10^6$	4.8×10^{10}	2×10^{6n}
cis-$Co(En)_2F_2^+$	5.4×10^8	6.0×10^8	$\leq 5 \times 10^6$	4.9×10^{10}	...
cis-$Co(En)_2Cl_2^+$	1.91×10^{9i}	2.3×10^{9i}	5.9×10^{8i}	7.3×10^{10}	...
trans-$Co(En)_2Cl_2^+$	2.3×10^{9i}	2.6×10^{9i}	$8.3 \times 10^{8i,j}$	7.7×10^{10}	...

[a] In units of M^{-1} sec^{-1}. All solutions contained 0.02 M MSO_4, 1×10^{-3} M CH_3OH, plus the complexes in different concentration and were at pH 5–6. The reactions of M^+ were followed at 310 mμ and of e_{aq}^- at 575 mμ without MSO_4. The maximal standard deviation is ±15%. The rate constants for the reaction of hydrogen atoms are from the literature (ref 9–11). [b] Measured at pH 4.0. [c] From ref 23. [d] Measured at pH 6.6. [e] Measured at pH 7.1. [f] Measured at pH 7.6, standard deviation ±25%. [g] Measured at pH 10.0. [i] Measured at 350 mμ. [j] Standard deviation ±25%. [k] Measured at 350 mμ. [l] The products of the reaction had a relatively large absorption, which decayed slowly and could not be identified, decreasing the accuracy; the results have therefore an accuracy of ±25%. Due to the large residual absorption the rate of the reaction $Ni^+ + Co(NH_3)_5$ fumarate$^+$ could not be determined. [m] Reference 9. [n] Reference 10. [o] Reference 11.

reaction 9 by following the disappearance of M^+. Reactions 10 and 11, in the absence of Co(III) complexes, have been studied earlier.[14] It was found that one can determine the specific rate constant of reaction 9, k_9, by introducing a small correction for reactions 10 and 11.[14] In the case where the final light transmission was slightly larger after the reaction than before the pulse, due to the decomposition of the Co(III) complex, an additional correction due to reactions 5 and 7 must be added.

The specific rates of reaction of Zn^+, Cd^+, Ni^+, and e_{aq}^- with a series of Co(III) complexes are summarized in Table I. The known corresponding rates of reaction of hydrogen atoms with the same complexes are included for comparison. It should be mentioned that the rates of reaction of Zn^+, Cd^+, and Ni^+ were measured in solutions containing 2×10^{-2} M of M^{2+} SO_4^{2-}, having therefore an ionic strength, $\mu = 0.08$.

The rates of reaction of the hydrated electron with the Co(III) complexes seem to be all diffusion controlled and therefore one can learn very little from the small differences in rates between the different complexes. Most of these rates are in fair agreement with other results cited in the literature.[20-23]

The diffusion-controlled rate of reaction between M^+ and a divalent cation has been calculated by means of the Debye equation for two extreme cases: (1) the radius of M^+ is 3.0 Å, assuming that it is fully hydrated, and (2) the radius of M^+ is 0.8 Å, assuming that it is not hydrated when reacting. After correcting for the salt effect it was found that the diffusion-controlled rate for such a reaction will range between 4 and 1×10^9 M^{-1} sec^{-1}, respectively. From the results in Table I it can be seen that some of the reactions have a rate of about 2×10^9 M^{-1} sec^{-1} and it can be assumed that these reactions are diffusion controlled, or at least approach this limit.

From the results it is evident that for the series of the $Co(III)(NH_3)_5X$ complexes the order of reactivities is $Zn^+ \geq Cd^+ > Ni^+$, the same order found for the reactions of these cations with other oxidants studied earlier.[14] However, for the series $Co(III)(En)_2XY$ the order of reactivities is $Cd^+ \geq Zn^+ > Ni^+$ with the exception of $Co(En)_3^{3+}$ and $Co(En)_2FH_2O^{2+}$. This change in the relative reactivities of Zn^+ and Cd^+ toward these two groups of very similar oxidants seems to suggest a difference in the mechanism of reduction by these cations.

It is generally accepted that the reduction of $Co(NH_3)_6^{3+}$ and $Co(En)_3^{3+}$ proceeds *via* the outer-

(20) J. H. Baxendale, E. M. Fielden, C. Capellos, J. M. Francis, J. V. Davies, M. Ebert, C. W. Gilbert, J. P. Keene, E. J. Land, A. J. Swallow, and J. Nosworthy, *Nature*, **201**, 468 (1964).

(21) A. Szutka, J. K. Thomas, S. Gordon, and E. J. Hart, *J. Phys. Chem.*, **69**, 289 (1965).

(22) J. H. Baxendale, E. M. Fielden, and J. P. Keene, *Proc. Roy. Soc.*, **A286**, 320 (1965).

(23) M. Anbar, E. M. Fielden, and E. J. Hart, unpublished results cited in M. Anbar and P. Neta, *Int. J. Appl. Radiation Isotopes*, **18**, 493 (1967).

sphere mechanism.[3,5] It is evident from these results that Zn^+ and Cd^+ are very efficient reducing agents through this mechanism. The results also suggest that Ni^+ is a much weaker reducing agent *via* this mechanism. The fact that the rates of reduction of $Co(NH_3)_6^{3+}$ and $Co(En)_3^{3+}$ by Zn^+ are within one order of magnitude of the diffusion-controlled limit naturally diminishes the effects of changing the ligands, and therefore decrease, even more than usual, the possibility to deduce from them the mechanism of reduction. The same is true to a lesser degree also for Cd^+. Still it seems that some suggestions can be made based on the effect of ligands on the reaction rates.

It is suggested that Zn^+ reacts mainly *via* the outer-sphere mechanism. This is reasonable in view of the very high rates of reaction with $Co(NH_3)_6^{3+}$ and $Co(En)_3^{3+}$ and the behavior of the aquo relative to the hydroxo complex.[3] The fluoro and acetate complexes are less reactive than the $Co(NH_3)_6^{3+}$ complex, also suggesting an outer-sphere mechanism. Still one cannot exclude the possibility that a contribution of the inner-sphere mechanism exists in some of the Zn^+ reductions.

For Cd^+ it is suggested that most of the reductions are *via* the inner-sphere mechanism or at least have a large contribution of it. This is in accordance with the fact that the hydroxo complex is reduced faster than the aquo complex,[3] and the relatively large effect of fluoride as a ligand. Furthermore, this explains the fact that Cd^+ and Zn^+ change their relative reactivities when passing from the $Co(NH_3)_5X$ group to the $Co(En)_2XY$ group. If Zn^+ is really mainly an outer-sphere reducing agent, the effect of changing the ligands on the oxidant is expected to be relatively small, whereas for Cd^+ as an inner-sphere reductant the effect should be larger.[5] This effect is naturally larger for the $Co(En)_2XY$ group as the rate of reduction of $Co(En)_3^{3+}$ is lower than that of $Co(NH_3)_6^{3+}$. It is therefore reasonable that the rate of reduction of $Co(En)_2XY$ complexes, where X and/or Y are good bridging groups, would be higher by Cd^+ than by Zn^+. It is further suggested that as Cd^+ reduces Pb^{2+} faster than Zn^+,[16] that Cd^+ reacts in this case mainly *via* the inner-sphere mechanism.

The relative rates of reaction of Ni^+ with the different complexes suggest that it is an inner-sphere reducing agent. The effect of the ligands in this case is large, changing the rates of reaction by several orders of magnitude, though the absolute rates are high. Furthermore, the rate of reduction of the hydroxo complex is higher than that of the aquo complex.[3] When comparing the specific rates of reaction of Cd^+ and Ni^+ with those of hydrogen atoms, which has been suggested to be an inner-sphere reducing agent,[9-11] the similarity in the effects of ligands is evident, especially for Ni^+. It might be added that the rate of reaction of Cd^+ with the fumarato complex is significantly lower than would be expected from the comparison with the hydrogen atoms; this may be due to the latter adding to the double bond on the ligand.

The suggestion that Zn^+ and Cd^+ are good outer-sphere reductants is reasonable as they have one electron in an S orbital,[14] and it is also expected that Zn^+ would be a better reducing agent by this mechanism, as it is expected that in the Zn, Cd, and Hg group the stability of the lower oxidation state will increase with the atomic weight. On the other hand, the larger cation Cd^+ is more polarizable and therefore probably a better reducing agent *via* the inner-sphere mechanism in accordance with the experiment. The added electron in Ni^+, having a $3d^9$ configuration,[14] is located in an inner orbital and it is reasonable therefore that Ni^+ is less reactive than Zn^+ and Cd^+.

If the suggestion that Cd^+ and Ni^+ do react with some of the complexes *via* the inner-sphere mechanism is true, it has to be concluded that the rate of exchange of the water molecules in the inner hydration shell with the bulk is at least of the order of 5×10^6 sec^{-1}, as reactions with half-lives of the order of 1×10^{-6} sec have been observed.

Finally, it is of interest to note that the effects of ligands on the rate of reduction are similar for these very fast reactions with a large $-\Delta F$ to those found for other reducing agents which act by the same mechanisms but at much lower reaction rates[3-8] (*e.g.*, compare the relative rates of reduction by Cd^+ and $Co(CN)_5^{3-}$ which both react *via* the outer- and inner-sphere mechanism). As expected, though the order of reactivities is kept, the relative effects of the ligands decrease as the reaction rates approach the diffusion-controlled limit. Still, it is found that the ratio

$$R = \frac{k_{Red} + Co(NH_3)_6^{3+}}{k_{Red} + Co(En)_3^{3+}}$$

equals 3.4 and 10.7 for Red = Zn^+ and Cd^+, respectively, very similar values to those found for the relative rates of reduction of these two complexes by Cr^{2+}, V^{2+}, Eu^{2+}, and $Cr(Bipy)_3^{2+}$,[5] where $R = 4.5$, 19, 4.0, and 3.8, respectively, though the specific reaction rates of the latter reductions are five to thirteen orders of magnitude lower than those for Zn^+ and Cd^+. The fact that R is not changed over such a wide range of reactivities can be used as an argument in favor of the Marcus theory, relating the rates of reaction *via* the outer-sphere mechanism to the free-energy gain in the reactions.[24] This agreement with the Marcus theory might be fortuitous as most other Co(III) reductions do not fit the theory, presumably due to the change in the spin multiplicity when reducing Co(III) to Co(II).[3,25]

(24) R. A. Marcus, *J. Phys. Chem.*, 67, 853 (1963).

(25) F. Basolo and R. G. Pearson, "Mechanism in Inorganic Reactions," John Wiley and Sons, Inc., New York, N. Y., 1967, p 507.

Acknowledgments. We are indebted to Dr. M. S. Matheson for his encouragement and discussions throughout this work, to Professor H. Taube, Professor J. Halpern, Professor F. Basolo, and Dr. G. Navon for providing the complexes thus enabling this study, to Professor M. Anbar for helpful discussions, and to Dr. M. C. Sauer for his assistance in the use of his computer program. We wish also to thank the Linac group for their careful operation and Mr. S. Petrek for maintaining the electronic equipment.

Transport in Concentrated Solutions of 1:1 Electrolytes

by P. C. Carman

National Chemical Research Laboratory, South African Council for Scientific and Industrial Research, Pretoria, South Africa *(Received July 1, 1968)*

By neglecting the relaxation effect in concentrated solutions, it is shown that ionic mobilities determined from ionic self-diffusion coefficients give a consistent interpretation of conduction and diffusion measurements. Ionic hydration is assumed and is found to lead to hydration numbers which are reasonably constant over wide ranges of concentration and are consistent with the known behavior of the ions concerned. Where ionic hydration occurs, it should affect transport numbers, and the corresponding relationship is derived and applied. Empirically determined electrophoretic factors agree with those calculated by the Onsager–Fuoss model up to the highest concentrations for neutral salts and only fail for the highest concentrations of HCl. The values of a which must be assumed can be used for accurate calculation of equivalent conductivities in dilute solutions.

Introduction

In the classical paper of Onsager and Fuoss[1] on diffusion and conduction in electrolytes, it was recognized that, except in very dilute solutions, solution viscosity and solvation of ions had to be taken into account as well as interionic effects. Much later, Robinson and Stokes[2] presented a theory of diffusion in concentrated electrolyte solutions which recognized that, apart from solvation effects, diffusion of free solvent must be allowed for. Consequently, if each diffusing species possesses an intrinsic mobility, the appropriate reference frame is that proposed independently by Darken[3] and by Hartley and Crank.[4] A severe limitation to application of this theory is that the intrinsic mobility q_i of ion i is calculated by dividing the limiting mobility q_i^0 by the relative viscosity of the solution, η_r. Basically the same theory was applied by Tamás and Újszászy,[5] but they used self-diffusion coefficients D_i^* to calculate intrinsic mobilities and thereby found that interdiffusion coefficients D_{12} for such electrolyte solutions as could be tested could be correlated excellently up to concentrations of 3–4 gfw/l. This diffusion theory neglected interionic effects, though self-diffusion coefficients are subject to a relaxation correction and interdiffusion coefficients to an electrophoretic correction. Unfortunately, these corrections can be calculated accurately only in very dilute solutions, so that a rigorous approach is not possible. However, it is well known that the electrophoretic correction is small if the ions involved do not differ widely in mobility, so that if relaxation corrections in self-diffusion are also small in concentrated solutions, the theory is well based. Evidence for this assumption is discussed in the following section.

The present paper is based on the same assumptions, applied to the correlation of equivalent conductivities and transport numbers as well as of diffusion coefficients.

Relaxation Corrections and Intrinsic Ionic Mobilities

In conduction, the time of relaxation effect gives rise to a field ΔE_c opposed to the applied field E. The limiting value of $\Delta E_c/E$ derived by Onsager is given by

$$-\frac{\Delta E_c}{E} = \frac{|z_1 z_2|\, e^2 \kappa}{3DkT} \frac{q}{(1-q)} (1 - \sqrt{q}) \qquad (1)$$

where e is the electronic charge, z_i is valence of ion i, D is the dielectric constant of the solvent, and k is the Boltzmann gas constant. κ is the reciprocal mean

(1) L. Onsager and R. M. Fuoss, *J. Phys. Chem.*, 36, 2689 (1932).
(2) R. A. Robinson and R. H. Stokes, "Electrolyte Solutions," 2nd ed, Butterworth and Co. Ltd., London, 1959, p 325.
(3) L. S. Darken, *Trans. Amer. Inst. Min. Met. Eng.*, 175, 184 (1948).
(4) G. S. Hartley and J. Crank, *Trans. Faraday Soc.*, 45, 801 (1949).
(5) J. Tamás and K. Újszászy, *Act. Chim. Hung.*, 49, 377 (1966).

thickness of the ionic atmosphere, given by

$$\kappa^2 = \frac{4\pi e^2}{DkT} \sum n_i z_i^2 \qquad (2)$$

where n_i is number concentration of ions i, while q is a complex function of valence and mobility of ions in solution. For (1:1) electrolytes $q = 1/2$, so that $q/(1 - q) = 1$, and, for aqueous solutions at 25°

$$\kappa = 0.329\sqrt{c} \times 10^8 \qquad (2a)$$

$$-\frac{\Delta E_c}{E} = 0.229\sqrt{c} \qquad (1a)$$

where molarity c is in gram-formula weights per liter. Thus, for $c = 1$, this represents a correction of 23%. In fact, while eq 1 is correct in limiting dilutions, its valid range is very small. If account is taken of a, the distance of closest approach between ions, Falkenhagen and Kelbg[6] divided the limiting value by the factor $(1 + \kappa a)(1 + \sqrt{q}\kappa a + q\kappa^2 a^2/3)$. Thus, for a typical value of a of 3.5 Å, the correction is reduced to a rather flat maximum of only about 5.2% at $\kappa a \simeq 0.9$, corresponding to $c \simeq 0.6$. It would be somewhat smaller for larger values of a and vice versa. In a solvent with low dielectric constant, *e.g.*, methanol at 25°, the limiting law should give a very large effect, namely, $\Delta E_c/E = 0.83\sqrt{c}$, and even the Falkenhagen correction for the same value of a gives a maximum correction of 18.6% for $c \simeq 0.25$.

Actually, the factor is not valid beyond $\kappa a \simeq 0.1$ corresponding to $c \simeq 0.01$. A similar factor was confirmed by Onsager and Fuoss[7,8] as a "first approximation," while extremely complex calculations for a further approximation were only valid to $\kappa a \simeq 0.2$ and did not much alter the magnitude of the correction in this range.

In the case of ionic self-diffusion, a retarding field ΔE^* is set up by the diffusing ion i^* and the driving force X_i^* is reduced by $e_i \Delta E^*$, with an Onsager limiting value[9,10] given by

$$-\frac{e_i \Delta E^*}{X_i^*} = \frac{z_i^2 e^2 \kappa}{3DkT}(1 - \sqrt{q^*}) \qquad (3)$$

The close similarity to eq 1, especially for 1:1 electrolytes, is obvious. If the ions involved do not have widely different mobilities, q^* for 1:1 electrolytes usually lies between 0.4 and 0.6, so that eq 1 and 3 give closely similar values for the same solution. Further, by extending the method of calculation of Onsager and Kim[11] to take a into account, it is found that a factor exactly analogous to that of Falkenhagen is also applicable, with a similar valid range.

Thus, apart from a strong tendency to give much smaller values than the Onsager limiting law, it is not possible from theory to predict relaxation effects above very small concentrations. It is necessary to turn to experimental studies of self-diffusion coefficients, since conductivity measurements involve an increasingly dominant electrophoretic effect. Unfortunately, measurements of high accuracy are difficult to achieve, so that there are few suitable data. Mills and Godbole[12] measured D_{Na}^* in NaCl solutions from $c = 0.0002$ to 0.097 and showed that the limiting law is valid only to $c \simeq 0.002$. The limiting value D_{Na}^0 is 1.334×10^{-5} cm²/sec and the value obtained at the highest concentration was 1.28×10^{-5} cm²/sec, which agrees almost exactly with a correction for $\eta_r = 1.01$ and a Falkenhagen relaxation correction with $a = 3.5$ Å. The Onsager correction gives 1.25×10^{-5} cm²/sec. An earlier accurate measurement by Mills[13] gave 1.30×10^{-5} cm²/sec at $c = 0.1$ for D_{Na}^*, which would indicate that even the Falkenhagen relaxation correction is excessive. Data of Mills[13,14] assembled by Robinson and Stokes[15] for D_{Na}^* in NaCl and of D_{Cl}^* in various chlorides correspond on the whole to relaxation corrections at c = 0.1 which are decidedly less than the Falkenhagen correction. For $c \geqslant 0.5$, these are the data used in this paper.

Kraus and coworkers[16,17] measured D_{Na}^* for $m = 0.1$ gfw of NaCl or $NaClO_4$/kg of solvent in mixtures of water with methanol, ethanol, propanol, glycol, and glycerol, all of which have low dielectric constants. They confirmed $D_{Na}^* = 1.28 \times 10^{-5}$ cm²/sec for water. Accurate data to calculate limiting values D_{Na}^0 from limiting equivalent conductivities of Na^+ ions are available only for 50 mol % methanol, pure methanol, and ethanol, and these are given in Table I,[18] together with values corrected (i) for viscosity due to solute alone and (ii) for both viscosity and the Falkenhagen relaxation factor.

Except for $m = 0.1$ in pure methanol, simple viscosity corrections give values close to the experimental one and, even for this solvent, the value of Ellard, *et al.*,[19] for $m = 0.04$, given in the last column, shows similar agreement. The further use of the Falkenhagen correction gives a good correlation in the exceptional case, but is decidedly excessive for the others. In the other solvents, which covered an enormous range of dielectric

(6) H. Falkenhagen and G. Kelbg, *Z. Elektrochem.*, **58**, 653 (1954).
(7) R. M. Fuoss and L. Onsager, *J. Phys. Chem.*, **61**, 668 (1957).
(8) R. M. Fuoss and F. Accascina, "Electrolytic Conductance," Interscience Publishers, Inc., New York, 1959.
(9) L. Onsager, *Ann. N. Y. Acad. Sci.*, **46**, 263 (1945).
(10) A. W. Adamson, *J. Phys. Chem.*, **58**, 514 (1954).
(11) L. Onsager and S. K. Kim, *ibid.*, **61**, 215 (1957).
(12) R. Mills and E. W. Godbole, *J. Amer. Chem. Soc.*, **82**, 2395 (1960).
(13) R. Mills, *ibid.*, **77**, 6116 (1955).
(14) R. Mills, *J. Phys. Chem.*, **61**, 1631 (1957).
(15) Reference 2, p 317.
(16) A. E. Marcinkowsky, H. O. Phillips, and K. A. Kraus, *J. Phys. Chem.*, **69**, 3968 (1965).
(17) A. E. Marcinkowsky, H. O. Phillips, and K. A. Kraus, *ibid.*, **72**, 1201 (1968).
(18) L. G. Longsworth and D. A. MacInnes, *ibid.*, **43**, 239 (1939).
(19) J. A. Ellard, W. D. Williams, and L. R. Dawson, *Trans. Kentucky Acad. Sci.*, **18**, 8 (1957).

Table I: D_{Na}^* in Various Solvents

	Solvent			
	50 mol % methanol	Methanol	Ethanol	Methanol
	Concn, m			
	0.1 NaCl	0.1 NaCl	0.1 $NaClO_4$	0.04 NaCl
η_r, solvent	1.48[a]	0.606[a]	1.228	0.606
η_r, solution	1.515	0.645	(1.33)[b]	(0.622)[b]
$D_{Na}^* \times 10^5$ cm²/sec (exptl)	0.755	0.98	(0.53)[b]	1.15
$D_{Na}^0 \times 10^5$ cm²/sec	0.787	1.204	0.541	1.204
$D_{Na}^* \times 10^5$ cm²/sec (calcd)[c]	0.77	1.13	0.50	1.17
κa, $a = 3.5$ Å	0.426	0.500	0.580	0.317
$D_{Na}^* \times 10^5$ cm²/sec (calcd)[d] with relaxation	0.72	1.01	0.46	1.07

[a] Data from ref 18. [b] Extrapolated or interpolated values. [c] $D_{Na}^0 \times (\eta_r$ solvent$)/(\eta_r$ solution$)$. [d] Further correction of (c) with Falkenhagen factor.

constants and viscosities, limiting equivalent conductivities for NaCl were available but not transport numbers. By assuming reasonable values for these, it was found throughout that simple viscosity corrections, using $\eta_r^{0.7}$, were sufficient to correlate self-diffusion coefficients and limiting conductivities. As in three of the four cases in Table I, any relaxation corrections must have been far less than calculated values. This is not surprising when it is noted that κa values in Table I are far above the valid limit of 0.1.

In brief, even at these relatively low concentrations, it seems that relaxation corrections are smaller than any calculated value. Kraus[17] has suggested that intrinsic mobilities are larger than expected from the limiting values, and that this masks relaxation effects. This is a possibility, but on the whole, it seems preferable to adopt the view that relaxation effects tend to become small and even to disappear at higher concentrations, so that D_i^* gives a direct measure of intrinsic mobility

$$q_i = D_i^*/RT \tag{4}$$

In fact, it offers the only possibility of measuring this specific property. For the aqueous solutions of 1:1 electrolytes considered here, $c = 0.5$ is the lowest concentration used. The units used in eq 4 for RT are joules/gram-formula weight.

In the case of ions of valence above one, even derivation of a "first approximation" valid to $\kappa a \simeq 0.1$ necessitates doubtful assumptions, and for, say, $CaCl_2$, this corresponds to $c < 0.003$. Experimental data are lacking, so that the present discussion is limited to 1:1 electrolytes, thereby enabling equations to be much simplified. It is sufficient to note here that Tamás and Újszászy[5] could interpret diffusion data for $CaCl_2$ up to $c \simeq 3$ with available self-diffusion coefficients.

Electrophoretic Effect

In the following, the independently transported components are electrolyte (1) and water (2), while the actual species undergoing transport are hydrated cations (3), hydrated anions (4), and free water (5). Concentrations are in gram-formula weights per cubic centimeter, so that the molarity $c = 1000c_1$. It is often convenient to replace the ratio c_1/c_2 by m/m_2, where m is molality and $m_2 = 55.5$.

In a 1:1 electrolyte $c_3 = c_4 = c_1$, valence $z_3 = -z_4 = 1$, and, if ions are hydrated with h_3 and h_4 molecules of water, respectively, so that hydration of 1 formula-weight of electrolyte is h

$$h = h_3 + h_4 \tag{5}$$

$$c_5 = (c_2 - hc_1) \tag{6}$$

The driving force acting on a species i is

$$X_i = -(\nabla\mu_i - z_iEF) \tag{7}$$

where μ_i is chemical potential in joules per gram-formula weight, F is the Faraday in coulombs, and E is any electrical field involved in the transport in volts per centimeter.

Then, if there were no electrophoretic effect, the flux of hydrated ion i would be given on a Darken reference frame by

$$J_i^h = c_iq_iX_i^h = c_1q_iX_i^h \tag{8}$$

The electrophoretic correction arises from volume forces acting upon all ions in the diffuse double layer surrounding ion i, and therefore depends upon both X_3^h and X_4^h. According to Onsager and Fuoss,[1] the corrected equation for J_i^h is

$$J_i^h = c_i\left[q_iX_i^h - \frac{\kappa \times 10^7}{6\pi\eta(1 + \kappa a)} \frac{z_i(z_ic_iX_i^h + z_jc_jX_j^h)}{(n_iz_i^2 + n_jz_j^2)}\right] \tag{9}$$

which, for aqueous solutions of 1:1 electrolytes at 25° reduces to

$$J_i^h = c_1\left[q_iX_i^h - \frac{\beta_0}{2\eta_r}(X_i^h - X_j^h)\right] \quad (i, j = 3, 4; j \neq i) \tag{9a}$$

where

$$\beta_0 = 3.24 \times 10^{-9} \times \frac{\sqrt{c}}{1 + \kappa a} \qquad (10)$$

Onsager and Fuoss[1] also introduced a second more complex correction term, with an opposite sign, but its theoretical basis is open to question, and it has had no well-based experimental confirmation, so that it has been omitted.

Equation 9 is only valid for $\kappa a \ll 1$, so that, for the relatively large values of κa corresponding to the concentrations discussed here, the form of eq 3 has been retained, but with an empirical electrophoretic factor β to replace β_0/η_r, *i.e.*

$$J_i^h = c_1\left[q_i X_i^h - \frac{\beta}{2}(X_i^h - X_j^h)\right] \quad (i, j = 3, 4; j \neq i) \qquad (11)$$

Ionic Phenomenological Coefficients

Equation 11 employs conjugate forces and fluxes and its coefficients thus conform to the phenomenological coefficients of nonequilibrium thermodynamics. The driving forces are, however, expressed in terms of hydrated ions, whereas thermodynamic activity coefficients for electrolytes are referred to unhydrated electrolytes. Thus, if X_i is the driving force for unhydrated ion i, we have

$$X_i^h = X_i + h_i X_5 \qquad (12)$$

$$X_5 = X_2 \qquad (13)$$

so that, by using the simplifying assumption that ions are uniformly hydrated, the flux for total ion i, J_i^0, and for total water, J_2^0, are given by

$$J_i^0 = J_i^h = c_1\left[\left(q_i - \frac{\beta}{2}\right)X_i + \frac{\beta}{2}X_j + \left\{h_i q_i - (h_i - h_j)\frac{\beta}{2}\right\}X_2\right] \quad (i, j = 3, 4; j \neq i) \qquad (14)$$

$$J_2^0 = h_3 J_3^0 + h_4 J_4^0 + q_5(c_2 - hc_1)X_2 \qquad (15)$$

We have thus a set of symmetrical l_{ij}^0 phenomenological coefficients

$$l_{ii}^0 = c_1\left(q_i - \frac{\beta}{2}\right) \qquad (16)$$

$$l_{34}^0 = l_{43}^0 = c_1\frac{\beta}{2} \qquad (17)$$

$$l_{2i}^0 = l_{i2}^0 = c_1\left\{h_i q_i - (h_i - h_j)\frac{\beta}{2}\right\} \qquad (18)$$

$$l_{22}^0 = c_2 q_5\left(1 - h\frac{m}{m_2}\right) + h_3 l_{23}^0 + h_4 l_{24}^0 \quad (i, j = 3, 4; j \neq i) \qquad (19)$$

Transformation from Darken frame to a solvent-fixed frame requires use of the equation[20]

$$l_{ij}^r = l_{ij}^0 - \frac{c_i}{c_2}l_{2j} - \frac{c_j}{c_2}l_{2i} + \frac{c_i c_j}{c_2^2}l_{22}^0 \qquad (20)$$

giving

$$l_{ii}^r = c_1\left[\left(q_i - \frac{\beta}{2}\right) - \frac{2m}{m_2}\left\{h_i q_i - (h_i - h_j)\frac{\beta}{2}\right\} + \frac{m}{m_2}\frac{l_{22}^0}{c_2}\right] \quad (i, j = 3, 4; j \neq i) \qquad (21)$$

$$l_{34}^r = c_1\left[\frac{\beta}{2} - \frac{m}{m_2}\{h_3 q_3 + h_4 q_4\} + \frac{m}{m_2}\frac{l_{22}^0}{c_2}\right] \qquad (22)$$

These correspond to the l_{ij} coefficients of Miller[21] for 1:1 electrolytes. Clearly, though such coefficients can be used as a means of expressing experimental data, they are not simple physical quantities, but are relatively complex functions of mobilities of ions and of water, of electrophoretic corrections, and of hydration numbers. In the following sections, eq 16–22 will be used to derive expressions for equivalent conductivity, Λ, transport number, t_3, and interdiffusion coefficient, D_{12}, in terms of these fundamental quantities.

Equivalent Conductivity and Electrophoretic Factor

As $X_i = z_i EF$, $E = 1$, and $X_2 = 0$

$$J_i^0 = z_i(l_{ii}^0 - l_{34}^0)F \qquad (i = 3, 4) \qquad (23)$$

and hence

$$\Lambda = \frac{F}{c_1}(J_3^0 - J_4^0) = \frac{F^2}{c_1}(l_{33}^0 + l_{44}^0 - 2l_{34}^0) \qquad (24)$$

i.e.

$$\Lambda = F^2(q_3 + q_4 - 2\beta) \qquad (25)$$

As Miller[21] has pointed out, Λ is reference-frame independent, and hence is not affected by hydration or solvent transport. This is confirmed by writing

$$\Lambda = \frac{F^2}{c_1}(J_3^r - J_4^r) = \frac{F^2\alpha}{c_1}$$

where we find

$$\alpha = l_{33}^r + l_{44}^r - 2l_{34}^r = l_{33}^0 + l_{44}^0 - 2l_{34}^0 \qquad (26)$$

From eq 25, if q_3 and q_4 are obtained from D_i^*, β can be evaluated. Even if the assumption that relaxation corrections can be neglected is not true, these are so nearly equal for conduction and self-diffusion that values of β calculated from eq 25 would be little affected.

(20) P. C. Carman, *J. Phys. Chem.*, **72**, 1707, 1713 (1968).
(21) D. G. Miller, *ibid.*, **70**, 2639 (1966).

Transport Numbers

These are measured on a solvent-fixed frame, so that

$$t_3 = \frac{J_3^r}{(J_3^r - J_4^r)} = \frac{l_{33}^r - l_{34}^r}{\alpha} \tag{27}$$

On substituting from eq 21 and 22

$$t_3 = \frac{(q_3 - \beta)[1 - h(m/m_2)]}{q_3 + q_4 - 2\beta} + h_4 \frac{m}{m_2} \tag{28}$$

As in the case of Λ, any relaxation corrections for q_i in conduction and self-diffusion tend to cancel out.

According to eq 28, transport numbers are affected by ionic hydration, a point which has been overlooked in the past due to use of solvent-fixed frames, whereas the Darken frame should have been employed for intrinsic mobilities. The Stokes type of equation[22] is obtained if hydration terms are omitted and we express $q_3 = q_3^0/\eta_r$, $\beta = \beta_0/\eta_r$, *i.e.*

$$t_3 = \frac{(q_3^0 - \beta_0)}{(q_3^0 + q_4^0 - 2\beta_0)} \tag{29}$$

Diffusion and Hydration Numbers

If J_1^r is the flux of total salt relative to a solvent-fixed frame and is represented by

$$J_1^r = L_{11}^r X_1 \tag{30}$$

then

$$D_{12}' = 2RT \frac{L_{11}^r}{c_1} \tag{31}$$

where

$$D_{12} = D_{12}'\left(1 + \frac{\partial \ln \gamma_\pm}{\partial \ln m}\right) \tag{32}$$

$\gamma_\pm$ being the mean ionic activity coefficient for molalities,[21] m. To obtain L_{11}^r, we have

$$J_1^0 = J_1^h = c_1 q_1 X_1^h = c_1 q_1 (X_1 + hX_2) \tag{33}$$

where q_1 is the effective intrinsic mobility of the whole salt. Further

$$J_1^0 = J_3^0 = J_4^0$$

and $X_1 = X_3 + X_4$, whence, from eq 14, X_3 and X_4 can be eliminated, giving eq 33 with

$$q_1 = \frac{q_3 q_4 - (\beta/2)(q_3 + q_4)}{q_3 + q_4 - 2\beta} \tag{34}$$

$$= \frac{q_3 q_4}{q_3 + q_4} - \frac{\beta}{2} \frac{(q_3 - q_4)^2}{(q_3 + q_4)(q_3 + q_4 - 2\beta)} \tag{34a}$$

Again, from eq 15

$$J_2^0 = hJ_1^0 + q_5(c_2 - hc_1)X_2$$

whence we obtain the coefficients

$$\left.\begin{aligned} L_{11}^0 &= c_1 q_1; \qquad L_{12}^0 = hc_1 q_1 \\ L_{22}^0 &= c_2\left(1 - h\frac{m}{m_2}\right)q_5 + h^2 c_1 q_1 \end{aligned}\right\} \tag{35}$$

Finally, transforming to a solvent-fixed frame

$$L_{11}^r = L_{11}^0 - 2\frac{m}{m_2} L_{12}^0 + \frac{m^2}{m_2^2} L_{22}^0 \tag{36}$$

Substituting from eq 35 and 36 in eq 31, we obtain

$$D_{12}' = 2RT\left[q_1\left(1 - h\frac{m}{m_2}\right)^2 + \frac{m}{m_2} q_5\left(1 - h\frac{m}{m_2}\right)\right] \tag{37}$$

Now, the self-diffusion coefficient of water is determined partly by mobility of free water, *i.e.*, a fraction $[1 - h(m/m_2)]$ of total water and partly by water bound to ions, so that

$$D_2^* = RT\left[q_5\left(1 - h\frac{m}{m_2}\right) + \frac{m}{m_2}(h_3 q_3 + h_4 q_4)\right] \tag{38}$$

Substituting $q_5[1 - h(m/m_2)]$ in eq 37, we obtain effectively the same equation as Tamás and Újszászy[5] for the special case of 1:1 electrolytes, if the electrophoretic factor β in q_1 is omitted.

Equation 37 is to be compared with that given by Robinson and Stokes,[2] which may be written

$$D_{12}' = \frac{1}{\eta_r}\left[(D_{12}^0 + \Delta_1 + \Delta_2)\left(1 - h\frac{m}{m_2}\right)^2 + \frac{2m}{m_2}(D_2^*)^0\left(1 - h\frac{m}{m_2}\right)\right] \tag{39}$$

They are based on the same assumptions, but instead of using self-diffusion coefficients to calculate mobilities, viscosity-corrected limiting values are employed. Thus, it is assumed that

$$q_5 = q_5^0/\eta_r = (D_2^*)^0/\eta_r RT$$

where $(D_2^*)^0$ is the self-diffusion coefficient of pure water, and that

$$q_1 = \frac{1}{2\eta_r RT}(D_{12}^0 + \Delta_1 + \Delta_2)$$

$$= \frac{1}{\eta_r}\left[\frac{q_3^0 q_4^0}{q_3^0 + q_4^0} - \frac{\beta_0}{2}\frac{(q_3^0 - q_4^0)^2}{(q_3^0 + q_4^0)^2} + \frac{\Delta_2}{2RT}\right]$$

the limiting mobilities q_i^0 being obtained from limiting equivalent conductivities. It can be seen that the Δ_1 term corresponds to the electrophoretic correction term in eq 34a, while Δ_2 represents a second correction of

(22) Reference 2, p 156, and R. H. Stokes, *J. Amer. Chem. Soc.*, 76, 1988 (1954).

Table II: Data for NaCl Solutions

c	m	Λ	t_3		$D_3^* \times 10^5$	$D_4^* \times 10^5$	$D_2^* \times 10^5$	$D_{12} \times 10^5$	$1 + \partial \ln \gamma_\pm / \partial \ln m$	η_r
0.5	0.506	93.62	0.375	0.377	1.279	1.854	2.32	1.474	0.930	1.049
1.0	1.022	85.76	0.369	0.375	1.234	1.772	2.24	1.484	0.979	1.094
1.5	1.549	79.86	0.365	0.372	1.180	1.677	2.14	1.501	1.040	1.158
2.0	2.086	74.71	0.362	0.371	1.134	1.614	2.05	1.518	1.108	1.219
2.5	2.635	70.02	0.359	0.369	1.081	1.525	1.97	1.542	1.189	1.294
3.0	3.197	65.51		0.368	1.030	1.440	1.87	1.564	1.276	1.382
4.0	4.360	57.23		0.366	0.932	1.25	1.68	1.594	1.472	1.588
5.0	5.589	49.46		0.364	(0.836)[a]	1.07	(1.50)[a]	1.590	1.685	1.862
Reference		26	29	28	13	14, 30	31, 32, 33	27		34

[a] Parenthesized values have been obtained by extrapolation.

Table III: Calculations for NaCl Solutions

c	m/m_2	$q_3 \times 10^9$	$q_4 \times 10^9$	$\beta \times 10^9$	$\beta_0/\eta_r \times 10^9$ $a = 3.2$ Å	$D_{12} \times 10^5$ cm²/sec, calcd	t_3, calcd $h_4 = 0$	t_3, calcd $h_4 = 0.1$
0.5	0.0092	5.16	7.46	1.28	1.28	1.42	0.381	0.382
1.0	0.0184	4.96	7.15	1.46	1.44	1.43	0.369	0.371
1.5	0.0279	4.75	6.75	1.50	1.49	1.45	0.362	0.365
2.0	0.0376	4.55	6.50	1.52	1.52	1.47	0.357	0.361
2.5	0.0474	4.35	6.15	1.50	1.50	1.51	0.354	0.359
3.0	0.0576	4.15	5.80	1.46	1.46	1.53	0.349	0.355
4.0	0.0785	3.75	5.04	1.32	1.34	1.58	0.349	0.357
5.0	0.1005	3.37	4.31	1.18	1.18	1.60	0.352	0.362

opposite sign which, as discussed earlier, has been omitted here. Equation 39 was applied successfully to several 1:1 halides up to c = 1, but, as will appear in the following, use of actual mobilities in concentrated solutions leads to hydration numbers which apply over wider ranges and are often more realistic.

Since the small term containing h_3 and h_4 in eq 38 plays little part, eq 34, 37, and 38 give the total hydration number h. With regard to the electrophoretic term in eq 34a, this has not been applied to NaCl, KCl, LiCl since values of q_3 and q_4 are comparable and therefore the resulting correction is very small. Further, if a second electrophoretic term were used, as in eq 39, it would tend to cancel the β correction or even reverse its sign. Finally, if a relaxation correction were not negligible, q_3 and q_4 should have somewhat larger values, so that omission of a negative electrophoretic correction tends to compensate for this. There is indeed no decisive experimental foundation for electrophoretic corrections in salt solutions.[10,23] Stokes[23] applied the corresponding correction to dilute solutions of $CaCl_2$ with apparent success, but the D_{12} values which he used were later shown to be too small.[24] In this and other cases, as good an agreement could be found by omitting electrophoretic corrections as by using any theoretically derived values.

In the case of HCl, the electrophoretic correction term is too large to be ignored and has therefore been employed.

Solutions of NaCl at 25°

There is a great paucity of the data for concentrated solutions required for this discussion, namely, Λ, t_3, D_3^*, D_4^*, D_2^*, D_{12}, $\gamma_\pm$, density, and relative viscosity. Only in fact for aqueous NaCl solutions at 25° are complete data of satisfactory accuracy available. In this and the following sections, the valuable compilation of data by Miller[21] for Λ, t_3, D_{12}, $\gamma_\pm$, and relations between c and m has been utilized in full, so that his critique of sources need not be repeated. Where possible, data have been extended to higher concentrations, even when short extrapolations of existing data are necessary. This is feasible, since self-diffusion coefficients and relative fluidities plotted against c are usually linear or nearly linear over wide ranges. All values of $[1 + (\partial \ln \gamma_\pm / \partial \ln m)]$ in this and the following sections have been obtained from Miller[21] or have been derived from the compilation of osmotic coefficients given by Robinson and Stokes.[25] Relative viscosities, except where otherwise indicated, were obtained from the "International Critical Tables."

For NaCl, values of Λ[26] and of D_{12}[27] are available to

(23) R. H. Stokes, *J. Amer. Chem. Soc.*, **75**, 4563 (1953).

(24) H. S. Harned and H. W. Parker, *ibid.*, **77**, 265 (1955).

(25) Reference 2, pp 476 and 483.

(26) J. F. Chambers, J. M. Stokes, and R. H. Stokes, *J. Phys. Chem.*, **60**, 985 (1956).

(27) V. Vitagliano and P. A. Lyons, *J. Amer. Chem. Soc.*, **78**, 1549 (1956).

$c = 5.0$, and Smits and Duyvis[28] give values of t_3 to saturation. These are a little larger than those of Currie and Gordon, as corrected by Spiro,[29] and the latter may be equally valid, as the methods differed, but they extend only to $m \simeq 2.5$. The ionic self-diffusion coefficients have been repeatedly measured, and the diaphragm cell values of Mills may be regarded as accurate.[13,14] For Na^+,[13] his values have been extrapolated to $c = 5.0$, while, for Cl^-, his data[14] agree well with Wang[30] so that the two have been combined to cover the whole range. For water, the three references[31-33] given agree on the ratio of D_2^* to that for pure water, and a value of 2.4×10^{-5} cm²/sec has been used for the latter. The values have been extrapolated from $c = 4.0$ to $c = 5.0$.

Table II summarizes the experimental data used,[34] and Table III contains the values calculated from these. Empirical values of β are compared with β_0/η_r, using eq 19 with $a = 3.2$ Å. They agree well, and β passes through a maximum which is clearly due to viscosity. This is further discussed later. Calculated values of D_{12} are then obtained, using q_1 uncorrected for electrophoresis and assuming $h = 1.5$. This is selected to give best agreement at the highest concentrations, which are most sensitive to variations in h. The calculated values at the lower concentrations are somewhat too small, but as they are relatively little affected by changes in h, the corresponding values of q_3 and q_4 are presumably too low. This can be accounted for if we assume that self-diffusion coefficients at $c = 0.5$ are in fact still subject to a relaxation correction of about 2% and that this decreases to zero at higher concentrations. As relaxation corrections counterbalance in conduction and self-diffusion, this would not affect β or t_3.

Finally, the values of β and h so obtained are used to calculate t_3 by eq 28. With $h_4 = 0$, it is found to give results somewhat below the experimental ones. By taking $h_4 = 0.1$, values are obtained which tend to lie between those of Currie and Gordon and of Smits and Duyvis. In brief, the data accord with the accepted view that it is the Na^+ ion which is hydrated and that hydration of Cl^- is minimal. Smits and Duyvis[27] found their t_3 agreed very well with the Stokes eq 29 over the whole concentration range, using $a = 5.2$ Å. As eq 28 uses a larger value of β and a hydration factor, both of which give smaller values of t_3, it is of interest to note the reason for the approximate agreement between eq 28 and 29, namely, that q_3 decreases less rapidly than q_4, thereby tending to increase t_3.

Low Concentrations

A surprising feature of Table II is that the experimental values of β agree so well with the simple Onsager electrophoretic correction up to high concentrations. The seat of the volume forces involved is at a distance of $[a + (1/\kappa)]$ from the center of ion i, and this has a value of only 4.8 Å for $c = 4.0$ and $a = 3.2$ Å. Thus, ordinary hydrodynamic laws apparently still afford a reasonably good approximation at these dimensions. This is, indeed, consistent with the observation by Robinson and Stokes[35] that ions with a radius in excess of about 5 Å have limiting equivalent conductivities conforming to Stokes' law, both in magnitude and in agreement with Walden's rule.

At high dilutions, $1/\kappa$ is large, so that the Onsager correction is valid. Since a is an arbitrary parameter, the significance of the foregoing agreement in concentrated solutions is strengthened if it can be shown that the same value of a is applicable to cases when $\kappa a < 0.1$, where theoretical calculations are valid. If, in this range, we assume that ionic mobilities are equal to viscosity corrected limiting mobilities and use the Falkenhagen relaxation correction, then, at 25°

$$\Lambda = \frac{1}{\eta_r}\left(\Lambda_0 - \frac{60.2\sqrt{c}}{1 + \kappa a}\right) \times \left[1 - \frac{0.229\sqrt{c}}{(1 + \kappa a)(1 + 0.71\kappa a + \kappa^2 a^2/6)}\right] \quad (40)$$

The agreement between experimental and calculated values of Λ is shown in Table IV up to $c = 0.05$. Up to $c = 0.01$, corresponding to $\kappa a = 0.105$, agreement is good, and the total correction is large enough to be affected by a seriously incorrect value of a. At $c = 0.05$, the calculated value is somewhat low, indicating that the Falkenhagen relaxation correction is already excessive.

KCl Solutions at 25°

For three other 1:1 electrolytes, $D_{Cl^-}^*$ has been measured with sufficient accuracy for the present calculations, namely, KCl, LiCl, HCl,[14,15] and all other data,

Table IV: Equivalent Conductivities in Dilute NaCl Solutions at 25°

c	κa, $a = 3.2$ Å	Λ_{exptl}	Λ_{calcd}
0	...	126.45	...
0.0001	0.0107	125.59	125.56
0.0005	0.0237	124.50	124.52
0.001	0.0333	123.70	123.75
0.005	0.075	120.65	120.70
0.01	0.105	118.51	118.41
0.05	0.237	111.06	110.50

(28) L. J. M. Smits and E. M. Duyvis, *J. Phys. Chem.*, **70**, 2747 (1966).
(29) M. Spiro, *J. Chem. Phys.*, **42**, 4060 (1965).
(30) J. H. Wang, *J. Amer. Chem. Soc.*, **74**, 1612 (1952).
(31) D. W. McCall and D. C. Douglass, *J. Phys. Chem.*, **69**, 2001 (1965).
(32) J. H. Wang, *ibid.*, **58**, 686 (1954).
(33) L. Devell, *Acta. Chem. Scand.*, **16**, 2177 (1962).
(34) L. L. Ezrokhi, *J. Appl. Chem. USSR*, **25**, 917 (1952).
(35) Reference 2, pp 125–130.

Table V: Data for KCl Solutions

c	m	Λ	t_3	$D_1^* \times 10^5$	$D_2^* \times 10^5$	$D_{12} \times 10^5$	$1 + \partial \ln \gamma_\pm / \partial \ln m$	η_r
0.5	0.509	117.27	0.489	1.963	2.42	1.850	0.892	0.999
1.0	1.033	111.87	0.488	1.955	2.40	1.892	0.905	0.999
1.5	1.574	108.27	0.487	1.931	2.38	1.943	0.931	1.004
2.0	2.133	105.23	0.487	1.907	2.36	1.999	0.963	1.010
3.0	3.310	99.46	0.486	1.841	2.33	2.112	1.037	1.036
4.0	4.587	93.46	(0.486)[a]	1.774	2.28	(2.205)[a]	1.085	1.073
Reference		26	37	14	5, 31	38		34

[a] Extrapolated values.

Table VI: Calculated Values for KCl Solutions

c	m/m_2	$q_4 \times 10^9$	$q_3 \times 10^9$	$\beta \times 10^9$	$\beta_0/\eta_r \times 10^9$ $a = 3.07$ Å	$D_{12} \times 10^5$ cm²/sec $h = 0$ (calcd)
0.5	0.0091	7.92	7.62	1.47	1.33	1.75
1.0	0.0186	7.88	7.60	1.75	1.63	1.81
1.5	0.0283	7.78	7.57	1.81	1.78	1.87
2.0	0.0383	7.69	7.38	1.89	1.87	1.97
3.0	0.0596	7.42	7.10	1.92	1.99	2.16
4.0	0.0826	7.15	6.85	1.98	2.00	2.28

except for self-diffusion data for the cations, are also available. In the case of KCl, Friedman and Kennedy[36] measured D_i^* for both ions, but later measurements of Mills[14] showed $D_{Cl^-}^*$ to be too large, and the values of $D_{K^+}^*$ must therefore also be suspect.

It is possible to make calculations for the foregoing three electrolytes on a trial and error basis, namely, to adopt a possible hydration number, to calculate q_3 and β from this, using Λ and t_3, and then to see if this gives reasonably correct values of D_{12} over a wide range of concentrations. The procedure has naturally a greater margin of error than direct determination of q_3.

This has been applied to KCl in Tables V[37,38] and VI. Table V gives the experimental data up to c = 4.0, the value for D_{12} at $c = 4.0$ being subject to a short extrapolation. As minimal hydration is to be expected for both K^+ and Cl^- ions, the calculated values in Table VI have been based simply on the assumption that $h = 0$. In this case, Fuoss and Accascina[39] have shown that a value of $a = 3.07$ Å gives an excellent correlation for very accurate measurements in dilute solutions, so that values of β_0/η_r have been calculated with this value and can be seen to show a good agreement with β. Thus, here, no arbitrary parameters for concentrated solutions have been introduced. The agreement between experimental and calculated values of D_{12} at the lower concentrations are distinctly poorer than in the case of NaCl. To explain this in the same way would indicate that a rather large relaxation correction for q_i had been neglected. Potassium halides represent one case in which a positive second electrophoretic term, which has been omitted here, can make a well-defined correction to D_{12} since the first term is effectively zero, due to almost equal mobilities of anions and cations.[38]

LiCl Solutions at 25°

The case of LiCl is of interest since the cation is strongly hydrated. Table VII[40-42] summarizes the available data up to $c = 4.0$. It includes small extrapolations for t_3 from $c = 2.95$ to $c = 3.0$ and for D_{Cl}^* from $c = 3.74$ to $c = 4.0$. The results of the calculations appear in Table VIII, on the assumption that $h = 3.5$ and that only the Li^+ ion is hydrated. From $c = 0.5$ to $c = 3.0$, β and q_3 were calculated as described above, and the calculated values of D_{12} are seen to agree well with experiment for the whole range. There is a single experimental check available, since the value for q_3 at $c = 2.0$ corresponds to $D_{Li}^* = 0.87 \times 10^{-5}$, which agrees well with the value of 0.89×10^{-5} at $m = 2.0$, obtained by Andreev[43] using a diaphragm cell. At $c = 4.0$, as no value was available for t_3, the nearly linear plot of q_3 *vs.* c was extrapolated, and the value obtained used to calculate t_3 and D_{12}. The former fits well on the extrapolated curve of t_3 *vs.* c and the latter

(36) A. M. Friedman and J. W. Kennedy, *J. Amer. Chem. Soc.*, **77**, 4499 (1955).

(37) T. Shedlowsky and D. A. MacInnes, *ibid.*, **59**, 503 (1937).

(38) L. Gosting, *ibid.*, **72**, 4418 (1950); H. S. Harned and R. L. Nuttall, *ibid.*, **71**, 1460 (1949).

(39) Reference 8, p 203.

(40) M. Jacopetti, *Gazz. Chim. Ital.*, **72**, 241 (1942).

(41) G. Jones and B. C. Bradshaw, *J. Amer. Chem. Soc.*, **54**, 138 (1932).

(42) V. Vitagliano, *Gazz. Chim. Ital.*, **90**, 876 (1960).

(43) G. A. Andreev, *Dokl. Akad. Nauk SSSR*, **145**, 358 (1962).

Table VII: Data for LiCl Solutions

c	m	Λ	t_3	$D_4^* \times 10^5$	$D_3^* \times 10^5$	$D_{12} \times 10^5$	$1 + \partial \ln \gamma_\pm / \partial \ln m$	η_r
0.5	0.506	81.36	0.299	1.815	2.28	1.272	1.013	1.075
1.0	1.022	72.77	0.286	1.678	2.16	1.302	1.142	1.152
1.5	1.548	66.90	0.276	1.588	2.03	1.337	1.275	1.237
2	2.085	61.79	0.269	1.494	1.91	1.369	1.433	1.327
3	3.197	52.80	(0.256)[a]	1.300	1.66	1.426	1.819	1.527
4	4.369	44.87	(0.245)[b]	(1.12)[a]	1.44	1.466	2.246	1.764
Reference		40	41	14	31	42		

[a] Extrapolated values. [b] Calculated from extrapolated value of q_3.

Table VIII: Calculated Values of LiCl

c	m/m_2	$q_4 \times 10^9$	$q_3 \times 10^9$ (calcd)	$\beta \times 10^9$	$\beta_0/\eta_r \times 10^9$ $a = 3.0$ Å	$D_{12} \times 10^5$ cm²/sec $h = 3.5$ (calcd)
0.5	0.0091	7.32	3.97	1.28	1.26	1.25
1.0	0.0185	6.78	3.74	1.36	1.42	1.30
1.5	0.0279	6.42	3.62	1.44	1.46	1.32
2	0.0376	6.03	3.50	1.47	1.45	1.37
3	0.0576	5.24	3.21	1.39	1.37	1.43
4	0.0788	4.51	(2.95)[a]	1.32	1.24	1.47

[a] Extrapolated value.

agrees with experiment. Further extrapolations were not attempted, as the values obtained would be questionable. Actually, as the fraction of water bound to cations, $h(m/m_2)$, is already 0.274 at c = 4.0, it is unlikely that the assumption of constant h could hold much further.

Values of β followed a similar course to those for NaCl and corresponded to β_0/η_r for $a = 3.0$ Å, except at the highest concentration. In Table IX, calculated and observed values of Λ in dilute solutions using this value of a in eq 40 are seen to be in excellent agreement up to $c = 0.01$, but, at $c = 0.05$, the Falkenhagen relaxation correction is excessive.

In this case, the hydration factor in eq 28 for t_3 plays a large rôle, so that the excellent agreement obtained provides good support for the equation. It is not possible to represent t_3 over the whole concentration range by means of a simple Stokes eq 29 with any single value of a.

Table IX: Equivalent Conductivities in Dilute LiCl Solutions at 25°

c	κa, $a = 3.0$ Å	Λ_{exptl}	Λ_{calcd}
0	...	115.03	...
0.0001	0.01	114.16	114.17
0.0005	0.0222	113.11	113.14
0.001	0.0313	112.37	112.40
0.005	0.070	109.34	109.35
0.01	0.099	107.28	107.22
0.05	0.222	100.13	99.47

HCl Solutions at 25°

Data are presented in Table X[44–47] up to $c = 4.0$, which is as far as D_{Cl}^* and D_{12} are available, and Table XI gives the results of calculations based on the assumption that both H^+ and Cl^- are unhydrated. In this case, the electrophoretic correction in eq 34a was applied to calculate D_{12}, since this is too large to be ignored in the case of hydrogen ions. The agreement between observed and calculated values of D_{12} is good except at the highest concentrations, and these could have been brought into agreement by assuming a small amount of hydration, *e.g.*, $h \simeq 0.4$, without affecting the agreement at lower concentrations. Owing to other uncertainties in the calculations, the introduction of additional parameters h_3 and h_4 was not considered justified.

Unlike the cases of KCl and LiCl, where q_3 could be and should be measured, the present indirect calculation of q_3 is the only way of determining mobilities of hydrogen ions in concentrated acid solutions, since, owing to exchange with water, measurement of self-diffusion coefficients with labeled ions is impossible.

Though the assumptions made in the calculations mean that there must be some degree of error in the values of q_3 and β, three important observations in

(44) B. B. Owen and F. H. Sweeton, *J. Amer. Chem. Soc.*, 63, 2811 (1941).

(45) H. S. Harned and E. C. Dreby, *ibid.*, 61, 3113 (1939).

(46) J. Giber, S. Lengyel, J. Tamás, and P. Tahi, *Acta. Chim. Hung.*, 32, 429 (1962).

(47) R. H. Stokes, *J. Amer. Chem. Soc.*, 72, 2243 (1950).

Table X: Data for HCl Solutions

c	m	Λ	t_3	$D_4^* \times 10^5$	$D_3^* \times 10^5$	$D_{12} \times 10^5$	$1 + \partial \ln \gamma_\pm / \partial \ln m$	η_r
0.5	0.506	360.9	0.838	1.931	2.40	3.184	1.034	1.03
1.0	1.022	332.3	0.841	1.878	2.36	3.453	1.185	1.06
1.5	1.549	306.1	0.842	1.821	2.34	3.744	1.349	1.09
2	2.086	281.7	0.843	1.764	2.27	4.045	1.522	1.12
3	3.196	237.7	0.843	1.640	2.14	4.643	1.901	1.19
4	4.351	200.1	0.836	1.554	2.05	5.170	2.297	1.26
Reference		44	45, 46	15	31	47		

Table XI: Calculated Values for HCl Solutions

c	m/m_2	$q_4 \times 10^9$	$q_3 \times 10^9$	$\beta \times 10^9$	$\beta_0/\eta_r \times 10^9$ $a = 1.8$ Å	$D_{12}/RT \times 10^5$ cm²/sec $h = 0$
0.5	0.0091	7.79	33.96	1.51	1.57	3.13
1.0	0.0185	7.59	31.88	1.90	1.94	3.46
1.5	0.0279	7.35	29.81	2.16	2.12	3.81
2.0	0.0376	7.10	27.83	2.35	2.25	4.16
3.0	0.0576	6.62	24.11	2.61	2.34	4.89
4.0	0.0785	6.28	20.7	2.76	2.38	5.70

connection with transport of hydrogen ions are definite. First, the mobility of hydrogen ions decreases considerably more rapidly with concentration than expected from viscosity, in sharp contrast with the behavior of Na^+, K^+, and Li^+. The chloride ion mobility, on the other hand, decreases much more nearly in inverse proportion to η_r, just as for the other chlorides.

Second, the calculations are based on zero hydration and it is certainly unnecessary to postulate any large hydration number. This is in accord with the general behavior of the chloride ion and with the fact that the high mobility of hydrogen ions is attributed to a mechanism of proton jumps from one water molecule to another. Such a mobility is unlikely if protons had to transport water molecules with them.

Third, the values of β are very large and, even at the lower concentrations, only approximate to β_0/η_r if we take $a = 1.8$ Å, corresponding to the crystal radius of an unhydrated chloride ion. This is, in fact, not unreasonable if a proton jump mechanism is assumed. Indeed, as shown in Table XII, the use of $a = 1.8$ Å in eq 40 for very low concentrations gives a good correlation between calculated and observed values of Λ up to $c = 0.01$. As in the previous cases, the relaxation correction is excessive above this.

Table XII: Equivalent Conductivities in Dilute HCl Solutions at 25°

c	κa, $a = 1.8$ Å	Λ_{obsd}	Λ_{calcd}
0	...	426.50	...
0.0001	0.0059	424.84	424.92
0.0005	0.0133	422.91	423.03
0.001	0.0188	421.46	421.65
0.005	0.0421	415.81	416.14
0.01	0.0594	412.02	411.97
0.05	0.133	399.12	397.6$_P$
0.10	0.188	391.34	388.20

At the highest concentrations, however, values of β could only be accounted for with smaller values of a, which are not conceivable. This can well be expected. At $c = 1.0$, the seat of the volume forces is at $[a + (1/\kappa)] = 4.8$ Å, corresponding to the highest concentrations for the previous electrolytes. Ordinary hydrodynamic laws must cease to be even approximately applicable for a closer approach to a proton moving by a jump mechanism.

The significance of the foregoing points is seen most clearly by comparing with calculations by Robinson and Stokes,[2] using eq 39. For concentrations up to $c = 1.0$, a hydration number $h \simeq 2$ was used, though this seems improbable for hydrogen ions. We now see that the low hydrogen ion mobilities and, more particularly, the large electrophoretic factors which are required to account for conductivity measurements are able to predict diffusion coefficients up to $c \simeq 4.0$ with reasonable accuracy, even if no hydration at all is assumed.

The results seem to be general. If eq 39 or its equivalent is applied to diffusion in HBr and in H_2SO_4 solutions up to $c \simeq 1$, it is also necessary to invoke hydration numbers of about 2 per hydrogen ion. On the other hand, if the mobilities and β values obtained in HCl are applied at equivalent ionic strengths and viscosities, diffusion coefficients for these two acids can be calculated with surprising accuracy without assuming any hydration.

Discussion

To summarize, though ionic self-diffusion coefficients are subject to relaxation effects, the limited experi-

mental evidence available suggests that such effects do not ever amount to more than a few per cent of the total, and that they tend to become negligible in concentrated solutions. In the aqueous solutions of the four 1:1 electrolytes discussed here, the assumption that D_i^* gives a good direct approximation to ionic mobility when $c \geq 0.5$ seems well justified.

Three points of general interest deserve attention. First, electrophoretic factors based on the simple Onsager–Fouss model are applicable for a single value of a from dilute solutions up to surprisingly high concentrations. The model breaks down for the higher concentrations of HCl studied, but up to $c \simeq 2$, it applies very well, using a value of a equal to the radius of a chloride ion.

Second, transport numbers depend upon the degree of hydration. This is particularly exemplified by LiCl solutions, for which the Stokes equation, having no hydration factor, is not applicable over the whole range of concentrations for any single value of a.

Third, the hydration numbers used for NaCl and LiCl, the virtual lack of hydration of KCl and HCl, and the values of a used for all four do not agree with values of a and h calculated by Stokes and Robinson from thermodynamic activities.[48] These were based on the assumption that an electrolyte solution is an ideal solution of hydrated ions, except for electrostatic interaction of the ions. This is to be contrasted with solutions of the nonelectrolyte, sucrose, where hydration calculated from thermodynamic activity could be used to calculate the diffusion coefficient.[49] It is very open to question, however, whether such a simple model is applicable for the thermodynamic properties of solutions of ions. The values of h and a obtained in this study are much smaller than those of Robinson and Stokes, but are at least reasonably consistent with ionic radii. For NaCl, $a = 3.2$ Å and $h = 1.5$, while the sum of the ionic radii is 2.76 Å. For LiCl, the ionic radii add to 2.41 Å, compared to $a = 3.0$ Å and $h = 3.5$. Perhaps in this case a is less than expected from the degree of hydration. In the case of KCl and HCl, where no hydration is assumed, the values of a used agree well with the ionic radii, if the hydrogen ion in transport is regarded as a bare proton.

(48) R. H. Stokes and R. A. Robinson, *J. Amer. Chem. Soc.*, 70, 1870 (1948); ref 2, p 246.

(49) P. C. Carman, *J. Phys. Chem.*, 71, 2565 (1967).

Ionization Potentials, Electronic and Molecular Structures of Metal Halides from Extended Hückel Theory

by J. W. Hastie and J. L. Margrave

Department of Chemistry, Rice University, Houston, Texas 77001 *(Received October 2, 1968)*

An extended Hückel (EH) method utilizing single-exponent one-electron Slater orbitals has been applied to the calculation of ionization potentials, electronic structures, and bond angles for many of the halides of groups I, IIa, IIIa, and IVa. The results compare very well with available experimental data and indicate a useful applicability of the EH method to these ionic molecules. In fact, the success of the calculations relates largely to the ionic nature of halides permitting only a minimum of orbital overlap which suggests that even crude atomic orbitals can lead to a reasonable molecular orbital scheme. The method also proves useful in predicting the electronic properties of radical species such as SiF, SiF_2, AlF_2, etc. Many of the species dealt with are outside of the present molecular size range of Hartree–Fock methods.

Introduction

Recent mass spectrometric and optical spectroscopic measurements have allowed the characterization of a considerable number of metal halides having a variety of valencies, thermodynamic, ionization, and structural properties.[1] For many diatomic halides both dissociation energies[2,3] and ionization potentials[4] can be predicted from simple ionic models. However, triatomic and higher polyatomic halides cannot be described by such simple models owing to an increased covalency, and a more sophisticated approach such as that provided by MO calculations is required to under-

(1) For example, see J. L. Margrave, Ed., "The Characterization of High Temperature Vapors," John Wiley and Sons, Inc., New York, N. Y., 1967; also subsequent references given in this paper.

(2) D. L. Hildenbrand, "Bond Energy Relationships in Polyvalent Metal Fluorides," in "Advances in High Temperature Chemistry," Vol. I, L. Eyring, Ed., Academic Press, New York, N. Y., 1967.

(3) (a) J. L. Margrave, *J. Phys. Chem.*, 58, 258 (1954); (b) K. S. Krasnov and N. V. Karaseva, *Opt. Spectrosc.*, 19, 14 (1965).

(4) J. W. Hastie and J. L. Margrave, *Fluorine Chem. Rev.*, 2, 77 (1968).

stand more fully their electronic structure. Both Hartree–Fock[5–8] (HF) and related extended Hückel[9–12] (EH) methods have proved useful in this respect, though the complexity of the former method, at present, restricts its application to lower molecular weight molecules.

Allen and Russell[9] have made a comparative analysis of the EH and HF methods. In particular they found similarity in the order of energy levels and molecular shape, the changes in hybridization and ionization potential (I.P.) with bond angle, but not good agreement however, of molecular orbital coefficients and molecular I.P.'s. A number of applications of EH theory to the prediction of molecular shape have been made.[9,10,12,13]

The inability of EH theory to predict more accurate ionization potentials must be partly due to the somewhat arbitrary method of correcting the valence state ionization energies (VSIE) on the central metal atom (or its ion) for the effect of the ligand field.[11,14] In fact, the EH theory should provide reasonable I.P. data even though one-electron orbitals are used, particularly as simple Hückel theory has proven useful in calculating I.P. data for organic and aromatic systems.[15]

It is the aim of this work to show the applicability of the EH method to the calculation of ionization potentials and structure for inorganic molecules and that satisfactory agreement between the calculated and experimental data can be obtained and hence a number of unknown I.P.'s and structural data can be predicted. Such I.P. predictions have particular relevance to mass spectrometric identification of new species in reducing or high-temperature systems (*e.g.*, SiF_3) where the ion (SiF_3^+) may have several precursors (Si_2F_6, SiF_4, SiF_3) and the detection of the radical (SiF_3) therefore requires a knowledge of its approximate I.P. In addition, the availability of I.P.'s for inorganic radicals (*e.g.*, AlF_2, BF_2, SiF_3, etc.) should lead to the estimation of new bond dissociation energies by the electron or photon impact methods. Often the use of fragment-ion appearance potentials is limited by the difficulty of assigning unambiguously the correct electron or photon impact process. The availability of reasonable estimates or semiempirically calculated bond energy and ionization potential data should reduce this problem. A combination of data from suitable electron or photon impact reactions can then lead to more accurate bond energy and ionization potential data.

Even a crude knowledge of bond angles or molecular structure is of importance in the interpretation of ir spectra and for the calculation of free energy functions to supplement thermodynamic data, particularly that obtained from mass spectrometry. Further, a useful systematization of the current experimental data for metal halides may be possible from this type of simple semiempirical MO treatment.

Method

The form of the extended Hückel method most commonly in use is essentially that of Hoffmann.[10] Actually, it has recently been shown[16] that this method can be thought of as a reduced form of the LCAO molecular Hartree–Fock method. However, unlike the HF method it is not possible to determine *ab initio* dissociation energies due largely to the neglect of electron–electron interactions implied by the use of one-electron wave functions.

The LCAO approach, for which Slater orbitals suffice, requires a solution to the secular determinant

$$| H_{ij} - EG_{ij} | = 0$$

where the diagonal Hamiltonian terms are usually assumed to be the negative values of valence-state ionization energies (VSIE), with a correction due to the coulombic field. The off-diagonal (H_{ij}) terms are approximated by the Ballhausen and Gray modification[17] of the Wolfsberg–Helmholtz approximation, *i.e.*

$$H_{ij} = KG_{ij}(H_{ii}H_{jj})^{1/2}$$

K is a somewhat arbitrary proportionality constant but generally has values between -1.6 and -2.0.[18] This semiempirical approximation is thought to compensate for the neglect of the difference between nuclear and electronic repulsion energies in the resonance integral.[10,19] Different approximations have more recently been suggested.[13,19]

Parameters. The diagonal H_{ii} terms of the secular determinant may be taken (a) as the VSIE's of the free atom[20–22] or (b) as the VSIE's of the totally or

(5) A. D. McLean, *J. Chem. Phys.*, **39**, 2653 (1963).

(6) K. D. Carlson and C. Moser, *ibid.*, **46**, 35 (1967).

(7) W. M. Huo, *ibid.*, **43**, 624 (1965).

(8) R. J. Buenker and S. D. Peyerimoff, *ibid.*, **45**, 3682 (1966).

(9) L. C. Allen and J. D. Russell, *ibid.*, **46**, 1029 (1967).

(10) R. Hoffmann, *ibid.*, **39**, 1387 (1963).

(11) F. A. Cotton, *Rev. Pure Appl. Chem.*, **16**, 175 (1966).

(12) R. L. Oakland and G. H. Duffey, *J. Chem. Phys.*, **46**, 19 (1967).

(13) L. C. Cusachs, *ibid.*, **43**, S 157 (1965).

(14) L. C. Cusachs and B. B. Cusachs, *J. Phys. Chem.*, **71**, 1060 (1967); M. D. Newton, *J. Chem. Phys.*, **45**, 2716 (1966); L. C. Cusachs, *ibid.*, **45**, 2717 (1966).

(15) N. S. Hush and J. A. Pople, *Trans. Faraday Soc.*, **51**, 600 (1955); A. Streitwieser, Jr., *J. Amer. Chem. Soc.*, **82**, 4123 (1960).

(16) G. Blyholder and C. A. Coulson, *Theoret. Chim. Acta* (Berlin), **10**, 316 (1968); M. D. Newton, F. P. Boer, and W. N. Lipscomb, *J. Amer. Chem. Soc.*, **88**, 2353 (1966); F. P. Boer, M. D. Newton, and W. N. Lipscomb, *Proc. Natl. Acad. Sci. U. S.*, **52**, 890 (1964); M. D. Newton, F. P. Boer, W. E. Palke, and W. N. Lipscomb, *ibid.*, **53**, 1089 (1965).

(17) C. J. Ballhausen and H. B. Gray, *Inorg. Chem.*, **1**, 111 (1962).

(18) P. Ros and G. C. A. Schmit, *Theoret. Chim. Acta*, **4**, 1 (1966).

(19) D. G. Carroll and S. P. McGlynn, *J. Chem. Phys.*, **45**, 3827 (1966).

(20) (a) C. E. Moore, "Atomic Energy Levels," National Bureau of Standards Circular 467, U. S. Government Printing office, Washington, D. C., 1949, 1952, 1958; (b) D. DeVault, *J. Chem., Educ.*, **21**, 575 (1944).

(21) H. B. Gray, "Electrons and Chemical Bonding," W. A. Benjamin, Inc., New York, N. Y., 1965.

(22) H. Basch, A. Viste, and H. B. Gray, *Theoret. Chim. Acta* (Berlin), **3**, 458 (1965).

partially charged ion, as given by Basch, *et al.*,[22] with a coulombic field correction for ionic molecules. For the latter case the charge is taken such that it is self-consistent with the value obtained in the Mulliken charge distribution analysis[23] which utilizes the overlap integrals (G_{ij}) and the eigenvectors of the solution to the secular determinant. The ligand field correction cannot be made *a priori* and the values usually assumed[11] are smaller than one would calculate from the potential energy of the metal–ion ligand system. The arbitrariness of this correction reduces the significance of the self-consistent charge (SCC) nature of choice (b). It is likely that choice (a) while not as aesthetically pleasing may well be just as satisfactory, particularly as the H_{ii} at the calculated charge are often close to those for the uncharged atoms.[24] Apparently there is no definite reason why atomic SCF functions should be better basis orbitals for a molecular calculation of this type.[25]

Exponents (α) to the Slater orbitals were the optimized values calculated by Clementi and Raimondi.[26] Alternatively, Slater's rules[27] were utilized where estimations were necessary. Internuclear separations (r) were taken as the experimental or estimated equilibrium distances.[21,25] Calculations were made for several molecules using a range of H_{ii}, K, α, and r values to test the effect of uncertainties in these parameters on the MO results.

Results and Discussion

Effect of Variable K Parameter. There is no *a priori* manner of obtaining a best value for the K parameter. Hence, as the extent to which the various dissimilar orbitals interact is very dependent on K, the effect of a variable K on the output data was recorded.

The output data can best be summarized, for the present applications, by (a) the molecular ionization potential, which by Koopmans' theorem[29] for SCF calculations is given approximately by the orbital energy of the highest (lowest energy in magnitude) occupied molecular orbital, abbreviated as HOMO throughout this paper, (b) the character of this orbital, in terms of the proportion (as obtained from the square of the eigenvectors) of each AO used in its formation, and (c) the charge separation of the molecule which results essentially from the overlap integrals, the eigenvectors, and the eigenvalues of the secular equation.

The variation of these data with K is indicated by Figure 1 for typical di- and triatomic species dealt with in this work. The value of $K = -1.75$ (indicated by the broken line in Figure 1), chosen by Hoffmann[10] as the most satisfactory value for his calculations, fits remarkably well with the value that best agrees with the experimental I.P.'s for the molecules considered in Figure 1. The magnitude of K also indirectly determines the extent to which effective compensation is made for neglect of nuclear and electronic repulsion in the EH method. The relative dissociation energy curves of Figure 1 indicate that the value of K which produces the best nuclear repulsion compensation falls in the -1.8 to -2.2 region. Cotton and Harris[24] considered a value between -1.7 and -1.8 to best reproduce, by calculation, an experimentally observed energy difference in the MO scheme. Contrary to previous experience,[30] we shall assume initially, for the purpose of simplicity, that K has the same value (*i.e.*, -1.750) for all other metal halides to be dealt with in this paper.

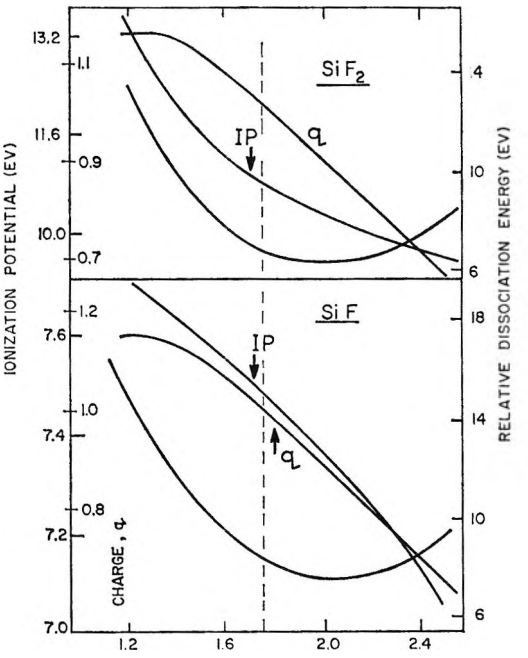


Figure 1. Variation of ionization potential, charge separation, and relative dissociation energy with K. Experimental I.P. and expected q values are indicated by arrows. The dashed line passes through the value of $K = -1.75$.

The nature of the variation of ionization energy with K, indicated by Figure 1, is typical of all metal halides where the HOMO is mainly localized about the metal nucleus. For such cases the ionization potentials of the diatomic halides vary by about 0.10 eV for a 10% change in K and the charge alters by about 10% also. Polyatomic species (*e.g.*, SiF_2) are more sensitive to the value of K due to increased orbital overlap. Both the ionization potential and the energy separation of

(23) R. S. Mulliken, *J. Chem. Phys.*, 23, 1833 (1955).

(24) F. A. Cotton and C. B. Harris, *Inorg. Chem.*, 6, 376 (1967).

(25) R. Hoffmann and W. N. Lipscomb, *J. Chem. Phys.*, 36, 2179 (1962).

(26) E. Clementi and D. L. Raimondi, *ibid.*, 38, 2686 (1963).

(27) J. C. Slater, "Theory of Atomic Structure," Vol. I, McGraw-Hill Book Co., Inc., New York, N. Y., 1960.

(28) L. E. Sutton, Ed., "Interatomic Distances," and Supplement Special Publication No. 11 and 18, The Chemical Society, London, 1958, 1965.

(29) T. Koopmans, *Physica*, 1, 104 (1933); G. G. Hall and J. Lennard-Jones, *Proc. Roy. Soc.*, A202, 155 (1950); see also ref 14; also M. D. Newton, *J. Chem. Phys.*, 48, 2825 (1968).

(30) F. A. Cotton and T. E. Haas, *Inorg. Chem.*, 3, 1004 (1964).

Table I: Self-Consistent Charge and Non-SCC Calculations

Input Data[b]

Atom	Valency orbital	VSIE, eV Atom	VSIE, eV Ion (−ve)	Slater exponent Atom	Slater exponent Ion	H_{ii}, eV[a] Ion (−ve)
			Molecules BeF and BeCl			
Be	2s	9.62	18.2	0.62	0.55	6.5 and 7.6
Be	2p	6.72		0.55		
F	2s	40.0		2.564		
F	2p	18.7	2.8	2.55	2.55	14.5
Cl	3s	25.3		2.356		
Cl	3p	13.7	3.0	2.039	2.039	13.6
			Molecules MgF and MgCl			
Mg	3s	7.7	15.0	0.95	1.1	6.2 and 7.1
	3p	...				
F	2s	40.0		2.6		
	2p	18.7	2.8	2.6	2.55	11.6
Cl	3s	25.3		2.03		
	3p	13.8	3.0	2.03	2.039	10.9
			Molecule KF			
K	3p	...	38.5	2.575	2.70	32.5
	4s	4.34	11.6	0.87	0.762	5.6
F	2s	40.0	24.7	2.564	2.425	30.7
	2p	18.7	2.8	2.55	2.425	8.8

Results

Molecule	I.P., eV	I.P.,[f] exptl, ±0.3	Orbital character (%)[e]	Charge of M in MX	Charge of M in $(MX)^+$	Exp[d] (in MX)
BeF	8.73	9.1	82.8Be(2s) + 16.0Be(2p) + 1.2F(2s)	1.0	2.0	1.0
BeF[c]	6.49	9.1	100Be(2s)	1.0	2.0	1.0
BeCl	8.3	11.2	66.8Be(2s) + 28Be(2p) + 1.05Cl(3s) + 4.15Cl(3p)	0.84	...	0.8
BeCl[c]	7.4	11.2	96.5Be(2s) + 3.5Cl(3p)	0.98	...	0.8
MgF	6.6	7.8	97Mg(3s) + 2.5F(2s) + 0.5F(2p)	1.0	2.0	1.9
MgF[c]	6.08	7.8	97.5Mg(3s) + 2.5F(2p)	0.99	1.98	1.0
MgCl	4.87	9.2	85Mg(3s) + 9.15Cl(3s) + 5.85Cl(3p)	0.98	2.96	0.92
MgCl[c]	6.29	9.2	85.3Mg(3s) + 14.7Cl(3p)			
KF	18.7	9.3	100F(2p)	1.01	1.01	1.0
KF[c]	8.76	9.3	99.84F(2p) + 0.16K(3p)	1.01	1.01	1.0

[a] Calculated assuming H_{ii} = VSIE (M^+ or X^-) ± P.E. where P.E. is obtained from: $-\text{P.E.} = D(MX) + \text{I.P.}(M) - \text{E.A.}(X)$. [b] The following internuclear separations, in Å units, were used: BeF, 1.361; BeCl, 1.78; MgF, 1.75; MgCl, 2.20; KF, 2.139.[28] The group IIa halide separations are those listed or estimated by Krasnov and Karaseva.[3] [c] These represent SCC calculations. [d] Taken from the ionic character *vs.* electronegativity difference curve of Dailey and Townes,[31] using Pauling's[32] electronegativities. [e] σ symmetry for p orbitals. [f] See ref 4.

occupied and nonoccupied orbitals vary by several electron volts for K values in the range −1.2 to −2.0. This variation indicates the apparent difficulty of attempting to predict quantitatively the energies of excited orbitals.

It has been previously indicated[4] that for diatomic metal halide species only the alkali halides are not of this character and we find that the ionization potential and charge separation are only slightly dependent on the magnitude of K (over the range −1.5 to −2.5).

Effect of Choice of H_{ii} (Coulomb Integral). The initial success of the Hückel method using the VSIE values of the neutral atoms rather than the partially charged ions warrants a comparison of the effect of both choices on the calculated MO's. The results for several typical molecules are compared in Table I.[31,32]

(31) B. P. Dailey and C. H. Townes, *J. Chem. Phys.*, 23, 118 (1955).
(32) L. Pauling, "The Nature of the Chemical Bond," 3rd ed, Cornell University Press, Ithaca, N. Y., 1960.

Table II: Ionization Potentials of Copper Halides

Input Data

Atom	Valency orbital	VSIE[a] −ve, eV	Slater exponent
Cu	4s	7.70	1.46
	3d	10.70	4.4
F	2s	40.0	2.564
	2p	18.7	2.550
Cl	3s	25.3	2.356
	3p	13.7	2.039
Br	4s	24.0	2.638
	4p	12.3	2.257

Results

Molecule	I.P., eV	I.P.,[b] exptl	Orbital character (%)	Charge M	Charge M, exptl
CuF[c]	10.67	10.5 ± 0.3	0.12Cu(4s) + 99.55Cu(3d) + 0.01F(2s) + 0.22F(2p)	1.02	0.97
CuCl[d]	10.64	10.8 ± 0.6	0.6Cu(4s) + 98.2Cu(3d) + 1.2F(2p)	0.91	0.55
CuBr[d]	10.65	10.7 ± 0.6	0.7Cu(4s) + 97.4Cu(3d) + 1.9F)2p)	0.83	...

[a] References 18 and 19. [b] Reference 4. [c] Internuclear separation from ref 28. [d] Internuclear separations, estimated from r (CuF) and the relative ionic radii of Cl^-, Br^-, and F^- are r(CuCl) = 1.863 Å, r(CuBr) = 2.013 Å.

For non-SCC calculations the H_{ii} were taken to be equal to the VSIE of the atoms. The H_{ii} used for the so-called SCC calculations were either the VSIE for the singly charged ions or a value of VSIE corrected for the potential field in the molecule, as indicated in Table I.

For the group IIa halides considered, both SCC and non-SCC calculations indicate almost complete ionic character for the fluorides and the calculated ionic character of both fluorides and chlorides is in good agreement with the predictions of Dailey and Townes[31] which are based on nuclear quadrupole resonance measurements.

The calculated I.P. data are mostly not in very good agreement with the experimental data. Neither the SCC or non-SCC calculations predict the correct trend of increasing I.P.'s with increasing ligand size. It is not surprising that poor agreement with experimental I.P.'s is found owing to the difficulty in correcting the H_{ii} (free ion) to an H_{ii} (ion in molecule) term. The corrections of 11.7 eV and 10.6 eV used for BeF and BeCl, respectively, appear to be several ev too high for good agreement of calculated and experimental I.P.'s to be obtained.

It appears that there is no way of correcting H_{ii} (free ion) to H_{ii} (ion in molecule) terms without an uncertainty of at least several eV and hence attempts to arrive at accurate ionization potential data by this SCC method are not very profitable. The original non-SCC approach appears to be at least as useful. One finds that for these essentially ionic molecules, both methods predict the correct degree of ionicity and a plausible electronic character for the ionizing molecular orbital.

SCC Calculations for Alkali Halides. SCC results could be obtained using +1, −1 charge separations for MX. Slater's rules[27] were used for the exponents on the ions and the VSIE values of Basch, *et al.*,[22] for ions were used. If overlap of only occupied M^+ or X^- orbitals was considered, the calculated I.P.'s had values very nearly equal to the H_{ii} value of the p orbitals on X^-. Thus if the free-ion values were used, *e.g.*, for $F^-(2p)$ H_{ii} = −2.88 eV, the calculated I.P. was only 2.7 eV. If the $H_{ii}(X^-)$ was corrected for the effect of the presence of M^+ then the I.P. was also close to this corrected value, as indicated by the example of KF in Table I. Mulliken overlap population analyses indicated the charge distribution in MX to be +1, −1 and in $(MX)^+$ to be +1, 0. These data agree with a previous conclusion[4] that the I.P.'s of alkali halides correlated well with a corrected VSIE for the p shell on X^-.

Similarly, if non-SCC calculations are made, *i.e.*, the neutral atom VSIE's are used as the H_{ii}, then the calculated I.P. is approximately equal to the VSIE of X(p). Population analyses again indicate MX to be M^+X^- and $(MX)^+$ to be M^+X^0.

These results suggest that current approximations for correcting VSIE values for neighboring charge effects are inadequate for the alkali halides. That is, while it has been suggested[11] for some cases that the VSIE on the ligand or the central atom require an adjustment of only several eV per charge, for the case of the alkali halides corrections of the order of 10 eV per charge are required—depending on the internuclear separation in the molecule.

Effect of Variable K on SCC Calculations. The SCC–ligand field corrected MO results, in contrast to those given in Figure 1, do not depend significantly on the value of K over the range −1.5 to −2.0. As seen in Table I for BeF or BeCl, the SCC calculation indi-

Table III: Ionization Potentials for Group IIIa Halides

Input Data[a]

Atom	Valency orbital	VSIE[c] (−ve)	Slater[b] exponent
B	2s	14.0	1.288
	2p	8.28	1.211
Al	3s	11.2	1.372
	3p	5.93	1.355
Ga	4s	12.0	1.767
	4p	5.8	1.555
In	5s	10.5	2.0 or 2.5
	5p	5.8	1.6 or 2.0
Tl	6s	12.0	2.2 or 2.8
	6p	6.1	1.7 or 2.2

Results[e]

Molecule[g]	I.P., eV	I.P.,[d] exptl, ±0.3 eV	Orbital character (%)[f]	Charge M	Charge M, exptl
BF	11.49	11.4	65.9B(2s) + 27.1B(2p) + 1.3F(2s) + 5.7F(2p)	0.98	0.95
BCl	10.57	10.4	43.0B(2s) + 38.4B(2p) + 0.14Cl(2s) + 18.46Cl(2p)	0.29	0.4
BBr	10.36	9.3–10.3	35.8B(2s) + 40.2B(2p) + 24Br(4p)	0.07	~0.2
AlF	9.74	9.5	85Al(3s) + 0.5Al(3p) + 1.98F(s) + 2.52F(2p)	1.1	1.0
AlCl	8.83	8.6–9.1	61.3Al(3s) + 25.8Al(3p) + 2.77Cl(3s) + 10.13Cl(3p)	0.77	0.82
AlBr	8.89	8.3–10.3	60.4Al(3s) + 19.9Al(3p) + 1.1Br(4s) + 18.6Br(4p)	0.73	0.75
GaF	10.51	10.4	87.2Ga(4s) + 6.36Ga(4p) + 2.16F(2s) + 4.28F(2p)	1.09	0.98
GaCl	9.27	9.8–11.0	59.9Ga(4s) + 18.3Ga(4p) + 2.1Cl(3s) + 20.1Cl(3p)	0.72	0.78
InF	9.64	9.6	91In(5s) + 4.84In(5p) + 0.95F(2s) + 3.51F(2p)	1.08	1.0
	(or 9.95[h])		[or 94.4In(5s) + 2.4In(5p) + 0.5F(2s) + 2.7F(2p)]	(or 1.05)	(1.0)
InCl	8.89	9.5–10.5	70.8In(5s) + 14.4In(5p) + 1.3Cl(3s) + 13.5Cl(3p)	0.86	0.75
TlF	11.01	10.5	92Tl(6s) + 3.18Tl(6p) + 1.31F(2s) + 3.51F(2p)	1.07	1.0
	(or 11.43[h])		[or 94.31Tl(6s) + 1.45Tl(6p) + 0.58F(2s) + 3.66F(2p)]	(or 1.04)	(1.0)
TlCl	9.79	≲9.9	62Tl(6s) + 12.5Tl(6p) + 1.4Cl(3s) + 24.1Cl(3p)	0.83	0.65
BF_2 (123°)	9.35	≲9.4	41B(2s) + 50B(2p) + 1.9F(2s) + 7.1F(2p)	1.91	<1.9
BCl_2 (130°)	7.47	7.20	13.8B(2s) + 61.8B(2p) + 24.4Cl(3p)	0.49	<0.4
AlF_2 (linear)	6.37	<9 ± 1	83.6Al(3s) + 9.13F(2s) + 8.37F(2p)	2.0	≲2.0
AlF_2 (130°)	7.8	<9 ± 1	64.1Al(3s) + 27.5Al(3p) + 3.9F(2s) + 2.3F(2p) + 2.2F($2p_y$)	2.0	
$AlCl_2$ (130°)	6.65	≪9	30.8Al(3s) + 2.0Cl(3s) + 8.7Cl(3p) + 1.9Cl($3p_y$)	1.44	

[a] Data for F, Cl, Br same as given in Table I. [b] Clementi and Raimondi's[26] values for B, Al, and Ga orbitals. Extrapolation of those data suggested the exponent values used for In and Tl. Slater's rules for estimating the exponents for In and Tl led to much smaller values which resulted in calculated I.P.'s that were of the order of 1 eV higher than those given in Table III. Clementi, *et al.*, *J. Chem. Phys.*, 47, 1300 (1967), have recently extended their calculations to give the following exponents: In(5s) = 1.9023, In(5p) = 1.694, Tl(6s) = 2.1366 and Tl(6p) = 2.0423. Recalculation of the data using these values does not significantly alter the present results. [c] Reference 21 or 22. [d] References: for diatomic species, Hastie and Margrave;[4] AlF_2, T. C. Ehlert and J. L. Margrave, *J. Am. Chem. Soc.*, 86, 3901 (1964); BCl_2, W. S. Koski, J. J. Kaufman, and C. F. Pachucki, *ibid.*, 81, 1326 (1956); BF_2 is isoelectronic with NO_2 which has IP of 9.8 eV[35] and an indirect experimental value of ≲9.4 eV appears to be correct, W. C. Steele, L. O. Nichols, and F. G. A. Stone, *ibid.*, 84, 1154 (1962). [e] Alternative VSIE values as suggested by Lohr and Lipscomb[34] of F(2s) = 37.24 eV and F(2p) = 18.86 eV were also tried but did not significantly alter the results. Likewise alteration of the exponents by ~20% did not significantly affect the results. [f] p orbitals have σ symmetry, *i.e.*, p_z, unless otherwise indicated as p_x or p_y. For molecules where more than one halogen group is involved the F or Cl orbital character contribution represents the total. [g] Experimental internuclear separations were used as given by Gray[21] and Sutton.[28] For BF_2 the geometry used was that given by Pople, *et al.*[36] Estimated internuclear separations of BCl_2 = 1.70, AlF_2 = 1.654, and $AlCl_2$ = 2.13 Å were used. Bond angles were estimated on the basis of Pople's calculated value for BF_2 and Walsh's predictions for 17-electron molecules. [h] Using the higher values of the two sets of exponents listed in the input data.

cates that the first molecular ionization potential is approximately the value of H_{ii} for the Be(2s) orbital. However, as this I.P. value is several eV lower than the experimental value the ligand field correction to VSIE is apparently overestimated. This is not surprising as the assumption of forces between point charges neglected shielding by electrons about the ions. It is not unexpected that K has a minimal effect for SCC calculations where the orbital overlap is very small.

Ionization Potentials

Group I Halides. For group Ia species where ionization is largely from the anionic part of the molecule, reasonable ionization potentials could only be calcu-

lated, as indicated above, if a significant correction was applied to the free-ion or -atom H_{ii} of X. On the other hand, for cases such as group IIa halides, where the VSIE values of the valence orbitals on M are more comparable with those of X, it appears reasonable to use the atomic VSIE energies as representing H_{ii}. Thus for the group Ib CuX molecules, where the atomic VSIE values are much lower than for group Ia, the experimental I.P. values are very close to the Cu(3d) VSIE value, indicated in Table II. A Hückel calculation verifies that ionization seems to arise largely in the Cu(3d) orbital and the calculated I.P. value agrees with the experimental data as indicated in Table II.

Group IIa Halides. As indicated in an earlier study[4] these molecules ionize mainly from an orbital on M^+ in M^+X^-. In this study the data suggested that, for fixed M and variable X, the I.P. increases with increasing size of X. However, one cannot predict this effect from the Hückel approach without arbitrarily altering the H_{ii} of M or M^+ in MX for various X. Generally, the Hückel calculated I.P. values are several eV lower than the experimental data. The results shown in Table I are typical data for this group and the nature of the ionizing MO is mostly M(s,p) with the s character of the orbital predominating. Chlorides and bromides have an additional several per cent X(s,p) character. These results do not vary significantly with changes of the order of 1 eV in the H_{ii} terms. They also indicate that the s nature of the ionizing MO increases from BeX to MgX to CaX.

For MX_2 we find that ionization occurs from an orbital localized mainly on X and the I.P. is very nearly equal to VSIE(X). The experimental I.P. value[33] of 14.7 ± 0.4 eV for BeF_2 indicates that the free atom VSIE(F) value of 18.7 eV requires a significant molecular-field correction.

Group IIIa Halides. For this group of molecules the H_{ii} were taken as the VSIE (neutral atom) values. The data used and results obtained are given in Table III.[34-36] Remarkable agreement between the calculated and experimental I.P. values is found for all species. Such an agreement for a variety of species would seem to support the assumption that neutral atom VSIE values best represent the H_{ii} terms in the interaction of atoms to form group IIIa halide molecules. Also of importance is the good agreement of calculated ionic character with the Dailey and Townes predictions.[31]

More extensive and accurate Hartree–Fock calculations have been made for BF by Huo[7] and a comparison of these data can be made with the results of the Hückel calculations. Huo calculates an I.P.(BF) value of 11.26 or 11.0 eV using a "Nesbet set" or "atomic built-up set," respectively. These compare well with the present calculated value of 11.49 eV and the experimental value of 11.4 ± 0.3 eV.

As may be seen in Table III, the character of the ionizing MO's shows considerable s–p mixing on the metal nucleus with the s contribution increasing markedly with the size of *M*, *i.e.*, from 65.9% for BF to 92% for TlF. This is in keeping with the accepted view that the lone s-pair stability increases from B to Tl with a resulting tendency for the monovalent state to be stable. These trends, however, do not readily explain the decreasing stability of the molecule-ions for increasing size of M.[4] For example, if TlF is considered as Tl^+F^- and ionization of the molecule is from the Tl(6s) orbital then one would expect the molecule-ion to have a considerable charge separation approximating $Tl^{2+}F^-$. The coulombic stability of such a species would be at least several eV as compared with the experimental molecule-ion dissociation energy of only a few tenths of an eV.

Group IVa Halides. Ionization potentials have been experimentally established for the mono-, di- and tetravalent fluorides of this group.[37] Hence, this group of molecules provides a wide range of electronic properties for useful testing of the EH method.

The results, as shown in Table IV, are generally in good agreement with experiment. Fair agreement is obtained for SiF_4 if only s and p orbitals are considered. Inclusion of Si(3d) orbitals, of the neutral-atom type and using Slater's rules[27] to estimate the orbital exponent, does not alter the calculated result. This oversimplified picture of the SiF_4 molecule is most certainly in error as one can only rationalize the unusual chemical properties of this species if Si(3d) orbitals are considered. A major difficulty is the unavailability of an optimized value for the 3d orbital exponent. Usually for these metal halides, particularly the lower valence species, the 3d (VSIE) values differ sufficiently from the other valence orbitals that their H_{ii} terms are unaffected and therefore the EH results are not significantly affected by the exclusion of the 3d orbitals. However, it seems that the major contributions to the ionization potential of SiF_4 are the Si(3s, 3p) and F(2s, 2p) orbitals. One notes that if each F atom is assumed to have a charge of only −0.15 and the VSIE is calculated for this partially charged group and used in the MO calculation, then the experimental I.P. of SiF_4 can be reproduced.

The general agreement of calculated and experimental ionization potentials suggests that, for the cases where

(33) D. L. Hildenbrand and E. Murad, *J. Chem. Phys.*, **44**, 1524 (1966).

(34) L. L. Lohr, Jr., and W. N. Lipscomb, *ibid.*, **38**, 1607 (1963).

(35) G. Herzberg, "Molecular Spectra and Molecular Structure, III," D. van Nostrand, Co., Inc., Princeton, N. J., 1966.

(36) J. A. Pople, D. L. Beveridge, and P. A. Dobosh, *J. Chem. Phys.*, **47**, 2026 (1967).

(37) K. Zmbov, J. W. Hastie, R. Hauge, and J. L. Margrave, "Thermodynamics of Vaporization of GeF_2, SnF_2 and PbF_2 and Bond Dissociation Energies of Group IVA Fluorides," Third International Symposium on High-Temperature Technology, Asilomar, 1967.

Table IV: Ionization Potentials for Group IVa Halides

Input Data[a]

Atom	Valency orbital	VSIE, eV[c] −ve	Slater[b] exponent	Atom	Valency orbital	VSIE, eV[c] −ve	Slater[b] exponent
C	2s	19.3	1.608	Sn	5s	14.0	2.2
	2p	10.6	1.570		5p	7.4	2.0
Si	3s	14.8	1.634	Pb	6s	15.3	2.4
	3p	7.75	1.428		6p	7.4	1.9
Ge	4s	14.8	2.011				
	4p	7.75	1.695				

Results

Molecule[d]	I.P., eV	I.P.,[e] exptl	Orbital character (%)[f,i]	Charge X −ve	Charge X, exptl −ve
CF	9.93	8.9	92.2C(2p) + 7.8F(2p)	0.68	0.82
CF_2	12.4	11.86 ± 0.1	33.9C(2s) + 47.7C(2p) + 1.26F(2s) + 15.96F(2p) 1.18F($2p_y$)	0.72	<0.82
CF_3 (120°)	8.98	9.25 ± 0.2	85.9C(2p) + 14.1F(2p)	...	≪0.82
CF_3 (112°)	6.7	9.25 ± 0.2	8.9C(2s) + 62.5C(2p) + 29.6F(2p)	0.11	≪0.82
CF_4	18.4	<15	∼100F(2p)	...	...
SiF	7.49	7.3	97.7Si(2p) + 2.3F(2p)	1.01	0.97
SiF_2	10.82	11.3 ± 0.2	60.6Si(3s) + 26.9Si(3p) + 2.64F(2s) + 7.1F(2p) + 2.76F($2p_y$)	1.01	<0.97
SiF_3 (120°)	6.85	8.5 ± 1	93Si(3p) + 7F(2p)	0.97	≪0.97
SiF_3 (112°)	6.11	8.5 ± 1[g]	15.9Si(3s) + 66.4Si(3p) + 17.7F(2p)	0.28	≪0.97
SiF_4	18.57	15.4	∼100F(2p)	...	...
GeF	7.56	7.8	98.32Ge(4p) + 1.68F(2p)	1.01	0.97
GeF_2	11.48	11.8 ± 0.1	67.5Ge(4s) + 18.6Ge(4p) + 2.47F(2s) + 7.56F(2p) + 3.87F($2p_y$)	1.0	<0.97
SnF	7.3	7.8	99.17Sn(5p) + 0.83F(2p)	1.01	0.97
SnF_2	11.97	11.5	81.2Sn(5s) + 6.82Sn(5p) + 2.42F(2s) + 5.13F(2p) + 4.43F($2p_y$)	1.01	<0.97
PbF	7.03	7.4	98.54Pb(6p) + 1.46F(2p)	0.97	0.97
PbF_2	12.93	11.5	85.3Pb(6s) + 7.12Pb(6p) + 2.24F(2s) + 5.34F(2p)	1.04	<0.97
CCl	9.74	9.2–10.7	78C(2p + 22Cl(3p)	+0.36	0.2
CCl_2 (110°)	10.79	...	10.8C(2s) + 48.6C(2p) + 40.6Cl(3p)	0	<0.2
CCl_3 (120°)	8.43	8.78 ± 0.05	68.3C($2p_z$) + 31.7Cl($3p_z$)	0.13	≪0.2
CCl_3 (112°)	5.3	8.78 ± 0.05	4.6C(2s) + 49.5C(2p) + 45.9Cl(3p)	+0.37	≪0.2
CCl_4	12.18	11.47	∼55Cl($3p_z$) + 45Cl($3p_y$)	+0.27	≪0.2
SiCl	7.36	∼7.6	94.3Si(3p) + 5.7Cl(3p)	0.6	0.64
$SiCl_2$	9.86	10 ± 0.5	38.7Si(3s) + 34.3Si(3p) + 0.74Cl(3s) + 21.6Cl(3p) + 4.66Cl($3p_y$)	0.63	<0.64
$SiCl_4$	13.35	12.06	∼100% Cl(3p)	0.65	≪0.64
GeCl	7.28	∼8.2	92.1Ge(4py) + 7.9Cl($3p_y$)	0.46	0.65
$GeCl_2$	9.5	...	30.4Ge(4s) + 41.1Ge(4p) + 0.6Cl(3s) + 25.4Cl(3p) + 2.5Cl($3p_y$)	0.53	<0.65
$PbCl_2$	10.3	10.4 ± 0.2	∼45Pb(6s) + 8Pb(6p) + 47Cl(3s, 3p)	0.73	<0.64

[a] Data for F, Cl, Br same as given in Table I. [b] Clementi and Raimondi's[26] values for C, Si, and Ge with data for Sn and Pb estimated by extrapolation of those values. More recently these authors (see footnote *b*, Table III), have calculated exponents, Sn(5s) = 2.1257, Sn(5p) = 1.8204, Pb(6s) = 2.35 and Pb(6p) = 2.0655, which are in satisfactory agreement with the estimates used here. [c] Data of Gray[21] or Basch, *et al.*[22] [d] The following experimental or estimated molecular geometries were used: CF, r = 1.271;[28] CF_2, r = 1.30 and angle 104°;[38] CF_3, r = 1.32, CF_4, r = 1.36;[21] SiF, r = 1.603;[28] SiF_2, r = 1.591, angle 101°;[39] SiF_3, r = 1.57; SiF_4, r = 1.54;[21] GeF, r = 1.74 (Johns, *et al.*, 1958, see footnote *g*, Table V); GeF_2, r = 1.74, angle 95°;[37] SnF, r = 1.95 (Johns, *et al.*, 1958); SnF_2, r = 2.04, angle 95° (L. Brewer, G. R. Somayajulu, and E. Brackett, *Chem. Rev.*, **63**, 111 (1963)); PbF, r = 2.10 (Johns, *et al.*, 1958); PbF_2, r = 2.08, angle 95° (Brewer, *et al.*, 1963); CCl, r = 1.75; CCl_2, r = 1.75, angle 110°; CCl_3, r = 1.75; CCl_4, r = 1.761;[21] SiCl, r = 2.10; $SiCl_2$, r = 2.10, angle 100°; $SiCl_4$, r = 2.02;[21] GeCl, r = 2.10; $GeCl_2$, r = 2.10, angle 100° and $PbCl_2$, r = 2.46, angle 100° (Brewer, *et al.*, 1963). [e] References for diatomics, Hastie and Margrave;[4] CF_2, R. F. Pottie, *J. Chem. Phys.*, **42**, 2607 (1965); CF_3, C. Lifshitz and W. A. Chupka, *ibid.*, **47**, 3439 (1967); CF_4, SiF_4, $SiCl_4$, R. W. Kiser, "Introduction to Mass Spectrometry and Its Applications," Prentice-Hall Inc., Englewood Clifis, N.J., 1965; SiF_2, J. D. McDonald, C. H. Williams, J. C. Thompson, and J. L. Margrave, "Silicon–Fluorine Chemistry V," to be published; GeF_2, SnF_2, PbF_2;[37] $SiCl_2$, M. Uy and J. L. Margrave, to be published; $PbCl_2$, J. W. Hastie, H. Bloom, and J. D. Morrison, *J. Chem. Phys.*, **47**, 1580 (1967); CCl_3, Koski, *et al.*, 1956, see footnote *d* Table III. [f] For cases where more than one F group is involved the F(2s) or F(2p) orbital character represents the sum of the contributions from all of the F atoms. [g] The analogous CF and SiF species differ by about 1.6 eV in their experimental I.P.'s; it is likely that CF_3 and SiF_3 do likewise. Hence a reasonable value for I.P.(SiF_3) by comparison with CF_3 is approximately 8.5 ± 1 eV. [h] Electron spin resonance measurements on CF_3 [R. W. Fessenden and R. H. Schuler, *J. Chem. Phys.*, **43**, 2704 (1965)] suggest an angle of ∼111° and Pople, *et al.*,[36] calculate ∼112°. [i] p orbitals are σ-symmetry unless otherwise indicated, *i.e.*, as p_z or p_y.

experimental data are not available, the calculated data may be used with confidence. Thus, the predicted ionization potential of the yet to be isolated species, SiF_3, is 6.1 ± 1.5 eV. The large error limits are necessary because of the strong dependence of the calculated I.P. value on the choice of geometry which is not yet exactly known.

Significant errors occur only where the metal has acquired a full electron configuration and ionization takes places mainly from the ligands, *e.g.*, CF_4, SiF_4, BeF_2, etc. For these cases correction to the F(2s) and F(2p) H_{ii} terms, similar to that suggested for the alkali halides, is required. Excellent agreement is obtained for cases where ionization occurs from an orbital that is mainly localized about the metal nucleus.

Variation of Energy with Bond Angle

The group IVa divalent fluorides are known to have bond angles in the region 90–110° which decrease with increasing size of M.[37–39] Also, the ionic nature of these difluorides increases markedly with increasing atomic number.

Extended Hückel calculations were carried out for various bond angles over the range 60–180° with the parameters listed in Table IV. The equilibrium bond angles were determined as those for which the total valency-orbital energy of each species was a maximum, corresponding to a minimum in the potential energy surface. A basic assumption of this method is that the sum of the orbital energies is proportional to the total energy and that the proportionality is not affected by different bond angles. On this basis the following bond angles were determined with an estimated interpolation uncertainty of ±5°: CF_2, 101°, SiF_2, 85°, GeF_2, 85°, and SnF_2, 85°, which compare satisfactorily with the known experimental values of CF_2(104°), SiF_2(101°), and GeF_2(95°). For CCl_2 an angle of 112° was determined. These bent configurations were found to be much more stable than their linear counterparts and the depth of the potential minimum was in the range 4–7 eV for these species. The disparity in the values for SiF_2 could possibly be removed with an adjustment to the VSIE or K parameters.

The energy variation of the various MO's with bond angle was also found to be in qualitative agreement with Walsh's predictions for 18 electron AB_2 species.[35,40] For each of these molecules, at their calculated equilibrium bond angle, an electronic ground state configuration of $\ldots (1a_1)^2 (1b_2)^2 (2b_2)^2 (2a_1)^2 (1b_1)^2 (3b_2)^2 (1a_2)^2 (3a_1)^2 (4a_1)^2 (2b_1)^0 (4b_2)^0 (5a_1)^0$ was found. The coordinate and symmetry notation given by Herzberg[35] (p 319) and others[8,40] was used. Of the occupied orbitals only the $(4a_1)$ was strongly angle sensitive, showing an increased stability with decreasing bond angle. For SiF_2, for example, a decrease of 40° in the bond angle resulted in a 1–1.5 eV energy increase for the $(4a_1)$ orbital. The antibonding $(4b_2)$ and $(5a_1)$ orbitals, which correlate with the π_u orbital of the linear molecule case, also varied considerably with bond angle. A consequence of the relative angle sensitivity of the occupied $(4a_1)$ and insensitivity of the unoccupied $(2b_1)$ orbitals is that an electron transition from the $(4a_1)$ to the $(2b_1)$ would result in a significant increase in the bond angle. This behavior has in fact been found experimentally for the $^1B_1 \leftarrow {}^1A_1$ transitions of CF_2, SiF_2, and GeF_2.

Excited States

The above results show that one can reliably calculate the ionization potential provided the orbital being ionized is localized mostly on the electropositive part of the molecule. Similarly, it should be possible to predict the position of electronically excited levels for these molecules. In the excitation of these localized electrons to a higher level it must be assumed that the other levels remain essentially unaltered in energy and the following data (*e.g.*, Table V) seem to verify this approximation.

It has recently been established spectroscopically that the divalent group IVa halides have an excited state located about 4 to 5 eV above the ground state. The MO calculations also show the presence of a nonbonding orbital several eV above the HOMO and a comparison of the energy separation (ΔE) for this orbital and the experimental observation of the $^1B_1 \leftarrow {}^1A_1$ transition energy is given in Table V. The agreement is sufficiently good that one can predict the approximate spectral regions for molecules where the transitions have not yet been studied. It appears that the heavier fluorides should give rise to an absorption further to the vacuum uv region than the lighter ones, while the absorption by the chlorides should fall nearer the visible than for the corresponding fluorides.

The results for the group IVa dihalides also indicate the $(4b_2)$ level to be significantly different in energy from the $(2b_1)$ (*i.e.*, 5.2 eV for SiF_2) and therefore the $^1B_2 \leftarrow {}^1A_1$ transition would occur at much higher energies than the $^1B_1 \leftarrow {}^1A_1$. Hence, the observed electronic transitions for these halides can certainly be ascribed to $^1B_1 \leftarrow {}^1A_1$ as previously suggested.[41]

For the group IIIa dihalides the EH results indicate a ground state of $^2A_1$: $\ldots (4a_1)^1 (2b_1)^0 (5a_1)^0$. These states are entirely analogous to those observed in the corresponding hydrides[55] for which energy separations of about 1.6 and 1.88 eV have been observed in BH_2 and AlH_2, respectively. The $^2A_1 \leftarrow {}^2B_1$ separation in the halides is likewise in the energy range of 1–2 eV, as shown in Table V.

On the other hand, for the trihalides of group IVa,

(38) (a) F. X. Powell and D. R. Lide, Jr., *J. Chem. Phys.*, **45**, 1067 (1966); (b) C. W. Mathews, *ibid.*, **45**, 1068 (1966).

(39) V. M. Rao, R. F. Curl, Jr., P. L. Timms, and J. L. Margrave, *ibid.*, **43**, 2557 (1965).

(40) A. D. Walsh, *J. Chem. Soc.*, 2260 (1953).

(41) J. P. Simons, *ibid.*, 5406 (1965).

Table V: Comparison of Calculated and Experimental Energy Separation of the Ground and First Excited States

Molecule	ΔE_{calcd}, eV	ΔE_{exptl}, eV
	Transition $^1B_1 \leftarrow X\ ^1A_1$	
CF_2	3.3 (4.9)[i]	4.68[a]
SiF_2	3.6	5.47[b]
GeF_2	4.1	5.43[c]
SnF_2	4.7	5.14[d]
PbF_2	5.7	~5.1[d]
CCl_2	1.67	~3.1[i]
$SiCl_2$	2.9	~3.5[e]
$GeCl_2$	2.7	4.0[d]
$SnCl_2$	...	4.4[d]
$PbCl_2$	3.5	3.4[d]
	Transition $^1\Pi$–$X\ ^1\Sigma$	
BF	3.91 (5.5)[i]	6.36[f]
AlF	3.99	5.47[f]
GaF	4.85	4.10[f]
InF	3.93	3.78[f]
TlF	5.0	5.64[f]
BCl	3.28	4.55[f]
AlCl	3.28	4.75[f]
GaCl	3.76	3.67[f]
InCl	3.34	3.44[f]
TlCl	3.96	3.85[f]
BBr	3.01	4.2[f]
AlBr	3.23	2.96[f]
	Transition $^2\Sigma$–$X\ ^2\pi$	
CF	4.93	5.31[f]
SiF	6.06	~6.4[g]
GeF	4.79	4.35[h]
SnF	5.42	4.3[f]
PbF	5.77	5.6[f]
CCl	2.87	4.45[f]
SiCl	4.0	4.24[e]
GeCl	3.7	4.20[f]
SnCl	...	3.59[e]
PbCl	...	4.36[f]
	Transition $^2\Pi$–$X\ ^2\Sigma$	
CaF	2.43	2.06, 2.35[f]
CaCl	2.1	2.0, 2.09[f]
	Transition $^2B_1$–$X\ ^2A_1$	
BF_2	2.0	...
AlF_2	0.8	...
BCl_2	1.35	...
$AlCl_2$	1.32	...
CF_3	7.0	>5.9[g]
SiF_3	6.1	...
CCl_3	5.3	...

[a] B. A. Thrush and J. J. Zwolenik, *Trans. Faraday Soc.*, **59**, 582 (1963). [b] V. M. Khanna, G. Besenbruch, and J. L. Margrave, *J. Chem. Phys.*, **46**, 2310 (1967). [c] R. Hauge, V. M. Khanna, and J. L. Margrave, *J. Mol Spectrosc.*, **27**, 143 (1968). [d] J. W. Hastie, R. Hauge, and J. L. Margrave, *J. Phys. Chem.*, **72**, 3510 (1968); also *J. Mol. Spectrosc.*, **29**, 152 (1969). [e] P. K. Asundi, M. Karim, and R. Samuel, *Proc. Phys. Soc.*, **50**, 581 (1938). [f] R. W. B. Pearse and A. G. Gaydon, "The Identification of Molecular Spectra," 3rd ed, John Wiley and Sons, Inc., New York, N. Y. [g] J. W. C. Johns and R. F. Barrow, *Proc. Phys. Soc.*, **71A**, 476 (1958). [h] E. B. Andrews and R. F. Barrow, *ibid.*, **63A**, 185 (1950). [i] D. C. Milligan, D. E. Mann, M. E. Jacox, and R. A. Mitsch, *J. Chem. Phys.*, **41**, 1199 (1964). [j] Bracketed values obtained by correcting for a $2s^2$ correlation energy of 1.6 eV.[42]

the energy separations for the analogous states are large, as shown in Table V.

The agreement with experiment appears best for radicals and for heavy metal halides. This is probably due to the neglect of electron-pair correlation energy in the ground states of the group IVa dihalides and group IIIa monohalides and also to the inability of the method to compensate for nuclear–nuclear repulsion in the lighter species, such as BF and CF. If the $2s^2$ correlation energy in the B and C atoms, which has been calculated[42] to fall in the region of 1.6 eV, is considered in the singlet–singlet transitions of BF and CF_2, then the calculated energy differences are in good agreement with the experimental data. Also, the tendency for the calculated ΔE of the heavier metal halides (*e.g.*, SnF_2 and InF) to be in better agreement with experiment could be due to the ns^2 correlation energy becoming less for the heavier, more ionic, species.

Ionic Character

The charge separations resulting from the Mulliken population analysis procedure are in good agreement, as shown in Figure 2, with values interpolated from the ionic character *vs.* electronegativity difference curve proposed by Daily and Townes[31] (shown in Figure 2) on the basis of nuclear quadrupole coupling constant measurements. Their curve is based on the electronegativity values calculated by Huggins.[43] We have used Pauling's[32] values which do not differ from these by more than 0.1 unit of the Pauling system.

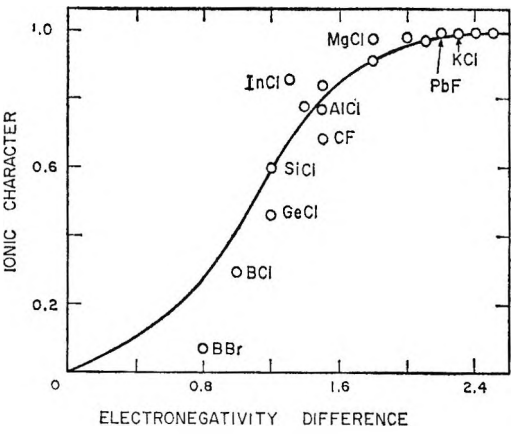


Figure 2. Comparison of calculated ionic character for diatomic metal halides (indicated by the circles) with the Dailey and Townes curve.

The general agreement found for the wide range of molecules considered here supports both the basis of the Dailey and Townes curve and also the choice of the charge sensitive K parameter for the MO calculations. However, it appears that the increasing tendency for

(42) L. C. Allen, E. Clementi, and H. M. Gladney, *Rev. Mod. Phys.*, **35**, 465 (1963).

(43) M. L. Huggins, *J. Amer. Chem. Soc.*, **75**, 4123 (1953).

deviation of the MO results from the Dailey and Townes curve, in the low electronegativity difference region, is significant and reflects the need to reduce K as the extent of overlap, or covalency, increases. Independent support for the Dailey and Townes curve in this strong overlap region is given by the AgCl molecule which has been shown experimentally[44] to have an ionic character of 52%, in agreement with the curve.

The calculations also predict, correctly, the increased covalent nature of chlorides and bromides as compared with fluorides as well as the increasing covalency with n for MX_n ($n = 1, 2, 3, 4$). The ability to calculate fairly reliable charge separations without great refinement of the LCAO calculations was predicted by Mulliken.[23]

Orbital Character

The orbital character for the HOMO seems to be in accord with the known chemical nature of the species. For example, the group IIIa monohalides show considerable mixing of the s and p levels for the first members (*e.g.*, BX) of the group but much less for InX and TlX. The predominant s character, interpreted as a lone pair of electrons, for the latter species is in keeping with the tendency for the heavier metals of group IIIa to form monovalent rather than trivalent compounds. Similarly, Table IV indicates that the group IVa divalent species have an increasing tendency to form a lone s pair of electrons from CX_2 to PbX_2, which agrees with both the increasing stability of the divalent over the tetravalent species and the decreasing bond angle of MX_2 for increasing size of M.

These data also tend to support the valence state hypothesis of Hildenbrand.[2] For example, the dissociation energies for the group IIa difluoride, BeF_2, may be interpreted as indicating a valence state of approximately 30% $sp + 70\% s^2$. Also the sp character decreases markedly from BeF_2 to BaF_2. The data of Table I show a similar trend for the MF species of this group. Similarly the group IIIa monohalides have been predicted[2] to have a considerable sp^2-hybrid bonding character as well as the expected pure p character. The data of Table III verify this considerable s–p orbital character.

The order of the energy levels for the group IVa monohalides, as obtained from the eigenvalues and eigenvectors, is found to be $\ldots (\sigma_s^b)^2 (\sigma_s^*)^2 (\pi_y^b)^2 (\pi_x^b)^2 (\sigma_z^b)^2 (\pi_y^*)^1 (\pi_x^*)^0 (\sigma_z^*)^0$ (using the notation given by Gray[21]). One would then expect ionization of these species to produce a more favorable bonding situation due to the removal of an antibonding π_y^* electron from the system. In fact the molecule-ion dissociation energies have been found to be higher than for the neutral molecules.[4] This stability increase on ionization probably results in a reduced internuclear separation for the molecule-ion. The Franck–Condon principle would therefore require the vertical ionization potential (as measured by electron impact ionization) to be greater than the adiabatic value (determined spectroscopically). Experimentally this difference has been found for the monofluorides to be of the order of several tenths of 1 eV.[4]

For group IIIa monohalides the highest occupied orbital is the σ_z^b bonding orbital. Removal of an electron from this level to produce the molecule-ion should therefore result in a reduced bond strength. In fact, the molecule-ion species have been shown experimentally to be of much lower stability than their un-ionized counterparts.

On the other hand, the dihalides of group IIIa (for example, BF_2) have the following electronic structure $^2A_1$: $\ldots (1b_2)^2 (1a_1)^2 (2b_2)^2 (2a_1)^2 (1b_1)^2 (3b_2)^2 (1a_2)^2 (3a_1)^2 (4a_1)^1 (2b_1)^0 (5a_1)^0 (4b_2)^0$, and the antibonding character of the $(1a_2)^2$, $(3a_1)$ and $(4a_1)$ orbitals must significantly reduce the stability of the molecules. The ion (*e.g.*, BF_2^+) would be expected to retain considerable stability due to the loss of an antibonding electron. In fact, use of a thermochemical cycle involving the stability of BF_2 and the ionization potentials of B and BF_2 indicates that BF_2^+ is only 1 eV less stable than BF_2.

The orbital character for CF_3, as shown in Table IV, varies considerably with bond angle. The C(2s) to C(2p) proportion at 112° is the same order of magnitude as that calculated from esr measurements (see footnote *h*, Table IV). Exact agreement is obtained if an angle of 109° is used for the EH calculation.

Conclusions

In applying the extended Hückel method to the calculation of ionization potentials, charge distribution, and geometry for inorganic molecules, it appears that the most reliable data are obtained for species where ionization is from an orbital which is mainly localized on the metal atom (or ion). Thus its application is most useful for radicals (*e.g.*, SiF, SiF_3) or molecules for which the metal ion is not of an inert gas configuration in its electron complement (*e.g.*, SiF_2, AlF, etc.). The implication of this is that H_{ii} (metal) terms of the Hamiltonian matrix are very well approximated by "VSIE free-atom" energies but that the H_{ii} (ligand or more electronegative group) terms require a correction to the VSIE free-atom energies, particularly for fluorides. Also the correction should be in the direction such that the H_{ii} (ligand) energies are less than the VSIE (free atom) values.

This ability of the EH method to yield reliable ionization potentials for molecules where the H_{ii} terms can be approximated by "VSIE free atom" energies, suggests that, for cases where this not so, one may correct the H_{ii} terms until the proper molecular I.P. is found. A similar method of adjustment has been

(44) L. C. Krisher and W. G. Norris, *J. Chem. Phys.*, 44, 391 (1966).

applied[13] to the H_2O molecule where use of uncorrected H_{ii} terms leads to a linear structure, while corrected terms predict the correct bent structure. Hence the availability of experimental I.P. data for a molecule can be used to assist in making the best choice of H_{ii} for an EH calculation which should predict a fairly reliable molecular and electronic structure.

A striking feature of the calculated I.P.'s is that ionization occurs mainly from significantly localized orbitals. Also, most of the experimental I.P. data used for comparison with these values were obtained by the electron impact method, which has been stated by Berry[45] to represent ionization also from localized orbitals. Small deviations, of the order of a few tenths of an electron volt, between experimental and MO data are to be expected due to the contribution of vibrational energy to the measured values. The MO results assume no change of internuclear separation in the ionization process.

The agreement of calculated and experimental data for the heavier metal halides such as TlX and PbX_n (n = 1 or 2) suggests that one can successfully extrapolate Clementi and Raimondi's[26] Slater exponents to the heavier elements. In favor of this is the increased tendency for the heavy metal halides to be ionic, and hence the extent of orbital overlap, which is greatly determined by the size of the Slater exponent, is much less and is not critical for these cases. This property of ionic molecules also allows one to formally assume that the orbital exponent for a particular AO does not vary significantly in different molecular environments. The assumption is known[46] to be invalid for covalent species.

The results also indicate that the energy of the HOMO can be used as a good approximation to indicate the ionization potential of the molecule. The deviations that do occur are probably partly due to the restriction in these calculations to a constant K for all molecules. K is not really a constant but one concludes from experience that, for molecules of the type dealt with in Figure 1, the ionization potential does not vary significantly for small variations of K. The suggestion that K should vary according to the magnitude of the overlap integral is probably a reasonable improvement.[13,19] However, we have tested this suggestion on several of the halides dealt with in this work, using the formula proposed by Cusachs,[13,14] and found only small differences in the results.

The data given in Tables III and IV for the group IIIa, MF and group IVa, MF_2 species—where the metal has essentially a nonbonding lone pair of s electrons—suggest a comparison of molecular lone pair energies with atomic lone pair energies. For the MF species the molecular lone pair energy is only about 1–2 eV lower than the free atom lone pair energy but for MF_2 the difference is 3–4 eV. SCF calculations have indicated that one can expect lone-pair ionization energies in a molecule to be close to those in the atom.[47]

Finally, the results for several of the diatomic species dealt with in this work may be compared with available SCF wave functions of "close to Hartree–Fock accuracy" as tabulated by McLean and Yoshimine.[48] For example, from the energies of the HOMO and assuming Koopman's theorem to be valid the following comparison of ionization potentials (in electron volts) is made; AlF = 9.5 ± 0.3 (exp), 9.74 (EH) and 9.15 (SCF); BF = 11.4 ± 0.3 (exp), 11.49 (EH) and 11.0 (SCF) and KF = 9.5 ± 0.3 (exp), 8.76 (EH) and 10.9 (SCF). The disagreement for KF seems to indicate that Koopman's theorem may not be a good approximation where the ionized electron has a strong bonding character in the molecule. A number of transition metal complexes where ionization is apparently from the ligands, show[49] similar disagreement with Koopman's theorem.

Acknowledgments. This work was supported by the Robert A. Welch Foundation. Mr. David Bonnell assisted with the computations which were carried out on an IBM-7040 computer.

(45) See R. S. Berry, "Ionization in High Temperature Gases," "Progress in Astronautics and Aeronautics," Vol. 12, K. E. Shuler, Ed., Academic Press, New York, N. Y., 1963 p 3; also in *Compt. Rend. Conf. Intern. Phenomenes Ionization Gas, 6e, Paris*, **1**, 13 (1963).

(46) D. B. Boyd and W. N. Lipscomb, *J. Chem. Phys.*, **46**, 910 (1967).

(47) D. Peters, *J. Chem. Soc.*, 2908 (1964).

(48) A. D. McLean and M. Yoshimine, "Tables of Linear Molecule Wave Functions," 1967, available from the authors, address San Jose Res. Lab, IBM Corp., San Jose, Calif.

(49) S. M. Schildcrout, R. G. Pearson, and F. E. Stafford, *J. Amer. Chem. Soc.* **90**, 4006 (1968).

The Role of Polar Factors in Collision Complex Models for the Solvent and Concentration Dependence of Nuclear Magnetic Resonance Parameters

by Raymond L. Schmidt, Robert S. Butler,[1] and J. H. Goldstein

Department of Chemistry, Emory University, Atlanta, Georgia 30322 *(Received September 26, 1968)*

A detailed experimental study of the nmr parameters of α-chloroacrylonitrile (α-CAN) has been carried out in seven solvents over the entire concentration range. The results have been interpreted on the basis of a collision complex model using least-squares methods to determine the association constants and nmr parameters for each postulated species. Parameter values appear reasonable and account for the observed parallel behavior of shifts and couplings in α-CAN. It has been shown that the influence of dielectric constant on the nmr parameters can be related to the influence of the solvent dipolar cohesive energy in the equilibrium constant of the collision complex model. The effect of reaction electric fields on chemical shifts has been introduced as a virial-type expression involving a Stockmayer intermolecular potential. This procedure accounts for previously observed nonlinearity in the dependence of the shift on an Onsager-type reaction field.

Introduction

A large number of theoretical and experimental studies concerning the interpretation of solvent effects in high-resolution nuclear magnetic spectroscopy have appeared in recent years.[2] The total experimentally observed proton chemical shift is considered as the sum of various contributions,[3] $\sigma = \sigma_G + \sigma_B + \sigma_A + \sigma_W + \sigma_E + \sigma_C$, where σ_G is the chemical shift of an isolated gas molecule, σ_B the shift due to the bulk diamagnetic susceptibility of the medium,[4] σ_A the shift arising from the anisotropic diamagnetic susceptibility of the neighboring molecules,[5] σ_W that due to van der Waals interactions between surrounding molecules,[6] σ_E the shift originating from the electric fields in the medium caused by the effect of polar solute molecules on the polarizable surroundings,[7,8] and σ_C is the shift due to specific intermolecular interactions (complex formation).[9] In this paper we shall be specifically concerned with the interpretation of the electric field and specific interaction terms.

The electric field term, σ_E, has been shown by Marshall and Pople[7] and Buckingham[3a] to depend on the component of the local field along the X–H bond direction

$$\sigma_E = -AE\cos\lambda - BE^2 \qquad (1)$$

where $E\cos\lambda$ is the projection of the local electric field, E, on the bond direction, and A and B are parameters which depend on the nature of the species forming the bond. The numerical values for these parameters have been reported by a number of workers.[3a,7,10] The contribution of σ_E to the total chemical shift is significant when protons experience fields of $\sim 10^6$ statV/cm.

The value of the electric field, E, appearing in eq 1, has frequently been assumed to be given by the Onsager relation, $E = (\mu_{solute}/\alpha_{solvent})Z(\epsilon_{solvent})$, where $Z(\epsilon)$ is usually taken to be $(\epsilon - 1)/(2\epsilon + 2.5)$. In view of the relatively small magnitude of B in eq 1, for a given solute, the observed chemical shift is expected to correlate linearly with $Z(\epsilon)$ for a series of solvents of varying dielectric constant.[11–15] However, many of the reported correlations of σ *vs.* $Z(\epsilon)$ exhibit considerable curvature. Schaefer and coworkers have proposed that this curvature may be the result of specific solute–

(1) NASA Graduate Trainee, Emory University, 1967–1970.

(2) Most of the earlier work is summarized by (a) J. A. Pople, W. G. Schneider, and H. J. Bernstein, "High Resolution Nuclear Magnetic Resonance," McGraw-Hill Book Co., Inc., New York, N. Y., 1959; (b) J. W. Emsley, J. Feeney, and L. H. Sutcliffe, "High Resolution Nuclear Magnetic Resonance Spectroscopy," Vol. 1 and 2, Pergamon Press, London, 1965; (c) P. Laszlo in "Progress in Nuclear Magnetic Resonance Spectroscopy," Vol. 3, J. W. Emsley, J. Feeney, and L. H. Sutcliffe, Ed., Pergamon Press, London, 1967.

(3) (a) A. D. Buckingham, *Can. J. Chem.*, **38**, 300 (1960); (b) A. D. Buckingham, T. Schaefer, and W. G. Schneider, *J. Chem. Phys.*, **32**, 1227 (1960).

(4) Ref 2a, p 81.

(5) J. C. Schug, *J. Phys. Chem.*, **70**, 1816 (1966).

(6) B. B. Howard, B. Linder, and M. T. Emerson, *J. Chem. Phys.*, **36**, 485 (1962).

(7) T. W. Marshall and J. A. Pople, *Mol. Phys.*, **1**, 199 (1958).

(8) J. I. Musher, *J. Chem. Phys.*, **37**, 34 (1962).

(9) (a) R. J. Abraham, *Mol. Phys.*, **4**, 369 (1961); (b) W. G. Schneider, *J. Phys. Chem.*, **66**, 2653 (1962); (c) J. V. Hatton and W. G. Schneider, *Can. J. Chem.*, **40**, 1285 (1962).

(10) (a) L. Petrakis and H. J. Bernstein, *J. Chem. Phys.*, **37**, 2731 (1962); (b) L. Petrakis and H. J. Bernstein, *ibid.*, **38**, 1562 (1953); (c) F. H. A. Rummens and H. J. Bernstein, *ibid.*, **43**, 2971 (1965).

(11) F. Hruska, E. Bock, and T. Schaefer, *Can. J. Chem.*, **41**, 3034 (1964).

(12) (a) V. S. Watts, G. S. Reddy, and J. H. Goldstein, *J. Mol. Spectrosc.*, **11**, 325 (1963); (b) V. S. Watts and J. H. Goldstein, *J. Chem. Phys.*, **42**, 228 (1965); (c) V. S. Watts, J. Loemker, and J. H. Goldstein, *J. Mol. Spectrosc.*, **17**, 348 (1965); (d) V. S. Watts and J. H. Goldstein, *ibid.*, **21**, 260 (1966); (e) L. S. Rattet, A. D. Williamson, and J. H. Goldstein, *J. Phys. Chem.*, **72**, 2954 (1968).

(13) (a) K. M. McLauchlan, L. W. Reeves, and T. Schaefer, *Can. J. Chem.*, **44**, 1473 (1966); (b) G. Kotowycz and T. Schaefer, *ibid.*, **45**, 1093 (1967); (c) H. M. Hutton and T. Schaefer, *ibid.*, **45**, 1111 (1967); (d) F. Hruska, D. W. McBride, and T. Schaefer, *ibid.*, **45**, 1081 (1967).

(14) P. Laszlo and J. I. Musher, *J. Chem. Phys.*, **41**, 3906 (1964).

(15) B. Fountaine, M. Chenon, and N. Lumbroso-Bader, *J. Chim. Phys.*, **62**, 1075 (1965).

solvent interactions in solvents of higher dielectric constant.

Specific interaction models have also been proposed by several authors to account for solvent effects.[16-18] In view of the relatively poor performance of the reaction field theory and the lack of a clear distinction between specific interactions and "bulk effects," Kuntz and Johnston[19] have suggested that most, if not all, of the "polar solvent effects" can be treated by specific interaction (collision complex[20]) models where the lifetime of the complex is larger than the time between collisions in the liquid state (10^{-11} sec).

The net result of the two approaches has been to implicate both polar factors (solvent dielectric constant, solute dipole moment) and complex formation. In this report we describe a study of solvent effects on nmr parameters, based upon the collision complex model, in which the role of polar factors has also been reasonably well established. Experimental data are presented using α-chloroacrylonitrile (α-CAN) as a probe molecule in a series of solvents whose dielectric constants cover a wide range (ϵ = 2–45). An expression for the electric field which includes the solvent dipole is presented which semiquantitatively explains the curvature in reaction field correlations.

Specific Interaction Model

Following the method of Saunders and Hyne[21] for treating the association of polymers containing n monomers, it is possible to write down a general expression[22] for the chemical shift as a weighted average of shifts characteristic of a molecule in a variety of complexed states

$$\sigma_{obs} = \sum_{i=1}^{p} (n_i K_i \sigma_i \prod_{j=1}^{r} X_j^{a_j}) / \sum_{i=1}^{p} (n_i K_i \prod_{j=1}^{r} X_j^{a_j}) \quad (2)$$

where p is the total number of complex states in which the molecule may exist, n_i is the number of probe molecules in the ith complex, K_i is the association constant for the formation of the ith complex, σ_i is the chemical shift characteristic of the molecule in the ith complexed state, r is the total number of ligands able to complex with the molecule, X_j is the equilibrium concentration of the jth ligand, determined from material balance equations, and a_j is the number of the jth ligand molecules in the complexed form. Considering the formation of polymers containing n monomer units, the above expression reduces to eq 9–128 of ref 2b.

For the analysis of the experimental data presented in this paper, we consider a two-component system (solute 1, solvent 2) able to form two complexed species, a solute–solute dimer (labeled 11) and a solute–solvent complex (labeled 12). Then the weighted average chemical shift is given by

$$\sigma_{obs} = \frac{X_1\sigma_1 + 2K_{11}\sigma_{11}X_1^2 + K_{12}\sigma_{12}X_1X_2}{X_1 + 2K_{11}X_1^2 + K_{12}X_1X_2} \quad (3)$$

where K_{11} is the association constant for the dimer formation, K_{12} is the association constant for the solute–solvent complex formation, X_1 is the equilibrium concentration of uncomplexed solute ($X_1 = X_1^0 - 2X_{11} - X_{12}$), and X_2 is the equilibrium concentration of the solvent ($X_2 = X_2^0 - X_{12}$). Thus the solvent dependence of the observed nmr chemical shift is described in terms of five parameters: the chemical shifts of the monomer, dimer, and a solute–solvent complex; and ΔG_i° values ($\Delta G_i^\circ = -RT \ln K_i$) for the monomer–dimer and the monomer-complex equilibria. This model has been applied to the nmr data obtained over the entire concentration range for α-CAN in seven solvents.

Electric Field Effect

Inasmuch as the Onsager reaction field is based upon a model of a polar solute in a polarizable but nonpolar solvent, there is some reason to expect that it may not be adequate for solvents of high dielectric constant. In an effort to involve explicitly the polarity of the solvent medium, we have employed the general theory of medium effects in imperfect gases as described by Raynes, Buckingham, and Bernstein,[23] in which the proton chemical shift is expressed as an expansion of the virial type ($\sigma = \sigma_0 + \sigma_1/V + \cdots$). Neglecting terms higher than first order in molar volume, the virial expression describes the initial deviation from ideal gas behavior. σ_1 is determined by binary molecular collisions and is given by

$$\sigma_1 = \tfrac{1}{2} N_a \int (\sigma_{pair}) \exp(-U/kT)\, d\tau_2 \quad (4)$$

where N_a is Avogadro's number, σ_{pair} is the screening constant of the molecule due to the presence of molecule 2, and U is the intermolecular potential energy. The integration volume element is

$$d\tau_2 = r^2 dr \sin\theta_1 d\theta_1 \sin\theta_2 d\theta_2 d\phi \quad (5)$$

Rummens, Raynes, and Bernstein[24] have applied this binary collision gas model to the calculation of the van der Waals contribution to the shift for a series of nonpolar, magnetically isotropic molecules in the liquid

(16) C. M. Huggins, G. C. Pimentel, and J. N. Shoolery, *J. Chem. Phys.*, 23, 1244 (1955).

(17) (a) A. L. McClellan, S. W. Nicksic, and J. C. Guffy, *J. Mol. Spectrosc.*, 11, 340 (1963); (b) A. L. McClellan and S. W. Nicksic, *J. Phys. Chem.*, 69, 446 (1965).

(18) B. B. Howard, C. F. Jumper, and M. T. Emerson, *J. Mol. Spectrosc.*, 10, 117 (1963).

(19) I. D. Kuntz, Jr., and M. D. Johnston, Jr., *J. Amer. Chem. Soc.*, 89, 6008 (1967).

(20) M. Horak, J. Moravec, and J. Pliva, *Spectrochim. Acta*, 21, 919 (1965).

(21) M. Saunders and J. B. Hyne, *J. Chem. Phys.*, 29, 1319 (1958).

(22) L. D. Homer, *Acta Biotheoret.*, 17, 125 (1967).

(23) W. T. Raynes, A. D. Buckingham, and H. J. Bernstein, *J. Chem. Phys.*, 36, 3481 (1962).

(24) F. H. A. Rummens, W. T. Raynes, and H. J. Bernstein, *J. Phys. Chem.*, 72, 2111 (1968).

state by using the appropriate liquid density in the virial expansion. In light of their success with the van der Waals term at liquid densities, it appeared worthwhile to consider also the virial theory expression for the electric field contribution under similar conditions.

Following the procedure outlined by Raynes, Buckingham, and Bernstein[23] for the electric field contribution in gaseous media, one can assume a Stockmayer intermolecular potential energy expression

$$U = 4\epsilon'[(r_0/r)^{12} - (r_0/r)^6] + \mu_1\mu_2 r^{-3}(2\cos\theta_1\cos\theta_2 + \sin\theta_1\sin\theta_2\cos\phi) \quad (6)$$

and neglect contributions to the electric field due to molecular quadrupole moments. ϵ' [25] and r_0 are constants with the dimensions of energy and length, respectively. Substitution of the appropriate expressions into eq 4, where σ_{pair} is given by eq 1, and integration over all configurations of molecule 2 yields

$$\begin{aligned}(\sigma_1)_E = &-(\pi N_a A\cos\lambda/6y^2)\mu_2\{(\tau/3)H_6(y) \\ &+ (y^4\tau^3/200)H_{12}(y)\cdots\} + (4\alpha_2\mu_1/r_0^3y^2) \\ &\times\{H_6(y) + (\tau^2y^4/40)H_{12}(y)\cdots\} \\ &- (\pi N_a B/3y^4)(2\mu_2^2/r_0^3)\{H_6(y) + (\pi^2y^4/40)H_{12}(y)\cdots\} \\ &+ (\alpha_2\mu_1\mu_2/r_0^6)\{y^2\tau H_{12}(y) + (y^6\tau^3/60)H_{18}(y)\cdots\} \quad (7) \\ \sigma_E = &\ (\sigma_1)_E/V\end{aligned}$$

where $\tau = \mu_1\mu_2/\epsilon r_0^3$, $y = 2(\epsilon/kT)^{1/2}$, $\epsilon = (\epsilon_1\epsilon_2)^{1/2}$, $r_0 = \frac{1}{2}(r_{01} + r_{02})$, μ_i and α_i are the component dipole moment and polarizability, V is the solvent molar volume, and the $H_n(y)$ functions are determined by the method given by Buckingham and Pople.[26] This expression, which explicitly contains the dipole moment of both solute and solvent species, was tested against the data obtained in this study.

Experimental Section

Cyclohexane, acetone, N,N-dimethylformamide (all Fisher Certified reagents), dimethyl sulfoxide (Matheson Coleman and Bell, spectroanalyzed) and *d*-chloroform (Diaprep Inc., Atlanta, Ga.) were used as solvents without further purification. Bromotrichloromethane and 4-heptanone (both Matheson Coleman and Bell, practical) were fractionally distilled through a spinning band column at atmospheric pressure. α-Chloroacrylonitrile (α-CAN) (Columbia Chemical Co.) was fractionally distilled through a spinning band column under reduced pressure to prevent polymerization during the purification. All solvents showed no detectable impurities in their nmr spectra even at the lowest solute concentrations used in this study.

All samples were prepared by weight in 10-ml glass vials and transferred into nmr sample tubes after addition of a small amount (less than 1%) of tetramethylsilane (TMS) to serve as the internal reference. When necessary the pure components were degassed with nitrogen before the samples were prepared.

All spectra were recorded at probe temperature (about 38°) on a Varian Associates A-60A nmr spectrometer and were calibrated by the usual side-band technique. Samples with N,N-dimethylformamide as solvent were also recorded at −58.5 and −19.5°. The observed frequencies were usually the average of one forward and one reverse sweep which produced sufficient accuracy except in the very dilute samples where at least two forward and two reverse sweeps were recorded. The nmr parameters (two chemical shifts and one coupling parameter) were corrected for second-order effects using a least-squares computer program. The mean deviation for each peak is in the range 0.00–0.07 Hz, and the estimated error in the shifts and coupling parameters is 0.05 Hz.

Results and Discussion

The pmr spectrum of α-chloroacrylonitrile ($H_2C{=}CClCN$) involves two chemical shifts (proton 1 is *cis* to Cl, proton 2 is *cis* to CN) and one H–H coupling, all of which are known to be sensitive to solvent and concentration. The spectrum is a simple AB pattern, which is easy to calibrate and analyze rigorously. For these reasons α-CAN serves as an ideal probe molecule in the investigation of solvent effects. Although solvent effects for this molecule have been reported before, it was highly desirable for the present study to obtain data over the entire concentration range for all solvents employed. The results obtained are illustrated in Figure 1 as plots of the chemical shift of proton 1 *vs.* concentration. The plots for the shift of proton 2 and J_{H-H} curves agree within experimental error with those reported previously.[12b] The chemical shift curves in solvents other than cyclohexane were about 1 Hz lower than previously reported; those in cyclohexane agree within experimental error.

Trial calculations indicated that all solvent systems considered could be adequately treated by considering the three species involved in eq 3: solute monomer, solute dimer, and solute–solvent complex. (The possibility that the two protons of α-CAN might show different complexing ability[17b] could not be substantiated since the dilution curves gave statistically identical equilibrium constants for all solvents.)

Because of the greater relative accuracy of the chemical shift data compared with the coupling values, the former were used to determine the equilibrium constants. Using these constants and three fitting parameters (J_1, J_{11}, J_{12}), it was possible to reproduce the

(25) The prime is introduced here to provide a distinction between this parameter of the Stockmayer potential and the ϵ used to designate the solvent dielectric constant. Since the letter ϵ is customarily used for both purposes, we hesitate to introduce radically new symbols for either.

(26) A. D. Buckingham and J. A. Pople, *Trans. Faraday Soc.*, 51, 1173 (1955).

Table I: Least-Squares Parameters of Eq 3[a]

Solvent	K_{11}	K_{12}	$\sigma_1(1)$	$\sigma_{11}(1)$	$\sigma_{11}(1)$	$\sigma_1(2)$	$\sigma_{11}(2)$	$\sigma_{12}(2)$	J_1	J_{11}	J_{12}	SE(σ)	SE(J)
Cyclohexane	1.05	0.27	−343	−395	−382	−344	−406	−403	−1.7	−3.8	−2.6	0.67	0.07
Bromotrichloromethane	0.73	0.40	−346	−401	−422	−349	−409	−434	−2.1	−3.7	−2.6	0.52	0.03
d-Chloroform	0.91	0.50	−348	−393	−400	−354	−399	−406	−2.1	−3.5	−2.8	0.57	0.03
4-Heptanone	0.49	0.39	−352	−399	−457	−358	−405	−473	−2.2	−3.8	−4.7	0.63	0.01
Acetone	0.43	0.41	−368	−374	−426	−382	−367	−424	−2.6	−3.2	−4.2	0.37	0.02
N,N-Dimethylformamide (35°)	0.26	0.71	−370	−373	−430	−384	−356	−435	−2.9	−2.8	−3.6	0.17	−0.03
(−19.5°)	0.19	0.76	−375	−366	−440	−390	−343	−446	−3.0	−2.3	−3.4	0.19	0.01
(−53.5°)	0.20	0.84	−376	−370	−448	−392	−348	−455	−3.1	−2.3	−3.2	0.29	0.03
Dimethyl sulfoxide	0.16	1.03	−368	−380	−419	−384	−348	−425	−3.0	−2.1	−3.4	0.19	0.03

[a] The dimensions of the quantities are: K, (mol fraction)$^{-1}$; σ, Hz; J, Hz; SE, Hz. SE is the standard error of the nonlinear least-squares fit.

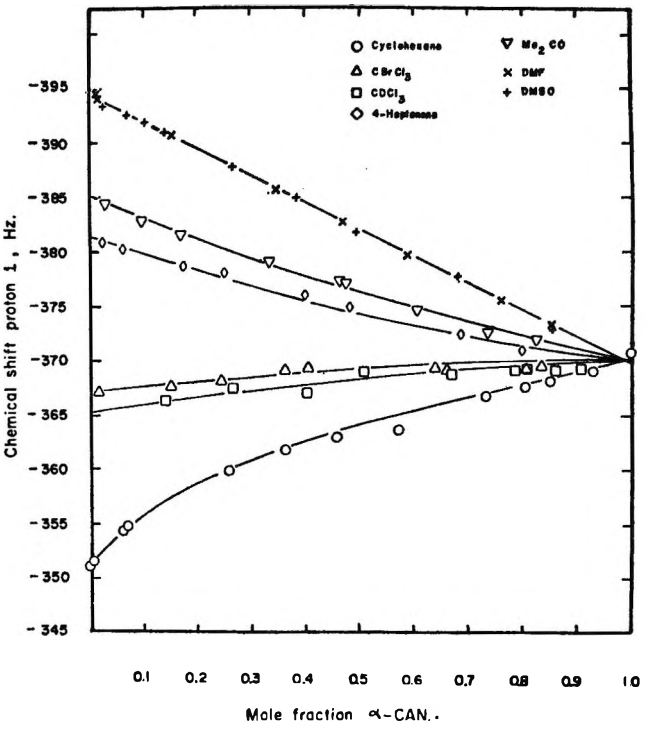


Figure 1. Dilution curves for proton 1 (*trans* to Cl substituent): (a) cyclohexane; (b) $CBrCl_3$; (c) $CDCl_3$; (d) 4-heptanone; (e) acetone; (f) dimethylformamide (probe temp); (g) dimethyl sulfoxide. Points are experimental and solid lines calculated.

observed concentration dependence of the coupling values reasonably well, considering the larger inherent uncertainty in the couplings. Such a result is considered to be very encouraging inasmuch as the generally parallel behavior of shifts and coupling in α-CAN suggest that common factors are involved in the solvent dependence of σ_1, σ_2, and J.

The model equation was fitted to the experimental data using nonlinear least-squares techniques involving the Marquardt algorithm,[27] the Hartley algorithm,[28] or a mixed Marquardt–Hartley algorithm to determine the parameters and the rate of convergence. The resulting least-squares parameters are presented in Table I. In most cases the root-mean-square error of the fit is less than 0.6 Hz except in cyclohexane and 4-heptanone where the error is only slightly greater than 0.6 Hz. For the higher dielectric constant solvents the root-mean-square errors are 0.2–0.3 Hz. The estimated error in the equilibrium constants is about 10% while the error in the shift parameters is generally less than 10 Hz. The relative errors in the coupling parameters (J_1, J_{11}, J_{12}) are much larger than those of the shift parameters (σ_1, σ_{11}, σ_{12}), which is to be expected in view of the corresponding uncertainties in the experimental couplings and shifts.

Correlation diagrams (σ *vs.* J) of the best least-squares parameters are given in Figure 2. These correlations

(27) D. W. Marquardt, *J. Soc. Ind. Appl. Math.*, 11, 431 (1963).
(28) H. O. Hartley, *Technometrics*, 3, 269 (1961).

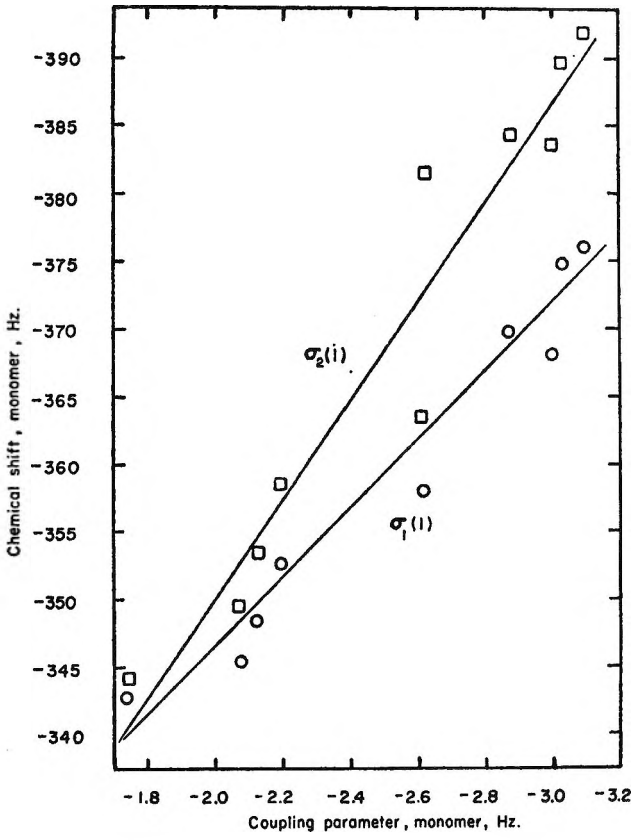


Figure 2. Correlation diagram of monomer, dimer, and complex parameters σ *vs.* J. Correlation coefficients are monomer: proton 1, 0.97, proton 2, 0.96; dimer: proton 1, 0.83, proton 2, 0.93; complex: proton 1, 0.70, proton 2, 0.64.

indicate that indeed the same association model may be simultaneously applied to both σ and J dilution curves and substantiates the proposal that similar factors are involved in solvent effects of both chemical shifts and coupling parameters.[12b]

It is necessary to caution the reader that satisfactory results in a statistical procedure such as that outlined above is of itself no guarantee that the model chosen is correct, unique, or even realistic. The feasibility of the model in the present case is substantiated by the reasonable values obtained for the least-squares parameters. The equilibrium constants are comparable to those obtained by other authors[19] and follow the expected trends on going from nonpolar to polar solvents. The chemical shift and coupling parameters are also of realistic magnitude and change in expected directions with variations in solvent polarity.

Watts and Goldstein[12b] have also presented correlations of observed dilute solution chemical shifts and coupling parameters with the solvent reaction field parameter, $Z(\epsilon)$. Such correlations show considerable scatter and are at best only a crude indication of the effect of the solvent on chemical shifts and coupling parameters. However, the parameters obtained in this study (see Table I) permit us to undertake a new, and hopefully more quantitative, investigation of these solvent effects. Thus, examination of the association constant data (Table I) indicates that they are, indeed, related to the corresponding solvent dielectric constants (see Table II). In fact, plots of ln K_{11} and ln K_{12} *vs.* ϵ (not given here) are approximately linear and of opposite slope. (There is some scatter in these plots in the region of small ϵ.) From this it follows that the free-energy differences for the corresponding equilibria are approximately linear in ϵ. In this connection, we note that Böttcher[29] has derived an expression for the dipolar contribution, $W(\epsilon)/RT$, to the cohesive free energy of a liquid. Moreover, there is a reasonably good correlation between our equilibrium constants and these dipolar cohesive free-energy values, as shown in Figure 3. In light of the transitory nature of the proposed collision complexes and the above correlation of ln K_{12} with $W(\epsilon)/RT$, it is possible to view the solvent–solute association model as a mechanism for including the solvent cohesive energy in the observed nmr solvent effects.

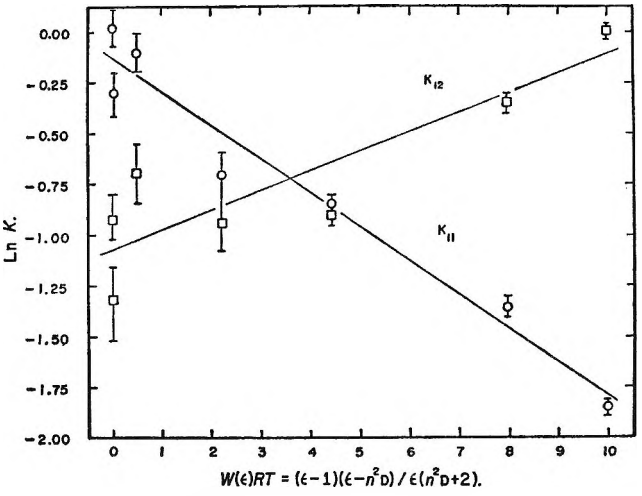


Figure 3. Correlation diagram of ln K *vs.* dipolar cohesive energy term. Correlation coefficients are ln K_{11} = 0.98, ln K_{12} = 0.87.

As has been previously mentioned, an unsatisfactory feature of the reaction field theory, to the approximation involved in the Onsager model, is its inability to account for the definitely nonlinear correlation of σ or J *vs.* $Z(\epsilon)$, as shown in Figure 4 for the chemical shift. Although a smooth curve has been drawn through the points in Figure 4, it is possible to represent these data by means of two straight line segments. The important point, however, is that in either case there is a sharp change in the dependence on $Z(\epsilon)$ at about the value of ϵ for α-CAN ($\epsilon \simeq 11.0 \pm 2.0$[30]).

Fröhlich[31] has shown that the Onsager reaction field

(29) C. J. F. Böttcher, "Theory of Electric Polarization," Elsevier Publishing Co., Amsterdam, 1952, eq 5.138.

(30) V. S. Watts, Ph.D. Dissertation, Emory University, 1965.

(31) H. Fröhlich, *Discussions Faraday Soc.*, 42A, 3 (1946).

Table II: Molecular Parameters for Virial Calculation

Solvent	Dielectric constant, ϵ	Molar volume, cc/mol	Refractive index, $n^{35}D$	Polarizability[i] $\times 10^{24}$, cc/molecule	Ionization potential[j] $\times 10^{12}$, ergs	ϵ'/k[l], °K	$10^8 r_0$[l], cm	Dipole moment, D
Cyclohexane	1.97[a]	100.04[d]	1.41848[d]	11.00	15.83	390.3[m]	6.78[m]	0.0
Bromotrichloromethane	2.38[c]	...	1.4983[b]	...	...	...	...	...
d-Chloroform[e]	4.59[a]	82.39[d]	1.43678[d]	8.55	18.30	539.7[n]	5.00[n]	1.05[r]
Iodomethane	6.62[b]	63.46[d]	1.52144[d]	7.66	15.28	538.8[v]	4.04	1.64[r]
Dichloromethane	8.53[b]	65.23[d]	1.41621[d]	6.49	18.18	734.2[o]	3.12[o]	1.59[r]
4-Heptanone	11.72[a]	142.58[b]	1.3998[b]	13.69	14.90[k]	...	...	2.70[s]
2-Pentanone	15.0[b]	108.63[f]	1.3828[d]	10.04	15.03	634.5[p]	3.31[p]	2.6[t]
2-Butanone	18.0[b]	91.48[f]	1.3711[d]	8.22	15.28	632.0[p]	3.95[p]	2.79[t]
Acetone	19.75[a]	75.05[d]	1.35157[d]	6.43	15.52	513.2[q]	3.93[q]	2.86[r]
Methanol	30.61[a]	41.17[d]	1.32277[d]	3.26	17.38	870.8[q]	2.70[q]	1.71[r]
N,N-Dimethylformamide	35.05[a]	77.40[f]	1.42240[b]	7.80	14.61	...	...	3.84[u]
Dimethyl sulfoxide	45.00[a]	71.92[g]	1.47165[h]	7.98	14.42[k]	...	...	3.90[u]
α-Chloroacrylonitrile	11 ± 2.0[w]	80.5[x]	1.4225[w]	8.32	...	...	...	3.32[y]

[a] V. S. Watts and J. H. Goldstein, *J. Chem. Phys.*, **42**, 228 (1965). [b] "Handbook of Chemistry and Physics," 46th ed, R. C. Weast, Ed., The Chemical Rubber Publishing Co., Cleveland, Ohio. [c] H. M. Hutton and T. Schaefer, *Can. J. Chem.*, **45**, 1111 (1967). [d] J. Timmermans, "Physicochemical Constants of Pure Organic Compounds," Vol. 1 and 2, Elsevier Publishing Co., New York, N. Y., 1950 and 1965. [e] Data for $CHCl_3$ was used as an approximation to $COCl_2$. [f] Estimated from data given in footnote *b*. [g] H. L. Clever and C. C. Snead, *J. Phys. Chem.*, **67**, 918 (1963). [h] Determined in this laboratory, L. L. Haynes. [i] Calcd by $\alpha = (3/4\pi)(M/\rho N_a)(M_0^2 - 1)/(M_0^2 + 2)$, M = molecular weight, ρ = density, N_a = Avagadro's number. [j] K. Watanabe, T. Nakayama, and J. Mettl, O.T.S.-U.S. Dept. of Commerce, Report no. PB-158-317 (1959). [k] Estimated from data of similar compounds. [l] Determined by a least-squares fit to second virial coefficient data, assuming a rigid dipolar molecular model by the method of A. D. Buckingham and J. A. Pople, *Trans. Faraday Soc.*, **51**, 1173 (1955), see also J. S. Rowlinson, *ibid.*, **45**, 974 (1949). [m] J. S. Rowlinson, *Proc. Roy. Soc. Ser. A*, **196**, 113 (1949). [n] P. G. Francis and M. L. McGlashan, *Trans. Faraday Soc.*, **51**, 593 (1955). [o] A. Perez Mosia and M. Diaz Pena, *An. Real. Soc. Espan. Fis. Quim., Ser. B*, **54**, 661 (1958); *Chem. Abstr.*, **53**, 17612c (1959). [p] J. K. Nickerson, K. A. Kobe, and J. J. McKetta, *J. Phys. Chem.*, **65**, 1037 (1961). [q] J. S. Rowlinson, *Trans. Faraday Soc.*, **45**, 974 (1949); also see footnote *m*. [r] A. L. McClellan, "Tables of Experimental Dipole Moments," W. H. Freeman and Co., San Francisco, Calif., 1963, gas phase. [s] Footnote *r*, CCl_4 solution. [t] Footnote *r*, estimated, benzene solution. [u] Footnote *r*, benzene solution. [v] P. G. T. Fogg, P. A. Hanks, and J. D. Lambert, *Proc. Roy. Soc., Ser. A*, **219**, 490 (1953). [w] Reference 30. [x] N. B. Lorette, *J. Org. Chem.*, **26**, 2324 (1961). [y] E. Bock and E. F. Dojack, *Can. J. Chem.*, **45**, 1097 (1967).

theory should be applicable only in solvents of low dielectric constant ($\epsilon < 9$). This limitation was pointed out in the early work on polar effects in nmr by Buckingham,[3a] but has been largely ignored in latter discussions. Thus, the observed behavior in Figure 6 is most likely due to the inadequacy of the Onsager reaction field expression in high dielectric constant solvents. While searching for a suitable expression for the field applicable to high dielectric constant solvents,[32-34] it was observed that curves similar in shape to those in Figure 4 were obtained from a variety of field expressions which explicitly contained the dipole moment and polarizability of the solvent in addition to the dipole moment of the solute. The model given in eq 7 contains these molecular parameters.

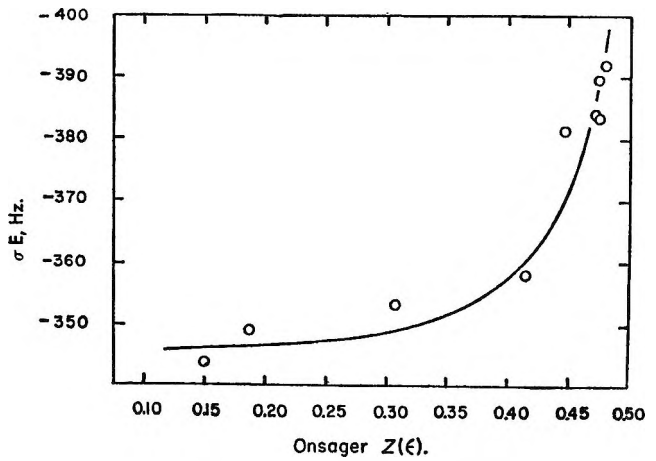


Figure 4. Correlation diagram of chemical shift proton 1 (monomer) *vs.* Onsager reaction field parameter, $Z(\epsilon)$.

The data frequently used for estimating the parameters ϵ'/k and r_0 of the Stockmayer potential are the second virial coefficients,[26] which were available for only three of the solvents used in this study. We have, therefore, extended the computations based on eq 7 to include additional solvents, listed in Table II, for which virial coefficient data were available. (These additional solvents are suitable media for nmr solvent studies, but their inclusion in this study would have been impractical.) The results of these calculations are presented in Figure 5, in which σ_E estimated from eq 7 is plotted against the Onsager $Z(\epsilon)$. As can be seen this curve has the correct general character of the experimental σ *vs.* $Z(\epsilon)$ graph (Figure 4), and the three experimental solvents used in this study lie very nicely on the curve. (An alternate representation of these

(32) C. O. Beckman and K. Cohen, *J. Chem. Phys.*, **4**, 784 (1936).
(33) A. J. Mukhedkar, *Z. Phys. Chem.* (Frankfurt am Main), **25**, 56 (1960); *J. Chem. Phys.*, **35**, 2133 (1961).
(34) O. E. Weigang, *ibid.*, **41**, 1435 (1964).

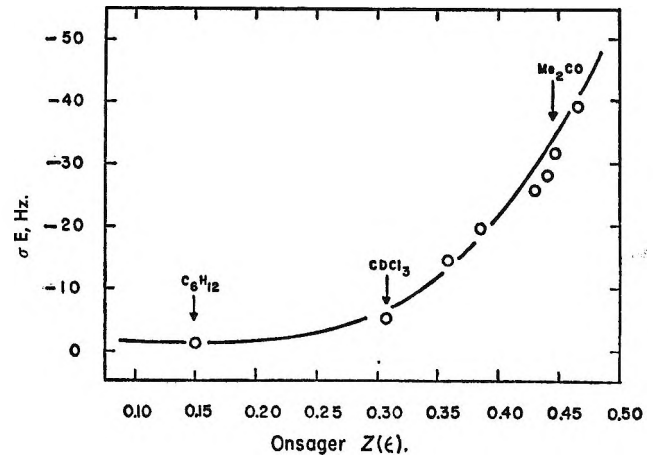


Figure 5. Correlation diagram of calculated electric field contribution (eq 7), σ_E, *vs.* Onsager reaction field parameter, $Z(\epsilon)$. ↑ solvents used in this study.

results can be obtained by plotting σ_{expt} *vs.* σ_E, yielding a straight line. However, Figure 5 has been preferred because it reproduces the nonlinear character of the σ *vs.* $Z(\epsilon)$ relationship.)

To calculate the electric field contribution given in eq 7 it is necessary to know the Stockmayer potential parameters $(\epsilon'/k, r_0)$ for the α-CAN solute molecule. To our knowledge, no experimental data for the second virial coefficients are available. Therefore, ϵ'/k was determined from the freezing point ($t_f = -54°$, $\epsilon'/k = 420°$),[35] and r_0 was determined by a least-squares fit of the data for the monomer and dimer chemical shift of the two protons of α-CAN to a model for the total chemical shift which consisted of a gas phase shift plus the electric field contribution given by eq 7. The r_0 parameter for α-CAN determined by this procedure was 8.66 Å, about 65% larger than expected from the molar volume. The error in the least-squares fit was 4.4 Hz for 12 data points. If one assumes a polarizable dipole model to determine the solvent Stockmayer potential parameters from second virial coefficient data, the value of r_0 for α-CAN is 54% larger than expected. The resulting gas phase shifts for the various states of the probe molecule are: $\alpha_1(1) = 340.4$ Hz, $\alpha_1(2) = 346.9$ Hz, $\sigma_{11}(1) = 400.0$ Hz, and $\sigma_{11}(2) = 403.5$ Hz (all ± 2.8 Hz). One cannot be overly concerned about the somewhat large value of r_0 for α-CAN required to reproduce the monomer and dimer chemical shifts because of the many problems involved in the precise determination of intermolecular forces from second virial coefficient data.[36]

Consideration was also given to the effect of van der Waals contribution to the chemical shifts, σ_w, following the methods given by Rummens, Raynes, and Bernstein.[24] These authors have indicated that their model is not applicable to polar media. The results described here are based on the assumption that the van der Waals contribution will not be significant in the cases studied.

On the basis of the above discussion and the results indicated in Figure 5, it appears that eq 7 accounts, in at least a semiquantitative way, for the electric field contribution to solute chemical shifts of a polar molecule in a polar solvent over a range of ϵ values for which the Onsager model is unsatisfactory. Moreover, the collision complex model, as applied here to α-CAN, also accounts for the observed parallel behavior of σ and J, with allowance being made for the relatively larger uncertainties in the values of the latter parameters. These results are available for use in other solvents as a further experimental test of these conclusions.

In a study of the temperature and solvent dependence of the proton-coupling parameter and chemical shift of α-CAN, McLauchlan, *et al.*,[13a] propose that there may be an association with N,N-dimethylformamide (DMF) which is strongly temperature dependent. The α-CAN–DMF system was observed at temperatures from -58.5 to 35° to investigate this possibility. Examination of Table I shows that there is a slight temperature dependence of the equilibrium constant for dimerization and complex formation, but the largest temperature effect is on the shift of the monomer, dimer, and complex. The shifts of the monomer and dimer are also included in Figure 4, using the values of the DMF dielectric constant at the appropriate temperature. For the monomer, σ becomes more positive with increasing temperature and for the dimer the reverse is true. Inasmuch as ϵ decreases with temperature, this behavior is consistent with expectations based upon the σ *vs.* $Z(\epsilon)$ graph given in Figure 4. This suggests that in these systems the effect of temperature is primarily reflected through the variation of the dielectric constant.

Acknowledgment. This research was supported in part by grants from the National Science Foundation and the National Institutes of Health. The authors would also like to thank A. Ray Tarpley and Robert C. Long for assistance in the experimental phases of this work.

(35) J. O. Hirschfelder, C. F. Curtiss, and R. B. Bird, "Molecular Theory of Gases and Liquids," John Wiley and Sons, Inc., New York, N. Y., 1954, Chapter 4.

(36) E. A. Mason and L. Monchick in "Intermolecular Forces," "Advances in Chemical Physics," Vol. 12, J. O. Hirschfelder, Ed., Interscience Publishers, New York, N. Y., 1967, p 370.

Analysis of the Proton Nuclear Magnetic Resonance Spectrum of Trimethylene Selenide

by William B. Moniz

Naval Research Laboratory, Washington, D. C. 20390 *(Received October 18, 1968)*

That the rapid ring inversions of nonplanar cyclic molecules do not cause the *cis* and *trans* proton coupling constants to become equal has been well established. Consequently, in four-membered ring systems, both planar molecules such as cyclobutanone and rapidly inverting nonplanar molecules such as trimethylene selenide constitute spin systems of the AA'BB'B''B''' type rather than the A_2B_4 type. Because the ring skeleton of trimethylene selenide inverts rapidly and symmetrically about a planar configuration, the effective symmetry of the spin system can be considered to be C_{2v} for purposes of the nmr analysis. The spectral parameters derived from an iterative computer analysis of the 100-MHz proton data yielded calculated spectra which were excellent fits to the 100-MHz and 60-MHz experimental spectra. As expected, the α protons are more shielded than the β protons due to the lower electronegativity of selenium relative to carbon.

Introduction

Proton nmr spectral parameters have been reported for the four-membered heterocycles trimethylene oxide,[1,2] trimethylenimine,[1] and trimethylene sulfide.[1] In addition, the spectra of two cyclobutane derivatives, cyclobutanone and 1,1-dicarbomethoxycyclobutane, have been analyzed.[1,3,4] Another member of this series, trimethylene selenide (TMSe), has recently been the subject of extensive infrared studies.[5,6] TMSe is interesting from the nmr point of view as it is the first of the four-membered heterocycles to contain an atom less electronegative than carbon.

Considerable attention has been devoted to the determination of ring-puckering vibrations and barriers to inversion of these and related molecules as characterized by their microwave spectra and infrared absorption, especially in the far-infrared region.[7] Cyclobutanone[8,9] and trimethylene oxide[10–12] are planar or nearly so, while trimethylene sulfide[8,9,13] and TMSe[5,6] are puckered. In analogy to cyclobutane,[14] 1,1-dicarbomethoxycyclobutane is most probably puckered. The barriers to the ring inversions in these molecules are low, the largest, that for TMSe, being about 1.1 kcal/mol.[5,6] Consequently, the ring inversions are rapid at normal temperatures.

With regard to vicinal and cross-ring proton–proton spin coupling, the *cis* and *trans* conformations are uniquely defined in the planar and near-planar molecules. On the other hand, for a puckered, rapidly inverting ring skeleton, the *cis–trans* distinctions can become blurred, as in the case of cyclohexane. However, despite the chair–chair inversions of cyclohexane-type ring systems, where relative C–H bond angular reorientations of as much as 120° may occur (a → e; e → a), $({}^3J_{cis})_{av}$ is not equal to $({}^3J_{trans})_{av}$,[15] because the "before" and "after" relationships for *cis* coupling (ea, ae) are not the same as those for *trans* coupling (aa, ee).

More limited angular reorientations occur in the ring inversions of the four-membered cyclic molecules. The most puckered of the four-membered ring compounds considered, TMSe, has a dihedral angle of less than 35°,[6] hence relative C–H bond angular reorientations of less than 70° occur in the conversion of one puckered conformation to another. Examination of a model shows that the *cis* and *trans* distinctions are not lost as a consequence of the inversions. Of course, since there is some averaging of the *cis* and *trans* couplings by virtue of the ring inversions, the nmr spectrum will reflect this fact.

Nonetheless, because the vicinal *cis* and *trans* couplings do not become equal, nor do the cross ring *cis* and *trans* couplings, these spin systems must be analyzed as AA'BB'B''B''' types, and not as A_2B_4 types, regardless of the degree of ring puckering. Thus, the

(1) J. A. Ferretti, Ph.D. Thesis, University of California, Berkeley, Calif., Aug 1965; UCRL-16349.

(2) E. Lustig, E. P. Ragelis, and N. Duy, *Spectrochim. Acta*, **23A**, 133 (1967).

(3) B. Braillon and J. Barbet, *Compt. Rend.*, **261**, 1967 (1965); B. Braillon, *J. Mol. Spectrosc.*, **27**, 313 (1968).

(4) L. H. Sutcliffe and S. M. Walker, *J. Phys. Chem.*, **71**, 1555 (1967).

(5) A. B. Harvey, J. R. Durig, and A. C. Morrissey, *J. Chem. Phys.*, **47**, 4864 (1967).

(6) A. B. Harvey, J. R. Durig, and A. C. Morrissey, submitted for publication; A. B. Harvey, private communication.

(7) For a recent summary, see J. Laane and R. C. Lord, *J. Chem. Phys.* **48**, 1508 (1968).

(8) J. R. Durig and R. C. Lord, *ibid.*, **45**, 61 (1966).

(9) T. R. Borgers and H. L. Strauss, *ibid.*, **45**, 947 (1966).

(10) S. I. Chan, T. R. Borgers, J. W. Russell, H. L. Strauss, and W. D. Gwinn, *ibid.*, **44**, 1103 (1966).

(11) A. Danti, W. J. Lafferty, and R. C. Lord, *ibid.*, **33**, 294 (1960).

(12) S. I. Chan, J. Zinn, J. Fernandez, and W. D. Gwinn, *ibid.*, **33**, 1643 (1960).

(13) D. O. Harris, H. W. Harrington, A. C. Luntz, and W. D. Gwinn, *ibid.*, **44**, 3467 (1966).

(14) A. Almenningen, O. Bastiensen, and P. N. Skancke, *Acta Chem. Scand.*, **15**, 711 (1961); J. D. Dunitz and V. Schomaker, *J. Chem. Phys.*, **20**, 1703 (1952).

(15) H. Booth, *Tetrahedron*, **20**, 2211 (1964); E. Lustig, E. P. Ragelis, N. Duy, and J. A. Ferretti, *J. Amer. Chem. Soc.*, **89**, 3953 (1967).

A_2B_4 treatment of cyclobutanone,[16] ruled out because the molecule is planar,[4] would have been invalid even if the molecule were not planar.

It is noteworthy that C_{2v} symmetry can be assumed in analyzing the AA'BB'B''B''' spin systems of these puckered four-membered ring compounds because the ring skeleton vibrates symmetrically about a planar conformation; this applies even in the case of trimethylenimine, for the nitrogen atom inverts rapidly on the nmr time scale.[1]

Experimental Section

Sample Preparation. The preparation of TMSe has been described elsewhere.[6] Because of the tendency of TMSe to polymerize readily, especially in the absence of oxygen,[17] neat samples could not be employed for the nmr measurements. Suitable long term stability was obtained in a vacuum-degassed solution containing 25 vol % TMSe in CCl_4 doped with 5 vol % tetramethylsilane.

Nmr Spectra. The 100-MHz proton spectra were obtained using a Varian HA-100 nmr spectrometer in the field-lock mode. All resolvable peaks were individually calibrated by multiple-period averaging of the frequency difference between the lock channel and analytical channel oscillators. The reproducibility of calibration was found to be ±0.03 Hz.

In the 60-MHz spectrum, obtained with a Varian A60 (courtesy of Dr. E. Lustig, Food and Drug Administration), only a few lines were calibrated in order to verify the sweep calibration and linearity.

Spectral Analysis. Even at 100 MHz, the spectrum of TMSe is far from first order (Figure 1, top). It is possible to discern, however, highly perturbed triplet character (upfield portion) and quintet character (downfield portion), which suggested that the α protons are more shielded than the β protons, as would be expected since selenium is less electronegative than carbon. The iterative analysis showed that this is indeed the case. Despite the tight coupling within the spin system due to the relatively small $\Delta\nu$, useful analytical information may be extracted from the spectrum. As noted in the Introduction, the spin system is of the AA'BB'B''B''' type, and C_{2v} symmetry may be assumed. The symmetry properties of the C_{2v} point group allow for factorization, so that the energy levels for $F_z = \pm 3$ and ± 2 of the A_1 species can be found explicitly. Manipulation of the appropriate submatrices involving these levels leads to the following analytical expressions involving the corresponding four A_1 transitions ν_1, ν_2, ν_3, and ν_4.[18]

$$J_{cis} + J_{trans} = [(\nu_2 - \nu_1) + (\nu_4 - \nu_3)]/3$$

and

$$2(\Delta\nu)^2 = (\nu_3 - \nu_1)^2 + (\nu_4 - \nu_2)^2 - (\tfrac{9}{2})(J_{cis} + J_{trans})^2$$

The transition frequencies ν_1, ν_2, ν_3, and ν_4 are characteristic and, with the aid of their calculable intensities, may be picked out of the experimental spectrum quite easily.[18] These lines are indicated in Figure 1, top. For TMSe at 100 MHz, one obtains $\Delta\nu = 18.4$ Hz, and $(J_{cis} + J_{trans}) = 15.2$ Hz. With this information and trial parameters based upon those of trimethylene sul-

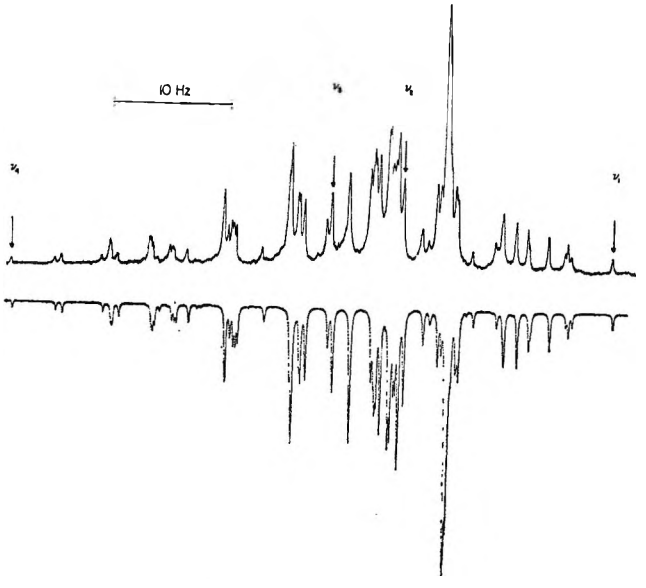


Figure 1. The 100-MHz ^{1}H spectrum of trimethylene selenide. Top: experimental spectrum. The lines ν_1–ν_4 corresponding to the transitions among the $F_z \pm 2$, ± 3 levels are indicated. Bottom: computer-plotted spectrum based on refined parameters.

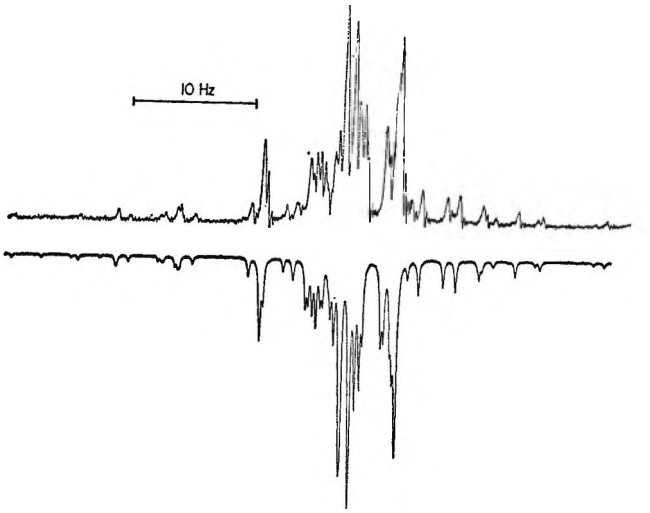


Figure 2. The 60-MHz ^{1}H spectrum of trimethylene selenide. Top: experimental spectrum. Bottom: computer-plotted spectrum based on refined parameters.

(16) L. L. Combs and L. K. Runnells, *J. Chem. Phys.*, **44**, 2209 (1966).

(17) R. F. Cozzens and A. B. Harvey, to be published.

(18) E. Lustig, private communication.

Table I: Nmr Spectral Parameters for Trimethylene Selenide

Coupling constant, Hz		Chemical shift (ppm: TMS = 0)	
$^2J_\alpha(gem)$	−7.91	H_α	3.115
$^2J_\beta(gem)$	−12.10	H_β	3.299
$^3J_{cis}$	8.70[a]		
$^3J_{trans}$	6.47		
$^4J_{cis}$	0.82		
$^4J_{trans}$	−0.41		

[a] The larger vicinal coupling constant is arbitrarily assigned to the *cis* configuration, in keeping with the observation that *cis* ^3J's are usually larger than *trans* ^3J's for a large number of cyclobutane derivatives [I. Fleming and D. H. Williams, *Tetrahedron*, **23**, 2747 (1967)].

fide,[1] iterative analyses were carried out with NMRIT-NMREN[19] and the 100-MHz data. However, presumably because line overlap prevented sufficiently accurate assignments in some portions of the spectrum, satisfactory convergence could not be obtained. Since the 60-MHz spectrum contains even fewer resolved lines, its analysis was not attempted. Instead, LAOCOON III[20] was employed with the 100-MHz data. After many cycles of line reassignments and iterations, good convergence was obtained, as evidenced by low rms error (0.023 Hz; 75 lines iterated) and excellent agreement of the computer-plotted spectrum with the experimental spectrum (Figure 1). In Figure 2 are shown the 60-MHz spectrum and the computer-plotted 60-MHz spectrum based on the 100-MHz analysis. Again, excellent agreement is obtained.

Coupling between ^{77}Se and protons may account for several lines of very low intensity which apparently are not a part of the analyzed spectrum. Because many of the lines which would be expected to arise from such coupling are undoubtedly buried in the abundance of "normal" lines, no effort was made to extract ^{77}Se–H coupling information.

Discussion

The refined spectral parameters for TMSe are listed in Table I. They are similar to those of the other four-membered heterocycles except for the expected reversal in the shielding of H_α and H_β.

The convergence of the computed spectrum to an excellent fit of the experimental spectrum while retaining $^3J_{cis} \neq {}^3J_{trans}$ and $^4J_{cis} \neq {}^4J_{trans}$ can be regarded as confirmation of the argument that ring inversions do not cause *cis* and *trans* coupling constants to become equal. It may be possible to correlate the dihedral angle in these ring systems with the partially averaged *cis* and *trans* coupling constants.[21]

With the determination of the spectral parameters of TMSe, the homologous four-membered ring compounds for which proton nmr analyses have been reported now encompass three contiguous periods as well as three contiguous groups of the Periodic Table. The trends in the nmr parameters of these molecules are under active consideration and will be the subject of a future report.

Acknowledgments. The author is especially grateful to Dr. A. B. Harvey for furnishing the trimethylene selenide, and to Drs. J. A. Ferretti and E. Lustig for valuable consultations concerning computer programs and aspects of the spectral analysis.

(19) J. D. Swalen and C. A. Reilly, *J. Chem. Phys.*, **37**, 21 (1962).
(20) S. Castellano, private communication.
(21) J. B. Lambert, *J. Amer. Chem. Soc.*, **89**, 1836 (1967).

Thermodynamics of Solutions with Liquid Crystal Solvents. II. Surface Effects with Nematogenic Compounds

by Laurence C. Chow and Daniel E. Martire

Department of Chemistry, Georgetown University, Washington, D. C. 20007 *(Received November 1, 1968)*

Differential scanning calorimetry and gas–liquid chromatography are used in a thermodynamic investigation of surface effects with two nematogenic liquid crystals (*p*-azoxyanisole and 4,4′-dihexyloxyazoxybenzene). Studied are bulk samples (film thickness of about 4×10^{-2} cm) and samples where the compound is spread on various common chromatographic support materials (film thicknesses ranging from 40 to 2200 Å). It is found that surface effects are absent at the solid–liquid crystal interface. However, at the gas–liquid crystal interface small surface effects are sometimes present with two-component systems (*i.e.*, when nonmesomorphic solute is added), but may be neglected provided that the film thickness is at least 1000 Å.

Introduction

Differential scanning calorimetry[1–3] (dsc) and gas–liquid chromatography[4,5] (glc) have been used recently to obtain thermodynamic information about liquid crystals. The former technique provides temperatures and enthalpies of solid → mesophase, mesophase → mesophase, and mesophase → liquid transitions; the latter method yields infinite dilution solute activity coefficients and partial molar excess enthalpies and entropies of solution in the anisotropic mesophase(s) and the isotropic liquid phase of liquid crystal solvents. The most recent glc work,[6] which dealt with the cholesteric type substance cholesteryl myristate, was reported in paper I of this series. We now direct our attention to nematic type liquid crystals.

An important problem that has not yet been directly approached is the effect of the contacting solid surface and the thickness of the liquid crystal layer on the determination of bulk thermodynamic properties for nematogenic compounds. It is not inconceivable that surface interactions could influence the molecular arrangement (and, hence, the thermodynamic properties) of the nematic and isotropic liquid phases through some sort of cooperative ordering or disordering phenomenon. If that were the case, the measured temperatures and heats of transition would depend on the nature of the solid surface in contact with the liquid crystal and/or the film thickness of the sample. Accordingly, by comparing the dsc values for a bulk sample with those for samples having film thicknesses orders of magnitude smaller and consisting of the substance in contact with several different types of surfaces (*e.g.*, common chromatographic solid support materials), a useful study could be made.

Furthermore, consider the glc experiment which involves a stationary phase (the liquid crystal) with a high surface area-to-bulk volume ratio (small film thickness). The possibility exists that appreciable solute adsorption could occur at the carrier gas–liquid crystal interface and, hence, that the glc results could depend on the surface-to-volume ratio.[6] Thus, before one can claim that thermodynamic information obtained from glc measurements reflects the behavior of the bulk liquid crystal, the absence of noticeable Gibbs solute surface excess concentrations and the validity of the usual assumption of a simple two-phase (gas/bulk liquid) glc partitioning process must be verified. This can be accomplished by establishing that for both nonpolar and polar solutes the specific retention volumes are independent of the weight per cent of stationary phase on the column packing (*i.e.*, the film thickness) and the nature of the solid support with both the nematic and isotropic liquid phases.

The foregoing provides the rationale for the present study in which dsc and glc are used to determine what surface effects (in a thermodynamic sense), if any, are found with nematogenic compounds.

Preparation of Materials

Liquid Crystals. The nematogenic compounds 4,4′-dimethoxyazoxybenzene or *p*-azoxyanisole (PAA) and 4,4′-dihexyloxyazoxybenzene (DHAB) were obtained from Frinton Laboratories and were purified by the

(1) E. M. Barrall, II, R. S. Porter, and J. F. Johnson, *J. Phys. Chem.*, **71**, 895 (1967).

(2) E. M. Barrall, II, R. S. Porter, and J. F. Johnson, *ibid.*, **71**, 1224 (1967).

(3) E. M. Barrall, II, R. S. Porter, and J. F. Johnson, *Mol. Cryst.*, **3**, 299 (1968).

(4) H. Kelker and E. von Schivizhoffen, "Advances in Chromatography," J. C. Giddings and R. A. Keller, Ed., Vol. 6, Marcel Dekker, Inc., New York, N. Y., 1968, pp 247–297.

(5) D. E. Martire, P. A. Blasco, P. F. Carone, L. C. Chow, and H. Vicini, *J. Phys. Chem.*, **72**, 3489 (1968).

(6) D. E. Martire, "Progress in Gas Chromatography," J. H. Purnell, Ed., Interscience Publishers, New York, N. Y., 1968, pp 93–120.

Table I: Surface-Coated Liquid Crystals

Liquid crystal	Solid support	Liquid crystal wt %	Surface area, A_L, (m^2/g of material)	Approximate film thickness, τ (cm $\times 10^6$)[c,d]	Use
PAA	Chromosorb P (60–80 Mesh)	7.63	2.3[a]	3	*e,f*
		16.74	1.9[a]	8	*e,f*
	Chromosorb W (60–80 Mesh)	9.51	0.7[a]	12	*f*
		15.25	0.6[a]	22	*e*
	Tee Six (60–70 Mesh)	~3	~7[b]	0.4	*e*
DHAB	Chromosorb W (60–80 Mesh)	7.63	0.7[a]	9	*f*
		10.00	0.7[a]	12	*f*

[a] Values interpolated from Figure 2 of ref 10. [b] Estimated from values of J. J. Kirkland, *Anal. Chem.*, 35, 2003 (1963). [c] Estimated by using a mean liquid crystal density of 1.15 g/ml (value reported in ref 11). [d] Film thickness of bulk sample used in the dsc experiment was about 4×10^{-2} cm. [e] Dsc experiment. [f] Glc experiment.

hydrogen peroxide oxidation procedure described by Dewar and Goldberg,[7] followed by triple recrystallization from hot ethanol. A Perkin-Elmer differential scanning calorimeter, Model DSC-IB, was employed to determine the purity of the compounds by comparing the peak for the solid → nematic transition with the melting peak for indium, using the analytical procedure described in the manufacturer's literature.[8] The dsc measurements (to be described later in more detail) yielded estimated purities of 99.7% for PAA and 99.6% for DHAB.

Coating of Supports. The solid support materials used in this study were: (a) Johns-Manville 60–80 mesh, acid washed and DMCS-treated Chromosorb W; (b) Johns-Manville 60–80 mesh, acid washed and DMCS-treated Chromosorb P; (c) Analabs 60–70 mesh Tee Six, made from specially processed tetrafluoroethylene. These supports were coated with the liquid crystal compounds by using methylene chloride as the dissolving solvent, followed by gradual solvent elimination through either rotary vacuum evaporation under slight heat or natural evaporation from a large diameter pan. Summarized in Table I are the properties of the surface-coated liquid crystal samples (packings) that were prepared. An exact weight percentage was not determined for the Tee Six sample. For the others, the weight per cent of liquid crystal in each sample was found by taking the average of at least three gravimetric determinations, with about 1 g of sample, done both before and after combustion of the organic liquid crystal.[9] The specific surface areas of the materials were estimated through interpolation of the measurements made by Pecsok, *et al.*,[10] in the range 0–20 liquid wt %. The film thicknesses were then estimated by assuming a mean liquid crystal density of 1.15 g/ml. (the value reported for PAA at the nematic–isotropic transition[11]).

Differential Scanning Calorimetry

Experimental Section

A Perkin-Elmer Model DSC-IB was used for the calorimetric studies. The dsc was purged continuously at a slow and constant flow rate with dry nitrogen gas. Using a scanning rate of 1.25 deg/min, the temperature axis was carefully calibrated in the range 54 to 156° with the known triple points of the eight standards listed in Table II. Each sample, containing from 5 to 10 mg of the standard, was weighed to the nearest 0.002 mg with a microbalance and then hermetically sealed in an aluminum pan.

Table II: Calibration of Dsc Temperature Axis

Std compound	Triple point, °C	Temp correction[d], ΔT (°C)
Indium[a]	156.2	−0.2
Adipic acid[b]	151.4	−0.8
Dimethylterephthalate[b]	139.7	0.0
Benzoic acid[c]	122.4	1.4
Acetanilide[b]	114.3	3.2
p-Dibromobenzene[b]	87.3	5.9
Naphthalene[c]	80.3	6.7
p-Dichlorobenzene[b]	54.2	11.4

[a] Supplied by Perkin-Elmer. [b] Zone-refined, from J. Hinton. [c] Fisher Certified Ther Metric Standard. [d] $\Delta T = T_{actual} - T_{obs}$.

(7) M. J. S. Dewar and R. S. Goldberg, *Tetrahedron Lett.*, 24, 2717 (1966).

(8) Thermal Analysis Newsletters, No. 1 to 7, Perkin-Elmer Corp., Norwalk, Conn.

(9) D. E. Martire and P. Riedl, *J. Phys. Chem.*, 72, 3478 (1968).

(10) R. L. Pecsok, A. de Yllana, and A. Abdul-Karim, *Anal. Chem.*, 36, 452 (1964).

(11) W. A. Hoyer and A. W. Nolle, *J. Chem. Phys.*, 24, 803 (1956).

Liquid crystal samples for dsc were prepared by accurately weighing from 5 to 10 mg of bulk compound and from 10 to 15 mg of surface-coated compound. Each sample was melt-recrystallized at least once before the three runs used in the determinations were carried out. The transition temperatures (T) were found with the aid of a calibration curve constructed from the results in Table II. The heats of transition (ΔH) were determined by the usual method[8] of comparing the chart peak area per milligram of sample with that of a known weight of standard (indium). The areas were measured with a compensating polar planimeter (K & E Model 62-0015) by taking the average value determined from three sweeps of each peak. The previously quoted purities were estimated from the thermograms of the bulk liquid crystal samples.

Table III: Comparison of Temperatures and Heats of Transition

p-Azoxyanisole (PAA)
Solid → Nematic Transition

	Temp, °C	Heat, cal/g
Reference 12	...	27.4
Reference 1	117.6	28.1 ± 0.9
Bulk[a]	117.5 ± 0.3	28.1 ± 0.3
7.63% on Chromosorb P[a]	117.2 ± 0.3	27.9 ± 0.9
16.74% on Chromosorb P[a]	117.3 ± 0 3	...
15.25% on Chromosorb W[a]	117.2 ± 0 3	...

Nematic → Isotropic Transition

	Temp, °C	Heat, cal/g
Reference 12	...	0.64
Reference 1	133.9	0.68 ± 0.02
Bulk[a]	134.2 ± 0.2	0.70 ± 0.02
15.25% on Chromosorb W[b]	134.0 ± 0.5[c]	...
~3% on Tee Six[b]	134.6 ± 0.5[c]	...

4,4′-Dihexyloxyazoxybenzene (DHAB)
Solid → Nematic Transition

	Temp, °C	Heat, cal/g
Reference 12	...	24.9
Reference 7	81	...
Bulk[a]	81.0 ± 0.4	26.1 ± 0.5

	Temp, °C	Heat, cal/g

Nematic → Isotropic Transition

	Temp, °C	Heat, cal/g
Reference 12	...	0.91
Reference 7	128	...
Bulk[a]	128.2 ± 0.3	0.90 ± 0.03

[a] Scanning rate of 1.25 deg/min. [b] Scanning rate of 10.0 deg/min. [c] Determined by comparison with the thermogram of a bulk sample run at a scanning rate of 10.0 deg/min.

Table IV: Heats of Transition for Bulk Samples—Complete Thermal Behavior[a]

p-Azoxyanisole (PAA)

Transition	Heat, cal/g
Solid I → nematic[b]	28.1
Nematic → isotropic[b]	0.70
Solid II → nematic[b]	21.8
Nematic → solid II[c]	28[d]
Solid II → solid I[c]	4[d]

4,4′-Dihexyloxyazoxybenzene (DHAB)

Transition	Heat, cal/g
Solid → nematic[b]	26.1
Nematic → isotropic[b]	0.90
Nematic → smectic[c]	Small[e]
Smectic → solid[c]	Large[e]

[a] See Figure 1. [b] Scanning (heating) rate of 1.25 deg/min. [c] Scanning (cooling) rate of 10.0 deg/min. [d] Heats estimated to the nearest cal/g. [e] Heats could not be estimated because the two peaks overlapped.

Results

The calorimetric results are set out in Tables III and IV and in Figure 1. The agreement between our dsc bulk values and those of others[1,7] is excellent; however, the dsc heats of transition are somewhat higher than those obtained from classical calorimetry.[12] Some difficulty was encountered (due to the appearance of small broad peaks) in the ΔH measurements with the support-coated liquid crystal samples; however, one decent value was eventually obtained (see Table III).

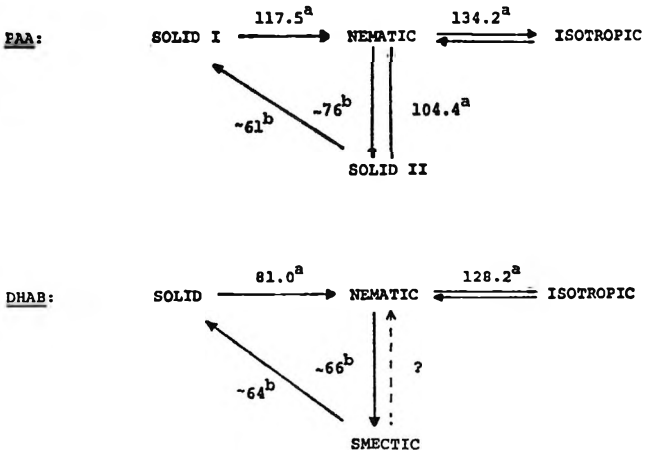


Figure 1. Thermal behavior of PAA and DHAB: superscript a, scanning (heating) rate of 1.25 deg/min; superscript b, scanning (cooling) rate of 10.0 deg/min and temperatures estimated to the nearest degree, without any calibration correction.

(12) H. Arnold, *Z. Physik. Chem.* (Leipzig), **226**, 146 (1964).

Table V: Composition of Glc Columns

Column No.	Liquid crystal	Solid support[a]	Total wt (g) of packing	Total wt (g) of liquid crystal	Wt % of liquid crystal
1	PAA	Chromosorb W	9.3224	0.8866	9.51
2	PAA	Chromosorb P	10.1230	1.6946	16.74
3	PAA	Chromosorb P	9.7866	0.7467	7.63
4	DHAB	Chromosorb W	6.7473	0.6750	10.00
5	DHAB	Chromosorb W	10.0072	0.7636	7.63

[a] All 60–80 mesh.

The detailed thermal behavior of bulk PAA and bulk DHAB, summarized in Table IV and Figure 1, is worth further mention. We have deduced that the intermediate state obtained on cooling the nematic phase was solid for PAA and liquid-crystalline[13] for DHAB. This was because the ΔH's are generally large for liquid crystal → solid transitions and small for liquid crystal → liquid crystal transitions.[1-3] All phase changes noted in Figure 1 were independent of the heating or cooling rates. Despite several attempts, we were unable to obtain a smectic → nematic transition in DHAB because of the short smectic range (~2°), whereas for PAA the solid II → nematic transition was always attainable at 104.4 ± 0.3°.

Gas–Liquid Chromatography

Experimental Section

The compositions of the five columns used in this study are given in Table V. All columns were made from 1/4-in. o.d. copper tubing; they were conditioned, with a gentle flow of helium, at about 150° for 24 hr. The glc unit employed was a dual column Perkin-Elmer Model 880 with dual flame ionization detectors. The detector temperature was maintained at about 200° and the injection port temperature at about 300°. The column temperature was determined at several points by using copper–constantan thermocouples attached to a Leeds and Northrup Type K-4 potentiometer which was equipped with a dc null detector and an Eppley standard cell. The maximum temperature difference along the column was found to be less than 0.3°; the average column temperature remained constant to within 0.1°. The helium carrier gas flow was regulated with Negretti–Zambra precision pressure regulators, Model R/182. The flow rates, which ranged from 35 to 50 ml/min, were measured with a soap-film meter at the column outlet and were chosen to give convenient elution times and reasonable column efficiencies. The inlet pressures were measured to the nearest 0.05 psi with a calibrated Series 1400 U. S. Test Gauge (range, 0–30 psig). The outlet pressure (atmospheric) was determined from a barometric reading. A 1-mV Leeds and Northrup

Table VI: Specific Retention Volumes (V_g^0) in PAA

Solute	Column no.[a] 1	2	3
A. Nematic Phase (123.8°)			
n-Undecane	49.41	50.14	51.28
n-1-Undecene	59.80	60.45	61.13
1-Bromohexane	56.00	56.01	56.13
o-Xylene	57.83	57.88	57.71
n-Butylbenzene	119.4	119.3	119.3
B. Isotropic Phase (140.8°)			
n-Undecane	44.54	44.95	45.57
n-1-Undecene	53.57	53.84	54.33
1-Bromohexane	51.35	59.10	51.40
o-Xylene	53.67	53.82	53.75
n-Butylbenzene	103.9	103.8	104.1
o-Dichlorobenzene	187.1	188.0	187.6

[a] See Table V.

Table VII: Specific Retention Volumes (V_g^0) in DHAB (Nematic Phase Only)

Solute	Column no.[a] 4	5
n-Heptane[b]	20.86	20.80
n-Octane[b]	43.67	43.69
n-Nonane[b]	90.73	90.86
2-Methyloctane[b]	65.17	65.18
2,2-Dimethylheptane[b]	42.69	42.64
n-Decane[c]	133.4	133.5
Tetrachloroethylene[c]	62.03	62.20
p-Xylene[c]	112.2	112.1
Cumene[c]	125.8	125.4

[a] See Table V. [b] T = 91.3°. [c] T = 102.3°.

(13) We have referred to this state as a smectic state because C. Weygand and R. Gabler, *J. Prakt. Chem.*, 155, 332 (1940), have indicated that a monotropic nematic → smectic transition occurs on cooling.

Table VIII: Surface and Bulk Contributions to Retention for Two Solutes in PAA[a]

Solute	Phase	V_g^0(bulk)[b]	Percentage of surface contribution to the total retention[c] Column 1	Column 2	Column 3
n-Undecane	Nematic[d]	48.8	1.2	2.7	4.8
	Isotropic[e]	44.3	0.5	1.4	2.8
n-1-Undecene	Nematic[d]	59.3	0.8	1.9	3.0
	Isotropic[e]	53.4	0.3	0.8	1.7

[a] All other systems gave no clear evidence of solute adsorption. [b] Determined by method outlined in ref 10, 15, and 16. [c] Calculated from eq 1 and Results in Table VI. [d] $T = 123.8°$. [e] $T = 140.8°$.

"Speedomax W" recorder, with a chart speed of 2 in./min, was utilized. The solutes studied were used without further purification; the chromatograms indicated that no major impurities were present. Individual liquid samples were injected with a 10-μl Hamilton syringe, using the smallest detectable sample size. The solute peak retention times past methane were determined by taking the average of from 3 to 5 measurements. Early measurements were reproducible at the end of the experiment to within the accuracy of the measurement; also, the use of an internal standard indicated that no bleeding loss of the stationary phase had occurred. It was established that the solute retention times were independent of sample size, hence that operation was taking place in the Henry's law region (*i.e.*, infinite dilution).

Results

Specific retention volumes (V_g^0) were calculated from the corrected peak retention times and the column operating conditions by using the well-known expression of Littlewood, *et al.*[14] The results for several representative solutes in PAA and DHAB are set out in Tables VI and VII.

Only *n*-undecane and *n*-1-undecene in PAA clearly exhibit the upward trend of V_g^0 with decreasing film thickness that is indicative of solute adsorption at the gas–liquid interface.[6] To estimate the extent of this adsorption contribution to the total retention, the glc results for these two systems were further analyzed by the method proposed by Martin[15] and successfully employed by others.[10,16] Utilizing the values in Tables I, V, and VI and the suggested plotting procedure,[15] we have determined the bulk phase contribution to the specific retention volume (*i.e.*, the value for the limit of infinite film thickness) and the approximate percentage of the surface phase contribution, *i.e.*, the value for

$$\frac{V_g^0(\text{measured}) - V_g^0(\text{bulk})}{V_g^0(\text{measured})} \times 100 \qquad (1)$$

The results are set out in Table VIII.

Discussion

From the results in Table III it is evident that there are no discernible differences between the values for the bulk and support coated samples of PAA. Therefore, considering the wide range of film thickness covered in the dsc experiment (a factor of about 10^5), it is apparent that the support materials studied have little or no effect on the heats and temperatures of transition.

The absence of solid surface effects does not, of course, preclude the possible presence of liquid surface effects with two-component systems (*i.e.*, when solute is added). A large Gibbs surface excess concentration for the solute component coupled with a high liquid surface-to-volume ratio for the solvent component can lead to appreciable solute adsorption at the gas–liquid interface.[6] Such has been observed with glc for binary systems consisting of nonpolar solutes and polar liquid phases.[10,15] It also takes place, but to a much smaller extent, with two solutes (the two least polar and polarizable ones) in PAA. The observed effects (see Table VIII) with the nematic phase are larger than (roughly double) those with the isotropic liquid phase, as would be expected for the more ordered (*i.e.*, "polar") phase.[10,15] However, for a high enough weight percentage (about 15%) of PAA on 60–80 mesh Chromosorb W, it appears that these effects may be neglected for all solutes, with minimal resulting error (less than 1%). The lack of any observable liquid surface effects for the paraffin solutes on DHAB could be due either to experimental error obscuring trends in the results or to the possibility that the ten additional methylene groups per molecule (compared with PAA) may lower the solvent surface free energy sufficiently to diminish the surface excess concentration of the solutes.[6]

In summary, one may conclude that, for all the solid supports and film thicknesses studied, surface effects are either absent or negligible at the solid–liquid crystal interface. Furthermore, at the gas–liquid crystal

(14) A. B. Littlewood, C. S. G. Phillips, and D. T. Price, *J. Chem. Soc.*, 1480 (1955).

(15) R. L. Martin, *Anal. Chem.*, **33**, 347 (1961).

(16) D. E. Martire, *ibid.*, **38**, 244 (1966).

interface, small surface effects are present in some cases, but they may be neglected in the glc experiment provided that a large enough film thickness (greater than about 1000 Å) is used. These encouraging findings now allow one to proceed with a detailed thermodynamic glc study of solutions involving these nematogenic solvents with confidence that the results will provide information about *bulk* liquid crystal behavior.

Acknowledgment. This work was supported through a basic research grant from the U. S. Army Research Office, Durham, North Carolina.

Physical Properties and Chemical Reactivity of Alternant Hydrocarbons and Related Compounds. XVI.[1] Electronic Absorption and Phosphorescence Spectra of Aryl Phenyl Ketones

by C. Párkányi,[2]

Institute of Physical Chemistry, Czechoslovak Academy of Sciences, Prague, Czechoslovakia

E. J. Baum,

Oregon Graduate Center for Study and Research,[3] Portland, Oregon

J. Wyatt, and J. N. Pitts, Jr.

Department of Chemistry, University of California, Riverside, California 92502 *(Received September 24, 1968)*

Spectral properties of eight aryl phenyl ketones were investigated by Pariser–Parr–Pople type LCI–SCF–MO calculations. Reasonable agreement is found between calculated ($S_0 \rightarrow S_1$) excitation energies and wavelengths of absorption band maxima of the ketones. Phosphorescence emission spectra for six of the ketones were obtained, and reasonable agreement is found between calculated ($S_0 \rightarrow T$) excitation energy and wavelength of the 0–0 emission band for those compounds assigned to have a lowest-lying (π, π^*) triplet state. The position of the 0–0 band was confirmed by phosphorescence excitation methods where possible. In all cases, the predicted transition energy was found to be too low. Calculated values were found to deviate equally from observed values for both singlet and triplet transitions resulting in accurate predictions of S–T splittings for the lowest (π, π^*) excited states. Major contributions to this error would be made by choice of calculation parameters for the keto group, deviations from planarity of the compounds studied, and solvent dependence of the spectral band positions.

Introduction

An earlier paper in this series discussed the correlation of HMO characteristics with physicochemical properties of aryl phenyl ketones.[4] Among other results, linear correlations were found between calculated transition energies and the positions of maxima in the long wavelength electronic absorption bands of these ketones. The present paper reports the results of LCI–SCF–MO calculations of singlet–singlet transition energies and oscillator strengths for ketones I–VIII. The values are compared with those derived from experimental absorption curves. Furthermore, phosphorescence emission and phosphorescence excitation spectra are presented, and calculated values of triplet–singlet transition energies are compared with experimentally determined values. Prominent features of the emission and excitation spectra along with phosphorescence lifetimes are

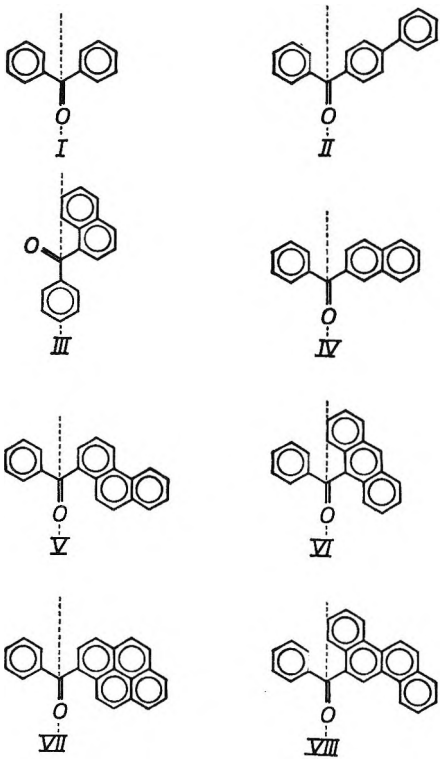
(1) Presented in part at the 2nd IUPAC International Symposium on Photochemistry, Enschede, The Netherlands, July 16–22, 1967. Part XV: C. Párkányi, Z. Dolejšek, and R. Zahradník, *Collect. Czech. Chem. Commun.*, 33, 1211 (1968).

(2) Gates and Crellin Laboratories of Chemistry, California Institute of Technology, Pasadena, Calif. 91109.

(3) 9340 S. W. Barnes Road, Portland, Ore. 97225.

(4) C. Párkányi, V. Horák, J. Pecka, and R. Zahradník, *Collect. Czech. Chem. Commun.*, 31, 835 (1966).

used to characterize the low-lying triplet states of ketones I–VIII.



Experimental Section

LCI–SCF–MO Treatment. The usual version of the Pariser–Parr–Pople LCI–SCF–MO method was used. The parametrization and method have been described elsewhere.[5] Interactions between monoexcited configurations formed by promotion of one π electron from one of the four highest occupied MO's to one of the four lowest unoccupied MO's were considered. The systems studied were assumed to be planar and to have idealized geometry. All C–C bond lengths and all bond angles (including the C–C–O bond angle) were assigned to be 1.40 Å and 120°, respectively. The C–O bond length was taken as 1.20 Å. SCF MO's were used as the basis for the CI calculations. Only resonance integrals between nearest neighbors were considered. The following parameters were used (values in eV).

Atom	I_μ	A_μ	$\gamma_{\mu\mu}$	Z_μ	$\beta_{C-\mu}$
C	11.22	0.69	10.53	1	−2.318
O	13.60	2.30	11.30	1	−2.318

I_μ and A_μ are the ionization potential and electron affinity of atom μ in the atomic valence state, respectively. The monocentric electronic repulsion integrals and core resonance integrals between nearest neighbors are represented by $\gamma_{\mu\mu}$ and $\beta_{C-\mu}$, respectively, and Z_μ is the core charge at atom μ. The bicentric electronic repulsion integrals have been calculated by the Mataga–Nishimoto formula[6]

$$\gamma_{\mu\nu} = \frac{14.399}{R_{\mu\nu} + 1.328} \text{ eV}$$

where $R_{\mu\nu}$(Å) is the distance between atoms μ and ν.

The calculations were performed on a National Elliott 503 computer.

Spectroscopic Methods. The apparatus for measuring phosphorescence spectra has been described elsewhere.[7,8] Ketones were dissolved in 4:1 ethanol–methanol solvent (saturated solutions at room temperature), and the solutions were degassed by the freeze–pump–thaw method in 7-mm Pyrex tubes. After sealing under vacuum, the samples were cooled to 77°K in the phosphoroscope Dewar. Phosphorescence spectra were obtained with excitation wavelengths $\lambda > 300$ mμ and were not corrected for spectral bandpass or wavelength response of the analyzing monochromator–photomultiplier section.

$S_0 \rightarrow T$ spectra of benzophenone in 4:1 ethanol–methanol glass and of 2-naphthyl phenyl ketone in 16:4:1 ethanol–methanol–ethyl iodide glass were obtained at 77°K by phosphorescence excitation techniques[8–10] (the phosphorescence excitation spectrum of 2-naphthyl phenyl ketone was measured on an Aminco-Bowman spectrophosphorimeter). The phosphorescence emission was monitored at the wavelength of maximum phosphorescence intensity, I_P, while the excitation wavelength was scanned. The excitation spectra were not corrected for the spectral distribution of exciting light intensity. The intensity was reasonably constant over the wavelength region of interest.

Phosphorescence decay curves were obtained with a Tektronix 535A oscilloscope, equipped with a Polaroid land camera, connected to the phosphoroscope. Phosphorescence lifetimes, τ_P, were found graphically from plots of ln I_P *vs.* time (slope $= -1/\tau_P$).

The fluorescence spectra of 9-anthryl phenyl ketone and 1-pyrenyl phenyl ketone in methanol (at room temperature) were obtained on an Optica Milano CF 4 NI spectrophotometer by the usual technique.

Materials and methods of purification were the same as those employed in earlier studies.[4] The $S_0 \rightarrow S$ absorption spectra of ketone–methanol solutions at room temperature were obtained previously.[4,11]

(5) J. Koutecký, P. Hochman, and J. Michl, *J. Chem. Phys.*, **40**, 2439 (1964).

(6) N. Mataga and K. Nishimoto, *Z. Phys. Chem.* (Frankfurt am Main), **13**, 140 (1957).

(7) J. G. Calvert and J. N. Pitts, Jr., "Photochemistry," John Wiley and Sons, Inc., New York, N. Y., 1966, pp 806–808.

(8) D. R. Kearns and W. A. Case, *J. Amer. Chem. Soc.*, **88**, 5087 (1966).

(9) R. F. Borkman and D. R. Kearns, *J. Chem. Phys.*, **46**, 2333 (1967).

(10) A. P. Marchetti and D. R. Kearns, *J. Amer. Chem. Soc.*, **89**, 768 (1967), and references therein.

(11) C. Párkányi, R. Zahradník, and M. Nepraš in "Absorption Spectra in the Ultraviolet and Visible Region," Vol. VI, L. Láng, Ed., Akadémiai Kiadó, Budapest, and Academic Press, Inc., New York, N. Y., 1966.

Table I: Results of LCI Calculations[a]

Ketone	ΔE^{1}[b]	f[c]	cos Φ[d]	Predominant configuration i, j[e]	Predominant configuration Wt	Second most important configuration[f] i, j[e]	Second most important configuration Wt	ΔE^{3}[g]
Benzophenone (I)	4.413	0.028	0.000	4, −1	0.528	1, −3	0.155	2.264
	4.422	0.002	−1.000	3, −1	0.578	1, −4	0.146	3.196
	4.521	0.347	1.000	1, −1	0.895	...	...	3.575
	4.724	0.491	0.000	2, −1	0.830	4, −1	0.132	3.715
	5.595	0.276	0.000	1, −3	0.476	4, −1	0.318	3.719
	5.629	0.037	0.000	1, −2	0.916	...	...	3.863
	5.695	0.328	−1.000	1, −4	0.413	3, −1	0.374	4.567
	6.171	0.062	1.000	2, −2	0.362	3, −4	0.270	4.572
4-Phenylbenzophenone (II)	4.100	1.041	−0.611	1, −1	0.929	...	...	2.404
	4.512	0.094	0.164	4, −1	0.526	2, −1	0.136	3.230
	4.595	0.389	0.569	2, −1	0.691	4, −1	0.084	3.627
	4.768	0.007	−0.005	3, −1	0.422	1, −3	0.194	3.939
	5.193	0.114	0.421	1, −2	0.865	2, −1	0.094	4.257
	5.622	0.264	0.155	1, −3	0.402	4, −1	0.179	4.637
	5.759	0.771	0.969	1, −4	0.448	3, −1	0.270	4.714
	5.931	0.043	0.997	2, −2	0.826	4, −3	0.057	4.887
1-Naphthyl phenyl ketone (III)	3.690	0.432	0.597	1, −1	0.930	...	...	2.015
	3.979	0.010	0.621	3, −1	0.546	1, −3	0.375	2.822
	4.419	0.193	0.976	2, −1	0.798	...	...	3.515
	4.486	0.024	−0.266	4, −1	0.560	2, −4	0.190	3.587
	4.695	0.036	0.516	1, −2	0.903	2, −1	0.061	3.896
	5.184	1.014	−0.919	1, −3	0.461	3, −1	0.410	4.022
	5.494	0.151	0.325	1, −4	0.293	4, −1	0.222	4.218
	5.556	0.190	0.860	2, −2	0.724	1, −4	0.070	4.384
2-Naphthyl phenyl ketone (IV)	3.815	0.104	−0.315	1, −1	0.641	1, −3	0.101	2.240
	4.115	0.086	−0.232	1, −2	0.288	1, −1	0.273	2.664
	4.465	0.036	0.032	4, −1	0.489	2, −4	0.159	3.402
	4.617	0.521	0.912	2, −1	0.496	3, −1	0.243	3.622
	4.804	1.044	0.410	1, −2	0.478	3, −1	0.337	3.810
	5.191	0.184	−0.940	1, −3	0.269	2, −2	0.221	3.917
	5.386	0.791	0.042	2, −2	0.485	1, −3	0.347	4.144
	5.660	0.257	−0.718	2, −4	0.312	4, −1	0.311	4.625
1-Phenanthryl phenyl ketone (V)	3.630	0.408	−0.109	1, −1	0.847	2, −1	0.050	2.206
	3.856	0.153	0.144	2, −1	0.418	1, −2	0.280	2.824
	4.463	0.410	−0.769	3, −1	0.606	4, −1	0.099	3.310
	4.533	0.060	−1.000	4, −1	0.503	3, −4	0.159	3.581
	4.578	0.390	0.994	1, −2	0.576	3, −1	0.187	3.632
	4.766	0.547	−0.741	2, −2	0.342	1, −3	0.272	3.851
	5.032	0.774	0.360	2, −2	0.477	1, −3	0.413	3.952
	5.412	0.434	−0.400	2, −3	0.812	1, −2	0.057	4.508
9-Anthryl phenyl ketone (VI)	2.977	0.535	0.518	1, −1	0.965	...	...	1.372
	3.669	0.020	−0.889	3, −1	0.592	1, −3	0.373	2.715
	3.992	0.008	−0.922	1, −2	0.737	2, −1	0.228	3.338
	4.132	0.058	−0.836	2, −1	0.620	1, −2	0.204	3.705
	4.336	0.016	−0.880	4, −1	0.864	2, −1	0.073	3.771
	4.733	1.617	−0.846	1, −3	0.545	3, −1	0.328	3.878
	4.999	0.025	−0.974	1, −4	0.930	...	...	4.494
	5.190	0.760	−0.688	2, −2	0.910	...	...	4.583
1-Pyrenyl phenyl ketone (VII)	3.149	0.883	0.254	1, −1	0.950	...	...	1.738
	3.515	0.041	0.079	2, −1	0.407	1, −3	0.267	2.638
	4.142	0.016	0.998	4, −1	0.687	1, −2	0.150	3.261
	4.286	0.331	0.984	1, −2	0.615	4, −1	0.145	3.474
	4.415	0.241	0.514	3, −1	0.650	4, −1	0.133	3.664
	4.708	0.941	−0.929	1, −3	0.552	2, −1	0.391	4.140
	5.174	0.724	0.339	2, −2	0.800	3, −1	0.062	4.173
	5.359	0.152	−0.971	1, −4	0.616	3, −4	0.170	4.619

Table I (*Continued*)

Ketone	ΔE^{1b}	f^c	cos Φ^d	Predominant configuration i, j^e	Wt	Second most important configuration^f i, j^e	Wt	ΔE^{3g}
6-Chrysenyl phenyl ketone (VIII)	3.375	0.757	−0.137	1, −1	0.959	...	...	1.994
	3.659	0.014	−0.954	2, −1	0.583	1, −3	0.376	2.748
	4.334	0.059	−0.866	1, −2	0.697	4, −1	0.209	3.193
	4.385	0.090	0.754	3, −1	0.846	...	...	3.339
	4.538	0.156	−0.971	4, −1	0.493	1, −2	0.139	3.714
	4.654	1.399	−0.886	1, −3	0.390	2, −1	0.260	3.976
	4.897	0.216	0.878	1, −4	0.849	4, −1	0.072	4.146
	5.064	0.531	−0.509	2, −4	0.262	2, −3	0.221	4.452

[a] Additional theoretical quantities concerning the models of compounds given in Table I can be obtained at request from the authors (C. P.). [b] Excitation energies (eV) for the eight lowest excited singlet states. [c] Oscillator strength. [d] Φ is the angle formed by the positive direction of the axis shown in the formula and the direction of the transition moment vector read clockwise. [e] A combination of two figures is used to label a configuration. A positive number refers to an orbital occupied in the ground state, a negative number to a virtual orbital. [f] Only configurations with more than 5% weight. [g] Excitation energies (eV) for the eight lowest excited triplet states.

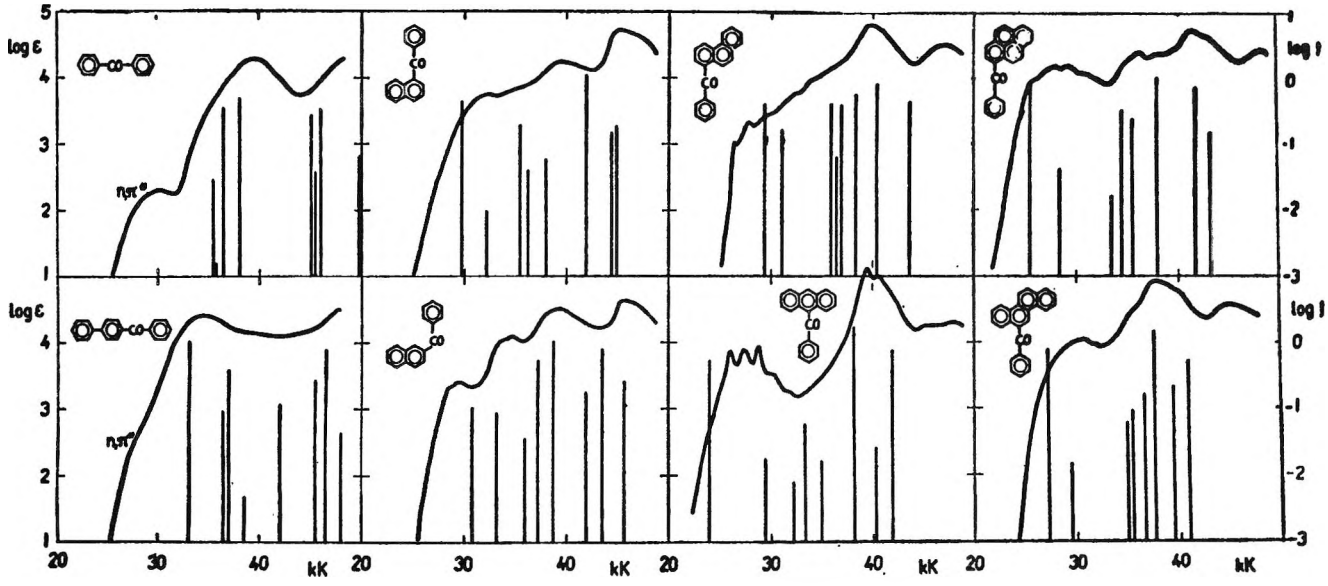


Figure 1. Ultraviolet absorption spectra of ketones I–VIII (methanol solutions). Calculated LCI transition energies and intensities are shown as full straight lines. Scale for the calculated oscillator strength is shown on the right-hand side.

Results and Discussion

Calculations. The results of the LCI–SCF–MO calculations of the spectral properties of the ketones I–VIII are summarized in Table I.

Electronic Absorption Spectra. Absorption curves of the aryl phenyl ketones, R–CO–C_6H_5, are similar to those of the corresponding parent hydrocarbons, R–H, with less fine structure and a more intense band in place of the weak α hydrocarbon band. Thus, the long wavelength region of the absorption spectra of aryl ketones shows only one band with a slight indication of structure rather than the original two bands in benzenoid hydrocarbons.[4]

The experimental absorption curves for ketones I–VIII are compared with the results of LCI–SCF–MO calculations in Figure 1. The locations of the first excited singlet states are summarized in Table II. It is seen from Figure 1 that acceptable agreement is usually obtained between theoretical and experimental values of oscillator strengths and band maxima positions with the exception of some longest wavelength bands. For example, the longest wavelength band of 9-anthryl phenyl ketone VI is predicted to be more intense and to lie further to the red than is experimentally observed. Lack of agreement could be ascribed to noncoplanarity in aryl phenyl ketones. (However, *cf.* a similar paper dealing with aryl phenyl methyl cations.[12]) Also, there is no way of accounting for solvent shifts in the calculations. Improvement of the correlation might be obtained by altering the parameters used for the keto

(12) V. Horák, C. Párkányi, J. Pecka, and R. Zahradník, *Collect. Czech. Chem. Commun.*, 32, 2272 (1967).

Table II: Location of the Lowest Excited (n, π^*) and (π, π^*) Singlet and Triplet States[a]

Compound	Observed (n, π^*) singlet state energy[b]	Observed (π, π^*) singlet state energy[c]	Observed (n, π^*) triplet state energy[d]	Observed (π, π^*) triplet state energy[d]	Phosphorescence bands 0–0		0–1	Phosphorescence lifetime, τ_P, sec
Benzophenone (I)	27.0	39.6	24.6[e]	...	24.1		22.4	4.7×10^{-3}[f]
4-Phenylbenzophenone (II)	26.8	34.4	...	21.2[g]	21.2		19.8	0.28[h]
1-Naphthyl phenyl ketone (III)	26.7	32.6	...	20.1[g]	20.1	19.5 sh	18.6	0.51[i]
2-Naphthyl phenyl ketone (IV)	...	34.2	23.8(?)	21.3	20.7	20.3 sh	19.2	1.01
1-Phenanthryl phenyl ketone (V)	...	32.5	...	20.7	20.7		19.3	0.92
9-Anthryl phenyl ketone (VI)	...	26.1	...	...	...		...	...
1-Pyrenyl phenyl ketone (VII)	...	26.3	...	...	...		...	...
6-Chrysenyl phenyl ketone (VIII)	...	28.5	...	18.9	18.9		17.5	0.59

[a] Energies are given in kK. [b] From ref 14, in ethanol–diethyl ether (2:1) at 77°K. [c] In methanol at room temperature, taken from ref 4. [d] Observed (n, π^*) and (π, π^*) triplet state energies for the compounds I and IV determined from their phosphorescence excitation spectra. For other compounds, the wave numbers of the phosphorescence 0–0 bands are given. [e] Reference 8 gives 24.7 kK. [f] Taken from ref 14, ref 8 gives $\tau_P = 4 \times 10^{-3}$ sec; *cf.* also ref 15, 22. [g] In agreement with ref 14. [h] Reference 14 gives $\tau_P = 0.30 \pm 0.02$ sec. [i] Reference 14 gives $\tau_P = 0.74 \pm 0.03$ sec.

group. The values employed here are those found suitable for planar phenalenones.[13]

Aryl phenyl ketones are not exactly planar. This complicates the comparison of theoretical and experimental transition energies. However, conjugation is reduced only slightly if deviations from planarity are small. It is found empirically that the energies of the maxima of the longest wavelength bands of the ketones studied here are roughly linearly correlated with calculated HMO $E(N \rightarrow V_1)$ energies.[4]

For certain of the ketones, the LCI calculations predict considerable mixing of configurations, even of those of low energy. The squares of the expansion coefficient for the $\chi_{1,-1}$ configuration in the CI function for the first excited state are 0.929, 0.930, 0.641, 0.847, 0.965, 0.950, and 0.959 for ketones II–VIII, respectively (*cf.* Table I). Generally, there is a close correlation between experimental and theoretical values for the energies of the first excited singlet states (Figure 2).

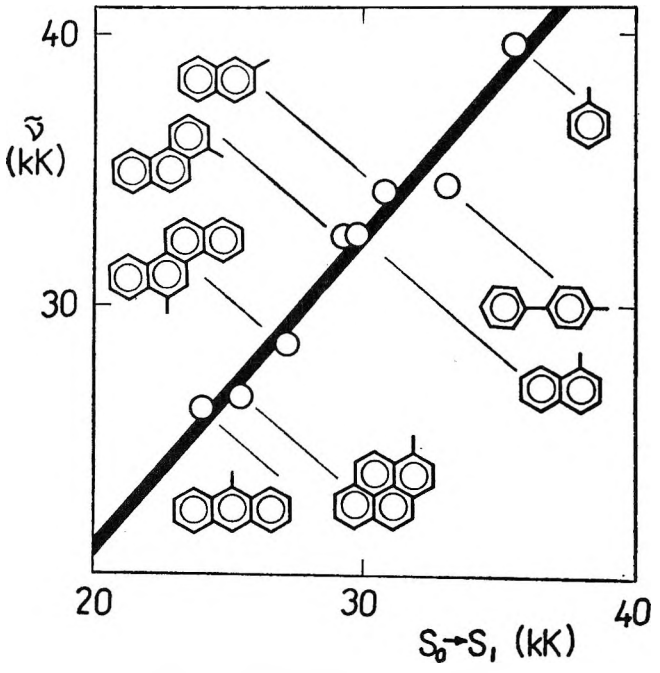


Figure 2. Plot of experimental ($\tilde{\nu}$) against theoretical LCI ($S_0 \rightarrow S_1$, see text) excitation energies for aryl phenyl ketones. Regression line: $\tilde{\nu}$ (kK) = 1.170 $S_0 \rightarrow S_1$ (kK) − 2.619; correlation coefficient $r = 0.979$, number of compounds $n = 8$. All values are significant on 1% probability level.

Phosphorescence Emission and Phosphorescence Excitation Spectra. Triplet states of aromatic ketones may be designated as either (n, π^*) or (π, π^*). The ketones can then be classified according to which of the two triplet types lies lowest in energy. The criteria used to distinguish between $S_0 \rightarrow T_{n,\pi^*}$ and $S_0 \rightarrow T_{\pi,\pi^*}$ transitions are summarized in Table III.[8]

Phosphorescence spectra of ketones I–V and VIII are shown in Figure 3, along with phosphorescence excitation spectra of ketones I and IV. We were not able to obtain excitation spectra of the other ketones discussed. The location of the lowest triplet states and phosphorescence lifetimes, τ_P, are summarized in Table II.

Benzophenone (I). The lowest-lying triplet state of benzophenone is an (n, π^*) state. (This is in accord with previous assignments.[8,14,15]) The phosphorescence lifetime is of the order of 10^{-3} sec, singlet–triplet splitting is ~2400 cm^{-1}, and a prominent 1700 cm^{-1} vibrational progression is observed in the spectrum; the positions of the 0–0, 0–1, 0–2, and 0–3 bands are 24.125, 22.470, 20.885, and 19.325 kK, respectively. No heavy atom solvent effect was noted on the intensity of the $S_0 \rightarrow T_{n,\pi^*}$ transition.

2-Naphthyl Phenyl Ketone (IV). The lowest-lying triplet state of compound IV was assigned as a (π, π^*) state on the basis of its phosphorescence spectrum and lifetime (singlet–triplet splitting ~12.9 kK, irregular

(13) R. Zahradník, M. Tichý, and D. H. Reid, *Tetrahedron*, 24, 3001 (1968).

(14) V. Ermolaev and A. Terenin, *J. Chim. Phys.*, 55, 698 (1958).

(15) G. Porter and P. Suppan, *Trans. Faraday Soc.*, 61, 1664 (1965).

Table III: Criteria Used to Distinguish between $S_0 \rightarrow T_{n,\pi^*}$ and $S_0 \rightarrow T_{\pi,\pi^*}$ Transitions

Spectroscopic feature	Transition type: $S_0 \rightarrow T_{n,\pi^*}$	Transition type: $S_0 \rightarrow T_{\pi,\pi^*}$
S–T splitting of 0–0 bands	~2000 cm^{-1}	Large (no definite position relative to $S \rightarrow S_{n,\pi^*}$ band)
Heavy atom solvent influence	Little or no enhancement	Increases absorption intensity
Lifetime of phosphorescence, τ_P	10^{-3} to 10^{-2} sec	10^{-1} sec or greater
Fine structure	C=O vibrational progression	Generally complex; no C=O progression

structure, τ_P = 1.01 sec). We were able to measure the phosphorescence excitation spectrum only in the presence of ethyl iodide.

Besides the 0–0 band of the $S_0 \rightarrow T_{\pi,\pi^*}$ transition at 21.3 kK, a second, poorly resolved band was observed at 23.8 kK in the excitation spectrum of IV. The large splitting between the two S–T bands (~2500 cm^{-1}) and the high intensity of the second (23.8 kK) band suggests that it is not due to the 0–1 band of the $S_0 \rightarrow T_{\pi,\pi^*}$ transition. One would expect the $S_0 \rightarrow S_{n,\pi^*}$ transition of 2-naphthyl phenyl ketone to occur at about 26.7 kK (the $S_0 \rightarrow S_{n,\pi^*}$ transitions of benzophenone, 4-phenylbenzophenone, and 1-naphthyl phenyl ketone are observed at 27.0, 26.8, and 26.7 kK, respectively). If the 23.8-kK band is assumed to be due to the $S_0 \rightarrow T_{n,\pi^*}$ transition, a reasonable value of 2900 cm^{-1} for the

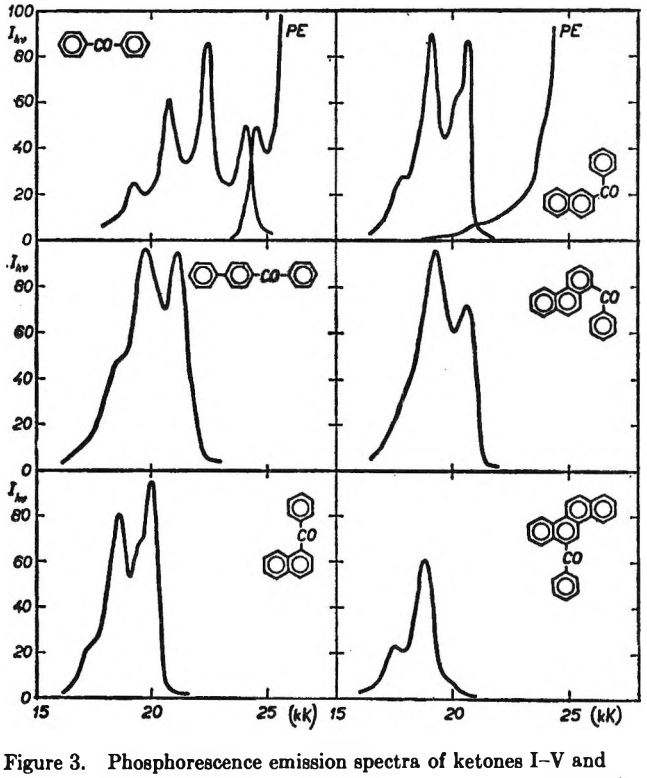


Figure 3. Phosphorescence emission spectra of ketones I–V and VIII. For the ketones I and IV, phosphorescence excitation (PE) spectra are shown also. Relative phosphorescence intensity, $I_{h\nu}$, is given.

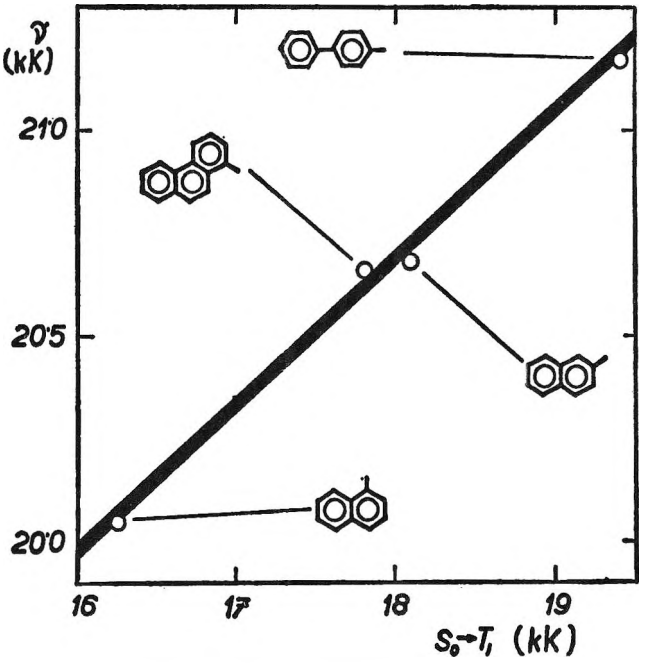


Figure 4. Plot of experimental ($\tilde{\nu}$) against theoretical LCI ($S_0 \rightarrow T_1$) excitation energies for aryl phenyl ketones. The position of the 0–0 phosphorescence band is used in the correlation. The point for ketone VIII does not fit the line.

(n, π^*) S–T splitting is obtained. However, this assignment is not unequivocal as the 23.8-kK band also lies within 11.2 kK of the $S_0 \rightarrow S_{2\pi,\pi^*}$ transition of 2-naphthyl phenyl ketone (*cf.* Figure 1). The expected S–T splitting for the second (π, π^*) state is about 12.9 kK.

Ketones II, III, V, and VIII. Phosphorescence lifetimes for these compounds are of the order of 0.1–1 sec. No characteristic vibrational structure resembling that for benzophenone was noted in the phosphorescence spectra. Singlet–triplet splittings are all larger than 9000 cm^{-1}. The lowest-lying triplet states are assigned as (π, π^*) for ketones II, III, V, and VIII. This is in agreement with earlier assignments for 4-phenylbenzophenone (II) and 1-naphthyl phenyl ketone (III).[15,16]

The positions of the 0–0 phosphorescence bands for

(16) V. Ermolaev and A. Terenin, *Soviet Phys. Usp. (English Transl.)*, 3, 423 (1960); *Usp. Fiz. Nauk*, 71, 137 (1960).

ketones II–V can be plotted against theoretical values of the energy of the lowest-lying triplet state of these compounds (Figure 4). A good regression line is obtained; however, the absolute values of the calculated energies are much lower than those experimentally observed. Nevertheless, the predictions are about equally good for the $S_0 \rightarrow S_1$ and $S_0 \rightarrow T_1$ transitions of the same molecule (Table IV). As a result of this, the S–T splittings for the lowest excited (π, π^*) states are remarkably accurate, even when the predictions of the absolute positions of bands are not good.

Table IV: Energy Difference, ΔE, between Calculated and Observed Transition Energies and the Singlet–Triplet Splittings for the Lowest Excited (π, π^*) States of the Ketones II–V and VIII (Values in eV)

	ΔE			
Compound	$S_0 \rightarrow S_{1\pi,\pi^*}$	$S_0 \rightarrow T_{1\pi,\pi^*}$	$\Delta E_{S,T\ obsd}$	$\Delta E_{S,T\ calcd}$
II	0.16	0.23	1.63	1.70
III	0.35	0.47	1.55	1.68
IV	0.42	0.40	1.60	1.58
V	0.40	0.36	1.46	1.42
VIII	0.15	0.35	1.19	1.38

We did not observe any phosphorescence from ketones VI and VII. It follows from Figure 4 and theoretical values of triplet levels for ketones VI and VII (1.371 and 1.378 eV, respectively) that the expected values of the 0–0 phosphorescence bands of these compounds should be 18.19 and 19.25 kK, respectively (*i.e.*, 550 and 520 mμ). However, we observed a weak fluorescence of 9-anthryl phenyl ketone with $\tilde{\nu}_{max}$ at 22.6 kK (442 mμ). The theoretical $S_0 \rightarrow S_1$ value for VI is 2.977 eV, *i.e.*, 24.1 kK. The agreement in this case is somewhat better than with the longest wavelength absorption band. A good fluorescence spectrum was obtained for 1-pyrenyl phenyl ketone (VII) which is a mirror image of its absorption spectrum (Figure 5).

Photochemical reactivity of aryl ketones can be correlated with relative ordering of their (n, π^*) and (π, π^*) triplet states. It has been demonstrated that (n, π^*) states are more reactive than (π, π^*) states toward hydrogen atom abstraction reactions. Quantum yields of photoreduction are of the order of 10 to 100 times larger for compounds having lowest-lying (n, π^*) triplet states than for those having lowest-lying (π, π^*) triplet states.[17]

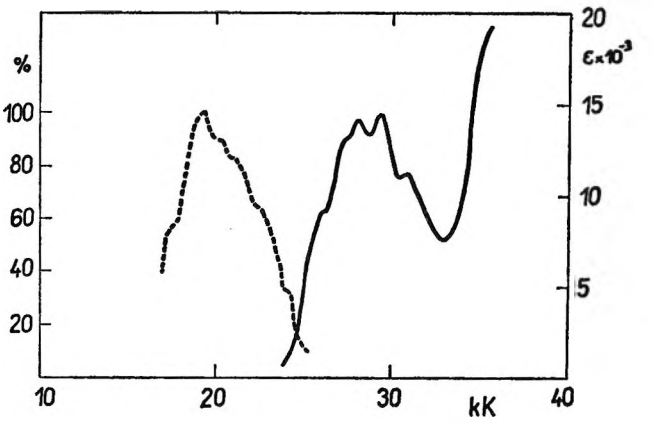


Figure 5. Comparison of the absorption and fluorescence emission spectra of 1-pyrenyl phenyl ketone (methanol). $\tilde{\nu}_{max}$ of fluorescence 19.4 kK (515 mμ). Absorption spectrum is represented by the full, fluorescence spectrum by the dashed line.

Thus, 4-phenylbenzophenone (II) is less reactive than benzophenone (I) toward intermolecular hydrogen atom abstraction (quantum yields of ketone consumption in isopropyl alcohol solution are 0.2 and 2.0, respectively, for these compounds).[18] It follows from our results that aryl phenyl ketones III–VIII should be less reactive than benzophenone as well, their reactivity approaching that of 4-phenylbenzophenone toward photoreduction.

The results of a recent photochemical study of the reduction of aryl phenyl ketones with sodium borohydride in dimethylformamide show that, under these conditions, the reactivity of 4-phenylbenzophenone resembles that of benzophenone rather than that of other aryl phenyl ketones.[19] However, these results may be complicated by the increased donating ability of sodium borohydride compared to that of alcohols. It has been shown that good hydrogen donors, such as tributyltin hydride, efficiently reduce photoexcited ketones having lowest-lying (π, π^*) triplet states.[20–22]

(17) See N. J. Turro, "Molecular Photochemistry," W. A. Benjamin, Inc., New York, N. Y., 1965, and ref 7 for detailed discussions.

(18) J. N. Pitts, Jr., H. W. Johnson, Jr., and T. Kuwana, *J. Phys. Chem.*, **66**, 2456 (1962).

(19) V. Horák and J. Pecka, private communication.

(20) G. S. Hammond and P. A. Leermakers, *J. Amer. Chem. Soc.*, **84**, 207 (1962).

(21) G. S. Hammond and P. A. Leermakers, *J. Phys. Chem.*, **66**, 1148 (1962).

(22) C. Parker and C. G. Hatchard, *Analyst*, **87**, 664 (1962).

Aromatic Hydroxylation Catalyzed by Fenton's Reagent. An Electron Paramagnetic Resonance Study. I. Furans

by Takeshi Shiga

Department of Physicochemical Physiology, Medical School, Osaka University, Osaka, Japan

and Akio Isomoto

College of General Education, Osaka University, Toyonaka, Osaka, Japan *(Received October 18, 1968)*

Unstable intermediate free radicals of furan, 2-furoic acid, 2-furfural, and 2-furfuryl alcohol, produced by Fenton's reagent (Fe(II) + H_2O_2), have been detected by electron paramagnetic resonance. The observed hyperfine structures were analyzed and molecular structures were assigned on the basis of Hückel MO calculations. Most of the free radicals were hydroxylated adducts: at position 5 of furan, 2-furfural, and 2-furfuryl alcohol, and at position 4 of furoic acid. The hydroxylation occurred at the position possessing minimal localization energy for radical attack and maximal free valence. A Ti(III) + H_2O_2 system attacked the same position of furan derivatives as Fenton's reagent, giving the same adducts, while the reagents abstract a hydrogen from different sites in the case of saturated hydrocarbons. The reactive species involved in these oxidation systems is therefore expected to be free radical in nature.

Introduction

Hydroxylation of aromatic compounds takes place in various oxidation systems, including many biological processes.[1,2] Most studies of hydroxylation have been concentrated on the product analyses of substrates, and the conclusions have been scattered. Since the final products of the reaction consist of various products resulting from many secondary reactions, even the position of initial attack cannot be determined with certainty. Therefore, it is desirable to identify an unstable intermediate during the hydroxylation reaction, before it undergoes successive reaction.

Unstable aliphatic free radicals produced by Fenton's reagent (Fe(II) + H_2O_2),[3-5] as well as by a Ti(III) + H_2O_2 system,[6-10] were detected successfully by electron paramagnetic resonance (epr) spectroscopy. Analyzing the hyperfine structures, the molecular structure of the intermediates was determined and the nature of the reactive species involved in the oxidation systems was discussed.[11]

Using aromatic compounds as substrates, the hydroxylation reaction occurs, instead of hydrogen abstraction as observed with the saturated compounds. Therefore, a free radical, a hydroxylated adduct, is expected to be detectable during the reaction, and was recently observed by Dixon and Norman[12,13] employing the Ti(III) + H_2O_2 system as an oxidant.

Fenton's reagent should also produce a detectable amount of such intermediate free radicals. The determination of their molecular structures is important for finding the relationship between the reactive site of substrates and the molecular properties, especially the quantum chemical indices. Further, these results may be significant for determining the nature of various reactive species.

In this paper, epr studies of the intermediate free radicals of furan derivatives are presented. The hyperfine structures of the free radicals are analyzed and the molecular structures are identified on the basis of Hückel calculations. The reaction of the Ti(III) + H_2O_2 system is also studied. Finally, the theoretical reactivity indices and the positions of the attack are compared.

Materials and Methods

Apparatus. A Varian V-4500 epr spectrometer with 100-kcps modulation unit was used. The design and characteristics of the continuous flow system have been described previously.[3,11] The pH of the solutions was

(1) See H. S. Mason, *Advan. Enzymol.*, **19**, 79 (1957).

(2) See R. O. C. Norman and J. R. Lindsay Smith in "Oxidases and Related Redox Systems," Vol. I, T. E. King, H. S. Mason, and M. Morrison, Ed., John Wiley and Sons, Inc., New York, N. Y., 1965, p 131.

(3) T. Shiga, *J. Phys. Chem.*, **69**, 3805 (1965).

(4) T. Shiga, A. Boukhors, and P. Douzou, *ibid.*, **71**, 3559 (1967).

(5) T. Shiga, A. Boukhors, and P. Douzou, *ibid.*, **71**, 4264 (1967).

(6) (a) W. T. Dixon and R. O. C. Norman, *J. Chem. Soc.*, 3119 (1963); (b) W. T. Dixon, R. O. C. Norman, and A. Buley, *ibid.*, 3625 (1964); (c) W. T. Dixon and R. O. C. Norman, *ibid.*, 4850 (1964); (d) R. O. C. Norman and R. J. Pritchett, *J. Chem. Soc. B*, 1329 (1967); (e) A. L. Buley, R. O. C. Norman, and R. J. Pritchett, *ibid.*, 849 (1968).

(7) P. Smith, J. T. Pearson, P. B. Wood, and T. C. Smith, *J. Chem. Phys.*, **43**, 1535 (1965).

(8) H. Fisher, *Z. Naturforsch.*, **19a**, 866 (1964).

(9) H. Yoshida and B. Rånby, *J. Polymer Sci.*, **C16**, 1333 (1967).

(10) J. R. Steven and J. C. Ward, *Aust. J. Chem.*, **20**, 2005 (1967).

(11) T. Shiga, A. Boukhors, and P. Douzou in "Recent Development of Magnetic Resonance in Biological Systems," S. Fujiwara and L. H. Piette, Ed., Hirokawa Publishing Co., Tokyo, 1968, p 146.

(12) (a) W. T. Dixon and R. O. C. Norman, *Proc. Chem. Soc.*, 97 (1963); (b) W. T. Dison and R. O. C. Norman, *J. Chem. Soc.*, 4857 (1964).

(13) C. R. E. Jefcoate and R. O. C. Norman, *J. Chem. Soc., B*, 48 (1968).

adjusted by a Hitachi F-5 pH meter. All the reactants, substrates, and salts were of reagent grade and were not purified further.

Method. The solvents were 0.1 *N* H_2SO_4, 0.2 *M* acetate buffer (pH 4 and 5), and 0.1 *M* phosphate buffer (pH 6 and 7). The solution of Fe(II) (5 m*M*) and ethylenediaminetetraacetic acid (EDTA) (molar ratio of 1:1) and the solution of H_2O_2 (0.1%) and substrates (3–5%) were mixed in the flow cell. In acid solution, EDTA was not added. Both solutions were bubbled with nitrogen gas in order to remove the dissolved oxygen.

The epr spectra were recorded 10–50 msec after mixing the two solutions. The hyperfine coupling constants and g values were measured by comparing the signals with a spectrum of Fremy's salt, which was sealed in a capillary and inserted beside the flow cell. The g values of the observed free radicals were about 2.004. The errors in the coupling constant measurements were within 5% in most cases. The 100 kcps modulation amplitude could not be reduced below 0.4 G because of a poor signal-to-noise ratio.

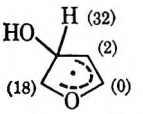
Calculations. A NEAC 2200-500 digital computer was used for Hückel MO calculations. The Hückel parameters employed are listed in Table I. Most of these values were chosen according to the suggestion of Yonezawa, *et al.*,[14] and were slightly modified considering the inductive effect. The calculation of hydroxylated adducts was carried out for the fragment of the molecule, which was used for computing the localization energies of Wheland. The theoretical proton coupling constants (A) were converted from the calculated spin densities (ρ), using the following equations: $A = Q^{H}_{CH} \times \rho$, where $Q^{H}_{CH} = -22.5$ G for the ring protons,[15] and $A = Q^{H}_{-CH(OH)-}(\rho_X + \rho_Y)$, where $Q^{H}_{-CH(OH)-} = 40$ G for a proton of hydroxylated position, –X–CH(OH)–Y– (see Discussion).

Table I: Hückel Parameters

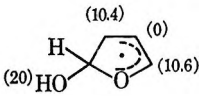
	Coulomb integral		
	Heteroatom	Neighbor(C)	Bond integral
—OH	1.70	0	0.60
=O	1.50	0.20	1.40
—O—	1.60	0.20	0.80
—C(OOH)	−0.15	0.10	0.90
—C(HO)	−0.15	0.10	0.90
$=H_2$, $=H_3$	−0.20	−0.10	2.00

Results

Furan. The epr spectrum of the furan free radical is shown in Figure 1. Both Fenton's reagent (at pH 7) and the Ti(III) + H_2O_2 system (at pH 1) produce the same free radical, whose spectrum consists of 4 proton hyperfine splittings (21.0, 14.8, 14.0, and 2.0 G). Two alternative structures, (I) and (II), can be assigned to this free radical. The theoretical coupling constants are



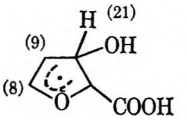
(I)



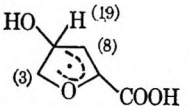
(II)

Therefore, the observed free radical is identified as the adduct (II).

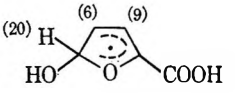
2-Furoic Acid. Fenton's reagent (at pH 7) and the Ti(III) + H_2O_2 system (at pH 1) produce the same free radical, with an epr spectrum consisting of three proton hyperfine splittings (19.1, 10.2, and 2.2 G) (Figure 2). The calculated coupling constants for three possible structures are



(III)



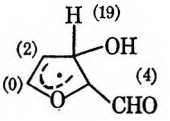
(IV)



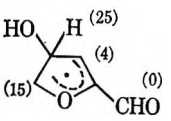
(V)

Thus adduct IV fits the observed spectrum.

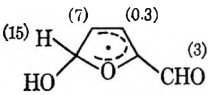
2-Furfural. At pH 5 and 7, Fenton's reagent gives a spectrum shown in Figure 3a, consisting of three proton hyperfine splittings (6.3, 3.2, and 1.0 G). However, at pH 1, both reagents produce the same free radical, whose spectrum is shown in Figure 3b. The proton hyperfine coupling constants are 17.1, 8.3, 3.5, and 1.9 G. The calculated coupling constants for three possible structures are



(VI)



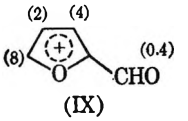
(VII)



(VIII)

Therefore, adduct VIII is produced in acidic medium.

Concerning the free radical produced at pH 7, the above adducts are not compatible with the spectrum of Figure 3a, but a free radical (IX) might explain the observed spectrum.



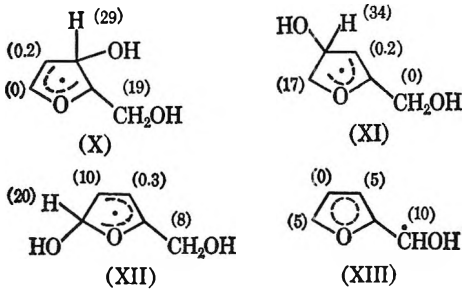
(IX)

2-Furfuryl Alcohol. Both oxidation systems produce the same free radical in acidic medium (Figure 4). Fenton's reagent gives the same free radical at pH 5. The coupling constants are 20.5, 12.9, 8.3, 7.5, and 1.9 G. The calculated coupling constants of the possible free

(14) T. Yonezawa, *et al.*, "Introduction to Quantum Chemistry," Kagaku, Kyoto, 1963, p 55.

(15) H. M. McConnell and D. B. Chesnut, *J. Chem. Phys.*, **28**, 107 (1958).

radicals are



Therefore, adduct XII is produced. According to this assignment, a few minor peaks cannot be interpreted, and the two proton coupling constants of $-CH_2OH$ are dissimilar. (See Discussion.)

At pH 7, only three peaks (separation 4.6 G) appear in the epr spectrum, for which we can give no explanation.

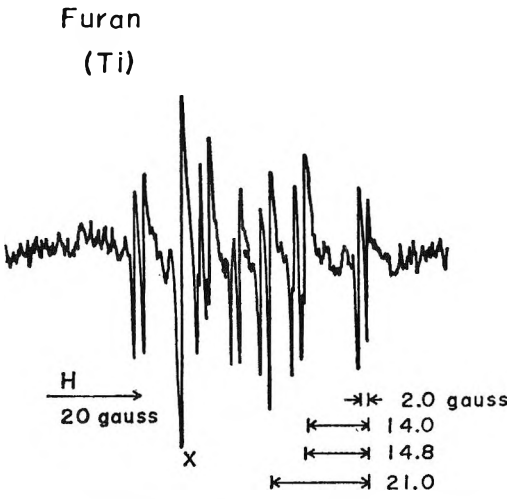


Figure 1. Epr spectrum of furan free radical, produced by Ti(III) + H_2O_2 system at pH 1. Conditions: microwave power 5 db; modulation 100 kcps, 0.8 G; time constant 0.3 sec; magnetic field scanning 30 G/min; temperature 18°. The marked peak (X) is the signal arising from the Ti(III) + H_2O_2 system itself.

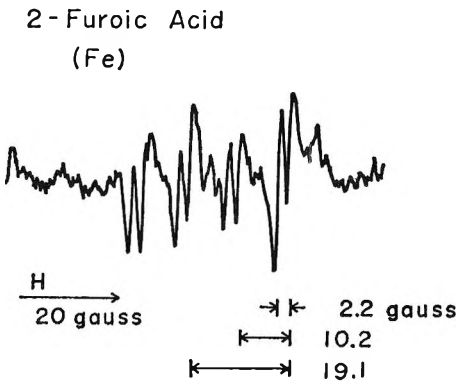


Figure 2. Epr spectrum of 2-furoic acid free radical, produced by Fenton's reagent at pH 7. Conditions: microwave power 5 db; modulation 100 kcps, 0.5 G; time constant 0.3 sec; magnetic field scanning 30 G/min; temperature 18°.

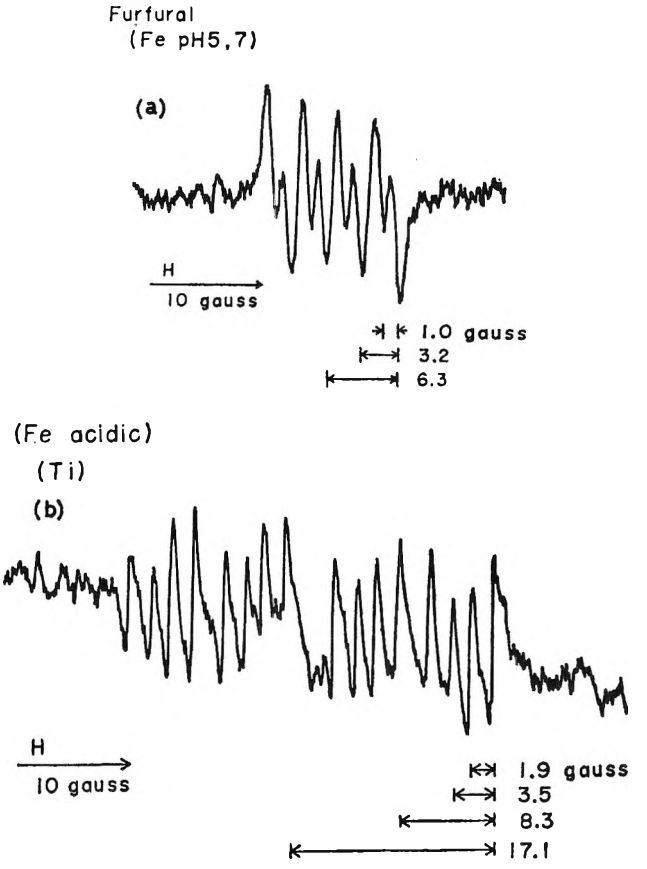


Figure 3. (a) Epr spectrum of 2-furfural free radical, produced by Fenton's reagent at pH 7. Conditions: microwave power 5 db; modulation 100 kcps, 0.8 G; time constant 0.3 sec; magnetic field scanning 30 G/min; temperature 20°. (b) Epr spectrum of 2-furfural free radical, produced by Ti(III) + H_2O_2 system at pH 1. Conditions: microwave power 5 db; modulation 100 kcps, 0.5 G; time constant 0.3 sec; magnetic field scanning 30 G/min; temperature 20°.

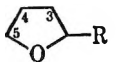
Discussion

Structure of Adducts. The structures of the free radicals cannot be uniquely assigned from the observed spectra, so that the observed coupling constants are compared with the estimated values of Hückel MO calculations. Since the substrates contain heteroatoms and substituents, the total number of electrons in the five-membered ring becomes ambiguous. Therefore, all the possible electronic structures of free radicals are calculated and compared with observed ring proton coupling constants; then the best fitting structures are chosen, keeping consistency among the four molecules studied. Finally, the following numbers of electrons are introduced into the π system: oxygen of position 1 gives 2 electrons, –COOH and –CHO groups donate 2 electrons, while each $-CH_2OH$ group contributes 4 electrons. The other possible combinations do not explain the observed coupling constants.

These choices of electron numbers, *i.e.*, of occupied energy levels, lead to good agreement between observed coupling constants (A) and calculated spin densities on the carbon atoms (ρ). As can be seen in Figure 5,

Table II: Reactive Indices of Furans

	Furan		Furoic acid			Furfural			Furfuryl alcohol		
	4	5	3	4	5	3	4	5	3	4	5
Localization Energy (Units of β)											
L(E)	2.454	2.172	2.518	2.512	2.914	2.067	1.987	1.860	2.454	3.553	2.310
L(R)	2.828	*2.230*	1.606	*1.588*	1.707	1.855	1.143	*1.721*	2.812	2.893	*2.571*
L(N)	3.242	2.288	0.695	0.664	0.500	1.643	2.299	1.582	3.160	2.233	2.832
Free Valence and Charge Density											
Fr	0.39	*0.56*	0.47	*0.69*	0.53	0.44	0.37	*0.54*	0.43	0.38	*0.55*
qr	1.01	1.08	1.55	1.12	1.36	1.54	1.06	1.32	1.16	1.04	1.18



$A = 27.4\rho$ fits well. When the coupling constants are small, a slight disagreement exists, because the present calculation does not take the negative spin density into account.

Although the Q parameter of the protons attached to the hydroxylated position, –X–CH(OH)–Y–, is unknown, $A = 40(\rho_X + \rho_Y)$ is used as a first approximation, assuming that the dihedral angle between the CH bond and the neighboring p_z orbital is 30° [thus $(B_0 + B\cos^2\theta) \doteqdot 40$ G], and disregarding the difference in orbital conformation of carbon and oxygen. Though the estimated coupling constants agree with the observed values, the exact molecular conformation is not certain.

The proton coupling constant of substituted –CHO can also be well predicted by $Q = -22.5$ G from the spin density of the carbon atom of aldehyde.

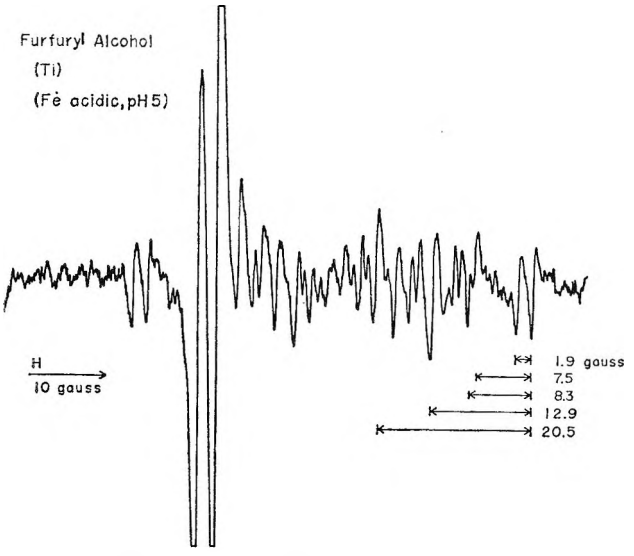


Figure 4. Epr spectrum of 2-furfuryl alcohol free radical, produced by Ti(III) + H_2O_2 system at pH 1. Conditions: microwave power 5 db; modulation 100 kcps, 0.6 G; time constant 0.3 sec; magnetic field scanning 30 G/min; temperature 20°. The two extreme peaks are the signals arising from the Ti(III) + H_2O_2 system itself.

The structure of the 2-furfuryl alcohol radical is peculiar; the two proton coupling constants of $-CH_2OH$ differ from each other, suggesting a hindrance of free rotation around the C_2–$C_{1'}$ axis. Correspondingly, the observed proton coupling constants (7.5 and 8.3 G) of substituents can be approximated by $A = 28\rho_{C_2}$, indicating that this coupling would be of hyperconjugative nature. Also, it was necessary to introduce four electrons from the substituent to the π system. These complications suggest that the alcoholic OH may be in some manner hydrogen-bonded to the ring oxygen, giving more electrons to the ring, and causing steric rotational hindrance of the substituted group. However, we do not intend to enter into this problem, since more evidence with similar molecules and further refinements of calculations seem to be needed.

Reactivity Indices and Reactive Sites. The structures of intermediate free radicals give more precise information about the reactive sites of substrates. In Table II,

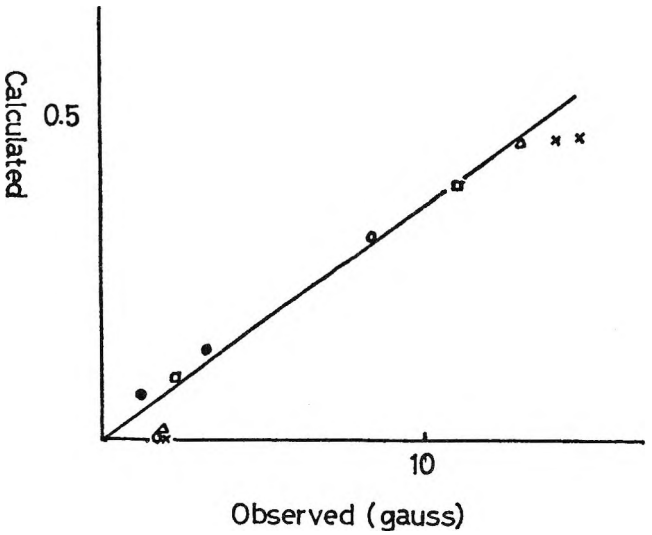


Figure 5. The relationship between the observed ring proton coupling constants and the spin densities on the carbon atoms: ×, furan; □, furoic acid; ○, furfural (adduct); ●, furfural (positive ion); △, furfuryl alcohol.

the localization energies of substrates for nucleophilic, radical, and electrophilic attack, as well as the free valences and π-electron densities of each position, are shown. The occupied energy levels are so determined as to give a good agreement with the structure of free radicals (*vide supra*).

All the hydroxylated positions, *i.e.*, position 5 (or 2) of furan, position 4 of furoic acid, position 5 of furfuryl, and position 5 of furfuryl alcohol, possess minimal localization energies for radical attack, and also maximal values of free valence (Table II). Therefore, it can be concluded that reactions of both oxidation systems, Ti(III) + H_2O_2 and Fe(II) + H_2O_2, involve radical species as a reactive intermediate.

For consistency, four electrons were introduced from CH_2OH to the ring of furfuryl alcohol. No other justification is offered at this time.

Nature of Reactive Species. The Ti(III) + H_2O_2 system has reactive properties similar to the OH radical with σ compounds, while Fenton's reagent possesses an opposite character as an oxidant.[3-5,11] However, concerning aromatic hydroxylation reactions, it is clearly shown that two oxidation systems behave similarly. The hydroxylated position of the intermediate free radical has been shown to be a most reactive site for radical attack of the original molecule. Similar results were obtained with phenol derivatives.[16]

The chemical nature of the reactive species involved in these oxidation systems is still unknown. OH-like species are proposed for the Ti(III) + H_2O_2 system as attacking agents, because Livingston and Zeldes[17] have shown that the intermediate free radicals obtained by photochemically generated OH radicals are similar to the intermediates produced by the Ti(III) + H_2O_2 system. A number of kinetic studies are now being carried out using epr.[18-22]

Despite considerable efforts to clarify the nature of the reactive species involved in Fenton's reagent since the 1930's, no definite conclusion has yet been reached. Recently, a series of epr studies demonstrated that Fenton's reagent possesses properties as an oxidant for saturated hydrocarbons[3-5,11] different from those of Ti(III) + H_2O_2. Taking as an example the oxidation of alcohols, Fenton's reagent extracts a hydrogen from the position farthest away from the alcoholic OH, while the Ti(III) + H_2O_2 system attacks the position nearest to the alcoholic OH. Therefore, it was concluded that the two oxidation systems involve different reactive species in the abstraction of hydrogen from saturated compounds. However, the present study demonstrates that both oxidants have similar properties in yielding hydroxylated adducts from furans. Further studies on aromatic hydroxylation are now in progress.

(16) T. Shiga, in preparation.

(17) R. Livingston and N. Zeldes, *J. Chem. Phys.*, **44**, 1245 (1966).

(18) L. H. Piette and G. Bulow, Preprints, 9,2-*c*, p c-9 American Chemical Society, 1967.

(19) F. Sicilio, R. E. Florin, and L. A. Wall, *J. Phys. Chem.*, **70**, 47 (1967).

(20) Y. S. Chiang, J. Craddock, D. Mickewich, and J. Turkevich, *ibid.*, **70**, 3509 (1967).

(21) H. Fischer, *Ber. Bunsenges. Phys. Chem.*, **71**, 685 (1967).

(22) K. Takakura and B. Rånby, *J. Phys. Chem.*, **72**, 164 (1968).

NOTES

Effect of Density and Electron Scavengers in Nitrous Oxide Radiolysis[1a]

by John T. Sears[1b]

Nuclear Engineering Department, Brookhaven National Laboratory, Upton, New York 11973 *(Received August 22, 1968)*

Primary processes in the irradiation-induced decomposition of nitrous oxide, which is a potential dosimetry system,[2,3] are still incompletely understood. The present investigation presents results of the irradiation of solid, liquid, and high density (to 0.7 g/cc) gas which emphasize the relative constancy of $G(N_2)$. Additional N_2O-scavenger experiments continue the investigation into the decomposition mechanism.

Experimental Section

All gases were simply purified by freeze–thaw vacuum techniques. Low-pressure γ-ray experiments were conducted in all-glass break-seal vessels (500 to 550 cc). In other experiments ^{222}Rn α rays (and daughter particles) were deposited internally in a 90-cc sealed vessel until the radon was exhausted. ^{210}Po α rays

(1) (a) This work was performed under the auspices of the U. S. Atomic Energy Commission. (b) Esso Research and Engineering Co., Linden, N. J. 07036.

(2) P. Harteck and S. Dondes, *Nucleonics*, **14**, 66 (1956).

(3) R. W. Hummel and J. A. Hearne, *Nature*, **188**, 734 (1960).

traveled through a stainless steel window into N_2O in a 605-cc vessel, which had a stopcock to allow periodic sampling. High density γ-ray experiments were conducted in 6-mm diam 3-cc sealed vessels; in gas-phase experiments, the vessels were situated inside stainless steel pressure vessels (7 cc), which were filled with N_2O to nearly the same density to equalize pressure, and irradiated in a controlled-temperature water bath.

Energy deposition by ^{210}Po α particles was calculated by Slater[4] from his semiconductor calibration of the source at various angles of emission, integrated over 2π radians. Energy deposition from radon decay was computer calculated by approximation of vessel geometry, α particle and recoil ranges in N_2O,[5,6] and assumed location on the vessel surface of daughter nuclei. *In situ* Fricke dosimetry with appropriate electron density corrections was used for ^{60}Co γ irradiation.

Noncondensible gases (at $-196°$) were collected over a Toepler pump and analyzed by a gas chromatograph (molecular sieve column) for N_2 and O_2. In ^{210}Po α-ray experiments, the irradiated gases were instead fed directly into a calibrated GPC. The products, NO and NO_2, were not measured in this study.

Results and Discussion

Table I summarizes the present results. All the pure N_2O results, in all phases below 40°, including the dense gas data at doses $>3 \times 10^5$ rads, demonstrate the remarkable relative constancy of $G(N_2)$ ($\approx$10 to 11.5). The ^{210}Po α-ray series gave $G(N_2) = 10.0 \pm 0.4$, in agreement with the value and analysis by Jones and Sworski [$G(N_2) = 10.0 \pm 0.2$].[7] Increase in dose above 4.4×10^6 rads (0.2% N_2) causes a decrease in nitrogen production rate until a new linear yield dose region (1 to 5% N_2) is obtained with $G'(N_2) = 6.7$;[8] the ^{222}Rn experiment was in reasonable agreement with these results. Irradiations of solid or liquid N_2O produced only slight increases in the gas yields (Table I). It is unclear why the present liquid phase results are slightly lower than those of Robinson and Freeman,[9] $G(N_2) = 12.9 \pm 0.2$, $O_2/N_2 = 0.2$. Oxygen yields also appear fairly stable; however, little mechanistic evidence should be deduced from this because of possible reaction during analysis[10] or scavenger attack (see results of additive-CCl_4 experiments).

Applied electric field experiments[7,10-12] and ethylene scavenger experiments[12] indicate that ionic recombination produces only small amounts of nitrogen ($G \ll 1$). It is then not surprising that geminate ionic recombination reactions, which may be prohibited because of the formation of negative molecular ions, and ionic cluster reactions[13] do not appear to be important above doses of 3×10^5 rads. The situation at low doses is unclear, and possible wall effects, etc., may be interfering.

Chemical reactions of atoms, excited molecules, and electrons (or negative ions) then have been postulated to produce decomposition. Present interest concerned electron reactions as deduced from scavenger-addition experiments. The present results, low and high density, indicate that $G(N_2)$ decreased by only $\approx G(e) = 3.05$ because of electron scavenging.

Thermal electrons might react to form nitrogen from the following over-all reaction[11]

$$e_{th}^- + N_2O \longrightarrow\longrightarrow N_2 + O^- \qquad (1)$$

It was then suggested that O^- further reacted[10]

$$O^- + N_2O \longrightarrow N_2 + O_2^- \qquad (2)$$

$$O^- + N_2O \longrightarrow NO + NO^- \qquad (3)$$

Reactions 1 and 2 were suggested[14] as the mechanism leading to N_2 formation in electron scavenger–hydrocarbon radiolysis. As preferential scavenging[14,15] of the electron by SF_6 and CCl_4 occurs, these additives should prohibit nitrogen formation *via* reactions 1 and 2, which have been estimated[16] from scavenger–alkane studies as

$$G(N_2) = [1 + k_2/(k_2 + k_3)]G(e) = 1.55G(e) = 4.7$$

in N_2O. Further, SF_6 should not interfere with positive ion reactions as its I.P. $\approx$ 19 eV.[17] Now carbon dioxide decreased the nitrogen yield in scavenger–alkane work to $G(e)$, which suggested[18] that reaction 2 was prohibited because of preferential formation of CO_3^-. In the present experiments, CO_2 only slightly decreased the nitrogen yield, while CCl_4, SF_6, and NO_2 decreased $G(N_2)$ by $\approx 3.2 \pm 0.5$. Reaction 1 seems to occur then, but the probability that reaction 2 is important is not supported by the present evidence. The suggestion by Burtt and Henis,[19] upon the observance of O_2^- from N_2O gas bombarded by O^- in a mass spectrometer, is often cited as evidence for reaction 2. However, Paulson[20] observed O_2^- also, but at a much

(4) L. Slater, *Intern. J. Appl. Radiation Isotopes*, in press.

(5) R. Evans, "The Atomic Nucleus," McGraw-Hill Book Co., New York, N. Y., 1955.

(6) D. L. Baulch and J. F. Duncan, *Aust. J. Chem.*, **10**, 112 (1957).

(7) F. T. Jones and T. J. Sworski, *J. Phys. Chem.*, **70**, 1546 (1966).

(8) J. Sutherland, private communication. Note that at these doses considerable product NO_2, etc., has formed, and it is tempting to compare the NO_2-addition experiments where $G(N_2)$ decreased to 6.8 and NO and O_2 were readily formed by photolysis/radiolysis of NO_2.

(9) M. G. Robinson and G. R. Freeman, *J. Phys. Chem.*, **72**, 1394 (1968).

(10) B. P. Burtt and J. F. Kircher, *Radiation Res.*, **9**, 1 (1958).

(11) H. Essex and N. T. Williams, *J. Chem. Phys.*, **16**, 1153 (1948).

(12) R. Gordon and P. Ausloos, *J. Res. Nat. Bur. Stand.*, **69A**, 79 (1965).

(13) J. L. Magee and K. Funabaski, *Radiation Res.*, **10**, 622 (1959).

(14) G. R. A. Johnson and J. M. Warman, *Nature*, **203**, 73 (1964).

(15) G. R. A. Johnson and J. M. Warman, *Trans. Faraday Soc.*, **61**, 1709 (1965).

(16) J. M. Warman, *J. Phys. Chem.*, **71**, 4066 (1967).

(17) R. W. Kiser, (AEC) TID-6142, 1960.

(18) J. M. Warman, *Nature*, **213**, 381 (1967).

(19) B. P. Burtt and J. Henis, *J. Chem. Phys.*, **41**, 1510 (1964).

(20) J. F. Paulson, Advances in Chemistry Series, No. 58, American Chemical Society, Washington, D. C., 1966, p 28.

Table I: Nitrous Oxide Irradiation

Series[a]	Description	Pressure or density	Temp, °C	Max dose, rads	Nominal source strength	$\%N_2$	O_2/N_2	Points	$G(N_2)$
I	^{210}Po α	440–680 Torr	25	4.27×10^6	209 mCi (1.0×10^5 rads/hr avg)	0.06–0.194	0.20 ± 0.01	9	10.0 ± 0.4[b]
II	^{222}Rn α	574 Torr	25	1.42×10^8	15 mCiRn (initially 1.05×10^6 rads/hr)	4.9	0.11	1	7.6
III	^{60}Co γ, gas	660–1000 Torr	10	4.4×10^5	1.2×10^5 rads/hr	to 0.02	0.18 ± 0.02	6	9.9 ± 0.5
IV	Solid	1.5 g/cc	−196	1.24×10^6	1.2×10^5 rads/hr	to 0.06	0.19 ± 0.01	5	10.6 ± 0.6
V	Liquid	1.19 g/cc	−78	1.18×10^6	1.2×10^5 rads/hr	to 0.06	0.20 ± 0.01	6	11.2 ± 0.5
VI[c]	Dense gas[d]	0.02 g/cc	38	1×10^6	6×10^4 rads/hr	to 0.05	0.16	4	11.2 ± 0.9
		0.035 g/cc					0.135	3	11.2 ± 0.8
		0.10 g/cc					0.15	2	10.6 ± 0.9
		0.30 g/cc					0.13	1	12.1
		0.40 g/cc					0.12	1	12.3
		0.55 g/cc					0.12	3	13.5 ± 0.6
		0.70 g/cc					0.15	4	11.6 ± 0.5
VII[e]	Additive	800 Torr of N_2O	10	9×10^5	1.2×10^5 rads/hr	to 0.03			
A	8–60 Torr of CO_2						0.23 ± 0.03	4	9.4 ± 0.6
B	0.1–8 Torr of SF_6						0.28 ± 0.04	15	7.25 ± 0.6
C	0.45–15 Torr of NO_2						(high O_2 from NO_2)	4	6.8 ± 0.4
D	1 Torr of CCl_4						0.16	3	7.7 ± 0.5
	3 Torr of CCl_4						0.12	2	6.7 ± 0.7
	8 Torr of CCl_4						0.11	7	6.7 ± 0.4
	14 Torr of CCl_4						0.04	1	6.8
VIII	Additive dense phase (0.5% SF_6)	0.7 g/cc	38	1.33×10^6	6×10^4 rads/hr	to 0.05		3	8.4 ± 0.3

[a] Linear yield–dose plots were obtained for series I, III, IV, VII(B), and VII(D, 8 Torr of CCl_4). [b] Much of this standard deviation error is energy absorption inaccuracy because of a folding defect in the thin stainless steel window (ref 4). [c] Below 3×10^5 rads, $G(N_2)$ increased to 13.5–18, although O_2/N_2 remained constant. Experiments in the stainless steel pressure vessel alone gave $G(N_2) \cong 11$ over all doses and densities, but little oxygen. The electron density correction seemed valid in glass [even at $\rho/d \cong 0.5$ g/cm^4, where the wall recoil electron effect could be important; see Y. Toi, D. B. Peterson, and M. Burton, *Radiation Res.*, **17**, 399 (1962)] although the evidence is very tentative [$G(N_2) \cong$ constant]. [d] $T_{critical} = 35.5°$; $\rho_{critical} = 0.451$ g/cc. [e] If no effect on G values upon additive concentration change was found, all experiments are reported here together.

reduced level compared with NO^- (reaction 3), and found that charge transfer from O^- to impurity level O_2 (and despite the decrease in electron affinity, 1.45 eV to 0.5 eV) could account for the O_2^- observed.

Energy dependence of electron reactions might be of importance in explaining this "excess" nitrogen in N_2O–alkane studies, for which reaction 2 has been proposed, as well as increased yields of N_2 in N_2O radiolysis under applied electric fields much lower than that required for secondary ionization.[7,10–12] Schulz[21] suggested that the following resonance reaction occurs in a mass spectrometer

$$e_{2.2\ eV}^- + N_2O_{(\nu=0)} \xrightarrow{\text{minor}} N_2^* + O^-$$

$$\xrightarrow{\text{predominate}} e_{th}^- + N_2O^*\ (\nu = i \ldots m) \quad (4)$$

If followed by N_2O^* $(\nu = i \ldots m)$ decomposition/reaction to form N_2, this process might be important if no other process competes for the energy of sub(electronic)-excitation electrons as the secondary electrons slow down. This could be the case in alkanes, as elastic collision–vibration excitation cross sections are low ($\ll 10^{-18}$ cm^2).[22] Other additives might compete for the secondary-electron energy or react with N_2O^* $(\nu = i \ldots m)$. In an applied field thermal electrons might be accelerated to react through (4) to form increased amounts of N_2. This specific reaction follows previous qualitative proposals.[7,12] Additional N_2 forms at $x/P \gtrsim 2$ V/cm-Torr;[7,10–12] secondary ionization occurs at $\approx$27 V/cm-Torr. The energy requirements then appear consistent. Thermal electrons (<0.1 eV) slowly react according to (1) in N_2O or N_2O–alkane, as recombination and other processes are much slower. Upon addition of high electron affinity compounds (SF_6, 1.57 eV; NO_2, 3.8 eV; CCl_4, 2.17 eV), the much faster attachment (or charge exchange) to these compounds occurs at thermal energies; but they do not compete with bulk N_2O for subexcitation electron energy. For instance, SF_6 has a resonance attachment cross section at thermal energies, $\sigma \cong 2.6 \times 10^{-14}$ cm^2,[23] but has a minute capture cross section for electrons at higher energies, $\leq 10^{-18}$ cm^2.

The specific proposed process is consistent, although not necessarily correct, and is a first step in considering energy dependent reactions in mechanisms. It is suggested that consideration of energy dependent cross sections of excited molecule, or electron, reactions in nitrous oxide systems and other radiation chemistry processes should be an increasingly fruitful approach.

Acknowledgment. The author extends his appreciative thanks to J. Sucher for his assistance with the experiments.

(21) G. J. Schulz, *J. Chem. Phys.*, **34**, 1778 (1961).
(22) A. Mozumder and J. L. Magee, *ibid.*, **47**, 939 (1967).
(23) B. H. Mahan and C. E. Young, *ibid.*, **44**, 2192 (1966).

The Dielectric Relaxation of Binary Liquid Mixtures

by K. Baba, T. Fujimura, and K. Kamiyoshi

Research Institute for Scientific Measurements, Tohoku University, Sendai, Japan *(Received October 2, 1968)*

According to the original suggestion by Schallamach[1] on the dielectric relaxation of liquid mixtures, the polar binary mixture in which the two components are both associative or both nonassociative has one common dispersion, whereas the mixture in which one is associative and the other nonassociative yields two regions of dispersion. This empirical rule was then confirmed experimentally by several authors,[2–5] but they observed the dielectric dispersion of liquid mixtures in a supercooled state at low temperature because they utilized a low-frequency apparatus. On the other hand, the dispersion of mixtures in a true liquid state at room temperature was observed by Garg and Kadaba[6] and by Smyth, *et al.*,[7,8] by utilizing a microwave apparatus. They found two regions of dispersion in the mixtures of

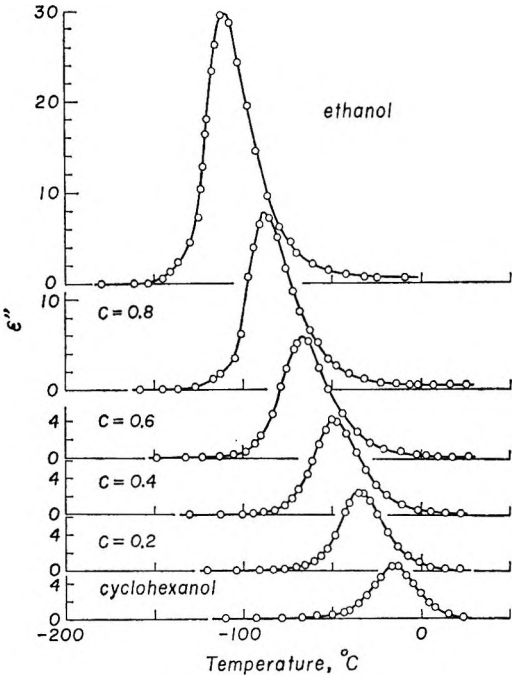


Figure 1. Dielectric relaxation of ethanol–cyclohexanol mixtures at 2 Mcps. C indicates the mole fraction of ethanol in the mixture.

(1) A. Schallamach, *Trans. Faraday Soc.*, **42**, 180 (1946).
(2) D. J. Denney and R. H. Cole, *J. Chem. Phys.*, **23**, 1767 (1955).
(3) D. J. Denney, *ibid.*, **30**, 1019 (1959).
(4) G. E. McDuffie, Jr., *ibid.*, **37**, 239 (1962).
(5) K. Kamiyoshi and T. Fujimura, *J. Phys. Radium*, **23**, 337 (1962).
(6) S. K. Garg and P. K. Kadaba, *J. Phys. Chem.*, **69**, 674 (1965).
(7) E. Forest and C. P. Smyth, *ibid.*, **69**, 1302 (1965).
(8) H. Kilp, S. K. Garg, and C. P. Smyth, *J. Chem. Phys.*, **45**, 2799 (1966).

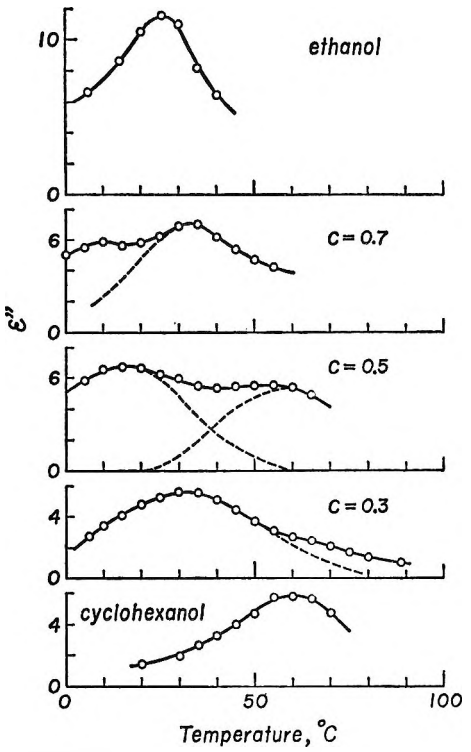


Figure 2. Dielectric relaxation of ethanol–cyclohexanol mixtures at 1000 Mcps. C indicates the mole fraction of ethanol in the mixture.

two associative liquids or of two nonassociative liquids. Consequently, Schallamach's rule seemed not to hold.

For the purpose of confirming clearly these contradictory results, the dielectric dispersion of mixtures of two associative polar liquids was observed both in a supercooled state and in a true liquid state. A mixture of ethanol and cyclohexanol was chosen in this experiment because they have a tendency to supercool easily and partly because they have a dielectric dispersion in a convenient frequency range. Hypersonics of 50 kcps, 100 W was applied to the solutions so as to make mixing as homogeneous as possible.

Figure 1 shows the dielectric dispersion observed at 2 Mcps (capacitance bridge) of pure ethanol, pure cyclohexanol, and mixtures of them at various concentrations. The concentration of ethanol in the specimen is indicated by the mole fraction C, in the figure. These experimental results show that two individual dispersions are no longer distinguishable in the mixtures.

Figure 2 shows the dielectric dispersion of the ethanol–cyclohexanol mixtures observed at 1000 Mcps (coaxial line) at temperatures above 0°. Two regions of dielectric dispersion appear clearly in this temperature range. The experimental curve may be considered to be the superposition of the two dispersions as shown by the dotted curve in the figure. The results also indicate that the dispersion corresponding to ethanol in the mixture shifts to the higher temperature, and that corresponding to cyclohexanol shifts to the lower temperature with the increase in the concentration of

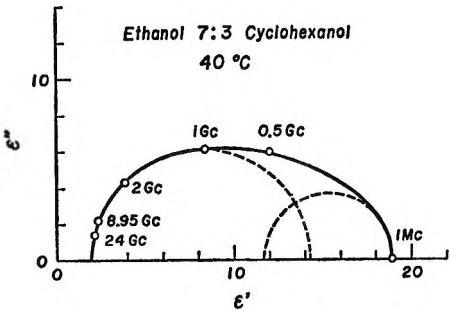


Figure 3. Cole–Cole plot of the dielectric relaxation of ethanol–cyclohexanol mixture (0.7:0.3 in mole fraction) at 40°.

ethanol. Figure 3 shows the Cole–Cole plot of the dispersion observed at 40° on the ethanol–cyclohexanol mixture whose concentration of ethanol is 0.7 mole fraction. The curve clearly contains two regions of dielectric dispersion. The experimental curve may be considered to be the superposition of the two semicircles as shown by the dotted circles in the figure, but Smyth, *et al.*,[8] suggest a new method concerning the separation of two superposed dispersions.

It is seen from these experimental results that two individual dielectric dispersions of the ethanol–cyclohexanol mixture are clearly distinguishable in the liquid state, whereas they are no longer distinguishable in the supercooled state.

Hyperfine and g-Tensor Anisotropy of the Tropenyl Radical[1]

by Walter V. Volland[2] and Gershon Vincow[3]

Department of Chemistry, University of Washington, Seattle, Washington 98105 *(Received October 9, 1968)*

Theories have been proposed for the hyperfine and g-tensor anisotropy of polycentric π-electron radicals.[4] These quantities also enter into the theory of esr line widths.[5] Comparison of theory with experiment has been very limited due to a paucity of measurements of these molecular parameters.[6] In this note we wish to report anisotropy parameters for the tropenyl radical,

(1) Supported by the U. S. Army Research Office (Durham).

(2) Department of Chemistry, Cornell University, Ithaca, N. Y.

(3) Alfred P. Sloan Research Fellow.

(4) (a) H. M. McConnell and J. Strathdee, *Mol. Phys.*, 2, 129 (1959); (b) W. Derbyshire, *ibid.*, 5, 225 (1962); (c) A. J. Stone, *ibid.*, 7, 311 (1964); (d) H. J. Silverstone, D. E. Wood, and H. M. McConnell, *J. Chem. Phys.*, 41, 2311 (1964).

(5) G. K. Fraenkel, *J. Phys. Chem.*, 71, 139 (1967).

(6) (a) C. Heller and T. Cole, *J. Chem. Phys.*, 37, 243 (1962); (b) H. C. Heller and T. Cole, *J. Amer. Chem. Soc.*, 84, 4448 (1962); (c) R. J. Cook, J. R. Rowlands, and D. H. Whiffen, *Mol. Phys.*, 7, 57 (1963); (d) S. H. Glarum and J. H. Marshall, *J. Chem. Phys.*, 44, 2884 (1966).

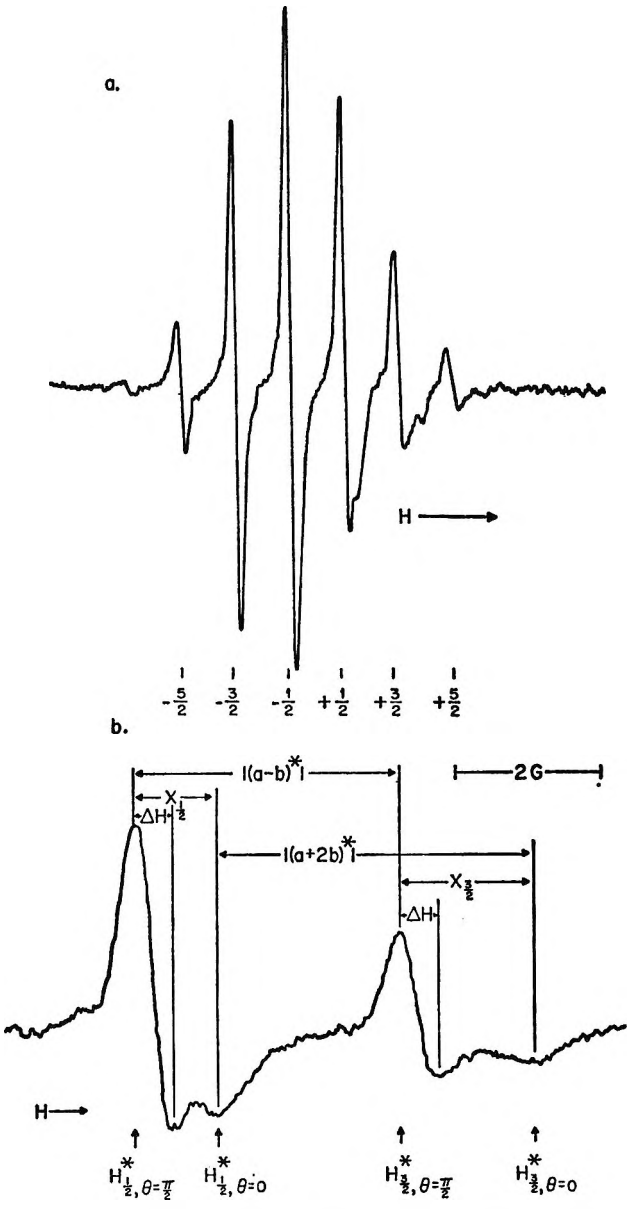


Figure 1. a. Tracing of the esr spectrum of $C_7H_7\cdot$ in polycrystalline $C_{10}D_8$ at room temperature. The outermost lines are obscured by noise. Components are labeled according to the value of M_I, the z component of the total nuclear spin angular momentum (units of $\hbar$); it is assumed that $a < 0$.
b. Tracing of the $M_I = +\frac{1}{2}$ and $+\frac{3}{2}$ components showing the various spacings which are measured. The quantity $X_{M_I} = [(g_\perp^* - g_{||}^*)/g_{||}^*]H_{M_I,\theta}^* - 3b^*M_I$ is a measure of the effect of anisotropy on component shape. $H_{M_I,\theta}^*$ designates the resonance field for radicals with angular momentum M_I and angle θ between the z axis and the applied field.

$C_7H_7\cdot$.[7] In addition, we report the first measurement of the temperature coefficient of a dipolar proton hyperfine splitting for a π radical.

The esr spectrum of $C_7H_7\cdot$ in solid polycrystalline naphthalene ($C_{10}H_8$) at room temperature consists of eight equally spaced, overlapped components with $\Delta H_{ms} \approx 1.7$ G and relative intensities close to the binomial ratios.[4d] It is inferred from the spectral shape that the tropenyl radical is reorienting rapidly about its sevenfold axis (but not about axes in the aromatic plane). Because of this motion the 7 protons are equivalent and $C_7H_7\cdot$ is effectively axially symmetric; *i.e.*, the in-plane components of the g and dipolar hyperfine tensors are averaged.

Principal values of the g and hyperfine tensors are designated $g_{||}$, $g_\perp$, and $g_\perp$ and $a + 2b$, $a - b$, and $a - b$, respectively. Corresponding principal axes are the sevenfold axis (z axis) and two mutually perpendicular axes in the molecular plane. Since $(g_\perp - g_{||})$ and b are relatively small, their effects are *masked* by the large line width, and the spectrum is similar to that of the radical in liquid solution.

We have prepared $C_7H_7\cdot$ in polycrystalline perdeuterionaphthalene, $C_{10}D_8$, in order to reduce the magnitude of the intermolecular dipolar interactions and hence the line width. The spectrum (Figure 1) is *strikingly different* from that of $C_7H_7\cdot$ in $C_{10}H_8$: hyperfine components are not overlapped, peak-height ratios differ markedly from binomial, and several components are quite asymmetric (Figure 1b).

The theory of polycrystalline line shapes, for the case of a radical with axial symmetry and infinitesimal line width, has been employed to indicate which resonance fields and spacings should be measured (see Figure 1b).[7c,8] We have also measured $g_\perp^*$ from the mean of $H^*_{-1/2,\theta=\pi/2}$ and $H^*_{+1/2,\theta=\pi/2}$. The stars denote that these are approximate values of the parameters which must be corrected for the effect of finite line width and the nuclear Zeeman interaction.

Results of our measurements (room temperature) are: $|(a-b)^*| = 3.69 \pm 0.01$ G, $X_{1/2} = 1.19 \pm 0.02$ G, $X_{3/2} = 1.74 \pm 0.04$ G, $g_\perp^* = 2.00294 \pm 0.00001$, and $\Delta H = 0.55 \pm 0.03$, 0.50 ± 0.02, 0.57 ± 0.02, 0.57 ± 0.01, 0.54 ± 0.01, and 0.54 ± 0.03 G for $M_I = -\frac{5}{2}$, $-\frac{3}{2}$, ... $+\frac{5}{2}$, respectively. Computer calculations of the polycrystalline line shape for the case of finite line width have been performed.[9] The following values lead to *excellent agreement* between calculated and experimental spectra: $a = -3.87$ G, $b = -0.18$ G, $g_\perp = 2.00286$, $g_{||} = 2.00236$, and the Gaussian line width equals 0.48 G.[10]

The z component of the dipolar hyperfine tensor is $2b = -0.36$ G ($\rho^\pi \approx \frac{1}{7}$). Corresponding values for $CH_3\cdot$[11] ($\rho^\pi \approx 1$) and $\cdot CH(COOH)_2$[12] ($\rho^\pi \approx 1$) are 0.5

(7) For previous work on tropenyl radical, see: (a) G. Vincow, M. L. Morrell, W. V. Volland, H. J. Dauben, Jr., and F. R. Hunter, *J. Amer. Chem. Soc.*, **87**, 3527 (1965); (b) M. L. Morrell, Ph.D. Thesis, University of Washington, Seattle, Wash., 1966; (c) W. V. Volland, Ph.D. Thesis, University of Washington, Seattle, Wash., 1967.

(8) R. Neiman and D. Kivelson, *J. Chem. Phys.*, **35**, 156 (1961).

(9) R. Lefebvre and J. Maruani, *ibid.*, **42**, 1480 (1965). We wish to thank Drs. Lefebvre and Maruani for sending us a copy of their program.

(10) These values are in good agreement with the isotropic splitting and g value (ref 7).

(11) M. T. Rogers and L. D. Kispert, *J. Chem. Phys.*, **46**, 221 (1967).

(12) T. Cole, T. Kushida, and H. C. Heller, *ibid.*, **38**, 2915 (1963).

and 0.8 G, respectively. It is evident that the contribution of nonadjacent carbon atoms in $C_7H_7\cdot$ is most important and is negative. Silverstone, Wood, and McConnell[4d] have made an approximate calculation of $2b$ for $C_7H_7\cdot$ and obtain -0.7 G, in fairly good agreement with our measurement.

Experiments on $C_7H_7\cdot$ in $C_{10}D_8$ have also been conducted at $-145°$. The most interesting result obtained is an approximate value of the temperature coefficient of $2b$, $\Delta(2b)/\Delta t \approx -0.5$ mG/°C. This increase in $|2b|$ with increasing temperature may be associated with the averaging of the dipolar tensor over the out-of-plane CH bending motion.

The value of $g_{||}$ is of interest since the trace of the g tensor of $C_7H_7\cdot$ (in general of C_nH_n) is anomalous relative to the value predicted using Stone's correlation for nondegenerate hydrocarbon radicals.[7b,13] It has been proposed that the vibronic near degeneracy of $C_7H_7\cdot$ might lead to an enhanced magnitude of the deviation of $g_{||}$ from the free-electron value.[4d] Stone has estimated that for all nondegenerate radicals $g_{||} = 2.00238$.[13a] From our experimental result, 2.00236, it is clear that the effect of the vibronic near degeneracy is negligible.

(13) (a) A. J. Stone, *Mol. Phys.*, **6**, 509 (1963); (b) B. G. Segal, M. Kaplan, and G. K. Fraenkel, *J. Chem. Phys.*, **43**, 4191 (1965).

Fluorescent Yields of 1,2,3,4-Tetrahydronaphthalene Excited in the 2850–3100-Å Region

by M. Grossman, G. P. Semeluk, and I. Unger

The Department of Chemistry, University of New Brunswick, Fredericton, New Brunswick, Canada
(Received October 21, 1968)

In recent years ample evidence has been accumulated demonstrating that benzene and benzene derivatives undergo intramolecular rearrangement when irradiated in the 2500-Å region.[1-4] It has been suggested that benzvalene is first formed when benzene is irradiated in the neighborhood of 2500 Å in both liquid and gas phases. In the gas phase the benzvalene rapidly rearomatizes to benzene, whereas in the liquid phase collisional deactivation stabilizes some of the benzvalene molecules.[5,6]

1,2,3,4-Tetrahydronaphthalene (tetralin), from the photochemical point of view, is very similar to an *ortho*-substituted benzene. Thus one might expect tetralin to show the same photochemical behavior as *o*-xylene[7] or *o*-difluorobenzene.[8] Should this be the case, then the irradiation of tetralin could in principle lead to *meta*- and *para*-bridged compounds. An investigation of this type should begin with an examination of

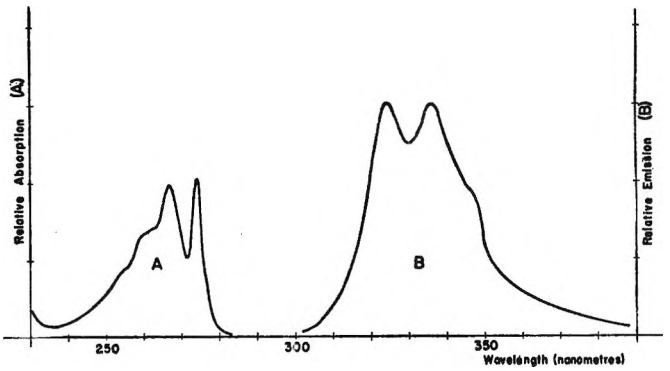


Figure 1. A, Absorption spectrum of tetralin in cyclohexane taken on a Coleman–Hitachi, Model EPS-3T spectrophotometer. B, Fluorescence spectrum of tetralin excited by 2900-Å radiation.

the relationship between singlet and triplet yields and exciting wavelengths. Presumably, at the exciting wavelength where the quantum deficit $[1 - (\Phi_S + \Phi_T)]$ is largest, benzvalene formation will be most likely to occur.[9] This note summarizes the results of such an investigation for tetralin excited in the 2850–3100-Å region.

All emission experiments were carried out in the liquid phase on a modified Aminco-Bowman spectrofluorometer.[9] The solvent used was fluorometric grade cyclohexane obtained from Aminco. The tetralin used in this study was purchased from the Fisher Scientific Co., fractionally distilled, and recrystallized from Freon 12 at $-120°$. Tetralin treated in this manner was found to contain less than 0.5% impurity by vpc. The biacetyl was obtained from the Aldrich Chemical Co. All solutions were thoroughly outgassed prior to use. The fluorescence yields reported here are based on a recently reported fluorescence quantum yield of benzene in cyclohexane solution.[10]

When tetralin is excited by light of 2850–3100 Å it exhibits a very strong fluorescent emission extending from 2800 Å to about 3800 Å; no phosphorescent emission is observed. Figure 1 shows a typical fluorescence spectrum along with the absorption spectrum. Exciting wavelengths below 2850 Å also produce a strong fluorescent emission. However, due to interference by scattered light, the quantum yield of fluorescence excited

(1) K. E. Wilzbach, J. S. Ritscher, and L. Kaplan, *J. Amer. Chem. Soc.*, **89**, 1031 (1967).
(2) I. Haller, *ibid.*, **88**, 2070 (1966).
(3) H. R. Ward and J. S. Wishnok, *ibid.*, **90**, 1085 (1968).
(4) D. Bryce-Smith, *Pure Appl. Chem.*, **16**, 47 (1968).
(5) K. E. Wilzbach, A. L. Harkness, and L. Kaplan, *J. Amer. Chem. Soc.*, **90**, 1116 (1968).
(6) L. Kaplan and K. E. Wilzbach, *ibid.*, **90**, 3291 (1968).
(7) W. A. Noyes, Jr., and C. S. Burton, *Ber Bunsenges. Physik. Chem.*, **72**, 146 (1968).
(8) J. L. Durham, G. P. Semeluk, and I. Unger, *Can. J. Chem.*, in press.
(9) F. W. Ayer, F. Grein, G. P. Semeluk, and I. Unger, *Ber Bunsenges. Physik. Chem.*, **72**, 282 (1968).
(10) I. B. Berlman, "Handbook of Fluorescence Spectra of Aromatic Molecules," Academic Press, New York, N. Y., 1965.

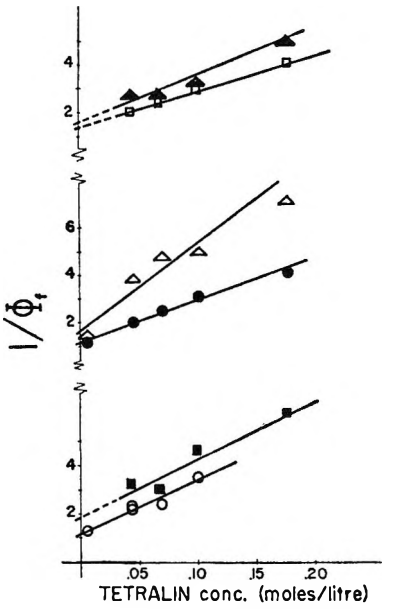


Figure 2. Variation of the reciprocal of fluorescent quantum yield of tetralin as a function of tetralin concentration at various exciting wavelengths: ○, 2850 Å; ●, 2900 Å; □, 3100 Å; ■, 3000 Å; △, 2950 Å; ▲, 3050 Å.

by wavelengths below 2850 Å could not be accurately determined. Plots of $1/\Phi_f$ *vs.* [tetralin] are linear for all the exciting wavelengths examined; see Figure 2. The extrapolated fluorescent quantum yields at infinite dilution are 0.88 ± 15% at λ_{ex} 2850 Å; 0.84 ± 10% at λ_{ex} 2900 Å; 0.59 ± 30% at λ_{ex} 2950 Å; 0.54 ± 30% at λ_{ex} 3000 Å; 0.60 ± 20% at λ_{ex} 3050 Å; 0.77 ± 10% at λ_{ex} 3100 Å. Thus the fluorescent quantum yield at several exciting wavelengths approaches unity within experimental error. It is also worth noting that the fluorescent yield for tetralin is far higher than the fluorescent yield for comparable molecules; *e.g.*, *o*-xylene in hexane has a fluorescent yield of 0.30.[11]

An attempt was made to determine triplet yields using the sensitized emission of biacetyl technique.[12] These experiments showed that tetralin did not excite a sensitized emission of biacetyl; they further showed that tetralin quenched the emission of biacetyl excited directly. Thus presumably if the process occurring is electronic energy transfer rather than chemical quenching,[13,14] the triplet state of tetralin is either equal to or lower in energy than the triplet of biacetyl which has been given as 56 kcal.[15]

Our findings lead us to suggest that the intersystem crossover in tetralin is not a very important process, which may be due to a large energy gap between the singlet and the triplet energy levels in this molecule.[16,17] We further suggest that intramolecular rearrangement in tetralin, though not excluded by our data, is not likely to occur to any significant extent at λ_{ex} 2850, 2900, and 3100 Å. Studies are currently underway in our laboratory on homologs of tetralin which should further elucidate the photochemical behavior of this series.

Acknowledgments. We wish to thank Dr. Z. Valenta of this department for suggesting this problem to us and for many valuable discussions. Financial assistance from the National Research Council of Canada and the Associated Alumni of the University of New Brunswick is gratefully acknowledged.

(11) J. G. Calvert and J. N. Pitts, Jr., "Photochemistry," John Wiley and Sons, Inc., New York, N. Y., 1966.

(12) H. Ishikawa and W. A. Noyes, Jr., *J. Chem. Phys.*, **37**, 583 (1962).

(13) H. L. J. Bäckström and K. Sandros, *Acta Chem. Scand.*, **12**, 823 (1958).

(14) H. L. J. Bäckström and K. Sandros, *ibid.*, **14**, 48 (1960).

(15) W. A. Noyes, Jr., and I. Unger, *Advan. Photochem.*, **4**, 49 (1966).

(16) R. Srinivasan, *J. Chem. Phys.*, **38**, 1039 (1963).

(17) M. Gouterman, *ibid.*, **36**, 2846 (1962).

Direct Observation of Intrinsic Diastereotopic Magnetic Nonequivalence

by G. Redl

Department of Chemistry, New York University, New York, New York 10453

and G. J. D. Peddle

Department of Chemistry, University of Alberta, Edmonton, Alberta, Canada *(Received October 28, 1968)*

The relative importance of the various factors contributing to the magnetic nonequivalence of the diastereotopic X groups in CX_2Y–CABC systems has been a subject of much discussion in recent years.[1]

Raban[1e] has formulated the ideas of earlier workers[1a,c] into the useful expression

$$\Delta\nu_{total} = \Delta\nu_{cp} + \Delta\nu_{id}$$

to indicate that the observed chemical shift difference ($\Delta\nu_{total}$) is made up of a temperature-dependent contribution due to unequal conformer populations ($\Delta\nu_{cp}$) and a temperature-independent contribution due to intrinsic diastereotopic nonequivalence ($\Delta\nu_{id}$).

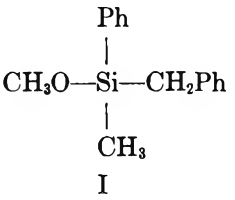
Attempts to observe $\Delta\nu_{id}$ directly by observing a high-temperature limit for $\Delta\nu_{total}$ have failed,[1f] and only indirect calculations of $\Delta\nu_{id}$ are available.[1c,1e,2] The calculated values of $\Delta\nu_{id}$ for CF_2Br–$CFBrCl$ and CF_2Br–$CHBrCl$ are 6.7[1c] and 55.3 cps,[1e,2] while the values of $\Delta\nu_{total}$ at the highest temperatures reported

(1) (a) J. S. Waugh and F. A. Cotton, *J. Phys. Chem.*, **65**, 562 (1961); (b) E. I. Snyder, *J. Amer. Chem. Soc.*, **85**, 2624 (1963); (c) H. S. Gutowsky, *J. Chem. Phys.*, **37**, 2196 (1962); (d) G. M. Whitesides, D. Holtz, and J. D. Roberts, *J. Amer. Chem. Soc.*, **86**, 2628 (1964); (e) M. Raban, *Tetrahedron Lett.*, 3105 (1966); (f) S. Seltzer and S. G. Mylonakis, *J. Phys. Chem.*, **72**, 754 (1968).

(2) R. A. Newmark and C. H. Sederholm, *J. Chem. Phys.*, **43**, 602 (1965).

are 46.5 and 187.8 cps, respectively. Both these calculated $\Delta\nu_{id}$ values are for nonequivalent fluorine nuclei and no observed or calculated values have been reported for protons. Indeed, it has been suggested that for protons $\Delta\nu_{id}$ will be close to zero.[1d]

We wish to report the direct observation of a high-temperature limit of $\Delta\nu_{total}$ for the diastereotopic benzylic protons in benzylmethylphenylmethoxysilane (I).



I

A norganosilicon compound was chosen for this study since because of the comparatively large covalent radius of silicon it was hoped that the limit of equal conformer population would be approached at a relatively lower temperature than for a carbon compound.

The pmr spectra of I were recorded on a Varian Associates HA100 spectrometer.[3] At temperatures below 100° a clear AB quartet was obtained for the benzylic protons ($J = 14.0 \pm 0.1$ cps). At temperatures above 100° the central lines of the quartet began to overlap and this together with a decrease in resolution at higher temperatures made it difficult to determine accurately the positions of the central doublet. However, since the position of the outer lines was not masked by overlap and the decrease in resolution, the chemical shift values were calculated from the outer line positions and $J = 14.0$ cps.

Table I: Variation of $\Delta\nu_{total}$ with Temperature

Temp, °C	Solvent	$\Delta\nu_{total}$, cps
−70	Toluene	17.7
−50	Toluene	15.4
−30	Toluene	13.7
−10	Toluene	12.3
10	Toluene	11.2
30	Toluene	10.3
40	Neat	10.0
50	Toluene	9.6
60	Neat	9.2
70	Toluene	9.1
80	Neat	8.7
80	Toluene	8.5
90	Toluene	8.2
100	Neat	8.0
120	Neat	8.0
140	Neat	7.7
160	Neat	7.3
170	Neat	7.1
180	Neat	7.1
190	Neat	6.9
200	Neat	7.1

The results obtained are shown in Table I. As the temperature increases from −70° the rate of change of $\Delta\nu_{total}$ decreases until finally the five values obtained between 160 and 200° are constant within experimental error. This value of 7.1 ± 0.2 cps should represent the chemical shift difference when conformer populations are approximately equal and thus may be assigned to the intrinsic diastereotopic nonequivalence of the benzylic protons of I. Since the maximum value observed for $\Delta\nu_{total}$ was under 20 cps, at least in I the contribution of $\Delta\nu_{id}$ to $\Delta\nu_{total}$ is a major one over the whole range of temperatures studied.

Acknowledgment. We thank the Petroleum Research Fund and the National Science Foundation for support of this research, and Mr. D. Gifford for providing the HA100 spectra.

(3) The variable temperature probe was calibrated using an iron–constantan thermocouple, and line positions were determined using an electronic counter in conjunction with a variable oscillator.

Ion–Solvent Interactions.

Relation to Solvent Dielectric Constant[1]

by C. N. Hammonds and M. C. Day

Department of Chemistry, Louisiana State University, Baton Rouge, Louisiana 70803 *(Received November 12, 1968)*

The importance of solvent dielectric constant on ionic conductance has long been recognized and was well demonstrated by the classic studies of Fuoss and Kraus on the conductivity of N(iamyl)$_4$NO$_3$ in dioxane–water mixtures,[2] but at the same time, specific ion–solvent interactions undoubtedly can play an important role. In some instances they may be more significant than the solvent dielectric constant. Gilkerson has clearly shown the importance of such interactions on the ion-pair equilibrium constant,[3] and examples of ion-size effects in which the ion must be treated as a solvated entity in order to correlate data are quite common.[4–6] A particularly good example of this latter case can be seen from the study of Griffiths and Scarrow on the ease of formation of the $NiBr_4^{2-}$ complex ion.[7] They propose that the Li^+ ion in acetone must be a larger entity than the (octyl$_3$propyl)N$^+$ ion.

(1) Reprint requests should be sent to M. C. Day.

(2) R. M. Fuoss and C. A. Kraus, *J. Amer. Chem. Soc.*, **55**, 21 (1933).

(3) W. R. Gilkerson, *J. Chem. Phys.*, **25**, 1199 (1956).

(4) F. Accascina, A. D'Aprano, and R. Triolo, *J. Phys. Chem.*, **71**, 3469 (1967).

(5) D. Nicholls, C. Sutphen, and M. Szwarc, *ibid.*, **72**, 1021 (1968).

(6) J. B. Ezell, and W. R. Gilkerson, *ibid.*, **72**, 144 (1968).

(7) T. R. Griffiths and R. K. Scarrow, "International Conference on Non-Aqueous Solvent Chemistry," Hamilton, Ont., Canada, June 1967.

Table I: Equivalent Conductance of $NaAlBu_4$–THF Solutions as a Function of Salt Concentration

	Concn of $NaAlBu_4$, M							
	0.05216	0.09525	0.1145	0.1674	0.2094	0.2881	0.3348	0.4687
Λ, mho cm^2	19.62	21.08	21.03	21.20	20.26	19.46	17.91	15.57

In spite of an awareness of the importance of these two quantities on ionic systems, the separation of the two effects has proven difficult. This is primarily because the usual procedures for altering the solvent dielectric constant also result in a change in the extent of ion–solvent interaction. Consequently, there is considerable interest in the independent correlation of the two effects with changes in conductance and, more importantly, with reaction rates which are observed to occur in going from one solvent to another. It would now seem that the solubility of sodium tetrabutylaluminate ($NaAlBu_4$) in saturated hydrocarbon solvents offers a somewhat unique approach to the problem. Nmr studies of the complexation of the Na^+ ion by tetrahydrofuran (THF) using cyclohexane as a solvent have shown that a very stable 1:1 complex exists with three additional molecules of THF in equilibrium with the 1:1 complex.[8] In the same manner, it has been shown that there is no significant interaction between the $NaAlBu_4$ and the hydrocarbon solvent. The solvent can thus be considered to be essentially a dispersing medium for the salt.[8] A knowledge of the nature of the THF complex with the Na^+ ion permits us to interpret the conductance curves of the system $NaAlBu_4$–cyclohexane–THF in a manner that indicates it is possible to distinguish between a specific ion–solvent interaction and a solvent dielectric constant effect. We wish to report here our studies on this system.

Experimental Section

The preparation of $NaAlBu_4$ and the solvents has been reported earlier.[8,9] The conductance measurements were made in conventional cells. Cell constants were determined with aqueous KCl solutions. For the different cells, these ranged between 0.01042 and 1.2238 cm^{-1}. The cells were filled in a nitrogen drybox and transferred to a constant temperature bath controlled at 25.00 ± 0.05° and containing a mineral oil, marcol.

Conductance measurements were made with a Leeds and Northrup Co. Model 4666 Jones modified conductivity bridge and an Industrial Instruments Inc. RC16 conductivity bridge. The RC16 bridge was used for resistance measurements in the range of 1×10^5 to 2.5×10^6 ohms. Solution and solvent densities were obtained with pycnometers calibrated with distilled water. Viscosities were measured with Cannon–Fenske viscosimeters calibrated with appropriate pure organic solvents.

All sample preparations and solution transfers were carried out in a nitrogen drybox. A circulating system passed the drybox atmosphere through a copper oven to remove oxygen and through 3A molecular sieves and a Dry Ice trap to remove moisture and organic vapors.

Results and Discussion

In Figure 1, the equivalent conductances of several different concentrations of $NaAlBu_4$ are shown as a function of the ratio of THF:salt using cyclohexane as a solvent. In all cases a peak occurs at a ratio of approximately 1:1 followed by a drop and short plateau. Analogous studies were made at salt concentrations of 0.209, 0.265, 0.288, and 0.468 M. Although different shapes of the peak and plateau regions occur, as well as considerably greater equivalent conductances, indicating possibly a different conductance mechanism at higher concentrations, the inflection point and rise in conductance are in general accord with those shown here.

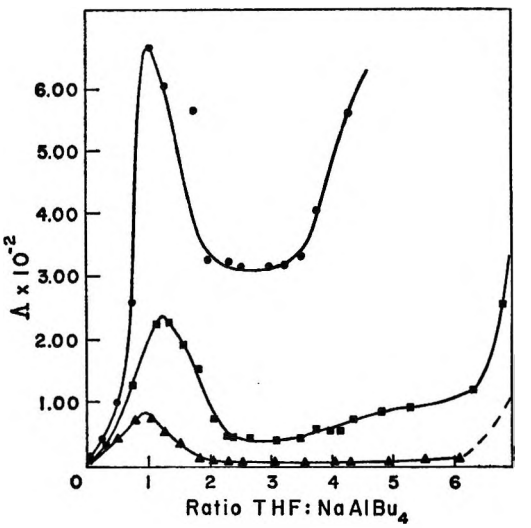


Figure 1. Equivalent conductance of $NaAlBu_4$ in cyclohexane–THF mixtures as a function of the mole ratio THF:salt: ●, 0.1525 M; ■, 0.09524 M; ▲, 0.05213 M $NaAlBu_4$.

At 25°, the dielectric constant of THF is 7.39 and that of cyclohexane is 2.05. Thus the addition of THF would be expected to increase the solvent dielectric

(8) E. Schaschel and M. C. Day, *J. Amer. Chem. Soc.*, 90, 503 (1968).
(9) M. C. Day, H. M. Barnes, and A. J. Cox, *J. Phys. Chem.*, 68, 2595 (1964).

constant. However, because of the stability of the 1:1 complex, it can be assumed that there is essentially no free THF up to the 1:1 ratio. Consequently, the increase in equivalent conductance up to this point cannot be attributed to an increase in solvent dielectric constant. Rather it is the result of the formation of a stable 1:1 complex between the Na^+ ion and the THF.

The decrease in equivalent conductance after the 1:1 ratio may be attributed to a decrease in mobility of the Na^+ ion arising from additional complexation. A rapid rise in equivalent conductance begins at or just prior to a 4:1 ratio of THF:salt and in all cases it rises to very nearly the same maximum in pure THF, as can be seen from the concentration dependent studies shown in Table I. In terms of the proposed equilibrium

$$[Na\cdot THF]^+ + 3THF \rightleftharpoons [Na\cdot 4THF]^+$$

in which a relatively stable 4:1 complex is formed, the rise in equivalent conductance after the 4:1 ratio would be expected because of the increase in solvent dielectric constant corresponding to the increase in free THF in the bulk solvent.

In Figure 2, the equivalent conductance of the 0.1525 *M* salt solution is extrapolated to that of pure THF as solvent. An increase is seen relative to the maximum at the 1:1 ratio of a factor of approximately 300.

Qualitatively, ion–solvent interaction may here be interpreted in terms of an ion-size effect. The stability of the ion aggregates will decrease with an increase in the effective cation size. This will result in an increase in the number of charge carriers, but complexation by a second THF molecule leads to a decrease in cation mobility. Thus the conductance behavior prior to the 4:1 ratio of THF:salt can be considered primarily in terms of ion size rather than solvent dielectric constant.

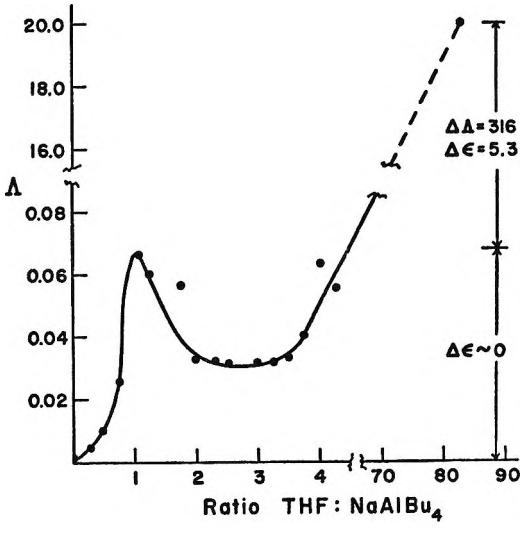


Figure 2. Comparison of the equivalent conductance of $THF:NaAlBu_4$ at low mole ratios to the equivalent conductance of $NaAlBu_4$ in pure THF.

The increase in equivalent conductance beginning at approximately the 4:1 ratio may then be attributed to an increase in solvent dielectric constant. However, in this region the separation of the two effects is not straightforward since the ion aggregates include the solvated rather than the free Na^+ ion, and a separation of the effects will require an analogous study as a function of cation size using sufficiently large cations that ion–solvent interaction can be neglected.

Acknowledgment. Support of this work by National Science Foundation Grant GP 6421 and a National Science Foundation Science Faculty Fellowship for C. N. Hammonds is gratefully acknowledged.

Nuclear Magnetic Resonance Study of Concentrated Lithium Chloride Solutions

by Robert G. Bryant

Department of Chemistry, Stanford University, Stanford, California 94305 *(Received June 21, 1968)*

Nuclear magnetic resonance has made significant contributions to the study of aqueous solutions containing electrolytes. While much of the work has employed proton resonance to observe changes in the solvent, an increasing amount of information is coming from the nuclear resonance of the solute ions.[1–5] Most work thus far has focused on the more dilute solutions and the data analysis has drawn heavily on models appropriate for the limit of infinite dilution. Although the theoretical treatments of more concentrated solutions are less precise, nuclear magnetic resonance measurements in concentrated solutions reflect the environment of the nucleus observed and thus provide useful information about the structure of the solution.

Since aqueous lithium chloride solutions may be made exceedingly concentrated, measurements of the $^7Li^+$ and $^{35}Cl^-$ resonances were made as a function of lithium chloride concentration to look for unusual behavior of the solute resonances at high concentrations. ^7Li and ^{35}Cl both possess a nuclear spin quantum number of $\frac{3}{2}$ and nuclear quadrupole moments of 0.1 and −0.079, respectively, so that the nuclear magnetic relaxation for both is usually dominated by the interaction of the nuclear quadrupole moment with random

(1) J. F. Hinton and E. S. Amis, *Chem. Rev.*, 67, 367 (1967).
(2) R. A. Craig and R. E. Richards, *Trans. Faraday Soc.*, 59, 1972 (1963).
(3) B. F. Fabricand and S. S. Goldberg, *Mol. Phys.*, 13, 323 (1967).
(4) P. A. Speight and R. L. Armstrong, *Can. J. Phys.*, 45, 2493 (1967).
(5) D. E. Woesner, B. S. Snowden, Jr., and A. G. Ostroff, *J. Chem. Phys.*, 49, 371 (1968).

fluctuations in the electric environment of the nucleus observed. In the limit of extreme narrowing, the relaxation time for a nucleus of spin $\frac{3}{2}$ is given by

$$\frac{1}{\pi T_1} = \frac{2\pi}{5}\left(1 + \frac{n^2}{3}\right)(e^2qQ)^2\tau_c \qquad (1)$$

where T_1 is the nuclear spin lattice relaxation time, q is the electric field gradient at the nucleus of quadrupole moment Q, n is the asymmetry parameter, and τ_c is the correlation time for reorientation of the field gradient with respect to the direction of the applied magnetic field.[6] In the limit of extreme narrowing the line width, $\Delta\nu$, measured in hertz as the full line width at half-height is equal to $1/\pi T_1$. Changes in the relaxation time or line width thus reflect either changes in the symmetry of the electric environment about a nucleus or changes in the average reorientation time for the nucleus with respect to the laboratory axis system. To a first approximation the correlation time is proportional to the bulk viscosity, η; however, the validity of this approximation depends critically on how exactly the bulk viscosity reflects the microscopic viscosity that dominates the τ_c term of eq 1. The quantity $1/T_1\eta$ is thus a measure of the remaining effects including terms strongly dependent on the electric symmetry at the observed nucleus.

Experimental Section

Lithium chloride purchased as Baker Analyzed reagent was recrystallized from water to remove a colored impurity apparent in concentrated solutions. Two solutions standardized by potentiometric titration with silver nitrate were used as stock solutions from which others were made volumetrically.

The nmr measurements were made on a Varian Model V-4300 nmr spectrometer operating at 4.33 MHz coupled with a Princeton Applied Research Model JB-4 Lock-in-Amplifier and audio amplifier built in this laboratory to permit various modulation and detection options. The ^{35}Cl line width was measured as the full width at half-height of the absorption signal displayed as the first side band at 550 or 750 Hz; the deviations reported are the average deviations from the mean calculated from at least eight measurements at each concentration. ^{7}Li T_1 measurements were made using adiabatic rapid-passage techniques. Recovery of the bulk magnetization was followed below saturation using a Model 151 Sanborn recorder. T_1 values reported are the average of at least three separate determinations and the deviations reported are the average deviations from the mean. Samples were contained in 14-mm o.d. Pyrex tubes and measured at the temperature of the magnet gap, 25 ± 2°. Values for the viscosity were obtained from the "International Critical Tables."

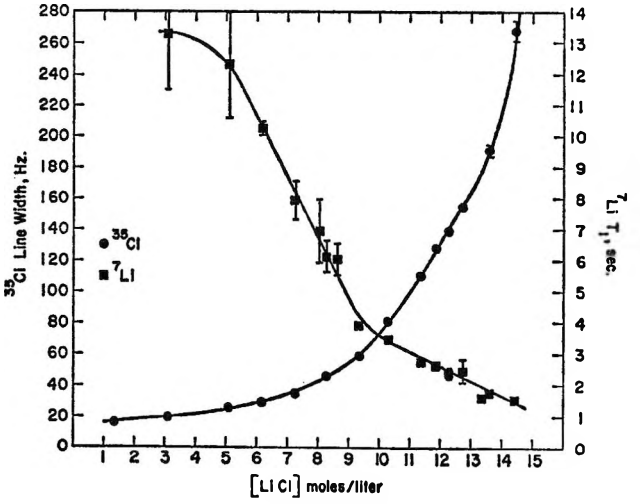


Figure 1. The ^{35}Cl line width and ^{7}Li longitudinal relaxation time *vs.* lithium chloride concentration.

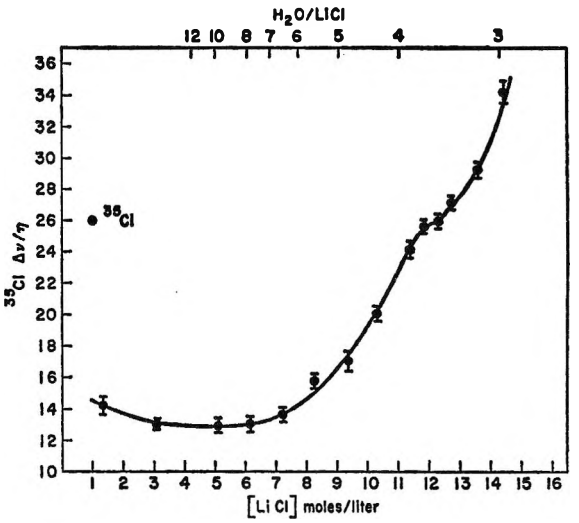


Figure 2. The ^{35}Cl line width divided by viscosity *vs.* lithium chloride concentration; the ratio of water molecules to lithium chloride molecules is indicated across the top.

Results and Discussion

The results of the $^{7}Li^{+}$ and $^{35}Cl^{-}$ measurements are presented in Figure 1. Although the changes in the slope of both plots in the region of 9 M are striking, interpretation is difficult since the data reflect changes in viscosity as well as changes in the electric environment of the nucleus observed.

The curves shown in Figures 2 and 3 represent the data in Figure 1 divided by the viscosity; the lithium T_1 data have been plotted as $1/T_1\eta$ so that it may be compared more directly with the chlorine line widths. The chloride plot reaches a minimum when the ratio of water molecules to lithium chloride molecules is approximately 12, and the curve shows a marked increase in slope at concentrations above which there are less than six water molecules per lithium chloride molecule. Because the $^{7}Li^{+}$ signal is weak at 4.3 MHz below

(6) A. Abragam, "The Principles of Nuclear Magnetism," The Clarendon Press, Oxford, 1961, p 314.

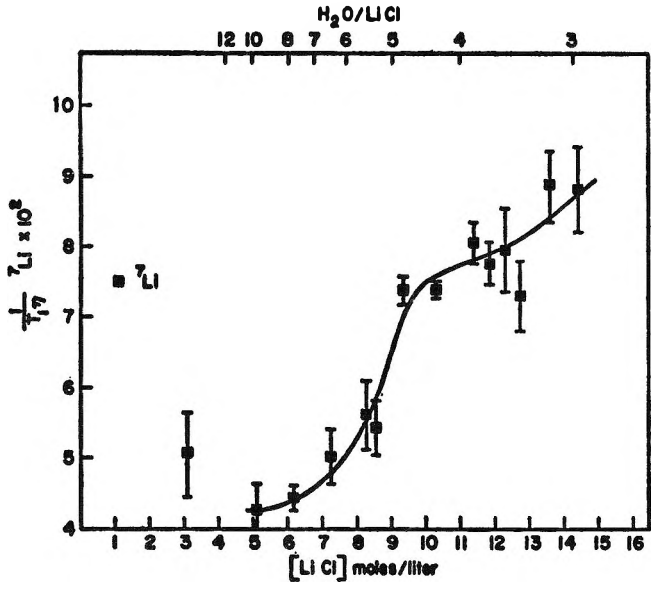


Figure 3. The reciprocal of the ^{7}Li longitudinal relaxation time divided by viscosity *vs.* lithium chloride concentration; the ratio of water molecules to lithium chloride molecules is indicated across the top.

concentrations of about 5 M, it is difficult to define the lithium $1/T_{1\eta}$ curve below this concentration. At approximately 8.5 M, however, there is a dramatic transition followed at higher concentrations by a region of almost zero slope. At concentrations above 13 M, where the water to lithium chloride ratio is less than 4, the slope again increases rapidly.

The general behavior of these curves suggests that the electrical environments of the nuclei observed experience significant changes at concentrations where the average number of water molecules available to associate with a lithium chloride molecule reaches critical values such as 12, 6, 5, or 4. That both resonances experience significant changes at concentrations where the water to lithium chloride ratio is less than 6 most likely indicates changes in the nature of ion pairing. The almost zero slope of the $1/T_{1\eta}$ curve between water to lithium chloride ratios of 5 and 4 suggests a primary coordination number for Li^+ of 4; however, such conclusions must be tempered with a realistic appraisal of the approximations involved.

To attribute the behavior of $1/T_{1\eta}$ or $\Delta\nu/\eta$ to changes in the environmental symmetry of a magnetic nucleus with a quadrupole moment is admittedly a very simplified interpretation of these results.[7] However, more detailed models for the relaxation mechanism of quadrupolar nuclei have drawn heavily on the asumption that the correlation time is linearly related to the viscosity and most measurements have confirmed this behavior.[8-10] Without making complex assumptions, these data imply that basic changes occur in lithium chloride solutions at high concentrations. While these measurements point to certain aspects of these changes, interpretation in terms of detailed ion-pairing schemes must be deferred until the solvent resonance data at these concentrations are more complete.

Acknowledgment. The author wishes to thank Professor John D. Baldeschwieler and the other members of his research group for very helpful discussions. Support of the National Institutes of Health under Grant GM 14752-02, the Center for Materials Research, Stanford University, and the National Science Foundation under Grant GP 4924x is gratefully acknowledged.

(7) Woesner, Snowden, and Ostroff[8] have shown that the dipole contribution to the $^7Li^+$ T_1 in aqueous solutions of lithium chloride is approximately equal to the quadrupole contribution. They have also shown that the quadrupole contribution dominates the shape of the curve $1/T_1$ *vs.* concentration. Therefore the treatment in terms of quadrupole relaxation is sufficient for this qualitative discussion.

(8) H. G. Hertz, *Z. Elektrochem.*, 65, 20 (1961).
(9) C. Deverell, D. J. Frost, and R. E. Richards, *Mol. Phys.*, 9, 565 (1965).
(10) K. A. Valiev and B. M. Khabibullin, *Russ. J. Phys. Chem.*, 35, 1118 (1961).

Diffusion of Alcohols and Amides in Water from 4 to 37° [1a]

by C. M. Gary-Bobo[1b] and Heather W. Weber

Biophysical Laboratory, Harvard Medical School, Boston, Massachusetts (*Received June 26, 1968*)

A large amount of data for the diffusion of small nonelectrolytes in water is scattered throughout the literature, but these data were obtained under such different conditions that their comparison is often difficult. Furthermore, there are very few data concerning diffusion in dilute solution that is pertinent to the diffusion and permeability measurements carried out today with radioactive tracers. The need for such a systematic study prompted our investigation. In the present work, the diffusion coefficients of a series of alcohols and amides were measured by the capillary-cell method designed by Wang and co-workers[2] using a modified technique described by Saraf, Witherspoon, and Cohen[3] and Witherspoon and Saraf.[4] The measurements were carried out at 4, 12.5, 24.8, and 37°. These temperatures were regulated within ±0.05. The solute concentration was fixed at 10^{-3} M (including ^{14}C-labeled and nonlabeled solute). The labeled solutes were obtained from New England Nuclear Corp., except *n*-butyramide and isobutyramide, which were obtained from International Chemical and Nuclear Corp.

(1) (a) This project was supported in part by the Atomic Energy Commission. (b) Laboratoire de Physiologie Cellulaire, Collège de France Paris Ve, France.
(2) G. H. Wang, *J. Amer. Chem. Soc.*, 73, 510, 4181 (1951); (b) J. H. Wang, C. V. Robinson, and I. S. Edelman, *ibid.*, 75, 466 (1953).
(3) D. N. Saraf, P. H. Witherspoon, and L. H. Cohen, *Science*, 144, 955 (1963).
(4) P. H. Witherspoon and D. N. Saraf, *J. Phys. Chem.*, 69, 3752 (1965).

Table I: Diffusion Coefficients of Alcohols

	$D \times 10^5$, cm²/sec ± S.E.			
	4°	12.5°	24.8°	37°
Methyl alcohol	0.80 ± 0.02	1.13 ± 0.03	1.70 ± 0.03	2.27 ± 0.04
Ethyl alcohol	0.67 ± 0.02	0.89 ± 0.03	1.26 ± 0.03	1.77 ± 0.03
n-Propyl alcohol	0.57 ± 0.02	0.76 ± 0.03	1.15 ± 0.04	1.56 ± 0.04
sec-Propyl alcohol	0.54 ± 0.02	0.73 ± 0.02	1.07 ± 0.03	1.52 ± 0.03
n-Butyl alcohol	0.51 ± 0.02	0.69 ± 0.02	1.00 ± 0.03	1.42 ± 0.05
t-Butyl alcohol	0.39 ± 0.02	0.60 ± 0.02	0.98 ± 0.02	1.31 ± 0.03

Table II: Diffusion Coefficients of Amides

	$D \times 10^5$, cm²/sec ± S.E.			
	4°	12.5°	24.8°	37°
Formamide	0.85 ± 0.02	1.17 ± 0.02	1.72 ± 0.03	2.20 ± 0.03
Acetamide	0.61 ± 0.02	0.83 ± 0.03	1.32 ± 0.03	1.75 ± 0.03
Propionamide	0.50 ± 0.02	0.73 ± 0.03	1.20 ± 0.03	1.60 ± 0.03
Butyramide	0.45 ± 0.02	0.65 ± 0.02	1.07 ± 0.03	1.45 ± 0.04
Isobutyramide	0.42 ± 0.02	0.63 ± 0.02	1.02 ± 0.04	1.41 ± 0.03

In the present experiment the major modification of Wang's original method is that no stirring takes place during the diffusion, in order to minimize the so called "Δl effect." Owing to the possible opposite error due to an unstirred layer effect in this condition, control experiments were carried out with THO at 5 and 24.8°. The diffusion coefficients obtained, respectively, $1.37 \pm 0.02 \times 10^{-5}$ and $2.41 \pm 0.03 \times 10^{-5}$, are in good agreement with the data reported by Wang[2b] for the same isotope.

The diffusion coefficients in cm²/sec ± S.E. are listed in Table I for alcohols and in Table II for amides. The results appear to be somewhat higher than those already reported in the literature.[5-7] These differences seem not to be attributable to the capillary cell method, but to the fact that a low solute concentration was used. With acetamide, measurements were carried out at 24.8° not only at 10^{-3} *M* but also between 0.1 and 1.0 *M*. The diffusion coefficients obtained in this range vary from 1.23×10^{-5} to 1.15×10^{-5}. They are in perfect agreement with the data obtained in the same concentration range by Christoffer and Kegeles[8] using the Gouy method. However, these authors, extrapolating their experimental results to zero concentration, obtained a diffusion coefficient $D = 1.249 \times 10^{-5}$ lower than our present value of 1.32×10^{-5} obtained at 10^{-3} *M*. This significant discrepancy would mean that the extrapolation to zero concentration of experimental data obtained above 0.1 *M* is not completely substantiated.

It appears that with respect to molecular volume, the amides, as a class, diffuse faster than the alcohols. One would expect the amides to be slower than the alcohols from the previous observations of Longsworth[6,7] and Gosting and coworkers.[9-11] However, Horowitz and Fenichel,[12] comparing the diffusion of a series of nonelectrolytes in formamide-swollen and water-swollen dextran gels, observed that in formamide the greater the number and strength of H bond formed by the solute with the solvent, the slower the diffusion; in water, the reverse is true. The authors, considering that the retardation effect of the solute–solvent H bonding must be operative in both solvents, assumed that in water the modification of the water structure by the solutes exercises a greater influence in the opposite direction. The present data, as well as the data obtained for the alkanes by Witherspoon and Saraf,[4] seem to give support to this assumption. Among these three series, the amides, which are strongly H bonded but appear to behave as "structure breakers," [13] diffuse faster than the alcohols which affect the water structure comparatively little, but seem to have an increasing structure promoting action with the increase of their hydrocarbon moiety.[14] The nonpolar alkanes, typically "structure-promoters," have the slowest diffusion.

It must be noted that in the temperature range investigated, there is no linear relationship between ln *D* and $1/T$ for the amides. For the alcohols a fairly good linear relationship is obtained only with ethanol and normal and *sec*-propanol. This brings additional evidence that a complex mechanism is operative in the diffusion of these nonelectrolytes in water.

(5) P. A. Johnson and A. L. Babb, *Chem. Rev.*, **56**, 387 (1956).
(6) L. G. Longsworth, *J. Amer. Chem. Soc.*, **75**, 5705 (1953).
(7) L. G. Longsworth, *J. Phys. Chem.*, **67**, 689 (1963).
(8) H. J. Christoffer and G. Kegeles, *J. Amer. Chem. Soc.*, **85**, 2562 (1963).
(9) L. J. Gosting and D. F. Akeley, *ibid.*, **74**, 2058 (1952).
(10) P. J. Dunlop and L. J. Gosting, *ibid.*, **75**, 5073 (1953).
(11) R. P. Wendt and L. J. Gosting, *J. Phys. Chem.*, **63**, 1287 (1959).
(12) S. B. Horowitz and I. R. Fenichel, *ibid.*, **68**, 3378 (1964).
(13) J. A. Rupley, *ibid.*, **68**, 2002 (1962).
(14) G. Wada and S. Umeda, *Bull. Soc. Chem. Jap.*, **35**, 646 (1962).

Adhesive Forces in Mixed Films of Cholesterol and Octadecyl Sulfate as Detected by Desorption

by M. Muramatsu[1] and N. L. Gershfeld

National Institute of Arthritis and Metabolic Diseases, U. S. Department of Health, Education, and Welfare, National Institutes of Health, Bethesda, Maryland 20014 *(Received June 27, 1968)*

The interaction between insoluble monolayers of cholesterol and soluble long-chain alkyl sulfates at the air–water interface has been studied by many investigators. Some have postulated the formation of a complex in the surface consisting of both components in definite molar ratios,[2–5] while others have argued against the likelihood of complex formation in the film.[6–8] Since monolayer desorption can provide information about the intermolecular forces in monolayers,[9–11] we have studied the kinetics of desorption of mixed films of sodium octadecyl sulfate (SOS) and cholesterol (COL), to test for the presence of interactions in the surface between the insoluble COL and the soluble SOS film molecules.

Experimental Section

The procedures were essentially the same as those described previously.[10–13] A Langmuir-type surface balance was used for measuring the surface pressure, π (dynes/cm), and the total film area, A_T (cm^2) of the surface layer occupied either by n moles of SOS or of the mixture of SOS and COL. The area was decreased manually with elapsing time, t, in order to maintain a constant π value. The surface potential of the monolayers, ΔV, was measured by a ^{226}RA electrode combined with an electrometer. The experiments were performed at 23.0 ± 0.1°.

The sample of SOS (mp 190–192°) was provided by Dr. V. Lamberti. Cholesterol was a pure sample of mp 148–148.5°. Each component and their equimolar mixture was spread from the solutions in a mixed solvent of benzene, isopropyl alcohol, and water (9:9:1 in volume ratio). To increase the precision of the measurements of film desorption (since SOS desorbs very rapidly at pH ≧3),[10] solutions of HCl at pH 2 were used as the subphase throughout. At this pH, the sulfate films appeared to be chemically stable since measured values of ΔV for 100% SOS films were in the range of −80 to −100 mV for values of π between 5 and 20 dyn/cm. These values of ΔV for SOS and pH 2 were similar to the values reported for SOS on 10^{-2} M NaCl, where SOS is considered to be highly ionized.[14] Moreover, ΔV remained sensibly constant (±15 mV) with time.

Results and Discussion

Figure 1 illustrates the A_T–t relationships for films of SOS and SOS + COL (spread as an equimolar mixture) at four different π values. For the SOS films alone, the linear portions of the desorption curves are considered to be due to the establishment of the steady state[10,15] in which k ($= -\mathrm{d} \ln A_T/dt$), the rate constant for film desorption, should obey the relation[9]

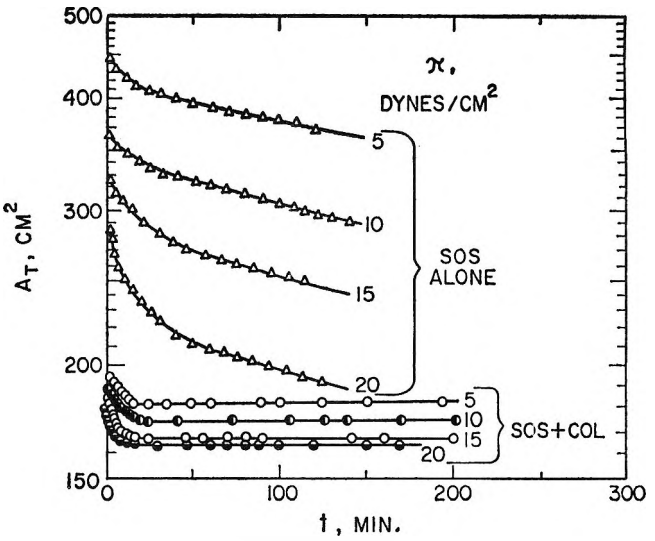


Figure 1. A_T *vs.* t relationships for SOS alone (triangles), and for SOS + COL equimolar mixture (circles), for total number of moles, $n = 10^{-7}$ film material added to surface at $t = 0$.

$$-\frac{\mathrm{d} \ln k}{\mathrm{d}\pi} = \frac{A}{RT} - C_s \qquad (1)$$

where A is the molar area, C_s is the compressibility of the film, R is the gas constant, and T is the temperature. This was indeed the case for the SOS system (triangles in Figure 1), in which $\mathrm{d} \ln k/\mathrm{d}\pi$ was found to be 0.11 cm/dyn; the values of 0.11–0.12 cm/dyn were obtained for $(A/RT - C_s)$ based on the π–A isotherm for SOS.[10] The time course of the curves for 100% SOS and the fact that eq 1 was obeyed indicate

(1) Visiting Scientist, NIH, 1967–1968, from Tokyo Metropolitan University Fukasawa-Cho, Setagaya-Ku Tokyo, Japan.

(2) (a) J. H. Schulman and A. H. Hughes, *Biochem. J.*, 29, 1243 (1935); (b) J. H. Schulman and E. K. Rideal, *Proc. Roy. Soc.*, B122, 29 (1937).

(3) R. Matalon, *J. Colloid Sci.*, 8, 53 (1953).

(4) E. D. Goddard and J. H. Schulman, *ibid.*, 8, 309, 323 (1953).

(5) D. G. Dervichian, "Surface Phenomena in Biology and Chemistry," J. F. Danielli, K. G. A. Pankhurst, and A. C Riddiford, Ed., Pergamon Press, New York, N. Y., 1958, p 80.

(6) E. Hutchinson, *J. Colloid Sci.*, 3, 413 (1948).

(7) F. M. Fowkes, *J. Phys. Chem.*, 65, 355 (1961).

(8) A. Matsubara, *Bull. Chem. Soc., Jap.*, 38, 1254 (1965).

(9) N. L. Gershfeld and C. S. Patlak, *J. Phys. Chem.*, 70, 286 (1966).

(10) N. L. Gershfeld in "Molecular Aggregation in Biological and Related Systems," Advances in Chemistry, Series, American Chemical Society, Washington, D. C., 1968.

(11) C. S. Patlak and N. L. Gershfeld, *J. Colloid Interface Sci.*, 25, 503 (1967).

(12) N. L. Gershfeld, "Proceedings of the IVth International Congress on Surface Active Substances," Vol. 2, Gordon & Breach, New York, N. Y., 1967, p 879.

(13) N. L. Gershfeld, *J. Phys. Chem.*, 66, 1923 (1962).

(14) J. Mingins and B. A. Pethica, *Trans. Faraday Soc.*, 59, 1892 (1963).

(15) L. Ter Minassian-Saraga, *J. Chim. Phys.*, 52, 181 (1955).

that the kinetics of desorption for SOS was diffusion controlled.[9-11]

In the mixed film, the kinetics of desorption for SOS should be unaffected by the presence of COL if no interactions between the two film components occur. However, the A_T–t relation for the mixed film system was unlike that for the 100% SOS monolayers in two major respects.

First, all the mixed films were characterized by an initial relatively rapid decrease in area. To compare the initial rate at which the area decreases for the pure and mixed SOS films, we used the function[15]

$$-\frac{d \ln A_T}{dt^{1/2}} = k_i \qquad (2)$$

where k_i is the rate constant in the initial stage of diffusion limited monolayer desorption. Estimates for k_i were obtained from the slopes of ln A_T–$t^{1/2}$ plots for the first 5 min of each of the curves in Figure 1. For example, k_i at $\pi = 10$ dyn/cm for 100% SOS was 0.012 $min^{-1/2}$, while the value for the mixed film was 0.036 $min^{-1/2}$. It should be noted that the latter value must be corrected for the initial 50% molar dilution of SOS in the surface.[16] At $t \leq 5$ min the correction factor will be about 2, and hence the apparent value of k_i for SOS in the mixed film becomes 0.072 $min^{-1/2}$, about sixfold greater than the value for the 100% SOS film. Approximately the same relative increase in k_i was observed for each mixed film at the other surface pressures.

The second major difference in the mixed film behavior was that the initial rapid decrease in area was followed by a period in which A_T was constant with time. Where SOS desorption should have been in the steady state (Figure 1), the mixed film was stable.

An estimate of the composition of the stable mixed film may be obtained by calculating the surface concentration of COL (assuming no loss of COL from the surface) from the final value of A_T and the amount of COL added initially. These values, at four surface pressures, are shown in Table I. column 3. For comparison the surface concentration of 100% COL films at the same values of π are shown in column 2 of Table I.

Table I: Surface Concentrations of Cholesterol, and Surface Potential ΔV, at Various Surface Pressures, π

(1)	(2)	(3)	(4)	(5)	(6)
	A^{-1}, mol/cm² × 10^{10}		ΔV, mV		
π, dyn/cm	COL (100%)	COL + SOS[a,b]	COL (100%)	COL[b] + SOS	$\Delta(\Delta V)$, mV (col 4 − col 5)
5	4.42	2.78	390	210	180
10	4.48	2.90	400	180	220
15	4.54	3.00	400	180	220
20	4.60	3.08	400	180	220

[a] Obtained from the horizontal portions of the curves in Figure 1. [b] Spreading solution contains an equimolar mixture of SOS and COL.

These values were obtained from the π–A isotherm of the pure COL film. The surface concentration of COL in the nondesorbing mixed film is about 35% lower than for the pure films of COL. We must conclude, therefore, that along with COL an additional component must still be in the film, namely SOS.

In support of this conclusion were the results of the ΔV measurements also given in Table I. ΔV values for 100% films of SOS are between −80 and −100 mV. Column 4 gives the surface potential for pure cholesterol films, while column 5 gives the values of ΔV obtained for the mixed film from which no desorption occurred. The decrease in ΔV of ~200 mV from the value for the pure cholesterol film (column 6) is consistent with the conclusion that a significant amount of SOS is present along with COL in the surface.[4]

The A_T–t results for the mixed film appear to be paradoxical. In the initial stages of the mixed film experiment SOS appears to desorb much more rapidly than from pure SOS films, while in the latter stages of the experiment SOS desorption is prevented. Perhaps the initial decrease in area for the SOS–COL system is due, in addition to desorption, to other mechanisms which can lead to contraction of the film such as a decrease in partial molecular areas or a rearrangement of the molecular packing. No quantitative assessment of these factors is possible without an independent measure of the mole fractions of each component in the surface.

However, whatever the stoichiometry of the SOS + COL system may be, the results indicate that adhesive forces do exist between COL and SOS, which are of sufficient magnitude to prevent desorption of SOS. This precludes consideration of this system as an ideal surface solution.[7] Whether this constitutes an example of molecular complex formation cannot be decided until additional evidence of the colligative properties of the system can be obtained.

(16) The actual correction factor is $1 + (n_{COL}\,\sigma_{COL})/(n_{SOS}\,\sigma_{SOS})$ where n refers to the number of moles (or molecules) per unit area of each film species at time t, and σ to the corresponding partial molar (or molecular) area.[12]

Kinetics of Hot Hydrogen Atoms from H_2S Photodissociation at 1850 Å[1a]

by L. E. Compton, J. L. Gole,[1b] and R. M. Martin

Department of Chemistry, University of California, Santa Barbara, California *(Received August 1, 1968)*

The H_2S 2000-Å vapor band shown in Figure 1 consists of a diffuse vibrational progression. This transi-

(1) (a) This work was supported in part by the Sulphur Institute and in part by the National Science Foundation under Grant GP-5834. (b) NSF Undergraduate Research Participant, Summer, 1967.

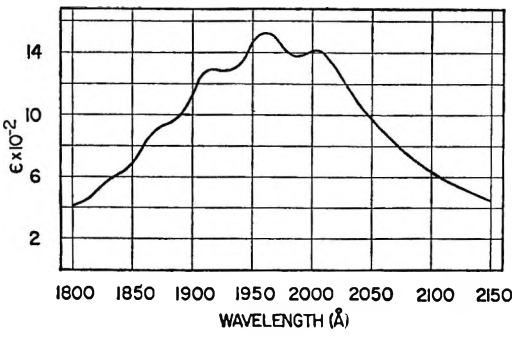


Figure 1. Absorption spectrum of H_2S at 25°.
Units for ϵ: l. mol^{-1} cm^{-1}.

tion has been qualitatively described as due to $4s_s \leftarrow 3p_s$ orbital excitation, and the vibrational intervals appear to be due to predominant excitation of the bending vibration.[2a] Gann and Dubrin[2b] have studied the photodissociation of H_2S at 2138 Å, which is in the continuous region before the first vibrational peak at 2000 Å, and by a comparison of hot hydrogen atom reaction yields they have shown that most of the excess energy of photochemical dissociation at 2138 Å appears as kinetic energy of separation of H and SH rather than internal energy of the SH radical. We have used the kinetic method to determine the average hydrogen atom energy from the photodissociation of H_2S at 1850 Å, which is between the fourth and fifth vibrational peaks of the 2000-Å band.

$HBr–C_4D_{10}$ and $H_2S–C_4D_{10}$ mixtures were irradiated with a low-pressure mercury lamp over a range of relative concentrations, and the resulting H_2/HD product ratio was plotted as a function of the HBr/C_4D_{10} or H_2S/C_4D_{10} reactant ratio, as shown in Figure 2. As has been observed previously for HI, HBr, and DBr photochemical hot atom systems,[3,4] the product ratio increases linearly with reactant ratio and positive intercepts are obtained when the line is extrapolated to a reactant ratio of zero. Reactants were prepared on a mercury-free vacuum line and pressures measured

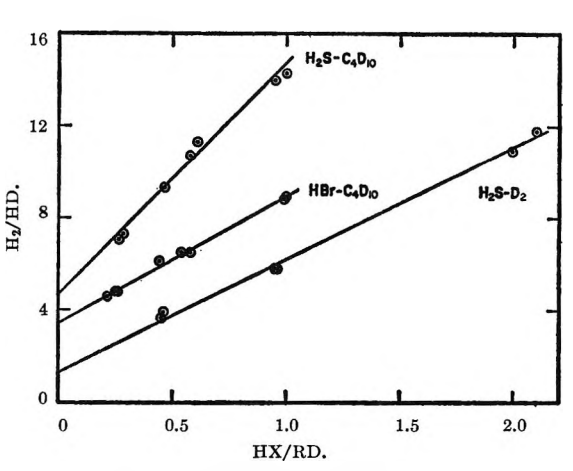


Figure 2. Product ratios as a function of reactant ratios for the 1849-Å photolysis of HX–RD mixtures at 25°.

with a Wallace and Tiernan FA 141 diaphragm gauge. Products were analyzed with a CEC 620 mass spectrometer calibrated with standard mixtures of the same composition range as the product mixtures. The H_2S spectrum in Figure 1 was taken on a Cary 15 spectrophotometer purged with nitrogen gas. The indicated extinction coefficients are the average of three determinations, which gave an average deviation ranging from 3.3% at 1800 Å to a minimum of 0.7% at 2000 Å.

The results of the 1850-Å photolyses are compared with those of Gann and Dubrin in Figure 3. The intercept I is interpreted as the H_2/HD ratio under conditions where C_4D_{10} is the only significant reactant for hot atoms above the $H + C_4D_{10}$ abstraction threshold energy, and the HBr or H_2S function as hot atom sources and as scavengers for atoms which are moderated below the $H + C_4D_{10}$ abstraction threshold energy. Therefore $(I + 1)^{-1} = HD/(H_2 + HD)$ indicates the fraction of the atoms which react to form HD before they are moderated below the threshold energy for abstraction with C_4D_{10}.[5] The ordinate of Figure 3 should go to zero at a threshold energy of

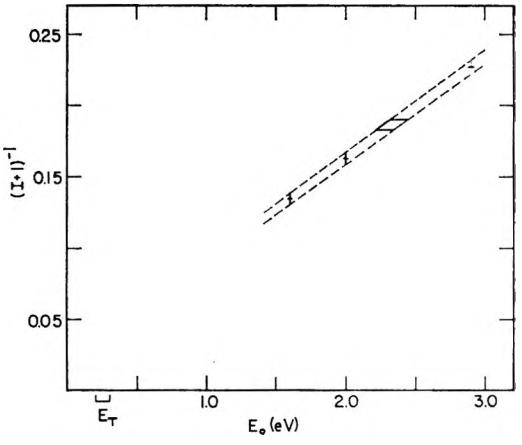


Figure 3. Abstraction probability $(I + 1)^{-1}$ for reaction with C_4D_{10} as a function of initial H atom energy. The values at 1.6 and 2.0 eV are those of ref 2b. The parallelogram indicates the range of average initial H atom energy from the photolysis of H_2S at 1850 Å, bracketed by the uncertainty in $(I + 1)^{-1}$ for H_2S and for HBr photolyzed at various wavelengths. $(I + 1)^{-1}$ will go to zero at the threshold energy E_T which is expected to be within the indicated range.

(2) (a) S. D. Thompson, D. G. Carroll, F. Watson, M. O'Donnell, and S. P. McGlynn, *J. Chem. Phys.*, **45**, 1367 (1966); (b) R. G. Gann and J. Dubrin, *ibid.*, **47**, 1867 (1967).

(3) R. L. Carter, W. H. Hamill, and R. R. Williams, *J. Amer. Chem. Soc.*, **77**, 6457 (1955).

(4) R. M. Martin and J. E. Willard, *J. Chem. Phys.*, **40**, 3007 (1964).

(5) Gann and Dubrin found that within experimental error $(I_0 + 1)^{-1}$ for H_2S was unaffected by substitution of HBr as the scavenger. However, at our higher energies some substitution, $H^* + C_4D_{10} \rightarrow C_4D_9H + D$, may occur; see C. C. Chou and F. S. Rowland, *J. Amer. Chem. Soc.*, **88**, 2612 (1966). The occurence of substitution rather than abstraction by the D atom with the scavenger could lead to error in the calibration curve at 2.9 eV. Based upon private communications with F. S. Rowland and D. R. Davis on abstraction/substitution ratios of hot and thermal H atoms, we estimate the possible error due to these effects to be less than 3%.

0.25–0.35 eV.[6] It is believed that only some 2% or less of the HBr photodissociations in the ultraviolet continuum yield $^2P_{1/2}$ Br atoms.[7] Such transitions will result in a lowering of the H atom recoil energy by about 0.45 eV. The predominant transition to ground-state Br atoms should give the H atom energies indicated in Figure 3 for the various wavelengths used. The three hot atom abstraction yields at 1.6, 2.0, and 2.9 eV using HBr as the source are consistent and indicate that the present data in this region are best represented as a linear increase of yield with initial energy. The observed H_2S–C_4D_{10} system ordinate of 0.18 then corresponds to an H atom energy of 2.3 ± 0.1 eV. The range of reported values of the H–SH bond dissociation energy is 4.1–3.7 eV,[8] giving 2.6–3.0 eV as the range of excess energy in the photochemical dissociation at 1850 Å. Therefore an average of at least 75% of the excess energy appears as kinetic energy of separation at 1850 Å. This indicates that the energy partitioning is similar at 1850 and 2138 Å despite the difference in initial vibrational state indicated spectroscopically, as Gann and Dubrin found that 80% or more of the excess energy goes to the H atom at the latter wavelength. A further conclusion of these results is that even at the high energy end of the 2000-Å band the main photodissociation process is $H_2S \rightarrow H + HS$ rather than $H_2S \rightarrow H_2 + S$. The upper limit on the occurrence of the latter process which is consistent with our results is a quantum yield of about 0.25, corresponding to a quantum yield of 0.75 for hot atom production with all of the excess energy going to kinetic energy of separation. We have determined the quantum yield for H_2 from H_2S at 1850 Å as 1.0 ± 0.1, but this does not distinguish between hydrogen atom and hydrogen molecule production in the primary process, since the fates of H and HS are expected to be $H + H_2S \rightarrow H_2 + HS$ and $HS + HS \rightarrow H_2S + S$.[9]

We have also studied the photolysis of H_2S–D_2 mixtures at 1850 Å, and a comparison of the present H_2S and HBr data with previous HBr data is presented in Table I. All of the systems in Table I have been found to follow the linear behavior $H_2/HD = A(HX/RD) + I$, where HX is either HBr or H_2S, over a wide range of (HX/RD). The second column of the table gives the reciprocal of the slope. With the reservations cited previously,[4,5] A^{-1} may be taken as an approximate measure of the average relative abstraction cross section ratio $\langle S_{RD}/S_{HX} \rangle$ over the relative energy distribution present in the system. Taking the ratio of the A^{-1} values for the HBr–D_2/HBr–C_4D_{10} systems and the H_2S–D_2/H_2S–C_4D_{10} systems gives values of $\langle S_{D_2}/S_{C_4D_{10}} \rangle$ of 2.7 and 2.0 where the initial hot atom energies are approximately 2.9 and 2.3 eV, respectively.

Table I: Hot Hydrogen Atom Kinetic Data for D Abstraction from Deuterated Reactants

System[a]	$(I + 1)^{-1}$	A^{-1}
HBr–D_2[b,c]	0.61	0.49
HBr–C_4D_{10}	0.23	0.18
HBr–C_2D_6[b]	0.14	0.085
HBr–CD_4[b]	0.062	0.012
H_2S–D_2[c]	0.43	0.20
H_2S–C_4D_{10}	0.18	0.10

[a] Data for photolysis at 1850 Å. [b] Data from ref 4. [c] Intercepts and slopes have been multiplied by 2 to correct for the HD assumed to be produced thermally from reaction with HBr or H_2S following the hot atom abstraction producing D.

It is interesting that the complex dynamics of monoenergetic atoms introduced into a thermal gas leads to the linear product dependence on reactant ratio which has now been observed with a variety of systems and initial energies. Further interpretation of such hot atom kinetics and the extraction of more definitive information on reaction cross section behavior above threshold requires more kinetic data than are presently available and the application of nonreactive cross section functions and statistical theory to describe the observed kinetics.

(6) B. A. Thrush, *Progr. Reaction Kinetics*, 3, 89 (1965).
(7) R. S. Mulliken, *J. Chem. Phys.*, 8, 382 (1940).
(8) T. L. Cottrell, "The Strengths of Chemical Bonds," Academic Press, London, 1958.
(9) D. deB. Darwent, R. L. Wadlinger, and M. J. Allard, *J. Phys. Chem.*, 71, 2346 (1967).

Activity Coefficients for Ionic Melts

by R. Haase

Institut für Physikalische Chemie, Rheinisch-Westfälische Technische Hochschule, Aachen, Germany *(Received August 26, 1968)*

While the definitions of activity coefficients for both nonelectrolyte solutions and electrolyte solutions are straightforward and well known, the situation with ionic melts is less clear and less well understood. It is true that most authors[1] proceed in the same way as they do with nonelectrolyte solutions, but it is by no means evident whether this is the adequate scheme of description. As a matter of fact, it will be shown that it is expedient to introduce activity coefficients for ionic melts that are different from those in nonelectrolyte and electrolyte solutions.

For simplicity's sake, we shall restrict the discussion to binary ionic melts such as the systems NaCl + KCl or $PbCl_2$ + $PbBr_2$. Reciprocal salt pairs of the type NaCl + KBr may also be treated as binary systems

(1) See, for example, H. Bloom, "The Chemistry of Molten Salts," W. A. Benjamin, Inc., New York, N. Y., 1967.

provided we either exclude heterogeneous equilibria or we consider the melt in equilibrium with a pure (*e.g.*, solid) phase.

The macroscopic description of any binary liquid mixture starts from the *chemical potentials* μ_1 and μ_2 of the two substances (denoted as components 1 and 2) as functions of thermodynamic temperature T, pressure P, and composition.

The *activity* a_1 or a_2 of component 1 or 2 is defined by

$$\ln a_i \equiv \frac{\mu_i - \mu_{0i}}{RT} \qquad (i = 1, 2) \tag{1}$$

where R is the gas constant and μ_{0i} the chemical potential of the pure liquid component i at the same values of T and P. Experimental values of the activities a_1 and a_2 are usually derived from vapor pressure measurements or electromotive force data.

The *macroscopic composition* of the ionic melt is described by the stoichiometric mole fraction x_1 or x_2 of component 1 or 2 ($x_1 + x_2 = 1$). We put $x \equiv x_2$, $1 - x \equiv x_1$, choosing x as the independent composition variable. Thus μ_1 and μ_2 or a_1 and a_2 may be considered to be functions of T, P, and x.

The *microscopic composition* of the melt is given by the true mole fractions x_j of all the species j actually present in the liquid. Let the subscript a refer to ions contained in component 1 only, the subscript b to ions common to both components, and the subscript c to ions occurring in component 2 only. Then the true mole fractions x_a, x_b, and x_c of the ionic species may, in principle, be expressed in terms of the independent mole fraction x. But these expressions are simple only for complete dissociation and absence of ionic complexes.

We denote the number of ions of kind a or b produced by one molecule of component 1 by ν_a or ν_b, respectively, and the number of ions of kind b or c produced by one molecule of component 2 by ν_b' or ν_c, respectively. We use the abbreviations

$$r_b \equiv \frac{\nu_b'}{\nu_b}; \qquad \nu_1 \equiv \sum_a \nu_a + \sum_b \nu_b;$$
$$\nu_2 \equiv \sum_b \nu_b' + \sum_c \nu_c \tag{2}$$

and write for the limiting values of the true mole fractions of the ionic species in the pure liquid components

$$x_a^0 \equiv \lim_{x\to 0} x_a; \qquad x_b^0 \equiv \lim_{x\to 0} x_b;$$
$$x_b^{0\prime} \equiv \lim_{x\to 1} x_b; \qquad x_c^0 \equiv \lim_{x\to 1} x_c \tag{3}$$

Then there follows, if we assume complete dissociation and ignore ionic complexes

$$\frac{x_a}{x_a^0} = \frac{\nu_1(1-x)}{\nu_1 + (\nu_2 - \nu_1)x}; \tag{4a}$$

$$\frac{x_b}{x_b^0} = \frac{\nu_1[1 + (r_b - 1)x]}{\nu_1 + (\nu_2 - \nu_1)x}$$

$$\frac{x_b}{x_b^{0\prime}} = \frac{\nu_2}{r_b \nu_1} \frac{1 + (r_b - 1)x}{\nu_1 + (\nu_2 - \nu_1)x}; \tag{4b}$$

$$\frac{x_c}{x_c^0} = \frac{\nu_2 x}{\nu_1 + (\nu_2 - \nu_1)x}$$

These relations will be used later. We first continue to give some perfectly general formula.

The chemical potentials μ_1 and μ_2 of components 1 and 2 are related to the chemical potentials μ_a, μ_b, μ_c of the ionic species a, b, c by the equations

$$\mu_1 = \sum_a \nu_a \mu_a + \sum_b \nu_b \mu_b;$$
$$\mu_2 = \sum_b \nu_b' \mu_b + \sum_c \nu_c \mu_c \tag{5}$$

For the limiting values of the chemical potentials of the ionic species in the pure liquid components we introduce a notation analogous to that in (3)

$$\mu_a^0 \equiv \lim_{x\to 0} \mu_a; \qquad \mu_b^0 \equiv \lim_{x\to 0} \mu_b;$$
$$\mu_b^{0\prime} \equiv \lim_{x\to 1} \mu_b; \qquad \mu_c^0 \equiv \lim_{x\to 1} \mu_c \tag{6}$$

Bearing in mind the definition of μ_{01} and μ_{02} we derive from (1), (5), and (6)

$$RT \ln a_1 = \sum_a \nu_a(\mu_a - \mu_a^0) + \sum_b \nu_b(\mu_b - \mu_b^0) \tag{7a}$$

$$RT \ln a_2 = \sum_b \nu_b'(\mu_b - \mu_b^{0\prime}) + \sum_c \nu_c(\mu_c - \mu_c^0) \tag{7b}$$

In addition to this, there is the general condition

$$(1 - x)\left(\frac{\partial \ln a_1}{\partial x}\right)_{T,P} + x\left(\frac{\partial \ln a_2}{\partial x}\right)_{T,P} = 0 \tag{8}$$

following from the Gibbs–Duhem relation.

We now introduce a standard type of ionic melts in a similar way as one usually does in the case of nonelectrolyte solutions, but we take account of the fact that the primary units are the ionic and molecular species actually present in the melt. Writing for the chemical potential μ_j of any species j in the whole composition range

$$\mu_j = \mu_{0j} + RT \ln x_j \tag{9}$$

we define an *ideal ionic melt*. This is the natural ex-

tension of the concept of an "ideal mixture" to ionic melts. It should be stressed that μ_{0j} is the chemical potential of the hypothetical pure liquid species j at the given values of T and P. Thus we have in particular

$$\mu_a = \mu_{0a} + RT \ln x_a; \qquad \mu_b = \mu_{0b} + RT \ln x_b; \qquad \mu_c = \mu_{0c} + RT \ln x_c \tag{10}$$

where

$$\mu_{0a} \equiv \lim_{x_a \to 1} \mu_a; \qquad \mu_{0b} \equiv \lim_{x_b \to 1} \mu_b; \qquad \mu_{0c} \equiv \lim_{x_c \to 1} \mu_c \tag{11}$$

in contrast to expressions 6.

We derive from (3), (6), (10), and (11)

$$\mu_a^0 = \mu_{0a} + RT \ln x_a^0; \qquad \mu_b^0 = \mu_{0b} + RT \ln x_b^0 \tag{12a}$$

$$\mu_b^{0'} = \mu_{0b} + RT \ln x_b^{0'}; \qquad \mu_c^0 = \mu_{0c} + RT \ln x_c^0 \tag{12b}$$

Inserting (10) and (12) into (7), we find

$$\ln a_1 = \sum_a \nu_a \ln \frac{x_a}{x_a^0} + \sum_b \nu_b \ln \frac{x_b}{x_b^0} \tag{13a}$$

$$\ln a_2 = \sum_b \nu_b' \ln \frac{x_b}{x_b^{0'}} + \sum_c \nu_c \ln \frac{x_c}{x_c^0} \tag{13b}$$

all these relations holding for ideal ionic melts.

Now a standard type of ionic melt, as a reference system for actual melts, is useful only if the activities a_1 and a_2 can be given *explicitly* in terms of the independent variables T, P, and x. Therefore, we decided to choose the *completely dissociated ideal melt* as our reference system since here, in view of (4), the true mole fractions can be expressed as functions of x. We repeat that, in deriving (4), we assumed both complete dissociation and absence of ionic complexes. Introducing the abbreviations

$$\nu_0 \equiv \sum_a \nu_a; \qquad \nu \equiv \sum_c \nu_c \tag{14}$$

we obtain from (4) and (13)

$$a_1 = a_1^{\mathrm{id}}; \qquad a_2 = a_2^{\mathrm{id}} \tag{15}$$

the functions a_1^{id} and a_2^{id} being defined by

$$\ln a_1^{\mathrm{id}} \equiv \nu_1 \ln \nu_1 + \nu_0 \ln(1 - x) - \nu_1 \ln [\nu_1 + (\nu_2 - \nu_1)x] + \sum_b \nu_b \ln[1 + (r_b - 1)x] \tag{16a}$$

$$\ln a_2^{\mathrm{id}} \equiv \nu_2 \ln \nu_2 - \sum_b \nu_b' \ln r_b + \nu \ln x - \nu_2 \ln[\nu_1 + (\nu_2 - \nu_1)x] + \sum_b \nu_b' \ln[1 + (r_b - 1)x] \tag{16b}$$

Thus a_1^{id} and a_2^{id} are the activities of components 1 and 2 in a completely dissociated ideal melt. They only depend on x and no longer on T and P. The condition following from (8)

$$(1 - x) \frac{\mathrm{d} \ln a_1^{\mathrm{id}}}{\mathrm{d}x} + x \frac{\mathrm{d} \ln a_2^{\mathrm{id}}}{\mathrm{d}x} = 0 \tag{17}$$

can be shown to be valid for expressions 16.

We accordingly define the *activity coefficients* f_1 and f_2 of components 1 and 2 in any ionic melt by

$$f_i \equiv a_i / a_i^{\mathrm{id}} \qquad (i = 1, 2) \tag{18}$$

The quantities f_1 and f_2 are functions of T, P, and x. They measure the deviations from the behavior of a completely dissociated ideal melt. If $f_i \neq 1$ the melt is either ideal with incomplete dissociation or nonideal with any degrees of dissociation.

From (8) and (17) we find

$$(1 - x) \left(\frac{\partial \ln f_1}{\partial x} \right)_{T,P} + x \left(\frac{\partial \ln f_2}{\partial x} \right)_{T,P} = 0 \tag{19}$$

Furthermore, we have according to (1), (16), and (18)

$$\lim_{x \to 0} f_1 = 1; \qquad \lim_{x \to 1} f_2 = 1 \tag{20}$$

The relations (19) and (20) are analogous to those for nonelectrolyte solutions.

The usual definition[1] of "activity coefficients" γ_1 and γ_2

$$\gamma_1 \equiv a_1/1 - x; \qquad \gamma_2 \equiv a_2/x$$

only coincides with our convention (18) for simple cases such as NaCl + KCl or $K_2CO_3 + K_2SO_4$.

There are three main reasons for using f_1 and f_2 instead of γ_1 and γ_2.

(1) The procedure of fixing a reference system is analogous to that already known from "associated ideal mixtures" in the case of nonelectrolyte solutions.

(2) Complicated ionic melts often can be described to a first approximation by $f_i = 1$ but not by $\gamma_i = 1$ $(i = 1, 2)$. Thus the melting point diagram of $AgNO_3$ (1) + K_2SO_4 (2) seems to indicate[2] that this system is nearly a completely dissociated ideal melt since the relations resulting from (15) and (16)

$$\ln a_1 = 2 \ln \frac{2(1 - x)}{2 + x}; \qquad \ln a_2 = 3 \ln \frac{3x}{2 + x}$$

are fulfilled to a good degree of approximation within a considerable range of compositions (pure silver nitrate being the solid phase).

(2) Y. Doucet, "Les aspects modernes de la cryométrie," Mém. Sciences Phys., Fascicule LIX, Gauthier-Villars, Paris, 1954.

(3) Series expansions of $\ln f_1$ and $\ln f_2$ in powers of x, the simplest case of which is

$$\ln f_1 = Bx^2; \qquad \ln f_2 = B(1 - x)^2 \qquad (21)$$

where B depends on T and P, are correct only for f_1 and f_2 but not for γ_1 and γ_2 (unless f_i coincides with γ_i). This is due to the fact that the proper form of the limiting laws for infinite dilution[3,4] results from an expansion such as (21) and this implies logarithmic terms for the functions $\ln \gamma_1$ and $\ln \gamma_2$ in general. More details have been given elsewhere.[5]

(3) R. Haase, Comptes rendus de la 2e Reunion Chimie Physique, Paris, 1952, p 131.

(4) R. Haase, "Thermodynamik der Mischphasen," Springer, Berlin–Göttingen–Heidelberg, 1956.

(5) R. Haase, *Z. Phys. Chem.* (Frankfurt am Main) **63**, 95 (1969).

Determination of Water Activities of Dilute Electrolyte Solutions

by S. Amdur

Israel Atomic Energy Commission, Soreq Nuclear Research Centre, Yavne, Israel *(Received October 3, 1968)*

The problem of integrating the McKay–Perring equation for ternary systems using isopiestic measurements has recently been under consideration.[1] Difficulties arise especially in the range of very dilute solutions, *i.e.*, less than 0.1 *m* where measurements are not available. Therefore, a method of water activity determination in this range is suggested.

The method is an osmometric one; the rate of water vapor adsorption by a drop of solution in a solvent atmosphere is determined potentiometrically.[2,3] Generally speaking, this procedure may not be considered better than the usual isopiestic method; however, it was found to be relatively fast and to increase the range of measurements down to 0.02 *m*.

Measurements were taken using an isothermal molecular weight apparatus[4] which contains a dc Wheatstone bridge and a null detector. Two branches of the bridge are glass covered thermistors of 100,000 ohms resistance each; a rheostat is connected in series with one of them. The thermistors are located in a glass container containing the solvent. The entire apparatus is enclosed in a thermostat maintained at 25°. The original instrument was improved in two ways: the thermostat was adjusted to control the temperature to within ±0.001°, and the original syringes were replaced by micrometer syringes permitting control of the volume of a drop to within ±1%.

The procedure is as follows. A drop of water is deposited on one thermistor and a drop of fixed volume of solution is deposited on the other thermistor. Due to the absorption of water vapor by the solution, there is an increase in temperature and decrease in resistance of the solution-bearing thermistor. This decrease in resistance is balanced with the rheostat (range of 0–1100 ohms and accuracy of ±0.1 ohm); a measured ΔR is obtained. The temperature increases with time and after several minutes reaches a plateau. This condition remains constant for a relatively long time (over 10 min) in the range of molalities measured, ΔR is read at this stage, and no extrapolation is done to zero time.

An equilibrium of heat content of the drop is assumed to be at the plateau condition at which the heat absorption is assumed to be

$$\frac{dQ_a}{dt} = k_1 S(p_0 - p) \qquad (1)$$

where k_1 is a constant, S is the surface area of the drop, p_0 is the vapor pressure of the solvent, and p is the vapor pressure of the solution. The rate of heat dissipation is assumed to be

$$\frac{dQ_d}{dt} = k_2(T - T_0) \qquad (2)$$

Table I: Water Activities and ΔR Values for KCl and NaCl Solutions

Molality	ΔR	a_w, standard	$a_w{}^a$	$\%\Delta^a$	$a_w{}^b$	$\%\Delta^b$
0.02075 KCl	16.7	0.99928	0.99935	+0.007	0.99926	−0.002
0.04026 NaCl	29.9	0.99863	0.99869	0.006	0.99867	0.003
0.06070 KCl	45.7	0.99795	0.99790	−0.005	0.99793	−0.002
0.07929 NaCl	58.5	0.99735	0.99726	−0.009	0.99732	−0.003
0.09956 KCl	70.5	0.99666	0.99666	0	0.99673	+0.007
0.15639 NaCl	108.4	0.99484	0.99476	−0.008	0.99479	−0.005
0.20402 KCl	137.0	0.99323	0.99333	0.010	0.99325	+0 002

[a] Calcd from eq 8. [b] Calcd from eq 9.

(1) C. Pan, *J. Phys. Chem.*, 72, 2548 (1968).

(2) A. P. Brady, H. Huff, and J. W. McBain, *J. Phys. Colloid Chem.*, 55, 304 (1951).

(3) E. E. Schrier, *J. Chem. Educ.*, 45, 176 (1968).

(4) Manufactured by Arthur H. Thomas Co., Philadelphia, Pa.

where k_2 is a constant, T is the temperature of the drop, and T_0 is the bath temperature. At the plateau

$$k_1S(p_0 - p) = k_2(T - T_0) \quad (3)$$

The termistors' resistance decreases exponentially with temperature, so, for a narrow range it may be assumed that

$$R = R_0e^{-k_3(T-T_0)} \quad (4)$$

where R and R_0 are the resistance of the thermistor at T and T_0, respectively, and k_3 is a constant. This equation leads directly to the logarithmic form

$$\ln (1 - \Delta R/R_0) = -k_3(T - T_0) \quad (5)$$

By combining eq 3 and 5 one gets

$$\ln (1 - \Delta R/R_0) = k_4(a_w - 1) \quad (6)$$

where

$$k_4 = k_1k_3p_0S/k_2$$

Expanding the logarithmic term into a series will result in a polynomial form

$$a_w = A_1 + A_2\Delta R + A_3(\Delta R)^2 + \cdots \quad (7)$$

$$A_1 = 1; \quad A_2 = -1/k_4R_0; \quad A_3 = -1/2k_4R_0^2$$

Measurements were taken on solutions of KCl and NaCl. Standard water activities as a function of solution concentration were calculated by interpolation from the tables of Robinson and Stokes[5] using a computer program. By the method of least squares the following expressions were obtained for a_w as a function of ΔR

$$a_w = 1.000186 - 0.500564 \times 10^{-4}\Delta R \quad (8)$$

$$a_w = 0.999996 - 0.431769 \times 10^{-4}\Delta R - 0.444668 \times 10^{-7}(\Delta R)^2 \quad (9)$$

For each ΔR, a_w values were calculated according to eq 8 and 9, and the deviations, in per cent (% Δ), of the calculated from the standard water activities were computed. The results are tabulated in Table I.

The permitted error of $\pm 0.15\%$ in molality demanded in isopiestic measurements is equivalent to an error (% Δ) of $\pm 0.0045\%$ in water activity in dilute solutions. The scattering reported largely falls within this range. It is evident that eq 9 is adequate describing the results by average deviation of $\pm 0.0034\%$ Δ which is lower than the isopiestic limit of error. The ratio of A_2/A_3 according to eq 9 is 10^3 instead of the theoretic value of 2×10^5 (R_0 is equal to 10^5 ohms). However, the method is useful no matter if the theory is exact or not.

Experiments with solutions of up to 0.6 m KCl and NaCl show larger Δa_w values. At higher molalities the plateau was not obtained.

The osmometric method may be used together with the isopiestic one in dilute solutions of <0.2 and permits extension of the measurements range down to 0.02 m. As a result the accuracy of graphical extrapolations to pure solvents may also be improved.[1]

(5) R. A. Robinson and R. M. Stokes, "Electrolyte Solutions," Butterworth and Co. Ltd., London, 2nd ed, 1965, pp 476, 481.

Negative Partial Molal Volumes in the Critical Region. Mixtures of Ethylene and Vinyl Chloride

by Paul Ehrlich[1] and Robert H. Fariss

Central Research Department, Monsanto Company, St. Louis, Missouri 63166 *(Received October 8, 1968)*

The qualitative features of binary phase equilibria at temperatures just above the critical temperature of one component and well below that of the other have been described[2a] and the nature of the critical locus in such systems has been reviewed recently.[2b] In mixtures of ethylene with polar compounds of low molecular weight one can observe regions of retrograde condensation and critical pressures of the mixture which are greatly in excess of those of either component.[3,4] When one component is a high polymer[5,6] the asymmetry of the phase diagrams can become extreme, even in nonpolar systems.

Elgin and Chappelear[4] observed that in mixtures of chlorotrifluoromethane with liquids the mean molar volume of the liquid phase showed minima near the critical composition and that the partial molal volume of the less volatile component became negative at temperatures slightly above the critical temperature of the more volatile component (chlorotrifluoromethane).

The data to be reported show that in mixtures of vinyl chloride with ethylene ($T_c = 9.7°$) at 30° and near the critical composition the partial molal volume of vinyl chloride can reach values larger by one order in absolute magnitude and opposite in sign to that of the molal volume of the pure component, even in the one-phase region. This conclusion is permissible in spite of the limited accuracy of the data to be presented and suggests that precise volume measurements in the critical region should provide a highly sensitive index

(1) Department of Chemical Engineering, State University of New York at Buffalo, Buffalo, N. Y. 14214.

(2) (a) W. B. Kay, *J. Phys. Chem.*, **68**, 827 (1964); (b) W. B. Kay *Accounts Chem. Res.*, **1**, 344 (1968).

(3) D. B. Todd and J. C. Elgin, *A.I.Ch.E. J.*, **1**, 20 (1955).

(4) D. C. Chappelear and J. C. Elgin, *J. Chem. Eng. Data*, **6**, 415 (1961).

(5) P. Ehrlich and J. J. Kurpen, *J. Polymer Sci.*, **A1**, 3217 (1963).

(6) P. Ehrlich, *ibid.*, **A3**, 131 (1965).

of intermolecular forces and of molecular structure in mixtures of chemically dissimilar components.

Experimental Section

The data were obtained in two different stirred-autoclaves both about 1000 cc in volume, the P–V–T data in an Autoclave Engineers "Magne-Drive" reactor and the phase equilibria data in a windowed vessel of special design. The latter had three pairs of windows, the middle pair turned 90° with respect to the top and bottom pairs, such that the total volume of the vessel was visible. Direct observation of dew-point and bubble-point pressures at known composition was thus possible. The vessels contained a small "dead space" not exceeding 1% of their volumes which were determined both by direct measurement and by standardization agains the accurate P–V–T data of Michels and Geldermans for ethylene.[7] The amounts of components added were determined by direct weighing from storage tanks maintained at constant pressure. Densities as a function of composition could thus be determined directly at any desired pressures. Pressures were determined by means of Heise gauges accurate to ±1 psi and temperature control was estimated at ±0.1° in the "Magne-Drive" system and at ±0.3° in the windowed vessel. Measurements were made in psig, but are reported in atm. The components were pumped into the carefully evacuated vessels by means of modified Sprague S-213-c micropumps.

Results

Figure 1 shows dew-point and bubble-point data at 20–59°. The critical region is shown at temperature intervals of about 10° and nearly the complete isotherm

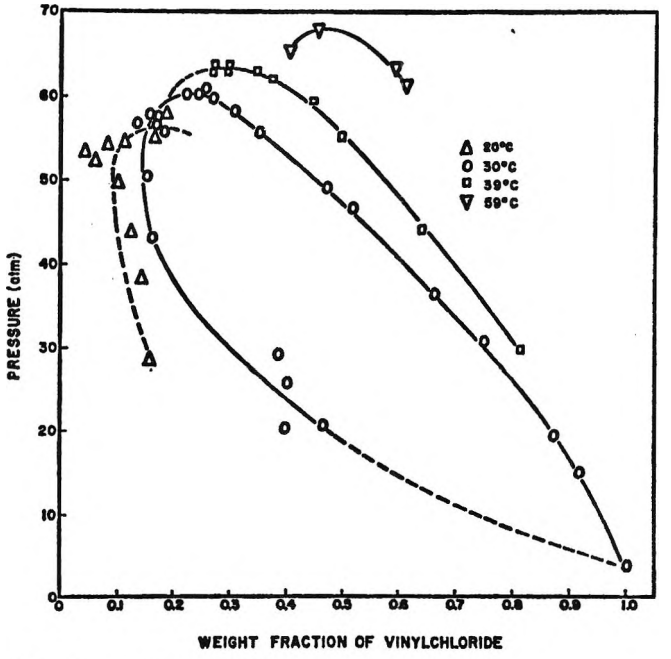


Figure 1. Isotherms at 30°.

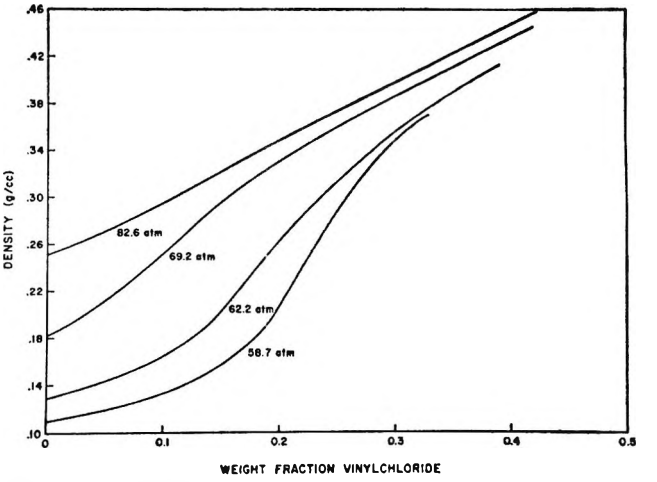


Figure 2. Density at 30° and at several pressures.

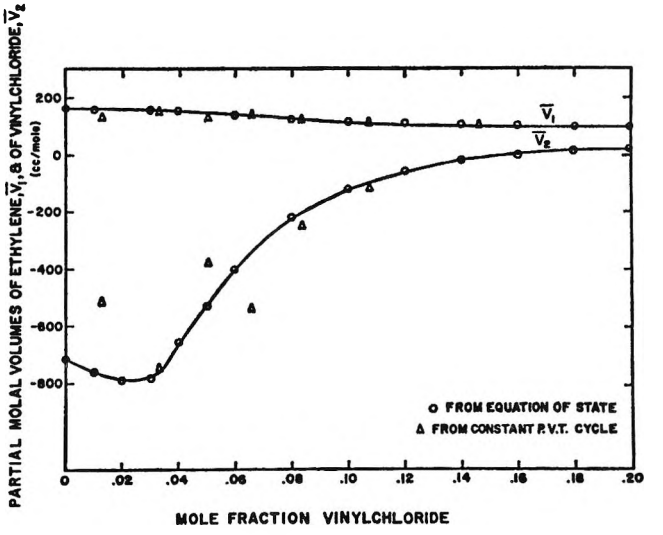


Figure 3. Partial molal volumes of both components obtained experimentally and calculated from the equation of state at 690 atm.

can be delineated at 30°. The major experimental limitations, reflected by the data, are the very large temperature sensitivity of the system at 20° and below, and the low density of the system along the dew-point line at high vinyl chloride content. (See Figure 2.)

Figure 3 is a smoothed plot of the experimental data of density *vs.* composition at several pressures in the one-phase region and at 30°. Particularly notable is the pronounced S shape of the curves as the critical pressure is approached.

A unique situation exists near the critical point as a result of the large negative partial molal volume of vinyl chloride. Here a two-step process can be carried out, resulting in a small change of composition at constant temperature, pressure, and volume. This allows a calculation of partial molal volumes by successively adding incremental amounts of the two components. It can be shown readily that at constant mole fraction x

(7) A. Michels and M. Geldermans, *Physica*, **9**, 967 (1942).

Table I: Data Obtained in Constant P–V–T Cycle at 30°[a]

P, atm	$+g_1$	$+g_2$	g_{1av}	g_{2av}	n_1	n_2	n	x_2	dn_1	dn_2	V/n	$\bar{v}_1$	$\bar{v}_2$
690	202	...	...	...	...	...	...	...	...	...	...	...	...
717	23.0	...	...	...	...	...	...	...	...	...	...	...	...
690	...	13.5	213.5	6.75	7.63	0.108	8.74	0.0124	0.823	0.216	126.8	134.7	−511
717	23.0	...	...	...	...	...	...	...	...	...	...	...	...
690	...	10.5	236.5	18.75	8.82	0.300	9.12	0.0329	0.823	0.168	121.4	150.8	−741
717	15.0	...	...	...	...	...	...	...	...	...	...	...	...
690	...	12.5	255.5	30.25	9.13	0.484	9.61	0.0503	0.536	0.200	115.3	141.4	−379
717	15.0	...	...	...	...	...	...	...	...	...	...	...	...
690	...	12.0	270.5	42.5	9.67	0.680	10.35	0.0657	0.536	0.192	107.0	142.7	−532
717	13.0	...	...	...	...	...	...	...	...	...	...	...	...
690	...	18.5	284.5	57.75	10.17	0.924	11.09	0.0834	0.465	0.296	100.0	123.0	−246
717	8.0	...	...	...	...	...	...	...	...	...	...	...	...
690	...	24.0	295	79.0	10.53	1.264	11.79	0.1073	0.286	0.384	94.0	115.7	−106.4
717	8.0	...	...	...	...	...	...	...	...	...	...	...	...
699	...	50	303	116	10.82	1.857	12.68	0.1468	0.286	0.80	87.4	108.8	−48.5

[a] Definition of symbols: subscripts 1 and 2 refer to ethylene and vinyl chloride, respectively; $+g$ is the weight of incremental component added; g_{av} is the average weight of component in given cycle; n is the moles present (average); dn is the incremental moles added.

and at constant T and P one has

$$\frac{(V/n) - \bar{v}_2 x}{\bar{v}_2(1 - x)} = -\frac{dn_2}{dn_1}$$

where V is the volume of the system, $\bar{v}_2$ is the partial molal volume of component 2 (vinyl chloride), n is the total number of moles present, dn_1, dn_2 are incremental moles of components 1 and 2 added in the cycle, and x is the mole fraction of component 2.

Some data were collected by this method and an example for such cycles performed near 700 atm and at 30°, *i.e.*, well in the one-phase region, is presented in Table I. The experimental error involved in the use of this method is high because of the great sensitivity of the partial molal volume of vinyl chloride to composition and temperature and because of the large weighing error caused by addition of incremental quantities.

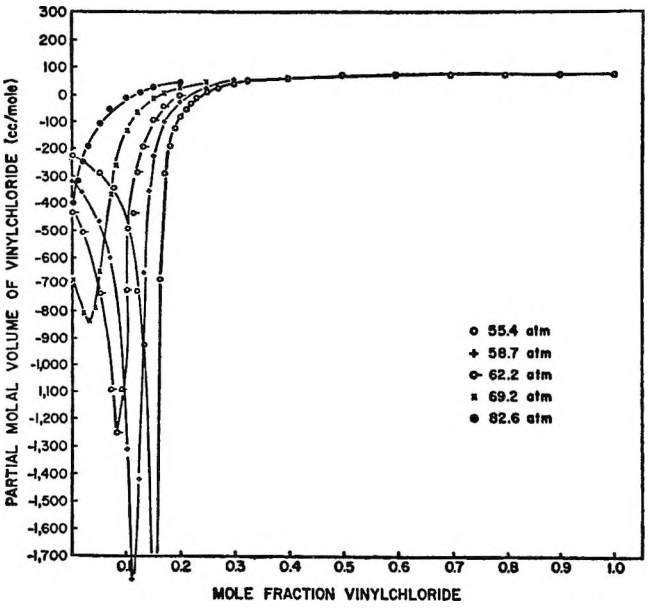


Figure 4. Partial molal volume of vinyl chloride calculated at several additional pressures.

Alternatively, partial molal volumes can be obtained from experimental volumetric data by first fitting the data with an analytical expression representing the equation of state and then differentiating its volume-explicit form. This procedure has been used here, the equational form being one recommended by Fariss[8] and found most capable of an accurate fit to the data of several which were investigated. This equation is of the form

$$V = (RT/P)[e^{-Q} + z'(1 - e^{-Q})] + D\exp(-\alpha\sqrt{P}) + E$$

where Q is a function of temperature and volume and z', D, and E are functions of the temperature. The foregoing parameters are expressed in terms of ten constants, determined by regression analysis. The constants were chosen to produce the best possible fit of the density data on pure components and mixtures at 30° (Figure 2) and 40° (not shown), taking into consideration the data of Michels and Geldermans for pure ethylene.[7]

Figure 3 allows a comparison of partial molal volumes obtained experimentally (Table I) and from the equation of state at 30° and approximately 700 atm. Figure 4 illustrates the variation of $\bar{v}_2$ with composition at several additional pressures near the critical composition, as calculated from the equation of state. The results, although probably only qualitatively correct, are consistent with the experimental points plotted in Figure 3 and with other qualitative observations made on pressure changes in constant volume systems upon

(8) R. H. Fariss, "Additive Volumes as a Route to Equations of State," presented at A.I.Ch.E. Symposium, St. Louis, Mo., April 1967.

addition of vinyl chloride. They indicate that $\bar{v}_2$ is strongly negative, extremely composition and pressure dependent near the critical point, and that no discontinuity exists at the phase boundary. The pronounced minima in the $\bar{v}_2$ *vs.* composition isobars near the critical point (accompanied by maxima in $\bar{v}_1$) are also consistent with the data (Figure 3).

It would therefore seem that strong ordering must occur over a rather broad region in solutions of this type both in the one-phase and in the two-phase region, accompanied by the formation of molecular clusters whose structure is highly composition and pressure dependent near the critical point.

Fluorescence of 2-Pentanone

by F. Sheldon Wettack[1]

Department of Chemistry, The University of Texas, Austin, Texas
(Received October 10, 1968)

The absolute fluorescent efficiency, Q_f, of 2-pentanone as a function of excitation wavelength and the effect of pressure and wavelength on this emission have been determined. The value of Q_f (number of quanta emitted by excited singlet state/number of quanta absorbed) obtained at 3130 Å agrees well with the relative (to biacetyl) value reported by Ausloos and Murad,[2] and the pressure dependence can be interpreted as confirming the wavelength effect noted[3] for the gas-phase Norrish type II reaction.

The method used for calculating Q_f is similar to method B of Noyes, Mulac, and Harter[4] for benzene except that integrations were performed over phototube sensitivity and filter transmission for the entire emission spectrum.[5]

Figure 1 shows the gas-phase emission spectrum[6] and Table I shows the measured values of Q_f. The overlap of the emission spectrum with the gas-phase absorption spectrum[5] indicates that the excited singlet energy is about 3.75 eV (3300 Å). The phosphorescence spectrum of 2-pentanone in EPA at 77°K has also been determined and the features are essentially the same as those reported by Borkman and Kearns[7] for acetone. Figures 2 and 3 show the effect of added 1,3-butadiene and *n*-butane on Q_f. Both gases tend to increase Q_f, which indicates that they are removing vibrational and not electronic energy.

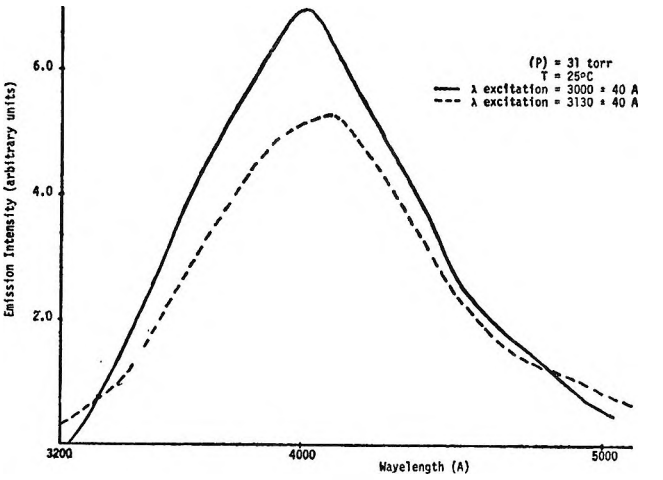


Figure 1. The gas-phase emission spectrum of 2-pentanone recorded with a Jarrell–Ash 3/4-m Czerny–Turner scanning spectrometer.

Table I: Fluorescence Efficiency of 2-Pentanone[a]

λ, Å	$Q_f \times 10^3$
3130	2.67 ± 0.29[b]
2925	2.01
2804	1.24
2730	1.34
2654	1.49

[a] 25 Torr at 25°. [b] Deviation from the mean for six measurements made with varying slit conditions. Values at $\lambda \neq 3130$ Å are relative to the 3130-Å value but have been corrected for any variation in phototube sensitivity.

Discussion

The values obtained for Q_f confirm that fluorescence is a minor process from the excited singlet state, and seem to substantiate that both fluorescence and part of the Norrish type II reaction occur from the same electronic state. As Q_f decreases by a factor of 2 in going from 3130 to 2700 Å, the quantum yield of type II from the singlet state, $^1\phi_{II}$, increases by a factor[3] of 2.2 over the same wavelength range. The increase in $^1\phi_{II}$ is based on the fraction of the type II yield which is unaffected by a high pressure of butadiene. Since the diolefin does not quench the ketone fluorescence in the pressure range studied it is assumed that the inhibited fraction of type II occurs from a triplet state while the uninhibited fraction has a singlet state precursor. This assumption is valid if fluorescence and type II from the singlet state are competitive. The present data do not prove this to be true, but the relationship between the decrease in Q_f and the increase in $^1\phi_{II}$ in going from 3130 to 2700 would seem to indicate that as type II becomes a more important singlet state process the singlet emission becomes less important.

(1) Department of Chemistry, Hope College, Holland, Mich. 49423.

(2) P. Ausloos and E. Murad, *J. Phys. Chem.*, 65, 1519 (1961).

(3) F. S. Wettack and W. A. Noyes, Jr., *J. Amer. Chem. Soc.*, 90, 3901 (1968).

(4) W. A. Noyes, Jr., W. A. Mulac, and D. A. Harter, *J. Chem. Phys.*, 44, 2100 (1966).

(5) For experimental details, see F. S. Wettack, Ph.D. Dissertation, The University of Texas at Austin, 1968.

(6) The author wishes to thank Dr. H. D. Mettee for help in obtaining this spectrum.

(7) R. F. Borkman and D. R. Kearns, *J. Chem. Phys.*, 44, 945 (1966).

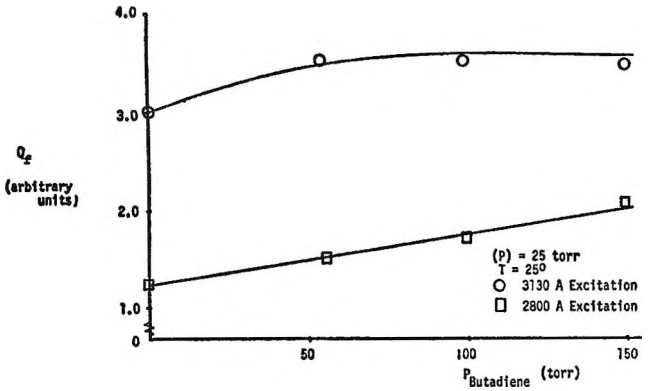


Figure 2. Effect of 1,3-butadiene on the fluorescence efficiency of 2-pentanone.

Thus one is tempted to conclude that each excited singlet molecule is capable of either fluorescing or undergoing the type II, and, hence, the two processes are competitive. However, such a conclusion is strictly valid only if both processes occur from the same vibronic states. That this condition is met in the 2-pentanone system cannot be rigidly established by the present data.

The question of competitiveness was raised recently[3] since the total type II quantum yield, ϕ_{II}, appears essentially independent of both wavelength and pressure but Q_f depends markedly on these parameters. However, ϕ_{II} may be a function of competition between formation of type II products and formation of the parent ketone from some intermediate other than the singlet formed by light absorption, while $^1\phi_{II}$ may be determined by competition within the singlet state between fluorescence and abstraction of a γ-hydrogen to form the intermediate.

The pressure dependence of Q_f substantiates the assumption made previously[3] regarding the loss of vibrational energy at long and short wavelengths. Furthermore, the similarity between the effect of 1,3-butadiene and *n*-butane provides evidence that the inhibition of the type II reaction by diolefins in the gas phase is due to an electronic energy transfer from the triplet state of the ketone as was assumed.[3] The electronic energy for the upper singlet state of diolefins is uncertain,[8] and a singlet transfer might be possible if fluorescence and singlet state type II are not competitive. This possibility seems to be negated by the present results.

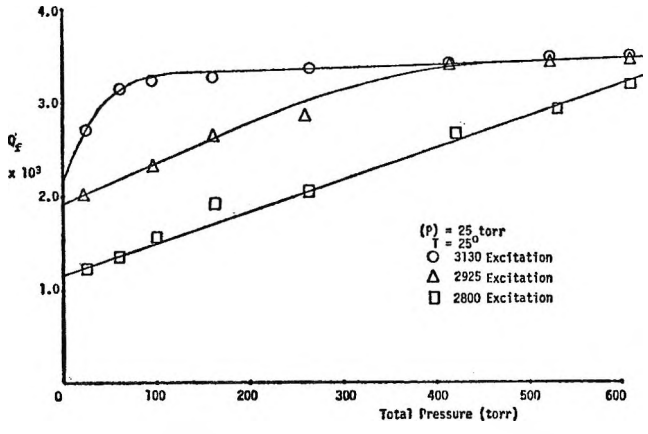


Figure 3. Effect of total pressure on the fluorescence efficiency of 2-pentanone. Added gas, *n*-butane.

The pressure dependence allows one to calculate[5] an effective cross section for removal of vibrational energy in a two-step mechanism at the various wavelengths. The resulting cross sections are 0.81 Å^2 (3130 Å) and 0.20 Å^2 (2800 Å). More than two steps are undoubtedly involved in the deactivation and so these values should represent maximum cross sections. At 3130 Å and 100 Torr such a cross section indicates that vibrational relaxation will occur in 2.9×10^{-8} sec, which is comparable to the mean lifetime of the singlet state, 2.8×10^{-8} sec, and that of the triplet state, 1.6×10^{-8} sec, as calculated from the rate constants reported in ref 3. These values show that vibrational relaxation should be complete at total pressures of about 100 Torr. At short wavelengths the vibrational energy would be equilibrated in 1.0×10^{-7} sec, but the singlet and triplet mean lifetimes are 1.0×10^{-8} sec^{-1} and 3.6×10^{-10} sec^{-1}, respectively. Thus high vibronic states will most certainly be involved in the reaction processes initiated with wavelengths below 2800 Å. It should be noted that the lifetimes mentioned are dependent on the assumptions regarding diolefin quenching and cannot be considered as absolute values, particularly at the shorter wavelengths.

In light of recent observations concerning the 0–0 band for the upper singlet state of diolefins, an interesting aspect of this work is that no quenching of Q_f by butadiene is observed. Quenching of singlet emission from benzene[9,10] and the xylenes[10] by diolefins has been observed, and indicates that the diolefin 0–0 band is at a wavelength longer than about 2650 Å (~4.7 eV). This conclusion assumes, of course, that the fluorescence quenching observed is due to an exothermic electronic energy transfer.

If singlet vibronic energy of the ketone is transferrable to the olefin as electronic excitation one might expect such a fluorescence quenching to occur when the ketone is excited in the region of 2800 Å. The lack of quenching indicates either (1) that the transfer does not occur or (2) that fluorescence and the transfer occur from two different excited states. If the latter is true and if the type II reaction attributed to the singlet state also occurs from a nonfluorescent state, the agreement between the $^1\phi_{II}$ increase and the Q_f decrease

(8) For example, see R. Srinivasan, *Advan. Photochem.*, **4**, 113 (1966).
(9) A. Morikawa and R. J. Cvetanovic, *J. Chem. Phys.*, **49**, 1214 (1968).
(10) W. A. Noyes, Jr., private communication.

is fortuitous. In this case the diolefin experiments at short wavelengths would have little meaning so far as triplet-state involvement in the type II process is concerned.

If option (1) is correct, one is led to the conclusion that the electronic energy of the first excited singlet state of butadiene is probably above 4.4 eV (2800 Å). If the energy is much less than 4.4 eV, one should observe energy transfer when the collision rate approaches the rate of dissipation of vibronic energy by other routes. The rates compared above indicate that vibrational relaxation is slow compared to reaction processes at 2800 Å. However, the concentration range investigated would seem sufficient to show the electronic energy transfer since Q_f does increase with increasing butadiene pressure in this range. This is presumably due to a relaxation of vibrational energy of the excited ketone through a collisional interaction. At 150 Torr of butadiene measurable vibrational relaxation has occurred but Q_f is still significantly lower than that found with 3130-Å excitation. Hence the collisional interaction is probably between a pentanone singlet possessing about 4.4 eV of vibronic energy and a ground-state diolefin.

Thus the effect of butadiene on Q_f and the relative changes in $^1\Phi_{II}$ and Q_f with decreasing wavelength indicate that collisions between 2-pentanone singlets and butadiene do occur but that energy transfer between the two does not occur following excitation at 2800 Å. This conclusion, coupled with the quenching observations[9,10] mentioned above, would seem to place the 0–0 band of butadiene between 2650 Å and approximately 2800 Å.

Acknowledgment. The author wishes to thank Professor W. A. Noyes, Jr., for guidance during the course of this work, which was supported by NSF Grant GP 6713.

The *cis–trans* Effect in the H-Atom Addition to Olefins

by Richard D. Kelley, Ralph Klein, and Milton D. Scheer

National Bureau of Standards, Washington, D. C. 20234
(Received October 14, 1968)

Gas-phase experiments at room temperature showed that hydrogen atoms add to *trans*-2-butene 20% faster than to *cis*-2-butene,[1] although earlier work using a molybdenum trioxide detector technique showed the reverse effect.[2] The room temperature gas-phase data were obtained for both *cis* and *trans*-2-butene by comparison of the rate of addition to the olefin with the rate of abstraction from *n*-butane. The ratio of the rates for *cis*-2-butene and *n*-butane and for *trans*-2-butene and *n*-butane were compared, the faster rate of addition to *trans* with respect to the *cis* being demonstrated. This result is rather surprising for not only are the two molecules identical with respect to electron density around the π bond, but the free energy of formation of the *cis*-2-butene, 67.588 kJ/mol (16.154 kcal/mol) is more positive than that of the *trans*-2-butene, 64.534 kJ/mol (15.424 kcal/mol).[3] Because of the small difference of the rates and the absence of a simultaneous comparison between the two olefins, further confirmation of a *cis–trans* effect was sought. For this purpose, we have utilized the low-temperature technique[4] and employed the compound *cis, trans*-2,6-octadiene. Since both functional groups are on the same molecule, certain possible extraneous effects, such as local concentration differences, are avoided and relative rates can be directly determined.

It has been demonstrated[4,5] that under the present experimental conditions of high dilution in propane at 90°K the only significant radical reactions are the disproportionation and combination reactions of two alkyl radicals. Combination of large alkyl radicals is small at low temperatures[4,6] and may be neglected. Thus the observed products result from the disproportionation of the C_8 radicals formed by H-atom addition.

A mixture of the three isomers of 2,6-octadiene was separated by gas chromatography, with each component being identified by ir absorption.[7] A 6-ft 20% glycerol (saturated with $AgNO_3$) column at 50° with a helium flow of 50 cc/min gave excellent resolution of the three components. The *cis, trans*-2,6-octadiene purified in this manner showed less than 0.1% of the *trans, trans* isomer and no detectable *cis, cis* isomer.

The reaction products of the H-atom addition to the 2,6-octadiene were observed by gas chromatography using a 20-ft 30% β,β'-oxydipropionitrile at 30° and a helium flow of 60 cc/min. No quantitative analysis was made of the product diolefins other than the 2,6-octadiene isomers.

The octadiene, diluted with propane in a 1 to 500 ratio at 90°K, was exposed to gas-generated hydrogen

(1) K. R. Jennings and R. J. Cvetanovic, *J. Chem. Phys.*, 35, 1233 (1961).

(2) P. E. M. Allen, H. W. Melville, and J. C. Robb, *Proc. Roy. Soc.*, A218, 311 (1953).

(3) F. D. Rossini, K. S. Pitzer, W. J. Taylor, J. P. Ebert, J. E. Kilpatrick, C. W. Beckett, M. G. Williams, and H. G. Werner, "Selected Values of Properties of Hydrocarbons," National Bureau of Standards Circular C461, U. S. Government Printing Office, Washington, D. C., 1947.

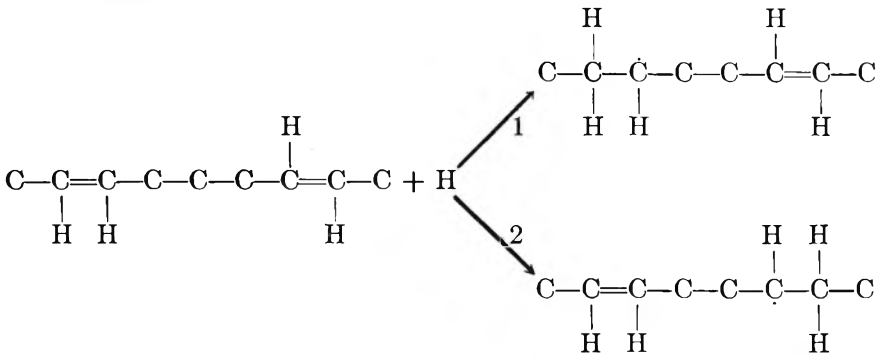
(4) R. Klein, M. D. Scheer, and R. Kelley, *J. Phys. Chem.*, 68, 598 (1964).

(5) R. D. Kelley, R. Klein, and M. D. Scheer, *ibid.*, 69, 905 (1965).

(6) R. Klein and M. D. Scheer, *ibid.*, 67, 1874 (1963).

(7) W. von E. Doering and W. R. Roth, *Tetrahedron*, 18, 67 (1962).

atoms. The initial reactions are



The H atoms can also add to the other carbon of the pair constituting the reacting olefinic bond.[5] The resulting radicals disproportionate in the usual way to give monoolefins and diolefins. It is evident that a *trans* monoolefin results from the H-atom reaction with the *cis* part of the diolefin and vice versa. The ratio of the *trans* to *cis* monoolefin at low conversions is thus a direct measure of the relative rate of the hydrogen atom addition to a *cis* and a *trans* double bond. The product monoolefins are also reactive to hydrogen atoms as evidenced by the formation of *n*-octane. In the process, some of the *cis*-2-octene is converted to the *trans* isomer *via* disproportionation of octyl radicals. The initial *trans* to *cis*-2-octene ratio must therefore be obtained by extrapolation. The value obtained is $k_{cis}/k_{trans} = 0.8$.

As a further check on the validity of the method, a sample of propane with 0.2% *trans*, *trans*-2,6-octadiene was exposed to H atoms. The only 2-octene isomer produced was the *trans* form. Similar experiments were done with *cis*, *cis*-2,6-octadiene. In this case, *trans*-2-octene may be formed from the initial products, *cis*-2-octene and *cis*, *trans*-2,6-octadiene. However, the ratio *trans*-2-octene/*cis*-2-octene extrapolates precisely to zero for zero conversion. (See Figure 1.)

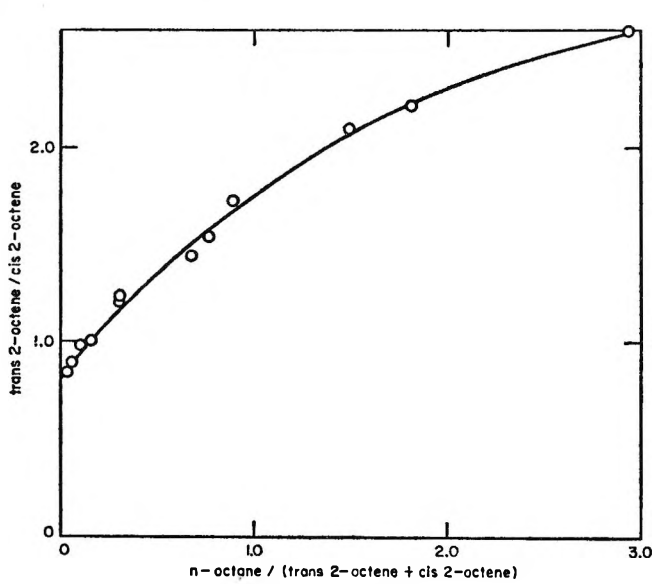


Figure 1. Variation of the product ratio *trans*-2-octene/*cis*-2-octene from the H-atom addition to *cis*, *trans*-2,6-octadiene (diluted 1:500 in C_3H_8) at 90°K.

The faster rate of the H-atom addition to the *trans* relative to the *cis* position measured by us at 90°K agrees with the value determined by Cvetanovic[1] at 300°K for *trans*- and *cis*-2-butene. We have also effected the H-atom reaction with *cis*, *trans*-2,6-octadiene at 143°K and found the ratio of addition to the *cis* relative to the *trans* olefinic bond to be 0.8. The absence of a temperature effect over the range 90 to 300°K implies that the rate difference between the H-atom addition to *cis* and *trans*-2-butene must be ascribed to steric effects, presumably associated with the methyl groups. It must be concluded that two methyl groups in the *cis* configuration are more effective in inhibiting the addition of a hydrogen atom than two methyl groups in the *trans* configuration.

Remarkably similar results have been found in the addition reactions of other species. Cvetanovic[8] has found that oxygen atoms add, at 25°, 20% faster to *trans*-2-butene than to *cis*-2-butene. Owen, Pearson, and Szwarc[9] have observed that CF_3 radicals also add 20% faster to *trans*-2-butene than to the *cis* isomer and further that there is no temperature effect in the range 65–180°. Since the *cis–trans* effect is a relative measurement, it is reasonable to conclude that the steric effects on the addition of CF_3 radicals, O atoms, and H atoms to *cis*- and *trans*-2-butene are similar.

(8) R. J. Cvetanovic, *Can. J. Chem.*, **38**, 1678 (1960).
(9) G. E. Owen, J. M. Pearson, and M. Szwarc, *Trans. Faraday Soc.*, **61**, 1722 (1965).

The Apparent Molecular Area of Adsorbed Carbon Tetrachloride

by W. D. Machin

Department of Chemistry, Memorial University of Newfoundland, St. John's, Newfoundland, Canada *(Received November 5, 1968)*

In the recent literature, different values for the molecular area of $CFCl_3$ and CCl_4, adsorbed on graphite

surfaces, have been recommended by various authors.[1-4] The basic source of disagreement involves the estimation of the monolayer capacity of the adsorbents, as the isotherms obtained in these studies do not yield reliable BET plots. In the present work other factors which may influence the molecular area of adsorbed molecules will be discussed.

The surface areas of a series of anhydrous transition metal sulfates have been measured using $CFCl_3$ at 20.0, 6.0, and $-10.0°$, and argon at 77°K.[5] In all cases, good BET plots were obtained. Using the molecular area of argon as 13.6 Å^2, the average molecular area of $CFCl_3$ on the series of adsorbents was found to be 29.7 ± 0.7 Å^2, in good agreement with the theoretical value[3] of 31.2 Å^2.

The use of CCl_4 as an adsorbate also gave isotherms of the same general shape as those obtained with $CFCl_3$, and which also gave good BET plots. The only exception was $ZnSO_4$, for which the isotherms were nearly linear, but which still gave reasonably good BET plots. In spite of this, the calculated surface areas generally gave poor agreement with the $CFCl_3$ and argon areas for the same adsorbents. Agreement could only be obtained by permitting the molecular area of CCl_4 to vary throughout the series of adsorbents. The CCl_4 apparent molecular areas for the series of adsorbents are shown in Figure 1. Also shown in this figure is the "unit cell area" for each adsorbent, which is the product of the orthorhombic unit cell parameters[6] to the two-thirds power, $(abc)^{2/3}$, a quantity which should be proportional to the average area of a M^{2+}, SO_4^{2-} pair in the surface.

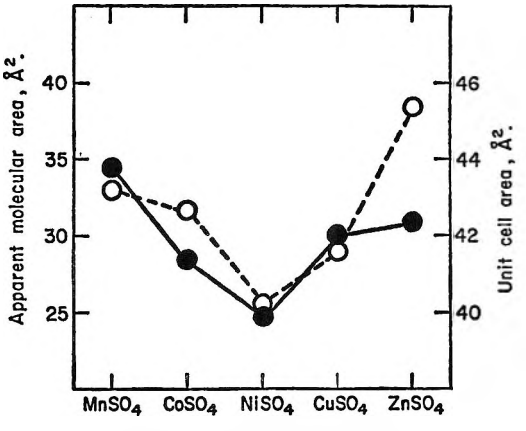


Figure 1. Variation of CCl_4 apparent molecular area (open points) and "unit cell areas" (solid points), through the series of adsorbents.

The variation of the adsorbate molecular area and the adsorbent "unit cell area" throughout the series of adsorbents strongly suggests that the apparent molecular area of the adsorbed CCl_4 is closely related to the adsorbent lattice parameters.

Differential molar entropy calculations for CCl_4 adsorbed on the various adsorbents suggest that the molecules are at least partially localized, in which case we might expect the apparent molecular area to show some dependence on the structure of the adsorbent. In contrast, similar calculations suggest that $CFCl_3$ behaves as a two-dimensional van der Waals gas on the same adsorbents,[5] and as we might expect, a mobile adsorbate would not show a similar dependence on the adsorbent lattice parameters.

As to why $CFCl_3$ appears to be mobile and CCl_4 does not, the reason may be that at the experimental temperatures, the reduced temperature of $CFCl_3$ is greater than the reduced temperature of CCl_4. Possibly, if CCl_4 isotherms were measured at higher temperatures, the variation in the apparent molecular area would be reduced. Unfortunately, the present design of the apparatus prohibits the measurement of isotherms above room temperature.

Acknowledgment. The author gratefully acknowledges financial support provided by the National Research Council of Canada.

(1) C. Pierce, *J. Phys. Chem.*, **72**, 1955 (1968).
(2) B. W. Davis and C. Pierce, *ibid.*, **70**, 1051 (1966).
(3) J. H. de Boer and J. C. P. Broekhoff, *Proc. Kon. Ned. Akad. Wetensch., Ser. B*, **70**, 333 (1967).
(4) W. D. Machin and S. Ross, *Proc. Roy Soc.*, **A265**, 455 (1962). The molecular area of CCl_4 as calculated from the data in this reference is 28.5 Å^2.
(5) W. D. Machin, *Trans. Faraday Soc.*, **65**, 529 (1969).
(6) R. W. G. Wyckoff, "Crystal Structures," Vol. 3, 2nd ed, John Wiley and Sons, Inc., New York, N. Y., 1965, pp 38–41.

Photolysis of 1,5-Cyclooctadiene Vapor. Molecular Elimination of Ethylene from 1,5-Dienes

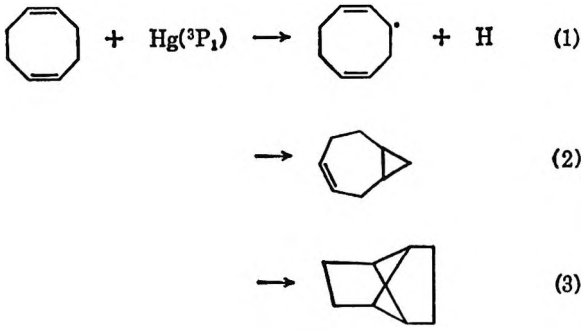
by Setsuo Takamuku and Hiroshi Sakurai

The Institute of Scientific and Industrial Research, Osaka University, Suita, Osaka, Japan *(Received October 29, 1968)*

The mercury-photosensitized isomerization of nonconjugated dienes has been extensively studied by Srinivasan and his coworkers.[1-5] It has been shown that all the nonconjugated dienes undergo three primary processes, which are (1) dissociation to free radicals, (2) production of cyclopropyl derivatives, and (3) bicyclo compound formation by internal cycloaddition. These reactions will be illustrated for the

(1) R. Srinivasan, *J. Amer. Chem. Soc.*, **85**, 819 (1963).
(2) R. Srinivasan, *ibid.*, **86**, 3318 (1964).
(3) I. Haller and R. Srinivasan, *ibid.*, **88**, 5084 (1966).
(4) R. Srinivasan and K. H. Carlough, *ibid.*, **89**, 4932 (1967).
(5) R. Srinivasan, *J. Phys. Chem.*, **67**, 1367 (1963).

case of 1,5-cyclooctadiene.[3]



In comparison with these extensive investigations of the photochemical isomerization, comparatively little attention has been given to the photodegradation of nonconjugated dienes.

In the present study, we wish to report the vapor phase photolysis of 1,5-cyclooctadiene which brings about molecular elimination of ethylene.

Experimental Section

In the presence of a small amount of mercury vapor, 1,5-cyclooctadiene (99.8% pure by gas chromatography) was irradiated with a low-pressure mercury lamp in a cylindrical quartz cell (5 cm in diameter and 5 cm long) at room temperature. The product gases volatile at −196 and −120° were separately collected by a Toepler pump into a gas buret in a greaseless vacuum system. The former was subjected to Pd thimble heated at 300° for hydrogen measurement and the latter was analyzed by gas chromatography (silica gel 3 m at 100°). The residual liquid fraction was also analyzed by gas chromatography (Squalane 7.5 m at 80–120°).

Quantum yields were determined by comparison with the decomposition of propane at 300 mm. The hydrogen yield from propane was assumed to be unity at low conversion (0.06%).[6,7]

Results and Discussion

Hydrogen, C_2H_4, C_2H_2, C_4H_6(1,3-butadiene), 1,3-CHD (1,3-cyclohexadiene), HT (*cis*- and *trans*-1,3,5-hexatriene), and benzene were observed as the photolysis product as well as photoisomers produced by processes 2 and 3. The yields of these products were significantly dependent on the exposure time as is shown in Figures 1 and 2. Acetylene formation diminished to nearly zero at shorter exposure times, whereas the rates of C_2H_4 and C_4H_6 formation increased rapidly. Therefore, C_2H_2 appears to be a secondary product, while C_2H_4 and C_4H_6 are primary products of the reaction. The further photolysis of C_2H_4 and C_4H_6 may lead to the formation of C_2H_2. In the liquid products (Figure 2), secondary reactions were also observed from the rapid decrease in the rate of formation of 1,3-CHD and HT, while yields of benzene and hydrogen still increased linearly with reaction time. These results are best explained by the further photolyses of 1,3-CHD and HT which give predominantly benzene and hydrogen, less probably C_2H_2 and C_2H_4.[8]

The initial rate of production of these products, required to the discussion of primary processes, is summarized in Table I with the quantum yield.

The yields of main products (C_2H_4, C_4H_6, and C_6 compounds) were only slightly affected by the addition

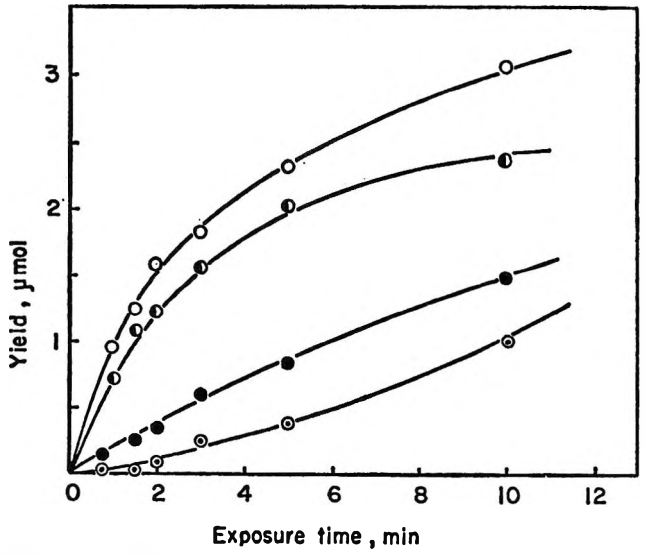


Figure 1. Yields, in micromoles, of gaseous products *vs.* exposure time in the mercury-photosensitized decomposition of 1,5-cyclooctadiene (pressure 3 mm): ●, hydrogen; ◐, ethylene; ⊙, acetylene; ○, 1,3-butadiene.

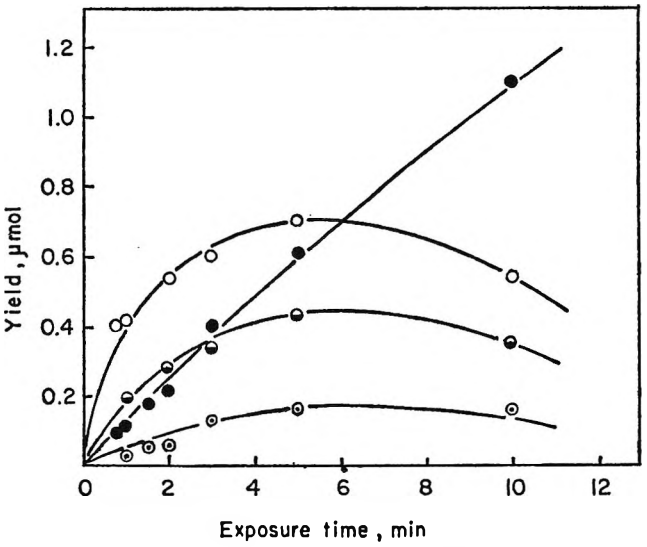


Figure 2. Yields, in micromoles, of liquid products *vs.* exposure time in the mercury-photosensitized decomposition of 1,5-cyclooctadiene (pressure 3 mm): ●, benzene; ○, 1,3-cyclohexadiene; ◒, 1,3,5-hexatriene; ⊙, C_6 unknown.

(6) R. A. Back, *Can. J. Chem.*, **37**, 1834 (1959).

(7) K. Yang, *J. Amer. Chem. Soc.*, **86**, 3941 (1964).

(8) The photolysis of 1,3-CHD and HT has been extensively studied by Srinivasan, and it has been shown that the main primary process is the dissociation to benzene and hydrogen through a common intermediate (see ref 9).

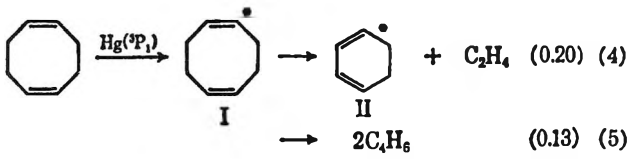
Table I: Initial Rate and Quantum Yield of Photolysis Product

Product	R^0, μmol min^{-1}	Φ^0	Product	R^0, μmol min^{-1}	Φ^0
H_2	0.20	0.05	Benzene	0.13	0.03
C_2H_4	0.77	0.20	1,3-CHD	0.38	0.10
C_2H_2	0.02	0.01	HT	0.21	0.05
C_4H_6	0.96	0.25	C_6 unknown	0.03	0.01

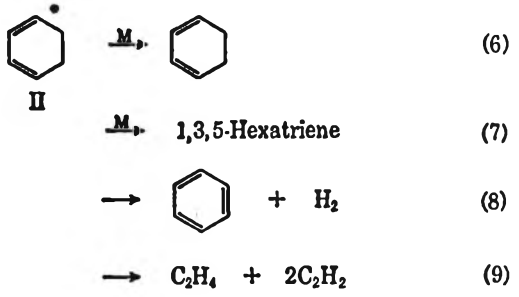
1,5-cyclooctadiene, 3 mm
C_4H_6, 1,3-butadiene; 1,3-CHD, 1,3-cyclohexadiene; HT, *cis*- and *trans*-1,3,5-hexatriene

of 8–12 mol% nitric oxide, arguing strongly for an intramolecular mechanism to the exclusion of a free-radical path for the formation of these products. Further, the formation of 1,3-CHD, HT, and benzene also suggested the presence of a common intermediate proposed in the photolysis of 1,3-CHD and HT.[9]

Thus the following possible primary dissociations may be considered for the mercury-photosensitized decomposition



followed by



where the numbers in parentheses give the quantum yield values at 3 mm. From this reaction mechanism, the following relations, $\Phi^0_{1,3\text{-CHD}} + \Phi^0_{HT} + \Phi^0_{benzene} = \Phi^0_{C_2H_4} - \Phi^0_{C_2H_2}$ and $\Phi^0_{benzene} = \Phi^0_{H_2}$ should hold. The data shown in the table supported the former, while the yield of hydrogen was higher than that of benzene indicating the presence of hydrogen formation other than (8), probably (1), though it was not studied in detail.

Effects of total pressure, studied by addition of krypton, are shown in Figure 3. By increasing the pressure of krypton, the photolysis was reduced owing to the deactivation of $Hg(^3P_1)$ and an activated 1,5-cyclooctadiene (I) by krypton as estimated from the decreases in the yields of C_2H_4 and C_4H_6. There was also a homogeneous decrease in the yield of benzene compared to those of 1,3-CHD and HT which increased a little at first, reached a maximum, and then began to

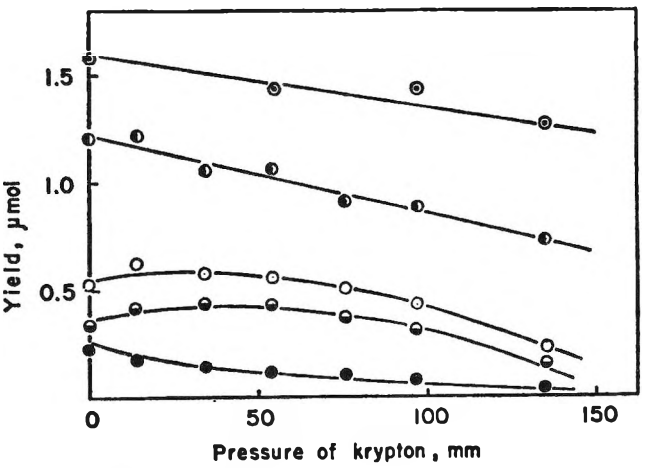
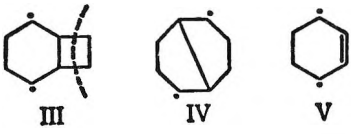


Figure 3. Effect of added krypton on the mercury-photosensitized decomposition of 1,5-cyclooctadiene (1,5-COD, 3 mm, irradiated for 2 min): ◐, ethylene; ⊙, 1,3-butadiene; ○, 1,3-cyelohexadiene; ◒, 1,3,5-hexatriene; ●, benzene.

decline in line with other products. The ratios 1,3-CHD/benzene and HT/benzene increased with pressure. It clearly demonstrates that the intermediate II, which undergoes dissociation to benzene and hydrogen otherwise, was also collisionally deactivated by krypton to give 1,3-CHD or HT. With the structure of II, there are still uncertainties that it is a common intermediate to both 1,3-CHD and HT; if so, it is cyclic or open chain. That the ratio 1,3-CHD/HT did not change under a variety of experimental conditions and the similarity to the intermediate in the photolysis of 1,3-CHD and HT seems to suggest the common intermediate.

A reaction of this type was also observed in an experiment with 1,5-hexadiene leading to the formation of equimolecular C_2H_4 and 1,3-butadiene.[10,11] From these results it may be concluded that II is of a cyclic structure when it is initially produced and its preferable precursor may be III.

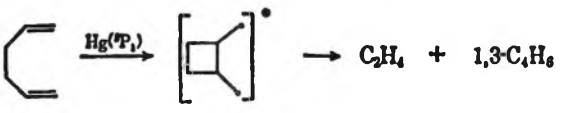


In the photoisomerization of 1,5-cyclooctadiene to bicyclo compound (process 3), IV was proposed as an intermediate by Srinivasan,[4] while the results here obtained indicate the presence of an alternate diradical III, even in a small amount.

(9) R. Srinivasan, *J. Amer. Chem. Soc.*, **82**, 5063 (1960); *ibid.*, **83**, 2806 (1961); *J. Chem. Phys.*, **38**, 1039 (1963).

(10) S. Takamuku, M. Utsunomiya, and H. Sakurai, *Chem. Comm.*, 173 (1969).

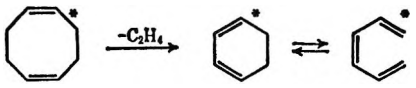
(11) The preferable mechanism may be



An intermediate V similar to II was reported to be produced by the photodecarbonylation of 7-ketonorbornene in liquid phase, forming 1,3-CHD and HT but not benzene.[12] The absence of benzene in the liquid phase supports the suggestion that benzene formation in the vapor phase proceeds from a vibrationally excited ground state molecule II, in agreement with the assumption by Srinivasan. Furthermore, this vibrational energy seems to contribute to the formation of HT because the formation of HT in the liquid phase was regarded as due to a further photolysis of 1,3-CHD different from these results mentioned above.[13]

(12) D. I. Schuster, F-T. H. Lee, A. Padwa, and P. G. Gassman, *J. Org. Chem.*, 30, 2262 (1965).

(13) These observations may suggest the presence of an equilibrium state between 1,3-CHD and HT with excess energy



COMMUNICATIONS TO THE EDITOR

Catalytic Synthesis of Ammonia over the Electron Donor–Acceptor Complexes of Alkali Metals with Graphite or Phthalocyanines

Sir: Some investigations have been carried out on the fixation of nitrogen in the solution by using some reduced transition metal compounds with alkali metals.[1] It was suggested previously[2] that graphite and various phthalocyanine (Pc) films exhibit marked catalytic activities for the hydrogen-activating reactions such as hydrogen chemisorption, hydrogen exchange reaction, and hydrogenation of olefins at room temperature when they are brought into contact with electron donors such as sodium. These reactions do not proceed even at higher temperatures over each of the phthalocyanines, graphite, and sodium.

When nitrogen gas was introduced to the potassium–graphite complex prepared by bringing vapor of alkali metal into contact with graphite in a glass tube in a vacuum, no detectable amount of nitrogen was adsorbed on the complex at room temperature, but as the temperature was raised, it began to be adsorbed. The decomposition of ammonia on the potassium– or sodium–graphite complex was studied. The changes in the pressure and the composition were measured by a mercury manometer and gas chromatography, respectively. When ammonia was introduced over the graphite–alkali metal complex at room temperature, a rapid uptake of ammonia occurred probably by the intercalation of ammonia into the complex. At the same time a considerable amount of hydrogen appeared in the gas phase. The evolution of hydrogen continued as the temperature was raised and nitrogen began to appear in the gas phase at 300°. No decomposition of ammonia to hydrogen and nitrogen took place over the evaporated film of the alkali metals in the conditions described above.

An attempt to get ammonia from the mixture of nitrogen and hydrogen gas was carried out as follows. A 1:1 mixture of hydrogen and nitrogen (total pressure *ca.* 15 cm) was introduced onto the potassium–graphite complex in a closed circulating system and was heated at various temperatures between 50 and 400°. The reaction products were collected by a U shape glass tube in the circulating system cooled by liquid nitrogen and was analyzed by the infrared spectroscopy. It is of great interest that the infrared spectra of the reaction products demonstrated the formation of ammonia. The reaction rate increased with increasing temperature and also with reaction time. The reaction proceeded similarly on the sodium–graphite complex.

When each (*ca.* 100 mg or 2×10^{-4} mol) of the phthalocyanines of such as iron, cobalt, nickel, chlorotitanium, molybdenum, platinum, copper, zinc, and metal-free was evaporated onto a sodium film on the wall of the glass vessel, deeply colored electron donor–acceptor (eda) complex films were formed *in vacuo* at room temperature. (The surface area of the complex films was estimated to be less than 1 m^2 by the BET method using nitrogen.) When 20 cm of nitrogen was introduced onto the eda complex films of Fe, Co, Ti, and Mo phthalocyanines, a considerable amount of nitrogen (1.6 ml STP) was chemisorbed in the tem-

(1) M. E. Vol'pin and V. B. Shur, *Nature*, 209, 1236 (1966); E. E. van Tamelen, G. Boche, and R. Greeley, *J. Amer. Chem. Soc.* 90, 1677 (1968), and references therein.

(2) A. Hérold, *Bull. Soc. Chim. Fr.*, 999 (1955); H. Inokuchi, N. Wakayama, T. Kondow, and Y. Mori, *J. Chem. Phys.*, 46, 837 (1967); M. Ichikawa, M. Soma, T. Onishi, and K. Tamaru, *Trans. Faraday Soc.*, 63, 1215 (1967); *J. Catal.*, 6, 336 (1966); 9, 418 (1967); *Bull. Chem. Soc. Jap.*, 41, 1739 (1968).

Table I: Ammonia Synthesis from N_2 and H_2 over the FePc–Na Complex Film[a]

N_2, cm	H_2, cm	T, °C	NH_3 formed in 20 hr, ml STP
10	30	110	0.26
10	30	170	0.92
10	30	240	3.64
10	30	260	4.60
30	10	240	1.80

[a] The complex film was heated at 200° for 20 hr prior to use and a mixture gas was circulated with a constant rate of 12.2 ml/min.

perature range between 25 and 240°. Hydrogen was also adsorbed to a considerable extent over these complex films. A mixture of N_2 and H_2 (the total pressure was less than 60 cm) with various relative molar ratio was circulated over the Fe phthalocyanine–sodium film in the temperature range between 25 and 260° for 20 hr. The volume of the closed circulating system was about 140 ml and ammonia produced was collected as in the case of graphite–potassium complex. An appreciable amount of ammonia was obtained at higher temperatures above 110° as shown in Table I. The catalytic activity of the complex film for the ammonia formation did not change appreciably in more than ten runs. No ammonia and other products were obtained when hydrogen was admitted to the Fe phthalocyanine complex film at above 280° in the absence of nitrogen gas. Ammonia was also formed to some extent above 170° over the Mo, Ti, and Co phthalocyanine eda complex films with sodium or potassium in the H_2–N_2 system. A negligible amount of ammonia, on the other hand, was formed over the Cu, Pt, Ni, Zn, and metal-free phthalocyanine eda complexes with sodium when a mixture of N_2 and H_2 was introduced onto these complex films above 200°, even though they are markedly active for the hydrogen activation reactions. A considerable amount of ammonia was sorbed and was decomposed into a mixture of N_2 and H_2 over Fe phthalocyanine eda complex film above 120°. The activity of the complex films was decreased considerably in the presence of oxygen, but it was almost completely restored by evacuation and hydrogen treatment at 100° for a long time.[3]

(3) It has been recently found in our laboratory that ammonia was formed slowly at room temperature from a mixture of N_2 (10 cm) and H_2 (45 cm) over the iron phthalocyanine–Na eda complex when the complex was deposited over the activated carbon to have a large surface area.

DEPARTMENT OF CHEMISTRY
THE UNIVERSITY OF TOKYO
HONGO, BUNKYO-KU, TOKYO, JAPAN

MIZUO SUDO
MASARU ICHIKAWA
MITSUYUKI SOMA
TAKAHARU ONISHI
KENZI TAMARU

RECEIVED NOVEMBER 7, 1968

Subnanosecond Observations of the Solvated Electron

Sir: The minimum time resolution obtained with conventional pulse-radiolysis systems has been about 2×10^{-9} sec (2 nsec).[1] Recently a new pulse-radiolysis system was described with a theoretical time resolution of about 20×10^{-12} sec (20 psec).[2] The growth and decay of the solvated electron in acidic aqueous solutions (e_{aq}^-) have now been detected with this new system.

The "stroboscopic" pulse-radiolysis technique[2] utilizes, as analyzing light, the Čerenkov light flashes produced in air by the fine-structure pulses of a 48-MeV linear accelerator (linac) operating at a frequency of 2.86×10^9 Hz. A train of 100 analyzing light flashes is produced by the 100 equispaced fine-structure pulses contained in a single 35-nsec linac output pulse. A simple optical delay varies the phasing between the fine-structure electron pulses and the analyzing light flashes. These light flashes are thus synchronized to "stop the action" of short-lived absorbing species in a manner similar to that of a stroboscope. Slow alterations of the optical delay allow the growth and decay of a short-lived absorbing species to be followed in the time interval between fine-structure electron pulses (0.35 nsec), using a conventional, "slow" photomultiplier detection system. The theoretical resolving time of this technique was estimated to be about 20 psec.[2] This limitation was due to the different velocities in the sample of the analyzing light flashes and the fine-structure electron pulses and also to the estimated width of the fine-structure electron pulses.

Some modifications have been made to the stroboscopic pulse-radiolysis system originally described.[2] A conical (axicon) lens was incorporated in the optical

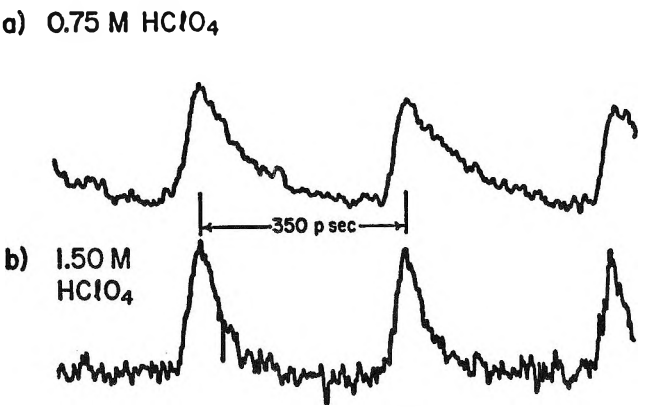


Figure 1. The formation and decay of e_{aq}^- in acidic aqueous solutions as observed by the stroboscopic technique. The periodicity in the patterns corresponds to a change of 10.5 cm in the optical path of the analyzing light. This distance is equivalent to the 350-psec spacing of the fine-structure pulses.

(1) J. W. Hunt and J. K. Thomas, *Radiation Res.*, 32, 149 (1967).
(2) M. J. Bronskill and J. W. Hunt, *J. Phys. Chem.*, 72, 3762 (1968).

system to improve focusing of the Čerenkov analyzing light. A signal-averaging computer (Fabritek Model 1062) was used to improve the signal-to-noise ratio of the absorption signal. The most significant improvements, however, were made to the Toronto linac, from which both higher currents and higher energies can now be obtained. The observations reported in this note were made with a 43-meV, 1.5-A beam pulse, 35 nsec in length, focused to a mean diameter of about 5 mm at the sample position. The absorbed dose per fine-structure pulse was measured to be about 170 rads, which produces an absorption signal of 2% (at 575 nm) for e_{aq}^-.

Figure 1a shows the rapidly decaying absorption signal observed at 625 nm in a 0.75 *M* $HClO_4$ solution. This signal was obtained by making 16 sweeps (of 20-sec duration) through the length of the variable optical delay of the stroboscopic system. The periodicity of this absorption corresponds to the time interval between fine-structure electron pulses, *i.e.*, to 350 psec. The apparent lifetime of this absorbing species could be altered by changing the concentration of perchloric acid to 1.5 *M* as shown in Figure 1b. The decays appear to be exponential; the apparent rate constants are compared in Table I to the values obtained by conventional pulse-radiolysis techniques. These rate constants are calculated from the slopes of the straight lines obtained by plotting log (absorbance) against time.

Table I

Concn of $HClO_4$, *M*	Av lifetime (τ_{37}), psec	$k_{e_{aq}^- + H_3O^+}$, M^{-1} sec^{-1}
0.75	61 ± 10	(2.2 ± 0.4) × 10^{10}
1.5	29 ± 5	(2.3 ± 0.4) × 10^{10}
	Published values	(2.06 ± 0.08) × 10^{10} [3]
		(2.26 ± 0.21) × 10^{10} [a]
		(2.36 ± 0.24) × 10^{10} [b]

[a] L. M. Dorfman and I. A. Taub, *J. Amer. Chem. Soc.*, 85, 1375 (1963). [b] S. Gordon, E. J. Hart, M. S. Matheson, J. Rabani, and J. K. Thomas, *ibid.*, 85, 2370 (1963).

Figure 2 shows the absorption spectrum of this species. Observations were limited to the region from 400 to 650 nm by the optical filters and photomultiplier tube used in the detection system. The known spectrum for e_{aq}^-, obtained in microsecond times,[3] is shown for comparison, normalized at 525 nm.

We conclude that the observed absorption is due to the solvated electron. The normal bimolecular rate constant for the reaction $e_{aq}^- + H_3O^+$ seems to describe the kinetics observed at subnanosecond times. The

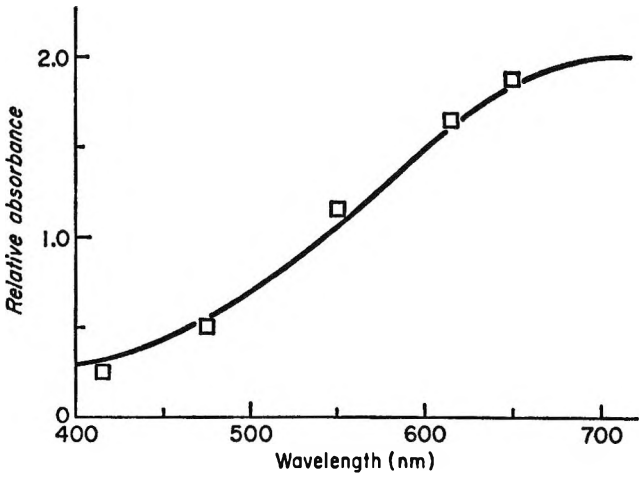


Figure 2. Measured spectrum of absorbing transient in Figure 1 (□), compared to known spectrum of e_{aq}^- (solid line).[3]

observed rise-time (10–90%) for the formation of the absorption signal observed in this system is less than 35 psec. Since the minimum resolving time for a 2 cm cell length is 20 psec,[2] it can be shown that the fine-structure electron pulse is less than 20 psec long.[4] This length is very close to the theroretically predicted values. The formation of e_{aq}^- is not observed and probably occurs in times shorter than the resolving time of the system. No evidence for nonhomogeneous short-lived "spur" type reactions has been observed to date.

Acknowledgments. We are indebted to Professor K. G. McNeill, Mr. E. W. Horrigan, and the operating team of the University of Toronto Linear Accelerator for their efforts in improving the linac beam. We also wish to thank Mr. Vince Terpstra of Ahearn and Soper, Toronto, for the loan of a demonstration Fabritek instrument computer. This work was supported by Grant No. A 4525 of the National Research Council of Canada and by the National Cancer Institute of Canada. M. J. B. is indebted to the National Cancer Institute of Canada for a Research Fellowship and R. K. W. is indebted to the Medical Research Council of Canada for a Studentship.

(3) J. P. Keene, *Radiation Res.*, 22, 1 (1964).

(4) The 35-psec rise time of the system is the convolution of the inherent rise time of the 2-cm cell (20 psec) with the identical distributions of the linac fine-structure and Čerenkov light pulses. Assuming a Gaussian distribution for the linac fine-structure pulse, we calculate that 50% of the high-energy electrons must occur within a burst 15 psec in length. The calculated pulse length would be even shorter if the solvation time for the subexcitation electron cloud, thought to be 10 to 20 psec, had been considered.

DEPARTMENT OF MEDICAL BIOPHYSICS
UNIVERSITY OF TORONTO
AND ONTARIO CANCER INSTITUTE
TORONTO 5, ONTARIO, CANADA

M. J. BRONSKILL
R. K. WOLFF
J. W. HUNT

RECEIVED JANUARY 7, 1969

Electron-Transfer Spectra and the II–III Oxidation Potentials of Some Lanthanide and Actinide Halides in Solution[1]

Sir: Interest in the stability of the 2+ valence state in the transplutonium element series and in the related II–III standard oxidation potentials has recently been stimulated by the demonstration of the existence of Md^{2+} and No^{2+} in aqueous media.[2,3] The purpose of the present communication is to put forward our estimates of the II–III standard oxidation potentials for this series. These estimates are based in part on the recently determined Md and No II–III oxidation potentials,[2,4,5] on Jørgensen's refined spin-pairing electronic energy theory[6] (some of the coefficients of the theory for the f^n electronic configurations are recorded incorrectly in ref 6a and these are corrected in ref 6b), and in part on measurements of the electron-transfer absorption bands of some of the tervalent lanthanide and actinide bromide and chloride complexes in anhydrous ethanol solution. The spectral measurements and oxidation potentials are interrelated on the basis of a calibration utilizing the known linear relationship between the standard II–III oxidation potential and the wave number of the lowest energy electron-transfer band.[7,8] In the application here of the refined spin-pairing electronic energy treatment to oxidation potentials, the calculations include secondary corrections accounted for by multiples of Racah's parameters of interelectronic repulsion, E^3, and first-order corrections accounted for by multiples of the Landé parameters, ζ. Values for both E^3 and ζ are available from $f \rightarrow f$ transition spectroscopy for each lanthanide and actinide case considered, making appropriate extrapolations where the data are as yet unknown.[6,9,10]

For the lanthanide series the II–III oxidation potentials of Sm, Eu, and Yb listed in the "measd" column of Table I were known. Fitting the three-parameter-refined spin-pairing energy theory to these points yielded $D = 0.664$ V, $E - A = 0.277$ V, and $W = 4.21$ V, and from these values the corresponding potential of every other member of the series was calculated. Only the lowest of these potentials, 2.4 V for Tm, however, is recorded in the "calcd" column of Table I since this is the only other case where the corresponding electron-transfer band is not in the uv cutoff and an independent experimental determination of the potential can be made.

The lowest energy wave numbers of the electron-transfer bands of the measurable lanthanide bromides, namely, Sm^{3+}, Eu^{3+}, Tm^{3+}, and Yb^{3+}, originally reported by Jørgensen,[6a] were remeasured in anhydrous ethanol solution, and these results are listed in the "measd" column of Table I. From the wave numbers for Sm, Eu, and Yb plotted against the corresponding II–III oxidation potentials, a linear calibration is obtained from which the II–III oxidation potentials of Tm and some of the transplutonium elements can be readily determined by measuring the wave number of the lowest energy electron-transfer absorption band. In the case of Tm an electron-transfer band is measured at 44,300 cm^{-1}, corresponding on the calibration plot to the potential 2.2 V reported in the "measd" column of Table I. This result is in excellent agreement with the above theoretical value of 2.4 V, or 46,200 cm^{-1} for the corresponding electron-transfer band position.

In the transplutonium series, from the theory and the known II–III oxidation potentials of Md and No presented in the "measd" column of Table I, the II–III oxidation potentials of Cm, Bk, Cf, Es, and Fm were calculated and the results are listed in the adjacent "calcd" column. It is important to recognize here that although we apply essentially a three-parameter phenomenological theory, where three known oxidation potentials or electron-transfer band wave numbers are required for a complete determination of the three unknown parameters and the II–III oxidation potentials for the entire series, only two of the three simultaneous equations describing the potentials of Md and No, in combination with Cm, Bk, Cf, Es, or Fm, are linearly independent. As a result, the three parameters of the theory are undetermined in these cases, but, notwithstanding, each of the above potentials is definitely determined from the values specified for Md and No.

Am presents a special case in these considerations. The three simultaneous equations describing the Md, No, and Am potentials are linearly independent, as they are in the analogous lanthanide case, so here at least one of the parameters, D, W, or $E - A$, of the theory must be known in order to determine the other two parameters and the Am potential. Since the Am potential cannot be determined from a measurement of the electron-transfer band, because the latter is ob-

(1) Research sponsored by the U. S. Atomic Energy Commission under contract with the Union Carbide Corp. This paper was presented by L. J. N. at the Seventh Rare Earth Research Conference, Coronado, Calif., Oct 28–30, 1968.

(2) J. Maly and B. B. Cunningham, *Inorg. Nucl. Chem. Letters*, **3**, 445 (1967).

(3) (a) J. Maly, T. Sikkeland, R. J. Silva, and A. Ghiorso, *Science*, **160**, 1114 (1968); (b) G. T. Seaborg, *Ann. Rev. Nucl. Sci.*, **18**, 53 (1968).

(4) E. K. Hulet, R. W. Lougheed, J. D. Brady, R. E. Stone, and M. S. Coops, *Science*, **158**, 486 (1967).

(5) R. J. Silva, T. Sikkeland, N. Nurmia, A. Ghiorso, and E. K. Hulet, *J. Inorg. Nucl. Chem.*, in press.

(6) (a) C. K. Jørgensen, *Mol. Phys.*, **5**, 271 (1962); (b) C. K. Jørgensen, *ibid.*, **7**, 17 (1963).

(7) J. C. Barnes and P. Day, *J. Chem. Soc.*, 3886 (1964).

(8) F. S. Dainton, Special Publication No. 1, The Chemical Society, London, 1954, p 18.

(9) C. K. Jørgensen, "Orbitals in Atoms and Molecules," Academic Press, New York, N. Y., 1962, pp 8–23, 146–157.

(10) (a) W. T. Carnall and P. R. Fields, Advances in Chemistry Series, No. 71, American Chemical Society, Washington, D. C., 1967, p 86; (b) W. T. Carnall, P. R. Fields, and K. Rajnak, *J. Chem. Phys.*, **49**, 4424, 4443, 4450 (1968).

Table I: Measured and Calculated Wave Numbers of the Absorption Maximum for the Lowest Energy Electron-Transfer Bands of Lanthanide and Actinide Bromides in Anhydrous Ethanol Solution and the Related Standard II–III Oxidation Potentials

	Wave number of the absorption maximum for the lowest energy electron-transfer band, cm^{-1}		Standard II–III oxidation potential, V	
	Measd	Calcd	Measd	Calcd
Samarium bromide[a]	40,300	Fitted	1.55 ± 0.02[f,g]	Fitted
Europium bromide[a]	30,300	Fitted	0.43 ± 0.01[f,g]	Fitted
Thulium bromide[b]	44,300	46,200	2.2	2.4
Ytterbium bromide[a]	35,300	Fitted	1.15 ± 0.01[f,g]	Fitted
Americium-243 bromide[c]		41,000		2.6
Curium-244 bromide[d]		61,100		5.0
Berkelium-249 bromide[d]		47,600		3.4
Californium-249 bromide[a]	35,700	36,500	1.9	2.0[j]
Einsteinium-253 bromide[a]	33,400	33,400	1.6	1.6[k]
Fermium bromide[e]		31,100		1.3
Mendelevium bromide[e]		21,600	0.15 ± 0.05[h,g]	Fitted
Nobelium bromide[e]		8,700	-1.45 ± 0.05[i,g]	Fitted

[a] The assignment in these cases is confirmed by observing the corresponding chloride electron-transfer band 6000 cm^{-1} higher. [b] The corresponding chloride electron-transfer band in these cases is not observed because it is in the uv cutoff. [c] Neither the bromide nor the chloride electron-transfer band is observable in this case—the former because it is obscured by strong f → d transitions and the latter because it is in the uv cutoff. [d] Neither the bromide nor the chloride electron-transfer band is observable in this case because they are in the uv cutoff. [e] In these cases a 20-μg minimum measurable sample is not yet available for the electron-transfer absorption measurements. [f] L. B. Asprey and B. B. Cunningham, *Progr. Inorg. Chem.*, **2**, 267 (1960). [g] These values were determined by standard methods that are independent of electron-transfer spectra. [h] References 2 and 4. [i] Reference 5. [j] On the basis of negative polarographic results B. B. Cunningham estimates a 1.4-V lower limit on this potential (private communication). [k] A lower limit of 1.1 V on this potential is estimated in ref 2.

scured in this case by strong f → d transitions, the best way to proceed is to extract a value of D from the theory and spectral analysis of the Am^{3+} $5f^6 \rightarrow 5f^6$ transitions.[9,10] From the latter one obtains $D = 0.714$ V, and from this the Am potential is calculated to be 1.7 V, a value clearly in conflict with other chemical evidence which indicates that the Am potential should be appreciably greater than the corresponding Cf potential.[11–13] This apparent discrepancy is resolved here by noting that a value for D similarly extracted from the theory and spectral analysis of the analogous Eu^{3+} $4f^6 \rightarrow 4f^6$ transitions is 0.777 V, a factor of 1.17 times the best value of D obtained above by fitting the lanthanide potentials to the theory. Applying the same correction factor to the transplutonium case gives $D = 0.610$ V, which in combination with the Md and No potentials yields $E - A = 0.946$ V, $W = 9.943$ V and the best value for the Am potential, 2.6 V, recorded in the "calcd" column of Table I.

From the above transplutonium potentials and the lanthanide calibration plot, properly shifted to apply to the actinides,[14] the wave number of the lowest energy electron-transfer band was determined in each case, and these values are listed in the "calcd" column of Table I. Of this series only $CfBr_3$ and $EsBr_3$ presently provide measurable electron-transfer bands in anhydrous ethanol solution. The others either have the electron-transfer band in the uv cutoff (Cm, Bk), have it obscured by strong f → d transitions (Am), or are not yet available in sufficient quantity to permit the absorption measurements (Fm, Md, and No). From the wave number of the measured $CfBr_3$ electron-transfer band and the actinide calibration plot, the Cf II–III potential was "measured" at 1.9 V and similarly, the Es II–III potential was "measured" at 1.6 V. These potentials are recorded in the "measd" column of Table I and they are in excellent agreement with the values calculated from the theory using the Md and No potentials.

In conclusion, the present work presents new and timely information consistent with recent chemical work[2–6,11–13] on the II–III oxidation potentials of some of the lanthanide and transplutonium elements, it indicates that a linear Barnes and Day type of lanthanide calibration plot shifted by +0.8 V can be applied to the transplutonium series, and it substantiates Jørgensen's spin-pairing energy treatment of electron-transfer spectra and related oxidation potentials. A complete description of this work will appear later with some new results in a full paper.

Acknowledgment. We express our appreciation to Dr. Jack L. Ryan for several helpful discussions on electron-transfer spectra.

(11) G. Bouissieres and Y. Legoux, *Bull. Soc. Chim. France*, 386 (1965).
(12) J. Maly, *Inorg. Nucl. Chem. Letters*, **3**, 373 (1967).
(13) F. David and G. Bouissieres, *ibid.*, **4**, 153 (1968).
(14) The origin of the calibration shift will be expounded in a later publication. It is +0.8 V here and this appears to be a characteristic difference between the lanthanides and actinides in several series of compounds.

TRANSURANIUM RESEARCH LABORATORY
OAK RIDGE NATIONAL LABORATORY
OAK RIDGE, TENNESSEE 37830
L. J. NUGENT
R. D. BAYBARZ
J. L. BURNETT

RECEIVED DECEMBER 2, 1968

Langmuir–Hinshelwood Mechanism as Revealed by Thermal Desorption Study. The Catalytic Decomposition of Methyl Formate on Copper Surface

Sir: Recently the thermal desorption method (tdm) has been applied to the study of adsorbed species and it has been found that various adsorbed states show different reactivities.[1] However, these species observed by tdm are not necessarily identical with those of real intermediates during reactions catalyzed by solid surfaces.

In the present work we have applied this method to the study of the decomposition of methyl formate over copper surface.[2] We have succeeded in revealing the details of this reaction which obeys the Langmuir–Hinshelwood mechanism by comparing the kinetic parameters determined by tdm with those obtained from conventional kinetics.

The study of decomposition kinetics was carried out in a pressure range 5–25 mm at temperatures between 100 and 170°. The copper catalyst was prepared from cupric hydroxide by reducing with hydrogen at 180° and was evacuated at 300°. The products were found to be CO, H_2, and traces of CO_2. The initial rate r_0 is expressed as

$$r_0 = kKP/(1 + KP)$$

where P is the initial pressure of methyl formate and k and K are constants. From the temperature dependences shown in Figure 1, k and K are found to be $5.4 \times 10^{27} \exp(-27{,}200/RT)$ molecules cm^{-2} sec^{-1} and $5.4 \times 10^{-10} \exp(14{,}300/RT)$ mm^{-1}, respectively.

When adsorption equilibrium is established for the reactant, it follows that K corresponds to the equilibrium constant, and the heat of "reactive" adsorption, Q, is 14.3 kcal/mol. Accordingly, the constant k has the physical meaning of the rate constant of surface reaction with the activation energy E_r of 27.2 kcal/mol.

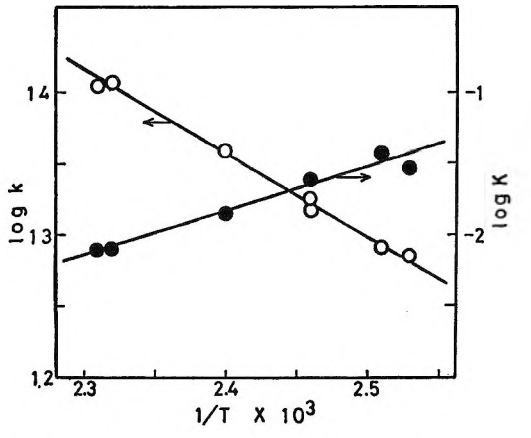


Figure 1. Temperature dependence of k and K.

The study on thermal desorption was carried out on the same catalyst as was used for the kinetic study. After a known amount of methyl formate was adsorbed on the catalyst, the temperature of the catalyst was raised at various rates (β) under evacuation of a constant speed (S). The pressure change due to desorbed gas was followed by means of a Pirani gauge. The composition of the gas phase was continuously analyzed by a mass spectrometer which was directly connected to the system. Large values of the S/β ratio were chosen to hold the condition under which the partial pressures of desorbed species are proportional to their respective rates of desorption.[3]

The desorption spectra shown in Figure 2 exhibit that there are several states in adsorbed methyl formate; since CO and H_2 were generated simultaneously in peak B, adsorbed methyl formate corresponding to this peak is likely responsible to the decomposition which gives CO and H_2.

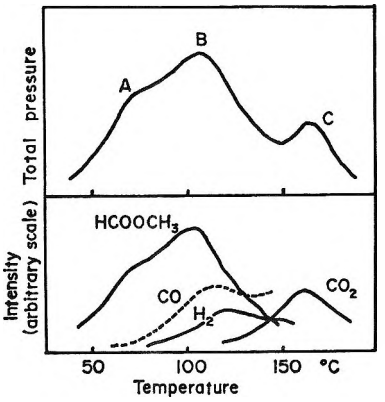


Figure 2. The desorption spectra of methyl formate (β = 0.13 deg sec^{-1}).

Both results of kinetics and of separated studies on thermal desorption of CO and H_2 adsorbed on Cu show that the desorption rates of CO and H_2 are much larger than that of decomposition of adsorbed methyl formate. Therefore on raising the temperature, methyl formate adsorbed at room temperature is supposed to change in the following way

$$HCOOCH_3(g) \xleftarrow[k_d]{} HCOOCH_3(a) \xrightarrow[k_r]{} CO(g) + H_2(g)$$

where k_d and k_r are the rate constants of the desorption and of the surface reaction, respectively. They are expressed in the forms $k_d = \nu_d \exp(-E_d/RT)$ and $k_r = \nu_r \exp(-E_r/RT)$, where ν's and E's are frequency factors and activation energies, respectively. When the adsorption of methyl formate is in a partial equilibrium ($k_d \gg k_r$), the following equations hold at temperatures

(1) Y. Amenomiya and R. J. Cvetanovic, *J. Catal.*, 9, 28 (1967).
(2) E. Miyazaki and I. Yasumori, *Bull. Chem. Soc. Jap.*, 40, 2012 (1967).
(3) P. A. Redhead, *Trans. Faraday Soc.*, 57, 641 (1961).

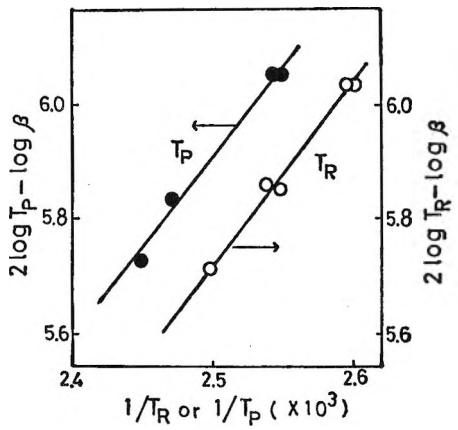


Figure 3. Plots of eq 1 and 2 for peak B.

T_R and T_P, which correspond to peak maxima of methyl formate and carbon monoxide, respectively.[4]

$$2 \log T_R - \log \beta = E_d/RT_R + \log (E_d/\nu_d R) \quad (1)$$

$$2 \log T_P - \log \beta = E_d/RT_P + \log (E_r/\nu_d R) \quad (2)$$

By measuring T_R and T_P for various β(0.13 − 0.31°/sec), the left-hand side of eq 1 (or 2) is plotted against $1/T_R$ (or $1/T_P$), as shown in Figure 3. From the slopes and the intercepts of these plots E_d, E_r, and ν_d were estimated, and these values are summarized in Table I. There is good agreement with corresponding values in the reaction scheme assumed above. The coincidence of a Q value with those of E_d suggests that the activation energy of adsorption for methyl formate is negligible.

Table I

	Kinetics	Thermal desorption
E_r, kcal/mol	27.2 ± 0.6	27.8 ± 1.3
Q or E_d, kcal/mol	14.3 ± 1.0	14.8 ± 0.7 (eq 1)
		14.6 ± 1.0 (eq 2)
ν_d, sec^{-1}	...	1.6×10^6
ν_r, molecules cm^{-2} sec^{-1}	5.4×10^{27}	...

It is therefore concluded that the adsorbed state corresponding to peak B is the true intermediate in the catalytic decomposition of methyl formate to CO and H_2 and that the surface reaction is the rate-determining step. Details and more general discussions for the case where the adsorption equilibrium is not established will be published later.

(4) Reference 3, p 655.

DEPARTMENT OF CHEMISTRY
TOKYO INSTITUTE OF TECHNOLOGY
OOKAYAMA, MEGURO, TOKYO, JAPAN

NAOHIRO MOMMA
IWAO YASUMORI

RECEIVED JUNE 7, 1968